

3. At 7
/ AECD-3646

THE REACTOR HANDBOOK

Volume 2

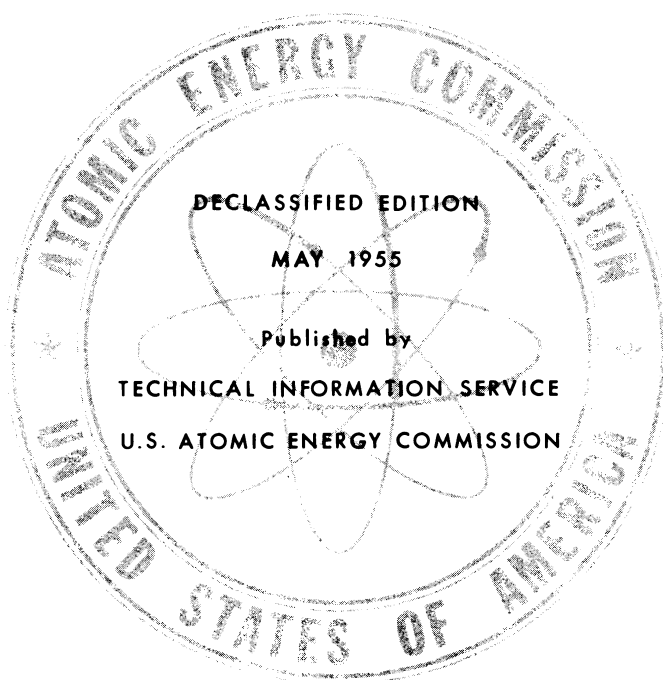
Engineering

UNITED STATES
ATOMIC
ENERGY
COMMISSION
MAY 1955
AECD-3646



THE REACTOR HANDBOOK

VOLUME 2 ENGINEERING



Contributors to the first edition:

ARGONNE NATIONAL LABORATORY

BATTELLE MEMORIAL INSTITUTE

BROOKHAVEN NATIONAL LABORATORY

KNOLLS ATOMIC POWER LABORATORY NORTH AMERICAN AVIATION, INC.

NUCLEAR DEVELOPMENT ASSOCIATES

OAK RIDGE NATIONAL LABORATORY

VITRO CORPORATION OF AMERICA

Reviewed on behalf of the Atomic Energy Commission by a
Review Board consisting of:

HARVEY BROOKS

Harvard University

S. LAWROSKI

Argonne National Laboratory

P. F. GAST

Nucleonics Division
General Electric Company

M. C. LEVERETT

ANP Project
General Electric Company

J. P. HOWE

North American Aviation, Inc.

W. H. ZINN, Chairman

Argonne National Laboratory

Program managed on behalf of the Division of Reactor
Development and the Technical Information Service by:

D. F. MASTICK

Division of Military Application*

**UNIVERSITY OF
ARIZONA LIBRARY**
Documents Collection

23 AUG 1955

Coordination and editing by:

J. F. HOGERTON and R. C. GRASS

Vitro Corporation of America

For sale by the Superintendent of Documents, U. S. Government Printing Office
Washington 25, D. C. - Price \$5.50 (Paper cover)

*Present address General Precision Equipment Corporation.

FOREWORD

With the rapid maturity of reactor technology and its growing application to industrial power reactors, there has developed an urgent need for a comprehensive and critical compilation of nuclear engineering data. At the request of Dr. L. R. Hafstad, Director of Reactor Development, and in accord with an over-all program for the organization and consolidation of AEC-developed technical information, the Commission's Technical Information Service has issued this Reactor Handbook for convenient reference use by scientists and engineers engaged on AEC reactor projects.

The material presented in this first edition of the Handbook represents the efforts of specialists in the various areas of reactor science and technology, and summarizes the accomplishments of the Commission's nuclear reactor program to date. Future editions are planned as continuing advances in this field may require.

The Commission extends its appreciation to all participants in the Reactor Program for the time and effort expended in the completion of this Handbook.

Lewis L. Strauss
Chairman
United States Atomic Energy Commission

REVIEW BOARD PREFACE

The Review Board was appointed by the Director of the Reactor Development Division in December of 1951. The Board found itself in agreement with the objective of preparing a reactor handbook at an early date, although it was recognized that this placed the effort under a considerable handicap as did the necessity of combining the efforts of numerous author groups.

The Board instituted a mechanism for review of the material as prepared by the author groups. In the work of review the members of the Board called upon many individuals in the various Laboratories for critical comments. Without this assistance the review could not have been performed in the two or three weeks usually available, and the members of the Board express their indebtedness and thanks to these reviewers.

The general format of the Handbook received consideration and the result is recognized as a compromise of what is most desirable in a handbook and what is practical under the present circumstances.

The ultimate success of the Handbook will depend a great deal upon the refinements in subject matter and presentation which will come about in subsequent revisions. It is expected that such revisions will profit enormously from suggestions from the users of the Handbook.

To the Editorial Coordinator, John F. Hogerton, to Donald F. Mastick who represented the Technical Information Service, and to William W. Galbreath who served as secretary, the Board expresses its appreciation for a cordial working relationship. Above all, thanks are due to the various author groups who made the task of review easier by their patience in receiving criticism and suggestions.

THE REVIEW BOARD

Harvey Brooks	Stephen Lawroski
Paul F. Gast	Miles C. Leverett
John P. Howe	W. H. Zinn, Chairman

EDITORIAL PREFACE

The purpose of the Reactor Handbook is to provide a condensed source of reliable data and reference information for those working in the reactor field. Work on this first edition, jointly sponsored by the Division of Reactor Development and the Technical Information Service, started in January 1952, with a fifteen-month publishing target. The authors, most of whom had heavy project commitments, had one month in which to plan their work, and three months to a year in which to survey the field and prepare their compilation. Those preparing large sections were called upon to submit their material in parts and were allowed on the average of one month for reworking a given part after review. The Review Board had the difficult task of reviewing the Handbook material in random increments, with two to three weeks in which to review a given increment. The schedule did not permit a second review following the author's reworking. The editors had from one to three weeks in which to prepare Handbook material for the publisher. To distribute the publisher's load at Oak Ridge, parts of sections were put into the publishing machinery while other parts were still in preparation by the authors.

To meet the schedule, it was necessary to make certain compromises which should be noted here:

1. A somewhat arbitrary approach has necessarily been taken on the problem of coverage, not only with respect to the subjects treated but also the data presented on a given subject. Before using a particular section for the first time, the reader should consult the author's preface which brings out any major limitations in the scope or treatment of the data presented.

2. The policy was adopted early in the program not to attempt a detailed documentation of the source of the data presented. Some specific references are given; however, source identification is restricted primarily to tables or figures which have been taken intact from project reports or the open literature.

3. It has not been possible to achieve the consistency one would like in the use of units. In general, the metric system is used where the data are considered to be of interest primarily to "scientists," and the English system is used where the data are considered to be of interest primarily to "engineers." An attempt has been made to include conversion factors in the body of tables and charts, and in some cases data are expressed in dual units.

4. To simplify page make-up and printing problems, the decision was made early in the program to eliminate the background grid from graphs. Data were to have been presented in tabular form in cases where it was considered important to retain accurate values. In actual practice some graphs have been reproduced with grid and it is felt that this practice can and should be extended in the next edition of the Handbook.

In the present edition of the Handbook, each volume is indexed separately. The organization is the same throughout. Sections are numbered consecutively within a volume; chapters consecutively within a section; and figures, tables, and formulae consecutively within a chapter.

The first edition combines elements of a "Handbook of Chemistry and Physics," a Marks' "Mechanical Engineer's Handbook," a Mellor's "Treatise on Inorganic Chemistry," and an industrial data book. This result is in some degree inherent in a work that cuts across a number of scientific and engineering disciplines; however, greater unity of presentation should be possible in future editions.

The editors are most appreciative of the attention their problems have received from the Review Board and the author groups, and from Alberto F. Thompson and Donald F. Mastick of the AEC staff. They are most appreciative, also, of the cooperation of William W. Galbreath of ANL, W. H. Sullivan of ORNL and Dennis Puleston of BNL, who did much to advance the Handbook effort at their respective sites, and of R. L. Cummins, E. C. Schulte, and their publishing personnel in the Technical Information Service at Oak Ridge.

John F. Hogerton and Robert C. Grass
VITRO CORPORATION OF AMERICA

A NOTE ON PREPARATION OF THE DECLASSIFIED EDITION

This declassified edition of the Reactor Handbook has been issued not only as a convenience to workers in the reactor field but also to help acquaint science and industry generally with techniques, processes and equipment which may find wider application.

In preparing the volumes of the declassified edition, deletions were made in the classified volumes according to security requirements. The remaining material was then assembled with the minimum editorial attention necessary for coherent presentation. Since this procedure has not, in general, provided for bringing the data up to date, users of these declassified volumes should consult section prefaces to determine how old the data is in each section.

TECHNICAL INFORMATION SERVICE

CONTENTS OF VOLUME 2-ENGINEERING

SECTION 1 - LIGHT- AND HEAVY-WATER-COOLED SYSTEMS	1
Authors' Preface	3
Chapter 1.1 General Reactor Characteristics	5
1.2 Heat Dissipation and Thermal Cycles	7
1.3 Physical and Thermodynamic Properties of Light and Heavy Water	21
1.4 Heat Transfer	43
1.5 Hydrodynamics	55
1.6 Spatial Distribution of Heat Generation	87
1.7 Steady-state Heat Removal	123
1.8 Transient Generation and Removal of Heat	141
1.9 Thermal-stress Analysis	165
1.10 Water Decomposition	175
1.11 Corrosion	193
1.12 Calculation of Water Activity	235
1.13 Fuel-element Design	239
 SECTION 2 - LIQUID-METAL-COOLED SYSTEMS	 245
Authors' Preface	247
Chapter 2.1 Liquid-metal Coolants for Nuclear Reactors	249
2.2 Properties of Liquid Metal Coolants	253
2.3 Heat-transfer Correlations for Liquid Metals	277
2.4 Handling of Liquid-metal Coolants	287
2.5 Reactor Cooling and Power Conversion Cycles	311
2.6 Mechanical Components and Design Considerations	321
2.7 Design and Construction of External Heat-transfer System	337
 SECTION 3 - GAS-COOLED SYSTEMS	 367
Authors' Preface	369
Chapter 3.1 General Reactor Characteristics	371
3.2 Thermal Cycles	375
3.3 Properties of Gas Coolants	381
3.4 Heat Transfer and Fluid Flow for Gases	409
3.5 Fuel Elements	451
3.6 Circulating Systems	461
3.7 Economic Comparison of Gas Coolants	477
3.8 Radioactivity in Coolants	483

SECTION 4 - AQUEOUS FUEL SYSTEMS	503
Authors' Preface	505
Chapter 4.1 General Reactor Characteristics	507
4.2 Neutron Chain Reactions in Aqueous Homogeneous Systems	511
4.3 Properties of Aqueous Solution Systems	555
4.4 Properties of Aqueous Slurry Systems	659
4.5 Properties of Aqueous Moderators	673
4.6 Nuclear Design Data	679
4.7 Engineering Design Information	691
SECTION 5 - LIQUID-METAL-FUEL SYSTEMS	741
Author's Preface	743
Chapter 5.1 General Reactor Characteristics	745
5.2 Composition and Properties of Liquid Metal Fuels	749
5.3 Engineering Design	771
SECTION 6 - FUSED-SALT SYSTEMS	799
Author's Preface	801
Chapter 6.1 General Reactor Characteristics	803
6.2 Composition of Fused-salt Systems	809
6.3 Properties of Fused-salt Systems	835
SECTION 7 - HANDLING AND CONTROL	851
Authors' Preface	853
Chapter 7.1 Remote Handling	855
7.2 Remote Viewing	875
7.3 Hot Laboratories	909
7.4 Nuclear Reactor Instrumentation and Control	925
SECTION 8 - REACTOR DESIGNS	983
Author's Preface	985
Chapter 8.1 Introduction	987
8.2 Graphite-moderated Heterogeneous Reactors	991
8.3 Beryllium-oxide-moderated Heterogeneous Reactors	1001
8.4 Light-water-moderated Heterogeneous Reactors	1005
8.5 Heavy-water-moderated Heterogeneous Reactors	1015
8.6 Miscellaneous Heterogeneous Reactors	1021
8.7 Unmoderated Heterogeneous Reactors	1023
8.8 Graphite-moderated Homogeneous Reactors	1029
8.9 Light-water-moderated Homogeneous Reactors	1033
APPENDIX	1039
INDEX	1049

Section 1

LIGHT- AND HEAVY-WATER-COOLED SYSTEMS

**Prepared by
REACTOR ENGINEERING DIVISION
ARGONNE NATIONAL LABORATORY**

AUTHORS' PREFACE

Considerable experience has been gained during the past ten years in the design and operation of reactors for service at slightly elevated temperatures. More recently many designs have been directed toward higher water temperatures.

This section contains much information applicable to the engineering of high-temperature reactors; in addition it contains pertinent engineering information on water-cooled reactors. Primary emphasis is placed on problems of heat transfer; conventional formulae and correlations for water, as well as discussions of two-phase flow, are presented in a form found useful by this author group. Discussions of the spatial distribution of heat generation are included (1) to characterize the power distribution found in these reactors, (2) to point out factors affecting the power distribution, (3) to present the usual methods used in computing distribution, and (4) to list design procedures followed to give optimum distributions. Methods of analyzing transient effects, both nuclear and thermodynamic, are included for simple cases.

Problems of thermal stress, water decomposition, and corrosion are discussed; formulae and data useful in reactor design are given. Typical fuel-element designs and a method of calculating water activity are included.

The author group recognized during the early stages of preparation that much of the available information was not readily amenable to a handbook style of presentation. In addition, the difficulties of organizing the many variables in reactor engineering into a concise but comprehensive formulation made some departure from usual handbook style necessary. Consequently, much of the information is presented in the form of general discussions or general design procedures, rather than as tabulated data or formulae.

The cutoff date for completion of data in this Section was July 1952. In some instances, however, additional data through February 1953 were included.

Individual chapters were prepared by and are the prime responsibility of the authors listed under each chapter heading. Over-all technical guidance was under the direction of A. Amorosi, J. R. Dietrich, H. Etherington, W. W. Galbreath, Jr., W. C. Gumprich, A. S. Jameson, and J. M. West.

Many members of the Reactor Engineering Division and the staff of Argonne National Laboratory have contributed in the preparation of this section; their help is gratefully acknowledged.

The help of the following people in obtaining and forwarding data on rather short notice or in reviewing the chapters aided greatly in the preparation of this section: W. L. Sibbitt, Purdue University, Chapter 1.3; H. S. Isben, University of Minnesota, Chapters 1.4 and 1.5; S. Krasik, Westinghouse Atomic Power Division and Paul H. Reinker, General Electric, Hanford Works, Chapter 1.6; D. J. DePaul, K. M. Goldman, A. Squire, and D. E. Thomas, Westinghouse Atomic Power Division, Chapter 1.11.

For the Reactor Engineering Author Group

H. Etherington*

W. W. Galbreath, Jr.†

*Present address, American Car & Foundry Industries, Inc., New York, N. Y.

†Present address, Vitro Engineering Division, New York, N. Y.

General Reactor Characteristics

H. Etherington

Two general types of water-cooled reactors have been developed and are in operation or under construction: in the first, water is used as both coolant and moderator; in the second, water is used primarily as the coolant, and graphite serves as the moderator (Hanford production reactors). A distinction is made in the first type between lumped reactors, in which natural or slightly enriched uranium is placed on lattice points, and reactors (here called quasi-homogeneous reactors) in which the coolant-moderator is rather uniformly interdispersed between fuel elements. Other types of reactors operating with boiling or at supercritical temperatures and pressures are being studied, but insufficient information is available for comprehensive treatment.

Both light and heavy water have good heat-transfer properties. The combination of high specific heat and good heat-transfer rates at design conditions make water a satisfactory heat-transfer media for thermal reactors. The specific heat of light water ranges from 1.0 to about 1.2 Btu/(lb)(°F) from 32° to 500°F; the specific heat of heavy water is slightly higher (about 1 percent) over the range 50° to 120°F. Heat-transfer coefficients (h) up to 10,000 Btu/(hr)(sq ft)(°F) are obtained with liquid water. Heat-transfer coefficients for heavy water calculated for the same mass velocity are about 10 percent higher.

The choice between light water and heavy water as a coolant-moderator is based primarily on physics and economic considerations rather than on heat transfer. Both are effective moderators. Light water is more effective in slowing down fast neutrons (i.e., it has a shorter slowing-down length), but it also has a much higher neutron absorption cross section. Heavy water is therefore more advantageous as a moderator where a very low thermal absorption cross section is of great importance, e.g., in natural-uranium reactors where neutron economy is important from the plutonium production standpoint (Savannah River Reactors) and in research reactors (CP-5) where it is desirable to produce a reactor of reasonably large size with very low critical mass to achieve a high ratio of thermal neutron flux to total power generation. Light-water moderation would be advantageous where very small reactors are desired or where there are strong limitations on the mass of water which may be contained in the reactor, e.g., water-cooled reactors which operate above the critical temperature. In general, if the application is one for which either light-water or heavy-water moderation is feasible, the superior nuclear performance of heavy water must be balanced against its higher cost. Clearly, the low absorption cross section of heavy water constitutes no particular advantage in reactors that contain high-cross-section materials, e.g., a highly enriched power reactor utilizing fuel elements clad with stainless steel. It has not been found possible to design light-water-moderated, natural-uranium reactors with sufficiently high reactivity to be of practical interest. In uranium-plutonium converter reactors, the choice between light- and heavy-water moderation depends upon an economic balance of the cost of enriching the uranium if light water is used vs the cost of heavy water, itself.

A simple comparison of light water and heavy water as coolant-moderator is made in the following generalization in which an idealized core is assumed with a given coolant-moderator/metal ratio utilizing the same constructional materials: Light water, by virtue of its large scattering cross section and relatively small leakage, reduces the amount of uranium necessary for criticality in small-radii, enriched reactors. This permits designing smaller reactors of the quasi-homogeneous type. On the other hand, as the size of the reactor is increased and the neutron leakage is correspondingly reduced, the critical mass of the D_2O reactor becomes less than that of the H_2O reactor.

The general advantages of water-cooled reactors are:

- (1) The use of water as a moderator permits the use of non-moderating construction materials.
- (2) The non-combustibility of water reduces handling problems.
- (3) Water has good heat-transfer properties.
- (4) Light water is cheap and readily available.
- (5) Reactors moderated and cooled by heavy water have a negative temperature coefficient.
- (6) Water-moderated reactors can be designed to have large negative temperature coefficients.
- (7) Radiation damage to water is relatively unimportant.
- (8) Water presents no freezing problems at normal temperatures.
- (9) Water is relatively easy to pump.
- (10) Water offers some lubrication.
- (11) Water offers the possibility of direct steam-generation in a boiling reactor.
- (12) Water technology is generally well known.

The general limitations for water reactors are:

- (1) Water corrodes uranium at low temperature and reacts vigorously with it at elevated temperature.
- (2) It is necessary to select materials that have adequate corrosion resistance at operating temperatures.
- (3) Pressurizing is necessary if the liquid phase is required above 212°F, and the critical temperature must not be exceeded.
- (4) The primary coolant circuit must be shielded to prevent activity produced by neutron reaction with oxygen.
- (5) Water may react with clad or constructional materials at very high temperatures.
- (6) The initial cost of heavy water and the economic necessity of reducing leakage and loss of heavy water to a minimum.

The over-all reactor design is a balance between many factors, some of which are discussed in the following chapters. Perhaps the most important, however, is the interrelation between good engineering design, the most advantageous utilization of fuel material, the cost and availability of fuel, and the cost of reprocessing spent fuel. Some of these factors, such as data on the cost and availability of fuels, are not included because of the obvious relationship with production figures; no attempt has thus been made to integrate these various factors. It is apparent, however, that, over and above the particular design of the machine, good reactor design must consider the feed material available, the cost of preparing the fuel into suitable elements, the cost of construction and operation of the reactor, the cost of reprocessing spent fuel, and the amount of strategic material held up during the various processes. A critical evaluation of the success of the operation and performance of a reactor must include the cost and supply of fuel material.

CHAPTER 1.2

Heat Dissipation and Thermal Cycles

E. K. Falls

Thermal energy generated in existing low-temperature water-cooled reactors, both production and research types, is dissipated to air or river water because the temperatures are too low for production of power. Reactors that heat the coolant to a temperature sufficiently above ambient temperature are able, if they can be operated in combination with appropriate thermodynamic cycles, to produce useful power. Although external heat dissipation can be accomplished in various ways, the manner in which the primary coolant absorbs the heat generated within the core is independent of the external systems. Accordingly, the problem of removing heat from the core is considered separately from that of disposing of or using the thermal energy. The power cycle is considered as a special application of heat dissipation.

HEAT REMOVAL FROM REACTOR

From heat-transfer considerations only, several water-cooling methods are available for removing thermal energy from the heat-generation section (core) of reactors, namely, (1) by sensible heat gain, (2) by boiling, and (3) by supercritical evaporation.

SENSIBLE HEAT GAIN

This water-cooling method utilizes an increase in temperature of the liquid coolant to remove the thermal energy generated within the core. The maximum permissible temperature of the water leaving the core is less than the saturation temperature corresponding to the absolute pressure of the primary-coolant system. Core cooling by sensible heat gain is a characteristic of the NRX, MTR, CP-3, STR, and Hanford water-cooled reactors. The method may utilize heavy or light water, forced or natural circulation, and atmospheric or pressurized systems.

BOILING

Compared with water-cooling by sensible heat gain, the two-phase boiling method offers, except in the region at and near the critical pressure, the advantages of higher heat-absorption rates per unit mass of cooling water and a lower circulation rate. Either natural or forced convection appears feasible. The use of forced circulation will provide closer control over the fluid-film temperature difference than can be obtained with natural convection but will of course require circulation pumps.

Steam generated in the core is separated from liquid water in the space above the core and can be disposed of in several ways: (1) condensation in an upper section of the reactor pressure vessel by an evaporative type of heat exchanger (shielded from the core) which evaporates water in a secondary-coolant circuit; (2) condensation in an external condenser which thus eliminates the need for shielding; and (3) utilization in a steam turbine as the thermodynamic fluid.

SUPERCRITICAL PRESSURE

Boiling-water reactors, owing to the large density changes accompanying evaporation, involve nuclear problems not encountered with reactors cooled by heating a liquid. To obviate these problems, reactors may be designed to operate at supercritical pressures and are therefore subject only to temperature changes of density.

HEAT DISSIPATION

ATMOSPHERIC OR LOW-PRESSURE SYSTEMS

At installations where the water supply is of high purity, the coolant may be pumped directly from the source, usually a river, through the reactor or heat exchanger, and discharged into the river downstream of the intake. Cooling water supplies that contain suspended solids can be clarified by the use of settling basins alone or in conjunction with coagulants. If the activity of the effluent is above accepted tolerance levels, retention basins must be provided to permit radioactive decay.

Elimination of all radioactive contamination from the effluent of a reactor installation requires an intermediate heat transfer; this can be accomplished in a closed-cycle primary system. Final dissipation of heat to the surroundings could then be accomplished with a water-to-air or water-to-water surface-type heat exchanger. Both heavy and light water reactor-coolants are used with this system. If it were not for losses by leakage followed by evaporation and release of radioactivity, a contact type of heat exchanger (such as a cooling tower) could be used to dissipate heat directly from the reactor coolant.

Light water in a secondary-coolant system can be utilized to dissipate the thermal energy (1) directly to the air by circulation through a cooling tower or (2) by an open cycle with no recirculation.

PRESSURIZED SYSTEMS WITH STEAM GENERATION

Regardless of the manner in which steam is generated when it is used in a turbine, a portion of the thermal energy of the steam is converted into mechanical energy in the turbine, and the remainder is rejected in the condenser and dissipated to the surroundings. Typical steam-generation installations are illustrated by the schematic line diagrams below.

A two-fluid coolant system with forced circulation of liquid primary coolant is illustrated by Fig. 1.2.1. An external heat exchanger is used to partially evaporate the secondary coolant. Steam separation occurs in the steam drum.

Two natural-circulation boiling-type reactors are illustrated by Fig. 1.2.2, which has an external heat exchanger, and Fig. 1.2.3, which has an internal heat exchanger. The condensing coil of Fig. 1.2.3 must be shielded from neutron activity which originates in the core. Both installations use a steam drum for steam separation in the secondary system.

Figure 1.2.4 illustrates a flooded-pressure-vessel, boiling, primary-coolant system with forced circulation and external steam space. The secondary-coolant system is similar to that of the two preceding illustrations.

Elimination of the temperature difference between the primary and secondary coolants in the water-to-water heat exchanger represents a thermodynamic gain. This can be accomplished by using the reactor coolant as the thermodynamic fluid. Dry steam (Fig. 1.2.5) is supplied directly to the turbine from the steam space of the reactor pressure vessel. The external part of the system is similar to typical steam plants except for problems of shielding and elimination of leakage.

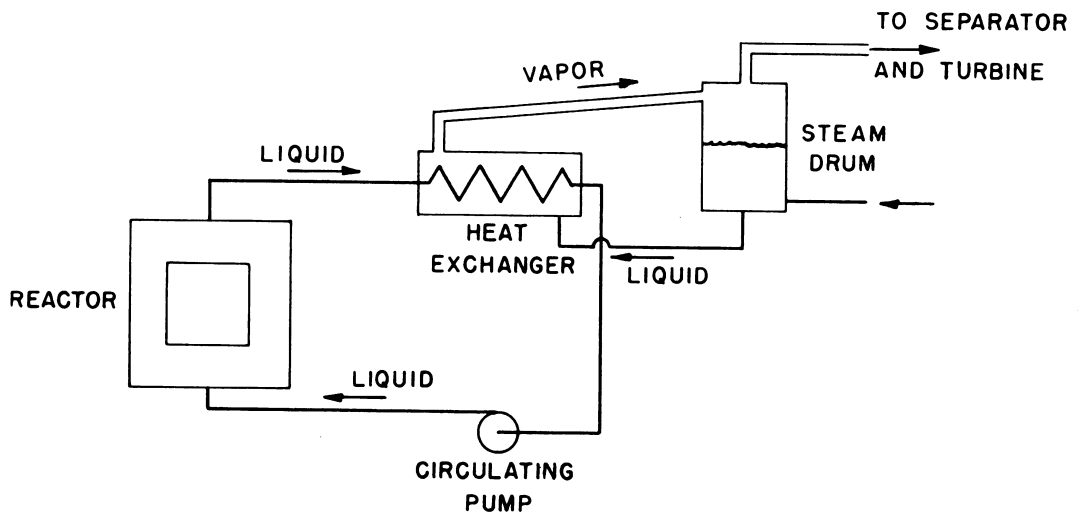


Fig. 1.2.1 — Forced Circulation of Liquid Primary Coolant External Heat Exchanger. Submitted by Argonne National Laboratory, Dec. 15, 1952.

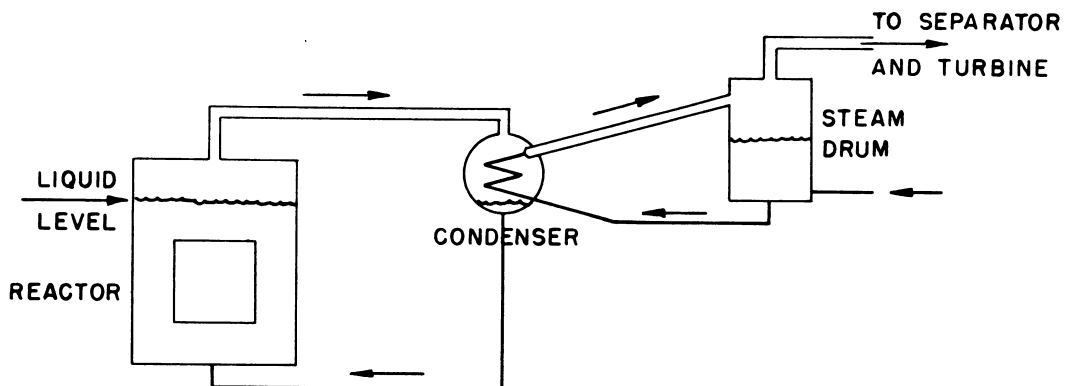


Fig. 1.2.2 — Natural-circulation, Boiling, Primary Coolant with External Evaporative Condenser. Submitted by Argonne National Laboratory, Dec. 15, 1952.

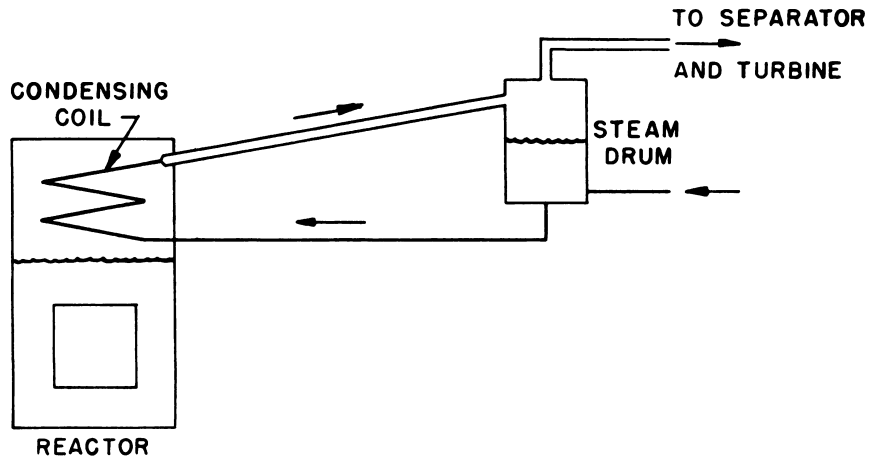


Fig. 1.2.3—Boiling Primary Coolant with Internal Evaporative Condenser.
Submitted by Argonne National Laboratory, Dec. 15, 1952.

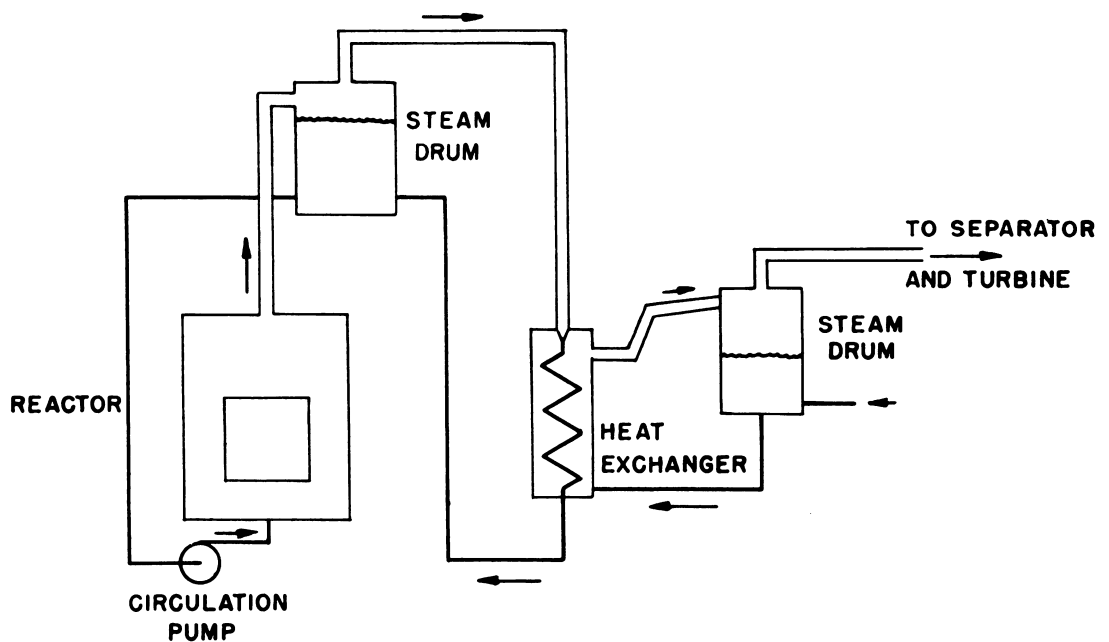


Fig. 1.2.4—Forced-circulation, Mixed-flow, Reactor Cooling with External Separation of Primary Coolant and Separate Evaporative Condenser. Submitted by Argonne National Laboratory, Dec. 15, 1952.

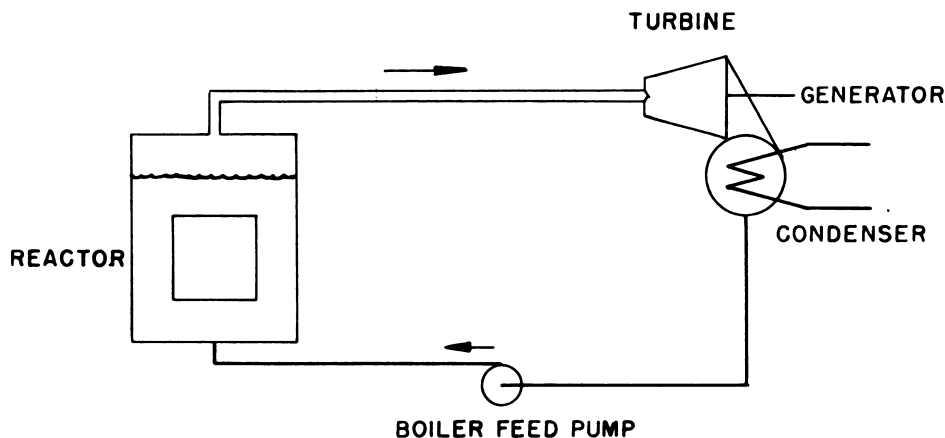


Fig. 1.2.5— Rankine Thermodynamic Cycle with Heat Exchanger Replaced by Reactor. Submitted by Argonne National Laboratory, Dec. 15, 1952.

STEAM CYCLES

Until the advent of regeneration and reheat practices, the Rankine cycle was considered the basic comparison for steam plants. This cycle consists of two isentropic work processes and two constant-pressure heat processes. The first work process increases the pressure on the fluid to that of the steam generator. The second process, that of constant-pressure heat addition, includes the sensible heat gain of the liquid, the latent heat, and (if used) the superheat of the vapor. The third process, isentropic expansion converts the available thermal energy into external work. The last process, rejects the unavailable thermal energy at constant pressure to a condenser. A discussion of the individual processes follows.

COMPRESSION PROCESS

The compression (pump) process increases the pressure on the liquid from atmospheric (or that pressure existing within the condenser) to the pressure within the steam generator. It may be accomplished in one step if feedwater is not heated, or in several steps as is common with the regenerative cycle.

The work input of the pumping process is obtained from the gross work output of the expansion process.

HEAT-ADDITION PROCESS

The heat-addition process of the several steam cycles includes the sensible heat gain of the liquid, evaporation of the liquid, and (if used) initial superheating of the steam. The sensible heat gain of the Rankine cycle process increases the liquid temperature to that of saturation; the thermal energy is supplied entirely by the heat source.

The modern central-station steam plant operates (1) on a regenerative steam cycle if the steam pressure is moderate or (2) on a regenerative-reheat steam cycle if the pressure is high (this assumes that initial superheat alone is insufficient to prevent a low-quality steam at the last stage of the turbine). In practice, steam withdrawn from the turbine at predetermined pressures serves as the heat source for the feedwater heaters.

EXPANSION PROCESS

The conversion from thermal energy to external work occurs during the expansion process. (Of the gross output of the turbine or engine, a portion is required to operate the auxiliary equipment). A Rankine cycle expansion process expands all the steam supplied at the turbine throttle from boiler pressure down to condenser pressure. With regard to the regenerative cycle, at each stage of extraction a portion of the initial supply to the turbine is removed from the turbine.

From practical considerations, the expansion process within the steam turbine is subject to limitations imposed upon the terminal state of the steam; the final temperature and pressure are established by the condenser, and the quality of the steam at the last row of turbine blades must be sufficiently high to prevent erosion of the blades; (a minimum of 86 to 90 percent should be maintained). These two limitations fix the state of the steam at the last turbine stage.

When initial superheating is used, it is not usually possible to maintain the minimum quality at the last turbine stage for straight-through expansion of steam initially at a high pressure. Proper operation is obtained, however, by removal of steam from the turbine at an intermediate pressure followed by drying and superheating (reheating) and reintroduction into the expansion process.

HEAT-REJECTION PROCESS

Only a part of the thermal energy added to the water and steam is utilized in a steam cycle. The heat-rejection process discards the remainder from the system. If a closed cycle is used, the condenser serves this purpose and returns the fluid to its initial state.

Condenser operation is a function primarily of coolant temperature and good design. In large condenser installations, the temperature of the cooling water may increase only 5° to 15°F with a temperature difference of 10° to 20°F between the condensing steam and the exit cooling water.

PLANT EFFICIENCIES

Plant efficiencies based on the Rankine cycle will not be considered here as this cycle has been largely displaced by the more efficient regenerative cycle. The ideal regenerative cycle assumes an infinite number of feedwater heaters; without superheating of the steam, it has the same thermal efficiency as a Carnot cycle operating between the same temperature limits. Although in practice, a finite number of feedwater heaters plus superheating is used, the ideal cycle serves as a basis for comparison. Efficiencies can be obtained from diagrams such as Fig. 1.2.6. Actual over-all plant efficiencies of representative steam plants are considerably lower than those shown but reflect the inherently higher efficiency of the regenerative cycle.

When the reactor and the cooling system of a nuclear-powered steam plant are considered simply as a source of heat and no allowance is made for the power required to control and cool the reactor, the over-all efficiency is practically that of conventional plants that operate on the same steam cycle. Allowance for the pumping requirements, however, decreases the over-all efficiency of the unit. Separate computation of the steam-plant efficiency permits the pumping-power requirements for one or more types of reactor and coolant system to be considered in combination with the steam plant.

A typical study which illustrates the effects of steam pressure, steam temperature, and temperature rise of the coolant through the reactor is illustrated by Figs. 1.2.7 through 1.2.10. Until the temperature rise drops to approximately 20°F, which corresponds to a relatively high circulation rate, the combined over-all efficiency of the reactor and steam plant is affected only slightly by changes of the coolant water differential temperature.

REACTOR APPLICATIONS

The feasibility and efficiency of a nuclear power plant are limited by the available temperature extremes. The lower temperature limit is the surrounding environment or the temperature of the cooling water supplied to the condenser. The upper temperature limit is set by stability of fuel elements, cladding, coolant, and other design limitations. The over-all temperature difference is a summation of temperature differentials throughout the system as shown in Fig. 1.2.11.

Inasmuch as a high over-all plant efficiency is desired, several conflicting factors must be compromised to obtain an optimum design: (1) a high differential temperature is desirable across the steam system in order to obtain a high thermal efficiency for the system; (2) a high differential temperature is desirable across the primary coolant-system elements; and (3) a large differential temperature across the heat exchanger keeps its size and cost to a minimum.

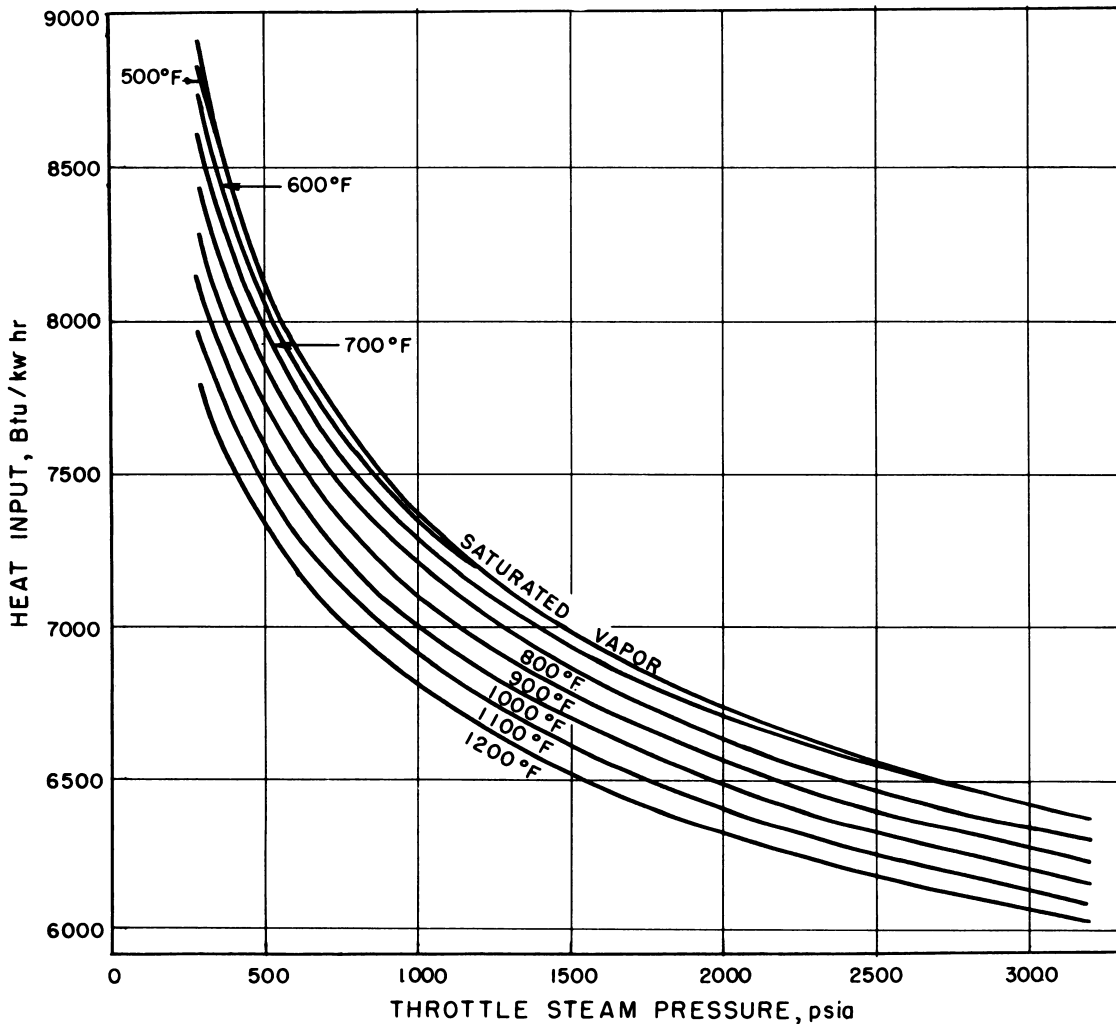


Fig. 1.2.6— Theoretical Regenerative Steam-cycle Heat Rates. Reprinted from A. M. Selvey and P. H. Knowlton, Theoretical Regenerative Steam-cycle Heat Rates, Trans. ASME 66, No. 6, Aug. 1944.

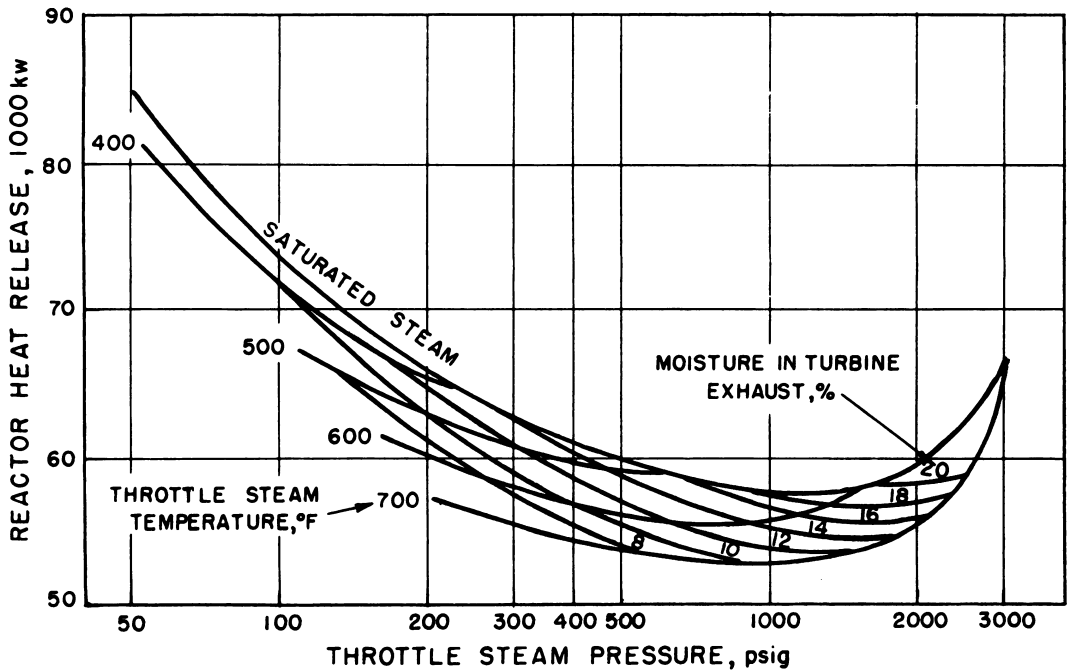


Fig. 1.2.7— Reactor Heat Release vs Turbine Steam Conditions. Redrawn from ORNL-133, 1948. Calculations based on reactor producing 70×10^3 kw with 50 Btu/lb heat rise. Steam leaving boiler must be 8 to 10% higher in pressure and 1% higher in temperature than steam at turbine throttle.

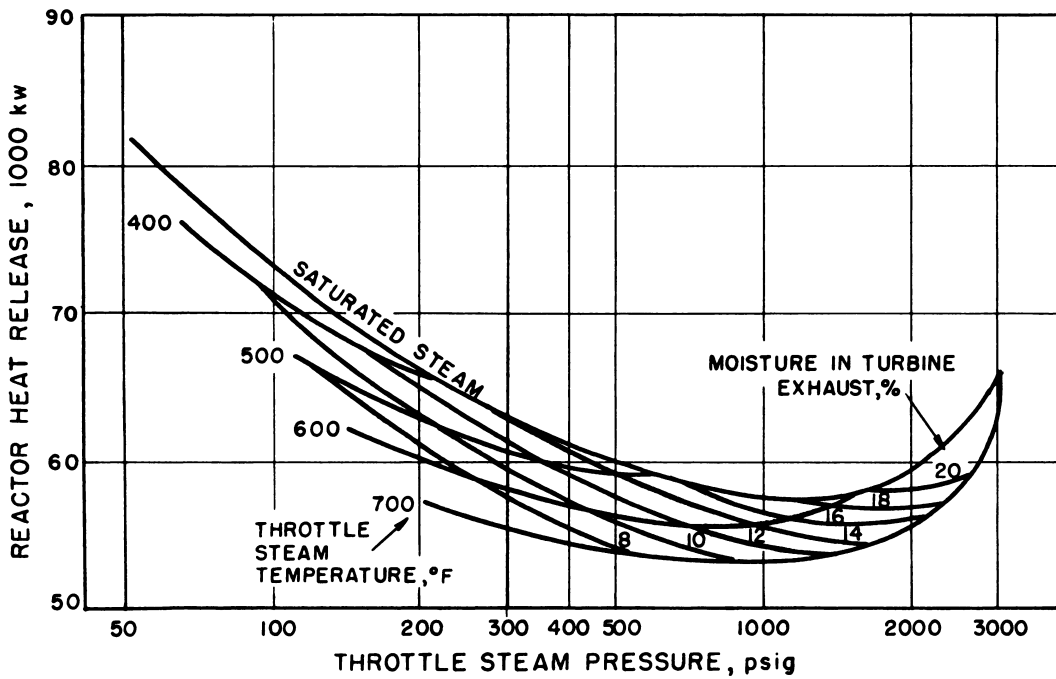


Fig. 1.2.8— Reactor Heat Release vs Turbine Steam Conditions. Redrawn from ORNL-133, 1948. Calculations based on reactor producing 70×10^3 kw with 40 Btu/lb heat rise. Steam leaving boiler must be 8 to 10% higher in pressure and 1% higher in temperature than steam at turbine throttle.

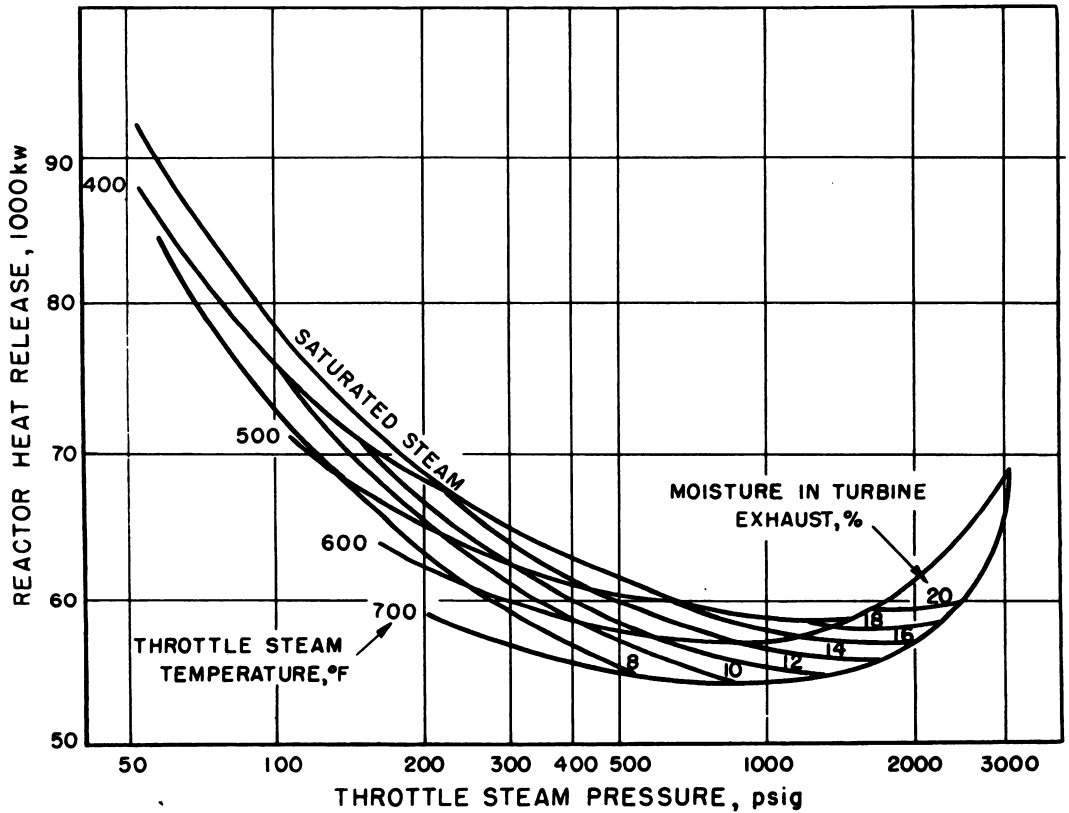


Fig. 1.2.9—Reactor Heat Release vs Turbine Steam Conditions. Redrawn from ORNL-133, 1948. Calculations based on reactor producing 70×10^3 kw with 30 Btu/lb heat rise. Steam leaving boiler must be 8 to 10% higher in pressure and 1% higher in temperature than steam at turbine throttle.

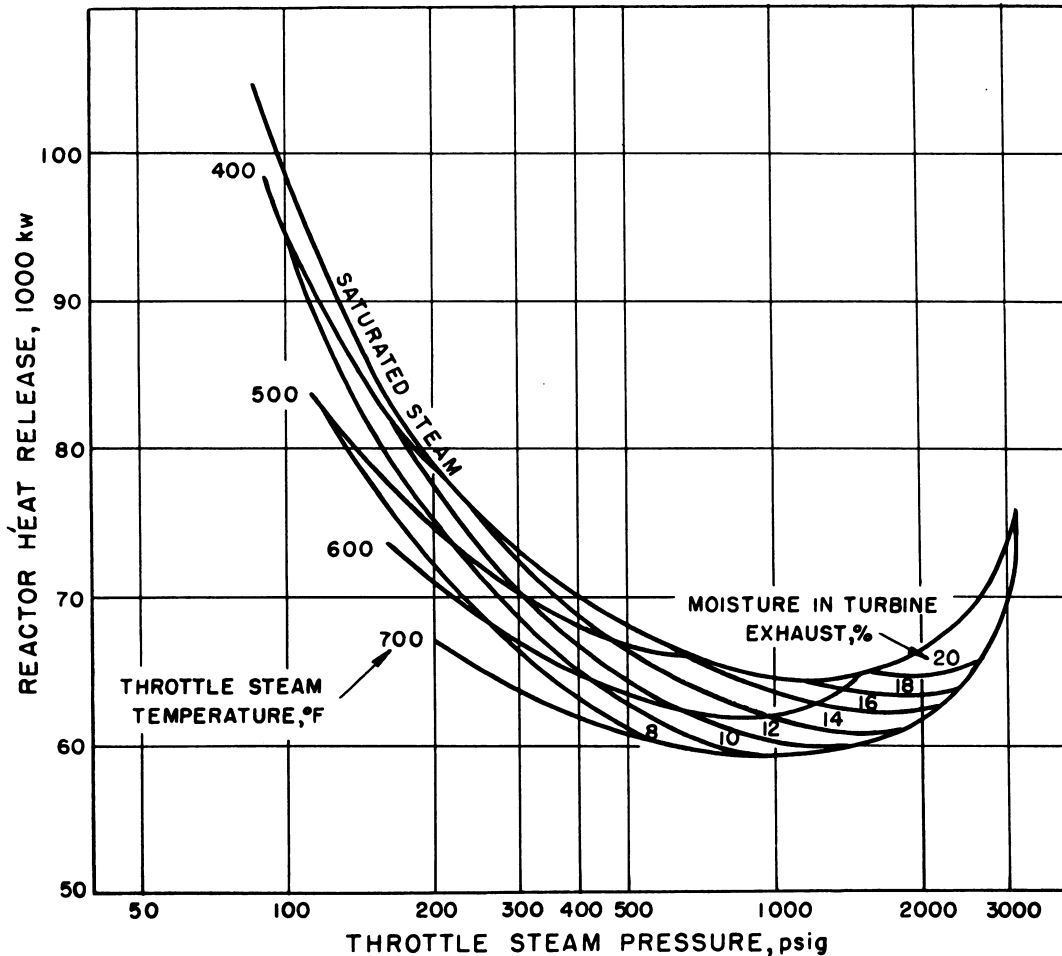


Fig. 1.2.10—Reactor Heat Release vs Turbine Steam Conditions. Redrawn from ORNL-133, 1948. Calculations based on reactor producing 70×10^3 kw with 20 Btu/lb heat rise. Steam leaving boiler must be 8 to 10% higher in pressure and 1% higher in temperature than steam at turbine throttle.

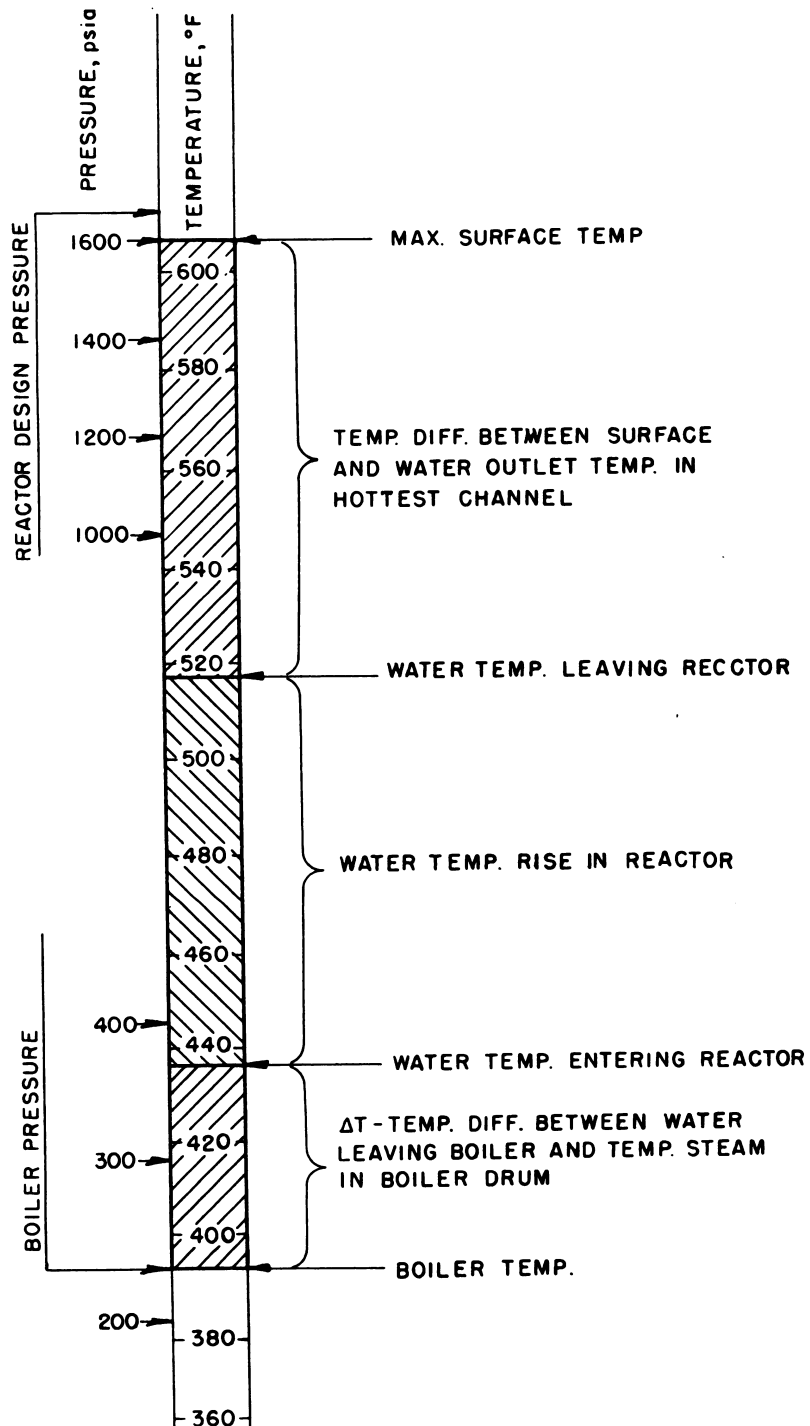


Fig. 1.2.11 — Representative Temperature Distribution in a Reactor-heated Power Cycle Showing Relationship with Pressure. Redrawn from ORNL-133, 1948.

SELECTED READING LIST

THERMODYNAMICS, H. E. Obert, 1st ed, McGraw-Hill Book Co., New York, 1948.

STEAM POWER STATIONS, G. A. Gaffert, 3rd ed, McGraw-Hill Book Co., New York, 1946.

APPLIED ENERGY CONVERSION, B.G.A. Skrotzki and W. A. Vopat, 1st ed, McGraw-Hill Book Co., New York, 1945.

THEORETICAL REGENERATIVE-STEAM-CYCLE HEAT RATES, A. M. Selvey and P. H. Knowlton, Trans. Am. Soc. Mech. Engrs. 66, No. 6, Aug. 1944.

THE STEAM-TURBINE REGENERATIVE CYCLE—AN ANALYTICAL APPROACH, J. Kenneth Salisbury, Trans. Am. Soc. Mech. Engrs. 64, April, 1942, p 231.

THERMODYNAMICS, J. H. Keenan, John Wiley & Sons, Inc., New York, 1941.

Physical and Thermodynamic Properties of Light and Heavy Water

P. A. Lottes

The properties of light and heavy liquid water and light-water vapor frequently used in heat transfer calculations are presented in tabular and/or graphic form. Heavy-water properties are available for relatively low temperatures only and are generally similar to those of light water. For most engineering calculations concerning heavy water at higher temperatures, the corresponding property of light water, with the exception of density, has been used since data are not available above approximately 100°F.

The data are presented by individual property. Critical properties, constant-pressure specific heat, thermal conductivity, dynamic viscosity, Prandtl number, density and latent-heat values are included when available; exception is made for the specific heat of light-water vapor and the latent heat of light liquid water because data presented in Keenan and Keyes¹ are the best available. In general, tabular compilations of the physical and thermodynamic properties for light and heavy liquid water are presented. Whenever possible, a graphical comparison of these properties is included. Graphs of frequently used properties of light-water vapor are included. Thermal conductivity data for heavy water are not available; consequently, thermal conductivity and the Prandtl number calculation, which includes the value of thermal conductivity, have been omitted.

A recent study by Wellman² presents a review of available data on the thermodynamic and physical properties of light liquid water in the form of tables of values; the study includes an evaluation of the accuracy of the values reported. These data were used in the preparation of this chapter with the exception that graphical data for the density and vapor pressure of light liquid water were taken from Keenan and Keyes.¹

The data of Kirshenbaum³ for heavy water have been recalculated into units used predominately in engineering heat transfer calculations.

Values for the properties of light-water vapor were provided by Sibbitt⁴ from an evaluation currently being made by Purdue University.

¹References appear at end of chapter.

Table 1.3.1 — Critical Properties of Light Water

Critical temperature	705.40	°F
	374.2	°C
Critical pressure	3206	psia
	218.2	atm
Critical density	19.9	lb/cu ft
	0.320	gm/ml

Table 1.3.2 — Critical Properties of Heavy Water

Critical temperature	700.7	°F
	371.5	°C
Critical pressure	3212	psia
	218.6	atm
Critical density	22.7	lb/cu ft
	0.363	gm/ml

Table 1.3.3 — Constant-pressure Specific Heat (c_p) of Liquid Light Water

(Conversion Factor: From Btu/(lb)(°F) to cal/(gm)(°C) multiply by 1)

Temperature, °F	c_p , Btu/(lb)(°F)						
	Saturated liquid	Pressure, psia, compressed liquid					
		1000	2000	3000	4000	5000	6000
32	1.0083	1.0032	1.0004	0.9979	0.9948	0.992	0.989
40	1.0048	1.0014	0.9986	.9959	.9926	.991	.988
50	1.0004	0.9991	.9963	.9933	.9899	.987	.984
60	0.9990	.9968	.9939	.9907	.9872	.984	.981
70	.9980	.9949	.9920	.9888	.9848	.982	.979
80	.9975	.9943	.9912	.9878	.9840	.981	.978
90	.9974	.9938	.9904	.9871	.9832	.980	.977
100	.9976	.9932	.9897	.9864	.9824	.978	.975
110	.9976	.9932	.9895	.9860	.9819	.978	.974
120	.9977	.9934	.9895	.9858	.9817	.978	.974
130	.9981	.9937	.9896	.9856	.9814	.977	.973
140	.9988	.9940	.9897	.9854	.9811	.977	.973
150	.9996	.9950	.9905	.9861	.9817	.978	.974
160	1.0004	.9959	.9913	.9868	.9823	.978	.974
170	1.0012	.9969	.9921	.9876	.9829	.978	.974
180	1.0022	.9980	.9931	.9885	.9836	.979	.975
190	1.0034	.9984	.9945	.9896	.9847	.980	.975
200	1.0047	1.0008	.9958	.9907	.9857	.981	.976
210	1.0061	1.0021	.9971	.9919	.9868	.982	.977
212	1.0064	1.0024	.9974	.9921	.9870	.982	.977
220	1.0079	1.0039	.9988	.9934	.9881	.983	.978
230	1.0097	1.0057	1.0005	.9951	.9896	.985	.980
240	1.0119	1.0075	1.0023	.9967	.9910	.986	.981
250	1.0142	1.0095	1.0041	.9984	.9925	.988	.983
260	1.0165	1.0117	1.0061	1.0003	.9943	.989	.984
270	1.0191	1.0140	1.0082	1.0023	.9961	.991	.986
280	1.0222	1.0163	1.0102	1.0042	.9979	.993	.988
290	1.0255	1.0194	1.0131	1.0069	1.0005	.995	.989

Table 1.3.3 — (Continued)

Temperature, °F	Saturated liquid	c_p , Btu/(lb)(°F)					
		Pressure, psia, compressed liquid					
		1000	2000	3000	4000	5000	6000
300	1.0289	1.0232	1.0166	1.0101	1.0037	.998	.992
310	1.0322	1.0270	1.0200	1.0132	1.0068	1.001	.995
320	1.0354	1.0307	1.0235	1.0164	1.010	1.004	.998
330	1.0404	1.0353	1.0278	1.0205	1.014	1.008	1.002
340	1.0455	1.0399	1.0322	1.0246	1.017	1.011	1.005
350	1.0511	1.0445	1.0365	1.0287	1.021	1.014	1.008
360	1.0564	1.0496	1.0411	1.0331	1.025	1.018	1.012
370	1.0614	1.0553	1.0461	1.0377	1.029	1.021	1.014
380	1.0669	1.0611	1.0510	1.0424	1.034	1.026	1.019
390	1.0728	1.0668	1.0560	1.0471	1.038	1.030	1.022
400	1.0794	1.074	1.062	1.053	1.043	1.035	1.027
410	1.0861	1.080	1.068	1.059	1.048	1.040	1.032
420	1.0941	1.087	1.075	1.065	1.053	1.045	1.037
430	1.1023	1.095	1.082	1.072	1.059	1.051	1.043
440	1.1114	1.105	1.091	1.079	1.066	1.057	1.048
450	1.1212	1.114	1.100	1.087	1.074	1.065	1.056
460	1.1319	1.124	1.109	1.095	1.081	1.071	1.061
470	1.1431	1.136	1.120	1.104	1.090	1.079	1.068
480	1.1545	1.149	1.131	1.114	1.099	1.087	1.075
490	1.1698	1.163	1.143	1.125	1.109	1.095	1.082
500	1.1861	1.176	1.154	1.135	1.118	1.102	1.088
510	1.21	1.19	1.171	1.551	1.132	1.115	1.100
520	1.23	1.21	1.188	1.166	1.146	1.127	1.110
530	1.25	1.23	1.205	1.182	1.160	1.139	1.121
540	1.28		1.225	1.199	1.175	1.152	1.132
550	1.31		1.252	1.218	1.192	1.168	1.147
560	1.34		1.278	1.238	1.209	1.182	1.158
570	1.37		1.304	1.257	1.227	1.198	1.172
580	1.41		1.341	1.283	1.246	1.216	1.189
590	1.46		1.382	1.310	1.265	1.230	1.200
600	1.51		1.448	1.346	1.290	1.25	1.21
610	1.58		1.52	1.385	1.317	1.27	1.23
620	1.65		1.62	1.441	1.352	1.29	1.25
630	1.71			1.509	1.392	1.32	1.27
640	1.88			1.597	1.442	1.36	1.31
650	2.09			1.701	1.505	1.40	1.34
660	2.34			1.817	1.576	1.43	1.36
670	2.84			2.14			
680	3.5			2.56			
690	5.5						

Accuracy for indicated temperature range, %

32–100	0.3	0.3	0.5	0.8	1.1	1.5	1.5
100–200	.2	.2	.4	.8	0.6	1.5	1.5
200–300	.2	.2	.4	.8	.6	1.5	1.5
300–400	.3	.3	.5	.9	.9	1.5	1.5
400–500	.3	.3	.5	.9	.9	1.5	1.5
500–530	1.0	1.0	.7	1.0	.5	1.5	1.5
530–600	1.5		.7	1.0	.5	1.5	1.5
600–620	1.5		1.5	1.0	.5	1.5	1.5
620–660	3.5			3.5	.5	1.5	1.5
660–680	4.0			4.0			
690	5.0						

Table 1.3.4—Specific Heat (c_p) of Liquid Heavy Water at 1 Atm*

(Conversion Factor: From Btu/(lb)(°F) to cal/(gm)(°C) multiply by 1)

Temperature		c_p , Btu/(lb)(°F)
°C	°F	
10	50	1.009
15	59	1.008
20	68	1.006
25	77	1.005
30	86	1.005
35	95	1.004

*Accuracy: $\pm 3.5\%$ Table 1.3.5—Thermal Conductivity (k) of Light Liquid Water

(Conversion Factor: From Btu/(hr)(ft)(°F) to cal/(sec)(cm)(°C) multiply by 0.00413379)

Temperature, °F	k , Btu/(hr)(ft)(°F)						
	Saturated liquid	Pressure, psia, compressed liquid					
		1000	2000	3000	4000	5000	6000
32	0.3185	0.3198	0.3211	0.3227	0.3246	0.3266	0.3286
40	.3245	.3260	.3275	.3294	.3314	.3335	.3358
50	.3319	.3337	.3356	.3377	.3398	.3422	.3447
60	.3397	.3414	.3433	.3454	.3476	.3500	.3528
70	.3472	.3487	.3508	.3530	.3551	.3576	.3604
80	.3532	.3537	.3570	.3590	.3616	.3640	.3665
90	.3589	.3608	.3629	.3651	.3676	.3700	.3723
100	.3641	.3659	.3680	.3703	.3727	.3751	.3777
110	.3689	.3707	.3727	.3760	.3773	.3797	.3822
120	.3733	.3751	.3771	.3792	.3815	.3839	.3862
130	.3772	.3790	.3810	.3831	.3853	.3877	.3900
140	.3810	.3828	.3847	.3868	.3891	.3914	.3938
150	.3836	.3855	.3875	.3897	.3920	.3944	.3968
160	.3861	.3880	.3902	.3924	.3948	.3973	.3997
170	.3884	.3903	.3925	.3947	.3971	.3996	.4020
180	.3905	.3924	.3945	.3968	.3992	.4017	.4041
190	.3923	.3942	.3964	.3986	.4010	.4034	.4059
200	.3935	.3957	.3980	.4003	.4027	.4051	.4074
210	.3943	.3970	.3995	.4017	.4044	.4067	.4088
212	.3944	.3972	.3998	.4020	.4047	.4070	.4091
220	.3950	.3977	.4003	.4028	.4055	.4079	.4103
230	.3957	.3983	.4010	.4037	.4064	.4091	.4118
240	.3961	.3988	.4016	.4043	.4071	.4099	.4127
250	.3964	.3992	.4021	.4048	.4077	.4106	.4135
260	.3964	.3992	.4021	.4048	.4077	.4106	.4135
270	.3962	.3991	.4020	.4048	.4078	.4107	.4136
280	.3959	.3987	.4018	.4048	.4079	.4109	.4140
290	.3955	.3984	.4015	.4047	.4078	.4110	.4141
300	.3952	.3981	.4013	.4045	.4076	.4109	.4141
310	.3948	.3975	.4006	.4038	.4069	.4102	.4137
320	.3944	.3969	.3998	.4029	.4060	.4094	.4131

Table 1.3.5—(Continued)

Temperature, °F	k, Btu/(hr)(ft)(°F)						
	Saturated liquid	Pressure, psia, compressed liquid					
		1000	2000	3000	4000	5000	6000
330	0.3933	0.3958	0.3988	0.4019	0.4050	0.4084	0.4122
340	.3921	.3947	.3977	.4009	.4040	.4075	.4114
350	.3906	.3933	.3965	.3997	.4031	.4069	.4108
360	.3891	.3919	.3951	.3984	.4020	.4059	.4101
370	.3876	.3904	.3936	.3970	.4006	.4046	.4089
380	.3857	.3885	.3919	.3954	.3991	.4031	.4077
390	.3834	.3863	.3900	.3937	.3975	.4017	.4063
400	.3809	.3840	.3880	.3920	.3960	.4000	.4043
410	.3783	.3817	.3860	.3903	.3944	.3983	.4021
420	.3753	.3787	.3833	.3877	.3920	.3960	.3999
430	.3724	.3757	.3806	.3850	.3894	.3936	.3976
440	.3693	.3728	.3776	.3821	.3865	.3907	.3947
450	.3670	.3697	.3745	.3791	.3836	.3880	.3922
460	.3640	.3664	.3713	.3761	.3809	.3857	.3904
470	.3608	.3630	.3678	.3727	.3775	.3823	.3872
480	.3575	.3595	.3642	.3689	.3738	.3784	.3832
490	.3535	.3553	.3603	.3650	.3698	.3744	.3791
500	.3494	.3510	.3562	.3611	.3658	.3705	.3750
510	.3446	.3461	.3519	.3574	.3626	.3677	.3725
520	.3397	.3410	.3475	.3535	.3591	.3645	.3697
530	.3348	.3356	.3424	.3486	.3545	.3602	.3657
540	.3298		.3371	.3437	.3499	.3559	.3617
550	.3246		.3318	.3386	.3452	.3515	.3577
560	.3189		.3256	.3328	.3398	.3465	.3530
570	.3130		.3190	.3265	.3339	.3410	.3478
580	.3064		.3118	.3198	.3277	.3354	.3429
590	.2997		.3045	.3130	.3215	.3298	.3380
600	.2919		.2962	.3056	.3146	.3232	.3318
610	.2839		.2875	.2979	.3074	.3167	.3257
620	.2753		.2778	.2892	.2997	.3100	.3199
630	.2662			.2800	.2916	.3030	.3137
640	.2565			.2700	.2831	.2953	.3068
650	.2454			.2588	.2736	.2869	.2993
660	.2335			.2469	.2634	.2779	.2914
670	.2198			.2319	.2516	.2679	.2830
680	.2056			.2161	.2395	.2577	.2744
690	.1854				.2242	.2463	.2661

Accuracy for indicated temperature range, %

32–100	0.7	1.0	1.0	1.0	1.0	1.0	1.2
100–200	.7	1.0	1.0	1.0	1.0	1.0	1.2
200–300	.6	1.0	1.0	1.0	1.0	1.0	1.2
300–400	.7	1.0	1.0	1.0	1.0	1.0	1.2
400–500	1.7	2.0	2.0	2.0	2.0	2.0	2.5
500–530	4.5	5.0	5.0	5.0	5.0	5.0	5.0
530–600	4.5		5.0	5.0	5.0	5.0	5.0
600–680	5.0		5.0	5.0	5.0	5.0	5.0
690	5.0				5.0	5.0	5.0

Table 1.3.6—Dynamic Viscosity (μ) of Light Liquid Water
(Conversion Factor: From lb/(hr)(ft) to poises multiply by 0.00413379)

Temperature, °F	μ , lb/(hr)(ft)						
	Saturated liquid	Pressure, psia, compressed liquid					
		1000	2000	3000	4000	5000	6000
32	4.340	4.309	4.279	4.248	4.218	4.187	4.157
40	3.742	3.721	3.699	3.677	3.656	3.643	3.613
50	3.169	3.154	3.140	3.126	3.111	3.097	3.082
60	2.731	2.722	2.714	2.705	2.696	2.688	2.679
70	2.372	2.369	2.365	2.361	2.357	2.354	2.350
80	2.084	2.084	2.083	2.083	2.082	2.082	2.081
90	1.847	1.848	1.850	1.851	1.853	1.854	1.855
100	1.650	1.654	1.658	1.663	1.667	1.671	1.675
110	1.487	1.492	1.498	1.503	1.509	1.514	1.519
120	1.353	1.360	1.366	1.373	1.380	1.387	1.394
130	1.236	1.244	1.252	1.259	1.267	1.275	1.283
140	1.137	1.145	1.154	1.162	1.170	1.179	1.187
150	1.050	1.059	1.068	1.077	1.086	1.095	1.103
160	0.970	0.979	0.988	0.997	1.006	1.015	1.024
170	.902	.912	.921	.930	0.939	0.949	0.958
180	.839	.849	.858	.868	.877	.887	.896
190	.786	.796	.806	.815	.825	.835	.845
200	.738	.748	.757	.767	.777	.787	.796
210	.702	.711	.721	.731	.740	.750	.760
212	.687	.697	.706	.716	.726	.735	.745
220	.660	.670	.680	.689	.699	.709	.718
230	.624	.633	.643	.652	.661	.671	.680
240	.595	.604	.614	.623	.632	.641	.650
250	.568	.578	.587	.596	.605	.614	.624
260	.542	.551	.560	.569	.578	.587	.596
270	.515	.524	.533	.541	.550	.559	.567
280	.494	.502	.511	.519	.528	.536	.545
290	.472	.480	.488	.496	.505	.513	.521
300	.452	.460	.468	.476	.484	.492	.500
310	.436	.442	.450	.459	.467	.475	.484
320	.420	.426	.433	.441	.449	.457	.464
330	.405	.411	.418	.426	.433	.440	.448
340	.391	.396	.404	.411	.418	.425	.432
350	.378	.384	.390	.396	.403	.407	.416
360	.366	.372	.378	.383	.390	.396	.401
370	.355	.361	.367	.372	.378	.384	.389
380	.346	.351	.356	.361	.366	.372	.377
390	.336	.340	.345	.350	.355	.360	.365
400	.327	.330	.335	.340	.345	.350	.355
410	.318	.321	.326	.331	.336	.340	.346
420	.310	.312	.317	.322	.327	.331	.336
430	.302	.304	.309	.313	.318	.322	.327
440	.294	.296	.301	.305	.310	.314	.319
450	.287	.289	.293	.298	.302	.306	.310
460	.280	.282	.286	.290	.294	.298	.302
470	.274	.276	.280	.284	.287	.291	.295
480	.267	.270	.273	.277	.280	.284	.288
490	.262	.263	.267	.270	.274	.278	.281

Table 1.3.6 — (Continued)

Temperature, °F	μ , lb/(hr)(ft)						
	Saturated liquid	Pressure, psia, compressed liquid					
		1000	2000	3000	4000	5000	6000
500	0.256	0.257	0.260	0.264	0.267	.271	0.274
510	.251	.251	.255	.258	.262	.266	.269
520	.246	.246	.249	.253	.256	.260	.264
530	.240	.241	.244	.248	.251	.255	.259
540	.235		.239	.243	.247	.250	.254
550	.230		.235	.239	.243	.247	.250
560	.225		.231	.234	.238	.243	.246
570	.221		.226	.229	.234	.238	.242
580	.217		.222	.225	.230	.234	.239
590	.214		.217	.221	.226	.230	.235
600	.210		.212	.217	.222	.227	.233
610	.205		.207	.212	.218	.224	.230
620	.200		.202	.208	.214	.220	.226
630	.195			.202	.209	.216	.222
640	.190			.196	.203	.211	.218
650	.183			.189	.197	.206	.215
660	.177			.182	.192	.202	.212
670	.169			.174	.186	.198	.210
680	.161			.166	.180	.194	.208
690	.148				.172	.188	.203

Accuracy for indicated temperature range, %

32-100	0.5	0.6	0.6	0.6	0.6	1.0	1.0
100-200	.7	.8	.8	.8	.8	1.0	1.0
200-300	1.5	2.0	2.0	2.0	2.0	2.5	2.5
300-400	1.5	2.0	2.0	2.0	2.0	2.5	2.5
400-500	3.0	3.5	3.5	3.5	3.5	4.0	4.0
500-530	4.0	4.5	4.5	4.5	4.5	5.0	5.0
530-600	4.0		4.5	4.5	4.5	5.0	5.0
600-620	7.0		7.0	7.0	7.0	8.0	8.0
620-680	7.0			7.0	7.0	8.0	8.0
690	7.0				7.0	8.0	8.0

Table 1.3.7 — Dynamic Viscosity (μ) of Heavy Liquid Water at 1 Atm*

Temperature		μ	
°C	°F	cp	lb/(hr)(ft)
5	41	1.988	4.809
10	50	1.684	4.074
15	59	1.450	3.508
20	68	1.260	3.048
25	77	1.102	2.667
30	86	0.972	2.352
35	95	.863	2.089

* Accuracy: $\pm 0.5\%$

Table 1.3.8—Prandtl Number ($c_p\mu/k$) for Light Liquid Water

Temperature, °F	$c_p\mu/k$						
	Saturated liquid	Pressure, psia, compressed liquid					
		1000	2000	3000	4000	5000	6000
32	13.74	13.52	13.33	13.14	12.93	12.72	12.51
40	11.59	11.43	11.28	11.12	10.95	10.80	10.63
50	9.55	9.44	9.32	9.19	9.06	8.93	8.80
60	8.03	7.95	7.86	7.76	7.66	7.56	7.47
70	6.82	6.76	6.69	6.61	6.54	6.46	6.38
80	5.89	5.86	5.78	5.73	5.67	5.61	5.55
90	5.13	5.09	5.05	5.01	4.96	4.91	4.87
100	4.52	4.49	4.46	4.43	4.39	4.36	4.32
110	4.02	4.00	3.98	3.94	3.93	3.90	3.87
120	3.61	3.60	3.59	3.57	3.55	3.53	3.52
130	3.27	3.26	3.25	3.24	3.23	3.21	3.20
140	2.98	2.97	2.97	2.96	2.95	2.94	2.93
150	2.74	2.73	2.73	2.72	2.72	2.71	2.71
160	2.51	2.51	2.51	2.51	2.50	2.50	2.49
170	2.33	2.33	2.33	2.33	2.33	2.32	2.32
180	2.15	2.16	2.16	2.16	2.16	2.16	2.16
190	2.01	2.02	2.02	2.02	2.03	2.03	2.03
200	1.88	1.89	1.89	1.90	1.90	1.90	1.91
210	1.79	1.80	1.80	1.80	1.81	1.81	1.82
212	1.75	1.76	1.76	1.77	1.77	1.77	1.78
220	1.69	1.69	1.70	1.70	1.70	1.71	1.71
230	1.59	1.60	1.60	1.61	1.61	1.61	1.62
240	1.52	1.53	1.53	1.54	1.54	1.54	1.55
250	1.45	1.46	1.47	1.47	1.47	1.48	1.48
260	1.39	1.40	1.40	1.41	1.41	1.41	1.42
270	1.33	1.33	1.34	1.34	1.34	1.35	1.35
280	1.27	1.28	1.28	1.29	1.29	1.30	1.30
290	1.22	1.23	1.23	1.24	1.24	1.24	1.24
300	1.18	1.18	1.19	1.19	1.19	1.19	1.20
310	1.14	1.14	1.15	1.15	1.16	1.16	1.16
320	1.10	1.11	1.11	1.11	1.12	1.12	1.12
330	1.07	1.07	1.08	1.08	1.08	1.09	1.09
340	1.04	1.04	1.05	1.05	1.05	1.05	1.06
350	1.02	1.02	1.02	1.02	1.02	1.01	1.02
360	0.993	0.997	0.996	0.993	0.994	0.994	0.991
370	.973	.977	.975	.972	.971	.968	.965
380	.956	.958	.954	.952	.949	.946	.942
390	.941	.939	.934	.930	.926	.922	.917
400	.927	.924	.918	.914	.908	.905	.902
410	.913	.909	.903	.898	.892	.889	.887
420	.903	.897	.890	.884	.877	.874	.872

Table 1.3.8 — (Continued)

Temperature, °F	$c_p \mu / k$						
	Saturated liquid	Pressure, psia, compressed liquid					
		1000	2000	3000	4000	5000	6000
430	.894	.886	.877	.872	.864	.861	.858
440	.886	.878	.869	.862	.854	.850	.846
450	.876	.871	.861	.854	.845	.841	.836
460	.871	.866	.855	.845	.835	.829	.822
470	.867	.863	.852	.840	.829	.822	.813
480	.863	.861	.849	.836	.824	.816	.807
490	.865	.862	.847	.833	.821	.812	.802
500	.870	.861	.844	.830	.816	.806	.796
510	.88	.86	.848	.832	.818	.805	.794
520	.89	.87	.852	.834	.819	.804	.792
530	.90	.88	.859	.841	.822	.806	.793
540	.90		.870	.848	.826	.811	.796
550	.93		.886	.859	.837	.820	.803
560	.95		.905	.871	.849	.828	.809
570	.97		.924	.882	.860	.837	.817
580	1.00		.953	.903	.874	.849	.827
590	1.04		.985	.925	.889	.859	.835
600	1.09		1.015	.954	.908	.879	.849
610	1.14		1.09	1.003	.934	.899	.869
620	1.20		1.18	1.034	.964	.916	.884
630	1.25			1.089	.997	.941	.901
640	1.39			1.158	1.034	.970	.933
650	1.56			1.241	1.086	1.006	.962
660	1.77			1.337	1.147	1.039	.990
670	2.19			1.61			
680	2.75			1.97			
690	4.40						

Maximum error for indicated temperature range, %

32-100	1.5	1.9	2.1	2.4	2.7	3.5	3.7
100-200	1.6	2.0	2.2	2.6	2.4	3.5	3.7
200-300	2.3	3.2	3.4	3.8	3.6	5.0	5.2
300-400	2.5	3.3	3.5	3.9	3.9	5.0	5.2
400-500	5.0	5.8	6.0	6.4	6.4	7.5	8.0
500-530	9.5	10.5	10.2	10.5	10.0	11.5	11.5
530-600	10.0		10.2	10.5	10.0	11.5	11.5
600-620	13.5		13.5	13.0	12.5	14.5	14.5
620-660	15.5			15.5	12.5	14.5	14.5
660-680	16.0			16.0			
690	17.0						

Table 1.3.9 — Absolute Density (ρ) of Heavy Liquid Water at 1 Atm*

Temperature		ρ	
°F	°C	Lb/cu ft	Gm/cc
41	5	69.0176	1.10555
50	10	69.0444	1.10598
51.8	11	69.0450	1.10599
53.6	12	69.0450	1.10599
55.4	13	69.0438	1.10597
59	15	69.0382	1.10588
68	20	69.0063	1.10537
77	25	68.9508	1.10448
86	30	68.8746	1.10326
95	35	68.7828	1.10179
104	40	68.6723	1.10002

* Accuracy: $\pm 0.003\%$

Table 1.3.10 — Vapor Pressure of Heavy Liquid Water

Temperature		Pressure	
°C	°F	Atm (absolute)	Psia
0	32	0.00480	0.0705
10	50	.01025	.1506
20	68	.0200	.2939
30	86	.0368	.5408
40	104	.0647	.9508
50	122	.1100	1.616
60	140	.1797	2.641
70	158	.2843	4.178
80	176	.4363	6.412
90	194	.6520	9.582
100	212	.9503	13.96
110	230	1.353	19.88
120	248	1.888	27.75
130	266	2.584	37.97
140	284	3.474	51.05
150	302	4.596	67.54
160	320	5.993	88.07
170	338	7.707	113.3
180	356	9.788	143.8
190	374	12.29	180.6
200	392	15.26	224.3
210	410	18.77	275.8
220	428	22.87	336.1
230	446	27.63	406.0
240	464	33.17	487.5
371.5	700.7	218.6	3212

Table 1.3.11 — Latent Heat of Vaporization of Heavy Water*

Temperature		ΔH	
°C	°F	Cal/gm	Btu/lb
3.82	38.9	554.66	998.39
10	50	549.47	989.05
25	77	541.53	974.76
40	104	531.50	956.69
60	140	519.86	935.75
80	176	507.98	914.36
100	212	495.65	892.16
120	248	482.76	868.98
140	284	469.08	844.35
160	320	454.70	818.47
180	356	439.28	790.69
200	392	422.70	760.86
220	428	404.63	728.33

* Accuracy: $\pm 0.3\%$

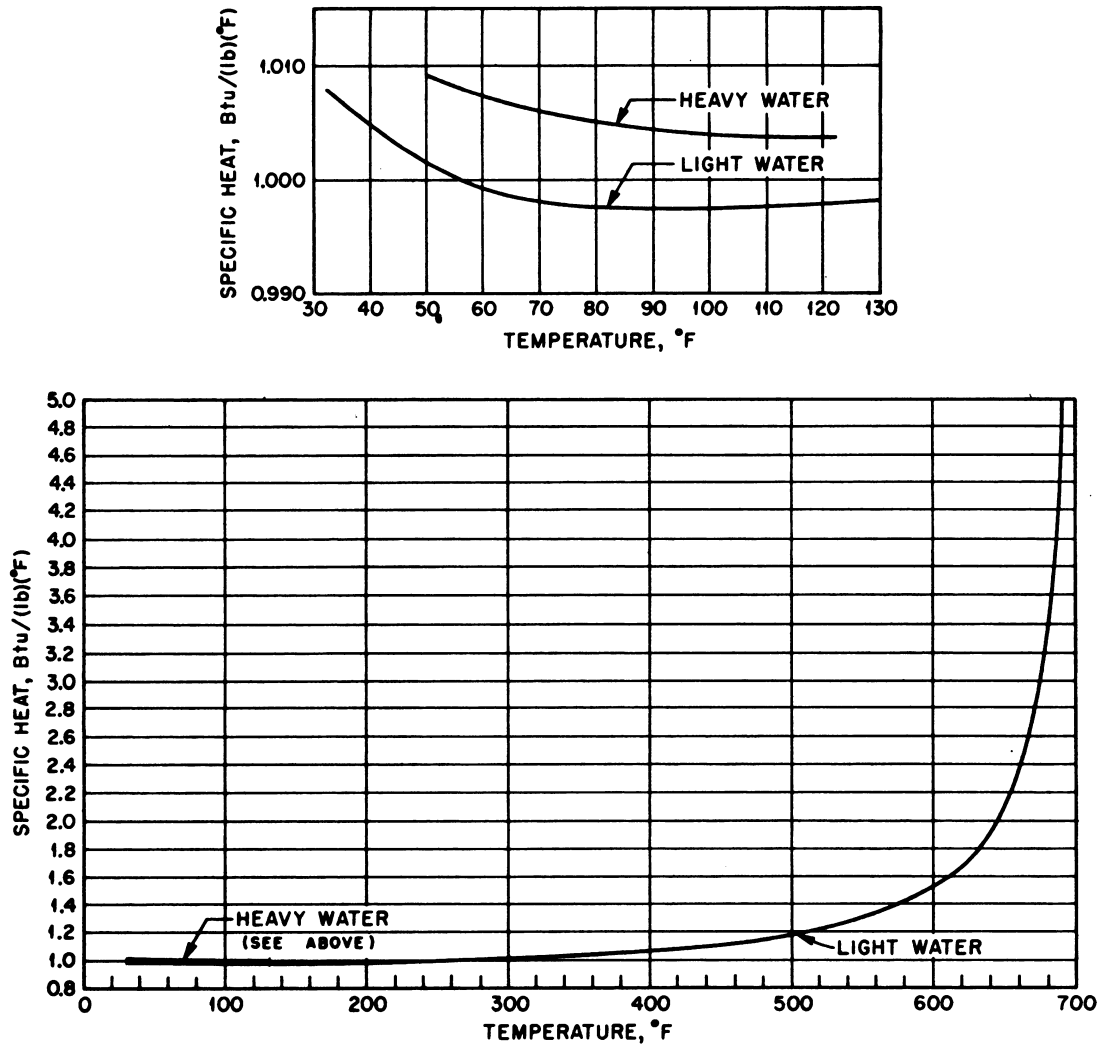


Fig. 1.3.1 — Graphical Comparison of Specific Heat Data for Light and Heavy Liquid Water. Drawn from values of Wellman² and Kirshenbaum³ by Argonne National Laboratory, June 15, 1952.

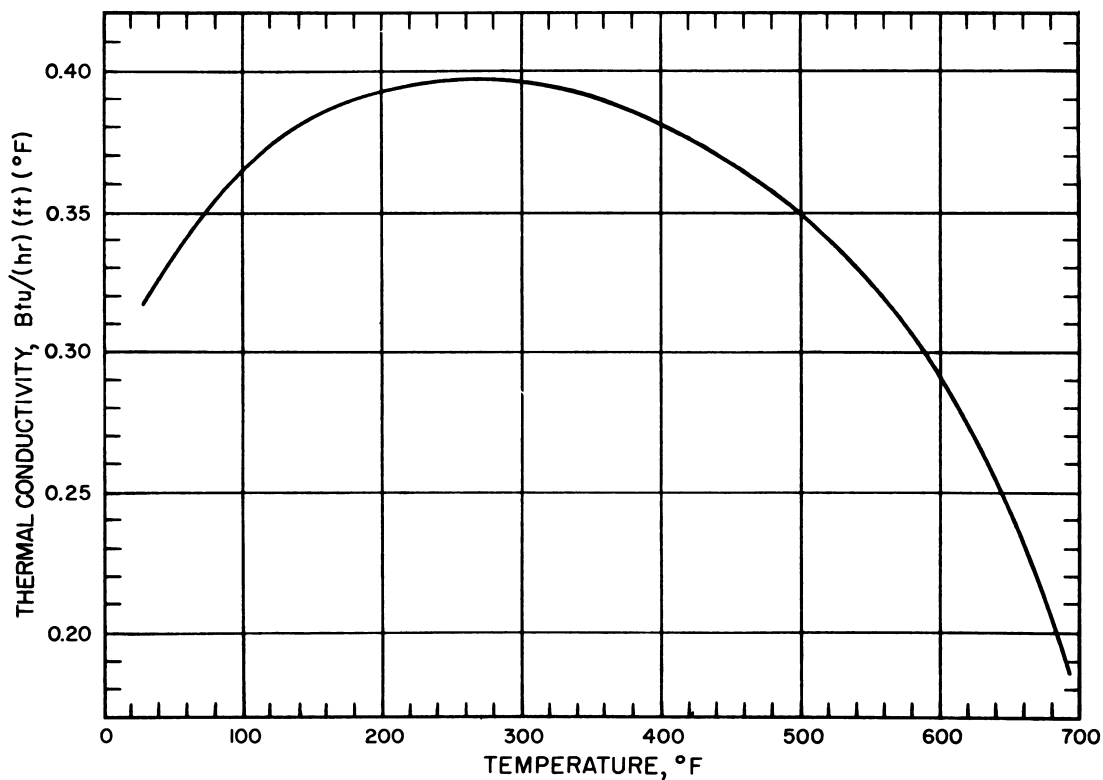


Fig. 1.3.2 — Graphical Presentation of Thermal Conductivity Values for Light Liquid Water. Drawn from values of Wellman² by Argonne National Laboratory, June 15, 1952.

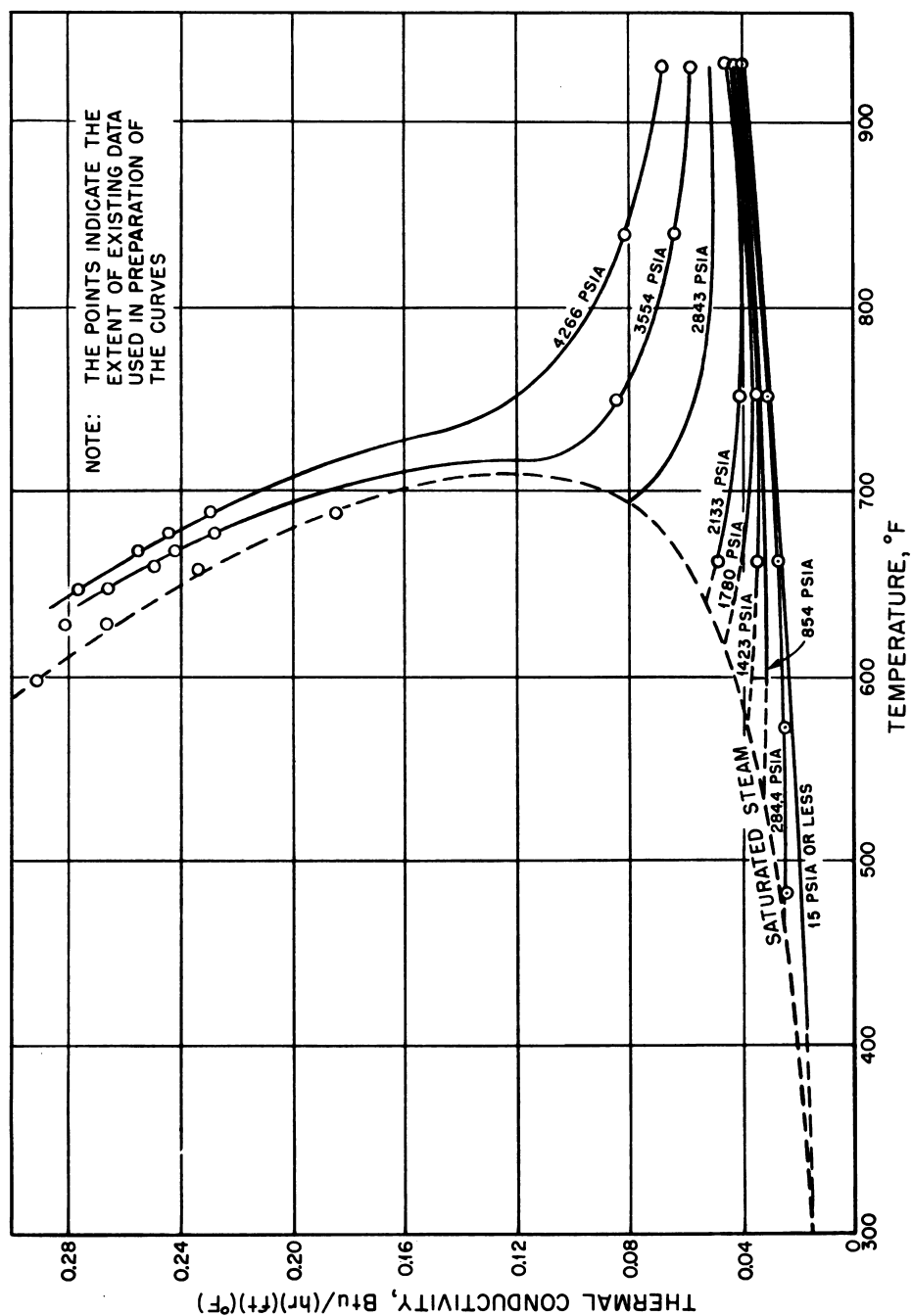


Fig. 1.3.3— Thermal Conductivity Data for Light-water Vapor. Submitted from data of Keyes and Sandell⁵ and from Timrot and Vargaftik⁶ by W. L. Sibbitt, Purdue University, June 23, 1952. Drawn by Argonne National Laboratory.

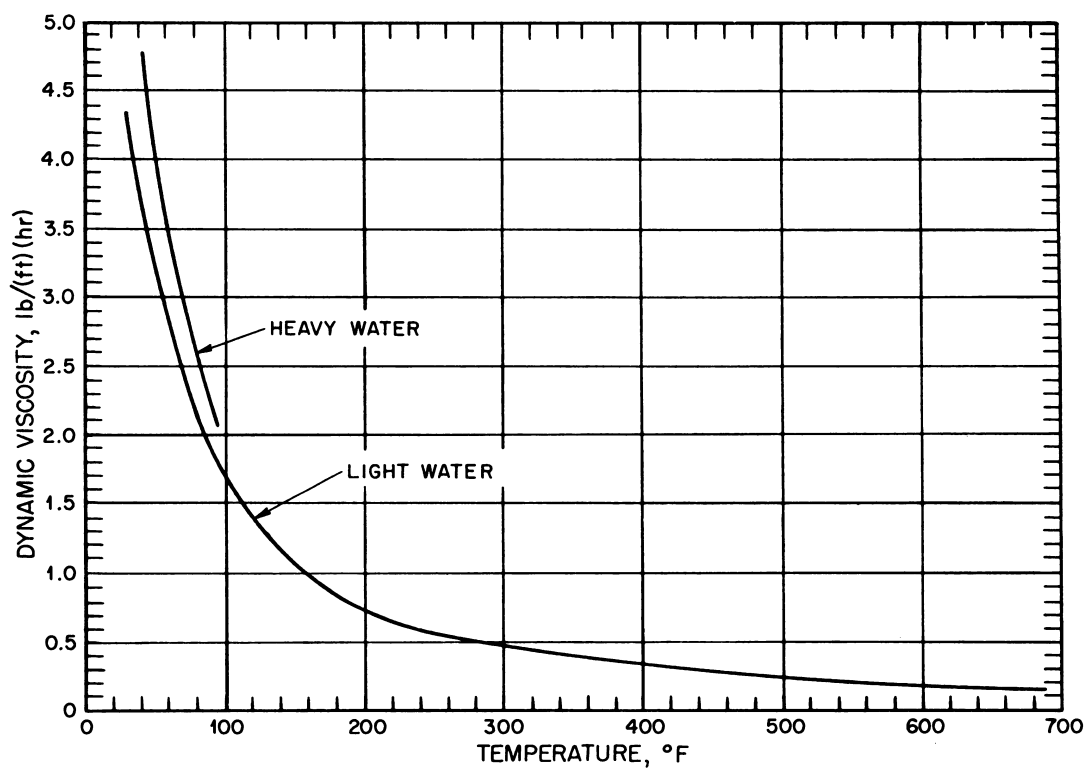


Fig. 1.3.4— Graphical Comparison of Dynamic-viscosity Data for Light and Heavy Liquid Water. Drawn from data of Wellman² and Kirshenbaum³ by Argonne National Laboratory, June 15, 1952.

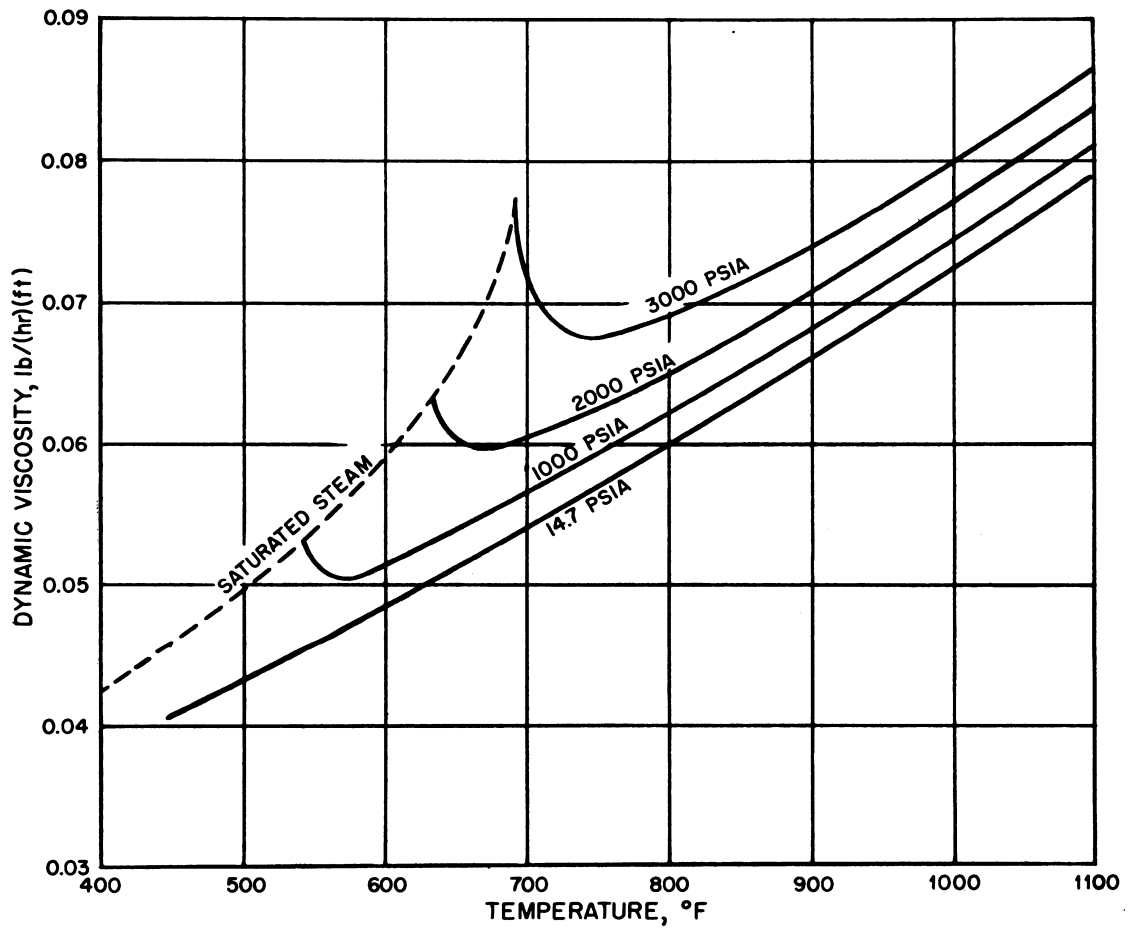


Fig. 1.3.5 — Dynamic-viscosity Values for Light-water Vapor. Submitted from data of Timrot¹ by W. L. Sibbitt, Purdue University, June 23, 1952. Drawn by Argonne National Laboratory.

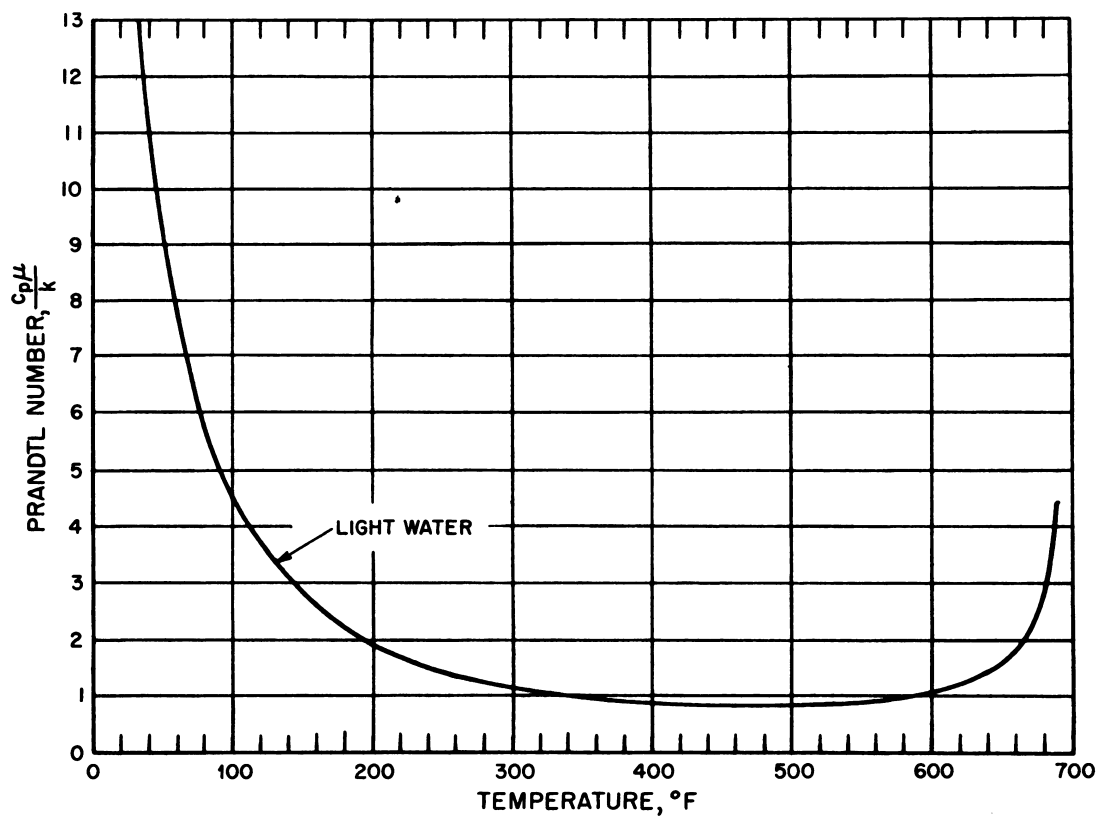


Fig. 1.3.6— Graphical Presentation of Prandtl Number Values for Light Liquid Water. Drawn from values of Wellman² by Argonne National Laboratory, June 15, 1952.

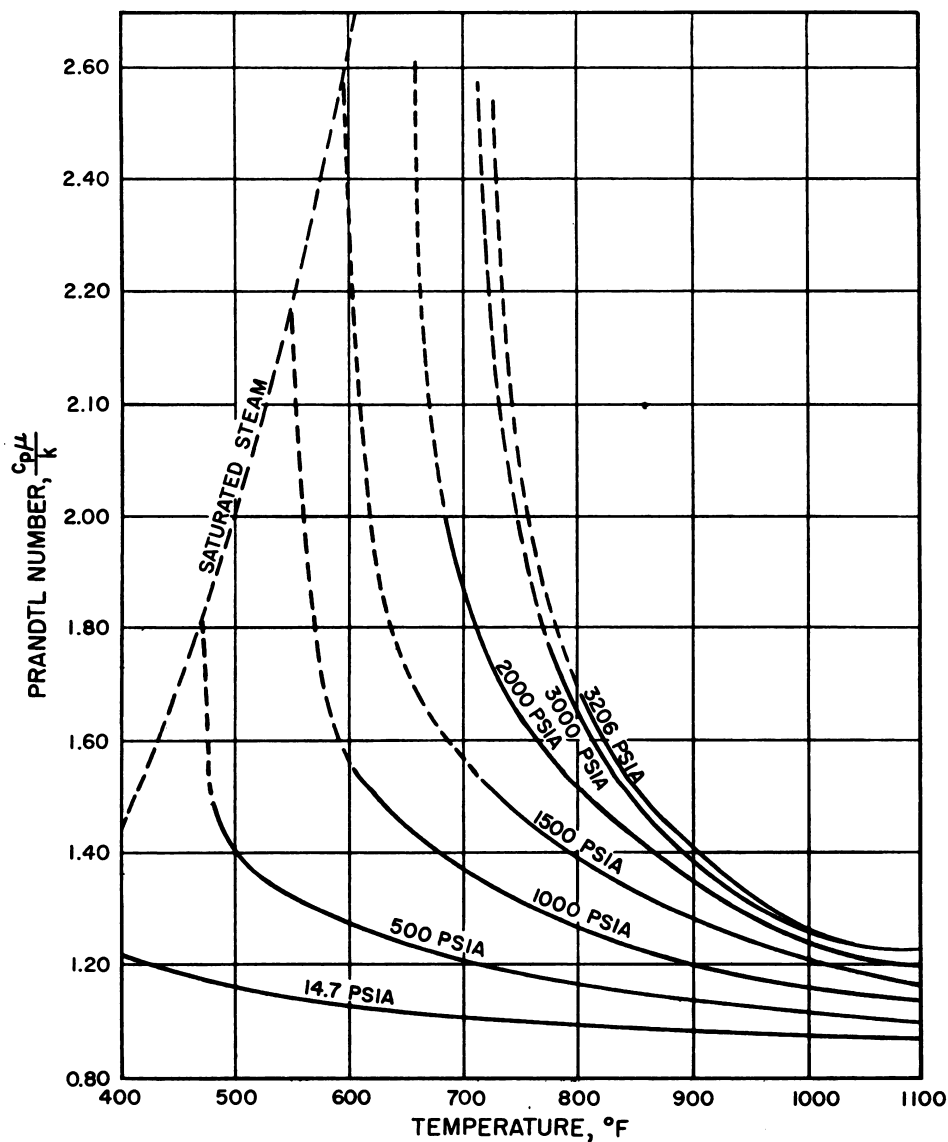


Fig. 1.3.7 — Graphical Presentation of Prandtl Number Value for Light-water Vapor. Drawn from calculations of W. L. Sibbitt,⁴ Purdue University, June 23, 1952, by Argonne National Laboratory.

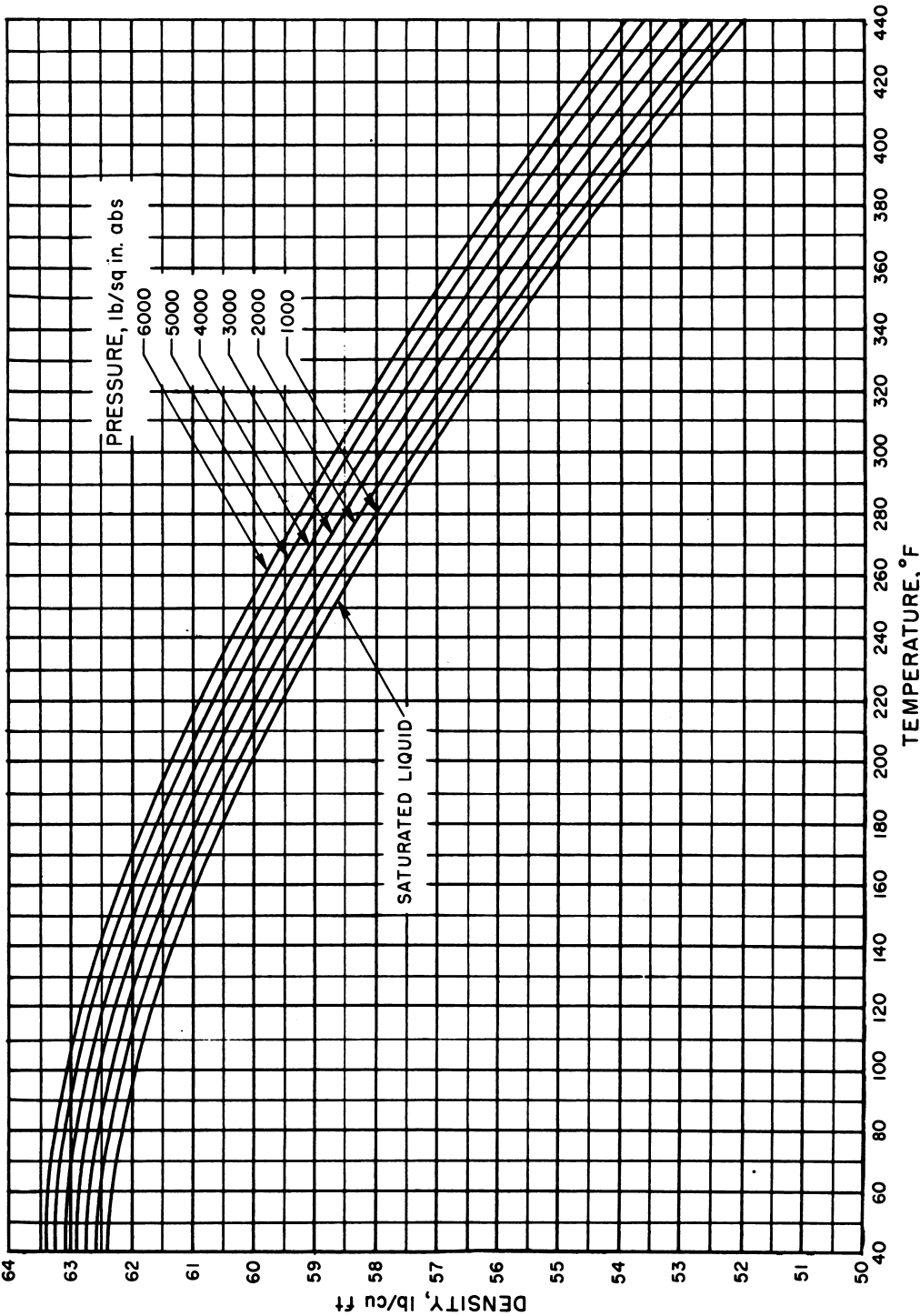


Fig. 1.3.8 — Graphical Presentation of Density Values for Light Water (40°–440°F).
Drawn from values of Keenan and Keyes¹ by Argonne National Laboratory, May 15, 1952.

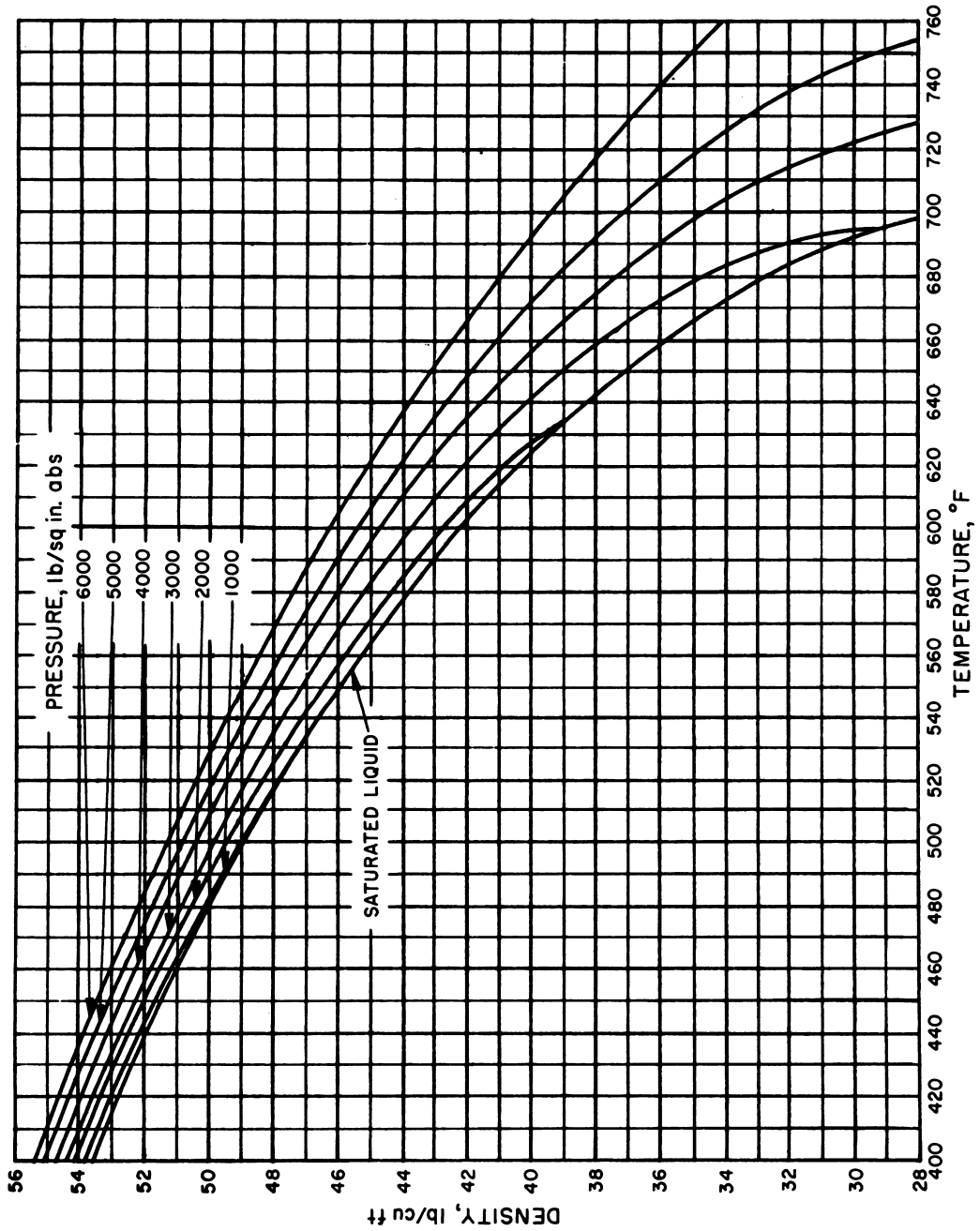


Fig. 1.3.9 — Graphical Presentation of Density Values for Light Water (400°-760°F).
 Drawn from values of Keenan and Keyes¹ by Argonne National Laboratory, May 15, 1952.

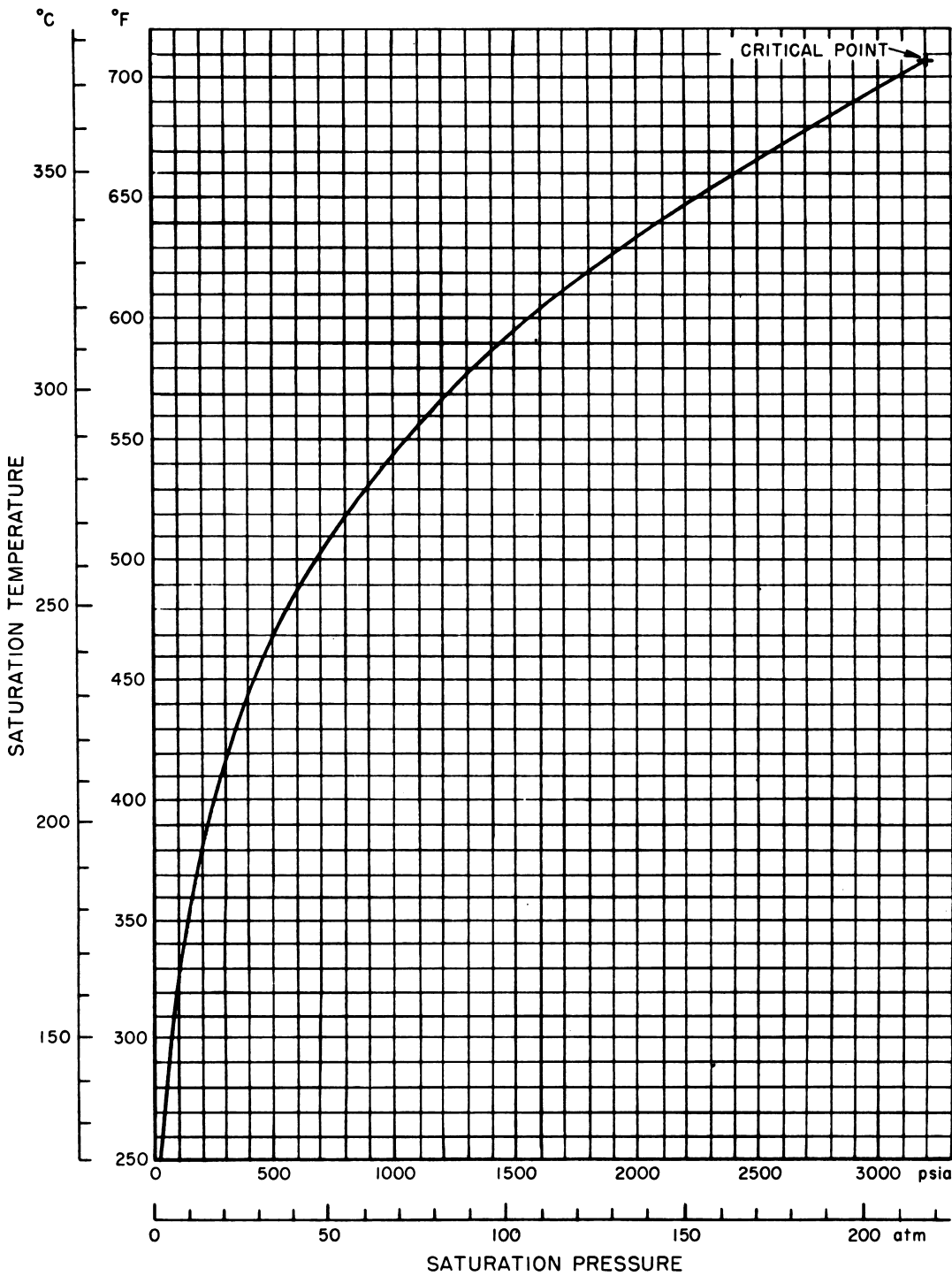


Fig. 1.3.10 — Graphical Presentation of Vapor-pressure Values for Light Water. Drawn from data of Keenan and Keyes¹ by Argonne National Laboratory, May 15, 1952.

REFERENCES

1. J. H. Keenan and F. G. Keyes, "Thermodynamic Properties of Steam," 1st ed., John Wiley & Sons, Inc., New York, 1936.
2. E. J. Wellman, "A Survey of the Thermodynamic and Physical Properties of Water," M.S. Thesis, Purdue University, January 1950.
3. I. Kirshenbaum, "Physical Properties and Analysis of Heavy Water," 1st ed., McGraw-Hill Book Company, Inc., New York, 1951.
4. W. L. Sibbitt, School of Mechanical Engineering, Purdue University, private communication.
5. F. G. Keyes and D. J. Sandell, Jr., "New Measurements of the Heat Conductivity of Steam and Nitrogen, Trans. Am. Soc. Mech. Engrs., 72: 767-778 (1950).
6. D. L. Timrot and N. B. Vargaftik, Heat Conductivity, Viscosity, and Thermodynamical Properties of Steam at High Temperatures and Pressures, Paper No. 10 in "Transactions of the Fourth World Power Conference, London, July 11-14, 1950," Vol. 3, pp 1642-1666, Percy Lund, Humphries & Co., Ltd., London, 1952.
7. D. L. Timrot, Determination of the Viscosity of Steam and Water at High Temperatures and Pressures, J. Phys. U.S.S.R., 2: 419-436 (1940).

SELECTED READING LIST

- PHYSICAL PROPERTIES AND ANALYSIS OF HEAVY WATER, I. Kirshenbaum, 1st ed., McGraw-Hill Book Company, Inc., New York, 1951.
- NEW MEASUREMENTS OF THE HEAT CONDUCTIVITY OF STEAM AND NITROGEN, F. G. Keyes and D. J. Sandell, Jr., Trans. Am. Soc. Mech. Engrs., 72: 767-778 (1950).
- HEAT CONDUCTIVITY, VISCOSITY, AND THERMODYNAMICAL PROPERTIES OF STEAM AT HIGH TEMPERATURES AND PRESSURES, D. L. Timrot and N. B. Vargaftik, Paper No. 10 in "Transactions of the Fourth World Power Conference, London, July 11-14, 1950," Vol. 3, pp 1642-1666, Percy Lund, Humphries & Co., Ltd., London, 1952.
- REVIEW OF DATA ON DYNAMIC VISCOSITY OF WATER AND SUPERHEATED STEAM, G. A. Hawkins, W. L. Sibbitt, and H. L. Solberg, Trans. Am. Soc. Mech. Engrs., 70: 19-23 (1948).
- HEAT CONDUCTION OF WATER AT HIGH TEMPERATURES, D. L. Timrot and N. B. Vargaftik, J. Tech. Phys. U.S.S.R., 10: 1063-1073 (1940).
- DETERMINATION OF THE VISCOSITY OF STEAM AND WATER AT HIGH TEMPERATURES AND PRESSURES, D. L. Timrot, J. Phys. U.S.S.R., 2: 419-436 (1940).
- PROPERTIES OF ORDINARY WATER-SUBSTANCE, N. E. Dorsey, Reinhold Publishing Corporation, New York, 1940.
- HEAT CONDUCTIVITY OF WATER VAPOR AT HIGH PRESSURES AND TEMPERATURES, N. B. Vargaftik and D. L. Timrot, J. Tech. Phys. U.S.S.R., 9: 63-70 (1939).
- THERMODYNAMIC PROPERTIES OF STEAM, J. H. Keenan and F. G. Keyes, John Wiley & Sons, Inc., New York, 1936.
- THERMAL CONDUCTIVITY OF LIQUIDS UNDER PRESSURE, P. W. Bridgman, Proc. Am. Acad. Arts Sci., 59: 141-169 (1923).

Heat Transfer

W. H. Jens and P. A. Lottes

The most common mode of heat transfer used to cool reactors is forced convection. Convection is defined as the transfer of heat from one place to another within a fluid by the mixing of one portion of the fluid with another. Convection is further subdivided into free convection and forced convection.

In free or natural convection, heat is transferred by the circulation of fluid due to density differences brought about by heating or cooling. In forced convection, the velocity of the main body of the fluid is usually large compared to the natural circulation currents. There is no sharp line of demarkation, however, between the two types of convection. In cases where the bulk velocity of the fluid is low, the transfer of heat will be governed mainly by the effect of temperature difference causing natural convection currents.

Forced convection is generally subdivided into laminar or turbulent flow. Laminar flow is generally considered to exist for values of Reynolds number ($D_e G/\mu$) of less than 2100 and turbulent flow for somewhat larger values. A transition region exists for Reynolds numbers between 2100 and 10,000.¹ Turbulent flow can safely be considered to exist at values above 10,000. For flow inside single tubes, turbulent flow exists for a Reynolds number above 3100. In the forced convection of water, the Reynolds number usually exceeds either of these critical values, and the flow is turbulent.

A film coefficient of heat transfer (h) is used in convection to determine the amount of heat transferred. It is defined as the heat transferred per unit area per unit time per unit temperature difference between the surface and the fluid. The thermal conductivity (k), the dynamic viscosity (μ), the density (ρ), and the constant-pressure specific heat (c_p) are the physical properties of the fluid that affect the film coefficient. Since these physical properties vary with temperature and pressure, the film coefficient is a function of temperature and pressure. The velocity of the fluid and the shape and spacing of the heating surface also affect the film coefficient; these variables may be adjusted to give the desired coefficient.

Heat-transfer nomenclature is presented in Table 1.4.1, and conversion factors are presented in Table 1.4.2.

BASIC EQUATIONS FOR FREE-CONVECTION HEAT TRANSFER

The following correlations² may be used to predict free-convection heat transfer from vertical metal surfaces to water. For the laminar range of $N_{Gr} \cdot N_{Pr} = 0.2 \times 10^8$ to 40×10^8 , the heat-transfer coefficient is given by the equation:

$$\frac{hL}{k} = 0.726 (N_{Gr} \cdot N_{Pr})^{1/4} \quad (1)$$

¹References appear at end of chapter.

Table 1.4.1 — Heat-transfer Nomenclature and Units

Symbol	Definition	Units*
A_f	Flow area	sq
b	Wetted perimeter	ft
C	Constant	None
c_p	Specific heat	Btu/(lb)(°F)
D_s	Diameter of sphere	ft
D	Outside diameter of pipe Eq. (4) and (5)	ft
D_e	Equivalent diameter equal to 4 times the flow area divided by the wetted perimeter, $\frac{4A_f}{b}$	ft
D_o	Outside diameter of cylinders	ft
f	Subscript used to designate that the physical properties should be evaluated at the film temperature	None
G	Mass velocity	lb/(hr)(sq ft)
G_{\max}	Mass velocity based on minimum free cross section across banks of tubes (either transverse to stream or on diagonal clearances, whichever is less)	lb/(hr)(sq ft)
G_s	Mass velocity per unit area of a bed of spheres	lb/(hr)(sq ft)
g	Gravitational acceleration, local, usually taken as standard value, 32.2	ft/(sec)(sec)
h	Heat transfer coefficient	Btu/(hr)(sq ft)(°F)
h_m	Mean value of heat transfer coefficient over entire surface of sphere or cylinder	Btu/(hr)(sq ft)(°F)
k	Thermal conductivity	Btu/(hr)(ft)(°F)
L	Length	ft
N	Number of tubes in direction of flow	None
N_{Gr}	Grashof number, $\frac{L^3 \rho^2 \beta g \Delta t}{\mu^2}$ or $\frac{D^3 \rho^2 \beta g \Delta t}{\mu^2}$	None
N_{Nu}	Nusselt number, hD_e/k	None
N_{Re}	Reynolds number, $D_e G/\mu$	None
N_{Pr}	Prandtl number, $c_p \mu/k$	None
P	Pressure	lb/sq ft
q''	Heat flux	Btu/(hr)(sq ft)
$q''_{B.O.}$	Burnout heat flux	Btu/(hr)(sq ft)
t_f	Film temperature, $\frac{t_w + t_s}{2}$	°F
t_s	Temperature of surface transferring heat	°F
t_{sat}	Saturation temperature	°F
t_w	Bulk water temperature	°F
β	Coefficient of thermal expansion	°F ⁻¹
ρ	Density	lb/cu ft
Δt	Temperature difference between surface and fluid	°F
Δt_{sat}	Temperature difference between temperature of surface transferring heat by boiling minus the saturation temperature	°F
Δt_{sub}	Temperature difference, saturation temperature minus the bulk water temperature	°F
μ	Viscosity† (dynamic)	lb/(hr)(ft)

*Lb used to represent pounds mass

†Viscosity as given in this chapter is given in units of lb/(hr)(ft) whereas in Chap. 1.5 the unit used is lb/(sec)(ft). Care should be taken in using proper units in equations

Table 1.4.2—Heat-transfer Conversion Factors

English Units × Multiplication Factor to Obtain		CGS Units
sq ft	929	cm ²
Btu/(lb)(°F)	1	cal/(gm)(°C)
ft	30.48	cm
lb/(hr)(sq ft)	1.356×10^{-4}	gm/(sec)(sq cm)
Btu/(hr)(sq ft)(°F)	1.356×10^{-4}	cal/(sec)(sq cm)(°C)
Btu/(hr)(sq ft)(°F)	5.676×10^{-4}	watt/(sq cm)(°C)
Btu/(hr)(ft)(°F)	4.133×10^{-3}	cal/(sec)(cm)(°C)
Btu/(hr)(ft)(°F)	1.73×10^{-2}	watt/(cm)(°C)
Btu/(hr)(sq ft)	7.535×10^{-5}	cal/(sec)(sq cm)
Btu/(hr)(sq ft)	3.154×10^{-4}	watt/sq cm
lb/(hr)(ft)	4.134×10^{-3}	gm/(sec)(cm)
lb/(hr)(ft)	4.134×10^{-3}	poise

For the turbulent range of $N_{Gr} \cdot N_{Pr} = 40 \times 10^3$ to 900×10^3 the heat-transfer coefficient is given by the equation:

$$\frac{hL}{k} = 0.0674 [N_{Gr}(N_{Pr})^{1.28}]^{1/2} \quad (2)$$

These equations represent experimental data on water and ethylene glycol to within ± 10 percent.

Free convection from single horizontal cylinders to water may be calculated within ± 10 percent according to Eq. (3)³ provided that the value of the outside diameter (D) of the cylinder is used as the characteristic length in the Nusselt and Grashof number:

$$\frac{hD}{k_f} = 0.53 [N_{Gr} \cdot N_{Pr}]^{0.25} = 0.53 \left[\frac{D^3 \rho_f^2 \beta g \Delta t}{\mu_f^2} \frac{c_p \mu_f}{k_f} \right]^{0.25} \quad (3)$$

The physical property constant $(\rho_f^2 \beta g / \mu_f^2)(c_p \mu_f / k_f)$ has been plotted as shown in Fig. 1.4.1 for saturated water as a function of temperature. The constant is practically independent of pressure. By multiplying this constant by the cube of the characteristic dimension, D^3 or L^3 , and by the temperature difference, Δt , the product $N_{Gr} \cdot N_{Pr}$ is obtained.

BASIC EQUATIONS FOR FORCED-CONVECTION HEAT TRANSFER

PIPES, NONCIRCULAR DUCTS, AND ANNULI

The heat-transfer coefficient for the turbulent flow of water through heated pipes, non-circular ducts, and annuli is calculated according to the equation:

$$\left[\frac{hD_e}{k} \right] = 0.023 \left[\frac{D_e G}{\mu} \right]^{0.8} \left[\frac{c_p \mu}{k} \right]^{0.4} \quad (4)$$

Equation (4) has been experimentally verified^{4,5,6} for water flowing in heated tubes up to 2500 psia and 600°F with heating rates up to 1,000,000 Btu/(hr)(sq ft) for Reynolds numbers of 50,000 to 700,000.

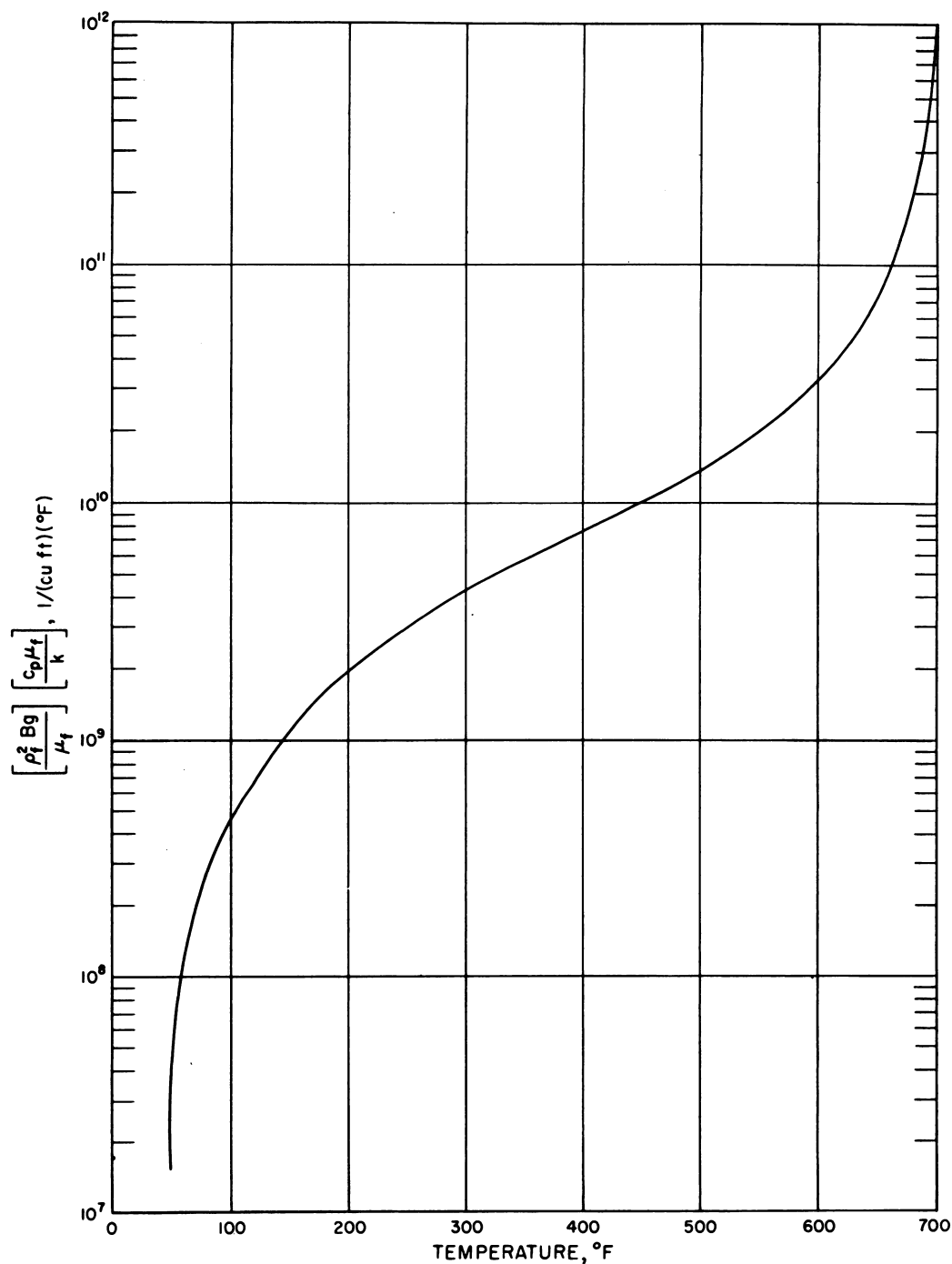


Fig. 1.4.1 — Relationship Between Free-convection Heat-transfer Physical Properties of Water, $(\rho_f^2 B g / \mu_f)(c_p \mu_f / k)$, and Temperature at Saturation Pressure. Submitted by Argonne National Laboratory, Sept. 15, 1952.

The heat-transfer coefficient calculated from Eq. (4) for water flowing through a channel with an equivalent diameter of 0.25 in. is shown as a function of water temperature and mass velocity in Fig. 1.4.2. Physical properties of water were evaluated at the saturation conditions. A correction factor to be used when calculating the heat-transfer coefficient for equivalent diameters other than 0.25 in. is included in Fig. 1.4.2. This correction factor is multiplied by the heat-transfer coefficient for an equivalent diameter of 0.25 in. to determine the heat-transfer coefficient for other equivalent diameters.

A comparison of the heat-transfer coefficients of light and heavy water is given in Fig. 1.4.3. The comparison is made for both constant linear and constant mass velocities of the two liquids. The physical properties presented in Chap. 1.3 of this section were used in this comparison with the exception of the thermal conductivity of heavy water. In the absence of values from the literature, the thermal conductivity values of heavy water were assumed to be the same as those for light water.

TUBE BANKS

FLOW PARALLEL TO AXIS

For turbulent flow outside tube banks with the liquid flowing parallel to the axis of the tubes, Eq. (4) is used. The equivalent diameter for this case is expressed as:

$$D_e = \frac{4A_f}{b} \quad (5)$$

FLOW NORMAL TO AXIS*

Use of the following equations^{3,7} is recommended for calculating the heat-transfer coefficient for the un baffled flow of water normal to banks of staggered tubes and for values of $(D_o G_{\max}/\mu_f)$ greater than 10,000:

$$\frac{h_m D_o}{k_f} = 0.33 \left[\frac{D_o G_{\max}}{\mu_f} \right]^{0.6} \left[\frac{c_p \mu_f}{k_f} \right]^{1/3} \quad (6)$$

The subscript *f* in the above equation indicates that the physical properties of the water should be evaluated at the film temperature, and h_m is the mean value of heat transfer coefficient over the entire surface of tubes.

For unstaggered tubes with values of $(D_o G_{\max}/\mu_f)$ greater than 10,000, the recommended equation is:

$$\frac{h_m D_o}{k_f} = 0.26 \left[\frac{D_o G_{\max}}{\mu_f} \right]^{0.6} \left[\frac{c_p \mu_f}{k_f} \right]^{1/3} \quad (7)$$

*The above formulas, correlated with data from gases at lower Reynolds numbers have been used generally as the basis for obtaining heat-transfer coefficients for water flowing across tube banks. It is recognized that the existing correlations must be extrapolated to much higher Reynolds numbers for use with water. In addition, Eqs. (7) and (8) are inconsistent. Work presently under way at Brookhaven for the flow of water across tube banks at high Reynolds number should be consulted.

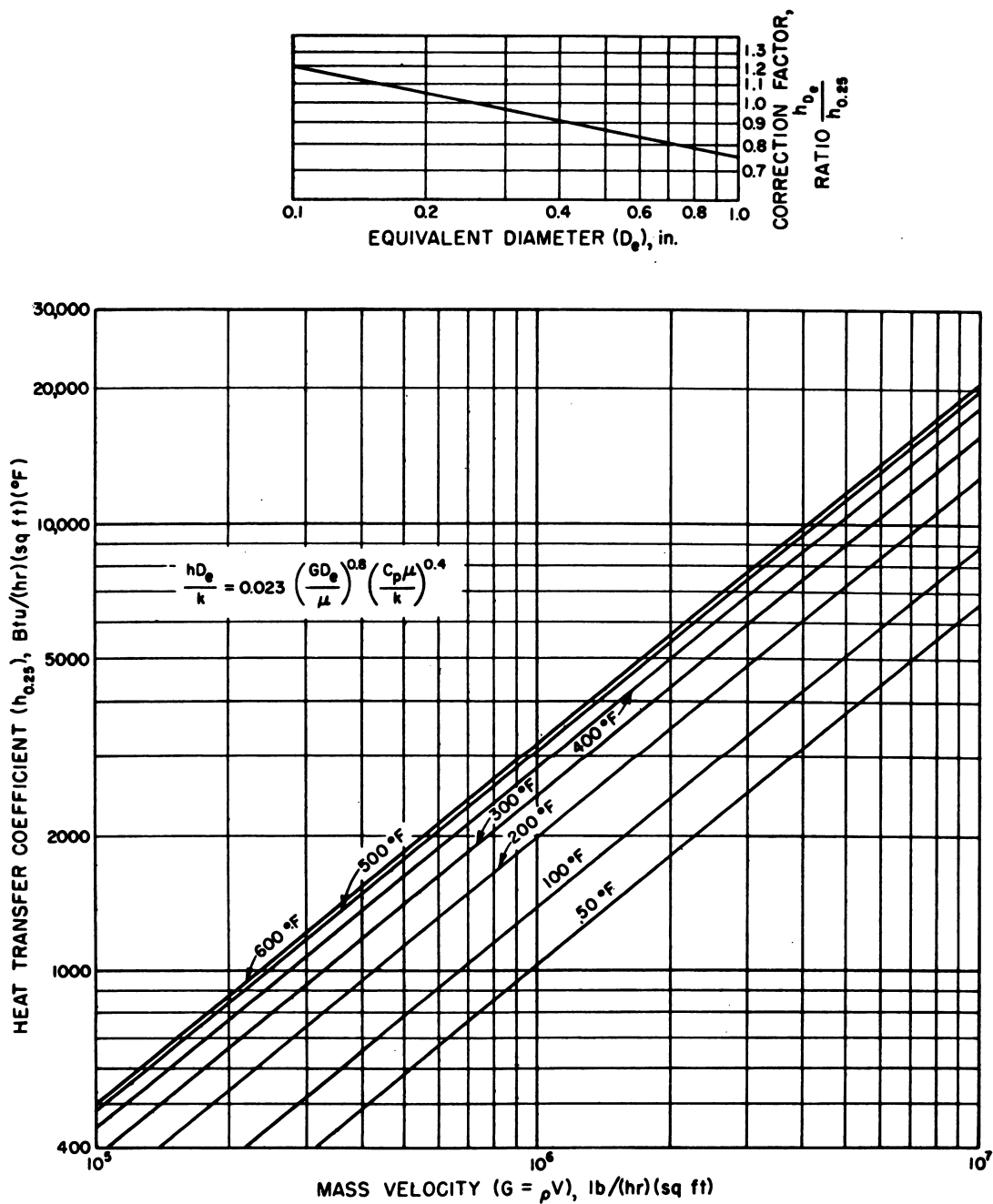


Fig. 1.4.2 — Heat-transfer Coefficient for Light Water. Submitted by Argonne National Laboratory, June 10, 1952.

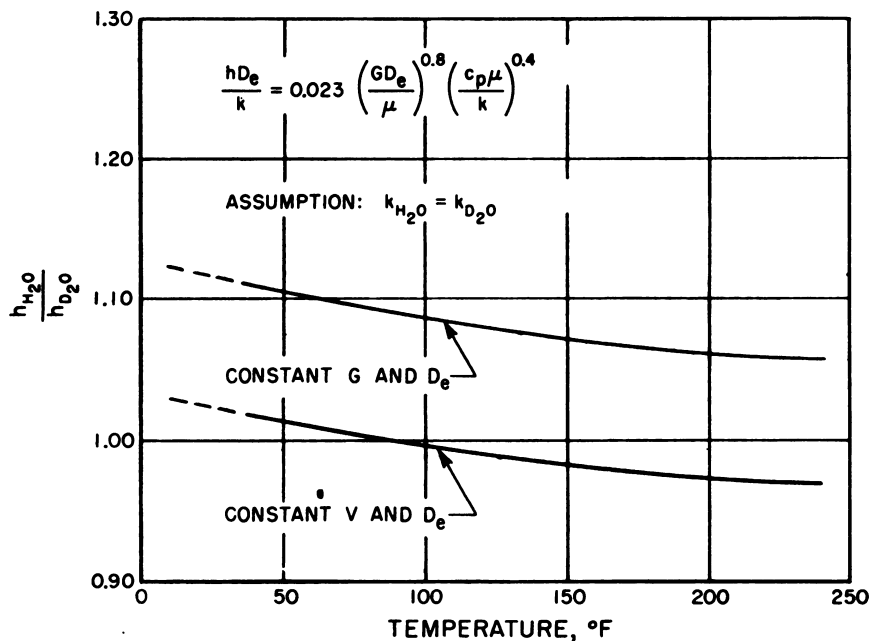


Fig. 1.4.3 — Relationship Between h_{H_2O} and h_{D_2O} . Submitted by Argonne National Laboratory, June 16, 1952.

Equations (6) and (7) apply only to ten or more rows of tubes. The coefficient h_m is the mean or average coefficient for all of the tubes. Table 1.4.3 gives the ratio of h_m for a tube bank N rows deep to that of a tube bank ten rows deep.

Table 1.4.3 — Effect of Number of Rows of Tubes on the Average Heat-transfer Coefficient (h_m)
(W. H. McAdams, "Heat Transmission," 2nd ed, McGraw-Hill Book Company, Inc., New York, 1942)

Number of rows	1	2	3	4	5	6	7	8	9	10
Ratio for staggered tubes		0.70	0.82	0.87	0.92	0.94	0.96	0.97	0.99	1.0
Ratio for in-line tubes	0.64	.76	.83	.87	.92	.94	.96	.97	.99	1.0

SINGLE CYLINDER - FLOW NORMAL TO AXIS*

The average heat-transfer coefficient for the flow of water normal to a single tube is given by:

$$\frac{h_m D_o}{k_f} = 0.26 \left[\frac{D_o G}{\mu_f} \right]^{0.6} \left[\frac{c_p \mu_f}{k_f} \right]^{0.3} \tag{8}$$

*The above formulas, correlated with data from gases at lower Reynolds numbers have been used generally as the basis for obtaining heat-transfer coefficients for water flowing across tube banks. It is recognized that the existing correlations must be extrapolated to much higher Reynolds numbers for use with water. In addition, Eqs. (7) and (8) are inconsistent. Work presently under way at Brookhaven for the flow of water across tube banks at high Reynolds number should be consulted.

for $D_o G / \mu_f$ from 1000 to 50,000. The coefficient will vary around the cylinder according to its angular position. The magnitude of this variation is estimated to be approximately 30 percent for water.

RANDOMLY PACKED SPHERES

The heat-transfer coefficient for the flow of water through beds of randomly packed spheres of equal diameters may be calculated according to the equation:⁸

$$\frac{h_m D_s}{k} = 0.58 \left[\frac{G_s D_s}{\mu} \right]^{0.70} \left[\frac{c_p \mu}{k} \right]^{0.30} \quad (9)$$

The correlation was based on experiments with air. The properties should be evaluated at the film temperature when large temperature differences exist between the sphere surface and the bulk of the fluid. No data are available on the local heat-transfer coefficient or the variation in the coefficient over the surface of a sphere.

BOILING HEAT TRANSFER

Heat transfer with a phase change from liquid to vapor is called boiling. This phase change may occur in the boundary layer next to the heat-transfer surface or in the bulk of the fluid. Boiling may occur in either a natural or forced-flow system. Boiling should occur whenever the surface temperature of the solid transferring heat exceeds the saturation temperature of the fluid by a specific amount, designated as Δt_{sat} . A further classification of the type of boiling is usually made. With the bulk temperature of the fluid below the saturation temperature of the fluid, the phase change is called nucleate or local boiling. With the bulk temperature of the fluid at the saturation temperature of the fluid, the phase change is called net boiling.

A typical plot of heat flux (q'') from a solid surface to a liquid is shown in Fig. 1.4.4 as a function of the difference between the surface temperature of the solid and the bulk temperature of the liquid. The curve has been verified in a static system; however, it is believed to hold also for a flowing system. The curve is drawn for constant pressure and constant bulk water temperature. At values of surface or wall temperature (t_s) below the water saturation pressure, the heat is transferred by convection and is proportional to the temperature difference ($t_s - t_w$). This is the region AB. As the surface temperature exceeds the saturation temperature of the fluid, the heat flux rises very rapidly for a small increase in temperature difference as shown by the nucleate or local-boiling region BC. Small vapor bubbles which form rapidly due to superheating of the surface and the liquid in a film adjacent to the surface also collapse very rapidly as soon as they grow and extend into the subcooled liquid beyond the superheated film. A further increase in wall temperature at point C or an increase in heat flux results in a blanketing of the surface with vapor due to the coalescing of the individual vapor bubbles. The heat flux curve in this region decreases with an increase in ($t_s - t_w$). In the region CD, however, the heat flux finally rises again, and the surface temperature becomes very high. The major share of the heat transfer in this region has been postulated to occur across the vapor space by conduction and radiation. The wall temperature in the region CD corresponding to the heat flux at C, the peak of the nucleate boiling region, is usually higher than the melting point of the metal surface. For this reason burnout usually accompanies an increase in heat flux above the peak value at point C. The heat flux at point C has been frequently called the burnout heat flux.*

*In water heat transfer, the burnout heat flux often corresponds to point C as shown in Fig. 1.4.4. However, burnout may occur at other values. In general, burnout heat flux is defined only as that heat flux at which burnout occurs for a given set of conditions.

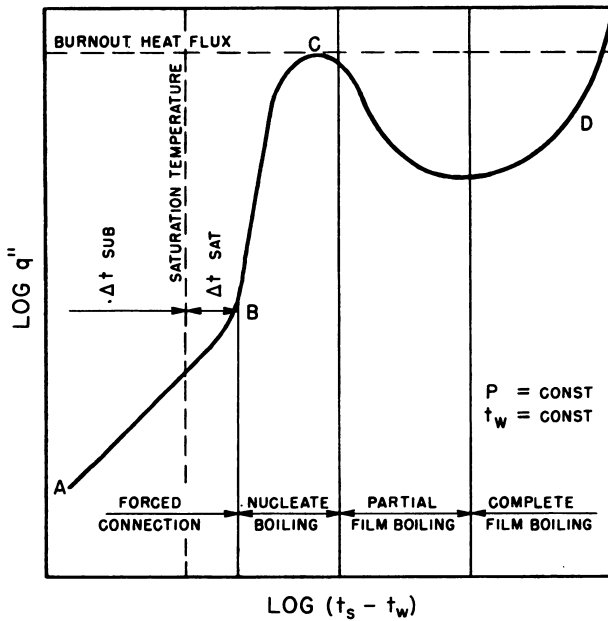


Fig. 1.4.4 — Boiling Heat Transfer from a Solid Surface to Water. Submitted by Argonne National Laboratory, July 15, 1952.

In reactors, heat is generated and transferred to the heat-transfer fluid independently of the amount of heat-transfer surface or the temperature of the fluid. For this reason it is comparatively easy to determine the surface temperature of the heat-transfer surface. The surface temperature is calculated based on a convection film coefficient. If the surface temperature as calculated does not exceed the saturation temperature of the fluid corresponding to the system pressure plus an additional temperature (termed ΔT_{sat}), the heat is transferred solely by convection and the surface temperature is as calculated. If the temperature of the surface as determined by dividing the heat flux by the calculated convection heat-transfer coefficient added to the fluid temperature is in excess of the saturation-temperature flux Δt_{sat} , then heat is being transferred by local boiling. The surface temperature under these conditions is not that which was calculated but is the saturation temperature plus Δt_{sat} . The heat flux, of course, must be less than the burnout heat flux for the specific conditions, otherwise the surface will burn out.

Numerous experiments^{4,5,9,10,11,12} have indicated that the heat flux in the nucleate boiling region does not depend significantly upon the fluid velocity, nor upon the temperature difference between the surface and the bulk water, but does depend upon the difference between the surface temperature and the saturation temperature corresponding to the system pressure, and upon the system pressure itself.

McAdams et al¹² correlated their local-boiling data at pressures from 30 to 90 psia for water flowing through an annulus. The relation is:

$$q'' = C \Delta t_{\text{sat}}^{3.88} \quad (10)$$

in which C varied from 0.189 for water containing 0.30 cc of dissolved air/liter of water to 0.074 for water containing 0.06 cc of dissolved air/liter of water.

The UCLA and MIT local-boiling data were correlated by means of the following equation:

$$\Delta t_{\text{sat}} = \frac{60(q''/10^6)^{1/4}}{e^{P/129600}} \quad (11)$$

The effect of dissolved gases,^{3,12,15} type of solid surface transferring heat,^{13,14,15} and cleanliness of the surface^{13,14,15} and of the water all affect Δt_{sat} , the effects being more pronounced at lower pressures. Very high values of Δt_{sat} have been obtained in a special apparatus⁵ in which high cleanliness was maintained.

The burnout heat flux^{5,6,9} has been investigated experimentally at pressures from 500 to 2000 psi at velocities from 5 to 30 ft/sec in a round seamless tube of 0.226 in. ID, using distilled water flowing upward through the tube. The equation expresses the condition that experimental burnout is always higher than that calculated by the derived equation. The maximum deviation was plus 23 percent. This equation results, therefore, in the minimum burnout heat flux for a round tube:

$$\frac{q'' \text{ B.O.}}{10^6} = C \left[\frac{G}{10^6} \right]^m (t_{\text{sat}} - t_w)^{0.22} \quad (12)$$

Values of "m" and C vs Pressure

Pressure, psia	m	C
500	0.16	0.817
1000	.275	.626
2000	.500	.445

This equation is limited to the conditions of the experiment. Other burnout experiments at lower velocities have demonstrated that burnout does not occur until very high steam qualities have been obtained. In these experiments, special apparatus was required to insure positive flow. Burnout at these high qualities would otherwise be difficult to anticipate since the flow would drop to very low values as steam is formed due to the high pressure drop associated with two-phase flow. If burnout is being predicted in any design, the pressure drop across the heated channel must be analyzed since it will probably be the determining factor in the burnout of the channel.

In pool boiling,^{12,14,15} burnout has been determined for horizontal wires and flat plates. In these cases, the water was at the saturation temperatures, and flow across the surface was by natural convection.

HEAT TRANSFER AT SUPERCRITICAL PRESSURE

To date, no correlations are available for predicting the heat-transfer coefficient of water under conditions where the water properties change radically with temperature, such as near the critical point. There is an increasing amount of analytical and experimental work currently being done toward obtaining a method of predicting the heat-transfer coefficient in these regions.¹⁶

The heat-transfer coefficient at supercritical pressures from metal surfaces to water in forced flow can be predicted from the previously mentioned equations provided that the water properties do not change radically with temperature.

REFERENCES

1. W. M. Kays and A. L. London, "Convective Heat Transfer and Flow Friction Behavior of Small Cylindrical Tubes—Circular and Rectangular Cross Section," Trans. Am. Soc. of Mech. Engrs., Preprint No. 51-A-130.
2. Y. S. Touloukian, G. A. Hawkins and M. Jacob, "Heat Transfer by Free Convection from Heated Vertical Surfaces to Liquids," Trans. Am. Soc. Mech. Engrs., 70: 13 (1948).
3. W. H. McAdams, "Heat Transmission," 2nd ed., McGraw-Hill Book Company, Inc., New York, 1942.

4. W. M. Rohsenow and J. A. Clark, "Heat Transfer and Pressure Drop Data for High Heat Flux Densities to water at High Subcritical Pressures," Massachusetts Institute of Technology (Contract Nos. N5ori-07827 and NR-035-267) DTC Project No. 6627, Progress Report No. 3, Apr. 1, 1951.
5. H. Buchberg et al., "Final Report on Studies in Boiling Heat Transfer," University of California, Department of Engineering, COO-24 (AEC Contract No. AT-11-1-Gen-9), March 1951.
6. H. L. McGill and W. L. Sibbitt, "Heat Transfer and Pressure Drop of Water Flowing in a Small Tube," ANL-4603, Part I, pp 1-58, February 1951.
7. W. M. Kays, A. L. London and R. K. Lo, "Heat Transfer and Friction Characteristics for Gas Flow Normal to Tube Banks—Use of a Transient Test Technique," Stanford University, Technical Report No. 15, to be issued.
8. W. H. Denton et al., "The Heat Transfer and Pressure Loss in Fluid Flow through Randomly Packed Spheres. I" United Kingdom, HPC-35, 44 pp, June 28, 1949.
9. W. H. Jens and P. A. Lottes, "Analysis of Heat Transfer, Burnout, Pressure Drop and Density Data for High-pressure Water," Argonne National Laboratory, ANL-4627, 71 pp, May 1, 1951.
10. F. C. Gunther, "Photographic Study of Surface—Boiling Heat Transfer to Water with Forced Convection," Trans. Am. Soc. Mech. Engrs., 73: 115-123, (1951).
11. F. Kreith and M. Summerfield, "Heat Transfer to Water at High Flux Densities with and without Surface Boiling," Trans. Am. Soc. Mech. Engrs., 71: 805-815 (1949).
12. W. H. McAdams et al., "Heat Transfer at High Rates to Water with Surface Boiling," ANL-4268, 78 pp, December 1948.
13. E. Schmidt et al., "Heat Transfer by Liquids Near the Critical State," AAF Translation, ATI No. 22433 (F-TS-527 RE), 15 pp, April 26, 1946.
14. M. T. Cichelli and C. F. Bonilla, "Heat Transfer to Liquids Boiling under Pressure," Trans. Am. Inst. Chem. Engr., 41: 755-787 (1945).
15. G. A. Hawkins, "A Brief Review of the Literature on Boiling Heat Transfer," University of California, Department of Engineering, COO-23 (AEC Contract No. AT-11-1-Gen-9), 50 pp, June 1950.
16. "Heat Transfer to Fluids with Temperature Dependent Properties," Nuclear Developments Assoc., White Plains, New York, April 1952.

SELECTED READING LIST

HEAT TRANSFER, A BIBLIOGRAPHY OF UNCLASSIFIED REPORT LITERATURE, A. T. Morphew, TID-3022, 53 p, March 18, 1952.

HEAT TRANSFER, A BIBLIOGRAPHY OF CLASSIFIED REPORT LITERATURE, A. T. Morphew, TID-3021, 66 p, January 31, 1952.

A BRIEF REVIEW OF THE LITERATURE ON BOILING HEAT TRANSFER, University of California, Department of Engineering, G. A. Hawkins, COO-23 (AEC Contract No. AT-11-1-Gen-9), 50 pp, June 1950.

HEAT TRANSFER, M. Jacob, Vol. 1, John Wiley and Sons, Inc., New York, 1949.

HEAT TRANSMISSION, W. H. McAdams, 2nd ed., McGraw-Hill Book Company, Inc., New York, 1942.

Hydrodynamics

W. H. Jens and P. A. Lottes

Hydrodynamics or fluid mechanics must be considered in the design of a nuclear reactor and its coolant system. For example: The pressure drop through the reactor and other parts of the coolant system must be known together with the required pumping power; the flow distribution to the coolant channels surrounding the fuel elements during normal operation must be properly evaluated; and the flow distribution during abnormal operation when boiling might occur must be understood so that the proper safeguards may be provided to prevent flow stoppage and burnout of a fuel element.

Fluid flow nomenclature used in the following equations is defined in Table 1.5.1, and appropriate conversion factors are listed in Table 1.5.2.

SINGLE-PHASE-FLOW PRESSURE DROP

APPLICATION TO REACTOR CORES AND HEAT EXCHANGERS

FLOW INSIDE TUBES, NON-CIRCULAR CHANNELS, AND ANNULI

The differential equation* for steady flow in tubes, ducts, or channels of constant cross section is:

$$v dP + \frac{d(V^2)}{2g_c} + \frac{g}{g_c} dz + \frac{fV^2}{2g_c D_e} dL = 0 \quad (1)$$

For flow of incompressible fluids, the integrated equation is:

$$\frac{1}{\rho} (P_1 - P_2) - \frac{g}{g_c} (z_2 - z_1) - \frac{fV^2 (L_2 - L_1)}{2g_c D_e} = 0 \quad (2)$$

where $\rho = 1/v$.

If the temperatures of the fluid varies, f will also vary, since it depends on the Reynolds number; this variation is generally very slight and is usually neglected.

For the case of varying friction factor, the mean friction factor (f_m) is:

$$f_m = \frac{1}{L_2 - L_1} \int_{L_1}^{L_2} f dL \quad (3)$$

* The friction factor (f) based on the equivalent diameter is used in this and subsequent equations; this friction factor is equal to four times the value used in the Fanning equation. Fanning used a hydraulic radius which is one fourth of the equivalent diameter.

Table 1.5.1—Hydrodynamic Nomenclature and Units

Symbol	Definition	Units*
A	Flow area	sq ft
b	Wetted perimeter	ft
d	Distance between channels	ft
D	Diameter (inside) of conduit	ft
D_e	Equivalent diameter of conduit	ft
D_o	Diameter (outside) of pipe	ft
D_s	Diameter of sphere	ft
f	Friction factor based on equivalent diameter	None
b'	Wetted perimeter per unit flow area	ft^{-1}
f_1	Friction factor for cross flow to tubes in Eqs. (7), (8), and (10)	None
f_2	Friction factor for randomly packed spheres in Eq. (11)	None
F_b	Frictional energy loss due to bends	$\text{ft-lb}_f/\text{lb}$
F_c	Frictional energy loss due to sudden contraction	$\text{ft-lb}_f/\text{lb}$
F_e	Frictional energy loss due to sudden expansion	$\text{ft-lb}_f/\text{lb}$
F_r	Frictional energy loss due to rough miter bend	$\text{ft-lb}_f/\text{lb}$
F_s	Frictional energy loss due to smooth miter bend	$\text{ft-lb}_f/\text{lb}$
F_v	Frictional energy loss due to valves	$\text{ft-lb}_f/\text{lb}$
g	Gravitational acceleration, local, usually taken as 32.2	$\text{ft}/(\text{sec})(\text{sec})$
g_c	Proportionality factor in Newton's law of motion equals 32.2	$[\text{lb}/\text{lb}_f][\text{ft}/(\text{sec})(\text{sec})]$
G	Mass velocity	$\text{lb}/(\text{sec})(\text{sq ft})$
x_l	Ratio of longitudinal pitch to outside tube diameter	None
x_t	Ratio of transverse pitch to outside tube diameter	None
z	Vertical distance above any arbitrary datum plane	ft
ΔH	Enthalpy of saturated liquid minus enthalpy of liquid, at inlet subcooling enthalpy	Btu/lb
ΔP	Pressure drop	$\text{lb}_f/\text{sq ft}$
ΔP_0	Friction pressure loss for flow of saturated water	$\text{lb}_f/\text{sq ft}$
ΔP_{TPF}	Friction pressure loss for flow of two-phase fluid	$\text{lb}_f/\text{sq ft}$
$\frac{(dP_{\text{TPF}})}{(dP_0)}$	Ratio of two-phase, frictional pressure gradient to saturated-water, frictional pressure gradient	None
$\frac{(\Delta P_{\text{TPF}})}{(\Delta P_0)}$	Ratio of two-phase, frictional pressure loss to saturated-water, frictional pressure drop	None
$\frac{\epsilon}{D}$	Relative roughness factor	None
θ	Angle of elevation with respect to the horizontal	Degrees
μ	Dynamic viscosity of liquid	$\text{lb}/(\text{sec})(\text{ft})$
μ_b	Dynamic viscosity of bulk water	$\text{lb}/(\text{sec})(\text{ft})$
μ_f	Dynamic viscosity of saturated water	$\text{lb}/(\text{sec})(\text{ft})$
μ_g	Dynamic viscosity of saturated steam	$\text{lb}/(\text{sec})(\text{ft})$
μ_m	Weighted viscosity of steam-water mixture in Eq. (31)	$\text{lb}/(\text{sec})(\text{ft})$
μ_w	Dynamic viscosity based on wall temperature	$\text{lb}/(\text{sec})(\text{ft})$
ρ	Density of fluid	$\text{lb}/\text{cu ft}$
$\bar{\rho}$	Average density of fluid	$\text{lb}/\text{cu ft}$
G_{max}	Maximum mass velocity based on minimum free area for cross flow through tube banks	$\text{lb}/(\text{sec})(\text{sq ft})$
G_{sonic}	Maximum mass discharge rate from a pipe	$\text{lb}/(\text{sec})(\text{sq ft})$
h_{fg}	Latent heat of vaporization	Btu/lb
K_b	Factor in bend-loss equation	None
K_c	Factor in contraction-loss equation	None
K_e	Factor in expansion-loss equation	None
K_r	Factor in rough miter bend-loss equation	None
K_s	Factor in smooth miter bend-loss equation	None
K_v	Factor in valve- and fitting-loss equation	None

Table 1.5.1 — (Continued)

Symbol	Definition	Units*
L	Length of pipe	ft
N	Number of rows in a bank of tubes	None
N_v	Number of velocity heads lost in friction, $f \frac{L}{D}$	None
N_{Re}	Reynolds number, GD_e/μ or $\rho v D_e/\mu$	None
P	Absolute pressure	lb _f /sq ft
P_v	Pressure equivalent of velocity head	lb _f /sq ft
Q	Total heat input	Btu/sec
r	Multiplication factor in Eq. (26)	None
v	Specific volume	cu ft/lb
\bar{v}	Average specific volume	cu ft/lb
v_f	Specific volume of saturated liquid	cu ft/lb
v_{fg}	Specific volume change due to vaporization	cu ft/lb
V	Velocity	ft/sec
W	Flow rate	lb/sec
x	Steam quality, fraction vaporized by weight	None

* Pounds mass used unless otherwise noted. Lb_f signifies pounds force

Table 1.5.2 — Hydrodynamic Conversion Factors

English units × multiplication factor = CGS units

sq ft	929	sq cm
ft	30.48	cm
ft-lb _f /lb	2.987×10^4	cm-dyne/gm
ft/(sec)(sec)	30.48	cm/(sec)(sec)
[lb/lb _f][ft/(sec)(sec)]	0.03105	[gm/dyne][cm/(sec)(sec)]
lb/(sec)(sq ft)	.488	gm/(sec)(sq cm)
Btu/lb	.5555	cal/gm
lb/sq in.	6.895×10^4	dyne/sq cm
Btu/sec	252	cal/sec
Btu/sec	1054.8	watts
cu ft/lb	62.42	cm ³ /gm
ft/sec	30.48	cm/sec
lb/sec	453.6	gm/sec
lb _f /sq ft	478.8	dyne/sq cm
lb/(sec)(ft)	14.88	gm/(sec)(cm)
lb/cu ft	1.602×10^{-2}	gm/cm ³

Generally, $f_m = f$ at $\frac{1}{2} (L_1 + L_2)$ and is sufficiently accurate for most calculations.

For cases in which the channel is horizontal or where the difference in hydrostatic head between the ends of the channel is negligible, Eq. (2) reduces to:¹

$$\Delta P = \frac{f G^2 L}{2 \bar{\rho} g_c D_e} \left[\frac{\mu_w}{\mu_b} \right]^{0.14} = \frac{f V^2 \bar{\rho} L}{2 g_c D_e} \left[\frac{\mu_w}{\mu_b} \right]^{0.14} \quad (4)$$

The term $[\mu_w/\mu_b]^{0.14}$ accounts for a change in viscosity of the fluid at the wall and of the bulk fluid, as caused by heat transfer. This term can generally be neglected when the bulk water temperature is greater than 200°F.

For pipes:

$$D_e = \text{pipe diameter} \quad (5)$$

For non-circular ducts and annuli:

$$D_e = \frac{4 \times \text{flow area}}{\text{wetted perimeter}} \quad (5a)$$

An approximation for parallel plates is:

$$D_e = 2 \times \text{distance between confining boundaries} \quad (5b)$$

For a circular annulus:

$$D_e = \text{outside diameter minus inside diameter of annulus} \quad (5c)$$

Equation (2) has been used in the past for geometries other than pipes and has recently been re-examined and substantiated for annuli.²

An evaluation of relative roughness as a function of the equivalent diameter of tubes or channels may be made from Fig. 1.5.1. The friction factor is then obtained from Fig. 1.5.2 using this value of relative roughness. The friction factor may be obtained directly from Fig. 1.5.1 for complete turbulence in rough pipes. Following general practice, the relative roughness curves presented in Fig. 1.5.1 were extrapolated to the smaller equivalent diameters generally encountered in reactor design. For convenience in making pressure drop calculations, the Reynolds number is given in Fig. 1.5.3 as a function of the product of velocity and equivalent diameter for various water temperatures.

FLOW OUTSIDE TUBE BANKS

Flow Parallel to Axis

Pressure drop for turbulent flow outside tube banks with the liquid flowing parallel to the axis of the tubes is calculated by Eq. (4). The friction factor (f) is evaluated from Fig. 1.5.2. The Reynolds number is:

$$N_{Re} = \frac{G D_e}{\mu} = \frac{4W}{\mu b} = \frac{4G}{\mu b'} \quad (6)$$

where b' is the wetted perimeter per unit of flow area.

¹References appear at end of chapter.

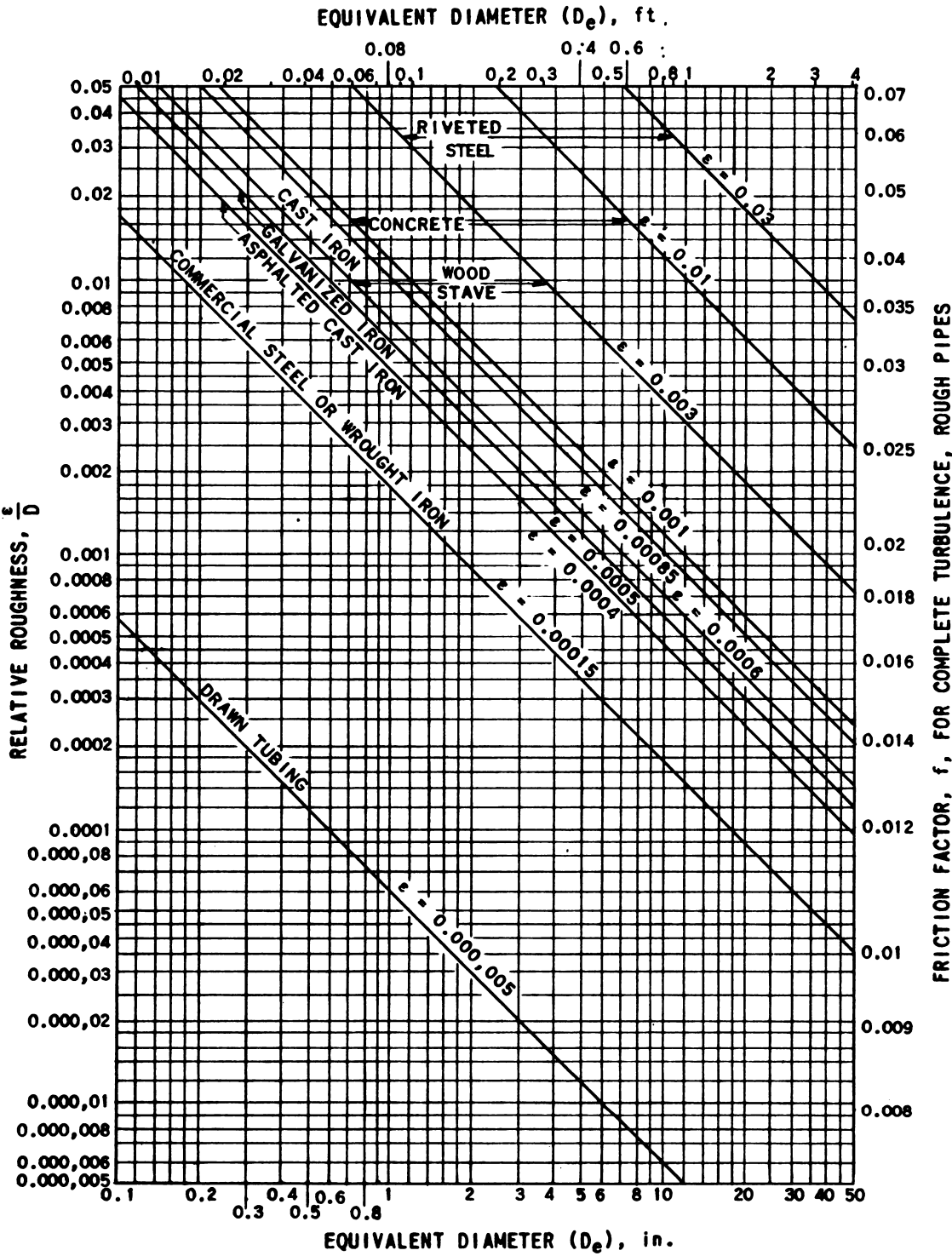


Fig. 1.5.1 — Relative Roughness vs Equivalent Diameter. Reprinted from L. F. Moody, Friction Factor for Pipe Flow, Trans. Am. Soc. Mech. Engrs., 66, 1944.

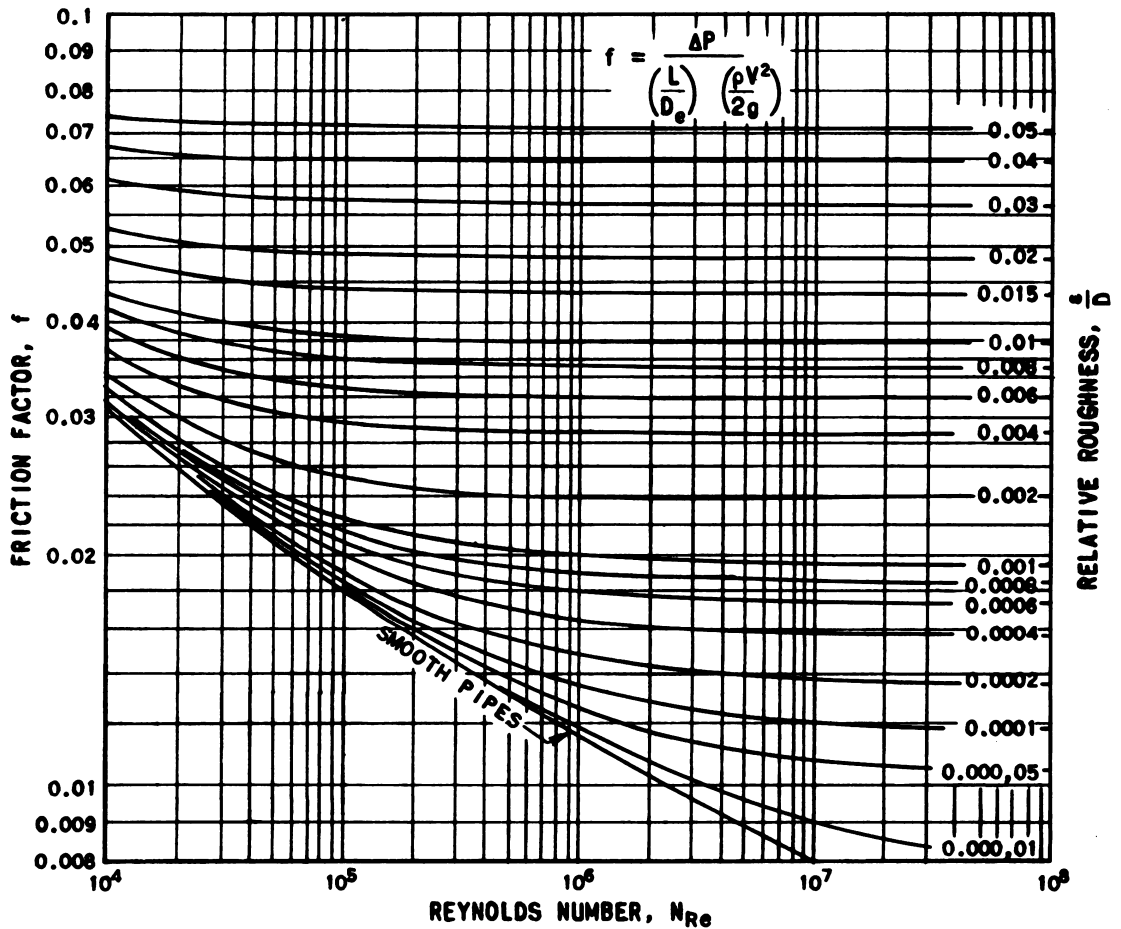


Fig. 1.5.2—Friction Factor vs Reynolds Number. Reprinted from L. F. Moody, Friction Factor for Pipe Flow, Trans. Am. Soc. Mech. Engrs., 66, 1944.

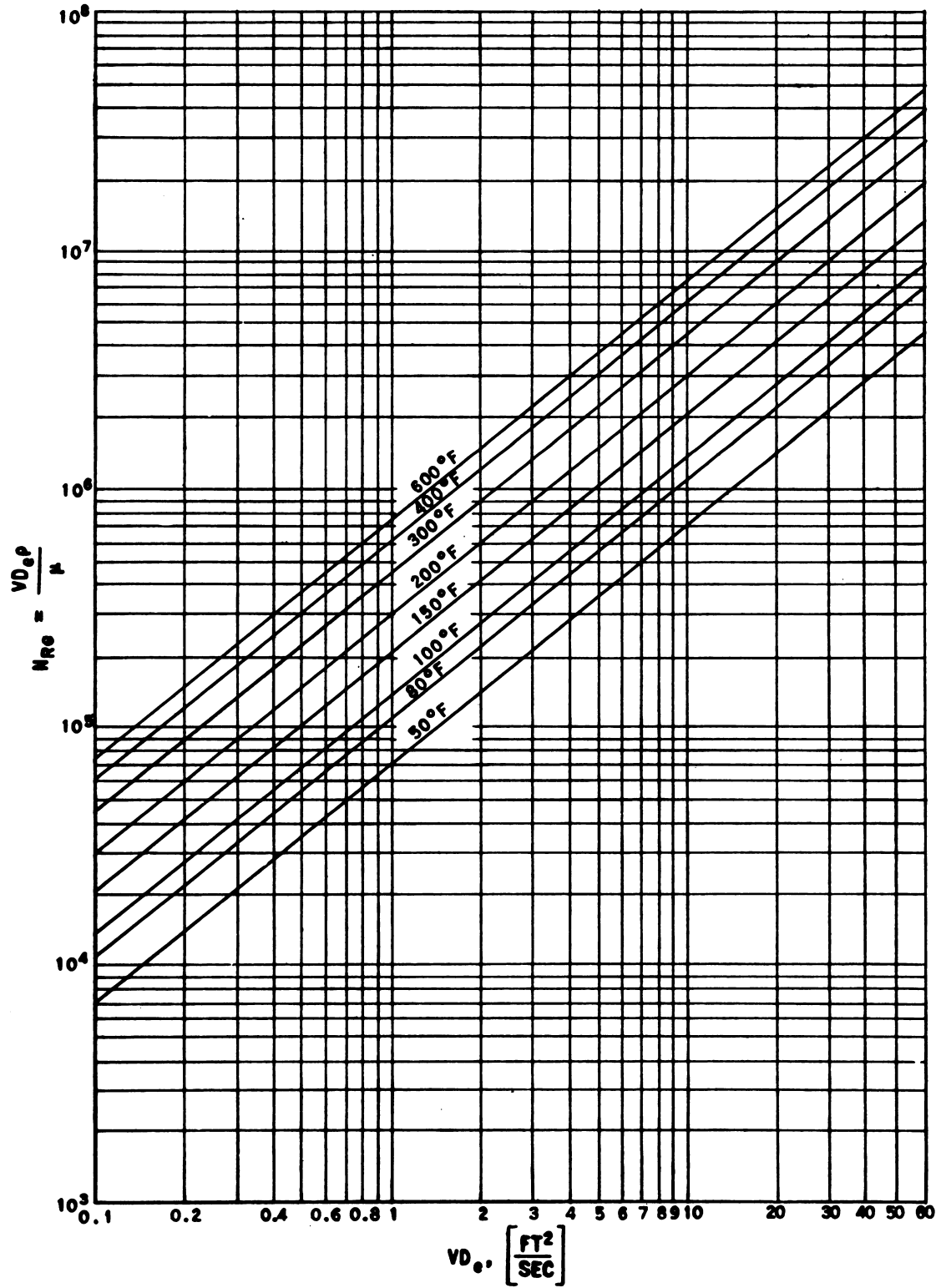


Fig. 1.5.3—Relationship Between Reynolds Number vs Velocity Times Equivalent Diameter for Various Water Temperatures. Submitted by Argonne National Laboratory, Sept. 12, 1952.

Flow Normal to Axis¹

The friction pressure drop for isothermal turbulent flow across tube banks is given by:

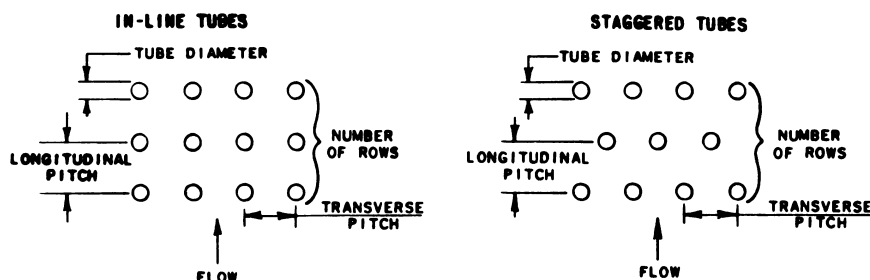
$$\frac{\Delta P}{\rho} = \frac{f_1 N V_{\max}^2}{2g_c} \quad (7)$$

where N = number of rows of tubes

V_{\max} = maximum velocity based on the minimum free area

The friction factors for unstaggered tubes are calculated from:

$$f_1 = 4 \left[0.044 + \frac{0.08 x_1}{(x_t - 1)^n} \right] \left[\frac{D_0 G_{\max}}{\mu_f} \right]^{-0.15} \quad (8)$$



where $n = 0.43 + 1.13/x_1$ (9)

x_1 = ratio of longitudinal pitch to tube diameter

x_t = ratio of the transverse pitch to tube diameter

Pitch is defined as the center-to-center distance between tubes.

The friction factors for staggered tubes are calculated from:

$$f_1 = 4 \left[0.23 + \frac{0.11}{(x_t - 1)^{1.08}} \right] \left[\frac{D_0 G_{\max}}{\mu_f} \right]^{-0.15} \quad (10)$$

RANDOMLY PACKED SPHERES

The local pressure gradient through a cylindrical bed of randomly packed spheres may be calculated according to the equation:³

$$\Delta P = \frac{f_2 L G^2}{2g_c \rho D_s} \quad (11)$$

where G is the apparent mass velocity based on the total cross section of the bed and D_s is the diameter of the spheres. Values of f_2 are shown in Fig. 1.5.4. At N_{Re} of about 50,000, f_2 approaches a constant value of 16, where all pressure loss arises from form resistance, causing changes in flow cross section.

APPLICATION TO PIPING AND PLENUMS

A convenient method of estimating pressure drop in a turbulent flow system is to use the velocity-head concept. In a turbulent flow system, friction losses can be visualized in terms of the kinetic energy of the fluid flowing. This can be shown from Eq. (4) since the kinetic energy per pound of fluid is:

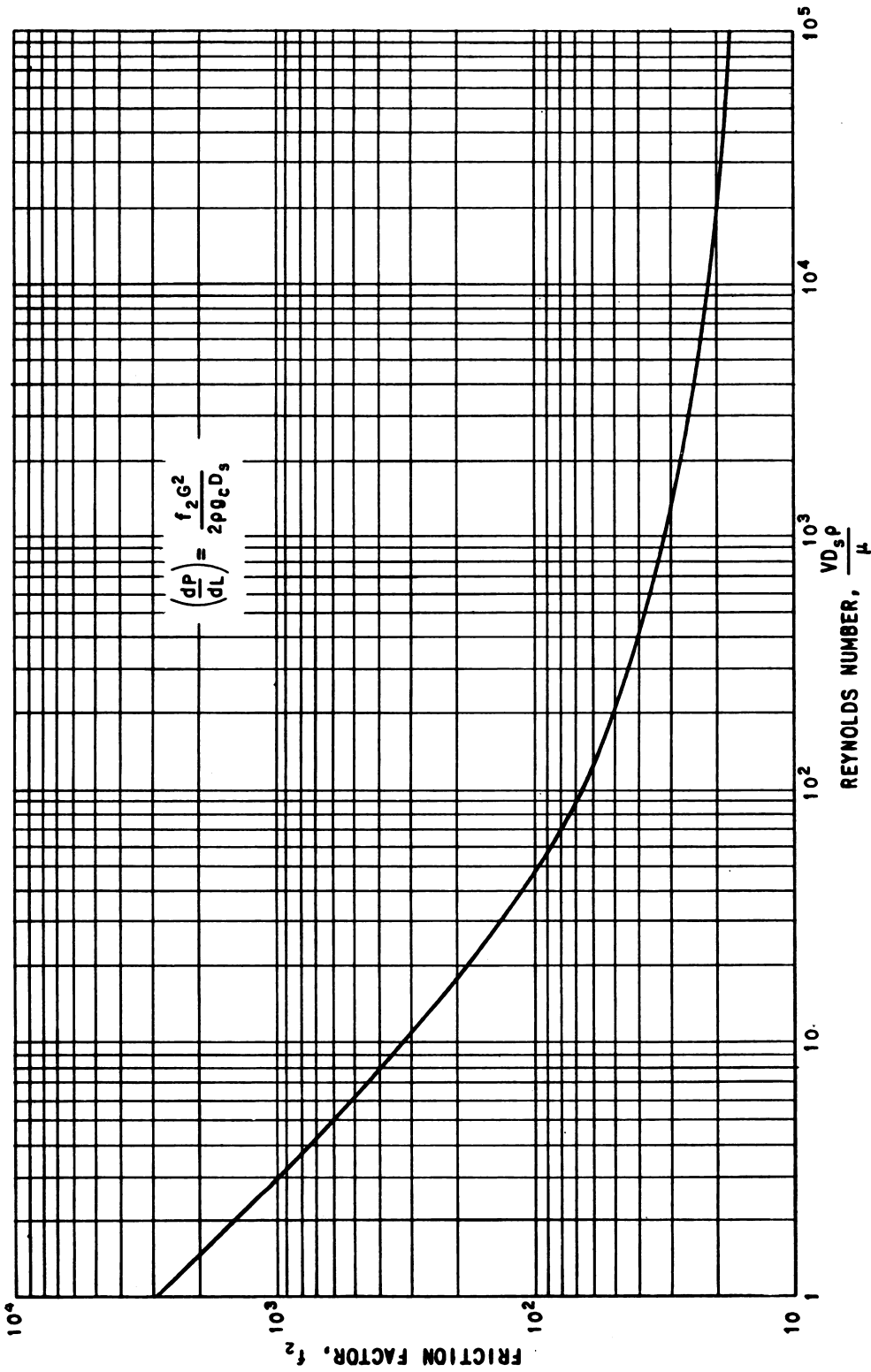


Fig. 1.5.4—Friction Factor (f_2) vs Reynolds Number for Randomly Packed Spheres. Reprinted from W. H. Denton et al, The Heat Transfer and Pressure Loss in Fluid Flow through Randomly Packed Spheres, I. United Kingdom HPC-35, June 28, 1949.

$$\frac{\text{kinetic energy}}{\text{pound}} = \frac{V^2}{2g_c} \quad (12)$$

and P is proportional to $V^2/2g_c$. The kinetic energy can, in turn, be expressed as a pressure differential by introducing density:

$$P_v = \frac{V^2}{2g_c} \quad (13)$$

where P_v is the velocity head in pounds force per square foot ($\text{lb}_f/\text{sq ft}$) for a fluid moving at a velocity V . A plot of velocity head for water expressed in pounds per square inch (psi) as a function of temperature and velocity is shown in Fig. 1.5.5.

FLOW IN PIPES

The isothermal frictional pressure drop can now be written in terms of velocity heads as:

$$N_v = \frac{\Delta P}{\rho V^2/2g_c} = f \frac{L}{D} \quad (14)$$

where N_v equals number of velocity heads lost and f is obtained from Fig. 1.5.1.

For rapid estimation of pipe-friction pressure drop in a flow system where N_{Re} lies in the range 5,000 to 1,000,000, an average value of f equal to 0.022 may be used for clean, commercial-steel pipe. Using this value of f in Eq. (14), an $L/D = 45$ is obtained; that is, a length of clean, commercial-steel pipe equivalent to 45 diameters will have approximately one velocity-head loss within plus or minus 40 percent.

Equation (1) for the flow of incompressible liquids can be revised for a general flow system in which a variety of frictional losses are encountered, providing the maximum velocity for each transition is the same:

$$\Delta P = (Z_1 - Z_2) \rho \frac{g}{g_c} + \frac{\rho V^2}{2g_c} (N_v + K_e + K_c + K_b + K_v + K_s + \dots) \quad (15)$$

where $N_v = f L/D$ and K_e , K_c , K_b , K_v , K_s are loss coefficients for enlargements, contractions, and the like.

ENLARGEMENT LOSSES

The frictional energy loss due to sudden and sharp enlargement of the flow cross section can be calculated according to the equation:

$$F_e = K_e \frac{V_1^2}{2g_c} = \left[1 - \frac{A_1}{A_2} \right]^2 \left[\frac{V_1^2}{2g_c} \right] \quad (16)$$

where V_1 = average linear upstream velocity

A_1/A_2 = ratio of upstream flow area to downstream flow area.

Values of K_e are shown as a function of A_1/A_2 in Fig. 1.5.6.

CONTRACTION LOSSES

The frictional energy loss due to sudden and sharp contraction of the flow cross section can be calculated with the equation:

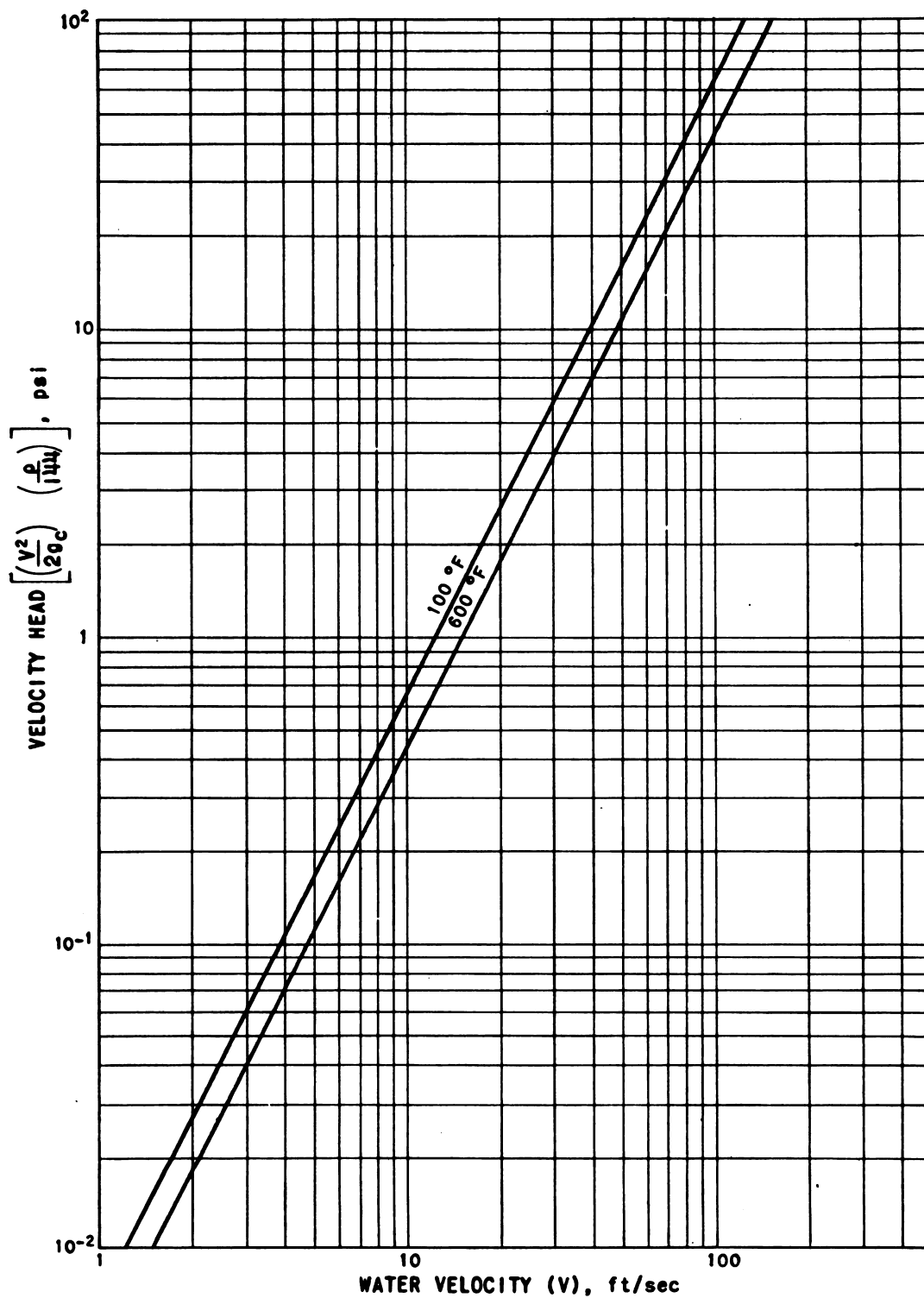


Fig. 1.5.5 — Velocity Head of Saturated Water as a Function of Velocity and Temperature. Submitted by Argonne National Laboratory, June 30, 1952.

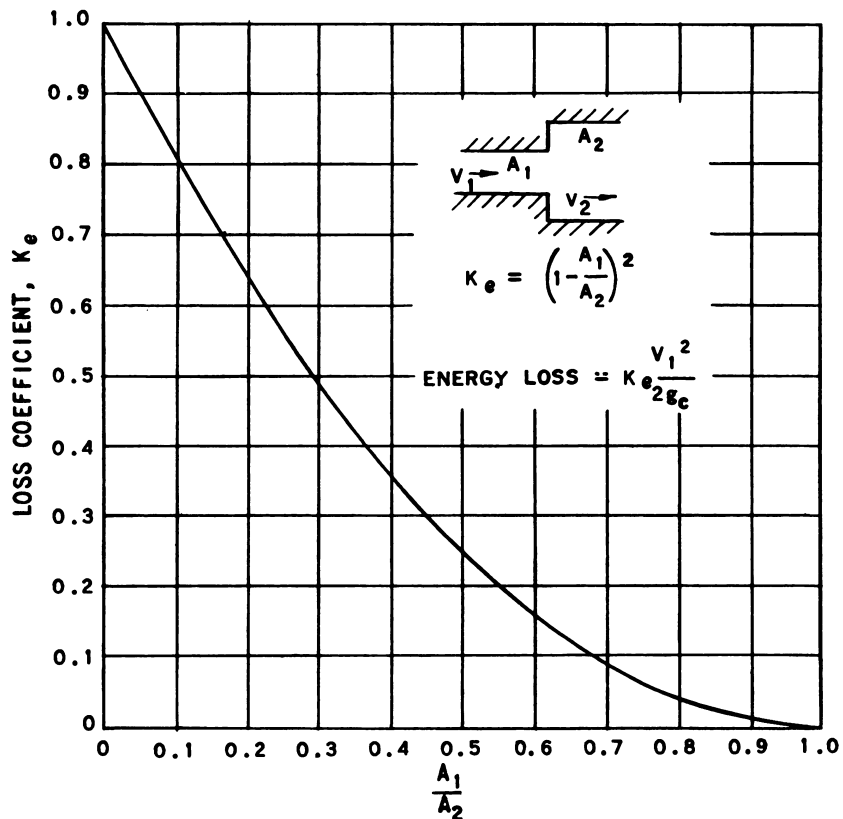


Fig. 1.5.6 — Loss Coefficient for Sudden Enlargement. Submitted by Argonne National Laboratory, June 30, 1952.

$$F_c = K_c \frac{V_2^2}{2g_c} \quad (17)$$

where V_2 = average linear downstream velocity.

Values of K_c are shown in Fig. 1.5.7.

RADIUS-BEND LOSSES

The frictional energy loss due to 90-degree bends may be calculated according to the equation:

$$F_b = K_b \frac{V^2}{2g_c} \quad (18)$$

Figure 1.5.8 shows values of K_b as a function of bend geometry. Values are shown plotted against the ratio of bend radius (from center of bend to centerline of pipe) to inside pipe diameter.

Figure 1.5.9 shows the effect of bend angle on K_b at $N_{Re} = 2.25 \times 10^5$.

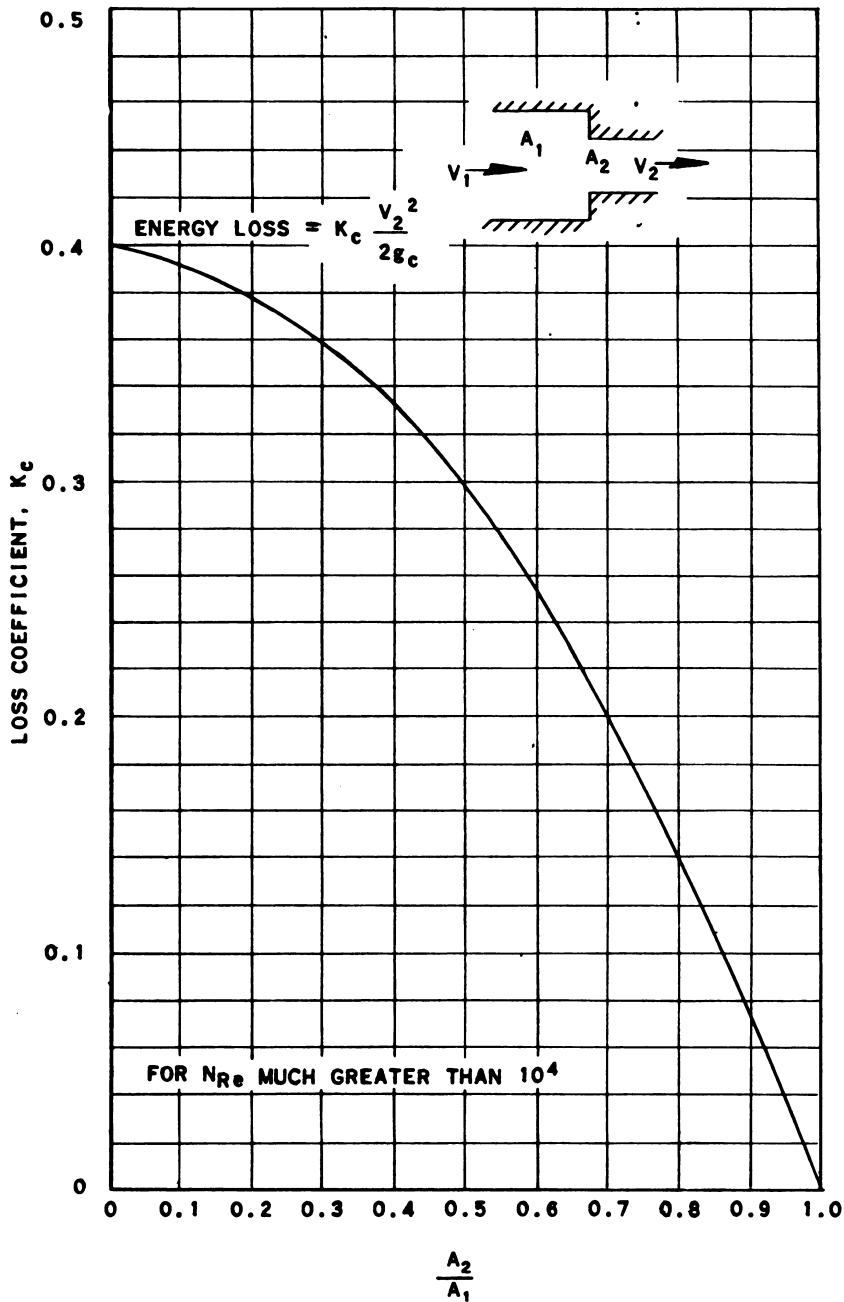


Fig. 1.5.7—Loss Coefficient for Sudden Contraction. Redrawn from W. M. Kays, Loss Coefficients for Abrupt Changes in Flow Cross Section with Low-Reynolds-Number Flow in Single- and Multiple-Tube Systems, Stanford University Technical Report No. 9, Jan. 1, 1950.

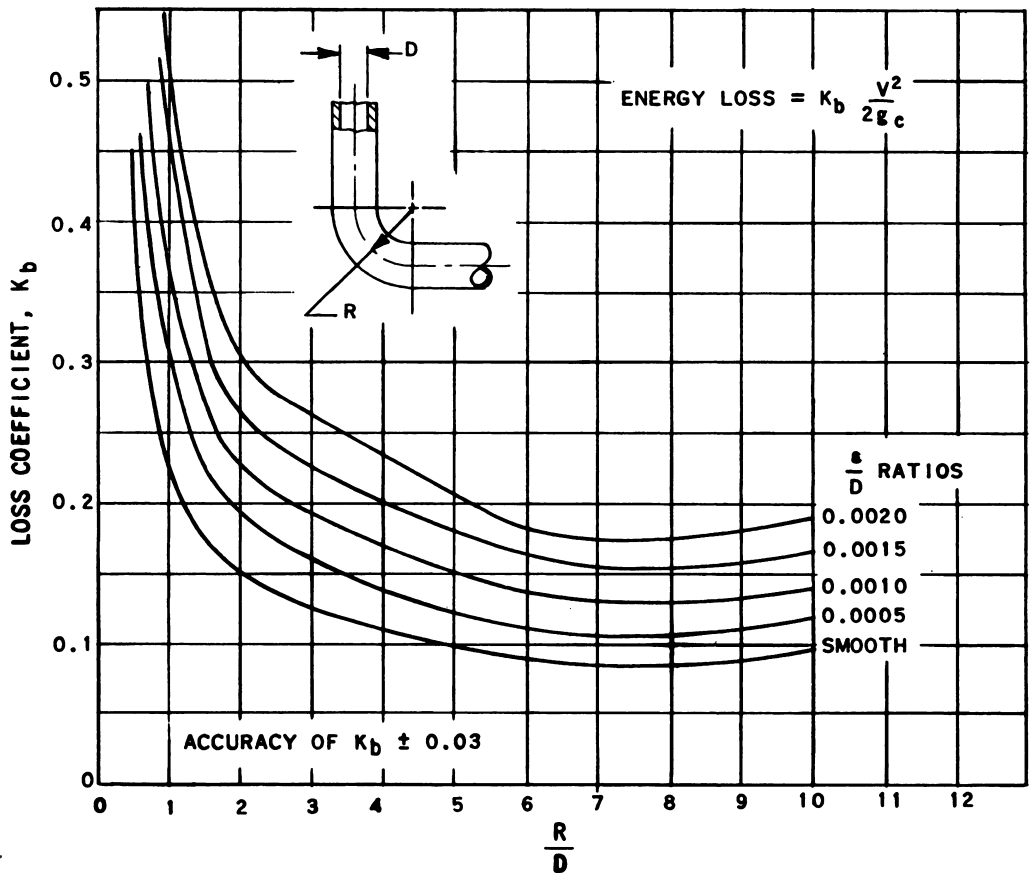


Fig. 1.5.8—Loss Coefficient for 90° Bends. Reprinted from Standards of Hydraulic Institute, 8th ed., Hydraulic Institute, New York, 1947.

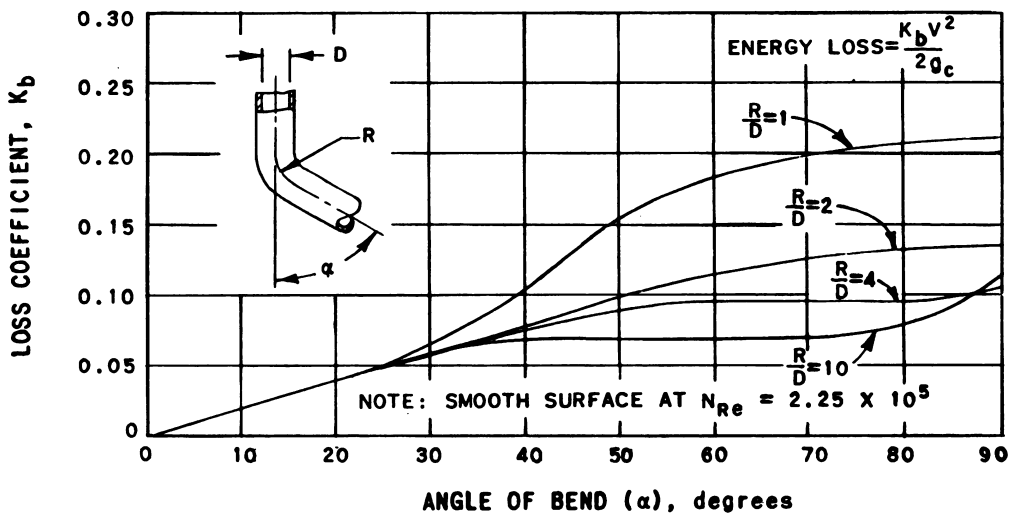


Fig. 1.5.9—Loss Coefficient for Bends vs Angle of Bend in Smooth Tubes. Reprinted from Standards of Hydraulic Institute, 8th ed., Hydraulic Institute, New York, 1947.

MITER-BEND LOSSES

The frictional energy loss due to miter bends may be calculated by means of the following equation:

$$F_s = K_s \frac{V^2}{2g_c} \text{ or } F_r = K_r \frac{V^2}{2g_c} \quad (19)$$

Figure 1.5.10 gives the values of K_s and K_r as a function of the angle of the miter bend and for various combinations of bends connected by straight pipe. The values are given for a Reynolds number of 2.25×10^6 .

LOSSES DUE TO VALVES AND FITTINGS

The frictional energy loss through screwed valves and fittings can be calculated according to the equation:

$$F_v = K_v \frac{V^2}{2g_c} \quad (20)$$

Values of K_v are given in Table 1.5.3 in the column designated "Equivalent Velocity Head."

TWO-PHASE-FLOW PRESSURE DROP**BASIC EQUATIONS**

The general equation for homogeneous (no slippage), two-phase flow may be written in differential form as:

$$-vdP = \frac{fV^2 dL}{2g_c D_e} + d \left[\frac{V^2}{2g_c} \right] + \frac{g}{g_c} dz \quad (21)$$

or:

$$-dP = \frac{vfG^2 dL}{2g_c D_e} + \frac{G^2 dv}{g_c} + \frac{g}{g_c} \frac{dz}{v} \quad (22)$$

The over-all pressure drop is then:

$$P_1 - P_2 = \frac{G^2}{2g_c D_e} \int_1^2 \frac{fdL}{\rho} + \frac{G^2}{g_c} \left[\frac{1}{\rho_2} - \frac{1}{\rho_1} \right] + \frac{g}{g_c} \int_1^2 \rho dz \quad (23)$$

The first two terms on the right hand side of Eq. (23) are the frictional pressure drop and momentum pressure drop, respectively. The last term is the change in hydrostatic head in the vertical direction "z." For vertical, two-phase flow upward with constant heat generation along a tube with saturated water at the inlet and equal steam and water velocities at any cross section (no slippage) with exit quality of x , the last term in Eq. (23) is evaluated as follows:

$$\int_1^2 \rho dz = \frac{1}{xv_{fg}} (z_2 - z_1) \log_e \left[1 + \frac{xv_{fg}}{v_f} \right] \quad (24)$$

The first two terms of Eq. (23) may be evaluated either according to the Martinelli-Nelson⁴ method or according to the method developed at Hanford.⁵









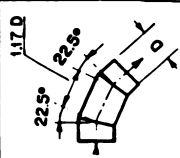
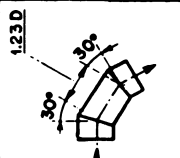
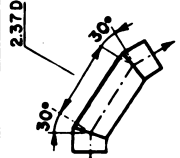
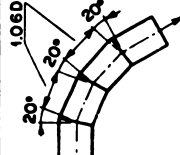
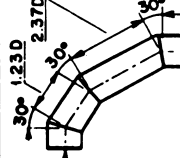
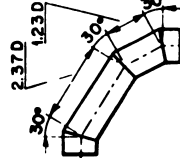
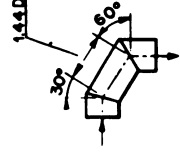
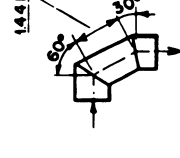
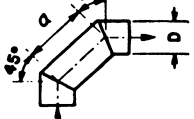
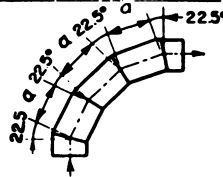
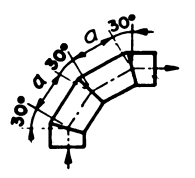
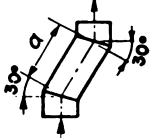
*OPTIMUM VALUE OF α INTERPOLATED																																																																																																																																	
K_s = RESISTANCE COEFFICIENT FOR SMOOTH SURFACE K_r = RESISTANCE COEFFICIENT FOR ROUGH SURFACE, $\frac{\epsilon}{D} \approx 0.0022$																																																																																																																																	
	$K_s = 0.016$ $K_r = 0.024$		$K_s = 0.034$ $K_r = 0.044$		$K_s = 0.042$ $K_r = 0.062$		$K_s = 0.066$ $K_r = 0.154$		$K_s = 0.130$ $K_r = 0.165$		$K_s = 0.236$ $K_r = 0.320$		$K_s = 0.471$ $K_r = 0.684$		$K_s = 1.129$ $K_r = 1.265$																																																																																																																		
	$K_s = 0.112$ $K_r = 0.284$		$K_s = 0.150$ $K_r = 0.268$		$K_s = 0.143$ $K_r = 0.227$		$K_s = 0.108$ $K_r = 0.236$		$K_s = 0.188$ $K_r = 0.320$		$K_s = 0.202$ $K_r = 0.323$		$K_s = 0.400$ $K_r = 0.534$		$K_s = 0.400$ $K_r = 0.601$																																																																																																																		
	<table><tr><th>α/D</th><th>K_s</th><th>K_r</th></tr><tr><td>0.71</td><td>0.507</td><td>0.510</td></tr><tr><td>0.943</td><td>0.350</td><td>0.415</td></tr><tr><td>1.174</td><td>0.335</td><td>0.384</td></tr><tr><td>1.42</td><td>0.261</td><td>0.377</td></tr><tr><td>1.50</td><td>0.280</td><td>0.376</td></tr><tr><td>1.86</td><td>0.289</td><td>0.390</td></tr><tr><td>2.36</td><td>0.356</td><td>0.429</td></tr><tr><td>3.14</td><td>0.356</td><td>0.460</td></tr><tr><td>4.89</td><td>0.369</td><td>0.455</td></tr><tr><td>6.59</td><td>0.392</td><td>0.444</td></tr><tr><td>6.28</td><td>0.369</td><td>0.444</td></tr></table>	α/D	K_s	K_r	0.71	0.507	0.510	0.943	0.350	0.415	1.174	0.335	0.384	1.42	0.261	0.377	1.50	0.280	0.376	1.86	0.289	0.390	2.36	0.356	0.429	3.14	0.356	0.460	4.89	0.369	0.455	6.59	0.392	0.444	6.28	0.369	0.444		<table><tr><th>α/D</th><th>K_s</th><th>K_r</th></tr><tr><td>1.186</td><td>0.120</td><td>0.294</td></tr><tr><td>1.40</td><td>0.125</td><td>0.254</td></tr><tr><td>1.50*</td><td>—</td><td>0.250</td></tr><tr><td>1.63</td><td>0.124</td><td>0.266</td></tr><tr><td>1.86</td><td>0.117</td><td>0.272</td></tr><tr><td>2.325</td><td>0.096</td><td>0.317</td></tr><tr><td>2.40</td><td>0.095</td><td>0.317</td></tr><tr><td>2.91</td><td>0.108</td><td>0.317</td></tr><tr><td>3.49</td><td>0.130</td><td>0.318</td></tr><tr><td>4.65</td><td>0.148</td><td>0.310</td></tr><tr><td>6.05</td><td>0.142</td><td>0.313</td></tr></table>	α/D	K_s	K_r	1.186	0.120	0.294	1.40	0.125	0.254	1.50*	—	0.250	1.63	0.124	0.266	1.86	0.117	0.272	2.325	0.096	0.317	2.40	0.095	0.317	2.91	0.108	0.317	3.49	0.130	0.318	4.65	0.148	0.310	6.05	0.142	0.313		<table><tr><th>α/D</th><th>K_s</th><th>K_r</th></tr><tr><td>1.23</td><td>0.195</td><td>0.347</td></tr><tr><td>1.44</td><td>0.196</td><td>0.320</td></tr><tr><td>1.67</td><td>0.150</td><td>0.300</td></tr><tr><td>1.70</td><td>0.149</td><td>0.299</td></tr><tr><td>1.91</td><td>0.154</td><td>0.312</td></tr><tr><td>2.37</td><td>0.167</td><td>0.337</td></tr><tr><td>2.96</td><td>0.172</td><td>0.342</td></tr><tr><td>4.11</td><td>0.190</td><td>0.364</td></tr><tr><td>4.70</td><td>0.192</td><td>0.360</td></tr><tr><td>6.10</td><td>0.201</td><td>0.360</td></tr></table>	α/D	K_s	K_r	1.23	0.195	0.347	1.44	0.196	0.320	1.67	0.150	0.300	1.70	0.149	0.299	1.91	0.154	0.312	2.37	0.167	0.337	2.96	0.172	0.342	4.11	0.190	0.364	4.70	0.192	0.360	6.10	0.201	0.360		<table><tr><th>α/D</th><th>K_s</th><th>K_r</th></tr><tr><td>1.23</td><td>0.157</td><td>0.300</td></tr><tr><td>1.67</td><td>0.156</td><td>0.378</td></tr><tr><td>2.37</td><td>0.143</td><td>0.264</td></tr><tr><td>3.77</td><td>0.160</td><td>0.292</td></tr></table>	α/D	K_s	K_r	1.23	0.157	0.300	1.67	0.156	0.378	2.37	0.143	0.264	3.77	0.160	0.292		
α/D	K_s	K_r																																																																																																																															
0.71	0.507	0.510																																																																																																																															
0.943	0.350	0.415																																																																																																																															
1.174	0.335	0.384																																																																																																																															
1.42	0.261	0.377																																																																																																																															
1.50	0.280	0.376																																																																																																																															
1.86	0.289	0.390																																																																																																																															
2.36	0.356	0.429																																																																																																																															
3.14	0.356	0.460																																																																																																																															
4.89	0.369	0.455																																																																																																																															
6.59	0.392	0.444																																																																																																																															
6.28	0.369	0.444																																																																																																																															
α/D	K_s	K_r																																																																																																																															
1.186	0.120	0.294																																																																																																																															
1.40	0.125	0.254																																																																																																																															
1.50*	—	0.250																																																																																																																															
1.63	0.124	0.266																																																																																																																															
1.86	0.117	0.272																																																																																																																															
2.325	0.096	0.317																																																																																																																															
2.40	0.095	0.317																																																																																																																															
2.91	0.108	0.317																																																																																																																															
3.49	0.130	0.318																																																																																																																															
4.65	0.148	0.310																																																																																																																															
6.05	0.142	0.313																																																																																																																															
α/D	K_s	K_r																																																																																																																															
1.23	0.195	0.347																																																																																																																															
1.44	0.196	0.320																																																																																																																															
1.67	0.150	0.300																																																																																																																															
1.70	0.149	0.299																																																																																																																															
1.91	0.154	0.312																																																																																																																															
2.37	0.167	0.337																																																																																																																															
2.96	0.172	0.342																																																																																																																															
4.11	0.190	0.364																																																																																																																															
4.70	0.192	0.360																																																																																																																															
6.10	0.201	0.360																																																																																																																															
α/D	K_s	K_r																																																																																																																															
1.23	0.157	0.300																																																																																																																															
1.67	0.156	0.378																																																																																																																															
2.37	0.143	0.264																																																																																																																															
3.77	0.160	0.292																																																																																																																															

Fig. 1.5.10—Loss Coefficient for Miter Bends of Various Angles and Straight Sections. Reprinted from Standards of Hydraulic Institute, 8th ed, Hydraulic Institute, New York, 1947.

Table 1.5.3 — Pressure Drop for Turbulent Flow Through Screwed Valves and Fittings

(Reprinted from "Velocity Head Simplifies Flow Computation," by
C. E. Lapple. By permission from Chem. Engr. 56, May 1949.)

Type of valve or fitting	Pressure drop*	
	Equivalent L/D	Equivalent velocity head (K_v)
Couplings	2	0.04
Unions	2	.04
Gate valves †		
Open	7	0.1
$\frac{3}{4}$ open	40	.8
$\frac{1}{2}$ open	200	4
$\frac{1}{4}$ open	800	15
Globe valves, † bevel seat		
Open	350	6
$\frac{1}{2}$ open	550	10
Composition disk		
Open	330	6
$\frac{1}{2}$ open	500	9
Plug disk		
Open	500	9
$\frac{3}{4}$ open	700	13
$\frac{1}{2}$ open	2000	35
$\frac{1}{4}$ open	6000	110
Angles valves †		
Open	170	3
Y or blow-off valves †		
Open	170	3
Check valves ‡		
Swing	110	2
Disk	500	10
Ball	3500	65
Water meters		
Disk	400	8

* Pressure drop is expressed as straight pipe of same nominal size as the fitting.

Where the pressure drop is expressed as L/D , L is the equivalent length (feet) of straight pipe and D is the inside diameter (feet). Where the pressure drop is expressed as velocity heads, the velocity in the pipe is based on the nominal diameter of the fitting

† Flow direction through valves has negligible effect on pressure drop

‡ Values apply only when check valve is fully open, which generally is attained at pipe velocities over 3 ft/sec for water

MARTINELLI-NELSON METHOD OF PREDICTING TWO-PHASE PRESSURE DROP

The friction pressure drop for two-phase isothermal flow may be written as:

$$\Delta P_{\text{TPF}} = \Delta P_0 \left[\frac{dP_{\text{TPF}}}{dP_0} \right] \quad (25)$$

Values of $[dP_{\text{TPF}}/dP_0]$ as a function of pressure and quality are given in Fig. 1.5.11. Equation (25) may be used to calculate frictional pressure drop of a constant-quality mixture flowing through a horizontal tube of constant diameter. The velocity of the water and steam are not necessarily equal in this correlation.

For the specific case of a horizontal, uniformly heated tube with constant heat input per unit length and saturated water at the inlet:

$$\Delta P_{\text{TP}} = \Delta P_0 \left[\frac{\Delta P_{\text{TPF}}}{\Delta P_0} \right] + r \frac{G^2}{g_c} \quad (26)$$

where r is a multiplication factor accounting for slippage of the steam in water as it affects the change in momentum pressure drop.

Values of $[\Delta P_{\text{TPF}}/\Delta P_0]$ as a function of pressure and exit quality are given in Fig. 1.5.12. This figure is the result of integrating the frictional term as indicated by Eq. (23) using point values of friction factor as given by Fig. 1.5.11. For equal velocities of water and steam, r in Eq. (26) is equal to the change in specific volume of the mixture during the acceleration. This is evident from a comparison of Eq. (23) and (26). For unequal velocities (slippage), values of r may be obtained from Fig. 1.5.13. For vertical tubes, the friction and acceleration losses from Eq. (26) may then be added to the loss in hydrostatic head to give total pressure drop.

HANFORD METHOD OF PREDICTING TWO-PHASE PRESSURE DROP

Hanford⁵ has developed a method for evaluating pressure drop of two-phase flow with heating through a horizontal tube. The method involves a stepwise calculation along a tube with a summation to give the total pressure drop.

This method involves the use of the equation:

$$\Delta P = C_1 W^{1.8} \mu_m^{0.2} L V + C_2 W^2 \left[\frac{1}{\rho_2} - \frac{1}{\rho_1} \right] \quad (27)$$

where:

$$C_1 = \frac{C_3}{2g_c A^{1.8} D_e^{1.7}} \quad (28)$$

$$C_2 = \frac{1}{A^2 g_c} \quad (29)$$

The constant C_3 in Eq. (28) is defined by McAdams¹ in the equation for turbulent flow:

$$f = \frac{C_3}{(N_{\text{Re}})^{0.7}} \quad (30)$$

where f is given in Fig. 1.5.1.

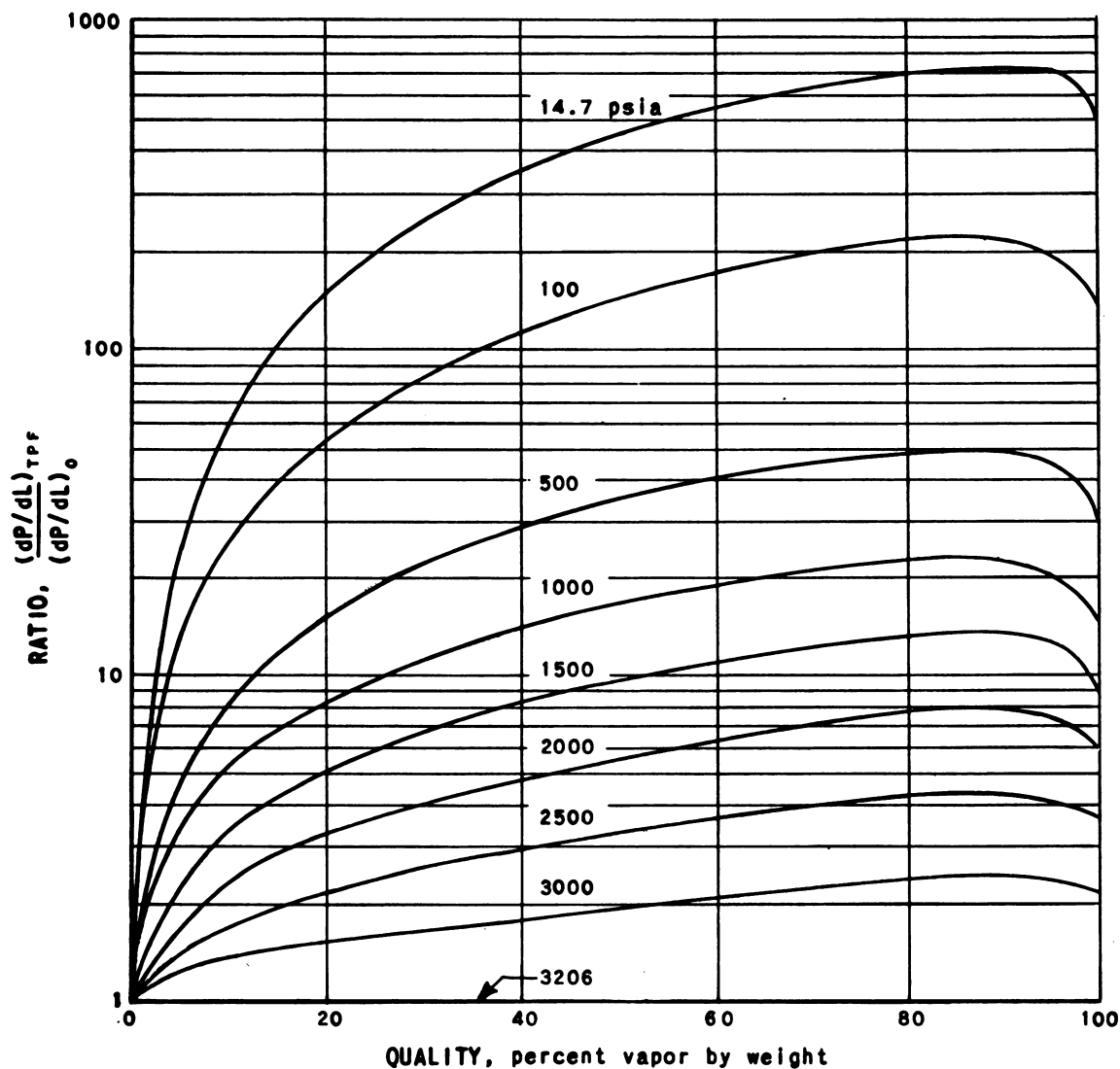


Fig. 1.5.11—Ratio of Local Two-phase Pressure Gradient to Pressure Gradient for 100 Percent Liquid Flow as a Function of Quality and Pressure. Reprinted from R. C. Martinelli and D. B. Nelson, Prediction of Pressure Drop During Forced Convection Boiling of Water, Trans. Am. Soc. Mech. Engrs., 70, (1948).

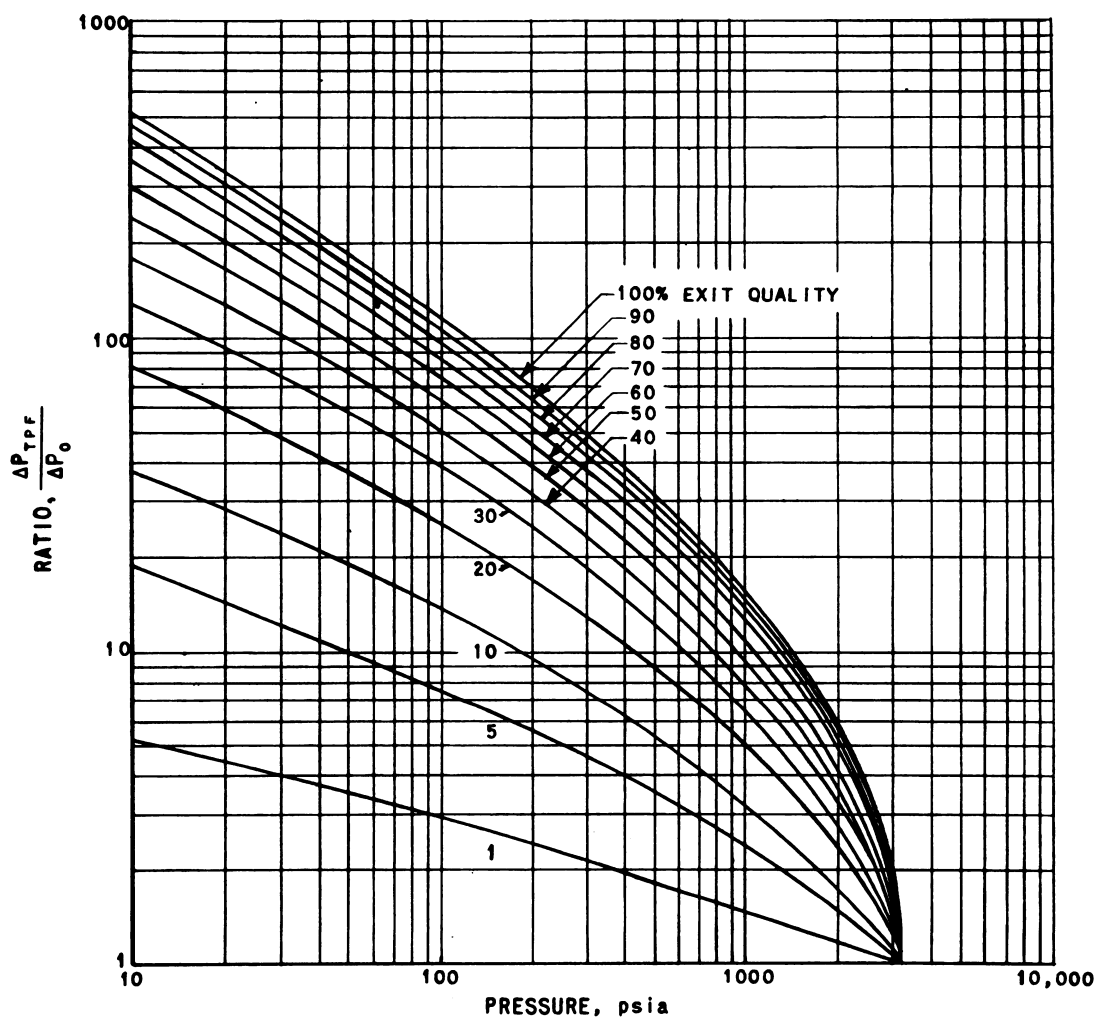


Fig. 1.5.12—Ratio of ΔP_{TPF} to ΔP_0 as a Function of Exit Quality and Pressure. Reprinted from R. C. Martinelli and D. B. Nelson, Prediction of Pressure Drop During Forced Convection Boiling of Water, Trans. Am. Soc. Mech. Engrs., 70, (1948).

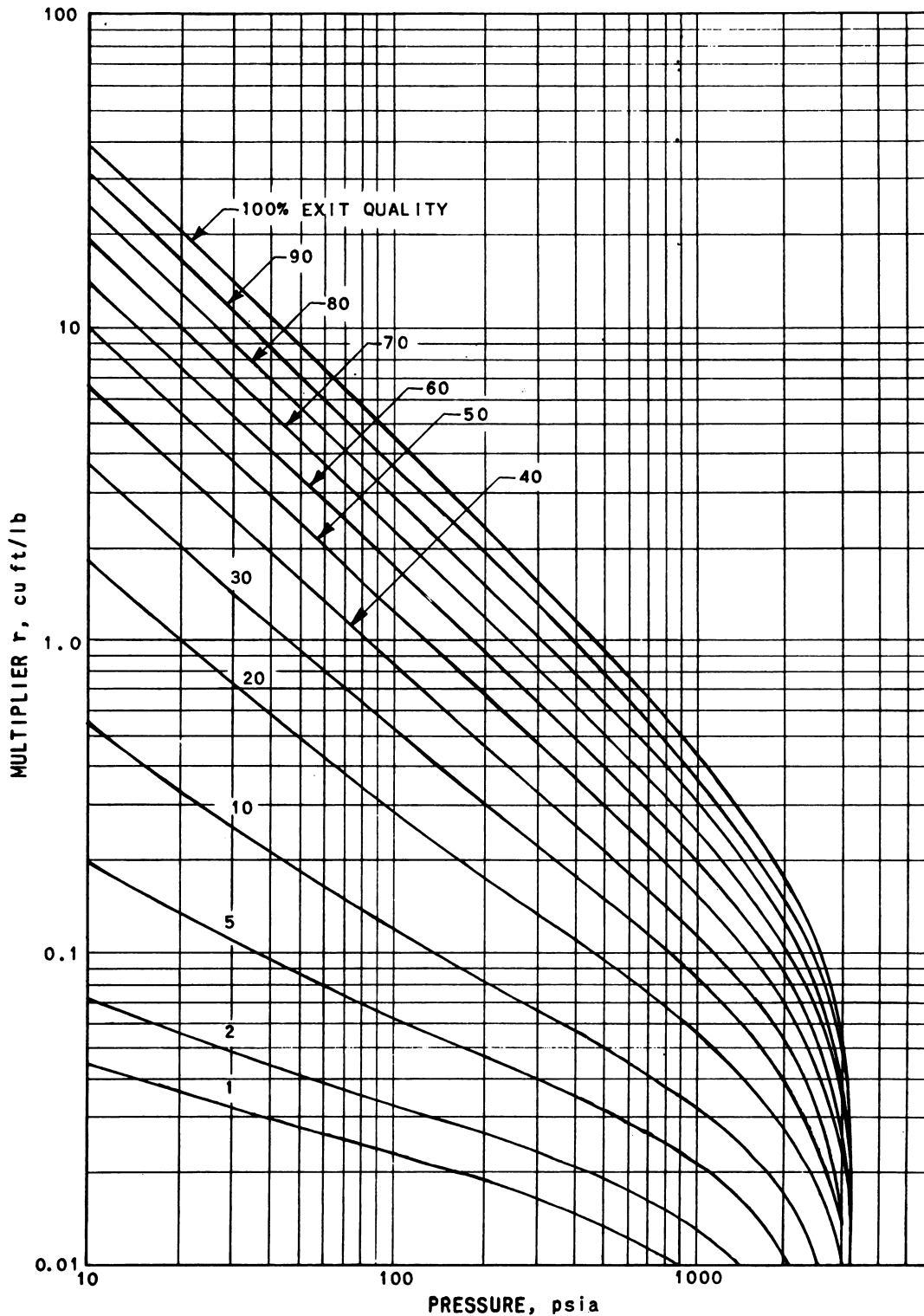


Fig. 1.5.13—Multiplier (r) vs Pressure for Various Exit Qualities. Reprinted from R. C. Martinelli and D. B. Nelson, Prediction of Pressure Drop During Forced Convection Boiling of Water, Trans. Am. Soc. Mech. Engrs., 70, (1948).

For smooth tubes, the value of C_3 in Eq. (30) is 0.184 for a range of N_{Re} from 5,000 to 200,000.

Equation (27) is of the same form as Eq. (23). The first term is the frictional drop. The dynamic viscosity is evaluated as:

$$\frac{1}{\mu_m} = \frac{1-x}{\mu_f} + \frac{x}{\mu_g} \quad (31)$$

The second term in Eq. (27) is the pressure loss due to the change in momentum of the flowing fluid and is based on equal steam and water velocities (no slippage). The constants C_1 and C_2 include the flow area.

CALCULATION FOR POSSIBILITY OF SONIC FLOW

In making any two-phase pressure-drop calculation, it should be determined that the exit velocity is less than the sonic velocity. If sonic flow (G_{sonic}) exists within a channel, the Martinelli-Nelson method may be used to evaluate the two-phase pressure drop up to the position where the sonic velocity exists. The pressure loss at the end of a channel due to sonic flow can be evaluated from Fig. 1.5.14. For a given flow and given exit enthalpy, Fig. 1.5.14 shows the pressure just inside the exit, independent of the back pressure:

$$vdP + \frac{VdV}{g_c} = 0 \quad (32)$$

or:

$$G_{sonic} = \sqrt{-g_c \frac{dP}{dv}} \quad (33)$$

Values of G_{sonic} as a function of quality and pressure are shown in Fig. 1.5.14. It was assumed that (dP/dv) should be evaluated at constant entropy.

EFFECT OF LOCAL BOILING

The general effect of local boiling is to increase pressure drop above that existing without boiling. The increase is dependent upon pressure, subcooling, and heat flux and is, at this time, unpredictable. However, the increases are small compared to the increases that occur with net boiling.⁶

FLOW IN PARALLEL CHANNELS

In heat exchange equipment containing many flow channels in parallel, each channel receives a share of the flow, the amount of which depends upon channel geometry, the orientation of the channels with respect to each other (as determined by the connecting headers), and the pressure-drop flow characteristic of each channel. The flow is governed by the total pressure drop across the channels. If the resistance to flow through any particular channel changes, the flow in that channel will change. This problem is obviously of primary importance in a heat exchange system of parallel channels using boiling water as the method of heat transfer, but it also is important in a system transferring heat to liquid water by forced convection. Careful analysis of the latter systems should be made since the accidental formation of steam in one channel of a heated parallel-channel arrangement may decrease the flow of liquid water in this channel, thereby causing more steam to form. The additional resistance to flow may even cause the flow of liquid water to stop entirely, and burnout of a reactor channel may result. The condition for burnout, therefore, must be con-

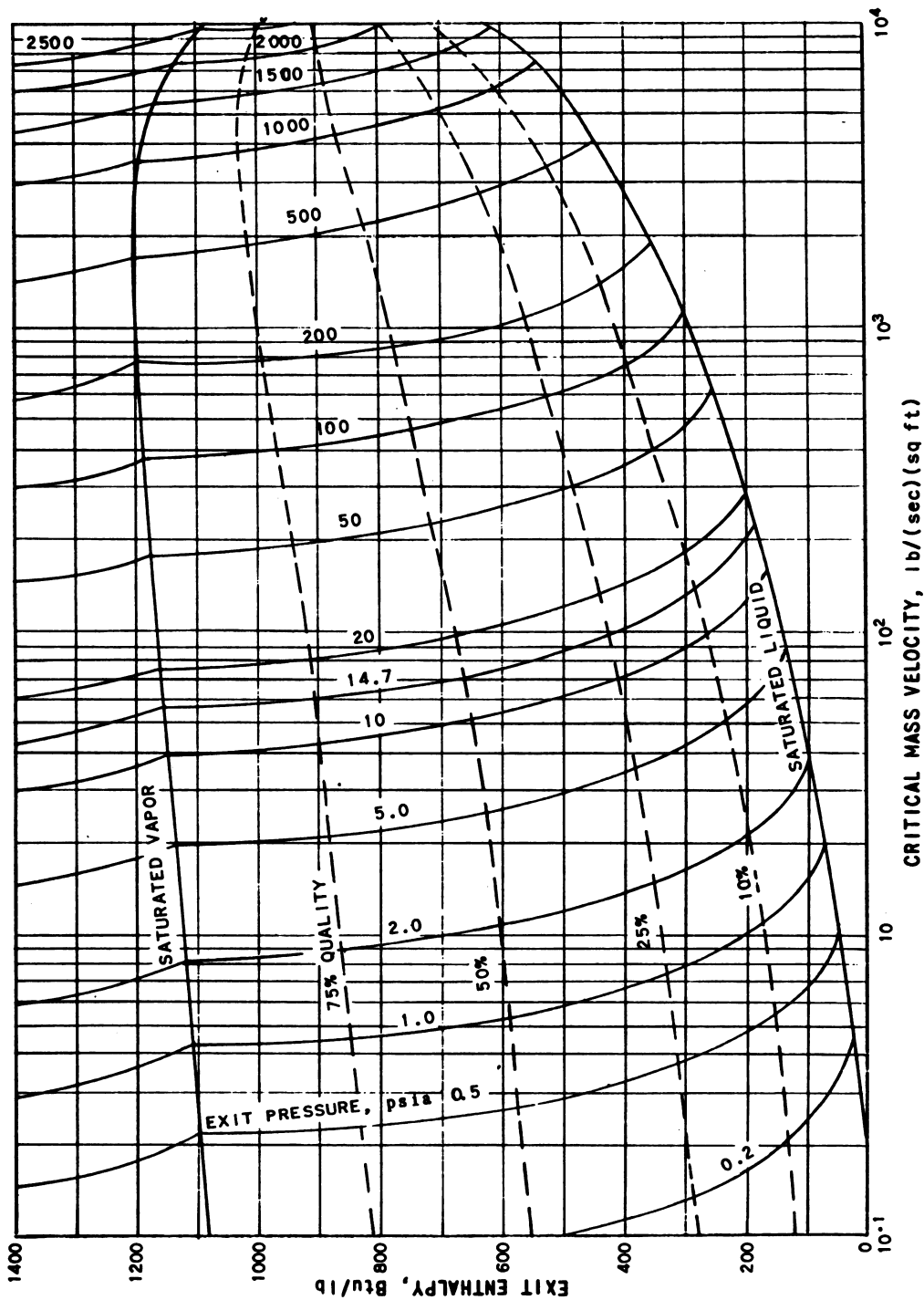


Fig. 1.5.14—Critical Mass Velocity vs Exit Enthalpy, Quality, and Pressure. Submitted by Argonne National Laboratory, June 30, 1952.

sidered as part of the parallel-channel flow problem. In the case of a natural-circulating system, a more complicated problem is encountered where steam formed in one channel causes a flow stoppage in another channel. This case is discussed in this chapter under "Parallel Flow Channels in Same Vertical Plane."

No analytical methods are available in the literature for the solution of two-phase flow in parallel channels. There are procedures, however, for avoiding flow instabilities and dangerous operating conditions. The general practice is to design each channel for stable flow by introducing properly sized orifices in series with each flow channel, provided that an analysis of single-flow channels indicates the need for such orifices.

PRESSURE DROP VS FLOW CHARACTERISTICS

A typical curve for two-phase flow is shown in Fig. 1.5.15 for a given geometry, heat flux, inlet subcooling, and pressure. Also shown are the pressure-drop curves for liquid flow and vapor flow. It is recommended that the Martinelli-Nelson method be used to calculate the two-phase region of this curve. Although the shape of this type of curve has been experimentally verified, the analytical methods presently available do not check quantitatively to the experimentally measured pressure drops in all cases.

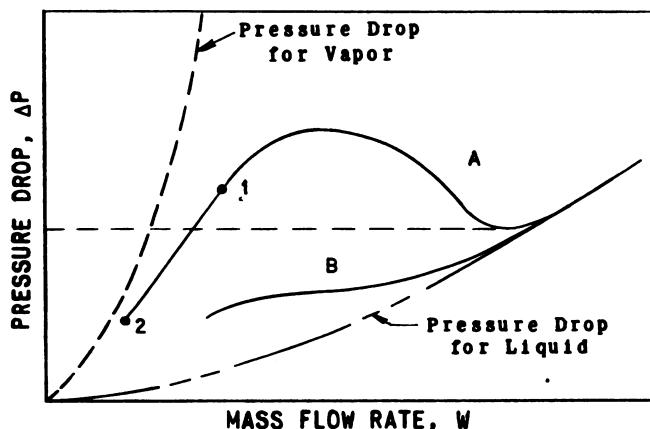


Fig. 1.5.15—Typical Flow Curves for Heating Water. Submitted by Argonne National Laboratory, June 2, 1952.

At high flow rates the characteristic curve follows the liquid line. As the flow is reduced with heat flux held constant, net boiling occurs, and the curve departs from the liquid line. Further reduction in flow causes more steam formation, and the curve approaches the vapor line. The manner in which the curve passes through the two-phase region depends upon the above mentioned variables. Fig. 1.5.15 shows two such paths: Curves A and B.

Points 1 and 2 on Curve A indicate two possible conditions of flow at which the channel could burn out or overheat. At flows greater than given by points 1 or 2, the heat is being transferred either by boiling or forced convection with surface temperatures not greatly in excess of saturation. At flows lower than given by points 1 and 2, the heat transfer coefficient decreases to a very low value, and surface temperature increases to very high values. These points cannot be calculated with presently available data and must be determined experimentally. In vertical channels with L/D ratios greater than 50 and heat fluxes less than 200,000 Btu/(hr)(sq ft), this overheating occurs when the steam quality is between 80 to 100 percent.

The general shape of the characteristic pressure-drop flow curve for each of the individual channels in parallel is the criteria for flow stability. The pressure drop across the parallel channels is also the pressure drop across each individual channel. The intersection of a horizontal line, representing the header pressure drop or the pressure drop across the parallel channels, with the characteristic curve of each channel determines the flow and the character of the flow in each channel. If the horizontal line representing this header pressure drop intersects a channel characteristic pressure drop curve at more than one point, an unstable condition is indicated. This possibility of instability exists with channels having a multivalued curve (such as A, Fig. 1.5.15). Channels represented by the single-value curve B, are considered to be stable channels.

Qualitatively, the general character of the pressure-drop curves can be obtained by integrating Eq. (22). The assumptions necessary in integrating the equation are a constant heat input, a horizontal tube, a constant friction factor for two-phase mixture, no slippage of steam through the water, no sonic discharge at the exit of the channel, and a sufficiently high absolute pressure so that the pressure drop across the channel will not appreciably affect the saturation pressure. The resulting Eq. (34) may be used to determine the effect of subcooling, pressure, and geometry. The equation should not be used where accurate values for two-phase drop are needed.

$$\Delta P = \frac{f}{2g_c D_e A^2} \left\{ L v_f W^2 + \left[\frac{Q L v_{fg}}{2 h_{fg}} \left(W - \frac{2 \Delta H W^2}{Q} + \frac{\Delta H^2 W^3}{Q^2} \right) \right] \right\} + \frac{v_{fg} Q}{h_{fg} g_c A^2} \left(W - \frac{\Delta H W^2}{Q} \right) \quad (34)$$

Differentiating Eq. (34) with respect to W gives the inflection point in the pressure-drop flow curve as a function of friction factor, L/D ratio, pressure, and inlet enthalpy.⁷ The condition for stability is:

$$\Delta H \leq \frac{\left[\frac{fL}{g_c D_e} \right] \left[\frac{v_f h_{fg}}{v_{fg}} \right]}{\left[\frac{fL}{g_c D_e} \right] + \frac{2}{g_c} - 2 \sqrt{\frac{3}{2} \left[\frac{fL}{2g_c D_e} \right] \left[\frac{fL}{4g_c D_e} + \frac{1}{g_c} \right]}} \quad (35)$$

The equation is shown in Fig. 1.5.16. These curves give the maximum permissible inlet enthalpy for flow stability with a given ratio of L/D and given pressure. In a system in which heat is being transferred, the condition for instability is independent of the heat transferred. However, in an unstable condition, the degree of instability is dependent upon the heat transferred because the maximum pressure drop in the unstable region increases with heat input.

PARALLEL FLOW CHANNELS IN SAME HORIZONTAL PLANE

The condition of two-phase flow through parallel channels in the same horizontal plane is illustrated in Fig. 1.5.17. This figure shows two typical curves. Curve A is the pressure-drop flow characteristic of channels which are generating an average heat flux. Curve B is the pressure-drop flow characteristic of channels which have a higher-than-average heat generation.

The header pressure drop is defined as the difference in static pressure between the inlet header and the exit header. This pressure drop occurs across all channels since they are in parallel. If this pressure drop should fall as low as the minimum point on curve B of Fig. 1.5.17, the flow in the hot channel would be too greatly reduced, and the channel would burn out as defined above. Burnout occurs since the pressure drop at burnout is higher than the available pressure drop.

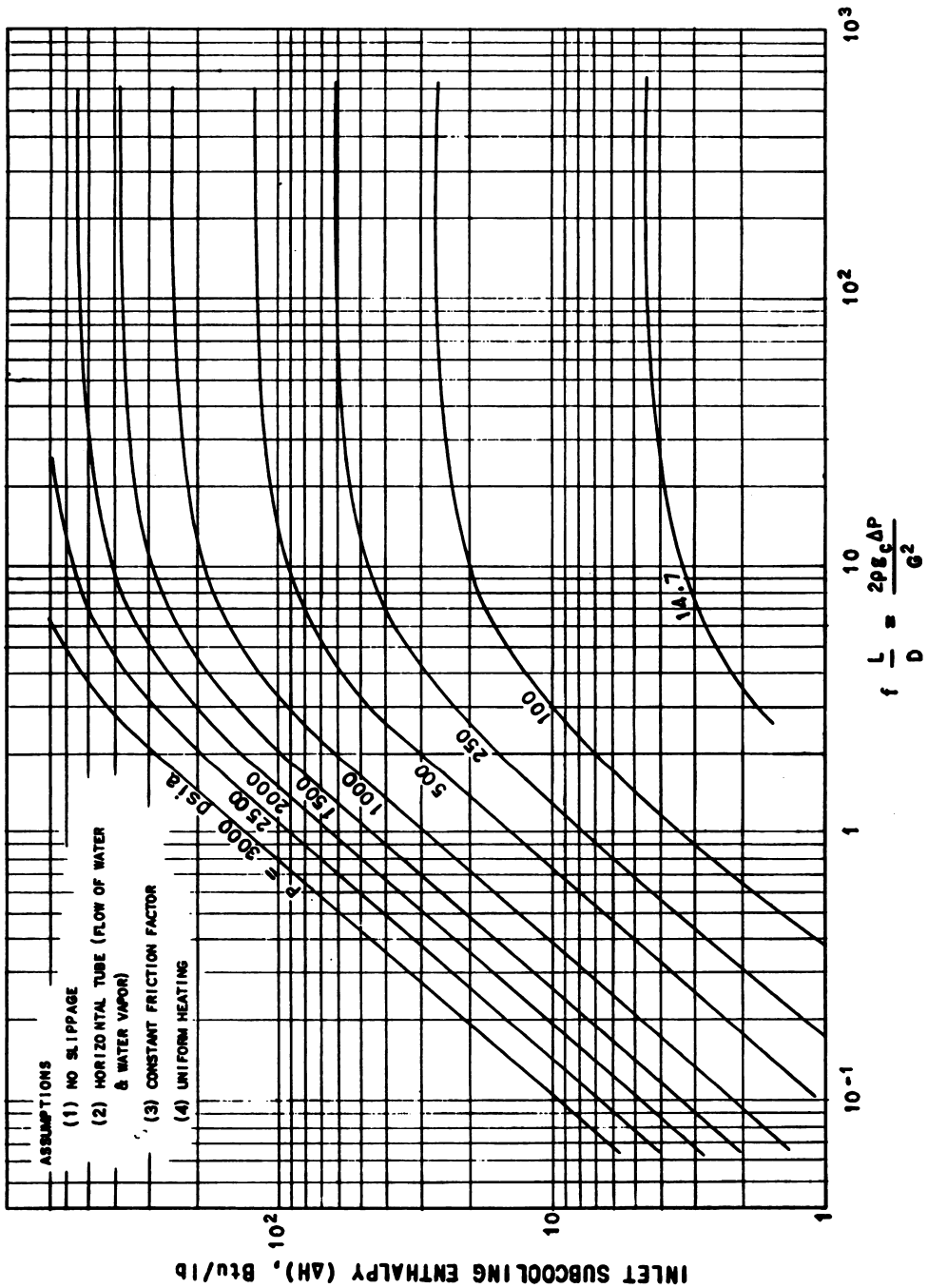


Fig. 1.5.16—Stability Condition for Forced Flow. Submitted by Argonne National Laboratory, June 30, 1952.

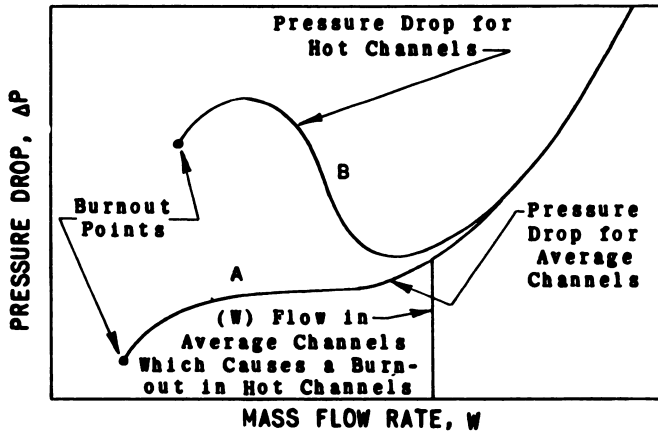


Fig. 1.5.17—Burnout with Two-phase Flow. Submitted by Argonne National Laboratory, July 2, 1952.

PARALLEL FLOW CHANNELS IN SAME VERTICAL PLANE

The parallel-flow problem is further complicated in that various orientations of the channels with respect to the vertical will affect the flow distribution in parallel channels. This is true in cases where the hydrostatic head becomes a sizeable amount compared to the friction and acceleration pressure losses, such as might occur in natural-circulating systems with steam generation. An example is the emergency cooling system of a water-cooled reactor.

If the channels are in any position other than vertical, density differences between the inlet and exit headers will affect the flow distribution. In fact, the flow may actually reverse in some channels.

In order to demonstrate the effect of headers, consider the two channels A and B in Fig. 1.5.18. The static pressure drop between points 1 and 2 through channel A is equal to sum of the dynamic pressure drop and hydrostatic pressure drop. The dynamic pressure drop is defined as the sum of the friction and acceleration losses:

$$P_1 - P_2 = \Delta P_A + \int_1^2 \rho_A \sin \theta \, dL \approx \Delta P_A + \bar{\rho}_A \sin \theta L \quad (36)$$

where $P_1 - P_2$ = total static pressure drop between points 1 and 2

ΔP_A = dynamic pressure drop between points 1 and 2

ρ_A = density of fluid at any point in channel A

θ = angle of orientation with respect to the horizontal

L = length along channel

$\bar{\rho}_A$ = average density in channel A.

If the headers are assumed large so that the velocities in the headers are small, the pressure drop between points 1 and 3 and between 2 and 4 will be largely hydrostatic pressure drop. Therefore:

$$P_1 - P_3 \approx -\rho_{in} d \cos \theta \quad (37)$$

$$P_3 - P_4 \approx \Delta P_B + \bar{\rho}_B L \sin \theta \quad (38)$$

$$P_4 - P_2 \approx d \rho_{out} \cos \theta \quad (39)$$

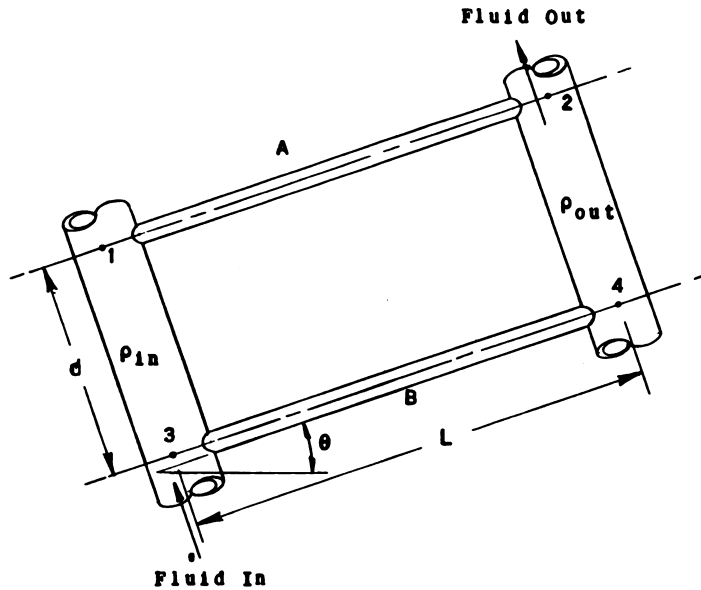


Fig. 1.5.18—Parallel Flow Channels. Submitted by Argonne National Laboratory, July 2, 1952.

Adding Eq. (37), (38), and (39):

$$P_1 - P_2 \approx \Delta P_B + \bar{\rho}_B L \sin \theta + d \cos \theta (\rho_{out} - \rho_{in}) \quad (40)$$

Equating (36) and (40):

$$\Delta P_A + \bar{\rho}_A L \sin \theta \approx \Delta P_B + \bar{\rho}_B L \sin \theta - d \cos \theta (\rho_{in} - \rho_{out}) \quad (41)$$

This equation could also have been written as:

$$(P_{in} - P_{out})_A = (P_{in} - P_{out})_B - d \cos \theta (\rho_{in} - \rho_{out}) \quad (42)$$

Equation (42) states that channel A has less pressure drop than channel B by an amount equal to the difference in hydrostatic head of the inlet and exit headers. If both channel A and B receive the same amount of heat, channel A will operate at a lower flow rate than channel B. A critical condition might occur if θ were small, ρ_{out} were small in comparison to ρ_{in} , and d were large. Under these conditions, the right side of Eq. (42) could become negative causing a reversal of flow in channel A with resulting burnout of channel A. In a single-phase system or in a system where the fluid is being pumped, this parallel flow problem probably does not exist.

EFFECT OF ORIFICES

In general, parallel-channel, water-cooled reactors operate in the non-boiling region. However, knowledge of the boiling characteristics of a particular reactor and an analysis of two-phase flow is essential to the safety of the reactor. A proper heat-transfer and fluid-flow analysis is the first step toward preventing burnout of any channel. The second step is to prevent reactor operation in an unstable flow region.

Orificing is one method of maintaining steady flow through a tube with a pressure-drop, flow-characteristic curve similar to that shown in Fig. 1.5.17, curve B.

If the pressure-drop, flow-characteristic curve for a heated channel is multivalued, it is probable that burnout would occur when the flow decreases or when the heat input increases to the point where boiling begins. Using an orifice at the entrance to the tube would change the pressure-drop flow characteristic of the orifice and tube. By proper selection of orifice size, the curve with the orifice then becomes single valued. Curve A in Fig. 1.5.19 is the

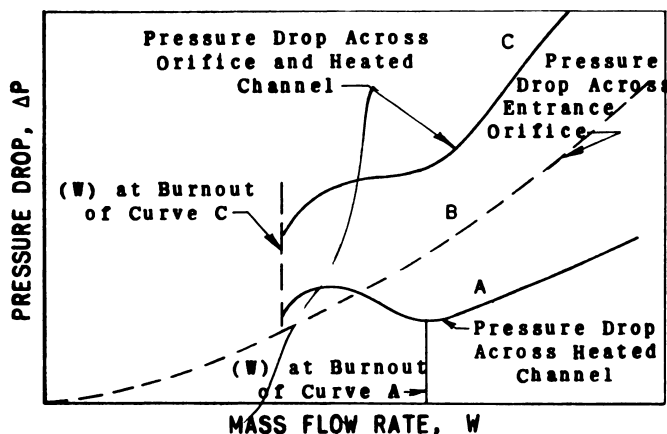


Fig. 1.5.19—Effect of Small Orifice on Pressure Drop. Submitted by Argonne National Laboratory, July 2, 1952.

pressure drop across the heated channel; curve B is the pressure drop across the entrance corrective orifice; and curve C is the sum of curves A and B or the pressure drop across the orifice and heated channel. Curve C is then the difference in header pressure between the entrance and exit header. The orifice for all of the channels is determined, therefore, by the orificing required for the channel with the maximum heat input, at the maximum possible power level expected. The flow which causes burnout is shown to have decreased by the installation of an orifice. This type of orifice will prevent unstable flow in all regions of operation. These tubes, therefore, could be designed to operate in the boiling region.

In many cases, the pressure drop, and consequently the pumping power, required to orifice for this much safety would be prohibitive, especially if the reactor were designed to operate in the single-phase region. Another method of orificing which does not require as much pressure drop across the orifice is based on the assumption of a momentary flow stoppage in a channel. Figure 1.5.20 shows the effect of a small orifice on pressure drop. The general practice is to design each channel for stable flow by ensuring that sufficient header pressure is available to sweep steam from the channel should boiling be initiated. It is postulated that the header pressure does not change but that some protection is needed to guard against the possibility of a momentary flow stoppage, such as that caused by a plugged channel.

The typical multivalued pressure-drop curve is shown as curve CAB. The orifice curve intersects curve CAB at the design operating point. If the flow should momentarily decrease to point E, the sum of the channel-pressure drop and orifice-pressure drop would be less than the header-pressure drop. The resulting excess pressure drop would restore the flow to point A.

If the header-pressure drop should decrease, it may be shown from Fig. 1.5.20 that the orifice curve would then intersect channel curve CAB in three points. Operation of the

channel in the boiling region would be unstable. This type of orifice does not necessarily provide protection for design operation in the boiling region. It does afford some protection for a reactor designed to operate in the non-boiling region. The header pressure drop must not be permitted to decrease, however. If, as was done in Fig. 1.5.19, the pressure drop across the orifice is added to the pressure-drop curve for the channel, the resulting curve will in all probability be multivalued.

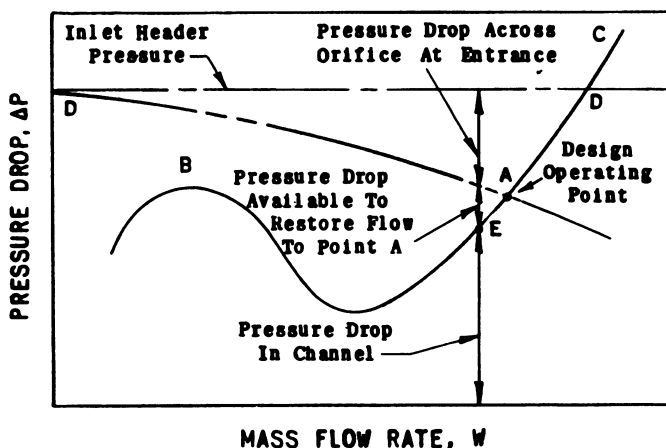


Fig. 1.5.20—Effect of Large Orifice on Pressure Drop. Submitted by Argonne National Laboratory, July 2, 1952.

A method recommended for sizing the orifice is to have an inlet header pressure, DD , a given percentage greater than the peak pressure, B , in the two-phase region. Several reactors are designed so that this increase is 30 percent. If the design operating point were at C or at higher flows, no orifices would be required for this method of protection.

Since unstable operation is probably caused by a sudden increase in power or decrease in flow (which in turn causes the formation of vapor by boiling), it is possible to prevent boiling over a wide range of conditions by pressurizing the system. The pressure may be established so that no boiling would occur between the design power and twice design power or any other overload figure set by the controllability of the reactor.

When mechanically feasible, advantage should also be taken of natural circulation in the design of a reactor cooling system. Natural circulation has a tendency to act as a protection, as do orifices. When steam is formed or water is heated it has a tendency to rise. It is possible that, even without the use of pumps, sufficient circulation could be induced to cool a reactor momentarily. For this reason, the flow should be upward. In upflow, the pressure-drop flow characteristic of a heated channel has less tendency to exhibit a multi-valued pressure-drop curve than downflow, and this also leads to a more stable condition.

REFERENCES

1. W. H. McAdams, "Heat Transmission," 2nd ed., McGraw-Hill Book Company, Inc., New York and London, 1938.
2. H. C. Clairborne, "A Critical Review of the Literature on Pressure Drop in Non-Circular Ducts and Annuli," ORNL-1248, May 22, 1952.
3. W. H. Denton, et al., "The Heat Transfer and Pressure Loss in Fluid Flow Through Randomly Packed Spheres," United Kingdom HPC-35, 44 pp, June 28, 1949.
4. R. C. Martinelli and D. B. Nelson, "Prediction of Pressure Drop During Forced Circulation Boiling of Water," Trans. Am. Soc. Mech. Engrs., 70 pp, 695-702, 1948.
5. Reactor Division, Hanford Works, Nucleonics Department, HDC-1565, November 30, 1949 (classified).

6. W. H. Jens and P. A. Lottes, "Analysis of Heat Transfer Burn Out, Pressure Drop, and Density Data for High Pressure Water," ANL-4627, (1951).
7. M. Ledinegg, "Instability of Flow During Natural and Forced Convection," Die Warme, 61, pp 891-898, (1938).

SELECTED READING LIST

- HANDBOOK OF ENGINEERING FUNDAMENTALS, O. W. Eshback, 2nd ed, John Wiley and Sons, New York, 1952.
- MECHANICAL ENGINEERS HANDBOOK, L. S. Marks, 5th ed, McGraw-Hill Book Co., Inc., New York, 1951.
- FLUID AND PARTICLE MECHANICS, C. E. Lapple et al, University of Delaware, Newark, Delaware, March 1951.
- MECHANICAL ENGINEERS HANDBOOK, R. T. Kent, 12th ed, Vol 2, John Wiley and Sons, New York, 1950.
- ENGINEERING HYDRAULICS, H. Rouse et al, John Wiley and Sons, New York, 1950.
- PREDICTION OF PRESSURE DROP DURING FORCED CIRCULATION BOILING OF WATER, R. C. Martinelli and D. B. Nelson, Trans. Am. Soc. Mech. Engrs., 70, pp 695-702, 1948.
- STANDARDS OF HYDRAULIC INSTITUTE, The Institute, 8th ed., New York, 1947.
- PIPING HANDBOOK, 4th ed, McGraw-Hill Book Company, Inc., New York, 1945.
- TUBE TURNS ENGINEERING DATA BOOK #111, Tube Turns, Inc., 1943.
- FLOW OF FLUIDS THROUGH VALVES, FITTINGS, AND PIPE, Crane Co., Technical Paper No. 409, Chicago, 1942.
- HEAT TRANSMISSION, W. H. McAdams, 2nd ed, McGraw-Hill Book Company, Inc., New York and London, 1942.
- FLUID MECHANICS FOR HYDRAULIC ENGINEERS, H. Rouse, 1st ed, McGraw-Hill Book Company, Inc., New York and London, 1938.
- FAN ENGINEERING, Buffalo Forge Co., 4th ed., Buffalo, New York, 1938.
- HYDRAULICS, E. W. Schoder and F. M. Dawson, 2nd ed, McGraw-Hill Book Company, Inc., New York and London, 1934.

Spatial Distribution of Heat Generation

J. R. Dietrich and D. Okrent

HEAT GENERATION IN FUEL ELEMENTS

The symbols used in this chapter are defined in Table 1.6.1.

Of the total useful primary energy emitted per fission, some 91 percent appears as kinetic energy of charged particles (fission fragments and beta particles—see Volume 1, Table 1.2.17). The fission-fragment energy is converted to heat within a few thousandths of a centimeter of the fission site, and the relatively unimportant beta energy is converted within about a centimeter of the fission site. Consequently, the spatial distribution of heat production in the fuel elements may be taken, with sufficient accuracy, to be the same as the distribution of fission density in the elements. In most water-cooled reactors, fissions are caused almost entirely by thermal neutrons, and the fission-density distribution is proportional to the distribution of the product of $\Phi(\text{thermal})$ and $\bar{\Sigma}_f(\text{thermal})$. Since the distribution of fissionable material in the fuel elements, and hence the spatial variation of Σ_f is generally known, determination of the power distribution in the fuel elements reduces to determination of the thermal neutron flux distribution. Indeed, all water-cooled reactors which have to date reached an advanced stage of design employ uniform density of fissionable material in the fuel elements, and the initial power distribution is just proportional to the thermal flux distribution. This initial distribution is modified somewhat with time as non-uniform burnup of fissionable material and, in converter reactors, non-uniform production of new fissionable material proceeds. This effect is not large for the degree of burnup designed into current reactors. The possibility of employing non-uniform fuel distribution to control the power distribution in fuel elements is discussed later.

QUASI-HOMOGENEOUS REACTORS

Included in this class are those reactors in which the fuel element-moderator-coolant structure is so fine-grained that no important change in neutron density occurs in going from, for example the center line of a typical fuel element, out through the fuel element, to the center line of the adjacent layer of moderator. This condition is met if at least one dimension of the typical fuel element is much less than one diffusion length. Most highly enriched reactors designed for high power density fall into this class. A typical example is the MTR. For such a reactor, the thermal flux distribution may be computed as though the fuel element-moderator matrix were an equivalent homogeneous region, and the power distribution in the fuel elements may be obtained from the product of the flux distribution and the local value of the fission cross section.

Table 1.6.1 — Symbols

Symbol	Definition	Units
A, B, C	Extrapolated lengths of sides of a bare rectangular reactor in x, y, and z directions, respectively	cm
A_e	Equivalent bare half-length of reflected finite cylindrical core = half-length of core plus reflector saving at one end	cm
$A_{\alpha i}$	Average absorption of neutrons to form α emitters of type i	$n/(cm^3)(sec)$
$A_{\beta i}$	Average absorption of neutrons to form β emitters of type i	$n/(cm^3)(sec)$
$A_{\gamma i}$	Average absorption of neutrons to form γ emitters of type i	$n/(cm^3)(sec)$
a	Radius of flattened zone of cylindrical core	cm
$E_{\alpha i}$	Energy of α particles from emitters of type i	mev
$E_{\beta i}$	Energy of β particles from emitters of type i	mev
$E_{\gamma i}$	Energy of γ photons from emitters of type i	mev
E_n	Fraction of total available energy per fission emitted as kinetic energy of neutrons (~ 0.027 for U^{235})	...
E_γ (prompt)	Fraction of total available energy per fission emitted as prompt γ energy (~ 0.027 for U^{235})	...
E_γ (delayed)	Fraction of total available energy per fission emitted as delayed γ energy (~ 0.032 for U^{235})	...
$J_0(\rho)$	Bessel function of the first kind, of argument ρ	...
k_{eff}	Multiplication constant of finite reactor, including effect of leakage	...
k_∞	Multiplication constant of an infinite medium having the same material properties as those of the finite reactor being considered	...
L^2	Thermal diffusion area for neutrons	cm^2
mfp	Neutron mean free path	cm
MTR	Materials Testing Reactor	...
$P(r)$	The local power density in a reactor core, computed as though the core were homogeneous	watts/cm ³
\bar{P}	Average power density over the entire reactor core	watts/cm ³
R_e	Equivalent bare radius of reflected cylindrical core = core radius + reflector saving	cm
r	Radial coordinate in cylindrical coordinate system	cm
x, y, z	Coordinates in the cartesian system	cm
$Y_0(\rho)$	Bessel function of the second kind, of argument ρ	...
β	Probability that a gamma photon, emitted inside a sample of material, will be absorbed inside the sample	...

Table 1.6.1 — (Continued)

Symbol	Definition	Units
κ^2	Reactor buckling in a given, specified direction	cm^{-2}
μ^2	Radial buckling of a cylindrical reactor = $\kappa_\infty^2 - 1/L^2 + \tau$ for an infinitely long cylinder in one-group theory	cm^{-2}
μ	Energy attenuation coefficient for gamma radiation	cm^{-1}
ξ	Logarithmic energy decrement for elastic scattering of fast neutrons	...
Σ_s	Macroscopic scattering cross section	cm^{-1}
$\Sigma_{\alpha i}$	Average macroscopic thermal cross section for absorption of neutrons to produce α emitters of type i	cm^{-1}
$\Sigma_{\beta i}$	Average macroscopic thermal cross section for absorption of neutrons to produce β emitters of type i	cm^{-1}
$\Sigma_{\gamma i}$	Average macroscopic thermal cross section for absorption of neutrons to produce γ emitters of type i	cm^{-1}
$\bar{\Sigma}_f$ (thermal)	Average macroscopic thermal fission cross section	cm^{-1}
$\Phi(r)$	Local neutron flux density	$\text{n}/(\text{cm}^2)(\text{sec})$
$\bar{\Phi}$	Neutron flux density averaged over reactor core	$\text{n}/(\text{cm}^2)(\text{sec})$
$\Phi_s, \Phi_{\text{thermal}}$	Thermal neutron flux density	$\text{n}/(\text{cm}^2)(\text{sec})$
$\Phi_f, \Phi_{\text{epithermal}}$	Epithermal neutron flux density	$\text{n}/(\text{cm}^2)(\text{sec})$
τ	Slowing down area for fission neutrons	cm^2

DISTRIBUTIONS IN BARE AND REFLECTED CORES

Most practical reactor shapes may be approximated by a rectangular parallelepiped or a right circular cylinder. Sometimes, for general analyses covering a range of variables, it is convenient to approximate practical shapes by a sphere. The thermal neutron flux distributions for homogeneous bare reactors of these three shapes are given in Table 1.6.2. The reactor dimensions are the extrapolated dimensions (Volume 1, Chapter 1.3).

Practical reactors almost always have a reflector of some kind which modifies the flux and power distributions. Usually, the power distribution in a reflected reactor is computed by solving one of the group approximations to the reactor equation in the core and reflector regions, with appropriate continuity conditions at the interfaces between regions. These methods are discussed in Volume 1, Chapter 1.4. This chapter gives a physical description of the effects of reflectors on power distribution, with illustrative examples.

Typical Features of Distribution in Reflected Reactor

The effect of a reflector on the criticality conditions in a reactor can be described in terms of a reflector saving (Volume 1, Chapter 1.5). The reflected reactor behaves, reactivity-wise, as the equivalent bare reactor; i.e., as a uniform reactor whose boundary lies at a distance equal to the reflector saving beyond the boundary of the active core of the real, reflected reactor. The concept of the equivalent bare reactor is useful also in describing the flux distribution in a reflected reactor. The thermal flux distribution in the core of such a reactor will be the same as that in the equivalent bare reactor (Table 1.6.2)

Table 1.6.2—Thermal Neutron Flux Distributions in Bare Homogeneous Reactors of Simple Shapes

Reactor geometry	Flux distribution*
Rectangular parallelepiped of extrapolated side length A, B, and C in x, y, and z directions. Axis of coordinates at center of reactor	$\Phi(x,y,z) = \Phi_0 \cos \frac{\pi x}{A} \cos \frac{\pi y}{B} \cos \frac{\pi z}{C}$
Right circular cylinder of extrapolated length H and extrapolated radius R. Axis of coordinates at center of reactor	$\Phi(z,r) = \Phi_0 \cos \frac{\pi z}{H} J_0 \left(\frac{2.405 r}{R} \right)$
Sphere of extrapolated radius R	$\Phi(r) = \frac{\Phi_0}{r} \sin \frac{\pi r}{R}$

* Φ_0 is in all cases the central value of the flux, determined by the power level at which the reactor is operating

to within a thermal diffusion length or two of the core-reflector boundary. In the regions closer to the boundary, the flux distribution will depend upon the detailed properties of both the core and the reflector. Typical features of the distribution in thermal reactors employing moderating reflectors are illustrated by the distributions shown in Fig. 1.6.1 which were computed for an H_2O reflected core composed of H_2O , zirconium and enriched uranium. From the center of the core out to about two diffusion lengths (7cm) from the core boundary, the radial thermal flux distribution follows very nearly the J_0 variation typical of the cylindrical reactor of the equivalent bare radius R_e (= radius of core + radial reflector saving), and the axial distribution follows nearly the cosine variation typical of the equivalent bare half-length A_e . Near the reflector, the thermal flux rises above the equivalent bare distribution, and in the case illustrated, peaks in the reflector. This relative increase in the thermal flux results from (1) the moderating effectiveness of the reflector being somewhat greater than that of the core and (2) the macroscopic thermal adsorption cross section in the reflector being less than that in the core. The ratio of the production rate of thermal neutrons in the reflector to the rate of loss (per unit thermal neutron flux) by absorption and leakage from the reflector is thus higher than the corresponding ratio in the core, and a maximum in the thermal neutron flux results. Evidently, the effect depends upon the relative magnitudes of the thermal and epithermal fluxes in the core as well as on the relative moderating effectivenesses and absorption cross section of the core and reflector (see below). Since the average epithermal flux in the case illustrated is almost four times the average thermal flux, the peaking in the reflector is pronounced.

Effect of Reflector Saving

It is evident from the above discussion that if the ratio of core dimension to reflector saving is large the ratio of the central thermal flux to the minimum thermal flux in the core will also be large. This effect is illustrated by Fig. 1.6.2A which shows thermal flux distributions in similar Be- H_2O cores¹ with different reflectors.

¹ References appear at end of chapter.

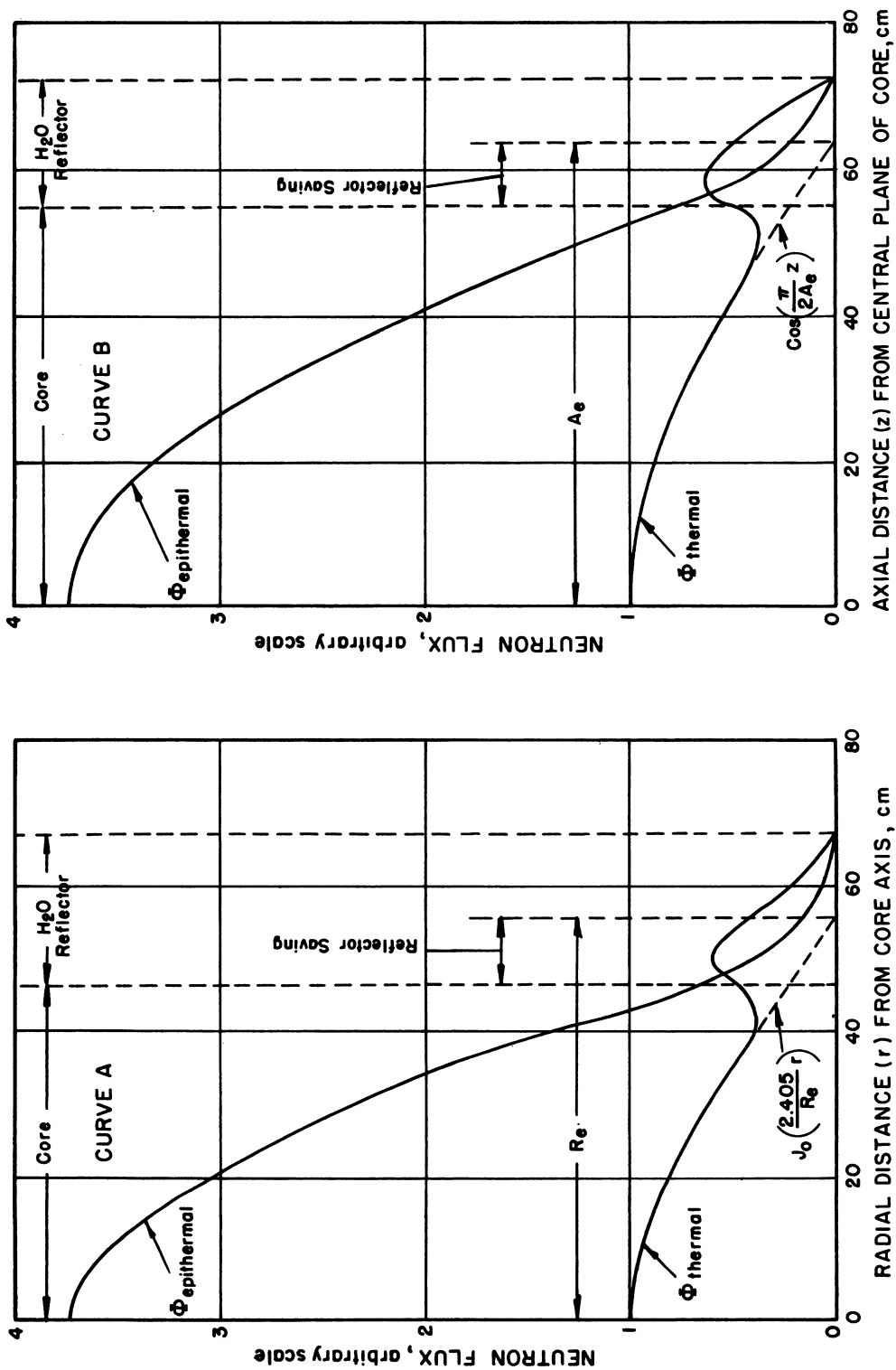


Fig. 1.6.1—Two-group Computed Thermal and Epithermal Flux Distribution in a Reactor Composed of an H₂O, Zirconium, and Enriched Uranium Core with Relatively High Thermal Absorption, Surrounded by an H₂O Reflector. Submitted by Argonne National Laboratory, Nov. 15, 1952. Curve A: radial distribution; Curve B: axial distribution.

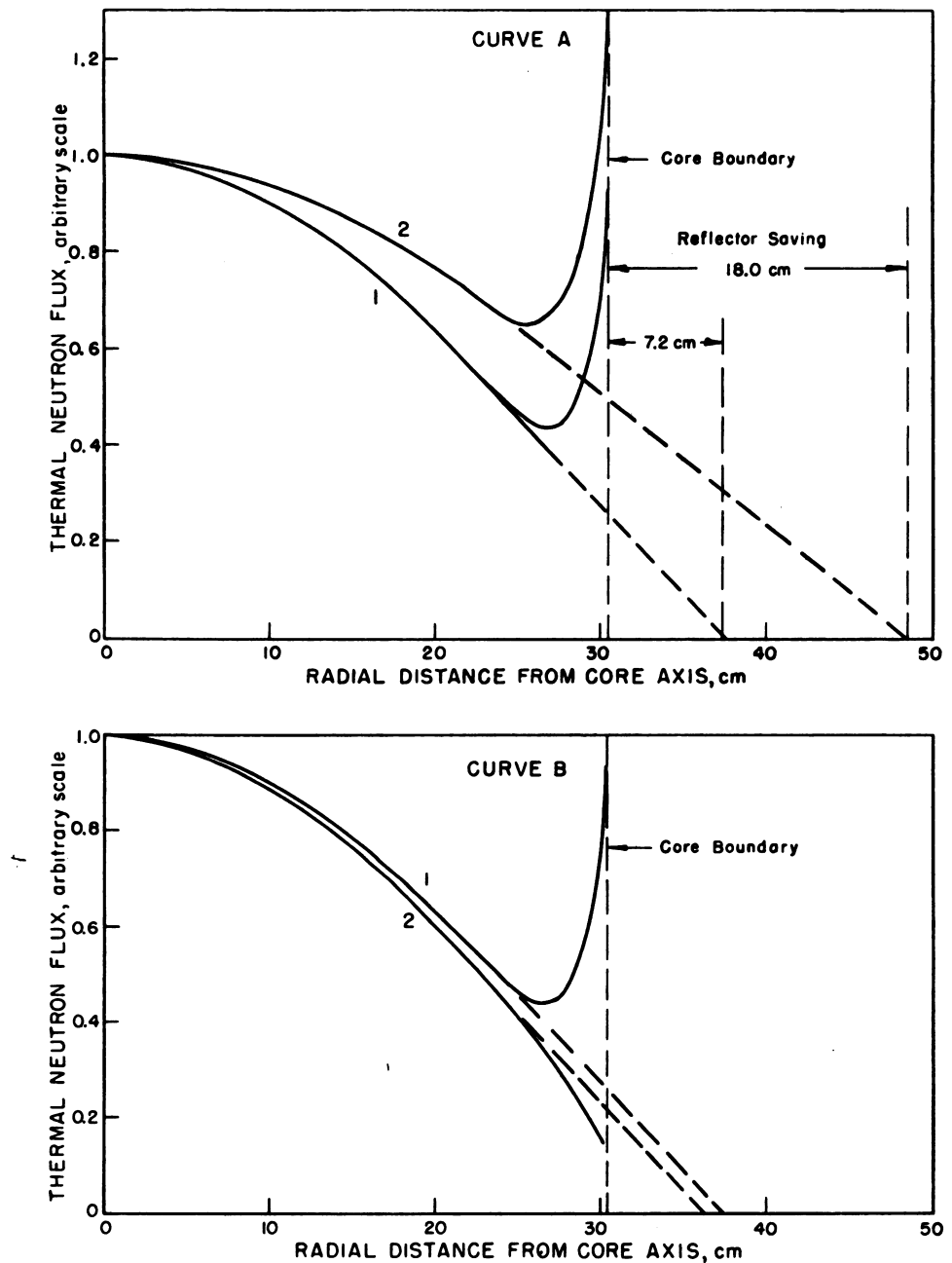


Fig. 1.6.2 — Computed Radial Thermal Flux Distributions in Cylindrical Be- U^{235} - H_2O Cores with Various Reflectors. Reprinted from ORNL-133, Sept. 1, 1948. BE: H_2O = 1:1 by volume; 416°F; length = diameter = 61 cm. Curve A, Effect of Reflector Saving: (1) 8-in.- H_2O reflector; core loading 20 kg U^{235} plus sufficient uniformly distributed absorber for criticality; (2) 8-in.-Be reflector; core loading 14 kg U^{235} plus sufficient uniformly distributed absorber for criticality. Curve B, Effect of Moderation in Reflector: (1) 8-in.- H_2O reflector; core loading 20 kg U^{235} plus sufficient uniformly distributed absorber for criticality; (2) 8-in.-Fe reflector; core loading 20 kg U^{235} plus sufficient uniformly distributed absorber for criticality.

In reactors designed for high average power density the use of a good, moderating reflector is often more important for the purpose of achieving a low maximum:average power ratio than for the purpose of reducing critical mass. Curve (2) of Fig. 1.6.2A illustrates the point that a moderating reflector with large saving, when used on a small core having a high ratio of epithermal to thermal flux, can cause the power peak at the edge of the core to exceed that at the center. This result is usually undesirable. The effect can be controlled by adjustment of the reflector thickness as well as by adjustment of the reflector composition.

Non-moderating Reflectors

If a non-moderating reflector is used, the thermal flux distribution does not rise above the curve for the equivalent bare reactor. If the thermal absorption cross section for such a reflector is relatively high (e.g., as for iron), the thermal flux may drop considerably below the equivalent bare distribution near the edge of the core. Figure 1.6.2B compares computed radial thermal flux distributions in water-reflected and iron-reflected cores. The two distributions differ widely near the core boundary even though the iron reflector saving is only slightly less than that of the water. It may be noted that a non-moderating reflector can provide appreciable reflector savings on a reactor having a high fast-neutron leakage even though the thermal absorption cross section of the reflector be large.

Effect of the Ratio $\Phi_{\text{epithermal}}/\Phi_{\text{thermal}}$

As pointed out above, the height of the thermal neutron peak in a moderating reflector relative to, for example, the general level of thermal flux in the core depends upon the relative magnitude of the epithermal leakage from the core into the reflector. This dependence can be illustrated by the change in thermal flux distribution resulting from a change in the (uniform) loading of fissionable material in a given reactor. As the loading is changed, the average epithermal flux in the reactor, and the epithermal leakage at a given fission rate (power level) will change only slightly. The average thermal flux at a given power level will, however, vary inversely as the loading [i.e., $\bar{\Phi}_{\text{thermal}} = \text{const} \times (\text{Reactor Power/Loading of Fissionable Material})$]. Thus, the ratio of thermal to epithermal flux will vary roughly inversely as the loading, and large changes in loading may produce marked effects on thermal flux distribution. Figure 1.6.3A shows computed radial thermal and epithermal distributions in a water-reflected beryllium-water core containing 2.6 kg of U^{235} (the clean critical mass). The maximum thermal flux is about 58 percent as high as the maximum epithermal flux. There is a marked divergence of the thermal flux from the equivalent bare distribution near the core boundary, but no peaking (i.e., the derivative of the flux remains negative in the core). Figure 1.6.3B shows the computed flux distributions in the same core loaded with 20 kg of U^{235} . (Sufficient thermal absorber is added to the core to maintain criticality.) The maximum thermal flux is now only 7.5 percent as high as the maximum epithermal. In fact, if the thermal flux is multiplied by the ratio 20 kg/2.6 kg the resulting product is in about the same ratio to epithermal flux as was the thermal flux in the 2.6-kg core, except near the core boundary. There is now a very pronounced rise in the thermal flux near the boundary.

Accuracy of Calculations of Flux Distribution

Figures 1.6.4 and 1.6.5 show comparisons of computed and measured thermal flux distributions in $\text{Al-H}_2\text{O}$ (MTR)² and $\text{Zr-H}_2\text{O}$ critical assemblies. The water-reflected reactors (Figs. 1.6.4A and 1.6.5) have been treated only by two-group calculations. Part

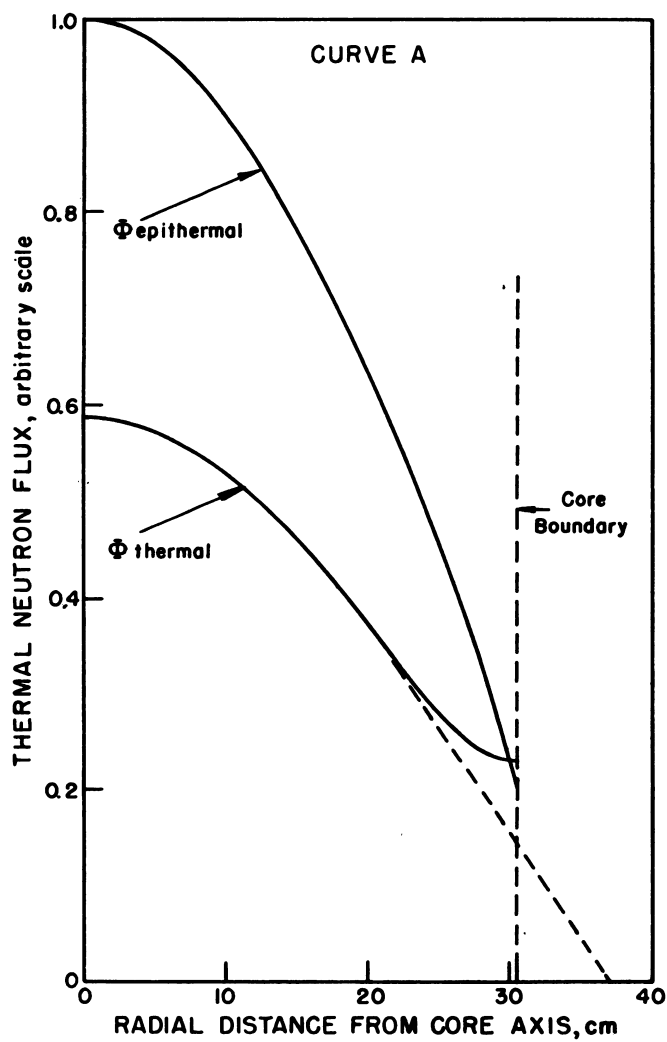


Fig. 1.6.3—See facing page for legend.

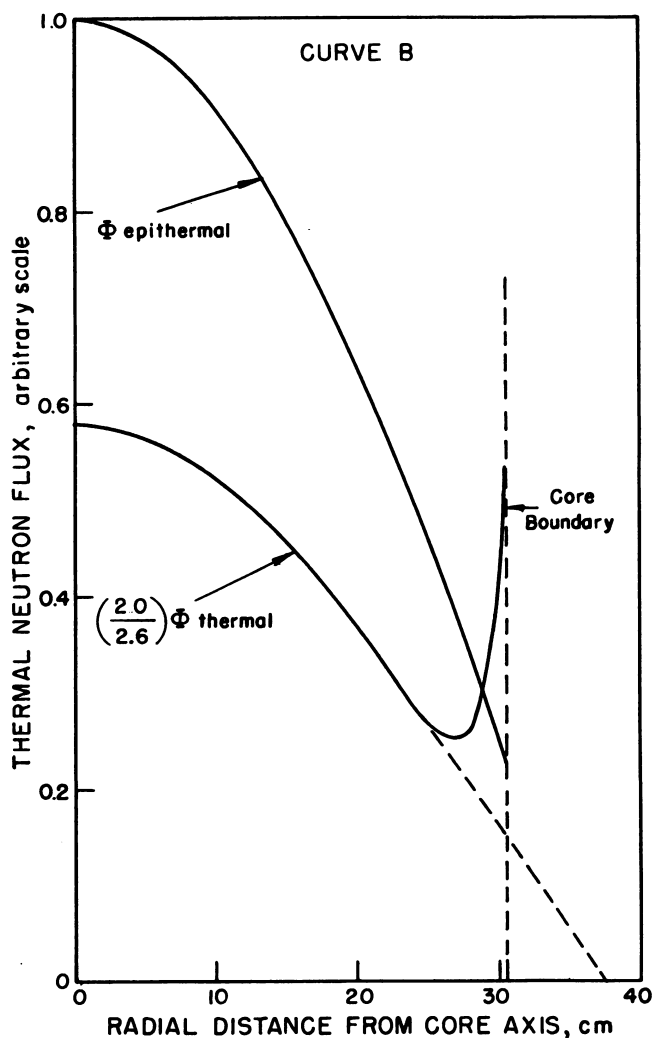


Fig. 1.6.3 — Computed Radial Thermal and Epithermal Flux Distributions in Cylindrical, Water-Reflected, Be- U^{235} - H_2O Cores with Different U^{235} Loadings. Reprinted from ORNL-133, Sept. 1, 1948. Be: H_2O = 1:1 by volume; 416°F; length = diameter = 61 cm; 8 in. H_2O reflector. Curve A, U^{235} loading = 2.6 kg (clean critical mass); reflector saving = 6.8 cm. Curve B, U^{235} loading = 20 kg plus sufficient uniformly distributed absorber for criticality; reflector saving = 7.2 cm.

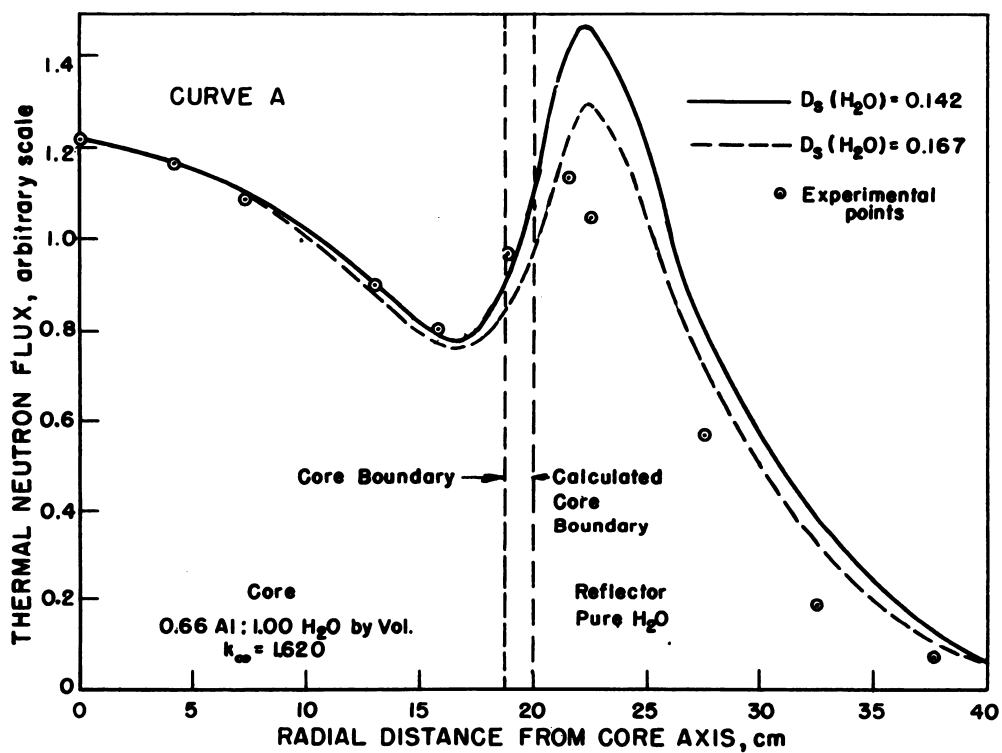


Fig. 1.6.4 — See facing page for legend.

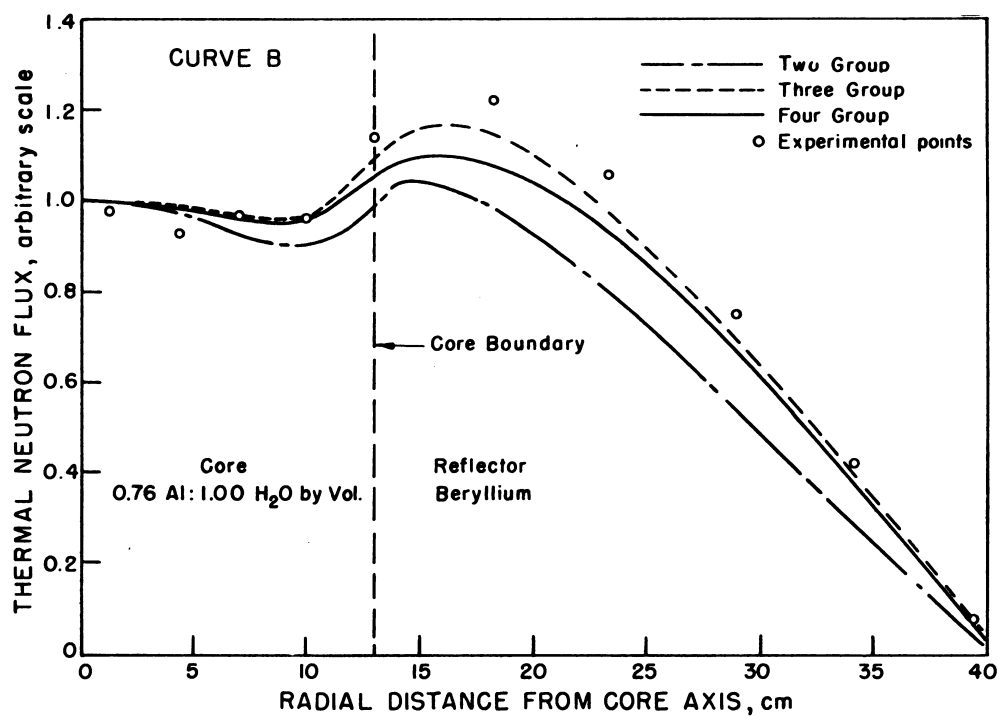


Fig. 1.6.4 — Measured and Calculated Radial Distributions of Thermal Neutron Flux in MTR Critical Assemblies. Reprinted from MonP-402, Oct. 29, 1947. Curve A, H₂O reflector, two-group calculations. Curve B, Be reflector, two-, three- and four-group calculations.

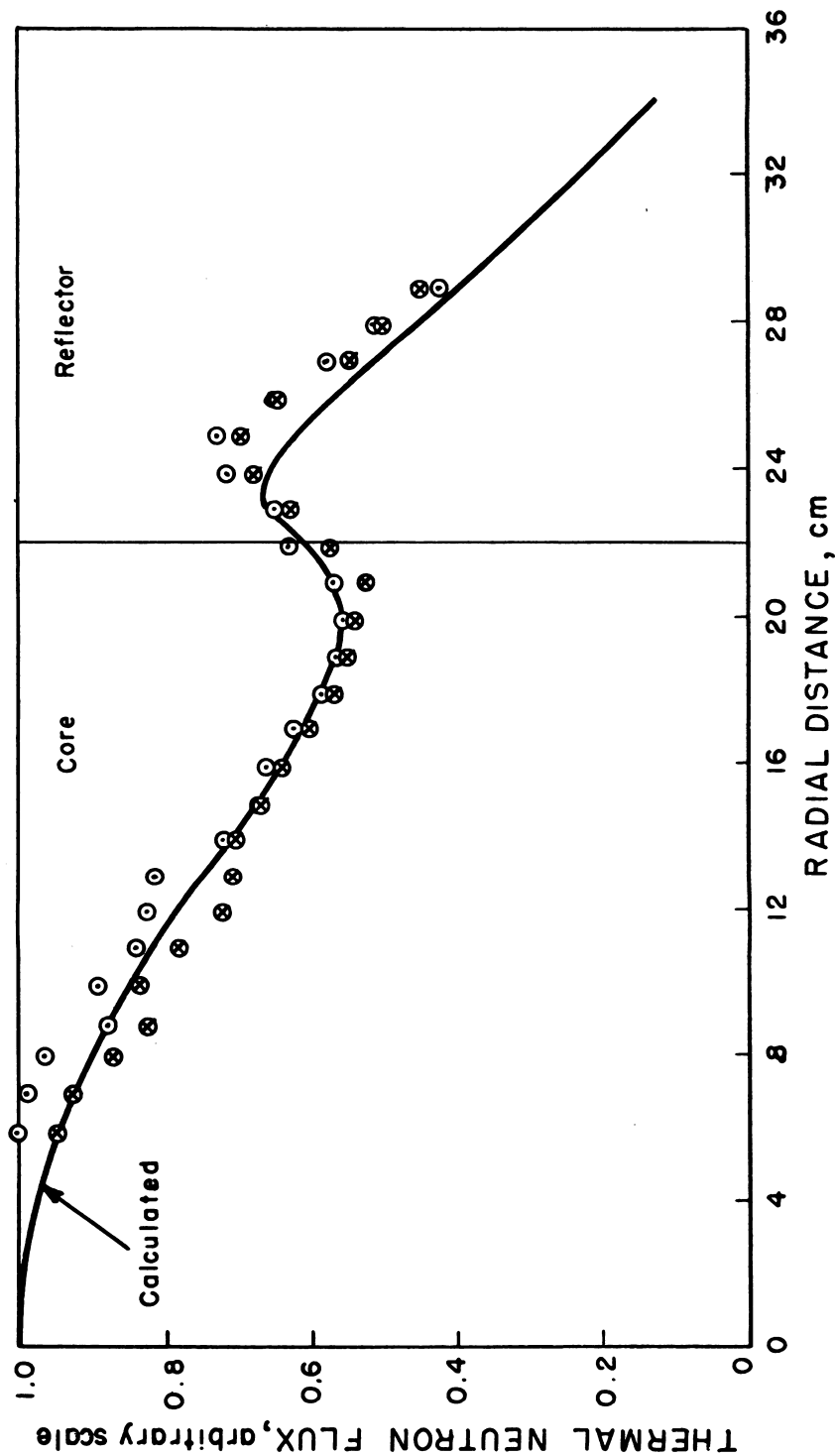


Fig. 1.6.5—Measured and Calculated Radial Distributions of Thermal Neutron Flux in an H_2O -reflected, $\text{Zr-H}_2\text{O-U}^{235}$ Critical Assembly. Based on data presented in ANL-4684, Aug. 24, 1951. The two sets of points were measured in two adjacent quadrants of the cylindrical assembly. The calculation is by the two-group model.

of the discrepancy between calculation and experiment in Fig. 1.6.4A results from the fact that the criticality calculation did not predict the correct position of the core boundary. Inasmuch as computation seems to predict too high a thermal flux peak in the reflector in Fig. 1.6.4A and too low a value in Fig. 1.6.5, it seems as likely that the discrepancies represent inaccuracies in reactor constants or in measurement as that they indicate inadequacy of the two-group model for flux computations. It may be noted that neutron transport calculations by the spherical harmonics method indicate that diffusion theory underestimates slightly the thermal flux rise near a boundary between water and core material (see Fig. 1.6.8).

When the equilibrium slowing-down distribution in the reflector material is much different than that in the core material, it is hardly surprising if two-group calculations fail to give correct flux distributions. Figure 1.6.4B compares two-, three-, and four-group calculations for such a case with the measured distribution. The three-group calculation fits the measured distribution better than either the two-group or the four-group. This result suggests that more may be gained by improving the constants to be used in three- or four-group theory than by using a larger number of groups.

It may reasonably be concluded from the relatively few cases in which calculated flux distributions have been checked by experiment, that if a two-group or multi-group calculation predicts critical mass correctly it will predict the power distribution in the core with sufficient accuracy for determining heat-removal requirements. An exception would be a reactor in which the power distribution near the core boundary is of primary importance, either because the power peak at the core boundary is the highest in the core, or because of thermal expansion difficulties arising from the steep power gradient.

Flux Distributions in D₂O-moderated Reactors

Few D₂O-moderated reactors in the quasi-homogeneous class have been investigated in detail. The general features of flux distributions discussed above hold also for D₂O-moderated reactors. In general, diffusion lengths in D₂O-moderated reactors will be considerably longer than those in H₂O-moderated reactors, and flux perturbations caused by the reflector will extend farther into the core. If reasonably thick D₂O reflectors are used, quite large reflector savings may be realized—up to perhaps 40 cm in practical cases. The combination of these two characteristics—long diffusion length and large reflector saving—makes it feasible to attain quite flat power distributions in simple D₂O-moderated cores up to three feet or more in diameter. Some measurements of flux distributions in U²³⁵-D₂O critical assemblies have been reported,³ and flux distributions in D₂O-reflected, H₂O-moderated reactors were made in connection with MTR critical experiments.⁴ A design study of a small, enriched, D₂O-moderated power reactor has been made which contains calculated power distributions,⁵ and subsequent studies of the same general type of reactor contain further computed (two-group) flux distributions and curves of reflector savings.⁶

EFFECTS OF CONTROL ELEMENTS

Since all types of control elements must be capable of varying the neutron balance in the reactor in order to fulfill their purpose, they will all modify the neutron flux distribution to a greater or lesser degree. To date, only absorbing rods and plates have been used as control elements in water-cooled reactors. They are usually, but not necessarily, black to thermal neutrons and may also have significant absorption in the resonance energy range. Since the effect of such a control element is to depress the thermal neutron flux in its vicinity, the elements should, in the interests of achieving flat power distribution, be installed in the regions of maximum thermal flux. The choice of the maximum flux regions is also dictated by control considerations since it results in maximum rod effectiveness (exception: if the maximum flux region is near the edge of the core—see discussion of

importance functions in Volume 1, Chapter 1.6 for more quantitative treatment of this subject). In fact, it can be shown that approximately maximum effectiveness can be obtained from a group of rods if the rods are so located in the reactor as to produce the flattest possible flux distribution.⁷

Symmetrical Calculations; Cell Approximations

If a single, round control rod at the center of the reactor is used, the resulting flux distribution can be computed by a straightforward application of two-group theory. If a reasonably large number of identical control rods are installed in a uniform lattice arrangement, the reactor region containing the control rods can be divided into a number of approximately equal "cells," each containing a control rod along its axis. The approximate flux distribution within a typical cell can be computed by a group method on the assumption that the neutron current is zero at the cell boundary. The gross flux distribution over the reactor can be computed on the assumption that the region of the reactor composed of the cells constitutes a separate, effectively homogeneous region with appropriate average properties. Detailed discussions of the cell method are contained in Volume 1, Chapter 1.6 and in reference (7).

Off-center Rods; the Nordheim-Scalett Method

If the number of control rods is small, if all the rods are not identical, or if the spacing is not such as to allow the identification of a typical "cell," a more general method of flux computation is required. The two-group Nordheim-Scalett method⁸ has been frequently employed. This method imposes no restrictions on the number, placement, or variation in size of control rods inserted in the axial direction in a cylindrical core. The labor of computation may, however, be great if many rods are used in an arrangement of poor symmetry. The method has two deficiencies: It usually applies the boundary condition on the thermal neutron flux at only one point on the rod surface, and it applies no boundary condition on the epithermal flux at the rod except that the flux remain finite at the rod center. The first of these deficiencies may not be serious if the rods treated are round, since the treatment inherently fits the boundary condition on an approximate circle if the condition is applied at one point on the circle. An extension of the method is available,⁹ which provides for boundary conditions at additional points. The second deficiency results in an apparent fast-neutron current into the rod which has no counterpart in fact. As a result, the calculation tends to overestimate the effectiveness of rods. The discrepancy can become quite large if the rods are large or if the epithermal flux in the reactor is very much higher than the thermal flux. It is generally advisable before applying the Nordheim-Scalett method to a complex arrangement of rods to test it against a straightforward two-group calculation for the case of a single rod installed on the reactor axis. It would seem reasonable to presume that if the size of "Nordheim-Scalett" rods is adjusted to give the same reactivity change as the actual rods the calculated resulting flux distributions would be reasonably accurate in most cases. More recent computation methods, which are fundamentally similar to the Nordheim-Scalett method, provide for a more realistic boundary condition on the epithermal flux.^{10,11}

Figure 1.6.6 is a flux distribution computed by the Nordheim-Scalett method for a water-reflected core composed of H₂O, zirconium, and enriched uranium, and containing six fully-inserted round control rods.¹² The flux flattening produced by the rods is evident if Fig. 1.6.6 is compared with Fig. 1.6.1A. The degree of flattening produced by such a ring of strong control rods (the rods are worth about 3 percent k_{eff} each) is quite sensitive to the distance from the core axis to the rod axes; a change in this distance of one diffusion length can change drastically the ratio of the height of the central flux peak to the height of the flux peak outside the ring of rods. The optimum rod position for flattening depends on the size and effectiveness of the rods and on the reactor constants.^{13,14}

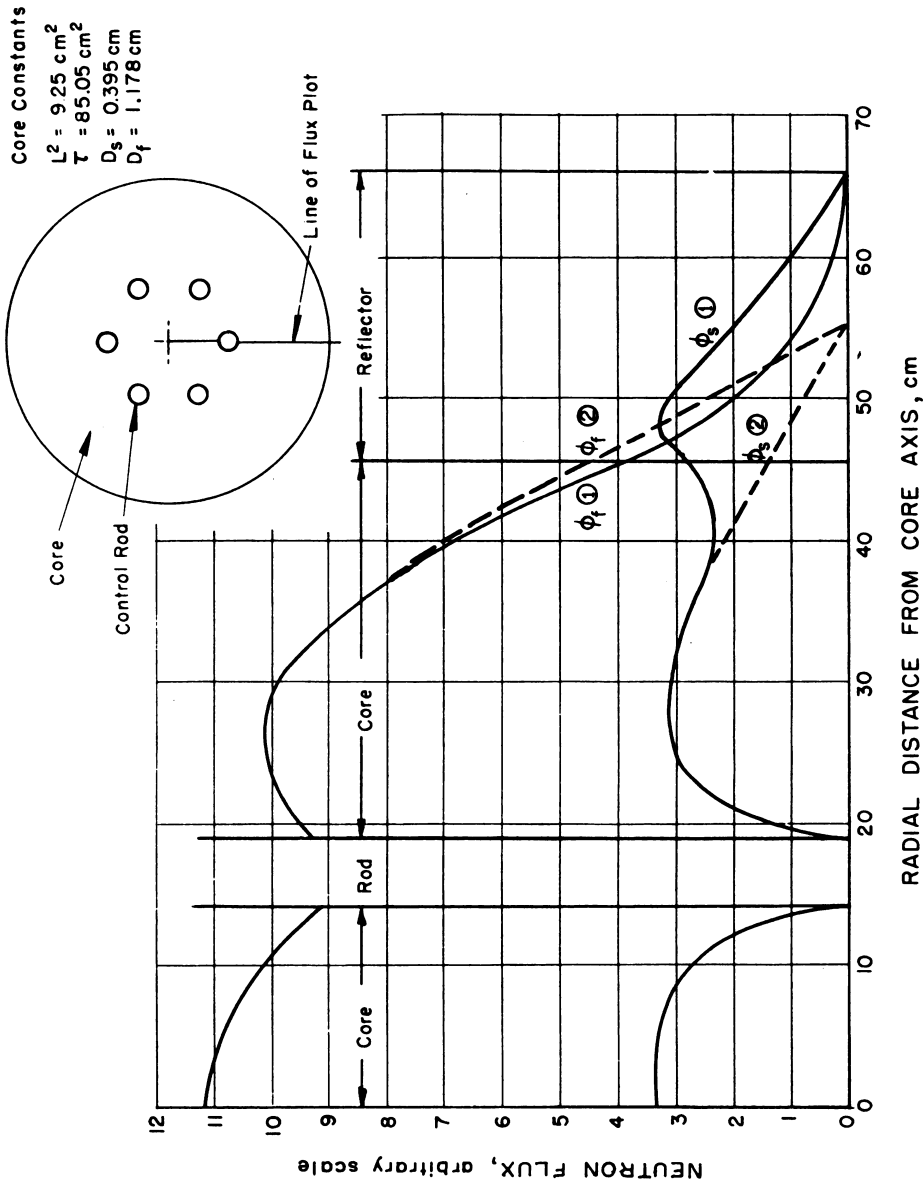


Fig. 1.6.6—Flux Distribution Through One Rod in a Reactor Composed of H_2O , Zirconium, and Enriched Uranium, and Containing Six Fully Inserted Round Rods in a Hexagonal Pattern. Computation by Nordheim-Scalettar method. Curve (1) is for a reactor with water reflector; curve (2) is for the equivalent bare reactor.

It is the usual practice to reduce the labor involved in computing flux distributions with control rods by solving the problem for the equivalent bare reactor, where the boundary of the equivalent bare reactor with rods is assumed to be the same as the boundary of the equivalent bare reactor without rods. In the case of Fig. 1.6.6, the equivalent bare computation gives a flux distribution that is identical with the reflected distribution except near the core boundary. This result would be expected so long as the rods are far from the core boundary.

Derivations of the Nordheim-Scalett equations and of the modified Nordheim-Scalett equations are available for a number of specific cases.^{9,15,16}

Non-circular Rods

In calculations of the heat-removal requirements of reactor fuel elements, the details of the flux depression very near the control rod are not usually important. Consequently, it is usually permissible to replace rods of inconvenient shape by equivalent circular rods, i.e., by circular rods which produce the same change in reactivity. If experimental data which indicate the correct equivalent circular rod are not available, estimates may be made by methods⁷ which neglect the slowing-down of fast neutrons near the rod, or a numerical computation may be made by relaxation techniques^{17,18} to determine the equivalent circular rod for any specified rod shape.

Figure 1.6.7 shows the result of a calculation by the relaxation method of a cross-shaped rod of $4\frac{3}{4}$ in. span.¹⁷ The calculated diameter of the equivalent circular rod is 3.68 in. Reference (7) would give 3.65 in. for the same rod. Experimental measurement in a H_2O reflected, $\text{Zr}-\text{H}_2\text{O}-\text{U}^{235}$ critical assembly showed an equivalent diameter of 3.5 in. The measured rods, a cadmium-silver alloy, absorbed appreciably in the resonance range, whereas the calculations were made for pure thermal absorbers.

PARTIAL INSERTION OF CONTROL RODS

Control rods when fully inserted do not affect the axial flux and power distributions in the reactor except insofar as the rods may change the reflector saving and the behavior of the thermal flux near and in the reflector. If the rods are only partially inserted, however, they tend to cause a depression in the general level of the flux in the region of the core penetrated by the rods in relation to the rest of the core. The resulting axial flux pattern, instead of having the basically cosinusoidal shape symmetrical about the central plane of the core, becomes unsymmetrical with the maximum displaced in the direction away from the control rods. Although a certain degree of asymmetry of this type may be beneficial for heat removal if properly integrated with the cooling design, a large effect, which may result if the partially-inserted rods control several percent reactivity, can result in a severe power peak.

No practical general method has been developed for calculating the three-dimensional flux distributions in reactors with partially inserted control rods. Ideally, the complete flux distribution could be computed for such a reactor by numerical methods such as the relaxation method. Such calculations are exceedingly laborious. As yet, no thorough investigation of the capabilities of high-speed automatic digital computers for this problem has been made. In many cases, approximate methods (see below) are considered sufficiently accurate for practical purposes.

Since absorbing control rods produce flux depressions rather than flux peaks in their vicinity, it is not usually necessary to know the detailed flux distribution near the control rods to design heat-removal systems. Often, satisfactory approximations to the general distribution can be computed by spreading the effects of the rods over a suitable volume, the boundaries of which are such as to simplify the application of boundary conditions, e.g., by extensions of the "cell" techniques.

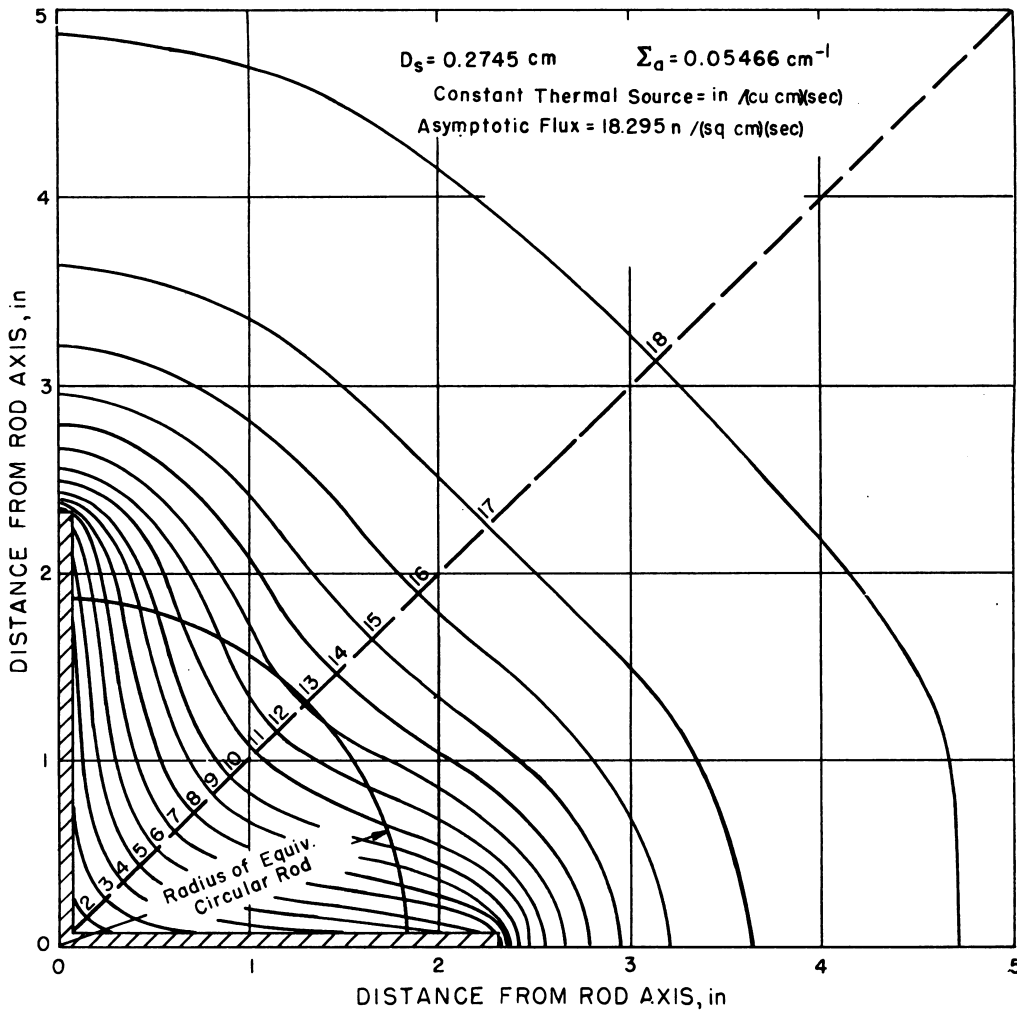


Fig. 1.6.7— Thermal Flux Contour Map Surrounding a Cross-type, Thermally-black Control Rod in an Infinite Medium of $\text{Zr-H}_2\text{O-U}^{235}$ Core Material. Redrawn from ANL-4795, Mar. 15, 1952. Computation by relaxation treatment of thermal neutron diffusion; slowing-down density assumed constant outside the rod. Numbers on contour lines indicate flux resulting from slowing-down density of 1 neutron/ $(\text{cm}^3)(\text{sec})$.

EFFECTS OF WATER HOLES

It has been pointed out above that if a core having a high ratio of epithermal to thermal flux is surrounded by a moderating reflector of relatively low cross section, a maximum will be produced in the thermal flux in the reflector, and a power peak will occur at the core-reflector boundary. For the same reasons, the presence of any sizeable lump of low-cross-section moderator (e.g., water) in the core will cause a thermal flux peak in the moderator and a power peak in the adjacent core material. Such power peaks may be quite serious if they occur in regions of the core where the power density is already high. The control-rod channels in water-cooled reactors constitute such flux-peaking "water holes" if they are allowed to fill with water as the control rods are withdrawn. This situation has been avoided in the MTR by attaching fuel elements to the ends of the absorbing

control rods located in the core. The control rod channel is thereby filled with material of approximately the same composition as the surrounding core when the control rod is withdrawn.

Computation with sufficient accuracy for practical purposes of the flux peaking caused by "water holes" has not proved particularly difficult. A spherical harmonic calculation (up to the ρ_7 term) has indicated that diffusion theory gives reasonably accurate thermal flux distributions around water slabs of thickness one mean-free-path in an infinite medium of Zr-H₂O-U²³⁵ core material.¹⁹ Figure 1.6.8 shows a comparison of thermal flux distributions computed by the spherical harmonic method and by diffusion theory. Flux distributions around single water holes of odd shapes can be computed by relaxation methods using diffusion theory. Because small water holes, although they may perturb the thermal neutron flux drastically, do not produce a large change in the total (fast plus thermal) neutron population (i.e., they do not represent large reactivity changes), it is possible to superimpose the local thermal flux peak owing to a water hole upon the unperturbed thermal flux distribution which would have existed if the water hole had been full of core material. It is also possible to superimpose to some extent the flux peaks resulting from neighboring water holes.

Reactor designs have not, to date, required any detailed investigation of the effects of water (D₂O) holes in D₂O-moderated reactors. D₂O slabs of 2- to 4-cm thickness have been computed by diffusion theory²⁰ for reactors having epithermal-to-thermal flux ratios of about two. The peaking at the core-D₂O boundary is about 8 percent and 20 percent, respectively, for the two slabs. The effects extend quite far in the core material because of the long diffusion length, and it might be expected that by employing judicious design the effects of D₂O holes might be kept unimportant in most D₂O-moderated cores.

METHODS OF IMPROVING POWER DISTRIBUTION

If the characteristics of a reactor do not change greatly with time (i.e., if the reactivity does not change much because of burnup of fissionable material, formation of fission-product poisons, or for other reasons during the life of the reactor), it is not difficult in theory to achieve quite a flat power distribution by proper design. Improvements beyond those obtained by the use of a good reflector and judicious placement of control rods may be made by non-uniform distribution of absorber, fissionable material, or (conceivably) moderator. These improvements may or may not result in the requirement of larger critical mass or improved fuel quality. It has been shown in Volume 1, Chapter 1.5 that the critical mass of the reactor can actually be minimized if the fuel is so distributed as to produce uniform thermal flux. This uniform flux distribution is achieved by concentrating the fuel near the center of the reactor. The power density is therefore not constant but rather concentrated near the reactor center. If, however, the core is made up of identical fuel subassemblies separated by moderator, the spacing of the subassemblies can be decreased near the center of the core to achieve a flat radial flux distribution with the result that the power output of all subassemblies is equal. This type of arrangement is of interest when moderator in excess of that required as coolant is necessary (for water-cooled reactors in the supercritical temperature range, and possibly for boiling reactors).

If the core is constructed of close-packed subassemblies, uniform power distribution can be achieved by varying the fuel content of the fuel elements. Figure 1.6.9 illustrates, for a spherical reactor, the effect on power distribution of various fuel distributions, from the uniform distribution to that producing uniform power distribution.²¹ The curves are normalized to the condition that the reactor power output is limited by the maximum power occurring at any point. The upper set of curves shows the assumed fuel distributions, and the middle set the corresponding thermal flux distributions. The lower set of curves, the power distributions, are the products of the other two sets of curves. Listed also on the figure is the ratio of critical mass, for each fuel distribution, to the critical mass with uniform fuel distribution.

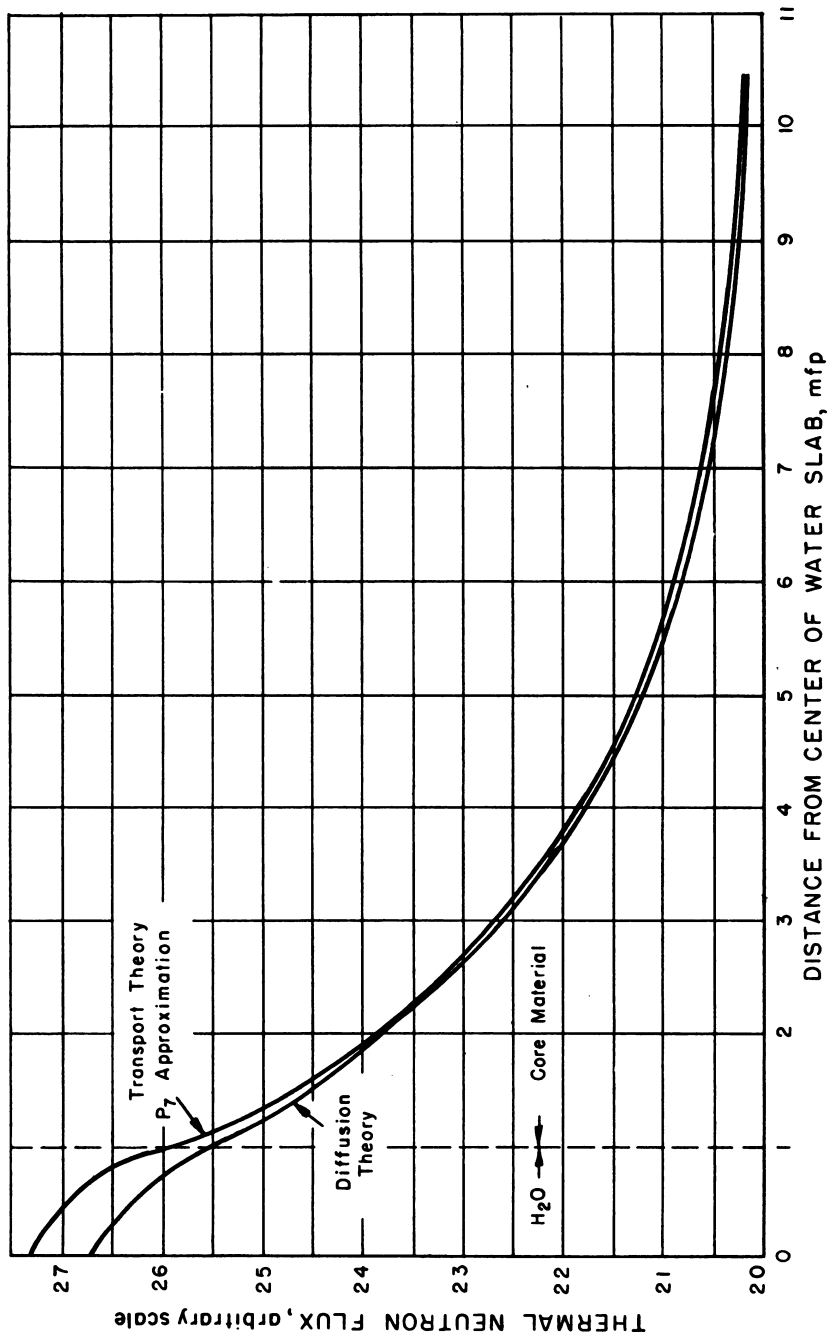


Fig. 1.6.8—Thermal Flux Distribution Near a Water Slab in Infinite Medium of $\text{Zr-H}_2\text{O-U}^{235}$ Core Material as Computed by Diffusion Theory and by the P_1 Spherical Harmonic Approximation to Transport Theory. Redrawn from ANL-4795, Feb. 15, 1952.

In a reactor which must provide for large changes in reactivity, the problem of providing continuous flat power distribution is much more difficult because most types of control elements cause changes in power distribution as they change reactivity. This effect is minimized if the source of control is an absorber of adjustable concentration distributed uniformly in the reactor core. This type of control might be achieved in water-cooled reactors if the absorber were dissolved in the coolant water. A practical system of this type has not been developed to date.^{22,23}

A second possibility for control of water-moderated reactors is to compensate for reactivity changes by adjustment of the average temperature and density of the water moderator.

HETEROGENEOUS (NATURAL-URANIUM AND LOW-ENRICHMENT) REACTORS

The heterogeneous design is used in natural-uranium and slightly enriched reactors to reduce the resonance absorption by U^{238} . The reactor core is periodic in structure and can be considered to be composed of "cells" symmetrical about the fuel element. The gross flux distributions in the reactor can be computed, as for homogeneous reactors, using appropriate average properties determined by detailed analysis of a typical cell. The detailed flux distributions can then be approximated by superimposing the distribution in a typical cell upon the gross distribution computed by homogeneous reactor theory. Such calculations are discussed in Volume 1, Chapter 1.5.

The principles governing the gross flux and power distributions in heterogeneous reactors are the same as those discussed above under "Quasi-homogeneous Reactors." The quantitative characteristics of heterogeneous reactors are, however, sufficiently different to emphasize different aspects of the power-distribution problem. These differences are most pronounced in graphite-moderated and D_2O -moderated reactors; some slightly enriched, H_2O -moderated designs begin to approach the compact structure characteristic of the quasi-homogeneous reactors.

Some important characteristics of most heterogeneous designs are:

(1) The size of the reactor core is usually rather large in comparison with the reflector saving; the reflector is less effective in flattening the power distribution than in the case of a small, highly enriched reactor.

(2) The epithermal flux is not usually much higher than the thermal flux, and the thermal flux peak at the core-reflector boundary is small or absent. This characteristic frequently does not apply to H_2O -moderated cases.

(3) In most cases, the cell structure is already so coarse that small departures from the typical structure (e.g., water holes) are not important. An exception occurs if the perturbation of structure exists very near the fuel element (see Wilkins Effect, in "Local Flux Distributions," below).

(4) Large changes in reactivity do not usually occur during operation of the reactor. It is therefore feasible, and customary, to employ spatial variations in the properties of the reactor to achieve advantageous power distributions.

The characteristics of heterogeneous reactor power distributions are discussed in more detail in the following.

RADIAL DISTRIBUTION

For an infinitely long, unreflected, cylindrical core of uniform composition, the radial distribution would be a Bessel function of the first kind, that is, a $J_0(\kappa r)$, where κ is determined by the L^2 , τ , and k_∞ of the lattice. Presumably k_∞ would be larger than necessary to supply the leakage out through the periphery, and control rods or some fixed thermal absorber would be distributed throughout the core to keep the reactor critical. To flatten the power, a redistribution of the thermal poison is made. By shifting enough of

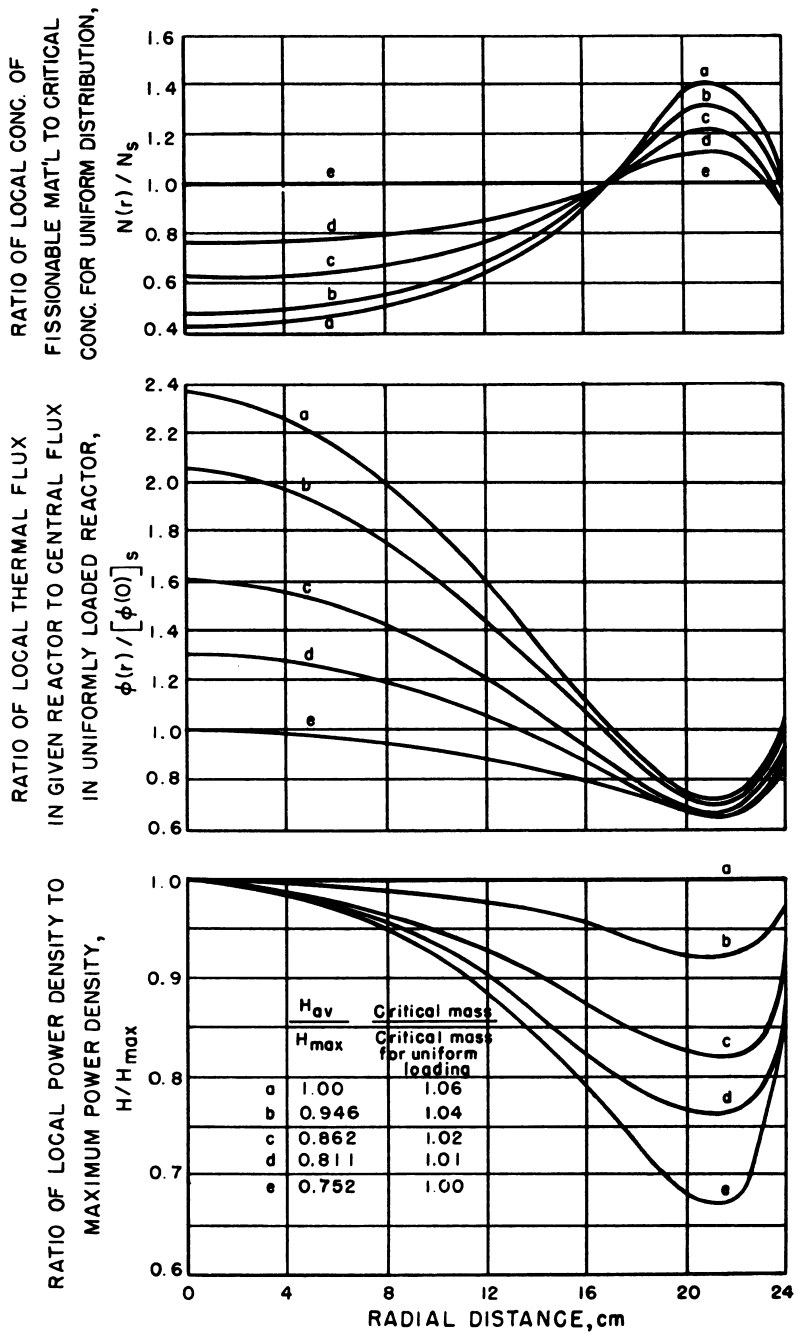


Fig. 1.6.9 — Distributions of Fuel, Thermal Flux, and Power in Spherical, Water-moderated, Water-reflected Reactors: Total Power Assumed Limited by Local Value of Power Density. Redrawn from NACA-RM-E52C11, 1952. Two-group calculations by electrical network reactor simulator. Numerical computation gives 3% higher critical mass than that tabulated for the case of uniform power distribution.

the absorber to the middle section of the core to make k_{∞} equal to unity there and by completely removing the poison from an annular band of thickness, t , which is determined by the L^2 , τ , and k_{∞} of the lattice, the reactor can be kept critical but the flux distribution changed so that it is flat across the middle and more highly buckled (or curved) near the periphery. A comparison of the flattened flux and J_0 for the infinite cylinder are given in Fig. 1.6.10. The proper radius, a , of the flattened zone is readily found from one-group diffusion theory.

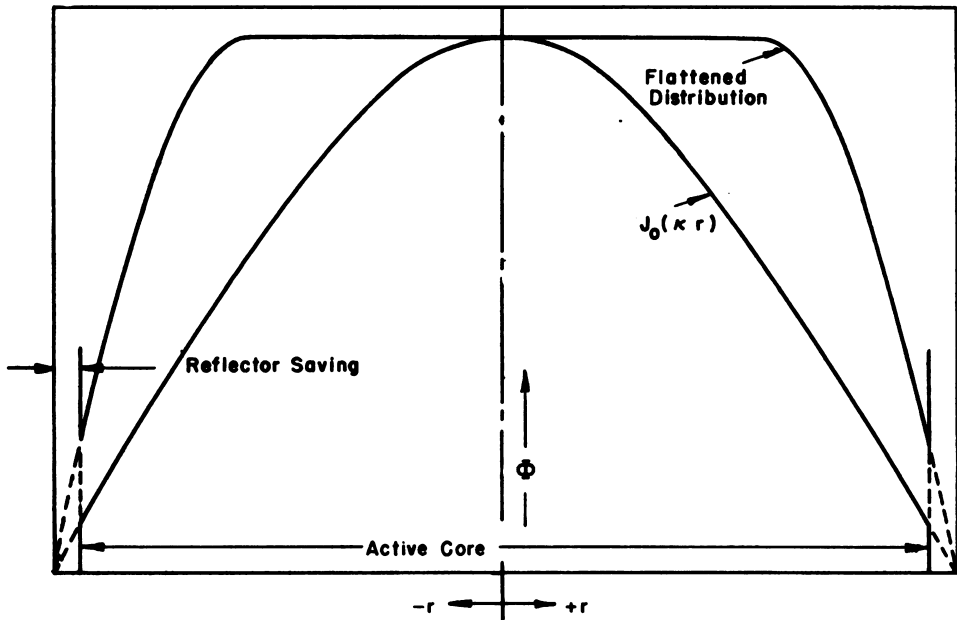


Fig. 1.6.10—Qualitative Comparison of Flattened Radial Flux Distribution with Unflattened [$J_0(kr)$] Distribution. Submitted by Argonne National Laboratory, Nov. 15, 1952.

The solution for the flux in the annular region is:

$$\Phi = AJ_0(\mu r) + Y_0(\mu r) \quad (1)$$

where:

$$\mu^2 = \frac{k-1}{L^2 + \tau}$$

and A is a constant to be determined. Since the flux goes to zero at the outer radius R :

$$A = -\frac{Y_0(\mu R)}{J_0(\mu R)} \quad (2)$$

Now $d\Phi/dr$ ($r = a$) must be zero for criticality. Hence:

$$\frac{Y_1(\mu a)}{J_1(\mu a)} = \frac{Y_0(\mu R)}{J_0(\mu R)} \quad (3)$$

If μ and R are known, this transcendental equation may be solved numerically for a .

If the reactor considered were a semi-infinite slab, the equation defining the thickness, t , of the buckled zone on each side of the flattened center would be:

$$t = \frac{\pi}{2} \sqrt{\frac{L^2 + \tau}{k - 1}} \quad (4)$$

If the reactor is not infinitely long, allowance must be made for leakage out the ends. Hence, k_{∞} in the flattened zone must be slightly greater than unity. Also, the thickness of the buckled zone will increase slightly if the lattice has the same k_{∞} , L^2 , and τ .

If the reactor has a radial reflector, usually the equivalent bare core is considered (i.e., actual core plus reflector saving). The thickness of the buckled zone is found as before, but now only part of it lies in the actual core.

It is noted that the one-group solution may differ significantly from the most accurate two-group solution, and the latter might best be employed to check design choices. In Fig. 1.6.11, the results of one-group and two-group solutions for a "flattened" reactor are compared. It is seen in this case that the smaller L^2 in the buckled zone causes the two-group thermal flux to fall off slightly at the edge of the flattened zone.

LOCAL FLUX DISTRIBUTIONS

A distinctive characteristic of heterogeneous reactors lies in the local flux variation around each fuel element which is superimposed on the over-all flux distribution. Although the reactor lattice is generally square or hexagonal, it is common practice to "cylindricize" the lattice cell for calculation purposes.

Another local perturbation on the thermal flux occurs in reactors using fuel elements in the shape of short slugs having end caps. The "Wilkins" effect^{24,25} occurs, whereby the small absorption and possibly large thermal mean-free-path of the end caps results in a higher flux at the ends of the slugs than the middle. This increase may range from 10 to 35 percent, depending on the particular geometry.

POWER DISTRIBUTIONS IN SPECIFIC REACTORS

MTR

Power distributions in the MTR are currently being measured. The radial distribution is variable according to the loading pattern used. Figure 1.6.4B is an approximation to the radial distribution with slab loading. The actual distribution is modified somewhat by the existence of various holes in the reflector.²⁶ The axial distribution in a freshly loaded MTR core is quite unsymmetrical because of the partial insertion of control rods. It is estimated that the limiting total power output of the fresh core is about half that of the core when depleted enough to allow complete withdrawal of the rods.

HEAT GENERATION IN OTHER CORE COMPONENTS AND MATERIALS

Although the density of heat production in other parts of the core is usually much lower than that in the fuel elements, its computation may be fully as important because it specifies the amount of cooling required for the non-fuel-bearing parts of the core as well as the thermal stresses and strains experienced by those parts.

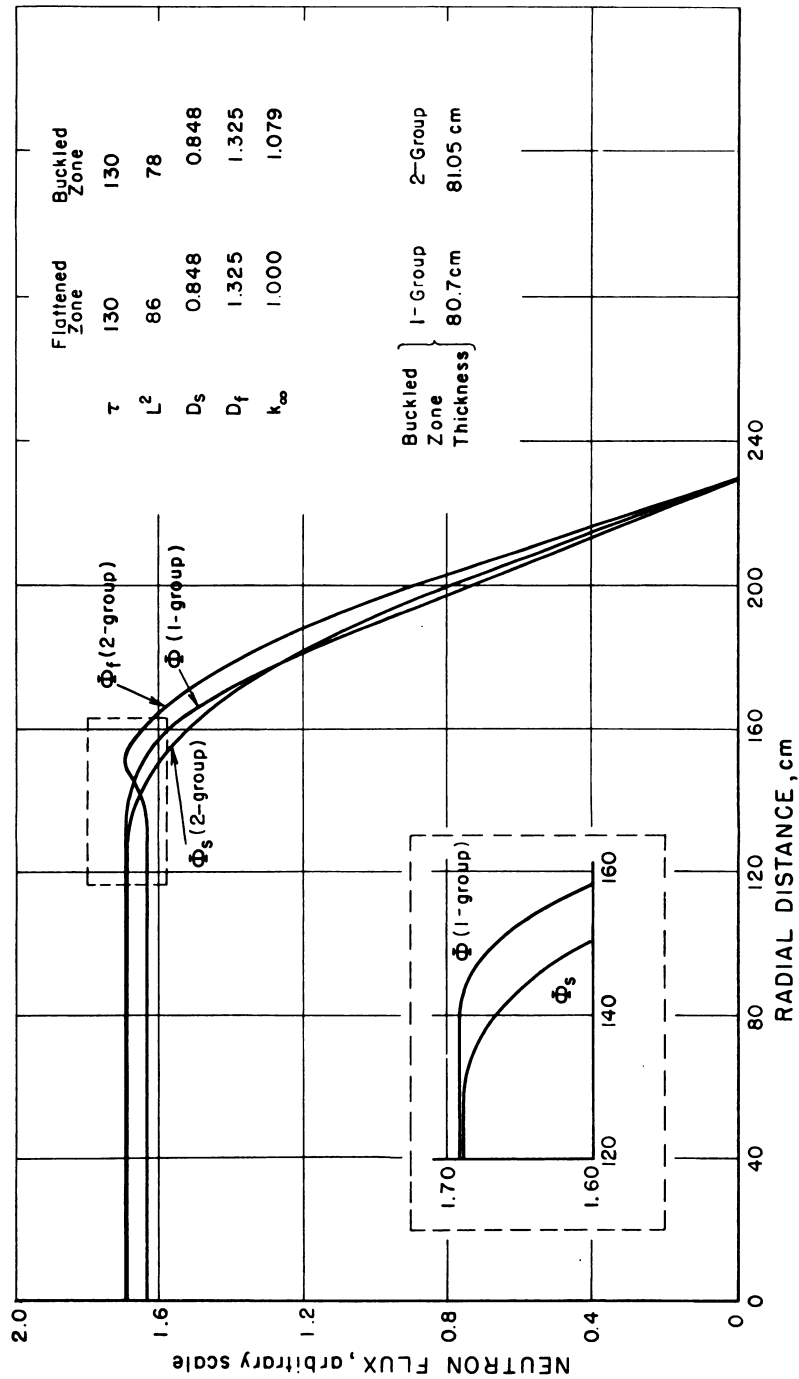


Fig. 1.6.11 — Flux Distributions in a Flattened, Bare, Cylindrical Core of Infinite Length as Computed by One-group and Two-group Theories. Submitted by Argonne National Laboratory, Nov. 15, 1952.

THE HEAT SOURCES

The immediate source of heat is, in all cases, a charged particle which is being slowed down in the material in question. The common classes of such charged particles are:

(1) High-speed electrons formed or ejected from atoms in the process of gamma-ray attenuation. The gamma rays may include secondary gammas from $n - \gamma$ reactions as well as the prompt and delayed fission gammas.

(2) Atomic nuclei knocked-on by fast-neutron collisions.

(3) α -particles formed in $n - \alpha$ reactions (e.g., in boron or lithium control rods).

(4) β -particles emitted in the decay of radioactive isotopes formed by neutron capture.

While these charged particles are the immediate heat sources, they all stem, ultimately, from the neutrons and gamma rays (prompt and delayed) emitted in connection with fission. The energies available in the primary fission gammas and neutrons are given in Volume 1, Table 1.2.10. The energies involved in secondary reactions ($n - \alpha$, $n - \beta$, $n - \gamma$) must be evaluated separately for the particular reactions in question.

APPROXIMATE GENERAL EXPRESSION FOR HEAT GENERATION IN A PIECE OF MATERIAL EMBEDDED IN THE REACTOR CORE

The following expression includes the common sources of heat in a sample of non-fissioning material embedded in a reactor core:

Heat production per cm^3 = (neutron energy loss per cm^3 owing to elastic collisions) + (absorption of fission-gamma energy per cm^3) + (absorption of energy from distributed secondary gammas per cm^3) + (absorption of energy per cm^3 from secondary gammas produced in the sample itself) + (energy per cm^3 of $n - \alpha$ and $n - \beta$ reactions in the sample).

The expression neglects inelastic scattering, which is usually unimportant in water-moderated reactors. The following gives approximate evaluations for the various terms of the above expression. The approximations are quite rough, and more accurate calculations should be made if the result is at all crucial. It is assumed that the following quantities are known or can be approximated for the reactor in question:

- (1) $P(r)$, the local total power density, computed as though the reactor were homogeneous, and including the energy of the fission fragments, in watts per cm^3 .
- (2) \bar{P} , the average total power density over the entire core, in watts per cm^3 .
- (3) $\Phi_s(r)$, the local thermal-neutron flux density.
- (4) $\Phi_f(r)/\bar{\Phi}_f$, the local distribution of fast-neutron flux.

NEUTRON ENERGY LOSS BY ELASTIC COLLISIONS

Approximations: All fast neutrons slow down in the core; energy absorption in any material proportional to $\xi \Sigma_s$ where Σ_s is evaluated at some "appropriate" energy:

$$(\text{Heating per cm}^3 \text{ at } r) = \bar{P} \frac{\Phi_f(r)}{\bar{\Phi}_f} \frac{(\xi \Sigma_s)_{\text{sample}}}{(\xi \Sigma_s)_{\text{core}}} E_n \text{ watts/cm}^3$$

Σ_s should be evaluated somewhere in the region between 0.5 mev and 2 mev. This expression gives only a rough estimate since Σ_s varies rather rapidly with energy in the neighborhood of 1 mev for the light elements. However, in many cases, the slowing-down energy is a small part of the total heating, and a rough estimate will suffice. If the rough relation indicates slowing-down energy to be important, more detailed calculations should be made.

ABSORPTION OF FISSION-GAMMA ENERGY

Approximations: Local gamma energy absorption per cm^3 in core material = local gamma energy production per cm^3 when core material is assumed homogeneous in composition:

$$(\text{Heating per cm}^3 \text{ at } r) = P(r) \frac{\mu_{\text{sample}}}{\mu_{\text{core}}} [E_{\gamma}(\text{prompt}) + E_{\gamma}(\text{delayed})] \text{ watts/cm}^3$$

where μ_{sample} and μ_{core} are the energy absorption coefficients for gammas in the sample and in the core, respectively. μ should be evaluated at 1 to 2 mev. The relation is good if the core is large and inhomogeneities (including the sample) small compared to $1/\mu$. As written, the relation applies when the reactor has operated long enough for the delayed γ -emitters to come to equilibrium. If this condition does not hold, $E_{\gamma}(\text{delayed})$ may be modified by application of the delayed gamma decay data (Volume 1, Chapter 1.2).

ENERGY FROM DISTRIBUTED SECONDARY-GAMMA SOURCES

Approximations: The core material, including the secondary-gamma emitters, is homogenized; local gamma energy absorption per cm^3 in core material = local gamma energy production per cm^3 :

$$(\text{Heating per cm}^3 \text{ at } r) = 1.6 \times 10^{-13} \frac{\mu_{\text{sample}}}{\mu_{\text{core}}} \Phi_s(r) \sum_i E_{\gamma i} \text{ watts/cm}^3$$

where the $\Sigma_{\gamma i}$ apply to the materials of the core.

In applying the relation, $\Phi_s(r)$ should be the equivalent homogenized value; e.g., local flux depressions less than $1/\mu$ should be ignored (unless caused by the secondary-gamma emitters themselves). The relation applies when the core is large and inhomogeneities (including the sample) small compared to $1/\mu$.

ENERGY FROM SECONDARY-GAMMA EMITTERS IN THE SAMPLE ITSELF

Approximations: Only the average heat production per cm^3 is evaluated. If the sample is a weak absorber (causes negligible flux depression):

$$(\text{Average heating per cm}^3 \text{ of sample at } r) = 1.6 \times 10^{-13} \beta \Phi_s(r) \sum_i \Sigma_{\gamma i} E_{\gamma i} \text{ watts/cm}^3$$

where the $\Sigma_{\gamma i}$ apply to the materials of the sample and β is the probability that a photon emitted in the sample will be absorbed in the sample. If the sample shape can be approximated by a sphere, an infinite cylinder, or an infinite slab, β can be read from Table 1.6.3.

If the sample is a strong absorber, the average absorption of thermal neutrons per cm^3 of sample per second ($A_{\gamma i}$) by the i^{th} type of γ -emitter must be calculated by appropriate means, and:

$$(\text{Average heating per cm}^3 \text{ of sample at } r) = 1.6 \times 10^{-13} \beta \sum_i A_{\gamma i} E_{\gamma i} \text{ watts/cm}^3$$

ENERGY FROM N- α AND N- β REACTIONS IN THE SAMPLE

Alphas and, unless the sample is very thin, most betas emitted in the sample will produce their heat in the sample. If the sample is a weak absorber:

$$(\text{Heating per cm}^3 \text{ of sample at } r) = 1.6 \times 10^{-13} \Phi_s(r) \sum_i (\Sigma_{\alpha i} E_{\alpha i} \Sigma_{\beta i} E_{\beta i})$$

Table 1.6.3 — Probability, β , That a Gamma Ray Emitted Inside a Sample Having Absorption Coefficient μ Will Be Absorbed Inside the Sample

μR	Source uniformly distributed ²⁷ over volume of sample			Source uniformly distributed over surface of sample
	Sphere of radius R	Infinite cylinder of radius R	Infinite slab of thickness R	Infinite slab of thickness R
0	0	0	0	0
0.5	0.295	0.405	0.61	0.336
1.0	.473	.594	.765	.425
1.5	.590	.700	.836	.463
2.0	.662	.765	.875	.481

If the sample is a strong absorber, the absorption of thermal neutrons per cm^3 of sample per second by the i^{th} type of alpha emitter ($A_{\alpha i}$) and by the i^{th} type of β emitter ($A_{\beta i}$) must be calculated by appropriate means, and:

$$(\text{Heating per cm}^3 \text{ at } r) = 1.6 \times 10^{-13} \sum_i (A_{\alpha i} E_{\alpha i} + A_{\beta i} E_{\beta i}) \text{ watts/cm}^3$$

The relations assume that all delayed emitters are in equilibrium.

HEATING OF THE MODERATOR

In water-cooled, water-moderated reactors, direct heating of the moderator is usually not of great importance. In graphite-moderated reactors, it may be important to know both the magnitude and the distribution of the heat produced in the moderator in order to provide proper cooling facilities. In large reactors, it may be assumed that all of the kinetic energy of the fission neutrons goes into the moderator. Primary and secondary gammas will be absorbed by both moderator and fuel slugs, roughly in the ratio $\mu_{\text{moderator}}/\mu_{\text{fuel slugs}}$ per unit volume. This procedure will overestimate the gamma heating of the moderator in lumped reactors because of the self-shielding of the fuel slugs. This effect can be estimated with the aid of Table 1.6.3.

The gross distribution of moderator heating will follow nearly that of fuel-element power in large reactors. More detailed, intracellular distributions are not generally calculated, but the methods are straightforward if such calculations are necessary.

HEATING OF CONTROL RODS

GENERAL METHODS

Generally, heat production in control rods has two main sources: gamma energy from distributed sources (fission and $n-\gamma$ reactions) in the surrounding core and energy from the neutron-absorbing reactions in the rod itself. Absorption of gammas from distributed sources may be estimated as indicated above. This procedure leads to some overestimate since it does not take account of the depression of both the fission rate and the $n-\gamma$ reaction rate near the rod. Reference (28) is an example in which this effect was computed.

In estimating the energy production from neutron reactions in the rod, the number of neutrons absorbed per second by the fully inserted rod is usually known from calculations of the rod effectiveness. If $n-\alpha$ reactions occur in the rod (e.g., boron, lithium), all of the emitted energy is absorbed in the rod. If $n-\gamma$ reactions occur, the fraction of the resulting energy absorbed in the rod must be computed. Simple cases can be estimated with the aid of Table 1.6.3. More complex cases must be computed in detail. If the shape of the rod is other than a circular cylinder, it may be necessary to compute the detailed distribution of neutron absorption in the rod, particularly if the reaction in the rod is $n-\alpha$, which will give a heat-production distribution identical with the neutron-absorption distribution. Such absorption distributions may be approximated by computations of the relaxation type (Fig. 1.6.7).

If the control is inserted completely through the core of the reactor, the distribution of heat production (owing to both core gammas and neutron-absorption reactions in the rod) along the length of the rod will be the same as the gross distribution of heat production in fuel elements along a line parallel to the rod axis. The absolute value of the heat production must, of course, be determined from the total neutron and gamma absorptions of the rod. If the rod is inserted only partway into the core, the axial distribution of heat in the rod, to within a diffusion length (core material) or two of the tip, will be nearly the same as the general distribution of heat production in fuel elements, in the direction parallel to the rod axis. This distribution may, of course, be influenced by the presence of the control rod or rods.

Far from the tip of a highly absorbing control rod, any given small length of the rod is "shadowed" by adjacent lengths. The material at the very tip of the rod is shadowed on only one side and consequently absorbs considerably more neutrons than the material a diffusion length or two from the tip. The tip of the rod receives also a relatively stronger dose of core gammas than do the points far from the tip. An estimate for the heating of the tip by core gammas can usually be made by ignoring the flux depression caused by the rod in the surrounding core material. This always gives an overestimate but usually not an unreasonable one.

Figure 1.6.12 shows the measured flux (copper foils) along a control rod slot in the CP-2 reactor.²⁹ The control "rod" was a flat cadmium strip, 3 in. wide. It is estimated that the flux at the tip of the rod is higher by a factor of 1.4 than the flux at a point 10 percent of the rod length back of the tip.

Figure 1.6.13 shows calculated values of the normal gradient of the neutron density (proportional to the current into the rod) around the tip of a cylindrical rod, with a tip shaped as indicated, half-inserted in a reactor core.³⁰ The calculation is by the one-group approximation (i.e., neutrons assumed to be born thermal), and the rod shape results from the characteristics of the calculation method. The total absorption in the last diametral length of the rod is 1.9 times that of one diametral length located 10 percent of the rod length behind the tip.

In a reactor having a diffusion length (L) considerably shorter than the slowing-down length ($\sqrt{\tau}$), e.g., in an H_2O -moderated reactor, a better approximation is probably obtained by assuming the epithermal flux is undisturbed by the presence of the rod and computing the thermal flux distribution around the tip by relaxation methods. Figure 1.6.14 shows such a distribution for a cylindrical rod cut off square at the end of a $Zr-H_2O-U^{235}$ core.

RODS IN SPECIFIC REACTORS

MTR

The estimated production of heat by absorption of core gammas in a foreign material placed at the center of the MTR core is $3.4 \text{ cal}/(\text{gm})(\text{sec})$.²⁸ This would produce $38 \text{ cal}/(\text{cm}^3)(\text{sec})$ in a thorium control rod at the maximum point. A thorium rod containing 0.1

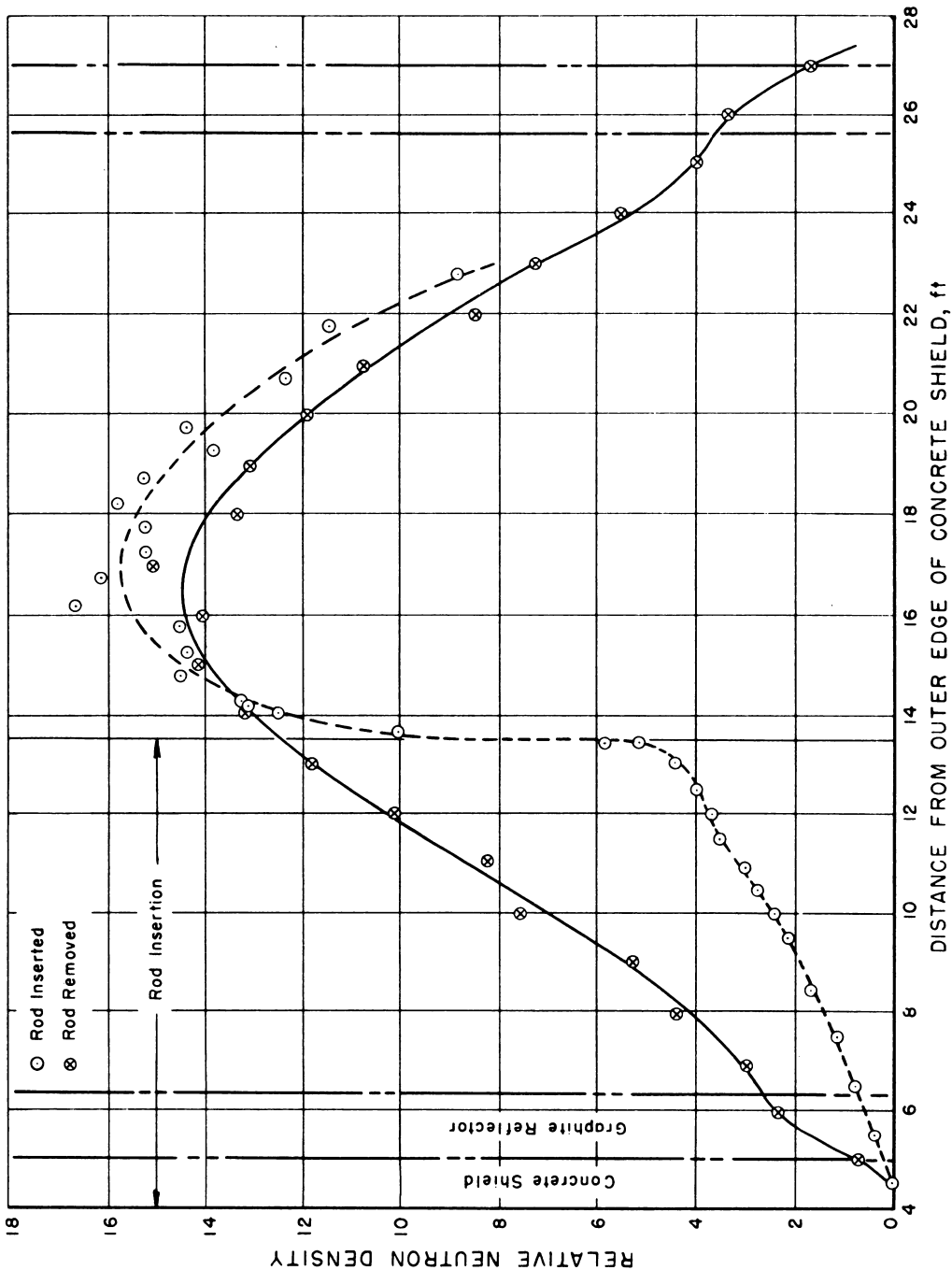


Fig. 1.6.12— Neutron Distribution in a Control Rod Slot in CP-2 as Measured by Copper Foils. Redrawn from CP-1088, Nov. 23, 1943. Control rod is a strip of cadmium 3 in. wide.

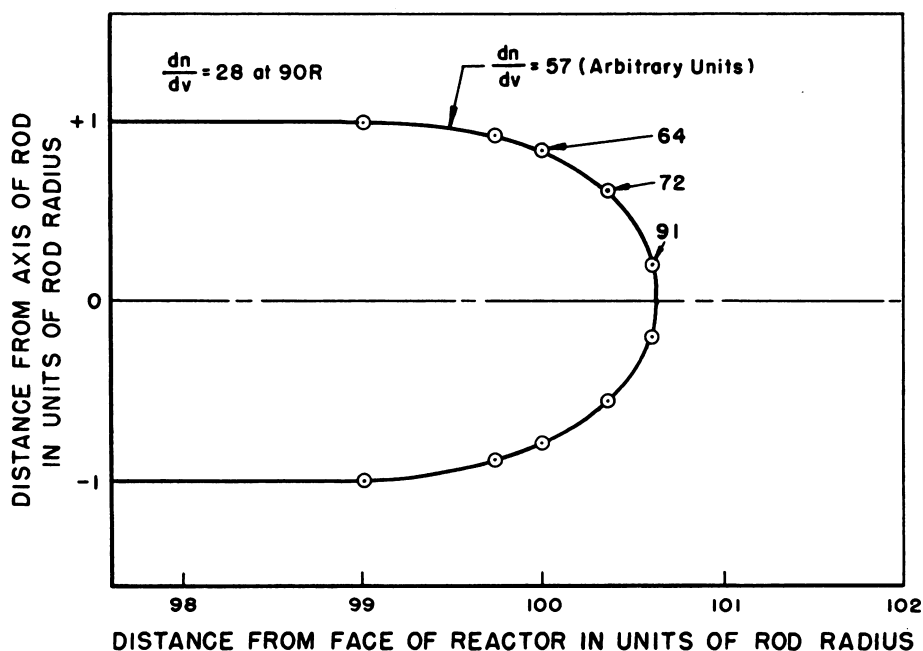


Fig. 1.6.13 — Calculated Relative Values of Normal Gradient of Neutron Flux (dn/dv) into a Cylindrical Rod with Tip Shaped as Indicated. Redrawn from CP-1235, Jan. 18, 1944. One-group calculation; rod black to all neutrons; rod of radius R is inserted axially to a depth of $100.6R$ into a bare cylindrical reactor of radius $100R$ and length $200R$.

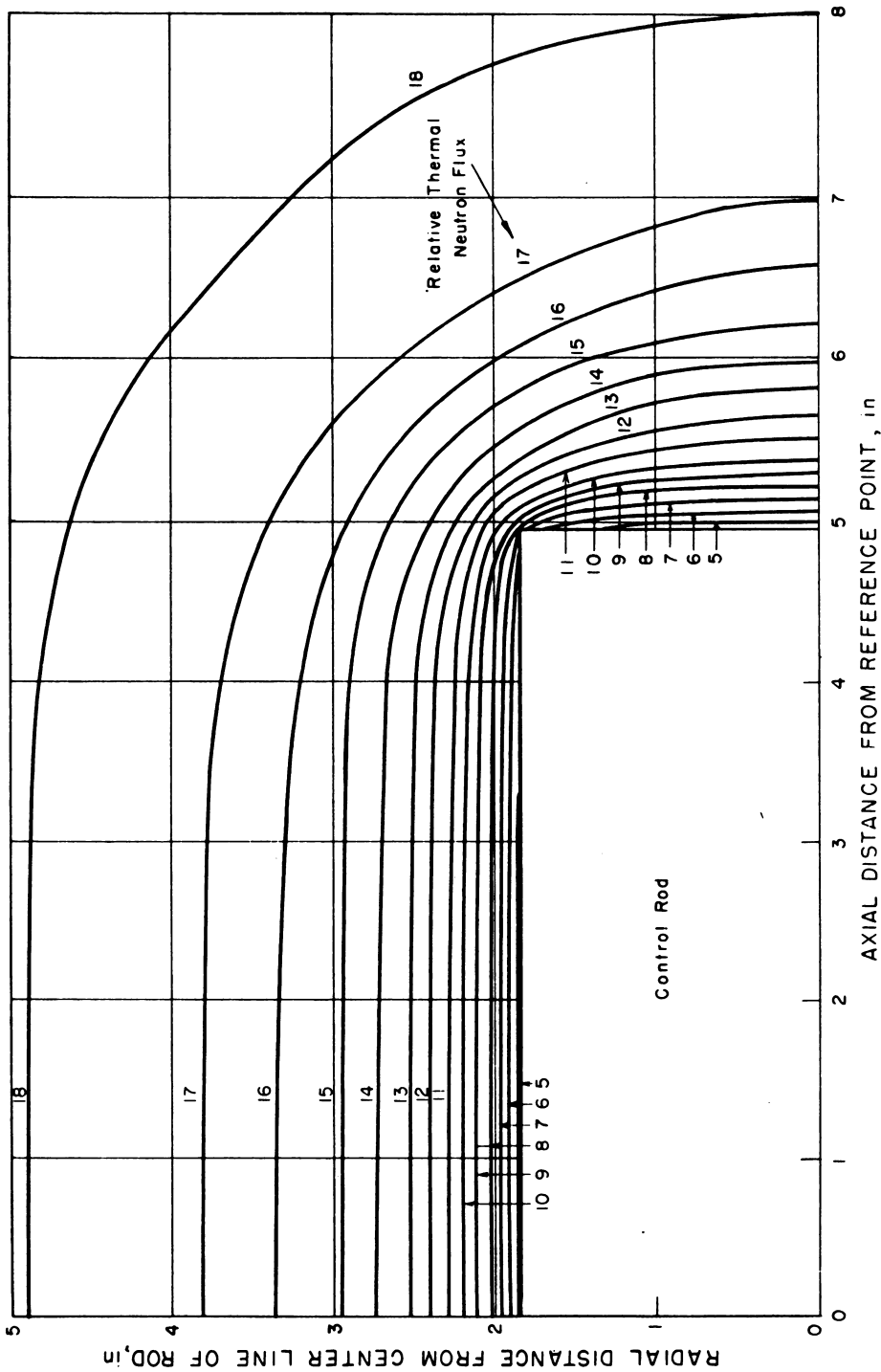


Fig. 1.6.14—Thermal Flux Contour Map Around Tip of Square-ended, Cylindrical Rod Which Is Black to Thermal Neutrons and Inserted in Infinite Medium of $\text{Zr-H}_2\text{O-U}^{235}$ Core Material. Redrawn from ANL-4795, Mar. 15, 1952. Computed by relaxation treatment of thermal-neutron diffusion; slowing-down density assumed constant outside the rod. Numbers on contour lines indicate thermal flux resulting from slowing-down density of one neutron/(cm^3)(sec).

percent converted U^{233} would produce 22 cal/(cm³)(sec) of fission heat at the same (maximum) point. Estimates for cadmium control rods are not given as their cooling is not crucial in the MTR design.

HEAT GENERATION IN REFLECTOR, THERMAL SHIELD, AND REACTOR VESSEL

Heat generation in the reflector is important for determination of cooling requirements if the reflector is composed of a solid material. Most high-power reactors require a thermal shield outside the reflector whose function is to attenuate the heat-producing radiations from the reactor for protection of either the reactor vessel, the biological shield material or both. The primary and secondary sources of heat energy are the same as those discussed above in connection with heating of core materials. The computation of heating of materials outside the core is often more difficult, however, because the transport of energy from the reactor core to the point in question, through the intervening material, must be calculated. The energy attenuation involved is often rather large (factors of 10 to 10³), and the additional processes of inelastic scattering and absorption of fast neutrons, which are negligible heat sources in most water-moderated cores, may have to be considered.

The methods of calculating heat generation in reflectors, thermal shields, and reactor vessels are the same as those presented in Volume 1, Chapter 2.9 for the shield in general and will not be treated here. Details of design calculations which have been checked by experiment do not exist in published form. Reference (31) contains detailed calculations of reflector heating, but confirming experiments have not been made. The remainder of this chapter presents experimental data and estimates for specific reactors.

ORNL LID TANK DATA

Many of the ORNL shielding data, from both the Lid Tank and the Bulk Shielding Facility, are useful for heating estimates. The Lid Tank data^{32,33} reproduced in Fig. 1.6.15 are particularly informative for water-moderated, water-reflected reactors. The gamma dose is plotted as a function of distance in water from the center of a thin-disc fission source. Plates of iron immersed in the water are interposed between the source and detector at various positions. The fission source, which covers an effective area of 3970 cm², operates at 6 watts. The effective power is reduced to about 3.6 watts by the shielding resulting from parts of the experimental assembly.³⁴ The heat production in a thin section of any material such as iron, which does not absorb neutrons strongly, is given by:

$$\text{Heat Production} = 3.3 \mu D \text{ ergs}/(\text{cm}^3)(\text{hr})$$

where μ is the gamma energy absorption coefficient and D is the gamma dose in mr/hr.

When the six iron slabs are placed immediately adjacent to the source they reduce the gamma dose by only a factor of 2.4 below that resulting from water alone. When the iron plates are moved back to leave 25.4 cm of water "reflector" between the source and the plates, the attenuation owing to the iron increases to a factor of 14.6. This is because much of the gamma intensity consists of secondary gammas arising from neutron absorption. The thick water reflector insures that most of the secondary gammas are formed at points where they can be attenuated by the iron plates. The addition of boron to the water in the "thermal shield" reduces the secondary gamma intensity still more, curve (d).

MTR REFLECTOR

Figure 1.6.16 shows the calculated heat production in the beryllium and graphite reflectors of MTR and the heat production measured in a critical assembly mock-up of the reactor.²⁸ Slab loading, which should result in maximum density of heat production, was used in the core.

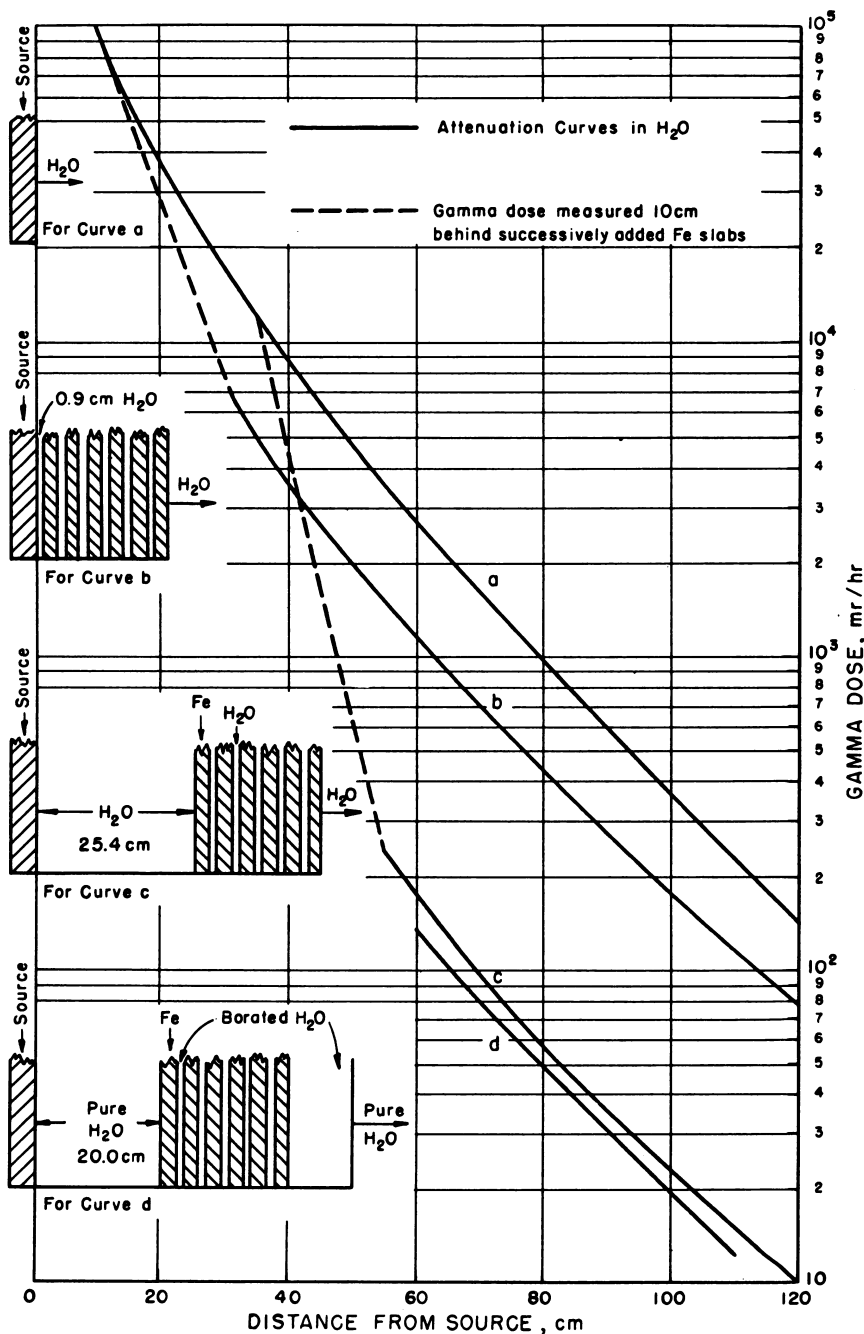


Fig. 1.6.15 — Gamma Dose Behind Thermal Shields Composed of 2.22-cm Iron Slabs Separated by 1.3-cm H₂O Layers. Drawn from Lid Tank Data from ORNL-CF-52-5-40 and ORNL-CF-52-5-41 both dated May 7, 1952.

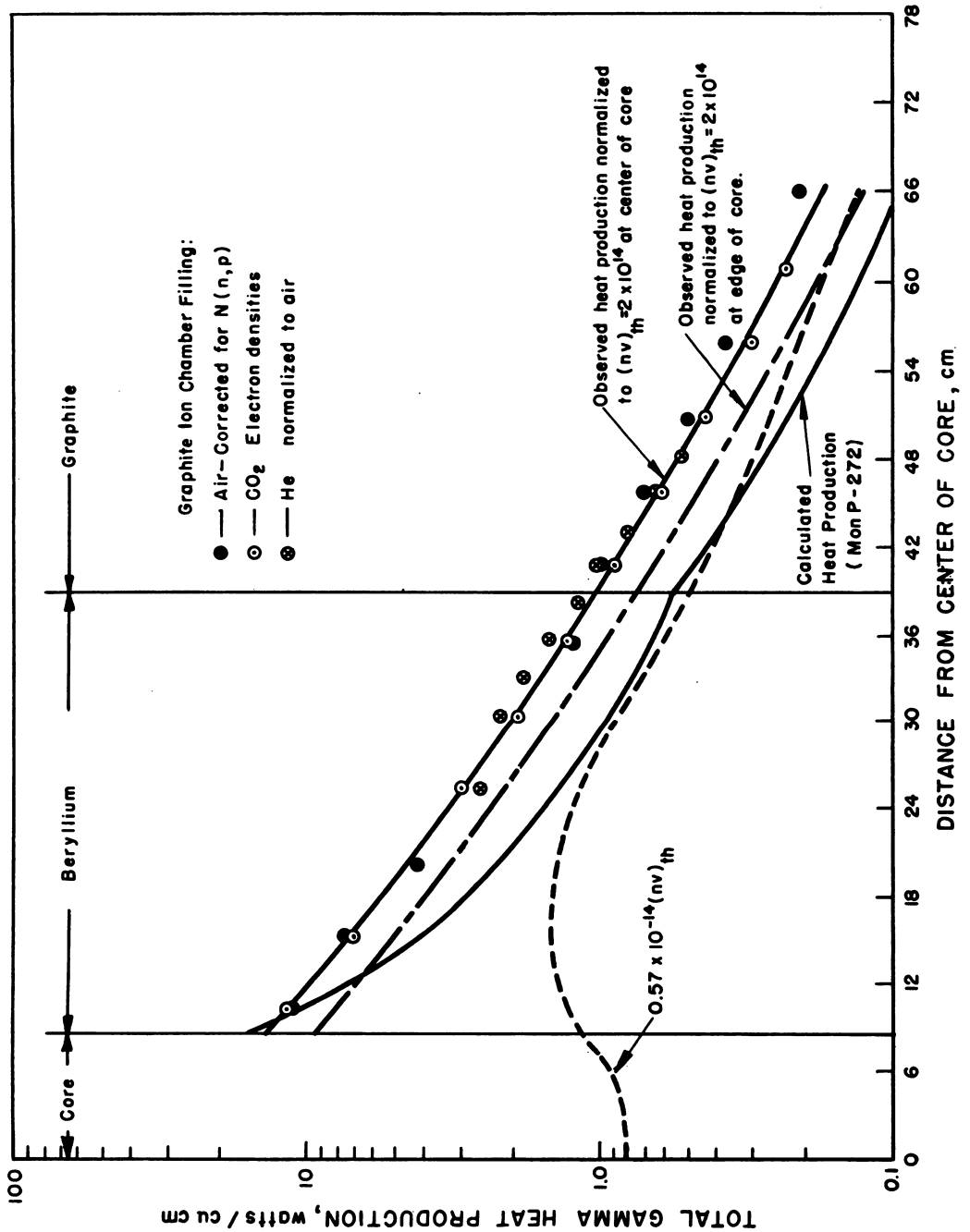


Fig. 1.6.16—Gamma Heat Production in Reflector as Measured in MTR Critical Experiments. Redrawn from ORNL-983, May 7, 1951. Slab loading: $71 \times 17 \times 66$ cm; 3 kg U^{235} .

REFERENCES

1. Oak Ridge Nat. Lab., ORNL-133, Sept. 1, 1948 (classified).
2. E. Greuling and B. Spinrad, Clinton Lab., MonP-402, Oct. 29, 1947 (classified).
3. A. H. Snell, Clinton Lab., MonP-454, Jan. 16, 1947 (classified).
4. M. M. Mann and A. B. Martin, Clinton Lab., MonP-357, Aug. 18, 1947 (classified).
5. Argonne Nat. Lab., ANL-4570, Feb. 1, 1951 (classified).
6. Argonne Nat. Lab., ANL-4683, Sept. 15, 1951, pp 99-102 (classified).
7. J. A. Wheeler, Metallurgical Lab., N-2292, June 28, 1944 (classified).
8. R. Scalettar and L. W. Nordheim, Theory of Pile Control Rods, Clinton Lab., MDCC-42, June 17, 1946.
9. H. L. Garabedian, Westinghouse Atomic Power Div., WAPD-18, Aug. 9, 1950 (classified).
10. L. N. MacKay, Nat. Res. Council of Canada, CRE-400-G, Sept. 1948 (classified).
11. J. Codd and C. A. Rennie, Two Group Theory of Control Rods in a Thermal Reactor, Atomic Energy Res. Establishment, AERE R/R 818, 1952.
12. Argonne Nat. Lab., ANL-4424, March 15, 1950, pp 14-24 (classified).
13. Argonne Nat. Lab., ANL-4898, Sept. 15, 1952, pp 10-12 (classified).
14. Argonne Nat. Lab., ANL-4455, June 15, 1950, p 88 (classified).
15. Clinton Lab., MonN-383, Appendix F., Sept. 15, 1947 (classified).
16. Oak Ridge Nat. Lab., ORNL-22, March 22, 1944, pp 28-36 (classified).
17. R. V. Southwell, Relaxation Methods in Theoretical Physics, Oxford Univ. Press, Oxford, 1946.
18. Argonne Nat. Lab., ANL-4795, March 15, 1952, pp 41-57 (classified).
19. Argonne Nat. Lab., ANL-4795, pp 30-42 (classified).
20. Argonne Nat. Lab., ANL-4729, Feb. 1, 1952, p 175 (classified).
21. R. R. McCready, R. B. Spooner, and M. F. Valerino, Nat. Advisory Comm. Aero., NACA-RM-E52C11, 1952 (classified).
22. Argonne Nat. Lab., ANL-4795, March 15, 1952, p 159 (classified).
23. Argonne Nat. Lab., ANL-4842, June 15, 1952, pp 107-113 (classified).
24. J. E. Wilkins, Jr., Metallurgical Lab., CP-1989, Aug. 3, 1944 (classified).
25. W. Karush, A. T. Monk and J. E. Wilkins, Jr., Metallurgical Lab., CP-2071, Aug. 16, 1944 (classified).
26. J. H. Buck and C. F. Leyse, Argonne Nat. Lab. and Oak Ridge Nat. Lab., ORNL-963, May 7, 1951 (classified).
27. C. W. J. Wende, E. L. du Pont de Nemours and Co., N-609(CP), Jan. 11, 1944 (classified).
28. Argonne Nat. Lab., ANL-4583, March 15, 1951, pp 16-17 (classified).
29. E. Fermi and Associates, Metallurgical Lab., CP-1088 (classified).
30. F. H. Murray, Absorption Near the Tip of a Control Rod, Metallurgical Lab., CP-1235, Jan. 18, 1944.
31. S. A. Kushneriuk and D. Hall, Atomic Energy of Canada, Ltd., Chalk River Project, CRT-504, April 28, 1952 (classified).
32. C. E. Clifford to E. P. Blizard, Oak Ridge Nat. Lab., ORNL-CF-5-40, May 7, 1952 (classified).
33. C. E. Clifford to E. P. Blizard, Oak Ridge Nat. Lab., ORNL-CF-52-5-41, May 7, 1952 (classified).
34. E. P. Blizard, Oak Ridge Nat. Lab., ORNL-CF-51-10-70, Mar. 7, 1952, pp 75-78 (classified)

CHAPTER 1.7

Steady-state Heat Removal

W. H. Jens and L. L. Kintner

Thermodynamic analysis of stationary-fuel reactor systems can be divided into two phases: (1) a macroscopic study of the over-all reactor cooling system in which the reactor may be treated as a heat source causing a temperature rise in the cooling water and (2) a microscopic study of the reactor itself in which a detailed examination is made of the fluid and metal temperatures that may occur within the reactor.

In all reactor systems, whether for production, power, or research, the power-density level is limited by the capacity of the heat-removal system. In all cases, the heat-removal system must be analyzed to determine optimum operating conditions.

The first (macroscopic) phase of the analysis is covered in Chapter 1.2, "Heat Dissipation and Thermal Cycles." In considering the complete system, the temperature of the heat sink, whether ambient air or cooling water, determines the lower temperature level of the entire reactor cooling system for a given reactor-system design and power level. Then, by relating successively the temperatures of the secondary and primary cooling fluids to the temperature of the heat sink, the fluid temperatures across the reactor as a point source of heat are finally obtained. The temperature of the heat source and the temperature level of the various intermediate heat flow paths to the heat sink establish themselves at levels required to transfer heat to the sink at the same rate as it is being generated at the heat source.

Nomenclature and units used in this chapter are given in Table 1.7.1 and conversion factors are given in Table 1.7.2.

A heat balance at the reactor relates the over-all reactor variables:

$$Q = (H_{\text{out}} - H_{\text{in}}) W \quad (1)$$

When only liquid-water phase is used as the coolant, this relation applies:

$$Q = W \int_{t_{\text{in}}}^{t_{\text{out}}} c_p dt \approx c_p (t_{\text{out}} - t_{\text{in}}) W \quad (2)$$

The variables may be determined by the requirements or purpose of the design or the design limitations.

As shown in Eq. (2), reactor power increases with an increase in (1) average water-temperature rise ($t_{\text{out}} - t_{\text{in}}$), (2) total flow rate (W), and (3) specific heat (c_p). Although the specific heat is fairly constant with temperature and is approximately equal to unity for water temperatures below 350°F, an increase in the outlet-water temperature (t_{out}) of the reactor beyond certain low limits will increase the cost because the wall thicknesses of piping and pressure vessels must be increased to contain the increased pressure necessary to prevent (or reduce) boiling.

Table 1.7.1 — Nomenclature and Units

Symbol	Definition*	Unit*
a	Flow area	sq ft
A	Area	sq ft
A_b	Mean heat flow area of bond	sq ft
A_c	Mean heat flow area of clad	sq ft
A_f	Outside heat flow area of fuel	sq ft
A_0	Outside heat flow area of scale	sq ft
A_s	Mean heat flow area of scale	sq ft
c_p	Specific heat	Btu/(lb)(°F)
F_m	Mixing factor, theoretical	None
F_0	Orificing factor	None
$F_{\Delta t}$	Ratio of the maximum water-temperature rise in a channel to the normal water-temperature rise in that channel	None
$F_{\Delta T}$	Ratio of the maximum temperature difference through a fuel element as compared to the normal temperature difference at this location	None
F_θ	Ratio of the maximum film-temperature difference between the fuel-element surface temperature and the water temperature to the normal temperature-difference at this location	None
h	Heat transfer coefficient	Btu/(hr)(sq ft)(°F)
H	Enthalpy	Btu/(lb)
k	Thermal conductivity	Btu/(hr)(ft)(°F)
k_b	Thermal conductivity of bond space or bond alloy	Btu/(hr)(ft)(°F)
k_c	Thermal conductivity of clad	Btu/(hr)(ft)(°F)
k_f	Thermal conductivity of fuel	Btu/(hr)(ft)(°F)
l	Length along fuel element to position designated by primes	ft
L	Length of fuel element	ft
p	Pressure	lb _f /sq ft
P_p	Pumping power	ft-lb _f /hr
q	Heat transfer per unit time	Btu/hr
q	Heat transfer per unit time per unit length of fuel element parallel to flow	Btu/(hr)(ft)
q''	Heat flux	Btu/(hr)(sq ft)
q'''	Volume heat generation	Btu/(hr)(cu ft)
Q	Total reactor power output	Btu/hr
r	Radius	ft
r_b	Radius of fuel element at the inner surface of clad	ft
r_c	Radius of fuel element at the outer surface of clad	ft
r_f	Radius of fuel element at the outer surface of fuel	ft
r_s	Radius of fuel element at the outer surface of scale	ft
R	Thermal resistance	(hr)(°F)/Btu
R_b	Thermal resistance of the bond between fuel and clad	(hr)(°F)/Btu
R_c	Thermal resistance of the clad	(hr)(°F)/Btu
R_f	Thermal resistance of fuel	(hr)(°F)/Btu
R_h	Thermal resistance of the water film	(hr)(°F)/Btu

Table 1.7.1 —(Continued)

Symbol	Definition	Unit*
R_s	Thermal resistance of the scale	(hr)(°F)/Btu
R'	Modified thermal resistance	(hr)(sq ft)(°F)/Btu
R'_b	Modified thermal resistance of bond	(hr)(sq ft)(°F)/Btu
R'_c	Modified thermal resistance of clad	(hr)(sq ft)(°F)/Btu
R'_f	Modified thermal resistance of fuel	(hr)(sq ft)(°F)/Btu
R'_h	Modified thermal resistance of water film	(hr)(sq ft)(°F)/Btu
R'_s	Modified thermal resistance of scale	(hr)(sq ft)(°F)/Btu
t	Water temperature	°F
T	Fuel-element temperature	°F
v	Velocity	ft/hr
W	Total flow rate	lb/hr
Δp	Pressure drop	lb _f /sq ft
Δt	Fluid temperature rise	°F
ΔT	Temperature difference through fuel element	°F
δ	Fraction of heat that enters channel up to certain point designated by primes	None
Δx	Thickness	ft
Δx_b	Thickness of bond	ft
Δx_c	Thickness of the cladding	ft
Δx_b	Thickness of fuel measured from the centerline	ft
Δs	Thickness of scale	ft
θ	Film temperature difference	°F
ϕ_a	Ratio of axial heat flux to the average heat flux as designated by primes	None
ϕ_r	Ratio of maximum transverse heat flux to the average transverse heat flux	None
Subscripts		
ave	Average	
in	Inlet	
max	Maximum	
out	Outlet	
Superscripts		
"	Position along the length of the channel at which the maximum surface-temperature occurs	
'''	Position along the length of the channel at which the maximum internal-temperature occurs	

* Pounds mass used unless otherwise noted; lb_f signifies pounds force

A decrease in inlet-water temperature (t_{in}) in the reactor is usually reflected by increased cost. When heat is rejected directly to the heat sink, a reduction in t_{in} will require the addition of a refrigeration system. If the primary-coolant system discharges the heat through a heat-exchanger to the heat sink, a reduction in t_{in} results in a lower temperature difference in the heat exchanger, a necessary increase in heat-exchanger size for the same power, and a consequent increase in cost. Where useful power is being produced, a reduction in inlet temperature results in a corresponding decrease in the steam pressure to the power turbine.

In the second (microscopic) phase of thermodynamic analysis of the reactor, the shape, size, number, and arrangements of fuel elements and the size and shape of the reactor,

Table 1.7.2—Conversion Factors

To convert from English unit	To CGS unit	Multiply by
sq ft	cm ²	929
Btu/(lb)(°F)	cal/(gm)(°C)	1
Btu/lb	cal/gm	0.5555
Btu/(hr)(sq ft)(°F)	cal/(sec)(sq cm)(°C)	1.356×10^{-4}
Btu/(hr)(sq ft)(°F)	watt/(sq cm)(°C)	5.676×10^{-4}
Btu/(hr)(sq ft)(°F)	cal/(sec)(cm)(°C)	4.133×10^{-3}
Btu/(hr)(ft)(°F)	watt/(cm)(°C)	1.73×10^{-2}
ft	cm	30.48
lb _f /sq ft	dyne/sq cm	479
ft-lb _f /hr	cm-dyne/gm	2.987×10^4
Btu/hr	cal/sec	7×10^{-2}
Btu/hr	watt	0.293
Btu/(hr)(ft)	cal/(sec)(cm)	2.295×10^{-3}
Btu/(hr)(ft)	watt/cm	9.62×10^{-3}
Btu/(hr)(sq ft)	cal/(sec)(sq cm)	7.53×10^{-5}
Btu/(hr)(sq ft)	watt/sq cm	3.15×10^{-4}
ft/hr	cm/sec	8.47×10^{-3}
lb/hr	gm/sec	0.126

itself, are determined consistent with the nuclear requirements. It is desirable to design the reactor with fuel elements and assemblies that are reliable and easily manufactured. The analytical procedure is usually one of trial and error in which a particular design is analyzed and the resulting temperatures, pressure drop, and pumping power determined. If certain nuclear or thermodynamic limitations (discussed later) are exceeded, modifications and another analysis are made. This procedure is followed until a successful design is obtained.

CALCULATION OF TEMPERATURE DISTRIBUTION

The basic law of steady-state uni-directional heat conduction¹ without heat generation is:

$$-q = kA \frac{\Delta T}{\Delta x} \quad (3a)$$

or:

$$\Delta T = \left(\frac{\Delta x}{kA} \right) (-q) \quad (3b)$$

The equation for steady-state heat transfer by convection is:

$$q = hA (T - t) \quad (4a)$$

¹Reference appears at end of chapter.

or:

$$(T - t) = \left(\frac{1}{hA} \right) (q) \quad (4b)$$

Both equations (3b) and (4b) state that the temperature difference is directly proportional to a thermal resistance and the quantity of heat being transmitted.

There are normally five resistances to heat flow in a fuel element, namely: the uranium fuel itself; the bond or lack of bond between the fuel clad and the uranium; the fuel clad; deposits, scale, or corrosion productions on the surface of the fuel element in contact with the water; and finally, the film heat-transfer coefficient.

For preliminary design work, it is usually assumed that all of the heat generated in the fission process is released as heat in the fuel core of the fuel element. Heat transfer is therefore that of heat conduction with internal heat generation. This assumption results in higher calculated fuel-element temperatures throughout the reactor. In more detailed calculations, a more realistic assumption is that most of the heat is generated in the fuel core and the remainder in the control rods, construction materials, coolant, and materials external to the core. Other assumptions usually made are that the thermal conductivity is constant (independent of temperature) and that the conductivity value is the mean value occurring within the material. It is also usually assumed that heat is generated uniformly within the fuel core and that no longitudinal heat conduction occurs along the fuel element.

Figure 1.7.1 shows three simple types of fuel elements. The temperature distribution in the fuel portion of each [with a uniform rate of heat generation rate in the fuel of q''' Btu/(ft³)(hr)] is parabolic, and the temperature differential through the fuel portion for each type is:

$$\text{Plates:} \quad T_u - T_f = \frac{(\Delta x_f)^2 q'''}{2k}$$

$$\text{Cylinders:} \quad T_u - T_f = \frac{r_f^2 q'''}{4k}$$

$$\text{Spheres:} \quad T_u - T_f = \frac{r_f^2 q'''}{6k}$$

The temperature differences stated above can be expressed in terms of the total heat, q , released from the fuel-element surface area, A_f , and a thermal resistance. Conversion of the above expressions results in:

$$\text{Plates:} \quad T_u - T_f = \frac{\Delta x_f}{2k_f A_f} (q) \quad (5)$$

$$\text{Cylinders and spheres:} \quad T_u - T_f = \frac{r_f}{2k_f A_f} (q) \quad (6) \quad \checkmark$$

The thermal resistance in the fuel is therefore $\Delta x_f / 2k_f A_f$ for plates and $r_f / 2k_f A_f$ for cylinders and spheres. Thermal resistances in series may be added, just as in the case of electrical resistances. This analogy is particularly helpful in the case of fuel elements in which several resistances are normally in series. The various thermal resistance (R)

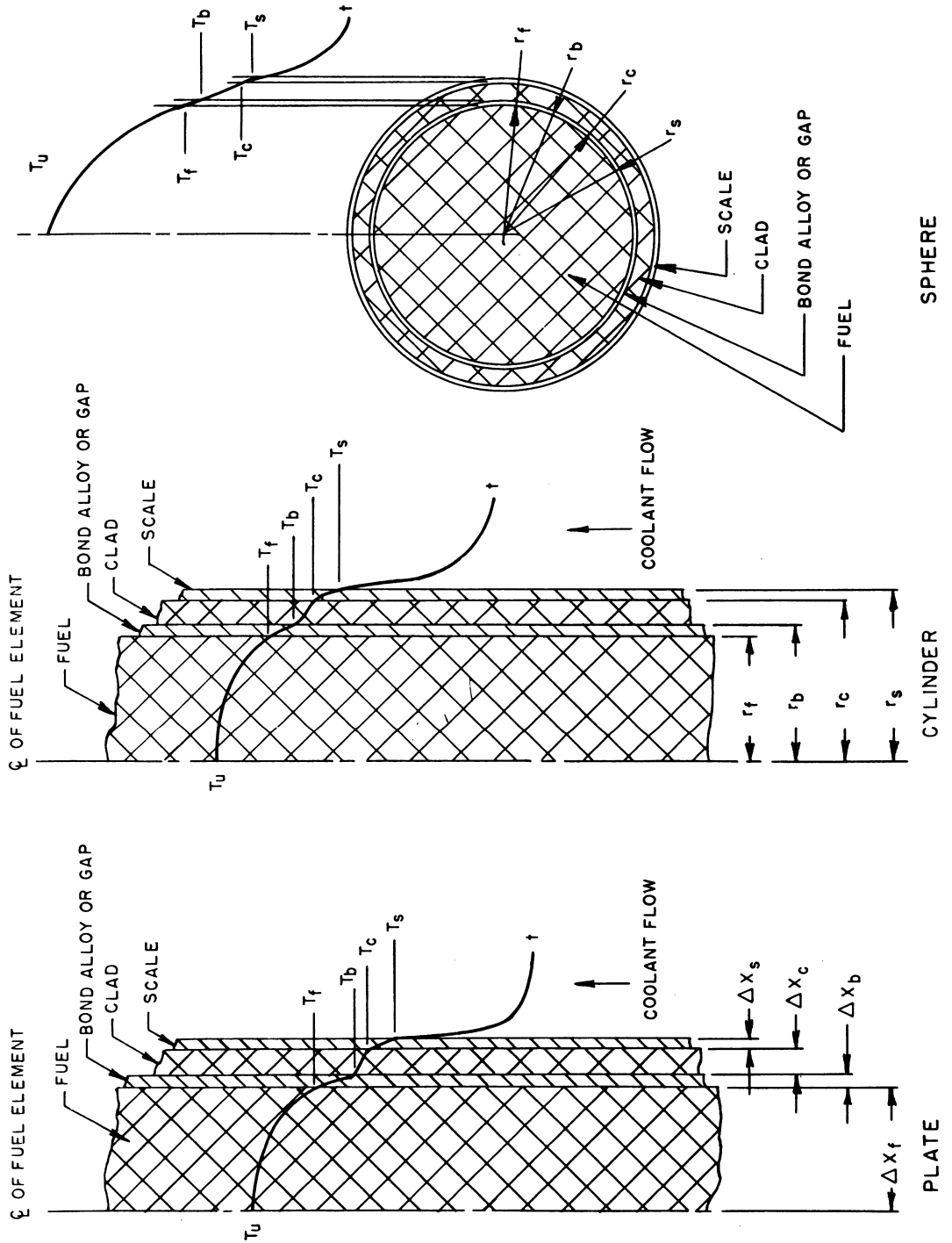


Fig. 1.7.1— Typical Fuel-element Geometries. Submitted by Argonne National Laboratory, Dec. 15, 1952.

formulae are given in Table 1.7.3 for the three simple fuel-element geometries sketched in Fig. 1.7.1.

The thermal-resistance term is used as follows: Two metal temperatures, namely, the surface temperature of the clad (T_c) and the internal fuel temperature (T_u), generally

Table 1.7.3 — Thermal-resistance Formulae for Plates, Cylinders, and Spheres

Type of resistance	Type of fuel element		
	Plane plate	Cylinder	Spheres
Film (R_h)	$\frac{1}{hA}$	$\frac{1}{2\pi r_s Lh}$	$\frac{1}{4\pi r_s^2 h}$
Scale (R_s)	$\frac{1}{k_s A / \Delta X_s}$	$\frac{1}{2\pi k_s L / \ln(r_s / r_c)}$	$\frac{1}{4\pi k_s} \left(\frac{1}{r_s} - \frac{1}{r_c} \right)$
Clad (R_c)	$\frac{1}{k_c A / \Delta X_c}$	$\frac{1}{2\pi k_c L / \ln(r_c / r_b)}$	$\frac{1}{4\pi k_c} \left(\frac{1}{r_c} - \frac{1}{r_b} \right)$
Bond (R_b)	$\frac{1}{k_b A / \Delta X_b}$	$\frac{1}{2\pi k_b L / \ln(r_b / r_f)}$	$\frac{1}{4\pi k_b} \left(\frac{1}{r_b} - \frac{1}{r_f} \right)$
Fuel (R_f)	$\frac{1}{2k_f A / \Delta X_f}$	$\frac{1}{4\pi k_f L}$	$\frac{1}{8\pi k_f r_f}$

limit a reactor design. It is usually desirable to relate these temperatures to the bulk-fluid temperature (t), as given below. Surface temperature of clad limiting:

$$T_c - t = (R_h + R_s) (q)$$

or:

$$q = \frac{T_c - t}{R_h + R_s} \quad (7)$$

Internal fuel temperature limiting:

$$q = \frac{T_u - t}{R_h + R_s + R_c + R_b + R_f} \quad (8)$$

The thermal resistance for cylinders and spheres may be simplified by using a mean heat-flow area for each thermal resistance, based on the arithmetic mean radius, if the radius ratios are less than 1.4 for cylinders and 1.2 for spheres. A modified thermal resistance may then be defined as $R \cong R'/A$ in which the area term is removed from the resistance term. Thus, Eqs. (7) and (8) in terms of modified resistance are:

$$q = \frac{A_0(T_c - t)}{R'_h + \frac{A_0}{A_s} R'_s} \quad (9)$$

$$q = \frac{A_0(T_u - t)}{R'_h + \frac{A_0}{A_s} R'_{hs} + \frac{A_0}{A_c} R'_c + \frac{A_0}{A_b} R'_b + \frac{A_0}{A_f} R'_f} \quad (10)$$

Where the mean area is defined as:

Mean area	For cylinders	For spheres
A_s	$\pi (r_s + r_c)L$	$\frac{4\pi}{2} (r_s + r_c)^2$
A_c	$\pi (r_c + r_b)L$	$\frac{4\pi}{2} (r_c + r_b)^2$
A_b	$\pi (r_b + r_f)L$	$\frac{4\pi}{2} (r_b + r_f)^2$
A_f	$2\pi (r_f)L$	$4\pi (r_f)^2$

The error introduced by this simplification is less than 1 percent. The values for the modified thermal resistance are therefore identical for the three simple fuel elements considered, if the Δx 's are considered as thickness of clad, bond, scale, and fuel. The values are given in Table 1.7.4.

Table 1.7.4—Modified Thermal-resistance Formulae for Plates, Cylinders, and Spheres

Type of resistance	Formula
Film (R'_h)	$\frac{1}{h}$
Scale (R'_s)	$\frac{1}{k_s/\Delta x_s}$
Clad (R'_c)	$\frac{1}{k_c/\Delta x_c}$
Bond (R'_b)	$\frac{1}{k_b/\Delta x_b}$
Fuel (R'_f)	$\frac{1}{2k_f/\Delta x_f}$

DESIGN LIMITATIONS AND CRITERIA

It is generally necessary to establish the effect of design variables on performance and operation in the initial design phase of a water-cooled, solid-fuel reactor. For convenience, design variables have been separated into two types: design limitations and design criteria. Values are assigned to some of these design variables (design limitations) to maintain consistency in the adjustment of the other variables (design criteria) in order to determine the best design for a specific reactor. Design limitations are imposed primarily by stress, temperature, and corrosion to assure successful reactor operation. Design criteria are used in evaluating pressure-vessel size, pumping costs, effect of scale on

heat transfer, and other conditions to assure a sound, economical, practical design. The particular objective of a reactor design will dictate the relative importance of the design limitations and the design criteria. In addition, the particular design will dictate the values that may be assigned to the various design limitations and the practicability of assigning various design criteria.

DESIGN LIMITATIONS

The following limitations are typical of the restrictions which may be imposed on a design by stress, corrosion, or heat-removal considerations:

MAXIMUM FUEL TEMPERATURE (T_u)

Fuel temperature is limited to prevent (1) phase changes in the fuel metal or alloy resulting in an excessive dimensional change in the fuel element or (2) exceeding the structural strength of the fuel. }

MAXIMUM SURFACE TEMPERATURE (T_s)

The temperature of the clad surface is limited to (1) the temperature corresponding to the maximum permissible rate for corrosion or (2) the saturation temperature corresponding to the static pressure necessary to prevent boiling of the coolant. }

MAXIMUM TEMPERATURE DIFFERENCE THROUGH A FUEL ELEMENT (ΔT_{max})

Temperature differences may be limited by the allowable thermal stress in the fuel element where extreme repeated temperature fluctuations are encountered or brittle materials are used. }

MAXIMUM COOLANT TEMPERATURE (t_{out})

The temperature of outlet fluid is limited to (1) maintain all liquid phase and prevent vapor binding of pumps or (2) prevent excessive corrosion of pressure vessels, piping, or other external equipment.

MAXIMUM WATER-TEMPERATURE RISE (Δt_{max})

The temperature rise may be limited by the maximum allowable thermal stresses or by distortions which may be developed in the reactor internal structure or in pressure vessels during sudden changes in power level.

BURNOUT OF A FUEL ELEMENT

Burnout occurs when a sufficient blanket of steam is formed on the heat-transfer surface to effectively insulate the fuel element and thus cause a rapid rise in metal temperature. In a reactor using net or local boiling as the heat-transfer mechanism, the design heat flux or power level should be limited to a value sufficiently below the burnout heat flux or power level.

DENSITY (ρ)

Density changes may be caused by corresponding periodic fluctuations in power level or by steady-state operation at various power levels. These density changes should be considered as functions of the compensation ability of the control system. In a reactor using net or local boiling as the heat-transfer mechanism, the amount of permissible density change should be considered as a design limitation.

MAXIMUM FLUID VELOCITY (V_{max})

Erosion of clad materials at high velocities should be considered in determining the maximum coolant velocity past the fuel elements. High coolant velocities in headers and plenum chambers may result in jetting of the fluid and maldistribution of flow.

DESIGN CRITERIA

Design criteria are general considerations in the design of a particular reactor and usually cannot be assigned specific values. Engineering judgment and evaluation of the specific design will dictate the relative importance of these criteria and their effect on the over-all design. The following criteria suggest some aspects of a design which may become critical.

THERMAL RESISTANCE OF CLADDING BOND ($\Delta x_b/k_b A_b$)

The bond between the clad and fuel alloy has a certain thermal resistance depending upon the type of bond obtained; generally, a mechanical bond has a significant resistance whereas a good metallurgical bond has a minimum resistance.

THERMAL RESISTANCE OF SCALE ON HEAT-TRANSFER SURFACE ($\Delta x_s/k_s A_s$)

Scale may be formed by corrosion products of clad material and/or by corrosion products formed elsewhere in the system and deposited on the heat-transfer surface. A value of the thermal resistance of the scale, based on these considerations, is used in calculating fuel-element temperatures.

MINIMUM THICKNESS OF FUEL ELEMENTS AND CLAD ($\Delta x_f, \Delta x_c$)

The minimum thickness is that which (1) may be practically achieved in manufacturing and (2) provides sufficient clad to protect the fuel from exposure to the coolant by corrosion or erosion.

PRESSURE (p)

The operating pressure for single-phase coolant systems is prescribed by the maximum surface temperature and is that pressure which will inhibit boiling at that location.

PRESSURE DROP (ΔP)

The permissible pressure drop is evaluated by consideration of (1) pressure stresses on fuel elements and fuel-element subassemblies and (2) the availability and size of pumps to produce desired flow at the given head loss.

PUMPING POWER (P_p)

The power available for pumping is determined by (1) percentage of total reactor power assigned for pumping or (2) amount of economically available power procured from outside facilities.

INLET- AND EXIT-HEADER SIZE

In designs using a pressure vessel, the number, size, and spacing of openings in the vessel effect the pressure stresses of the vessel. In designs incorporating a low static pressure, the problem is one of supplying large quantities of water to a relatively small plenum chamber with reasonable velocities and pressure drops in the ducts.

PRESSURE-VESSEL SIZE

The practical pressure-vessel size, particularly the diameter, is evaluated as a balance between design pressure and manufacturing and transportation facilities.

PLANT SIZE AND WEIGHT

For mobile application, minimum size and weight considerations are of primary importance and dictate stringent requirements during all phases of reactor design.

RELATIONSHIPS BETWEEN DESIGN LIMITATIONS AND DESIGN VARIABLES

Solid-fuel reactors can be subdivided into two general types, heterogeneous and quasi-homogeneous, based on nuclear considerations. In the heterogeneous type, fuel is lumped with the fuel elements being placed on the reactor lattice points. Cooling is provided by the circulation of water past these fuel elements. Thermodynamically, the flow channels surrounding the fuel elements can be treated individually. In the quasi-homogeneous type, fuel is distributed throughout the core of the reactor in a uniform manner, usually with alternate spacing of fuel element and coolant. In most cases, the fuel elements form individual flow channels such as those formed by parallel plates.

In the analyses, the performance of the reactor and the fuel elements is determined by the performance of a single channel, called the "hot channel." A hot channel is that flow channel (or fictitious flow channel in the case of discontinuous fuel elements) which contains the fuel element with greatest surface temperature, greatest temperature differences, and/or highest internal temperature in the reactor. This channel is usually the channel having the highest heat production owing to a non-uniform neutron-flux distribution.

In preliminary design work, approximate flux distributions are obtained as mathematical expressions by making simplifying assumptions. These expressions can be used in mathematical form to obtain the temperature distribution. However, these cases are very specific and generally very difficult to handle. It is simpler to graphically integrate the calculated flux-distribution curve to obtain the temperatures along the length of a channel. Figure 1.7.2 shows the typical temperature distribution in fuel elements in the direction of flow. In the case of discontinuous fuel elements, such as the flow across wires, the temperature distribution would be discontinuous; however, the equations to be given are also applicable.

Since the temperatures to be calculated are maximum temperatures, it is usually necessary to determine graphically where the maximum surface temperature and maximum internal temperature will occur along the channel. To simplify the analytical procedure, several quantities will be defined. The fraction of total heat input that enters the flow-stream up to the point where the maximum nominal surface temperature exists is defined as:

$$\delta'' = \frac{\int_0^{l''} q' dl}{\int_0^L q' dl} \quad (11)$$

The fraction of total heat that enters the flow-stream up to the point of maximum nominal internal temperature is:

$$\delta''' = \frac{\int_0^{l'''} q' dl}{\int_0^L q' dl} \quad (12)$$

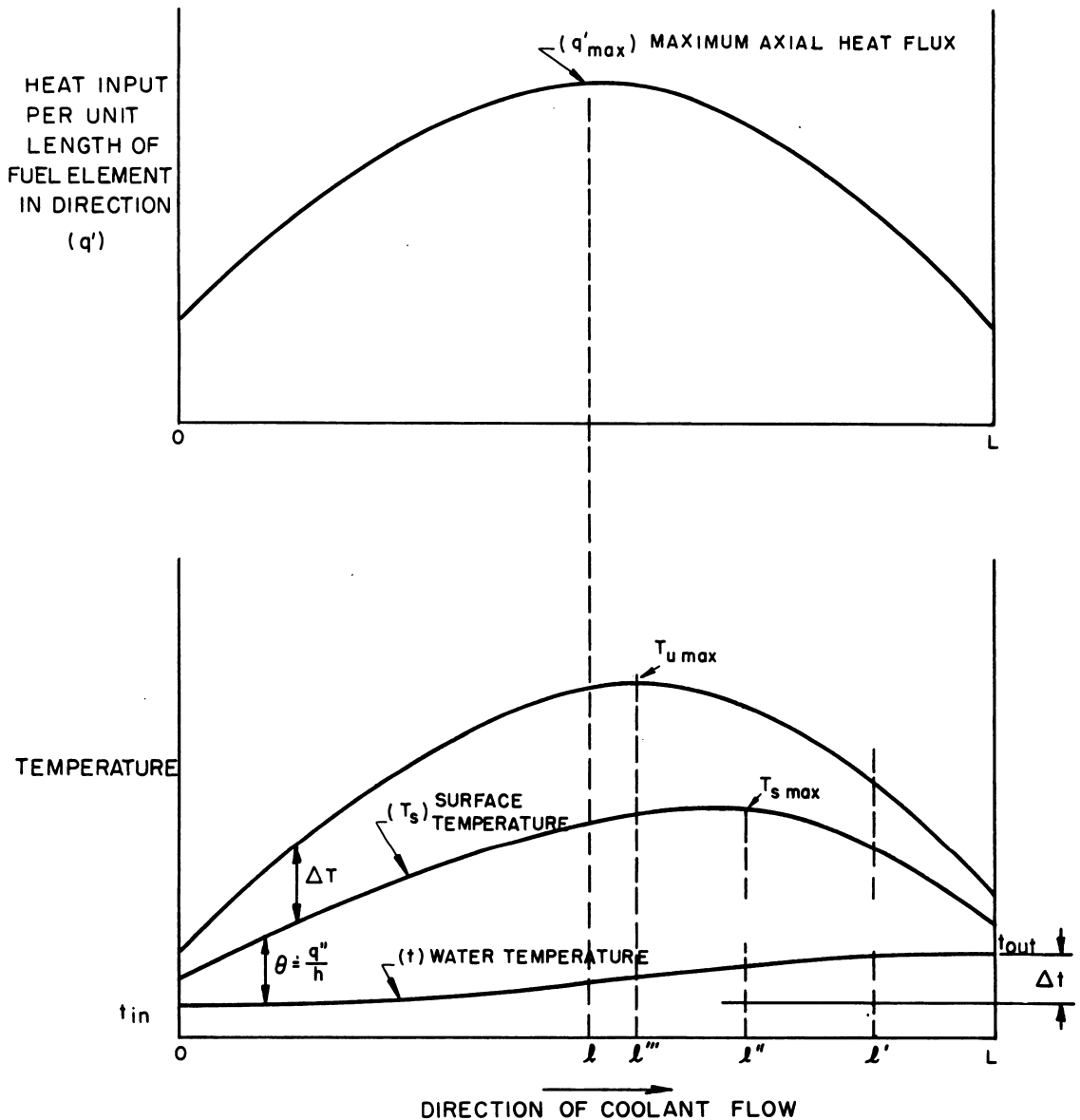


Fig. 1.7.2— Typical Temperature Distribution in a Fuel Element. Submitted by Argonne National Laboratory, Dec. 15, 1952.

Basically, the equations developed are expressions for three temperature differences: the water temperature rise (Δt), the film temperature difference (θ) between the bulk-water temperature and the metal surface, and finally, the temperature difference between the center and the surface of a fuel element (ΔT). The maximum nominal surface temperature is obtained by adding the appropriate water-temperature rise up to the position l'' and the film temperature difference at the position l'' to the inlet water temperature. Similarly, the maximum nominal internal temperature can be obtained by adding the appropriate

water-temperature rise up to the position l''' and the film temperature drop and temperature difference through a fuel element at the position l''' to the inlet-water temperature.

To estimate the maximum possible temperatures that may occur within the reactor and thereby maintain the temperatures within the specified design limitations, uncertainties in flow conditions, heat generation, fuel-element fabrication, and analytical variables must be anticipated. Typical variables that can produce higher-than-nominal temperatures are tabulated in Table 1.7.5, including an order of magnitude of each effect on the coolant-temperature rise, the film-temperature differential, and the temperature drop from center of fuel element to surface. The values shown in the table are intended to be used only as a guide in general reactor work, as the order of magnitude of the individual factors may be varied considerably and both the applicable factor and its magnitude depends on the particular reactor. In a particular design, it should be recognized that some of the factors are based on estimates of reactor operating conditions while others, such as the effect of manufacturing tolerances, are based on detailed physical analyses.

Table 1.7.5—Hot-spot Factors Used in Typical Design

Uncertainty or deviation from nominal condition	Order of magnitude of factor involved		
	$F_{\Delta t}$	F_{θ}	$F_{\Delta T}$
Effect of plenum-chamber conditions upon flow distribution to parallel reactor channels	1.02	1.02	...
Effect of warping	1.04	1.03	...
Combined effect of tolerances on core alloy in fuel element, both in thickness and concentration	1.08	1.21	1.21
Combined effect of tolerances on clad-thickness and water-channel dimension	1.40	1.26	...
Precision of flux-distribution calculation	1.20	1.20	1.20
Local variations in axial, heat-flux distribution, such as the Wilkins effect (this factor may be included as a flux-ratio factor)	...	1.10	1.10
Precision of flux distribution radially or through the thickness of a fuel element	1.10
Accuracy of the thermal conductivity of the fuel-element material	1.20
Precision of the correlation for the heat-transfer coefficient	...	1.20	...
Variation of heat-transfer coefficient on the fuel-element surface	...	1.50	...
Precision of power measurement resulting in deviations in design-power output	1.10	1.10	1.10
If the power output of each channel is monitored by noting its temperature rise, all of the individual factors for $F_{\Delta t}$ may be neglected except for one to account for inaccuracies in measuring each temperature rise	1.10
If the coolant channels should be interconnected, then most all factors on $F_{\Delta t}$, water temperature rise may be disregarded with the exception of a factor for deviations from theoretical mixing	1.3

It is assumed for conservative design that the individual effects all occur simultaneously in the same channel, the channel exposed to the highest heat generation. The use of hot-spot factors gives reasonable assurance that these temperatures will never exist within the reactor or that, if they do, they will occur only at certain limited, perhaps microscopic locations. This procedure is especially applicable to designs where the penalty for exceeding temperature limitations is severe.

The combined effect of all the individual variables is obtained as a composite product of the individual factors, to yield over-all hot-spot factors for water-temperature rise, $F_{\Delta t}$, film drop, F_θ , and fuel-element temperature differential, $F_{\Delta T}$. Their use, as shown below, then gives the maximum possible water-temperature rise in a channel and the maximum possible surface and fuel-element temperatures.

The average temperature rise in a reactor is obtained from Eq. (2) as:

$$\Delta t_{ave} = \frac{Q}{c_p W} \quad (13)$$

The water-temperature rise in the hottest channel or channel with the maximum heat input is obtained by multiplying the average water-temperature rise by the ratio of the maximum transverse flux to the average transverse flux.

The maximum possible water-temperature rise is obtained by multiplying the water-temperature rise in the channel with maximum heat input by the hot-spot factor for the water-temperature rise. If individual channels or groups of channels are orificed to proportion the flow according to the radial flux distribution or if the channels are interconnected, an additional factor must be allowed for this effect.

In symbols:

$$\Delta t_{max} = \Delta t_{ave} F_{\Delta t} \phi_r F_m F_\theta = \frac{Q}{c_p W} F_{\Delta t} \phi_r F_m F_\theta \quad (14)$$

where: $F_{\Delta t}$ = hot-spot factor for water-temperature rise

ϕ_r = ratio of maximum radial flux to the average radial flux

F_m = factor to account for theoretical mixing. For individual channels, $F_m = 1$. For flow in interconnected channels, F_m would be less than 1 but greater than $1/\phi_r$

F_θ = factor to account for orificing. Without orificing, $F_\theta = 1$. With orificing of each individual continuous channels, $F_\theta = 1/\phi_r$

The water temperature rises up to the points of maximum internal temperatures are given as:

$$\Delta t \text{ (to } t_{c \text{ max}}) = \frac{Q}{c_p W} F_{\Delta t} \phi_r F_m F_\theta \delta'' \quad (15)$$

$$\Delta t \text{ (to } T_{u \text{ max}}) = \frac{Q}{c_p W} F_{\Delta t} \phi_r F_m F_\theta \delta''' \quad (16)$$

It may be desirable in some cases to substitute the fluid velocity for the flow rate, especially in cases where the velocity is limiting. In general:

$$W = \rho V_a F_\theta \quad (17)$$

The average heat flux in a reactor is given as:

$$q''_{\text{ave}} = \frac{Q}{A} \quad (18)$$

Using the expression for the average heat flux, the film-temperature difference at the point of the maximum surface temperature can be written as:

$$\theta \text{ (at } t_{c \text{ max}}) = q''_{\text{ave}} F_{\theta} \phi_r \phi'_a (R'_b + R'_s) = \frac{Q}{A} F_{\theta} \phi_r \phi'_a (R'_b + R'_s) \quad (19)$$

and:

$$\theta \text{ (at } T_{u \text{ max}}) = q''_{\text{ave}} F_{\theta} \phi_r \phi'''_a (R'_b + R'_s) = \frac{Q}{A} F_{\theta} \phi_r \phi'''_a (R'_b + R'_s) \quad (20)$$

The maximum surface temperature can therefore be written as:

$$T_{c \text{ max}} = t_{\text{in}} + \Delta t \text{ (to } T_{c \text{ max}}) + \theta \text{ (at } T_{c \text{ max}}) \quad (21)$$

$$T_{c \text{ max}} = t_{\text{in}} + \frac{Q}{c_p W} F_{\Delta t} \phi_r F_m F_{\theta} \delta'' + \frac{Q}{A} F_{\theta} \phi_r \phi'_a (R'_h + R'_s) \quad (22)$$

The maximum internal temperature can be written as:

$$T_{u \text{ max}} = t_{\text{in}} + \Delta t \text{ (to } T_{u \text{ max}}) + \theta \text{ (at } T_{u \text{ max}}) + \Delta T \text{ (at } T_{u \text{ max}}) \quad (23)$$

$$= t_{\text{in}} + \frac{Q}{c_p W} F_{\Delta t} \phi_r F_m F_{\theta} \delta''' + \frac{Q}{A} F_{\theta} \phi_r \phi'''_a (R'_h + R'_s) + \frac{Q}{A} F_{\Delta t} \phi_r \phi_a (R'_c + R'_b + R'_f) \quad (24)$$

In the preliminary evaluation of the effect of design variables on a given design, it is usually sufficiently accurate to assume approximate values of ϕ'_a , ϕ'''_a , δ'' and δ''' . Estimates are also made of the hot-spot factors, $F_{\Delta t}$, F_{θ} , and $F_{\Delta T}$, and the mixing and orificing factors, F_m and F_{θ} . With these factors assumed, the equations reduce to a form in which the effect of the flow area of the reactor, the total heat transfer area, and the fuel-element geometry can be studied.

Another major consideration in reactor design is the pressure drop and pumping power required to obtain the desired heat-transfer performance. The formulas for pressure drop are given in Chapter 1.5. The formula for fluid pumping power is given as:

$$P_p = \frac{W \Delta p}{\rho} \quad (25)$$

Normally, three temperatures determined by the performance of the hottest channel are limiting in a design: the minimum inlet temperature (t_{in}), the maximum surface temperature (T_c), and the maximum internal fuel temperature (T_u).

Equations (22) and (24) demonstrate that a power increase will result in a proportional increase in the rise in water temperature (Δt), in the film temperature difference (θ), and in the temperature difference through a fuel element (ΔT). Since it is usually desired to increase the power of the reactor without a corresponding increase in the temperature differences between the surface and the inlet water ($T_c - t_{\text{in}}$) and the temperature difference between the internal fuel and the inlet water in the hot channel ($T_u - t_{\text{in}}$), changes

must be made in certain other variables. For maximum effectiveness, changes in design parameters should be made which reduce the largest of the contributing temperature differences in a particular design. A list of changes and the general results produced are given below. Each change is considered to occur without altering any of the other variables.

(1) Reactor channels may be orificed for proper flow distribution by adjusting the flow in each channel to obtain the same water-temperature rise in every channel. Another method, not commonly used, is to orifice each channel to permit the maximum surface temperature and the maximum internal temperature to occur simultaneously in all of the channels. Flow distribution by orificing reduces the amount of water needed for cooling and the thermal stress between fuel elements since the differences in the average temperature between individual fuel elements is minimized. For fuel elements in the form of rods, wires, spheres, or any other discontinuous form, orificing cannot be effectively used. For these cases, however, mixing will tend to equalize the outlet temperatures throughout the outlet-flow cross section.

(2) Increasing the flow rate decreases the water-temperature rise and decreases the film-temperature difference. For the same flow area, an increase in flow is accompanied by an increase in velocity. Therefore, the heat-transfer coefficient increases and the film-temperature-drop decreases. The pressure drop and pumping power increase with an increase in flow rate.

(3) Decreasing the flow cross section of the reactor, without altering the heat-transfer area or flow rate, increases the velocity. Therefore, as stated in (2), the film-temperature-difference decreases. The pressure drop and pumping power increase with a decrease in cross section.

(4) Increasing the number of passes of the coolant through the reactor by the use of baffling increases the velocity, thereby decreasing the film-temperature drop. The pressure drop and pumping power increase with an increase in the number of passes.

(5) Decreasing the amount of scaling or corrosion of the fuel-element surface decreases the thermal resistance of the scale and therefore decreases the film-temperature difference. Since the surface is smoother with less scale, the pressure drop and pumping power probably decrease.

(6) Decreasing the thickness of the fuel elements permits more heat-transfer area to be placed in the reactor volume with the same flow area. This change results in a decrease in the film-temperature difference and in the temperature drop through the fuel elements. The pressure drop and pumping power normally increase for a decrease in the fuel-element thickness.

(7) Decreasing the maximum-to-average heat-production distribution by the proper use of nuclear poisons or enriched fuels decreases the three temperature differences without increasing pressure drop or pumping power. In cases where the internal temperature is limiting and the fuel elements are relatively thick, as in production reactors, it is desirable to have the heat-generation distribution as uniform as possible in both the axial and transverse directions. This flattened-flux distribution not only reduces the temperature drop through the fuel element but also decreases the film-temperature difference and water-temperature rise in cases where orifices are not used.

(8) When the internal fuel temperature is not limiting and the fuel-element thicknesses are small, as in small enriched power reactors, it may be advantageous to use a roof-top flux distribution. Roof-topping involves adjusting the heat-generation distribution in the axial or flow direction to maintain surface temperature (T_c) constant at the maximum limiting value. The variation of the heat-transfer coefficient with water temperature along the length of the channel should be considered in determining the roof-topped flux distribution. If surface temperature is the only limitation, more power can be obtained from the hottest channel (and therefore the reactor) by roof-topping than with any other flux distribution.

(9) Decreasing the pressure of the system to permit local boiling decreases the film-temperature difference. However, pressure drop and pumping power probably increase, and the complexity of the problems associated with flow in parallel channels and flow stability increases. The density changes associated with local boiling may increase problems of reactor control. In general, the safety of the reactor decreases since the design condition is closer to the burnout conditions. If local boiling is to be employed as the heat-transfer mechanism to advantage, care should be taken to eliminate scale.

(10) Distribute the fuel and coolant in such a manner as to accomplish either a constant coolant temperature rise for each channel or a constant maximum fuel temperature, the result to be accomplished to depend on which limitation controls or which result gives the maximum power.

REFERENCES

1. M. Jakob, Heat Transfer, Vol. 1, John Wiley and Sons, Inc., New York, 1949.
2. Argonne Nat. Lab., ANL-4683, Sept. 15, 1951, p. 20 (classified).
3. R. N. Lyon and W. B. Harrison, Oak Ridge Nat. Lab., ORNL-CF-52-1-76 (classified).

CHAPTER 1.8

Transient Generation and Removal of Heat

J. P. Silvers and J. R. Dietrich

Chapter 1.6 of Volume 1 contains a comprehensive treatment of reactor dynamics. The following paragraphs contain some supplementary information of particular use in the treatment of water-cooled reactors. The nomenclature employed in these paragraphs is defined in Table 1.8.1.

TRANSIENTS WHEN REACTIVITY IS INDEPENDENT OF POWER LEVEL

In a supercritical or subcritical reactor, the power increases or decreases, respectively, with time. Although in the general case the spatial distribution of power generation as well as the power level may vary with time, it is entirely adequate for practical reactor design to assume that the spatial distribution remains the same as that for the critical reactor of the same configuration. Any departures from this distribution will exist for only a few average neutron-generation times and will be small in magnitude so long as the departure from criticality is limited to a few percent. By making this approximation, the spatial distribution of power generation may be treated by the methods discussed in Volume 2, Chapter 1.6, and if reactivity is independent of power level, the time variation of power level can be determined by solution of the space-independent one-group equation as discussed in Volume 1, Chapter 1.6. Since most water-cooled reactors have rather large temperature coefficients of reactivity, the assumption that reactivity is independent of power level is applicable only for power levels so low that they produce no important temperature increase in the reactor or for transients so rapid that large power changes may occur before the resultant heat can be transferred to the regions of the reactor which are effective in changing the reactivity. When the reactivity is independent of the power level, the important dynamic characteristics of the reactor depend upon only the effective neutron-generation time in the reactor and the characteristics of the available delayed-neutron emitters. Delayed-neutron data are contained in Volume 1, Table 1.2.16 (curves of use in solving the kinetic equation with the delayed neutrons characteristic of U^{235} are contained in Volume 1, Chapter 1.6). Reactors containing large quantities of D_2O or Be may have a small additional contribution to the delayed neutrons as a result of γ - η reactions involving delayed-fission gammas.

Neutron-generation times in existing H_2O -moderated reactors lie in a range around 10^{-4} second, while those in existing D_2O -moderated and graphite-moderated reactors are in the neighborhood of 10^{-3} second. Calculated generation times¹⁻⁵ for a number of specific re-

¹References appear at end of chapter.

Table 1.8.1 — Nomenclature and Units

Symbol*	Definition	Units
a, b, d	Physical measurements, constant	ft
A ₁ , A ₂ etc.	Equation constants	Dependent upon usage
A _w	Wetted surface area in core	sq ft
B ₁ , B ₂ , B ₃	Equation constants	Dependent upon usage
c	Heat capacity	Btu/(lb)(°F)
C ₁ , C ₂	Equation constants	Dependent upon usage
h	Coefficient of convective heat transfer	Btu/(hr)(sq ft)(°F)
k	Thermal conductivity	Btu/(hr)(ft)(°F)
k _{eff}	Multiplication constant of a finite reactor, including effect of neutron leakage	None
k _∞	Multiplication constant of an infinite medium having the same material properties as those of the finite reactor being considered	None
P	Total heat generated in the core per unit time	Btu/hr
q	Time-variable density of heat generation, = q(t)	Btu/(hr)(cu ft)
q''	Density of heat flow (flux)	Btu/(hr)(sq ft)
Q	Initial density of heat generation	Btu/(hr)(cu ft)
T	Temperature in excess of an arbitrary level	°F
U	Over-all coefficient of heat transfer from fuel element interior to coolant	Btu/(hr)(sq ft)(°F)
v	Velocity	ft/hr
V	Volume	cu ft
x	Space variable	ft
α	Reciprocal of period of exponential rise	hr ⁻¹
γ	Specific weight	lb/cu ft
Δ	Prefix indicating finite lumping	None
κ	Thermal diffusivity $\frac{k}{\rho c}$	sq ft/hr
ρ	Density	lb/cu ft
τ	Time	hr

***Subscripts**

i	Inlet
o	Outlet
m	Metal
w	Coolant
τ	Present time
τ + Δτ	Future time, one time-step later

Numbers or letters, in general, refer to points or different spatial regions

Superscripts

'(prime)	Future time, after one time-step
''(double prime)	Used with q to indicate heat flux (flow density)

actors are listed in Tables 1.8.2 and 1.8.3. Approximate experimental verifications of calculated generation times have been made only for the Chalk River zero-power reactor (ZEEP)³ and the Argonne graphite reactor (CP-5).⁵ High accuracy in determining the generation time is not usually necessary, as the generation time has an important effect only in very rapid transients, where other large uncertainties usually exist.

Table 1.8.2—Calculated Neutron-generation Times for Specific Reactors

Reactor	Fuel	Moderator	Neutron-generation time, sec
Argonne research reactor (CP-3')	Enriched U ²³⁵	D ₂ O	2.3×10^{-3}
New Argonne research reactor (CP-5)	Enriched U ²³⁵	D ₂ O	1×10^{-3}

Table 1.8.3—Calculated Neutron-generation Time in MTR⁴ as Function of k_{∞} and Core Size*

U ²³⁵ , kg	k_{∞}	Generation time, 10 ⁴ sec
0.98	1.606	2.36
1.88	1.432	1.52
2.61	1.373	1.26

*Vol aluminum/vol water = 0.75. The fuel density in core is constant; the total loading is varied by increasing the core size. Criticality is maintained by poisoning. The unpoisoned k_{∞} = 1.61

TEMPERATURE COEFFICIENT OF REACTIVITY

In enriched H₂O-moderated and D₂O-moderated reactors which do not contain important resonance absorbers, the temperature coefficient of reactivity results primarily from changes in the moderator temperature with, in some cases, small contributions from expansions of the reactor parts. The reactivity is therefore insensitive to the fuel-element temperature and varies with moderator temperature. In D₂O-moderated reactors, the coefficient is negative in all practical cases (reactivity decreases with increasing temperature) and is larger for small reactors (high buckling) than for large reactors (low buckling). In small H₂O-moderated reactors, the coefficient is negative. At low temperatures (MTR) where the density of water does not change rapidly with temperature, the coefficient results primarily from the change of microscopic cross sections with neutron temperature. At high temperatures, the change in water density with temperature makes the most important contribution to the temperature coefficient. At such temperatures, the negative coefficient decreases as reactor size is increased and may presumably become positive if the size is increased to the point where the increased absorption caused by an incremental increase in H₂O density is more important to the neutron balance in the reactor than is the accompanying decrease in neutron leakage.

In natural-uranium and slightly enriched reactors, there is a negative contribution to the temperature coefficient from the doppler broadening of the U^{238} resonance lines. This component of the coefficient is associated with the fuel temperature. All other contributions to the coefficient are associated with the moderator or the coolant temperature. The important contributions are usually from change in resonance escape owing to change in slowing-down power of the moderator and, for the H_2O case, change in thermal utilization. Changes in leakage are usually of lesser importance since most reactors of this class have low total leakage. Reactors which are both cooled and moderated by D_2O will have negative coefficients in all practical cases. The possibility of net positive coefficients for H_2O -moderated reactors evidently exists, but this undesirable characteristic has been successfully avoided in the design studies to date. A strong positive component may be expected in the temperature coefficient of reactors cooled by H_2O and moderated by D_2O or graphite. This positive component is usually large enough to result in a net positive coefficient. Temperature coefficients of reactivity for some specific reactors are given below.

**ARGONNE D_2O -MODERATED, ENRICHED-URANIUM,
RESEARCH REACTOR (CP-3')**

The calculated temperature coefficient for CP-3' is -0.05 percent $k_{eff}/^{\circ}C$; this value is approximately confirmed in operation. Changes in the temperature of fuel elements alone do not affect reactivity appreciably; the coefficient is produced almost entirely by temperature changes in the D_2O and the reactor tank. Since heat is transferred from the fuel elements to the D_2O by natural convection (although the D_2O is circulated for heat removal), the temperature coefficient is relatively slow in action.

**NEW ARGONNE D_2O -MODERATED, ENRICHED-URANIUM,
RESEARCH REACTOR (CP-5)**

The temperature coefficient is calculated to be -0.06 to -0.07 percent $k_{eff}/^{\circ}C$. Essentially all of the coefficient results from moderator heating. About half of the coefficient results from the D_2O inside the fuel subassemblies and will, therefore, act fairly rapidly. The remainder results from the D_2O surrounding the subassemblies and will act quite slowly.

MATERIALS TESTING REACTOR (MTR)⁶

Calculated temperature coefficients for three different core radii are given in Table 1.8.4. The average measured value of the temperature coefficient between 36° and $54^{\circ}C$ on the MTR mockup (LITR), for which $k_{\infty} = 1.58$, is $-13 \times 10^{-3}\%$ $k_{eff}/^{\circ}C$.

Table 1.8.4—Calculated Temperature Coefficients of
Reactivity in MTR at $20^{\circ}C$

Reactor r, cm	12.78	17.85	21.12
k_{∞}	1.606	1.432	1.373
Expansion of fuel plates, $10^3\%$ $k_{eff}/^{\circ}C$	-1.6	-1.4	-1.3
Expansion of water, $10^3\%$ $k_{eff}/^{\circ}C$	-3.8	-3.0	-2.8
Change in microscopic cross sections with temperature, $10^3\%$ $k_{eff}/^{\circ}C$	-15.7	-10.5	-8.9
Total, $10^3\%$ $k_{eff}/^{\circ}C$	-21	-15	-13

TEMPERATURE DISTRIBUTIONS WITH EXPONENTIAL POWER RISE

In fixed-fuel reactors having temperature coefficients associated primarily with the coolant temperature, very rapid power transients, such as those which may be postulated in reactor accidents, can raise the fuel element temperatures to dangerously high levels before sufficient heat flows into the coolant to change its temperature appreciably. During this part of the power transient, the reactivity may be considered independent of the power level, and, in fact, the power rise will in many cases be nearly exponential over an important fraction of the transient. When these conditions hold, the transient is usually so fast that transport of heat by coolant flow is unimportant, and the transient temperature distribution of interest is that associated with the transfer of heat from the sources in the fuel element to the coolant. The estimation of this distribution of interest may be relatively simple when the power transient is exponential. Equations for the temperature distribution in some specific idealized configurations are given in the following. This applicability to any given reactor must be evaluated for the particular case of interest. See Table 1.8.1 for definition of symbols.

UNCLAD FUEL PLATE IN STAGNANT COOLANT⁷

The period is assumed to be so fast that convection is negligible, and heat flows from fuel plate to coolant by conduction alone. Fuel plate and coolant are initially both at temperature 0; at $t = 0$, uniform heat generation, $q = Qe^{\alpha\tau}$ cal/(cm³)(sec) begins in the fuel plate. The fuel plate (region 1) and coolant channel (region 2) are considered slabs infinite in two dimensions. The center of coordinates ($x = 0$) is at the central plane of the fuel plate; the fuel plate-coolant boundary is at $x = a$; the central plane of the coolant channel is at $x = b$ (see Fig. 1.8.1A). The temperature distribution is, in the fuel plate:

$$T_1(x, \tau) = \frac{Q}{\alpha\rho_1c_1} e^{\alpha\tau} \left[1 - \frac{\beta \sinh \sqrt{\frac{\alpha}{\kappa_2}} (b-a) \cosh \sqrt{\frac{\alpha}{\kappa_1}} x}{g(\sqrt{\alpha})} \right] - \frac{Q}{\alpha\rho_1c_1} \left[1 + \beta \frac{\frac{b-a}{\sqrt{\kappa_2}}}{\frac{a}{\sqrt{\kappa_1}} + \beta \frac{(b-a)}{\sqrt{\kappa_2}}} \right] + \frac{\beta Q}{\rho_1c_1} \sum_{j=1}^{\infty} \frac{2 \sin \lambda_j \frac{b-a}{\sqrt{\kappa_2}} \cos \frac{\lambda_j x}{\sqrt{\kappa_1}} e^{-\lambda_j^2 \tau}}{\lambda_j (\lambda_j^2 + \alpha) \frac{d}{d\lambda} [g(\lambda)]_{\lambda = i\lambda_j}} \quad (1)$$

and in the coolant:

$$T_2(x, \tau) = \frac{Q}{\alpha\rho_1c_1} e^{\alpha\tau} \frac{\sinh \sqrt{\frac{\alpha}{\kappa_1}} a \cosh \sqrt{\frac{\alpha}{\kappa_2}} (b-x)}{g(\sqrt{\alpha})} + \frac{Q}{\rho_1c_1} \frac{\frac{a}{\sqrt{\kappa_1}}}{\frac{a}{\sqrt{\kappa_1}} + \beta \frac{(b-a)}{\sqrt{\kappa_2}}} - \frac{Q}{\rho_1c_1} \sum_{j=1}^{\infty} \frac{2 \sin \lambda_j \frac{a}{\sqrt{\kappa_1}} \cos \frac{\lambda_j}{\sqrt{\kappa_2}} (b-x)}{\lambda_j (\lambda_j^2 + \alpha) \frac{d}{d\lambda} [g(\lambda)]_{\lambda = i\lambda_j}} e^{-\lambda_j^2 \tau} \quad (2)$$

where $i\lambda_j$ satisfies:

$$g(i\lambda_j) = 0$$

g is defined as:

$$g(\sqrt{s}) = \sinh \sqrt{\frac{s}{\kappa_1}} a \cosh \sqrt{\frac{s}{\kappa_2}} (b-a) + \beta \cosh \sqrt{\frac{s}{\kappa_1}} a \sinh \sqrt{\frac{s}{\kappa_2}} (b-a)$$

with:

$$\beta = \frac{k_2 \sqrt{\kappa_1}}{k_1 \sqrt{\kappa_2}}$$

and:

$$\kappa = \frac{k}{\rho c}$$

In both Eqs. (1) and (2), all terms beyond the first become negligible after a few periods, and the spatial temperature distribution assumes a characteristic asymptotic form (dependent on the period) which is maintained as long as the heat generation rises as $e^{\alpha\tau}$ (that is, the temperature at every point in the fuel plate and coolant rises also as $e^{\alpha\tau}$).

CLAD FUEL PLATE IN STAGNANT COOLANT[†]

Again, heat flow from fuel plate to coolant is assumed to be by conduction alone. All regions are initially at temperature 0; at $\tau = 0$, uniform heat generation, $q = Qe^{\alpha\tau}$ cal/(cm³)(sec), begins in the fuel plate. The fuel plate (region 1), cladding (region 2), and coolant channel (region 3) are slabs infinite in two dimensions. The center of coordinates ($x = 0$) is at the central plane of the fuel plate; the fuel plate-cladding interface is at $x = a$; the cladding-coolant channel interface is at $x = b$; and the central plane of the coolant is at $x = c$ (see Fig. 1.8.1B). The temperature distribution is, for the fuel plate:

$$T_1(x, \tau) = \frac{Q}{\alpha \rho_1 c_1} e^{\alpha\tau} \left[1 + \frac{N\sqrt{\alpha}}{D\sqrt{\alpha}} \cosh \sqrt{\frac{\alpha}{\kappa_1}} x \right] + \frac{Q}{\alpha \rho_1 c_1} \left[\frac{\frac{b-a}{\sqrt{\kappa_2}} + \beta \frac{(c-b)}{\sqrt{\kappa_3}}}{\frac{b-a}{\sqrt{\kappa_2}} + \beta \frac{(c-b)}{\sqrt{\kappa_3}} + \frac{\gamma a}{\sqrt{\kappa_1}}} - 1 \right]$$

$$- \frac{Q}{\rho_1 c_1} \sum_{j=1}^{\infty} \frac{2N(i\lambda_j) e^{-\lambda_j^2 \tau}}{i\lambda_j (\lambda_j^2 + \alpha) \frac{d}{d\lambda} [D(\lambda)]_{\lambda = i\lambda_j}} \cos \frac{\lambda_j}{\sqrt{\kappa_1}} x \quad (3)$$

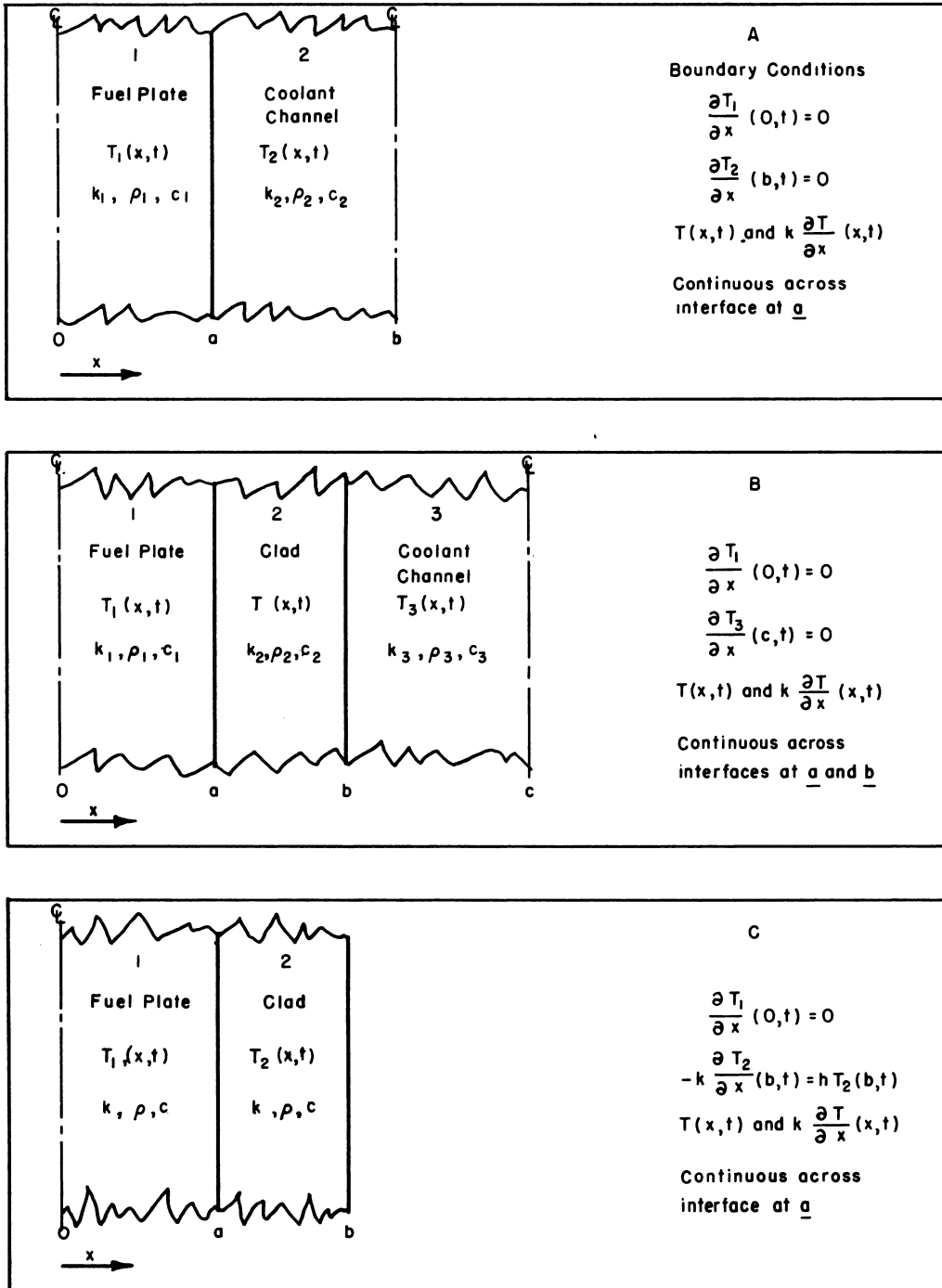


Fig. 1.8.1 — Geometrical Arrangements for Calculation of Temperature Distributions in Slab Fuel Elements Under Exponential Power Increases. Submitted by Argonne National Laboratory, Nov. 15, 1952. (A) Unclad fuel plate in stagnant coolant; (B) elad fuel plate in stagnant coolant; and (C) clad fuel plate in flowing coolant.

for the clad:

$$\begin{aligned}
 T_2(x, \tau) = & \frac{Qe^{\alpha\tau}}{\alpha\rho_1c_1} \left[\frac{\gamma \sinh \sqrt{\frac{\alpha}{\kappa_1}} a \sinh \sqrt{\frac{\alpha}{\kappa_2}} (b-a) \cosh \sqrt{\frac{\alpha}{\kappa_3}} (c-b)}{-D(\sqrt{\alpha})} \right] \cdot \left[\cosh \sqrt{\frac{\alpha}{\kappa_2}} (b-x) \right. \\
 & \left. + \beta \tanh \sqrt{\frac{\alpha}{\kappa_3}} (c-b) \sinh \sqrt{\frac{\alpha}{\kappa_2}} (b-x) \right] - \frac{Q}{\alpha\rho_1c_1} \frac{\frac{a}{\gamma\sqrt{\kappa_1}}}{\frac{b-a}{\sqrt{\kappa_2}} + \frac{\beta(c-b)}{\sqrt{\kappa_3}} + \gamma\frac{a}{\sqrt{\kappa_1}}} \\
 & - \frac{Q}{\rho_1c_1} \sum_{j=1}^{\infty} e^{-\lambda_j^2\tau} \left[\frac{4\gamma \sin \frac{\lambda_j}{\sqrt{\kappa_1}} a \sin \frac{\lambda_j}{\sqrt{\kappa_2}} (b-a) \cos \frac{\lambda_j}{\sqrt{\kappa_3}} (c-b)}{i\lambda_j (\lambda_j^2 + \alpha) \frac{d}{d\lambda} [D(\lambda)]_{\lambda = i\lambda_j}} \right] \\
 & \left[\cos \frac{\lambda_j}{\sqrt{\kappa_2}} (b-x) - \beta \tan \frac{\lambda_j}{\sqrt{\kappa_3}} (c-b) \sin \frac{\lambda_j}{\sqrt{\kappa_2}} (b-x) \right] \quad (4)
 \end{aligned}$$

and for the coolant:

$$\begin{aligned}
 T_3(x, \tau) = & \frac{Q}{\alpha\rho_1c_1} e^{\alpha\tau} \left[\frac{2\gamma \sinh \sqrt{\frac{\alpha}{\kappa_1}} a \sinh \sqrt{\frac{\alpha}{\kappa_2}} (b-a)}{-D(\sqrt{\alpha})} \right] \cosh \sqrt{\frac{\alpha}{\kappa_3}} (c-x) \\
 & - \frac{Q}{\alpha\rho_1c_1} \frac{\frac{a}{\gamma\sqrt{\kappa_1}}}{\frac{b-a}{\sqrt{\kappa_2}} + \beta \frac{(c-b)}{\sqrt{\kappa_3}} + \gamma\frac{a}{\sqrt{\kappa_1}}} - \frac{Q}{\rho_1c_1} \sum_{j=1}^{\infty} \frac{4\gamma \sin \frac{\lambda_j}{\sqrt{\kappa_1}} a \sin \frac{\lambda_j}{\sqrt{\kappa_2}} (b-a) \cos \frac{\lambda_j}{\sqrt{\kappa_3}} (c-x)}{i\lambda_j (\lambda_j^2 + \alpha) \frac{d}{d\lambda} [D(\lambda)]_{\lambda = i\lambda_j}} \quad (5)
 \end{aligned}$$

where D and N are defined by:

$$\begin{aligned}
 D(S) = & \cosh \frac{S}{\sqrt{\kappa_1}} a \cosh \frac{S}{\sqrt{\kappa_3}} (c-b) + \beta\gamma \sinh \frac{S}{\sqrt{\kappa_1}} a \sinh \frac{S}{\sqrt{\kappa_3}} (c-b) \\
 & - \gamma \sinh \frac{S}{\sqrt{\kappa_1}} a \sinh \frac{2S}{\sqrt{\kappa_2}} (b-a) \cosh \frac{S}{\sqrt{\kappa_3}} (c-b) \\
 & - \beta\gamma \sinh \frac{S}{\sqrt{\kappa_3}} (c-b) \cosh \frac{2S}{\sqrt{\kappa_2}} (b-a) \sinh \frac{S}{\sqrt{\kappa_1}} a \\
 & - \beta \cosh \frac{S}{\sqrt{\kappa_1}} a \sinh \frac{2S}{\sqrt{\kappa_2}} (b-a) - \cosh \frac{S}{\sqrt{\kappa_1}} a \cosh \frac{2S}{\sqrt{\kappa_2}} (b-a) \cosh \frac{S}{\sqrt{\kappa_3}} (c-b)
 \end{aligned}$$

(Note: D(S) is inherently negative for real S)

$$N(S) = \left[\cosh \frac{2S}{\sqrt{\kappa_2}} (b-a) - 1 \right] \cosh \frac{S}{\sqrt{\kappa_3}} (c-b) + \beta \sinh \frac{2S}{\sqrt{\kappa_2}} (b-a) \sinh \frac{S}{\sqrt{\kappa_3}} (c-b)$$

$i\lambda_j$ are the successive roots of $D(\lambda) = 0$ and:

$$\beta = \frac{k_3}{k_2} \frac{\sqrt{\kappa_2}}{\sqrt{\kappa_3}}$$

$$\gamma = \frac{k_1}{k_2} \frac{\sqrt{\kappa_2}}{\sqrt{\kappa_1}}$$

Again the solutions contain terms which describe an asymptotic spatial temperature distribution which is independent of time. The calculated asymptotic distributions for clad aluminum fuel plates (similar to MTR plates) in water are shown in Figs. 1.8.2 and 1.8.3 for periods of 0.01 sec and 0.001 sec, respectively.⁸

CLAD FUEL PLATE IN FLOWING COOLANT⁹

Heat is assumed to be transferred from the fuel-plate clad to the coolant by the usual forced-convection process, characterized by a heat-transfer coefficient h cal/(cm²)(sec)(°C). The heat capacity of the bulk coolant is assumed effectively infinite (i.e., the bulk coolant temperature does not change), and the heat capacity of the boundary layer is assumed negligible. These assumptions lead to the simple mathematical boundary conditions tabulated on Fig. 1.8.1C. All regions are initially at temperature 0; at $t = 0$, uniform heat generation, $q = Qe^{\alpha\tau}$ cal/(cm³)(sec), begins in the fuel plate. The fuel plate (region 1) and the cladding (region 2) are slabs infinite in two dimensions. The center of coordinates ($x = 0$) is at the central plane of the fuel plate; the fuel plate-cladding interface is at $x = a$; and the cladding-coolant channel interface is at $x = b$. Since the coolant is regarded as a constant-temperature heat sink, its extent is effectively infinite (see Fig. 1.8.1C). The fuel plate and the cladding are assumed to have identical thermal properties (except for the sources, which are confined to the fuel plate). Only the asymptotic distribution has been derived. The distribution is, in the fuel plate:

$$T_1(x, \tau) = \frac{Qe^{\alpha\tau}}{\alpha\rho c} \left[1 - \frac{\cosh \frac{k}{h} \sqrt{\frac{\alpha}{\kappa}} + \sqrt{\frac{\alpha}{\kappa}} (b-a)}{\cosh \left[\frac{k}{h} \sqrt{\frac{\alpha}{\kappa}} + \sqrt{\frac{\alpha}{\kappa}} b \right]} \cosh \sqrt{\frac{\alpha}{\kappa}} x \right] \quad (6)$$

and in the clad:

$$T_2(x, \tau) = \frac{Qe^{\alpha\tau}}{\alpha\rho c} \frac{\sinh \sqrt{\frac{\alpha}{\kappa}} a}{\cosh \left(\frac{k}{h} \sqrt{\frac{\alpha}{\kappa}} + \sqrt{\frac{\alpha}{\kappa}} b \right)} \sinh \left[\frac{k}{h} \sqrt{\frac{\alpha}{\kappa}} + \sqrt{\frac{\alpha}{\kappa}} (b-x) \right] \quad (7)$$

Neglecting the heat capacity of the boundary layer in deriving the above equations may prove serious for the case of very rapid transients. For that case, the assumption of stagnant coolant (see above) may be a more valid approximation.

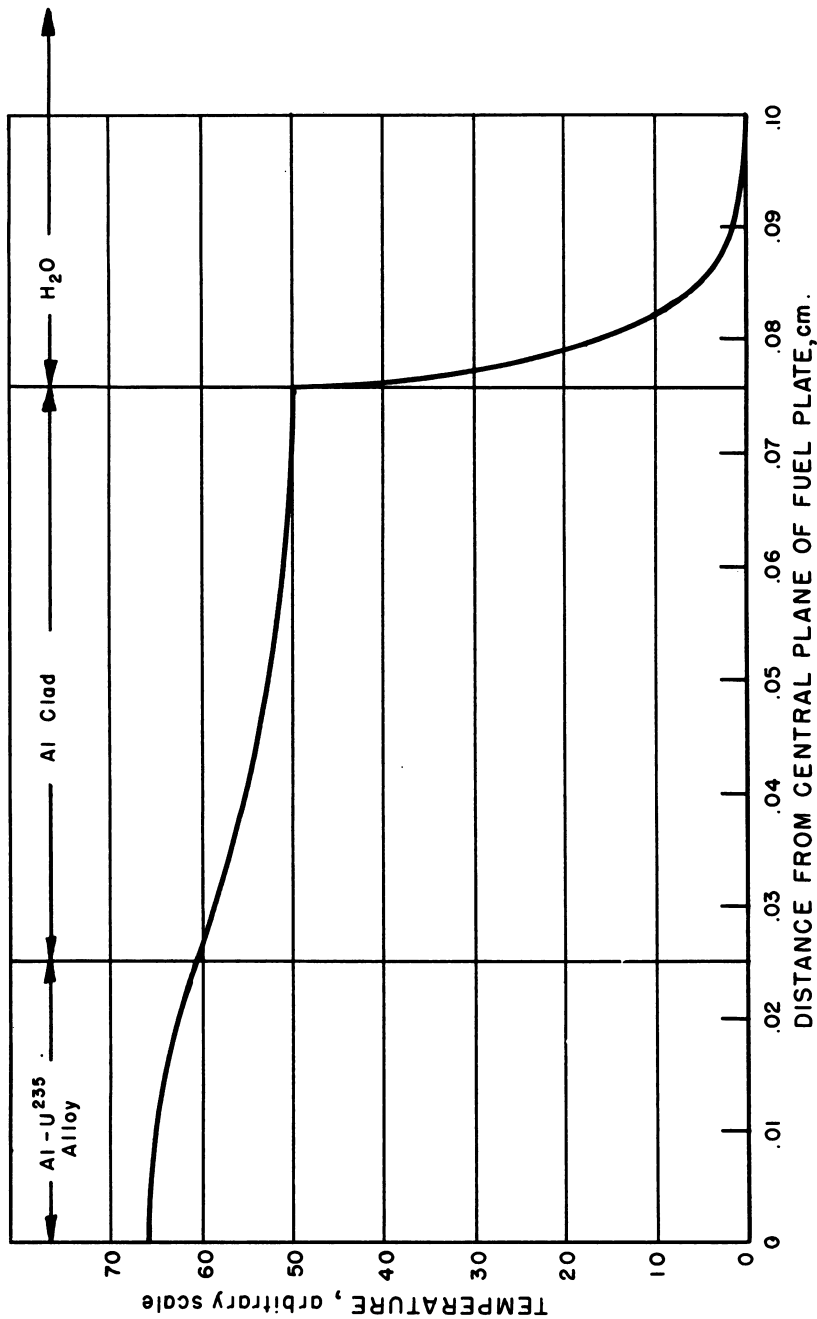


Fig. 1.8.2 — Calculated Asymptotic Temperature Distribution in Clad Aluminum Fuel Plate in Stagnant Coolant with Exponential Power Increase on 0.01-sec Period. Redrawn from ANL-4921, Nov. 12, 1952.

Constants Used in Calculation

	Al-U ²³⁵	Al Clad	H ₂ O
k, cal/(cm)(sec)(°C)	0.40	0.50	0.00143
ρ, gm/cm ³	3.44	2.70	1.0
c, cal/(gm)(°C)	0.22	0.23	1.0

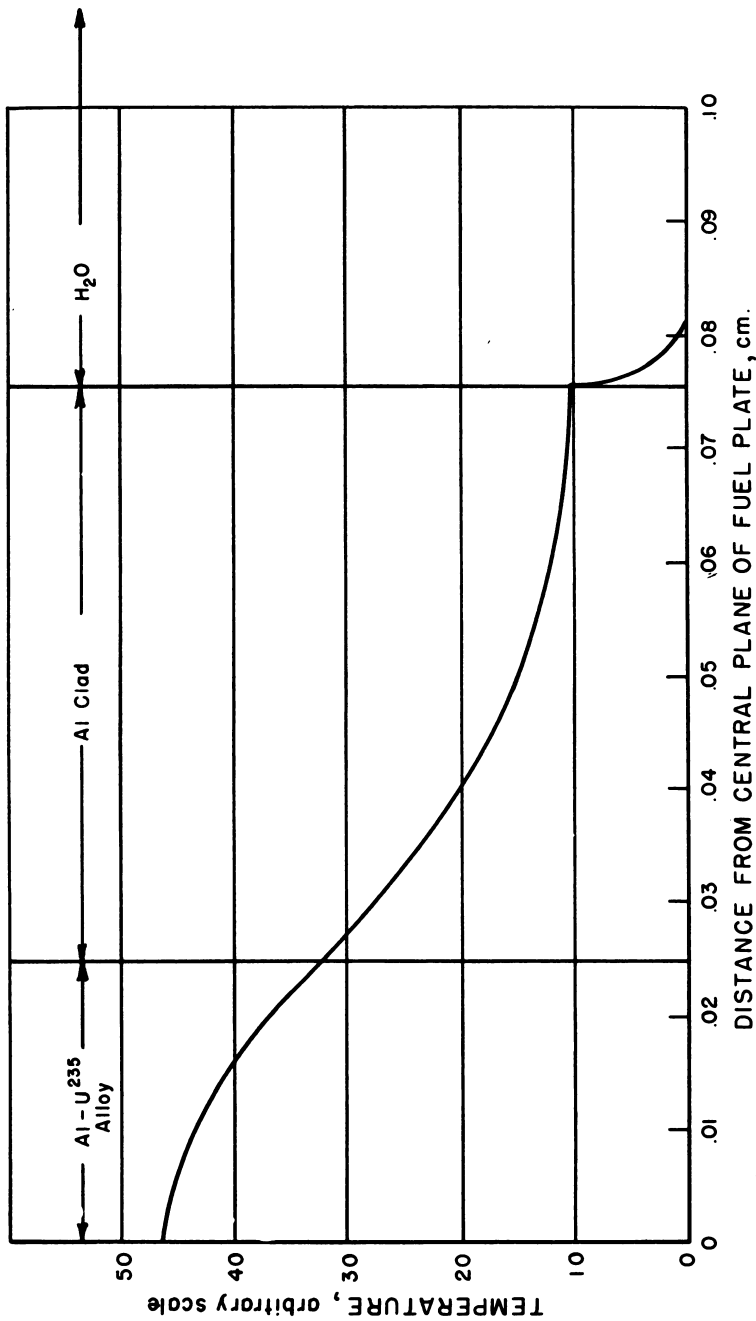


Fig. 1.8.3 — Calculated Asymptotic Temperature Distribution in Clad Aluminum Fuel Plate in Stagnant Coolant with Exponential Power Increase on 0.001- sec Period. Redrawn from ANL-4921, Nov. 12, 1952.

Constants Used in Calculation			
	Al-U ²³⁵	Al Clad	H ₂ O
k, cal/(cm)(sec)(°C)	0.40	0.50	0.00143
ρ, gm/cm ³	3.44	2.70	1.0
c, cal/(gm)(°C)	0.22	0.23	1.0

TEMPERATURE DISTRIBUTION FOR ARBITRARY POWER GENERATION

In the general case of reactor power variation for which the reactivity is coupled to the power level via the temperature coefficient of reactivity, it is not possible to treat the kinetics of heat generation and heat flow separately. This circumstance arises from the non-linearity of the differential (reactor kinetics) equations which describe the time variation of power generation. If, however, the power transients to be investigated are confined to small variations about a steady value, the reactor kinetics equations can be linearized, as discussed in Vol. 1, Chapter 1.6. This approximation is quite useful in analyzing the stability of reactor control systems. In the linearized treatment, the equations of transient heat flow may be handled separately from those of reactor kinetics, and for this application, methods of computing temperature distributions resulting from arbitrary power variations, especially sinusoidal power variations, are useful.

For cases in which the linearized treatment is inadequate, both automatic digital computers^{10,11} and analog computers¹² have been used successfully. When these methods are applied, methods of computing temperature distributions resulting from arbitrary power variations are again useful; they may be employed in specifying satisfactory electrical analogs for use in analog computers and in arriving at approximations which simplify the formulation of the computation for a digital computer.

The following summarizes simple and general analytical methods for approximating the temperature distributions resulting from arbitrary, specified power variations. These methods can be used for making broad estimates on a wide variety of physical cases in a minimum of time. More accurate and less general methods (as above) are used frequently for obtaining solutions in individual applications; references to solutions for more of these are given in the Selected Reading List.

There are two usual points of interest in connection with reactor thermal transients; (1) calculation of local fuel-element temperatures and (2) the over-all mean core temperature response, including the transfer function of the core.

FUEL-ELEMENT TEMPERATURES

The analytical method shown is that of lumped parameters. This consists of "lumping" space or time or both into discrete subdivisions and assuming that conditions are uniform within a space lump and constant within a time lump. The most general approach by this method (that of using completely irregular lumping) has been slighted in the literature, most authors having preferred to describe special refinements obtainable with special circumstances. Many of these specialized treatments may be found in the Selected Reading List. Dusenberre¹³ and, to some extent, Ingersoll and Zobel¹⁴ have taken the trouble to deal with irregular and non-homogeneous lumping in a clear and unsophisticated way. Since a refined approach is not generally useful when a fast solution is desired, the crude form of lumping treatment will be given here.

Consider a fuel element of plate form (Fig. 1.8.4) with a heat-generating region in the center protected by metal and cooled by a liquid at the clad surface. Assume, for simplicity, that only one-dimensional heat transfer need be considered. (The method is quite general and may be applied to different geometrical arrangements and two- or three-dimensional heat flow.) The lumping may be done arbitrarily in a manner suited to the purposes of the analysis and the geometry of the element. In general, a finer subdivision gives more accurate results, and it will often be found that less complicated as well as more accurate equations result from the use of uniform spacing in the lumps. In Fig. 1.8.4, a non-uniform spacing is inferred for generality of presentation.

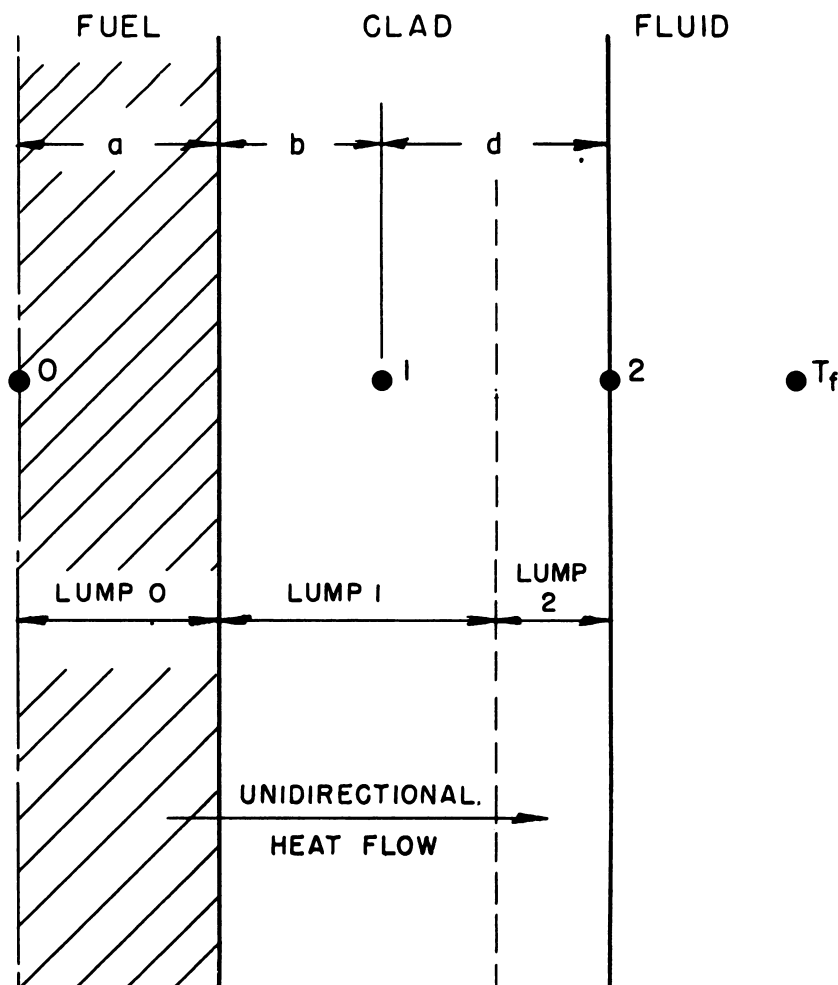


Fig. 1.8.4 — An Example of Coarse, Non-uniform Lumping in a Plate-type Fuel Element. Submitted by ANL, Dec. 15, 1952.

EQUATION FOR LUMPED SPACE AND CONTINUOUS TIME

A heat balance is written upon the center lump surrounding point 0. Since this lump is at the center line of the plate, it is assumed that (because of symmetry) heat flows only to the right of point 0, none passing through the plate centerline. Heat flowing through the right face of the lump is assumed directly proportional to the temperature difference between points 0 and 1 (and the unit area of the surface) and inversely proportional to the heat-flow resistance of the path between the points:

$$q''_{\text{out}} = \frac{A}{\frac{a}{k_a} + \frac{b}{k_b}} (T_1 - T_0)$$

The heat generated within the lump is expressed by (aQA) . The product of heat capacity of the core lump and the time rate of temperature change at point 0 is set equal to the rate

of heat gain and/or loss by conduction plus the heat gain by power generation:

$$Aa\gamma_a C_a \frac{dT_0}{d\tau} = \frac{A}{\frac{a}{k_a} + \frac{b}{k_b}} (T_1 - T_0) + aq A \quad (8)$$

This is the equation for the core lump. It will be observed that the effect of lumping in the space variable is to remove that variable from the equation leaving in this case an ordinary time-dependent differential equation. Similar equations may be written for each of the other lumps (cancelling the unit area):

$$(b+d/2) \gamma_b C_b \frac{dT_1}{d\tau} = \frac{1}{\frac{a}{k_a} + \frac{b}{k_b}} (T_0 - T_1) + \frac{k_b}{d} (T_2 - T_1) \quad (9)$$

$$\frac{d}{2} \gamma_b C_b \frac{dT_2}{d\tau} = \frac{k_b}{d} (T_1 - T_2) + h(T_w - T_2) \quad (10)$$

The bulk fluid temperature, T_w , is left as a specified quantity here and therefore does not require an equation.

The problem of estimating the transient thermal response of the fuel element is now reduced to the simultaneous solution of three ordinary differential equations. Such equations may often be solved with analogue computing equipment, or explicit analytical solutions may often be found for certain simply expressed types of perturbation such as step or sine function charges of T_f or Q . However, a different solution must be worked out for each case. For flexibility and the inclusion of arbitrary types of parameter variations, a totally numerical approach is often useful.

EQUATIONS FOR LUMPING IN BOTH THE SPACE AND TIME VARIABLES

The totally numerical solution is made by lumping the time variable as well as the space variable. This can be done in different ways; three representative solutions are discussed below:

Explicit Numerical Equations

The first solution is obtained by expressing a future temperature at a point as an explicit function of the past temperatures at the same and surrounding points. An imaginary space-time grid is shown in Fig. 1.8.5. [In the figures showing grids of this type, dots (•) represent known temperatures, crosses (x) represent unknown future temperatures, and circled crosses (⊗) represent the unknown points for which solution is to be made. All points marked in one of these ways represent temperature values which enter into the computation of a temperature at a particular point.] The time lumping is illustrated with an equation of the form of Eq. (8) above:

$$\frac{dT_0}{d\tau} = C_1 (T_1 - T_0) + C_2 q$$

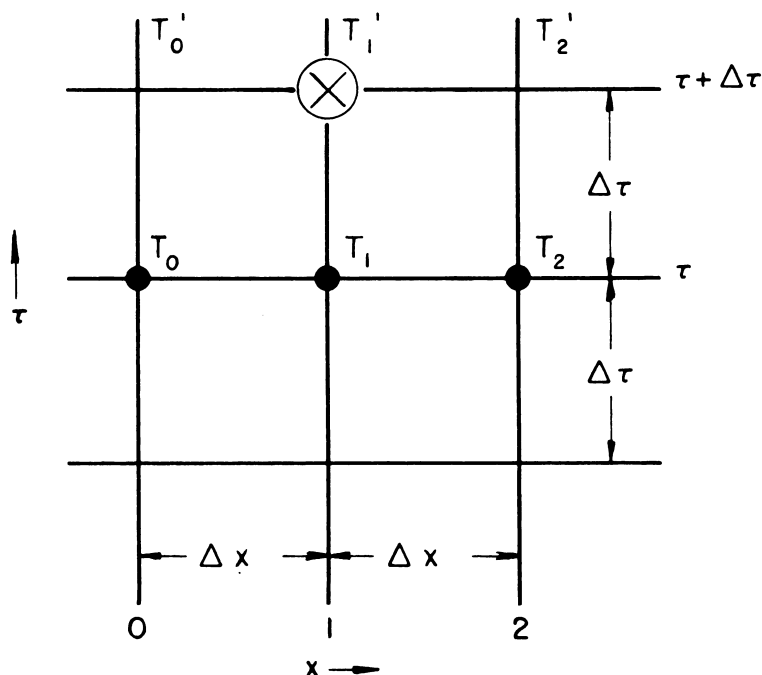


Fig. 1.8.5— Space Time Coordinate Grid Showing the Temperature Points which Enter into Explicit Computation of T'_1 . Submitted by ANL, Dec. 15, 1952.

The time derivative is lumped by replacement with a difference quotient:

$$\frac{dT_0}{d\tau} = \frac{T'_0 - T_0}{\Delta\tau} = \frac{T_{0, \tau + \Delta\tau} - T_{0, \tau}}{\Delta\tau}$$

Making this substitution, and solving for T'_0 gives:

$$T'_0 = (1 - C_1\Delta\tau) T_0 + C_1\Delta\tau T_1 + C_2\Delta\tau q \quad (11)$$

With equations of type (11), for each point, the calculator chooses a $\Delta\tau$ value (subject to restrictions explained below) and evaluates the constants. Starting with a specified initial temperature distribution, future temperatures can be computed indefinitely by time-steps of size $\Delta\tau$. The computer inserts proper specified initial values into the explicit equation for each point and thus computes a complete new set of T values. The new values are re-substituted in the proper equations and the process repeated indefinitely. (Representative results of calculations performed in this way may be seen in Figs. 1.8.6 to 1.8.9).

The computer does not have a completely free hand in the choice of a $\Delta\tau$ value. The restricting criterion is roughly as follows: With the finite difference (or lumped) equation solved explicitly for T'_0 , collect all T_0 terms on the right side of the equation. The resulting coefficient of T_0 must be greater than or equal to zero. Thus in Eq. (11), if $\Delta\tau$ is chosen

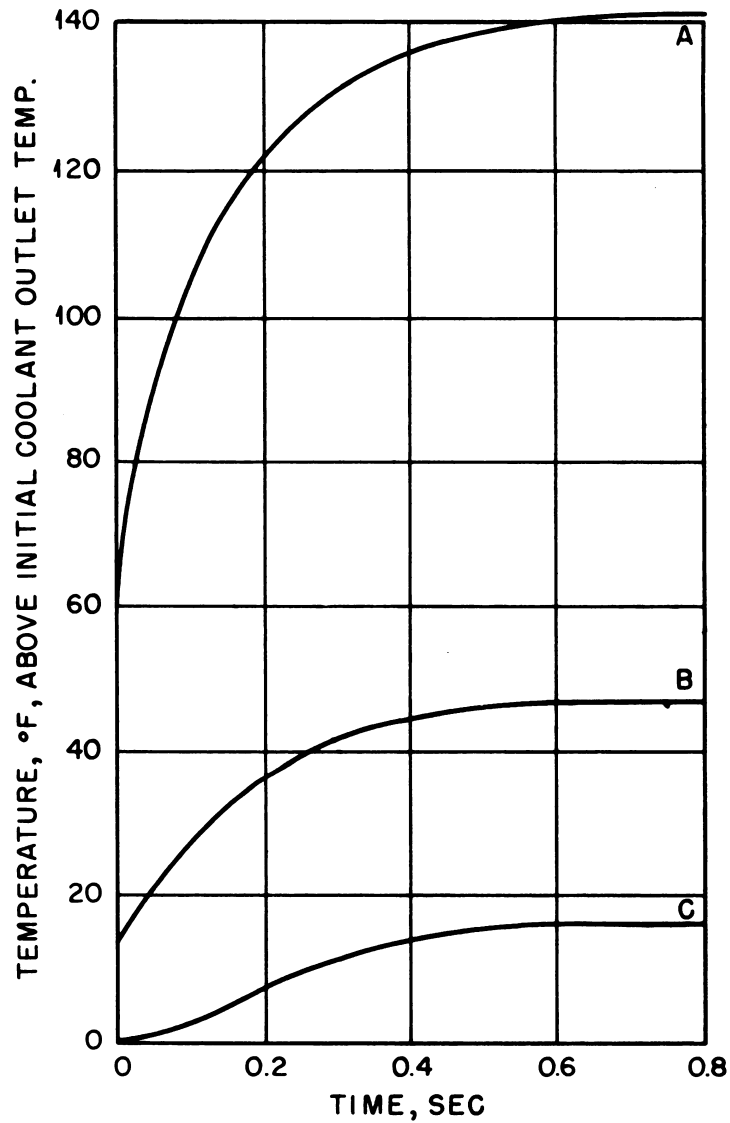


Fig. 1.8.6—Transient Temperature Response of the Metal and Coolant in a Reactor Pass with a Perturbation in Power Production. Redrawn from ANL-4810, April 10, 1952. Reactor power instantaneously doubled from normal full-power value; coolant flow held constant at full-flow level and coolant inlet temperature maintained constant; channel of average power production and non-uniform flux distribution in the second reactor pass; metal temperature taken at a point of about twice the average full-power flux, approximately $\frac{1}{3}$ the distance through the pass. Curve (A), fuel-element (centerline); curve (B), fuel-element (surface); curve (C); coolant (pass outlet). Ordinate scale shows temperature difference only.

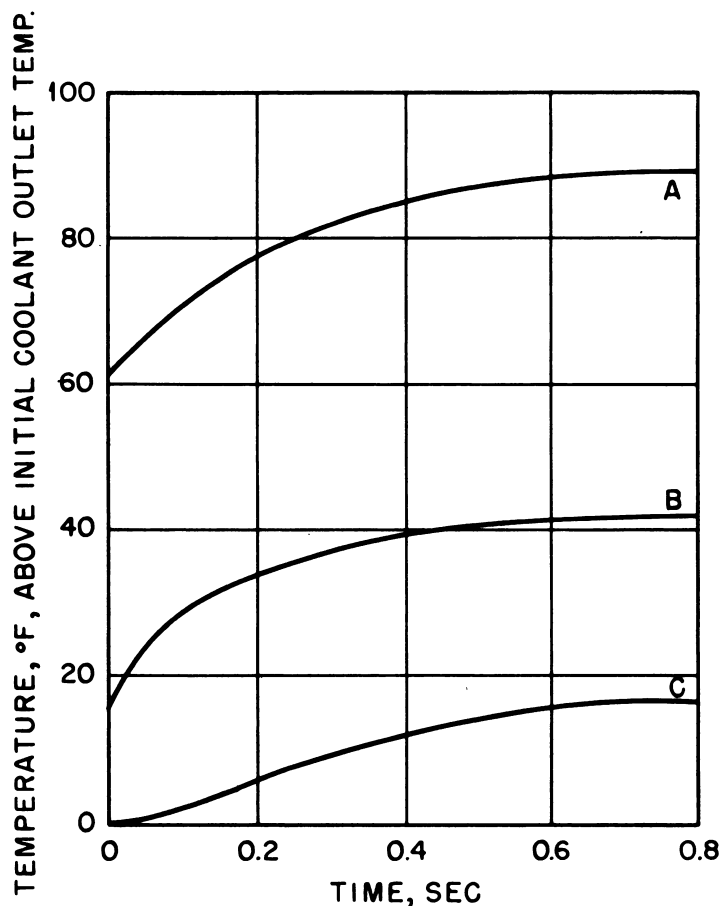


Fig. 1.8.7—Transient Temperature Response of the Metal and Coolant in a Reactor Pass with a Perturbation in Coolant Flow. Redrawn from ANL-4810, April 10, 1952. Coolant flow instantaneously halved from a normal full-flow value; reactor power held constant at full power and coolant inlet temperature maintained constant; channel of average power production and non-uniform flux distribution in the second reactor pass; metal temperatures taken at a point of about twice the average full-power flux, approximately $\frac{1}{3}$ the distance through the pass. Curve (A), fuel-element (centerline); curve (B), fuel-element (surface); curve (C), coolant (pass outlet). Ordinate scale shows temperature difference only.

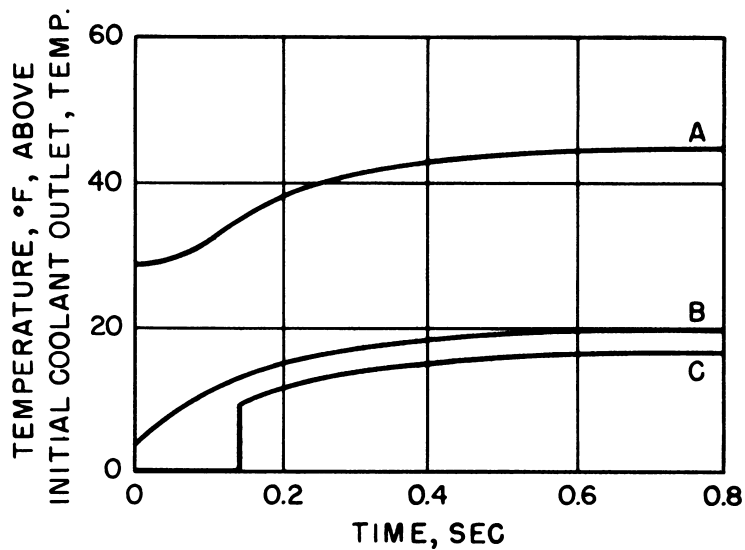


Fig. 1.8.8—Transient Temperature Response of the Metal and Coolant in a Reactor Pass with a Perturbation in Coolant Inlet Temperature. Redrawn from ANL-4810, April 10, 1952. Pass inlet coolant temperature instantaneously increased by 16.5°F; reactor power and coolant flow maintained at normal full-power levels; channel of average power production and uniform flux distribution, in the first reactor pass; average metal temperatures given. Curve (A), fuel-element (centerline); curve (B), fuel-element (surface); curve (C), coolant (pass outlet). Ordinate scale shows temperature difference only.

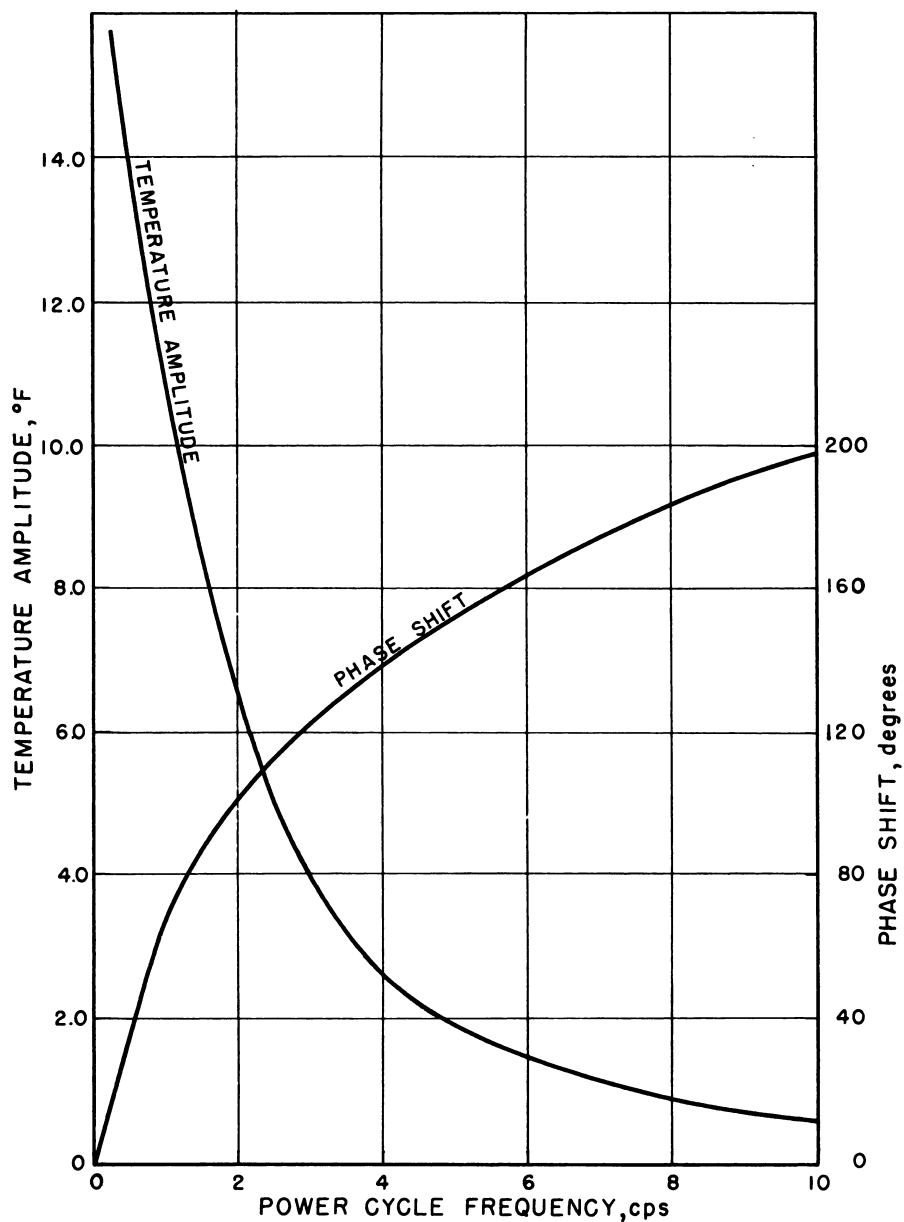


Fig. 1.8.9 — Calculated Outlet Coolant Temperature Variation of a Single Reactor Pass in Response to Sinusoidal Variations in Power Level. Redrawn from ANL-4810, April 10, 1952. Power cycled between zero and twice full power; reactor channel of average power generation and uniform flux distribution; flow and pass inlet coolant temperature held constant at normal full-power levels.

such that $C_1 \Delta \tau > 1$, the equation becomes unstable. Choosing $C_1 \Delta \tau$ too close to unity even though stable will sometimes cause unsatisfactory oscillations. The value of $\Delta \tau$ is thus restricted, and it may often be found that this restriction necessitates an impractical amount of calculation.

Implicit Numerical Equations

A second way to lump the time variable is to express the desired unknown future temperature as an implicit function of its own past value and the unknown future values at surrounding points. This procedure is shown diagrammatically in Fig. 1.8.10. In this case, Eq. (8) would be stated:

$$\frac{T'_0 - T_0}{\Delta \tau} = C_1 (T'_1 - T'_0) + C_2 q' \quad (12)$$

Solved for T'_0 :

$$T'_0 = \frac{T_0 + C_1 \Delta \tau T'_1 + C_2 \Delta \tau q'}{1 + C_1 \Delta \tau} \quad (13)$$

With this type of equation, it can be seen that unknown temperatures appear on both sides of the equation. It is therefore necessary to make a simultaneous solution of the equations of all points at each time step. This is not a great disadvantage where only a few points are involved, whereas a great advantage accrues to this method in being able to take unlimited values of $\Delta \tau$ without incurring instability. If the number of equations is only five

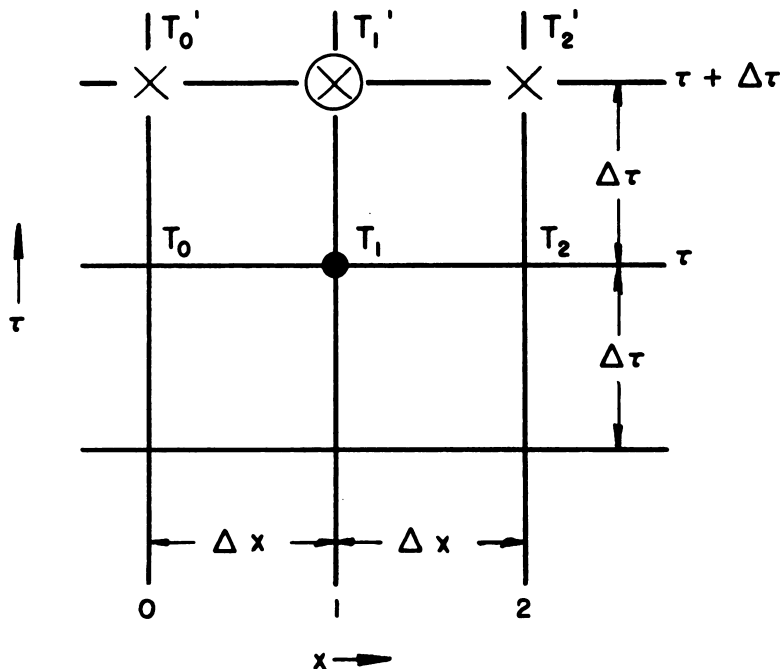


Fig. 1.8.10 — Space-time Coordinate Grid Illustrating an Implicit Finite Difference Computation Scheme. Submitted by Argonne National Laboratory, Dec. 15, 1952.

or so, the unknowns may be eliminated algebraically prior to computation; for example, with three equations such as Eqs. (8), (9), and (10), each point would reduce to the explicit form (T'_w and Q' specified):

$$T'_0 = A_1 T_0 + A_2 T_1 + A_3 T_2 + A_4 T'_w + A_5 q'$$

The computation would then proceed in a straightforward manner, beginning with a specified initial temperature distribution and continuing by time-steps of $\Delta\tau$ duration.

An interesting solution can be made with the implicit computational pattern (Fig. 1.8.10) in any transient case wherein both initial and final temperature distributions are known. Equation (12) can be solved for T_0 instead of T'_0 :

$$T_0 = (1 + C_1 \Delta\tau) T'_0 - C_1 \Delta\tau T'_1 - C_2 \Delta\tau q' \quad (14)$$

Note that this equation is explicit for the past temperature of T_0 in terms of future temperatures. If the final temperatures are known, they may be inserted for the prime (') or future values, and the temperatures for one increment $\Delta\tau$ in the past may be evaluated. The procedure is then repeated until the solution closes upon the known initial values. This solution does not require simultaneous elimination of variables and is stable for all values of $\Delta\tau$. The accuracy with which it closes on the initial values can also afford some idea of the accuracy of the solution.

Judgment must be used in choosing the size of $\Delta\tau$ even where its value is not limited by instability; too large a choice will still destroy the accuracy of solution. Comparing the results of two sets of computations, each performed with different values of $\Delta\tau$, will indicate reasonable values; if the results are not greatly different, the larger choice probably affords sufficient accuracy for estimating purposes.

Time Average Implicit Numerical Equations

A third set-up has the advantage of stability for large values of $\Delta\tau$ and is somewhat more accurate. This consists of expressing the desired future temperature in terms of its own past value and the average of present and past values at surrounding points, as illustrated in Fig. 1.8.11.

In this case, Eq. (8) would be stated as follows:

$$\frac{T'_0 - T_0}{\Delta\tau} = C_1 \frac{(T'_1 + T_1 - T'_0 - T_0)}{2} + C_2 \frac{(q' + q)}{2}$$

Solved for T_0 :

$$T'_0 = \frac{(1 - C_1 \Delta\tau/2)T_0 + C_1 \Delta\tau/2 (T'_1 + T_1) + C_2 \Delta\tau/2 (q' + q)}{1 + C_1 \Delta\tau/2} \quad (15)$$

Equations of type (15) are then applied for the numerical solution in the same manner as the fully implicit equations described previously.

CORE RESPONSE

Lumping may also be employed to estimate the temperature response or transfer function of the entire core. The core may be represented by two gross lumps of material as shown in Fig. 1.8.12. One lump represents all the core metal, while the other represents all the coolant within the core. An over-all coefficient of heat transfer from metal to water is evaluated by combining the resistance of the mean fluid film coefficient and the mean

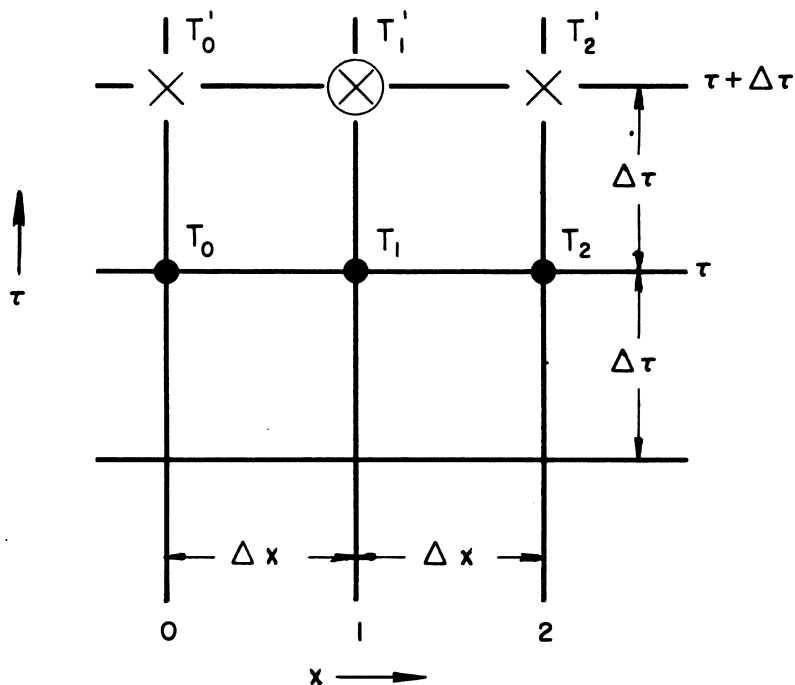


Fig. 1.8.11 — Space-time Coordinate Grid Illustrating the Time Average Implicit Computational Scheme for Computation of T'_1 . Submitted by Argonne National Laboratory, Dec. 15, 1952.

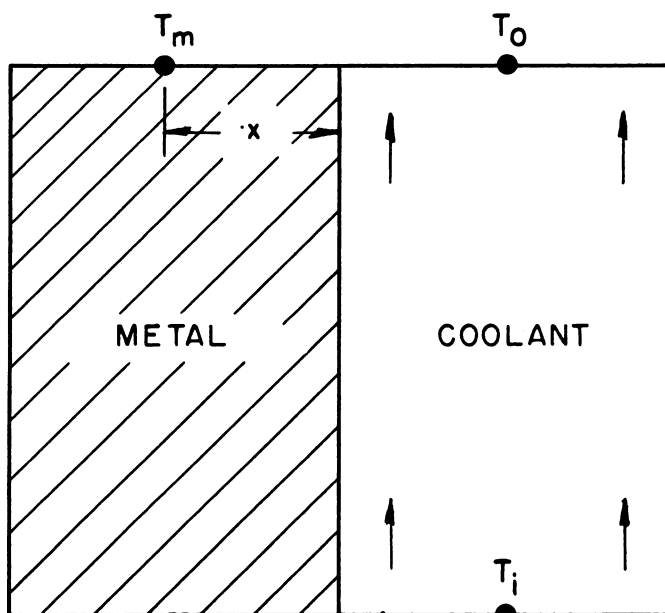


Fig. 1.8.12 — A Schematic Example of Gross Lumping of all the Fuel and all the Coolant in a Reactor Core. Submitted by Argonne National Laboratory, Dec. 15, 1952.

length of heat conduction path (x) from within the fuel elements to their surface. (As a simple example, with plate-type fuel elements, x would be roughly $\frac{1}{4}$ the plate thickness.) Using broad assumptions, heat balances are written upon each lump:

$$V_m \gamma_m c_m \frac{dT_m}{d\tau} = UA_w (T_0 - T_m) + P \quad (16)$$

$$V_w \gamma_w c_w \frac{dT_0}{d\tau} = UA_w (T_m - T_0) + v \gamma_w c_w (T_i - T_0) \quad (17)$$

These equations may be solved by any of the previously mentioned methods. In making a specific analysis of the core response, this crude lumping was found to give results not greatly different from considerably more detailed work.¹⁵ This method does not faithfully transmit a step function of coolant inlet temperature but instead smooths it out as shown in Fig. 1.8.13. This is a rare discontinuity, however. The effects of step changes in

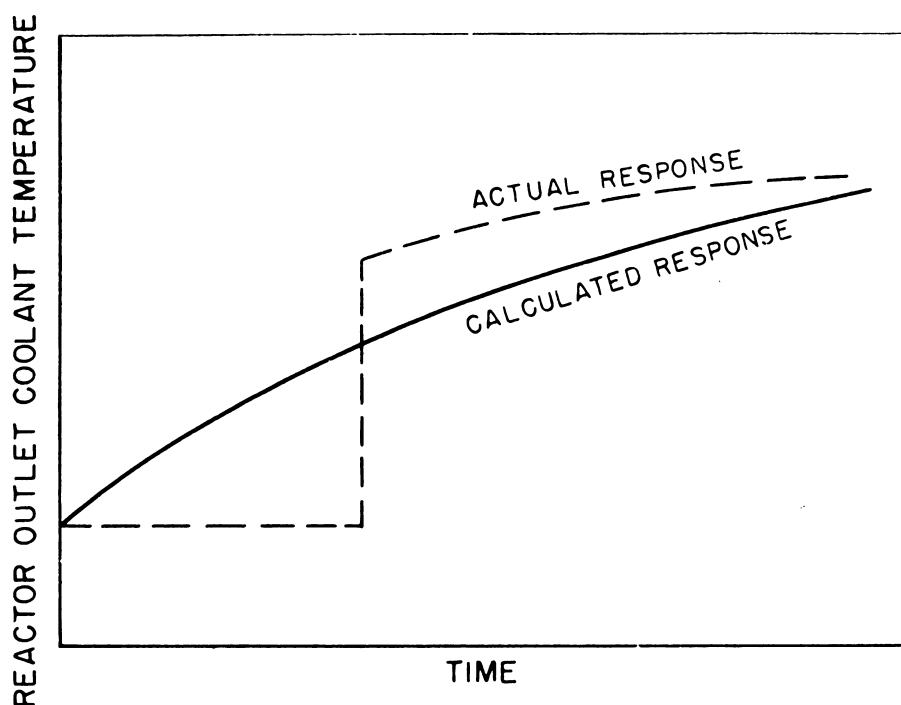


Fig. 1.8.13 — The Effect of Gross Reactor Lumping on the Transmission of a Jump in Inlet Temperature. Submitted by Argonne National Laboratory, Dec. 15, 1952.

P and v are represented with sufficient accuracy for estimating purposes.

The two equations may be combined into one, eliminating T_m if so desired, with the following result:

$$\frac{d^2 T_0}{d\tau^2} + \left(B_3 + \frac{v}{V} + B_1 \right) \frac{dT_0}{d\tau} + \left(\frac{1}{V_w} \frac{dv}{d\tau} + \frac{B_1 v}{V_w} \right) T_0 = \frac{v}{V_w} \frac{dT_i}{d\tau} + \left(\frac{1}{V_w} \frac{dv}{d\tau} + \frac{B_1 v}{V_w} \right) T_1 + B_2 P \quad (18)$$

where:

$$B_1 = \frac{UA_w}{V_m \gamma_m c_m}$$

$$B_2 = \frac{1}{V_m \gamma_m c_m}$$

$$B_3 = \frac{UA_w}{V_w \gamma_w c_w}$$

In most cases to be analyzed, not all the parameters (v , P , T_i) will be allowed to vary simultaneously, and Eq. (18) would usually be considerably simplified in application.

It will be noticed that in Eqs. (16) and (17) the coolant lump storage is based on the core outlet temperature, T_0 , rather than the average coolant temperature. The metal-to-fluid heat transfer is also expressed relative to T_0 . Setting the equations up in this manner lends stability to the numerical solution and does not greatly affect the estimates derived from them. In solving, however, it should be understood that T_m of Eq. (16) is not the average metal temperature but is higher by about $0.5 (T_0 - T_i)$.

The q and P terms in the above equations represent heat generation and power terms which, of course, are proportional to the fissions occurring in the reactor. Any equations of reactor physics which represent these quantities may be inserted in the above equations to further generalize their application.

REFERENCES

1. M. M. Mills, Reactor Sci. Tech. 1, No. 1, TID-71, April 1951, pp 55-81 (classified).
2. E. F. Fricke et al, Argonne Nat. Lab., ANL-4810, April 10, 1952 (classified).
3. C. W. Gilbert and G. J. Fergusson, Nat. Res. Council of Canada, CRP-377, May 20, 1948 (classified).
4. E. Greuling, H. Soodak, and A. M. Weinberg, Clinton Lab., MonP-272, Mar. 27, 1947, p 28 (classified).
5. J. M. Harrer, R. E. Boyar, and D. Krucoff, Transfer Function of Argonne CP-2 Reactor, Nucleonics 10, No. 8, Aug. 1952, pp 33-36.
6. J. H. Buck and C. F. Leyse, Argonne Nat. Lab. and Oak Ridge Nat. Lab., ORNL-963, May 7, 1951, pp 4.19 and A4.36 (classified).
7. Argonne Nat. Lab., ANL-4951, Dec. 15, 1952 (classified).
8. J. R. Dietrich, D. C. Layman, and O. A. Schulze, Argonne Nat. Lab., ANL-4921, Nov. 12, 1952 (classified).
9. Westinghouse Atomic Power Div., WAPD-55 (Section 2 - Appendices), April 20, 1951, pp 186-188 (classified).
10. A. F. Henry, Westinghouse Atomic Power Div., WAPD-28, March 1951 (classified).
11. A. F. Henry, Westinghouse Atomic Power Div., WAPD-37, Aug. 1951 (classified).
12. J. C. Simons, Jr., Westinghouse Atomic Power Div., WAPD-34, Vol. I and II, Feb. 1952 (classified).
13. G. M. Dusenberre, Numerical Analysis of Heat Flow, 1st ed, McGraw-Hill Book Co., New York, Chapters 5, 6, and 11, 1949.
14. L. R. Ingersoll, O. J. Zobel, and A. C. Ingersoll, Heat Conduction, 1st ed, McGraw-Hill Book Co., New York, Chapter 11, 1948.
15. Argonne Nat. Lab., ANL-4537, Dec. 15, 1950, pp 101-103 (classified).

SELECTED READING LIST

- HEAT TRANSFER, M. Jacob, Vol I, 1st ed, John Wiley & Sons, Inc., New York, Chapters 18 and 19, 1949.
- NUMERICAL METHODS OF ANALYSIS IN ENGINEERING, L. E. Grinter, 1st ed, Macmillan Co., New York, 1949.
- ENGINEERING EXPERIMENTAL STATION BULLETIN NO. 98, Purdue University, G. A. Hawkins and G. T. Agnew, March 1947.
- A STUDY OF THE NUMERICAL SOLUTION OF PARTIAL DIFFERENTIAL EQUATIONS, G. G. O'Brien, M. A. Human, and S. Kaplan, Jour. Math. and Phys. 24, No. 4, Jan. 1951, p 223.
- MEASUREMENT OF CP-2-REACTOR TRANSFER FUNCTION, Argonne Nat. Lab., J. M. Harrer, R. E. Boyar, and D. Krucoff, ANL-4373, Jan. 1952.
- FORMULAS AND TABLES OF COEFFICIENTS FOR NUMERICAL DIFFERENTIATION WITH FUNCTION VALUES GIVEN AT UNEQUAL-
LY SPACED POINTS AND APPLICATION TO SOLUTION OF PARTIAL DIFFERENTIAL EQUATIONS, Lewis Flight Propulsion Lab.,
Chung-Hua Wu, NACA-TN-2214, Nov. 1950, 104 pp.

CHAPTER 1.9

Thermal-stress Analysis

R. A. Daane

Thermal stresses occur in all parts of a reactor core as a result of the internal heat generated in the fissionable material and, to some extent, in all irradiated components. Removal of the heat produces temperature distributions which cause thermal stresses. Nuclear characteristics, strength, corrosion resistance, and economy considerations in many designs require a conjunction of various materials with different coefficients of expansion. When large parts are connected by elements of small cross section, the resulting expansion differences may produce great strain concentrations.

Rational determination of stresses and strains and their significance would require, in addition to complicated mathematical operations, knowledge of the behavior of the construction materials complete enough to permit the macroscopic mechanical condition of the material to be predicted for any conditions of temperature, stress, and stress history encountered in operation. Such extensive knowledge and, especially, mathematically useable laws formulated from such knowledge is not currently available, even for commonly used materials. The theory of elasticity, based primarily on the rule that stress is proportional to strain, provides a satisfactory approximation to these laws for most materials under restricted conditions, but the conditions accompanying thermal stresses in reactors often fall outside this restricted area.

The primary object of this chapter is to provide a skeletal basis for attacking thermal stress problems in reactor designs by presenting thermal-stress formulas for a few simple but frequently encountered cases, by indicating methods of analysis for other problems, and by listing some general relationships that show the order of magnitude of thermal stresses for selected shapes and temperature distributions. Material behavior characteristics which should be considered in analyzing thermal stresses and in applying the results to reactor designs are also pointed out. A Selected Reading List is also presented which is grouped as follows: general methods of stress analysis, items (1) through (20); design data in the form of solutions to and methods of analysis of specific types of problems, items (29) through (44); and the mechanical behavior of materials under conditions related to thermal-stress problems, items (14) through (28).

THERMAL-STRESS FORMULAS, RULES, AND RELATIONSHIPS

The following formulas relate to elastic thermal stresses occurring at the boundary surfaces* of simple shapes heated internally by a constant heat generation (q) per unit volume, cooled uniformly on the surface, and at steady-state temperature. Heat generation resulting from irradiation is not constant but is attenuated toward the interior of the

* Boundary surface stresses are usually the significant stresses since it is at the boundary surface that fatigue cracking usually originates.

material. However, this attenuation is negligible for small thicknesses and, when considered, results in a smaller maximum thermal stress for the cases given here. Nomenclature and units are presented in Table 1.9.1.

Table 1.9.1—Stress Analysis Nomenclature and Units

Symbol	Definition	Units
a	Inside radius of tube	in.
b	Outside radius of tube	in.
C	Curvature	1/in.
d	Diameter of solid cylinder	in.
E	Modulus of elasticity	psi
k	Thermal conductivity	Btu/(hr)(in.)(°F)
q	Heat generation per unit volume	Btu/(hr)(cu in.)
t	Thickness of flat plate	in.
T	Temperature excess with respect to reference temperature such that when T is uniformly zero, there is no stress	°F
T_{ave}	Mean temperature rise	°F
T_1, T_a , etc.	Temperature at surface denoted by subscript	°F
x, y	Rectangular coordinates	in.
α	Coefficient of thermal expansion	in./(in.)(°F)
ϵ	Unit strain	in./in.
ν	Poisson's ratio	None
σ_a	Longitudinal and circumferential stress at the inside surface of a tube	psi
σ_b	Longitudinal and circumferential stress at the outside surface of a tube	psi
σ_s	Stress at the boundary in a cross sectional plane of a prismatical shape	psi
σ_z	Longitudinal stress in cylinder	psi
σ_1	Stress in any direction parallel to the surface on side 1 of flat plate	psi
σ_θ	Circumferential stress in cylinder	psi

SIMPLE SHAPES

LONG, SOLID ROD

The maximum stresses, except for stresses near the ends (i.e., at a distance from the end less than or equal to the diameter of the cylinder), are at the boundary surface.

$$\text{Max Stress, } \sigma_\theta = \sigma_z = \frac{E\alpha q d^2}{32k(1-\nu)} \quad (1)$$

FIXED PLATE (NOT FREE TO BEND), COOLED ON ONE OR BOTH SURFACES, WITH TEMPERATURE T_1 ON SURFACE NO. 1 AND T_2 ON SURFACE NO. 2

• The maximum stress is at the surface with the lower temperature, T_1 . At the surface with temperature T_1 :

$$\text{Max Stress, } \sigma_1 = \frac{E\alpha}{2(1-\nu)} \left[\frac{qt^2}{6K} + (T_2 - T_1) \right] \quad (2)$$

FREE PLATE (FREE TO BEND)

The maximum stress is at the surface of the plate and is the same at both surfaces.

$$\text{Max Stress, } \sigma_1 = \sigma_2 = \frac{E\alpha q t^2}{12k(1-\nu)} \quad (3)$$

HOLLOW TUBE

The maximum stress, except for stresses near the ends, is at either the inside or the outside surface of the tube wall.

$$\text{Max Stress, } \sigma_a = \frac{\alpha E}{1-\nu} \left\{ \frac{q}{8k} \left[b^2 + a^2 - \frac{b^2 - a^2}{\log_e b/a} \right] + (T_b - T_a) \left[\frac{b^2}{b^2 - a^2} - \frac{1}{\log_e b^2/a^2} \right] \right\} \quad (4)$$

$$\sigma_b = \frac{\alpha E}{1-\nu} \left\{ \frac{q}{8k} \left[b^2 + a^2 - \frac{b^2 - a^2}{\log_e b/a} \right] + (T_b - T_a) \left[\frac{a^2}{b^2 - a^2} - \frac{1}{\log_e b^2/a^2} \right] \right\} \quad (5)$$

THIN-WALLED TUBE

When the thickness of the tube wall is less than about one-tenth of the inner radius, thermal stresses not near the ends are approximately the same as those for a flat plate, fixed against bending, whose thickness is equal to that of the tube wall. The stresses in this case are given by Eq. (2).

If there are no surface forces or restraint forces, the maximum stresses near the ends are, for cylinders, somewhat larger than those given above by a factor which depends on the thickness of the tube wall. The percentage increase in maximum stress near the ends varies from about 10 percent for a solid rod to about 20 percent for a thin-walled tube.^{1,2}

No simple formulas can be derived for calculating thermal stresses in more complicated cases. In general, solutions must be obtained by methods such as those described in items (1) through (20) of the Selected Reading List.

DISTORTIONS OF LONG PRISMATICAL SHAPES

Another frequently encountered problem in reactor stress analysis is the calculation of the distortions of parts the function of which would be impaired by large changes in shape. Reactor control rods are examples. The shapes of many such members approximate long prisms with temperatures constant in the z (longitudinal) direction. For such objects, the distortion consists of:

- (1) Pure bending (i.e., uniform curvature of the member in a longitudinal plane with no warp of cross-sectional planes and no twist).
- (2) Uniform longitudinal expansion.
- (3) Cross-sectional distortions within cross-sectional planes.

Considering the curvature assumed by the bar as made up of two components of curvature, C_x and C_y (the curvature in x - z and y - z planes, respectively), these components are given by (assuming elastic conditions):

$$C_x = \frac{\alpha \int T x dA}{I_y} \quad C_y = \frac{\alpha \int T y dA}{I_x} \quad (6)$$

where the integrations are to be made over the complete area of cross section of the member, I_y and I_x are the moments of inertia about the y and x axes, respectively, and the

¹References appear at end of chapter.

x and y axes are principal centroidal rectangular coordinate axes for the cross-sectional area.

Uniform expansion of the longitudinal centroidal axis is given by:

$$\epsilon_{z,0} = \frac{\alpha \int T dA}{\text{Area}} = \alpha T_{\text{ave}} \quad (7)$$

where T_{ave} is the mean temperature rise over the cross section, compared with a reference temperature for which $T = 0$.

Cross-sectional distortions may be calculated for each particular case, using the equations of elasticity for plane strain, superposing on these results the cross-sectional deformations:

$$-\nu(\epsilon_{z,0} + x \cdot C_x + y \cdot C_y)$$

STRESSES IN PRISMATICAL SHAPES WITH CONSTANT AXIAL TEMPERATURES, NOT NEAR THE ENDS

Boundary surface stresses are usually the most important thermal stresses. For elastic stresses at a boundary surface, Hooke's law reduces to:

$$\begin{aligned} \sigma_z - \nu \sigma_s &= E \epsilon_z \\ \sigma_s - \nu \sigma_z &= E \epsilon_s \end{aligned} \quad (8)$$

from which:

$$\sigma_z = \frac{E}{1 - \nu^2} (\epsilon_z + \nu \epsilon_s) \quad (9)$$

The strain, ϵ_z is:

$$\epsilon_z = \alpha T_a + x \cdot C_x + y \cdot C_y - \alpha T \text{ (at the point considered).} \quad (10)$$

If the temperature distribution in the prismatical shape is such that $C_x = C_y = 0$ (which would be the case when the temperatures are symmetrical with respect to a pair of x and y axes) or if the bar is restrained against bending, then:

$$\sigma_z = \frac{E \alpha (T_{\text{ave}} - T)}{1 - \nu^2} \left(1 + \nu \frac{\epsilon_s}{\epsilon_z} \right) \quad (11)$$

The stress σ_s and the strain ϵ_s depend on the cross-sectional shape and are not, in general, limited to any simply expressed value. However, if the cross-sectional shape is simple (i.e., does not involve thin webs or flanges) and if we are considering a point on a relatively smooth part of the boundary, then, in general:

$$\epsilon_s \cong \epsilon_z$$

so that:

$$\sigma_z = \frac{E \alpha (T_{\text{ave}} - T)}{1 - \nu} \quad (12)$$

EFFECT OF AXIAL TEMPERATURE GRADIENTS IN PRISMATICAL SHAPES

If there are no resultant forces or moments acting over any complete cross section in a thermal-stress problem, then, for a prismatical shape, by St. Venants' principle,³ the stresses at any point depend only on the temperature distribution within a short distance of the point (approximately a distance equal to the major dimension of the cross section). This is only a general rule, applicable to reasonably simple shapes.

Accordingly, axial temperature differences do not cause appreciable stresses when the variation of temperature along the axis is rather gradual. The elastic stress resulting from an axial variation in temperature is generally less than:

$$\frac{1}{2}E\alpha(\Delta T)_d$$

where $(\Delta T)_d$ is the difference in temperature occurring over a length equal to a major cross-sectional dimension. Even then, there must be a change in axial temperature gradient near the point considered in order to have this large a stress. (Further information will be found in items (39) and (40) of the Selected Reading List.)

GENERAL CONSIDERATIONS

THE NATURE OF THERMAL STRESSES

The system of thermal stresses developed in an unrestrained body is that equilibrium system of stresses which produces strains at each point such that the total unit deformations (thermal expansions plus strains) constitute a compatible set of deformations. In other words, temperature differences within a body produce strain differences and associated stress differences which keep the elementary parts of the body fitting together. Temperatures which vary linearly with respect to rectangular coordinates do not produce any stress in a free body because the associated expansions constitute a compatible system.

Temperature differences do not give rise to boundary surface loads. Thus, in an unrestrained body, thermal stresses must be so distributed that the resultant shear force, normal force, and bending and twisting moments acting over any complete cross section* of the body are zero.

These considerations apply to a multiply connected body considered in its entirety as well as to simply connected bodies. However, in a multiply connected body or in a group of mechanically connected parts, resultant loads and moments may act on some cross sections. Special attention should be given to thermal stresses in multiply connected components having large parts connected by relatively small sections since large resultant forces or moments may exist in these small sections. Reactor core structures usually involve such problems. The calculation of thermal stresses in multiply connected objects usually requires all of the considerations made in a statically indeterminate structure analysis. Items (6) through (9) and (38) of the Selected Reading List pertain to such analyses.

THE ORDER OF MAGNITUDE OF THERMAL STRESSES AND STRAINS

In accordance with the nature of thermal stresses, the largest thermal strain occurring in an unrestrained body of fairly regular† shape with a non-linear temperature distribution

* The term complete cross section is used to designate a cross section or the sum of cross sections cutting the body into two separate parts. In a multiply connected body, it is possible to make a complete cut over a cross section (interior surface completely bounded by the external surface of the body) without separating the body into two parts.

† "Regular" is used to refer to shapes not having sections which are thin compared with other parts of the body. In such thin sections, concentrated strains may occur.

has an order of magnitude equal to the product of the coefficient of expansion (α) and the maximum temperature difference (ΔT) existing in the body. Then for elastic conditions, the order of magnitude of the maximum stress is:

$$\text{Stress} \cong E\alpha\Delta T$$

It is emphasized that these expressions are approximations and cannot be used indiscriminately for precise calculations. The actual stress and strain depends upon the three-dimensional distribution of expansions, stresses, and strains existing in the body, taking into account the effect of strains in directions normal to the strain considered. The more irregular the geometry of the body, the more in error these rules may be. However, as an approximate rule of thumb for simple regular shapes, this estimate of maximum stress or strain may justify disposing of the thermal stress problem without further analysis.

If the material is ductile and if the temperature differences are large enough to cause strains above the elastic limit,* then the order of magnitude of the strain for a simple shape is still that given by the above rule. However, the stress may be considerably smaller than $E\alpha\Delta T$, since for plastic strains a lot less stress is required to produce a given strain than for elastic strains. Unlike stresses caused by sustained mechanical loads where resultant forces and moments must be balanced by definite stresses in the material regardless of the strain that occurs, thermal stresses above the elastic limit must be calculated according to a reasonably realistic theory of plasticity, even though the mathematical difficulties encountered in such calculations make it necessary to use a greatly simplified and approximate idealization of plastic behavior.

In recent years, much work has been done to develop applicable theories of inelastic stress analysis. Applicable discussions are presented in items (10) through (20) of the Selected Reading List.

THE SIGNIFICANCE OF THERMAL STRESSES

The significance of the results of thermal-stress calculations, aside from the design significance of the thermal strains and distortions which must be determined as a part of the stress analysis, is their indication of the probability that the component will fracture under stresses combined with mechanical loads. Thermal stresses are predominately biaxial or triaxial. Stress problems in reactors usually concern materials at elevated temperatures. Cyclic thermal stresses usually consist of large stresses with a relatively small number of cycles occurring during the life of the reactor.

For these conditions, sufficient information is not available to allow accurate prediction of either static or fatigue fractures. However, some probable relationships between thermal stresses and different types of failure are presented in Table 1.9.2. Items (17) through (26) of the Selected Reading List are representative of the available information of this type.

*"Elastic limit" is the largest stress or strain which may occur in a material without causing a permanent deformation; when strains are below the elastic limit strain, stress is proportional to strain, and the strain or deformation does not depend on time. These rules of behavior form the principal basis of the theory of elasticity. Except for a few materials such as bronze and mild steel, this usage of the term "elastic limit" is a simplifying idealization of the behavior of materials. For most materials, some permanent strain will result from even the smallest stress, and the stress-strain curve is actually curved from the outset, but the deviations from the idealized elastic behavior are very small for low stresses and gradually increase as the stresses increase. Also, at higher stresses, flow may occur; i.e., the strain increases with time while the stress remains constant. Thus "elastic limit" is usually taken to mean a conventional elastic limit, below which the stresses may be calculated according to the theory of elasticity to a degree of approximation permissible for the given problem. Above this conventional elastic limit, the material behavior is described as being plastic.

Table 1.9.2—Effects of Thermal Stress

Mode of failure	Type of component	Material property of primary importance	Significant stress or strain combination measuring probability of failure
Static rupture	Brittle material	Ultimate strength	Maximum elastic tensile stress
Static rupture	Regular shape ductile material	...	No rupture is likely
Static rupture	Ductile material irregular shape, especially when multiply connected, where concentrated strain may occur	Ductility (elongation and reduction of area)	Unknown for combined stresses Maximum strain for uniaxial stress
Creep buckling (or other distortions in excess of elastic or short time plastic distortions)	Fuel plates, webs, flanges or thin sections of irregular shapes and multiply connected bodies	Creep rate for stress and temperature encountered	Intensity of stress (decreasing as creep occurs): $\sqrt{(\sigma_1 - \sigma_2)^2 + (\sigma_2 - \sigma_3)^2 + (\sigma_3 - \sigma_1)^2}$ where σ_1 , σ_2 and σ_3 are principal stresses. Inelastic stress
Creep	Regular shape	...	No appreciable effect is likely to occur
Fatigue	Any part	Endurance, or cycles to failure for specific combination of stress and temperature encountered. For the most part, unknown for high combined stresses and elevated temperature	Stress intensity of biaxial boundary surface stresses, $\sqrt{2(\sigma_1^2 - \sigma_1\sigma_2 + \sigma_2^2)}$ where σ_1 and σ_2 are the principal stresses at the boundary surface. Elastic or inelastic stress

IRRADIATION EFFECTS

Data on the effects of irradiation on the behavior of materials are presented in Sect. 3.2, "Radiation and Thermal Effects," Volume 3.

In some materials, such as uranium and graphite, irradiation produces growth or unit deformations. Such deformations may give rise to stresses in the same manner that differential expansions produce stresses but may be much greater than the differential thermal expansions encountered. Consequently, stresses and distortions of this type should be considered in a reactor design.

Irradiation in reactors may change the properties of the component materials. An increase in notch sensitivity has been found to occur in some boiler steels. These changes in properties may not only determine what the allowable stresses are but may also affect the method of analysis and especially the significance of thermal stresses.

REFERENCES

1. S. Timoshenko, *Theory of Elasticity*, 1st ed, Engineering Societies Monograph, McGraw-Hill Book Company, Inc., New York, 1934, pp 151 and 174.
2. F. H. Murray, *Thermal Stresses and Strains in a Finite Cylinder with No Surface Forces*, AECD-2966, Jan. 9, 1945.
3. Timoshenko, loc cit, p 31.

SELECTED READING LIST

1. THEORY OF ELASTICITY, S. Timoshenko, 1st ed, Engineering Societies Monograph, McGraw-Hill Book Company, Inc., New York, 1934.
2. SOME PRACTICALLY IMPORTANT STRESS SYSTEMS IN SOLIDS OF REVOLUTION, R. V. Southwell, *Proc. Roy. Soc., London*, A, 180, 1942, pp 367 and 396.
3. RELAXATION METHODS APPLIED TO ENGINEERING PROBLEMS, VII D, STRESS DISTRIBUTION IN ELASTIC SOLIDS OF REVOLUTION, D. N. de G. Allen, L. Fox and R. V. Southwell, *Phil. Trans. Roy. Soc., London*, Series A, Vol. 239, 1945, pp 501-537.
4. RELAXATION METHODS IN ENGINEERING SCIENCE, R. V. Southwell, Oxford Press, 1946.
5. RELAXATION METHODS IN THEORETICAL PHYSICS, R. V. Southwell, Oxford Press, 1946.
6. STRENGTH OF MATERIALS, S. Timoshenko, 2nd ed, Vols. I and II, D. Van Nostrand, Inc., 1930.
7. THEORY OF ELASTIC STABILITY, S. Timoshenko, Engineering Societies Monograph, McGraw-Hill Book Company, Inc., New York, 1936.
8. THEORY OF PLATES AND SHELLS, S. Timoshenko, Engineering Societies Monograph, McGraw-Hill Book Company, Inc., New York, 1940.
9. THEORY OF STRUCTURES, S. Timoshenko and D. H. Young, 1st ed, McGraw-Hill Book Company, Inc., New York, 1945.
10. RECENT DEVELOPMENTS IN THE MATHEMATICAL THEORY OF PLASTICITY, W. Prager, *Jour. Applied Phys.*, Vol. 20, March 1949, pp 235-241.
11. THEORY OF PERFECTLY PLASTIC SOLIDS, W. Prager, *Applied Mathematics Series*, John Wiley & Sons, Inc., New York, 1951.
12. THE INELASTIC BEHAVIOR OF ENGINEERING MATERIALS AND STRUCTURES, A. M. Freudenthal, John Wiley & Sons, Inc., New York, 1950.
13. THE MATHEMATICAL THEORY OF PLASTICITY, R. Hill, Oxford University Press, 1950.
14. GENERAL STRESS-STRAIN LAWS OF ELASTICITY AND PLASTICITY, A. Gleyzal, *Jour. Applied Mech.*, Vol. 13, Dec. 1946, pp A261-264.
15. CORRELATION OF TENSION CREEP TESTS WITH RELAXATION TESTS, E. P. Popov, *Jour. Applied Mech.*, Vol. 14, 1947, pp A135-142.
16. BIBLIOGRAPHY ON PLASTICITY, IT'S THEORY AND APPLICATIONS, ASME—Metals Engineering Division, The Society, 1950.
17. PLASTICITY, A. Nadai and A. M. Wahl, McGraw-Hill Book Company, Inc., New York, 1931.
18. THE INTERPRETATION OF CREEP TESTS FOR MACHINE DESIGN, C. R. Soderberg, *Trans. Am. Soc. Mech. Engr.*, Nov. 1936, p 733.

19. THEORY OF FLOW AND FRACTURE OF SOLIDS, A. Nadai, 2nd ed, McGraw-Hill Book Company, Inc., New York, 1950.
20. HANDBOOK OF EXPERIMENTAL STRESS ANALYSIS, Edited by M. L. Hetenyi, Chapter 10, "Working Stresses," C. R. Soderberg, John Wiley and Sons, Inc., New York, 1950, pp 438-458.
21. FATIGUE OF METALS, H. F. Moore and J. B. Kommers, 1st ed, McGraw-Hill Book Company, Inc., New York, 1927.
22. ABSTRACTS OF ARTICLES ON FATIGUE OF METALS UNDER REPEATED STRESS, JULY 1, 1928 TO JUNE 30, 1930, Prepared by the A. S. T. M. Research Committee on Fatigue of Metals, Philadelphia, Pennsylvania, 1929-1931.
23. PREVENTION OF THE FAILURE OF METALS UNDER REPEATED STRESS, Battelle Memorial Institute, John Wiley & Sons, Inc., New York, 1941.
24. FAILURE OF METALS BY FATIGUE, University of Melbourne, University Press, Melbourne, Australia, 1947.
25. AN INVESTIGATION OF THE ABILITY OF ZIRCONIUM TO WITHSTAND STRESSES CAUSED BY THERMAL CYCLING, Westinghouse Atomic Power Division, D. D. Frederick, WAPD-EM-167, Classified, April 23, 1952, p 24.
26. AN INVESTIGATION OF THE ABILITY OF TYPE 347 STAINLESS STEEL TO WITHSTAND STRESSES CAUSED BY THERMAL CYCLING, Westinghouse Atomic Power Division, D. D. Frederick, WAPD-EM-159, Jan. 31, 1952.
27. CYCLIC HEATING TEST OF MAIN STEAM PIPING BETWEEN FERRITIC AND AUSTENITIC STEELS—SEWAREN GENERATING STATION, H. Welsberg, ASME Trans., 71, Aug. 1949, pp 643-664.
28. THERMAL SHOCK AND OTHER COMPARISON TESTS OF AUSTENITIC AND FERRITIC STEELS FOR MAIN STEAM PIPING—A SUMMARY REPORT, W. C. Stewart and W. G. Schreitz, ASME Paper No. 52-A-35, presented at Annual Meeting, Dec. 1952.
29. MEMOIRES PAR DRIVERS SAVANTS, J. M. C. Duhamel, French Academy, Vol. 5, Paris, 1838, p 440.
30. ON THE STRESSES IN SOLID BODIES DUE TO UNEQUAL HEATING, AND ON THE DOUBLE REFRACTION RESULTING THEREFROM, Lord Rayleigh, Phil. Mag., Series 6, Vol. I, 1901, pp 169-178.
31. THE CALCULATION OF TEMPERATURE STRESSES IN TUBES, ENGINEERING, L. H. Barker, Vol. 124, 1927, p 443.
32. THERMAL STRESSES IN SPHERES AND CYLINDERS PRODUCED BY TEMPERATURES VARYING WITH TIME, C. H. Kent, Trans. Am. Soc. Mech. Engr., Vol. 54, No. 18, 1932, p 185.
33. THE THERMAL STRESSES IN SPHERES AND CYLINDERS PRODUCED BY TEMPERATURES VARYING WITH TIME, C. H. Lees, Trans. Am. Soc. Mech. Engr., Vol. 54, No. 18, 1932, p 185.
34. A GENERAL PROPERTY OF TWO-DIMENSIONAL THERMAL STRESS DISTRIBUTION, M. A. Boit, Phil. Mag., Vol. 19, 1935, p 540.
35. THERMAL STRESSES IN PLATES, J. L. Maubetsch, Jour. Applied Mech., Vol. 2, No. 4, Dec. 1935.
36. TEMPERATURE STRESS IN FLAT RECTANGULAR PLATES, AND IN THIN CYLINDRICAL TUBES, J. Franklin Institute, Aug. 1936, p 149.
37. THERMAL STRESSES, J. N. Goodier, Trans. Am. Soc. Mech. Engr., Vol. 59, Paper A-33, 1937.
38. FORMULAS FOR STRESS AND STRAIN, R. J. Roark, 2nd ed, McGraw-Hill Book Company, Inc., New York, 1943.
39. STRESSES IN LONG THIN-WALLED CYLINDERS, DUE TO AN AXIAL TEMPERATURE GRADIENT, G. Horvay and W. P. Manger, KAPL-390, Aug. 15, 1950.
40. CIRCULAR CYLINDER STRESSES, M. Kornhauser, Jour. Am. Soc. Nav. Engrs., 62, No. 1, 1950, pp 55-62.
41. THERMAL STRESSES AND STRAINS IN A FINITE CYLINDER WITH NO SURFACE FORCES, F. H. Murray, AECD-2966, Jan. 9, 1945.
42. THERMAL BUCKLING OF PLATES, M. L. Gossard, Paul Seide, W. M. Roberts, NACA-TN-2771, Aug. 1952.
43. THE PLANE STRESS PROBLEM OF PERFORATED PLATES, G. Horvay, Jour. Applied Mech., 19, No. 3, Sept. 1952, pp 355-360.
44. STRESSES IN PERFORATED SHEETS DUE TO NON-UNIFORM HEATING, G. Horvay, KAPL-566, Aug. 17, 1951.

CHAPTER 1.10

Water Decomposition

H. O. Monson

Water subjected to reactor irradiation undergoes decomposition. In general, the amount of decomposition is extremely small and, for practical purposes, often may be assumed negligible. Among the aspects of decomposition most frequently suggested as representing possible practical problems are the following: effect of the decomposition products on corrosion resistance of containing vessels; requirements of degasification equipment for removing decomposition products; requirements of burner (catalytic) equipment for recombining the decomposition products to reform water; formation of explosive mixtures by accumulation of gaseous decomposition products; effect of bubbles of gaseous decomposition products on heat-transfer characteristics or on reactor reactivity; and loss of heavy water. Experience with reactors has shown that some of these possible problems never are manifested, while others, although they should be considered under some circumstances, are relatively minor in magnitude and rather easily handled in practice.

The mechanism of water decomposition is complicated. There are many variables involved in the decomposition process, and the effects of some of these have not yet been completely investigated. Although the qualitative picture is fairly well developed, particularly for water at ordinary temperature, much uncertainty remains with respect to many of the quantitative considerations. The intent here is to provide, first, a general qualitative description of the decomposition process, and second, a brief survey of quantitative experimental data.

The treatment presented here is meant to apply only to water employed for cooling or moderating stationary-fuel reactors, not to water used for carrying fuel. This limitation, in effect, limits the types of radiation absorbed by the water to gamma radiation and neutron radiation.

A qualitative description of decomposition is given under the following headings: **GENERAL CONSIDERATIONS**, an approximate picture of the gross process; **THE MECHANISM**, the role of ionization and the principal chemical reactions involved; and **MAJOR FACTORS**, the major variables and their effects upon decomposition. Finally, under **PRACTICAL CONSIDERATIONS**, general observations on decomposition which are of interest to the reactor designer, general rules for minimizing decomposition, and specific decomposition data obtained from in-reactor experiments and from full-sized reactors are presented.

GENERAL CONSIDERATIONS

For water at high temperatures (above about 200°F), the end products of decomposition are gaseous hydrogen* and oxygen. At ordinary temperatures, the end products are gaseous

* For heavy water (D_2O), all references to hydrogen are to be interpreted as deuterium.

hydrogen, gaseous oxygen, and hydrogen peroxide in solution. This temperature dependency of the nature of the decomposition end products results from breakdown of the peroxide at high temperatures to form oxygen (and water).

The instantaneous **RATE OF DECOMPOSITION** of water is equal to the difference between two separate rates of reaction; viz, the rate of the **FORWARD REACTION**, which converts water to decomposition products, and the rate of the **BACK REACTION**, which converts decomposition products to water.

When water is first irradiated, no back reaction exists initially since there are no decomposition products present to be converted to water. The initial rate of decomposition is therefore equal to the rate of the forward reaction. If the decomposition is allowed to proceed within a closed system, accumulation of decomposition products leads to a back reaction by which some of the products are converted to water; the rate of decomposition, accordingly, is reduced. As the concentrations of decomposition products increase, the rate of the back reaction also increases in accordance with the mass-action law, and the rate of decomposition is eventually reduced to zero; that is, an **EQUILIBRIUM CONDITION** is achieved in which the rate of the back reaction exactly equals the rate of the forward reaction, the rate of decomposition equals zero, and the decomposition-product concentrations remain constant at their maximum, equilibrium values.

On the other hand, if the decomposition is allowed to proceed (hypothetically) within a completely open system, i.e., a system from which the decomposition products are removed immediately upon being formed (with the result that the concentrations of the products never become greater than zero), the rate of decomposition remains constant with time and equal to the initial, maximum rate.

Actually, the conditions most often applying to water used to cool or moderate reactors lie somewhere between these two extremes. The gaseous decomposition products normally are being continuously removed from the water, but at too low a rate to maintain zero product concentrations within the water. The product concentrations therefore increase to some intermediate value, while the rate of decomposition (or rate of gas generation) decreases correspondingly. Often, an essentially constant rate of removal of decomposition products exists, so that the system ultimately reaches a **STEADY-STATE CONDITION** in which the rate of decomposition (gas generation) equals the rate of removal and the decomposition product concentrations remain constant.

Sometimes, one or more decomposition products are also generated in the water by some extraneous process (as, for example, generation of hydrogen by corrosion of container materials). The steady-state condition in such a case results when the total rate of generation (rate of extraneous process plus rate of decomposition) exactly equals the rate of removal. In practice, the decomposition products are removed from the water continuously by deliberate, mechanical degasification or by natural diffusion from the water to a gas space above the water surface.

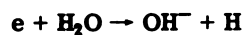
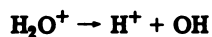
The preceding description illustrates the general picture of water decomposition, but the picture as presented is not rigorously correct. One discrepancy is that not all decomposition products enhance the rate of the back reaction (hydrogen does, but oxygen or hydrogen peroxide in excess actually inhibits the back reaction). A more accurate picture must consider not only this discrepancy but also a number of other factors which affect the decomposition process. Before taking up these factors, the general mechanism of water decomposition is described.

THE MECHANISM

Decomposition of water by reactor radiations occurs primarily because of the ionizing abilities of the radiations. Fission recoils, alpha particles, protons (or deuterons), gamma rays, and beta rays are all present within a reactor, and all are potentially capable

of ionizing water. However, in stationary-fuel reactors employing water solely for cooling or moderating (as opposed to fuel carrying), only protons and gamma rays are effective, the other radiations being almost completely absorbed by fuel elements and structural materials before reaching the water. Protons appear in the water as a result of collisions between epithermal neutrons and the nuclei of hydrogen atoms of the water; the neutrons undergo a loss in energy, and the nuclei are ejected from their atoms as energetic protons. The protons ionize water molecules directly, by virtue of their charge and speed. The gamma rays do not ionize directly but are absorbed within the water by photoelectric effect, Compton effect, or pair-production, each type of absorption resulting in production of high-speed electrons. The electrons thus produced then ionize the water molecules directly.

In brief, the epithermal-neutron flux within a reactor is responsible for the production of protons in the water. The protons, together with the electrons produced by gamma rays, ionize molecules of the water to give H_2O^+ ions and secondary electrons. Starting with these ions, a series of chemical reactions then automatically ensues which finally results in decomposition. The initial chemical reactions are:



which have the net result:



The free radicals, H and OH, then may react according to:

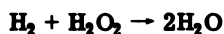


and these are the processes which constitute the forward reaction converting water to decomposition products (the H_2O_2 being further decomposed at high temperatures to O_2 and water).

The free radicals of Eq. (1) may also react, however, according to:



with the net result:

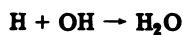


and these are the processes which constitute the back reaction converting decomposition products to water. This reaction is a chain reaction which, presumably, proceeds indefinitely unless interrupted by some sort of chain-termination reaction.

There are also other reactions in which the free radicals, H and OH, may take part:



with the net result:



or:

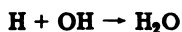


with the same net result. The effect of these processes is to reduce the back-reaction rate, thereby promoting decomposition by removing H and OH radicals which are necessary to the back-reaction processes of Eqs. (4) and (5).

The free radicals may also become involved in reactions with ionic impurities in the water. A number of such processes are possible, one example being:



with the net result:



Regardless of the exact mechanisms involved, the effect of processes of this type is always to reduce the back-reaction rate and promote decomposition, again by removing the necessary H and OH radicals.

A reaction which complements the back reaction of Eqs. (4) and (5) is:



This reaction may be considered both as radiation-induced and as a catalyzed thermal reaction (catalysis being effected by certain impurities in the water, as discussed later).

With the above general mechanism in mind, various factors which have important effects on the decomposition of water may be examined.

MAJOR FACTORS

Primarily, the instantaneous rate of water decomposition and the equilibrium concentrations of decomposition products within water (and therefore the maximum partial pressures exerted by the gaseous products) are dependent upon four major factors:

- (1) The nature and intensity of the radiation.
- (2) The temperature of the water.
- (3) The nature and extent of ionic impurities in the water.
- (4) The concentrations of the decomposition products in the water.

These four factors are discussed briefly below, both with regard to water irradiated at elevated temperature and water irradiated at moderate temperature. Since hydrogen peroxide has not been detected experimentally in water irradiated at high temperature, the chemical reactions which result in decomposition at elevated temperature probably differ somewhat from those which produce decomposition in water irradiated at moderate temperature; therefore, data pertaining to water at moderate temperature may not be applied unqualifiedly to water at elevated temperature.

EFFECT OF NATURE AND INTENSITY OF RADIATION

The ionizing ability of a charged particle is a result of its charge and its motion. For a moving particle with a given charge, the probability of its ionizing molecules lying in its path becomes greater as the velocity of the particle becomes smaller (down to a velocity where the particle either has become neutralized or has insufficient energy to effect ionization). Since the magnitude of the charge of a proton is the same as that of an electron and since its velocity, for the same energy, is much smaller, the probability of ionizing water molecules lying in the path of a proton (produced by an epithermal neutron) is much greater than for an electron (produced by a gamma ray). Accordingly, the ionization density [and therefore the local concentration of H and OH free radicals formed in accordance with Eq. (1)] along the tracks of protons coursing through water is very much greater than along the tracks of electrons.

Since gamma (electron) radiation results in the formation of free radicals only at widely separated intervals along the radiation tracks, the free radicals get little chance to react with each other to form decomposition products in accordance with Eqs. (2) and (3). Instead, many drift away from the tracks into the bulk of the water and become available for reacting with decomposition products (to form water) in accordance with Eqs. (4) and (5). The ratio of the number of pairs of free radicals which form decomposition products to the number of pairs which become available for recombining the decomposition products is about one to four. This results in a weak forward reaction and a very strong back reaction, and in pure water, gamma radiation alone produces no decomposition. In fact, gamma radiation provides a reserve of recombination potential, and radiation of another nature which may tend to produce decomposition must first overcome this excess capacity for recombination before any decomposition can result.

On the other hand, epithermal neutron (proton) radiation results in the formation of relatively close free radicals. Many of these radicals have the opportunity therefore to combine in accordance with Eqs. (2) and (3) to produce decomposition products before becoming dispersed. Relatively few radicals drift away from proton tracks and become available for the back reaction of Eqs. (4) and (5). The ratio of the number of pairs of free radicals which form decomposition products to the number which become available for recombining the decomposition products is comparatively high (the exact value of the ratio not yet having been determined). Consequently, a strong forward reaction, together with a weak back reaction, results, and epithermal-neutron irradiation of pure water produces appreciably high rates of decomposition.

When water is irradiated by gamma rays and epithermal neutrons simultaneously, the rate of decomposition is greatly reduced from that which would exist if neutron radiation alone were present. This important effect occurs, as indicated above, because the free radicals formed by the gamma rays and dispersed into the bulk of the water by diffusion help to convert the decomposition products produced by the epithermal neutron radiations to water through Eqs. (4) and (5). As the intensity of epithermal-neutron radiation is increased from zero for a given gamma-radiation intensity, the rate of decomposition remains at zero until the neutron-radiation intensity is sufficient to overcome the reserve recombination capacity of the gamma radiation. Further increase in the neutron-radiation intensity then results in a progressively higher (initial) rate of decomposition. The minimum neutron-radiation intensity required to effect decomposition, of course, is increased as the gamma-radiation intensity is increased.

In brief, the decomposition effects on reactor water subjected to epithermal neutron and gamma fluxes simultaneously are these: both the instantaneous rate of decomposition and the equilibrium concentrations of decomposition products increase with increase in epithermal neutron flux (unless the flux remains below the minimum value required to produce decomposition); both decrease with increase in gamma flux (unless the flux was initially

high enough to prevent any decomposition); of most importance, *under the average neutron- and gamma-flux levels existing in cooling water or moderating water of present reactors, both the instantaneous decomposition rates and the maximum concentrations of decomposition products are very close to zero (for initially gas-free, relatively pure water).*

LOW TEMPERATURE

Experimental evidence indicating the relative effects of epithermal neutron and gamma fluxes has been obtained. Figure 1.10.1 relates the total pressure exerted by gaseous decomposition products (or, effectively, the concentration of the gaseous products) to the

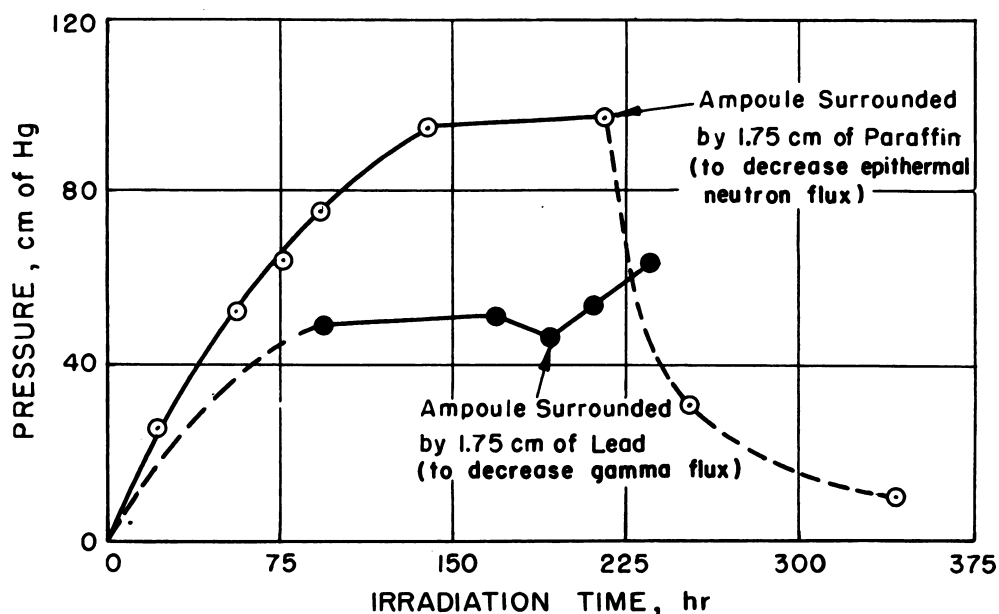


Fig. 1.10.1 — Effect of Change in Nature and Intensity of Radiation upon Water Decomposition Product Equilibrium Pressure as Observed with Partially Filled Ampoules Irradiated in Oak Ridge X-10. Redrawn from ORNL-130, Oct. 11, 1949.

irradiation time for water irradiated in a quartz ampoule at 77°F in the ORNL X-10 reactor.¹ The slope of the curve is quantitatively indicative of the rate of decomposition; where a slope equals zero, equilibrium exists. On one run (upper curve) after equilibrium was established, a shield of paraffin was placed around the ampoule to decrease the epithermal neutron flux without appreciably changing the gamma flux. Upon introduction of the shield, the pressure fell rapidly as a result of the reduction in the forward-reaction rate, Eqs. (2) and (3), without an accompanying reduction in the back reaction rate. On the other run (lower curve) after equilibrium was established, a shield of lead was placed around the ampoule to decrease the gamma flux without impairing the neutron flux. On inserting the lead shield, the pressure rose rapidly as a result of the reduction in the back-reaction rate, Eqs. (4) and (5), and consequent resumption of decomposition. The difference between the equilibrium pressures shown for the two runs was caused by a difference in water purity and has no bearing on the present discussion.

¹References appear at end of chapter.

The back reaction is augmented by another type of product recombination; viz, radiation-induced recombination of hydrogen and oxygen to form water in accordance with Eq. (13). Experimental evidence¹ indicates that, at low temperature, the back reaction is substantially bolstered by this process (when the concentrations of hydrogen and oxygen are high) in liquid water but does not occur in the vapor phase. The effect of such recombination is to reduce the decomposition rate (except for the initial, maximum rate), as well as the decomposition-product equilibrium concentrations.

HIGH TEMPERATURE

Experimental results^{2,3} indicate that the rate of recombination of hydrogen and oxygen in accordance with Eq. (13) while under irradiation at high temperature is appreciable. Figure 1.10.2 shows, as a function of time, the total partial pressure of hydrogen and oxygen added to the vapor phase of an ampoule containing both liquid- and vapor-phase

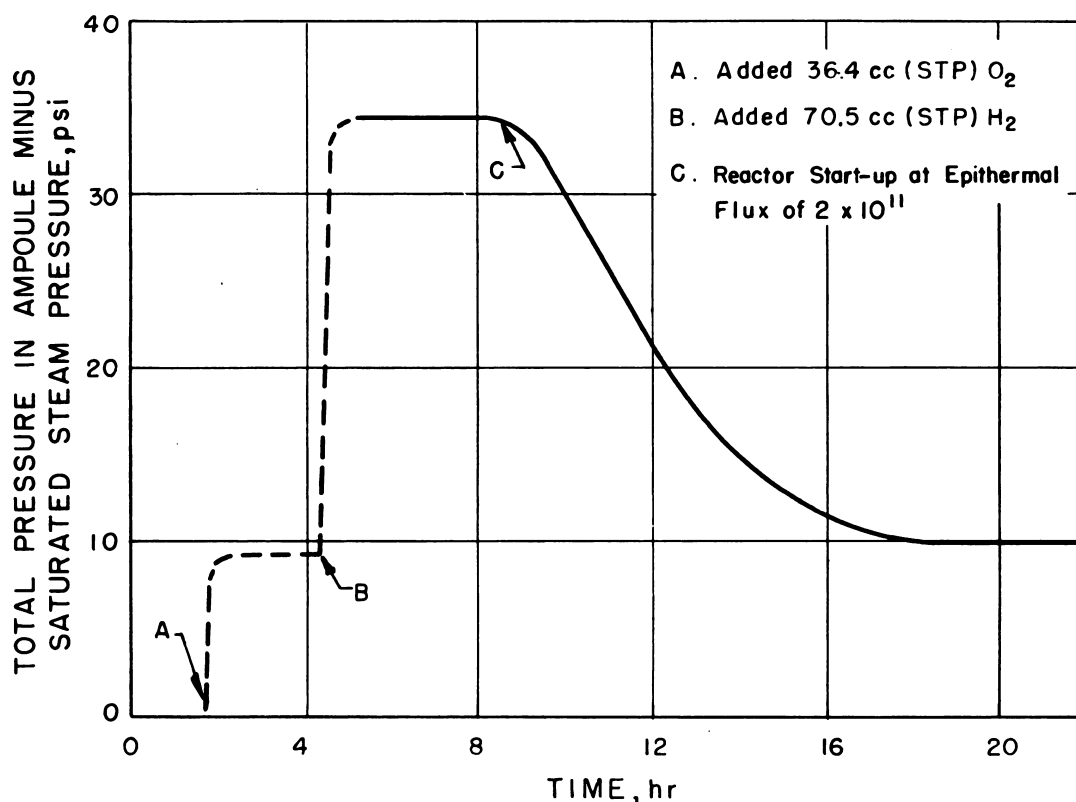


Fig. 1.10.2— Radiation-induced Recombination of Hydrogen and Oxygen in an Ampoule Partially Filled with Water. Redrawn from ANL-4628, May 1, 1951.

water at 202°F.² Although the pressure remained constant in the absence of irradiation, a rapid reduction in pressure, indicating recombination, commenced upon start-up of the reactor. At high temperature, contribution to the back reaction by Eq. (13) seems to occur in both liquid- and vapor-phase water.³ Again, the result is reduction in the decomposition rate and equilibrium concentrations.

EFFECT OF TEMPERATURE

The important effect of temperature is that *in general, increased temperature results in reduced decomposition rates and equilibrium concentrations of decomposition products.*

Temperature does not affect the forward-reaction rate and, consequently, does not affect the initial, maximum decomposition rate. It does, however, influence the rate of back reaction expressed by Eqs. (4) and (5), an increase in temperature producing an increase in back-reaction rate. Therefore, the rate of decomposition experienced with concentrations of decomposition products anywhere between zero (where the initial, maximum decomposition rate occurs) and the equilibrium value (where the decomposition rate equals zero) is reduced by increase in temperature; similarly, the equilibrium concentrations of decomposition products are reduced.

Experimental results have been obtained which suggest that the rate of radiation-induced recombination of hydrogen and oxygen by the process of Eq. (13) also may be influenced by temperature. At elevated temperature, the rate of this reaction apparently becomes fairly high and is effective in reducing the rate of decomposition and the equilibrium concentrations of decomposition products.

LOW TEMPERATURE

In one experiment⁴ utilizing relatively pure water in a quartz ampoule, increasing the water temperature from 97°F to 230°F reduced the equilibrium partial pressure (effectively, gaseous decomposition-product concentration) from 14 to 1.2 psi. Much of this effect is probably attributable to an increased rate of the back reaction of Eqs. (4) and (5). A graph of the data from this experiment is shown in Fig. 1.10.3.

HIGH TEMPERATURE

A recent series of experiments⁵ suggests that the rate of radiation-induced recombination of hydrogen and oxygen in accordance with Eq. (13) in an ampoule containing both liquid- and vapor-phase water increases with increase in temperature up to about 300°F. Above about 300°F, the rate of this recombination reaction seems to be fairly high and essentially independent of temperature. A graph of some of the data obtained in these experiments is shown in Fig. 1.10.4.

EFFECT OF IMPURITIES

The important effect of ionic impurities is that, *in general, the presence of ionic impurities results in increased decomposition rates and equilibrium concentrations of decomposition products, some impurities producing slight increases and others producing very large increases.*

Ionic impurities in water have no effect upon the forward-reaction rate. Many types of such impurities, however, have been shown to reduce the back-reaction rate. The ionic impurity reacts with the free radicals H and OH by some scheme of the type illustrated by Eqs. (10), (11), and (12), thereby removing free radicals which are required for the back reaction of Eqs. (4) and (5). Consequently, almost any ionic impurity capable of reacting with H and OH radicals increases the rate of decomposition (except for the initial, maximum rate which is not affected) by reducing the back-reaction rate and also increases the equilibrium concentrations of decomposition products.

Apart from ionic impurities, suspended or colloidal impurities may be present in water. Like ions, such impurities have no effect upon the forward-reaction rate. Unlike ions, however, these impurities do not reduce the rate of the back reaction of Eqs. (4) and (5), because they do not readily react with and remove H and OH free radicals. Consequently,

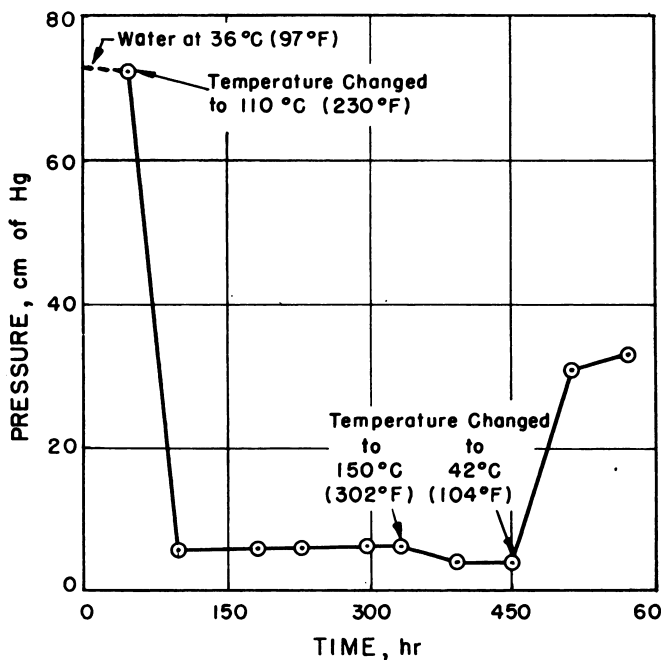


Fig. 1.10.3— Effect of Temperature on the Equilibrium Pressure of Water Decomposition Products as Observed with a Partially Filled Ampoule Irradiated in Oak Ridge X-10 Reactor. Redrawn from ORNL-130. Oct. 11, 1949. Pressures measured at room temperature during periodic removal of ampoule from reactor.

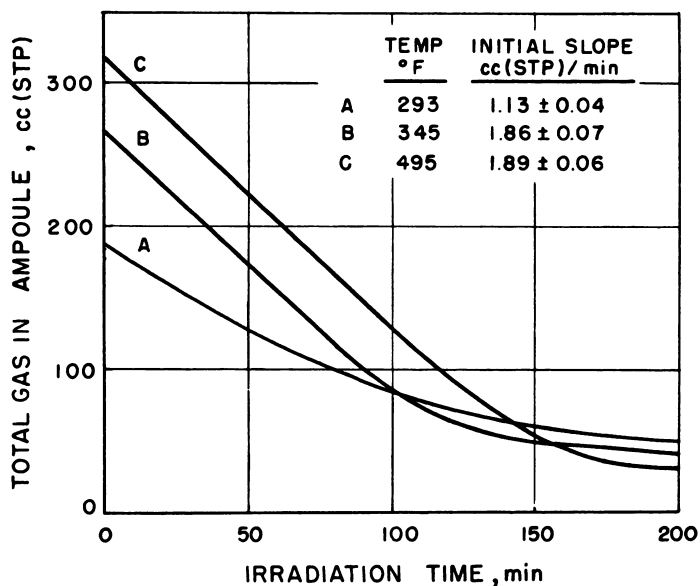


Fig. 1.10.4— Effect of Temperature upon Rate of Combination of Hydrogen and Oxygen in an Ampoule Partially Filled with Water and Under Irradiation in the Chalk River Reactor (NRX). Redrawn from ANL-5004, March 1953. Initial ratios of hydrogen to oxygen only approximately stoichiometric.

in general, the presence of suspended or colloidal impurities does not result in increased decomposition rates or equilibrium concentrations of decomposition products.

There are, however, a few suspended or colloidal impurities (cited below) which have been shown to catalyze the recombination of hydrogen and oxygen in accordance with Eq. (13). Here, obviously, the effect is to reduce the decomposition rate and the equilibrium concentrations. Such catalysis is strongly dependent upon temperature, being considerably greater at higher temperatures.

Organic materials form a special class of impurities in that they readily break down under irradiation to liberate free hydrogen and other products. The hydrogen thus evolved sometimes aids in reducing the rate of decomposition, as described later.

LOW TEMPERATURE

Experimental evidence¹ indicates that some ionic impurities have a much greater effect on decomposition than others. Solutions of KBr, KI, CuSO₄, KCl, HCl, H₂SO₄, and K₂SO₄, among others, provide ions that react with H and OH; of these, Br⁻, I⁻, and Cu⁺⁺ ions are the most reactive and, even with very dilute solutions, result in extremely high equilibrium concentrations and decomposition rates. With neutron- and gamma-flux conditions which in relatively pure water would produce equilibrium partial pressures (concentrations) of less than 10 psi, solutions of KBr, KI, and CuSO₄ may produce partial pressures of more than 1500 psi. Under the same flux conditions, a 0.0088N solution of HCl produces a pressure of 350 psi; a 1.03N solution of H₂SO₄ produces 155 psi; and a 0.0095N solution of H₂SO₄ has little effect, producing about the same equilibrium pressure as relatively pure water.

Experimental evidence has been obtained⁴ which shows that undissolved impurities, at least in the range from a few to 16 ppm, have no effect upon decomposition.

HIGH TEMPERATURE

Although few details are available at present, exploratory work⁵⁻⁶ has shown that certain impurities strongly catalyze the recombination process of Eq. (13) at high temperature. Among these impurities are copper, rhodium, palladium, platinum, silver, iodine, and (to a lesser extent) tin, iron, and titanium. This effect is important only at temperatures above 400°F.

EFFECT OF DECOMPOSITION PRODUCT CONCENTRATIONS

As indicated earlier, many of the reactions involving decomposition products are dependent upon the availability of the free radicals H and OH, this availability being primarily a function of the intensity of the existing gamma flux. Because the average gamma-flux intensity within present stationary-fuel reactors is relatively high, the effects of such reactions are of considerable importance. It should be kept in mind, however, that in a case where the gamma-flux intensity is low, these reactions would be expected to be relatively ineffective. The same comment is applicable to reactions involving ionic impurities, as described above.

Although the concentrations of decomposition products in water have little or no effect upon the forward-reaction rate, they may greatly affect the rate of decomposition by virtue of their effect upon the rates of the processes contributing to the back reaction. The process of Eqs. (4) and (5) is greatly influenced by the concentrations of hydrogen and hydrogen peroxide in the water. As the concentration of hydrogen is increased, the rate of this process is increased (by the mass-action law) and back reaction is promoted. As the concentration of hydrogen peroxide is increased, however, a twofold effect occurs: The increase tends to increase the rate of the back reaction (again, by mass action); simultaneously, it tends to decrease the rate of the back reaction by removing, through the process of Eqs. (6) and (7), the H and OH free radicals necessary to Eqs. (4) and (5). In other words,

the presence of hydrogen peroxide tends to inhibit decomposition on the one hand, and enhance it on the other. The net effect has been shown to be a function of the ratio of the hydrogen concentration to the hydrogen peroxide concentration. The importance of this ratio is described below.

The effect of oxygen concentration is roughly comparable to that of hydrogen peroxide: Oxygen tends to decrease the rate of the back reaction by removing, through the process of Eqs. (8) and (9), the H and OH free radicals necessary to Eqs. (4) and (5); simultaneously, oxygen tends to bolster the back reaction by recombining with the hydrogen present in accordance with Eq. (13).

LOW TEMPERATURE

In relatively pure water* at low temperature (where appreciable concentrations of hydrogen peroxide are possible), an important criterion for the effect of hydrogen and hydrogen peroxide on decomposition is the hydrogen-to-hydrogen peroxide ratio at the start of irradiation. Experimental evidence¹ indicates that the effect upon equilibrium concentrations of decomposition products is as follows: For high ratios, very little decomposition occurs, and the equilibrium concentration of hydrogen is low, the hydrogen peroxide concentration very low, and the oxygen concentration effectively zero; for a ratio of unity, more decomposition occurs, the equilibrium concentrations of hydrogen and hydrogen peroxide are higher, and the concentration of oxygen becomes appreciable; for low ratios, the equilibrium concentrations of all the decomposition products are relatively high. The decomposition rates effected follow the same pattern, being very low in the case of high hydrogen-to-hydrogen peroxide ratio and relatively high for low ratios.

When initially gas-free, relatively pure water is irradiated within a closed system (a system such that decomposition products formed must remain in the water), the resulting decomposition rates and equilibrium concentrations are comparable to those for the unity-ratio case, above. However, if such water is irradiated within a system which permits some of the gaseous hydrogen to escape from the water, as by mechanical degasification or by diffusion from the water to a gas space above the water, the decomposition rates and equilibrium concentrations become much greater as a consequence of the lowered hydrogen-to-hydrogen peroxide ratio. In either case, *at low temperature, decomposition is so repressed by excess hydrogen that virtually no decomposition occurs at average neutron and gamma irradiation levels in present reactors if hydrogen equivalent to 5 to 10 psi partial pressure is initially dissolved (and maintained) in otherwise relatively pure water.*

The presence of oxygen in water at low temperature promotes decomposition, principally through the effect of Eqs. (8) and (9) on Eqs. (4) and (5) when hydrogen and hydrogen peroxide are present in low concentrations. At high concentrations, it is probable that the same result is effected through some different process. However, as indicated above, maintenance of excess hydrogen precludes formation of oxygen by decomposition, and promotion of decomposition by the presence of oxygen may be avoided by using initially oxygen-free, hydrogenated water.

HIGH TEMPERATURE

The general decomposition mechanism and the effects of the various decomposition-product concentrations on decomposition of water have received much less study for high-temperature water than for low-temperature water. It is probable, however, that both the

* The term "relatively pure water" is used in this chapter to denote water which has been treated by distilling, demineralizing, and degasifying so as to leave only trace amounts of impurities, including organics. Very approximately, a minimum specific resistance of 200,000 ohm-cm and a maximum gas content of 0.1 ml/liter are implied. The term "pure water" is reserved for the hypothetical case of water with no impurities.

general mechanism and the concentration effects are similar for both cases, the chief differences being those which stem from the rapid breakdown of hydrogen peroxide and consequent formation of oxygen at high temperature. Because of this rapid thermal decomposition, hydrogen peroxide is present at high temperature only in negligibly low concentrations, and the hydrogen-to-hydrogen peroxide concentration ratio always is extremely high. With much excess hydrogen, some tendency to repress decomposition would be expected. In addition, both radiation-induced and catalytic thermal recombination of oxygen with hydrogen in accordance with Eq. (13) are very effective at high temperature, further tending to repress decomposition. Finally, the low oxygen concentration found in high-temperature water under irradiation, as discussed below, aids in reducing decomposition. The total effect, with relatively pure water at very high temperature, is almost complete elimination of decomposition.

If initially gas-free, relatively pure water at high temperature is irradiated by epithermal neutrons and gamma rays, an equilibrium condition should quickly be reached in which the hydrogen peroxide concentration is (effectively) zero, the oxygen concentration very low, and the hydrogen concentration about twice that of the oxygen. Practically, this condition seldom is realized. Because the vapor pressure of water at elevated temperature is extremely high, almost any vessel or piping system designed to contain water within a reactor must be constructed of some metal with which there is associated a certain corrosion rate, or rate of reaction between the metal and the water. One result of such a corrosion process is the liberation of hydrogen into the water without liberation of oxygen. The excess hydrogen thus introduced tends to combine with oxygen present, repress decomposition still further, and still further lower the oxygen concentration (normally, to a point well below half the hydrogen concentration, although a portion of this effect is a result of loss of oxygen to corrosion of containing materials and impurities). Of course, as long as corrosion continues and no water is gasified either mechanically or by diffusion into a gas space, the hydrogen concentration continues to rise. Consequently, an equilibrium or steady-state condition is never attained under these circumstances. Normally, however, some degasification does occur and a steady-state condition is achieved in which the rate of hydrogen formation is equal to the rate of degasification and in which the hydrogen concentration (as well as that of oxygen) remains constant. If the rate of degasification is initially so high that the hydrogen concentration is prevented from rising above a very low value, decomposition takes place at some constant rate which is primarily dependent upon this steady-state hydrogen concentration, and the rate of degasification is equal to the steady-state rate of hydrogen formation by decomposition plus that by corrosion; however, if the rate of degasification is initially sufficiently low, the hydrogen concentration increases to a value where the decomposition rate becomes zero, and the steady state is achieved only if the rate of degasification is equal to the rate of hydrogen formation by corrosion (if the rate of degasification is higher than this, the preceding case results; if lower, a steady-state condition is not realized because the hydrogen concentration continues to increase).

The most important observation concerning effects of decomposition-product concentrations is that *at high temperature, initial introduction (and maintenance) of a hydrogen concentration equivalent to 5 to 10 psi partial pressure reduces decomposition of (otherwise) relatively pure water subjected to average neutron- and gamma-irradiation levels in a reactor virtually to zero and effectively maintains the oxygen concentration very close to zero.*

PRACTICAL CONSIDERATIONS

The data presented in the following, if extrapolated in accordance with the principles discussed above, should permit an engineer to estimate the decomposition problems that may be expected in a contemplated reactor. If a precise estimate of the extent of decom-

position is required or if the assumed irradiation conditions are far removed from those in existing reactors, the reader is urged to refer to the references listed.

GENERAL OBSERVATIONS

(1) If pure water were irradiated in a reactor by neutron and gamma flux only, it is very probable that no decomposition of the water would occur because of the relatively high gamma flux normally associated with the average epithermal-neutron flux in a reactor.

(2) In practice, some decomposition of water irradiated in a reactor usually does take place because of certain ionic impurities in the water, the effect of the impurities being sufficient to override the repressive effect of the gamma flux. The amount of decomposition occurring depends upon the amount and type of ionic impurities present. The impurities may have been contained in the initial charge of water or they may be introduced as discussed below in paragraph (3).

(3) The material used to contain the water in the reactor may readily introduce appreciable amounts of ionic impurities into the water. Because such impurities are continuously introduced, some of which promote decomposition, a means must be provided to remove them continuously from the system if decomposition must be eliminated or reduced to a very low value. The use of initially relatively pure water is not a sufficient precaution, in itself, to assure negligible decomposition.

(4) The decomposition of water in any of the existing or currently planned reactors may be completely or very nearly eliminated by a combination of the following: using initially relatively pure water; continuously removing impurities inadvertently introduced during operation; maintaining a small amount of excess hydrogen (or deuterium) in the water.

(5) In certain reactors, the effects of water decomposition are negligible even though no precautions are taken for minimizing decomposition; in other reactors, the effects represent minor problems to which the solutions are readily available.

MEANS OF MINIMIZING DECOMPOSITION

The chief interest of the reactor designer with regard to water decomposition lies in reducing or, if possible, eliminating it. Based on theoretical considerations and supporting experimental evidence already discussed, the following are known to be effective in minimizing decomposition:

(1) Maintain the water free of all ionic impurities which promote decomposition.^{1,4,9-12,14} In addition to removing impurities before the water is charged, a method for continuous removal (such as by by-passing a portion of the water flow through an ion-exchange bed) should be employed. It is especially important that Br^- , I^- , and Cu^{++} ions be removed from water to undergo irradiation at low temperature; even slight traces of Br^- or I^- left in the water may be sufficient to cause a high rate of decomposition.

The specific resistance of water is, at best, a qualitative indication of the ionic content with respect to the particular ions of importance in water decomposition. Nevertheless, regulating the specific resistance can be employed to advantage to keep the general ion content as low as possible and, thereby, hold the undesirable ion content to a reasonably low value.^{4,10,14} In general, the higher the specific resistance of the water, the less the decomposition. In most existing reactor systems, the specific resistance of the water is normally maintained within the megohm-cm range.

(2) Maintain a certain concentration of hydrogen (or deuterium) in the water.^{1,3,9,11,15} The presence of a small amount of hydrogen is normally sufficient to reduce the decomposition to zero, or very nearly zero. The exact amount required depends upon a variety of other conditions, e.g., epithermal-neutron and gamma flux intensities, temperature, and ionic impurity content. In the usual case, with water of high specific resistance, a hydrogen partial pressure of a few psi is sufficient.

(3) In systems at ordinary temperature, reducing the hydrogen peroxide (or deuterium peroxide) and oxygen concentrations as far as possible aids in reducing decomposi-

tion.^{1,4,9,11,15} This is best accomplished by initially removing all oxygen from the water and dissolving a small amount of hydrogen in the water before the start of irradiation; the presence of the hydrogen (which must be continuously maintained if any sort of degasification takes place during operation) then prevents appreciable formation of peroxide or oxygen. If excess hydrogen is not deliberately maintained in the water, large gas spaces should be avoided into which any hydrogen generated can diffuse from the water and, thereby, help to establish high hydrogen peroxide concentration.

(4) Usually, the presence of undissolved solids in the water is not important.⁴ Introduction of certain suspended materials, such as copper, rhodium, palladium, platinum, silver, and iodine^{5,6,7} is known to reduce decomposition at high temperature, mainly above about 400°F; however, the practicability of using such materials, especially in view of possible detrimental effects unconnected with decomposition, has not yet been established.

Two additional means of minimizing decomposition, of possible application to in-reactor experimental equipment, although of little use in reactor design, are mentioned below.

(5) Decrease the epithermal-neutron flux and increase the gamma flux within the water as much as possible.^{1,9,10} Normally, both these fluxes are firmly fixed by other considerations, and no range of manipulation of either is available for reduction of decomposition. It is remotely possible, however, that a choice of water passage location may be made to favor zones of low neutron flux or high gamma flux. In some instances, it may be possible to use alternate structural materials or structural configuration to promote intensity of the gamma flux within the water.

(6) Increase the temperature of the water under irradiation to as high a value as possible.^{1,10-13} Again, the water temperature usually is dictated by other considerations and cannot easily be increased solely for the purpose of reducing decomposition. In those cases where temperature could be increased, the problems of increased corrosion rates of containing materials and of providing additional structural strength to withstand the increased water vapor pressure would have to be weighed against the benefit in the decomposition problem.

THE PRACTICAL DECOMPOSITION PROBLEM IN REACTORS

To illustrate the problems of water decomposition encountered in practice and the means available for combating them, the CP-3 class of reactor is discussed below.

CP-3 CLASS OF REACTOR

The CP-3 class of reactor is characterized by: use of a RECIRCULATING water system; irradiation of the water at LOW TEMPERATURE; use of heavy water. In addition to CP-3, other reactors of the same general type are NRX and CP-5. Additional reactors which properly are classed with CP-3, although they employ light water instead of heavy water, are MTR, LITR, and the ORNL Research Reactor. The use of light water does not materially change decomposition considerations except to eliminate concern over possible loss of water and eliminate possible need for recombination equipment. Practically all decomposition data available to date on the CP-3 type of reactor have been obtained from CP-3 (CP-3') or NRX.

CP-3 (Argonne Heavy-water Reactor)

Heavy water at low temperature is used for both cooling and moderating. The system is closed, the same water being continuously recirculated through the reactor. The core consists of an aluminum tank in which cylindrical, aluminum-clad fuel rods are suspended, and through which all the heavy water flows. A large gas space filled with helium is present over the surface of the water within the tank. Within the reactor, the containing

material is all aluminum and external to the reactor, primarily stainless steel. Approximate values of pertinent operating conditions are as follows:

Epithermal neutron flux	$4 \times 10^{11} \text{ cm}^{-2} \text{ sec}^{-1}$
Water temperature	100°F
Volume of water under irradiation	5000 liters
Volume of water in system	6000 liters
Flow rate in main system	27,000 liters/hr
Water pressure	15 psia
Reactor power (heat)	275 kw
Surface area of water-gas interface	30 ft ²
Surface area of aluminum	450 ft ²
Surface area of stainless steel	200 ft ²

In this reactor, the following conditions tend to promote decomposition: fairly high epithermal-neutron flux; low water temperature; high ionic-impurity content; high initial oxygen content; lack of introduction of excess deuterium into the water prior to and during irradiation; the presence of a large gas space into which the deuterium initially formed can escape from the water, thereby aiding establishment of a high deuterium peroxide concentration.

Aside from the fairly high gamma flux which would be expected, there are no outstanding conditions present tending to repress decomposition.

A factor which increases the importance of any decomposition which might result is that the decomposition products tend to accumulate since the water is irradiated repeatedly instead of being discharged after one passage through the reactor. A sufficiently high accumulation of oxygen or deuterium peroxide could conceivably pose a corrosion problem; a sufficiently high total gas concentration could conceivably produce bubbles capable of interfering with desirable heat-transfer characteristics or with reactor reactivity control. Other factors are possible formation of explosive mixtures in the gas space within the tank, and the fact that appreciable decomposition may require provisions for water degasification and recombination of deuterium and oxygen (because loss of heavy water is economically objectionable).

The original operation of CP-3 was carried out under the above conditions. A considerable amount of decomposition occurred,^{10,14} and recombination of deuterium and oxygen was necessary. This was accomplished by continuously recirculating the helium-deuterium-oxygen mixture through the gas space in the reactor tank and through an unheated platinum-catalyst recombiner outside the reactor. The water was degasified adequately by natural diffusion into the gas space within the tank. A helium flow of 6 cfm was found more than sufficient to preclude possible formation of explosive mixtures (although it probably should be pointed out that nitrogen impurity in the helium was observed to form nitric acid in the reactor water). During this initial operation, because the water system was closed and because additions of ammonium hydroxide were made regularly for pH control, the ionic-impurity content of the water was very high. At one time, the water contained about 1200 ppm of ammonium nitrate in addition to about 100 ppm of aluminum, 50 ppm of lead, and appreciable amounts of copper, chloride, and other metals. At that time, the following conditions existed:

Water conditions:

Specific resistance	10,000 ohm-cm
Deuterium peroxide concentration	10 – 15 ppm
Deuterium concentration	Not observed
Oxygen concentration	Not observed

Water decomposition rate:

<i>Rate of formation of deuterium</i>	60,000 – 100,000 ml/hr
<i>Rate of formation of oxygen</i>	30,000 – 50,000 ml/hr

The reactor (now known as CP-3') is being currently operated under the same conditions except that the water is kept relatively free of impurities.^{10,14} A mixed-bed ion-exchange system, through which a small fraction (about 230 liters/hr) of the main system flow is by-passed, continuously removes ionic impurities from the water and maintains the total dissolved solids content at about 1 ppm. This change has resulted in the following conditions:

Water conditions:

Specific resistance	1,000,000 ohm-cm
Deuterium peroxide concentration	<1 ppm
Deuterium concentration	0.08 ml/liter
Oxygen concentration	0.01 ml/liter

Water decomposition rate:

<i>Rate of formation of deuterium</i>	200 ml/hr
<i>Rate of formation of oxygen</i>	Negligible

The rates of formation of gas shown include the effects of corrosion processes.

In this type of reactor, as indicated earlier, the inherent irradiation conditions would be expected to favor extensive decomposition. The original operation of CP-3 has shown that appreciable decomposition does occur, but that of the several possible detrimental effects of such decomposition cited at the beginning of the chapter, the only ones of practical significance are: a possibility of formation of explosive mixtures by accumulation of the gaseous decomposition products; the necessity of providing burner equipment for catalytic recombination of the gaseous products to reform heavy water; a possibility of increased aluminum corrosion resulting from deuterium peroxide in the water.

Present operation of CP-3' has shown that all of the above effects are eliminated by maintaining high specific resistance of the water through the use of a by-pass, mixed-bed ion-exchange system. In spite of the many other conditions tending to promote decomposition, the one precaution which assures low ionic content in the water is sufficient to virtually eliminate decomposition. It is highly probable that decomposition (by irradiation) would be totally eliminated if a few psia partial pressure of deuterium were maintained in the gas space of the reactor tank so as to keep the concentration of deuterium in the water at a relatively high level.

In brief, the CP-3 class of reactor tends to produce appreciable water decomposition unless precautions are taken to maintain high water purity. The only problems of practical significance resulting from such decomposition are: possible formation of explosive mixtures by accumulation of gaseous decomposition products; loss of heavy water; and possible increased aluminum corrosion because of deuterium peroxide in the water.

The first two of these problems are satisfactorily handled by maintaining an inert-gas blanket over the reactor water surface and by circulating the gas, together with the decomposition products, through a simple platinum-catalyst recombiner. If no gas space exists within the reactor, one may be provided in the system outside the reactor to serve the same purpose; alternatively, some other sort of degasifier may be used, again in conjunction with a recombiner. The third problem disappears when steps are taken to reduce the decomposition to a low level. Decomposition may be completely eliminated, or very nearly so, by installation of a by-pass, mixed-bed, ion-exchange system to maintain the specific resistance of the water at a very high value (1,000,000 ohm-cm or higher). It is very probable that maintaining dissolved deuterium in the water in an amount on the order of several milliliters per liter, together with a high specific resistance of the water, would

completely eliminate decomposition (by irradiation). The available data suggest that, with-in a factor of about five, the rate of generation of deuterium in the CP-3 type of reactor (in milliliters STP per hour per liter of water volume under irradiation) is equal to 10^5 divided by the specific resistance of the water in ohm-cm (within the approximate range 20,000 to 700,000 ohm-cm). Of course, this relation could not be expected to apply to water containing other than the normal types of impurities.

REFERENCES

1. A. O. Allen and associates, Oak Ridge Nat. Lab. ORNL-130, Oct. 11, 1949 (classified).
2. J. R. Humphreys, E. L. Abers, P. E. Brown, and associates, Argonne Nat. Lab., ANL-4628, May 1, 1951 (classified).
3. J. R. Humphreys, E. L. Abers, and Y. Solomon, Argonne Nat. Lab., ANL-5004, Mar. 1953 (classified).
4. H. G. Heal, A. R. Van Dyken, T. J. Hardwicke, and R. F. S. Robertson, Atomic Energy of Canada, Ltd., CRC-494, Feb. 8, 1952 (classified).
5. Oak Ridge Nat. Lab., ORNL-630, pp 129-131 (classified).
6. Oak Ridge Nat. Lab., ORNL-1153, pp 93-96 (classified).
7. Oak Ridge Nat. Lab., ORNL-1360, pp 89, 116-118, 121-127 (classified).
8. Oak Ridge Nat. Lab., ORNL-1221, pp 122-123 (classified).
9. A. O. Allen, Mechanism of Decomposition of Water by Ionizing Radiations, BNL-1080, April 1952.
10. M. Sivetz and C. H. Scheibelhut, TID-2002, Aug. 1952 (classified).
11. A. O. Allen, BNL-1012, Jan. 15, 1952 (classified).
12. Oak Ridge Nat. Lab., ORNL-630, pp 5,40-41, 47-48 (classified).
13. L. W. Fromm, Oak Ridge Nat. Lab., ORNL-404, Sept. 16, 1949 (classified).
14. Nat. Res. Council of Canada, Atomic Energy Project, CRR-479, Oct. 5, 1951 (classified).
15. Oak Ridge Nat. Lab., ORNL-65, p 116 (classified).

SELECTED READING LIST

AN INTRODUCTION TO RADIATION CHEMISTRY, M. Burton, Jour. Chem. Ed. 28, 1951, p 404.

THE DECOMPOSITION OF WATER BY RADIATION, Univ. Cal. Rad. Lab., W. J. Toulis, UCRL-583, Feb. 10, 1950.

DECOMPOSITION OF TRITIUM OXIDE UNDER ITS OWN RADIATION, Oak Ridge Nat. Lab., J. A. Ghormley and A. O. Allen, ORNL-128, Sept. 1, 1948.

RADIATION CHEMISTRY OF AQUEOUS SOLUTIONS, A. O. Allen, Jour. Phys. and Colloid Chem. 52, p 479.

CHEMICAL REACTIONS OF ORGANIC COMPOUNDS WITH X-RAY ACTIVATED WATER, H. Fircke, E. J. Hart, and H. P. Smith, Jour. Chem. Phys. 6, 1938, p 299.

CHAPTER 1.11

Corrosion

A. H. Roebuck

GENERAL CONSIDERATIONS

Corrosion is the destruction of a metal by chemical or electrochemical reaction with its environment. The selection of materials for water-cooled reactor systems involves establishing the effect of the environment on the corrosion of a material and the effect of contamination by that material on the specific environment, that is, corrosion studies for reactor systems should attempt to determine the inter-related effects of the corrosion process and maintenance of water purity.

Primary considerations in the corrosion of aqueous reactor systems, in addition to those normally encountered in industrial corrosion problems, include the following:

- (1) Materials must be satisfactory for long service to provide a maximum of reliability without periodic inspection.
- (2) The dissociation of water accompanying reactor irradiation provides a constant source of oxygen and other decomposition products for corrosion processes. The concentration of dissolved oxygen is a very important factor in steel corrosion.
- (3) If continuous and appreciable corrosion is possible, removal of the resulting corrosion product must be considered to minimize preferential deposition on heat-transfer surfaces or in high-flux zones.
- (4) Water purity should be maintained within limits dictated by radioactivity tolerances, shielding requirements, accessibility of primary components for repair, and decomposition problems.
- (5) The effects of irradiation on corrosion processes, although probably of secondary importance, should be evaluated.
- (6) The effects that impurities produced by corrosion processes have on the dissociation of water must be taken into consideration.
- (7) Materials should be resistant to water that contains such additives as corrosion inhibitors or poisons for excess reactivity.

Materials are, for convenience, generally classified as fuel-element materials or construction materials. Fuel-element materials include fuel materials and cladding or can materials. The most frequently used clads are aluminum and zirconium, but stainless-steel and beryllium clads have also been considered in design studies. Construction materials of primary interest are the general engineering materials and special alloys used for pressure vessels or containing tanks, piping, fuel-assembly supports, control elements, core-drive mechanisms, thermal and neutron shields, and the like. The primary construction material for low-temperature reactors is aluminum; stainless steel, zirconium, and other corrosion-resistant metals are used in high-temperature reactor applications.

FUEL-ELEMENT MATERIALS¹

In current water-cooled reactor design, the fuel material is clad to prevent corrosive attack of the uranium or its alloy. Alloys containing high percentages of uranium are attacked rapidly in water at temperatures above 300°F.

Corrosion and scale formation are limiting factors in fuel-element design because the maximum coolant temperature and maximum fuel-element surface temperature are dictated by the corrosion characteristics of the cladding. Burn-up effects and other irradiation phenomena influence performance but in most cases are not limiting. An analytical discussion of these effects is presented in Chapter 1.7.

Although the primary purpose of the fuel-element cladding in water-cooled reactors is to prevent the coolant from attacking the fuel alloy, the cladding must also prevent fuel-alloy fission products from dispersing into the coolant, and in some cases it must also provide structural strength. The cladding must therefore have sufficient corrosion resistance to protect the fuel alloy for the core life or cycle time.

CONSTRUCTION MATERIALS

General corrosion leading to large amounts of corrosion products in the coolant stream is to be avoided. Corrosion products in the coolant tend to deposit on high-temperature heat-transfer surfaces, in dead spaces (sometimes in areas of high flux), and often in small constrictions (e.g., instrumentation lines) causing total or partial plugging. Deposition of suspended material in or around close-fit moving parts may cause them to fail or malfunction, e.g., close-fitting shaft and sleeve mechanisms may freeze if excessive amounts of corrosion products accumulate in the shaft-sleeve gap. Insoluble corrosion products in the coolant have an erosive action on impellers and/or sharp elbows. Corrosion products in the coolant stream, especially from high-cross-section materials, may also cause changes in the nuclear characteristics of a reactor.

An appreciable amount of corrosion may cause positive or negative changes in dimensions. If an adherent insoluble oxide is formed as the metal corrodes, the dimension change may be positive. If, however, the corrosion product is soluble or nonadherent, dimension changes will be negative. Either change may cause malfunction of close-fitting mechanisms.

A higher level of corrosion can be tolerated from parts of limited surface area. Materials having desirable physical properties but not normally acceptable corrosion resistance may be used in this instance. Application of these materials is limited to mechanisms where close tolerance is not necessary and to sizes or areas where the higher corrosion rate will not introduce excessive impurity.

FACTORS AFFECTING SYSTEM CORROSION

TEMPERATURE

Corrosion rates generally increase with increasing temperatures, but the corrosion rate vs temperature curve is usually logarithmic, not linear. The temperature range in which the increase in corrosion rate becomes critical depends upon the specific material. For example, the corrosion rate of AISI type 300 stainless steels does not generally increase radically from 500° to 650°F, whereas the corrosion rate of uranium increases rapidly from 300° to 450°F. A small increase in water temperature above that normally considered

¹ References appear at end of chapter.

to be the maximum for satisfactory corrosion resistance may result in a large increase in corrosion rate.

The exact temperature dependence of corrosion is not always readily predictable as corrosion processes may be influenced by other factors which are themselves dependent on temperature. Such factors include dissolved-oxygen concentration and corrosion-product solubility.

IMPURITIES

Water purity, a major factor in the corrosion resistance of reactor systems may be controlled. Soluble ions that promote galvanic corrosion and dissolved gases that are similarly deleterious should be held to a minimum. In addition, insoluble corrosion products that would accelerate corrosion, erosion, or deposition on heat-transfer surfaces must be carefully controlled.

Additives to water might be desirable for certain applications, such as: (1) addition of soluble solutions of high-cross-section materials to effect emergency shutdown or control excess reactivity; (2) addition of buffer solutions to adjust the pH and improve corrosion behavior; and (3) addition of gases to increase the pressure or to provide chemical potential, such as adding hydrogen to force oxygen recombination.

INSOLUBLE PARTICLES

Insoluble particles may generally be removed by mechanical methods or sedimentation. Filters are commonly used in closed-cycle high-temperature reactor systems, either by inserting them directly into the system or by utilizing the retention of insoluble particles in ion-exchange resins and their protective screens.

DISSOLVED GASES

Oxygen

The corrosion resistance of some engineering metals and alloys depends markedly on the concentration of dissolved oxygen in the reactor system. Most metals can be placed in one of two broad classifications: Maximum corrosion resistance is exhibited (1) either in the absence of oxygen or (2) in the presence of a particular (and usually large) oxygen concentration. There is evidence that some metals can be placed into both classifications; these metals show high corrosion susceptibility between two oxygen concentration regions where low or minimum corrosion is observed. Such behavior is exhibited by some of the stainless steels and probably always involves corrosion mechanisms which change with changing oxygen concentration.

Hydrogen

Certain metals exhibit exceptionally high corrosion resistance in high-temperature water systems containing large amounts of dissolved hydrogen (more than 50 ml/l). AISI type 300 stainless steels show the most pronounced effect; tensile tests on samples exposed to 500°F water containing hydrogen have not shown changes in physical properties. High-temperature aqueous systems containing large excesses of hydrogen have been found to be essentially free of dissolved oxygen. Most of the metals which exhibit high corrosion resistance in the presence of excess hydrogen also show high resistance in systems of minimum oxygen content. The effect of dissolved hydrogen on corrosion is thus postulated to be related to the effect of hydrogen on the oxygen concentration.

Control of Gas Content

Dissolved gases may be removed or their concentrations reduced by several methods. Mechanical degasification may be accomplished by spraying the water into the vapor phase and continually venting a small amount of vapor. The concentration of dissolved oxygen, for instance, may be reduced to 0.2 ml/l or less by this method depending on the efficiency of the degasifier, how long it is operated, and the concentration of dissolved oxygen in the make-up water used.

Oxygen may also be removed by the addition of excess hydrogen and by the use of oxygen-absorbing resins.² The introduction of hydrogen in amounts greater than 50 ml/l has been found to shift the equilibrium of the reaction:



toward the right. The use of an oxygen-absorbing resin is also effective, but because the resin contains metallic copper, precautionary measures must be taken to remove any copper ions introduced into the coolant.

SOLUBLE SALTS

Of particular concern to reactor performance is the presence of chloride ions and the soluble salts of heavy metals. Soluble salts of any kind will usually intensify general attack and perhaps cause other undesirable effects. Special care, however, must be exercised to ensure the absence of chloride ions. Concentrations exceeding a few ppm may greatly increase corrosion. Stainless steels, beryllium, aluminum, and aluminum alloys are particularly susceptible to attack by chloride ions. Soluble salts of heavy metals such as copper, cadmium, cobalt, gold, lead, and silver intensify local attack and pitting. Heavy metals tend to deposit or plate out in metallic form and provide bi-metallic systems in which the heavy metal is the cathode.

Soluble-ion content may be reduced appreciably by demineralization, and conventional practice is to bypass a certain amount of the coolant through resin beds. In high-temperature water systems, the bypass flow must be cooled to approximately 140°F, the maximum operating temperature of ion-exchange resins. Values for the specific resistance in systems operating with demineralizers are given in Chapter 1.10 "Water Decomposition."

EFFECT OF pH

In reactor systems composed of various types of metals, a pH useful in controlling the corrosion of one material may accelerate that of another. Metal combinations and assemblies should therefore be thoroughly tested under the proposed pH conditions before they are used in reactors.

Alkaline conditions are useful in reducing the corrosion of steels and ferrous alloys. Alkaline systems (high pH) are often used industrially to control corrosion in steel boiler-condenser systems. These systems are generally not required to meet rigid water specifications on allowable ion content or specific resistance such as are often necessary for reactors.

Slightly acid conditions are useful in controlling the corrosion of metals such as aluminum and aluminum alloys (see later discussion of aluminum and aluminum alloys).

EFFECT OF IRRADIATION

Data on samples of engineering materials tested in high-temperature water loops in operating reactors indicate that irradiation does not significantly affect the corrosion rate of these materials for general reactor application. The water velocity in these tests was about 10 ft/sec, and the maximum temperature studied was 540°F. Various materials have

been tested under an integrated neutron flux of up to 10^{18} nvt thermal and 10^{17} fast. Control samples were tested in these loops under the same conditions except that they were not under reactor irradiation. While a tendency toward preferential deposition of corrosion products in high-flux zones has been noted, no corrosion effects on the samples directly attributable to irradiation were observed.

COUPLE AND CREVICE EFFECTS

Active metals are defined as metals high in the electromotive force series. They usually show a tendency to oxidize or corrode easily. Inactive (noble) metals, on the other hand, are defined as metals low in the electromotive force series and are metals usually resistant to corrosion. If an active metal is placed in contact with an inactive metal, electrons flow from the active to inactive metal. This imposes a more positive charge on the active metal and causes it to corrode even more rapidly than it ordinarily would.

It is desirable to avoid contacts between metals widely separated in the electromotive force series. Contacts between any two metals which do not build up protective films of high electrical resistance should also be avoided. Such contacts will increase the tendency of the active metal to corrode and will correspondingly protect the more noble metal. A corroding bi-metallic couple in an aqueous system may be thought of schematically as three resistances in series:

- (1) Anodic resistance
- (2) Cathodic resistance
- (3) Solution resistance

Any process which will increase these resistances will reduce corrosion. Anodic resistances may be increased by film build-up, and the solution resistance may be increased by demineralization. In systems containing high-resistivity water, the solution resistance is very high; this high resistance prevents extensive galvanic corrosion which might otherwise be introduced by couples or crevices.

Certain couples tend to pitting of the contact faces and should be avoided except for limited-surface applications. Nickel, nickel-base alloys, AISI type 400 stainless steels, copper, and copper alloys behave in this fashion when coupled to most other metals in oxygenated water at 200°F and higher. Nickel and nickel alloys exhibit the most pronounced effect.

Gaps or crevices in a system should be avoided if possible. In static systems or in dead spots such as close-fitting, non-moving parts in dynamic systems, corrosion products build up at the mouth of fine crevices or gaps. In some cases, blisters form; in others, ridges of corrosion products are produced. Corrosion product build-up on close-fitting shaft-sleeve mechanisms may cause sticking or freezing. A larger shaft-sleeve clearance lessens the tendency for freezing; the proper clearance depends on:

- (1) Length of shaft contact with sleeve
- (2) Temperature, coolant, severity of conditions, and the like
- (3) Diameter of the shaft
- (4) Frequency of use (continuous or intermittent)

At 500°F in degassed water, a clearance of 2 to 3 mils has been found satisfactory for a $\frac{1}{2}$ -in.-diameter shaft in a $\frac{3}{4}$ -in.-long sleeve which is moved continuously or at least once a week. If longer periods between movement are anticipated, the clearance should be doubled to prevent freezing. In general, the required clearance of shaft sleeves for working parts increases with (1) increased contact length and shaft diameters and (2) corresponding temperature rises. However, the ratio of the required clearance per inch of shaft diameter to the shaft diameter decreases with increasing diameter of the shaft. Before acceptance, the assembly should be tested under the proposed conditions.

Small gaps or fine crevices are not open to circulation if they are of any depth. For this reason, the ion concentration builds up in these areas, and the oxygen concentration is

depleted. The increased ion concentration results in a lower specific resistance of the medium in the gap and increases the possibility of galvanic attack. If system flow does not wash away corrosion products, the oxygen concentration in the crevice will be depleted, and the corrosion process will often be self-limiting. Systems containing water having a high specific resistance are less susceptible to galvanic attack.

If system water does not have high specific resistance and if the dissolved oxygen concentration is depleted locally, the metal contacted by the depleted water will develop a different potential than the adjoining metal. This leads to increased corrosion and is known as the "oxygen cell effect." Gaps and crevices are susceptible to this effect.

EFFECT OF COOLANT VELOCITY

Erosion may be defined as the destruction or loss of metal or other material by the abrasive action of liquid, vapor, or gas. The presence of suspended solids usually increases the erosive action of a medium; care must therefore be exercised to remove these solids from high-velocity systems.

Metals which resist water corrosion at temperatures up to 500°F are unaffected by flow rates up to 30 ft/sec. Metals in this class include stainless steels, zirconium and zirconium alloys, cobalt alloys, and several silver-platinum-cobalt alloys; aluminum and aluminum alloys are also unaffected by these flow rates provided the temperature and pH do not exceed the range where aluminum has satisfactory corrosion behavior. Materials which are susceptible to corrosion or which have limited corrosion resistance almost always show increased corrosion rates under flow. Thorough testing is recommended before specifying such materials for reactor use.

The rate of flow is apparently important in determining the amount of corrosion product deposition. Heaviest deposition occurs mainly in stagnant areas or areas of low flow rate. At 500°F, heavy deposition occurred at velocities less than 2 ft/sec.

CORROSION DATA FOR REACTOR MATERIALS

Table 1.11.1 presents a tabulation of the relative corrosion resistance of various metals and classes of metals in high-purity degassed water up to 650°F. The table is used only to indicate the general class of materials that may be considered for water systems operating at the indicated temperatures. The corrosion behavior of specific metals and alloys under various test conditions simulating reactor conditions are presented under subsequent headings. Table 1.11.2 lists some terms and test conditions used in the following discussions.

Judgement must be exercised in extrapolating test data to select reactor materials since water purity, water composition, and velocity effects may differ considerably. For instance, the magnitude of oxygen concentration (usually low) predicted for a new reactor is difficult to simulate during a test program. In addition, oxygen concentrations may not be uniform in all sections of a reactor or test apparatus.

In evaluating test data weight-change rates and visual observations of the amount and type of corrosion products formed were used as primary criteria for accepting materials. No attempt was made to remove corrosion products after the test or between test periods. The corrosion behavior of many highly resistant materials was not reflected in the rates of weight change. Visual examination, however, indicated typical corrosion behavior since adherent oxide films were rather readily distinguished from loose flaky films and/or pitting, couple effects, and the like; accordingly, the reported data contain descriptions of typical corrosion products. In general, a material having a rate of weight change of less than 0.3 mg/(cm²)(mo) and showing a thin adherent corrosion film has been considered satisfactory.

Table 1.11.1—General Corrosion Resistance of Metals in Degassed Water

Material	Corrosion resistance*					
	200°F	300°F	400°F	500°F	600°F	650°F
Aluminum	G	G	D	P	P	P
Beryllium	G	D	P	P	P	P
Chromium plate	G	G	G	P	P	P
Cobalt alloys	G	G	G	G	G	G†
Copper	G	G	D	P	P	P
70-30 copper-nickel	G	G	G	G	P	P
Bronze	G	G	D	P	P	P
Gold	G	G	G	G	G	G†
Magnesium	D	P	P	P	P	P
Nickel	G	G	G	D	P	P
Nickel alloys						
Monel	G	G	G	G	D	P
Inconel	G	G	G	G	D	P
Hastelloy	G	D	P	P	P	P
Platinum	G	G	G	G	G	G†
Steels						
Carbon	D	D	P	P	P	P
Stainless						
Austenitic	G	G	G	G	G	G†
Ferritic	G	D	D	P	P	P
Heat resisting	G	G	G	G	G	G†
Martensitic	G	G	G	D	P	P
Precipitation hardening	G	G	G	G	D	P
Silver	G	D	D	P	P	P
Titanium	G	G	G	G	G	G†
Thorium	D	P	P	P	P	P
Uranium	D	P	P	P	P	P
Zirconium (crystal-bar)	G	G	G	G	G	D
Zirconium-tin alloys						
2½% tin	G	G	G	G	G	D
1½% tin + trace elements	G	G	G	G	G	G†

*G = Good – Appearance: no apparent corrosion products; clean tarnish film.

Weight change: less than 0.3 mg/(cm²)(mo)

D = Doubtful – (1) Appearance: no apparent corrosion products; clean tarnish film.

Weight change: greater than 0.3 mg/(cm²)(mo)

– or (2) Appearance: some apparent corrosion products on surface or moderate amount of pitting and spalling

Weight change: less than 0.3 mg/(cm²)(mo)

P = Poor – Appearance: heavy deposit of corrosion products on surface, or general deep pitting and spalling

Weight change: greater than 0.3 mg/(cm²)(mo)

†Recent tests show that these materials have satisfactory corrosion resistance in 750°F superheated steam

Table 1.11.2—Terms and Test Conditions

Corrosion rate	The amount of metal penetration or weight of metal lost per unit area per unit time [(inch/yr, mils/mo, mg/(cm ²)(mo)]. A distinction is made between a corrosion rate and a weight-change rate. The corrosion rate may be determined from the metal corroded vs time curve as illustrated in Fig. 1.11.1; the corrosion rates usually reported are taken from the slope of the linear portion of such a curve. Inclusion of accelerated corrosion resulting from initial surface conditions is thus avoided in this interpretation, and such rates may be extrapolated to longer periods of time.
Weight change	The change in weight of a sample per unit area (mg/cm ²). In determining a weight change, the original sample is weighed without any attempt to remove adherent corrosion products. Weight change may express weight loss (minus) or weight gain (plus).
Weight-change rate (Rate of weight change)	The weight change per unit area divided by time under test [mg/(cm ²)(mo)]. In determining the rate of weight change, the original sample is weighed after each test period without any attempt to remove adherent corrosion products.
Gas concentrations	Gas volumes are calculated for solutions at room temperature and atmospheric pressure and are expressed as milliliters of gas per liter of water (ml/l).
Degassed water	Routine laboratory test water, degassed by boiling, has an oxygen content of about 0.1 to 1 ml/l. In special tests employing deoxygenating resins, the oxygen content is reduced to less than 0.05 ml/l.

ALUMINUM AND ALUMINUM ALLOYS*

Aluminum and aluminum alloys have excellent corrosion resistance in many aqueous environments. Commercially-pure 2S aluminum is useful in reactors as cladding and tubing. No significant amount of information about corrosion rates of aluminum in nearly pure water exists in the open literature, and all of the results presented here are from project sources. Differences in the corrosion rates of aluminum in neutral or slightly acid solutions caused by such variables as solution flow rate, hydrogen peroxide concentration, calcium-, magnesium-, and several mixed-salts, the presence of soluble oil, dissolved oxygen content, several metal surface pre-treatments, and irradiation during exposure were unmeasurable with the methods used. It was generally agreed that dilute hydrogen peroxide and the higher flow rates (above 10 ft/sec) decreased the prevalence of pitting.³⁻²⁴

EFFECT OF TEMPERATURE AND pH AT TEMPERATURES ABOVE 100°C (212°F)

The corrosion of 2S aluminum in relatively pure water is shown in Fig. 1.11.1. After an initial period of relatively rapid corrosion, the rate diminishes to a constant value. The

* This sub-section on aluminum and aluminum alloys was prepared by J. E. Draley, Metallurgy Division, Argonne National Laboratory.

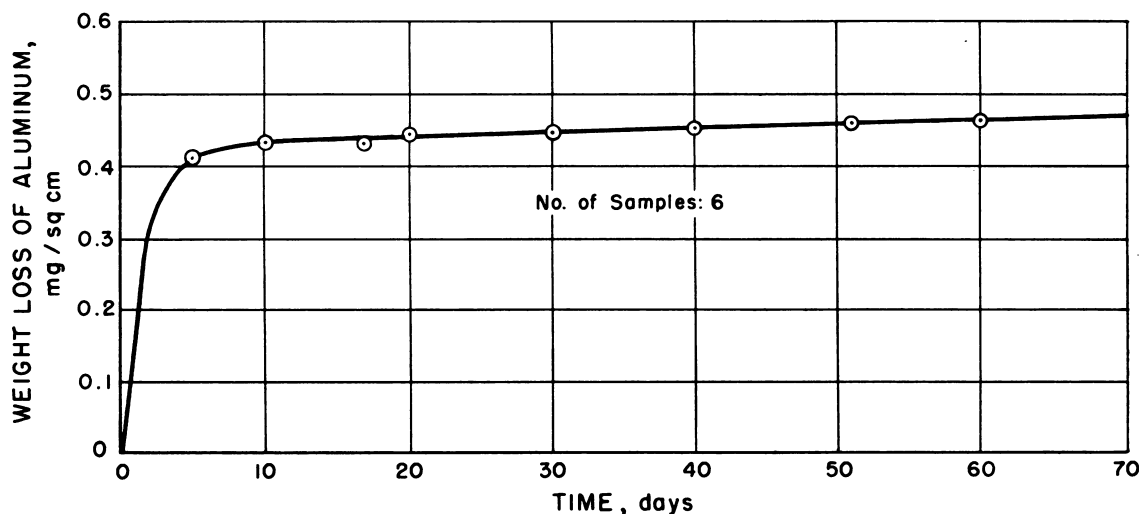


Fig. 1.11.1 — Corrosion of 2S Aluminum in Oxygen-saturated Distilled Water at 50°C (122°F). Submitted by Argonne National Laboratory, Sept. 16, 1952.

slope of this linear portion of the curve is often called the corrosion rate, since it can be extrapolated to long times.

Such corrosion rates are plotted in Figs. 1.11.2 and 1.11.3 as a function of temperature. In Fig. 1.11.2, three curves have been drawn: one for approximately neutral distilled water, one for dilute potassium hydroxide solution (pH 8 to 9), and one for dilute sulfuric acid (pH 4.0 to 4.4). Inaccuracies in the data plotted are such that considerable care should be taken in their interpretation. Points are given, at temperatures below 100°C (212°F), for water containing hydrogen, helium, or oxygen. Points used for the neutral water curve are the helium and hydrogen-saturated cases. At 200° and 275°C (392° and 527°F), the water was not changed for the duration of individual exposures. After seven days at higher temperature, the water pH had risen to above 8, and an intergranular attack had apparently started by ten days, as shown in Fig. 1.11.4. Subsequent to that time, more rapid attack and general disintegration occurred. Rates before eight and after ten days are plotted in Fig. 1.11.2 for that temperature.

Examination of the curves in Fig. 1.11.2 shows straight-line relationships between log corrosion rate and $1/T$, with sharp changes in slope between 100°–150°C (212° and 300°F). These breaks perhaps correspond to the transition in the composition of the corrosion product as the temperature is changed. The product at elevated temperatures is the alpha monohydrate of aluminum oxide. At lower temperatures, the composition is usually the beta trihydrate. Apparently, the transition between the two oxides is a function not only of temperature but also of water purity or solution composition. The high-temperature data will soon be issued in topical report form.¹⁸

EFFECT OF pH, WATER COMPOSITION, AND VELOCITY BELOW 100°C (212°F)

Aluminum suffers rapid attack in either alkaline or strongly acid media. The rate of corrosion is seen to be lowest in the general pH region of 4.5 to 7.0, with a minimum at about 6.5 (see Fig. 1.11.5). Within that range, the temperature and flow rate caused no large variation in corrosion rate. However, the presence of only 2 ppm chloride ion caused a noticeable increase in pitting, the effect beginning at about pH 6 and increasing as the pH was decreased. No pitting was observed in the absence of chloride ion and very

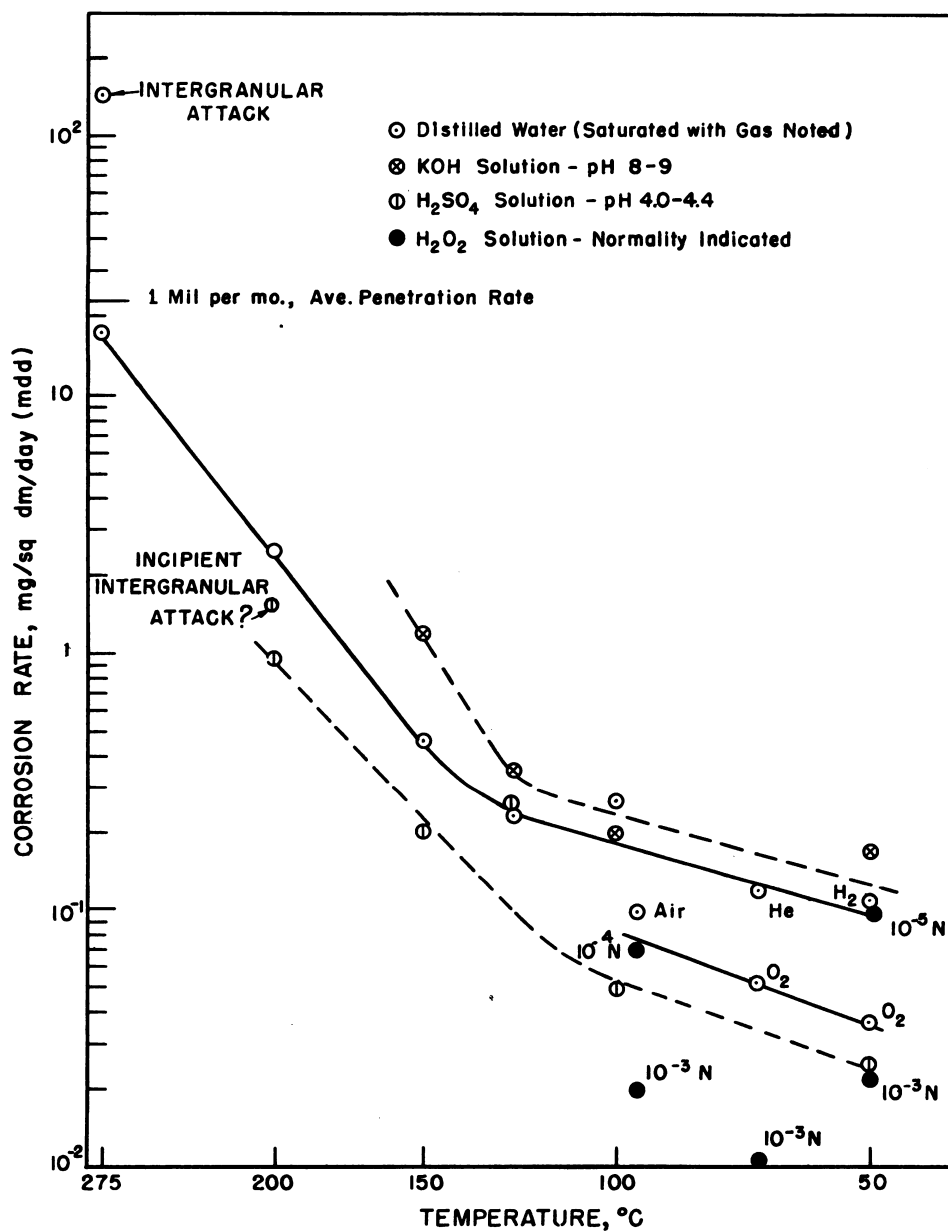


Fig. 1.11.2—Aqueous Corrosion of 2S Aluminum. Submitted by Argonne National Laboratory, Sept. 16, 1952.

little when it was present at a concentration of 1 ppm. At pH above 7 and below 4.5, corrosion rates are seen to increase sharply. In both regions, a positive dependence of corrosion rate on flow rate is exhibited. Above pH 7, increasing the temperature from 70° to 95°C (158° and 203°F) increases the corrosion rate; below pH 4, the reverse seems to be true.

These data were obtained in recirculating systems to which was continuously added fresh solution of suitable composition. Water composition thus remained constant. Solution flow rates past specimens were from 9 to 38 ft/sec. Within the pH range of 5 to 7, the solute concentrations varied throughout the following ranges from one test to another: chloride, 0 to 2 ppm; hydrogen peroxide, 0 to 10^{-3} M; sulfate, up to 100 ppm; magnesium, 0 to 6 ppm; calcium, 0 to 20 ppm. These variations did not have a consistent significant effect on the corrosion rate. Dilute hydrogen peroxide and the higher flow rates (above 10 ft/sec) decreased the prevalence of pitting. Slightly lower corrosion rates are typically observed in good quality distilled water (ca. 1 megohm-cm specific resistance) because of the presence of hydrogen peroxide at 50° to 95°C (122°–203°F). See Fig. 1.11.2.

Halide ions are generally deleterious to aluminum in water, corroding it in decreasing severity in the order: chloride ion, bromide ion, and iodide ion. Fluoride ion usually does not cause as rapid corrosion as the other halides. The harmful effect of the chloride ion is enhanced by the presence of small amounts of ions of heavy metals such as copper and iron. Even under conditions where the over-all corrosion rate is not significantly increased, these ions often cause severe local attack or pitting. Such behavior spoils the usefulness of the metal in many applications where perforation of the piece cannot be tolerated.

EFFECT OF ALLOYING

It is generally true that the commercial alloys of lowest additive content are most corrosion resistant. Although a certain minimum silicon content may be essential for the best corrosion resistance, commercial alloys have more than this minimum amount. Most metallic constituents are relatively insoluble in aluminum at ordinary temperatures and usually are present in a separate phase. If this separate phase has a markedly different solution potential than the aluminum matrix, local galvanic cell action is intensified, often resulting in considerably increased corrosion.

The corrosion resistance of aluminum alloys other than 2S in high-purity water has not been thoroughly investigated. The corrosion of 63S aluminum is very much like that of 2S at 200° and 115°C (392° and 239°F) in boiled distilled water.¹⁸ Alloys 52S and 61ST corrode similarly to 2S at 35° and 70°C (95° and 158°F).¹³ The 72S alloy corrodes at approximately the same rate as 2S, but with a greater pitting susceptibility, at temperatures from 70° to 94°C (158° to 201°F).¹³ Alloys containing much more than the minimum critical amount of silicon generally corrode somewhat more rapidly than 2S and exhibit a greater susceptibility to pitting attack.^{13,20}

COUPLE EFFECT

Aluminum is an active metal and would be expected to corrode more rapidly when exposed to the corroding medium while electrically connected to most other metals. In many aqueous media, this phenomenon does occur. Coupling to a cathodic material such as copper, brass, stainless steel, or graphite frequently causes rapid pitting of aluminum. Depending on the conditions, the attack may be largely adjacent to the cathodic metal or spread out over most of the aluminum surface. In Columbia River water, real and simulated, severe aluminum corrosion results from coupling to graphite.²⁰ In distilled water, aluminum is generally highly resistant to the anodic attack although it is anodic to most metals.²¹ In the absence of oxygen, the corrosion rate of 2S aluminum is perhaps somewhat reduced by coupling to graphite.²² At temperatures above the boiling point, no signifi-

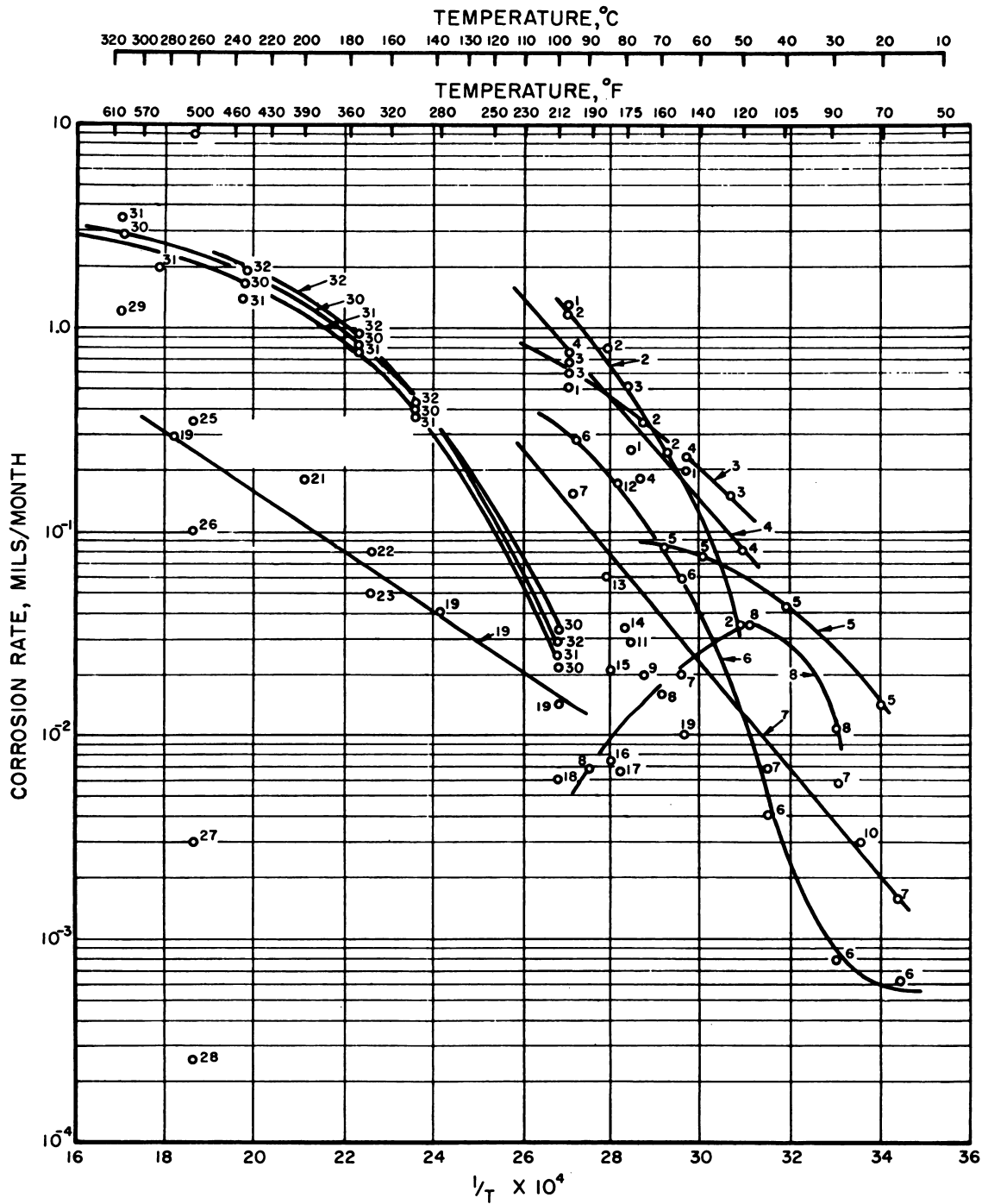


Fig. 1.11.3— See facing page for legend.

Fig. 1.11.3—Corrosion Rate of Various Aluminum Alloys as a Function of Temperature and Water Condition. Reprinted from NAA-SR-94, 1950.

LEGEND*

Test No.	Type of aluminum	Water flow, ft/sec	Type of water	pH	Additives	Other water data	Test time, hr†
1	2S-72S clad	20	Demineralized	7.5	Dichromate	Degassed	500
2	2S-72S clad	20		6.5	500
3	2S-72S clad	20	Demineralized	6.5	...	Degassed	500
4	2S-72S clad	20		7.5	Dichromate	...	500
5	2S	20		7.5	Dichromate	Degassed	6000
6	2S	...		7.5	Dichromate	...	4500
7	72S	...		7.5	Dichromate	...	4500
8	356	Static	Demineralized	6.0	0.005M H ₂ O ₂	...	1000
9	2S	Static	Distilled	5.9	720
10	2S	...	Distilled	6.0	Sat. CO ₂	...	342
11	2S	15	Distilled	6.0	0.00001N H ₂ O ₂	...	700
12	356	7	Demineralized	6.0	0.0005M H ₂ O ₂	...	1000
13	356	7	Demineralized	6.0	...	Degassed	1000
14	356	7	Demineralized	6.0	0.005M H ₂ O ₂	...	1000
15	356	Static	Demineralized	6.0	...	Degassed	1000
16	356	Static	Demineralized	6.0	0.005M H ₂ O ₂	...	1000
17	356	Static	Demineralized	6.0	0.0005M H ₂ O ₂	...	1000
18	2S	3	Distilled	5.7	...	Degassed	120
19	2S	Static	Distilled	6.5	...	Degassed	48
20	2S	3	Distilled	4.8	0.05M H ₂ O ₂	Degassed	285
21	2S	Convect.	Distilled	6.5	...	Degassed	48
22	2S	3	Distilled	5.7	...	Degassed	150
23	2S	3	Distilled	5.7	0.0001M H ₂ O ₂	Degassed	55
24	2S	27	Distilled	6.5	-O ₂	...	470
25	2S	27	Distilled	6.5	-H ₂	...	650
26	2S	Static	Distilled	6.5	...	Degassed	720
27	2S	Static	Distilled	6.5	-H ₂	...	720
28	2S	Static	Distilled	6.5	-H ₂ O ₂	...	20
29	Alclad	Static	Distilled	6.0	...	Degassed	140
30	72S	Static	Distilled	6.5	...	Degassed	48
31	24S	Static	Distilled	6.5	...	Degassed	48
32	2S	Static	Distilled	6.5	...	Degassed	48

*Points are estimated mean values for corrosion rates; deviations as high as a factor of 2 are often encountered

†The tests run at 212°F were for 1000 hr duration instead of 48 hr. In general, corrosion rates of Al measured over short periods of time are too high



Fig. 1.11.4—Section of 2S Aluminum Sample at Corroded Surface Showing Intergranular Attack after Ten Days in Distilled Water at 275°C (526°F). Reprinted from ANL-4581, Dec. 31, 1950. (magnification 250×)

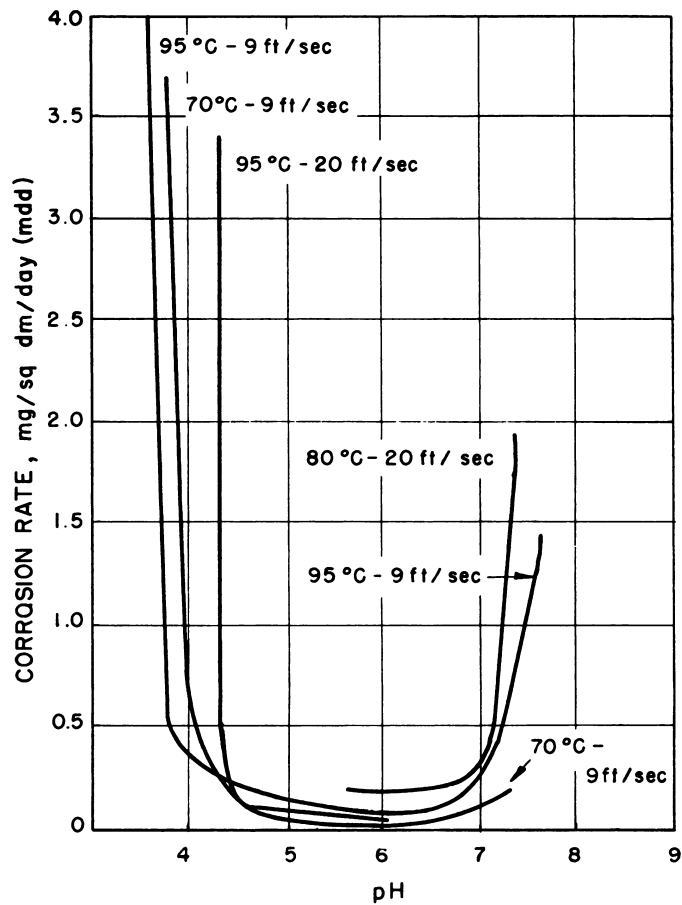


Fig. 1.11.5—Effect of pH and Other Variables on the Aqueous Corrosion of 2S Aluminum. Reprinted from CT-3027, Reference (11), June 19, 1945.

cant galvanic effect is observed when it is coupled to graphite. At 100°C (212°F) or lower, no significant galvanic effect is observed where the aluminum is in open contact with water, but considerable attack occurs within the crevice formed by fastening the piece of aluminum to a piece of graphite or stainless steel.²³ It is possible that such crevice effects are the result of increased alkalinity caused by the corrosion reactions in the very small amount of water stagnant within the crevice. The effect does not occur in 10⁻³N hydrogen peroxide solution at 40°C (104°F). Couples with graphite and with stainless steel tested in 10⁻³N hydrogen peroxide showed no attack, even in the crevice.²⁴

IRRADIATION EFFECT

Tubes fabricated from 2S aluminum are now in use in several reactors. No evidence of increased corrosion caused by irradiation effects upon the metal has been noticed.

PROTECTIVE MEASURES

Protective methods used to prevent rapid corrosion of aluminum include the use of inhibitors. Those used most are oxidizing agents, with chromate or dichromate being outstanding. Substances in this category are added to the corroding solution and apparently help to repair breaks in the protective oxide film, thereby stifling any reaction at the local anodes on the metal surface.

Another method used is the application of a protective layer on the metal before it is exposed to the corrosive environment. Such coats include paints and the products of chemical or electrochemical treatment. Chemical baths are used to form a coat of low porosity and solubility, such as aluminum phosphate. In the electrochemical treatment, the metal is "anodized" in one of a variety of solutions; this treatment applies a layer of aluminum oxide to the surface. All pretreatments have the disadvantage that the effect is not permanent. If the applied coating is perforated either by mechanical or chemical means, the resulting penetration of the base metal may be worse than if it had not been so "protected."

Aluminum is also protected from severe corrosion by "cathodic protection." A current is passed to the metal from a separate electrode in a direction that increases the rate of the reduction reactions at the aluminum surface and limits oxidation reactions, or corrosion. If a sufficiently high current is used, anodic reactions of aluminum are prevented and no corrosion occurs.

Protection from penetrating pits is sometimes achieved through the use of "Alclad" parts. A thin layer of an anodic aluminum alloy is metallurgically bonded to the surface of the structural alloy which is to be subjected to the corrosive environment. If pitting proceeds through the clad to the base metal, penetration stops because the cladding sacrificially protects the base metal. This is a special case of cathodic protection.

BERYLLIUM

Beryllium has corrosion properties similar to those of aluminum and magnesium. Its corrosion rate depends upon the history of the sample. In general, the expected corrosion rate in water at 300°F is approximately 0.5 to 1 mg/(cm²)(mo), i.e., 2 to 4 × 10⁻³ in./yr. Corrosion is more rapid at higher temperature, and at 500°F the corrosion rate increases to approximately 2 to 4 mg/(cm²)(mo).²⁵⁻³⁵ Best corrosion resistance is achieved in de-gassed or hydrogenated water. In water containing dissolved oxygen, resistance is decreased.

The most resistant type of beryllium is the BP-QMV grade, a high-purity beryllium, cast by vacuum methods into billets, then pulverized and hot-pressed into blocks. This type of beryllium is being used in the MTR.

Beryllium is susceptible to galvanic attack when coupled to stainless steel AISI type 347 or to 2S aluminum. Pitting and general intergranular attack are the primary mechanisms of corrosion.

Beryllium oxide, a loose white powder, is the corrosion product formed when beryllium corrodes appreciably. An adherent oxide coating, apparently impervious, forms on resistant metal. The presence of localized impurities in the metal increases corrosion.

Foreign ions in the test water lead to increased corrosion. The most deleterious are chloride ions, copper ions, iron ions, or sulfate ions. Inhibitors, however, such as NaNO_3 (3–4 ppm) or Na_2CrO_4 (5 ppm), reduce corrosion.

Various surface treatments and fabrication methods have been investigated in an effort to improve corrosion resistance in 500°F water. None have resulted in any marked improvement. Besides cleaning all grease and other attached impurities from the metal before use, no special pretreatment is recommended.

CHROMIUM

Chromium is very corrosion resistant in a passive condition.^{36,37} Tests indicate that when properly prepared it may be used in high-resistivity water up to 650°F. In distilled demineralized water containing 10 ml/l of oxygen, the rate of weight change is about 0.15 mg/(cm²)(mo) at 500°F and about 0.4 mg/(cm²)(mo) at 650°F.³⁸

Chromium is used chiefly as a plating for wear surfaces. Such parts exhibit maximum resistance when in motion and when used in high-resistivity water. The use of chromium in low-resistivity water or water containing dissolved salts should be avoided because of the tendency to pit and promote galvanic corrosion.

In the preparation of chromium-plated parts, it is extremely important to avoid pits, pores, cracks, or other such flaws in the plate. Flaws that allow the coolant media to penetrate the plate will lead to galvanic attack and increased corrosion. Chromium is cathodic to most other metals and tends to accelerate corrosion rate if coupled. Applications with chromium in contact with metals of doubtful corrosion resistance should be avoided. Many chromium-plated parts are ground before use. The only additional surface cleaning suggested is degreasing.

COBALT AND COBALT ALLOYS

Cobalt metal has low corrosion resistance;³⁹ many cobalt alloys, however, have high resistance.^{40–42} In general, tests indicate that cobalt alloys having primary alloying constituents of 35 to 55 percent cobalt, 18 to 33 percent chromium, 5 to 16 percent tungsten, and small percentages of silicon, manganese, nickel, and iron,* have satisfactory corrosion resistances in water up to 650°F. Weight-change rates are lower in hydrogenated or thoroughly degassed water than in oxygenated water. There is a tendency for these alloys to lose weight rather rapidly during the first several weeks of exposure. Subsequent to the initial period, weight changes are small and general corrosion behavior satisfactory.

Other cobalt alloys containing approximately the same alloying elements as those mentioned above but with reduced cobalt contents of 27 to 34 percent† are less resistant. They do not exhibit good resistances at 500°F but may be used in water up to 250°F.

*Trade marks for alloys tested are:

Haynes Stellite Division: Stellite 1, Stellite 3, Stellite 4, Stellite 6, Stellite 12, Stellite 19, Stellite 21, Stellite 26 and Haynes Alloy 25

Vascalloy-Ramet Corporation: Vascalloy-Ramet 171 and Vascalloy-Ramet 192

Elgin National Watch Company: Elgiloy

†Trade marks for alloys tested are:

Haynes Stellite Division: Stellite 98M2 and Stellite Star J

Cobalt alloys are generally not susceptible to serious couple effects. Couples tested up to 500°F without deleterious effects are listed in Table 1.11.3.

The exact mechanism of the corrosion process is unknown, but in high-temperature water, initial weight-change rates of cobalt alloys are negative, indicating that there is a certain amount of metal dissolution before a corrosion-resistant film is formed. The negative corrosion rate indicates that proper precautions should be taken to minimize the presence of cobalt corrosion product in the coolant system.

The surface preparation recommended for cobalt alloys is a clean machining and/or an HF-HNO₃ pickle.⁴² Nitrided cobalt alloys have been tested and found subject to spalling and couple effects; their use is not recommended for 500°F water.

COPPER AND COPPER ALLOYS

Copper and its alloys are not recommended for general service in water-cooled reactors except where absolutely necessary.⁴³⁻⁴⁷ Such uses include applications where anti-fouling properties are necessary. Copper and copper alloys do not have exceptionally high corrosion resistance, and their corrosion resistance, and their corrosion products have a strong tendency to deposit or "plate" out of the coolant stream in other parts of the system. The deposit may be copper oxide or metallic copper depending on the individual conditions.

Several copper alloys tested at 500°F contained 9 to 11 percent aluminum, approximately 3 to 4 percent iron, and 85 to 88 percent copper;* these alloys exhibited good corrosion resistance. Cupro-nickel alloys containing at least 30 percent nickel had fair resistance at 500°F. Their rate of weight change at this temperature is about $-0.3 \text{ mg}/(\text{cm}^2)(\text{mo})$. Increasing the nickel content gave added corrosion resistance.

Copper, aluminum bronze, phosphorus bronze, silicon bronze, and two alloys† having a composition of 9 to 10 percent aluminum, 1 to 3 percent iron, and about 85 percent copper showed poor corrosion resistance in 500°F water but were satisfactory at temperatures up to 200°F.

Generally speaking, copper and copper alloys have a higher resistance in hydrogenated or thoroughly degassed water than in oxygenated water.⁴⁸

Alloys containing more than 50 percent copper tend to cause undesirable coupling effects when in contact with other metals.⁴⁹ This effect is especially bad with phosphor, silicon, and aluminum bronzes at elevated temperatures. Aluminum in contact with copper and its alloys suffers severe pitting. Caution should be exercised in the use of bronzes or brasses because of their susceptibility to stress corrosion.^{50,51}

Copper and its alloys can develop an adherent oxide film but tend to go directly into solution; their corrosion rates increase with increasing temperature. In order to prevent an undesirable build up of copper corrosion products in systems containing copper or copper alloys, counter-measures (such as the use of ion exchangers) must be taken to remove them.

GOLD AND PLATINUM AND THEIR ALLOYS

Pure gold and platinum are metals of extremely high corrosion resistance.⁵²⁻⁵⁶ Corrosion rates for both metals are low, and they have been tested at temperatures up to 650°F in water with satisfactory results. Alloys of gold and platinum, high in either metal, also have good corrosion resistance. These, however, require individual study and no specific conclusions are drawn.

*Trade marks for alloys tests are:

Ampco Metals Corporation: Ampco 15, Ampco 18, and Ampco 23

†Trade marks for alloys tested are:

Ampco Metals Corporation: Ampcoloy A-3 and Ampcoloy 45

Table 1.11.3—Cobalt Alloy Couples of Satisfactory Tested Resistance*
(Compiled from ANL and WAPD Data)

Cobalt alloy	Coupled to
Stellite 6, Stellite 3, or Haynes Alloy 25	Type 304
	US Steel - Stainless W
	US Steel - Stainless W, nitrided
	US Steel - Stainless W, chrome plated
	Type 347
	Type 347, chrome plated
Haynes Alloy 25	Armco 17-4 PH
	Stellite 6
	Type 347, chrome plated
	Armco 17-4 PH, nitrided
Stellite 3	Stellite 3
	Graphitar 14
	Type 304, chrome plated

*When motion must take place for proper operation of adjacent parts, it is recommended that these parts be moved at least once a week in order to prevent crevice corrosion product build up and subsequent freezing. This tendency is prevalent for even the most resistant couples

Gold and platinum and their alloys tend to accentuate couple effects of other metals. These noble metals owe their corrosion resistance to their chemical inactivity. They are at the bottom of the emf series. When coupled to more active metals they cause increased galvanic attack of the active metal.

In any use, a clean surface is recommended for best service. A surface machining operation or a dilute nitric-hydrofluoric acid pickle is satisfactory in most cases.

MAGNESIUM AND MAGNESIUM ALLOYS

The corrosion rate for commercial-grade magnesium in aerated, boiling, distilled water is about 4 mils/mo, i.e., 18 mg/(cm²)(mo). The rate increases rapidly with temperature. Corrosion resistance of magnesium and its alloys may be improved by increasing the pH to between 9 and 11. To date, magnesium has not been used as a major constructional material or fuel-element clad because of its high corrosion rate and the resulting large amount of corrosion products.⁵⁷⁻⁶⁴

Alloy additions or impurities affect the corrosion resistance of magnesium. Impurities such as iron, nickel, and copper,⁵⁹ if present in amounts above tolerance limits, decrease corrosion resistance. Typical data showing the change of corrosion rate with temperature for a magnesium alloy containing 6.5 percent Al, 0.2 percent Mn, and 1 percent Zn are shown in Table 1.11.4.

Magnesium and magnesium alloys are subject to galvanic attack when coupled to other metals lower in the emf series. They are anodic to most other metals and are often used as sacrificial anodes to prevent or reduce corrosion of other metals. Magnesium tends to

pit in stagnant water. The attack is fairly uniform in dynamic or freely flowing water if the flow rate is not excessive. At flow rates greater than 25 ft/sec, magnesium is sometimes subject to erosion.

NICKEL AND NICKEL ALLOYS

Nickel and its alloys show limited corrosion resistance at 500°F⁶⁵⁻⁶⁹ and poor corrosion resistance above this temperature. Rates of weight change in degassed 500°F water for the more resistant alloys are about $-0.4 \text{ mg}/(\text{cm}^2)(\text{mo})$ or less, depending on the oxygen content. Nickel and nickel alloys exhibit their highest corrosion resistance in degassed

Table 1.11.4—Aqueous Corrosion of a Magnesium Alloy

Temperature, °F	Corrosion rate	
	Mils/month	Mg/(cm ²)(mo)
95	0	0
150	0.27	1.2
180	.75	2.9
212	2.9	13

water or in water containing only small amounts of dissolved oxygen. Nickel alloys exhibit good resistance in 500°F water containing hydrogen. The compositions of alloys that show the best resistance in tests at 500°F are shown in Table 1.11.5. Nickel alloys show better resistance at lower temperatures. Most nickel alloys containing more than 50 weight-percent nickel have weight-change rates of less than $-0.2 \text{ mg}/(\text{cm}^2)(\text{mo})$ at 200°F in degassed water.

Nickel alloys exhibit a tendency toward pitting in high-temperature oxygenated systems. Nickel is above copper and below iron in the emf series. Nickel alloys may increase galvanic corrosion when coupled to another metal unless used with discretion. Nickel does not readily discharge hydrogen in water in the absence of oxygen or other oxidizing agents; it exhibits an overvoltage of about 0.5 volts. For this reason, it has fair to good corrosion resistance in media not containing depolarizers such as dissolved oxygen.

There are various pickles for nickel alloys. A clean machined surface or a pickled surface is recommended for best service.

SILVER AND SILVER ALLOYS

Silver has good corrosion resistance in water up to about 250°F. In 500°F water, it corrodes at a rate of approximately $40 \text{ mg}/(\text{cm}^2)(\text{mo})$, and its corrosion products deposit readily on other metallic surfaces.⁷⁰⁻⁷³ Silver corrodes with the formation of an oxide film, but this film is non-protective and corrosion products tend to disperse into the coolant stream and plate out in other parts of the system. Several alloys containing cadmium, platinum, and gold have shown satisfactory resistance in 500°F water; these are listed in Table 1.11.6. Other alloys containing 60 to 70 percent silver, 30 percent cadmium, and from 3 to 9 percent copper have not shown satisfactory resistance in 500°F water. Silver and silver alloys accentuate couple effects. The same precautions suggested for the use of dissimilar metals in contact with gold and platinum alloys should be employed for silver or silver alloys.

Table 1.11.5—Composition of Nickel Alloys Showing Good Corrosion Resistance in 500°F Water

Alloy	Composition, wt-%								Trade mark	Manufacturer	
	Ni	Cr	Fe	Cu	C	Mn	Si	Mo			Others
1	66.0		1.50	30.0	0.20(max)				Al - 3.5	K Monel	International Nickel Company
2	73.0	15.0			.04	0.5	0.4		Cb - 1.0, Ti - 3.5	Inconel X	International Nickel Company
3	56.0	22.5	6.5	6.5	.2	1.25	.65	6.4	Ti - 0.2	Illium G	Illium Corporation
4	56	23		8.0		1.0		4.0	W - 2.0	Durco D-10	Duriron Company
5	63	3		.	0.1	1.0	1.0	32		Chlorimet 2	Schleier Pump Company
6	75/85	8/14							B - $\frac{2}{3}$, (Fe, Si, C - 8 max)	Colmonoy 4	Wall-Colmonoy Corporation

Table 1.11.6—Composition of Silver-Cadmium Alloys of
Good Resistance in 500°F Water
(ANL-4729)

Alloy	Alloying elements, wt-%						
	Ag	Cd	Pd	Au	Cu	Sn	Al
1	60	30	10				
2	50	30	20				
3	40	30	30				
4	66.5	30			3		0.5
5	30	50		20			
6	30	60				10	

PLAIN-CARBON AND LOW-ALLOY STEELS

Metals in this class have high corrosion rates and are not generally used in water-cooled reactors at any temperature.⁷⁴⁻⁷⁸ They are susceptible to severe local attack and pitting. Mild steel corrodes at a rate of about 20 mg/(cm²)(mo) in 140°F water containing an oxygen concentration of 3.9 ml/l.⁷⁸

The corrosion of steels is very sensitive to the presence of chloride ions as well as to pH and dissolved carbon dioxide and oxygen. The concentration of dissolved oxygen has been found to be critical at higher temperatures in distilled demineralized water.

The primary corrosion process of a metal and water is thought to involve a reaction between the metal and the dissolved oxygen present in the water. The reaction for iron and oxygen takes place in a stepwise fashion:



The oxides formed are no doubt hydrated. The degrees of hydration depend on the conditions of formation and are not indicated in the above equations. Fe₂O₃ and Fe₃O₄ are stable oxide forms of iron and are the usual corrosion products. These compounds are only slightly soluble in water, even at high temperatures, and may be suspended in the coolant as colloids or suspensions or may precipitate out as powdery deposits. FeO is not stable in water in the presence of dissolved oxygen, readily oxidizing to Fe₂O₃ or Fe₃O₄.

STAINLESS STEELS

As a class, stainless steels are corrosion-resistant and versatile structural materials for use in high-temperature water-cooled reactors.⁷⁹⁻⁸⁴ They have been classified into five groups for this discussion: (1) AISI 300 series -austenitic, (2) AISI 400 series -martensitic, (3) AISI 400 series -ferritic, (4) precipitation hardening and (5) high-alloy steels and heat-resistant alloys.

Stainless steels owe their corrosion resistance to the presence of chromium and nickel as alloying elements. The austenitic and high-alloy steels have the highest corrosion resistance of the stainless steels; recent tests indicate good corrosion properties at temperatures up to 700°F in degassed water. Corrosion increases slightly in oxygenated

water. The corrosion rates for austenitic and high-alloy stainless steels vary from 0.01 to 0.1 mg/(cm²)(mo) in demineralized 600°F water containing dissolved oxygen (about 5 ml/l). Carbide precipitation at grain boundaries, caused by welding or heat treatment, does not affect the corrosion resistance of the 300 series in water up to 500°F. The precipitation-hardening stainless steels are the next most resistant; they are slightly less corrosion resistant than the 300 series steels but are susceptible to stress corrosion cracking in high-temperature water. The martensitic and ferritic stainless steels are the least resistant. These steels have good resistance up to 200°F in carefully degassed water. With the exception of types 430, 442, 443, and 446, their general corrosion resistance is poor in 500° or 600°F water; they are susceptible to pitting and galvanic attack. Table 1.11.7 presents a comparative tabulation of the corrosion resistance of stainless steels.

300 SERIES—AUSTENITIC

The austenitic AISI 300 series stainless steels have very high corrosion resistance in high-temperature water; they are characterized by a high chromium-nickel content, nominally 18-8, 25-12, and 25-20 (Cr-Ni) and a relatively low carbon content, 0.25 percent or less. The stable austenitic phase gives ductility and corrosion resistance. Types 304, 309, 310, 316, 321, and 347 have the highest corrosion resistance⁸⁴⁻⁸⁸ and are weldable without appreciable loss of corrosion resistance.⁸⁹⁻⁹⁴ Figures 1.11.6, 1.11.7, and 1.11.8 show weight-change vs time data for AISI type 347 stainless steel at various gas concentrations.* Types 304, 309, 310, 316, and 321 behave in a similar manner.

In evaluating the behavior of a material, appearance as well as weight change should be considered. The general corrosion effect noted for these materials in high-temperature water is the formation or development of an adherent oxide film except in media containing more than 50 ml of dissolved hydrogen per liter. With hydrogen addition, the specimen appearance remains bright during exposure, indicating little or no film formation. In media containing oxygen in amounts of more than 0.5 ml/liter, a thicker and darker oxide builds up which eventually turns black. This oxide may appear dull and have a loose, powdery overlay of corrosion product deposited from the system water.

Heat treatment after welding is unnecessary except as required to improve physical properties. Intergranular or grain-boundary corrosion resulting from carbide precipitation in unstressed 300 series stainless steels is not experienced in high-temperature water. Stresses in the range of 0 to 10,000 psi does not affect their resistance in water

400 SERIES—MARTENSITIC

The martensitic 400 series stainless steels contain up to 2½ percent nickel and 12 to 17 percent chromium. The hard martensitic phase is developed by heat treatment at 1700° to 1900°F. These steels are not as resistant as the 300 series steels at 500° and 600°F in oxygenated water. There is some evidence indicating that steels such as AISI type 410 are more resistant at temperatures of 650° and 680°F than at 500°F. Figures 1.11.9 and 1.11.10 show weight-change vs time data for several of the martensitic steels. It is emphasized that weight-change data alone does not allow complete evaluation of the behavior of a material but must be considered with the appearance. The 400 series martensitic steels tend to develop a thick, black oxide film and are frequently covered with heavy deposits of corrosion product.

* The degassed water prepared for these tests was boiled and passed through a deoxygenating resin. The resulting oxygen concentration was about 0.01 ml/l.

Table 1.11.7—Corrosion Resistance of Stainless Steels in 500°F Distilled Water Compared to AISI Type 347

Same typical performance*	Unsatisfactory performance†
302	403
303	405
304	410
304L	414
305	420
309	430‡
310	431
316	440A
318	440B
321	440C
USS Stainless W	442‡
Armco 17-4 PH	443‡
Armco 17-7 PH	446‡
Carpenter 20	501
Durimet 20	

*“Same typical performance” indicates the same relative corrosion resistance as shown by AISI type 347

†“Unsatisfactory performance” indicates a lower general corrosion resistance than AISI type 347 and probable exclusion from general use in 500°F water

‡Tests have indicated that these metals are the best of the 400 series ferritic. Under some conditions they show fairly good resistance at 500°F

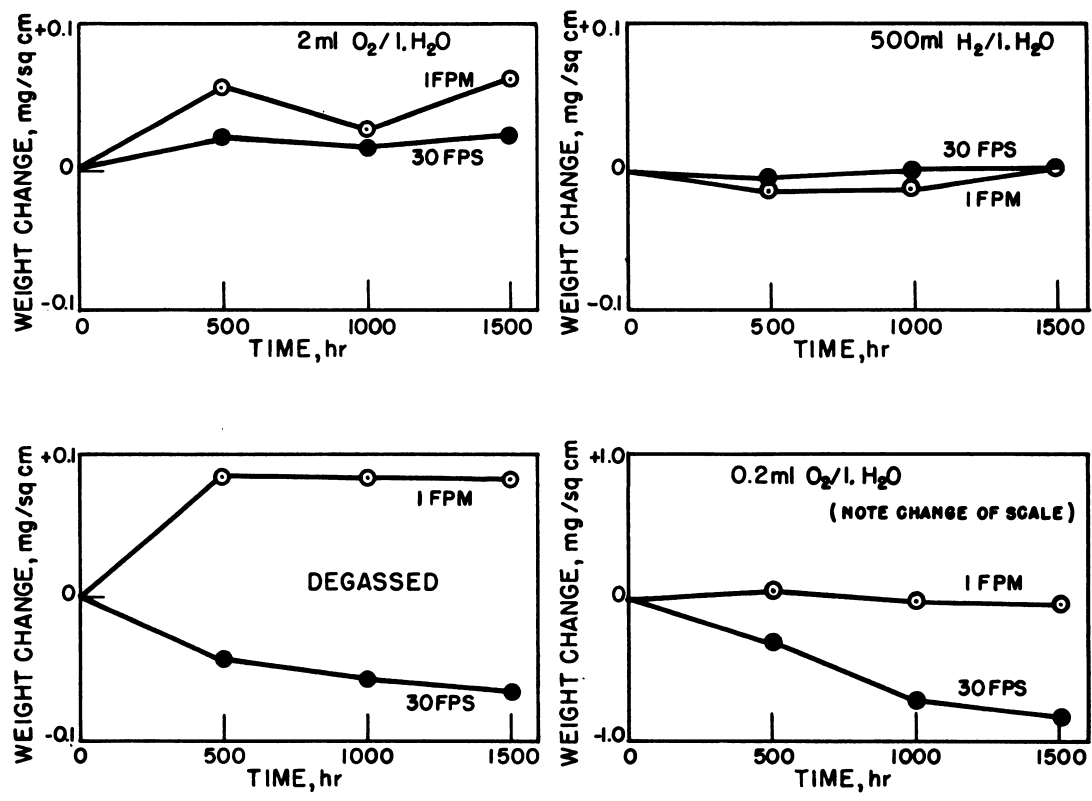


Fig. 1.11.6—Weight Change of AISI Type 347 Stainless Steel in Demineralized Water Containing Various Gas Additions. Plotted from Babcock and Wilcox data, Nov. 10, 1952. Dynamic loop tests: temperature, 500°F; pressure, 2000 psig.

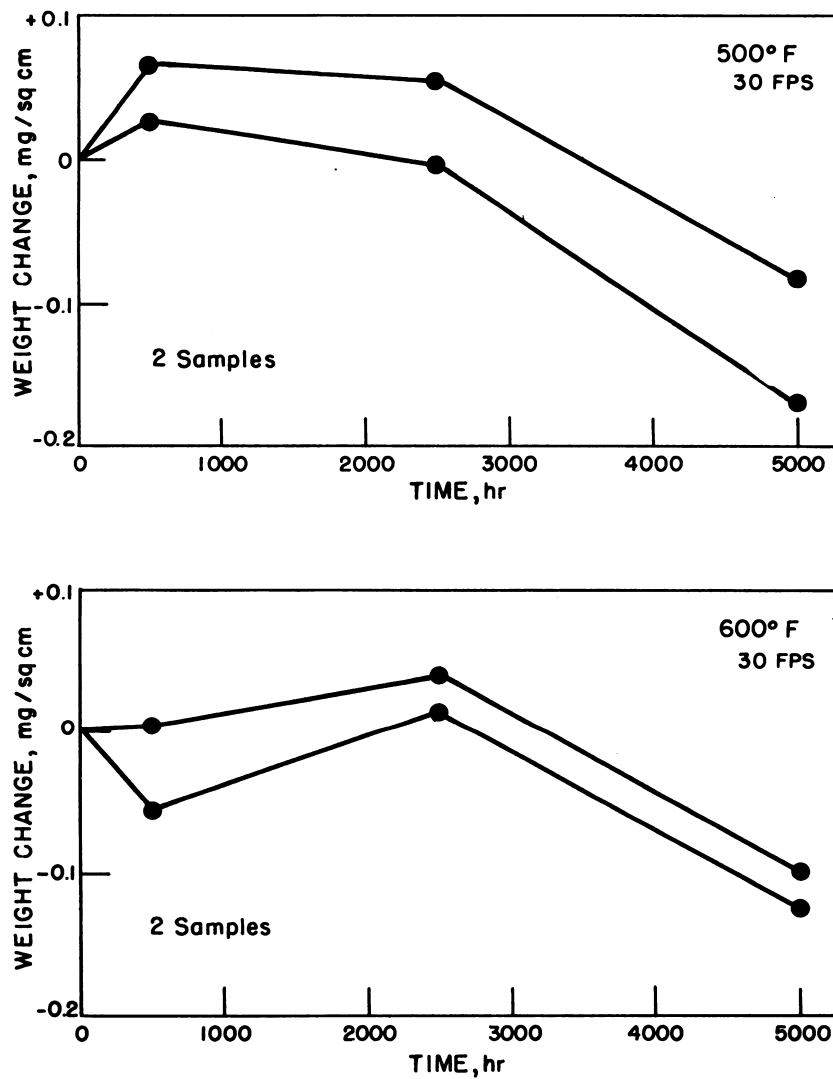


Fig. 1.11.7—Weight Change of AISI Type TS347A Stainless Steel in De-mineralized Water at 500° and 600°F. Plotted from Babcock and Wilcox data, Nov. 10, 1952. Dynamic loop test: pressure, 2000 psig; dissolved oxygen, 30 ml/l.

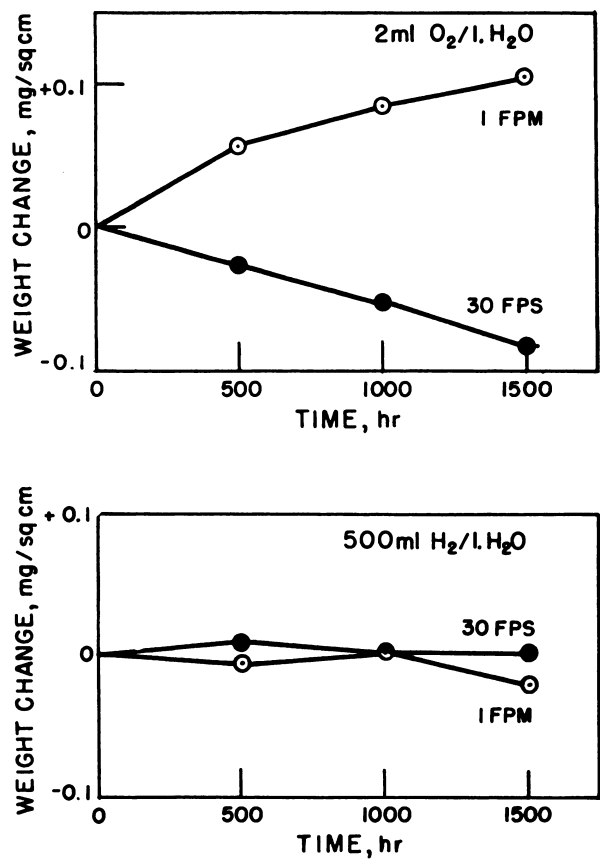


Fig. 1.11.8—Weight Change of AISI Type TS347A Stainless Steel in De-mineralized Water Containing Various Gas Additions. Plotted from Babcock and Wilcox data, Nov. 10, 1952. Dynamic loop test: temperature, 500°F; pressure, 2000 psig.

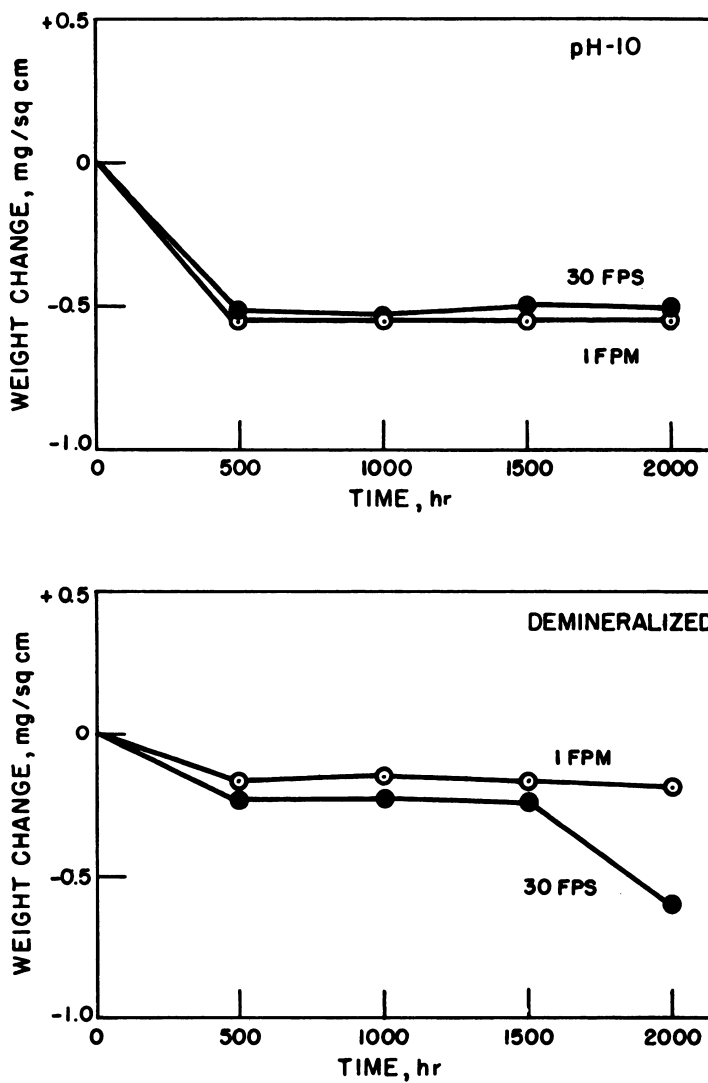


Fig. 1.11.9—Weight Change of AISI Type 410 Stainless Steel (Hardened) in Water Containing NaOH and in Distilled, Demineralized Water. Plotted from Babcock and Wilcox data, Nov. 10, 1952. Dynamic loop test: temperature, 500°F; pressure, 2000 psig; dissolved oxygen, 2 ml/l.

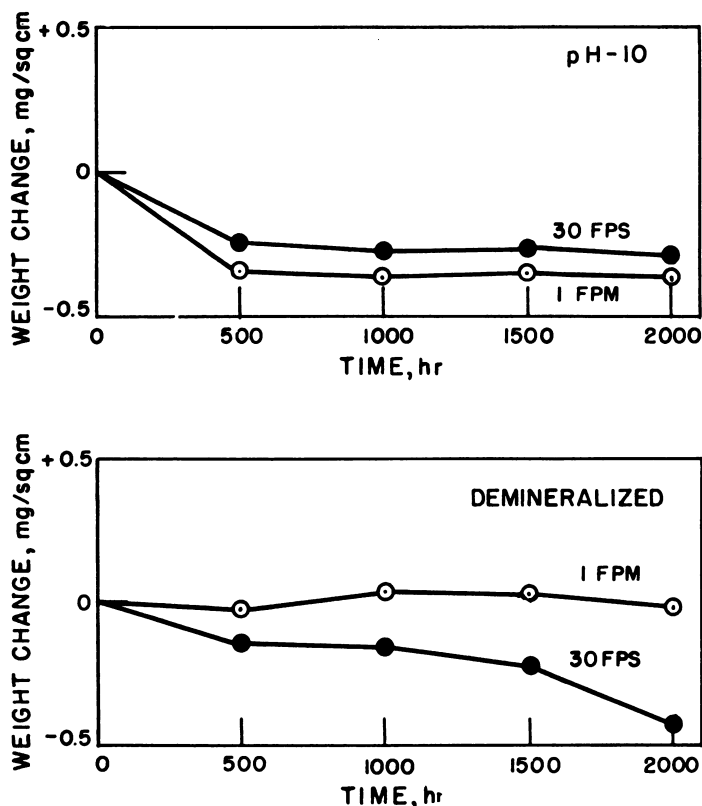


Fig. 1.11.10— Weight Change of AISI Type 440C Stainless Steel (Hardened) in Water Containing NaOH and in Distilled Demineralized Water. Plotted from Babcock and Wilcox data, Nov. 10, 1952. Dynamic loop test: temperature, 500°F; pressure, 2000 psig; dissolved oxygen, 2 ml/l.

400 SERIES—FERRITIC

The ferritic 400 series stainless steels contain 18 to 30 percent chromium and no nickel; they are not hardenable by heat treatment or mechanical working. These steels have a slightly higher corrosion resistance than the martensitic type 400 series steels, but the corrosion resistance is not comparable to the 300 series steels. AISI types 430 and 446 are the most resistant of the ferritic stainless steels; type 442 and 443 are slightly less resistant.

AISI 400 series metals are readily susceptible to pitting and local couple effects; if used as working parts, they should be kept in motion for best service.

PRECIPITATION-HARDENING STAINLESS STEELS

The precipitation-hardening stainless steels contain small amounts of one or more alloying elements such as titanium, aluminum, or copper. The most resistant alloys tested are of the austenitic or essentially austenitic type.* In 500°F hydrogenated water (50 ml/l or more of hydrogen) for periods up to 500 or 1000 hr, the weight-change rates range from -0.4 to -1.5 mg/(cm²)(mo); after this initial period, the rate of weight change is small.

*Trade marks for steels tested are:

Armco Steel Corporation; Armco 17-4 PH, Armco 17-7 PH

United States Steel Corporation; USS Stainless W

Corrosion is approximately 1 to 4 times more rapid than the 300 series in 500°F degassed water.

The precipitation-hardening steels hold up well as gear and bearing materials if kept in motion. These metals show a tendency for galvanic attack in stagnant water, especially if the ion-impurity concentration increases; in high-purity water, performance is more satisfactory.

HIGH-ALLOY AND HEAT-RESISTANT STEELS

The high-alloy and heat-resistant steels contain alloying elements in amounts greater than normally associated with 300 series, 400 series, or precipitation-hardening stainless steels and possess high resistance to oxidation and thermal shock. Recent tests on two alloys containing approximately 29 percent nickel, 20 percent chromium, 2 percent molybdenum, 3 percent aluminum, and the balance iron* have indicated good corrosion resistance at temperatures up to 650°F.

FACTORS AFFECTING THE CORROSION OF STAINLESS STEELS

Effect of Oxygen Concentration

The corrosion rate of stainless steels in high-temperature distilled water is markedly dependent on the amount of dissolved oxygen present. Low rates are observed when no oxygen is present. Corrosion increases rapidly with increasing oxygen concentrations from a few tenths of a milliliter per liter to about 15 ml/l. Above this range, corrosion increases slowly and has a tendency to level off until oxygen concentrations of the order of magnitude of about 1000 ml/l are reached. At these higher concentrations, corrosion decreases slightly.

The addition of hydrogen (50 ml/l or more) is effective in reducing corrosion. Many stainless steels show no visible corrosion when tested at 500°F in water containing dissolved hydrogen. It is postulated that the hydrogen effectively removes dissolved oxygen from the water and is a means of deoxygenating a system. In operating systems containing hydrogen, the most beneficial effects are obtained by introducing the desired amount of hydrogen at room temperature before bringing the system to operating temperature and pressure. The appearance of type 347 samples after test in 500°F water containing various gas additions is shown in Fig. 1.11.11.

The use of hydrogen in systems previously run under oxygen should be considered with caution. There is some evidence that oxide scale previously formed under oxygen is loosened and partially dispersed into the system-water stream by dissolved hydrogen. The descaling is only partial, and stainless-steel surfaces are not completely deoxidized. The role of hydrogen in high-temperature water systems is not completely understood at this time; therefore, it is recommended that a complete evaluation be made before using hydrogen in any contemplated system.

Surface Treatments

The cleanliness of the stainless-steel surface is an important factor in corrosion resistance. For maximum resistance, the surface should be machined clean with a sharp clean tool or pickled in a nitric-hydrofluoric acid solution; oxide scale should be removed before pickling. A scaled surface, or one which has been rough machined, has a much lower resistance to corrosion.

* Trade marks for steels tested are:
Carpenter Steel Corporation; Carpenter 20
Duriron Company; Durimet 20

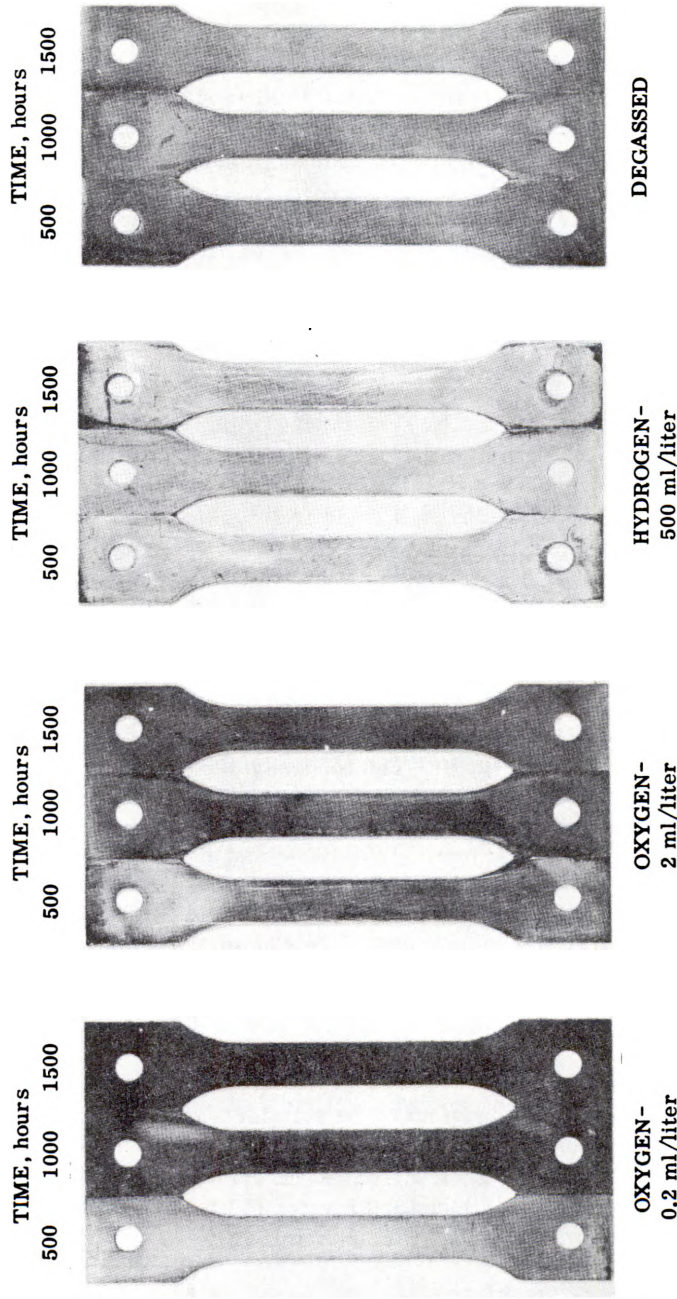


Fig. 1.11.11 — Appearance of AISI Type 347 Stainless Steel Samples Tested Under Various Gas Conditions in 500°F Demineralized Water. Photographs of samples tested at Babcock and Wilcox Feb. 1953. Dynamic loop tests at 2000 psig.

Effect of Nitriding

Stainless steels having nitrided surfaces show varying corrosion resistance. In some instances, a nitrided surface will show extremely high resistance; in others, pitting and spalling are prevalent and over-all corrosion resistance is low. Precipitation-hardening steels that have been nitrided show corrosion resistances slightly superior to most other nitrided stainless steels. Data indicate that the corrosion resistance of nitrided steels increases with temperature up to 500°F and varies inversely with the oxygen concentration at room temperature. The presence of carbon dioxide in the water accelerates corrosion. Increased pH or decreased resistivity increases the corrosion. Although general corrosion resistance is unchanged by water velocity, localized attack and pitting apparently decrease with increased velocity.

Surface treatments prior to nitriding and after nitriding are important. For best service, it has been found that the surface should be lapped or ground after nitriding in order to remove the top of the nitrided layer, sometimes known as "the white layer." Passivating the nitrided surface with nitric acid or dichromate solutions was not found to improve corrosion resistance in 500° and 600°F water. The tendency of nitrided steels to pit, spall, and accentuate couple effects demands thorough test before selection as reactor materials.

Effect of Heat Treatment

Heat treatments, as such, do not appear to affect the corrosion resistance of the 300 series stainless steels in high-temperature water. The 400 series and precipitation-hardening steels show slightly increased resistance in their hardened condition. Resistances of the high-alloy steels vary with heat treatment, depending on composition.

Velocity Effect

No appreciable effect of velocity has been noted on stainless-steel corrosion. Tests have been made at water velocities up to 30 ft/sec at 500° and 600°F without any appreciable erosion; higher velocities have not been investigated. Rates of weight change in Figs. 1.11.6 through 1.11.10 show that high-velocity water (30 ft/sec) has more of a tendency to remove corrosion products than low-velocity water (1 ft/sec).

Use of Inhibitors

Inorganic inhibitors, such as hydroxides, chromates, molybdates, tungstates, and the like, are effective in changing the corrosion characteristics of stainless steels. Hydroxides and ammonia or basic amine inhibitors are widely used in the boiler industry for corrosion control. The addition of traces of certain polyfunctional acidic substances, such as SiO_2 , V_2O_5 , or borates, improves the resistance of most stainless steels.¹ Organic inhibitors are probably unsatisfactory for use in high-temperature-water reactors because of thermal and radiation instability. No experimental data are reported on specific beneficial effects of inhibitors in high-temperature-water stainless-steel reactor systems. In general, the use of inhibitors offers a possibility of improving corrosion resistance; tests on the effect of various inhibitors on corrosion of the materials must be made in and out of reactors to establish feasibility.

THORIUM AND THORIUM ALLOYS

Thorium metal has inferior corrosion resistance. Rates of weight change vary from -1.5 to approximately 4 mg/(cm²)(mo) in distilled water at temperatures of 212° to 284°F. Rates of weight change increase sharply to approximately -500 mg/(cm²)(mo) at 350°F.

Ames* thorium shows a rate of weight change of approximately $-5 \text{ mg}/(\text{cm}^2)(\text{mo})$ at 160°F in simulated river water flowing at 25 ft/sec and containing H_2O_2 (0.006N). The effect of aeration or hydrogenation on corrosion is nil. The low corrosion resistance prevents the use of unclad and unalloyed thorium in direct contact with water. Alloys of thorium containing additions of 1 to 2 percent beryllium, small amounts of silicon, or more than 5 percent niobium or iron have increased resistance.⁹⁵⁻¹⁰²

Thorium and thorium alloys corrode with the formation of an adherent, lustrous, protective film or a porous coating of thorium oxide. If H_2O_2 is present in the water, an over-laying white floc is formed.

The method of surface preparation is important and may cause initial corrosion rates to vary as much as 300 percent. The most satisfactory surface is one which is ground and pickled. Anodizing thorium in a H_2SO_4 - H_3PO_4 bath produces an oxide film which is not protective in boiling distilled water. Thorium can be coated by dipping at 1470°F in molten aluminum (grade 2S). The corrosion resistance of the aluminum-coated thorium is approximately the same as aluminum metal.

TITANIUM

Commercially pure titanium has good corrosion resistance up to 680°F in water and is one of the most resistant metals.¹⁰³⁻¹⁰⁹ In 500°F water, the rate of corrosion is about twice as great in oxygenated as in degassed water. The average rate of weight change is about $0.03 \text{ mg}/(\text{cm}^2)(\text{mo})$ in 600°F air-saturated water. Titanium is resistant in 750°F , 1500 psig steam but reacts with steam at 1500°F .¹⁰⁹

Titanium is not ordinarily susceptible to couple effect. Exposure to high-temperature water builds up an oxide film of high electrical resistance; the resultant film prevents free flow of electrons from coupling metals and reduces the tendency of couple attack. Titanium, as are most metals that are easily anodically polarized, is not usually susceptible to galvanic attack or couple effects.

Titanium should be machined clean or pickled in a hydrofluoric-nitric acid mixture.

URANIUM

Uranium has very low corrosion resistance in water;¹¹⁰⁻¹²¹ consequently, the metal has been clad for reactor use. The log of the rate of attack of unalloyed uranium varies linearly with the reciprocal of the temperature from 100° to 440°F in hydrogen-saturated water as shown in Fig. 1.11.12. The corrosion rate is approximately $1900 \text{ mg}/(\text{cm}^2)(\text{mo})$, i.e., $2.7 \text{ mg}/(\text{cm}^2)(\text{hr})$ in boiling distilled water as shown in Fig. 1.11.12. In aerated water at temperatures less than 160°F , the initial corrosion rate is low and less than in the hydrogenated water at the same temperature (possibly because a temporary protective oxide is formed in the air-saturated water). See Fig. 1.11.13. After longer exposure, this rate increases.

ZIRCONIUM AND ZIRCONIUM ALLOYS

Zirconium of proper purity has high corrosion resistance and low thermal neutron cross section. At 600°F in oxygenated water, unalloyed high-purity zirconium has a weight change of about 0.01 to $0.1 \text{ mg}/(\text{cm}^2)(\text{mo})$ for periods up to 6 months. Recently developed zirconium alloys have shown good corrosion resistance at temperatures up to 650°F in water and 750°F in superheated steam.

The corrosion product for resistant zirconium exposed to high-temperature water is black and adherent; that for non-resistant zirconium is white and powdery. On long ex-

* Prepared by Iowa State College, Ames, Iowa.

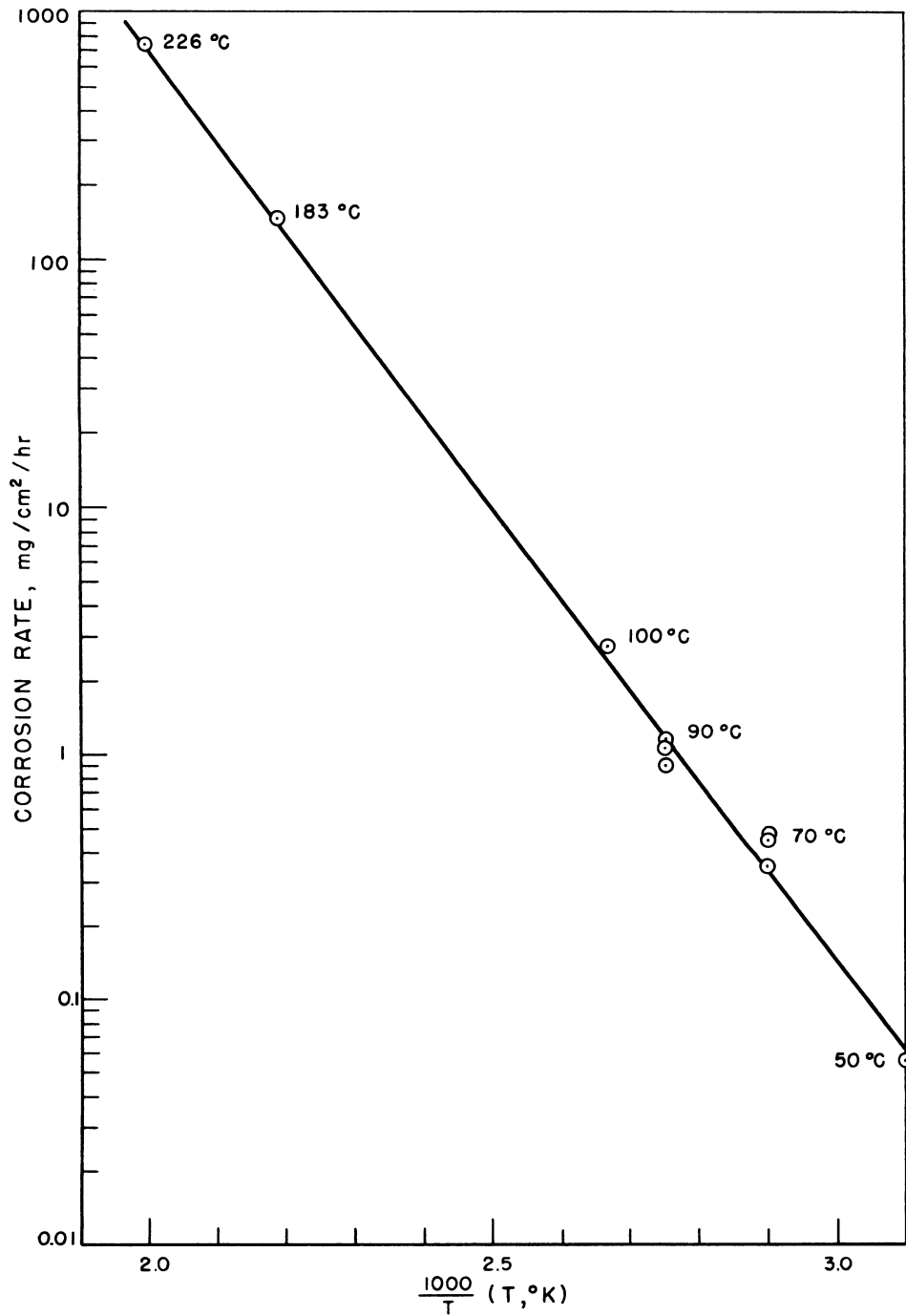


Fig. 1.11.12—Corrosion Rate of Standard Uranium in Hydrogen-saturated Water vs the Reciprocal of the Temperature. Reprinted from ANL-4862, May 14, 1952.

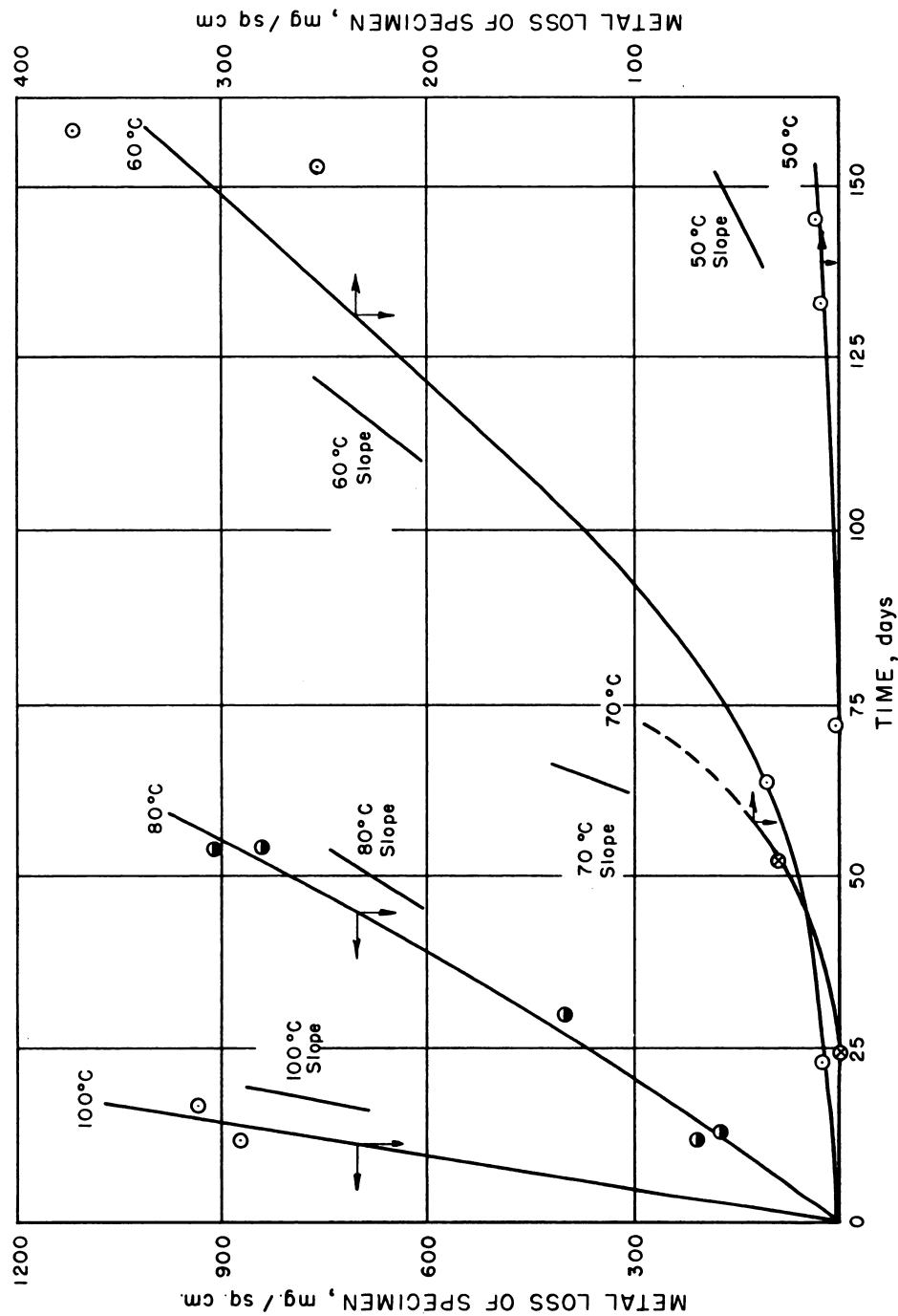


Fig. 1.11.13 — Corrosion of Standard Uranium in Aerated Distilled Water.
Reprinted from ANL-4862, May 14, 1952.

posure to high-temperature water, zirconium exhibits what is referred to as "breakaway" corrosion, i.e., a much increased corrosion rate after a period of relatively little corrosion. The time required to reach the point of breakaway in 600°F water varies from less than two weeks to more than two years depending on the purity of the metal and the surface condition.

UNALLOYED ZIRCONIUM

In high-temperature water, the corrosion resistance of unalloyed zirconium depends mainly on impurity content. Two types of zirconium are available, sponge zirconium¹²² and crystal-bar zirconium.

The sponge zirconium produced until recently generally had a higher impurity content than crystal-bar zirconium and was not as uniformly or as highly corrosion resistant as crystal-bar zirconium. Corrosion tests at temperatures up to 500°F for periods up to 6 months resulted in rate of weight changes of about 0.01 to 0.2 mg/(cm²)(mo); above this temperature, corrosion resistance may decrease rapidly. Sponge metal recently produced by the Bureau of Mines has shown a very low impurity content and high corrosion resistance. Three grades, A, B, and C, are assigned to the sponge metal based on its final position in the reaction vessel. The A and B grades contain iron as an impurity from the retort.¹²² C grade is, however, contaminated with most of the calcium and magnesium from the reduction; these light-metal impurities are removed from C grade by distillation.

Crystal-bar zirconium is the purest unalloyed zirconium and shows a more uniform and generally higher corrosion resistance than sponge zirconium.^{123,124} Tests at temperatures up to 650°F show weight-change rates of 0.02 to 0.2 mg/(cm²)(mo).

ALLOYED ZIRCONIUM

Alloyed zirconium is not thought to have corrosion resistance superior to that of the pure unalloyed metal. The resistance of pure zirconium is very sensitive to traces of impurities, improper handling, or fabrication techniques. Alloys have corrosion resistances which are not as sensitive to trace impurities as pure zirconium. Two general objectives in alloying zirconium with regard to its corrosion resistance are:

- (1) Decreasing the sensitivity of pure crystal-bar zirconium to trace impurities.
- (2) Improving uniformity of the corrosion resistance of sponge zirconium.

These objectives are not intended to improve such physical characteristics as hardness, ductility, weldability, and the like. Some of the more promising elements used in binary alloys of zirconium, and the most promising composition ranges in tests are:¹²⁵

Element	Weight-percent
Tin	1.5 to 5
Tantalum	0.1 to 0.5
Iron	Trace to 0.25
Nickel	Trace to 3
Niobium	0.5 to 3
Chromium	Trace to 1.0

Other elements, when added to zirconium to form binary alloys, decrease corrosion resistance. Results indicate that binary alloys of zirconium containing aluminum, beryllium, carbon, magnesium, nitrogen, and tungsten have low corrosion resistance over all composition ranges. Tests on binary alloys of zirconium containing approximately 5 percent antimony,¹²⁶ arsenic, bismuth, calcium, cerium, copper, germanium, gold, iron, lead, lanthanum, manganese, molybdenum, neodymium, praseodymium, vanadium, silver, and

zinc have lower resistance than unalloyed zirconium. Except for some narrow composition ranges, binary zirconium-titanium alloys have low corrosion resistance. Two zirconium-tin alloys have been extensively tested as possible cladding materials. One is a binary alloy of sponge zirconium containing $2\frac{1}{2}$ percent tin.* The presence of tin has been thought to prevent small amounts of nitrogen (about 200 ppm) from having deleterious effects on corrosion resistance. The other is a sponge zirconium alloy containing 1.5 percent tin, 0.1 to 0.15 percent iron, 0.1 percent chromium, 0.05 percent nickel, and less than 0.006 percent nitrogen.† This alloy is more resistant than the $2\frac{1}{2}$ tin alloy, and 2030-hr tests at 680°F have indicated a rate of weight change of 0.1 to 0.3 mg/(cm²)(mo). Tests have also been run at 750°F in superheated steam for 2000 hr without film breakdown. The 750°F test is much more severe than the 680°F test.

GENERAL COMMENTS

The corrosion resistance of zirconium is thought to result from the formation of a thin protective surface film tightly adherent to the metal surface and growing in thickness as the metal corrodes.¹²⁷ The film, initially thin, shows interference colors from gold to dark blue or green and as corrosion continues grows in thickness and finally turns black. During the initial stages of corrosion, the thickness of the film may be approximated by its color. The uniformity of color indicates uniform film thickness and uniform corrosion. This is in contrast with aluminum which also protects itself by a thin film but suffers from localized attack. Zirconium is not usually attacked by pitting.

Long exposure to high-temperature water may lead to film breakdown. At breakdown the lustrous adherent black film turns white, becomes flaky or powdery, and loses the protective ability. After film breakdown, further exposure results in accelerated corrosion. The film is non-healing and does not repair after breakdown. Initial x-ray diffraction studies of the thin colored-oxide film, the thicker black oxide, and the white oxide breakdown product showed monoclinic zirconium dioxide. Recent studies give evidence of tetragonal zirconium dioxide.¹²⁸

SURFACE PREPARATION

Before use, the zirconium surface should be freed from impurities. This is best accomplished by a clean machining followed by a pickle in a bath containing 35 percent by weight nitric acid, 1 to 2 percent by weight hydrofluoric acid, and the remainder water; this bath removes approximately 0.3 mil/min at 85°F. Removal of approximately 1 to 2 mils of zirconium surface is recommended. X-ray spectrometer line-broadening data indicate that surface working by machining operations may extend approximately 2 mils into the surface of the metal; corrosion resistance of a machined piece is best after this metal has been removed. The resistance of pure zirconium metal is affected by its surface condition to a much greater extent than that of alloys such as Zircaloy 2.

In 500°F degassed distilled water, there is no apparent correlation between corrosion resistance and the following finishes (pickled after finishing): rough machining, smooth machining, screw threading, knurling, honing, polishing, and vapor blasting. Dry grinding, polishing, sand blasting or other rough finishes without a subsequent pickle produce a less-corrosion-resistant surface.

EFFECT OF WATER PURITY

Corrosion resistance has been found not to be dependent on pH in the range 5.5 to 8.5. Tests indicate that dissolved oxygen or hydrogen, in amounts up to 200 ml/l has a tem-

* Zircaloy 1, a Westinghouse Atomic Power Division designation.

† Zircaloy 2, a Westinghouse Atomic Power Division designation.

porary effect on the corrosion resistance. From the weight-change data obtained from samples tested in degassed water for comparative purposes, it is evident that dissolved oxygen increases initial corrosion while dissolved hydrogen reduces it. After this initial effect, corrosion proceeds at about equal rates in degassed, oxygenated, or hydrogenated water.

Additions of small amounts (less than 0.1 molar) of NaNO_3 , $\text{Na}_2\text{Cr}_2\text{O}_7$, NaOH , KOH , or LiOH have not shown appreciable effects on the resistance of zirconium in 500°F degassed water. However, additions of NaF in amounts of 0.01M or greater cause greatly increased corrosion.

EFFECT OF COUPLING

No appreciable galvanic effects have been noted in tests made on coupled zirconium. The metal resists galvanic attack and does not accentuate this effect in other metals. As an anode, zirconium polarizes readily to high values; as a cathode it polarizes to the same approximate value as other metals. Coupling zirconium to noble metals does not appreciably affect the corrosion rate.

EFFECT OF VELOCITY AND STRESS

The resistance of zirconium to corrosion by 500°F water has been found not to be affected by the velocity of the water or the stress imposed. Specimens tested at water velocities up to 35 ft/sec under stresses of 5000 psi have shown no effects attributable to these conditions.

EFFECT OF HEAT TREATMENT

No appreciable effect has been noted.

EFFECT OF IRRADIATION

Data on samples of zirconium tested in high-temperature water in reactors indicate that for engineering purposes irradiation does not affect the corrosion resistance. Integrated thermal neutron fluxes of up to 10^{18} nvt have been experienced without effect; tests have been made on samples in circulating water loops placed in reactors at water velocities up to 10 ft/sec and maximum water temperatures of 540°F.

REFERENCES

1. ANL-4950, Dec. 15, 1952 (classified).
2. G. F. Mills and B. N. Dickinson, Oxygen Removal From Water by Amine Exchange Resins, *Ind. Eng. Chem.* 41, 1949, p 2842.

Aluminum

3. J. M. Bryan, Aluminum and Aluminum Alloys in the Food Industry, Dept. of Science and Industry Research (Brit.): Food Investigation, Special Report No. 50, London, 1948.
4. H. B. Linford, Literature Survey on the Corrosion of Aluminum in Dilute Solutions, Columbia University, DuPont Subcontract, May 1, 1952.
5. R. L. Loftness and M. H. Feldman, North American Aviation, Inc., NAA-SR-94, 1950 (classified).
6. B. J. Borgmier, HW-21166, May 22, 1951 (classified).
7. R. B. Briggs, CE-973, Oct. 9, 1943 (classified).
8. W. P. Jesse, M. C. Leverett, W. D. B. Spatz, and R. B. Briggs, Clinton Labs., CT-1440, May 15, 1944 (classified).
9. M. C. Leverett and R. B. Briggs, Clinton Labs., CE-1644 (A-2485), June 22, 1944 (classified).
10. A. O. Allen, M. G. Bowman, N. Goldowski, R. G. Larsen, and L. Treiman, CC-1677 (A-2413), July 6, 1944 (classified).
11. S. Kuniatsky and R. B. Briggs, CT-1853 (A-2678), July 15, 1944 (classified).
12. R. B. Briggs, Clinton Labs., CE-2818, April 7, 1945 (classified).
13. J. E. Draley et al, CT-3027, June 19, 1945 (classified).
14. W. W. Binger, CT-3030, June 2, 1945 (classified).
15. R. B. Briggs, Clinton Labs., M-3893 (classified).

16. R. B. Briggs, Clinton Labs., M-3878 (classified).
17. D. G. Reid and L. P. Bornwasser, Clinton Labs., MONT-348, July 24, 1947 (classified).
18. J. E. Draley and W. E. Ruther, Aqueous Corrosion of 2S Aluminum at Elevated Temperatures, ANL 5001, Feb. 1, 1953.
19. ANL-4576, Jan. 31, 1951, pp 81-85 (classified).
20. J. L. English, Clinton Labs., ORNL-681, July 20, 1950 (classified).
21. R. B. Hoxeng, CT-3023, May 2, 1945 (classified).
22. Roy A. U. Huddle, BI-102, Oct. 26, 1946 (classified).
23. ANL-4664, July 19, 1951, pp 107-109 (classified).
24. ANL-4923, 1953 (classified).

Beryllium

25. H. R. Nelson, BMI-HRN-1, Oct. 1, 1947 (classified).
26. M. C. Udy, H. L. Shaw, and F. W. Boulger, BMI-T-14, July 15, 1949 (classified).
27. J. P. Howe et al, CT-752, Part III, June 26, 1943 (classified).
28. F. Foote et al, CT-M-3011, May 1945 (classified).
29. H. L. Logan and H. Hessing, Nat. Bu. of Stds. NBS-6, April 14, 1949 (classified).
30. Nat. Bu. of Stds., NBS-P-12, Dec. 9, 1948 (classified).
31. J. L. English, ORNL-298, March 17, 1949 (classified).
32. J. L. English, ORNL-772, Jan. 23, 1951 (classified).
33. A. R. Olsen, ORNL-1146, April 1, 1952 (classified).
34. BMI-64, April 1, 1951, pp 29-33 (classified).
35. J. Reed, ORNL-942, Jan. 9, 1953 (classified).

Chromium

36. M. Kolodney, Chromium Plating, Information Release 4, War Metallurgy Committee of the National Research Council, 1943.
37. W. L. Pinner, G. Soderberg, and E. M. Baker, Modern Electroplating, The Electrochemical Society, 1942, pp 235-274.
38. Private Communication, D. J. DePaul and A. Squire, Westinghouse Atomic Power Division, Jan. 1953.

Cobalt and Cobalt Alloys

39. H. H. Uhlig, The Corrosion Handbook, John Wiley and Sons, New York, 1948, pp 57-59.
40. K. Rose, Highly Corrosion Resistant Spring Material Finds Varied Use, Materials and Methods, Vol. 32, No. 3, Sept. 1950, pp 54-55.
41. R. F. Waindie, New Uses for Cobalt-Base Spring Alloy, Met. Prog. 56, No. 6, Dec. 1949, pp 808-811.
42. R. H. Hill, M. A. Cook, W. M. Fassell, and R. B. Parlin, Studies on Surface Chemistry: Progress Report on Research Project, AECU-117, Nov. 27, 1950.

Copper and Copper Alloys

43. E. Voce, Copper and Copper Alloys: Technical Progress in 1949, Metallurgia 41, Nos. 242 and 243, Jan. 1949, pp 96-101, 150-152.
44. Corrosion Resistance of Copper and Copper Alloys, Chem. Eng. 58, Jan. 1951, pp 108-111.
45. J. R. Freeman, Jr. and A. W. Tracy, Comparative Corrosion Resistance of Some Copper Alloy Condenser Tubes, Corrosion 5, No. 8, Aug. 1949, pp 245-248.
46. G. R. Hill, Corrosion of Copper in Aqueous Solution, Univ. of Utah, Tech. Report No. 1, NP-1256, Dec. 15, 1949.
47. C. L. Bulow, Wrought Copper and Copper-Base Alloys, Ind. Eng. Chem. 42, Oct. 1950, pp 1970-77.
48. C. R. Breden, S. Greenberg, R. M. Robinson, A. H. Roebuck, V. F. Saitta, and C. C. Scott, Water Corrosion of Structural Materials, October 1948-June 1951, ANL-4519, July 15, 1951.
49. C. W. Borgmann and R. T. Koenig, Bimetallic Corrosion in Neutral Electrolytes; First Technical Report, Colorado University Engineering Experiment Station, NP-3047; ONR BOS-2322, Dec. 1, 1947.
50. R. Settler, A Brief Survey of Stress and Corrosion Cracking in Brass, Sheet Metal Ind. 27, No. 274, Feb. 1950, pp 119-122.
51. J. T. Clenny, Stress Corrosion of Cast Bronzes Evaluated, Iron Age 167, No. 25, June 21, 1951, pp 85-89.

Gold and Platinum

52. H. W. Russell, H. R. Nelson, and R. W. Dayton, BMI-P-33, Oct. 1, 1950 (classified).
53. WAPD-MR-16 (modified) May 1, 1951 (classified).
54. C. R. Breden, S. Greenberg, R. M. Robinson, A. H. Roebuck, V. F. Saitta, and C. C. Scott, Water Corrosion of Structural Materials, October 1948-June 1951, ANL-4519, Reactor Engineering Div., July 15, 1951, pp 62 and 123.
55. Hanford Works, HW-19301, Nov. 6, 1950 (classified).
56. BMI-P-33, Oct. 1, 1950 (classified).

Magnesium and Magnesium Alloys

57. Bibliography of the Corrosion of Magnesium and Its Alloys, Dept. of Mines and Resources, Canada, Jan. 1949.
58. ANL-4755, Sec. IV, Jan. 30, 1952 (classified).
59. N. B. Harvey, The Corrosion and Protection of Magnesium Alloys, I. Birmingham Met. Soc., England 30, No. 1, 1950, pp 26-40.
60. Finishing Magnesium, Products Finishing 3, No. 3, London, Mar. 1950, pp 74-85.
61. M. Lewis and S. Goldsmith, HW-23082, Dec. 19, 1951 (classified).

62. Preparation of High Purity Magnesium and a Study of the Effect of Non-Metallic and Alkali Metal Impurities on the Corrosion Characteristics of Pure Magnesium, Dow Chemical Co. Biennial Report, COO-85, Dec. 1, 1949–Nov. 30, 1951.
63. K. Lohberg, Corrosion of Intermetallic Compositions, Dow Annual Report COO-21 (15198) December 1, 1949–November 30, 1950, Z. Metallkunde, Germany, Vol. 41, No. 2, Feb. 1950, pp 56-59.
64. Magnesium Alloy Dissimilar Metal Corrosion, Consolidated Vultee Aircraft Corp., Board of Trade, Tech. Inf. and Docs. Unit, ORR 360/50, PB99964, Report FGT-442, May 1946.

Nickel and Nickel Alloys

65. H. O. Teeple, Nickel and High-Nickel Alloys, Ind. Eng. Chem. 42, No. 10, Oct. 1950, pp 1990-2001.
66. Corrosion-Resistance of Stainless, Monel, and Nickel Castings, Materials & Methods 29, No. 5, May 1949, pp 79-81.
67. W. Z. Friend and F. L. LaQue, Corrosion-Resisting Nickel Alloys and Chemical Progress, Ind. Eng. Chem. 44, May 1952, pp 965-971.
68. BMI-726, pp 43-56 of Progress Report for month of January 1952 (classified).
69. J. R. Gilbreath and O. C. Simpson, ANL-4427, Chemistry Division, Section C-II, July 28, 1950 (classified).

Silver and Silver Alloys

70. WAPD-MR-16 (modified) (classified).
71. ANL-4729, Feb. 1, 1952, pp 117, 118 (classified).
72. ANL-4795, Mar. 15, 1952, pp 103, 104 (classified).
73. ANL-4898, Sept. 15, 1952, p 56 (classified).

Plain-carbon and Low-alloy Steels

74. R. Corey and T. Finnegan, The pH, Dissolved Iron Concentration, and Solid Product Resulting From Reaction Between Iron and Pure Water at Room Temperature, Proc. Am. Soc. Testing Materials 39, 1939, p 1242.
75. F. G. Frese, Effect of Oxygen on the Corrosion of Steels, Ind. Eng. Chem. 30, 1938, pp 83-85.
76. G. Skaperdas and H. Uhlig, Corrosion of Steel by Dissolved Carbon Dioxide and Oxygen, Ind. Eng. Chem. 34, 1942, p 748.
77. W. Whitman, R. Russell, and V. Altieri, Effect of Hydrogen Ion Concentration on the Submerged Corrosion of Steel, Ind. Eng. Chem. 16, 1924, p 665.
78. H. H. Uhlig, The Corrosion Handbook, John Wiley and Sons, New York, 1948, pp 120-143.

Stainless Steels

79. V. W. Whitman, Stainless Steel—Its Development and Use, Iron Steel Engr. 27, No. 11, Mar. 1950, pp 70-73.
80. M. G. Fontana, Fundamental Corrosion Research, Summary Tech. Report on Office of Naval Research Contract N6-ori-17, T.O. II, May 10, 1949.
81. T. H. Arnold and C. V. Mills, Developments in Alloy Steels, Metallurgia 41, No. 242, Dec. 1949, pp 75-78.
82. R. L. Loftness and M. H. Feldman, North American Aviation, Inc., NAA-SR-94, 1950 (classified).
83. A. R. Olsen, The Corrosion Resistance of Various Stainless Steels in Aqueous Solutions in the Presence of Dowex No. 50 Resin, ORNL-804, Sept. 15, 1950.
84. ANL-4898, Sept. 15, 1952 (classified).
85. G. T. Colegate, The Corrosion of the Austenitic Stainless Steels, Metallurgia 41, Jan. No. 243, pp 147-150; Mar. No. 245, pp 259-262; Apr. No. 246, pp 305-308, May No. 247, pp 362-366; 1950.
86. R. S. Stewart and S. F. Urban, Aluminum Decreases Corrosion Resistance of Austenitic Stainless, Iron Age 166, No. 7, Aug. 17, 1950, pp 91-95.
87. R. Franks, J. W. Juppenlatz, V. N. Krivolbok, F. L. LaQue, and E. A. Schoefer, Data on Corrosion and Heat-Resistant Steels and Alloys—Wrought and Cast, ASTM Special Tech. Publ. No. 52A, May 1950.
88. C. W. Borgmann and R. T. Koenig, Bimetallic Corrosion in Neutral Electrolytes; First Technical Report, Colorado University Engineering Experiment Station, NP-3047; ONR BOS-2322, Dec. 1, 1947.
89. H. Thielsch, Physical Metallurgy of Austenitic Stainless Steels, Welding Jour. 29, Dec. 1950, pp 5775-6215.
90. L. Piatti, The Influence of Precipitations at the Grain Boundaries on the Resistance of Chromium Nickel Steels to General Corrosion, Engrs. Digest 11, No. 9, Sept. 1950, p 11.
91. A. Thomas, Extra Low Carbon Stainless Steel, Corrosion (News Section) 6, No. 5, May 1950, p 1.
92. H. W. Gillett, Present Knowledge of Low-Carbon 18-8, Am. Soc. Testing Matls., Special Tech. Publ. No. 93, pp 41-54, Symposium on Evaluation Tests for Stainless Steel, May 1950.
93. L. G. Cook, W. M. Campbell, and G. C. Lawrence, Chalk River Proj. PR-CE-13 (classified).
94. C. J. Lancaster, Corrosion Tests of Sixteen Materials in 500°F Water at High and Low Velocities, U. S. Naval Engineering Experiment Station, E.E.S. Report 4a(21)966870, Nov. 18, 1952.

Thorium and Thorium Alloy

95. CS-I(T)-2498, Dec. 19, 1944 (classified).
96. A. R. Olsen, ORNL-1066, Dec. 19, 1951 (classified).
97. D. E. Hamley, ORNL-1090, Dec. 7, 1951 (classified).
98. J. E. Draley, ANL-4908, Oct. 3, 1952 (classified).
99. R. B. Briggs, Clinton Lab. M-3893 (classified).
100. J. G. Feibig, CT-C-2715, April 25, 1945 (classified).
101. J. W. Arendt, W. W. Binger, J. Hopkins, and F. Nelson, CT-C-3036, June 23, 1945 (classified).
102. CT-BMI-3054, June 1, 1945 (classified).

Titanium

103. C. I. Bradford, J. P. Catlin, and E. L. Wemple, Properties of Wrought Commercially Pure Titanium Prepared by Arc-Melting and Casting, *Metal Progress* 55, Mar. 1949, pp 348-350.
104. W. L. Williams and W. C. Stewart, Fatigue and Corrosion of Sintered and Rolled Titanium, *Metal Progress* 55, 1949, p 348.
105. H. Adenstedt, Mechanical Properties, Weldability and Corrosion of Commercially Pure Titanium, *Air Materiel Command*, AF-TR-5935, Oct. 1949.
106. M. G. Fontana, Fundamental Corrosion Research; Summary Technical Report, Ohio State University, NP-993, May 10, 1949.
107. E. C. Miller, ORNL-267, July 19, 1949 (classified).
108. Battelle Memorial Institute—Douglas Aircraft Co., Inc.—Project Rand, (RA-15080), April 2, 1948 (classified).
109. H. H. Uhlig, *The Corrosion Handbook*, John Wiley and Sons, 1948, p 329.

Uranium and Uranium Alloys

110. A. Dravnieks and H. J. McDonald, Electropotentials in Growing Halide and Oxide Layers on Metals, *Trans. Electrochemical Soc.* 93, 1948, pp 177-191.
111. N. B. Pilling and R. E. Bedworth, Oxidation of Calcium and Magnesium, *Jr. Inst. for Metals* 29, 1923, p 577.
112. A. S. Covert and M. Kolodoney, LA-313, June 18, 1945 (classified).
113. E. A. Gulbransen and J. W. Hickman, *AIMME Trans.* 171, 1946, p 330.
114. S. Katz, CT-2454, Nov. 11, 1944 (classified).
115. J. J. Katz and E. Rabinowitz, Chemistry of Uranium, National Nuclear Energy Series, Div. VIII, Vol. 5, 1951, p 192.
116. A. B. Greninger et al, CT-1272, Part IV of report for month ending February 1, 1944 (classified).
117. J. E. Draley and G. C. English, CT-1943, July 1, 1944 (classified).
118. J. G. Feibig, CT-2715, April 25, 1945 (classified).
119. W. A. Mollison, G. C. English, and F. Nelson, CT-3055, June 23, 1945 (classified).
120. N. Benson, R. P. Straetz, and J. E. Draley, CT-3043, June 4, 1945 (classified).
121. G. Bitstanes, Alloys of Uranium and Silicon. II. The Epsilon Phase, CT-3309, Mass. Inst. of Tech., June 1945.

Zirconium

122. K. M. Goldman, WAPD-MM-140, (shows A, B, and C sponge diagrams), Oct. 6, 1952, p 26 (classified).
123. F. B. Litton, Ten Zirconium Alloys Evaluated, *Iron Age* 167, No. 15, April 12, 1951, p 112.
124. G. Miller, Zirconium, *Ind. Chemist* 26, No. 309, 1950, p 435.
125. Northwest Electrodevelopment Laboratory, Bureau of Mines, Albany, Oregon, BM II-39 (classified).
126. ISC-290, Sept. 20, 1952, p 12 (classified).
127. A. Charlesby, Ionic Currents in Thin Films of Zirconium Dioxide, Atomic Energy Research Establishment, M/R-1014, Sept. 23, 1952.
128. C. M. Schwartz, D. A. Vaughn, and G. G. Cocks, BMI-793, Dec. 17, 1952 (classified).

SELECTED READING LIST

- SYMPOSIUM ON WATER CORROSION, *Ind. Eng. Chem.* 44, No. 8, Aug. 1952, pp 1736-1795.
- COMPARISON OF CORROSION PROPERTIES OF ZIRCONIUM, TITANIUM, TANTALUM, STELLITE 6, AND TYPE 316 STAINLESS STEEL, E. Wick, *Materials and Methods* 35, (bibliog.) Jan. 1952, pp 115, 177.
- BIBLIOGRAPHIC SURVEY OF CORROSION—1946-1947, National Assoc. of Corrosion Engineers, Houston, Texas, 1951.
- CORROSION GUIDE, E. Rabald, Elsevier Pub. Co., New York, 1951.
- WATER CORROSION OF STRUCTURAL MATERIALS, Argonne National Laboratory, C. R. Breden, S. Greenberg, R. M. Robinson, A. H. Roebuck, V. F. Saitta, and C. C. Scott, ANL-4519, July 15, 1951.
- CORROSION TESTS OF METALS AND CERAMICS, compiled by L. D. Yates, Chem. Eng. Report No. 9 Tenn. Valley Auth., Wilson Dam, Ala., 1951.
- CORROSION DATA SURVEY, G. A. Nelson, Shell Development Co., San Francisco, 1950.
- ALUMINUM AND ALUMINUM ALLOYS IN THE FOOD INDUSTRY, J. M. Bryan, Her Majesty's Stationery Office, London, 1948.
- CORROSION HANDBOOK, H. H. Uhlig, J. Wiley and Sons, New York, 1948.
- METALLIC CORROSION, PASSIVITY AND PROTECTION, U. R. Evans, Longmans, Green, New York, 1948.
- CORROSION OF METALS, C. W. Borgmann, C. P. Larrabec, and W. O. Binder, Am. Soc. Metals, Cleveland, 1946.
- BIBLIOGRAPHIC SURVEY OF CORROSION—1945, R. D. Misch, J. T. Waber, H. J. McDonald, Illinois Institute of Technology, Chicago, Corrosion Research Lab., 1945.
- ENGINEERING ALLOYS, N. E. Woldman and R. J. Metzler, First Edition Revised, Am. Soc. Metals, Cleveland, 1945.
- CORROSION RESISTANCE OF METALS AND ALLOYS, R. J. McKay and R. Worthington, Reinhold Pub. Corp., New York, 1936.
- THE THERMOCHEMISTRY OF THE CHEMICAL SUBSTANCES, F. R. Bichowsky and F. D. Rossini, Reinhold Publishing Corp., New York, 1936.

Calculation of Water Activity

Marshall Grotenhuis and J. W. Butler

In designing a water-cooled reactor, it is necessary to know the induced activity of the water for shielding purposes. Several reactions leading to radioactive nuclides are possible, and others lead to stable nuclides.

The most important reaction is the $O^{16}(n,p)N^{16}$ reaction.¹ This reaction has a threshold energy of 9.5 mev and an effective energy of 10.3 ± 0.7 mev.^{2,3} The reaction cross section, averaged over the fission spectrum, is 0.014 mb.^{2,4} The half-life of the product, N^{16} , is 7.35 sec,⁴ and β rays of 3.8 mev (~40%), 4.3 mev (~40%), 4.6 mev (~2%), and 10.5 mev (18%),⁴ and γ rays of 6.2-7.0 mev (80%)^{5,6,7} are emitted.

The reaction $O^{17}(n,p)N^{17}$ is also an important reaction.¹ The threshold for this reaction is 7.9 mev, and the effective energy is ~10 mev.⁸ The half-life of the product, N^{17} , is 4.14 sec, and a 3.7-mev β and a 1-mev neutron are emitted.^{7,9,10} The cross section for this reaction is estimated to be 0.01 barns⁸ but with an uncertainty of a factor of ten.

The reaction $O^{18}(n,\gamma)O^{19}$ produces a radioactive product¹ that has a half-life of 29.4 sec.¹¹ It emits a 2.9-mev β (70%), 4.5-mev β (30%), and a 1.6-mev γ (70%)^{11,12}. The thermal absorption cross section for this reaction is 22 mb.¹³ This reaction is not nearly as important as the $O^{16}(n,p)N^{16}$ reaction in shielding work because the energy, as well as the rate of emission, of the gamma-ray is much lower.

Other reactions possible in water are: $H^2(n,\gamma)H^3$,¹ which has as its product a weak β -emitter (0.018 mev) and no γ rays; $O^{17}(n,\alpha)C^{14}$, also a weak β -emitter (0.155 mev) with no gamma-rays; and $O^{16}(n,\gamma)O^{17}$, $O^{17}(n,\gamma)O^{18}$, $O^{16}(n,\alpha)C^{13}$, and $H^1(n,\gamma)H^2$ with stable products.

The differential equations governing the buildup of activity in a fluid circulating in a reactor are, neglecting the burnup of active nuclides:

$$\frac{dA}{dt} = N(t) \sigma \phi(t) - \lambda A(t) \quad (1)$$

$$\frac{dN}{dt} = -N(t) \sigma \phi(t) \quad (2)$$

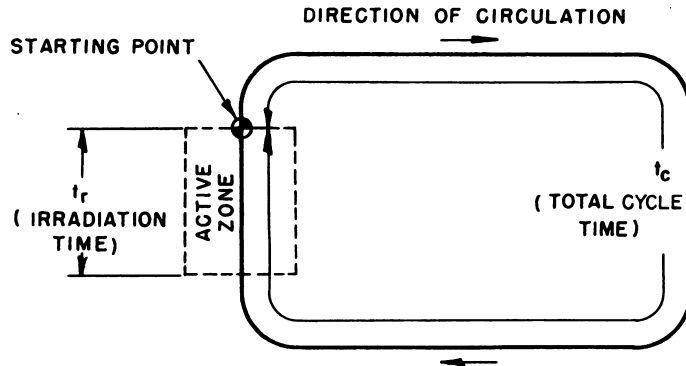
For many cases, the burnup of irradiated material is negligible. Under this condition, the differential equation governing the buildup of activity is:

$$\frac{dA}{dt} = N_0 \sigma \phi(t) - \lambda A(t) \quad (3)$$

¹References appear at end of chapter.

Rewriting Eq. (3):

$$\frac{d}{dt} \{e^{\lambda t} A(t)\} = N_0 \sigma \phi(t) e^{\lambda t} \quad (4)$$



Integrating Eq. (4) over one cycle of operation (see sketch), from:

$$t = (n-1) t_c \text{ to } t = n t_c$$

yields:

$$e^{n\lambda t_c} A(n t_c) - e^{(n-1)\lambda t_c} A(n t_c - t_c) = N_0 \sigma \int_{(n-1)t_c}^{n t_c} d\tau \phi(\tau) e^{\lambda \tau} \quad (5)$$

Let:

$$\phi(t) = \phi_0 \quad (n t_c - t_r \leq t \leq n t_c)$$

and:

$$\phi(t) = 0$$

at all other times. Then Eq. (5) becomes:

$$e^{n\lambda t_c} A(n t_c) - e^{(n-1)\lambda t_c} A(n t_c - t_c) = \frac{N_0 \sigma \phi_0}{\lambda} (1 - e^{-\lambda t_r}) e^{n\lambda t_c} \quad (6)$$

Defining:

$$B_n = A(n t_c) e^{n\lambda t_c}$$

and substituting in Eq. (6):

$$B_n - B_{n-1} = \frac{N_0 \sigma \phi_0}{\lambda} (1 - e^{-\lambda t_r}) e^{n\lambda t_c} \quad (7)$$

Summing up the recurring terms, assuming no initial activity [$A(0) = 0$]:

$$B_n = \frac{N_0 \sigma \phi_0}{\lambda} (1 - e^{-\lambda t_r}) \sum_{j=1}^n e^{j \lambda t_c} \quad (8)$$

$$B_n = \frac{N_0 \sigma \phi_0}{\lambda} (1 - e^{-\lambda t_r}) e^{\lambda t_c} \frac{1 - e^{n \lambda t_c}}{1 - e^{\lambda t_c}} \quad (9)$$

$$A(nt_c) = \frac{N_0 \sigma \phi_0}{\lambda} (1 - e^{-\lambda t_r}) \frac{1 - e^{-n \lambda t_c}}{1 - e^{-\lambda t_c}} \quad (10)$$

Equation (10) can be simplified if the number of cycles becomes very large:

$$A(nt_c) \rightarrow \frac{N_0 \sigma \phi_0}{\lambda} \frac{(1 - e^{-\lambda t_r})}{(1 - e^{-\lambda t_c})} \quad (n \rightarrow \infty) \quad (11)$$

Also, if λt_c (and hence λt_l) is a very small number:

$$A(nt_c) \sim \frac{N_0 \sigma \phi_0}{\lambda} \frac{t_r}{t_c} (1 - e^{-n \lambda t_c}) \quad (12)$$

and finally if n becomes large and t_c is small:

$$A(nt_c) \rightarrow \frac{N_0 \sigma \phi_0}{\lambda} \frac{t_r}{t_c} \quad (n \rightarrow \infty) \quad (13)$$

If it is desired to include the effect of burnup of the original atoms, an extension of the method used in the derivation of Eq. (10) can be applied to Eqs. (1) and (2). An approximate form of the result is:

$$A(nt_c) = \frac{N_0 \sigma \phi_0 \theta}{\lambda} (1 - e^{-\lambda t_r}) e^{-n \lambda t_c} \frac{1 - e^{n(\lambda t_c - \sigma \phi_0 t_r)}}{e^{-(\lambda t_c + \sigma \phi_0 t_r)} - 1} \quad (14)$$

where:

$$1 \leq \theta \leq e^{\sigma \phi_0 t_r}$$

Another treatment of this problem, including burnup, is given by Allard.¹⁴

By means of Eqs. (10) through (14), the number of active atoms per cubic centimeter of coolant may be calculated. It must be remembered that ϕ_0 was assumed not to vary with time and also that ϕ_0 is assumed to be a suitable average flux value. In the case of a threshold reaction, such as $O^{16}(n,p)N^{16}$, the determination of ϕ_0 is more difficult and may have to be done in part experimentally.^{15,16,17}

Equations (10) through (14) are also suitable for calculating radioactive atoms in coolant owing to irradiation of impurities in the water if N is the number of atoms of impurity per cubic centimeter of coolant. They can also be used for approximate calculation of activity owing to corrosion products in the water if it is remembered that N is then a function of time and that a suitable average value be substituted. For information concerning radioactive nuclides formed during neutron irradiation, see Volume 1, Chapter 1.2, Table 1.2.4, or charts.^{1,18,19}

Nomenclature and Units

Symbol	Definition	Units
$A(t)$	Active atoms per cubic centimeter in the system at time t	Atoms/cm ³
n	Number of complete cycles starting at the outlet of the active zone	None
$N(t)$	Atoms per cubic centimeter of material irradiated at time t	Atoms/cm ³
N_0	Atoms per cubic centimeter of material irradiated at time $t = 0$	Atoms/cm ³
t_c	Total time to complete cycle	Sec
t_r	Time in active zone	Sec
λ	Disintegration constant of active nuclide	Sec ⁻¹
$\phi(t)$	Neutron flux	Neutrons/(cm ²)(sec)
σ	Cross section producing active nuclide under consideration	Cm ²

REFERENCES

1. Nuclear Data, NBS-499, 1950.
2. Quarterly Progress Report, CF-3490, CF-1946 (classified).
3. E. Bleuler et al, β -Zerfall von N¹⁶, Helva. Phys. Acta. 20, 1947, p 96.
4. Quarterly Progress Report, CP-3574, 1946 (classified).
5. E. Bleuler et al, γ -Strahlung von N¹⁶, Helva. Phys. Acta. 19, 1946, p 421.
6. C. H. Millar et al, Gamma-rays from N¹⁶, Phys. Rev. 77, 1950, p 742.
7. G. T. Seaborg and I. Perlman, Table of Isotopes, Rev. Mod. Phys. 20, No. 4, 1948.
8. Charple et al, On the Delayed Neutron Emitter N¹⁷, Phys. Rev. 76, 1949, p 1255.
9. L. W. Alvarez, N¹⁷, A Delayed Neutron Emitter, Phys. Rev. 75, 1949, p 1127.
10. E. Hayward, The Energy Spectrum of the Delayed Neutrons from O¹⁷, Phys. Rev. 75, 1949, p 917.
11. A. H. Snell and N. W. Fulbright, Radiation from O¹⁹, CP-1357, 1944.
12. E. Bleuler and W. Zunti, Die Zerfallsenergien von O¹⁹, Na²⁶, Mg²⁷, Al²⁸, and K⁴², Helva. Phys. Acta. 20, 1947, p 195.
13. L. Seren et al, Absorption Curve of 31 sec O¹⁹ Beta-rays and Cross Section for Production by Thermal Neutrons, Phys. Rev. 70, 1946, p 561.
14. G. A. Allard, Activation of a Fluid Circulating through a Reactor, KAPL-665, 1951.
15. J. J. Taylor, STR Shield Design, WAPD-23, 1951 (classified).
16. N. M. Smith, Shielding of the External Water Pipes in the High Pressure Water Pile, Oak Ridge National Laboratory, CF-48-3-264, 1948 (classified).
17. M. C. Leverett, Aluminum Activity in Pile Water, Clinton Laboratory, CE-1632, 1944 (classified).
18. F. E. Sentele and W. S. Leavitt, Table for Calculating Activities Produced by Thermal Neutrons, Nucleonics 6, No. 5, 1950.
19. H. R. Kroeger, Thermal Neutron Cross Sections and Related Data, Nucleonics 5, No. 4, 1949.

CHAPTER 1.13

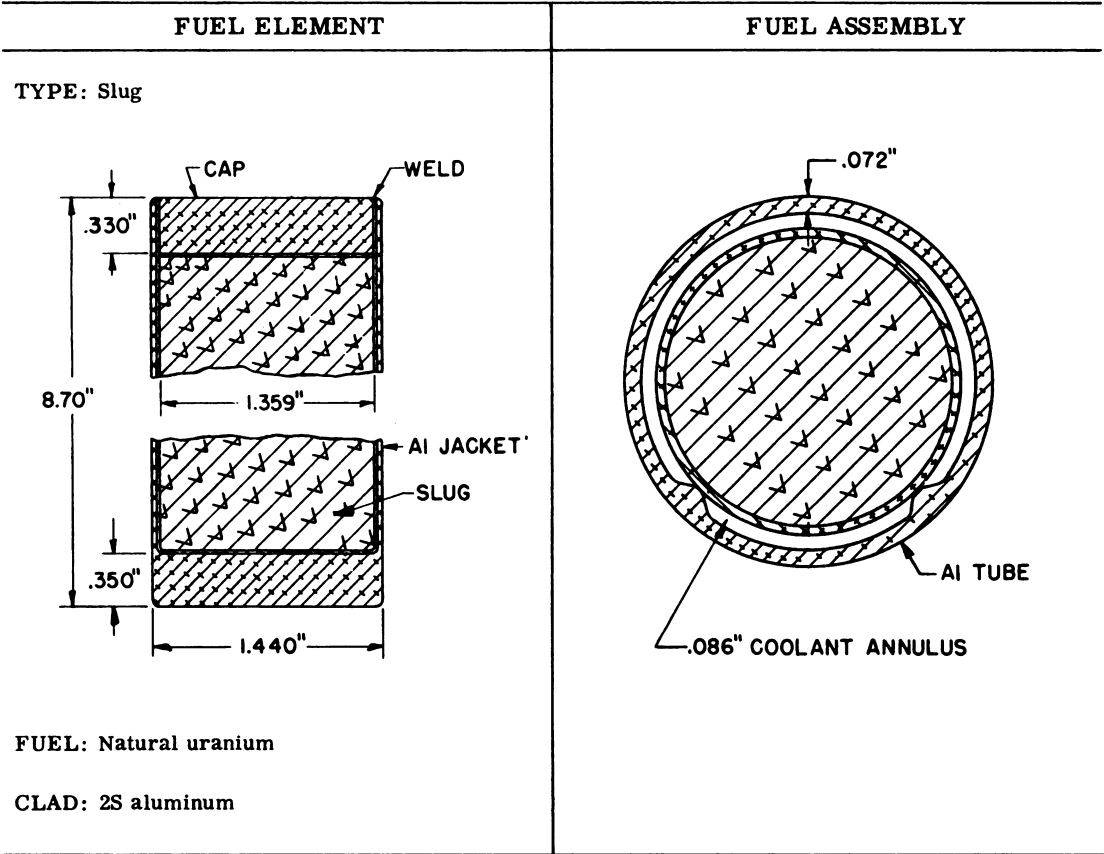
Fuel-element Design*

Reactor performance is a function of fuel-element design. Once nuclear requirements are satisfied, a fuel element is designed for efficient heat removal, mechanical stability, stability of materials, and fabricability as required by the specific reactor design. For example, power- and production-reactor fuel elements are designed to provide the maximum rate of heat removal compatible with efficient reactor operation. Low-power, research-reactor fuel elements, on the other hand, are designed to permit flexibility in loading, and heat removal is a less important consideration. In the first case, the trend in fuel-element design is toward large surface-to-volume ratios; in the latter, design is directed toward a unit for partial replacement or relocation of fuel elements or assemblies. The importance of mechanical stability, materials stability, and fabricability have been shown in previous chapters.

Fuel-element designs of water-cooled reactors which are in operation or under construction are shown in Figs. 1.13.1 through 1.13.5. The specific reactors and corresponding figure numbers of the fuel-element designs are as follows:

Reactor	Figure No.
Production	
Hanford-type Reactor	1.13.1
Savannah River (CP-6)	1.13.2
Research	
Argonne Heavy-water Reactor (CP-3')	1.13.3
Materials Testing Reactor (MTR)	1.13.5
Argonne Research Reactor (CP-5)	1.13.6

* This chapter is abstracted from Fuel Elements for Nuclear Reactors by J. B. Anderson, W. H. Cook, R. A. Daane, and R. E. Rice, ANL-4874, Nov. 1952.



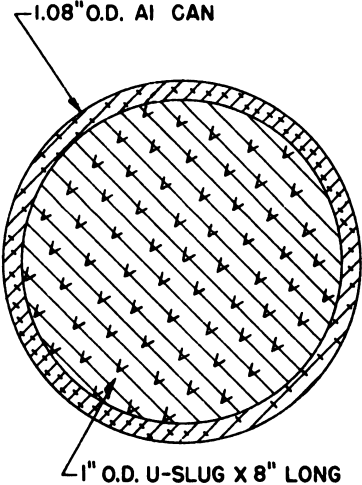
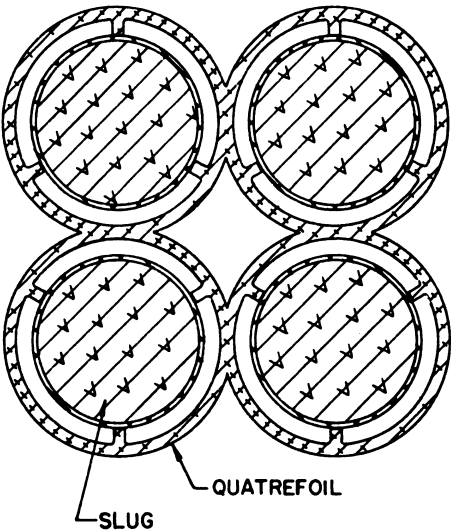
CORE CONFIGURATION: Process tubes set in graphite-block stack with square lattice spacing

COOLANT: H₂O

MODERATOR: Graphite

REACTOR APPLICATION: Plutonium production (Hanford-type reactor)

Fig. 1.13.1 — Hanford-type Reactor.

FUEL ELEMENT	FUEL ASSEMBLY
<p>TYPE: Slug</p>  <p>FUEL: Natural uranium</p> <p>CLAD: 2S aluminum</p>	

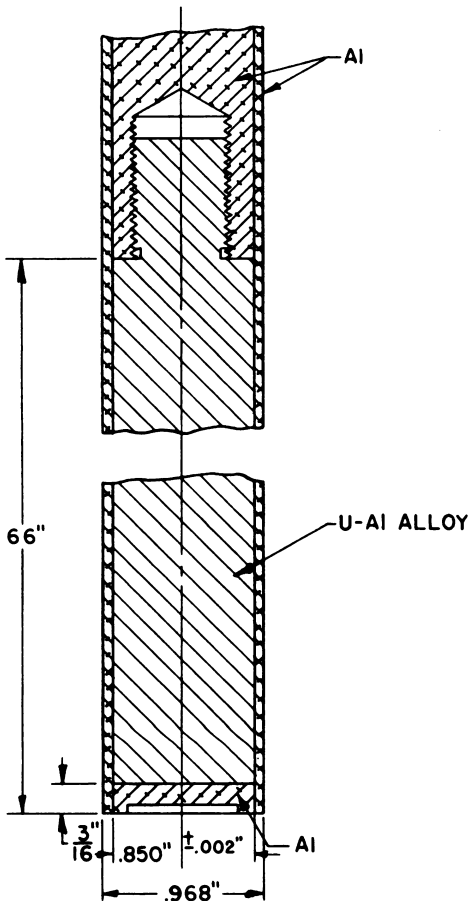
CORE CONFIGURATION: Quatrefoil process tubes placed on hexagonal lattice.

COOLANT: D_2O

MODERATOR: D_2O

REACTOR APPLICATION: Plutonium producer—Savannah River (CP-6)

Fig. 1.13.2 — Savannah River Reactor (CP-6).

FUEL ELEMENT	FUEL ASSEMBLY
<p>TYPE: Rod FUEL: 2 wt-% uranium ~ 90% U²³⁵ — aluminum alloy 0.850 in. diameter CLAD: Aluminum jacket 0.059 in. thick</p>	 <p>66"</p> <p>U-Al ALLOY</p> <p>Al</p> <p>0.850" ±.002"</p> <p>0.968"</p> <p>3/16"</p>

CORE CONFIGURATION: 116 2% U-Al rods + 2 special rods containing 29 in. of 6% U-Al alloy grouped on 5³/₈ in. centers in 6 ft diameter × 7 ft 9 in. effective height

COOLANT: D₂O

MODERATOR: D₂O

REACTOR APPLICATION: Argonne heavy water reactor (CP-3')

REFERENCE: ANL-WHZ-250

Fig. 1.13.3 — Argonne Heavy-water Reactor (CP-3').

FUEL ELEMENT	FUEL ASSEMBLY
<p>TYPE: Plate</p> <p>FUEL: 10 to 20 wt-% uranium ~ 90% U²³⁵ aluminum alloy, 0.021 in. thick</p> <p>CLAD: Aluminum, 0.020 in. thick</p> <p>LENGTH: Standard, 24⁵/₈ in. over-all Outside, 28⁵/₈ in. over-all Active, 23³/₄ in. over-all</p> <p>WIDTH: 2.845 in. before curving</p>	<p>2.996"</p> <p>COMB .064"</p> <p>15°</p> <p>.188"</p> <p>.079"</p> <p>3.071"</p> <p>3.169"</p> <p>.113" (ALL GAPS)</p> <p>.064"</p> <p>5.504" R.</p> <p>BRAZED JOINTS</p> <p>OUTSIDE FUEL PLATE</p> <p>STANDARD FUEL PLATE</p>

CORE CONFIGURATION: Subassemblies grouped into slab; active core approximately 9 in. wide by 27 in. long by 23³/₄ in. high; beryllium reflector

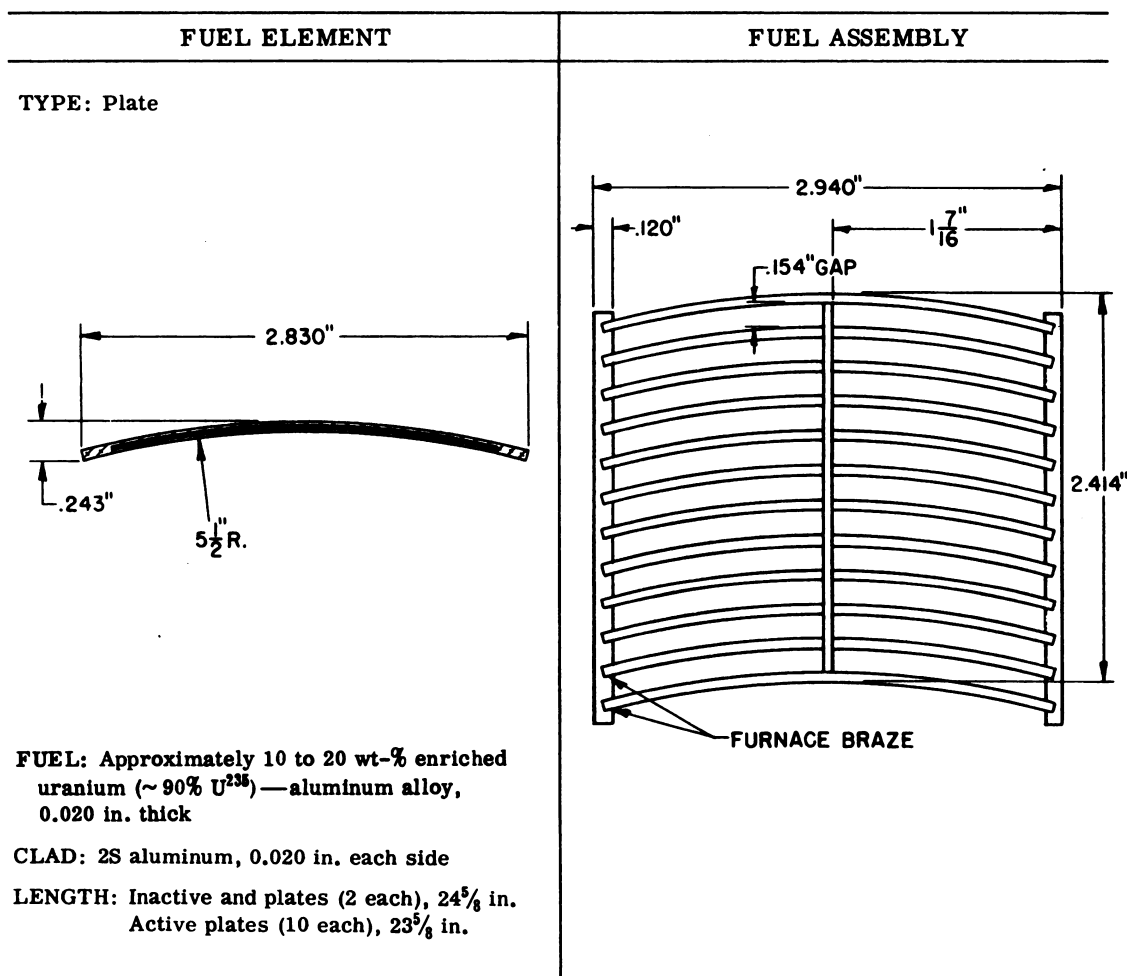
COOLANT: H₂O

MODERATOR: H₂O

REACTOR APPLICATION: Materials testing reactor (ARCO)

REFERENCE: ORNL-963

Fig. 1.13.4— Materials Testing Reactor (MTR).



CORE CONFIGURATION: Provisions for 17 subassemblies as shown; reactor start-up will be made using the 10 to 20% enriched uranium-aluminum subassemblies; estimated 12 required; two subassemblies added later for burn-up compensation; three additional subassemblies available for initial loading; subsequent reloadings to be made with less enrichment per subassembly to utilize all locations; subassemblies contained in 6-ft-diameter tank

COOLANT: D₂O

MODERATOR: D₂O

REACTOR APPLICATION: Argonne research reactor (CP-5)

REFERENCE: Communication from J. M. West

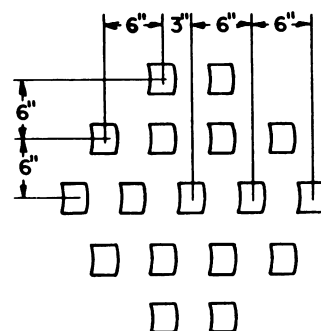


Fig. 1.13.5— Argonne Research Reactor (CP-5).

Section 2

LIQUID-METAL-COOLED SYSTEMS

Prepared under the direction of
R. W. LOCKHART
ENGINEERING AND PRODUCTION SECTION
KNOLLS ATOMIC POWER LABORATORY

Authors' Preface

Two liquid-metal-cooled reactors have been built and operated; one other is under construction. As coolants for these reactors, mercury was chosen, because of its non-moderating nuclear properties, for the experimental Fast Reactor at Los Alamos, and sodium-potassium alloy (NaK) was chosen, because of its good elevated-temperature heat-removal and low-moderating nuclear properties, for the Experimental Breeder Reactor at Arco.

Also under construction is the KAPL Submarine Intermediate Reactor (SIR) which is cooled by sodium; this coolant was chosen for its high-temperature heat-transfer properties and acceptable nuclear properties. An extensive program to develop the usefulness of Na and NaK has been in operation for over six years at KAPL. During this development period, an eight-million-Btu/hr non-radioactive heat-transfer system was operated for tens of thousands of hours with top (simulated reactor) temperature above 850°F; some runs were made up to 1200°F. Many other sites particularly ANL, ORNL, and Mine Safety Appliance Company have contributed to the liquid-metal technology of SIR design.

In addition to these reactors, numerous studies have been made or are in progress, and some preliminary design has been completed on other proposed liquid-metal-cooled reactors. These studies are mainly concerned with heat-removal properties at elevated temperatures (power production) and acceptable nuclear properties (fast- and intermediate-spectrum reactors). Most of the liquid-metal work has been conducted using Na and NaK; a limited amount of work has been expended on Pb, Pb-Bi, and Li.

The objectives of this section of the handbook are:

(1) To summarize the physical properties and "know-how" of the application of liquid-metal coolants; (2) to discuss the advantages and problems of using liquid metals as heat-transfer fluids, particularly with respect to their application as reactor coolants (examples of some of the possible cooling cycle arrangements are presented); (3) to present a summary of liquid-metal components and design considerations.

The design data in this section include experimental or operating data as well as predicted data, and reflects information available up to the end of December 1952. New and improved component designs are being studied, and future editions of this handbook should include information on such subjects as homopolar (generator-DC electromagnetic) pumps and electromagnetic null pressure gauges that can be used at elevated temperatures. Engineering units are used in all cases; where it was thought that CGS units would be convenient, dual units were used.

The editor wishes to express his appreciation to Miss Carol J. Ranney and Mr. Sheldon K. Friedlander, his assistant editors, for their administration of the details of this section of the handbook, and to Mr. Thomas Trocki for his help in outlining this section and reviewing some of the chapters. Recognition is also due to Miss B. L. Jones and Mrs. E. R. Supley who prepared most of the tracings, to the KAPL Engineering secretaries, and to the KAPL engineers, physicists, and metallurgists for the assistance rendered to the individual chapter authors.

Encouragement and information from Mr. A. P. Fraas (ORNL), Mr. H. Lichtenberger and Mr. M. Novick (ANL-EBR), and Mr. F. R. Lesch (SOO of the AEC) is acknowledged and gratefully appreciated.

Robert W. Lockhart

CHAPTER 2.1

Liquid-metal Coolants for Nuclear Reactors

R. W. Lockhart

During the past decade, great effort has been expended toward obtaining a knowledge of the physical properties of liquid metals and the necessary "know-how" which would permit their use as heat-transfer media. Reports in the classified and unclassified literature describe criteria for choosing such a coolant, and many of the early reports of the reactor-design groups describe criteria for a coolant for a nuclear reactor. The study of the operation of a mercury heat-transfer system, such as a binary-coolant power plant, is an example of elevated-temperature, liquid-metal, heat-transfer system technology carried out prior to reactor heat-removal considerations. Liquid-metal-cooled reactors are the EBR, LAPR, and SIR (see Section 8 of this volume).

A review¹ of completed and in-progress liquid-metal research indicates that the most effort has been applied to the alkali metals, particularly sodium and NaK (sodium-potassium alloy); a limited effort, in decreasing order, has been accorded Li, Pb, Bi, Pb-Bi alloy, and Hg. The results of this work indicate that Na and NaK rank high in the list of elevated-temperature coolants. When a reactor is used for power generation, the conversion-system efficiency is a function of outlet temperature of the reactor coolant. In general, the choice of a coolant depends on many compromises involving the physical properties of coolants. The choice of a nuclear reactor coolant emphasizes specifically those properties that (1) provide extreme reliability of the coolant system, (2) permit removal of heat from a concentrated heat source, and (3) affect the nuclear characteristics of the coolant. Some of these considerations are discussed below.

NUCLEAR PROPERTIES

The nuclear properties, such as moderating ratio, absorption cross section, activation (shielding required), and radiation stability, eliminate many coolants from further consideration.

MODERATING RATIO

If a thermal reactor is required, a coolant with high moderating ratio and low neutron absorption is necessary. Although these specifications are satisfied by light or heavy water, they do not exclude all liquid metals.

For an intermediate or fast reactor for mobile power plant or power breeder application, low-moderating-ratio coolants can be considered. Liquid-metal coolants have been success-

¹References appear at end of chapter.

fully applied in these cases (e.g., the fast reactor at Los Alamos, the EBR at Arco, and the SIR under construction at West Milton) and are, in fact, practically the only coolants that will satisfy the nuclear and heat-removal requirements for these reactors. Hydrogenous coolants would not be effective in such applications because of their moderating effect. The thermal-neutron moderating ratios of some coolants are compared in Table 2.1.1.

Table 2.1.1 — Thermal-neutron Moderating Ratios of Some Coolants

Coolant	Average loss of energy, ξ	Moderating ratio,* $\left(\frac{\sigma_s}{\sigma_a}\right) \xi$
Be	0.21	150
H	~ 1	140
Na	0.085	0.76
K	.051	.03
Hg	.01	0
Li	.26	0.006
Bi	.0096	4.2
Pb	.0097	0.39

* σ_s = scattering cross section; σ_a = absorption cross section

ABSORPTION CROSS SECTION

Since low critical mass is one of the important reasons for choosing a thermal reactor and since absorption cross sections are larger for materials when lower-energy neutrons are involved, many coolants that are practical for fast and intermediate reactors are not satisfactory for thermal reactors.

RADIATION DAMAGE

Many non-metal coolant mixtures suffer serious radiation damage that transforms or disassociates the molecules under the high reactor fluxes. Liquid metals are particularly resistant to such damage because of their simple structure; a portion of the liquid-metal coolant is activated, however, and transformed into another isotope, such as Na^{24} to Mg^{24} , but the amount transformed per life of the reactor at the present design fluxes is small.

ACTIVATION

When liquid metal coolants become activated they emit characteristic γ and/or β rays that have to be attenuated by biological shielding. If neutron distribution in the reactor is held constant, and the amount of coolant in this region is compared with the total amount of coolant circulating, an estimate of the amount of shielding required for each coolant can be obtained.

HEAT-REMOVAL PROPERTIES

The heat-removal capacity of a coolant is important to a reactor since a compromise has to be made between the coolant flow rate, the temperature rise through the reactor, and the volume of the reactor that can be made available for the coolant passages. A detailed discussion of the heat-removal properties of liquid metals is presented in Chapter

2.2. Generally, the specific heat per unit volume for liquid metals is lower than water, but at comparable pressure and temperature conditions above the critical point of water (705°F), most liquid metals are superior to water. This means that the use of liquid-metal coolants will require a lower product of coolant velocity and temperature rise to remove a given amount of heat.

High boiling points (or low vapor pressure) for liquid metals allow more flexibility in operation; for instance, in near emergency cases, the reactor coolant outlet temperature can be greatly increased without the possibility of a vapor burn-out.

Just above their respective melting points, liquid metals have relatively low viscosities, and their hydraulic characteristics (except for density effect) are not too different from those of water at ambient temperatures. Experience has shown that system pressure drops can be predicted by applying accepted methods of correlation.

STRUCTURES AND MATERIALS TO CONTAIN LIQUID METALS

Because of the low vapor pressure of liquid metals, system pressures have been determined by coolant-system pressure drops, which are usually less than 100 psi, and minimum absolute inlet pressure to the circulating pumps. Operating temperatures in excess of 700°F are possible with little worry about local boiling or serious changes in physical properties of the coolant.

The relatively high thermal conductivity of liquid metals not only minimizes the possibility of hot spots caused by local boiling and of large temperature gradients across coolant ducts that might warp the structure or bind moving parts but also reduces the thermal film drop to a nearly negligible value.

General statements about the thermal shock effect on structural material, corrosion, and purification treatment required when liquid metals are used are more difficult to make at this time, but such data are accumulating. These topics are treated in the following chapters of this section, but a more complete presentation of corrosion and purification is available in the second edition of the Liquid Metals Handbook. It is stated in the literature without qualification that in a closed system liquid Na and NaK are simpler to maintain than water for similar duty.

OTHER PROPERTIES

A freezing point above ambient temperature can be both an asset for a coolant as well as a liability. It is sometimes desirable to let the system or portions of the system freeze so that components may be replaced without draining the coolant system. Conversely, it is normally a liability to have to maintain the complete system above the melting point of the coolant before the coolant can be circulated.

The high electrical conductivity of the liquid alkali metals permits their use in completely sealed pumps (AC or DC, electromagnetic type) and EM flowmeters.

The availability of liquid metals is given in the Liquid Metals Handbook. Since the volume of a reactor coolant system is relatively small and recharging only infrequently required, the actual cost of the coolant is low. Sodium is reported to be the least expensive (0.16 \$/lb), with lead, zinc, and aluminum slightly more. Potassium is considerably more expensive (2.50 \$/lb).²

CONCLUSIONS

Liquid-metals have the best combination and range of physical properties for application as fast- or intermediate-spectrum nuclear-reactor coolants. The choice of the particular

coolant will depend on the application of the reactor. The following chapters in this section will discuss the properties of liquid-metal coolants, the heat-transfer correlations used with liquid metals, the purification, corrosion, and induced activities of some of the liquid metals, the reaction between alkali liquid metals and water, the various reactor-cooling and power-conversion cycles, the distribution and magnitude of heat generation in liquid-metal-cooled reactors, and the design and construction of reactors and associated heat-transfer systems.

Many of the systems and design details presented in this edition of Section 2, describe equipment that was tested in the project Genie liquid-metal test system that was operated by the KAPL. The presentation of one complete design seemed preferable to an attempt to generalize on the basis of two or three existing experimental designs, and, on the basis of this choice, much of the discussion is directed toward Na and NaK, since the most is known about these liquid-metal coolants.

REFERENCES

1. D. W. Lillie, Report No. WASH-89, April 16, 1952 (classified).
2. Liquid Metals Handbook, 2d edition, R. N. Lyon, editor, Dep't of the Navy, U. S. Atomic Energy Commission, June 1952, p 258.

CHAPTER 2.2

Properties of Liquid Metal Coolants

R. D. Brooks

The physical properties of various liquid metals are listed in Table 2.2.1 in English units and in Table 2.2.2 in metric units. The original references for most of these data are given in Chap. 2 of the "Liquid Metals Handbook." Unit prices as of 1951 are also included in Table 2.2.1.

Table 2.2.3 shows cross sections for the metals as they occur naturally, i.e., for the usual mixtures of isotopes. The macroscopic cross sections were calculated at the melting points.

In Figs. 2.2.1 to 2.2.8, the density, heat capacity, viscosity, and thermal conductivity are plotted vs. temperature for most of the elements of Table 2.2.1. The grid for each plot is marked in English units, but corresponding metric values are given on the opposite side of every page. The curves labeled "NaK (56,44)" refer to the alloy composed of 56 wt-% sodium and 44 wt-% potassium; a similar notation is used for the alloy composed of 22 wt-% sodium and 78 wt-% potassium.

Figures 2.2.9 to 2.2.12 show total cross sections as a function of neutron energy for several selected metals, namely, Na, K, Li, Pb, Bi, and Hg, which are of most interest at present. Similar plots for other metals can be found in Report AECU-2040.

A Mollier chart for mercury is given in Fig. 2.2.13. The original reference also includes a table of the thermodynamic properties of mercury. These data were published in 1949 and are currently being reviewed by L. F. Epstein and coworkers at Knolls Atomic Power Laboratory.

Table 2.2.1—Physical Properties of Liquid Metals (English Units)

(Liquid Metals Handbook, edited by R. N. Lyon, Department of the Navy and U. S. Atomic Energy Commission, NAVEXOS P-733, 2d ed., in preparation)

Metal	Atomic No.	Atomic wt	Melting point, °F	Latent heat of fusion, Btu/lb	Boiling point (760 mm Hg), °F	Latent heat of vaporization, Btu/lb	Vapor pressure		Density	
							Mm Hg	°F	°F	Lb/cu ft
Aluminum	13	26.97	1220.4	173	4442	5500	1	2799	1220	148.6
							10	3218	1292	147.9
							100	3778	1652	144.5
							400	4280	2012	141.2
Antimony	51	121.76	1167	69.0	2624	690	1	1627	1184	405
							10	1891	1292	403
							100	2233	1472	398
							200	2350	1778	393
Bismuth	83	209	520	21.6	2691	368	1	1683	572	626.2
							10	1953	752	619
							100	2295	1112	603
							200	2417	1476	587
Cadmium	48	112.41	609	23.8	1409	515	1	741	626	500
							10	903	662	499
							100	1132	752	495
							200	1216	932	488
Cesium	55	132.91	83.2	6.78	1301	263	1	532	83	114.9*
							10	729	211	112.2*
							100	959	285	110.7*
							200	1058	412	108.1*
Gallium	31	69.72	85.86	34.5	3601	1825	1	2399	90	380.4
							10	2727	574	368.6
							100	3139	1112	357.1
							200	3285	1483	349.9
Indium	49	114.76	313	12.26	3789	841	1	2280	327	438.6
							10	2671	381	437.1
							100	3193	442	435.4
							200	3385	520	433.2
Lead	82	207	621	10.6	3159	369	1	1809	752	656
							10	2133	932	649
							100	2583	1112	641
							200	2746	1472	627
Lithium	3	6.94	354	284	2403	8420	1	1373	392	31.7
							10	1634	752	30.6
							100	1983	1112	29.6
							200	2113	1472	28.5
Magnesium	12	24.32	1204	148	2017	2400	1	1150	1204	98.1
							10	1296	1252	96.8
							100	1668	1292	95.9
							200	1773	1328	94.3
							400	1893	1382	91.8

Table 2.2.1 — (Continued)

Specific heat		Viscosity		Thermal conductivity		Electrical resistivity		Volume change on fusion, % of solid volume	Unit price (Sept. 1951), \$/lb
*F	Btu/(lb)(*F)	*F	Lb/(ft)(hr)	*F	Btu/(hr)(ft)(*F)	*F	μ-ohms		
1220- 1832	0.259	1292 1472	7.0 3.4	1292 1454	59.8 70.2	1214 1238 1355 1485 1598	19.6 20.5 21.3 22.4 23.2	6.6	0.22
1202- 1742	0.0656	1296 1474 1652 1836	3.14 2.69 2.41 2.19	1166 1346	12.6- 12	1160 1292 1472 1562 1652	117.00 117.65 120.31 123.54 131.00	-0.94	0.44
520 752 1112 1472 1832	0.0340 .0354 .0376 .0397 .0419	579 844 1112	4.02 3.10 2.41	572 752 932 1112 1292	9.9 8.95 8.95 8.95 8.95	572 752 1112 1382	128.9 134.2 145.25 153.53	-3.32	2.25
610- 1292	0.0632	662 752 932 1112	5.74 5.23 4.45 3.73	671 676 716 815	25.6 25.4 25.4 28.8	617 752 932 1112 1292	33.7 33.7 34.12 34.82 35.78	4.74	2.55
83	0.060	83 211 285 412	1.655* 1.150* 0.9837* .8090*	83	10.6	86 99	36.6 37.0	2.6	4.00/gm
55- 392	0.082	127 574 756 932 1483	4.583 2.490 2.125 1.963 1.579	85.86	17- 22	85 86 114	25.9 27.2 28.4	-3.1	2.50/gm
314	0.0652			313	22- 29	309 359 432 536	29.10 30.11 31.87 34.84	2.5	32.8
621 752 932	0.039 .037 .037	826 853 1024 1296 1551	5.121 4.983 4.114 3.265 2.868	626 752 932 1112 1292	9.4 9.2 8.95 8.7 8.7	621 752 1112 1472 1832	94.6 98.0 107.2 116.4 125.7	3.6	0.17
392 572 752 932	1.40 1.23 1.09 1.00	362.1 379.8 420.8 483.4 545.9	1.432 1.391 1.308 1.190 1.098	424- 451	22	446	45.25	1.5	11
1204 1341 1701 1881 2048	0.317 .321 .332 .337 .342						98.4 103.2 114.2 127.5 135.5	4.2	0.245

Table 2.2.1—(Continued)

Metal	Atomic No.	Atomic wt	Melting point, °F	Latent heat of fusion, Btu/lb	Boiling point (760 mm Hg), °F	Latent heat of vaporization, Btu/lb	Vapor pressure		Density	
							Mm Hg	°F	°F	Lb/cu ft
Mercury	80	200.61	-37.97	5.0	675	125	1	259	-4.0	851.9
							10	363	68	845.7
							100	503	212	833.6
							200	555	392	818.8
							400	613	572	804.2
Potassium	19	39.096	147	26.3	1400	893	1	648	212	51.1
							10	829	482	48.9
							100	1078	752	46.6
							200	1175	1022	44.4
							400	1285	1292	42.2
Rubidium	37	85.48	102	11	1270	382	1	561	100	91.93*
							10	729	212	90.04*
							100	966	285	88.84*
							200	1056	354	87.73*
							400	1162	428	86.58*
Sodium	11	22.997	208	48.8	1621	1810	1	824	212	57.9
							10	1018	482	55.6
							100	1285	752	53.3
							200	1386	1022	51.0
							400	1499	1292	48.7
Thallium	81	204.39	577	9.06	2655	342	1	1517	584	704.8
							10	1801	620	702.6
							100	2185	626	702.3
							200	2325	632	702.6
							400	2487		
Tin	50	118.70	449	26.1	4118	1030	1	2718	768	426.6
							10	3097	973	422.1
							100	3574	1065	420.1
							200	3745	1198	416.7
							400	3931	1299	414.5
Zinc	30	65.38	787	44	1663	755	1	909	787	432.0
							10	1099	1112	425.1
							100	1357	1472	410.2
							200	1450		
							400	1551		
Sodium-potassium alloy 56 wt-% Na, 44 wt-% K		28.1 (calc.)	66.2		1517		1	720	212	55.3
							10	914	482	53.1
							100	1180	752	50.8
							200	1285	1022	48.6
							400	1400	1292	46.3
Sodium-potassium alloy (near eutectic) 22 wt-% Na, 78 wt-% K		33.9 (calc.)	12		1443		1	671	212	52.9
							10	856	482	50.6
							100	1117	752	48.4
							200	1218	1022	46.1
							400	1330	1292	43.9
Lead-bismuth alloy (eutectic) 44.5 wt-% Pb, 55.5 wt-% Bi		208 (calc.)	257		3038				392	653
									752	636
									1112	619
									1472	602
									1832	584

*E. N. da C. Andrade and E. R. Dobbs, Proc. Roy. Soc. London, A211: 12-30 (1952)

Table 2.2.1 — (Continued)

Specific heat		Viscosity		Thermal conductivity		Electrical resistivity		Volume change on fusion, % of solid volume	Unit price (Sept. 1951), \$/lb
°F	Btu/(lb)(°F)	°F	Lb/(ft)(hr)	°F	(Btu/(hr)(ft)(°F)	°F	μ-ohm		
32	0.03334	-4.0	4.48	32	4.74	122		3.6	2.56
212	.03279	32	4.07	140	5.59	212			
392	.03245	68	3.75	248	6.31	392			
572	.03234	212	2.93	320	6.75	572			
842	.03256	392	2.44	428	7.33	662			
167	0.1956	157.3	1.25	392	26.0	147	13.16	2.41	2.50
392	.1887	333	0.801	572	24.5	302	18.70		
752	.1826	482	.624	752	23.1	482	25.00		
1112	.1825	752	.462	932	21.7	572	28.2		
1472	.1884	1292	.329	1112	20.5	662	31.4		
102- 258	0.0913	100	1.630*	102	17	122	23.15	2.5	4.50/gm
		212	1.172*	122	18	167	25.32		
		284.9	1.000*			212	27.47		
		354.2	0.8794*						
		428.2	.7826*						
212	0.3305	218.7	1.66	212	49.71	212	9.65	2.5	0.16
392	.3200	334	1.22	392	47.10	392	13.18		
752	.3055	482	0.922	572	43.76	482	14.90		
1112	.2998	752	.651	752	41.15	572	16.70		
1472	.3030	1292	.440	932	38.61	662	18.44		
578- 932	0.0367			662	14.3	577	74.0	3.2	12.50
482	0.0580	464	4.62	464	19.4	449	47.6	2.6	1.03
2012	.0758	572	4.04	558	19.6	752	51.4		
		752	3.34	783	19.1	1112	56.8		
		932	2.86	928	18.9	1472	62.7		
		1112	2.54			1832	68.6		
787	0.1199	842	7.67	932	33.4	787	35.3	6.9	0.18
1112	.1173	932	6.73	1112	32.9	932	35.4		
1472	.1076	1112	5.42	1292	32.7	1112	35.0		
1652	.1044	1292	4.55			1282	35.65		
1832	.1012					1472	35.70		
212	0.269	219	1.32	212	14.9	122	33.0	2.5	2
572	.255	334	0.997	392	15.3	212	35.5		
932	.249	482	.765	572	15.7	302	38.0		
1112	.248	752	.567	752	16.0	392	41.0		
1472	.253	1292	.390	932	16.3				
32	0.238	219	1.13	212	14.1	122	37.5	2.5	2
392	.217	334	0.869	752	15.4	212	41.0		
752	.210	482	.675			302	44.0		
1112	.209	752	.496			392	47.0		
1472	.213	1292	.353						
291- 676	0.035	630	4.11	320	5.3	392	113	0.6	
		842	3.34	392	5.6	572	118		
		932	3.12	464	5.8	752	123		
		1022	2.98	572	6.3	932	128		
		1112	2.83	608	6.5				

Table 2.2.2—Physical Properties of Liquid Metals (Metric Units)

(Liquid Metals Handbook, edited by R. N. Lyon, Department of the Navy and U. S. Atomic Energy Commission, NAVEXOS P-733, 2d ed., in preparation)

Metal	Melting point, °C	Latent heat of fusion, cal/gm	Boiling point (760 mm Hg), °C	Latent heat of vaporization, cal/gm	Vapor pressure		Density	
					mm Hg	°C	°C	Gm/cc
Aluminum	660.2	96	2450	3050	1	1537	660	2.380
					10	1770	700	2.369
					100	2081	900	2.315
					400	2360	1100	2.261
Antimony	630.5	38.3	1440	383	1	886	640	6.49
					10	1033	700	6.45
					100	1223	800	6.38
					200	1288	970	6.29
Bismuth	271.0	12.0	1477	204.3	1	917	300	10.03
					10	1067	400	9.91
					100	1257	600	9.66
					200	1325	802	9.40
Cadmium	321	13.2	765	286.4	1	394	330	8.01
					10	484	350	7.99
					100	611	400	7.93
					200	658	500	7.82
Cesium	28.5	3.766	705	146.0	1	278	28.4	1.841*
					10	387	99.6	1.797*
					100	515	140.5	1.773*
					200	570	210.9	1.732*
Gallium	29.92	19.16	1983	1014	1	1315	32.4	6.093
					10	1497	301	5.905
					100	1726	600	5.720
					200	1807	806	5.604
Indium	156.4	6.807	2087	468	1	1249	164	7.026
					10	1466	194	7.001
					100	1756	228	6.974
					200	1863	271	6.939
Lead	327.4	5.89	1737	204.6	1	987	400	10.51
					10	1167	500	10.39
					100	1417	600	10.27
					200	1508	800	10.04
Lithium	179	158	1317	4680	1	745	200	0.507
					10	890	400	.490
					100	1084	600	.474
					200	1156	800	.457
Magnesium	651	82.2	1103	1337	1	621	651	1.572
					10	702	678	1.55
					100	909	700	1.536
					200	967	720	1.51
					400	1034	750	1.47

Table 2.2.2—(Continued)

Specific heat		Viscosity		Thermal conductivity		Electrical resistivity		Surface tension	
°C	Cal/(gm)(°C)	°C	Cp	°C	Cal (sec)(cm)(°C)	°C	μ-ohms	°C	Dynes/cm
660- 1000	0.259	700 800	2.9 1.4	700 790	0.247 .290	657 670 735 807 870	19.6 20.5 21.3 22.4 23.2	750	520
650- 950	0.0656	702 801 900 1002	1.296 1.113 0.994 .905	630 730	0.052- 0.05	627 700 800 850 900	117.00 117.65 120.31 123.54 131.00	635 675 725 800	383 384 383 380
271 400 600 800 1000	0.0340 .0354 .0376 .0397 .0419	304 451 600	1.662 1.280 0.996	300 400 500 600 700	0.041 .037 .037 .037 .037	300 400 600 750	128.9 134.2 145.25 153.53	300 350 400 450 500	376 373 370 367 363
321- 700	0.0632	350 400 500 600	2.37 2.16 1.84 1.54	355 358 380 435	0.106 .105 .105 .119	325 400 500 600 700	33.7 33.7 34.12 34.82 35.78	330 370 420 450 500	564 608 598 611 600
28.5	0.060	28.4 99.6 140.5 210.9	0.6837* .4753* .4065* .3343*	28.5	0.044	30 37	36.6 37.0		
12.5- 200	0.082	52.9 301 402 500 806	1.894 1.029 0.8783 .8113 .6524	29.92	0.07- 0.09	29.75 30.3 46.1	25.9 27.2 28.4	30- 40	735
156.4	0.0652			156.4	0.09- 0.12	154.0 181.5 222 280.2	29.10 30.11 31.87 34.83	170- 250	340
327 400 500	0.039 .037 .037	441 456 551 703 844	2.116 2.059 1.700 1.349 1.185	330 400 500 600 700	0.039 .038 .037 .036 .036	327 400 600 800 1000	94.6 98.0 107.2 116.4 125.7	350 400 450 500	442 438 438 431
200 300 400 500	1.40 1.23 1.09 1.00	183.4 193.2 216.0 250.8 285.5	0.5918 .5749 .5406 .4917 .4548	218- 233	0.09	230	45.25		
651 727 927 1027 1120	0.317 .321 .332 .337 .342							681 894	563 502

Table 2.2.2—(Continued)

Metal	Melting point, °C	Latent heat of fusion, cal/gm	Boiling point, (760 mm Hg), °C	Latent heat of vaporization, cal/gm	Vapor pressure		Density	
					Mm Hg	°C	°C	Gm/cc
Mercury	-38.87	2.8	357	69.7	1	126.2	-20	13.645
					10	184.0	20	13.546
					100	261.7	100	13.352
					200	290.7	200	13.115
					400	323.0	300	12.881
Potassium	63.7	14.6	760	496	1	342	100	0.819
					10	443	250	.783
					100	581	400	.747
					200	635	550	.711
					400	696	700	.676
Rubidium	39.00	6.1	688	212	1	294	38.0	1.4725*
					10	387	99.7	1.4423*
					100	519	140.5	1.4230*
					200	569	179.0	1.4053*
					400	628	220.1	1.3869*
Sodium	97.8	27.05	883	1005	1	440	100	0.928
					10	548	250	.891
					100	696	400	.854
					200	752	550	.817
					400	815	700	.780
Thallium	303	5.04	1457	189.9	1	825	306.5	11.289
					10	983	326.7	11.254
					100	1196	330.0	11.250
					200	1274	333.5	11.254
					400	1364		
Tin	231.9	14.5	2270	573	1	1492	409	6.834
					10	1703	523	6.761
					100	1968	574	6.729
					200	2063	648	6.671
					400	2169	704	6.640
Zinc	419.5	24.4	906	419.5	1	487	419.5	6.92
					10	593	600	6.81
					100	736	800	6.57
					200	788		
					400	844		
Sodium-potassium alloy: 56 wt-% Na, 44 wt-% K	19		825		1	382	100	0.886
					10	490	250	.850
					100	638	400	.814
					200	696	550	.778
					400	760	700	.742
Sodium-potassium alloy: (near eutectic) 22 wt-% Na, 78 wt-% K	-11		784		1	355	100	0.847
					10	458	250	.811
					100	603	400	.775
					200	659	550	.739
					400	721	700	.703
Lead-bismuth alloy (eutectic): 44.5 wt-% Pb, 55.5 wt-% Bi	125		1670				200	10.46
							400	10.19
							600	9.91
							800	9.64
							1000	9.36

*E. N. da C. Andrade and E. R. Dobbs, Proc. Roy. Soc. London, A211: 12-30 (1952)

Table 2.2.2—(Continued)

Specific heat		Viscosity		Thermal conductivity		Electrical resistivity		Surface tension	
				°C	Cal (sec)(cm)(°C)				
°C	Cal/(gm)(°C)	°C	Cp	°C		°C	μ-ohms	°C	Dynes/cm
0	0.03334	-20	1.85	0	0.0196	50	98.4	20	465
100	.03279	0	1.68	60	.0231	100	103.2	112	454
200	.03245	20	1.55	120	.0261	200	114.2	200	436
300	.03234	100	1.21	160	.0279	300	127.5	300	405
450	.03256	200	1.01	220	.0303	350	135.5	354	394
75	0.1956	69.6	0.515	200	0.1073	64	13.16	100-	86
200	.1887	167.4	.331	300	.1013	150	18.70	150	
400	.1826	250	.258	400	.0956	250	25.00		
600	.1825	400	.191	500	.0898	300	28.2		
800	.1884	700	.136	600	.0846	350	31.4		
39-	0.0913	38.0	0.6734*	39	0.07	50	23.15		
126		99.7	.4844*	50	.075	75	25.32		
		140.5	.4133*			100	27.47		
		179.0	.3634*						
		220.1	.3234*						
190	0.3305	103.7	0.686	100	0.2055	100	9.65	100	206.4
200	.3200	167.6	.504	200	.1947	200	13.18	250	199.5
400	.3055	250	.381	300	.1809	250	14.90		
600	.2998	400	.269	400	.1701	300	16.70		
800	.3030	700	.182	500	.1596	350	18.44		
393-	0.0367			350	0.059	303	74.0	327	401
500									
250	0.0580	240	1.91	240	.08	231.9	47.6	300	526
1100	.0758	300	1.67	292	.081	400	51.4	350	522
		400	1.38	417	.079	600	56.8	400	518
		500	1.18	498	.078	800	62.7	450	514
		600	1.05			1000	68.6	500	510
419.5	0.1199	450	3.17	500	0.138	419.5	35.3	510	785
600	.1173	500	2.78	600	.136	500	35.4	550	778
800	.1076	600	2.24	700	.135	600	35.0	600	768
900	.1044	700	1.88			700	35.65	640	761
1000	.1012					800	35.70		
100	0.269	103.7	0.546	100	0.0617	50	33.0	19-	110-
300	.255	167.5	.412	200	.0633	100	35.5	250	100
500	.249	250	.316	300	.0648	150	38.0		
600	.248	400	.230	400	.0662	200	41.0		
800	.253	700	.161	500	.0675				
0	0.238	103.7	0.468	100	0.0583	50	37.5	-11-	120-
200	.217	167.5	.359	400	.0636	100	41.0	250	110
400	.210	250	.279			150	44.0		
600	.209	400	.205			200	47.0		
800	.213	700	.146						
144-	0.035	332	1.7	160	0.022	200	113	800	367
358		450	1.38	200	.023	300	118	1000	356
		500	1.29	240	.024	400	123		
		550	1.23	300	.026	500	128		
		600	1.17	320	.027				

Table 2.2.3—Cross Sections of Naturally Occurring Mixtures of Isotopes
 (Neutron Cross Sections, edited by D. J. Hughes, AECU-2040, May 15, 1952, and
 "GE Chart of the Nuclides")

Element	10^{24} Nuclei/cc at m.p.	Thermal-pile-neutron cross section, barns		Macroscopic cross section at m.p., cm^{-1}	
		Absorption	Total	Absorption	Total
Aluminum	0.0530	0.22	1.6	0.012	0.085
Antimony	.0321	5.3	9.6	.17	.31
Bismuth	.0290	0.032	9	.00093	.26
Cadmium	.0429	3100	3100	130	130
Cesium	.00831	29	50	0.24	0.4
Gallium	.0525	2.8	7	.15	.4
Indium	.0341	190	192	6.48	6.55
Lead	.0306	0.17	11	0.0052	0.34
Lithium	.0441	67	68	2.95	3.0
Magnesium	.0389	0.059	3.6	0.0023	0.14
Mercury	.0409	360	370	14.7	15.1
Potassium	.0128	2.0	3.5	0.026	0.045
Rubidium	.0102	0.70	13	.0071	.13
Sodium	.0243	.49	4.5	.012	.11
Thallium	.0334	3.3	17	.11	.57
Tin	.0353	0.6	5	.02	.18
Zinc	.0638	1.0	4.6	.06	.29

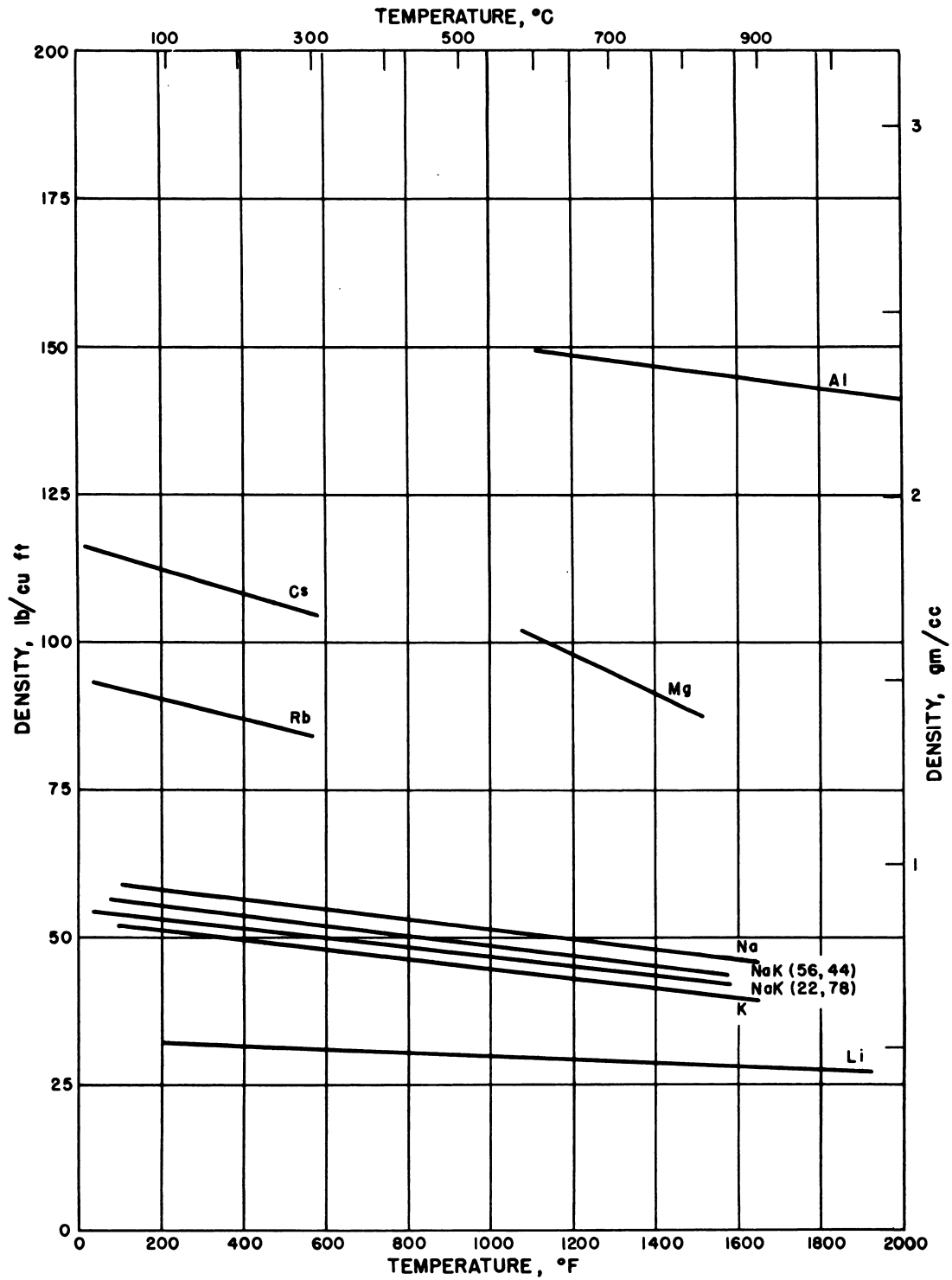


Fig. 2.2.1— Density as a Function of Temperature for Various Liquid Metals (Low Range). Submitted by Knolls Atomic Power Laboratory, July 14, 1952.

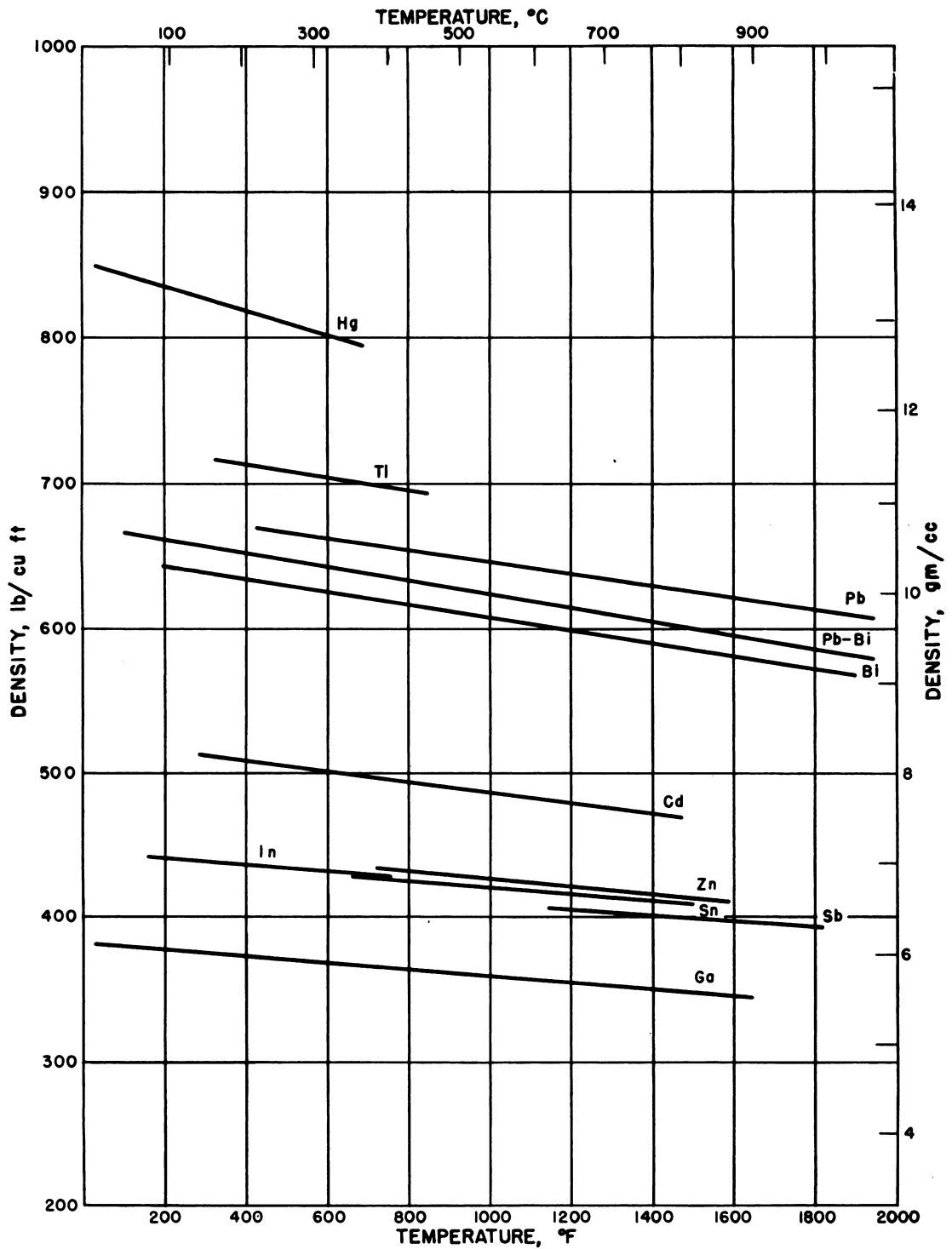


Fig. 2.2.2— Density as a Function of Temperature for Various Liquid Metals (High Range). Submitted by Knolls Atomic Power Laboratory, July 14, 1952.

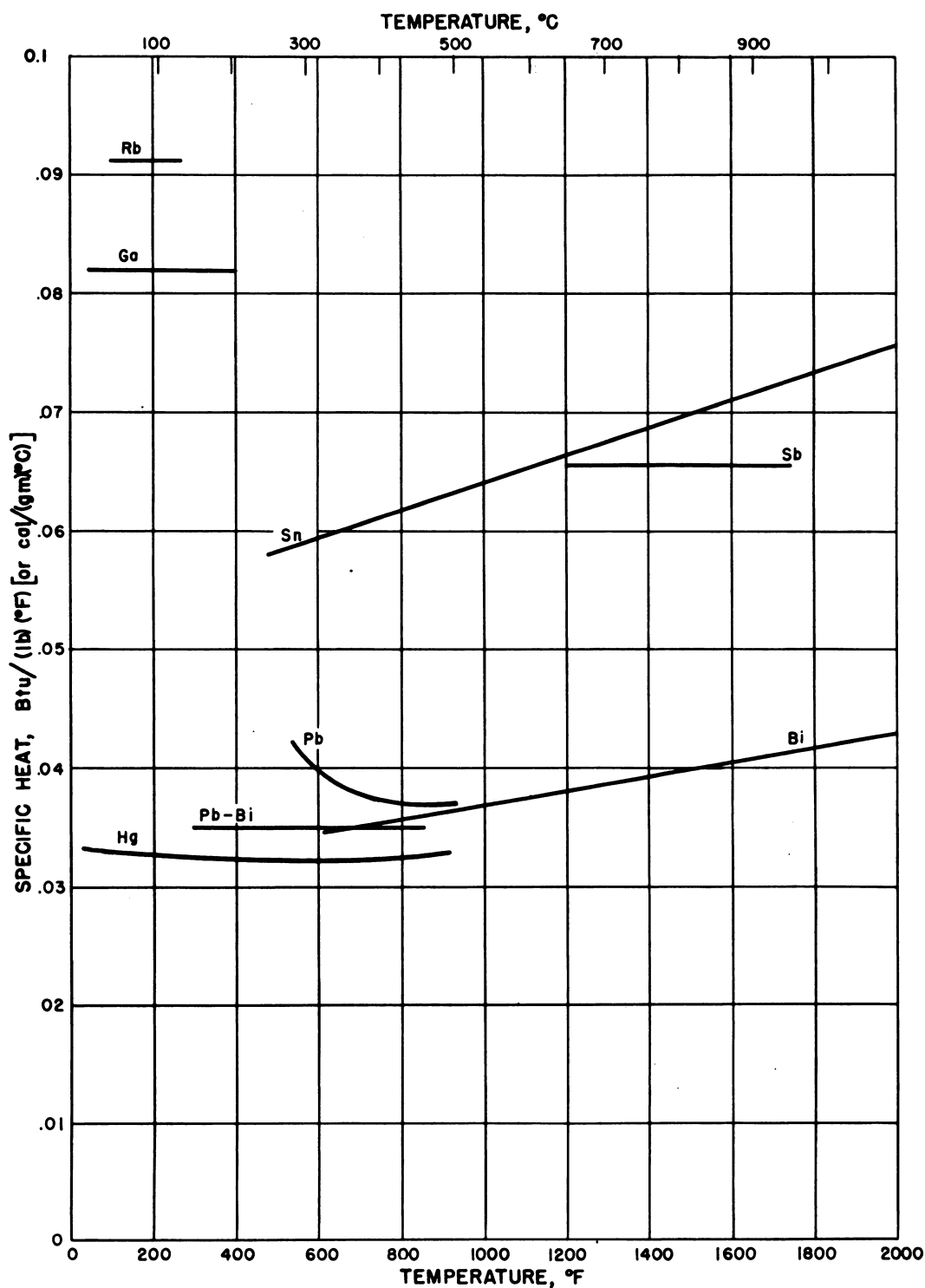


Fig. 2.2.3— Specific Heat as a Function of Temperature for Various Liquid Metals (Low Range). Submitted by Knolls Atomic Power Laboratory, July 14, 1952.

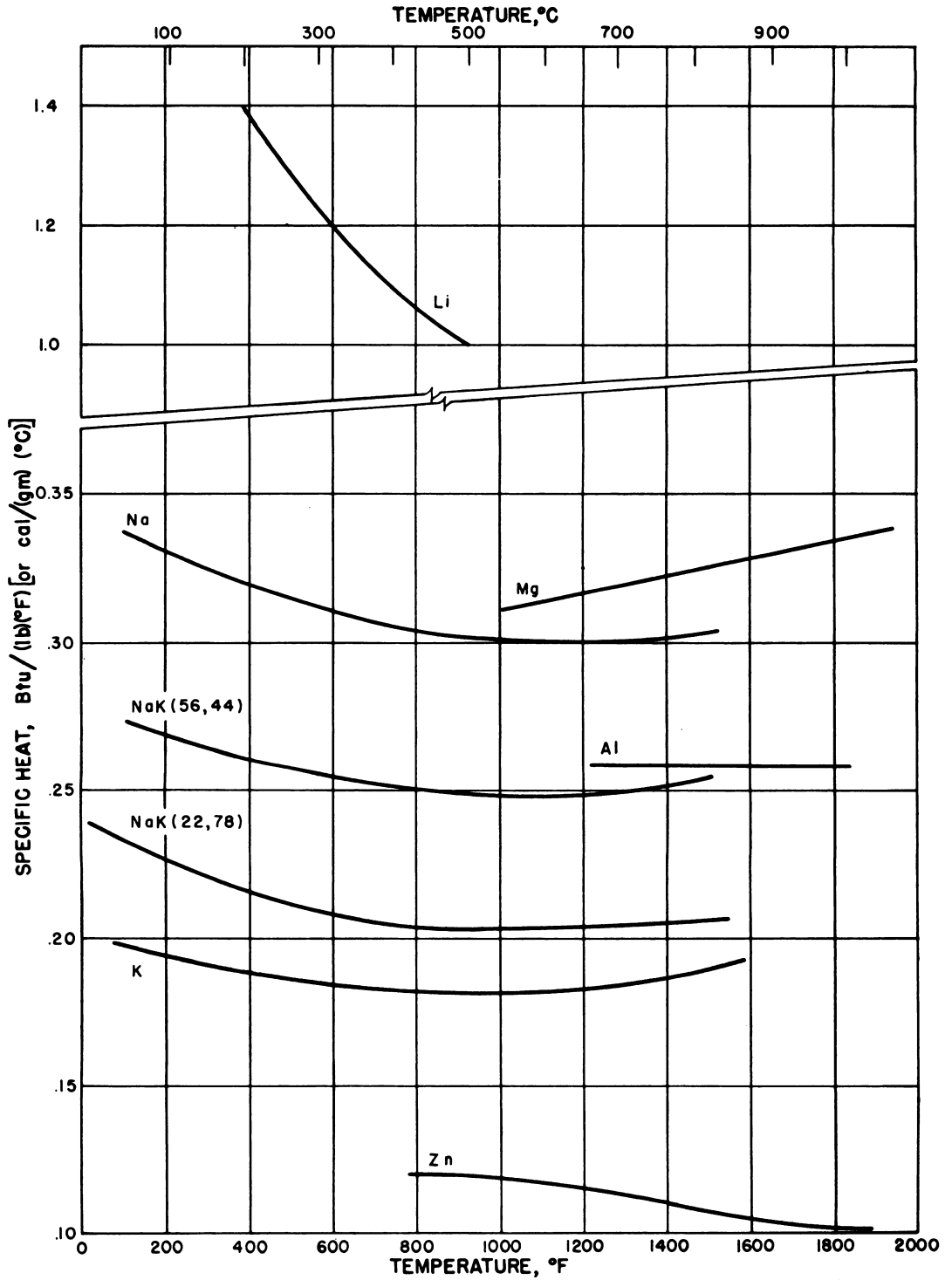


Fig. 2.2.4— Specific Heat as a Function of Temperature for Various Liquid Metals (High Range). Submitted by Knolls Atomic Power Laboratory, July 14, 1952.

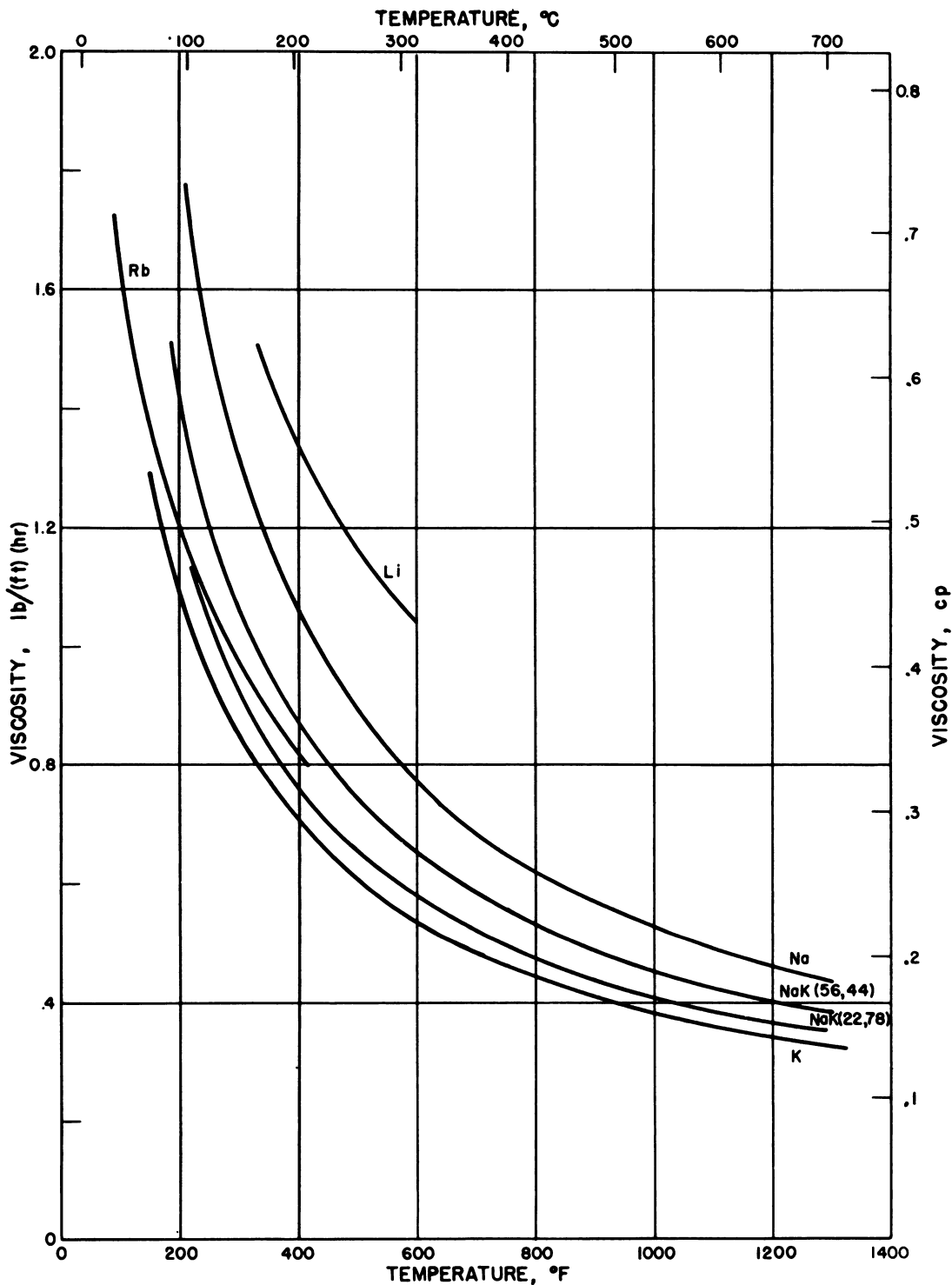


Fig. 2.2.5—Viscosity as a Function of Temperature for Various Liquid Metals (Low Range). Submitted by Knolls Atomic Power Laboratory, July 14, 1952.

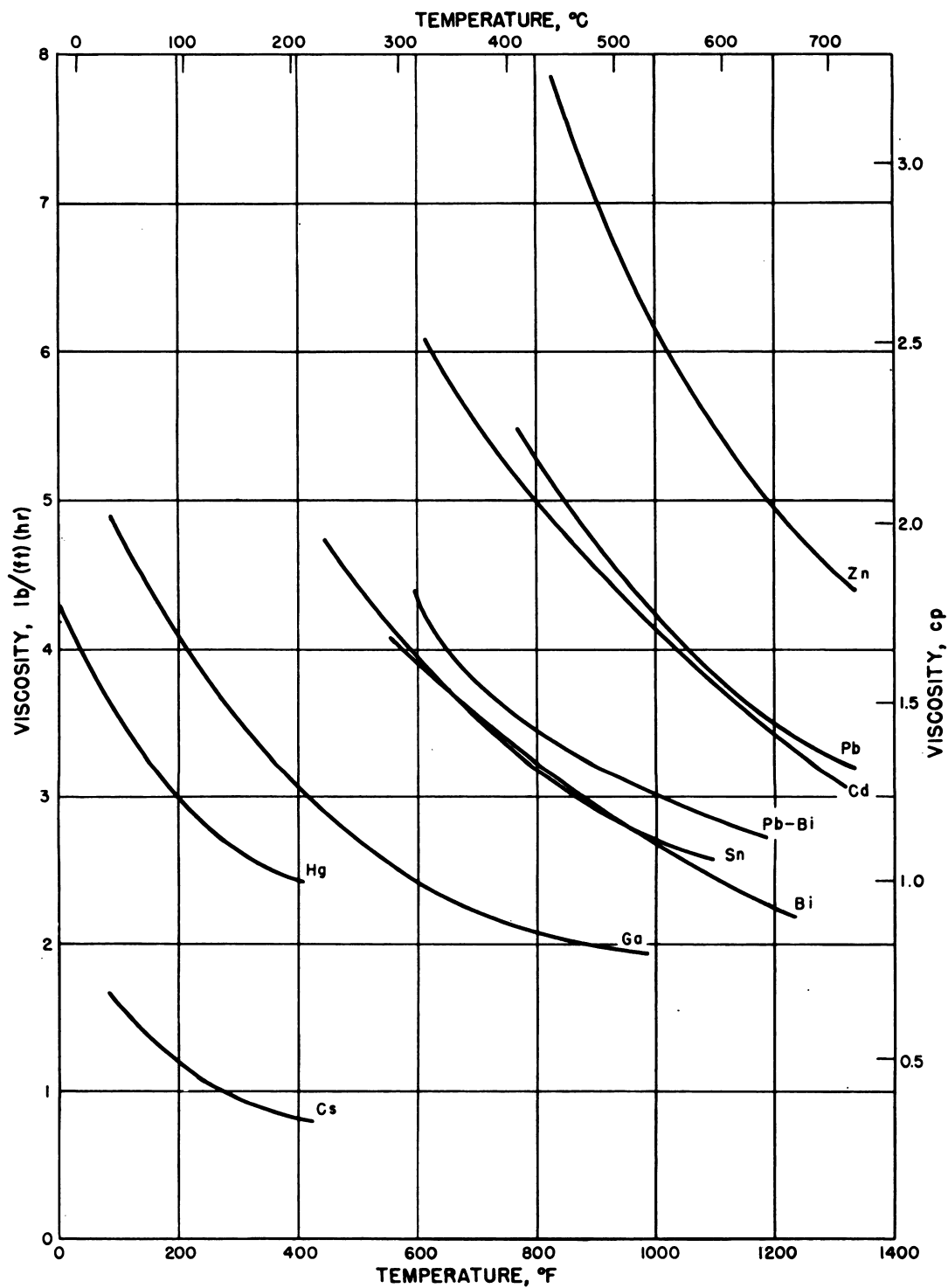


Fig. 2.2.6—Viscosity as a Function of Temperature for Various Liquid Metals (High Range). Submitted by Knolls Atomic Power Laboratory, July 14, 1952.

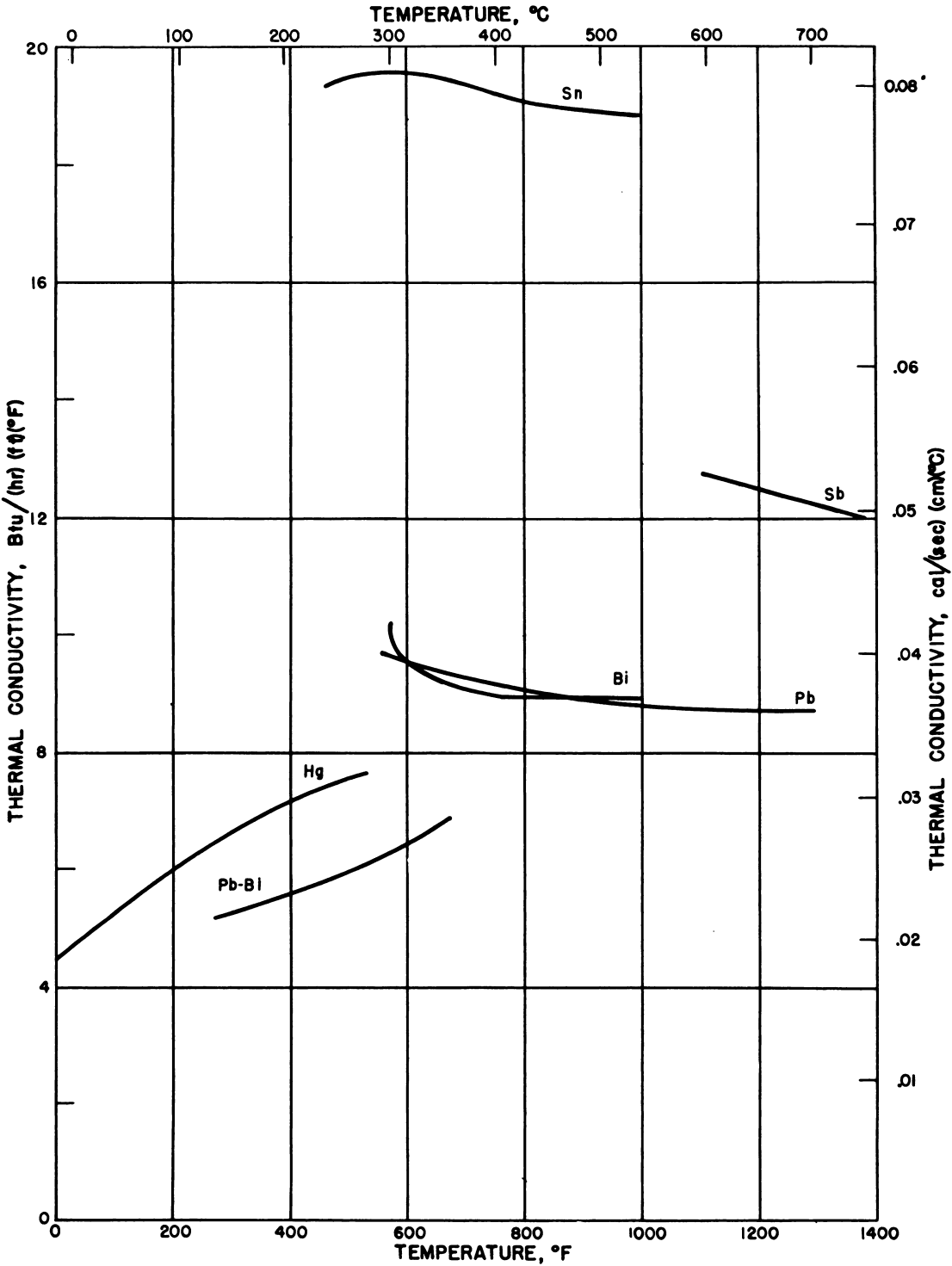


Fig. 2.2.7 — Thermal Conductivity as a Function of Temperature for Various Liquid Metals (Low Range). Submitted by Knolls Atomic Power Laboratory, July 14, 1952.

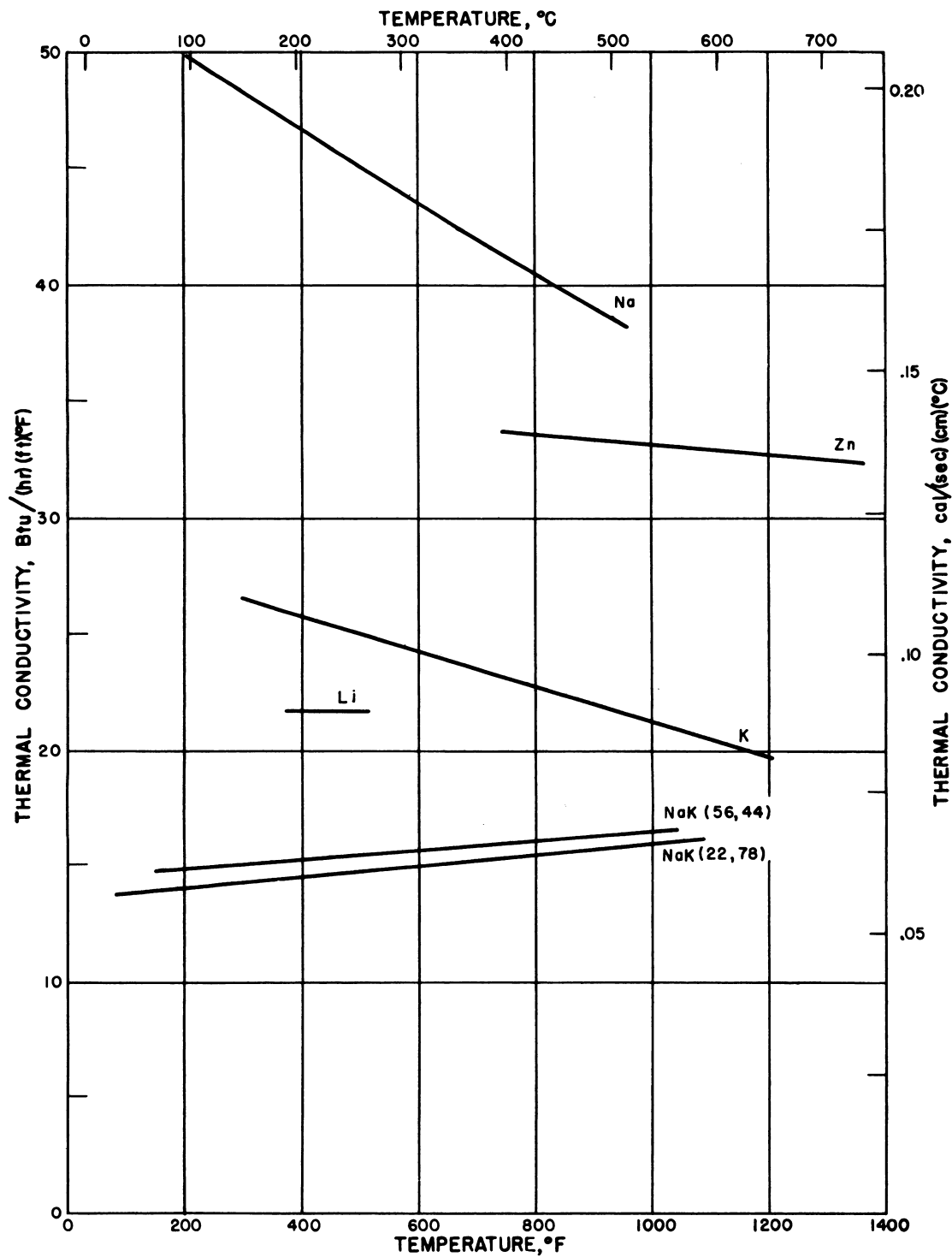


Fig. 2.2.8— Thermal Conductivity as a Function of Temperature for Various Liquid Metals (High Range). Submitted by Knolls Atomic Power Laboratory, July 14, 1952.

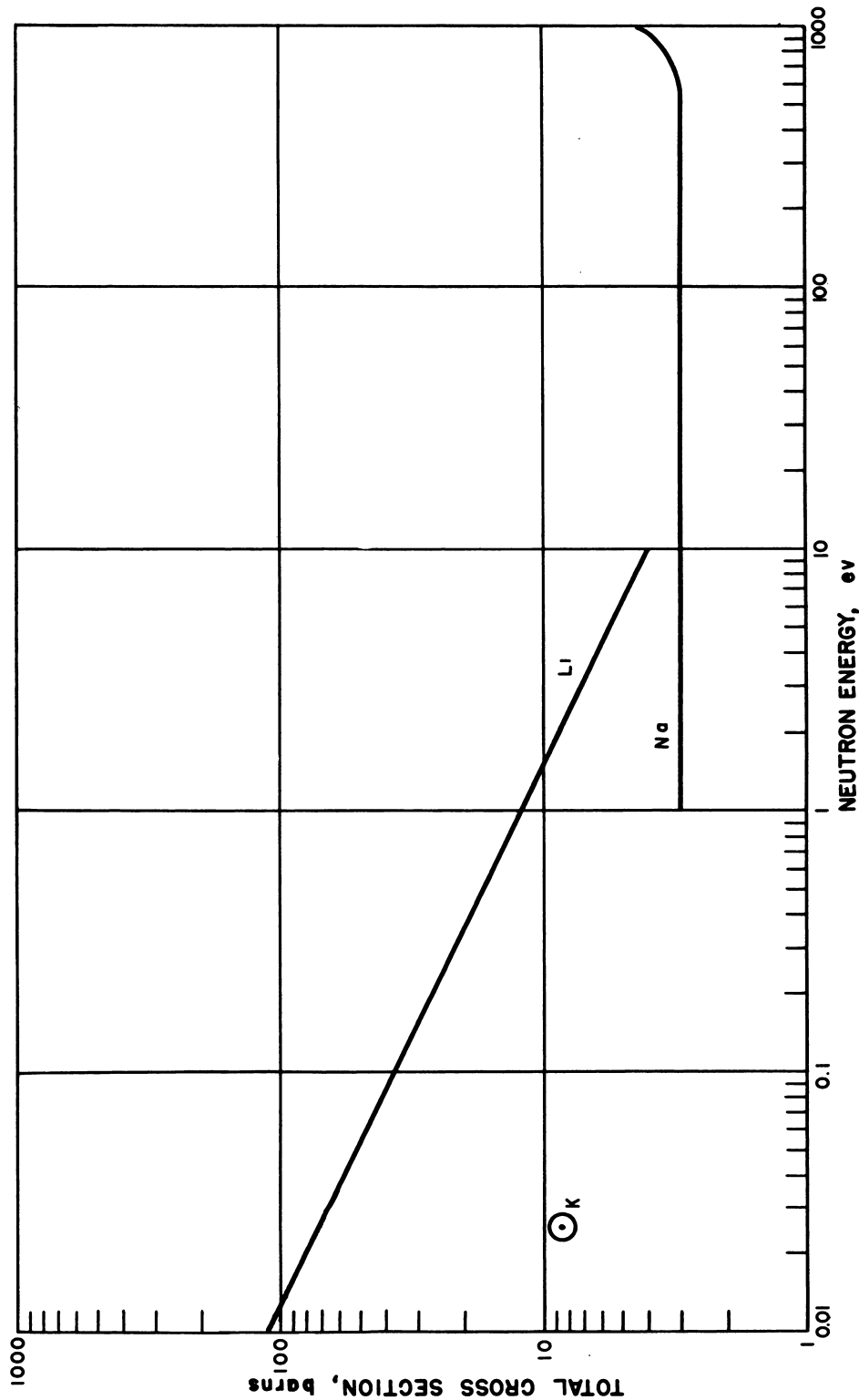


Fig. 2.2.9 — Cross Section as a Function of Neutron Energy for Na, K, and Li (Slow Neutrons). Based on Neutron Cross Sections, AECU-2040, May 15, 1952.

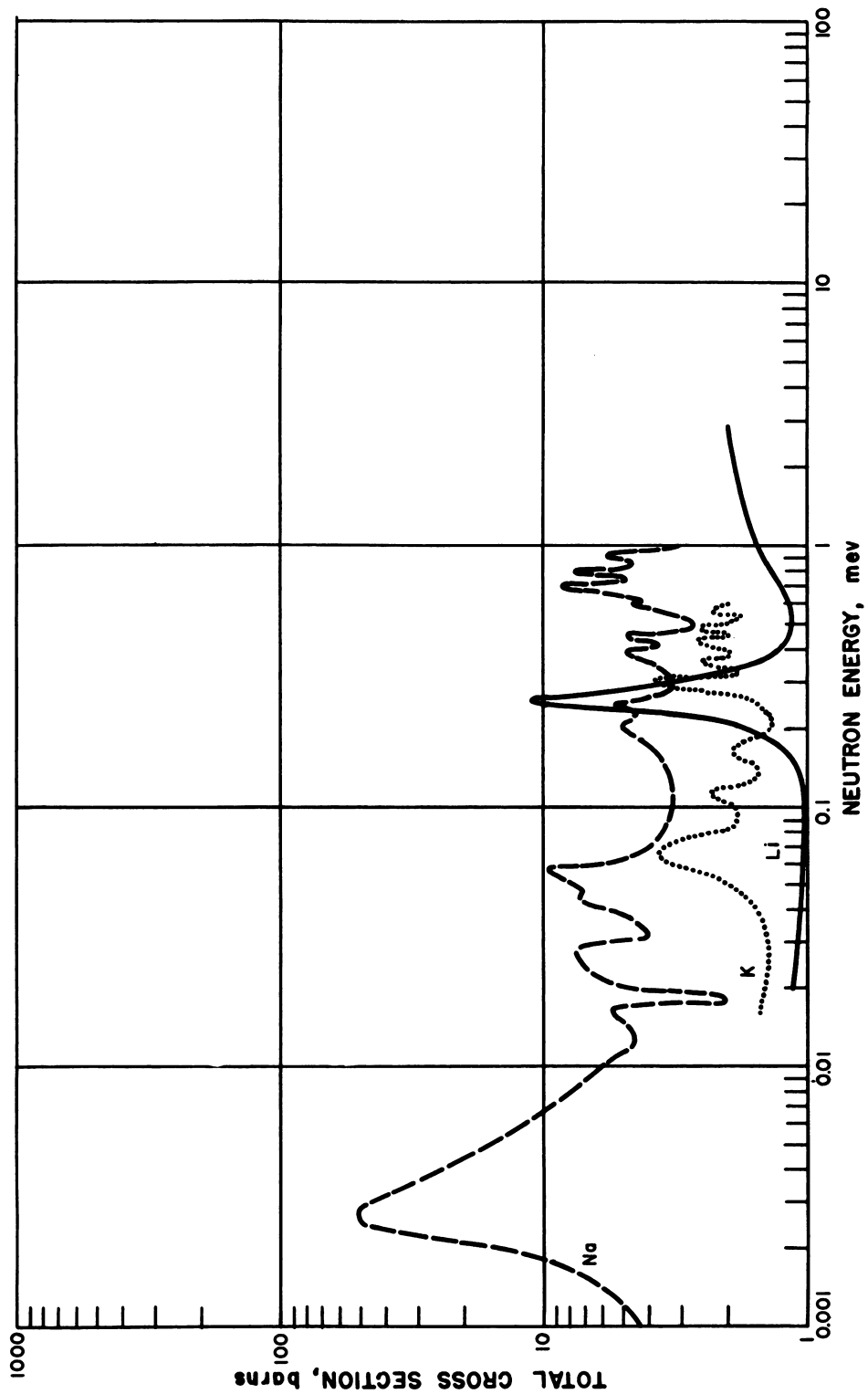


Fig. 2.2.10—Cross Section as a Function of Neutron Energy for Na, K, and Li (Fast Neutrons). Based on Neutron Cross Sections, AECU-2040, May 15, 1952.

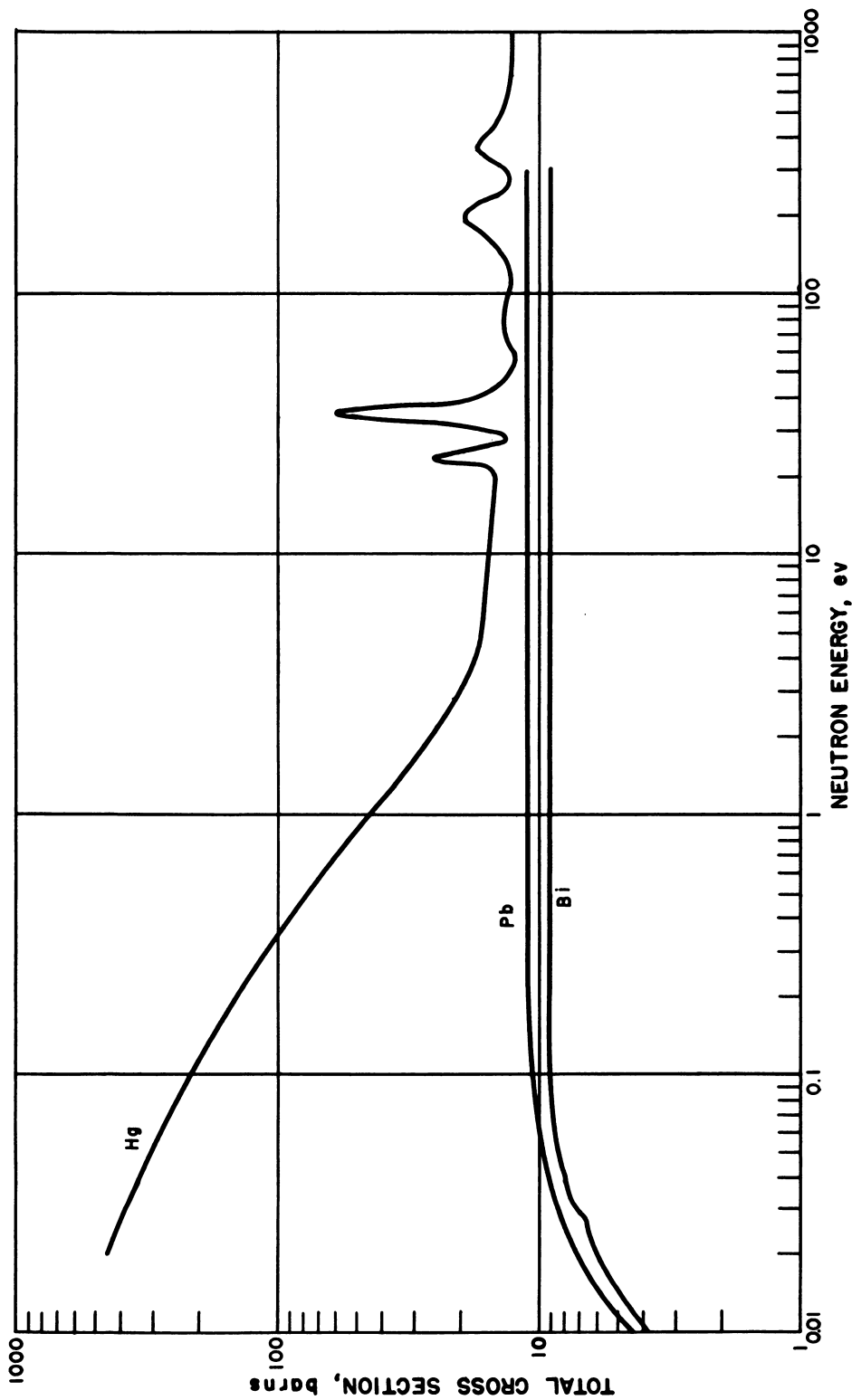


Fig. 2.2.11 — Cross Section as a Function of Neutron Energy for Pb, Bi, and Hg (Slow Neutrons). Based on Neutron Cross Sections, AECU-2040, May 15, 1952.

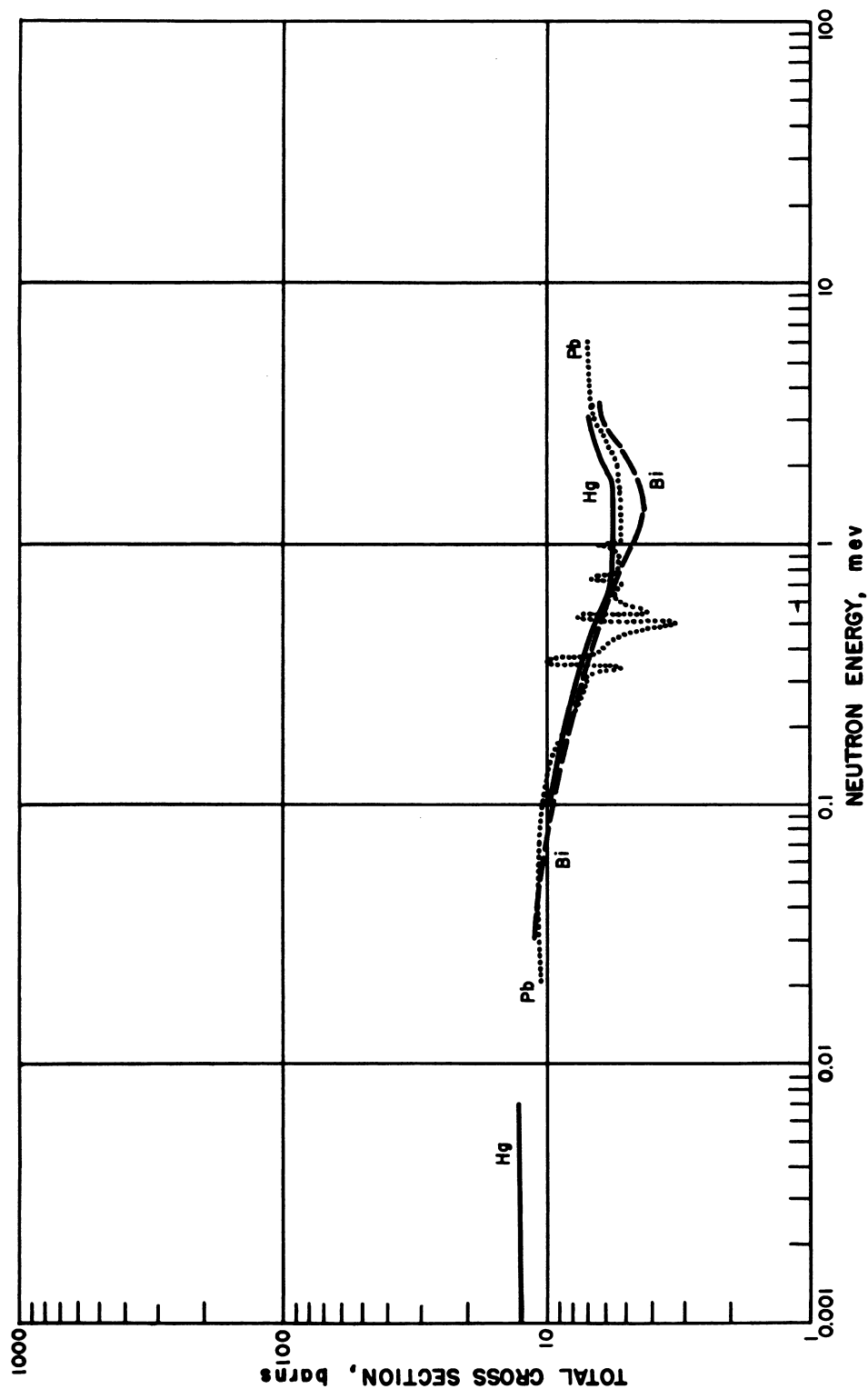


Fig. 2.2.12—Cross Section as a Function of Neutron Energy for Pb, Bi, and Hg (Fast Neutrons). Based on Neutron Cross Sections, AECU-2040, May 15, 1952.

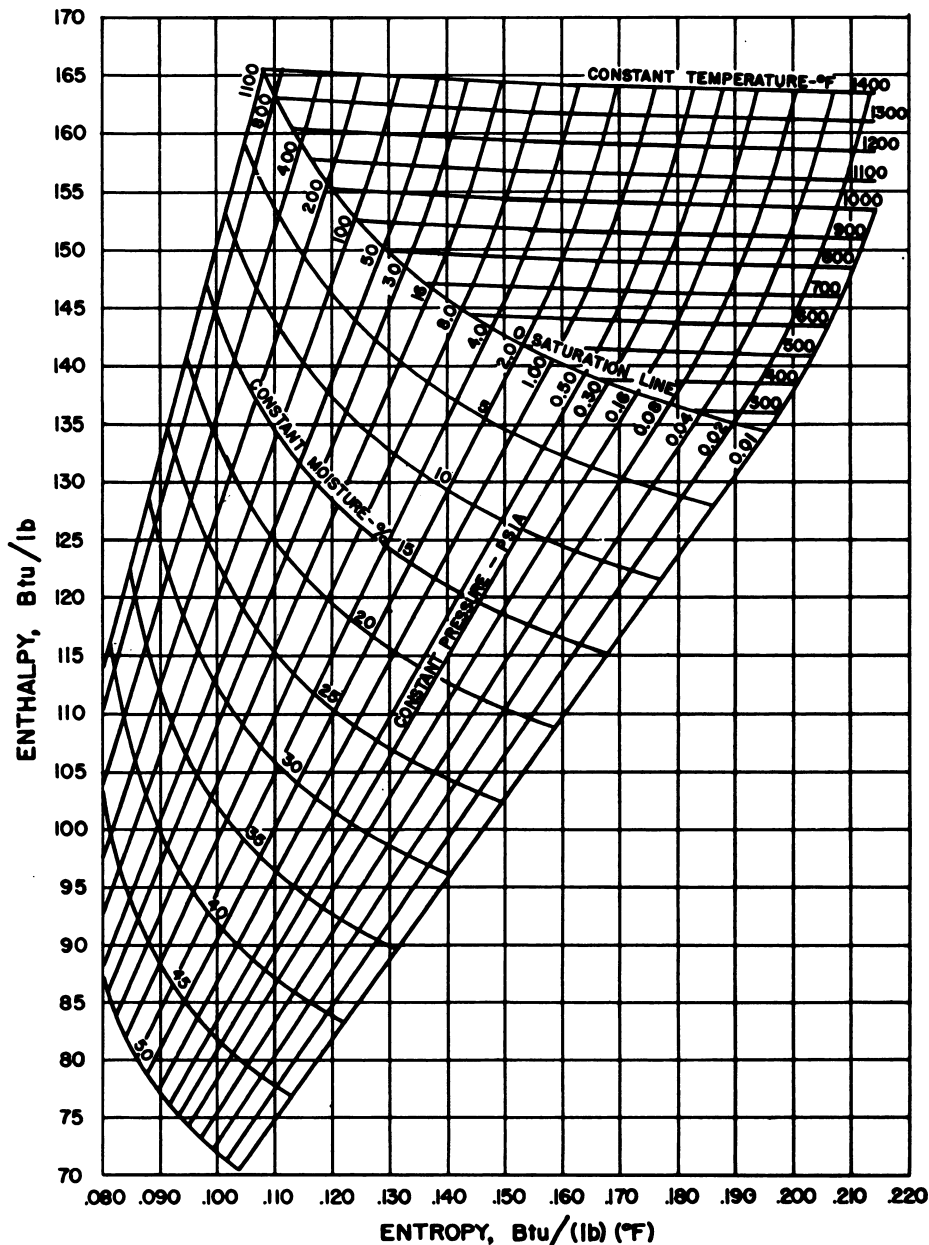


Fig. 2.2.13 — Total Heat-Entropy Diagram for Mercury. Reprinted from Thermodynamic Properties of Mercury Vapor, by L. A. Sheldon, Paper No. 49-A-30, presented at 1949 ASME Annual Meeting in New York, Nov. 27 to Dec. 2, 1949; Mech. Eng. 71: 1052 (1949). By permission from American Society of Mechanical Engineers.

SELECTED READING LIST

NEUTRON CROSS SECTIONS, edited by D. J. Hughes, AECU-2040, May 15, 1952.

THE VISCOSITIES OF LIQUID LITHIUM, RUBIDIUM AND CESIUM, E. N. da C. Andrade and E. R. Dobbs, Proc. Roy. Soc. London, A211: 12-30 (1952).

LIQUID METALS HANDBOOK, edited by R. N. Lyon, Department of the Navy and U. S. Atomic Energy Commission, NAVEXOS, P-733, 1st ed., June 1, 1950; 2d ed., June 1952.

THERMODYNAMIC PROPERTIES OF MERCURY VAPOR, L. A. Sheldon, Paper No. 49-A-30, presented at 1949 ASME Annual Meeting in New York, Nov. 27 to Dec. 2, 1949; Mech. Eng., 71: 1052 (1949).

CHART OF THE NUCLIDES, prepared by Knolls Atomic Power Laboratory, General Electric Company.

CHAPTER 2.3

Heat-transfer Correlations for Liquid Metals

R. D. Brooks and S. K. Friedlander

Heat-transfer correlations applicable to liquid metals are summarized in Table 2.3.1.* It will be noted that most of these expressions are based on theory and have not been confirmed experimentally. The correlations for pipe, parallel-plate, and annular flow under turbulent conditions were obtained from analyses of the Martinelli type with the assumption that $E_H = E_M$; they apply far downstream from the inlet where the temperature distribution is fully developed. Similar derivations for flow in non-circular ducts have been delayed because of a lack of information on velocity profiles; the correlations tabulated for these cases are based on slug flow.

The equations for laminar flow were derived from the Fourier-Poisson equation assuming a parabolic velocity distribution and neglecting the variation of the fluid properties with temperature. For oils and other fluids of high Pr , these expressions are generally modified empirically to correct for the variation of viscosity with temperature; this effect is probably of less importance in the case of liquid metals.

Prandtl numbers for some of the liquid metals have been calculated from the data of Chapter 2.2. These are plotted in Fig. 2.3.1.

TURBULENT FLOW THROUGH PIPES

Studies of heat transfer by forced convection have been made for the flow of mercury, lead-bismuth, and NaK through tubes. Of the three metal systems, mercury has been most thoroughly investigated by several different techniques in tubes ranging from 0.05-1.5 in. ID. A somewhat smaller number of tests have been made with lead-bismuth, while only two independent studies have been reported for NaK.

In general, the results for NaK and some of those for mercury are adequately correlated by the Lyon-Martinelli equation, which is plotted in Fig. 2.3.2 with some of the experimental data. The results for lead-bismuth and some of those for mercury have generally fallen below the theoretical line, most of the points being 25 to 50 percent less than predicted.

This deviation from theory and the variation in results observed by different investigators is often ascribed to a "thermal contact resistance" between solid surfaces and the non-wetting liquid metals, mercury and lead-bismuth. There is still considerable uncertainty concerning the value of this resistance, and the relative contribution of the scale or oxide film is not clearly understood; apparently, the addition of wetting or gettering agents increases the heat-transfer coefficients of these non-wetting liquid metals.

Several cooling runs have been made with sodium flowing down inside vertical tubes.²³

*A definition of all nomenclature as well as references on the theory of liquid-metal heat transfer are given at the end of this chapter.

Table 2.3.1 — Heat-transfer Correlations for Liquid Metals

Duct	Type of flow	Thermal conditions	E_H	Correlation	Based on		Estimated accuracy	Reference
					Theory	Exp.		
Pipe	Turbulent	Constant q	Equal to E_M	$Nu = 7 + 0.025(Pe)^{0.8}$	x	x	Very good (see text)	(1)(2)
Pipe	Turbulent	Constant t_w	Equal to E_M	$Nu = 4.8 + 0.025(Pe)^{0.8}$	x		Good	(3)
Shell side (unbaffled)	Turbulent	$Nu = 61.2(Pe(A_p/A_H)^{1/4})^{0.8}$ (both Nu and Pe based on tube D)	x		Good	(4)
Parallel plates	Turbulent	Heat through one plate	Equal to E_M	$Nu = 5.8 + 0.02(Pe)^{0.8}$ (based on $D_e = 2d$)	x		Good	(5)(6)
Parallel plates	Turbulent	Heat through both plates with each at same temperature	Equal to E_M	$Nu = 10.5 + 0.036(Pe)^{0.8}$ (based on $D_e = 2d$)	x		Good	Derived from Seban, ⁵ this reference also suggests a method for determining Q 's, h 's, and t 's with heat flow through both plates when at different temperatures
Annuli	Turbulent	Constant q through inner wall—outer wall insulated	Equal to E_M	For $D_o/D_i < 1.4$, use flat-plate correlations $Nu = (5.25 + 0.0175 Pe)(D_o/D_i)^{0.38}$ (Nu and Pe based on $D_e = D_o - D_i$)	x		Good	(7)
		$Nu = .80 Pe^{0.5}$			Fair	(9)
		Constant q	0	$Nu = 4.36$			Unknown	(10)(11)
		Constant t_w	0	$Nu_s = 1.615(Pe)^{1/4} (D/x)^{1/4}$ for $Pe (D/x) > 10$ based on $\Delta t_s = t_w - (t_1 + t_2/2)$			Unknown	(12)
Cross flow to cylinders	Turbulent	Constant q	0	$Nu = 6$ (based on $\Delta t_m = t_{mw} - t_m$ and $D_e = 2ab/a + b$)			Unknown	(12)
Pipe	Laminar	Constant q	0	$\Delta t_{corner} = q/12 \text{ kL to } t_m$			Unknown	(12)
Pipe	Laminar	Constant t_w	0	$Nu = 4$ (based on $\Delta t_m = t_{mw} - t_m$ and $D_e = 2a/3$)			Unknown	(12)
Rectangular cross section	Slug	Constant q	0	$\Delta t_{corner} = q/4 \sqrt{3KL} \text{ to } t_m$			Unknown	(12)
Triangular cross section	Slug	Constant q	0	$Nu = 3$ (based on $\Delta t_m = t_{mw} - t_m$ and $D_e = 0.637a$)			Unknown	(12)
Right-triangular cross section	Slug	Constant q	0	$\Delta t_{45^\circ \text{ corner}} = 0.236q/\text{kL to } t_m$			Unknown	(12)
Natural convection from horizontal cylinders	Laminar	$Nu = 0.53 [Pr/0.952 + Pr]^{1/4} (Gr \cdot Pr)^{1/4}$			$\pm 10\%$	(13)(14)

⁵ References appear at end of chapter

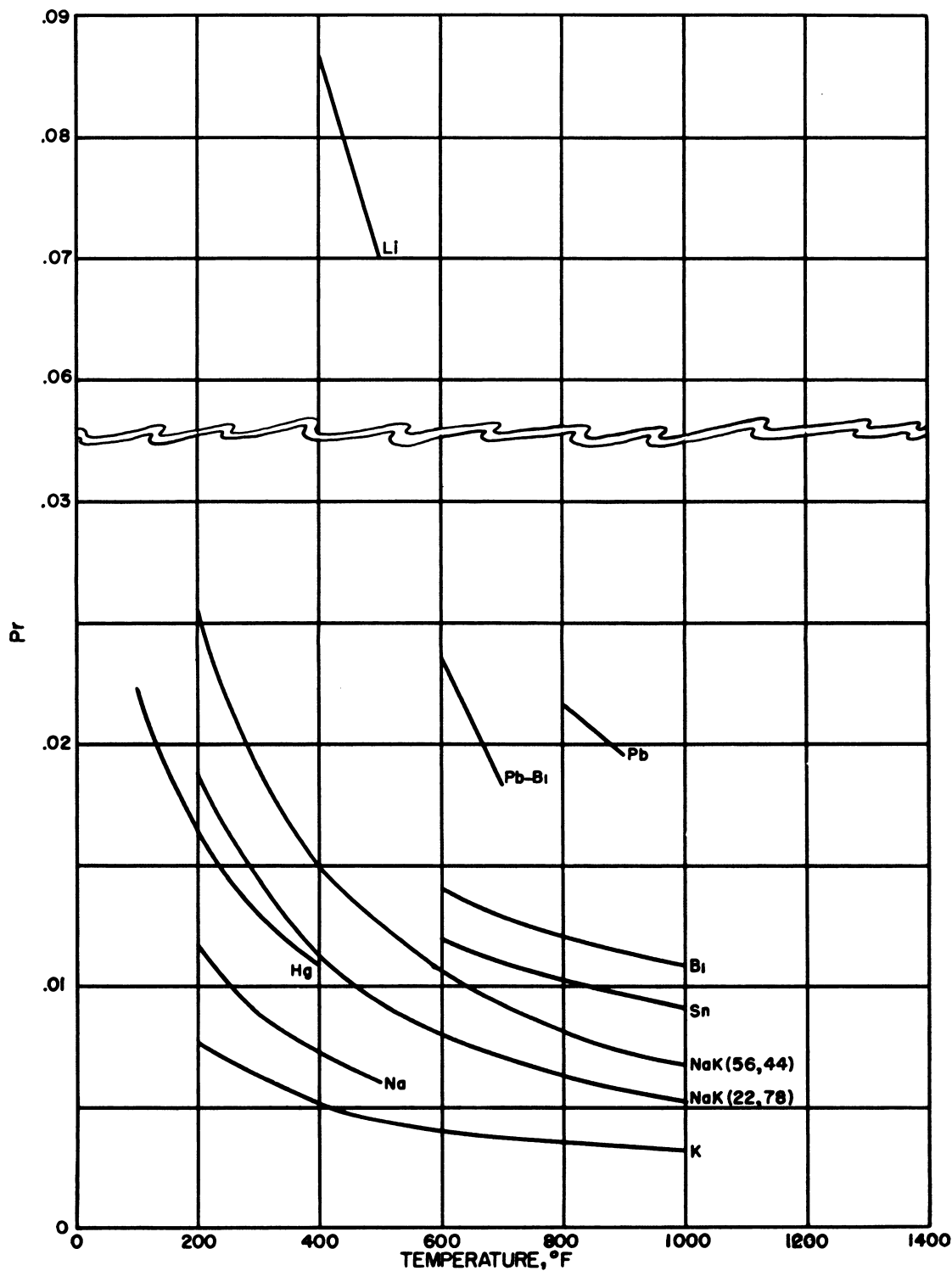


Fig. 2.3.1 — Prandtl Number as a Function of Temperature for Various Liquid Metals. Submitted by KAPL, Aug. 15, 1952.

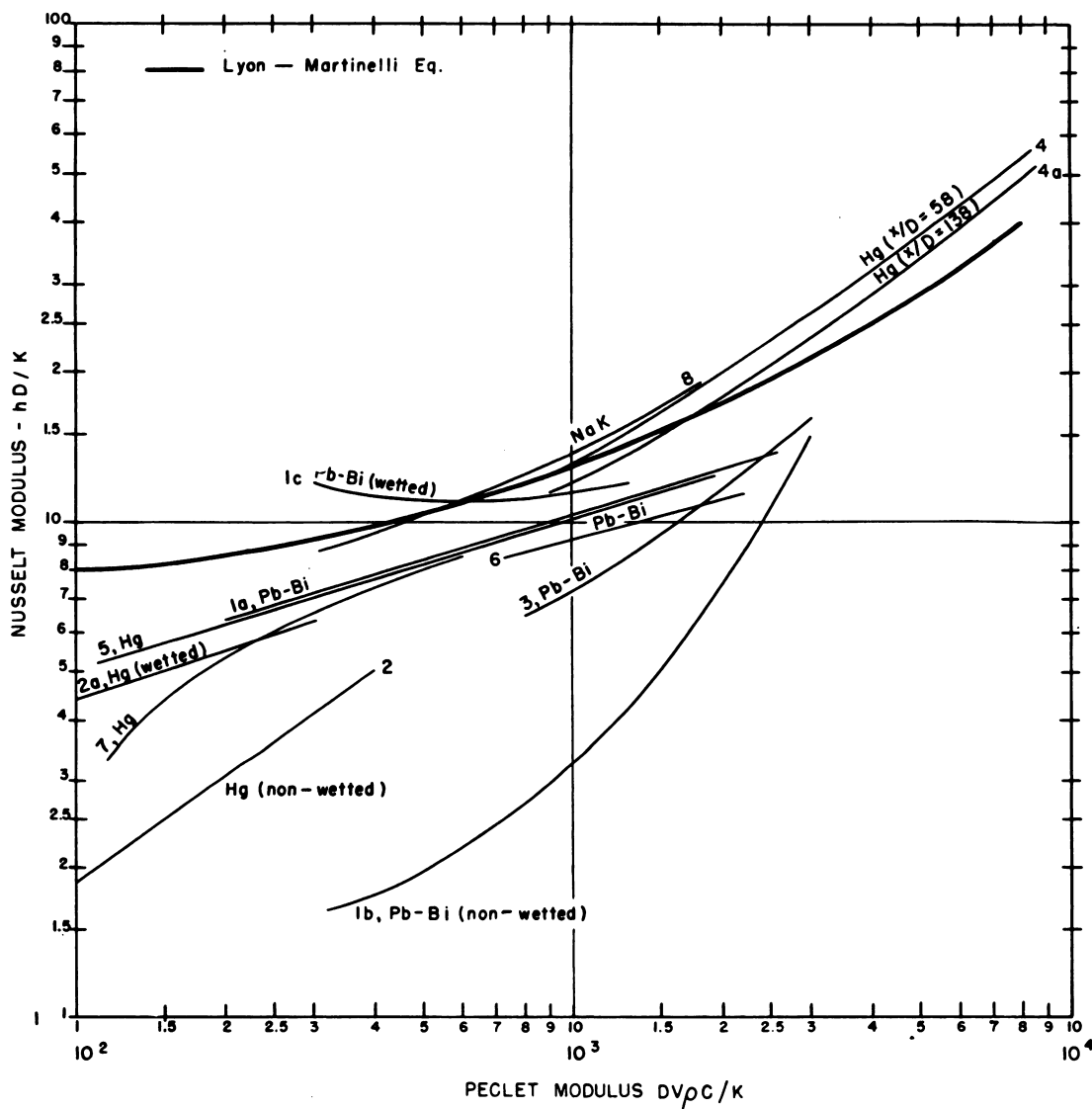


Fig. 2.3.2 — Nusselt Numbers for Turbulent Flow Inside Tubes. Reprinted from Liquid-Metals Handbook, Chapter 5, R. N. Lyon and H. F. Poppendiek, June 1952. Legend: 1a = Ref. (15); 1b = Ref. (15); 1c = Ref. (15); 2a = Ref. (16); 2b = Ref. (16); 3 = Ref. (17); 4a = Ref. (18); 4b = Ref. (18); 5 = Ref. (19); 6 = Ref. (20); 7 = Ref. (21); and 8 = Ref. (22).

The heat transfer coefficients at low velocities were considerably higher than those for similar tubes in the horizontal position. This effect is thought to result from the increased velocity of the cooler, heavier fluid descending near the wall, compared with that of the main body of the fluid.

FLOW THROUGH HEAT-EXCHANGER SHELLS

Calculated values from the correlation given in Table 2.3.1 are plotted in Fig. 2.3.3 along with experimental points. This equation is based on a series of tests with a horizontal shell-and-tube heat exchanger and two horizontal shell-and-tube evaporators. In each case, NaK flowed parallel to the tubes through an un baffled shell. The heat-exchanger tubes were $\frac{5}{8}$ -in. OD* and those of the evaporator $1\frac{3}{4}$ -in. OD* while the shells were about 1 ft in diameter.

An equation suggested by Donohue²⁴ has been used successfully by Tidball²⁵ to correlate his data for small, baffled exchangers ($\frac{1}{8}$ -in.-OD tubes and 0.87-in.-ID shell).

FLOW THROUGH NONCIRCULAR DUCTS

Table 2.3.1 includes several correlations for slug flow in noncircular ducts with heat transferred only by conduction. In the original reference, Claiborne also gives solutions for ducts with elliptical and circular cross sections. He concludes that slug flow solutions approximate liquid metal systems with $Pe \leq 100$.

Eckert and Low²⁶ have calculated temperature distributions in the fluid and in the walls of heat exchangers consisting of staggered series of rectangular or triangular passages. Their solutions are based on velocity profiles experimentally determined by Nikuradse and on the assumption of negligible eddy diffusivity of heat.

NATURAL CONVECTION

Figure 2.3.4 shows Eckert's theoretical curve for natural convection from a horizontal cylinder; the trends shown by the experimental data of Bonilla and co-workers are also shown. Lead-bismuth eutectic, lead, bismuth, sodium, and NaK were studied using tubes ranging from $\frac{1}{4}$ to $1\frac{1}{2}$ in. in diameter. Bonilla's results suggest that at high heat flow rates a turbulence develops around the tube with values of Nu larger than would be predicted from Eckert's theory. In tests with mercury under wetting and non-wetting conditions, no change was noted in the heat-transfer coefficient.

When a fluid having a fully developed velocity distribution enters a region the walls of which possess a new temperature distribution, the heat-transfer coefficient and boundary layer thickness adjust themselves to values characteristic of the new distribution. The distance which the fluid must flow before the coefficient and boundary layer thickness are within 1 percent of their final values is the "thermal entry length." Figure 2.3.5 shows how the average Nusselt number varies with Pe (D/x) for parabolic- and uniform-velocity profiles. These curves were determined from the Graetz^{10,11,13,14} theory which neglects the variation in fluid properties with temperature. Poppendiek^{27,28} has calculated point heat-transfer coefficients for Pe (D/x) above 1000 for turbulent flow with a velocity profile based on the $\frac{1}{4}$ power law. Heat transfer was assumed to occur by conduction alone, although a method is proposed for extending the conduction solutions to cases where the eddy diffusivity is small but not negligible.

*This includes an annulus for static liquid metal.

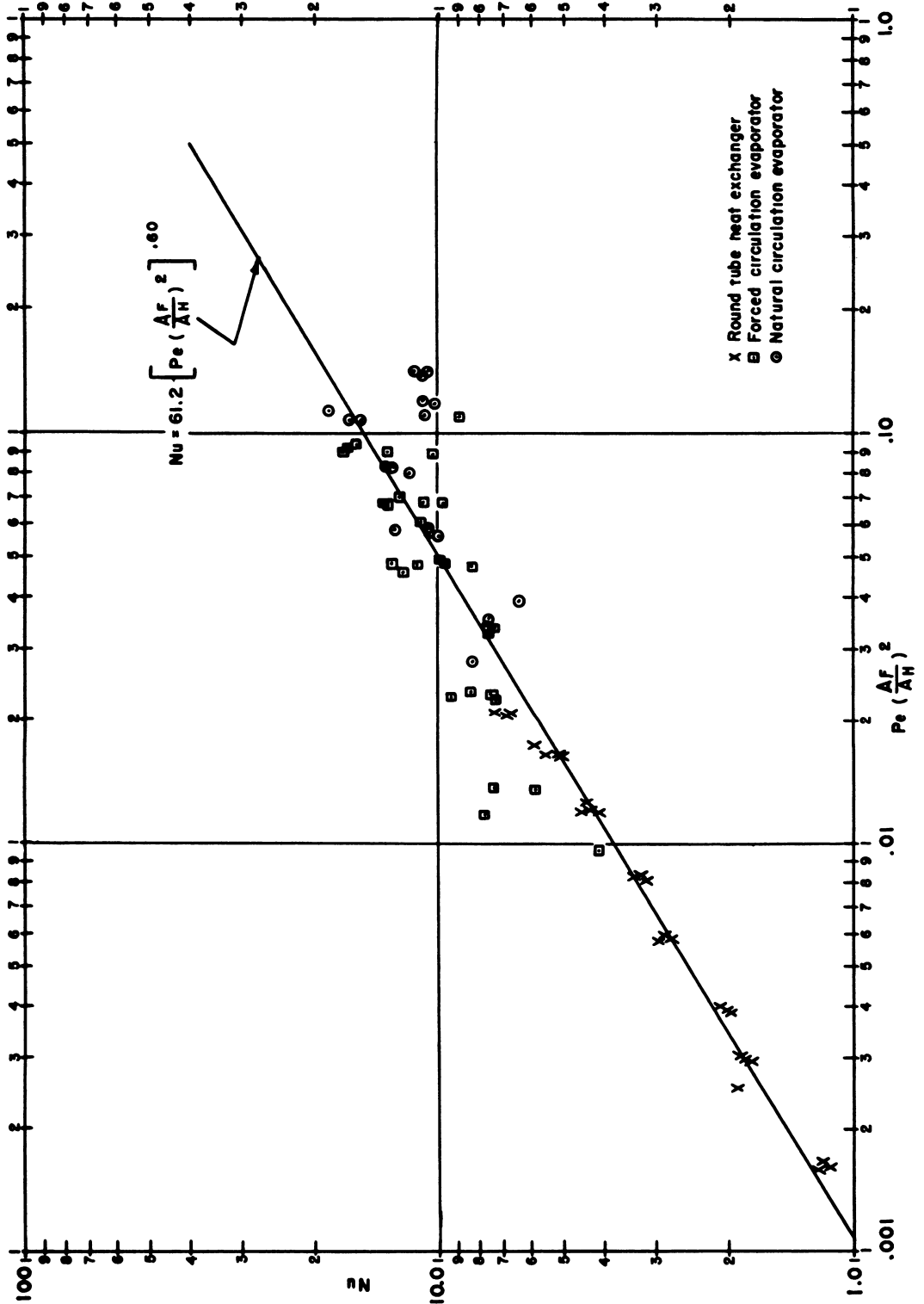


Fig. 2.3.3—Nusselt Numbers for Natural Convection from a Horizontal Cylinder. Submitted by KAPL, Aug. 15, 1952.

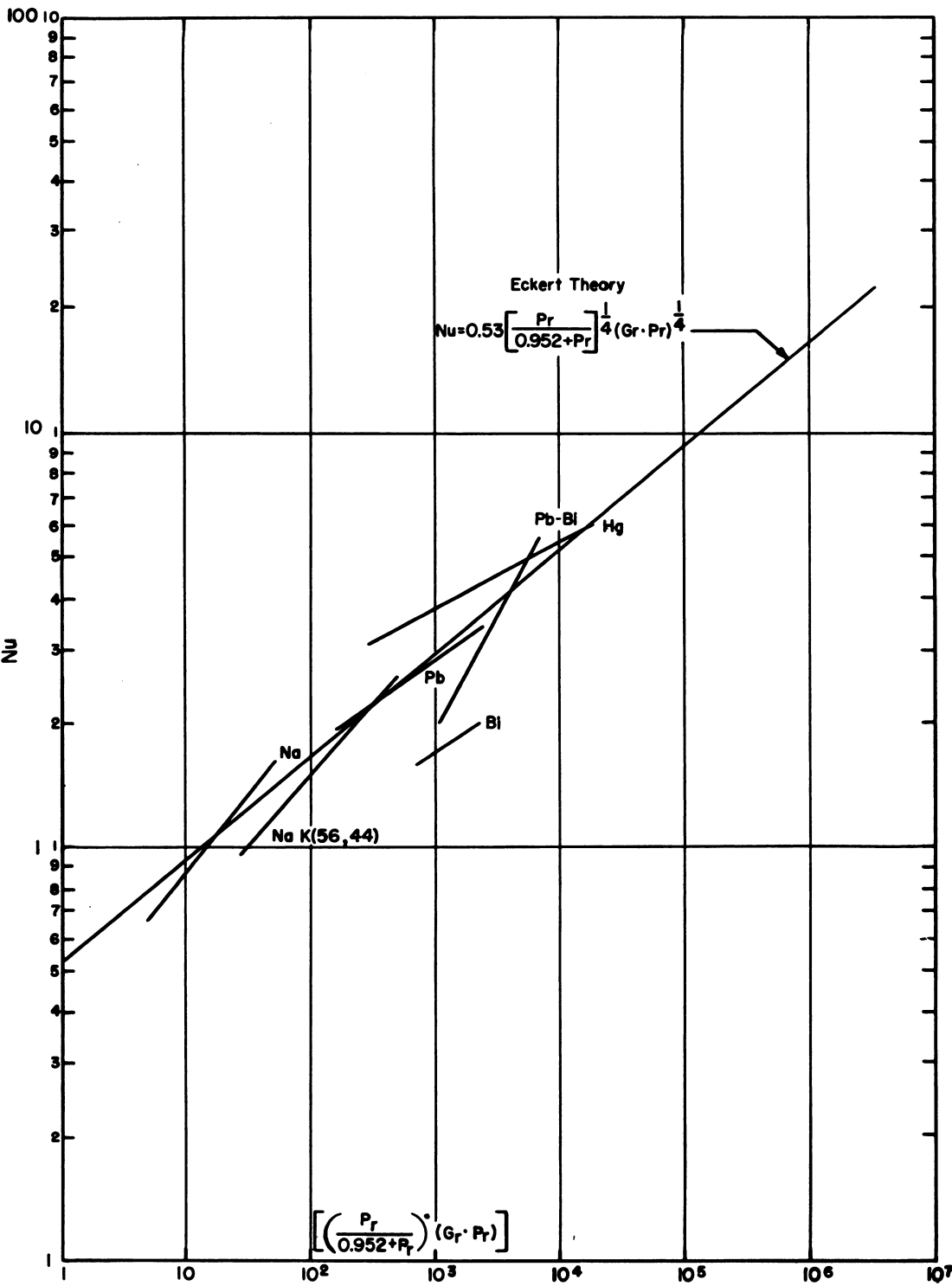


Fig. 2.3.4— Nusselt Numbers for Natural Convection from a Horizontal Cylinder. Submitted by KAPL, Aug. 15, 1952.

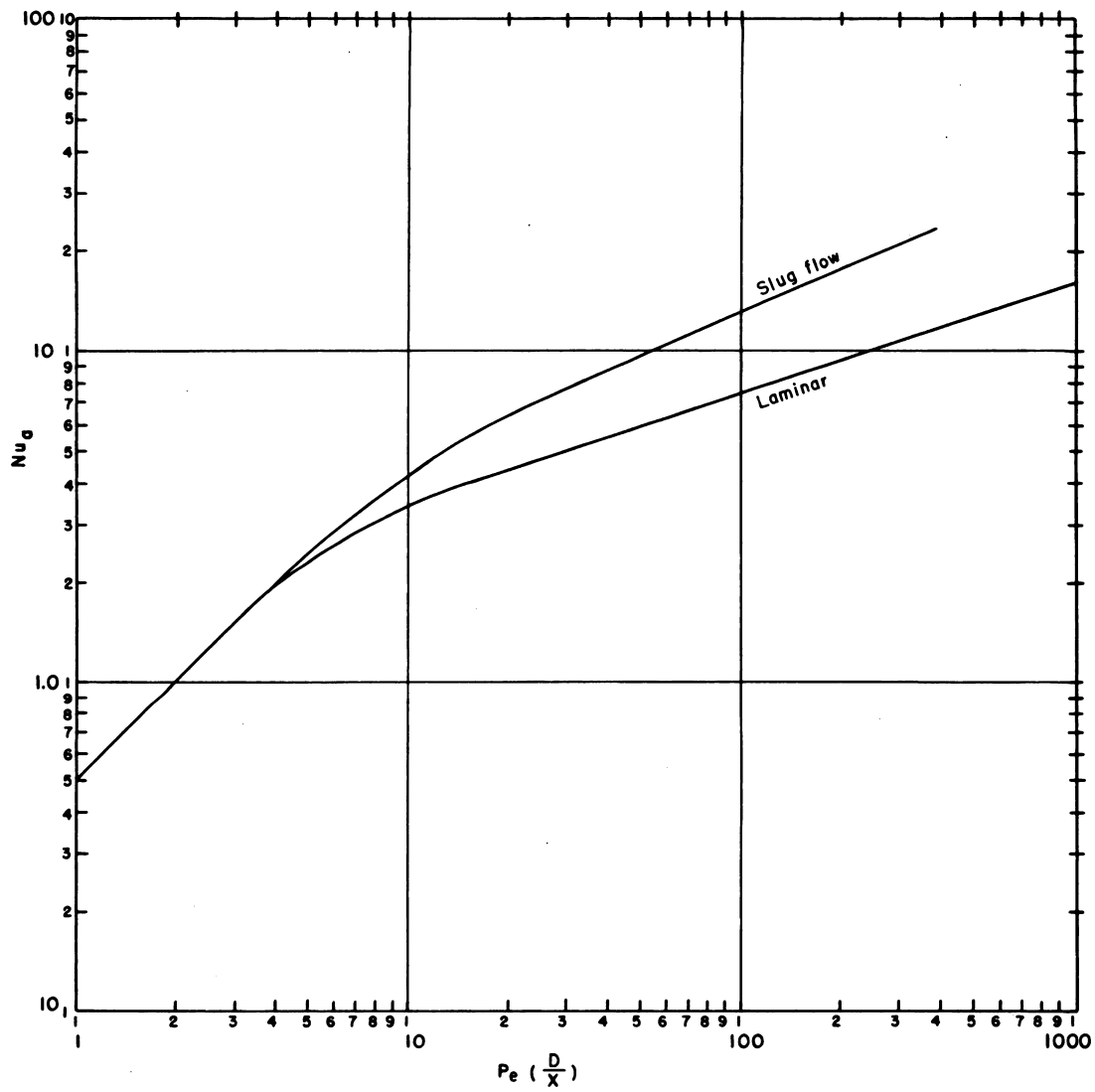


Fig. 2.3.5—Nusselt Numbers for Thermal Entry Regions. Submitted by KAPL, Aug. 15, 1952.

NOMENCLATURE

- Gr = Grashof number, $\frac{D^3 \rho^2 g \beta t}{\mu^2}$
- Nu = Nusselt number, hD/k
- Nu_a = Nusselt number based on average temperature difference, $t = t_w - \frac{t_2 + t_1}{2}$
- Pe = Peclet number, $DV\rho c/k$
- Pr = Prandtl number, $C\mu/k$
- a = Side of rectangle or triangle, ft
- b = Side of rectangle, ft
- A_F = Flow area in shell of exchanger, parallel to tube axis
- A_H = Area for heat transfer based on outside diameter of tubes
- β = Coefficient of volumetric expansion, $1/^\circ\text{F}$
- c = Specific heat, $\text{Btu}/(\text{lb})(^\circ\text{F})$
- d = Distance between parallel plates, ft
- D = Diameter, ft
- D_e = Equivalent diameter = $D_o - D_i$ for annulus, ft
- D_i = Inner diameter of annulus, ft
- D_o = Outer diameter of annulus, ft
- E_H = Eddy diffusivity of heat, $\text{K}/c\rho$
- E_M = Eddy diffusivity of momentum, μ/ρ
- g = Acceleration due to gravity, ft/sec^2
- h = Heat-transfer coefficient, $\text{Btu}/(\text{hr})(\text{ft})^2(^\circ\text{F})$
- k = Thermal conductivity, $\text{Btu}/(\text{hr})(\text{ft})(^\circ\text{F})$
- L = Duct length, ft
- μ = Viscosity, $\text{lb}/(\text{hr})(\text{ft})$
- V = Velocity, ft/hr
- q = Heat flux, $\text{Btu}/(\text{ft})^2(\text{hr})$
- ρ = Density, lb/ft^3
- Δt = Temperature difference, $^\circ\text{F}$
- t_m = Mean temperature, $^\circ\text{F}$
- t_w = Wall temperature, $^\circ\text{F}$
- t_{wm} = Mean wall temperature, $^\circ\text{F}$
- t_1 = Initial temperature of fluid, $^\circ\text{F}$
- t_2 = Final temperature of fluid, $^\circ\text{F}$
- x = Distance from duct entrance, ft

REFERENCES

1. R. C. Martinelli, Heat Transfer to Molten Metals, TASME 69, 1947, p 947.
2. R. N. Lyon, Liquid Metal Heat Transfer Coefficients, Chem. Eng. Progr. 47 (2), 1951, p 75.
3. R. A. Seban and T. Shimazaki, Heat Transfer to a Fluid Flowing Turbulently in a Smooth Pipe with Walls at Constant Temperature, Contract N7-onr-29523, Phase (2), Project NR35324, Univ. of Calif., Berkeley, Calif., 1949.
4. R. D. Brooks and A. L. Rosenblatt, Design and Performance of Liquid Metal Heat Exchangers and Steam Generators for Nuclear Power Plants, Preprint of paper to be published in TASME, 1952.
5. R. A. Seban, Heat Transfer to a Fluid Flowing Turbulently Between Parallel Walls with Asymmetric Wall Temperatures, TASME 72, 1950, p 789.
6. W. B. Harrison and J. R. Menke, Heat Transfer to Liquid Metals Flowing in Asymmetrically Heated Channels, TASME 71, 1949, p 797.
7. R. V. Bailey, Heat Transfer to Liquid Metals in Concentric Annuli, ORNL-521, June 13, 1950, 45 pp.
8. R. N. Lyon, Liquid Metals Handbook, 2d ed., Chap. 6, June 1952.
9. R. C. Martinelli, unpublished notes, Aug. 10, 1948.
10. R. H. Norris and D. D. Streid, Laminar Flow Heat Transfer Coefficients for Ducts, TASME 62, 1940, p 525.

11. T. B. Drew, *Mathematical Attacks on Forced Convection Problems: A Review*, *TAICHÉ* 26, 1931, p 26.
12. H. C. Claiborne, *Heat Transfer in Non-circular Ducts*, ORNL-985, May 14, 1951, 43 pp.
13. S. C. Hyman, C. F. Bonilla, and S. W. Ehrlich, *Natural Convection Transfer Processes*, *Preprints of Papers for Heat Transfer Symposium*, *AIChE*, Dec. 1951.
14. E. R. G. Eckert, *Introduction to the Transfer of Heat and Mass*, 1st ed., McGraw-Hill Book Co., New York, p 158.
15. H. A. Johnson, J. P. Hartnett, W. J. Clabaugh, *Heat Transfer to Molten Lead-Bismuth Eutectic in Turbulent Pipe Flow*, *Preprints of Papers, Heat Transfer and Fluid Mech. Inst., UCLA*, June 1952.
16. T. C. Doody and A. H. Younger, *Heat Transfer Coefficients for Liquid Mercury in Forced Convection*, *Preprints for Heat Transfer Symposium*, 44th Ann. Mtg., *AIChE*, Dec. 1951.
17. B. Lubarsky, *Experimental Investigation of Forced Convection Heat Transfer Characteristics of Lead-Bismuth Eutectic*, *NACA-E51G02*, Sept. 20, 1951.
18. S. E. Isakoff and T. B. Drew, *Heat and Momentum Transfer in Turbulent Flow of Mercury*, *Preprints for Heat Transfer Discussions*, London, England, 1951.
19. L. M. Trefethen, *Heat Transfer Properties of Liquid Metals*, ORNL, NP-1788, July 1950.
20. R. A. Seban, *Heat Transfer Measurements in Lead-Bismuth Eutectic in Turbulent Pipe Flow*, Contract N7-onr-29523, Phase (2), Project NR35324, Univ. of Calif., Berkeley, Calif., June 15, 1950.
21. *Heat Transfer Properties of Mercury*, *At. Energy Res. Est., Min. of Sup.*, Harwell, Berks, June 1950.
22. R. C. Werner, E. C. King, and R. A. Tidball, *Heat Transfer with Sodium-Potassium Liquid Alloys*, presented at Ann. Mtg. *AIChE*, Pittsburgh, Pa., Dec. 1949.
23. R. D. Brooks and A. L. Rosenblatt, *Design and Performance of Liquid Metal Heat Exchangers and Steam Generators for Nuclear Power Plants*, *Mech. Eng.*, 75: 363-368, May 1953.
24. D.A. Donohue, *Heat Transfer and Pressure Drop in Heat Exchangers*, *IEC* 41, 1949, p 2499.
25. R. A. Tidball, *Performance of Small Liquid Metal Heat Exchangers*, *Preprints of Papers for AIChE Heat Transfer Symposium* Dec. 5, 1952, p 199.
26. E. R. G. Eckert and G. M. Low, *Temperature Distribution in Internally Heated Walls of Heat Exchanger with Noncircular Flow Passages Using Coolants with Very Low Prandtl Number*, *Nat. Adv. Com. for Aer.*, *NaCa TN-2401*, Wash., July 1951.
27. H. F. Poppendiek, *Forced Convection Heat Transfer in Thermal Entrance Region, Parts I and II*, ORNL-913, May 20, 1952, 29 pp.
28. H. F. Poppendiek, *Forced Convection Heat Transfer in Thermal Entrance Region, Parts I and II*, *Ibid.*, ORNL-914, June 11, 1952, 22 pp.

SELECTED READING LIST

THEORETICAL PAPERS

- LIQUID-METALS HANDBOOK*, Chapter 6, R. N. Lyon, Department of the Navy and U. S. Atomic Energy Commission, 2d Edition, June 1952.
- HEAT TRANSFER TO MERCURY*, D. L. R. Bailey, W. F. Cope, G. G. Watson, *Heat Div. Paper No. 13*, ME Res. Lab., East Kilbride, Glasgow, July 1952.
- LIQUID METAL HEAT TRANSFER COEFFICIENTS*, R. N. Lyon, *TAICHÉ* 47, 1951, p 75.
- A PRELIMINARY INVESTIGATION OF THE ANALOGY OF TRANSFER OF VORTICITY TO THE TRANSFER OF HEAT FLUIDS OF LOW PRANDTL NUMBER*, R. G. Kennison, Jr., MS Thesis, RPI, May 25, 1950.
- HEAT TRANSFER PROPERTIES OF LIQUID METALS*, Oak Ridge Nat. Lab., L. M. Trefethen, NP-1788, July 1950.
- HEAT TRANSFER TO MOLTEN METALS*, R. C. Martinelli, *TASME*, 69, 1947, p 947.

Handling of Liquid-metal Coolants

W. H. Bruggeman and H. E. Stone

The principal handling problems encountered when liquid metals are used as reactor coolants are the results of corrosion, extreme chemical activity (particularly in the case of alkali metals), and induced radioactivity. Radioactive damage to the coolant does not occur since the liquid metals are monatomic.

PURIFICATION OF ALKALI METALS AND INERT BLANKET GASES

(W. H. Bruggeman)

Purity requirements and purification techniques for liquid-metal reactor coolants are well established only for sodium and NaK. Although it is reasonable to believe that many of these purification techniques are applicable to lithium, purification of this coolant is complicated by the necessity to remove corrosive Li_3N . Purification techniques for lead, lead-bismuth, and gallium have not been developed sufficiently to warrant detailed discussion at this time.

Metallic sodium is produced by the electrolytic decomposition of NaCl in the presence of CaCl_2 . The metal thus produced is filtered at the melting point to reduce the calcium content to 0.04 percent and to remove chlorides. Although most experience has been obtained with DuPont sodium, check analysis of the National Distillers' product indicates that its impurity content is comparable. As a commercial-grade product, metallic sodium is unusually pure.

The Mine Safety Appliances Company produces NaK by the high-temperature reaction of sodium with potassium chloride. The excess chloride is removed by filtration, and the resulting NaK is distilled to enrich the potassium content. As a result of the distillation step, NaK is generally somewhat lower in high-boiling impurities and, since it is packaged under inert gas, is less contaminated with oxides than sodium.

Table 2.4.1 shows the average impurities content of DuPont sodium and the NaK charge of the Experimental Breeder Reactor. These analyses do not include oxygen values which vary as a result of contamination by atmospheric oxygen.

THE EFFECT OF SPECIFIC IMPURITIES IN SODIUM AND NaK

NUCLEAR POISONS

On the basis of the average impurities content shown in Table 2.4.1 and assuming the total rare-earth content to be gadolinium, the impurities contribute less than $\frac{1}{2}$ percent to the thermal cross section of pure sodium. Nuclear poisons not shown in the sodium assay are not expected to be present in sufficient quantity to appreciably alter this figure. Because commercially available sodium and NaK have a minimum of high-cross-section impurities, removal of these impurities is not required.

IMPURITIES WHICH ACTIVATE

Trace impurities in sodium, however, cause a certain amount of contaminant activity to build up. For example, a test sample of commercial sodium was irradiated in a neutron flux for 30 days. After the sodium activity had decayed to 10^{-6} of its initial value, an impurity gamma-activity appeared with a half-life of about 50 days. This relatively long-lived residual activity indicates that systems must be designed so that they may be completely drained to allow accessibility for maintenance.

Table 2.4.1—Impurities in Commercial Sodium and NaK

Impurity	Average analysis of core of DuPont brick sodium, ppm	Analysis of MSA NaK in EBR primary circuit, ppm
Al	1.7	3.0
B	2	1
Bi	<1	
Ba	2	2
C	40	
Ca	350	30
Cd	<1	<1
Cl	190	15
Co	<1	<1
Cr	<1	<1
Cs	2	1
Cu	<1	5
Fe	0.5	2
Hg	2	<2
K	150	(77.7%)
Li	67	235
Mn	<1	<1
Ni	<1	<1
P	11	20
Pb	<1	4.8
S	35	34
Si	21	<1
Total rare- earth elements	<0.5	

HYDROGEN MODERATION

The presence of hydrogen in the coolant of an epithermal reactor system might cause excess reactivity as a result of moderation. The hydrogen content of brick sodium is generally about 0.006 weight-percent.* In addition, hydrogen (as NaH) can form in the coolant by contact with impurities in the inert blanket gases or (as NaOH) by contact with water. Little is known regarding the solubility of NaOH or NaH in sodium; however, the removal of hydrogen is relatively simple owing to the decomposition of NaH and NaOH at high temperatures. Excess hydrogen can be satisfactorily removed by heating the liquid to 800°–900°F under a vacuum or inert-gas purge.

*Analytical procedure by Pepkowitz and Proud.¹

¹References appear at end of chapter.

IMPURITIES AFFECTING CORROSION

The corrosion of structural materials by sodium and NaK is discussed later. In general, oxygen, carbon, and (to a lesser extent) calcium are important.

Oxygen

The reaction of sodium with oxygen yields the monoxide, Na_2O , which is extremely corrosive when pure. For temperatures up to 1000°F , sodium containing up to 0.02 weight-percent O_2 causes negligible corrosion with stainless steels. A more serious effect, however, is plugging of the system owing to the low solubility of Na_2O in Na.

Carbon

Additions of carbon to sodium result in carburization of the stainless-steel surfaces, but little work has been done on the behavior of carbon in sodium and on possible methods of removal. Carburization has not been observed with filtered commercial sodium unless carbon compounds were specifically added or unless the sodium was in contact with both carbon steel and stainless steel. In view of this, sodium- and NaK-cooled stainless-steel reactor systems should be designed to prevent carbon or oil additions to the coolant.

Calcium

Nickel forms intermetallic compounds with sodium containing free calcium. This has not been observed when commercial sodium is used (where the bulk of the 0.04 percent Ca is probably oxidized to CaO) or with NaK (where the Ca content is reduced to a low value by distillation). The attack on nickel components would be expected, however, if calcium were used as a getter for Na_2O . At temperatures above 1000°F , calcium-gettered sodium may also attack high-nickel alloys.

PLUGGING CAUSED BY ALKALI OXIDE

The solubility of Na_2O in sodium² and NaK³ is shown in Fig. 2.4.1. (In NaK, the sodium is preferentially oxidized, and apparently the NaK composition does not govern the solubility.) Figure 2.4.1 illustrates the relatively low solubility of oxide in alkali metal as well as the positive solubility coefficient and can be used to determine the amount of insoluble oxide in a system when the oxygen concentration, system temperature, and system volume are known.

Plugging can take place wherever insoluble alkali oxide is present. The mechanism is a combination of diffusion of oxide to cold walls, where deposition occurs, and of precipitation in the main fluid stream with subsequent crystal growth in cold restricted passages. The plugs are composed of a mixture of approximately 20 weight-percent Na_2O and 80 weight-percent sodium; thus, a relatively large plug can form with a small amount of insoluble oxide.

The amount of oxygen which will cause plugging in a given system depends on many factors. The volume of sodium or NaK in the system is important since a small percentage of insoluble oxide in a large sodium charge may be sufficient to plug small passages. In general, all cold-zone passages less than 0.5 in. in diameter should be considered as possible regions of plugging.

In view of the uncertainties regarding plugging, the only guarantee of protection is to operate with an oxide content below saturation at the lowest operating temperature. Since this may involve special precautions in applying the handling and purification techniques described herein, this criterion should be adopted only when necessary. Systems where some plugging is not serious do not require such stringent purity specifications.

Certain design features will minimize plugging if the oxide concentration should unavoid-

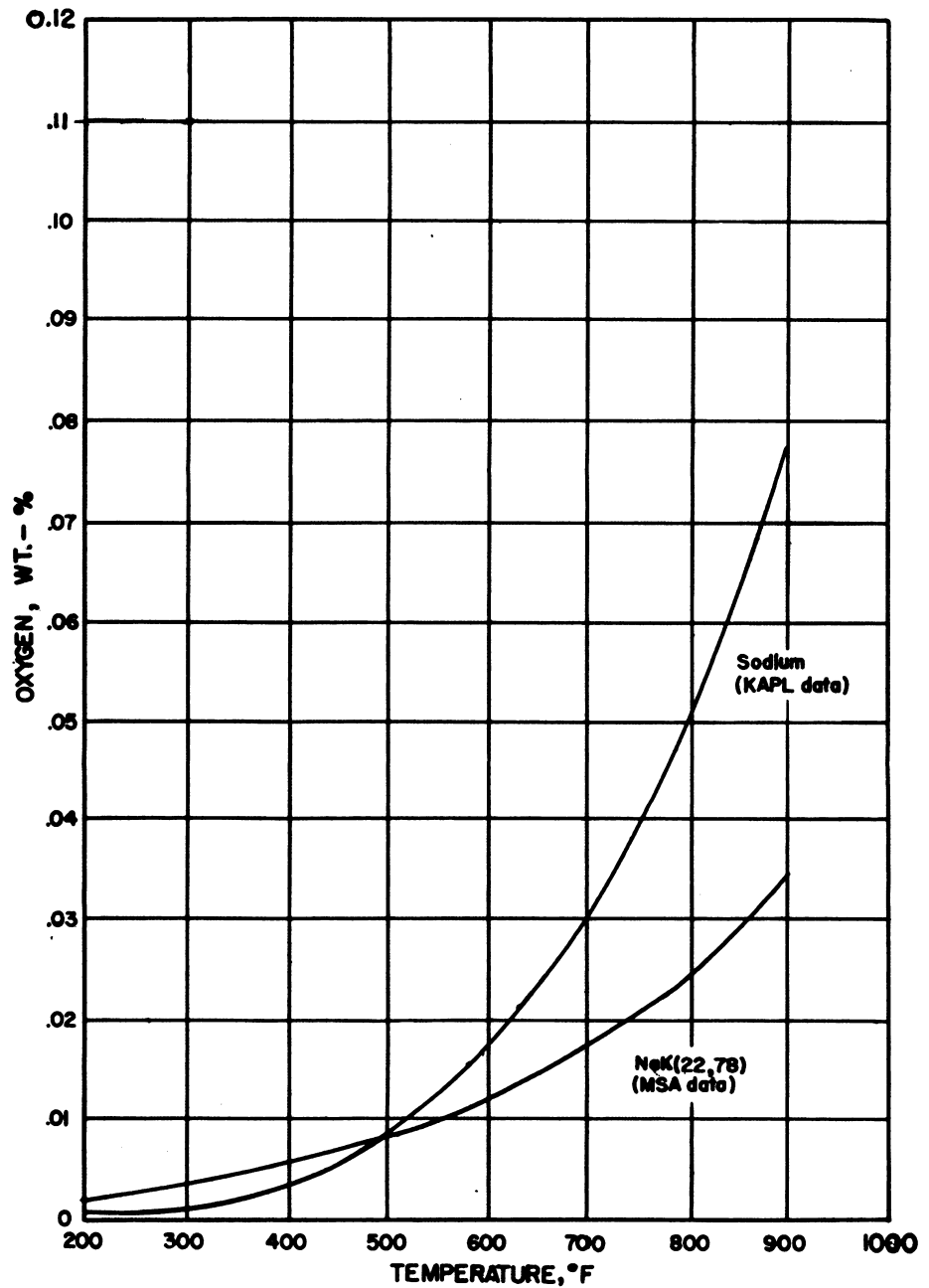


Fig. 2.4.1 — Oxygen Solubility in Sodium and NaK (22 : 78) as a Function of Temperature. Submitted by the Knolls Atomic Power Laboratory, Sept. 5, 1952.

ably rise above the desired limit. Included in these features are a minimum of restricted passages and the location of necessary restricted passages (streamlined, if possible) in warm zones. Cold stub ends should have a low temperature gradient per unit length and should be placed vertically to minimize oxide accumulation.

PURIFICATION OF LIQUID SODIUM AND NaK

Sodium is commercially available in 1-lb, $2\frac{1}{2}$ -lb, or $12\frac{1}{2}$ -lb bricks or, for very large quantities, cast in rail tankcars. The usual specification to which the sodium is sold is 0.04 percent calcium and 0.005 percent Cl, maximum. Variation of other trace impurities from those values given in Table 2.4.1 is normally quite small. To avoid the possibility of carburization, brick sodium should be purchased "dry mold," that is, without kerosene which is used as a mold release agent in the casting process.

MELT STATION

Brick sodium should be liquefied in a melt tank and pressured through a metallic filter element into the reactor system or the reactor system storage tank. Because of the accumulation of oxide from the brick crust, the melt tank should be designed for convenient cleaning. This can be accomplished by providing a large opening in the top (to vent H_2 from the sodium-water reaction) and by designing the unit to be relatively portable.

At KAPL, the filters used have been made of sintered stainless steel with an average porosity of 10 microns (similar to those supplied by the Micro-Metallic Corp.). On occasion, a 5-micron filter is used in series with the first filter, although the necessity for this has not been established. It should be possible to process about 500 lb of brick sodium per cubic foot of melt-tank volume before it is necessary to remove the excess oxide dross from the melt tank. The sintered metal filter tends to crack if sodium is frozen and remelted in the pores.

The throughput of the 10-micron metal filter varies as the filter cake builds up. An average throughput, however, at $230^\circ F$ and 15-psi differential pressure is 5 lb of Na/(min)(ft).² This melting and filtration (several degrees above the melting point) will remove the bulk of the alkali oxide and any additional insoluble material.

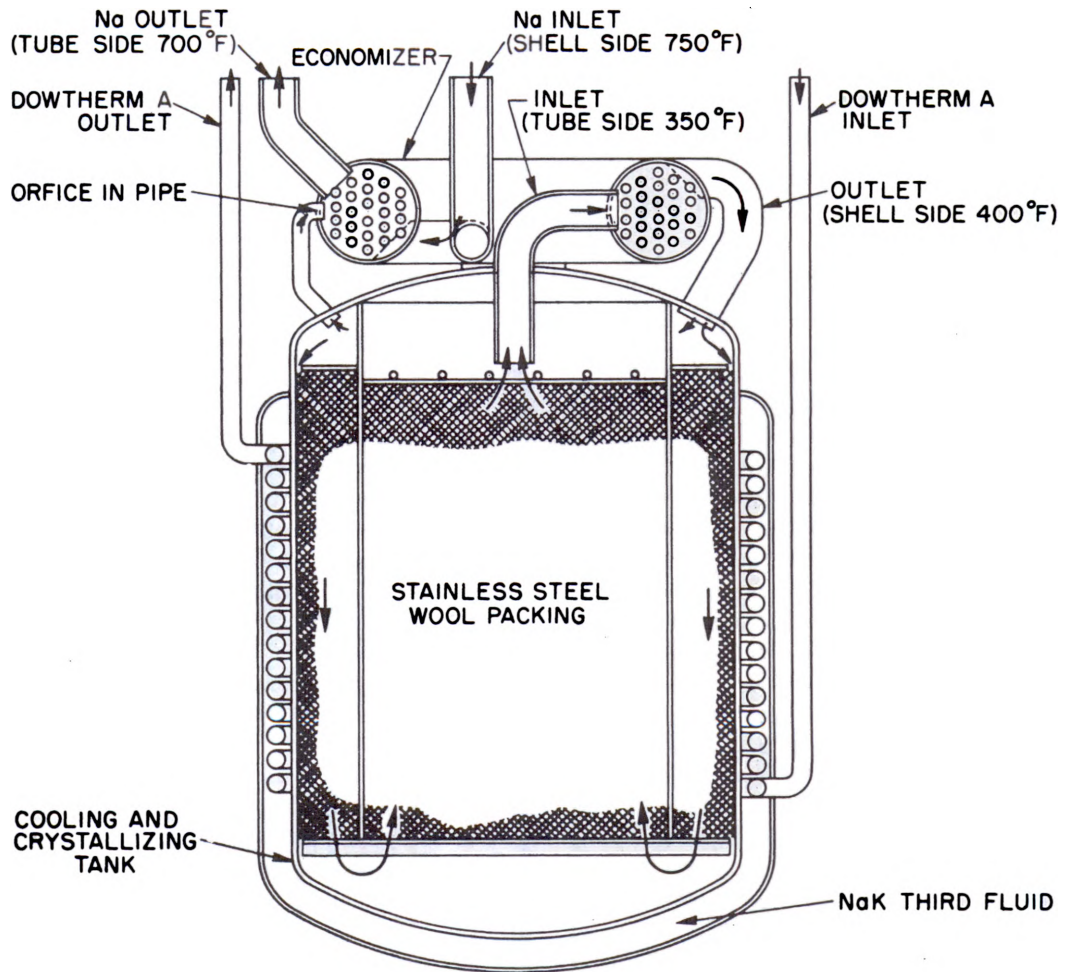
NaK is supplied by the Mine Safety Appliances Company in 230-lb containers. The specification on freezing point can be met to within $1^\circ F$. Since this material is shipped under inert gas, less oxide is present, and since the alloy is liquid at room temperature, no melting equipment is required. A sintered metal filter should be used between the shipping container and the vessel being filled.

OXYGEN-REMOVAL EQUIPMENT

Although the melt-station equipment can supply low-oxide sodium, periodic repurification of the coolant is necessary to remove oxide during system operation. Such repurification is required because it is impractical to remove all traces of H_2O and O_2 from a system prior to filling, because atmospheric oxygen tends to enter a reactor system during refueling or repair, and because of trace oxygen contaminants in the inert-gas blanket.

In addition to purifying the sodium or NaK charge, it is important that the entire system be thoroughly cleaned. Merely purifying the charge or introducing a fresh batch into contaminated equipment does not assure adequate purity in the circulating system. The most satisfactory method of cleaning both the system and the liquid metal is to purify a by-pass flow of the coolant while the system is maintained at an elevated temperature so that the oxide solubility is high. This may be accomplished by use of a "cold trap," for example, the Test Cold Trap (Fig. 2.4.2), which operates as follows:

The system is heated to $600^\circ - 750^\circ F$ to dissolve precipitated oxide, and a by-pass coolant flow of 20 gpm is removed from the system either by pump or by means of a system pres-



APPROXIMATE OVERALL DIMENSIONS (UNINSULATED AND UNSHIELDED) 4 X 3 FT. DIA.

Fig. 2.4.2—Test Cold Trap. Submitted by the Knolls Atomic Power Laboratory, Sept. 5, 1952.

sure differential. This hot sodium is cooled to 350°F in a regenerative heat exchanger by the effluent sodium from the cold trap; the "dirty" liquid metal from the system is passed through the shell side of the exchanger to prevent plugging. As a result of the rapid decrease in temperature, large numbers of very small Na_2O crystals are formed.

The sodium next passes to the crystallizing tank where it is cooled to 300°F by Dowtherm cooling coils. This unit is primarily a low-velocity section filled with stainless-steel wool. Here, the crystals of sodium oxide grow and deposit on the steel wool. For residence times of 5 min or more, the cold trap approaches an efficiency of 100 percent; i.e., the discharge is saturated at the temperature of the crystallizing tank.

The oxide capacity of the cold trap is at least 10 weight-percent Na_2O based on crystallizer-tank volume. Although stainless-steel wool of 3-mils fiber-diameter packed to a density of 15 lb/ft³ has been used successfully, knitted-type, stainless wire is recommended. This material, which is similar to York Company packing, is preferred, since there is less tendency for wire-fracture with subsequent introduction of loose ends into the system.

An important consideration for satisfactory operation is the location of the coldest spot in the crystallizing tank. Since the oxide will concentrate at this point, it should not be located at the tank discharge or similar places where oxide deposition may result in plugging.

Cold traps for different systems may have quite different configurations. The Test Cold Trap was designed for intermittent use, for compactness, and for ease of replacement when filled. Continuous units need not operate under such large temperature differences or flow velocities and as a result may not need the economizer. If large oxide capacities are required, the crystallizer volume must be increased. Systems which have a storage tank that operates at lower temperatures than the main fluid and through which a small by-pass is always directed have a build-in cold trap already available. If properly designed, this arrangement is satisfactory even without the steel-wool packing; however, sooner or later the problem of removing the accumulated oxide from this larger vessel must be faced.

SAMPLING AND ANALYSIS OF SODIUM AND NaK

Sampling of alkali metals to analyze for components not present in the atmosphere can be done with such standard apparatus as the thief tube, taking precautions to prevent burning in air. However, sampling for determination of oxygen or other atmospheric components requires special techniques. A device developed at KAPL for this purpose is described by Bruggeman and Billuris.⁴ This instrument is an inert-gas-filled steel box through which is passed a stream of the sodium to be sampled. The temperature of the sampling stream is maintained above that of the liquid metal being sampled to prevent oxide precipitation. Manipulators are attached for transferring sample cups from under the flowing stream into a sample carrier.

The oxide composition of the sample is determined by a modification of the Pepkowitz-Judd mercury-extraction procedure.⁵ The sample is extracted with mercury until no sodium is present in the amalgam discharged from the extraction chamber. The Na_2O which remains behind is dissolved in water and titrated.

INERT-GAS PURIFICATION

Owing to their reactivity, all free sodium or NaK surfaces must be blanketed with inert gas. The gas purity required for this purpose is a function of the volume of gas in contact with liquid metal and the operating time between liquid metal repurifications. In general, however, it is desirable to use the purest gas conveniently available. Argon, nitrogen, and helium have been used as blanket gases. Helium is preferred in reactor systems because it does not become radioactive. The cost of the highest grades of these gases in standard 230-ft³ cylinders is shown in Table 2.4.2.

These gases are generally available in either the lamp grade or high-purity grade to an impurity specification of less than 50 ppm (except for the nitrogen contained in argon). A somewhat lower cost for helium (\$1.30/100 cu ft) can be realized by purchasing the gas directly from the Bureau of Mines in 200,000-SCF rail cars (at 220 psig). The prices do not include shipping or handling charges.

Although Bureau-of-Mines helium is sold only to a method-of-manufacture specification, viz., double-charcoal purified, the impurity content shown in Table 2.4.3 generally can be expected.

Table 2.4.2—Cost of Inert Gases

Gas	\$/100 cu ft
N ₂	1.01
He	4.56
A	11.50

Table 2.4.3—Impurities in Bureau-of-Mines Helium

Impurity	Concentration, ppm
CO ₂	6
A	0.5
H ₂	.3
N ₂	16
CH ₄	0
O ₂	10–20
H ₂ O	5–10

If a transfer compressor is required for handling the gas, a water-lubricated unit supplemented by high-pressure drying with a suitable desiccant is recommended.

For additional removal of oxygen or water vapor, a NaK bubbler can be used. This is a tower packed with stainless-steel wool and filled with NaK. The tower is electrically heated to 500°F to promote the reaction of oxygen and water vapor with the NaK. The bubbler should be supplemented by a vapor trap.

VAPOR TRAPS

One of the problems associated with handling effluent gases from high-temperature, metal-cooled reactors is the entrainment of liquid-metal vapor. In addition to such vent gases carrying radioactivity to the atmosphere, sodium vapors condense and freeze, causing plugging at various types of fittings. The liquid-metal vapor can be removed by passing the gas through a NaK-filled, stainless-steel wool-packed column. The column should be cooled to 100°F and contain at least 18 in. of packing, the bottom 6 in. of which are covered with NaK. The column should operate below the loading or flooding point at the rated gas flow. When used to remove sodium vapor, a potassium-rich NaK should be employed to retard the elevation of the melting point of the NaK as sodium is absorbed. In operation, these units decrease the liquid-metal content of the vent gases to that corresponding to the equilibrium vapor pressure at the operating temperature of the vapor trap.

CORROSION*

One of the major factors limiting the development of high-temperature engineering systems is the inability of materials to withstand attack by liquid metals. The process of attack is generally termed corrosion although the phenomenon seems to be quite different from that of the common electrolytic corrosion.

Two of the most troublesome manifestations of attack by liquid metals are self-welding and thermal-gradient transfer. Self-welding is probably caused by diffusion across the contact interface with reduction of surface oxides and contact stresses contributing to the process. It generally increases with temperature and with the pressure under which the solid surfaces are held. Self-welding may be a major factor in the determination of the upper temperature of a liquid-metal system because of interference with the operation of valves, pumps, and flanged joints.

"Thermal-gradient transfer" is the term used to describe the transport of material from one region of a liquid-metal system to another; it results from the co-existence of a temperature gradient and an appreciable temperature coefficient of solubility. Even though the actual solubility is low, large amounts of a solid component may be dissolved from the zone of higher solubility and precipitated in the zone of lower solubility. This continual removal results in corrosion in some areas and plugging in others.

Evaluation of corrosion data is based in this discussion on the following criteria:

Rate of attack, mils/yr	Rating
< 1	Good
1-10	Limited
> 10	Poor

A summary of the resistance of materials to liquid metals is shown in Fig. 2.4.3. Four bar-charts (Figs. 2.4.4 through 2.4.7) are included showing the resistances of various materials to attack by sodium and NaK, mercury, lithium and lead-bismuth. These bar charts represent, for the most part, only a limited number of relatively small-scale, laboratory tests. The data do not in themselves warrant final selection of a material for a given application, but they can be used to eliminate many materials from consideration. The actual design of liquid-metal heat-transfer systems, particularly at higher temperatures, should be based on an experimental study duplicating the contemplated operating conditions.

SODIUM AND NaK

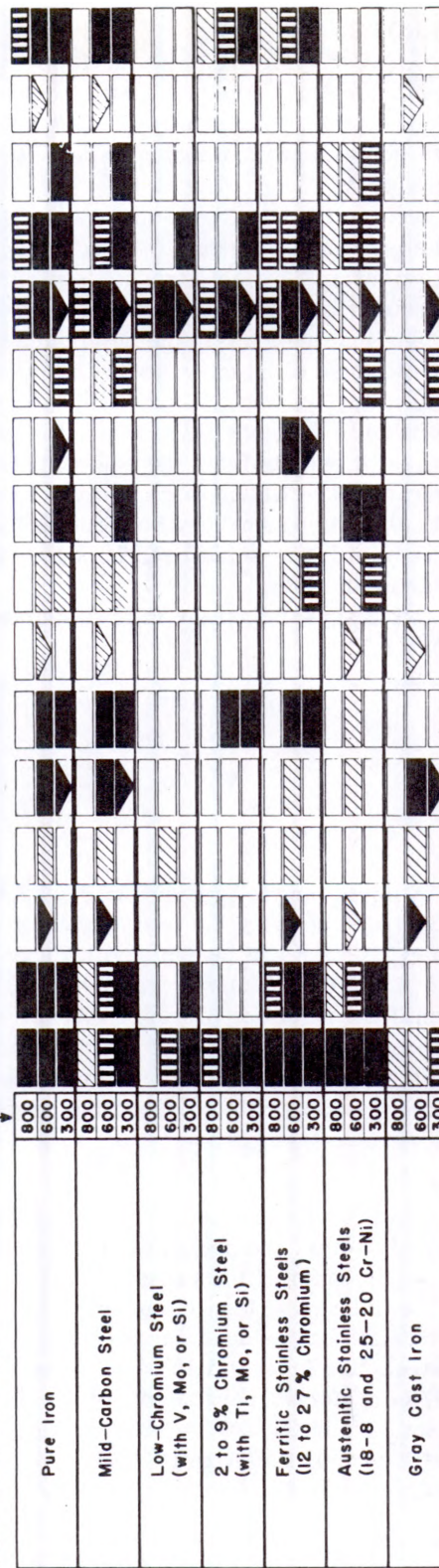
The resistances of various materials to attack by sodium and NaK are summarized in Fig. 2.4.4. It should be noted that the alloys of sodium and potassium behave similarly toward container materials throughout their entire composition range.

Recent engineering experience with sodium and NaK at high temperatures indicates that a large number of ordinary metals of construction can be used successfully as container materials. The 18-8, austenitic stainless steels are most widely used at present for NaK; of these, the columbium-stabilized type-347 is preferred because of its superior welding characteristics and greater metallurgical stability in the 1000°-1500°F range. Types 310 and 316 have been preferred by some investigators while Inconel X and a nickel-chromium alloy, Nichrome V, also resist attack by sodium or NaK. High-temperature, cobalt-base

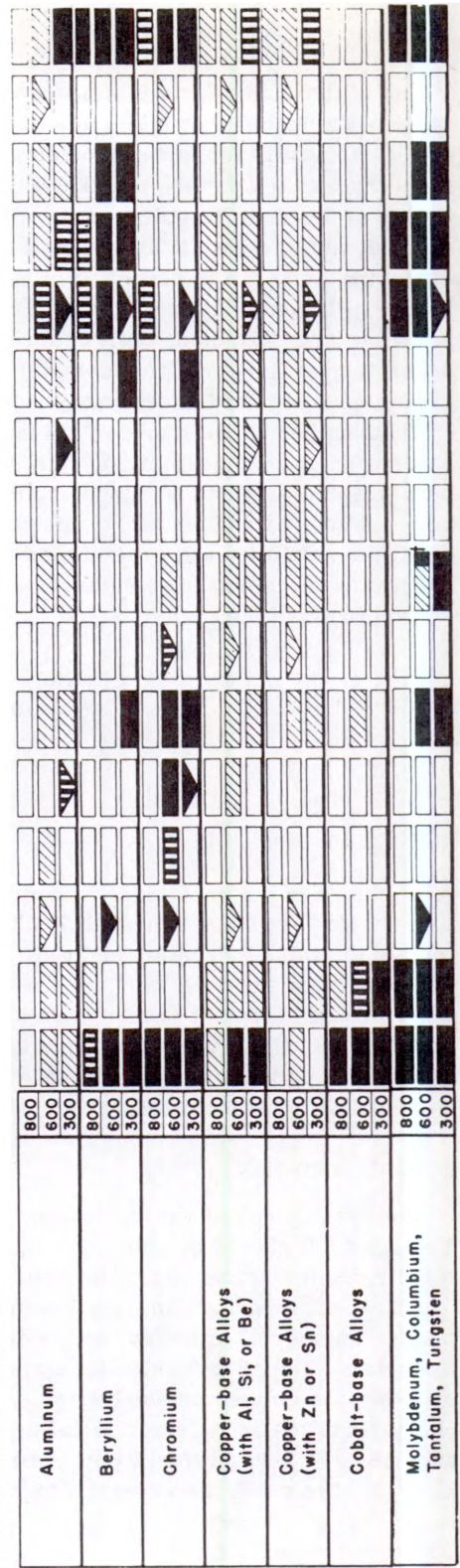
*This discussion is abstracted from the 2nd edition of the Liquid-Metals Handbook, June 1952.

LIQUID METAL	Na, K -12.3 to 98.3	Li	Mg	Zn	Cd	Hg	Al	Ga	In	Tl	Sn	Pb	Bi-Pb	Bi-Sn	Sb	Bi
MELTING POINT, °C	→	→	→	→	→	→	→	→	→	→	→	→	→	→	→	→
	186	651	419.5	321	-38.8	660	29.8	156.4	303	231.9	327	125	97	630.5	271.3	

FERROUS METALS



NONFERROUS METALS




[illegible]

NON-METALS

[illegible]

Resistance Ratings (These ratings refer to liquid-metal resistance only—not to temperature-dependent mechanical strength or metallurgical stability. See text for further discussion.): ■■■■—Good resistance; ■■■—limited resistance; ■■■—poor resistance; ■■■—unknown resistance.

—Liquid freezes above this temperature, shading in triangle indicates degree of resistance to liquid at the melting point.

* — Indicates: Poor with potassium, good with sodium; † — Tungsten, good; ‡ — Inconel, limited.

Fig. 2.4.3 — Condensed Summary of Resistance to Liquid Metals at 300°C, 600°C, and 800°C. Reprinted from Liquid-Metals Handbook, Edited by R. N. Lyon, Department of the Navy and U. S. Atomic Energy Commission, 2nd Ed., June 1952.

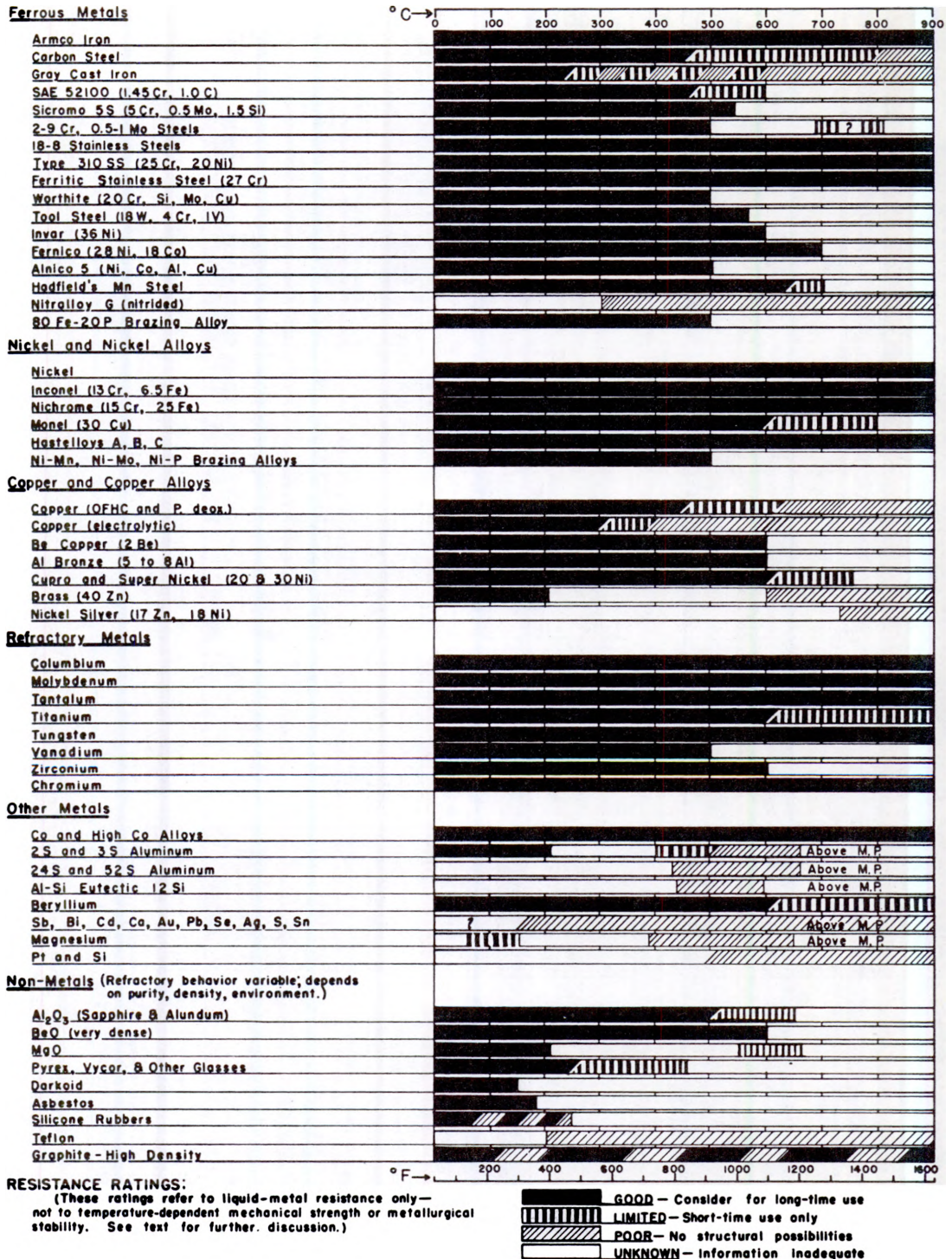


Fig. 2.4.4 — Resistance of Materials to Liquid Sodium and Sodium-Potassium Alloys. Reprinted from Liquid-Metals Handbook, Edited by R. N. Lyon, Department of the Navy and U. S. Atomic Energy Commission, 2nd Ed., June 1952.

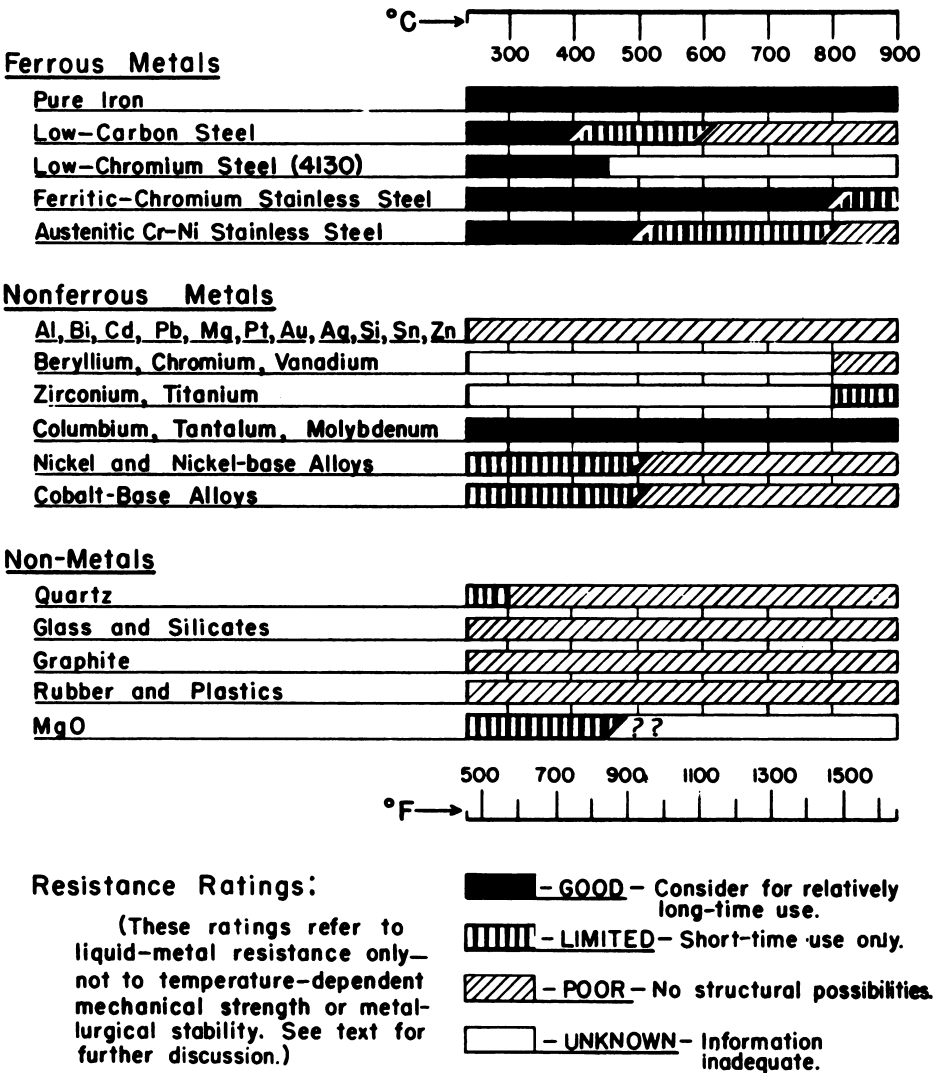


Fig. 2.4.5 — Resistance of Materials to Liquid Lithium. Reprinted from Liquid-Metals Handbook, Edited by R. N. Lyon, Department of the Navy and U. S. Atomic Energy Commission, 2nd Ed., June 1952.

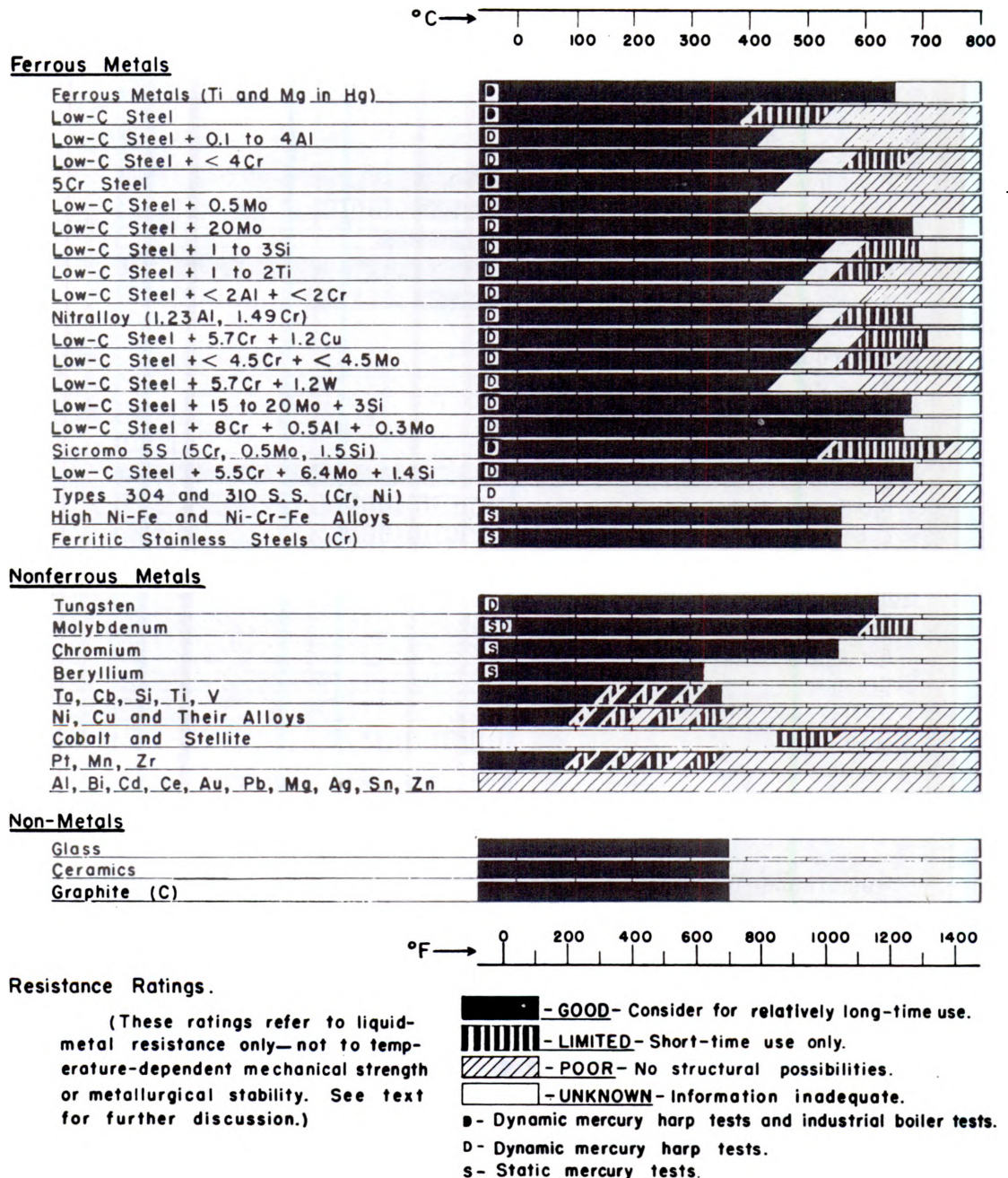


Fig. 2.4.6—Resistance of Materials to Liquid Mercury. Reprinted from Liquid-Metals Handbook, Edited by R. N. Lyon, Department of the Navy and U. S. Atomic Energy Commission, 2nd Ed., June 1952.

alloys, such as Haynes Alloy 25 and Allegheny Ludlum's V-36, have shown excellent resistance to sodium as well as good high-temperature strength.

During the last few years, a large amount of laboratory work has been done on the effects of temperature, impurities, thermal gradients and fluid velocity on corrosion by sodium and NaK. The results of these experiments are not in all cases directly comparable, since variables now known to be important were not always properly controlled. Some of the more recent data from static tests under closely controlled and comparable conditions are summarized in Table 2.4.4. The data in this table are largely limited to tests conducted at temperatures up to 932°F. Additional work has also been done on corrosion by sodium up to 2000°F and higher. In general, the materials which resist sodium at 1000°F also resist it at higher temperatures in static tests.

One of the most important factors affecting corrosion is oxygen content. The presence of oxygen in sodium in amounts less than 0.01 percent apparently has no serious consequences in stainless-steel systems up to 1000°F. In greater percentages, the oxygen, probably present as dissolved Na_2O , accelerates attack although it does not increase the solubility of the container material in sodium. This increased rate of attack is particularly serious in circulating systems because of thermal transfer. Both the corrosive action and the oxide solubility increase with temperature.

Many non-metallic materials have been subjected to static tests in sodium to study their possible use as valve seats, bearings, and insulators. Table 2.4.5 shows the results of selected static tests on a number of ceramic materials using aged and filtered sodium; Table 2.4.6 gives similar data for cemented carbides. Beryllia, zirconia, magnesia, alumina, molybdenum disilicide, and many cemented carbides resist sodium attack if sufficiently dense but are penetrated if porous. Temperature of test, character of ceramic binder, particle size, and firing temperature also affect corrosion. High-density material produced by hot pressing or by fusion may be susceptible to spalling rather than corrosion.

The elements, antimony, bismuth, cadmium, calcium, copper, gold, lead, selenium, silicon, silver, sulfur, and tin, are unsuitable as container materials because of high solubility in sodium and potassium. Magnesium has limited resistance to NaK at very low temperatures.

RECOMMENDATIONS FOR HANDLING THE REACTION BETWEEN ALKALI-TYPE LIQUID METALS AND WATER*

A study of the reaction of liquid metals with water has been carried on by the Mine Safety Appliances Company for approximately four years using NaK except for a few tests with sodium and potassium. All of the experiments have been made in closed, stainless-steel containers.

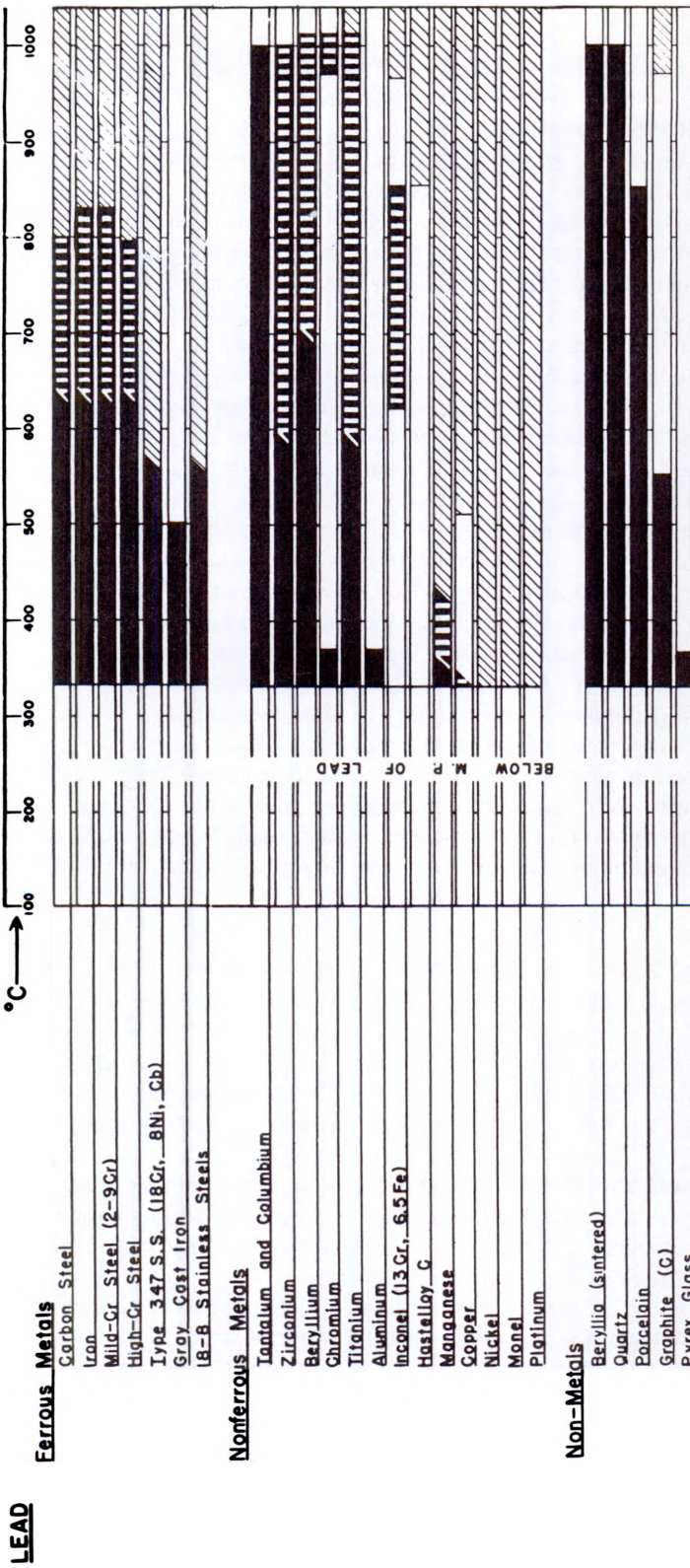
The reaction of a liquid metal and superheated steam showed no hazardous results. The most dangerous condition found exists in that section of an exchanger or boiler where liquid water and liquid metal may come together. From the information obtained to date, the following recommendations for handling the reaction are suggested:

(1) The liquid metal should be under pressure to minimize agitation at the reaction zone caused by hydrogen bubbles formed when water contacts the liquid metal; this permits continuous and uniform mixing of the liquid metal and water. The optimum pressure was found to be 200 psi or higher; however, 50 psi is deemed safe.

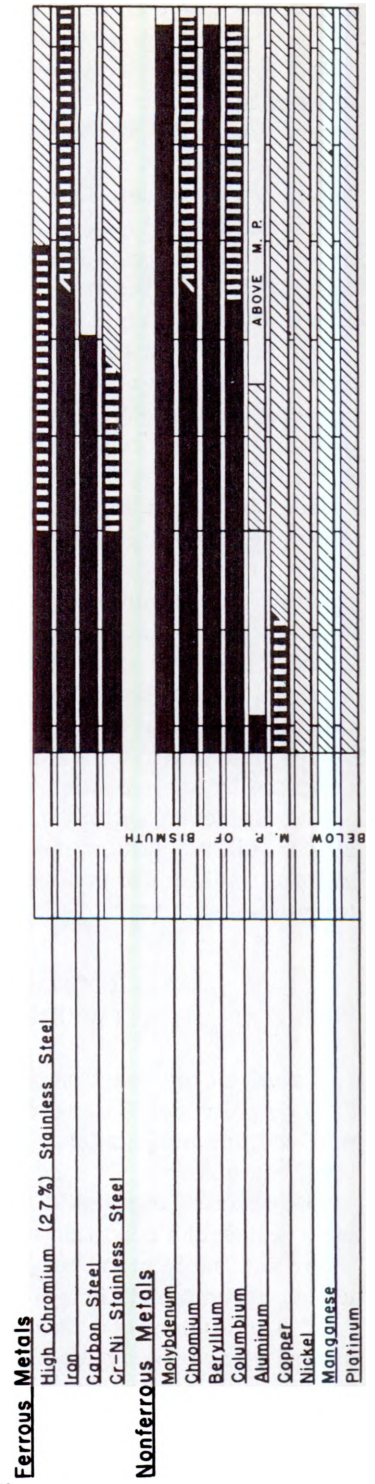
(2) If the liquid metal is at 600°F or higher, the formation of intermediate reaction products is greatly reduced. The accumulation of intermediate reaction products containing hydrogen can cause rather violent reaction in the presence of excess liquid metals.

(3) No difficulty has yet been experienced in venting the generated hydrogen through a relief valve when the above values of pressure and temperature are maintained.

*Memo by E. C. King, MSA.



BISMUTH



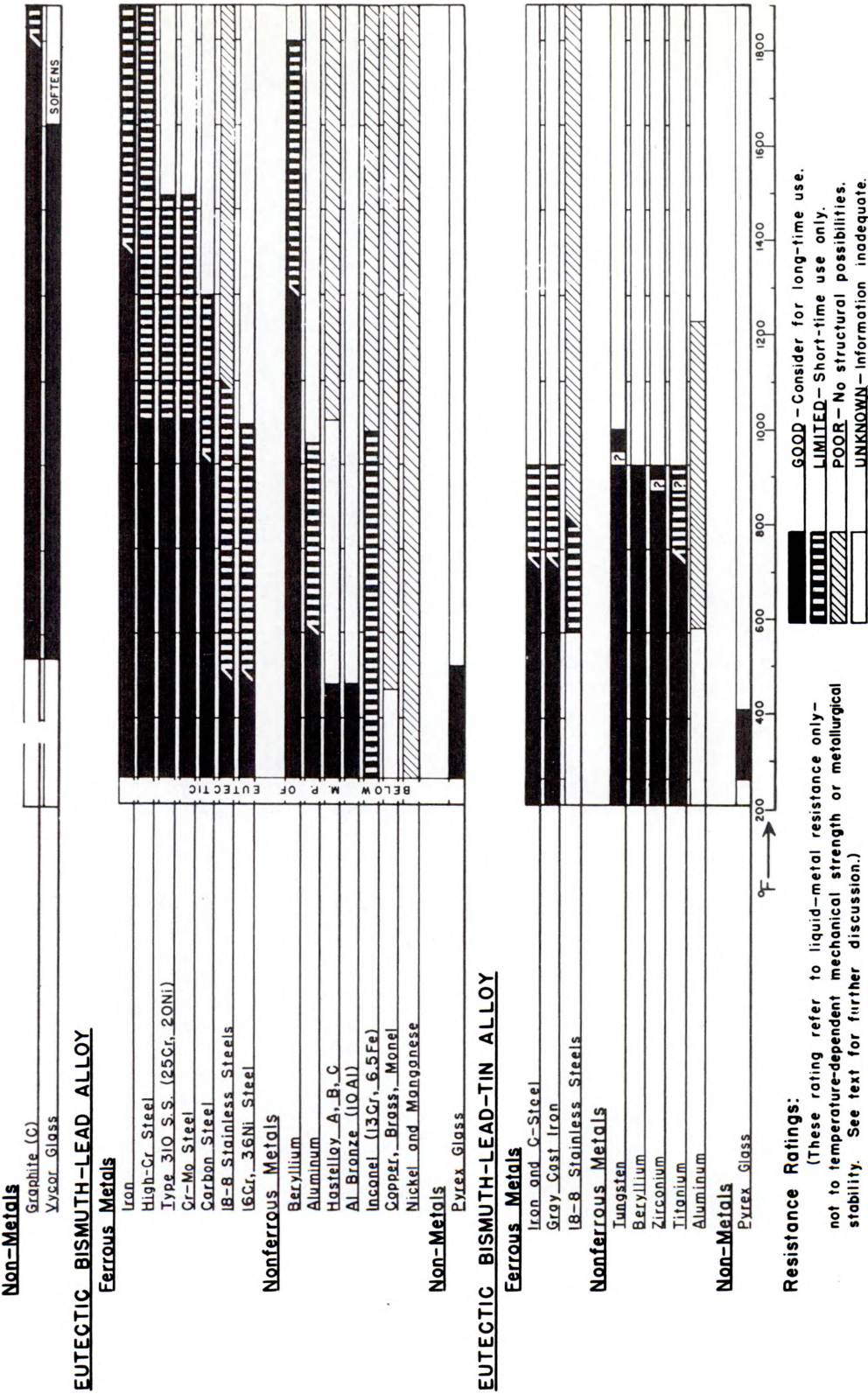


Fig. 2.4.7 — Resistance of Materials to Liquid Lead, Bismuth, Eutectic Bismuth-Lead, and Eutectic Bismuth-Lead-Tin Alloy. Reprinted from Liquid-Metals Handbook, Edited by R. N. Lyon, Department of the Navy and U. S. Atomic Energy Commission, 2nd Ed., June 1952.

**Table 2.4.4—Resistance of Some Metals to Attack by Sodium and NaK
in Static Corrosion Tests (KAPL)**

(Stainless-steel vessels used except where otherwise noted)

Metal	Temp., °C	Resistance
Aged and filtered (5-μ) sodium, probably containing 0.005–0.01 % oxygen		
Aluminum, 99.99% pure	427	Poor
Aluminum, 99.99% pure	500	Poor
Aluminum alloy 3S, 24S, 52S, 75S, 750	427	Poor
Aluminum bronze, cast	427	Good*
Armco iron	500	Good
Armco 17-7 PH stainless steel	427	Good*
Beryllium, warm-extruded rod	500	Good
Beryllium, chromium-plated	500	Good*
Fernico	500	Good
Inconel X	500	Good
Monel	500	Good
80Ni-20Cr	500	Good*
Nickel, "L"	500	Good
Nickel (1/4% Zr)	500	Good
Nickel (1/4% Zr in Ni container)	500	Good
Nitrided Nitralloy	500	Good*
Nitrided 347	500	Good*
SS 303, 304ELC, 321, 347, 347(+Ta), 347(carburized), T347(cyanided)	500	Good
Low-to-medium chrome-steel alloys		
1Cr:0.5Mo	500	Good
1Cr:1Mo:0.25V	500	Good
2Cr:0.5Mo	500	Good
2.25Cr:1Mo	500	Good
3Cr:1.5Si:0.5Mo	500	Good
5Cr:0.5Mo	500	Good
5Cr:0.5Mo:0.5Ti	500	Good
5Cr:1.5Si:0.5Mo	500	Good
7Cr:0.5Si:0.5Mo	500	Good
Carbon (0.5Mo)	500	Good
AISI-1019 steel	500	Good†
Zirconium	500	Good
98Zr:2Al	500	Good
98Zr:2Fe	500	Good
93Zr:7Mo	500	Good
92Zr:8Cr	500	Good
90Zr:10Ti	500	Good
Distilled sodium		
Aluminum, high-purity	450	Good
Aluminum, high-purity	500	Poor†
Aluminum alloy 2S	450	Good
Aluminum alloy 2S	500	Poor†
Stainless steel, 347	450	Good
Calcium-gettered sodium, probably containing less than 0.005% oxygen		
Aluminum, 99.99% pure	427	Poor
Aluminum alloy 3S, 24S, 52S, 75S, 750	427	Poor
Aluminum bronze, T-224	427	Good

Table 2.4.4—(Continued)

Metal	Temp., °C	Resistance
Beryllium, extruded	500	Good*
Beryllium, sintered	500	Good*
Copper, OFHC (in SS container)	427	Good*
Copper, OFHC (in Cu container)	400	Good
Durimet 20	427	Good
Inconel X	500	Good
Mechanite	427	Decarburized*
Monel, S	427	Good*
Nickel, L	500	Good
Ni-Mn, 40-60	500	Good*
Ni-Mn, 80-20	500	Good*
Ni Resist	427	Decarburized
Nitrided 347 stainless steel	500	Good
Tantung-Ni, 30-70	500	Good*
Tantung A166, A171, A192, A166 Spring	500	Good*
Titanium	500	Good*
Vanadium	500	Good‡
Zirconium	427	Good*
Zirconium	500	Good
SS, 302, 304, 310 (25 Cr-20 Ni), 316, 321, 347, 35-15-Ni-Cr	500	Good
SS, 416	427	Good*
SS, 440 C	427	Good*
52100 Steel	427	Good*
6-6-2 high-speed tool steel	427	Good*
18-4-1 high-speed tool steel	427	Good*
Gettered by calcium additions to test container		
Beryllium, extruded	500	Good
Beryllium, sintered	500	Good
Nickel, A (2% Ca added)	500	Limited
Nickel, A (10% Ca added)	500	Poor
Nickel, L (0.1% Ca added)	500	Good
Stainless steel, 347	500	Good
Filtered (5-μ) NaK (56K : 44Na)		
Aluminum, high purity	450	Good
Aluminum alloy 2S	450	Good
Stainless steel, 347	450	Good

*Tested in individual stainless-steel cans

†Decarburized

‡Flat specimens spaced $\frac{1}{16}$ in. from flat plates of stainless steel

§Tested in individual nickel cans

Table 2.4.5—Resistance of Selected Ceramics to Attack by Aged and Filtered Sodium

Ceramic (Mole compositions except as indicated)	Resistance	
	500°C (932°F)	750°C (1382°F)
Artificial periclase crystal	Good	Good
BeO	Good	...
Stabilized ZrO ₂	Limited	...
1BeO : 1Al ₂ O ₃	Good	...
1MgO : 4ZrO ₂	Good	Poor
1MgO : 8BeO : 1Al ₂ O ₃	Good	Limited
160BeO : 2Al ₂ O ₃ : 1ThO ₂ + 2% CaO	Limited	Limited
76BeO : 4Al ₂ O ₃ : 20ZrO ₂ + 2% CaO	Good	Good
3MgO : 90BeO : 1ZrO ₂	Good	Limited
Hot-pressed synthetic mica	Disintegrated	...
TiN	Spalled	...
TiC ₂	Disintegrated	...
CaZrO ₃	Poor	...
CiO	Disintegrated	...
ZnO		
TiC	Cracked	...
Be ₂ C (swelled due to hydration after test)	Limited	...
MoSi ₂	Disintegrated	...
B ₄ C, TaC, TiC, VC, ZrC	Good	...
Silicon carbide crystals, SiC	Good	...
Mixed carbides, B ₄ C and SiC	Limited	...
Carbon-titanium mixed borides	Good	...
Zirconium boride, ZrB ₂	Limited	...
Calcium boride, CaB ₆	Poor	...
Zirconium nitride, ZrN	Good	...
Beryllium nitride, Be ₃ N ₂	Limited	...
Titanium nitride, TiN	Poor	...
Beryllium oxide, BeO	Good	...
Chrysoberyl, BeO-Al ₂ O ₃	Good	...
Spinel (hot pressed), MgO-Al ₂ O ₃	Limited	...
Zirconium stab. with CaO	Limited	...

(4) It is recommended that all hydrogen relief be made from the water or steam side of the system if possible (see item 5). Very high temperatures have been experienced when water is forced for any length of time into areas of excess liquid metal.

(5) To adopt recommendation (4), liquid-metal systems must be designed to withstand full steam pressure until either the reaction area can be isolated from the rest of the system by quick-closing valves or all the water can be removed from the reaction.

(6) A dump valve or similar device should be included in the system to dump the water from the lowest point of the boiler or exchanger. This valve could be actuated by a sudden increase in pressure in the liquid-metal system.

INDUCED ACTIVITY

(H. E. Stone)

When the coolant passes through the core, reflector, and thermal blanket of a reactor, it is exposed to a neutron flux which may reach a value of $10^{14}/(\text{cm}^2)(\text{sec})$. As long as the coolant is in the flux, there is a continuous birth of radioactive atoms and also a continuous decay. After the fluid leaves the reactor, the activation stops although the decay continues.

Table 2.4.6—Resistance of Cemented Carbides to Attack by Aged and Filtered Sodium

Nominal composition, %	Resistance	
	500°C (932°F)	750°C* (1382°F)
30Ni: 8CbTiTaC ₃ : 62TiC	Good	Limited
20Ni: 15CbTiTaC ₃ : 55TiC	Poor	...
20Ni: 8CbTiTaC ₃ : 72TiC	Good	Good
20Co: 80TiC	Good	...
20Co: 15CbTiTaC ₃ : 65TiC	Good	...
5Co: 15CbTiTaC ₃ : 80TiC	Limited	...
100TiC	Good	Good
Co Bonded WC	Good	Good
20Fe: 80TiC	Good	...
10Co: 8CbTiTaC ₃ : 82TiC	Good	Limited
30Ni: 70TiC	Good	Limited
20Ni: 80TiC	Good	...
20Ni: 15CbTiTaC ₃ : 55TiC	Good	...

*The initial weights for the specimens which were rerun in sodium at 750°C were taken as their final weight after the 500°C run. This may have introduced some error.

Table 2.4.7—Induced Activities from Some Coolant Metals

Isotope	Natural element, %	Thermal cross section, barns	Radioactive product of (n,γ) reaction	Half-life	Energy of γ radiation, mev	Number γ's per neutron capture
¹¹ Na ²³	100	0.48	¹¹ Na ²⁴	14.9 hr	2.76, 1.38	1 each
¹⁹ K ⁴¹	6.8	1	¹⁹ K ⁴²	12.4 hr	1.51	0.25
⁸⁰ Hg ¹⁹⁶	0.155	2900	⁸⁰ Hg ¹⁹⁷	23 hr	96% 0.13, 0.16, 0.27	1 each
				64 hr	0.08	1 each
⁸⁰ Hg ¹⁸⁶	10.1	20	⁸⁰ Hg ¹⁸⁹	44 min	0.37	1
⁸⁰ Hg ²⁰²	29.6	2.4	⁸⁰ Hg ²⁰³	51 days	0.28	1
³ Li ⁷	92.6	0.033	³ Li ⁸	0.88 sec	13.4-mev β and Bremsstrahlung	

This decay or induced activity poses a shielding problem for the external heat-transfer system; it is most serious for high-energy gamma radiation or Bremsstrahlung. Table 2.4.7 shows the gamma- or X-radiation to be expected from some activated coolant metals.

General expressions can be derived for the specific activity of a fluid circulating through a neutron flux. These equations can be simplified under equilibrium conditions, i.e., when the number of atoms being activated is equal to the number of decaying atoms:

In all cases:

$$A(t) = A(t') e^{-\lambda(t-t')} \quad (1)$$

$$\bar{A} = \frac{A(t')}{\lambda(T-t')} [1 - e^{-\lambda(T-t')}] \quad (2)$$

For cyclical irradiation:

General Expressions

After k cycles:

$$A_k(t') = \frac{\lambda NF \sigma [1 - e^{-(F\sigma + \lambda) t'}] [1 - e^{-(k+1)(F\sigma t' + \lambda T)}]}{F\sigma + \lambda} \quad (3)$$

At equilibrium:

$$A_\infty(t') = \left(\frac{\lambda NF \sigma}{F\sigma + \lambda} \right) \left(\frac{1 - e^{-(F\sigma + \lambda) t'}}{1 - e^{-(F\sigma t' + \lambda T)}} \right) \quad (4)$$

$F\sigma \ll \lambda$

After k cycles:

$$A_k(t') = NF \sigma \frac{(1 - e^{-\lambda t'}) (1 - e^{-(k+1) \lambda T})}{1 - e^{-\lambda T}} \quad (5)$$

At equilibrium:

$$A_\infty(t') = NF \sigma \frac{1 - e^{-\lambda t'}}{1 - e^{-\lambda T}} \quad (6)$$

$F\sigma \ll \lambda$ and $\lambda T \ll 1$

After k cycles:

$$A_k(t') = NF \sigma \frac{t'}{T} [1 - e^{-(k+1) \lambda T}] \quad (7)$$

At equilibrium:

$$A_\infty(t') = NF \sigma \frac{t'}{T} \quad (8)$$

From these equations it can be seen that the activity of a coolant depends on the following variables:

- (1) Macroscopic capture cross-section (nuclei/cc \times cross section in cm^2), the probability of a neutron capture in the element—this is energy dependent.
- (2) Neutron flux and spectrum, as this affects the capture cross section.
- (3) Half-life of the radioactive isotope—the longer the half-life, the longer it takes to arrive at the equilibrium condition. A longer half-life also indicates a slower decay of the radioactive isotope.
- (4) Circulation time of the coolant.
- (5) Fraction of circulation time spent in the neutron flux.

In order to compare fluids from an activation point of view, all of the above parameters should be varied. For sodium and potassium, however, one can assume that the neutron flux, neutron spectrum, circulation time of coolant, and fraction of time spent in the radiation zone are equal.

From the values in Table 2.4.7, the ratio of the specific activity of sodium to that of potassium is found to be 12.6. A better indication of shielding requirements can be ob-

tained from the "dose" rate or energy flux as approximated by a semi-infinite sea of coolant:

$$D = \frac{AE}{4} \quad (9)$$

Thus:

$$D_{Na} = A_{Na} \left[\frac{2.76 \times 30.9}{4} + \frac{1.38 \times 21.4}{4} \right] = 28.8 A_{Na}$$

$$D_K = A_K \left(\frac{1.51}{4} \times \frac{22.4}{4} \right) = 2.11 A_K = \frac{A_{Na}}{12.6} \times 2.11 = 0.168 A_{Na}$$

and:

$$\frac{D_{Na}}{D_K} = \frac{28.8}{0.168} = 171$$

NOMENCLATURE

- A = Specific activity; disintegrations/(sec)(cm³ of fluid)
- A(t') = Value of A at the outlet from the neutron flux
- A(t) = Value of A as a function of time outside the neutron flux
- \bar{A} = Average value of A outside the neutron flux
- F = Neutron flux in energy range under consideration; neutrons/(cm²)(sec)
- k = Number of circulation cycles undergone by the cm³ of coolant under consideration.
- n = Number of activated nuclei under study per cm³ of fluid.
- N = Total number of nuclei under study per cm³ of fluid.
- t = Time measured from the instant the cm³ of fluid under consideration enters the neutron flux; t starts at zero again whenever the cm³ of fluid re-enters the flux.
- t' = Time of exposure of each nucleus in neutron flux; sec.
- T = Period of complete circulation cycle, i.e., time between two successive entrances of a particular nucleus into the neutron flux, assuming that all of the nuclei circulate at the same rate; sec.
- λ = Disintegration constant of activated nuclei ($\lambda = 1$ mean life = 0.693/half-life); sec⁻¹
- σ = Capture cross section of nuclei under consideration in energy range considered (where σ is assumed constant); cm²
- D = Dose rate; mev/(cm²)(sec)
- E = Energy of gamma ray; mev
- l = Mean free path of gamma ray; cm

REFERENCES

1. L. P. Pepkowitz and E. R. Proud, The Determination of Hydrogen—A New Universal Gasometric Method, KAPL-1, Sept. 1947, 4 pp.
2. Progress Report No. 42, Section III, Reactor Materials, KAPL-298, Jan. 1950, 39 pp.
3. S. L. Walters, Maximum Oxygen Content of Flowing Eutectic NaK in a Stainless Steel System, Tech. Rep. No. VIII, Mine Safety Appliance Co., NP-1942, Nov. 20, 1950, 14 pp.
4. W. H. Bruggeman and G. Billuris, Sampling of High-temperature Alkali Metals, AECU-2143, 16 pp, Unclassified.
5. L. P. Pepkowitz and W. C. Judd, Determination of Sodium Monoxide in Sodium, Anal. Chem. 22, 1950, p 1283.

SELECTED READING LIST**PURIFICATION**

INTERIM REPORT ON COLD TRAP INVESTIGATIONS, Knolls Atomic Power Laboratory, B. G. Voorhees and W. H. Bruggeman, KAPL-612, Oct. 1, 1951, 36 pp.

CORROSION

PROBLEMS IN THE USE OF MOLTEN SODIUM AS A HEAT TRANSFER FLUID, Jour. Met. and Cer., L. F. Epstein and C. E. Weber, TID-70-Part II, No. 6, Jan. 1951, 36 pp.

RESISTANCE OF MATERIALS TO ATTACK BY LIQUID METALS, Argonne National Laboratory, L. R. Kelman, W. D. Wilkinson, and L. Yaggee, ANL-4417, July 1950, 139 pp, Unclassified.

PROBLEMS IN THE USE OF MOLTEN SODIUM AS A HEAT TRANSFER FLUID, Jour. Met. and Cer., L. F. Epstein and C. E. Weber, TID-67-Part I, No. 3, May 1949, 85 pp.

INDUCED ACTIVITY

ACTIVATION OF A FLUID CIRCULATING THROUGH A NEUTRON FLUX, Knolls Atomic Power Laboratory, G. A. Allard, KAPL-665, Dec. 14, 1951, 16 pp, Unclassified.

Reactor Cooling and Power Conversion Cycles

T. Trocki and R. W. Lockhart

The operating conditions of a nuclear power-conversion system are a compromise between the requirements of the application and the limitation of the nuclear reactor. The application requirements vary according to whether the power plant is mobile or stationary or whether power or fuel production is the prime objective. The limitations of the nuclear reactor are similar to those of other heat sources except that they are more stringent because of the nuclear properties of the constituents, the difficulty of repairing or inspecting fixed reactor components because of radioactivity, or self-destruction (over-temperature) of the reactor core if the coolant is lost. Since liquid-metal cooling is more advantageous at higher temperatures, it has been studied mainly with respect to power production or for application to dual purpose reactors. However, the fact that liquid metals possess nuclear properties which might make them attractive for cooling a fast-spectrum fuel-production reactor near ambient temperatures should not be overlooked.

Since a reactor coolant not only becomes radioactive but for some applications is also not chemically compatible with the water-steam power-conversion cycle, intermediate heat-transfer cycles, usually utilizing liquid metals, are used to isolate physically and/or nuclearly the reactor and the power-conversion cycles. Liquid metals possess physical properties which allow high rates of heat transfer and therefore small heat-transfer equipment.

From a heat-transfer and power-production standpoint, the temperature rise of the reactor coolant is a design feature. To remove the same amount of heat from a given reactor, water usually requires the lowest temperature rise; liquid metals, because of their relatively lower specific heat, usually require a temperature rise several times as large, and gases require an even larger temperature rise. The design temperature rise results from a compromise among the following factors:

- (1) Percentage of coolant in reactor core.
- (2) Reasonable pressure drop and pumping power.
- (3) Allowable upper and lower coolant operating temperatures, or allowable temperature difference (as for thermal shock).

The maximum operating temperature for liquid metals is limited either by the corrosion or strength of the structural materials. The lowest allowable operating temperature or the maximum temperature difference can be set by one of the following factors:

- (1) Solidification or separation point of the coolant.
- (2) Corrosion by mass transfer between hot and cold portions of the cycle.

(3) Precipitation of impurities in the cold portion (such as sodium oxide from sodium at low temperature).

(4) Maximum allowable thermal shock upon reactor scram.

BASIC CYCLE EQUATIONS

Present applications of liquid-metal heat-transfer systems have been designed to deliver the heat to steam power-conversion systems. The following basic equations apply. The reactor heat output:

$$Q = WC_P(t_{out} - t_{in})$$

or in heat exchanger terms:

$$Q = Q_{IHE} = Q_S + Q_E + Q_F$$

or:

$$Q = (UA)_{IHE} \Delta t_{lmIHE}$$

or:

$$Q = (UA)_S \Delta t_{lmS} + (UA)_E \Delta t_{lmE} + (UA)_F \Delta t_{lmF}$$

Applications of these relationships are illustrated graphically in Figs. 2.5.1 through 2.5.4 and will be described in the following text. The first equation is basic for any single-phase coolant and indicates the relationship of the term that it contains. The remaining equations indicate the heat-exchanger relationships.

Figure 2.5.1 is an example of the effect of reactor outlet temperature and reactor coolant temperature rise on the required total steam-generator area. It is evident that smaller heat-transfer areas are required at higher reactor outlet temperatures and lower reactor coolant temperature rise. The steam-drum pressure was held constant for this comparison; the corresponding cycle diagram appears in Fig. 2.5.2. Similar curves can be calculated for any steam generator using the fourth equation. This curve can be used for an intermediate heat-exchanger system if the specifications indicated on the curve are maintained when the reactor symbols are replaced by intermediate fluid.

The following description of typical cycles illustrates some of the possible compromises that have been made to remove heat and generate power from a nuclear reactor.

TYPICAL CYCLES

The simplest reactor cooling cycle consists of a single fluid system which heats the fluid passing through the reactor and delivers its energy directly to a heat sink or power-conversion unit. Many of the existing non-power-production and experimental reactors are of this type (e.g., the Fast Experimental Reactor at Los Alamos which uses liquid-metal mercury cooling).

Water- and liquid-metal-cooled power reactors that are under construction may have two cycles between the reactor and the power-conversion unit. This added system isolates the radioactivity of the reactor coolant from the power-conversion cycle and allows different coolants or different purities of coolant to be used in each cycle. Fig. 2.5.2 shows the liquid-metal cycle and temperature conditions for a typical two-cycle system at rated power.

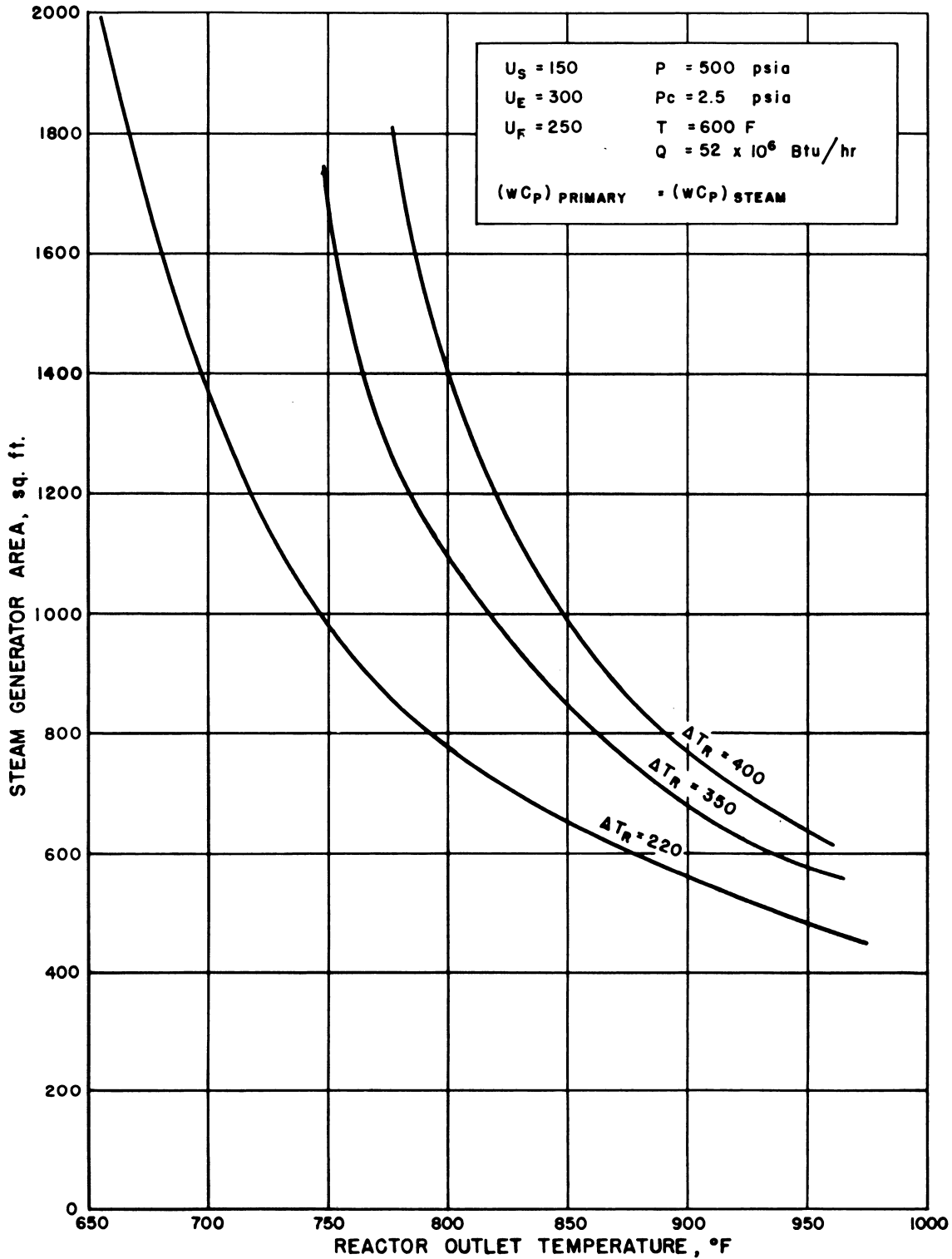


Fig. 2.5.1 — Predicted Effect of Reactor Outlet Temperature and Coolant Temperature Rise on Steam Generator Area for a Particular Application. Submitted by KAPL, Feb. 12, 1953.

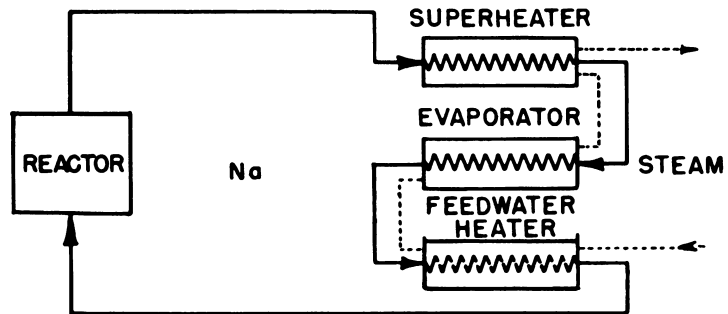
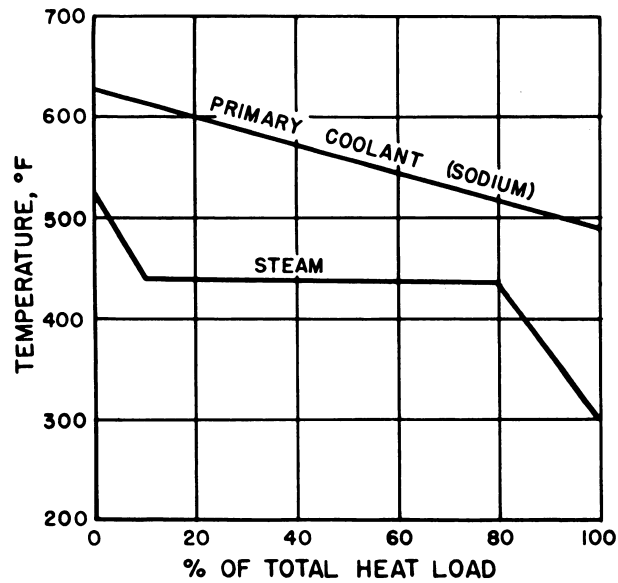


Fig. 2.5.2—Predicted Liquid-metal-water Cycle and Temperature Condition for a Particular Application. Submitted by KAPL, Feb. 12, 1953.

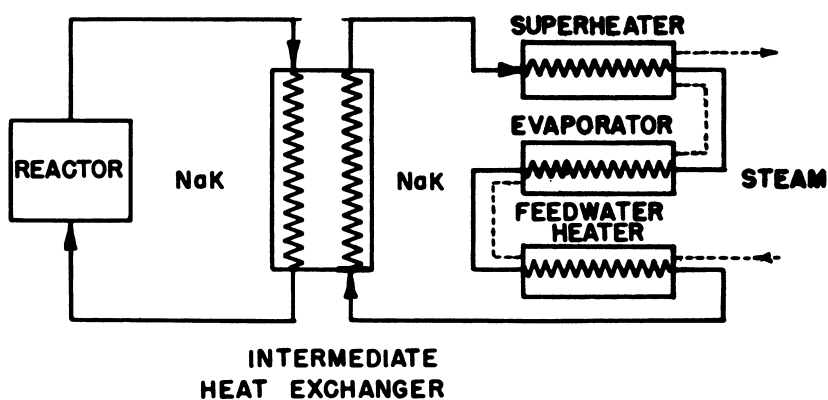
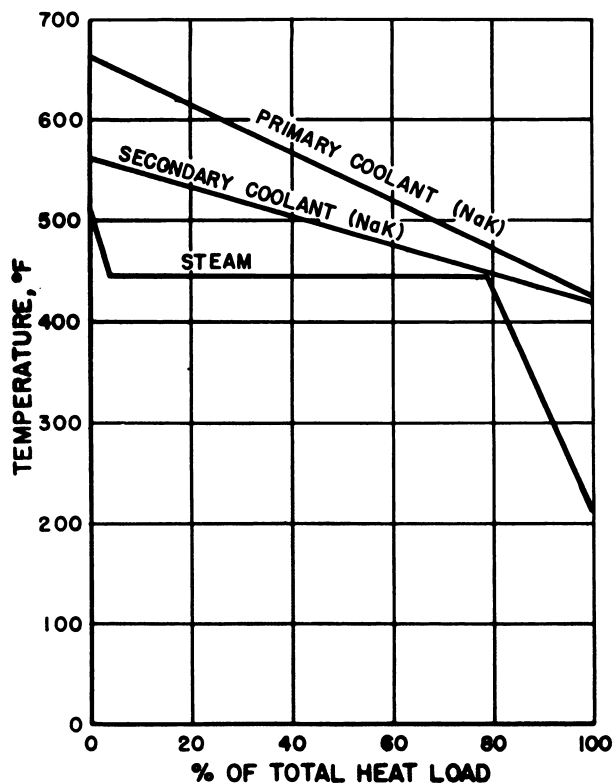


Fig. 2.5.3 — Intermediate-cycle System; Operating Temperature Conditions for EBR. Submitted by KAPL, Feb. 12, 1953.

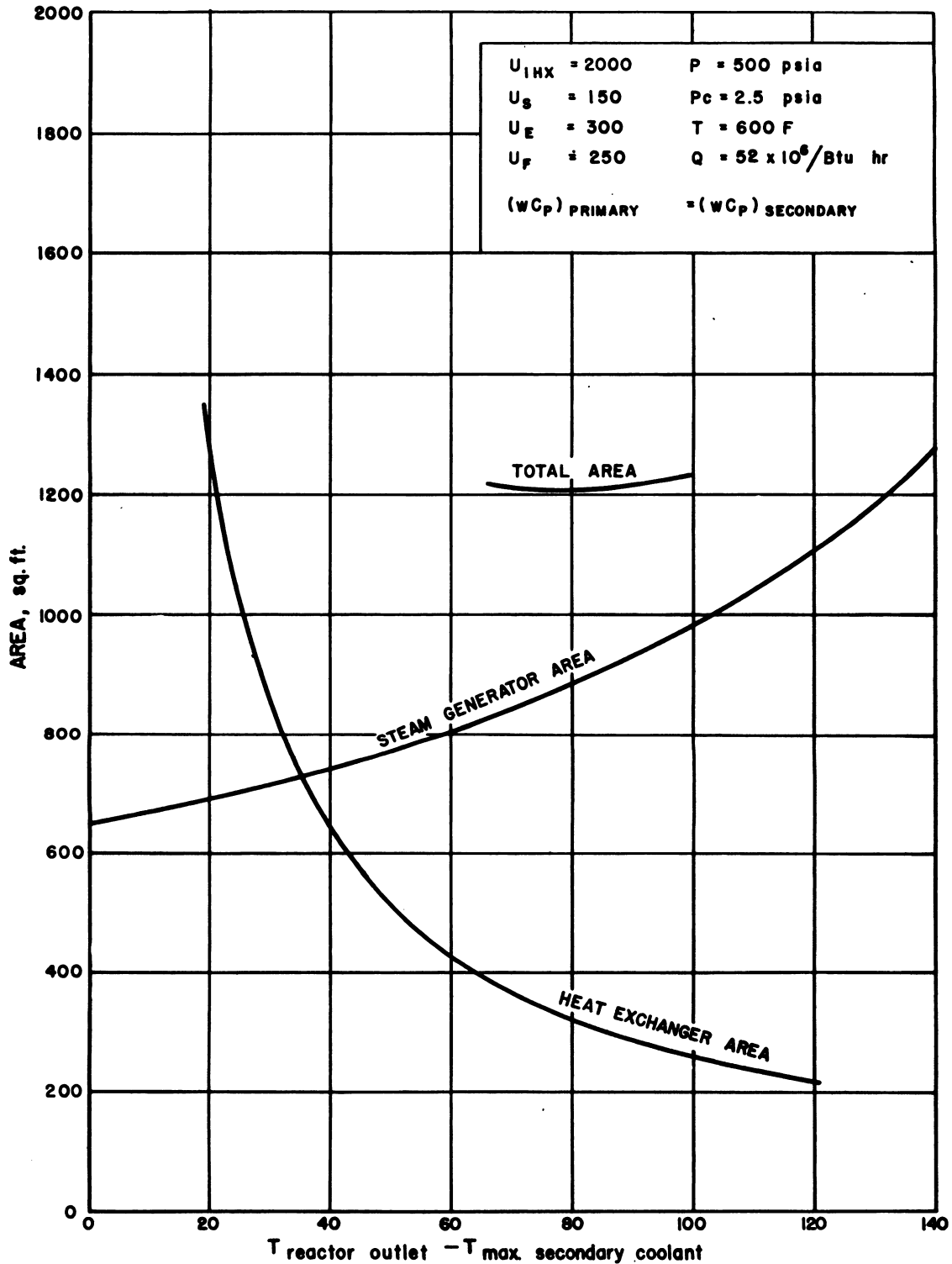


Fig. 2.5.4 — Calculated Steam-generator and Heat-exchanger Areas as a Function of the Difference Between Reactor Outlet Temperature and the Maximum Temperature of the Secondary Coolant. Submitted by KAPL, Feb. 12, 1953.

INTERMEDIATE-CYCLE SYSTEM

NO POWER CONVERSION OF INTERMEDIATE CYCLE

To reduce the volume of the primary (radioactive) coolant system, which in turn reduces the weight, volume, and cost of the coolant shielding, intermediate liquid-metal cycles have been inserted between the primary liquid-metal system and the steam system. This additional system reduces the danger of radiation damage to, or chemical reaction with, the water system, at the expense of additional equipment.

The Experimental Breeder Reactor cooling system is an example of this intermediate-cycle system (see Fig. 2.5.3). The temperatures shown represent operating power-production conditions. The cycle temperatures are reduced when power production is not required. The EBR-reactor and intermediate-cycle coolants are eutectic NaK.

Intermediate-cycle systems have the cycle disadvantages of larger temperature differences between the reactor outlet and the upper temperature of power conversion of the heat sink. It is practical to design the intermediate cycle with about the same water-equivalent flow rate as the reactor cycle, $(WC_p)_{\text{reactor}} = (WC_p)_{\text{intermediate}}$. If they are equal, the temperature level loss is the same as the log mean temperature across the intermediate heat exchanger (about 50° to 150°F).

The minimum total intermediate heat-exchanger and steam-generator area or the minimum intermediate heat-exchanger area can be calculated. An example of the solution presented in a design study is shown in Fig. 2.5.4.

POWER-CONVERSION OF INTERMEDIATE CYCLES

This system consists of the "basic-cycle" system firing a binary mercury-steam power-conversion system. This binary power cycle is the most efficient cycle used commercially for any size plant. Figure 2.5.5 compares mercury and steam plant net heat rates; the lower the heat rate or the higher the plant efficiency, the greater is the power produced per kilogram of fuel fissioned. A reactor binary power-production system is illustrated in Fig. 2.5.6. A liquid-metal outlet temperature of about 1100°F would be required to make this system feasible; an outlet temperature of 1200° to 1800°F would make this system very attractive.

NOMENCLATURE

- A = heat transfer area, ft²
- C_p = specific heat of primary coolant, Btu/(lb)(°F)
- E = evaporator
- F = feedwater heater
- IHX = intermediate heat exchanger
- Q = heat-transfer rate Btu/hr
- S = superheater
- U = over-all heat-transfer coefficient, Btu/(hr)(ft²)(°F)
- V = velocity, ft/hr
- W = mass flow rate of primary coolant, lb/hr
- t = temperature, °F
- Δt_{lm} = log mean temperature difference, °F
- ρ = density, lb/ft³
- Δt_R = temperature rise across the reactor

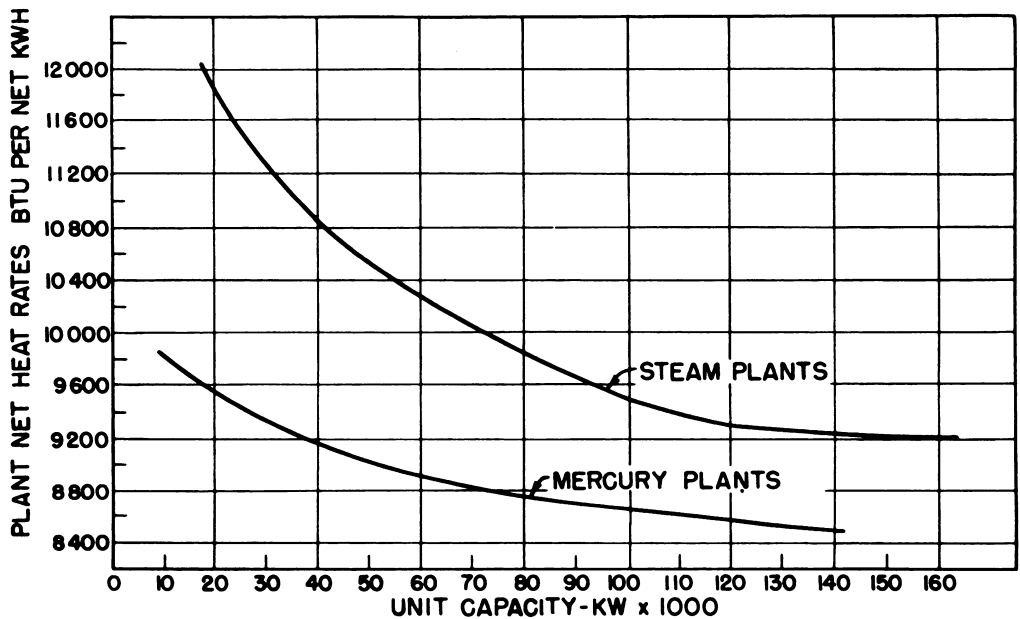


Fig. 2.5.5 — Comparison of Mercury and Steam Plant Net Heat Rates. Reprinted from Mercury-steam Power Plants, by H. N. Hackett, Mechanical Engineering 73, 1951. By permission from American Society of Mechanical Engineers.

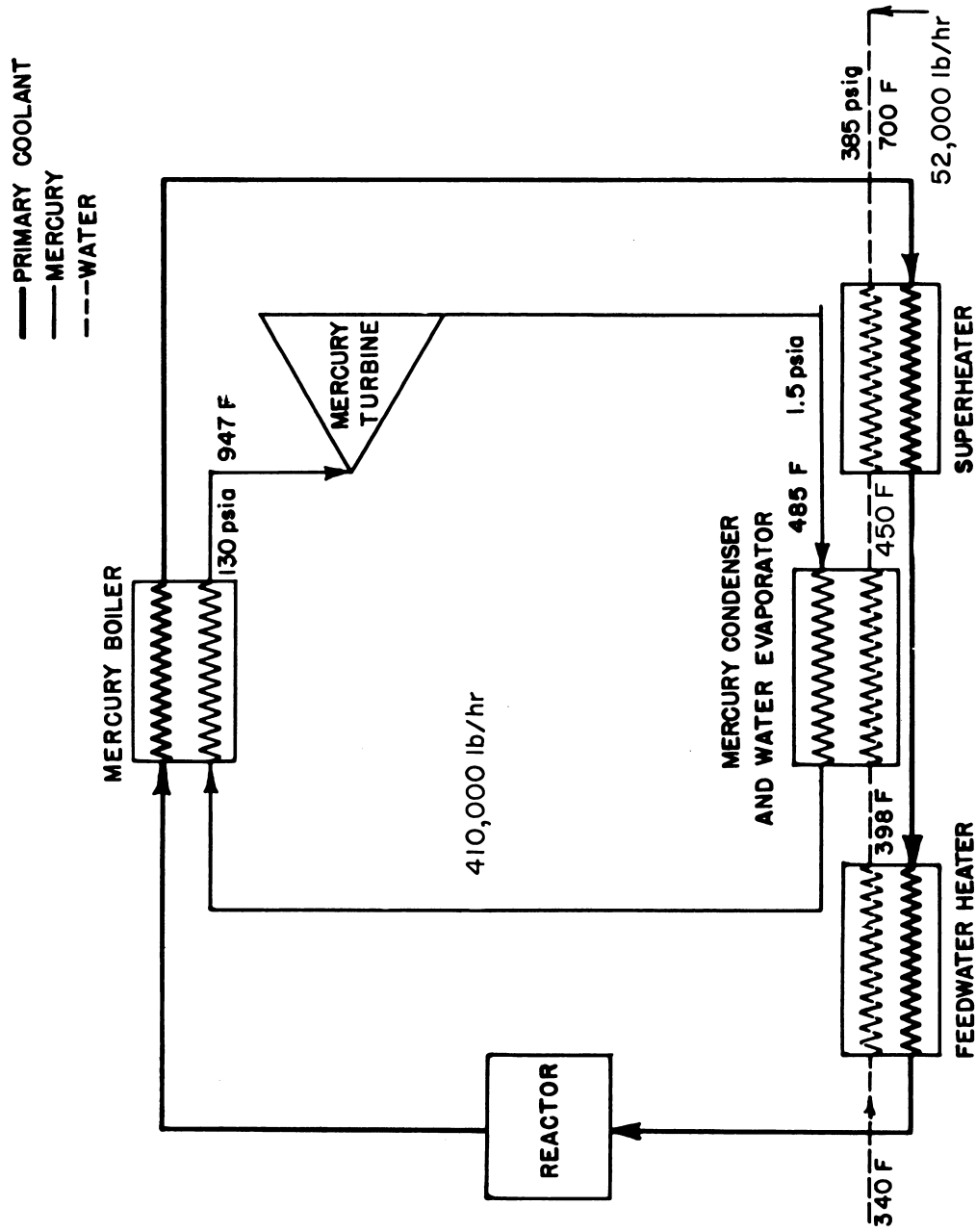


Fig. 2.5.6 — Power Cycle with Binary Mercury-water system. Submitted by KAPL, Feb. 12, 1953.

Mechanical Components and Design Considerations

REACTOR COMPONENTS

(J. H. Germer and C. R. Stahl)

FUEL ELEMENTS

REQUIREMENTS OF A FUEL ELEMENT

A fuel element is the basic unit which furnishes heat in an atomic power reactor. The element must be designed to work at reasonable stresses and internal temperatures. It must not be corroded by the coolant, nor should the fuel material corrode its container. In order that it may transmit a large amount of heat, it must have a large surface area and must have a low resistance to the coolant flow.

The fuel element should allow a reasonably large fraction of the fuel to be fissioned. Since some of the fission products are stable gases, the fuel element must be able to confine these gases either inside the fuel-element container or internally within the fuel solid. Evolution of these gases into the coolant stream is hazardous because of their inherent radioactivity.

From a nuclear standpoint, the fuel element should not contain excessive amounts of materials which readily absorb neutrons (B, Cd, Mn, Li, Co, and the like). The fuel should not be present in such large concentrations that it shields neutrons from itself. Finally, it is desirable that the fuel element should not become more reactive as its temperature or power increases.

As a structure, the fuel element must be reasonably easy and economical to fabricate, and it must be sufficiently sturdy to withstand any mechanical or fluid loads imposed upon it. Usually, it must also be replaceable in the reactor. To eliminate handling tremendous numbers of small individual fuel elements, the smaller elements are ordinarily assembled into fuel rods as units.

GENERAL TYPES OF FUEL ELEMENTS

(1) **Homogeneous.** In a homogeneous reactor, there are no individual fuel rods. The fuel is combined with the coolant, and the core consists essentially of an enlargement in the coolant stream. The fuel may exist as a solution in the coolant or as a slurry of a solid material in the coolant liquid.

(2) **Liquid Fuel Cooled by Secondary Fluid.** The fuel liquid in this case is not circulated but is present either inside or outside of tubes, from the other side of which the coolant liquid removes the heat. The fuel element may be an integral unit which can be removed individually, or it may be a permanent part of the reactor refueled by draining the fuel liquid.

(3) **Laminated Fuel and Structural Material.** Such materials as uranium-zirconium alloy clad on both sides with zirconium have been used with success. At present they are

used only in water-cooled reactors, but they could be applied to liquid-metal-cooled reactors.

(4) **Metal-filled Tubes.** This type is used as rather large elements in natural-uranium reactors but could be used in small, high-flux fuel elements. The use of a solid metal solves the gas-storage problem, since gaseous fission products are retained within the structure of the fuel. If the fuel element is to generate a high heat flux, there should be an intimate bond between the fuel and the tube. The fuel may be present either in the form of uranium metal or as an alloy such as uranium-zirconium. If a high percentage of fuel burnup is required, a dilute fuel alloy is preferred, since high burnup in uranium metal causes its disintegration.

(5) **Powder-filled Tubes (Pins).** This type of fuel element allows large burnup since disintegration of the fuel is not a problem; also, high temperatures in the fuel are less of a problem since they do not directly cause thermal stress. Normally, fission-product gases will be evolved from the powder, thereby requiring the element to be built as a pressure container.

CONTROL ELEMENTS

TYPES OF CONTROL

The power level of a reactor varies as the rate of fission. The power remains constant whenever the rate of neutron generation in the fission process is equal to the rate of neutron fission capture plus the neutrons lost through leakage and non-fission capture. Whenever this neutron balance is maintained, the reactor is said to be "at critical." If the rate of fission-neutron production is greater than the loss, the reactor is "above critical," and the power level rises. If it is less, the reactor is "below critical," and the power falls.

The purpose of the control element is to regulate this neutron balance. From the regulation standpoint, there are three basic types of controls which are often superimposed on a single control element.

(1) **Fine Control.** Maintains the reactor accurately "at critical," except when power is to be raised or lowered. Action may be rapid, but only over a small amplitude, and it may be operated automatically.

(2) **Shim Control.** Slowly regulates the control point over a wide range to compensate for large, long time effects such as fuel burnup and fission-product poisoning.

(3) **Safety Control (or "scram").** Rapidly shuts down the reactor in an emergency by causing it to be "below critical." This is usually accomplished both manually and automatically in case of too high a power level.

METHODS OF CONTROL

The neutron balance may be controlled by any of the following methods:

(1) Inserting neutron-absorbing rods into the reactor core (the usual method on thermal reactors).

(2) Inserting neutron-absorbing rods between the core and reflector.

(3) Removing fuel from the core.

(4) Moving portions of the reflector (either liquid or solid) which surround the core.

(5) Adding fluid poison to the coolant.

(6) Adding to the reactor core a "burnable poison" which is consumed at a rapid enough rate to compensate for the loss of reactivity.

(7) Removing moderator (such as heavy water) from core.

OTHER REACTOR COMPONENTS

SEALS

Normally, a reactor container must be penetrated to operate the control elements and to refuel. The control elements are usually operated through either rotating or reciprocating shafts. All such penetrations must be sealed to prevent the entrance of air and the exit of radioactive gases or coolant fluid. When liquid sodium is used as the coolant, seal construction is particularly important, since air which reacts strongly with sodium would thereby contaminate the system.

WELDED SEALS

A welded seal provides positive static sealing but may be inconvenient to remove. General practice has been to rely upon bolts for mechanical strength and to provide thin lips which can be welded without heating the body of the metal excessively.

Frozen Static Seals

When a coolant liquid with a melting point above ambient temperature is used, static sealing may be accomplished by allowing the liquid to freeze. This requires control of the temperature of the frozen zone. When the seal is to be removed, the frozen seal must be melted, but at the same time, the gas pressure must be maintained in order to prevent the liquid from freezing at a higher level. Melting may be accomplished electrically or by allowing the unit to heat from radioactive decay.

A frozen sodium seal should be blanketed by an inert gas to prevent corrosion of the sodium.

Frozen Rotating Seal (Fig. 2.6.1)

If the temperature gradient is maintained along the length of a frozen seal and if the other design conditions are favorable, a shaft will be free to rotate in the seal with low friction. Sodium under relatively high pressures has been sealed in this way. This type of seal cannot be relied upon, however, to seal against gas in the liquid metal.

Rubber Boot Seals (Fig. 2.6.1)

This seal system consists of a "rubber boot" in series with two rotating O-ring seals. A helium blanket is confined between the liquid-metal level and the seal to prevent sodium from reaching a level which would cause it to freeze. The rubber boot is a cylindrical piece of Type-GN Neoprene rubber of about 40 Durometer hardness, $4\frac{7}{8}$ in. OD, $3\frac{7}{8}$ in. ID, and $14\frac{5}{16}$ in. active length. The lower end is bonded to the rotating shaft, while the upper end is bonded to the stationary container. To enable the rubber boot to withstand a differential pressure on either side, metal rings are added for support. These rings are $\frac{3}{8}$ in. wide and are located on the inside and outside of the boot. The surface in contact with the rubber has rounded edges and is chrome-plated to reduce friction and wear between the rings and the boot. To enhance the bearing sliding characteristics between adjacent rings during twisting of the boot, alternate rings are made of bronze, so that a bronze:chrome-plated carbon-steel bearing surface exists between rings. A thin film of molybdenum disulfide is used as a lubricant. This seal was designed for 140° rotation. Leakage through the boot is caused only by diffusion and can be calculated from its diffusivity of $9 \times 10^{-8} \text{ cm}^3/(\text{min})(\text{cm})(\text{cm Hg})$. It is independent of flexing:

$$\text{Leakage } \frac{\text{cm}^3}{\text{min}} = \frac{\text{diffusivity} \times \text{area (cm}^2\text{)} \times \text{pressure across seal (cm Hg)}}{\text{thickness (cm)}}$$

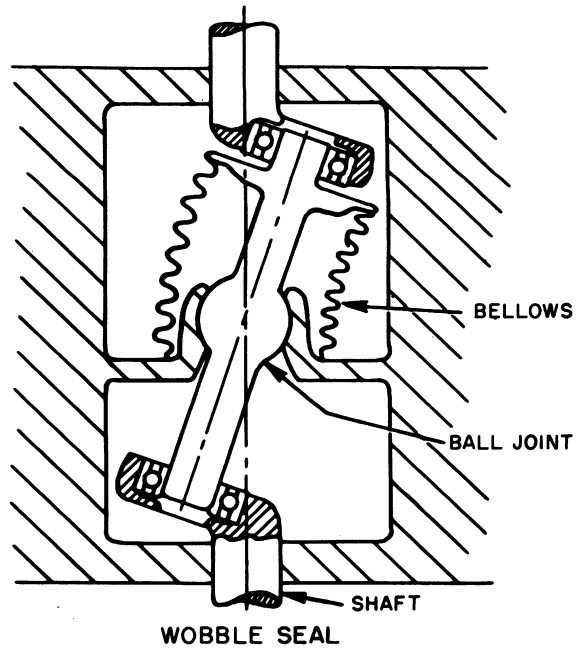
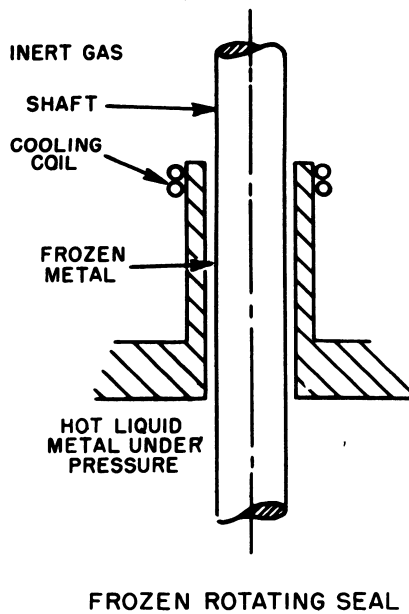
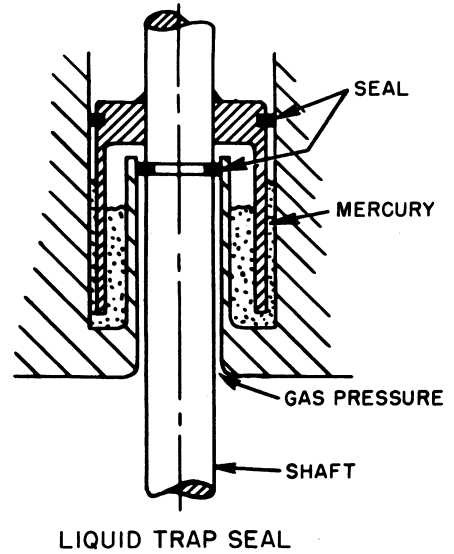
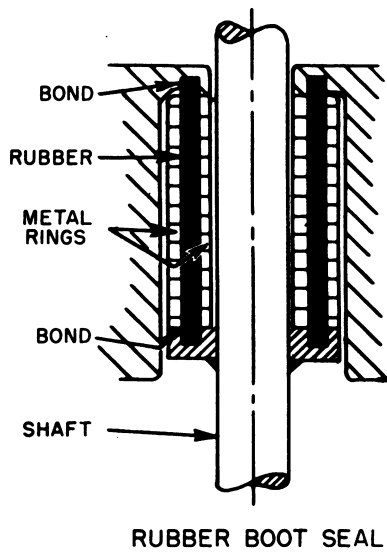


Fig. 2.6.1— Four Types of Seals Used in Reactors. Submitted by Knolls Atomic Power Laboratory, Feb. 27, 1953.

Liquid Trap Seals (Fig. 2.6.1)

A positive, diffusion-free seal can be made by requiring that any leakage gas pass through a trap filled with mercury or other liquid of extremely low gas diffusivity. Low pressure can be sealed with a seal in the form of a manometer; higher pressures can be sealed by a combination of liquid and a conventional sealing member.

Wobble Seals (Fig. 2.6.1)

Positive sealing of a reciprocating shaft can be accomplished with a welded metal bellows, but this method does not lend itself to a direct rotational seal. A rotating seal, however, can be made by converting rotational motion into a wobble motion or a reciprocating motion, passing it through a metal bellows, and then converting back to rotational motion. This seal tends to be rather bulky and to have a limited torque and thrust capacity.

BEARINGS

Only bearings operating under conditions unique to reactor operation and associated with liquid-metal-cooled reactors are considered here. Important factors in the design of such bearings are compatibility of the bearing materials, friction, stability under irradiation, and ease of manufacture.

Compatibility of Materials

Two materials which have been found to give satisfactory service in liquid metal for intermittent, light-load service are Type-138A Kennametal on 779 Carboloy. Bearings made of these materials have been run in sodium at 850° to 950°F under a loading of 50 psi with good results; the maximum friction coefficients found under these conditions were 0.31 running and 0.53 static.

Journal-Bearing Design

Reduction of Thermal Stresses

Since bearing materials which differ from the structural material (stainless steel) must be used, differential thermal expansion between materials could result in severe thermal stresses. This effect is eliminated by the design shown in Fig. 2.6.2 which makes use of conical surfaces. In this bearing, any dimensional change produced by temperature variation is radial from the "origin" which is located on the shaft center line. This eliminates any variation in the tightness of the bearing in its support as a result of relative thermal expansion. The only stresses introduced by a differential thermal expansion between the bearing and the shaft will be sliding stresses at the bearing-shaft interface owing to relative expansion between the bearing and the shaft materials.

Allowance for Misalignment

To minimize the effects of misalignment, the inner (journal) bearing surface is made slightly convex (15 in. radius). Small misalignment is possible with only a slight amount of curvature (less than spherical); a spherical surface would produce higher contact stresses but would be capable of large misalignment.

Clearance

The bearing was designed to give 0.0135 in. to 0.0145 in. diametrical clearance on the 4.5-in. contact diameter. This is based upon permissible play and freedom from binding.

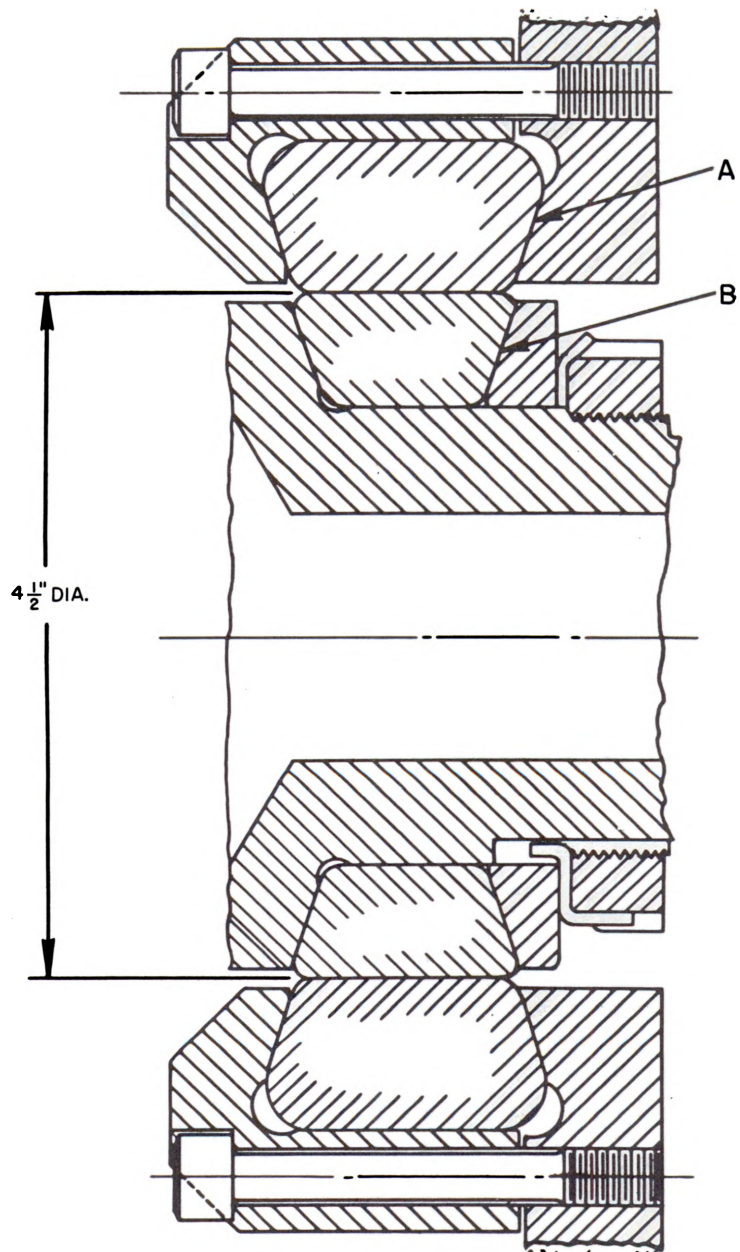


Fig. 2.6.2—Journal Bearing. Submitted by Knolls Atomic Power Laboratory, Feb. 27, 1953.

Materials

The inner race is made from 138A Kennametal and the outer race of 779 Carboloy.

Anti-Friction Bearings

Ball and roller bearings can be used if they are constructed of materials which will remain hard at high temperatures (such as 18-4-1 tool steel). They should be designed so that there is a minimum of sliding of the various parts of the bearing on each other. To accommodate axial and angular misalignment as in the journal bearing (Fig. 2.6.2), several bearing designs anti-friction have been developed (Figs. 2.6.3, 2.6.4, and 2.6.5). For small-angle oscillations, conventional needle bearings of 18-4-1 tool steel have been successful.

THERMAL SHOCK SHIELDS

(R. J. Fritz)

NEED FOR SHIELDS

It is well known that thermal gradients in structural members cause thermal stresses owing to unequal expansion of the various elements of the structure. When the thermal gradients are transient instead of steady state, determination of these stresses at any instant is unchanged. In the operation of nuclear reactors, where large quantities of heat are transferred to a fluid heat-transfer medium, thermal transients are generated in the fluid coolant and hence in the associated reactor structure when a constant relationship between the reactor power and the coolant flow rate is not maintained.

Probably the most severe thermal transient is caused by an emergency shutdown or scram of the reactor. Reactor power will generally decay more rapidly than the coolant flow rate decreases causing transient thermal stresses in the structure owing to the quenching action of the coolant. In systems using fluid capable of transferring very high transient heat flux rates, rather severe thermal gradients may be induced in the enclosing structure, depending on the coolant temperature changes involved. As the thermal transients are propagated into the material of the structure, the gradients are reduced or dissipated.

The presence of thermal gradients in a structural plate, which is restrained against bending, or in the wall of a long circular cylinder causes thermal stresses given by:

$$\sigma_x = \sigma_y = \frac{E\alpha}{1-\mu} (T_0 - T) \quad (1)$$

where σ_x and σ_y are biaxial stresses tangential to the surface taken in the principal directions. Equation (1) is not valid near the edges of the plate or cylinder. In the case of a cylinder, x and y are taken in the longitudinal and circumferential directions. The stress in the direction normal to the surface may normally be neglected. E is Young's modulus; α , the coefficient of linear thermal expansion; and μ , Poisson ratio for the material. The quantity $E\alpha/1-\mu$ is approximately 360 psi/°F for austenitic steels and about 220 psi/°F for ferritic steels. The temperature distribution in the structure will be generally a function of time and the normal distance from the coolant surface. T_0 is the average temperature of the plate or cylinder wall, and T is the temperature at the point for which the stresses are being evaluated. For a plate, the average temperature is given by:

$$T_0 = \frac{1}{e} \int_0^e T(x) dx \quad (2)$$

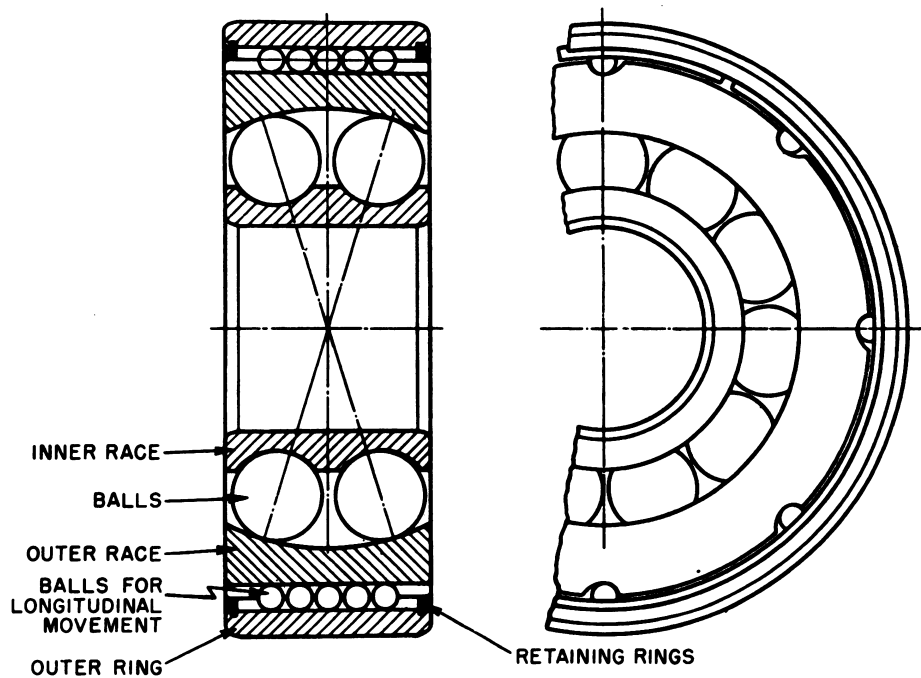


Fig. 2.6.3 — New Departure Bearing. Reprinted from Babcock and Wilcox Rept. 5065, J. S. Gilhart and W. Market, Jr., Rolling Contact Bearings for Oscillating Service in High-temperature Sodium, Oct. 30, 1952.

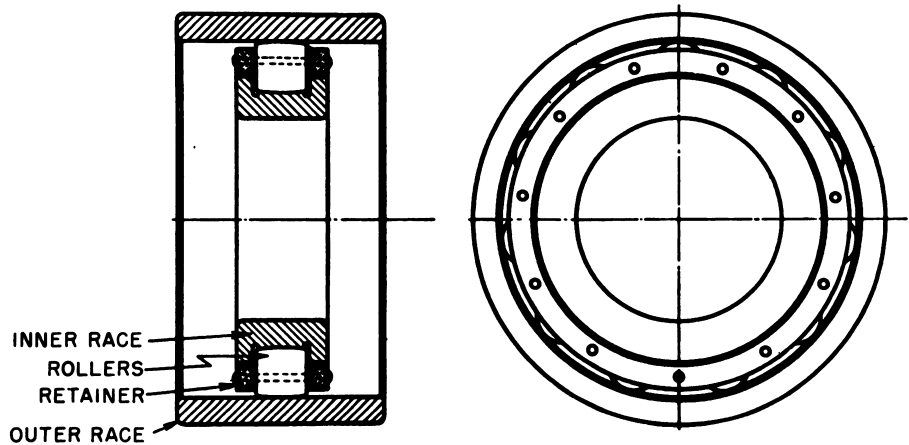


Fig. 2.6.4 — Shafer Bearing. Reprinted from Babcock and Wilcox Rept. 5065, J. S. Gilhart and W. Market, Jr., Rolling Contact Bearings for Oscillating Service in High Temperature Sodium, Oct. 30, 1952.

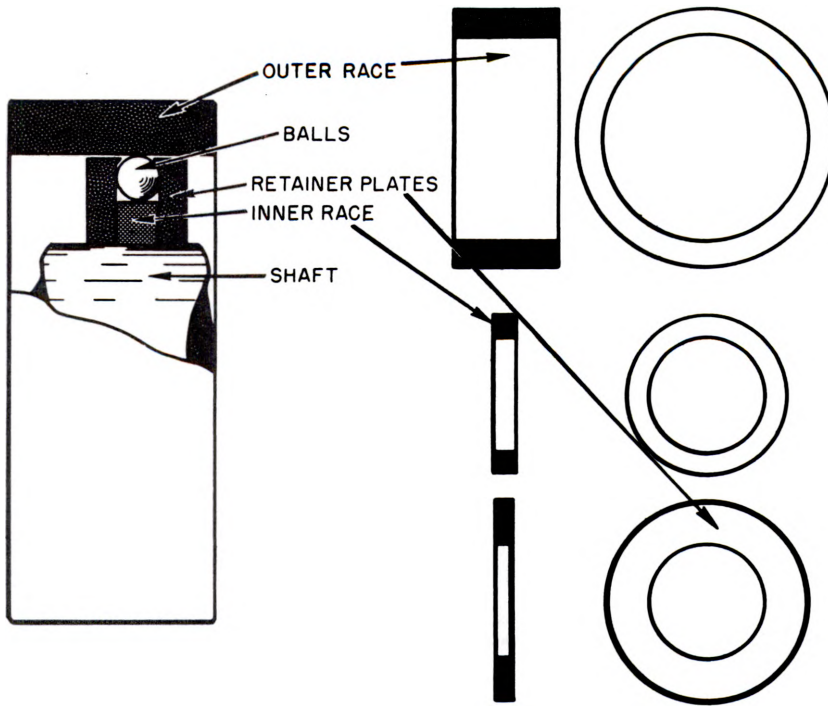


Fig. 2.6.5—De Groh Bearing. Reprinted from Babcock and Wilcox Rept. 5065, J. S. Gilhart and W. Market, Jr., Rolling Contact Bearings for Oscillating Service in High Temperature Sodium, Oct. 30, 1952.

where $T(x)$ is the temperature distribution as a function of the thickness coordinate x . For a cylindrical shell:

$$T_0 = \frac{2}{b^2 - a^2} \int_a^b rT(r)dr \quad (3)$$

where b and a are the outside and inside radii of the shell and $T(r)$ is the temperature distribution as a function of the radial coordinate r . For a pipe where the diameter is much larger than the wall thickness, Eq. (3) will reduce to Eq. (2).

This relation gives the actual stress if the proportional limit of the material is not exceeded. Otherwise, it gives merely an index to the thermal-shock severity.

When a thermal transient is impressed on the surface of a structure, the thermal gradients are most severe near the surface and become less severe with increasing distance from the surface. If it is desired to protect the structure from thermal-shock stresses, putting thin laminations or thermal shields between the coolant surface and the structure will filter out or attenuate severe gradients. It is possible by choosing the thickness of these laminations to limit the thermal stress in the structure.

A procedure that may be used to estimate the thermal stresses is as follows:

- (1) Determine the transient-temperature distribution in the structure wetted by the coolant. This temperature distribution is plotted with the distance normal to the wetted surface as abscissa and time as a parameter.
- (2) Determine the average temperature of the lamination T_0 , by Eq. (2) or (3), whichever applies. Equation (2) can be solved graphically by finding on the temperature-vs-distance plot the rectangle that gives the same area as the actual temperature distribution. The

height of the rectangle is the average temperature, T_0 , and the base is the plate thickness.

By a cut-and-try method, one can determine the lamination thickness to limit the maximum transient stress to a specified value. The problem is then to support these laminations so as to accommodate their shrinkage relative to their supports.

DESIGN BASIS FOR SHIELDS

DETERMINATION OF THERMAL SHOCK STRESS LIMITATIONS

The term "thermal shock" implies a thermal transient severe enough to cause failure within only a few cycles or even a single cycle. Fatigue failures may also occur after many cycles of fast- or slow-cycling of more moderate thermal stresses. Moreover, a thermal transient that causes a fatigue failure in one structural geometry could, in a different structural geometry, cause failure within only a few cycles. Hence, there is no inherent characteristic of the thermal transient that identifies it as being critical either from thermal-shock or thermal-fatigue standpoints.

Thermal stresses differ from the ordinary engineering stresses in that they represent a strain input rather than a load input. To accommodate very large thermal stresses such as those which may occur in a high specific-power nuclear reactor, extra care must be exercised in design to anticipate those factors that cause loss of ductility or embrittlement of the structure, such as corrosion, galling, stress concentrations, high stress gradients, low-quality material, poor welds, time-temperature aging, and nuclear radiation damage.

Notches, weldments, and structural discontinuities (as flanged pipes) which are present in power-plant structures cause loss of ductility. To test these factors, a thermal-shock test program has been jointly undertaken by Mine Safety Appliances Company and the Knolls Atomic Power Laboratory. The first specimen to be tested was a section of butt-welded 8-in., Schedule-40 (0.322-in. wall) stainless-steel (Type-347) pipe. The inside pipe surface was quenched 2500 times with NaK from 850°F to about 400°F in about one second. The pipe did not exhibit any operational deficiencies. Radiographic and liquid-penetrant tests did not reveal any defects. Subsequent examination by microphotographs, however, revealed that cracks that had formed during welding in the root section between the pipe and backup ring had propagated during the test. Cracks extending about 0.010 in. into the 0.322-in. wall were observed. This test provided evidence of the detrimental features of leaving backing rings in thermally-shocked butt-welded pipes.

Stresses (produced by thermal shock) in excess of the yield strength may be permitted in design provided the severity of the stress and the number of repetitions of thermal shock are known. When plastic flow of the metal results from severe thermal stress brought about by a particular reactor operating condition, a change in operating conditions can lead to a reversal both in stress and plastic flow. Consequently, the cycling of these operating conditions may result in failure by fatigue in severely loaded components. An experimental program* is being carried out at KAPL to assess the seriousness of the phenomenon and to reliably determine a satisfactory basis for design. Thin-walled, tubular, test specimens are subjected to cyclic uniaxial stresses induced by thermally shocking the specimen and constraining the specimen longitudinally. The temperature cycle is essentially a square wave with time. Heating is accomplished electrically with the specimen serving as its own resistance, and cooling is done with an air blast. The "hold time" is the time for which both the maximum and minimum temperatures are maintained in each cycle and is adjustable over limits. Test conditions have covered a wide range of thermal shock varied in magnitude, mean temperature, and cycling period.

*Details of this program are described in *An Apparatus for the Study of the Effects of Cyclic Thermal Stresses on Ductile Metals*, Knolls Atomic Power Laboratory, L. F. Coffin, Jr. and R. P. Wesley, KAPL-830, Oct. 27, 1952, Unclassified.

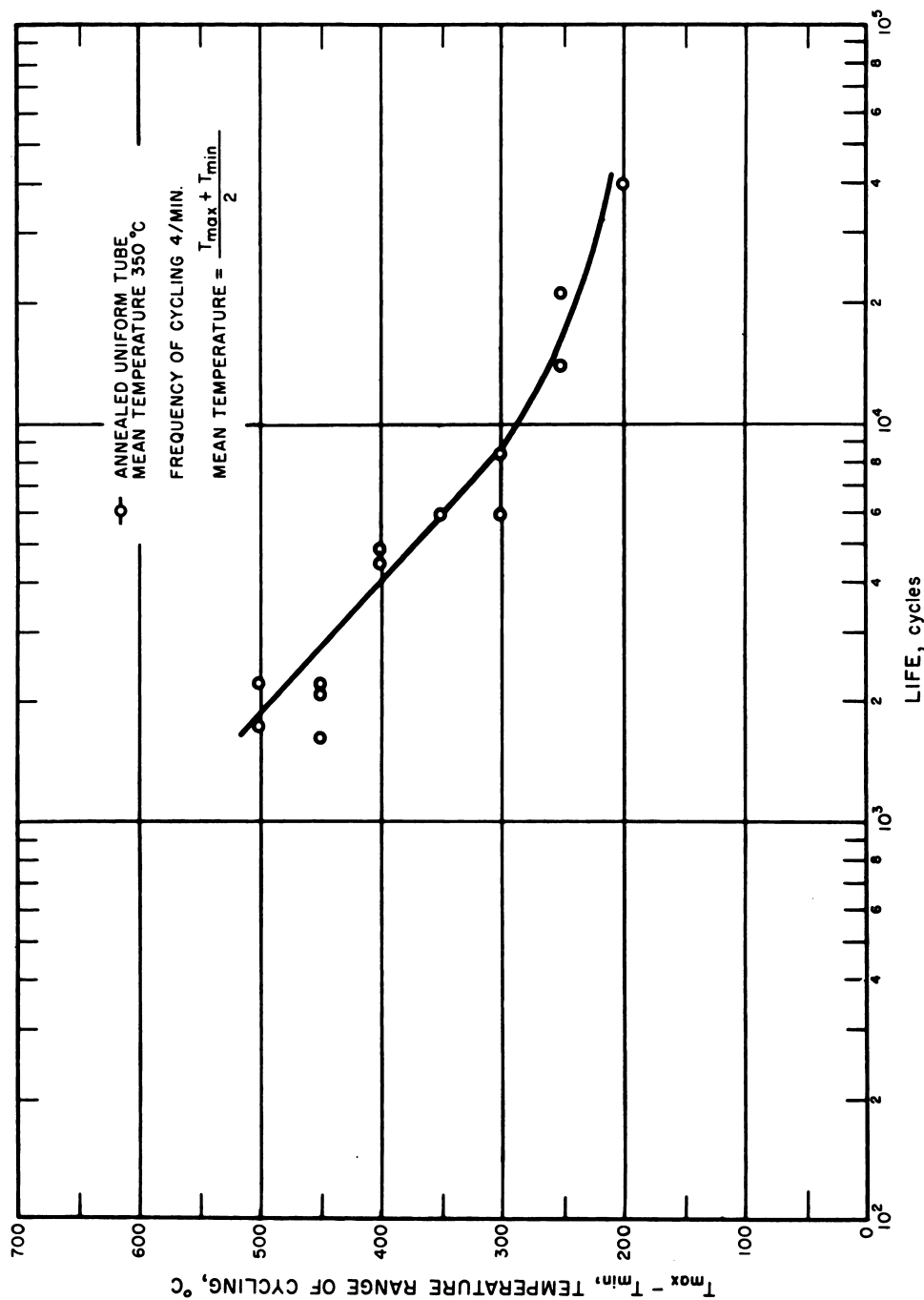


Fig. 2.6.6—Influence of Thermal Cycling with Uniaxial Constraint on Life of Type 347 Stainless Steel. Submitted by Knolls Atomic Power Laboratory, Feb. 27, 1953.

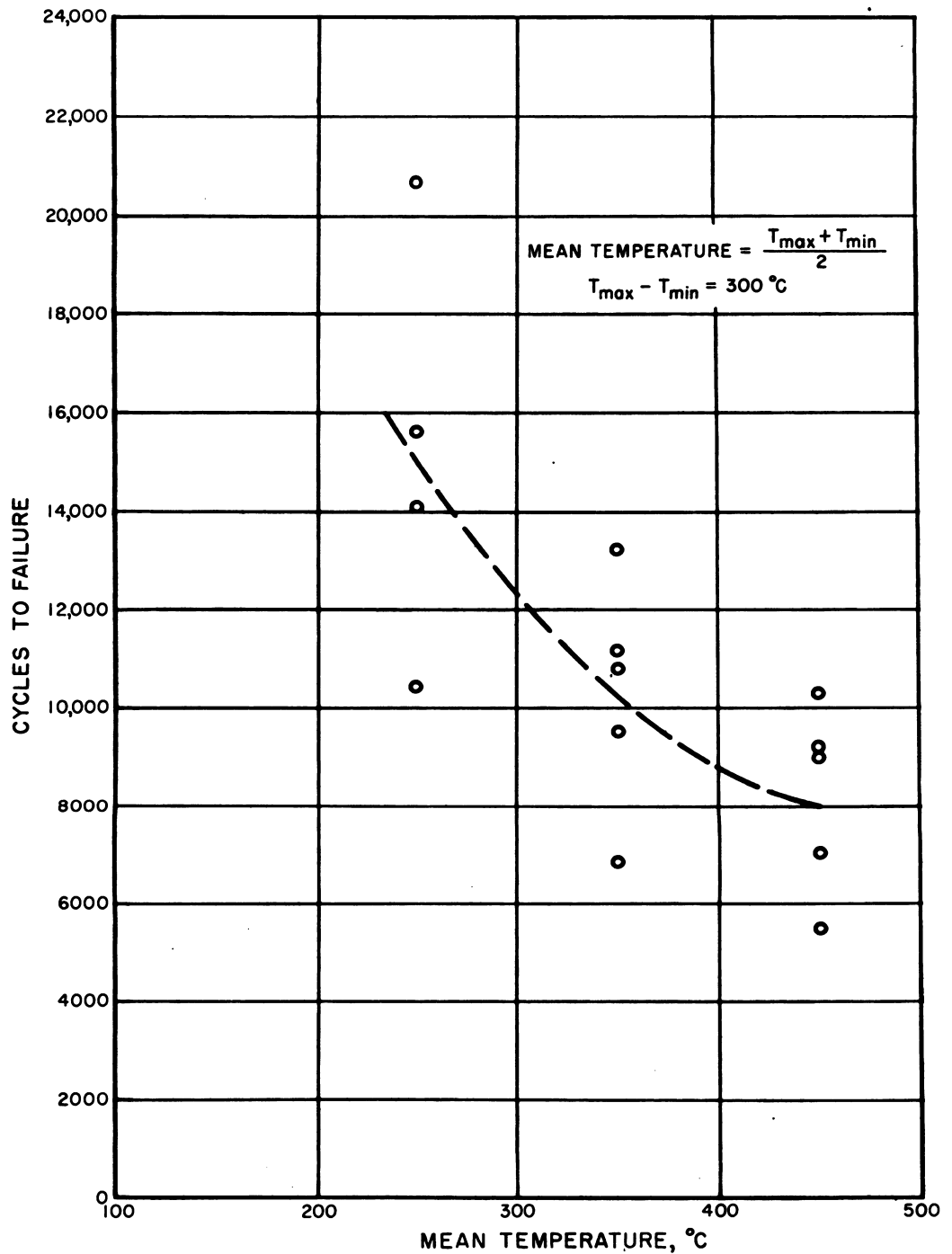


Fig. 2.6.7— Effect of Mean Temperature on Cycles-to-failure for Thermally-cycled Type 347 Stainless Steel. Submitted by Knolls Atomic Power Laboratory, Feb. 27, 1953.

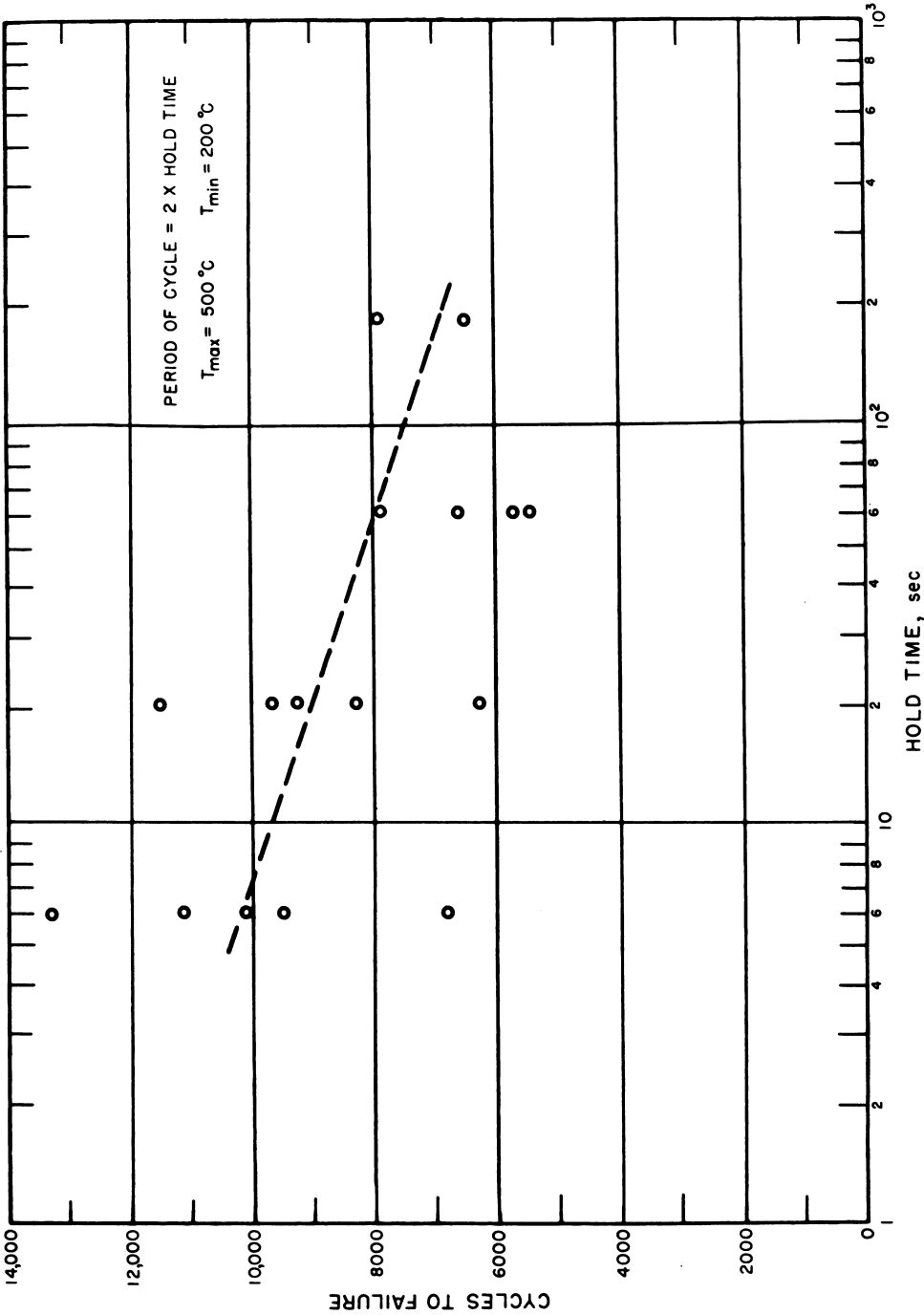


Fig. 2.6.8—Effect of Hold Time on Cycles-to-failure for Thermally-cycled Type 347 Stainless Steel. Submitted by Knolls Atomic Power Laboratory, Feb. 27, 1953.

A fairly thorough investigation of annealed Type-347 stainless steel has been carried out. Figure 2.6.6 shows the effect of the magnitude of repeated thermal shocks ($T_{\max} - T_{\min}$) in producing fatigue failures for this material. Here, the mean temperature [$(T_{\max} - T_{\min})/2$] of the shock is maintained at 350°C (662°F) with about 4 cycles of thermal shock per minute. Variation of the mean temperature while maintaining a thermal shock, which is fixed in magnitude (300°C), is shown in Fig. 2.6.7. Finally, in Fig. 2.6.8, the influence of the frequency of cycles on cycles-to-failure for a particular magnitude of thermal shock is shown.

RESIDUAL HEAT REMOVAL

[D. J. Oakley and G. E. Tate (Foster Wheeler)]

Residual or emergency cooling systems are required for any reactor that will produce sufficient heat, if the coolant flow is interrupted, to damage the structure by the effects of high temperature. Reliable systems have been designed and tested either to add coolant to a system or to implement circulation and heat removal from the reactor, or both. If the integrity of the reactor cooling system is high, the first problem can be dismissed. It is preferable to prevent a loss of coolant rather than to have a reservoir system with only a limited life.

SELECTED READING LIST

Reactor Components

ROLLING CONTACT BEARINGS FOR OSCILLATING SERVICE IN HIGH TEMPERATURE SODIUM, J. S. Gilhart and W. Market, Jr., Babcock and Wilcox Company, Rept. No. 5065, Oct. 30, 1952, 26 pp (classified).

INTERIM REPORT: CONTROL ROD GAS SEALS, W. A. Heywood and C. J. Hibbert, Knolls Atomic Power Lab., KAPL-669, Jan. 14, 1952, 83 pp.

Thermal Shock Shields (Thermal Stresses)

References specifically on thermal-shock shields as such are nonexistent. However, since thermal shock is but a special case of thermal stress the following works are recommended.

TEXTBOOKS

CONDUCTION OF HEAT IN SOLIDS, H. S. Carslaw and J. C. Jaeger, Oxford Press, 1947.

THEORY OF ELASTICITY, S. Timoshenko and J. N. Goodier, McGraw-Hill, 1951. Chapter 14 contains a thorough discussion of thermal stresses and their analysis. Discusses work by earlier authors on plates (Goodier, 1936; J. P. Den Hartog, 1936), cylindrical shells and cylinders (Den Hartog, *ibid*; C. H. Kent, 1931), modern general methods of analysis (M. A. Biot, 1935; Goodier, 1937; N. O. Myklestad, 1941).

HANDBOOK OF EXPERIMENTAL STRESS ANALYSIS, M. Hetenyi, John Wiley and Sons, 1950. Section S of Chapter of Analogies discusses Biot's work (1935) in reducing two-dimensional thermal stresses to dislocation theory; also suggests mechanical testing methods for thermal stresses.

HIGH-TEMPERATURE PROPERTIES OF METALS, Parker et al, Amer. Soc. Metals, 1950.

PROPERTIES OF METALS AT ELEVATED TEMPERATURES, G. V. Smith, McGraw-Hill, 1950.

WARMESPANNUNGEN, E. Melan and H. Parkus, Springer, Wien (announced for 1953).

SUMMARY REPORTS

BEHAVIOR OF METALS UNDER CONDITIONS OF THERMAL STRESS, S. S. Manson, Heat Transfer Symposium, Univ. of Mich., 1952.

THERMAL FATIGUE AND THERMAL SHOCK, H. Thielsch, Welding Res. Council Bull.

RECENT PAPERS AND REPORTS CONCERNED MOSTLY WITH ANALYSIS AND ELASTIC BEHAVIOR

THERMAL STRESSES IN SPHERES AND CYLINDERS PRODUCED BY TEMPERATURES VARYING WITH TIME, C. H. Kent, Trans. ASME, 1932.

- STRESSES IN BOILER TUBES SUBJECTED TO HIGH RATES OF HEAT ABSORPTION, W. L. De Baufre, Trans. ASME, 1932.
- THERMAL STRESSES IN LONG CYLINDRICAL BODIES, B. E. Gatewood, Phil. Mag., 1941.
- ON THERMAL STRESSES, STRAINS, AND WARPING, F. H. Murray and G. Young, AECD-2960, 1944.
- THERMAL STRESSES AND STRAINS IN A FINITE CYLINDER WITH NO SURFACE FORCES, F. H. Murray, AECD-2966, 1945.
- THERMAL STRESSES IN A RECTANGULAR PLATE CLAMPED ALONG AN EDGE, B. J. Aleck, J. A. M., 1949.
- STRESSES IN LONG, THIN-WALLED CYLINDERS, DUE TO AN AXIAL TEMPERATURE GRADIENT, G. Horvay and W. P. Manger, KAPL-390, 1940.
- THERMAL STRESSES IN PERFORATED PLATES, G. Horvay, Proc. First Nat'l. Congress of Applied Mech., KAPL P-780, 1950.
- THERMOELASTIC STRESS IN THE SEMI INFINITE SOLID, R. D. Mindlin and D. H. Cheng, J. A. Ph., 1950.
- THE EFFECT OF NON-UNIFORM TEMPERATURE DISTRIBUTIONS ON THE STRESSES AND DISTORTIONS OF STIFFENED-SHELL STRUCTURES, R. R. Heldenfels, NACA-TN2240, 1950.
- NUMERICAL METHOD FOR STRESS ANALYSIS OF STIFFENED-SHELL STRUCTURES UNDER NON-UNIFORM TEMPERATURE DISTRIBUTIONS, R. R. Heldenfels, NACA-TN2241, 1950.
- STRESSES IN PIPE BUNDLES, H. Poritsky and G. Horvay, J. A. M., 1951.
- TEMPERATURE AND STRESS DISTRIBUTION IN SPHERES, RODS, TUBES, AND PLATES IN WHICH SOURCE IS WITHIN THE BOUNDARIES OF THE SOLIDS, J. C. Carter, ANL-4690, 1951.
- TEMPERATURE STRESSES IN IRREGULAR SOLIDS, R. D. Hoyle, Nature, 1951.
- BIHARMONIC RELAXATION METHOD FOR CALCULATING THERMAL STRESSES, A. G. Holms, NACA-TN2434, 1951.
- TRANSIENT THERMAL STRESSES IN CIRCULAR DISKS, G. Horvay, KAPL-518, 1951.
- STRESSES IN PERFORATED SHEETS DUE TO NON-UNIFORM HEATING, G. Horvay, KAPL-566, 1951.
- THE PLANE STRESS PROBLEM OF PERFORATED PLATES, G. Horvay, J.A.M., KAPL P-769, 1952.
- EXPERIMENTAL AND THEORETICAL DETERMINATION OF THERMAL STRESSES IN A FLAT PLATE, R. R. Heldenfels and M. Roberts, NACA-TN2769, 1952.
- TRANSIENT THERMAL STRESSES, M. Heisler and E. Martin, NAA-SR-176, 1952.
- A GENERAL METHOD FOR DETERMINATION OF THE THERMAL STRESSES IN A COMPOSITE MEDIUM, J. Brandstatter, NAA-SR-184, 1952.
- SIMILARITY LAWS FOR STRESSING HEATED WINGS, H. S. Tsien, I.A.S., 1953.
- THERMAL BUNDLING OF PLATES, M. L. Gossard, P. Seide, and W. M. Roberts, NACA-TN2771, 1952.
- THERMAL STRESSES IN A PARTIALLY CLAMPED ELASTIC HALF-PLANE, J. H. Huth, J. A. Ph., 1952.
- TRANSIENT THERMAL STRESSES IN DISKS AND CYLINDERS, G. Horvay, Paper to be presented at Los Angeles meeting of the ASME, 1953.
- RECENT PAPERS AND REPORTS CONCERNED MOSTLY WITH PLASTICITY, CREEP, FATIGUE, SHOCK, AND EXPERIMENTAL METHODS AND DATA.**
- APPLICATION OF BAILEY'S THEORY OF TUBE STRESS CALCULATIONS, C. O. Rays, Proc. Am. Petroleum Inst., Vol. 19, 1938.
- CYCLIC HEATING TEST OF STEAM PIPING JOINTS BETWEEN FERRITIC AND AUSTENITIC SHELLS, H. Weisberg, Trans. ASME, 1949.
- ANALYSIS OF ROTATING DISKS OF ARBITRARY CONTOUR AND TEMPERATURE DISTRIBUTION IN THE REGION OF PLASTIC DEFORMATION, S. S. Manson, Proc. First Nat'l. Congress of Applied Mech., ASME, 1950.
- SAFETY MARGINS AND STRESS LEVELS IN HIGH-TEMPERATURE EQUIPMENT, E. L. Robinson, Trans. ASME, 1951.
- EXPERIENCE WITH AUSTENITIC STEELS IN HIGH-TEMPERATURE SERVICE IN PETROLEUM INDUSTRY, M. E. Holmberg, Trans. ASME, 1951.
- CENTRIFUGAL AND THERMAL STRESSES IN DISKS, AND STRESS CHANGES DUE TO PLASTIC FLOW AND CREEP, R. L. Brooking, J. Brown, and B. R. Atkins, Nat'l. Gas Turbine Establishment (Great Britain), Report R-122, 1952.
- AN APPARATUS FOR THE STUDY OF THE EFFECTS OF CYCLIC THERMAL STRESSES ON DUCTILE METALS, L. F. Coffin and R. P. Wesley, KAPL-830, 1952.
- STUDY OF THE EFFECTS OF CYCLIC THERMAL STRESSES IN A DUCTILE METAL, L. F. Coffin, KAPL, 1953.
- THERMAL-SHOCK AND OTHER COMPARISON TESTS OF AUSTENITIC AND FERRITIC STEELS FOR MAIN STEAM PIPING, W. C. Steward and W. G. Schreitz, ASME Transaction, Oct. 1950.

Design and Construction of External Heat-transfer System

The technology of sodium and NaK heat-transfer systems is comparatively well developed; both large- and small-scale systems have been operated over extended periods at temperatures up to 1000°F with a fluid temperature rise as high as 300°F. Power plants with mercury as the working fluid have been operated successfully for many years. Lithium and lead-bismuth coolants, on the other hand, have been studied only in small-scale laboratory systems.

Most experience with liquid metals has been limited to non-radioactive systems. To date, two liquid-metal-cooled reactors have been operated, viz., the NaK-cooled Experimental Breeder Reactor (EBR), which is a dual-purpose installation of power-plant scale, and the mercury-cooled fast-reactor at Los Alamos, from which the heat is removed without power production. Although transfer of radioactive material with liquid metal as the carrier has been noted in laboratory experiments, it was not observed at EBR after approximately 12 megawatt-days of operation.

The design and construction of liquid metal systems is based upon established high-temperature practice with special provisions for the unusual properties of the liquid metals:

(1) It is most important that the system be completely leak-tight to prevent escape of radioactive and/or chemically active coolant, or in-leakage of air. This requirement affects every component and is most significant in the design of pumps and valves, which entail shaft penetrations into the system. All-welded construction is recommended for piping and heat exchangers, and leak testing with sensitive instruments, such as the helium mass spectrometer, is advisable both during and after fabrication.

(2) A high degree of system cleanliness is essential. Internal surfaces must be kept free of welding scale, cutting oils, and dirt during assembly; the completed system should be degreased with an appropriate solvent, then flushed out and thoroughly dried.

(3) For metals with high melting points, e.g., sodium, lithium, or lead-bismuth, freezing and plugging difficulties are encountered, particularly in small lines, and provision must be made for preheating the entire system before circulation is started.

HEAT EXCHANGERS AND STEAM GENERATORS

(D. B. Nelson)

Units for the exchange of heat from one liquid metal circuit to another are used to isolate a reactor coolant from a non-radioactive system. These "intermediate heat exchangers" must be specially constructed to prevent leakage between circuits should the reactor coolant become highly radioactive. Since their normal operating pressures are low (less than 100 psi), some latitude in design configuration is available.

For liquid metal steam generators, the potentially violent reaction between water and the alkali metals necessitates special construction features. Moreover, design latitude is considerably restricted since steam pressures of 400-600 psi may be required.

Thus, most liquid-metal heat-transfer units, whether exchangers or steam generators, have been designed so that simultaneous faults in two separate circuits must occur before the fluids can mix. Several such installations have been operated in the Alplaus Heat Transfer Test System at the Knolls Atomic Power Laboratory. In these units, the conventional shell-and-tube configuration has been modified to include concentric tubes joined to individual tube sheets with a static liquid (thermal bond) in the annulus between tubes and in the space between tube sheets; sodium has been used as the static fluid in the heat exchangers and mercury in the steam generators. Leakage from either circuit can be detected from a variation of the pressure or the volume of the static fluid. Thermal expansion is taken up by bellows expansion joints or by using free-mounted hairpin tubes.

A heat exchanger and steam generator of different designs are used in the power conversion system of the Experimental Breeder Reactor.^{1,2} The heat exchanger is of the shell-and-tube type with hairpin tubes of "L" nickel and with seal-welded mechanical joints. The steam generator is composed of concentric nickel tubes; the annular spaces are filled with copper provided with minute longitudinal flutes to allow passage of gas. The presence of metal vapor or oxides in the gas permits detection of leaks.

Duplex tubes without an intermediate bonding medium and either with or without detection flutes are also under development.³

Completely separate circuits can also be maintained by passing each fluid through its own set of tubes. The two sets are intermeshed to form a bundle immersed in the static fluid which provides the thermal bond between the tubes. Differential expansion between the outer shell and both sets of tubes is absorbed by bending of the hockey-stick-shaped tubes (Fig. 2.7.1). Such units yield high over-all heat-transfer coefficients at relatively low pressure drops, since all circulation is inside tubes. Still further reduction in size has been gained by flattening the tubes to approach a flat-plate configuration. Shell-and-tube units of single-walled tube construction have been used in numerous cases where less assurance of leak tightness was required.

The performance of two liquid metal heat exchangers is illustrated by Fig. 2.7.2. The data⁴ are for sodium-to-NaK heat exchangers designed for 8×10^6 Btu/hr rating at a log mean temperature difference of 70°F. The over-all heat-transfer coefficient is plotted against flow rate when the ratio

$$\frac{W_{\text{NaK}} c_{p_{\text{NaK}}}}{W_{\text{Na}} c_{p_{\text{Na}}}} \text{ or } \frac{\Delta t_{\text{Na}}}{\Delta t_{\text{NaK}}} = 0.77, 1.0, \text{ and } 1.3$$

where W = mass flow rate, lb/hr
 c_p = specific heat, Btu/(lb)(°F)
 Δt = temperature rise, °F

These exchangers employed "L" nickel tubes and a sodium-filled annulus to obtain maximum thermal conductance of the walls and thereby capitalize on the high, liquid-metal, heat-transfer coefficients. Wall resistance still represents 30 to 50 percent of the total.

Steam-generator performance is illustrated by the Fig. 2.7.3 evaporator and superheater data of units described by Brooks and Rosenblatt.⁴ These are of concentric-tube construction with static mercury as the thermal bond. The steam circuits differ in that one is natural circulation and the other forced circulation. The values obtained indicate the general experience in producing steam at 500 psia and superheating to 760°F.

¹References appear at end of chapter.

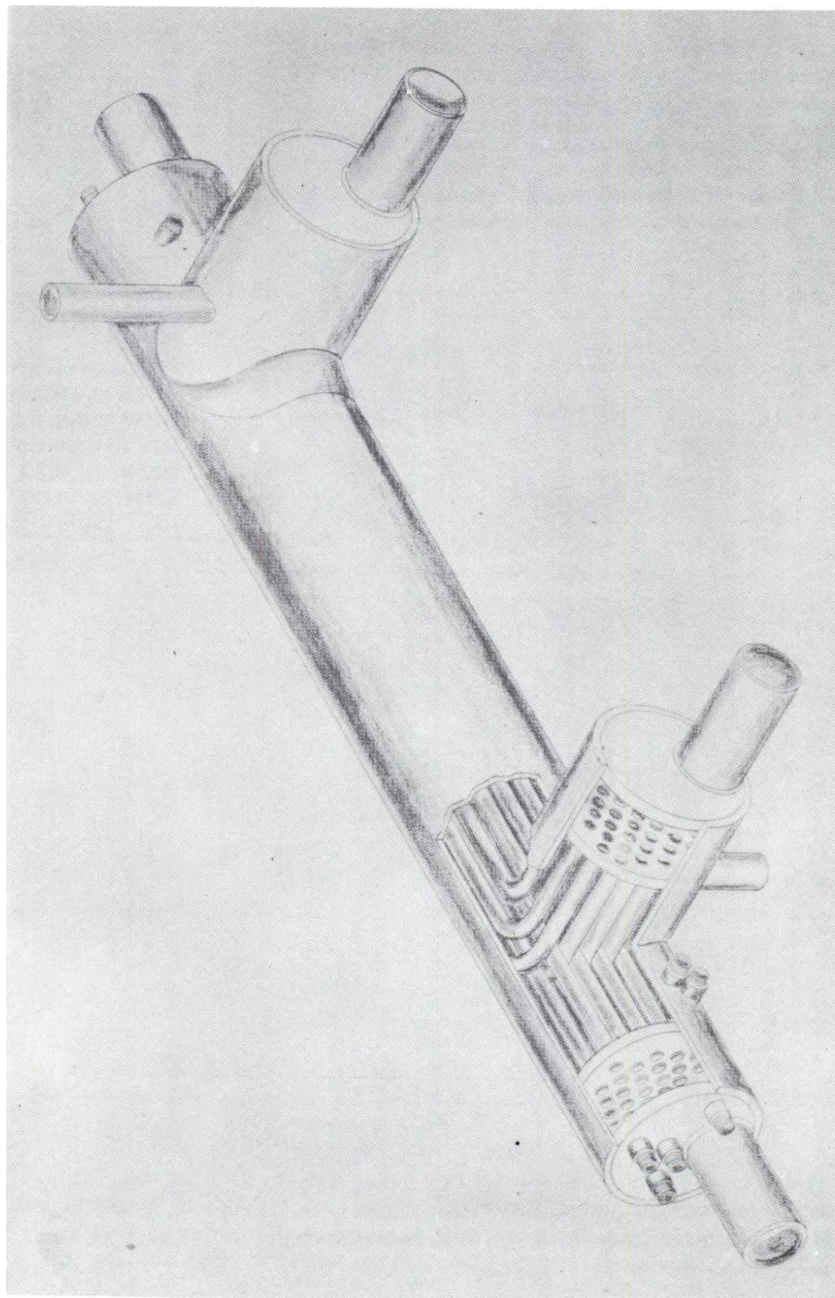


Fig. 2.7.1 — Flat-tube, Intermediate Heat Exchanger with "Hockey-stick" Arrangement. Submitted by Knolls Atomic Power Laboratory, Sept. 8, 1952.

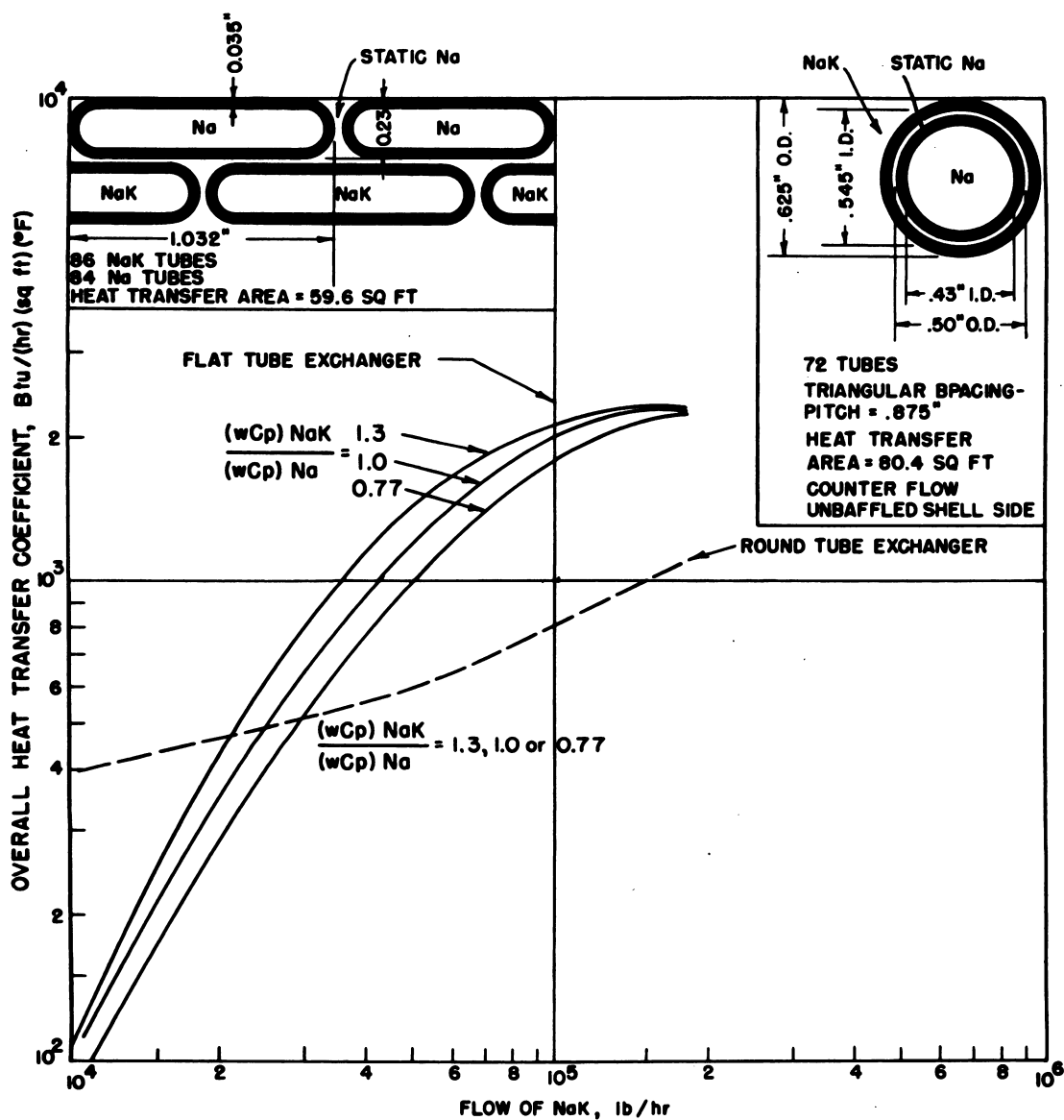


Fig. 2.7.2—Over-all Heat-transfer Coefficient as a Function of Weight Flow of NaK for two Alphas Liquid-metal Heat Exchangers. Submitted by Knolls Atomic Power Laboratory, Sept. 8, 1952. Sodium temperature at inlet for both exchangers was 950°F.

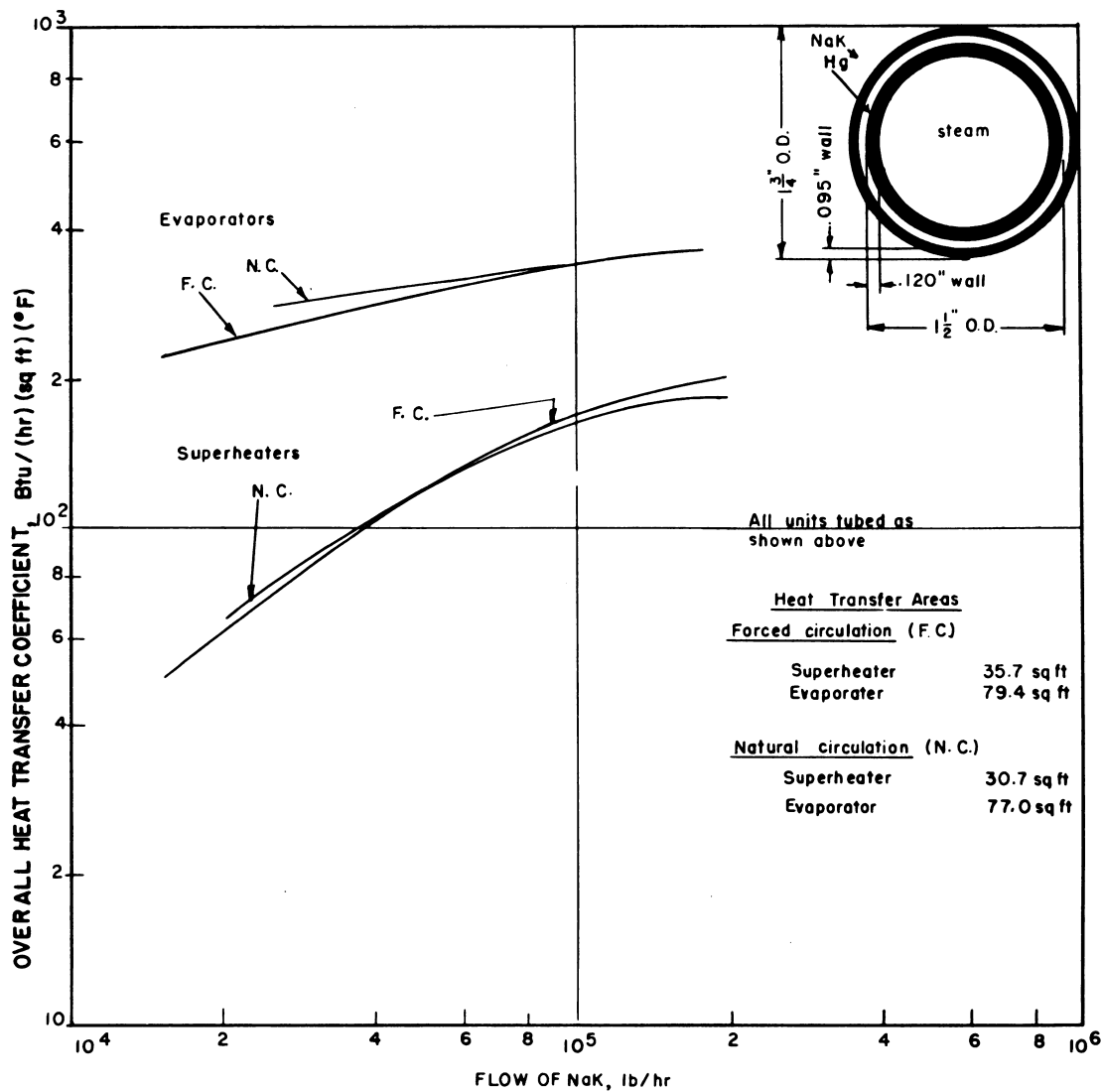


Fig. 2.7.3 — Over-all Heat-transfer Coefficient as a Function of Weight Flow of NaK for Alplauss Liquid-metal Steam Generators. Submitted by Knolls Atomic Power Laboratory, Sept. 8, 1952. NaK inlet temperature ranged from 790°F to 905°F.

The superheater of the Experimental Breeder Reactor is composed of four of the nickel-copper-nickel tubes described above. The NaK flows through the four tubes in parallel while steam makes the four passes in series. The tubes are 2 in. ID and 10 ft long with a total internal heat-transfer area of 20 sq ft. At a NaK rate of 278 gpm and a steam rate of 3160 lb/hr, the over-all coefficient was 95 Btu/(hr)(sq ft)(°F); the NaK entered at 560°F while the steam left at 510°F and 390 psig.

Tube diameter and tube spacing play a large part in determination of heat-transfer rates per unit volume of the tube bundle. Comparative performance factors, Btu/(hr)(°F)(cu ft), are shown in Fig. 2.7.4 for Na-heated water evaporators of a range of tube diameters and spacings. A basic configuration of Na inside the tubes, Hg-filled annuli, and boiling water in the shell is used for this comparison. The significance of tube-wall conductance is illustrated by the dotted family of curves in which Type-347 stainless steel has been replaced by nickel-zirconium as the tube material and the mercury in the annulus replaced by sodium.

Tubes of differing designs are compared in the bar chart of Fig. 2.7.5. All tubes shown are 0.83 in. ID with the sodium-side coefficient and the outside boiling-coefficient assumed constant. Spacing was assumed to be in accord with the Standards of the Tubular Exchanger Manufacturer's Association (see Fig. 2.7.4).

PUMPS AND VALVES

(J. F. Cage, Jr., and G. D. Collins)

PUMPS

From a purely hydraulic point of view, pumping of sodium and NaK is relatively easy. The physical properties (vapor pressure, density, and viscosity) are such that mechanical pumping is possible; the electrical resistivity and permeability of the fluids make them suitable for pumping by electromagnetic means. There are a large number of materials which are sufficiently corrosion resistant to be useable as structural materials in pumps for service up to about 1000°F. With the exception of the bearings, choice of materials is not usually a major problem in the design of pumps.

There are, however, general requirements which have made special design and development necessary for high-temperature sodium and NaK pumps. These are:

(1) Ability to pump high-temperature liquids. This is not a particularly unique problem, as it has been encountered in the pumping of high-temperature salts and oils in other applications. However, it calls for special features in the design of windings and drive motors which are more troublesome than those encountered in conventional pump design.

(2) Ability to operate for extended periods without maintenance. Since maintenance may be difficult because of radiation hazard, an attempt should be made to minimize or eliminate parts subject to wear and fatigue and components requiring adjustment.

(3) The necessity of leakless, or nearly leakless, operation. This is usually the governing factor in the design and selection of pumps and has led to the development of unusual means for sealing mechanical pumps as well as to the development of electromagnetic pumps which can be made inherently leakless.

In addition, the unique features of the application may dictate the type of pump to be used and greatly influence its design. Some of these features are:

(1) The space available for the pump.

(2) Source of power for the pump and space available for special power supplies.

(3) Available auxiliary systems—water or gas cooling systems, bearing oil supply systems, available provisions to vent bleed off gases, and the like.

(4) The relative importance of the weight of the pump in the over-all system design.

(5) The fluid circuit characteristics and location of free surfaces—whether the pump is required to pump from a sump into an overhead tank or to circulate in a closed system.

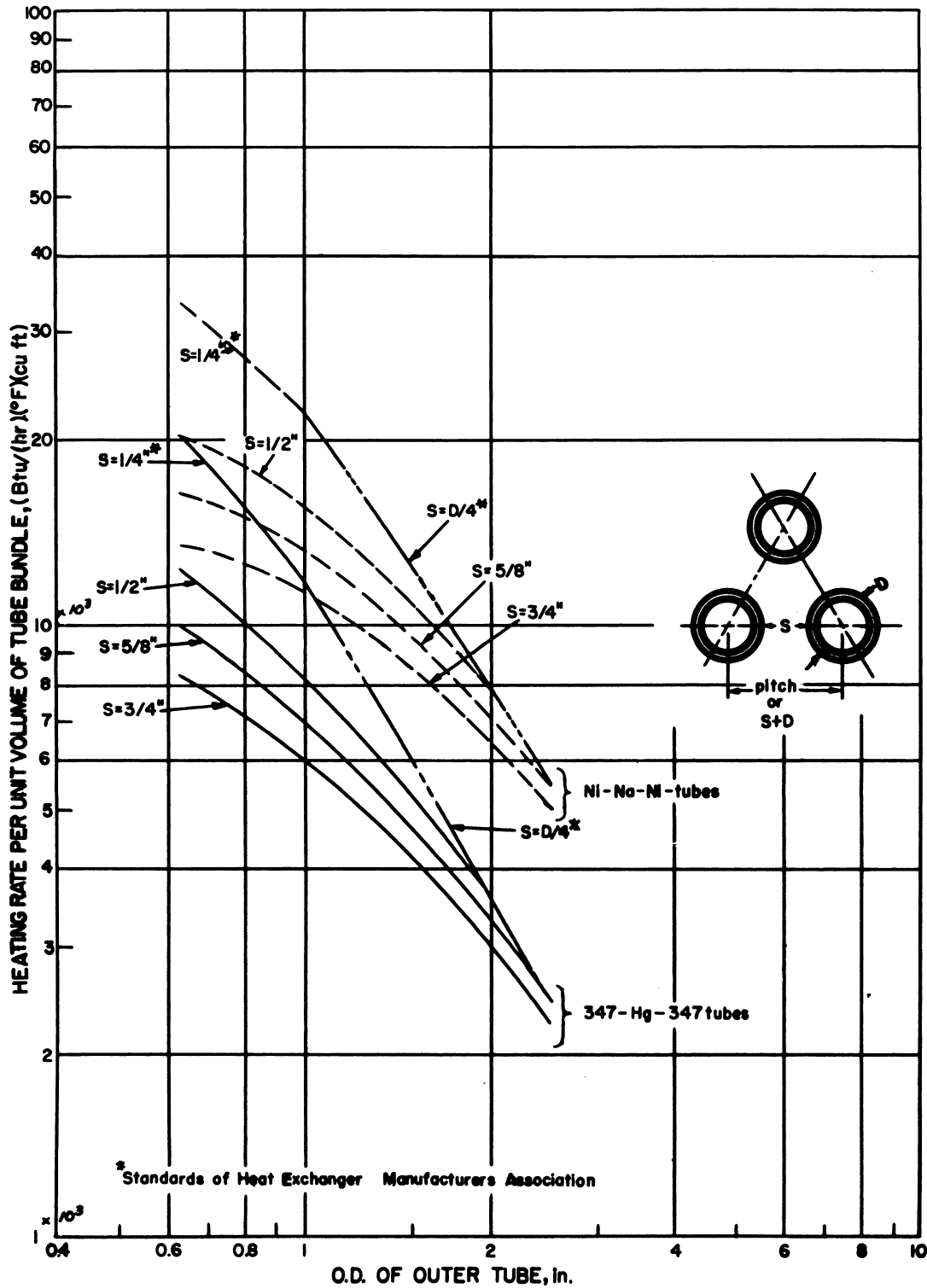


Fig. 2.7.4— Heating Rate per Unit Volume of the Tube Bundle as a Function of OD of Outer Tube for Two Types of Concentric Tubes. Submitted by Knolls Atomic Power Laboratory, Sept. 8, 1952.

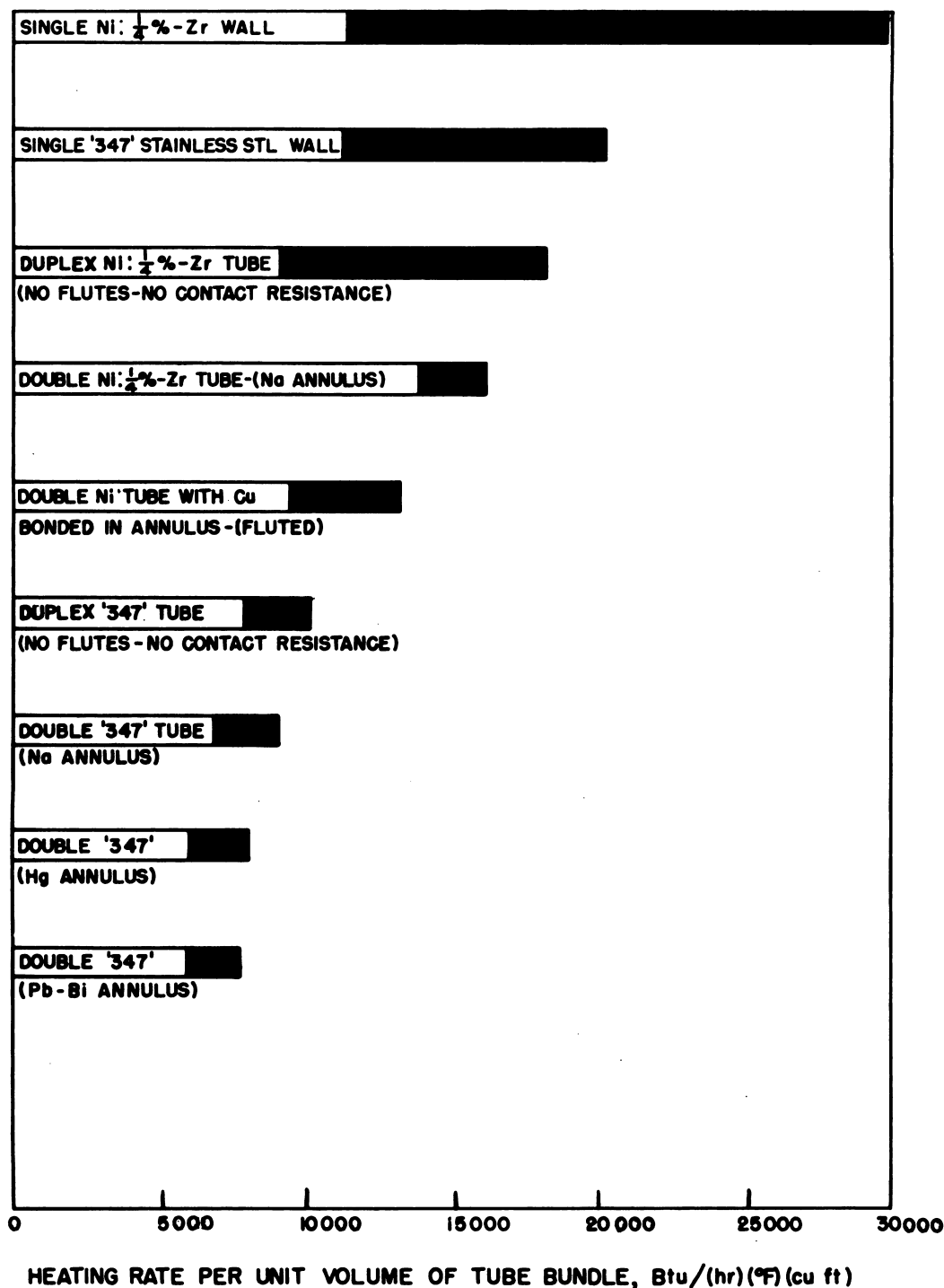


Fig. 2.7.5— Heating Rate per Unit Volume of Tube Bundle for Tubes of Various Designs. Submitted by Knolls Atomic Power Laboratory, Sept. 8, 1952. Spacing according to Tubular Exchanger Manufacturer's Association.

- (6) The pressure available at the pump inlet to prevent cavitation.
- (7) Method of speed control—whether the pump operates at constant flow or whether the flow is variable, and by what means this variation is obtained.
- (8) Whether the pump is stationary in space or is required to operate under conditions of pitch, roll, and mechanical shock expected in a mobile plant.

Liquid-metal pumps have been designed to meet unusual system requirements or to take advantage of different facilities. As a consequence, they vary widely both in type and in design depending on the application:

- (1) In the EBR, circulation through the reactor is maintained by gravity flow from an overhead tank into a sump. In this application, a DC Faraday-type pump is used to pump from the sump to the overhead tank.
- (2) In numerous test loops, where dependable operation is required and space for special power supplies is available, the DC Faraday-type electromagnetic pump has been widely and successfully used.
- (3) The characteristics of a number of electromagnetic and mechanical pumps considered for some of these applications are listed in Tables 2.7.1 and 2.7.2.

Sufficient development has been done on certain types of pumps to allow some general conclusions which are of interest whenever the application of a proposed pump to some future reactor cooling system is being considered. In this analysis, pumps are divided into two general groups, mechanical and electromagnetic.

MECHANICAL

The problems encountered in the design of pumps for sodium and NaK are, with certain exceptions discussed in the following paragraphs, those encountered in any pump design. Cavitation parameters in sodium and NaK appear to follow the laws governing this phenomenon in other fluids. It has been observed that during conditions of severe cavitation the rate of loss of material in 400°F sodium is several times that in water at room temperature.

The operation of bearings in sodium and NaK is difficult because of the increased tendency of materials to gall when rubbing in liquid metals. This markedly reduces the life of most antifriction bearings and limits the selection of materials for slider-type bearings. The wearing characteristics of approximately 400 pairs of materials have been evaluated in NaK at various temperatures up to about 850°F; the best of these are listed in Table 2.7.3.

The problem of obtaining an adequate shaft seal has led to a number of methods which so influence the pump design that mechanical pumps can be categorized by the method of sealing. Three such categories are discussed in the following paragraphs.

Shaft-seal Pumps

Pumps utilizing a shaft seal are the nearest in design to conventional pumps. The shaft can be driven by the most suitable means, such as an AC or DC motor, turbine, or other conventional prime mover, which allows maximum flexibility of control and minimizes or eliminates special power supplies. Conventional bearings are used and lubricated in a normal manner.

Shaft seals which seal the liquid metal directly have, for the most part, been found not suitable. A number of pumps have been built and operated which utilize a double-seal arrangement in which the leakage of liquid metal through one seal is accumulated in a reservoir under an inert gas blanket; the second seal serves to prevent leakage of the gas. A design of this sort is shown in Fig. 2.7.6. This arrangement requires an auxiliary system to accommodate the fluid leaking past the first seal and successful operation depends on the maintenance of proper fluid levels throughout the entire system. Effective periods between maintenance are usually limited by the operation of the gas seal.

Table 2.7.1 — Mechanical Pumps

Characteristic	Canned rotor	Canned rotor	Canned motor	Shaft seal, face type
Builder	Allis-Chalmers	Byron Jackson	Argonne National Lab.	General Electric Co.
Location	Milwaukee	Babcock & Wilcox	ARCO, EBR	Alplauss, KA PL
Capacity, gpm	3800	3625	500	400
Head, ft	125	126	53	126
Speed, rpm (min, rpm)	1690 (350)	900 (500)	1750 (...)	1750 (500)
Drive	Induction motor	Induction motor	Induction motor	DC motor
Power requirements	150 v, 60 cycles, 3 phase, 195 kw	460 v, 60 cycles, 3 phase, 135 kw	60 cycles, 3 phase, 8.2 kw	250 v, 20 hp amplidyne
Axial length, in.	80	102	86	108
Diameter, in.	35	50	50	52
Weight, lb	5400	~10,000		
NPSH, * psia	15	<15		15
Auxiliaries	None	Cooling oil pump	Liquid-level indicator and controller	Shaft cooler, seal lubrication, LM by-pass
Bearings	Liquid-lubricated, hydrostatic-pressurized by auxiliary impeller on main shaft	Sodium-lubricated ball bearings	Oil-lubricated ball bearings	Oil-lubricated
Cooling	Liquid-water heat exchanger, water jacket around stator	Forced oil-cooled windings	Self contained fan	Na-to-kerosene heat exchanger, ambient air circulation
Max. LM temperature	...	890°F	275°C	800°F
Control of flow	Vary frequency	Vary frequency	Constant	Vary voltage
Efficiency, %	45	55	54	50

*Net positive suction head

Table 2.7.2—Electromagnetic Pumps

Characteristic	Linear Induction General Electric KAPL	Linear Induction General Electric KAPL	Round Induction General Electric KAPL	DC Faraday Argonne National Lab. ARCO, EBR	EM Centrifugal Allis-Chalmers Milwaukee
Builder					
Location					
Capacity, gpm	1400	2500	400	500	275
Head, ft	100	100	54	50	55
Speed, rpm	1600
Power requirements	350 v, 60 cps, 3 phase, 80 kw	440 v, 60 cps, 3 phase, 130 kw	200 v, 25 cps, 3 phase, 28 kw	0.8 v, 18,000 amp, DC	25-hp drive, field ex- citation 30 amp
Dimensions	8.5 ft long 37 in. wide 24 in. high	7 ft, 8 in. long 37 in. wide 15.5 in. high	38 in. long 25 in. diameter
Weight, lb	6430	3900
NPSH, * psia	20	21
Cooling	Forced air, 2000 cfm	Forced water, 50 gpm	Forced air, 1000 cfm	None	Air
Insulation	Class B	Class H	Class B	Stainless steel	Class B
Thermal insulation	Phosphoasbestos	Stainless steel	Phosphoasbestos	None	...
Control of flow	Vary voltage	Vary voltage	Vary voltage	Vary current	Vary speed or ex- citation
Efficiency	37% Na	37% Na	20%	40% NaK	17% Na
Power factor	50% Na	35% Na	80%

*Net positive suction head

Table 2.7.3—Wearing Properties of Materials in NaK*

Fixed member	350°F				600°F				800°–950°F			
	Rotating member	Fixed member	Rotating member	Fixed member	Rotating member	Fixed member	Rotating member	Fixed member	Rotating member	Fixed member	Rotating member	Fixed member
Group I. Negligible wear, no apparent transfer of material, polishing of both specimens.												
Carboloy 55A	Carboloy 779	20% Fe-80% TiC	Carboloy 779	Kentanium K-138	Carboloy 779	Kentanium K-138	Carboloy 779	Kentanium K-138	Carboloy 779	Kentanium K-138	Carboloy 779	Carboloy 779
Tantung G	Carboloy 779	Kentanium K-138	Carboloy 779	Kentanium K-138	Carboloy 779	Kentanium K-138	Carboloy 779	Kentanium K-138	Carboloy 779	Kentanium K-138	Carboloy 779	Carboloy 779
6-6-2 HSTS	Carboloy 779	Kentanium K-138	Carboloy 779	Kentanium K-138	Carboloy 779	Kentanium K-138	Carboloy 779	Kentanium K-138	Carboloy 779	Kentanium K-138	Carboloy 779	Carboloy 779
18-4-1 HSTS	Carboloy 779	Kentanium K-138	Carboloy 779	Kentanium K-138	Carboloy 779	Kentanium K-138	Carboloy 779	Kentanium K-138	Carboloy 779	Kentanium K-138	Carboloy 779	Carboloy 779
Stellite J	Carboloy 779	Kentanium K-138	Carboloy 779	Kentanium K-138	Carboloy 779	Kentanium K-138	Carboloy 779	Kentanium K-138	Carboloy 779	Kentanium K-138	Carboloy 779	Carboloy 779
White cast iron	Carboloy 779	Kentanium K-138	Carboloy 779	Kentanium K-138	Carboloy 779	Kentanium K-138	Carboloy 779	Kentanium K-138	Carboloy 779	Kentanium K-138	Carboloy 779	Carboloy 779
17-4 PH s.s.	Carboloy 779	Kentanium K-138	Carboloy 779	Kentanium K-138	Carboloy 779	Kentanium K-138	Carboloy 779	Kentanium K-138	Carboloy 779	Kentanium K-138	Carboloy 779	Carboloy 779

Group II. Some smooth wear of the fixed specimen, no apparent transfer of material, polishing of the rotating specimen

Aluminum alloy 122	Carboloy 779	Copper	Carboloy 779	Carboloy 55A	Kentanium K-138A
Aluminum alloy 122	18-4-1 HSTS nitrided	Copper	Chrome plated 416 s.s.	Copper	Kentanium K-138
Aluminum 24ST4	SAE 52100	Copper	SAE 52100	Carboloy 907	
		Aluminum bronze	18-4-1 HSTS		

Group III. Smooth wear of the fixed specimen, minor transfer of material to sleeve, or smooth wear of the sleeve specimen, minor transfer of material to fixed specimen

Aluminum 24ST4	Carboly 779	Carboly 55A	Carboly 779	Kentanium K-138A	Carboly 779
Stellite 6	Carboly 779	Stellite J	Carboly 779	Molybdenum	Carboly 779
Aluminum bronze	Carboly 779	18-4-1 HSTS	Carboly 779	Firthe HT-77	Carboly 77B
Molybdenum	Carboly 779	Tantung G	Carboly 779	20% Fe-80% TiC	Kentanium K-138A
SAE 52100	Carboly 779	18-4-1 HSTS	Stellite 98M2	Kentanium K-138	Kentanium K-138A
Tantung G	18-4-1 HSTS nitrided	Tantung G	Stellite 98M2	Kentanium K-138	Kentanium K-138
Beryllium copper	18-4-1 HSTS (60 Rc)	Graph tung	Stellite 98M2	Carboly 44A	Kentanium K-138
Aluminum 24ST4	18-4-1 HSTS (60 Rc)	Stellite 98M2	Stellite 98M2	Kentanium K-151	Kentanium K-138
18-4-1 HSTS	18-4-1 HSTS (60 Rc)			Carboly 55A	Kentanium K-138
Aluminum 24S	18-4-1 HSTS (60 Rc)			18-4-1 HSTS	Kentanium K-138
Onyx spring steel	18-4-1 HSTS (60 Rc)			Colmonoy No. 6	Kentanium K-138
Leaded commercial bronze	Stellite J			Firthe HT-77	Firthe HT-77
Alloy die steel	Stellite J			Carboly 44A	Firthe HT-77
Tantung G	Stellite J			Carboly X304OD	Firthe HT-77
Type-347 s.s. nitrided	Stellite J			Carboly 77B	Firthe HT-77
Carboly 55A	SAE 52100			Carboly 55A	Firthe HT-77
				Carboly 907	Firthe HT-77
				Carboly 120	Firthe HT-77
				Carboly 78	Firthe HT-77
				Colmonoy No. 6	Colmonoy No. 6
				Kentanium K-12	Colmonoy No. 6
				Aluminum bronze	Stellite 98M2
				Stellite 98M2	Stellite 98M2
				Carboly 55A	Sintercast WF-87
				Carboly 78	Sintercast WF-87

*As determined by tests in which the end of a $\frac{5}{16}$ -in.-diameter right cylinder is loaded against the circumference of a $\frac{1}{8}$ -in.-diameter cylinder rotating at 900 rpm

Shaft seals employing frozen sodium have been used on small shafts with moderate success. Sodium is allowed to leak into a thin annulus surrounding the shaft; the temperature in this region is kept below the freezing point by means of forced cooling. As a result of friction, a thin film of molten sodium is maintained immediately around the shaft. The film can withstand moderate pressures without being expelled.

Canned-rotor Pumps

In canned-rotor pumps, sealing is accomplished by means of a thin cylindrical liner interposed in the air gap between the stator and the rotor of the induction motor which drives the pump. The end of the liner facing the impeller is welded to and open to the main pump body, which is made leak tight and filled with the liquid metal. The opposite end of the liner usually contains a radial bearing and is welded closed. Liquid metal generally fills the gap and surrounds the rotor; the liquid metal serves to remove rotor heat losses and lubricates the bearings, which are entirely internal. Forced cooling of the stator windings is necessary and is usually accomplished by a water jacket on the motor yoke. An auxiliary heat exchanger is required to remove the rotor losses from the liquid metal which flows through the gap; this portion of the liquid metal is kept separate from the main stream and maintained at as low a temperature as can be tolerated without causing an excessive concentration of oxides within the pump.

Canned-rotor pumps are generally compact. They require circulating-liquid cooling systems which occasionally must have special temperature control. The use of forced air or gas cooling simplifies the pump design but usually requires gas-monitoring systems and excessive shield penetrations. Since they are totally sealed, canned-rotor pumps require no vent or bleed off and are independent of the location of free surfaces in the system. Power must be supplied from a suitable AC source. If voltage control of flow variation is required, the drive motor must be oversize and must contain special design features. Speed variation is limited to a range of about 20 to 100 percent of full speed by bearing operation if either hydrodynamic or internally supplied pressure pad bearings are used. This range can be extended to substantially zero percent if externally supplied pressure pad bearings are used. Efficiencies up to 55 percent have been obtained with pumps of this type.

A canned-rotor pump using externally supplied pressure pad bearings and gas cooling is shown in Fig. 2.7.7.

Canned-motor Pump

In the canned-motor pump, the drive motor, pump shaft, and bearings are enclosed in a hermetically sealed vessel in which an inert-gas blanket covers the liquid metal; this avoids shaft penetrations of the gas blanket and its associated seal. Conventional bearings are usually used, and precautions are taken to prevent the diffusion of liquid-metal vapor into the bearings and motor.

Pumps of this type have been used in stationary applications, usually as a sump-type pump when liquid-level control can be maintained by gravity. Since these pumps are totally enclosed, vents and auxiliary systems are not required. The canned-motor pump is not particularly compact because the motor and gas vessel are gas-cooled. Because of the high wear of carbon brushes operated in the absence of water vapor, DC motors have not been required. The problems associated with the use of an induction motor are the same as for those using an induction motor driving a canned-rotor pump.

ELECTROMAGNETIC PUMPS

Electromagnetic pumps, which utilize the effect of electromagnetic forces on the liquid metal, have been the subject of extensive development for the past five years.

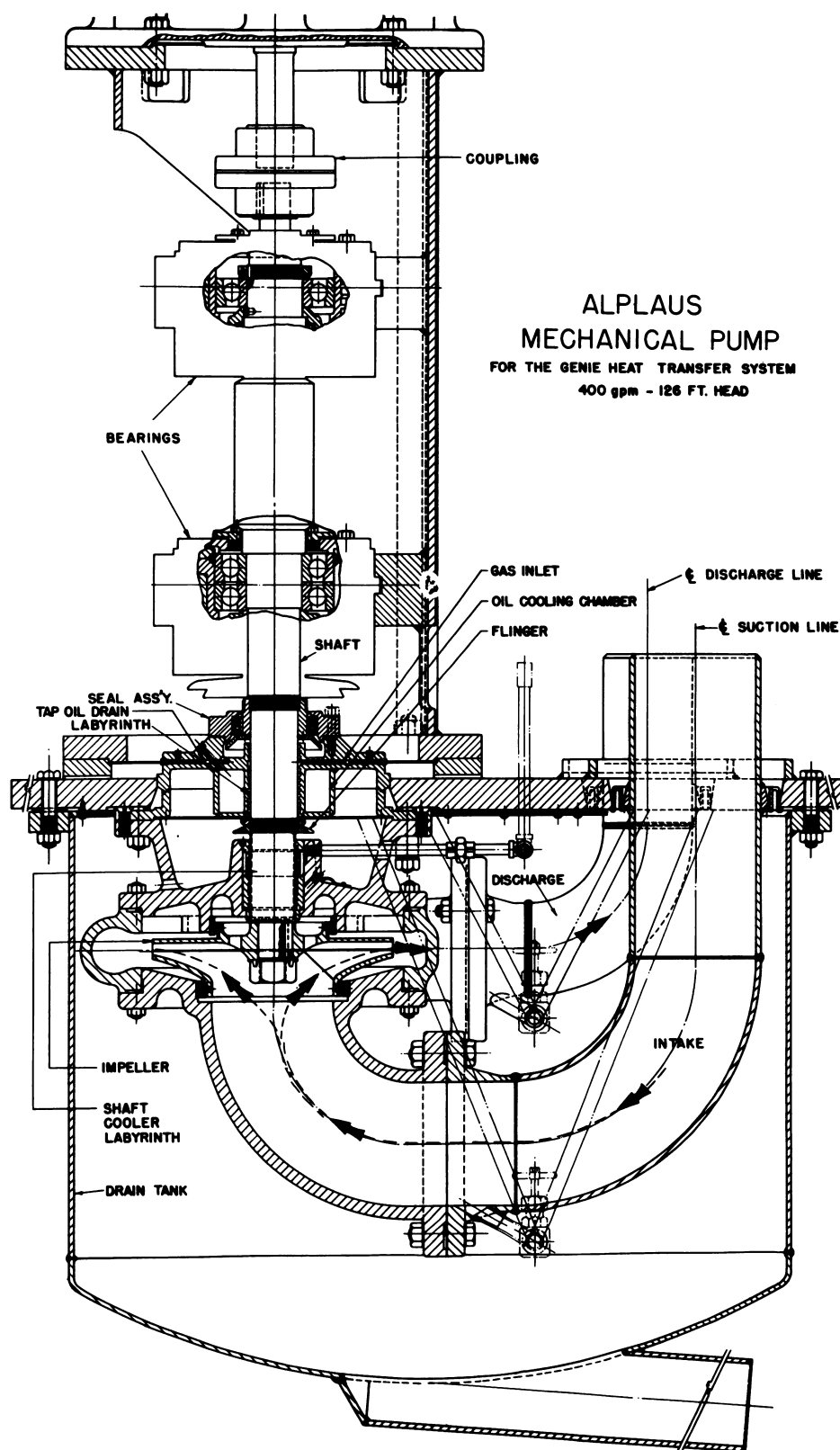


Fig. 2.7.6— Shaft-seal Pump Tested at Alplaus (400 gpm, 126-ft head). Submitted by Knolls Atomic Power Laboratory, Sept. 8, 1952.

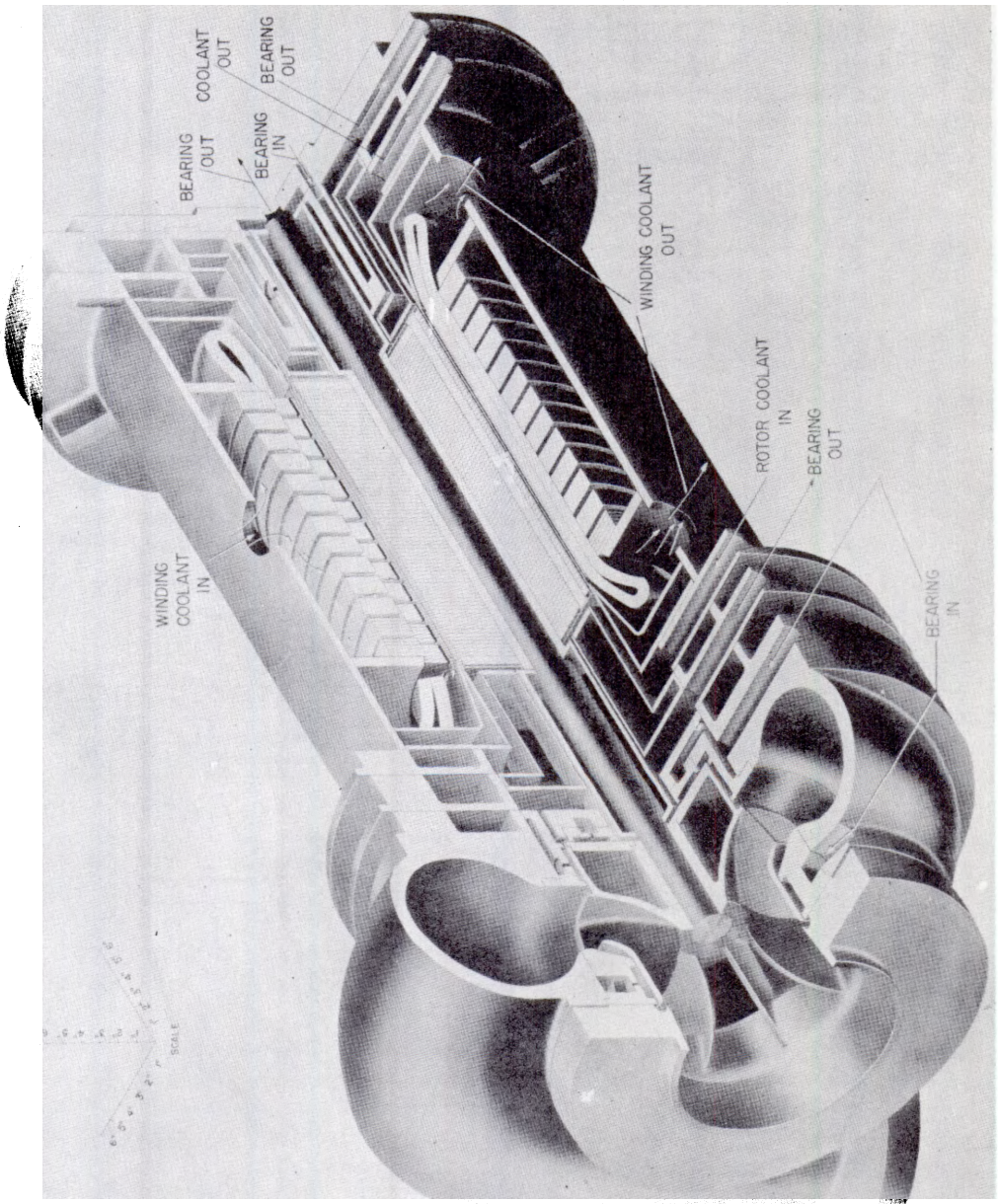


Fig. 2.7.7—Canned-rotor Pump. Submitted by Knolls Atomic Power Laboratory, Sept. 8, 1952.

All electromagnetic pumps have the desirable feature of requiring no penetration into the liquid metal which makes complete sealing possible. Their size and weight are of the same order of magnitude as mechanical liquid-metal pumps of the same rating. They require no venting or gas bleed lines, are independent of the location of free surfaces in the fluid system, and normally have characteristics which are independent of their orientation in space.

Electromagnetic pumps contain the liquid metal in ducts which vary in wall thickness from about 0.025 to 0.060 in. Normal practice is to provide secondary support for these thin-walled members so that they are not required to withstand operating pressures.

Cavitation of the fluid in the neighborhood of these thin-walled members must be avoided. Tests have shown that maintaining a total pressure at the pump inlet approximately 2.5 times the maximum velocity head in the pump is sufficient to prevent cavitation, provided that the hydraulic passages are reasonably well designed.

Three types of electromagnetic pumps which have been built and tested in various sizes and which are fairly well developed are the linear, AC, induction pump, the helical-flow induction pump, and the DC Faraday type. These are discussed in the following paragraphs and their characteristics are shown in Table 2.7.2.

Linear Induction Pump

This pump utilizes a multipole field traveling axially down the fluid duct. The field is produced by polyphase AC windings located on two sides of the duct, normally of rectangular cross section. Present practice is to limit fluid velocities to about 40 ft/sec or less and to maintain an aspect ratio in the duct cross section of about 24:1. A model of the linear induction pump is shown in Fig. 2.7.8.

Since the windings must be close to the hot liquid-metal duct, their cooling requires special attention. Pumps can be designed to use either gas or water cooling, and moderate winding temperatures can be maintained with reasonable quantities of coolant. A water-cooled pump (the 2500-gpm unit in Table 2.7.2) is shown in Fig. 2.7.9.

Efficiencies of about 40 percent have been obtained with pumps of this type, and values as high as 50 percent should be possible. The power factor is characteristically low, usually about 40 percent. Improvement in efficiency can be obtained at the expense of a reduction in power factor. Linear pumps can be designed to operate at 60 cps-voltages without severe design compromises. The performance of the 2500-gpm unit is given in Fig. 2.7.10.

The characteristics of the linear induction pump make it suitable for operation over a wide flow range using voltage control; AC power is, of course, required. The low power factor requires the use of either high-KVA-rating alternators or power-factor-correction equipment, such as capacitors. The only auxiliary system required is the winding cooling system, either water or gas. Temperature regulation of the coolant is not normally required.

Helical-flow Induction Pump

This pump is similar to the linear induction pump in principle; the fluid, however, is contained in a hollow cylindrical duct (Fig. 2.7.11), rather than in a flat duct of rectangular cross section. The helical-flow type is usually more compact than a linear pump of the same rating but normally about 50 percent heavier. The operational characteristics and cooling requirements for both are similar. The two differ in that the helical type usually requires a frequency less than 60 cps for optimum efficiency.

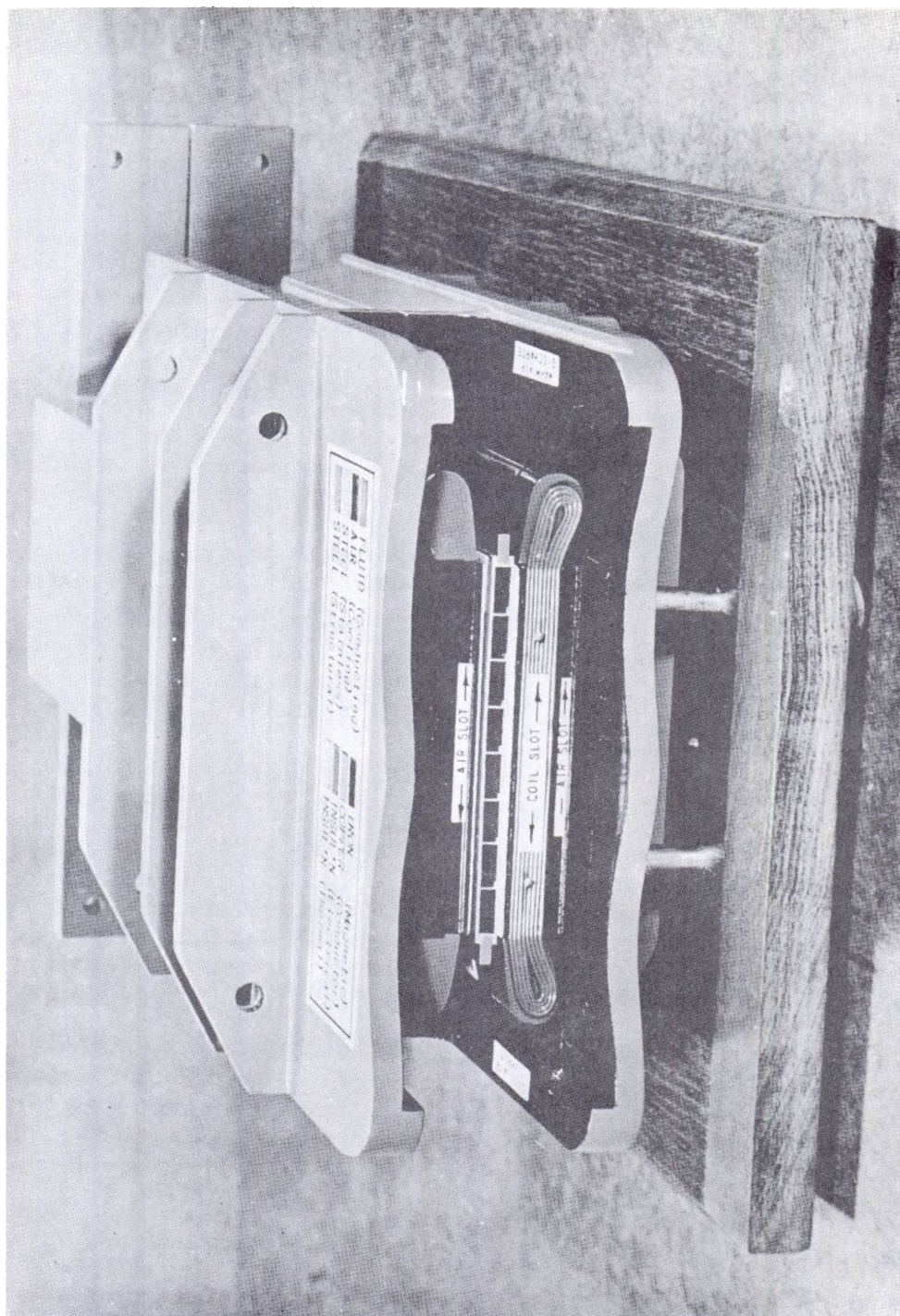


Fig. 2.7.8— Model of Linear Induction Pump. Submitted by Knolls Atomic Power Laboratory, Sept. 8, 1952.

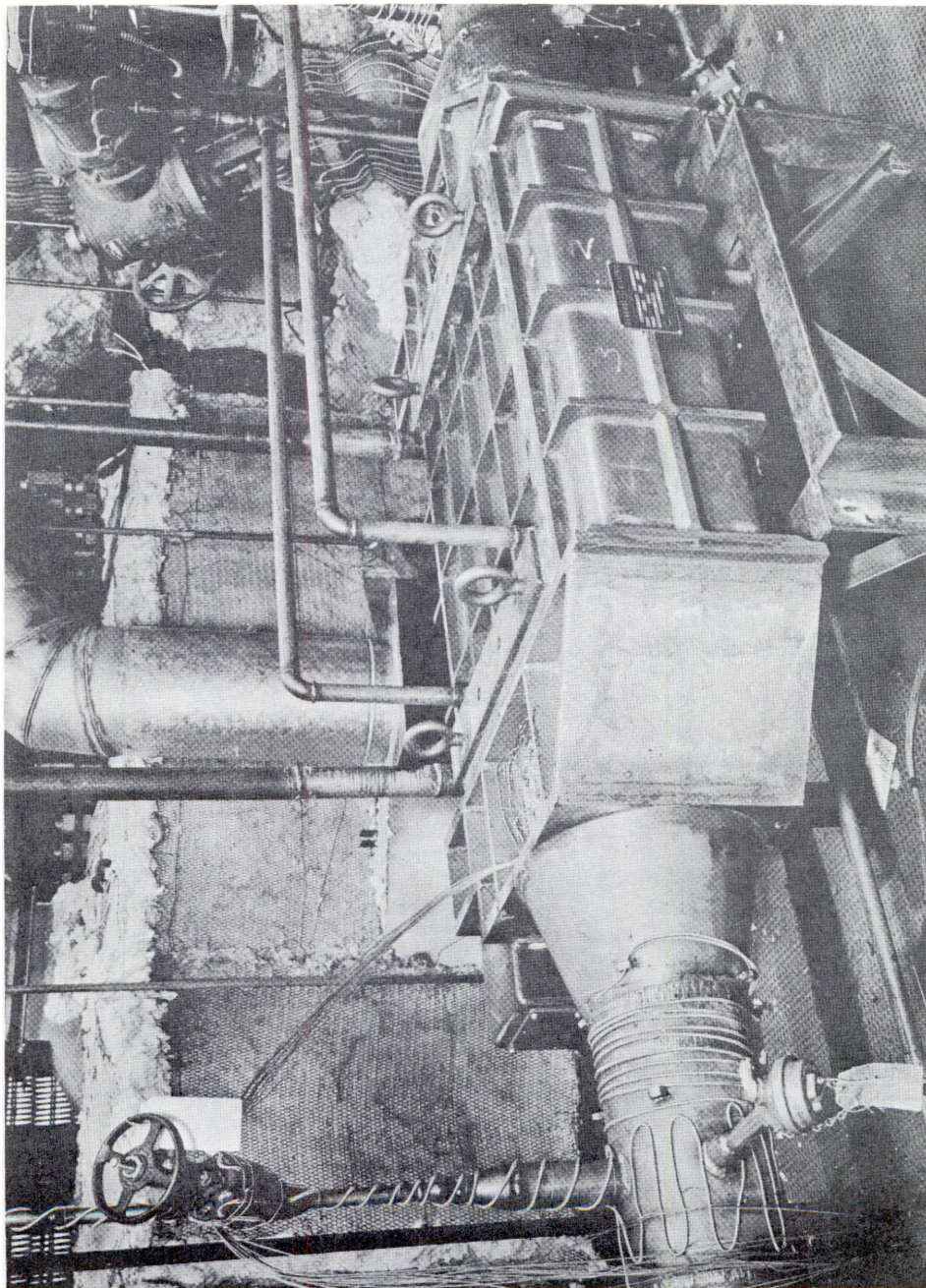


Fig. 2.7.9— Water-cooled Linear Induction Pump. Submitted by Knolls Atomic Power Laboratory, Sept. 8, 1952.

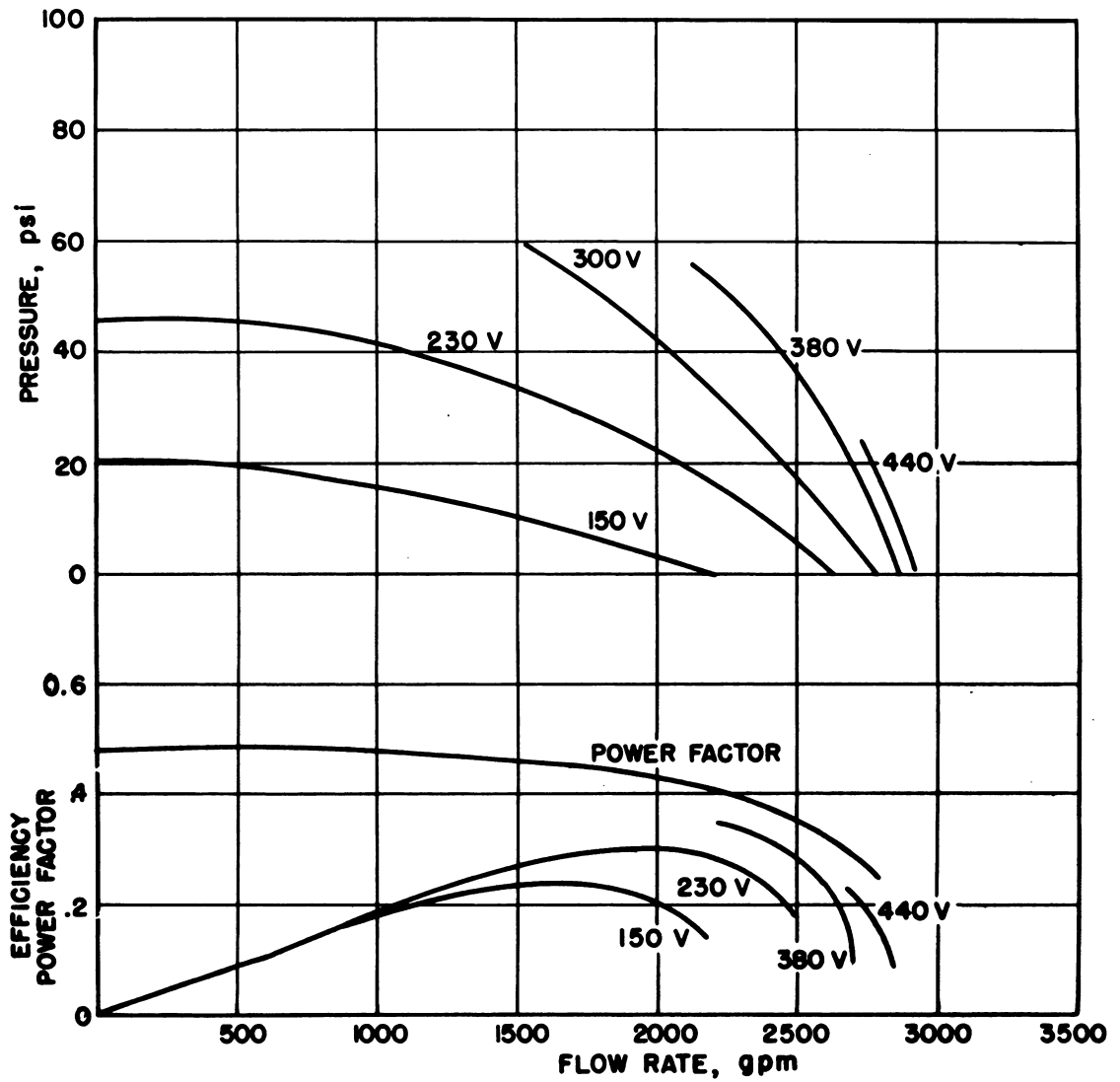


Fig. 2.7.10—Performance Characteristics of 2500-gpm Linear Induction Pump. Submitted by Knolls Atomic Power Laboratory, Sept. 8, 1952.

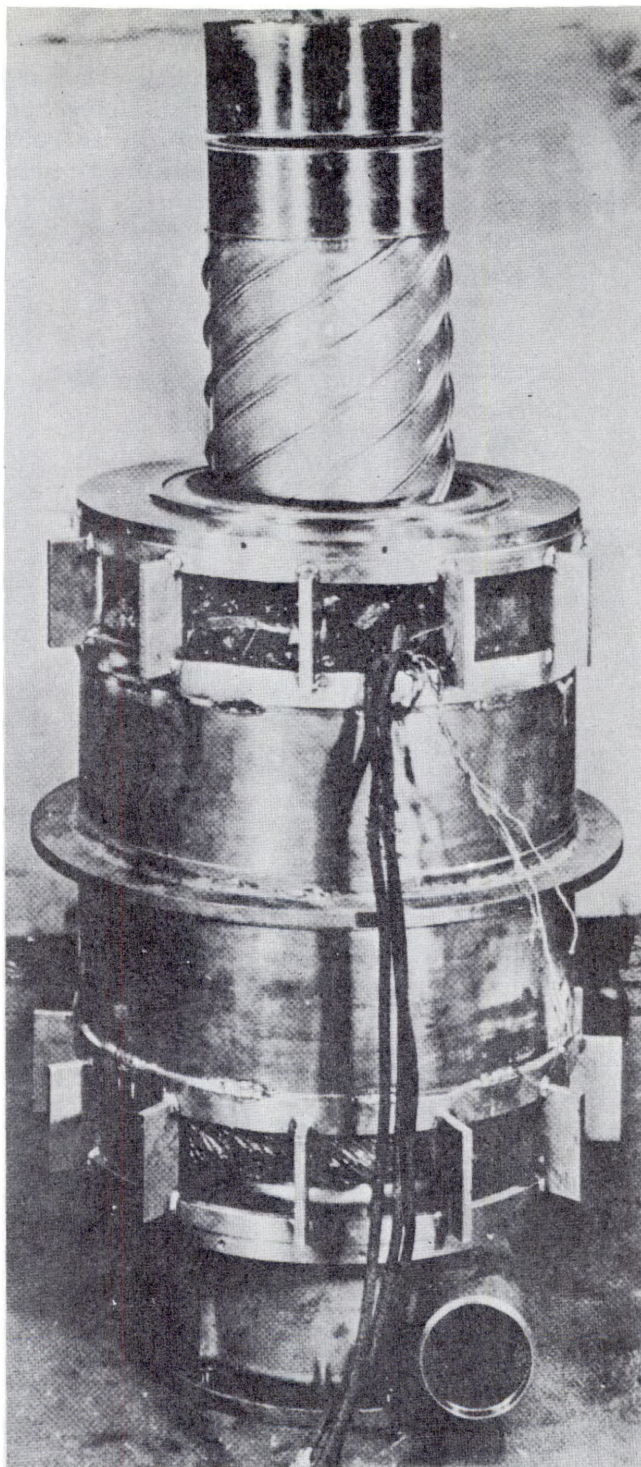


Fig. 2.7.11—Helical-flow Induction Pump. Submitted by Knolls Atomic Power Laboratory, Sept. 8, 1952.

DC Faraday Type

This is the most elementary of all the electromagnetic pumps and has the simplest construction. The fluid is contained in a thin-walled duct, usually of rectangular or square cross section, which is located in a constant field. Current is forced through the fluid in a direction perpendicular to the direction of the field and the direction of flow. This current is conducted into the fluid by electrodes which are normally brazed to the walls of the duct. These elements are shown schematically in Fig. 2.7.12.

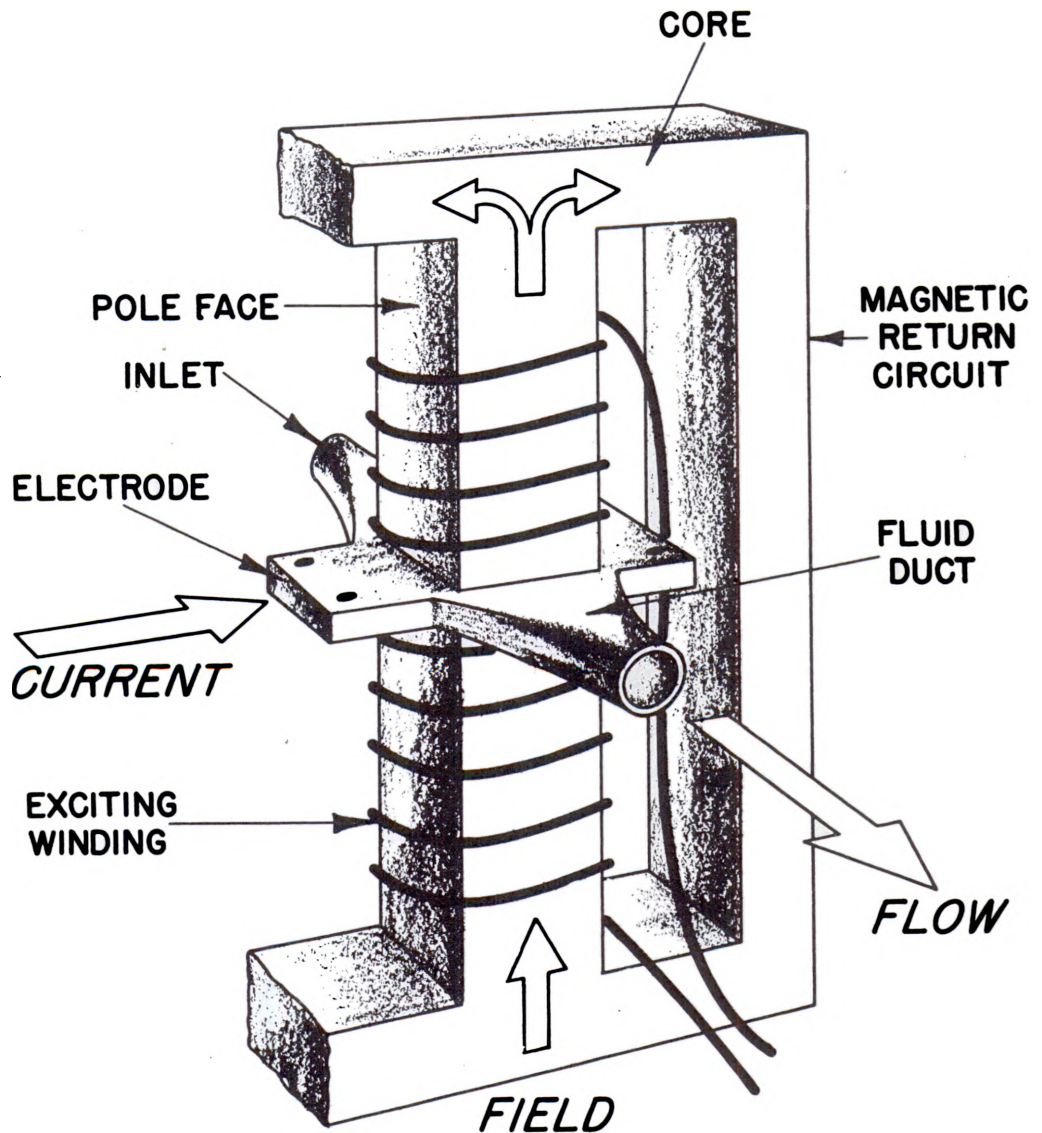


Fig. 2.7.12—Schematic Drawing of DC Faraday Pump. Submitted by Knolls Atomic Power Laboratory, Sept. 8, 1952.

The theory of operation of the DC pump is fairly well developed, and design parameters are understood well enough so that the design of a pump of this type is a reasonably straightforward process. Methods of compensating for the field distortion owing to the cur-

rent flowing in the fluid have not been worked out thoroughly, nor has a method for multiple re-entry of the current been successfully developed.

Efficiencies of about 50 percent have been obtained with this pump, and theoretical analyses have indicated that higher efficiencies should be possible. This type inherently has a low characteristic input impedance and requires a very-low-voltage, DC power source. Most DC Faraday pumps must operate at less than 2 volts.

DC Faraday pumps can be made with shunt or separately excited field coils which are cooled by natural convection and which utilize varnish-type insulation. Series-connected pumps have also been built which require no electrical insulation in the conventional sense, thereby avoiding cooling requirements altogether.

DC Faraday pumps are usually equivalent to helical-flow induction pumps in weights but are somewhat more bulky. Flow control over a wide range can be obtained by voltage variation, a stable satisfactory method. The unusual power requirements, however, are a handicap; the difficulty of supplying very large currents, plus the sheer bulk of bus-bar work to carry them, have prevented use of the DC Faraday type in applications where capacities above a few hundred gpm are required.

VALVES

Valves for service in liquid metal systems are usually distinguishable from conventional valves for high-temperature service only in that more attention is given to sealing the valve stem. Bellows are generally used, but occasionally, double bellows are employed.

Valve seats of conventional design are used for liquid metals; hard-facing materials such as stellite are satisfactory for sodium up to about 950°F. Conventionally designed and manufactured valve seats are not capable of completely stopping liquid sodium under moderate pressure, and freezing is generally used where a complete shut-off is required.

There has been little development of special valves for liquid-metal service since most requirements have been met using standard valves with little or no modification. Work on valves has largely been limited to testing of bellows to establish their probable life when used as stem seals. The dependability of valves is limited owing to the statistical probability of premature bellows failure.

AUXILIARY EQUIPMENT

Table 2.7.4 is a summary of the types of piping, insulation, and joints which have been used with some liquid metals.

INSTRUMENTATION

(F. O. Prescott)

Most of the development work in liquid-metal instrumentation has been done for sodium and NaK, but many of the instruments are applicable with some modification to lithium and lead-bismuth and possibly other liquid metals. Comparison of physical properties of a given liquid metal with those of sodium and NaK will indicate the possibility of applying these instruments.

The liquid-metal properties which affect instrumentation are:

(1) Thermal conductivity—high values are very advantageous in temperature measurements, affording fast time-constants and good, representative, mixed mean-temperature measurements.

(2) Electrical conductivity—high values permit the application of such devices as the magnetic flowmeters and resistance level-detectors.

Table 2.7.4—Auxiliary Equipment

Metal	Experience	Piping	Insulation	Joints
Na and NaK	Many thousands of hours of operating power-plant and laboratory-scale equipment	For temperature up to 1000°F, the austenitic stainless steels have proved satisfactory. Considerable experience has been accumulated with Types 316, 321, and 347	Commercial mineral wool insulation (fibrous slag from steel or lead furnaces) has proved satisfactory. It is relatively resistant to Na and NaK and tends to contain and smother leaks or spillage. Many of the usual insulations are highly reactive with freely burning Na or NaK	Flanges are unsatisfactory for operation over wide temperature ranges but may be used in inert-gas regions. Piping-Code welding procedures for pressure piping are recommended. Consideration should be given to the design of welded joints without backing rings to minimize the amount of liquid metal remaining in the system after draining
Li	Several thousand hours of laboratory-scale operation. Results to date have been unsatisfactory owing to plugging of cond. zone	Type-310 stainless steel is recommended between 1350° and 1800°F. Types 316 (particularly the extra-low-C grade) and 347 are recommended for temperatures up to 1350°F	Super-X and standard magnesia have been employed. Weber's plastic insulation has been used successfully up to 1500°F. In some experimental installations, polished stainless-steel radiation shields have been used in place of insulation. The shields were of two-piece construction and were attached to the pipes by clips to facilitate removal	Welded joints are preferred, especially above 1000°F. Standard ring-type flanges have proved satisfactory up to 1000°F. Flanged joints using soft-iron gaskets have been exposed to Li for over 100 hr at 800°F without leaking

Pb-Bi	Few thousand hours of laboratory-scale operation	Data on container materials are sparse. Up to 1200°F, the high-chrome, ferritic stainless steels, notably Type 430, give reasonably good service. Austenitic stainless steels (Types 310, 316, or 347) are less desirable since their stress rupture strength is appreciably lowered by Pb-Bi	It is believed that any of the usual, non-temperature-sensitive, insulating materials will be satisfactory because of the relative inactivity of Pb-Bi	Weld-connected, metallic-gasketed systems are believed essential for reliable, long-period service
Hg	Power-plant scale	Sicromono-5S is used for boiler tubes. In cooler passes, Croloy-3 or Croloy-2 are satisfactory

(3) Melting point—for sodium, the relatively high (as compared with NaK) melting point is both an advantage and disadvantage. In case of a small leak, as into a capillary tube, the sodium may freeze, thus reducing the hazard of fire, whereas the low melting point of NaK makes it a potential fire hazard under the same circumstances. On the other hand, NaK requires no heat source to keep sensing lines from plugging, while sodium lines must be heated and maintained at a temperature above the melting point.

(4) Vapor pressure—both sodium and NaK have sufficiently high vapor pressures at normal operating temperatures to cause difficulties. The vapors tend to condense out on the cooler surfaces of containers, sensing lines, and vent lines, eventually leading to plugging. This has been especially troublesome in systems which employ a pressure control on gas exhaust lines.

(5) The danger of plugging owing to thermal transport also necessitates heating of liquid-metal instrument lines.

TEMPERATURE

The precision attainable in temperature measurements above 500°F in high neutron fluxes has yet to be established. Thermocouples are most widely used since they do not appear to be grossly affected. Resistance thermometers, however, may drift as much as 5 to 10 percent from their calibration in a neutron field. It is believed that the drift is a result of stresses induced in the resistance element.

Besides calibration uncertainties, the effects of both gamma- and neutron-radiation upon electrical insulators have been a major problem. While a good deal of work is currently being done on this, at present the rather meager data available dictate the use of powdered inorganic insulators such as MgO or Al_2O_3 supported in a metal sheath.

For temperature measurements inside the neutron shield, KAPL is using a stainless-steel-clad, two-wire, chromel-alumel thermocouple with MgO insulation. These are manufactured by the General Electric Industrial Heating Division and can be obtained in units as small as $\frac{1}{16}$ in. OD. They are suitable for direct immersion in molten sodium and provide very fast time-constants.

Resistance thermometers are used outside the primary shield. The Leeds & Northrup Co. makes a unit which is accurate to $\pm 1^\circ F$ at 1000°F temperatures. Apart from special design considerations of response time and installation methods, these are standard elements. Connections to these units are made with General Cable's "MI" cable to bring the leads through the secondary shield.

PRESSURE

Conventional methods for measuring pressure are not applicable to sodium systems for several reasons. First, bourdon tube instruments, directly connected, plug very quickly even when adequately heated; second, bellows-type detectors or transmitters which have a sharp temperature gradient across them are vulnerable to calibration shifts owing to condensation of sodium vapors between convolutions of the bellows; third, any method involving the use of electrical heating is only as reliable as the heating circuit. Caution must be observed in heating techniques, for the cold-trap effect (cf. Chap. 2.4) may result in precipitation of impurities and plugging.

FLOWMETERS

The magnetic flowmeter of Kolin⁵ has been given much attention since the advent of liquid-metal-coolant systems. The unit is externally mounted on the pipe, making replacement a simple matter. There is no head loss associated with the magnetic flowmeter, for no power is drawn from it. Since the variable measured is velocity, the output varies linearly with flow.

The principle of operation is simply that of a DC generator. A permanent magnet, bolted to the pipe, sets up a magnetic field across the pipe, and liquid metal flow cutting the lines of force generates a voltage within itself. This voltage is picked up by a pair of electrodes fastened to the pipe in a plane which is at right angles to both that of flow and that of the magnetic field. A typical installation is shown in Fig. 2.7.13.

The following equation, derived by Elrod,⁶ checks very closely with experimental results:

$$E = BVd \times 10^{-8} \times \frac{2 \left(\frac{d}{D} \right)}{1 + \left(\frac{d}{D} \right)^2 + \frac{\rho_F}{\rho_W} \left[1 - \left(\frac{d}{D} \right)^2 \right]}$$

where E = output in volts

B = magnetic field strength in gauss

d = pipe ID in cm

D = pipe OD in cm

ρ_F = resistivity of fluid

ρ_W = resistivity of pipe material

v = velocity in cm/sec

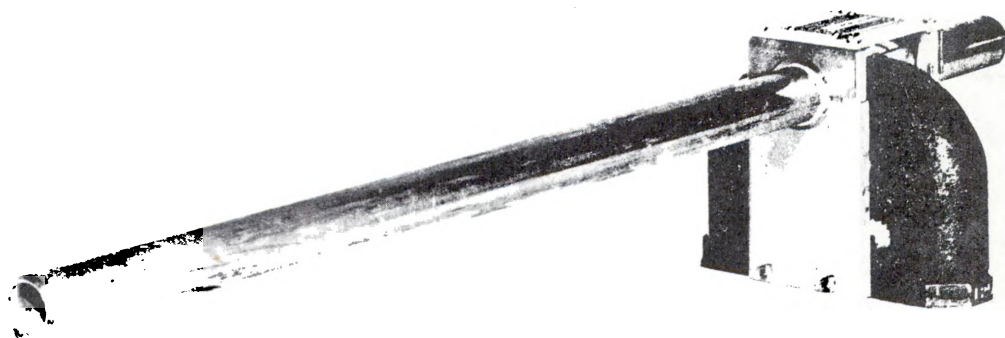


Fig. 2.7.13—Magnetic Flowmeter. Submitted by Knolls Atomic Power Laboratory, Sept. 8, 1952.

There are some problems and uncertainties associated with the use of the magnetic flowmeter. Wetting of the pipe surface is of vital importance in obtaining good flow measurement. It has been shown, however, that once a pipe has been initially brought up to wetting temperature, it remains wetted down to temperatures considerably below this value. Magnetic flowmeters are slightly affected by temperature of operation.

Another difficulty is that stainless steel is not a completely homogeneous material. Even though stainless-steel lead-wire may be used for electrodes, it may differ sufficiently from the pipe material to produce thermal emfs of sufficient magnitude to materially affect the indication. This difficulty has been solved by using electrodes made from the pipe material itself for electrodes, although even here thermal emfs have been detected.

There appears to be a limit on the physical size of a permanent magnet commensurate with a predictable accuracy. Since the practical application of the flowmeter depends upon a rather high flux density (and a uniform one), the size of the yoke and the cross-sectional area of the magnet increase tremendously as the air gap (pipe size) is increased. Attempts

are currently being made to resolve these problems for an 8-in.-pipe installation. It would seem that this approaches the practical size limitation.

Another uncertainty is the effect of radiation exposure on permanent magnets. Testing is currently under way to determine the magnitude of this effect.

LIQUID-LEVEL INDICATORS

Almost any conventional or commercially available liquid-level measuring device can be used for liquid metals in stationary plants if it can be adapted to meet the stringent requirements for leak tightness and temperature insensitivity.

A level-measuring instrument of the "resistance" type has been developed. A simple stainless-steel probe is immersed directly in sodium, and its resistance is measured as a function of level (Fig. 2.7.14). While the relationship between level and resistance (actually voltage is measured using a constant current source) is not linear, it is reproducible, and the effects of temperature can be calibrated. A curve showing the reproducibility and the general relationship between level and resistance for a test installation is shown in Fig. 2.7.15.

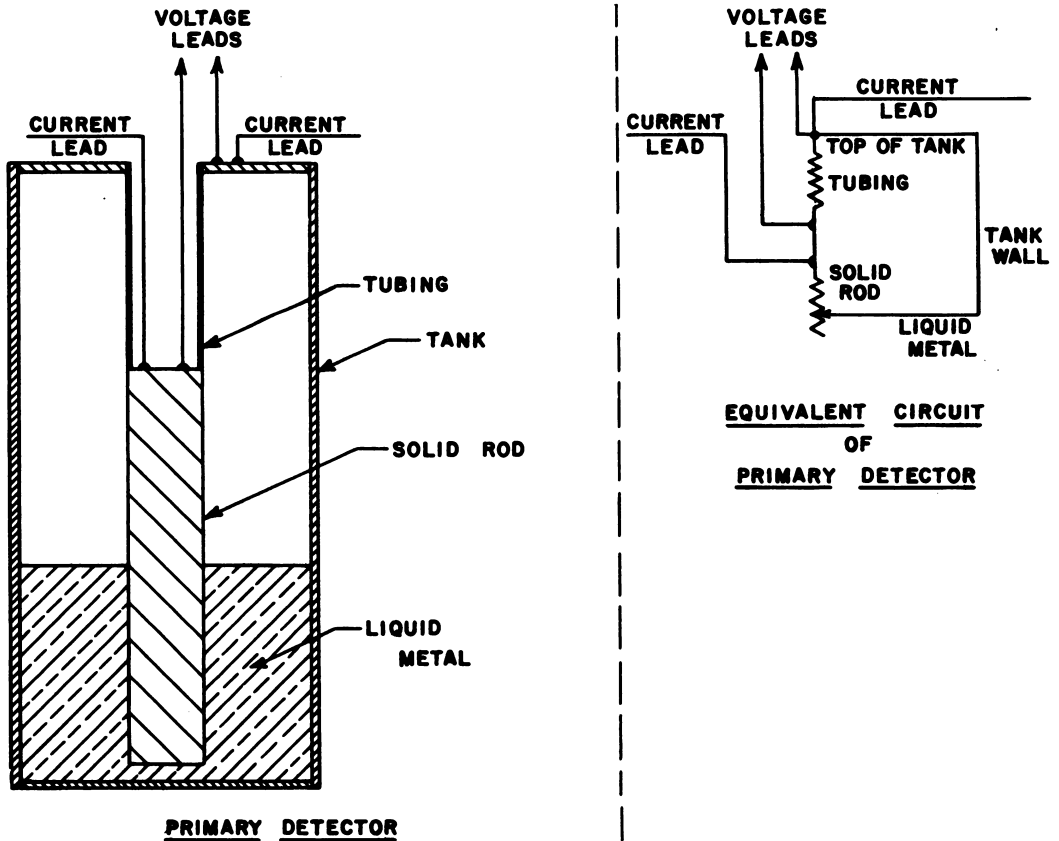


Fig. 2.7.14--Resistance-type Liquid-level Indicator. Submitted by Knolls Atomic Power Laboratory, Sept. 8, 1952.

An "impedance" type unit has been developed which shows promise for stationary applications; further work, however, is necessary to improve reliability and reduce temperature dependence. This unit is described in the second edition of *The Liquid-Metals Handbook*.

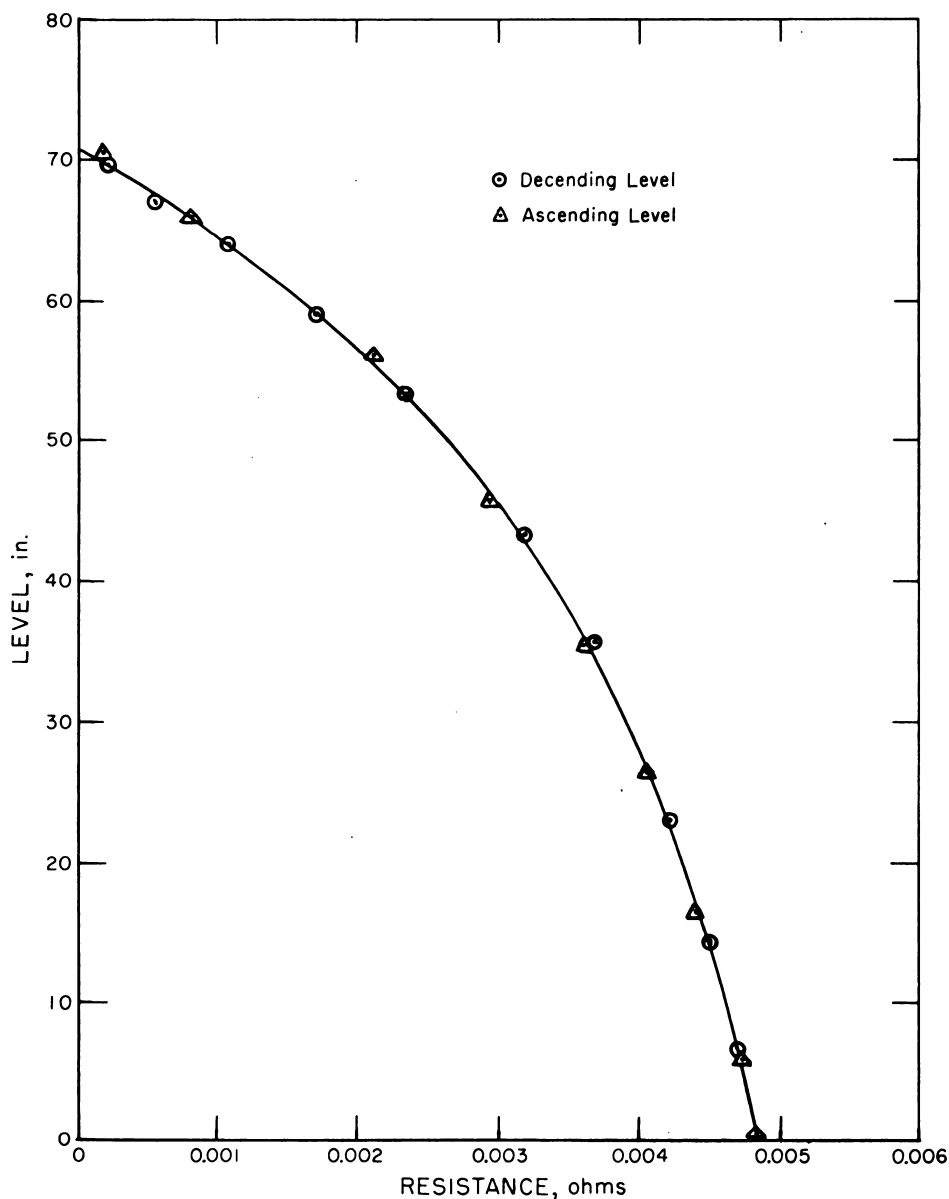


Fig. 2.7.15—Level in Inches as a Function of Resistance for a Liquid-level-indicator Test-installation. Submitted by Knolls Atomic Power Laboratory, Sept. 8, 1952.

REFERENCES

1. R. A. Cameron et al, Experimental Breeder Project Report for the Period February 1, 1950, Through March 31, 1951, ANL-4554, April 1, 1951, 60 pp.
2. W. H. Zinn, H. V. Lichtenberger, and M. Novick, Feasibility Report—Fast Neutron Pile for a Test of Conversion, ANL-4356, Oct. 14, 1949, 84 pp.
3. E. C. King and R. A. Tidball, Heat Fluxes from Liquid Metal to Boiling Water, MSA Tech. Rep. No. 16, Aug. 8, 1952, 22 pp.
4. R. D. Brooks and A. L. Rosenblatt, Design and Performance of Liquid Metal Heat Exchangers and Steam Generators for Nuclear Power Plants, submitted to ASME for Dec. 1952 annual meeting.
5. A. Kolin, An Alternating Field Induction Flowmeter of High Sensitivity, Rev. Sci. Inst. 16, 1945, p 109.
6. N. G. Elrod and R. R. Fouse, An Investigation of Electromagnetic Flowmeters, Babcock and Wilcox Tech. Rep. I-5206, NEPA-1451, June 12, 1950, 31 pp.

SELECTED READING LIST

Heat Exchangers and Steam Generators

DESIGN AND PERFORMANCE OF LIQUID METAL HEAT EXCHANGERS AND STEAM GENERATORS FOR NUCLEAR POWER PLANTS, R. D. Brooks and A. L. Rosenblatt, submitted to A.S.M.E. for Dec. 1952 Annual Meeting.

HEAT FLUXES FROM LIQUID METAL TO BOILING WATER, Mine Safety Appliance Co., E. C. King and R. A. Tidball, MSA Tech. Rep. No. 16, Aug. 8, 1952, 22 pp.

FEASIBILITY REPORT-FAST NEUTRON PILE FOR A TEST OF CONVERSION, Argonne National Laboratory, W. H. Zinn, H. V. Lichtenberger, and M. Novick, Oct. 14, 1949, 84 pp.

Pumps

OPERATION AND ANALYSIS OF A 100-PSI ELECTROMAGNETIC PUMP, G. D. Collins, KAPL-668, Jan. 19, 1952, 73 pp.

PUMPS FOR LIQUIDS (Bibliography), R. L. Morgan, TID-3015 (rev), Jan. 11, 1952, 10 pp.

DESCRIPTION AND TEST RESULTS OF A 400-GPM LIQUID METAL INDUCTION PUMP, J. F. Cage, Jr. and E. H. Schoch, KAPL-619, Oct. 23, 1951, 65 pp.

COMPATIBILITY OF MATERIALS IN LIQUID METAL, D. B. Vail, KAPL-589, Aug. 18, 1951, 103 pp.

TEST OF 1200-GPM LINEAR A-C ELECTROMAGNETIC PUMP, J. Barnard and G. D. Collins, KAPL-568, May 23, 1951, 65 pp.

EBR PROGRESS REPORT, FEBRUARY 1, 1950—MARCH 31, 1951, prepared by EBR Project Staff, ANL-4554, April 1, 1951, 60 pp.

CENTRIFUGAL AND AXIAL FLOW PUMPS, A. J. Stepanoff, John Wiley and Sons, New York, 1948.

DESIGN, CONSTRUCTION, AND ASSEMBLY OF A PROTOTYPE LIQUID METAL PUMP, J. J. Owens, Babcock and Wilcox Co., Report No. 5038, NP-3681, Sept. 19, 1951, 14 pp.

Valves

FIRST INTERIM REPORT ON DURABILITY AND SEAT LEAKAGE TESTS ON LIQUID METAL VALVES, H. J. Balhouse, KAPL-585, Aug. 3, 1951, 59 pp.

Instrumentation

INVESTIGATION OF THERMOCOUPLE DESIGN FOR REACTOR SERVICE, H. Robinson and R. G. Moss, General Electric, G. E. Gen. Eng. Lab. Rep. No. R52GL81, Mar. 14, 1952.

MAGNETIC FLOWMETER OUTPUT POTENTIALS, E. R. Astley, General Electric, G. E. Gen. Eng. Lab. Rep. No. R52GL42, Mar. 1, 1952, 13 pp.

MAGNETIC FLOWMETER CALIBRATION RESULTS, W. C. Gray, Knolls Atomic Power Laboratory, KAPL-613, Oct. 3, 1951, 9 pp.

AN INVESTIGATION OF ELECTROMAGNETIC FLOWMETER, N. G. Elrod, and R. R. Fouse, Babcock and Wilcox Co., Tech. Rep. I-5206, NEPA-1451, June 12, 1950, 31 pp.

AN ALTERNATE FIELD INDUCTION FLOW METER OF HIGH SENSITIVITY, A. Kolin, Rev. Sci. Inst. 16, 1945, pp., 109-116.

Section 3

GAS-COOLED SYSTEMS

Prepared by
W. R. PAGE AND E. GOODMAN
BROOKHAVEN NATIONAL LABORATORY

AUTHORS' PREFACE

It is the primary objective of the authors in preparing this section to make conveniently available data on the physical properties of gases usable for reactor cooling. Empirical equations, which have been developed for predicting heat transfer and pressure drop under conditions which are likely to be encountered in the physical situations best suited for reactor internal-surface configurations are also presented. This information has been incorporated in Chapters 3.3 and 3.4.

Other objectives were to outline the general distinctive characteristics of gas-cooled reactors (Chapter 3.1), to indicate the thermodynamic cycle systems in which it is possible to operate with such reactors (Chapter 3.2), to present information on fuel-element design (Chapter 3.5), to describe the feasible fuel loading configurations, gas passage shapes, and gas distribution within the reactor which lead to maximum net-power output (Chapter 3.6), to indicate the basis for choice of certain types of gases for reactor cooling (Chapter 3.7), and to present in outline form the factors which are involved in the solution of problems which arise in connection with the disposal of radioactivity in the gas streams leaving nuclear reactors (Chapter 3.8).

It may be possible in future editions of this section to provide more fundamental information on optimizing the various independent design factors. On the other hand, each gas-cooled reactor designed to date has had its own peculiarities and requirements; optimizing reactor weight, size, coolant flow area, and fuel-element dimensions (to mention only a few of the variables involved) has been and may yet continue to be based to some degree on a combination of intuitive judgment, past experience, and engineering fundamentals rather than on a set of detailed correlations of limited applicability.

The information in this Section is based upon data available up to about mid-1952.

The authors wish to acknowledge the assistance of the following people in the preparation and evaluation of the material presented in Volume 2, Section 3, Gas-Cooled System: A. Amorosi, ANL; E. J. Boyle, ORNL; J. Chernick, BNL; J. A. Cox, ORNL; Farrington Daniels, Allis Chalmers; R. W. Dayton, BMI; R. G. Deissler, NACA; L. Emlet, ORNL; H. Etherington, ANL; L. A. Evers, NACA; A. E. Focke, GE; E. F. Fricke, ANL; L. V. Humble, NACA; C. Lankton, GE; A. L. London, Stanford Univ.; W. H. Lowdermilk, NACA; S. V. Manson, NACA; R. L. Mela, NDA; E. W. Sams, NACA; E. Schmidt, GE; C. Starr, NAA; W. B. Thomson, GE; and G. Thornton, GE.

Valuable assistance was also given by M. L. Barad, HW, in reviewing Chap. 3.8 and by W. H. McAdams, MIT, and T. B. Drew, Columbia, in reviewing Chap. 3.4.

We also wish to acknowledge the assistance given by the following groups at Brookhaven National Laboratory: Technical Information, Libraries, Photography, Duplicating, and the Secretarial Staff of the Nuclear Engineering Department. We wish to express our gratitude to the following: G. Cox, J. Garfield, J. Herod, D. Puleston, M. Waisman, and all our other associates at BNL who helped with this section.

E. I. Goodman* and W. R. Paget

*Present address, Nuclear Science and Engineering Corporation, Pittsburgh, Pa.

†Present address, Dewey & Almy Chemical Company, Cambridge, Mass.

General Reactor Characteristics

Gas coolants for reactors provide certain advantages over liquids for some applications. Air is a convenient low-neutron-cross-section coolant for unenriched experimental reactors. Helium has potential application at high pressure as an inert, high-conductivity, low-neutron-cross-section coolant where the temperatures of the fuel elements and exhausting helium can be such as to provide high thermodynamic efficiency in a gas-turbine cycle.

However, compared with liquids, gas coolants are characterized by low volume heat capacity and low heat-transfer coefficients. For this reason, when used for land-based power reactors, they require larger flow passages through the reactor and higher fuel-element temperatures for a given reactor heat output and coolant pumping power than do liquids. Generally, these factors do not permit very compact reactor designs because of (1) the increase in the size of the reactor itself and (2) the comparatively large gaps required to allow the gas to pass through the shield. In some applications, the first disadvantage may be offset by simplifying the external heat-removal system; the second is also compensated for to some extent by the low volumetric neutron cross section of the gas. Since the coolant pressure drop varies inversely as the flow area to the 2.5 power,¹ a satisfactory design is possible. Another factor which helps to offset the poor heat-transfer characteristics of the gas is the chemical inertness of such coolants as helium, which permits the fuel elements to operate at a higher temperature than with liquid metal coolant. If this higher permissible temperature is used to obtain an increased temperature rise in the coolant by reducing the coolant flow rate, a considerable reduction in pumping power can be obtained, since the pumping power varies inversely as the cube of the coolant temperature rise for a given level of reactor power. By such techniques as pressurizing the gas and increasing the flow area and the allowable fuel-element temperature, the fraction of total reactor heat output expended as pumping power can be reduced to a tolerable value. A comparison of pumping-power requirements for the same flow cross section but with the use of a higher gas-coolant temperature rise and high gas pressures is shown in Fig. 3.1.1.

Figure 3.1.2 illustrates the advantage of high helium-exhaust temperature for a gas-turbine cycle. The efficiency given is over-all and takes into account the power required for recompressing the coolant.

Because high pressures are required to generate a significant amount of net power in a gas-cooled reactor, a leak-proof circulating system must be maintained and the amount of radioactivity in the coolant must be kept to a minimum. Considerable effort has been expended on design with these considerations in mind (see Chapters 3.6 and 3.8). Because a higher fuel-element temperature must be maintained with gas-cooled reactors than with liquid-cooled reactors to obtain an equivalent thermodynamic efficiency, fuel elements must be fabricated to withstand very high temperatures under irradiation without rupture, release of fission products, undue growth, creep, or warpage. This is one of the major concerns in the development of gas-cooled power reactors (see Chapter 3.5).

¹Reference appears at end of chapter.

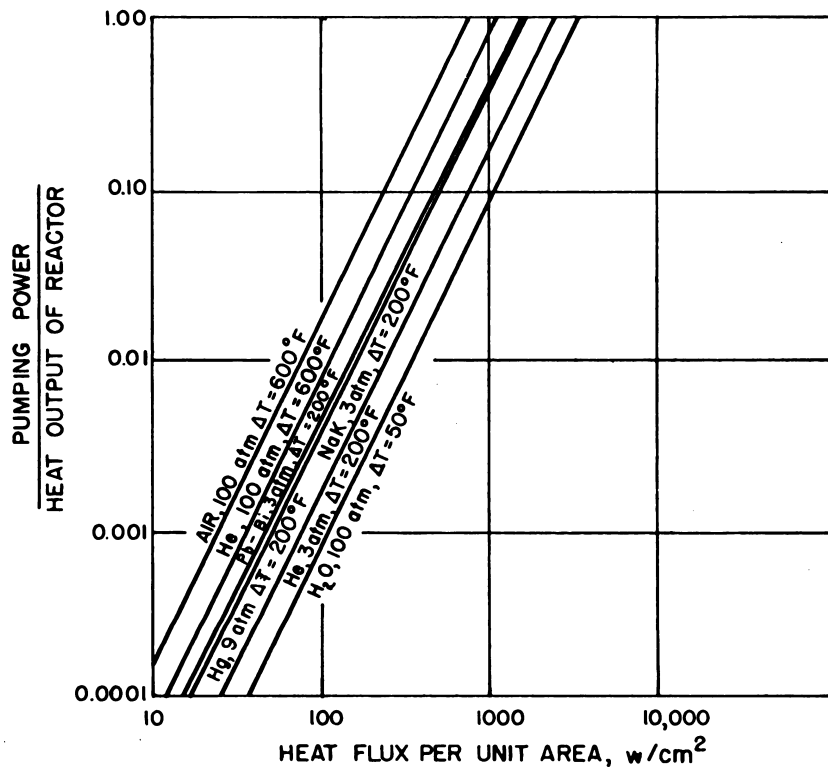


Fig. 3.1.1— Comparison of Pumping-power Requirements. Submitted by Knolls Atomic Power Laboratory, Feb. 19, 1948. Flow through channels 0.1 in. \times 1 in. \times 4 ft long; heated length = 1.5 ft; total pumping power = 2 \times reactor pumping power. Outlet temperatures: Air, 1300°F; He, 1300°F; molten metals, 950°F; H₂O, 450°F.

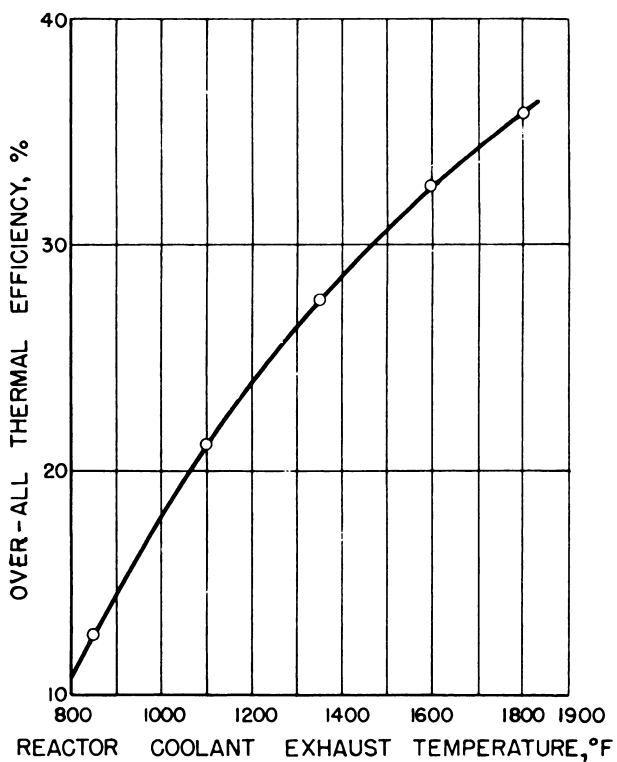


Fig. 3.1.2 — Thermal Efficiency as a Function of Reactor Exhaust Temperature for a Helium-cooled Reactor and Gas-turbine Power Cycle. Submitted by the Allis-Chalmers Manufacturing Company, Inc., Feb. 15, 1952.

REFERENCE

1. Martinelli, R. C., "Heat Transfer IV," Knolls Atomic Power Laboratory, KAPL-40, Secret, Feb. 19, 1948.

Thermal Cycles

Power is extracted from the gas of gas-cooled reactors by allowing either the hot reactor coolant or a secondary fluid, which is heated by the reactor coolant, to expand adiabatically through a turbine. In the gas-turbine cycle, the gas is then cooled and recompressed sufficiently to compensate for the pressure losses in the reactor and auxiliary ducting as well as for the turbine pressure drop.

The following are typical nuclear power cycles using gas as the reactor coolant:

- (1) Direct-air-cycle reactor.
- (2) Closed-cycle helium-cooled reactor.
- (3) Helium-cooled reactor using gas-turbine cycle.
- (4) Helium-cooled reactor using steam-turbine cycle.
- (5) Stationary unenriched uranium power-plant cycle (Fig. 3.2.1)

Four of the above five cycles use gas turbines to extract all or part of the available heat energy directly from the gas leaving the reactors. The other cycle transfers the gas heat energy to boiling water which in turn drives turbines. The relative efficiencies of the direct (gas-turbine) and the indirect (steam-turbine) cycles have been studied in detail¹ for application in a reactor, and the results are summarized in Fig. 3.2.2. A comparison of the data on cycles (3) and (4) shows that for the same shaft-horsepower the gas-turbine cycle has a considerable weight advantage over the steam-turbine design at a reactor exhaust temperature of 1100°F. The effect of gas-turbine pressure ratio on net plant thermal efficiency is illustrated in Fig. 3.2.3 for a cycle using both intercooler and regenerator. The merits of heat interchange between fluid streams at various points in the gas-turbine cycle are shown in Fig. 3.2.4, which presents thermal efficiencies for a simple cycle, a cycle with regenerator, a cycle with regenerator and intercooler, and a cycle with intercooler. The cycle with regenerator and intercooler offers significantly greater over-all efficiency.

The pumping power required for cycle (5) is an appreciable fraction of the total power generated because a low helium pressure is required in the necessarily large unenriched-uranium reactor.

¹Reference appears at end of chapter.

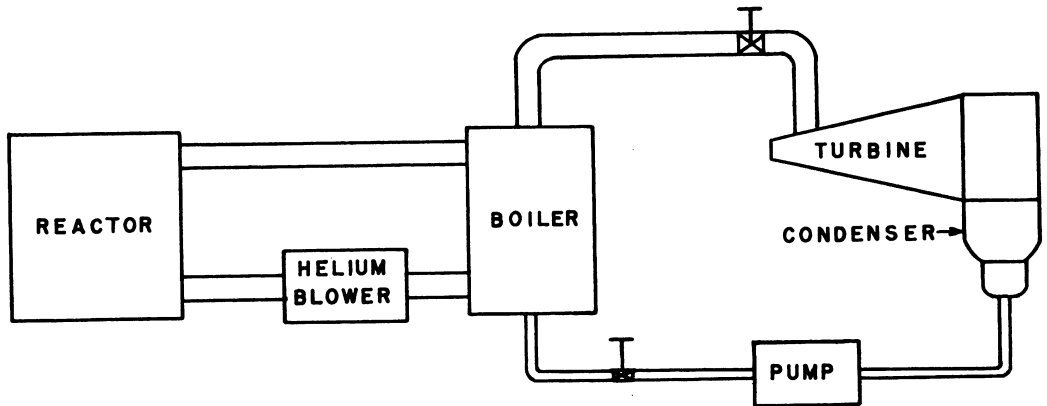


Fig. 3.2.1 — Helium-cooled Stationary Power Reactor. Presented by Commonwealth Edison Company and Public Service Company of Northern Illinois, CEPS-1101, May 1952.

Design Data:

Reactor heat output, kw = 350,000
 Coolant = Helium
 Pressure, reactor outlet, psia = 148
 Pressure, reactor inlet, psia = 153
 Gas temperature, reactor outlet, °F = 700
 Gas temperature, to boiler, °F = 650
 Gas temperature, from boiler, °F = 384
 Gas temperature, reactor inlet, °F = 403
 He flow rate, lb/sec = 908
 Steam flow rate, lb/sec = 236
 Water temperature to condenser, °F = 79
 Turbine steam pressure, psig = 250
 Turbine steam temperature, °F = 525
 Turbine exhaust pressure, mm Hg = 1
 Gross power, electric, kw = 67,300
 Auxiliary power, electric, kw = 15,000
 Auxiliary power, steam, kw (equiv) = 12,000
 Net power available for system = 52,300
 Internal turbine efficiency, % = 80
 Helium blower efficiency, % = 78
 Mechanical electrical losses, % = 5

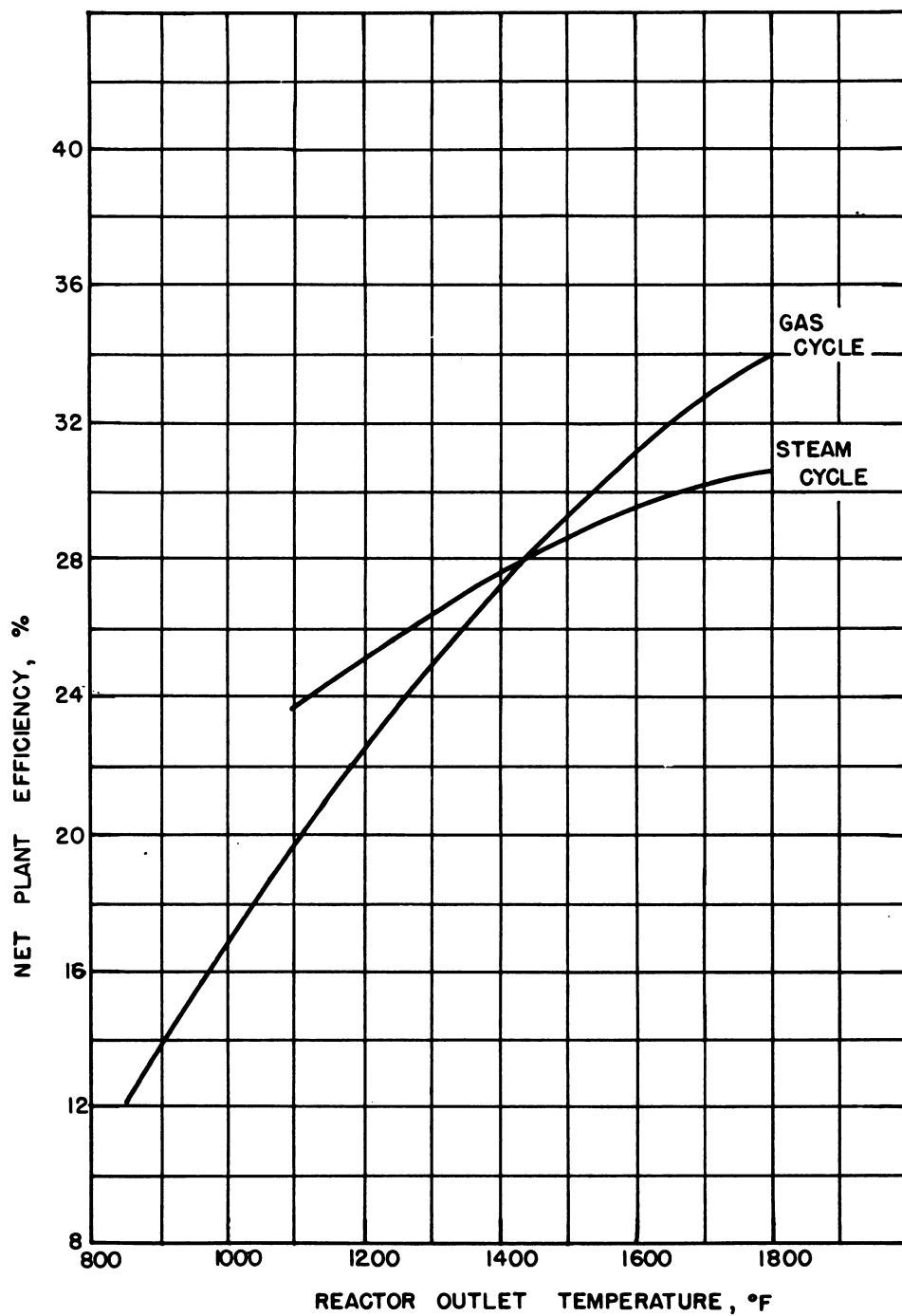


Fig. 3.2.2— Net Plant Efficiency vs Reactor Outlet Temperature for Closed Helium Gas and Steam Cycles. Reprinted from NP-3683, Jan. 1952.

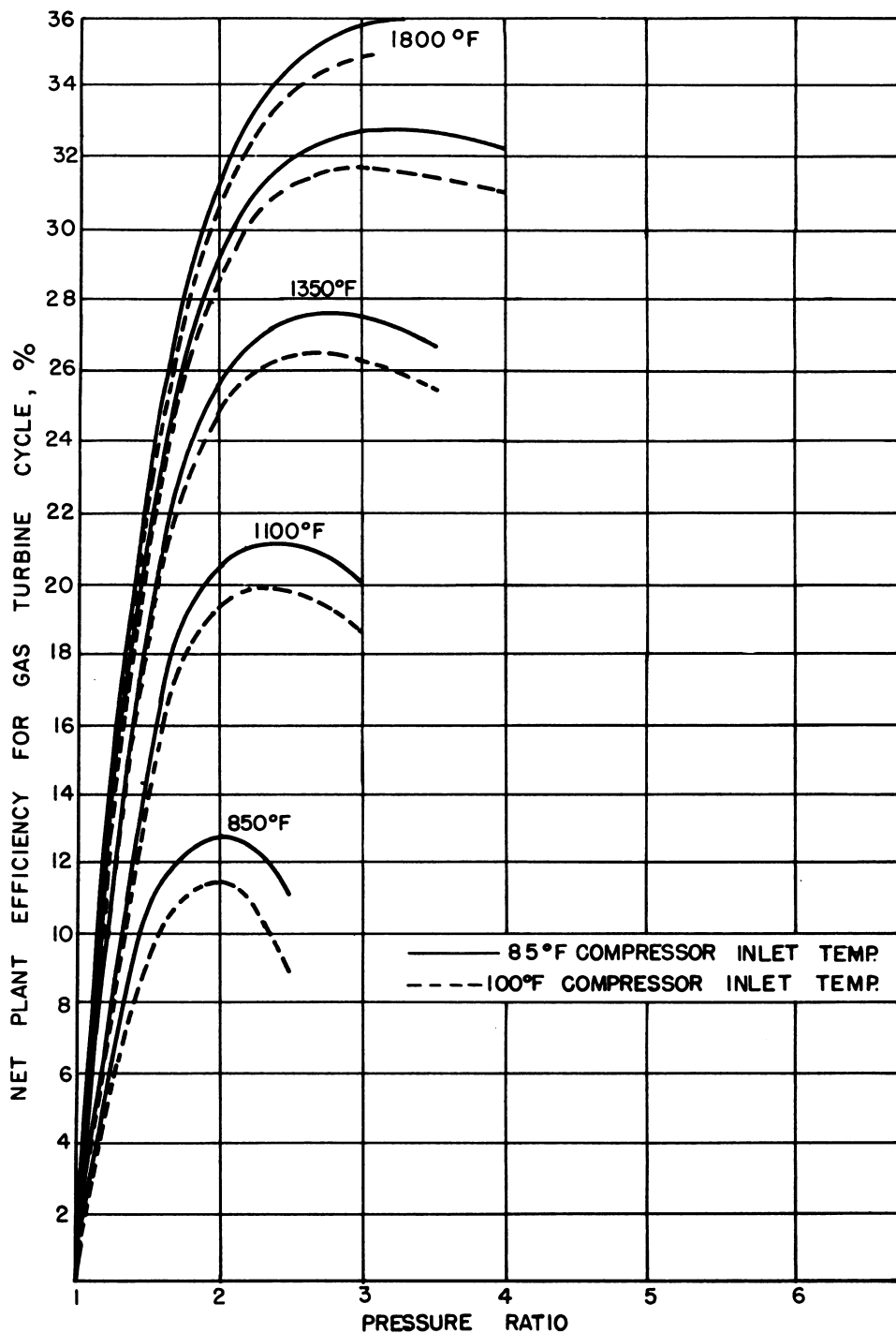


Fig. 3.2.3 — Thermal Efficiency vs Pressure Ratio for Helium. Reprinted from NP-3683, Jan. 1952. Component efficiencies, %: compressor, 80; turbine, 83; regenerator, 75.

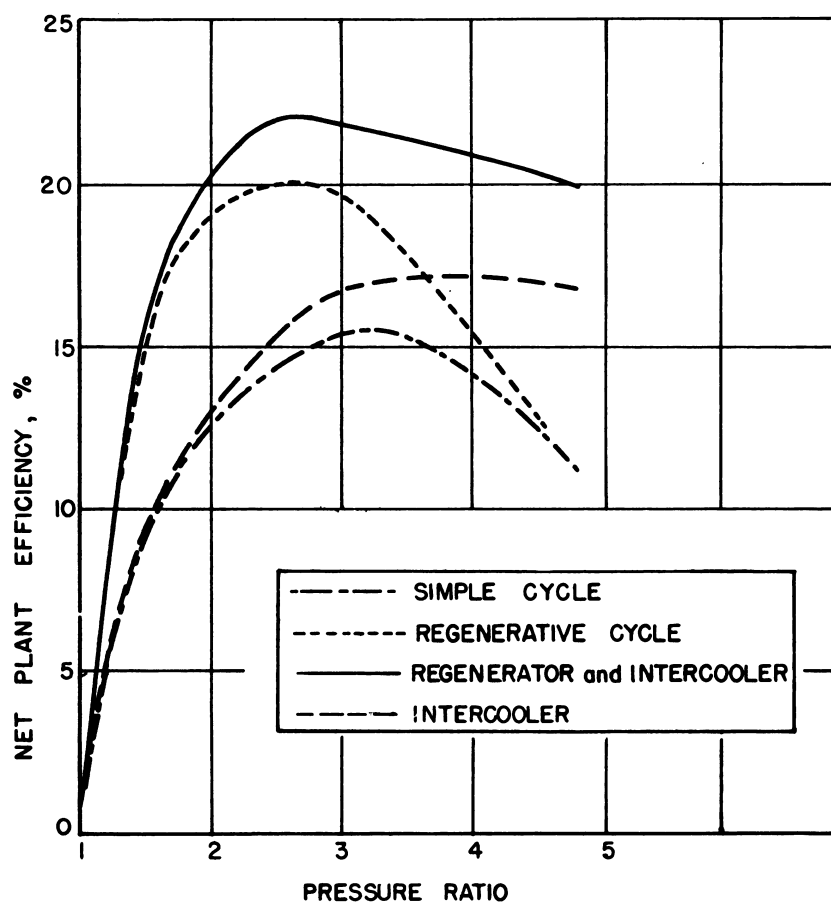


Fig. 3.2.4— Thermal Efficiencies for Various Cycles for Helium. Reprinted from NP-3683, Jan. 1952. Component efficiencies, %: turbine, 82; compressor, 80; regenerator, 50. Inlet temperatures, °F: turbine, 1350; compressor, 100.

REFERENCE

1. NP-3683, Allis-Chalmers Manufacturing Company, Final Report, Jan. 1952.

CHAPTER 3.3

Properties of Gas Coolants

The physical properties of air, helium, and carbon dioxide are given in detail since these gases have a combination of heat-transfer, nuclear, and chemical properties which makes them desirable as reactor coolants. (See Chap. 3.7, "Economic Comparison of Gas Coolants.") Less complete data are also given for other gases to permit evaluation of design parameters in coolant comparisons. Empirical correlations of the physical properties are included to facilitate extrapolation of existing data on gas coolants to reactor conditions.

Table 3.3.1 — Conversion Factors

Property	Multiply	By	To obtain
Density	gm/cc	62.4	lb/cu ft
	lb/cu ft	0.0160185	gm/cu cm
Entropy	cal/(gm)(°K)	1.00	Btu/(lb)(°R)
Internal energy	cal/gm	1.8	Btu/lb
	Btu/lb	0.5556	cal/gm
Pressure	atm	14.6959	lb/sq in
	atm	1.03323	kg/sq cm
	atm	760	mm Hg (0°C)
Specific heat	cal/(gm)(°C)	1.00	Btu/(lb)(°F)
Temperature	(°F-32)	5/9	°C
	°C	1.8	(°F-32)
Thermal conductivity	cal/(sec)(cm)(°C)	2901.0	Btu/(hr)(ft)(°F)
	Btu/(hr)(ft)(°F)	3.447×10^{-4}	cal/(sec)(cm)(°C)
Viscosity	cp	0.010	poises
	poises	1.000	gm/(sec)(cm)
	cp	0.000672	lb/(sec)(ft)
	cp	2.42	lb/(hr)(ft)

Table 3.3.2—Viscosity of Air at 1 Atm*

(Reprinted from "Chemical Engineers' Handbook," edited by J. H. Perry, 2d ed.
By permission from McGraw-Hill Book Company, Inc., New York, 1941)

T, °C	η , cp
0	0.018
100	.021
200	.025
300	.028
400	.031
500	.034
600	.037
700	.041
800	.043
900	.046
1000	.049

* See also Tables 3.3.22 and 3.3.23

Table 3.3.3—Physical Properties of Air at 10 Atm Pressure

(B. O. Newman, Physical Properties of Heat Transfer Fluids, GI-401, Nov. 10, 1947)

T, °F	Density, d, lb/cu ft	Viscosity, η , lb/(hr)(ft)	Specific heat, C_p , Btu/(lb)(°F)	Thermal cond., k, Btu/(hr)(ft)(°F)	Prandtl No., N_{Pr} , $c_p \eta / k$
0	0.863	0.0397	0.2398	0.0130	0.731
100	.709	.0461	.2403	.0157	.706
200	.602	.0520	.2412	.0182	.690
300	.523	.0577	.2427	.0205	.682
400	.462	.0628	.2449	.0228	.677
500	.413	.0680	.2476	.0250	.672
600	.371	.0730	.2505	.0272	.668
700	.342	.0769	.2534	.0293	.666
800	.315	.0811	.2566	.0314	.663
900	.292	.0849	.2598	.0334	.660
1000	.272	.0890	.2640	.0355	.658
1100	.254	.0926	.2660	.0376	.655

Table 3.3.4—Density of Air (Calculated)

(C. F. Curtiss and J. O. Hirschfelder, Thermodynamic
Properties of Air, CM-472, June 1, 1948)

T, °K	Density, gm/cc		
	1.0 atm	10 atm	100 atm
200	1.769×10^{-3}	1.807×10^{-2}	0.2312
250	1.413×10^{-3}	1.425×10^{-2}	.1506
273.2	1.293×10^{-3}	1.299×10^{-2}	...
300	1.177×10^{-3}	1.180×10^{-2}	0.1184
350	1.009×10^{-3}	1.009×10^{-2}	.09909
400	8.823×10^{-4}	8.804×10^{-3}	.08570
450	7.841×10^{-4}	7.820×10^{-3}	.07573
500	7.056×10^{-4}	7.034×10^{-3}	.06796
600	5.880×10^{-4}	5.860×10^{-3}	.05655
700	5.041×10^{-4}	5.023×10^{-3}	.04851

Table 3.3.5—Entropy of Air (Calculated)

(C. F. Curtiss and J. O. Hirschfelder, Thermodynamic Properties of Air, CM-472, June 1, 1948)

T, °K	Entropy, S, cal/(gm)(°K)		
	1.0 atm	10 atm	100 atm
200	1.5432	1.3815	1.1661
250	1.5970	1.4367	1.2554
300	1.6408	1.4813	1.3098
350	1.6779	1.5189	1.3519
400	1.7101	1.5514	1.3869
450	1.7387	1.5802	1.4172
500	1.7644	1.6061	1.4442
600	1.8094	1.6512	1.4905
700	1.8481	1.6899	1.5300

(J. O. Hirschfelder and C. F. Curtiss, Thermodynamic Properties of Air, II, CM-518, December 21, 1948)

T, °K	S - S ₀ , cal/(gm)(°K) [S ₀ = 1.6191. Dry air]					
	d/do* = 0.008	d/do = 0.04	d/do = 0.2	d/do = 1	d/do = 5	d/do = 25
273.2	0.3314	0.2210	0.1105	0	0.1115	0.2268
300	.3482	.2379	.1273	0.0167	-.0946	-.2098
400	.3978	.2874	.1769	.0663	-.0449	-.1600
500	.4369	.3265	.2161	.1055	-.0058	-.1205
600	.4699	.3594	.2489	.1384	+.0272	-.0871
700	.4982	.3878	.2774	.1669	.0556	-.0584
800	.5238	.4133	.3029	.1924	.0812	-.0327
900	.5469	.4364	.3260	.2156	.1044	-.0093
1000	.5682	.4578	.3473	.2367	.1257	+.0120

S - S ₀ , cal/(gm)(°K) [S ₀ = 1.6233, 0.5% moisture]						
273.2	0.3318	0.2212	0.1106	0	-0.1105	0.2202
300	.3479	.2374	.1267	0.0161	-.0948	-.2067
400	.3978	.2872	.1765	.0658	-.0452	-.1580
500	.4370	.3265	.2157	.1051	-.0061	-.1192
600	.4686	.3580	.2474	.1379	+.0268	-.0863
700	.4986	.3879	.2773	.1667	.0554	-.0577
800	.5242	.4136	.3028	.1923	.0811	-.0320
900	.5474	.4367	.3261	.2156	.1044	-.0088
1000	.5689	.4582	.3476	.2368	.1257	+.0128

S - S ₀ , cal/(gm)(°K) [S ₀ = 1.6276, 1% moisture]						
273.2	0.3323	0.2216	0.1107	0	-0.1107	-0.2206
300	.3487	.2379	.1270	0.0161	-.0949	-.2070
400	.3986	.2879	.1770	.0661	-.0452	-.1582
500	.4379	.3272	.2162	.1055	-.0060	-.1193
600	.4709	.3601	.2492	.1385	+.0270	-.0863
700	.4998	.3891	.2781	.1671	.0559	-.0575
800	.5254	.4145	.3038	.1928	.0816	-.0317
900	.5487	.4379	.3273	.2162	.1049	-.0085
1000	.5702	.4596	.3487	.2377	.1263	+.0132

S - S ₀ , cal/(gm)(°K) [S ₀ = 1.6592, 5% moisture]						
273.2	0.3376	0.2250	0.1125	0	-0.1123	-0.2237
300	.3541	.2416	.1290	0.0164	-.0963	-.2100
400	.4054	.2929	.1803	.0677	-.0453	-.1599
500	.4457	.3331	.2206	.1080	-.0051	-.1201
600	.4797	.3671	.2545	.1419	+.0289	-.0861
700	.5090	.3964	.2839	.1714	.0582	-.0567
800	.5353	.4228	.3102	.1976	.0846	-.0303
900	.5595	.4470	.3343	.2218	.1086	-.0063
1000	.5816	.4691	.3564	.2439	.1308	+.0160

* do is the density of air at 1 atm pressure and 0°C

Table 3.3.6—Internal Energy of Air (Calculated)

(J. O. Hirschfelder and C. F. Curtiss, Thermodynamic Properties of Air, II, CM-518, December 21, 1948)

T, °K	μ , cal/gm [Dry air]					
	d/do = 0.008	d/do = 0.04	d/do = 0.2	d/do = 1	d/do = 5	d/do = 25
273.2	45.767	45.765	45.756	45.712	45.492	44.394
300	50.366	50.364	50.356	50.314	50.104	49.057
400	67.633	67.631	67.624	67.586	67.398	66.458
500	85.188	85.186	85.179	85.143	84.965	84.075
600	103.20	103.20	103.19	103.16	102.97	102.11
700	121.74	121.74	121.73	121.70	121.53	120.68
800	140.84	140.84	140.83	140.80	140.63	139.79
900	160.49	160.49	160.48	160.45	160.28	159.45
1000	180.67	180.67	180.66	180.63	180.46	179.65

T, °K	μ , cal/gm [0.5% Moisture]					
	d/do = 0.008	d/do = 0.04	d/do = 0.2	d/do = 1	d/do = 5	d/do = 25
273.2	36.026	36.020	36.012	35.968	35.744	34.620
300	40.641	40.635	40.627	40.584	40.367	39.277
400	57.958	57.953	57.945	57.912	57.731	56.827
500	75.566	75.562	75.554	75.523	75.348	74.470
600	93.627	93.622	93.614	93.585	93.414	92.558
700	112.23	112.23	112.23	112.19	112.03	111.18
800	131.40	131.40	131.38	131.35	131.19	130.36
900	151.11	151.12	151.11	151.09	150.92	150.09
1000	171.38	171.37	171.37	171.34	171.17	170.36

T, °K	μ , cal/gm [1% Moisture]					
	d/do = 0.008	d/do = 0.04	d/do = 0.2	d/do = 1	d/do = 5	d/do = 25
273.2	26.253	26.239	26.240	26.187	25.958	24.806
300	30.880	30.867	30.869	30.816	30.591	29.461
400	48.250	48.238	48.239	48.200	48.027	47.160
500	65.914	65.902	65.904	65.865	65.693	64.828
600	84.033	84.021	84.022	83.984	83.815	82.969
700	102.69	102.68	102.69	102.65	102.48	101.65
800	121.92	121.92	121.92	121.88	121.72	120.90
900	141.72	141.71	141.72	141.69	141.52	140.70
1000	162.05	162.05	162.04	162.01	161.84	161.03

T, °K	μ , cal/gm [5% Moisture]					
	d/do = 0.008	d/do = 0.04	d/do = 0.2	d/do = 1	d/do = 5	d/do = 25
273.2	-53.348	-53.339	-53.359	-53.413	-53.687	-55.058
300	-48.606	-48.597	-48.617	-48.677	-48.970	-50.433
400	-30.810	-30.800	-30.812	-30.836	-30.951	-31.521
500	-12.702	-12.691	-12.706	-12.736	-12.887	-13.641
600	+ 5.886	+5.896	+5.882	+5.850	+5.696	+4.923
700	25.049	25.059	25.045	25.013	24.857	24.083
800	44.825	44.789	44.795	44.766	44.610	43.838
900	65.141	65.150	65.145	65.116	64.961	64.188
1000	86.052	86.045	86.052	86.023	85.866	85.098

Table 3.3.7—Pressure of Air (Calculated)

 (J. O. Hirschfelder and C. F. Curtiss, Thermodynamic Properties of
Air, II, CM-518, December 21, 1948)

T, °K	p, atm [Dry air]					
	d/do = 0.008	d/do = 0.04	d/do = 0.2	d/do = 1	d/do = 5	d/do = 25
273.2	0.0080059	0.040029	0.20012	1.0001	4.9890	24.651
300	.0087916	.043958	.21977	1.0986	5.4856	27.245
400	.011722	.058611	.29308	1.4657	7.3358	36.877
500	.014653	.073264	.36636	1.8327	9.1854	46.481
600	.017583	.087916	.43967	2.1997	11.034	56.069
700	.020514	.10257	.51294	2.5668	12.883	65.650
800	.023444	.11722	.58623	2.9337	14.732	75.234
900	.026375	.13187	.65950	3.3009	16.580	84.811
1000	.029305	.14653	.73278	3.6676	18.428	94.381

T, °K	p, atm [0.5% Moisture]					
	d/do = 0.008	d/do = 0.04	d/do = 0.2	d/do = 1	d/do = 5	d/do = 25
273.2	0.0080059	0.040029	0.20013	1.0001	4.9887	24.643
300	.0087913	.043957	.21976	1.0985	5.4851	27.236
400	.011722	.058609	.29307	1.4656	7.3356	36.869
500	.014652	.073261	.36634	1.8326	9.1851	46.467
600	.017583	.087913	.43966	2.1996	11.033	56.051
700	.020513	.10257	.51293	2.5667	12.883	65.636
800	.023445	.11722	.58621	2.9336	14.730	75.211
900	.026374	.13187	.65948	3.3004	16.578	84.783
1000	.029306	.14652	.73276	3.6674	18.427	94.362

T, °K	p, atm [1% Moisture]					
	d/do = 0.008	d/do = 0.04	d/do = 0.2	d/do = 1	d/do = 5	d/do = 25
273.2	0.0080065	0.040028	0.20013	1.0001	4.9882	24.635
300	.0087919	.043955	.21977	1.0985	5.4846	27.227
400	.011722	.058607	.29305	1.4655	7.3347	36.856
500	.014653	.073259	.36635	1.8326	9.1840	46.452
600	.017584	.087911	.43966	2.1996	11.033	56.039
700	.020514	.10256	.51293	2.5664	12.880	65.616
800	.023445	.11721	.58623	2.9336	14.730	75.195
900	.026376	.13187	.65951	3.3003	16.577	84.767
1000	.029306	.14652	.73281	3.6674	18.425	94.332

T, °K	p, atm [5% Moisture]					
	d/do = 0.008	d/do = 0.04	d/do = 0.2	d/do = 1	d/do = 5	d/do = 25
273.2	0.0080068	0.040035	0.20015	1.0001	4.9864	24.572
300	.0087922	.043962	.21980	1.0985	5.4828	27.162
400	.011723	.058618	.29309	1.4657	7.3330	36.782
500	.014654	.073272	.36640	1.8326	9.1818	46.366
600	.017584	.087926	.43967	2.1996	11.031	55.936
700	.020515	.10258	.51302	2.5667	12.877	65.502
800	.023446	.11724	.58630	2.9336	14.726	75.060
900	.026377	.13189	.65962	3.3007	16.574	84.624
1000	.029307	.14655	.73289	3.6674	18.421	94.173

Table 3.3.8—Composition of Air at Sea Level
(C. F. Curtiss and J. O. Hirschfelder, *Thermodynamic Properties of Air*, CM-472, June 1, 1948)

Component	Fraction by volume
N ₂	0.780881
O ₂	.209495
A	.009300
CO ₂	.000300
Ne	.000019
He	.000005

Table 3.3.9 — Specific Heat of Air at Constant Volume (Calculated)

(J. O. Hirschfelder and C. F. Curtiss, Thermodynamic Properties of Air, I, CM-472, June 1, 1948)

T, °K	c_v , cal/(mole)(°C)			[Dry air]
	1 atm	10 atm	100 atm	
200	4.9582	5.0100	6.5830	
250	4.9603	4.9884	5.4732	
300	4.9708	4.9845	5.1985	
350	4.9936	5.0041	5.1149	
400	5.0296	5.0368	5.1003	
450	5.0791	5.0850	5.1241	

(J. O. Hirschfelder and C. F. Curtiss, Thermodynamic Properties of Air, II, CM-518, December 21, 1948)

T, °K	c_v , cal/(gm)(°C)						[Dry air]
	d/do* = 0.008	d/do = 0.04	d/do = 0.2	d/do = 1	d/do = 5	d/do = 25	
500	0.1777	0.1777	0.1777	0.1777	0.1777	0.1780	
600	.1827	.1827	.1827	.1828	.1828	.1830	
700	.1883	.1883	.1883	.1883	.1883	.1884	
800	.1938	.1938	.1938	.1938	.1938	.1939	
900	.1993	.1993	.1993	.1993	.1993	.1995	
1000	.2043	.2044	.2044	.2044	.2043	.2044	

c_v , cal/(gm)(°C)						[0.5% Moisture]
500	0.1782	0.1782	0.1782	0.1782	0.1783	
600	.1833	.1833	.1833	.1833	.1833	.1835
700	.1889	.1885	.1889	.1889	.1889	.1891
800	.1944	.1945	.1945	.1945	.1945	.1946
900	.2000	.1999	.2001	.2001	.2000	.2001
1000	.2052	.2050	.2050	.2050	.2051	.2052

c_v , cal/(gm)(°C)						[1% Moisture]
500	0.1787	0.1787	0.1787	0.1787	0.1787	
600	.1838	.1839	.1839	.1839	.1839	.1841
700	.1895	.1895	.1895	.1896	.1896	.1897
800	.1952	.1952	.1952	.1953	.1952	.1953
900	.2008	.2008	.2007	.2008	.2007	.2008
1000	.2058	.2058	.2058	.2058	.2056	.2059

c_v , cal/(gm)(°C)						[5% Moisture]
500	0.1833	0.1833	0.1833	0.1832	0.1828	
600	.1887	.1887	.1887	.1887	.1887	.1887
700	.1948	.1945	.1946	.1946	.1946	.1946
800	.2005	.2005	.2006	.2006	.2006	.2006
900	.2062	.2064	.2064	.2064	.2064	.2064
1000	.2118	.2116	.2118	.2117	.2117	.2117

* do is the density of air at 1 atm pressure and 0°C

Table 3.3.10—Specific Heat of Air at Constant Pressure (Calculated)

(J. O. Hirschfelder and C. F. Curtiss, Thermodynamic Properties of Air, I, CM-472, June 1, 1948)

T, °K	c _p , cal/(mole)(°C)			[Dry air]
	1 atm	10 atm	100 atm	
200	6.9694	7.2532	16.264	
250	6.9619	7.1224	9.3501	
300	6.9675	7.0662	8.1454	
350	6.9873	7.0572	7.7078	
400	7.0216	7.0721	7.5138	
450	7.0699	7.1086	7.4316	

(J. O. Hirschfelder and C. F. Curtiss, Thermodynamic Properties of Air, II, CM-518, December 21, 1948)

T, °K	c _p , cal/(gm)(°C)						[Dry air]
	d/do* = 0.008	d/do = 0.04	d/do = 0.2	d/do = 1	d/do = 5	d/do = 25	
500	0.2463	0.2463	0.2463	0.2465	0.2472	0.2510	
600	.2513	.2513	.2513	.2515	.2521	.2552	
700	.2569	.2569	.2569	.2569	.2575	.2600	
800	.2624	.2624	.2624	.2624	.2629	.2651	
900	.2679	.2679	.2679	.2679	.2683	.2704	
1000	.2729	.2730	.2730	.2730	.2733	.2751	
c _p , cal/(gm)(°C)							[0.5% Moisture]
500	0.2469	0.2469	0.2470	0.2471	0.2479	0.2515	
600	.2520	.2520	.2521	.2522	.2527	.2558	
700	.2577	.2573	.2577	.2578	.2582	.2609	
800	.2631	.2632	.2633	.2634	.2638	.2659	
900	.2687	.2686	.2689	.2689	.2692	.2712	
1000	.2740	.2737	.2739	.2738	.2742	.2760	
c _p , cal/(gm)(°C)							[1% Moisture]
500	0.2476	0.2476	0.2476	0.2477	0.2485	0.2519	
600	.2527	.2528	.2528	.2529	.2535	.2565	
700	.2584	.2583	.2584	.2586	.2591	.2616	
800	.2641	.2640	.2641	.2643	.2646	.2668	
900	.2697	.2697	.2696	.2698	.2700	.2720	
1000	.2747	.2747	.2746	.2747	.2749	.2768	
c _p , cal/(gm)(°C)							[5% Moisture]
500	0.2532	0.2532	0.2533	0.2533	0.2536	0.2554	
600	.2586	.2586	.2587	.2588	.2594	.2623	
700	.2647	.2645	.2646	.2647	.2651	.2677	
800	.2705	.2705	.2706	.2706	.2711	.2732	
900	.2761	.2763	.2764	.2764	.2768	.2787	
1000	.2817	.2815	.2817	.2817	.2820	.2836	

* do is the density of air at 1 atm pressure and 0°C

Table 3.3.11 — Ratio of Specific Heats of Air (Calculated)

(J. O. Hirschfelder and C. F. Curtiss, Thermodynamic Properties of Air, I, CM-472, June 1, 1948)

T, °K	$\gamma = c_p/c_v$		
	1 atm	10 atm	100 atm
200	1.4056	1.4477	2.4706
250	1.4035	1.4278	1.7083

(J. O. Hirschfelder and C. F. Curtiss, Thermodynamic Properties of Air, II, CM-518, December 21, 1948)

T, °K	$\gamma = c_p/c_v$ [Dry air]					
	d/do* = 0.008	d/do = 0.04	d/do = 0.2	d/do = 1	d/do = 5	d/do = 25
273.2	1.409	1.409	1.409	1.412	1.422	1.444
300	1.406	1.406	1.406	1.409	1.418	1.440
400	1.396	1.396	1.396	1.398	1.404	1.425
500	1.386	1.386	1.386	1.387	1.391	1.410
600	1.376	1.376	1.376	1.376	1.379	1.395
700	1.365	1.365	1.365	1.365	1.368	1.380
800	1.354	1.354	1.354	1.354	1.357	1.367
900	1.344	1.344	1.344	1.344	1.346	1.356
1000	1.336	1.336	1.336	1.336	1.338	1.346
$\gamma = c_p/c_v$ [0.5% Moisture]						
273.2	1.411	1.411	1.409	1.412	1.418	1.453
300	1.408	1.408	1.406	1.409	1.415	1.448
400	1.397	1.397	1.396	1.398	1.403	1.429
500	1.386	1.386	1.386	1.387	1.391	1.411
600	1.375	1.375	1.376	1.376	1.379	1.394
700	1.364	1.365	1.364	1.365	1.367	1.380
800	1.354	1.353	1.354	1.354	1.356	1.367
900	1.344	1.344	1.344	1.344	1.346	1.356
1000	1.335	1.335	1.336	1.336	1.337	1.345
$\gamma = c_p/c_v$ [1% Moisture]						
273.2	1.411	1.411	1.411	1.411	1.418	1.459
300	1.408	1.408	1.408	1.408	1.415	1.453
400	1.397	1.397	1.397	1.397	1.403	1.431
500	1.386	1.386	1.386	1.386	1.391	1.411
600	1.375	1.375	1.375	1.375	1.379	1.393
700	1.364	1.363	1.364	1.364	1.367	1.379
800	1.353	1.353	1.353	1.353	1.356	1.366
900	1.343	1.343	1.343	1.344	1.345	1.355
1000	1.335	1.335	1.334	1.335	1.337	1.345
$\gamma = c_p/c_v$ [5% Moisture]						
273.2	1.403	1.407	1.407	1.408	1.417	1.462
300	1.401	1.404	1.404	1.405	1.414	1.456
400	1.392	1.393	1.393	1.394	1.401	1.434
500	1.382	1.382	1.382	1.383	1.388	1.412
600	1.371	1.371	1.371	1.372	1.375	1.390
700	1.359	1.360	1.360	1.360	1.362	1.376
800	1.349	1.349	1.349	1.349	1.352	1.362
900	1.339	1.339	1.339	1.339	1.341	1.350
1000	1.330	1.330	1.330	1.331	1.332	1.340

* do is the density of air at 1 atm pressure and 0°C

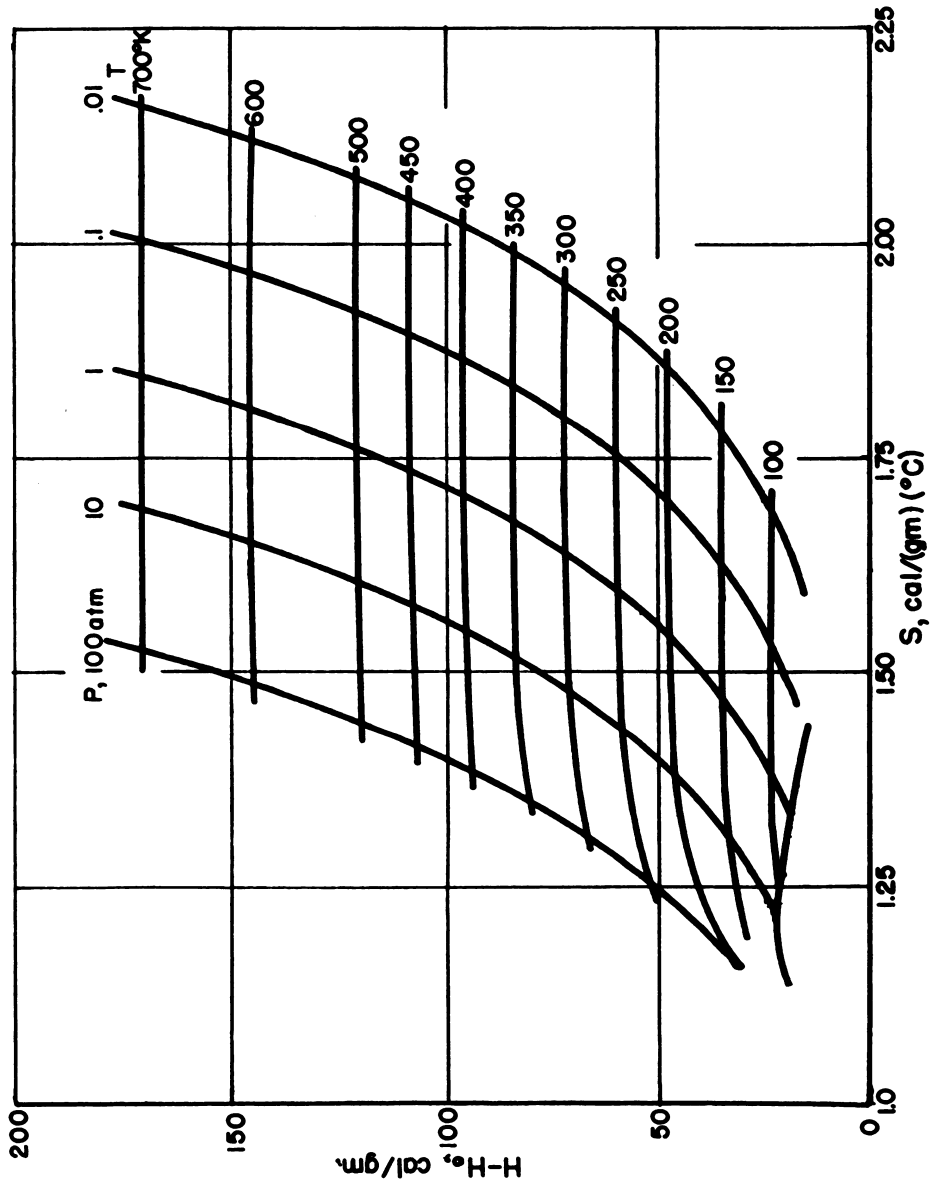


Fig. 3.3.1 — Mollier Diagram for Dry Air. Submitted by the University of Wisconsin, May 1947.

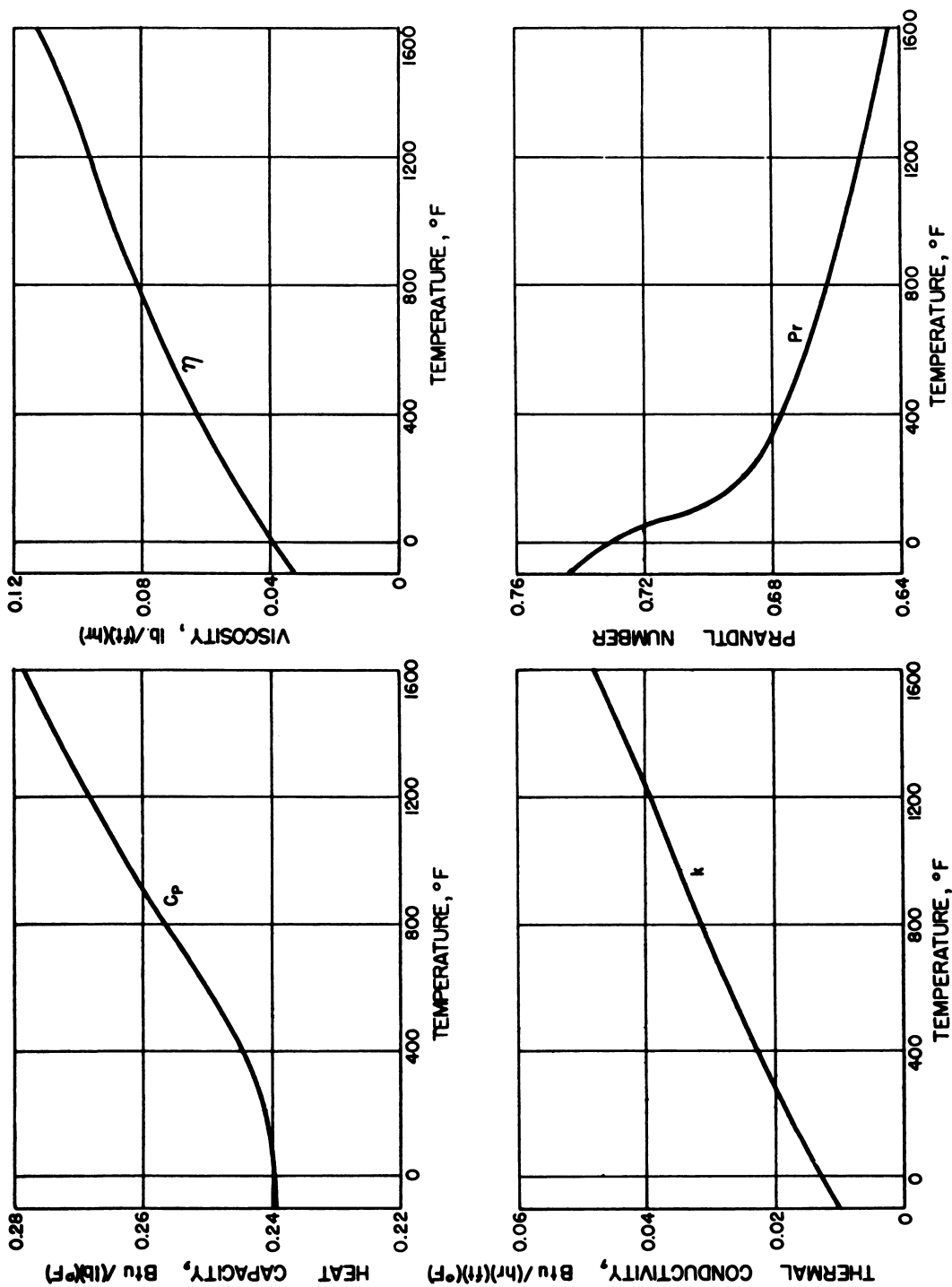


Fig. 3.3.2 — Physical Properties of Air, Submitted by Oak Ridge National Laboratory, April 1949.

Table 3.3.12—Physical Properties of Helium at 10 Atm Pressure
(B. O. Newman, Physical Properties of Heat Transfer Fluids, GI-401, Nov. 10, 1947)

T, °F	Density, d, lb/cu ft	Viscosity, η , lb/(ft)(hr)	Specific heat,* c_p , Btu/(lb)(°F)	Thermal cond.,† k, Btu/(ft)(hr)(°F)	Prandtl No., N_{Pr} , $c_p\eta/k$
32	0.1117	0.0457	1.248	0.083	0.687
100	.0974	.0495	1.248	.090	.687
200	.0827	.0555	1.248	.100	.687
300	.0718	.0605	1.248	.110	.686
400	.0635	.0653	1.248	.119	.684
500	.0569	.0700	1.248	.128	.682
600	.0516	.0743	1.248	.136	.679
700	.0475*	.0780	1.248	.145	.675
800	.0430*	.0821	1.248	.153	.671
900	.0399*	.0859	1.248	.160	.667
1000	.0373*	.0889	1.248	.167	.662
1100	.0351*	.0918	1.248	.175	.656

* Extrapolated

† Atmospheric pressure

Table 3.3.13—Thermodynamic Properties of Helium
(S. W. Akin, Thermodynamic Properties of Helium at High Pressures and Temperatures, NP-124, May, 1947)

Pressure, psia	Property*	0°F	100	200	300	400	500	600°F
		255.38°K	310.94	366.49	422.05	477.60	533.16	588.72°K
14.696	v	83.971	102.23	120.487	138.743	157.00	175.258	193.515
	d	.0119088	.0097820	.0082997	.0072076	.0063694	.0057059	.0051676
	h	577.92	707.73	827.56	952.38	1077.20	1202.02	1326.83
	s	6.5965	6.8421	7.0472	7.2233	7.3776	7.5149	7.6386
50	v	24.717	30.085	35.451	40.817	46.183	51.549	56.915
	d	.040457	.033239	.028208	.024500	.021653	.019399	.017570
	h	578.26	703.08	827.90	952.72	1077.54	1202.36	1327.18
	s	5.9885	6.2342	6.4393	6.6153	6.7697	6.9070	7.0307
150	v	8.2735	10.063	11.8522	13.6407	15.4293	17.2183	19.008
	d	.120868	.099372	.084372	.073310	.064812	.058078	.052610
	h	579.25	704.08	828.91	953.73	1078.55	1203.37	1328.19
	s	5.4429	5.6886	5.8937	6.0698	6.2241	6.3614	6.4852
400	v	3.1347	3.8062	4.4775	5.1487	5.8197	6.4905	7.1616
	d	.31901	.26273	.22334	.194225	.171831	.154072	.139633
	h	581.72	706.58	831.42	956.24	1081.06	1205.88	1330.70
	s	4.9555	5.2013	5.4065	5.5827	5.7371	5.8744	5.9981
600	v	2.1067	2.5546	3.0023	3.44995	3.8973	4.3449	4.7923
	d	.47468	.39146	.33308	.28986	.25658	.23016	.20867
	h	583.60	708.49	833.33	958.15	1082.97	1207.79	1332.61
	s	4.7539	4.9998	5.2050	5.3813	5.5357	5.6730	5.7968
900	v	1.4211	1.7200	2.0187	2.3173	2.6157	2.91399	3.2124
	d	.70369	.58139	.49537	.43154	.38230	.34317	.31129
	h	585.09	710.29	835.38	960.40	1085.42	1210.42	1335.36
	s	4.5521	4.7981	5.0035	5.1797	5.3342	5.4715	5.5953

Table 3.3.13 — Continued

Pressure, psia	Property*	0°F	100	200	300	400	500	600°F
		255.38°K	310.94	366.49	422.05	477.60	533.16	588.72°K
1500	v	.87224	1.05192	1.2314	1.4108	1.58994	1.7690	1.9483
	d	1.14647	.95064	.81207	.70880	.62897	.56528	.51328
	h	590.08	715.54	840.77	965.88	1090.92	1215.94	1340.97
	s	4.2974	4.5437	4.7475	4.9257	5.0801	5.2176	5.3414
2500	v	.54224	.65044	.75847	.86635	.97410	1.08176	1.18947
	d	1.84420	1.53741	1.31845	1.15427	1.02659	.92442	.84071
	h	598.60	724.37	849.73	974.95	1100.10	1225.22	1350.29
	s	4.0420	4.2887	4.4928	4.6712	4.8258	4.9634	5.0873
4000	v	.35574	.42377	.49161	.55932	.62694	.69444	.76191
	d	2.8110	2.3598	2.0341	1.78789	1.59503	1.44000	1.31248
	h	610.24	736.48	862.24	987.70	1113.12	1238.46	1363.73
	s	3.8058	4.0531	4.2576	4.4363	4.5912	4.7287	4.8530
6000	v	.25126	.29696	.34253	.38796	.43325	.47849	.52369
	d	3.9800	3.3675	2.9195	2.5776	2.3081	2.0899	1.9095
	h	625.80	752.49	878.58	1004.32	1129.96	1255.54	1381.03
	s	3.6017	3.8385	4.0535	4.2327	4.3879	4.5259	4.6503

* v = cu ft/lb; d = lb/cu ft; h = Btu/lb; s = Btu/(lb)(°F).

Table 3.3.14 — Impurities in Grade A (99.99%) Helium

(W. M. Deaton, U. S. Bureau of Mines,
Personal Communication, 1952)

Impurity	Concentration, ppm (by weight)
H ₂	5
H ₂ O	45
Air	73

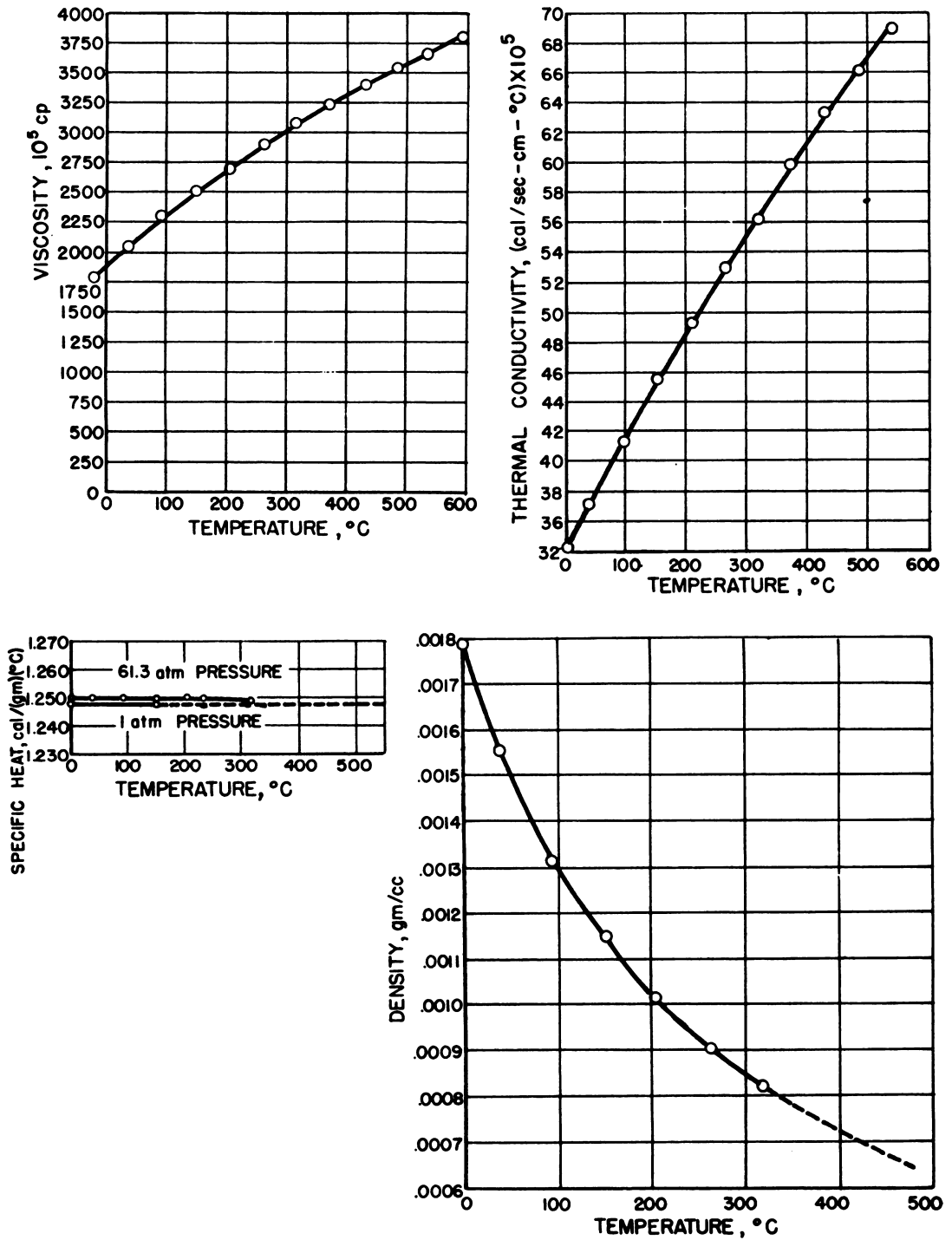


Fig. 3.3.3 — Physical Properties of Helium. Submitted by the General Electric Company, November 1947.

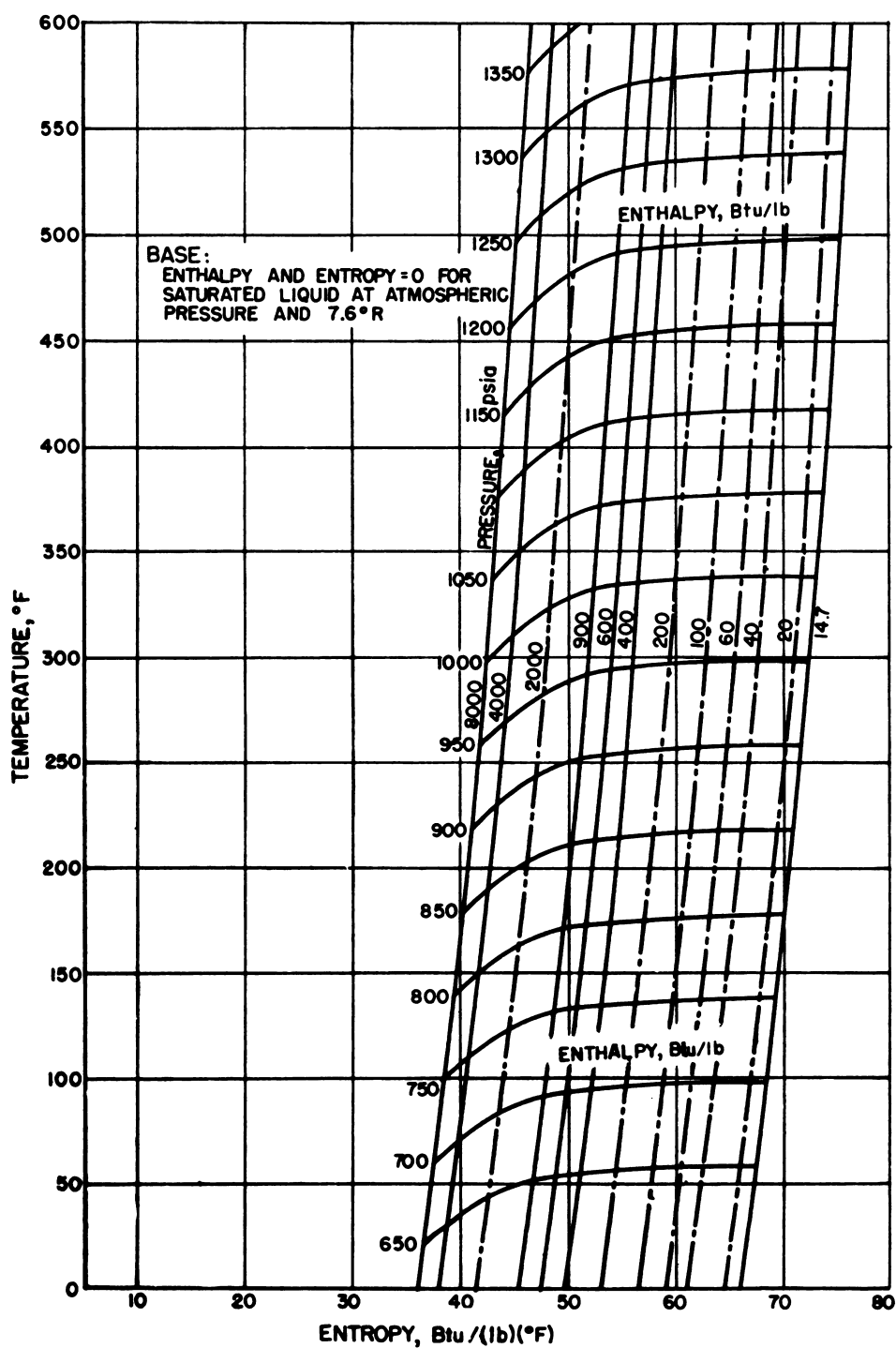


Fig. 3.3.4 — Temperature-Entropy Diagram for Helium. Submitted by the General Electric Company, May 1947.

Table 3.3.15—Properties of Superheated Carbon Dioxide

[Reprinted from "Chemical Engineers' Handbook," edited by J. H. Perry, 3rd ed., McGraw-Hill Book Company, Inc., New York, 1950, by permission. Data from Sweigert, Weber, and Allen, Ind. Eng. Chem., 38: 185 (1946), with permission.]

Pressure, psia	Property*	-75°F	-50	0	50	100	150	200	300	400	600	800	1000	1200	1400	1600	1800°F
1.00	v	93.90	100.0	112.2	124.4	136.6	148.8	161.0	185.4	209.7	258.5	307.2	356.0	404.8	453.6	502.3	551.0
	h	283.2	288.0	297.8	307.7	318.0	328.4	339.1	361.4	384.7	434.4	487.1	542.4	599.6	658.6	718.8	780.0
	s	1.4772	1.4892	1.5112	1.5316	1.5506	1.5684	1.5852	1.6165	1.6451	1.6969	1.7423	1.7829	1.8197	1.8533	1.8838	1.9123
10.0	v	9.280	9.902	11.15	12.38	13.61	14.84	16.06	18.51	20.96	25.85	30.73	35.61	40.49	45.36	50.24	55.11
	h	282.6	287.5	297.3	307.3	317.7	328.2	339.0	361.3	384.6	434.4	487.1	542.4	599.6	658.6	718.8	780.0
	s	1.3733	1.3853	1.4073	1.4277	1.4467	1.4645	1.4813	1.5126	1.5412	1.5930	1.6384	1.6790	1.7158	1.7494	1.7799	1.8084
20.0	v	4.586	4.904	5.542	6.119	6.778	7.407	8.016	9.247	10.47	12.92	15.36	17.80	20.24	22.68	25.11	27.55
	h	281.9	287.0	296.8	306.8	317.3	327.9	338.8	361.1	384.5	434.3	487.1	542.4	599.6	658.6	718.8	780.0
	s	1.3417	1.3538	1.3759	1.3964	1.4154	1.4332	1.4500	1.4813	1.5099	1.5617	1.6071	1.6477	1.6845	1.7181	1.7486	1.7771
40.0	v	2.239	2.404	2.738	3.053	3.363	3.668	3.993	4.615	5.230	6.458	7.688	8.901	10.12	11.37	12.56	13.78
	h	280.6	285.9	295.8	305.9	316.5	327.4	338.4	360.9	384.3	434.2	487.0	542.4	599.6	658.6	718.8	780.0
	s	1.3088	1.3211	1.3435	1.3642	1.3834	1.4014	1.4184	1.4499	1.4787	1.5305	1.5759	1.6165	1.6533	1.6869	1.7174	1.7459
80.0	v	...	1.154	1.335	1.498	1.657	1.828	1.982	2.298	2.608	3.226	3.839	4.448	5.060	5.670	6.281	6.887
	h	...	283.8	293.8	304.1	315.1	326.4	337.7	360.2	383.9	434.0	486.9	542.3	599.5	658.6	718.8	780.0
	s	...	1.2778	1.3044	1.3284	1.3480	1.3679	1.3855	1.4177	1.4468	1.4991	1.5446	1.5852	1.6220	1.6556	1.6861	1.7146
120	v	0.8665	0.9799	1.088	1.208	1.311	1.525	1.734	2.148	2.559	2.966	3.373	3.781	4.188	4.592
	h	291.7	302.2	313.6	325.4	337.0	359.7	383.5	433.8	486.8	542.3	599.5	658.6	718.8	780.0
	s	1.2833	1.3086	1.3297	1.3488	1.3666	1.3993	1.4285	1.4808	1.5263	1.5669	1.6037	1.6373	1.6678	1.6963
160	v	0.6305	0.7207	0.8033	0.8986	0.9760	1.139	1.297	1.610	1.918	2.224	2.530	2.836	3.141	3.445
	h	289.7	300.4	312.1	324.4	336.3	359.1	383.1	433.6	486.6	542.2	599.5	658.6	718.8	780.0
	s	1.2666	1.2928	1.3154	1.3350	1.3529	1.3957	1.4151	1.4675	1.5133	1.5539	1.5907	1.6243	1.6548	1.6833
200	v	0.4891	0.5652	0.6376	0.7125	0.7748	0.9075	1.035	1.287	1.534	1.779	2.024	2.269	2.513	2.757
	h	287.7	298.6	310.6	323.4	335.6	358.5	382.7	433.4	486.5	542.2	599.5	658.5	718.8	780.0
	s	1.2519	1.2805	1.3038	1.3239	1.3421	1.3753	1.4049	1.4574	1.5033	1.5439	1.5807	1.6143	1.6448	1.6733
240	v	0.3948	0.4614	0.5237	0.5886	0.6407	0.7832	0.904	1.071	1.273	1.482	1.687	1.891	2.095	2.297
	h	285.6	296.7	309.1	322.4	334.9	358.0	382.3	433.1	486.4	542.1	599.5	658.5	718.8	780.0
	s	1.2395	1.2694	1.2940	1.3145	1.3350	1.3671	1.3963	1.4490	1.4948	1.5356	1.5724	1.6060	1.6365	1.6650
300	v	0.3563	0.4100	0.4636	0.5065	0.5985	0.6868	0.8556	1.021	1.186	1.349	1.513	1.676	1.838
	h	294.0	306.9	320.9	333.9	357.1	381.6	432.8	486.2	542.0	599.4	658.5	718.7	780.0
	s	1.2562	1.2813	1.3029	1.3219	1.3560	1.3862	1.4389	1.4848	1.5256	1.5624	1.5960	1.6265	1.6550
360	v	0.2858	0.3341	0.3780	0.4171	0.4958	0.5693	0.7212	0.8502	0.9874	1.125	1.261	1.397	1.533
	h	291.2	304.6	319.4	332.8	356.3	381.0	432.5	486.0	541.9	599.4	658.5	718.7	779.9
	s	1.2436	1.2699	1.2925	1.3134	1.3475	1.3779	1.4307	1.4766	1.5174	1.5542	1.5878	1.6183	1.6468

440	v	0.2216	0.2652	0.3040	0.3358	0.4022	0.4633	0.5817	0.6950	0.8079	0.9201	1.032	1.142	1.255
	h	287.6	301.6	317.4	331.4	355.1	380.2	432.1	485.8	541.7	599.3	658.4	718.6	779.9
	s	1.2282	1.2559	1.2797	1.3006	1.3370	1.3681	1.4215	1.4675	1.5083	1.5451	1.5787	1.6092	1.6377
520	v	0.1772	0.2174	0.2513	0.2795	0.3374	0.3901	0.4912	0.5881	0.6832	0.7785	0.8733	0.9672	1.062
	h	283.9	298.7	315.4	330.0	354.0	379.4	431.7	485.5	541.5	599.2	656.3	718.6	779.9
	s	1.2148	1.2438	1.2687	1.2905	1.3281	1.3599	1.4138	1.4599	1.5007	1.5375	1.5711	1.6010	1.6301
600	v	0.1452	0.1823	0.2123	0.2383	0.2898	0.3363	0.4250	0.5093	0.5921	0.6747	0.7571	0.8385	0.9202
	h	280.3	295.7	313.4	328.6	352.8	376.6	431.1	485.3	541.4	599.0	658.2	718.6	779.8
	s	1.2020	1.2323	1.2583	1.2809	1.3198	1.3525	1.4071	1.4534	1.4942	1.5310	1.5646	1.5951	1.6236
800	v	0.1196	0.1483	0.1712	0.2126	0.2489	0.3173	0.3812	0.4436	0.5080	0.5680	0.6292	0.6906
	h	288.2	308.4	325.1	350.0	376.5	430.1	484.7	541.0	598.8	658.0	718.4	778.7	839.0
	s	1.2111	1.2391	1.2631	1.3041	1.3380	1.3935	1.4404	1.4812	1.5180	1.5516	1.5821	1.6106
1000	v	0.1101	0.1310	0.1663	0.1966	0.2526	0.3048	0.3547	0.4049	0.4545	0.5037	0.5528
	h	303.4	321.6	347.1	374.5	429.1	484.0	540.6	598.5	657.8	718.3	778.6
	s	1.2218	1.2472	1.2903	1.3258	1.3928	1.4302	1.4712	1.5080	1.5416	1.5721	1.6006
1200	v	0.1042	0.1356	0.1621	0.2096	0.2531	0.2953	0.3374	0.3789	0.4199	0.4609
	h	318.4	344.2	372.5	428.1	483.5	540.2	598.2	657.7	718.2	779.5
	s	1.2343	1.2791	1.3158	1.3740	1.4216	1.4628	1.4996	1.5332	1.5637	1.5922
1400	v	0.1136	0.1375	0.1788	0.2160	0.2529	0.2892	0.3249	0.3601	0.3951
	h	341.4	370.4	427.0	482.9	539.8	598.0	657.5	718.0	779.5
	s	1.2703	1.3078	1.3668	1.4145	1.4558	1.4927	1.5263	1.5568	1.5853
1600	v	0.1191	0.1557	0.1898	0.2211	0.2530	0.2843	0.3153	0.3461
	h	367.6	426.0	482.3	539.5	597.7	657.2	717.9	779.4
	s	1.3002	1.3602	1.4083	1.4497	1.4867	1.5193	1.5508	1.5793
1800	v	0.1047	0.1377	0.1675	0.1964	0.2249	0.2528	0.2804	0.3079
	h	364.0	424.9	481.7	539.1	597.4	657.0	717.8	779.3
	s	1.2930	1.3539	1.4023	1.4440	1.4812	1.5148	1.5453	1.5738
2200	v	0.1120	0.1368	0.1605	0.1840	0.2070	0.2296	0.2522
	h	421.7	480.5	538.4	596.9	656.6	717.5	779.2
	s	1.3426	1.3925	1.4344	1.4720	1.5057	1.5362	1.5647
2600	v	0.1156	0.1357	0.1557	0.1752	0.1945	0.2137
	h	479.3	537.6	596.4	656.3	717.2	779.1
	s	1.3834	1.4260	1.4640	1.4981	1.5286	1.5571
3000	v	0.1001	0.1176	0.1349	0.1519	0.1687	0.1856
	h	478.1	536.8	595.8	656.0	717.0	778.8
	s	1.3752	1.4183	1.4569	1.4915	1.5220	1.5505

*v = cu ft/lb; h = Btu/lb; s = Btu/(lb)(°R). To make the enthalpies of saturated CO₂ consistent with those of superheated CO₂, add 143.3 Btu/lb to h_{sat}

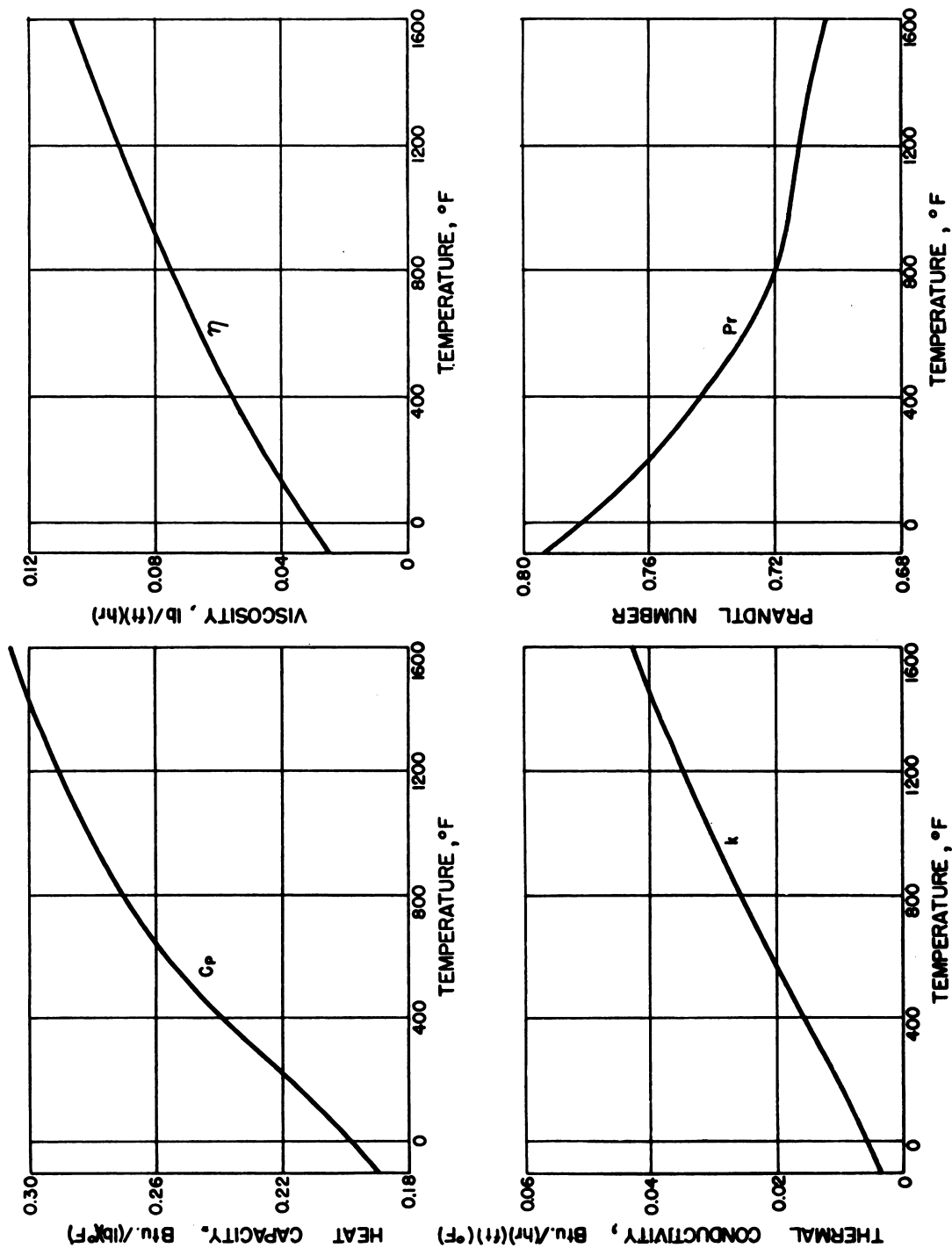


Fig. 3.3.5 — Physical Properties of Carbon Dioxide. Submitted by Oak Ridge National Laboratory, April 1949.

Table 3.3.16—Properties of Gas Coolants Listed in the International Critical Tables

Gas	Density		Specific heat		Viscosity		Thermal conductivity	
	Volume	Page	Volume	Page	Volume	Page	Volume	Page
Helium	3	3	1	102	5	2	5	213,214
Carbon dioxide	3	3,11	7	243	5	4	5	214,215
Air	1	102	1	103	1	102	2	312
	2	312	5	80,81				
	3	3						

Table 3.3.17—Viscosities of Gases

(Reprinted from "Chemical Engineers' Handbook," edited by J. H. Perry, 3rd ed.
By permission from McGraw-Hill Book Company, Inc., New York, 1950)

Gas	X*	Y*	Gas	X*	Y*
Acetic acid	7.7	14.3	Freon-113	11.3	14.0
Acetone	8.9	13.0	Helium	10.9	20.5
Acetylene	9.8	14.9	Hexane	8.6	11.8
Air	11.0	20.0	Hydrogen	11.2	12.4
Ammonia	8.4	16.0	3H ₂ + 1N ₂	11.2	17.2
Argon	10.5	22.4	Hydrogen bromide	8.8	20.9
Benzene	8.5	13.2	Hydrogen chloride	8.8	18.7
Bromine	8.9	19.2	Hydrogen cyanide	9.8	14.9
Butene	9.2	13.7	Hydrogen iodide	9.0	21.3
Butylene	8.9	13.0	Hydrogen sulfide	8.6	18.0
Carbon dioxide	9.5	18.7	Iodine	9.0	18.4
Carbon disulfide	8.0	16.0	Mercury	5.3	22.9
Carbon monoxide	11.0	20.0	Methane	9.9	15.5
Chlorine	9.0	18.4	Methyl alcohol	8.5	15.6
Chloroform	8.9	15.7	Nitric oxide	10.9	20.5
Cyanogen	9.2	15.2	Nitrogen	10.6	20.0
Cyclohexane	9.2	12.0	Nitrosyl chloride	8.0	17.6
Ethane	9.1	14.5	Nitrous oxide	8.8	19.0
Ethyl acetate	8.5	13.2	Oxygen	11.0	21.3
Ethyl alcohol	9.2	14.2	Pentane	7.0	12.8
Ethyl chloride	8.5	15.6	Propane	9.7	12.9
Ethyl ether	8.9	13.0	Propyl alcohol	8.4	13.4
Ethylene	9.5	15.1	Propylene	9.0	13.8
Fluorine	7.3	23.8	Sulphur dioxide	9.6	17.0
Freon-11	10.6	15.1	Toluene	8.6	12.4
Freon-12	11.1	16.0	2,3,3-trimethylbutane	9.5	10.5
Freon-21	10.8	15.3	Water	8.0	16.0
Freon-22	10.1	17.0	Xenon	9.3	23.0

* Coordinates for use with Fig. 3.3.8

Table 3.3.18—Thermal Conductivities of Gases and Vapors

(Reprinted from "Heat Transmission," by W. H. McAdams, 2d ed. By permission from McGraw-Hill Book Company, Inc., New York, 1942)

[The extreme temperature values given constitute the experimental range. For extrapolation to other temperatures, it is suggested that the data given be plotted as $\log k$ vs. $\log T$, or that use be made of the assumption that the ratio $C_p\eta/k$ is practically independent of temperature (or of pressure, within moderate limits).]

Substance	T, °F	k, Btu/(hr)(ft)(°F)	Substance	T, °F	k, Btu/(hr)(ft)(°F)
Acetone ¹	32	0.0057	Dichlorodifluoromethane	32	0.0048
	115	.0074		122	.0064
	212	.0099		212	.0080
	363	.0147		302	.0097
Acetylene ²	-103	0.0068	Ethane ^{2,5}	-94	0.0066
	+32	.0108		-29	.0086
	122	.0140		+32	.0106
	212	.0172		212	.0175
Air ¹	-148	0.0095	Ethyl acetate ¹	115	0.0072
	+32	.0140		212	.0096
	-212	.0183		363	.0141
	392	.0226	Ethyl alcohol ¹	68	0.0089
	572	.0265		212	.0124
Ammonia ²	-76	0.0095	Ethyl chloride ¹	32	0.0055
	+32	.0128		212	.0095
	122	.0157		363	.0135
	212	.0185		413	.0152
Benzene ¹	32	0.0052	Ethyl ether ¹	32	0.0077
	115	.0073		115	.0099
	212	.0103		212	.0131
	363	.0152		363	.0189
	413	.0176		413	.0209
Butane (n-) ³	32	0.0078	Ethylene ²	-96	0.0064
	212	.0135		+32	.0101
Butane (iso-) ³	32	0.0080		122	0.0131
	212	.0139		212	.0161
Carbon dioxide ⁴	-58	0.0068	Heptane (n-) ¹	392	0.0112
	+32	.0085		212	.0103
	212	.0133	Hexane (n-) ³	32	0.0072
	392	.0181		68	.0080
	572	.0228	Hexene ¹	32	0.0061
Carbon disulfide ²	32	0.0040		212	.0109
	45	.0042	Hydrogen	-148	0.065
Carbon monoxide ^{2,5}	-312	0.0041		-58	.083
	-294	.0046		+32	.100
	+32	.0135		122	.115
Carbon tetrachloride ²	115	0.0041		212	0.129
	212	.0052		572	.178
	363	.0065	Hydrogen and carbon dioxide ⁷	32	
Chlorine ⁶	32	0.0043	0% H ₂		0.0083
Chloroform ²	32	0.0038	20%		.0165
	115	.0046	40%		.0270
	212	.0058	60%		.0410
	363	.0077	80%		.0620
Cyclohexane	216	0.0095	100%		.10

Table 3.3.18—(Continued)

Substance	T, °F	k, Btu/(hr)(ft)(°F)	Substance	T, °F	k, Btu/(hr)(ft)(°F)
Hydrogen and nitrogen ^f	32		Nitric oxide ²	-94	0.0103
0% H ₂		0.0133		+32	.0138
20%		.0212			
40%		.0313	Nitrogen ^{2,8}	-148	0.0095
60%		.0438		+32	.0140
80%		.0635		122	.0160
				212	.0180
Hydrogen and nitrous oxide ^f	32		Nitrous oxide ^{2,8}	-98	0.0067
0% H ₂		0.0092		+32	.0087
20%		.0170		212	.0128
40%		.0270			
60%		.0410	Oxygen ⁹	-148	0.0095
80%		.0650		-58	.0119
Hydrogen sulfide ²	32	0.0076		32	.0142
Mercury ⁶	392	0.0197		122	.0164
Methane ^{2,3,5}	-148	0.0100		212	.0185
	-58	.0145	Pentane (n-) ^{1,3}	32	0.0074
	+32	.0175		68	.0083
	122	.0215	Pentane (iso-) ¹	32	.0072
Methyl alcohol ¹	32	0.0083		212	.0127
	212	.0128			
Methyl acetate ¹	32	0.0059	Propane ³	32	0.0087
	68	.0068		212	.0151
Methyl chloride ¹	32	.0053	Sulfur dioxide ⁸	32	0.0050
	115	.0072		212	.0069
	212	.0094			
	363	.0130	Water vapor ^{1,5,10,11}	115	0.0120
	413	.0148		212	.0137
Methylene chloride ¹	32	0.0039		392	.0187
	115	.0049		572	.0248
	212	.0063		752	.0315
	413	.0095		932	.0441

*1. Moser, Dissertation, Berlin, 1913.

*2. Eucken, A., Physik, Z., 12: 1101-1107 (1911); 14: 324 (1913).

3. Mann, W. B., and B. G. Dickens, Proc. Roy. Soc. (London) A 134: 77-96 (1931).

4. Sherrat, G. G., and E. Griffiths, Phil. Mag., 27: 68-75 (1939).

5. Chilton, T. H., and R. P. Generaux, personal communication, 1940.

6. "International Critical Tables," McGraw-Hill Book Company, New York, 1929.

7. Ibbs, T. L., and A. A. Hirst, Proc. Roy. Soc. (London), A 123: 134-142 (1929).

8. Dickens, B. G., Proc. Roy. Soc. (London), A 143: 517-540 (1934).

9. Gregory, H. S., and J. H. Marshall, Proc. Roy. Soc. (London), A 118: 594 (1928).

10. Milverton, S. W., Proc. Roy. Soc. (London), A 150: 287 (1935).

11. Vargaftik, N., and J. Timrot, J. Tech. Phys. (USSR) 9: 963-970 (1939).

*Data from Eucken and Moser are measurements relative to air. Data in this table from these sources are based on the thermal conductivity of air at 32°F of 0.140 Btu/(hr)(sq ft)(deg F per ft).

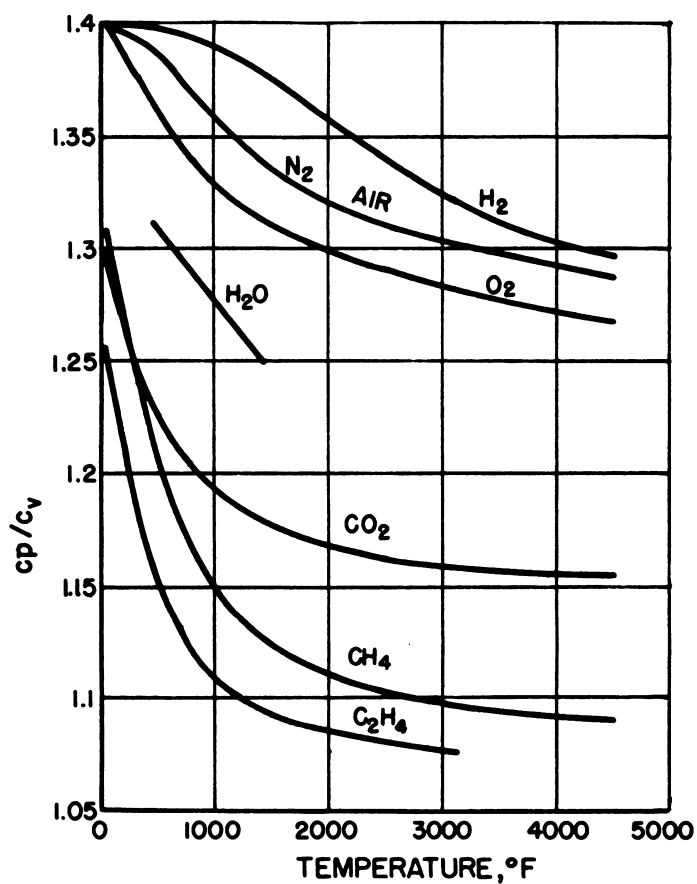


Fig. 3.3.6— Specific Heat Ratio vs Temperature for Air, CO_2 , H_2 , H_2O , CH_4 , C_2H_4 , N_2 , O_2 . Submitted by Clinton Works, May 29, 1947.

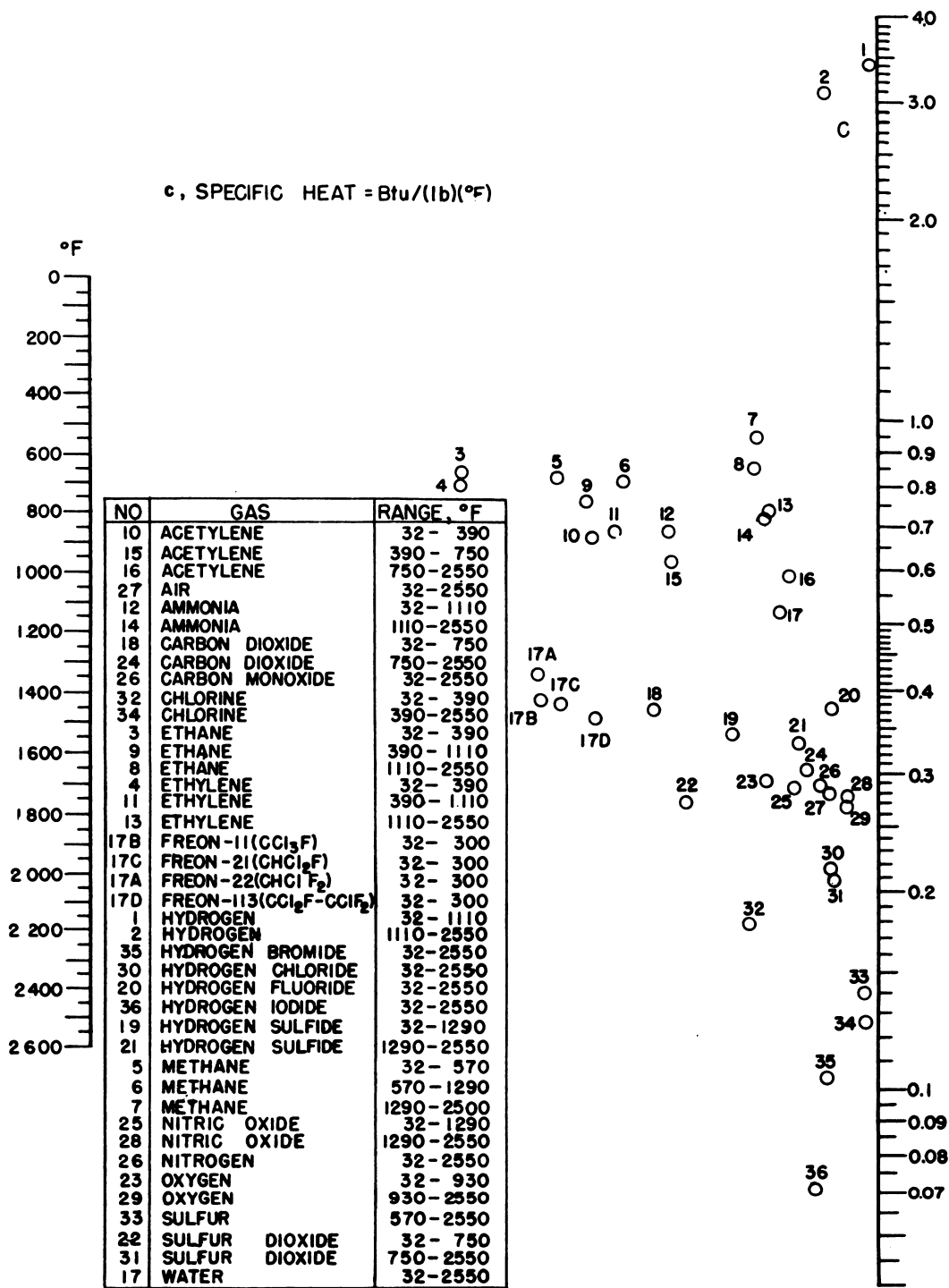


Fig. 3.3.7 — True Specific Heats of Gases and Vapors at 1 atm Pressure. Reprinted from "Heat Transmission," by W. H. McAdams, 2d. ed. By permission from McGraw-Hill Book Company, Inc., New York, 1942. Draw a straight line between point as given in table and required temperature. Intersection of this straight line with right hand scale is desired specific heat.

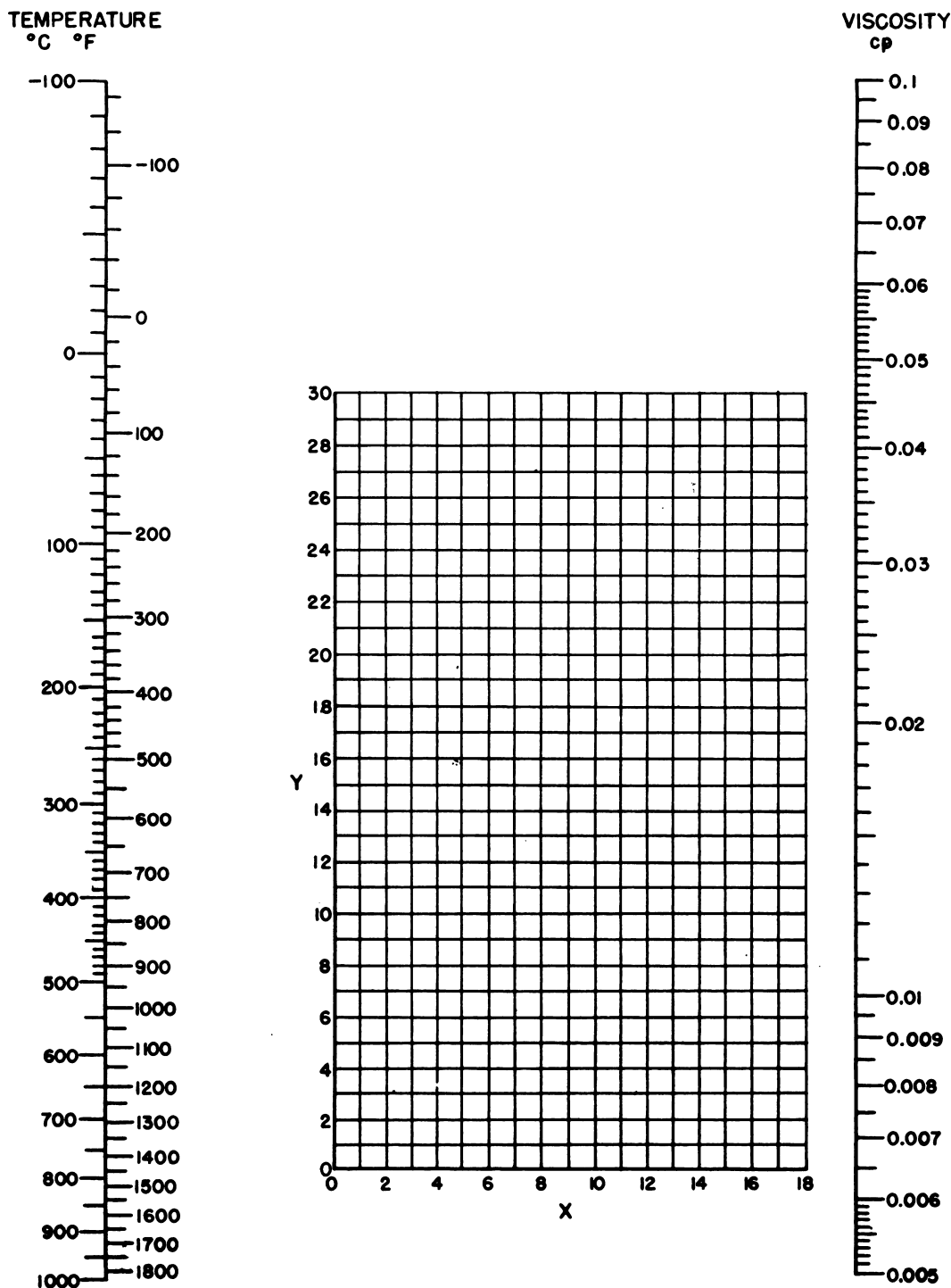


Fig. 3.3.8 — Viscosities of Gases and Vapors at 1 atm Pressure. Reprinted from "Heat Transmission," by W. H. McAdams, 2d. ed. By permission from McGraw-Hill Book Company, Inc., New York, 1942. Draw a straight line between point (coordinates of point given for materials in Table 3.3.17) and required temperature. Intersection of this straight line with right hand scale is desired viscosity.

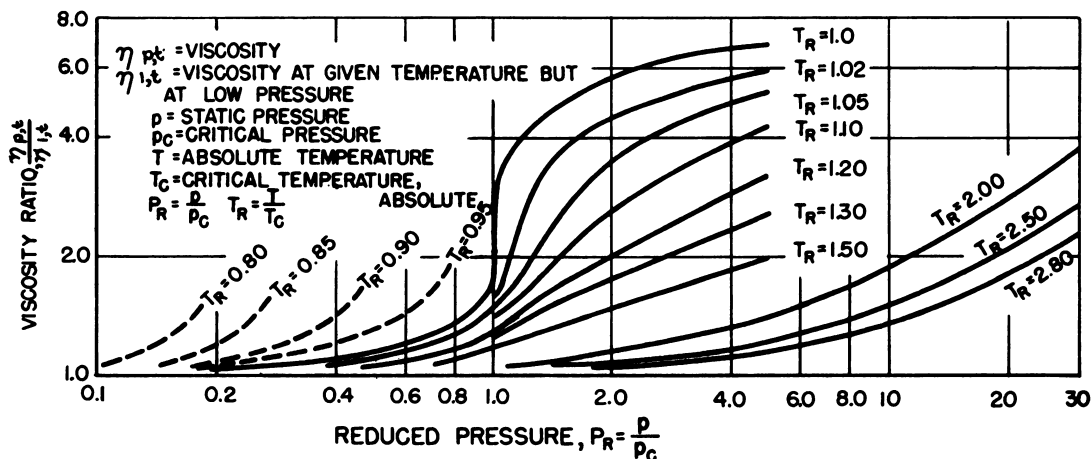


Fig. 3.3.9—Effect of Pressure on Viscosities of Gases at Several Temperatures. Reprinted from "Heat Transmission," by W. H. McAdams, 2d ed. By permission from McGraw-Hill Book Company, Inc., New York, 1942. Data from Comings, E. W., and R. S. Egley, Ind. Eng. Chem., 32: 714-718 (1940).

Table 3.3.19—Constants for Thermal-conductivity Correlation*

Gas	C_0	C	C_1
He	2.35	43.5	10
CO ₂	4.61	6212	10
Air	0.632	245	12

* These constants are used in the following equation to correlate the thermal conductivities of gases in the temperature range of 15° to 375°K:

$$10^5 k = \frac{C_0 \sqrt{T}}{1 + \frac{C/T}{10^{C_1/T}}}$$

Table 3.3.20—Thermal Conductivities Calculated by the Eucken Equation*

(J. M. Wright, Calculated Thermal Conductivities of Pure Gases and Gaseous Mixtures at Elevated Temperatures, HW-21741, July 18, 1951)

Gas	T, °K	k, 10 ⁻⁵ cal/(sec)(cm)(°C)	
		Calculated	Experimental
He	273.1	35.3	34.1
	375.7	43.4	40.9
	400.0	45.2	
	600.0	58.7	
	800.0	70.8	
CO ₂	273.1	3.32	3.40
	400.0	6.13	
	600.0	9.53	
	800.0	12.30	
N ₂	273.1	5.6	5.66
	400.0	7.67	
	600.0	10.4	
	800.0	12.9	

$$* k = \frac{1}{4} [9 C_D/C_V - 5] \eta C_V$$

Table 3.3.21—Viscosity Correlations for Gases at Low Pressures*

Gas	T, °K	Correlation for viscosity, η , in poises
He	140-373	$10^6 \eta = \frac{1.805 \sqrt{T}}{251} \left(1 + \frac{T}{10^{\frac{10}{T}}} \right)$
Air	90-1845	$10^6 \eta = \frac{1.488 \sqrt{T}}{122.1} \left(1 + \frac{T}{10^{\frac{1}{T}}} \right)$
CO ₂	198-1686	$10^6 \eta = \frac{1.554 \sqrt{T}}{246.0} \left(1 + \frac{T}{10^{\frac{1}{T}}} \right)$

*A Summary of Viscosity and Heat-conduction Data for He, A, H₂, O₂, N₂, CO, CO₂, H₂O, and Air, by F. G. Keyes. Trans. Am. Soc. Mech. Engrs., 73: 589-596 (1951). By permission from American Society of Mechanical Engineers.

Table 3.3.22—Constants for Viscosity Correlations of Gases*

(Reprinted from "Chemical Engineers' Handbook," edited by
J. H. Perry, 3rd ed. By permission from McGraw-Hill
Book Company, Inc., New York, 1950)

Gas	$\frac{\eta}{\eta_0} = (273.1 + C/T + C)(T/273.1)^{1/2} \dagger$		$\frac{\eta}{\eta_0} = (T/273.1)^{N \dagger}$		
	C	Range °C	N	Range °C	η_0 , cp
Air	114	0–300	0.768	0–100	0.01709
CO ₂	239.7	–21–302	.935	–20–140	.0137
	274	15–100			.0137
He	78.2	–61–184	0.647	–258–19	.0187
	80.3	15–185	.685	15–100	.0187
H ₂	83	–60–185	.695	–183–21	.0084
	71.7	–21–302			.0084

* The empirical relations, if not applicable directly, can serve as a method of extrapolating to get orders of magnitude, not precise results

† Given by Perry as applicable to gases other than H₂ or He

‡ Given by Perry as applicable to H₂ and He

SELECTED READING LIST

A SUMMARY OF VISCOSITY AND HEAT-CONDUCTION DATA FOR He, A, H₂, O₂, N₂, CO, CO₂, H₂O, and AIR, F. G. Keyes, Trans. Am. Soc. Mech. Engrs., 73: 581-595 (1951).

CALCULATED THERMAL CONDUCTIVITIES OF PURE GASES AND GASEOUS MIXTURES AT ELEVATED TEMPERATURES, Hanford Works, J. M. Wright, HW-21741, Secret, July 18, 1951.

CHEMICAL ENGINEERS' HANDBOOK, edited by J. H. Perry, 3d ed., McGraw-Hill Book Company, Inc., New York, 1950.

THERMODYNAMIC PROPERTIES OF AIR, University of Wisconsin, C. F. Curtiss and J. O. Hirschfelder, CM-472, 50 pp, June 1, 1948.

HEAT TRANSFER IN MANHATTAN DISTRICT AND ATOMIC ENERGY COMMISSION LABORATORIES: A CRITICAL SURVEY, Oak Ridge National Laboratory, W. B. Harrison, ORNL-156, Secret, Oct. 1, 1948.

THERMODYNAMIC PROPERTIES OF AIR II, University of Wisconsin, J. O. Hirschfelder and C. F. Curtiss, CM-518, 121 pp, Dec. 21, 1948.

GAS TABLES, J. H. Keenan and Joseph Kaye, 2d ed., John Wiley and Sons, Inc., New York, 1948.

THERMODYNAMIC PROPERTIES OF HELIUM AT HIGH PRESSURES AND TEMPERATURES, Schenectady Works, S. W. Akin, NP-124, May 1947.

PHYSICAL PROPERTIES OF HEAT TRANSFER FLUIDS, Schenectady Works, B. O. Newman, GI-401, 70 pp, November 10, 1947.

HEAT TRANSMISSION, W. H. McAdams, 2d ed., McGraw-Hill Book Company, Inc., New York, 1942.

INTERNATIONAL CRITICAL TABLES, McGraw-Hill Book Company, Inc., New York, 1926-1933.

Heat Transfer and Fluid Flow for Gases

To compete with liquids as reactor coolants, gases must operate under more severe conditions of temperature and pressure. To avoid hot spots and high surface temperatures, local and over-all heat-transfer coefficients, which are lower generally than those of liquid-cooled reactors, must be known accurately because of the high temperature difference required between the reactor wall and fluid. The high ratio of surface temperature to coolant bulk temperature encountered in gas-cooled reactors called for new analytical approaches and new experimental data.

The use of irregularly shaped fuel elements also made additional data necessary. Data were selected to show the effects of high heat flux and surface temperatures. Roughness, porosity, turns in flow lines, entrance and exit effects, and heat-transfer and fluid-flow characteristics of packed beds are all pertinent to the removal of heat from nuclear reactors and to the effective utilization of this heat energy. This chapter presents such basic design data for gas-cooled reactors.

GENERAL EQUATIONS UTILIZING HEAT-TRANSFER AND PRESSURE-DROP DATA

The nomenclature for the following equations is defined in Table 3.4.1.

HEAT TRANSFER

The heat-transfer coefficient is utilized in the equation:

$$Q = h A \Delta t \quad (1)$$

Data for h are usually presented in the dimensionless ratios hD/k and $h/c_p G$.

PRESSURE DROP

The general differential equation for steady-flow pressure drop is:

$$-vdp = \frac{g}{g_c} dZ + \frac{VdV}{g_c} + \frac{fV^2 dL}{2g_c r_m} \quad (2)$$

Simplified methods for calculating pressure drops for compressible fluids are presented N.A.C.A.¹⁻⁴ The methods outlined are essentially solutions to Eq. (2). Equation (2) becomes:

$$-dp = \frac{G^2 dv}{g_c} + \frac{G^2 f dL}{2g_c r_m} \quad (3)$$

¹References appear at end of chapter.

Table 3.4.1—Nomenclature

Symbol	Definition	Unit
A	Heat-transfer surface area	Sq ft
a	Constant of integration	Dimensionless
b	Roughness factor	Dimensionless
c	Specific heat	Btu/(lb)(°F)
c_p	Specific heat at constant pressure	Btu/(lb)(°F)
$c_{p,b}$	Average specific heat at constant pressure	Btu/(lb)(°F)
D	Inside diameter of conduit	Ft
D_H, D_E	Hydraulic diameter or equivalent diameter	Ft
D_o	Outside diameter	Ft
d	Symbol for differentiating	Dimensionless
d	Density	Lb/cu ft
d_f	Average density of fluid	Lb/cu ft
d_h	Hydraulic diameter of fin passage	Ft
F_c	Friction loss due to sudden contraction	Lb/sq ft
F_e	Friction loss due to sudden enlargement	Lb/sq ft
f	Friction factor	Dimensionless
f_{APP}	Experimentally determined friction factor	Dimensionless
f_f	Friction factor evaluated at average temperature of fluid	Dimensionless
f_{K-N}	Friction factor calculated from equation of Von Karman and Nikuradse	Dimensionless
G	Mass velocity	Lb/(sec)(sq ft)
G_{max}	Mass velocity based on smallest flow-area	Lb/(sec)(sq ft)
g	Local gravitational acceleration	Ft/(sec)(sec)
g_c	Conversion factor, 32.2	(ft)(lb-mass)/(sec) ² (lb-force)
h	Coefficient of heat transfer	Btu/(hr)(sq ft)(°F)
h_e	Local coefficient of heat transfer	Btu/(hr)(sq ft)(°F)
h_L	Coefficient of heat transfer based on log mean of temperature difference at entrance and exit	Btu/(hr)(sq ft)(°F)
h_m	Average heat-transfer coefficient	Btu/(hr)(sq ft)(°F)
h_{mi}	Heat-transfer coefficient referring to an average value based on initial temperature	Btu/(hr)(sq ft)(°F)
h_x	Local coefficient of heat transfer at point x	Btu/(hr)(sq ft)(°F)
K_c	Empirical constant for contraction losses	Dimensionless
K_e	Empirical constant for expansion losses	Dimensionless
k	Thermal conductivity	Btu/(hr)(ft)(°F)
k_f	Average thermal conductivity	Btu/(hr)(ft)(°F)
L	Length	Ft

Table 3.4.1 — (Continued)

Symbol	Definition	Unit
L	Subscript indicating based on log mean average	Dimensionless
M	Mach number	Dimensionless
Nu	Nusselt number	Dimensionless
Nu _{av}	Average Nusselt number	Dimensionless
n	Empirical constant	Dimensionless
Pr	Prandtl number, $c_p \eta / k$	Dimensionless
p	Absolute pressure	Lb/sq ft
p ₀	Stagnation pressure	Lb/sq ft
q	Heat flow rate at any given point	Btu/(hr)(sq ft)
q ₀	Heat flow rate at inside wall	Btu, (hr)(sq ft)
Re	Reynolds number, DG/η	Dimensionless
r _m	Hydraulic radius	Ft
St	Stanton number, $h/c_p G$	Dimensionless
T	Absolute temperature	°R or °K
T _{av}	Average absolute temperature	°R or °K
T _b	Average temperature of fluid	°R or °K
T ₀	Stagnation temperature	°R or °K
T _s	Surface temperature of wall	°R or °K
t	Temperature	°R or °K
t ₀ , t _w	Inside wall temperature	°R or °K
t _b	Bulk temperature of fluid	°R or °K
t _f	Film temperature, $0.5 (t_0 - t_b) + t_b$	°R or °K
t _{0.4}	Film temperature, $0.4 (t_0 - t_b) + t_b$	°R or °K
u	Time average velocity	Ft/sec
u _b	Bulk average velocity	Ft/sec
u ⁺	Velocity parameter, $u/\sqrt{\tau_0/d_0}$	Ft/sec
V, V _b	Average velocity	Ft/sec
v	Specific volume	Cu ft/lb
v _m	Mean specific volume	Cu ft/lb
w	Fluid-flow rate	Lb/sec
x	Distance from conduit entrance	Ft
y	Distance from tube wall	Ft
y ⁺	Wall/distance parameter, $y\sqrt{\tau_0/d_0/\eta_0/d_0}$	Ft
y ₀	Distance between flat plate and wavy plate	Ft
Z	Distance (vertical)	Ft
α	Dimensionless ratio	Dimensionless
β	Heat-transfer parameter $\frac{q_0 \sqrt{\tau_0/d_0}}{c_p q t_0}$	Dimensionless
Δ	Difference	Dimensionless
η	Absolute viscosity	Lb sec/sq ft
η ₀	Absolute viscosity at wall	Lb sec/sq ft
η _b , η _f , η _m	Average absolute viscosity	Lb sec/sq ft
η _s	Absolute viscosity at surface	Lb sec/sq ft
κ	Kappa, Karman constant	Dimensionless
σ	Flow contraction ratio	Dimensionless
τ	Shear stress in fluid	Lb/sq ft
τ ₀	Shear stress in fluid at wall	Lb/sq ft
ζ	Four times the friction factor, f	Dimensionless

for the pressure drop of a compressible fluid in a constant-area passage with the combined effects of heat transfer and friction, elevation changes being neglected.

An integrated form of Eq. (3), with f assumed constant, is:

$$\Delta p = p_1 - p_2 = \frac{G^2(v_2 - v_1)}{g_c} + \frac{G^2 f v_m L}{2g_c r_m} \quad (4)$$

where:

$$v_m = \frac{1}{L} \int_0^L v dL \quad (4a)$$

For a perfect gas:

$$v_m = v_1 \frac{p_1 T_{av}}{p_{av} T_1} \quad (4b)$$

where p_{av} can be taken as an arithmetic average of p_1 and p_2 if $\Delta p \ll p_1$ and T_{av} can be taken as an arithmetic mean if the Δt between wall and fluid is constant. If this Δt varies, then $T_{1ma} = T_s - \Delta t_{1m}$ should be used for T_{av} .

The more usual application of Eq. (4a) as applied to reactors is for the case where the temperature can be expressed as a function of passage length, L . Rewriting Eq. 4(a) with the introduction of 4(b):

$$v_m = \frac{p_1 v_1}{L T_1 p_{av}} \int_0^L T dL \quad (4c)$$

The evaluation of the integral in Eq. (4c) proceeds from a heat balance where q is the heat input per unit length:

$$q dL = w c dT \quad (4d)$$

Solving for dT and integrating:

$$\int dT = \int_0^L \frac{q}{w c} dL \quad (4e)$$

Substituting in Eq. (4c):

$$v_m = \frac{p_1 v_1}{L T_1 p_{av} w c} \int_0^L \left[\int_0^L q dL \right] dL \quad (4f)$$

The value of v_m can now be evaluated if q is known as a function of L . This function is set by the physics of the reactor and can readily be obtained.

In practice, another integrated form of Eq. (2) has been used successfully.⁵ A log mean average specific volume is assumed, Eq. (4g):

$$v_m = \frac{v_2 - v_1}{\ln \frac{v_2}{v_1}} \quad (4g)$$

which leads to Eq. (4h):

$$1 - \frac{p_2}{p_1} = \left(\frac{G^2 v_1}{g_c p_1} \right) \left[\frac{(T_2/T_1)}{(p_2/p_1)} - 1 \right] \left[1 + \frac{(fL/2r_m)}{\ln \left(\frac{T_2/T_1}{p_2/p_1} \right)} \right] \quad (4h)$$

$$= \left(\frac{G^2 v_1}{g_c p_1} \right) \left[\frac{v_2}{v_1} - 1 \right] \left[1 + (fL/2r_m)/\ln \left(\frac{v_2}{v_1} \right) \right]$$

The basic differential equation is also expressed in terms of Mach number, stagnation pressure, and stagnation temperature as follows:⁶

$$dp_0/p_0 = \frac{-kM^2}{2} \left[\frac{dT_0}{T_0} + \frac{f dL}{r_m} \right] \quad (5)$$

Data and correlations on pressure drop are presented as friction factor, f , as a function of Reynolds number. The more important correlations are summarized in Tables 3.4.2 and 3.4.3. The text should be consulted for the restrictions on these correlations and the physical properties to be used.

Table 3.4.2—Data and Correlations for h , the Coefficient of Heat Transfer

Flow	Type of coefficient	Fig. No. or equation	Notes
Turbulent	Local	Fig. 3.4.2	High-flux data
Turbulent	Local	$h_c/c_p G = 0.033(DG/\eta_m)^{-0.23}$ Fig. 3.4.5	Equation fits data to within ± 7 percent
Turbulent	Local	Fig. 3.4.6 and 3.4.7	Coefficients near an entrance
Streamline	Local	$h_x D/k = 1.75 + 0.65 \sqrt{wc_p/kx}$ Fig. 3.4.4	$8 < x/D < 80$ $5 < wc_p/kx < 400$
Streamline	Average	$(h_{mi}/c_{pb} G)(c_p \eta/k)_b^{1/2} = 0.664(LG/\eta)_b^{-0.5}$ Fig. 3.4.9	Constant surface temperature; average deviation 10 percent; $5 < L/D < 63$
Turbulent	Average	$hD/k_f = 0.034(d_f V_b D/\eta_f)^{0.8} \times (c_{pf} \eta_f/k_f)^{0.4} (L/D)^{-0.1}$ Fig. 3.4.10	High-flux data; constant q/A ; $30 < L/D < 120$
Turbulent	Average	$h_L/c_{pL} G = 0.026(DG/\eta)_b^{-0.20} \times [1 + (L/D)^{-0.70}]$ Fig. 3.4.13	$1 < L/D < 68.4$; constant surface temperature
Turbulent		Fig. 3.4.14	High-pressure data; constant surface temperature

Table 3.4.3—Data and Correlations for f , the Friction Factor and Pressure Loss

Flow	Type	Fig. No. or equation	Notes
Turbulent	Local	Fig. 3.4.3	High-flux data
Turbulent	Local	Fig. 3.4.8	Friction factors near an entrance
Turbulent	Average	$1/\sqrt{8f_f/2} = 2 \log_{10} (d_f V_b D/\eta_f \sqrt{8f_f/2})^{-0.8}$ Fig. 3.4.15	High-flux data; $30 < L/D < 120$; heating or cooling
Laminar and turbulent	Local	Fig. 3.4.16	Entrance and exit losses

LOCAL HEAT-TRANSFER COEFFICIENT AND PRESSURE-DROP DATA

VELOCITY DISTRIBUTION

Basic data on velocity distribution are presented in Fig. 3.4.1, which also shows the equations representing the distribution near the wall and in the bulk of the fluid. In the Reynolds number range 10,000-200,000, theoretical analysis and experimental data for air (taken with an 0.87-in. Inconel tube with $L/D = 100$) indicated that variable shear stress across the tube and compressibility without heat transfer altered the velocity distribution curve approximately $2\frac{1}{2}$ percent.⁷

HEAT TRANSFER—TURBULENT FLOW

Figure 3.4.2 presents a plot of Nusselt number versus Reynolds number obtained with high surface temperature/bulk temperature ratios, t_0/t_b . The data and analysis are correlated well by evaluating the physical properties at $t_{0.4} = 0.4(t_0 - t_b) + t_b$. Thermal conductivities and viscosities for air were both assumed proportional to the 0.68 power of the absolute temperature.

PRESSURE DROP—TURBULENT FLOW

Figure 3.4.3 presents data for the friction factor versus Reynolds number with the physical properties also evaluated at $t_{0.4}$. Theoretical analysis also indicated only slight effect of variable shear stress and heat transfer across the tube on the velocity profile for turbulent flow with variable fluid properties.⁸ A similar method of analytically deriving local heat-transfer coefficients to fluids with temperature-dependent properties is also presented by Goldmann.⁹

HEAT TRANSFER—STREAMLINE FLOW

Data for local coefficients with streamline flow are presented in Fig. 3.4.4 for 0.0625-in.-diameter Inconel tubes. The data are correlated within 22 percent by the equation:

$$\frac{h_x D}{k} = 1.75 + 0.65 \sqrt{\frac{w c_p}{k_x}} \quad (6)$$

in the range of x/D from 8 to 80, and $w c_p / k_x$ from 5 to 400.¹⁰ The data for the physical properties of air are from the "Gas Tables."¹¹ Further analysis of Kroll's temperature data is presented by Klein and Tribus¹² who also present analytical methods for predicting heat transfer from non-uniform temperature surfaces.

HEAT-TRANSFER COEFFICIENT INDEPENDENT OF TEMPERATURE DRIVING FORCE

A heat-transfer coefficient defined by:

$$h_e = \frac{dq}{dA} \frac{1}{t_w - t_{aw}} \quad (7)$$

is found to be independent of temperature difference between wall and fluid, where t_w is the surface temperature with heat transfer and t_{aw} is the corresponding temperature the surface would assume in the absence of heat transfer. Figure 3.4.5 presents the correla-

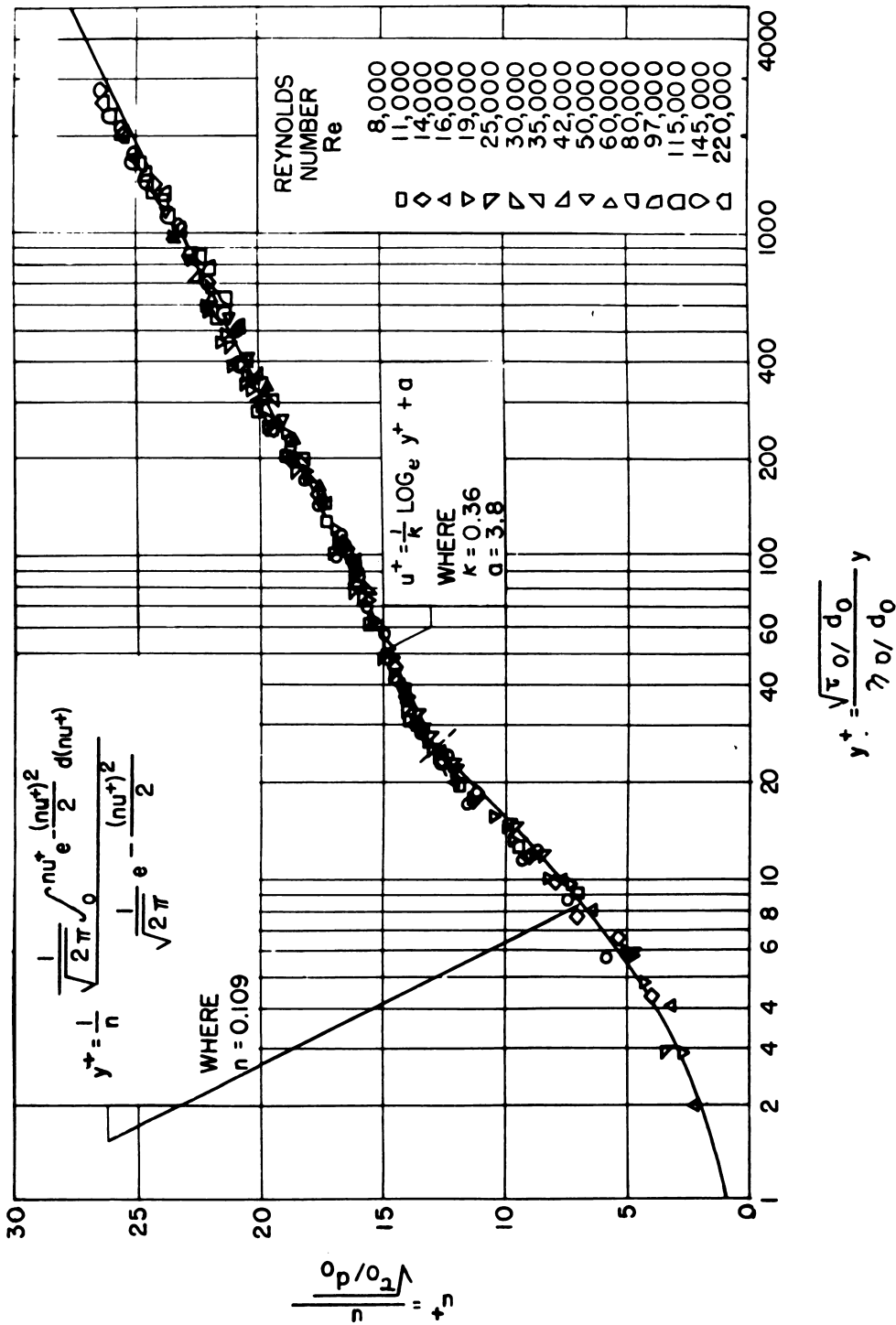


Fig. 3.4.1— Velocity Distribution Curve. Reprinted from NACA-TN-2138, July 1950.

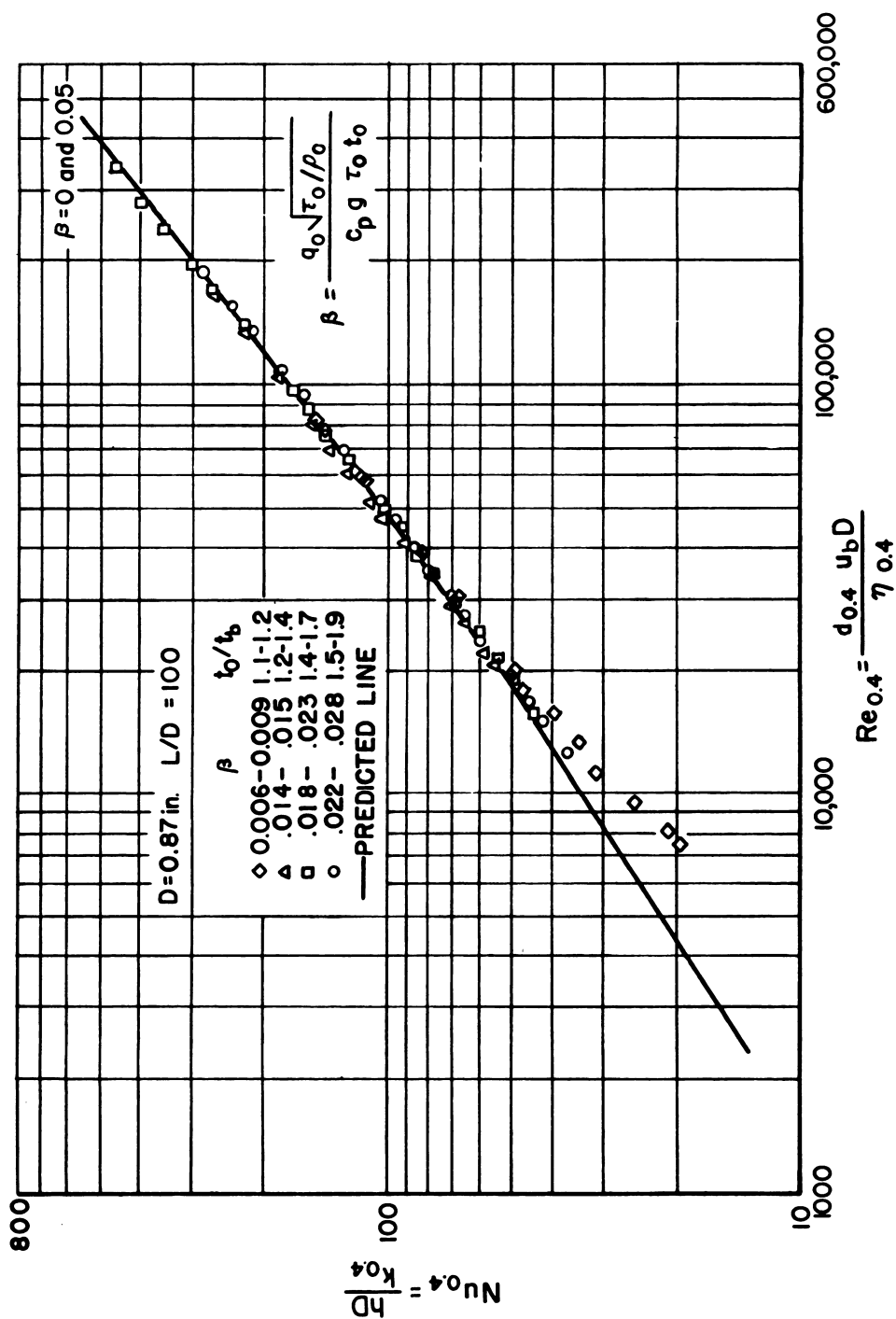


Fig. 3.4.2 — Heat-transfer Correlation. Reprinted from NACA-TN-2629, Feb. 1952.

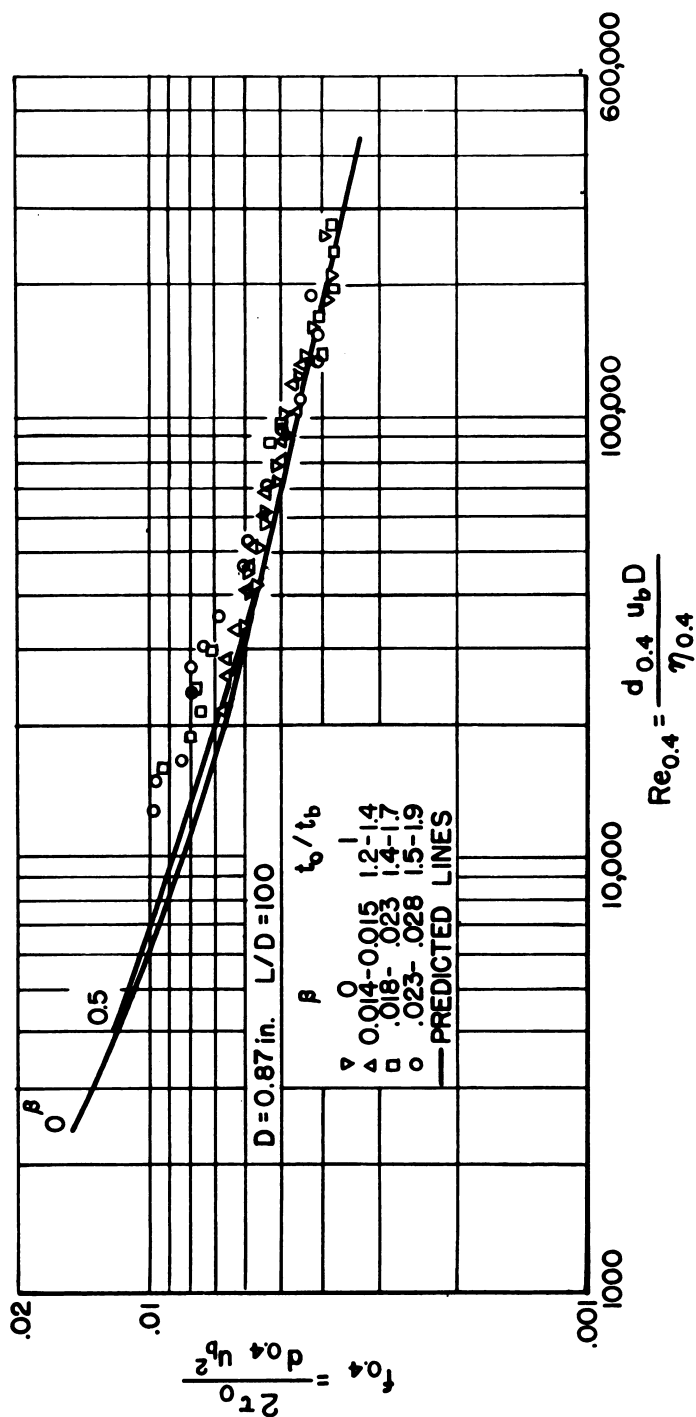


Fig. 3.4.3—Friction-factor Correlation. Reprinted from NACA-TN-2629, Feb. 1952.

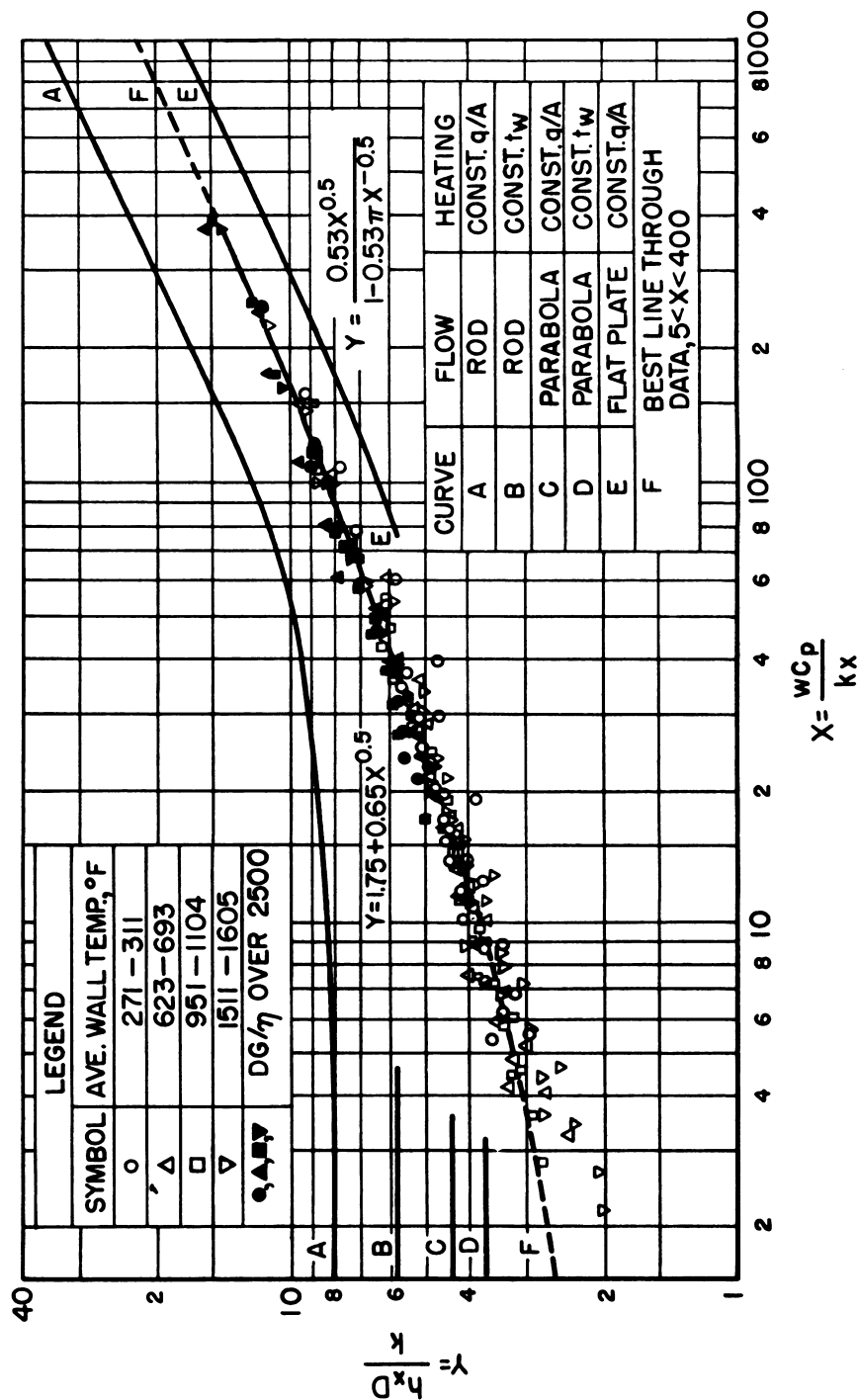


Fig. 3.4.4. — Heat-transfer Correlation. Reprinted from NEPA-1688, Dec. 1950.

tion obtained for h_e . All data given on Fig. 3.4.5 are represented within ± 7 percent by the equation:

$$\frac{h_e}{c_p G} = 0.033 \left(\frac{DG}{\eta_m} \right)^{-0.23} \quad (8)$$

where the physical properties of air are taken from the NACA data¹³ and cover the following ranges of variables:

Diameter, in.	0.28 – 0.99
Pressure, atm.	.2 – 3
Temperature difference, °F	10 – 400
Mach number	0 – 1
Reynolds number	10,000 – 400,000

HEAT-TRANSFER COEFFICIENTS NEAR ENTRANCE

Data on local heat-transfer coefficients near the entrance to a tube are presented in Figs. 3.4.6 and 3.4.7. Analytical methods by Boelter et al¹⁴ are also presented for predicting the local coefficient of heat transfer near the entrance of round tubes. In addition to Figs. 3.4.6 and 3.4.7, local heat-transfer coefficient data are given by Boelter¹⁴ on the systems shown in Table 3.4.4.

Data on entrance coefficients have also been presented by Cholette¹⁵ for the Reynolds-number range 678 to 18, 250.

TUBE ENTRANCE PRESSURE DROP

Data on friction factors near the entrance to tubes are presented in Fig. 3.4.8 for air. The value of the friction factor remains within 5 percent of that given by the Karman-Nikuradse relation, Eq. (11), beginning at approximately 40 to 60 diameters downstream from the entrance.¹⁶ Entrance and exit effects as well as turning losses are discussed elsewhere in this chapter.

AVERAGE HEAT-TRANSFER COEFFICIENT AND PRESSURE-DROP DATA

The latest data of interest on average heat-transfer coefficients and pressure drop are those obtained with high surface temperatures and low L/D ratios. The usual correlations are modified by evaluating the physical properties at some temperature intermediate to the bulk temperature of the fluid and the wall temperature. The L/D ratio is also incorporated in the equations to obtain correlations.

HEAT TRANSFER—STREAMLINE FLOW

Heat-transfer data for small L/D ratios, constant surface temperature, and laminar flow are presented in Fig. 3.4.9. These data are correlated with an average deviation of 10 percent by the Pohlhausen equation for flat plates:

$$\frac{h_{mi}}{c_{pb} G} \left(\frac{c_p \eta}{k} \right)_b^{1/3} = 0.664 \left(\frac{L G}{\eta} \right)_b^{-0.5} \quad (9)$$

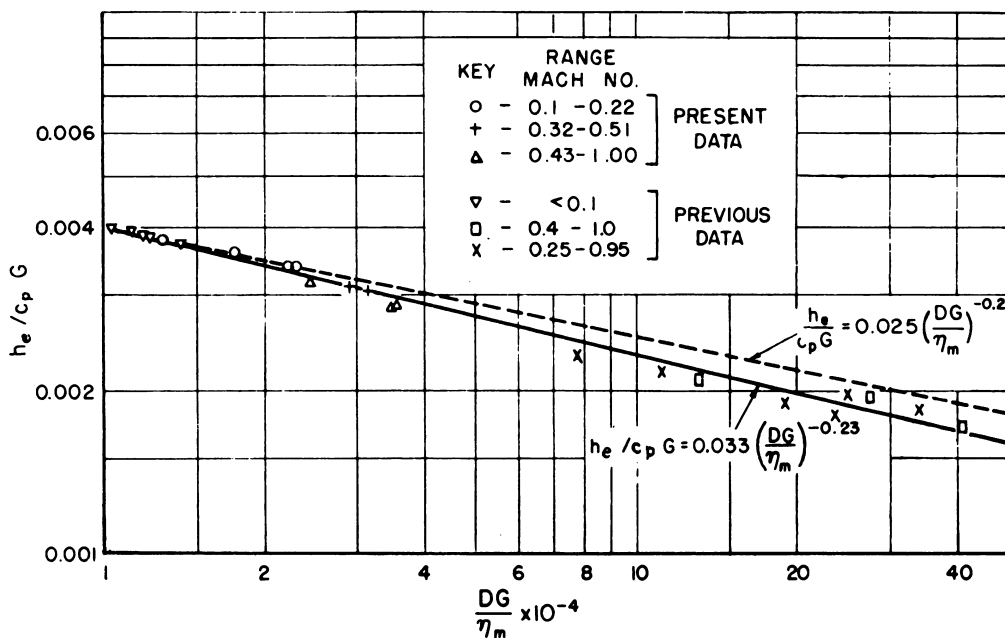


Fig. 3.4.5 — Heat-transfer Correlation. Reprinted from NACA-TN-985, June 1945.

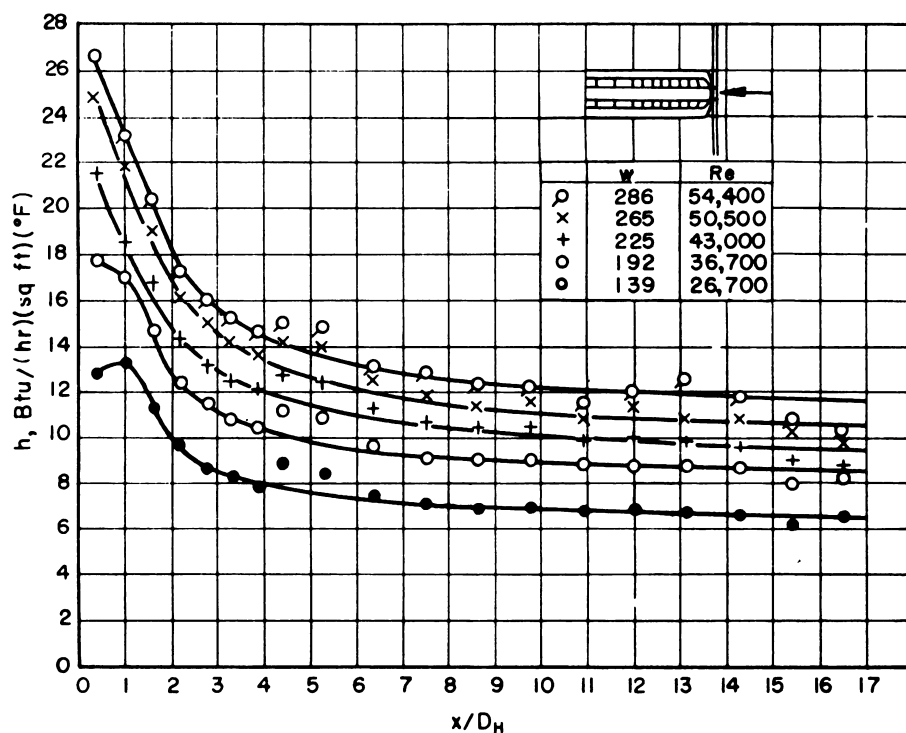


Fig. 3.4.6 — Entrance Heat-transfer Data Using Right-angle-edge Entrance. Reprinted from NACA-TN-1451, July 1948.

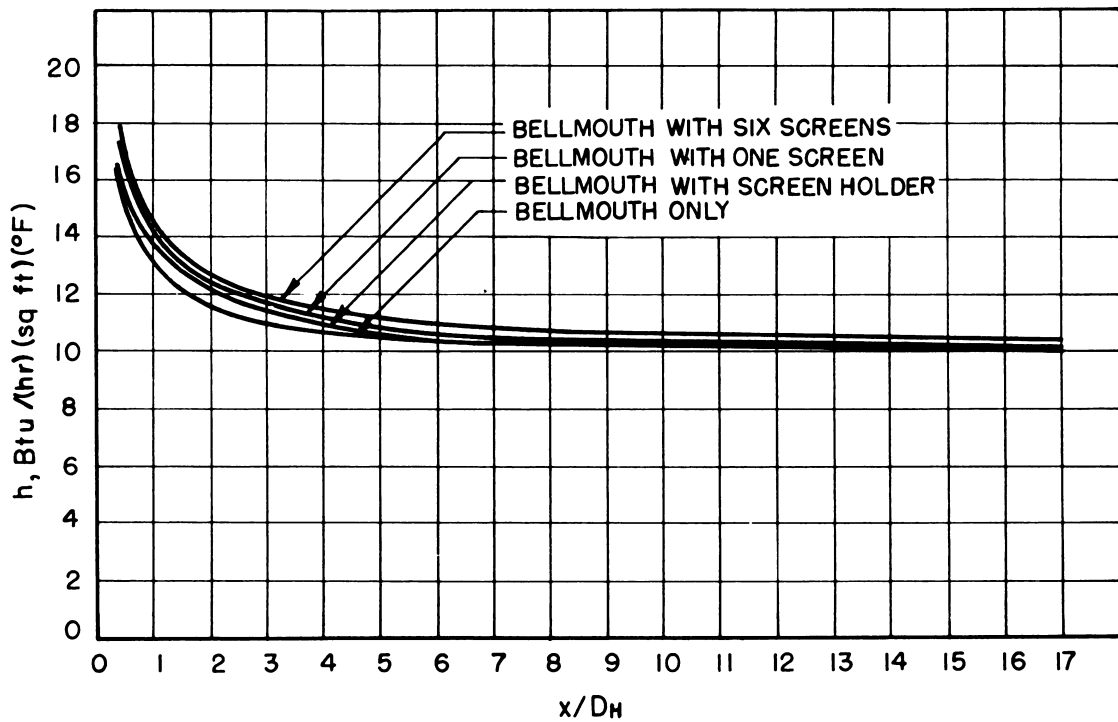


Fig. 3.4.7 — Curves of Entrance Heat-transfer Data Using Various Entrances.
Reprinted from NACA-TN-1451, July 1948.

Table 3.4.4 — Configurations on Which Entrance Heat-transfer-coefficient
Data are Presented by Boelter et al

- (1) Circular tube with bellmouth at entrance
- (2) Circular tube with bellmouth and one screen at entrance
- (3) Circular tube with bellmouth and screen holder at entrance
- (4) Circular tube with bellmouth and six screens at entrance
- (5) Circular tube with bare sharp-edge entrance
- (6) Circular tube with large orifice at entrance
- (7) Circular tube with small orifice at entrance
- (8) Circular tube with short calming section at entrance
- (9) Circular tube with long calming section at entrance
- (10) Circular tube with 45°-angle bend at entrance
- (11) Circular tube with right-angle bend at entrance
- (12) Circular tube with right-angle bend and long calming section at entrance
- (13) Circular tube with 45° round bend at entrance
- (14) Circular tube with 90° round bend at entrance
- (15) Circular tube with 180° round bend at entrance

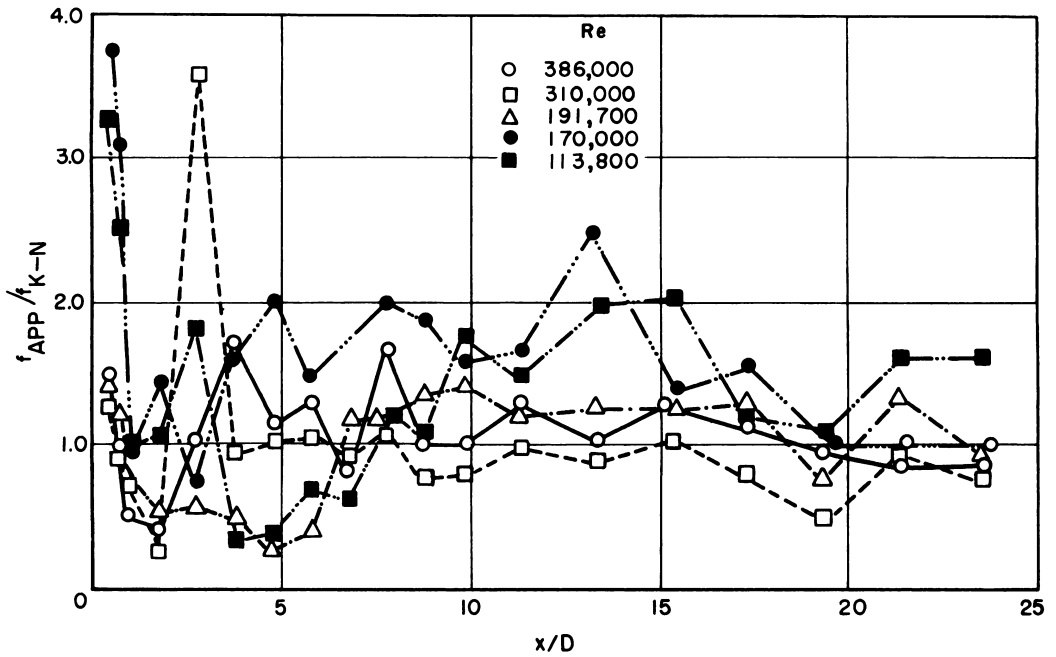


Fig. 3.4.8 — Entrance Friction-factor Data. Reprinted from NACA-TN-1785, Nov. 1948.

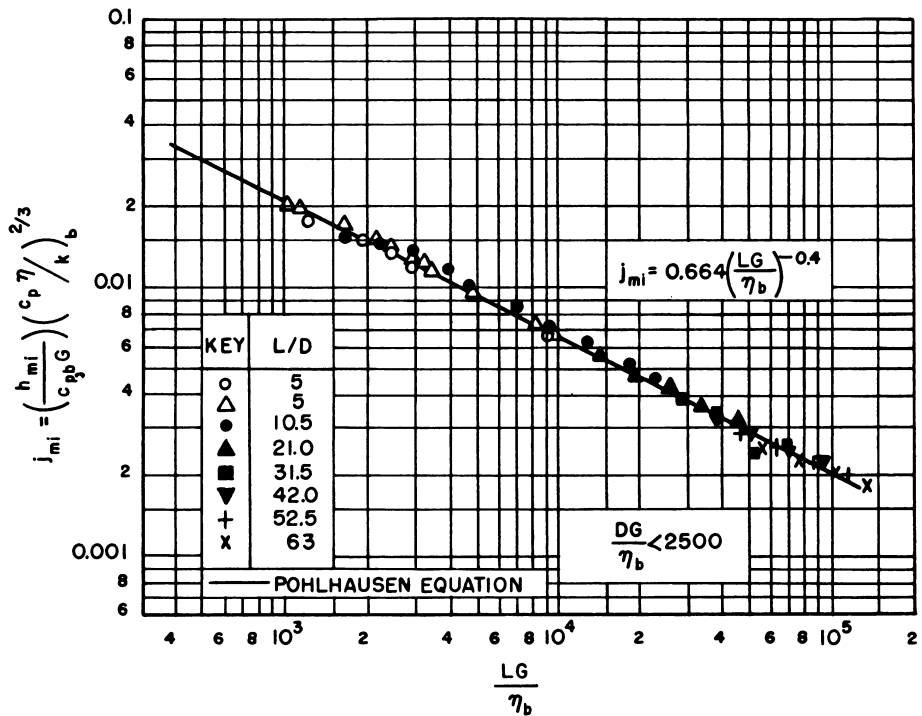


Fig. 3.4.9 — Heat-transfer Correlation for Stream-line Flow. Reprinted from NEPA-1688, Dec. 1950.

In this correlation, the physical properties of air are taken from the “Gas Tables” by Keenan and Kaye.

HEAT TRANSFER—TURBULENT FLOW

Figure 3.4.10 presents a correlation over wide range of surface temperatures, bulk temperatures, and length-to-diameter ratios at constant q/A . Diameters of 0.402 in. and 0.525 in. were used. The velocity in the Reynolds number is evaluated at the bulk temperature, the physical properties of air at a film temperature which is the average of the bulk and wall temperatures. The NACA physical properties for air were utilized. In addition, the thermal conductivity of air is assumed directly proportional to the square root of the absolute film temperature.¹⁷

In contrast, Fig. 3.4.11 presents low-flux data for air where the L/D ratio is not important, although a trend is shown and the physical properties are evaluated at the bulk temperature of the fluid. Since the correlation obtained is good, the surface temperature effect does not seem important in these data.

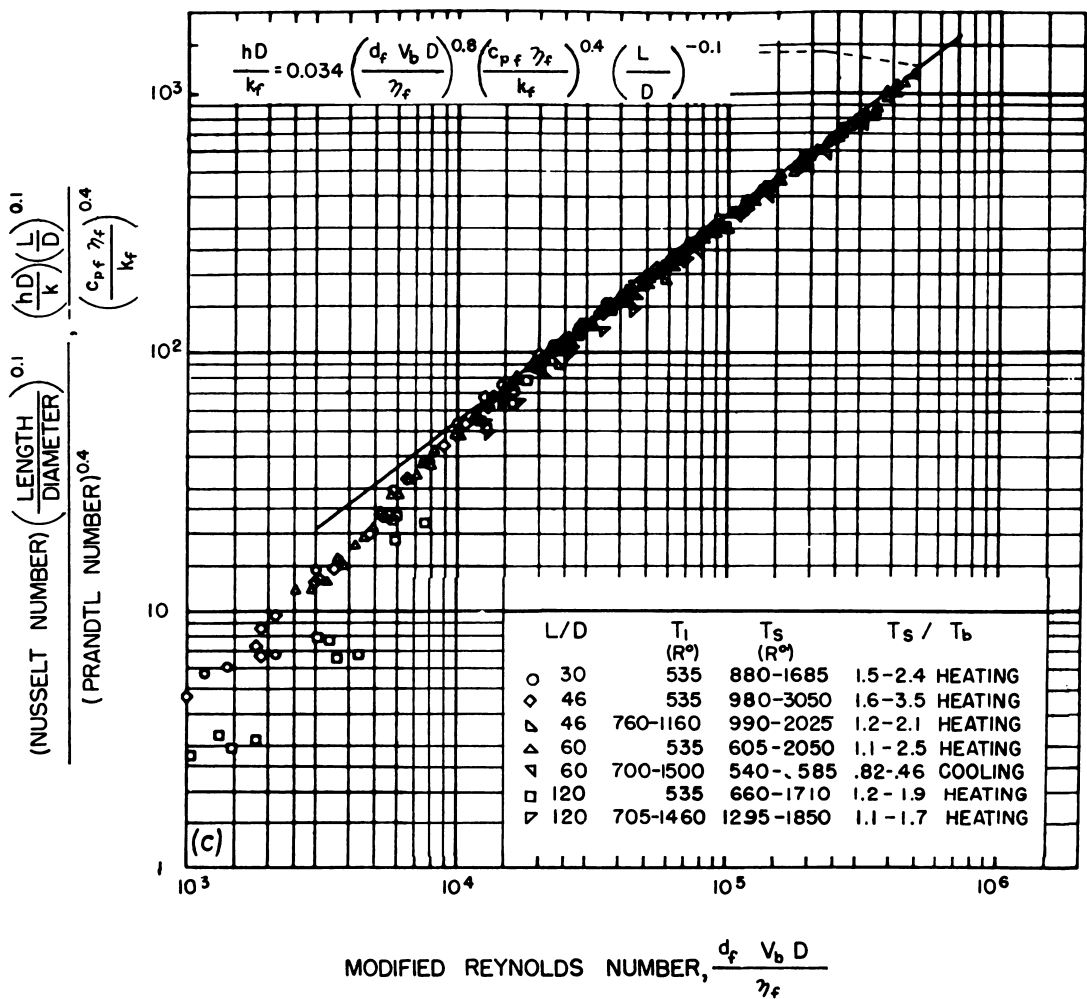


Fig. 3.4.10— Heat-transfer Correlation for Turbulent Flow. Reprinted from NACA-1020, 1951.

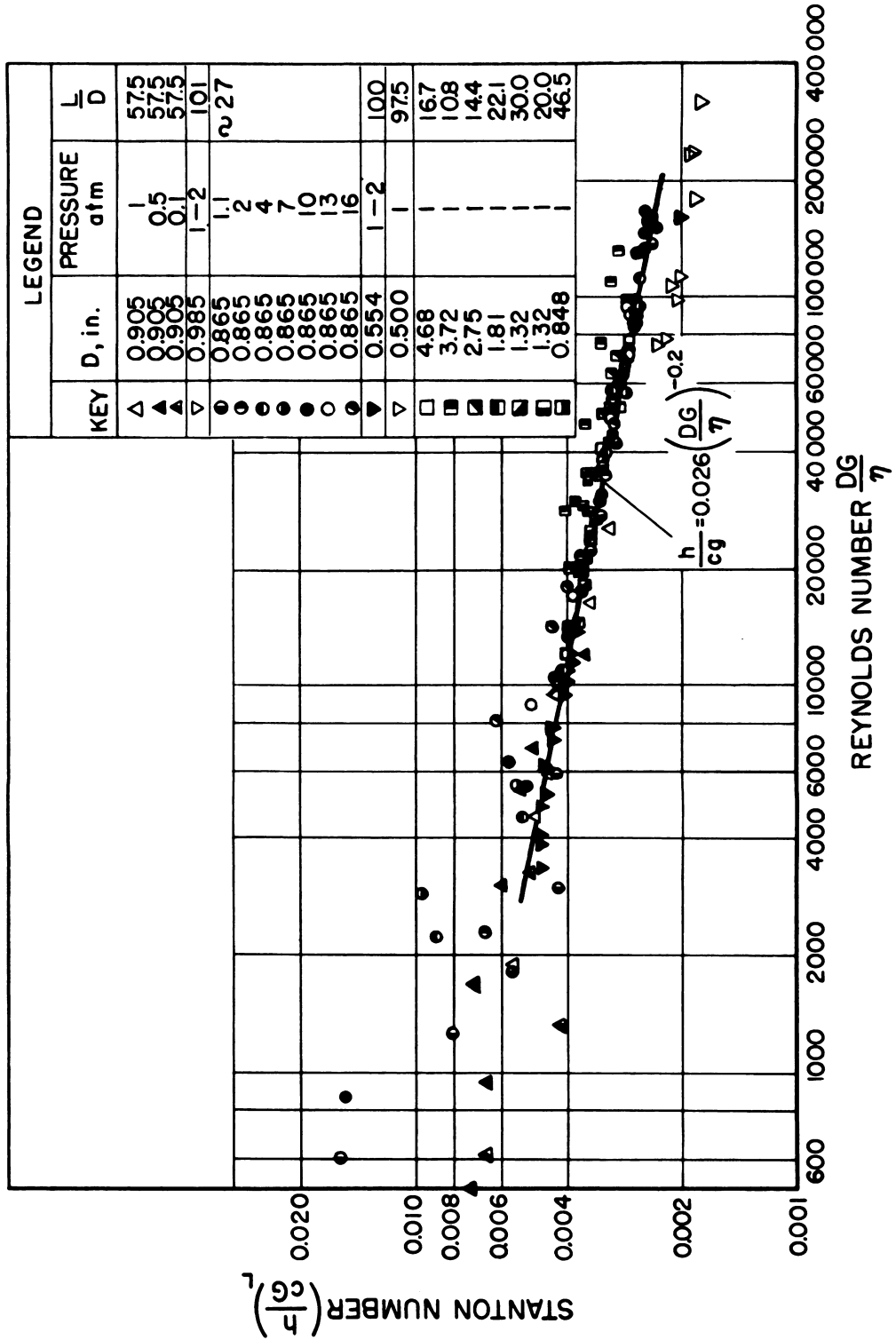


Fig. 3.4.11 — Heat-transfer Correlation Independent of Length-to-diameter Ratio. Reprinted from NACA-ARR-4F28, Feb. 1945.

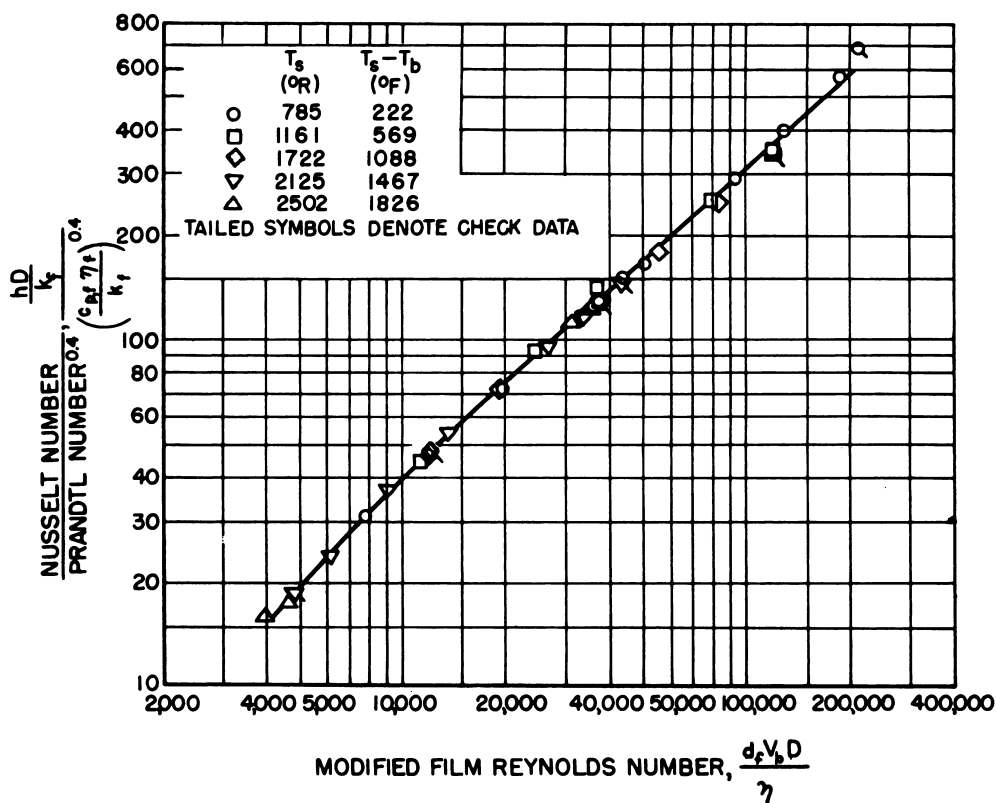


Fig. 3.4.12—Heat-transfer Correlation for Turbulent Flow. Reprinted from NACA-RM-E9D12, June 23, 1949.

Figure 3.4.12 demonstrates the validity of obtaining the heat-transfer coefficient with high surface-to-bulk temperature ratios by evaluating the physical properties at the film temperature. Fair correlation was also obtained evaluating the physical properties at the surface temperature of the wall.

Figure 3.4.13 presents further data obtained for turbulent flow with low L/D ratios and low heat flux. These data are correlated with a maximum deviation of 17 percent by the equation:

$$\frac{h_L}{c_{p,b} G} = 0.026 (DG/\eta)_b^{-0.20} [1 + (L/D)^{-0.70}] \quad (10)$$

where the physical properties of air were taken from the "Gas Tables" by Keenan and Kaye.

HEAT-TRANSFER DATA FOR OTHER GASES

Heat-transfer data for helium are presented by Lyon.¹⁸ The precision of the data is not sufficient to detect any significant difference from that predicted by the Colburn or Dittes-Boelter equations. Figure 3.4.14 presents data obtained for a 3:1 hydrogen-nitrogen mixture at various pressures as well as for air. In this correlation, ϕ is a function of Reynolds and Prandtl numbers. These data indicate that low-pressure data may be utilized to obtain high-pressure data as long as the physical properties at the high pressure are known.

A simplified equation for quickly calculating the heat-transfer coefficient for gases in turbulent flow as presented by McAdams¹⁹ is:

$$h = 0.027 c_p G^{0.8} \eta^{0.2} / D^{0.2} \quad (10a)$$

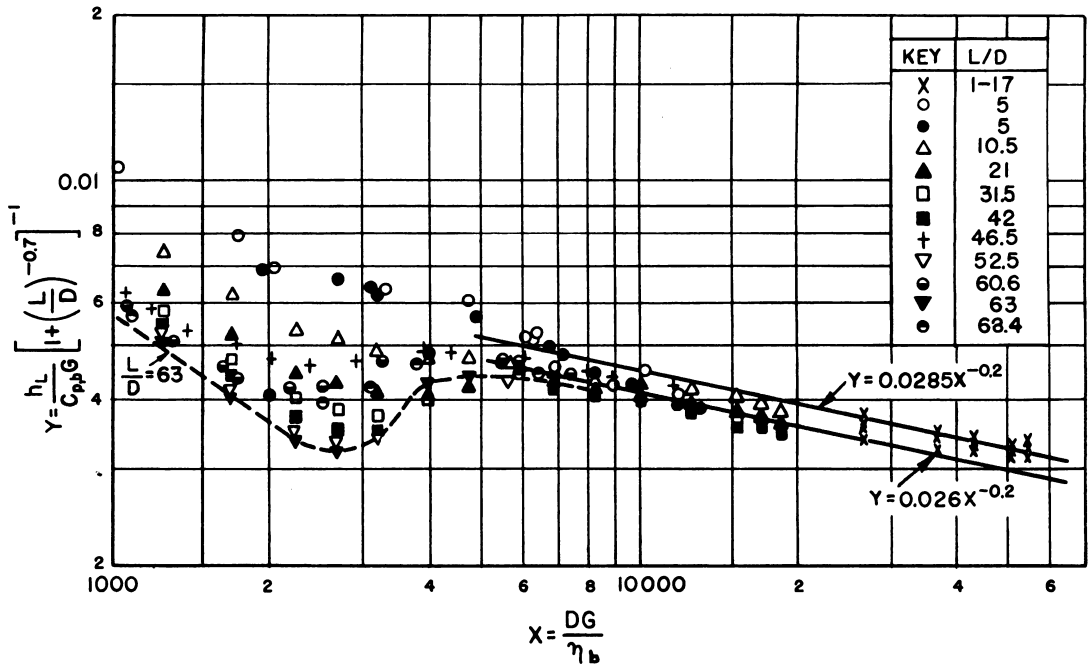


Fig. 3.4.13—Heat-transfer Correlation for Low L/D . Reprinted from NEPA-1688, Dec. 1950.

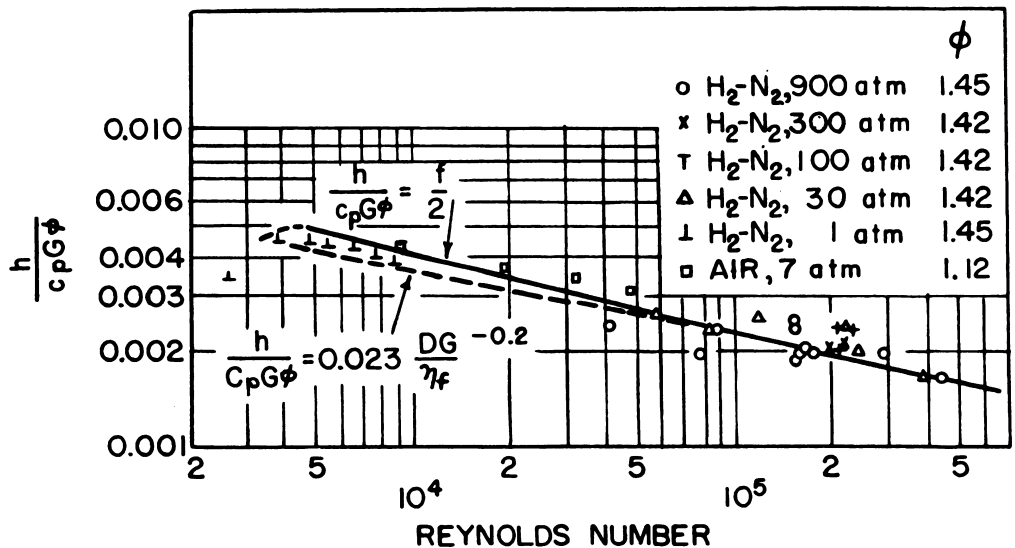


Fig. 3.4.14—Heat-transfer Data for 3:1 H_2-N_2 Mixtures and for Air. Reprinted from A. P. Colburn et al, Ind. Eng. Chem. 39, No. 8, 1947, p 960.

PRESSURE DROP—TURBULENT FLOW

Figure 3.4.15 illustrates the effect of the following on the average friction factor:

- (1) Effect of entrance configuration with heat addition.
- (2) Effect of L/D and inlet air temperature with heat addition.
- (3) Effect of heat extraction.

The Karman-Nikuradse relation for smooth tubes, Eq. (11), best represents the data:

$$\frac{1}{\sqrt{8 \frac{f_f}{2}}} = 2 \log \left(\frac{d_f V_b D}{\eta_f} \sqrt{8 \frac{f_f}{2}} \right) - 0.8 \quad (11)$$

The density and viscosity are evaluated at the film temperature using NACA and Keenan and Kaye's "Gas Tables" data.

The von Karman semi-theoretical treatment can be used in the determination of friction factor at any Reynolds number in the turbulent range provided the mean height of the surface irregularities of the conduit is known.²⁰

ENTRANCE AND EXIT EFFECTS ON PRESSURE DROP

The friction caused by a sudden contraction at an entrance or exit is usually given by:

$$F_c = \frac{K_c V_2^2}{2g_c} \quad (12)$$

where K_c is the function of the ratio of the new cross-sectional area to the original area, σ , the flow area contraction ratio. Similarly, expansion losses are given by:

$$F_e = K_e \frac{V_3^2}{2g_c} \quad (13)$$

Figure 3.4.16 presents a method of evaluating K_e and K_c , knowing the Reynolds number and the porosity, for the following types of flow passages:

- (1) Circular multiple-tube system.
- (2) Two-dimensional infinitely wide gap.
- (3) Square-tube plate-fin system.
- (4) Equilateral-triangular plate-fin system.

These plots are derived for non-compressible flow, and experimental results have confirmed the predictions of this analysis.²¹

For non-adiabatic Flow, Kays' correlations hold if the velocity is evaluated at the bulk temperature of the fluid with the physical properties of the fluid evaluated at the wall temperature.²² Turning losses are discussed elsewhere in this chapter.

FINNED SURFACES

The design of gas-cooled finned surfaces requires the calculation of heat transfer and pressure drop as related to design conditions such as cylinder diameter, width and spacing of the fins, and roughness of the surface, and to operating conditions such as velocity of coolant and temperature differences. Detailed treatment of finned surfaces is given in the A.S.M.E. Transactions,²³ but the data presented are not directly applicable where the fin is made from the fuel elements.

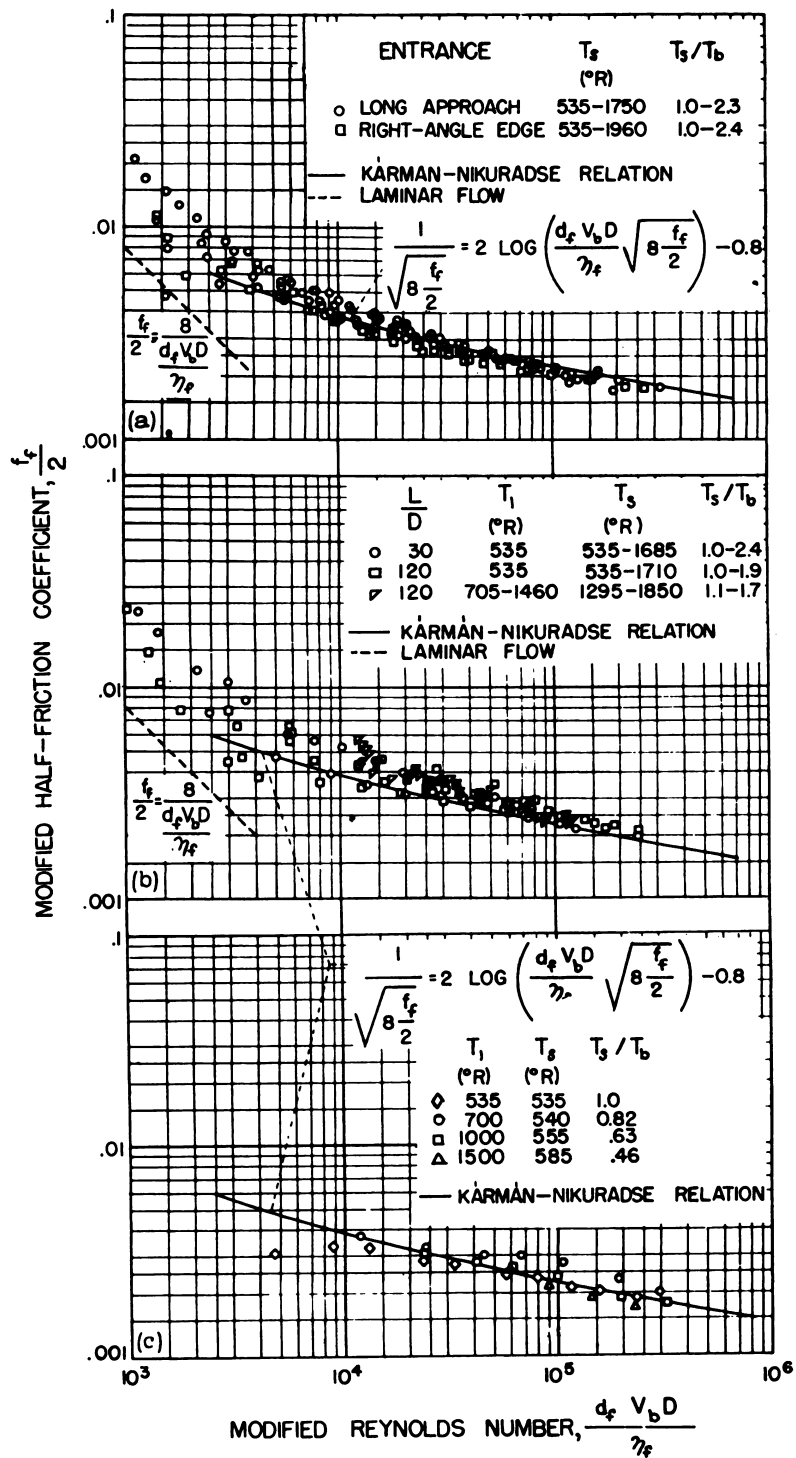


Fig. 3.4.15— Friction-factor Correlation for Turbulent Flow. Reprinted from NACA-1020, 1951.

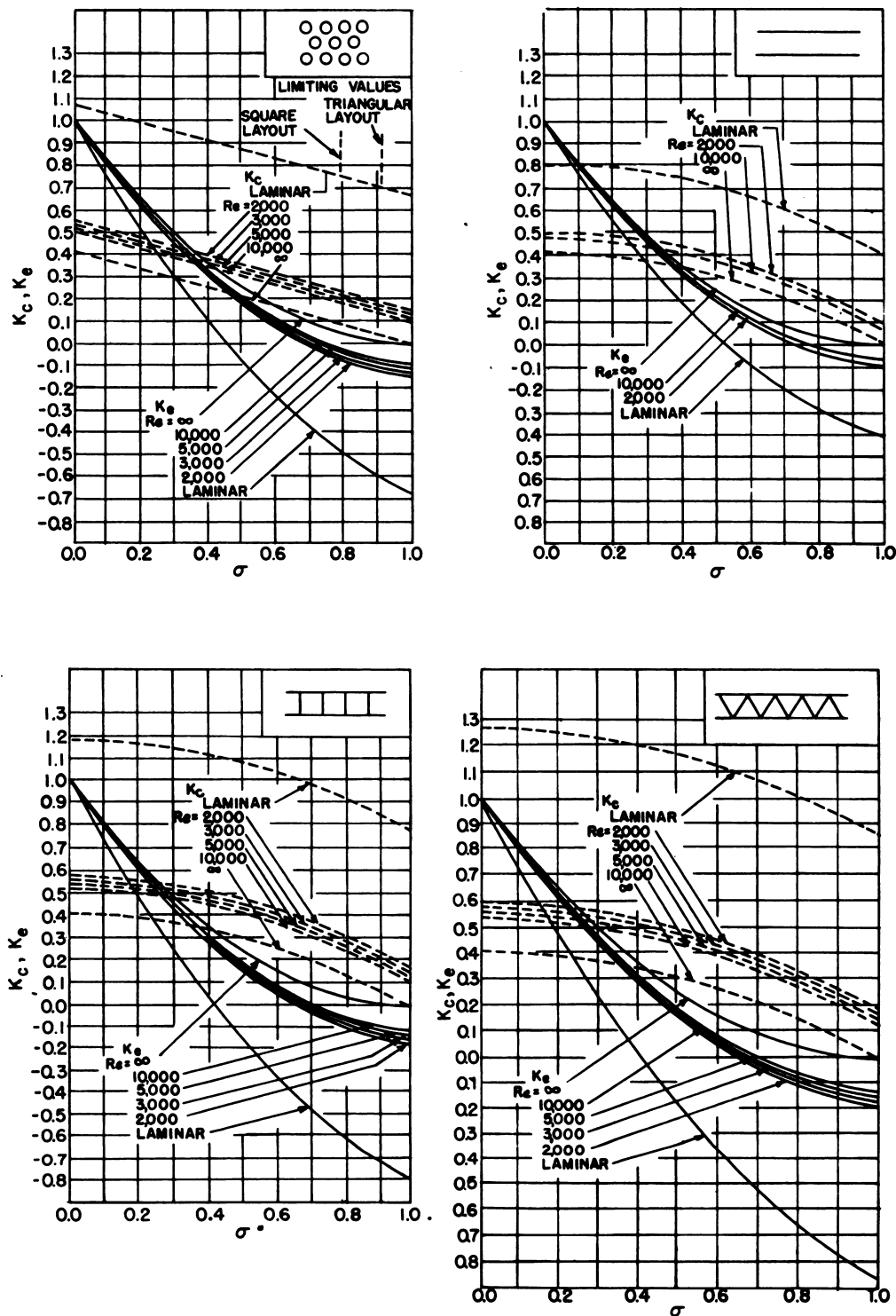


Fig. 3.4.16—Constants for Entrance and Exit Pressure Loss. Reprinted from NP-3901, Jan. 1, 1950.

The general conclusions deduced from many independent sources of fin data are:²⁴

- (1) For a given Reynolds number, the Stanton numbers, $h/c_p G$, usually increase with increase in fin spacing for both rectangular and triangular fins.
- (2) For a given Reynolds number, the Stanton numbers usually increase with increase in fin width for rectangular fins, but decrease with increase in fin width for triangular fins.
- (3) Cylindrical diameter has no effect on the coefficient of heat transfer.
- (4) Temperature difference has a negligible effect on the surface heat-transfer coefficient, in the range of available data where the maximum t was approximately 200°F.
- (5) There is an indication in the data that rough or wavy surfaces:
 - (a) Increase the Stanton number for a given Reynolds number.
 - (b) Increase the heat-transfer coefficient for a given pumping power per unit surface.
 - (c) Increase the heat-transfer coefficient slightly for a given pressure drop.

Interrupted plane fins staggered in successive rows have been utilized where high heat-transfer coefficients were desirable. These fins do not allow the boundary layer in the fluid to develop fully because of the interruption in the fins. High heat-transfer coefficients are the result. Figure 3.4.17 is a schematic diagram of interrupted plane fins, with S , the transverse wall-to-wall spacing between fins in the same row, λ , the length of fin in direction of fluid flow, δ , the thickness of fin metal, and σ , the transverse stagger spacing between the fins in successive rows indicated.

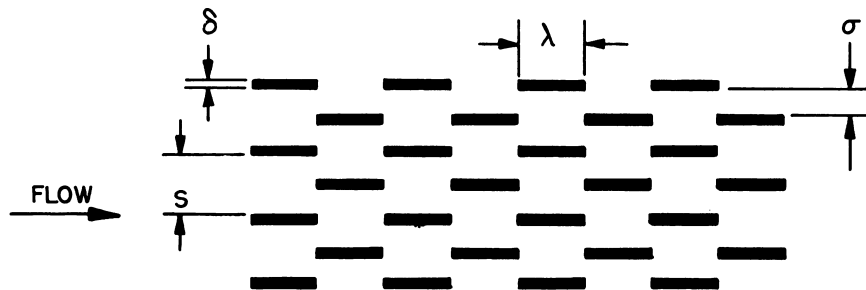


Fig. 3.4.17—Schematic Diagram of Interrupted Plane Fins. Reprinted from NACA-TN-2237, Dec. 1950.

Figure 3.4.18 presents heat-transfer data over the wide range of fin characteristics indicated. The equations representing the line are:

$$\frac{h}{c_p G} \text{Pr}^{1/3} = \frac{0.60}{\sqrt{\frac{\lambda}{d_h} \left(\frac{G d_h}{\eta} \right)}} \quad (14)$$

for $\lambda/d_h \leq 3.5$, and:

$$\frac{h}{c_p G} \text{Pr}^{1/3} = \frac{0.60}{\sqrt{3.5 \left(\frac{G d_h}{\eta} \right)}} \quad (15)$$

for $\lambda/d_h > 3.5$. In these equations, d_h is the hydraulic diameter of the fin passage equal to four times the cross-sectional area divided by the wetted perimeter.

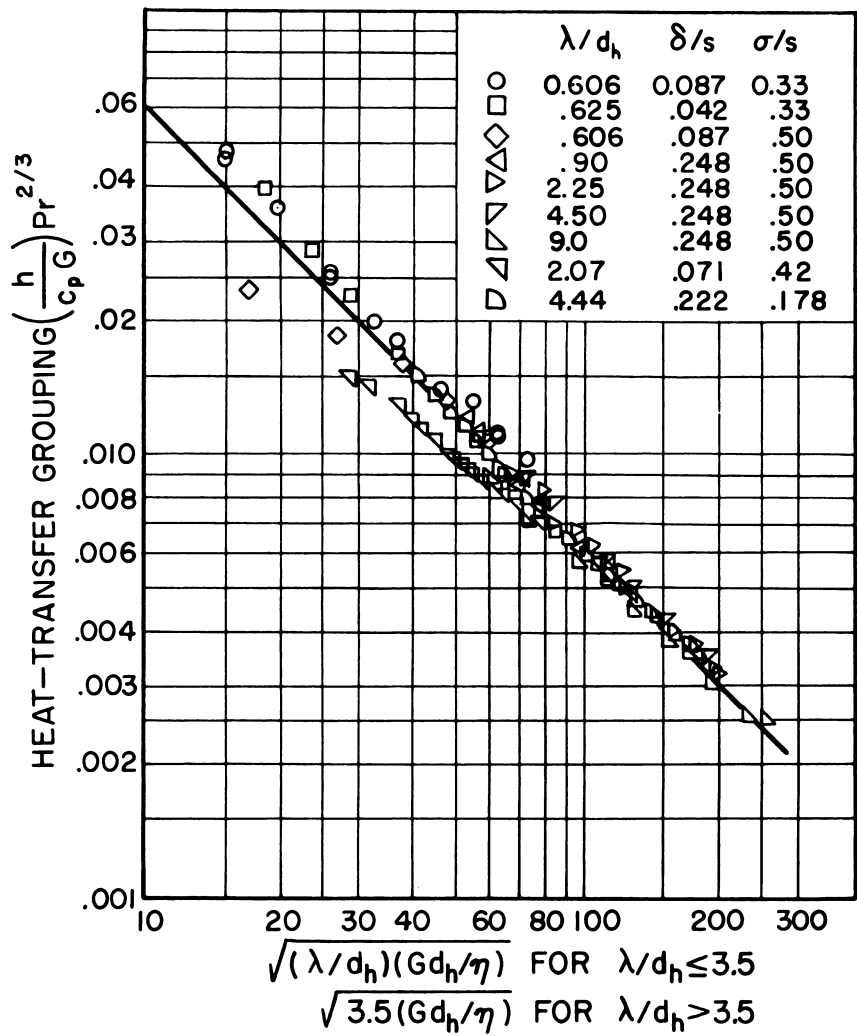


Fig. 3.4.18—Heat-transfer Data for Interrupted Plane Fins. Reprinted from NACA-TN-2237, Dec. 1950.

Figure 3.4.19 presents the data for the friction factor for Reynolds numbers less than or equal to 3500 and for Reynolds numbers greater than 3500. The correlating equations for the friction coefficients for Reynolds numbers ≤ 3500 are:

$$f = \frac{11.8}{\frac{\lambda}{d_h} \left(\frac{G d_h}{\eta} \right)^{0.67}}$$

(16)

for $\lambda/d_h \leq 3.5$, and:

$$f = \frac{11.8}{3.5 \left(\frac{G d_h}{\eta} \right)^{0.67}}$$

(17)

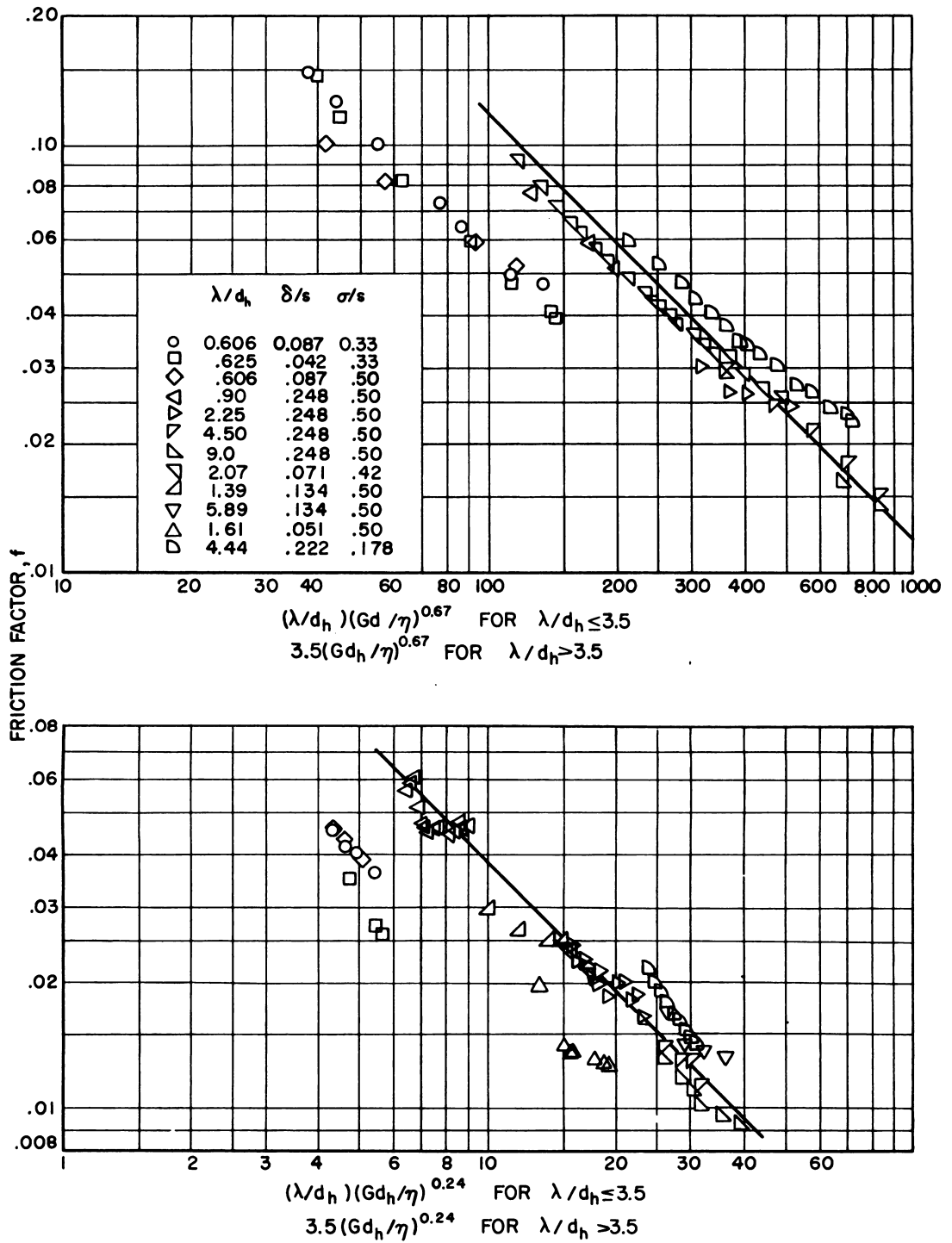


Fig. 3.4.19—Friction-factor Data for Interrupted Plane Fins. Reprinted from NACA-TN-2237, Dec. 1950.

for $\lambda/d_h > 3.5$. For Reynolds numbers > 3500 :

$$f = \frac{0.38}{\frac{\lambda}{d_h} \left(\frac{Gd_h}{\eta} \right)^{0.24}} \quad (18)$$

for $\lambda/d_h \leq 3.5$, and:

$$f = \frac{0.38}{3.5 \left(\frac{Gd_h}{\eta} \right)^{0.24}} \quad (19)$$

for $\lambda/d_h > 3.5$. More recent fin data are presented by Kays et al.²⁵

TURNING LOSSES

In reactors using split flow of coolant and in folded reactors (Chapter 3.6), turning losses are an important fraction of the total pressure drop of the coolant. It is difficult to extrapolate the turning-loss data obtained with models because of the inadequate theory describing the losses.

Figure 3.4.20 presents data for turning losses with various slot widths and illustrates the effect of using bellmouths at the entrance to the channels. The channels had the finned fuel elements shown in Fig. 3.5.5 in them. The air flowed down the slot and turned into the 2.67-in.-ID channels on 8-in. centers normal to the slot as shown in Fig. 3.4.21. Table 3.4.5 lists the various operating conditions for Fig. 3.4.20.

The data presented in Fig. 3.4.22 are for normal flow and turning flow. The data are for relatively short passages and exhibit a slope of minus one-half instead of minus one because of the entrance effects. The losses caused by flowing through two 90° turns are indicated by the separations between these curves. The turning losses decrease with increased Reynolds number.

The estimate that a turning loss is equivalent to one velocity head is shown by the above data to be conservative. Turning losses from 0.61 to 1.47 velocity heads have also been reported²⁶ and may be kept to the minimum value by the proper design of passage entrance and exits.

FLOW IN CHANNELS OF IRREGULAR SHAPES

HEAT TRANSFER—RECTANGULAR DUCTS

Heat-transfer data from many sources are plotted in Fig. 3.4.23 for rectangular ducts. The data for high L/D ratios fall below the curves. This is attributed to inaccurate temperature measurements because of poor mixing of the stream. The correlations in Fig. 3.4.23 are therefore only valid for L/D ratios below 80.

HEAT TRANSFER—RECTANGULAR AND TRAPEZOIDAL DUCTS

Data plotted in Fig. 3.4.24 for rectangular and trapezoidal ducts fall 30 to 35 percent below the usual correlation.²⁷

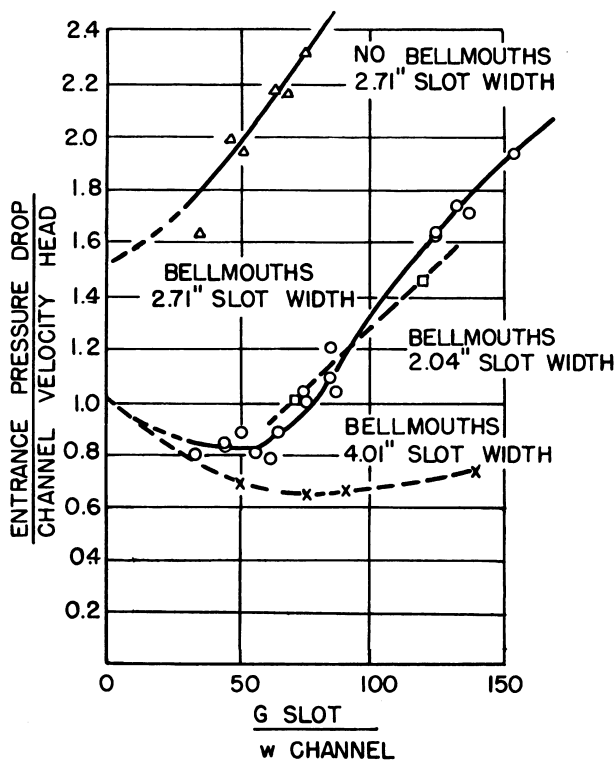


Fig. 3.4.20—Turning-loss Data. Reprinted from BNL-23, Oct. 1, 1949, Secret. Channel-entrance pressure drop expressed as fraction of channel velocity head vs the ratio of the mass velocity, G , in the feed slot to the weight rate of flow, w , through the channel.

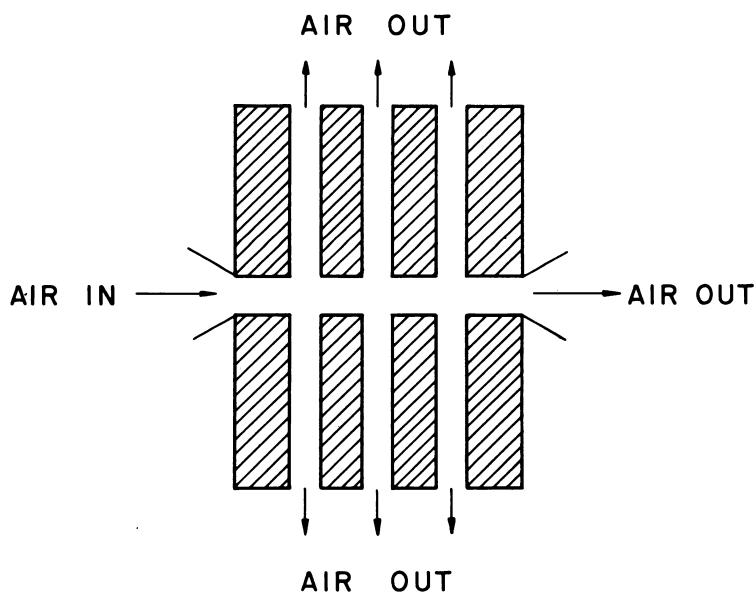
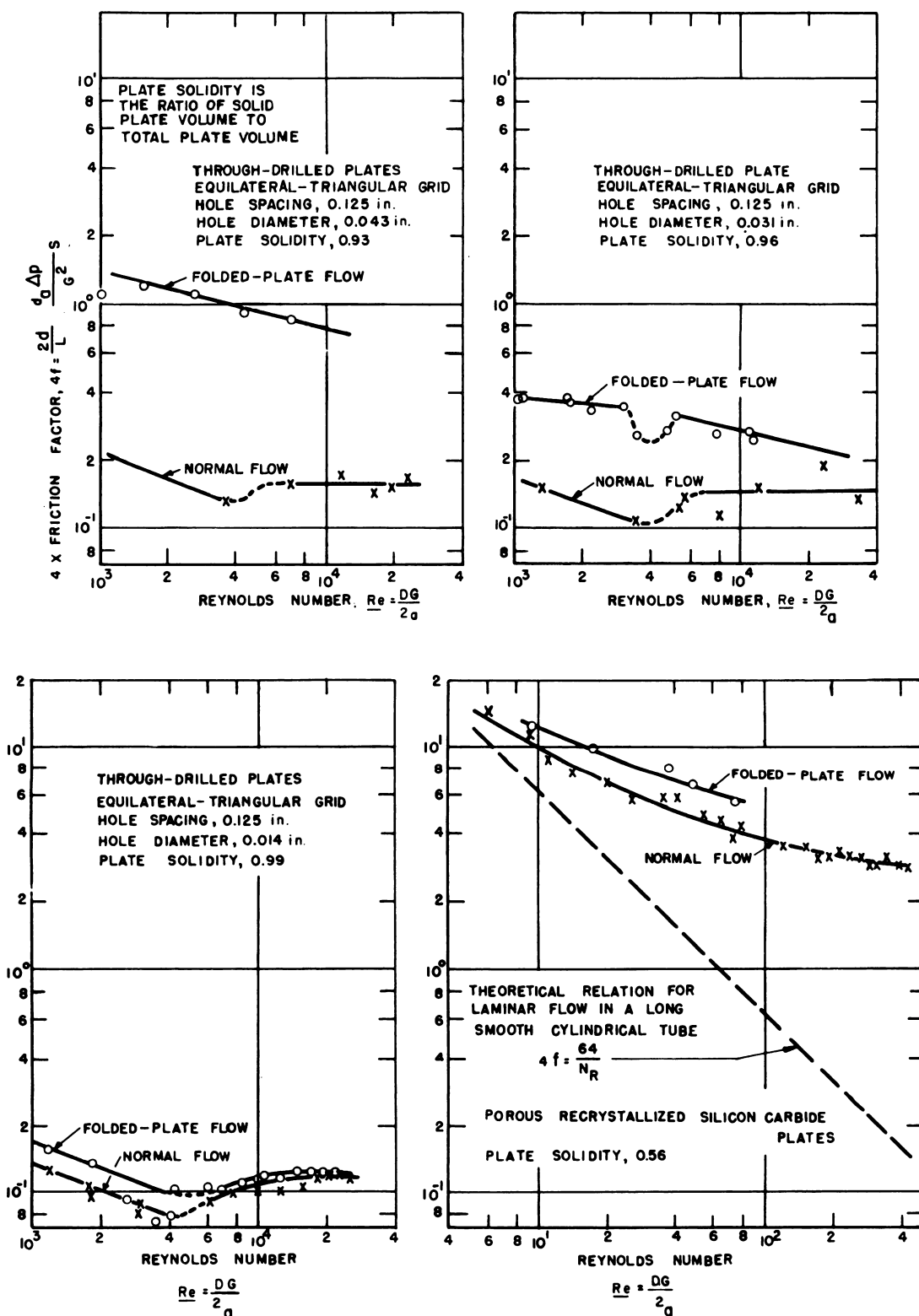


Fig. 3.4.21—Schematic of Turning Flow. Reprinted from BNL-23, Oct. 1, 1949, Secret. The pressure drop was measured from an average position in the slot to 10 in. downstream in a channel.

Table 3.4.5—Channel-entrance Pressure-drop Data and Results

Run No.	Weight rate of flow through channel, lb/hr	Average air velocity passing channel, ft/sec	Static pressure upstream of channel,* in. H ₂ O	Static pressure down-stream of channel,* in. H ₂ O	Average static pressure at channel entrance,* in. H ₂ O	Static pressure in channel 10 in. from drop, in. H ₂ O	Entrance pressure drop, in. H ₂ O	Channel velocity head, in. H ₂ O	Ratio of entrance pressure drop to channel velocity head	Mass velocity in slot, lb/(hr)(sq ft)	Ratio of slot mass velocity to channel weight rate of flow
Without bellmouths—2.71-in. slot width											
1	863	118	5.59	4.76	5.17	9.13	3.96	2.44	1.62	31100	36.0
2	843	151	6.77	5.95	6.36	11.00	4.64	2.34	1.98	39700	47.1
3	842	169	10.43	8.89	9.66	14.17	4.51	2.34	1.93	44100	52.3
4	833	208	13.37	11.48	12.42	17.42	5.00	2.32	2.16	53900	64.8
5	830	221	12.60	11.22	11.91	16.85	4.94	2.30	2.15	57400	69.2
6	816	240	15.84	14.25	15.04	20.20	5.16	2.24	2.30	61900	76.0
With bellmouths—2.71-in. slot width											
7	873	112	5.83	4.81	5.32	7.29	1.97	2.49	0.79	29600	33.9
8	861	146	77.20	5.90	6.55	8.58	2.03	2.43	.84	38400	44.7
9	858	147	7.56	6.70	7.13	9.10	1.97	2.41	.82	38600	45.0
10	846	182	9.09	8.11	8.60	10.67	2.07	2.35	.88	42700	50.5
11	816	240	16.43	14.56	15.49	17.70	2.21	2.23	.99	61700	75.7
12	808	270	18.62	16.63	17.62	20.25	2.63	2.20	1.19	69000	85.4
13	808	276	18.50	16.43	17.46	19.70	2.24	2.20	1.02	70600	87.3
14	550	119	4.30	3.74	4.02	4.80	0.78	0.97	0.80	31500	57.3
15	540	128	5.12	4.57	4.85	5.58	.73	.95	.77	33800	62.6
16	538	134	5.43	4.41	4.92	5.75	.83	.94	.88	35400	65.8
17	526	148	6.50	5.28	5.89	6.81	.92	.90	1.03	39000	74.2
18	515	166	8.03	6.89	7.46	8.39	.93	.86	1.08	46300	84.7
19	487	234	12.60	11.97	12.28	13.54	1.26	.78	1.61	60600	124.5
20	488	234	12.40	11.06	11.73	13.00	1.27	.78	1.62	60900	125.0
21	480	250	14.26	13.66	13.96	15.27	1.31	.76	1.72	63700	133.0
22	480	254	13.81	12.80	13.30	14.60	1.30	.76	1.70	65700	137.0
23	469	285	18.23	17.13	17.68	19.10	1.42	.74	1.92	72800	155.0
With bellmouths—4.01-in. slot width											
24	850	165	7.36	6.50	6.93	8.53	1.60	2.35	0.68	43300	51.0
25	820	247	13.82	12.45	13.13	14.56	1.43	2.23	.64	63700	77.7
26	510	177	8.23	7.60	7.91	8.47	0.56	0.85	.66	46400	91.0
27	480	248	14.75	13.85	14.30	14.85	.55	.76	.72	63800	38.0
With bellmouths—2.04-in. slot width											
28	518	140	7.32	6.30	6.81	7.68	0.87	0.873	1.00	36800	71
29	480	223	14.20	12.80	13.50	14.62	1.12	.761	1.47	57700	120

* All static pressures are given as inches of water below atmospheric



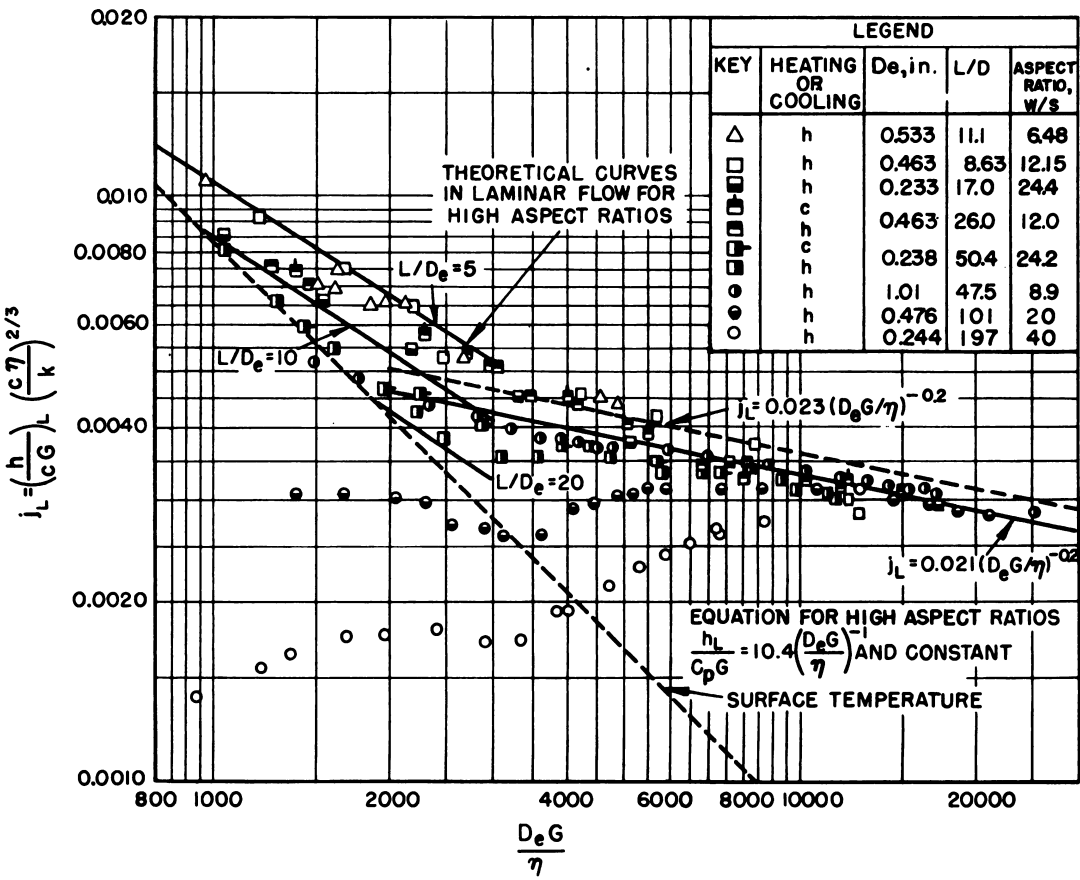


Fig. 3.4.23 — Heat-transfer Correlation for Rectangular Ducts. Reprinted from NACA-ARR-4F28, Feb. 1945.

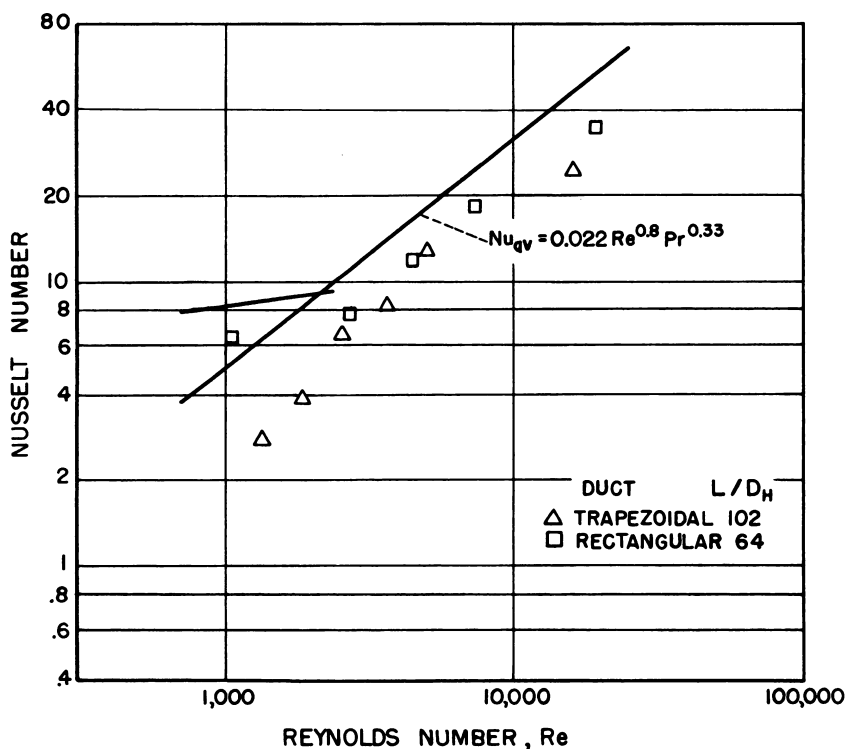


Fig. 3.4.24—Heat-transfer Data for Rectangular and Trapezoidal Ducts. Reprinted from NACA-TN-2524, Nov. 1951.

PRESSURE DROP—RECTANGULAR AND TRAPEZOIDAL DUCTS

Friction-factor data are presented in Fig. 3.4.25 for trapezoidal and rectangular ducts. The pressure drops are predictable to within 20 percent by the following equations:

$$\zeta = 4f = \frac{64}{Re} \quad (20)$$

for $Re \leq 1800$, and:

$$\zeta = 4f = \frac{0.176}{Re^{0.20}} \quad (21)$$

for $Re > 1800$.

WAVE-SHAPED PLATES

The analysis of heat-transfer and pressure-drop data for wavy plates indicates an approximate doubling of the heat-transfer rate for a narrow duct. The pressure drop was increased by a factor of ten over that for a straight duct. Figure 3.4.26 is an example of the data obtained. A tabulation of the systems studied with wave-shaped plates is presented in Table 3.4.6.²⁸

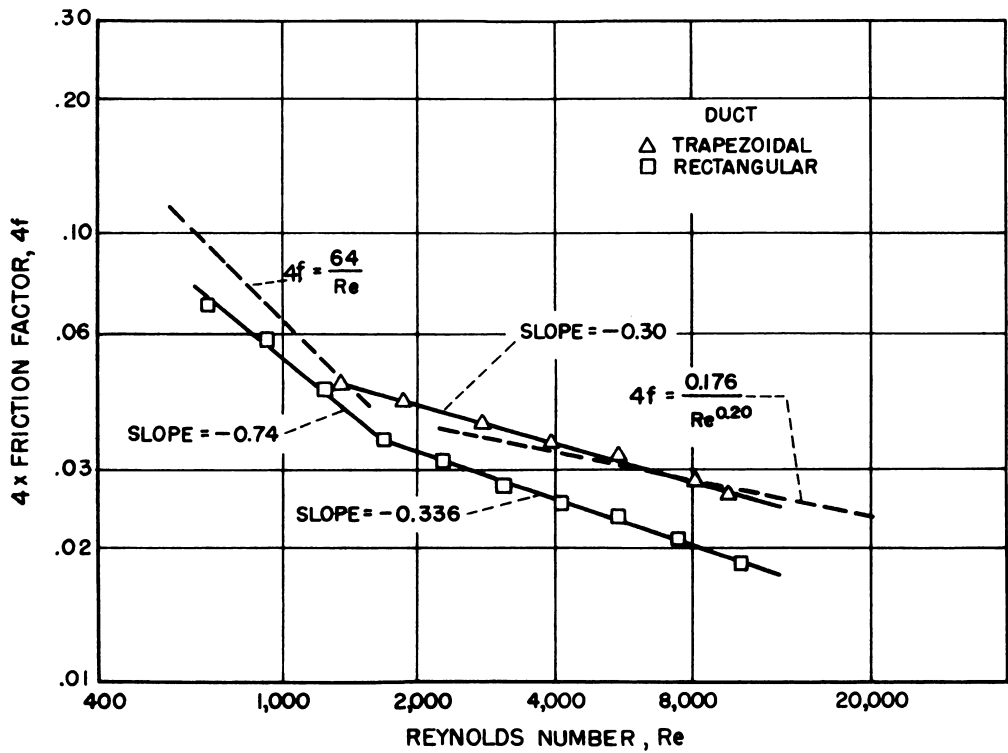


Fig. 3.4.25 — Friction-factor Data for Rectangular and Trapezoidal Ducts. Reprinted from NACA-TN-2524, Nov. 1951.

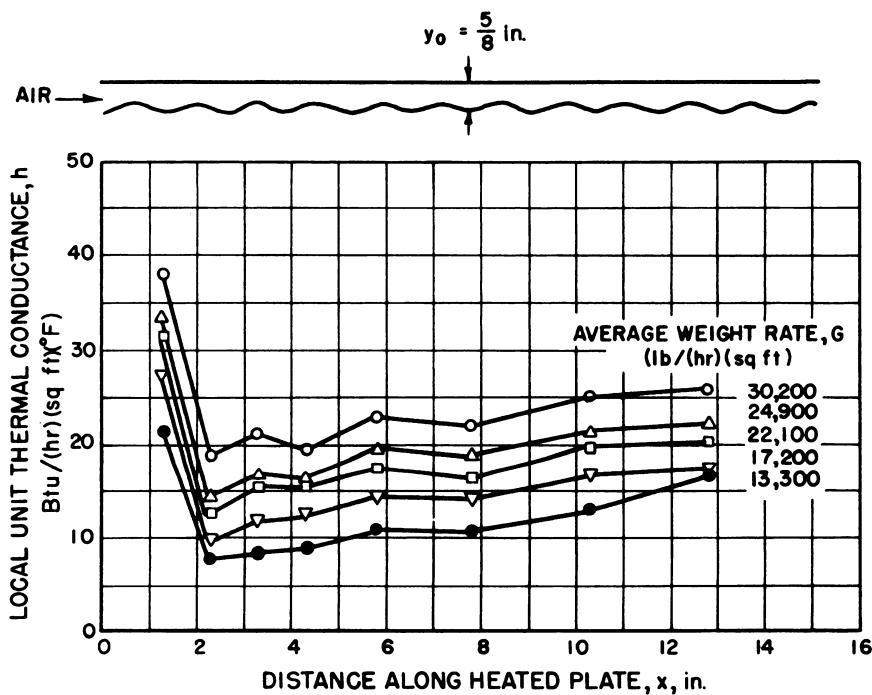


Fig. 3.4.26 — Local Heat-transfer Coefficients for Wavy Plates. Reprinted from NACA-TN-2426, Aug. 1951.

Table 3.4.6 — Systems Studied with Wave-shaped-plates by Boelter*

Small wave plate	$y_0 = \frac{7}{8}$ in.
Small wave plate	$y_0 = 1\frac{5}{8}$ in.
Small wave plate	$y_0 = 3\frac{1}{8}$ in.
Large wave plate	$y_0 = \frac{7}{8}$ in.
Large wave plate	$y_0 = 1\frac{5}{8}$ in.
Large wave plate	$y_0 = 3\frac{1}{8}$ in.

* Variation of heat-transfer coefficient with distance and pressure drop vs flow rate studied for the systems in this table

VELOCITY DISTRIBUTION IN TRIANGULAR PASSAGES

Figure 3.4.27 presents measured velocity contours in a triangular passage. Analytical methods are presented for determining temperature distributions.²⁹

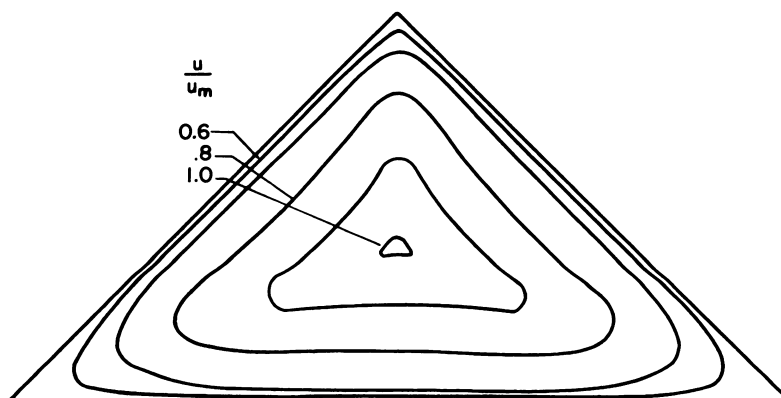


Fig. 3.4.27 — Velocity Contours in a Triangular Passage. Reprinted from NACA-TN-2257, Jan. 1951.

ANNULI AND NON-CIRCULAR DUCTS

Information on heat transfer and fluid flow for annuli and non-circular ducts is available.^{30,31}

PRESSURE DROP—FUEL ELEMENT CHANNELS

Data are available for the pressure drop across various fuel-element channels,^{32,33} but these treatments are too specific to be of widespread interest.

PRESSURE DROP—HEADERS, DUCTS, AND DUCT COMPONENTS

Detailed information is available for predicting pressure drop for headers and ducts of various shapes as well as for duct components.^{26, 34-38}

POROUS BODIES

PRESSURE DROP—STREAMLINE FLOW

Streamline flow through porous bodies follows the equation:

$$f = \frac{16}{\text{Re}} + b \quad (22)$$

where b , called a roughness factor, is a constant for the sample. Figure 3.4.28 presents experimental data obtained with hydrogen and nitrogen. The limit of the experimental error in determining the friction factor is less than ± 1 percent. In other experimental work on heat transfer, the temperature ratio of solid to coolant temperature was not known precisely enough to determine heat-transfer coefficients.³⁹

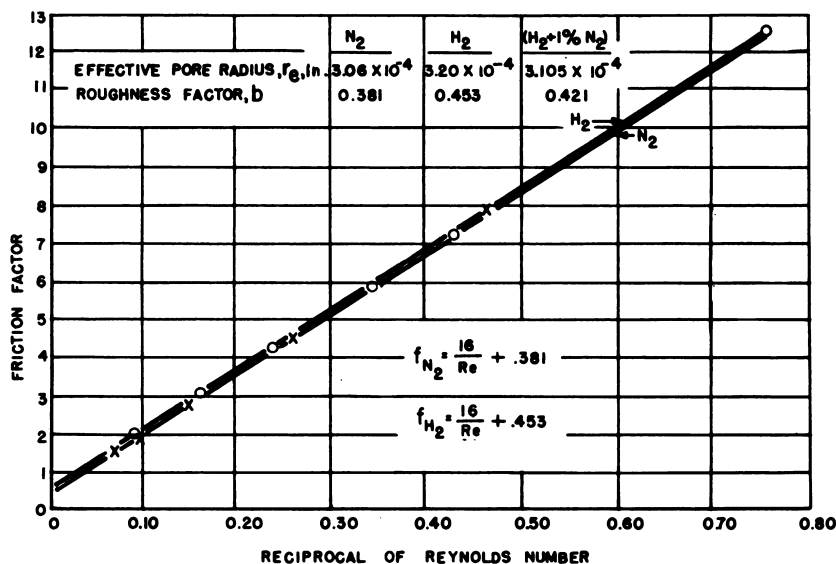


Fig. 3.4.28—Pressure-drop Correlation for Streamline Flow Through Porous Bodies. Reprinted from R-111, Aug. 10, 1948, Secret.

PRESSURE DROP—TURBULENT FLOW

A modified fluid-flow equation, which was verified experimentally, is:

$$\Delta P = \frac{\text{LB}'G^2}{4r_e d_a} + \frac{8\eta LG}{d_a r_e^2 + 5.00 r_e \eta (d_0/P_0)^{1/2}} \quad (23)$$

for which the nomenclature is defined in Table 3.4.7. Equation (23) has been verified⁴⁰ for many porous materials using nitrogen and hydrogen under conditions that approximate the flow of gases at high temperatures through the body. Figure 3.4.29 is an example of the correlation obtained. The deviation between calculated and experimental curves is less than 8 percent.

Table 3.4.7—Nomenclature for Equation (23)

Symbol	Definition	Unit
B'	Constriction factor	Dimensionless
d_a	Average density of fluid	gm/cu cm
d_0	Density of fluid at exit	gm/cu cm
G	Mass flow per unit area at cross section	gm/(sq cm)(sec)
L	Length or thickness of body	cm
P_0	Exit pressure of fluid	dynes/sq cm
ΔP	Pressure drop	dynes/sq cm
r_e	Effective pore radius	cm

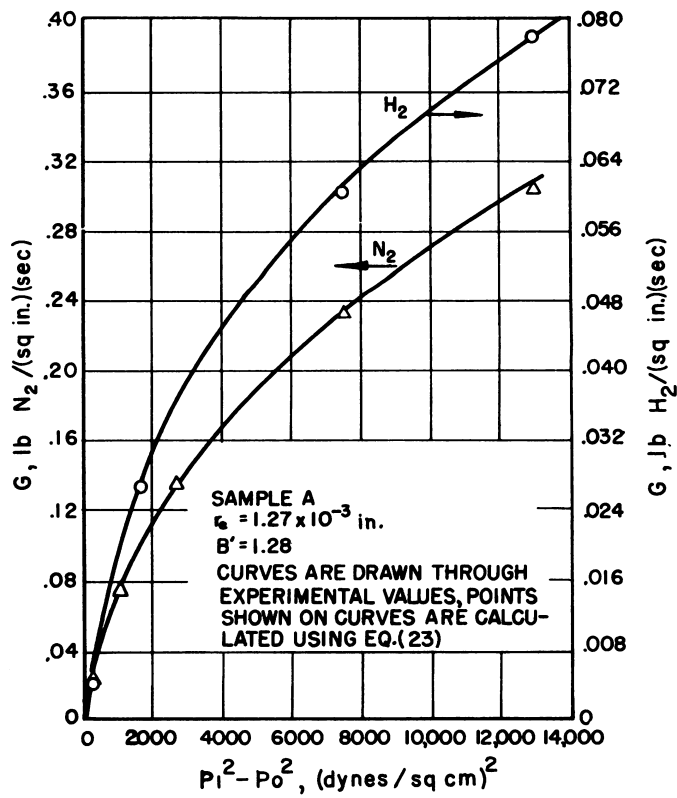


Fig. 3.4.29—Pressure-drop Correlation for Turbulent Flow Through Porous Bodies. Reprinted from R-128, Jan. 1949.

PACKED BEDS

Heat-transfer and friction-factor data for spheres are presented in Figs. 3.4.30 and 3.4.31, respectively. These data are valid for gases having Prandtl numbers of approximately 0.73. Curves previously reported in the literature^{41,42} are also indicated. A new method of analysis for estimating heat-transfer coefficients and friction factors based on the properties of a single particle is presented by Ranz,⁴³ which correlates the data of Gamson.⁴²

Work on stacked and separated screens having porosities of 0.34 to 0.84 in the Reynolds number range of 10 to 1000 has been in progress at Stanford, and the data will be published in late 1952.*

ROUGHNESS

HEAT TRANSFER

The equation:

$$\frac{hD}{k_f} = 0.040 \left(\frac{d_f V_\tau D}{\eta_f} \right)^{1.0} \left(\frac{c_{p,f} \eta_f}{k_f} \right)^{0.4} \quad (24)$$

correlates the data taken within ± 15 percent for tubes having square-thread-type roughness. The properties of the fluid are evaluated at the film temperatures from NACA data and the "Gas Tables." Figure 3.4.32 presents the data under the conditions listed in Table 3.4.8.

The roughness ratio, e/r , is defined as the ratio of the height of the thread to the radius of the tube. V_τ , the friction velocity, is defined as the product of the velocity and the square root of one-half the friction factor:

$$V_\tau = V_b \sqrt{f_t/2}$$

PRESSURE DROP

The friction factors observed were higher than for conventional smooth tubes. They were correlated by the introduction of roughness parameters as indicated in Eq. (25):

$$f_t/2 = 0.0036 (s/W)^{0.80} (e/W)^{1.70} \quad (25)$$

where: s = distance between threads
 W = thread width
 e = thread height

Figure 3.4.33 presents the data as correlated by Eq. (25). This correlation applied only to turbulent flow.

*A. L. London, personal communication, Oct. 5, 1952.

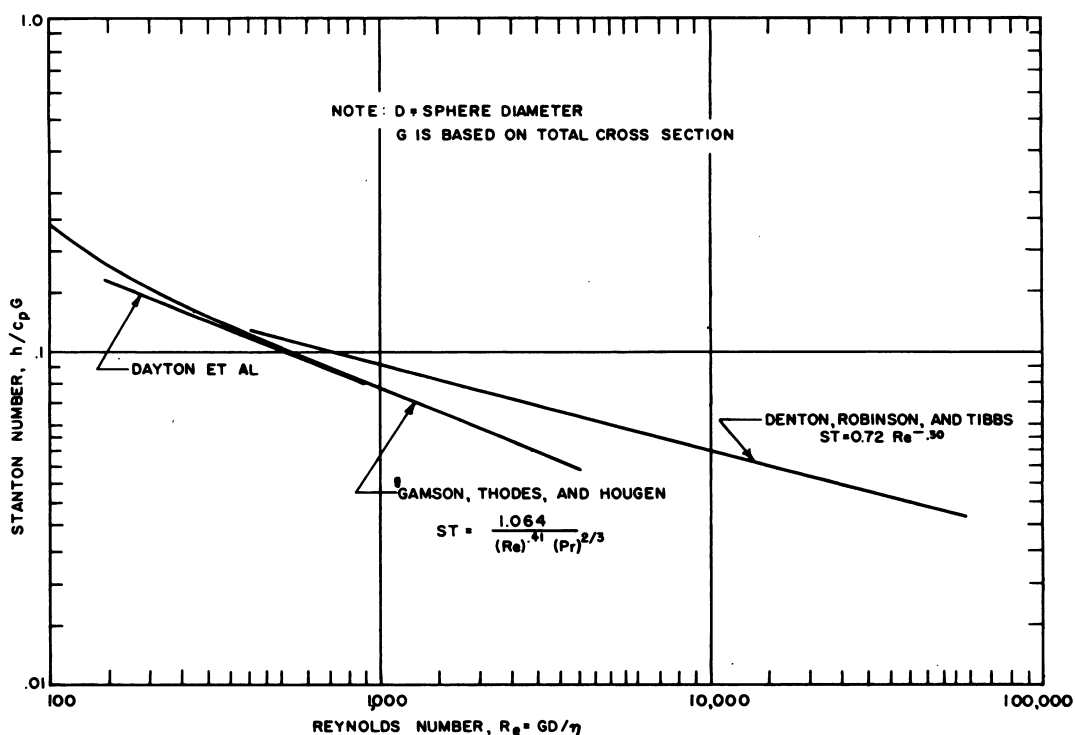


Fig. 3.4.30—Stanton Number vs Reynolds Number for Heat Transfer Between Packed Spheres and Air. Submitted by BMI, Nov. 1952.

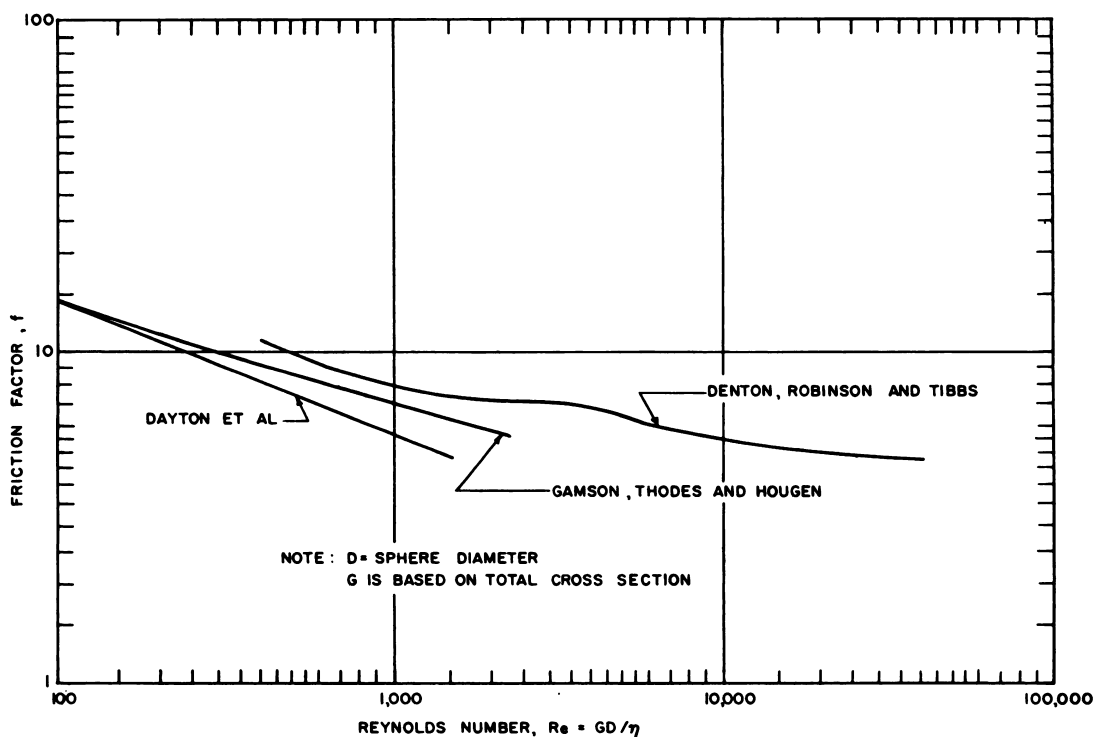


Fig. 3.4.31—Friction Factors for Air Flowing Through Packed Spheres. Submitted by BMI, Nov. 1952.

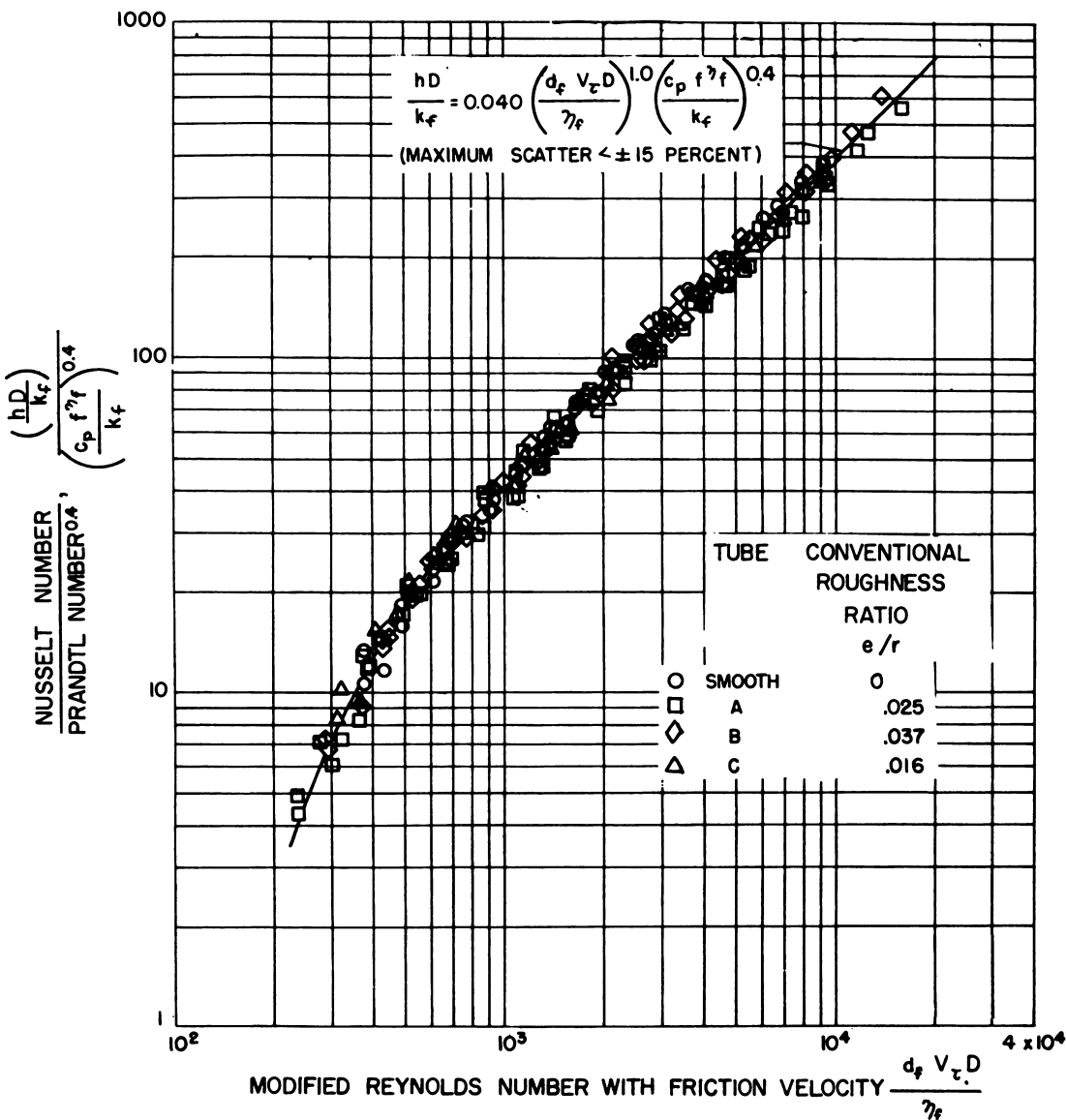


Fig. 3.4.32—Heat-transfer Correlation for Tubes Containing Square-thread-type Roughness. Reprinted from NACA-RM-E52D17, June 27, 1952.

Table 3.4.8 — Conditions for Heat-transfer and Pressure-drop Data in Roughness Study

Roughness ratio	0 to 0.037
Reynolds number	Up to 350,000
Tube-wall temperature	Up to 1950°F
Heat-flux	Up to 115,000 Btu/(hr)(sq ft)

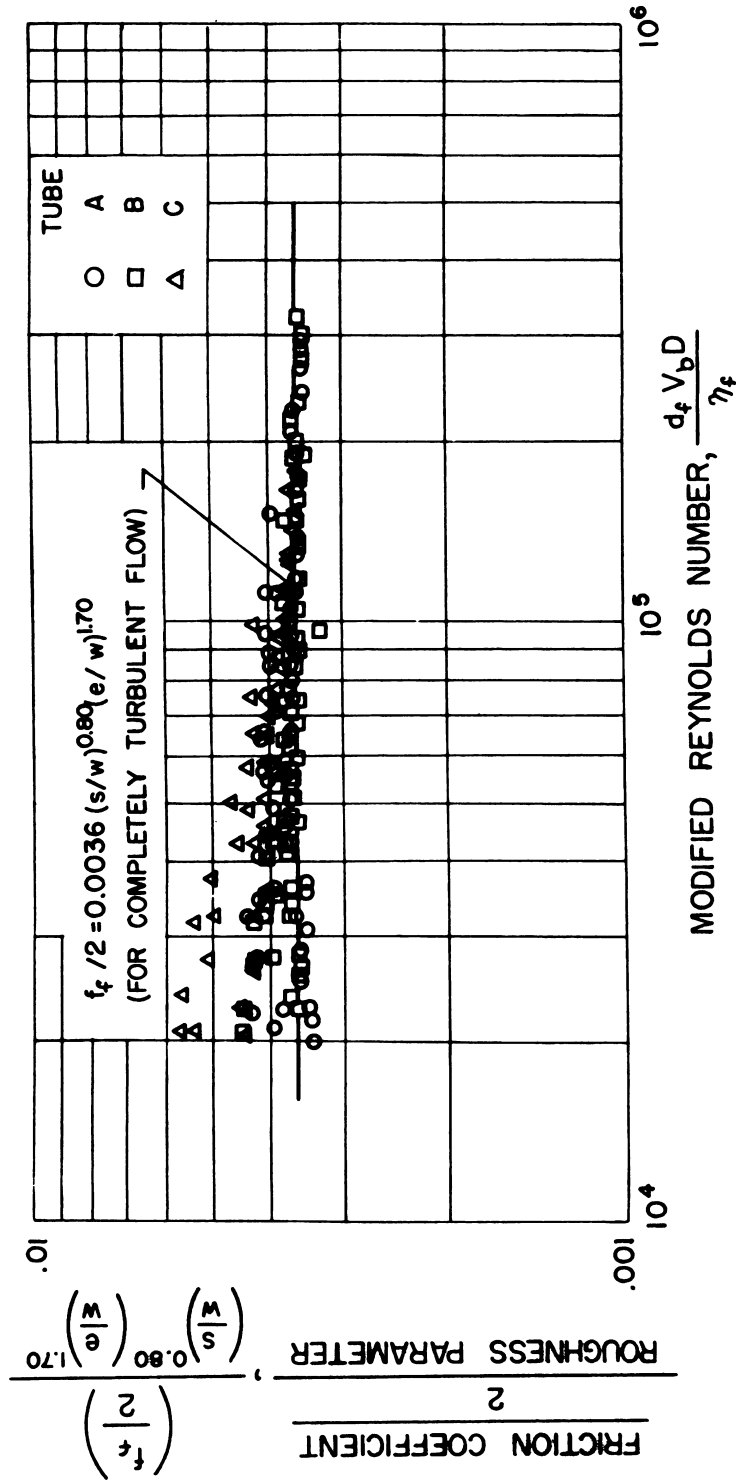


Fig. 3.4.33—Correlation of Friction Factor to Roughness Parameters. Reprinted from NACA-RM-E52D17, June 27, 1952.

FLOW ACROSS TUBES

HEAT TRANSFER—TURBULENT FLOW

Equation (26) is recommended for gases flowing normal to banks of staggered tubes. For banks of tubes in line, it is recommended that Eq. (26) be used with the constant reduced to 0.26:¹⁹

$$\frac{h_m D_0}{k_f} = 0.33 \left(\frac{c_p \eta_f}{k_f} \right)^{1/3} \left(\frac{D_0 G_{\max}}{\eta_f} \right)^{0.6} \quad (26)$$

As given in Eq. (26), h_m is for tubes that are 10 or more rows deep. Table 3.4.9 gives the correction factors for h_m for N rows deep.

Table 3.4.9 — Ratio of h_m for N Rows Deep to That for 10 Rows Deep

(Reprinted from "Heat Transmission," by W. H. McAdams.
By permission from McGraw-Hill Book Company, Inc.,
New York, 1942)

Tube geometry	$h_m(N \text{ rows})/h_m(10 \text{ rows})$									
	$N = 1$	$N = 2$	$N = 3$	$N = 4$	$N = 5$	$N = 6$	$N = 7$	$N = 8$	$N = 9$	$N = 10$
Staggered		0.73	0.82	0.88	0.91	0.94	0.96	0.98	0.99	1.0
In-line	0.64	.80	.87	.90	.92	.94	.96	.98	.99	1.0

HEAT TRANSFER—LAMINAR FLOW

Investigations limited to pitch-to-diameter ratios of 1.25 and 1.5 have indicated the correlation:

$$\left(\frac{h}{c_p G} \right) \left(\frac{c_p \eta}{k} \right)^{2/3} \left(\frac{\eta_s}{\eta} \right)^{0.14} = 1.3 \left(\frac{DG}{\eta} \right)^{-0.64} \quad (27)$$

for Reynolds numbers below 200.⁴⁴

PRESSURE DROP—TURBULENT FLOW

Nomograms valid for Reynolds numbers from 2,000 to 40,000 are given in Perry,⁴⁵ which correlate the friction factor with Reynolds number and tube geometry. Useful data on the cross-flow of gases over tubes are also reported by Grimison.⁴⁶

REFERENCES

1. M. F. Valerino and R. B. Doyle, Method for Determining Pressure Drop of Monatomic Gases Flowing in Turbulent Motion Through Constant-Area Passages with Simultaneous Friction and Heat Addition, NACA-TN-2328, April 1951.
2. B. Pinkel et al, Method for Determining Pressure Drop of Air Flowing Through Constant-Area Passages for Arbitrary Heat-Input Distributions, NACA-TN-2186, Sept. 1950.
3. M. Sibulkin and W. K. Koffel, Chart for Simplifying Calculations of Pressure Drop of a High-Speed Compressible Fluid Under Simultaneous Action of Friction and Heat-Transfer—Application to Combustion-Chamber Cooling Passages, NACA-TN-2067, Mar. 1950.
4. R. L. Turner et al, Charts for the Analysis of One-Dimensional Steady Compressible Flow, NACA-TN-1419, Jan. 1948.
5. NEPA-1767, n.d. (classified).
6. A. H. Shapiro and W. P. Hawthorne, The Mechanics and Thermodynamics of Steady One-Dimensional Gas Flow, NEPA-979-IER-13, June 1, 1949.
7. R. G. Deissler, Analytical and Experimental Investigation of Adiabatic Turbulent Flow in Smooth Tubes, NACA-TN-2138, July 1950.
8. R. G. Deissler and C. S. Eian, Analytical and Experimental Investigation of Fully Developed Turbulent Flow of Air in a Smooth Tube with Heat Transfer with Variable Fluid Properties, NACA-TN-2629, Feb. 1952.
9. K. Goldmann, Heat Transfer to Fluids with Temperature Dependent Properties, NDA, April 1952.
10. C. L. Kroll, Sc. D. thesis in chemical engineering, MIT, 1951.
11. J. H. Keenan and J. Kaye, Thermodynamic Properties of Air, Wiley, New York, 1947 (revised 1950).
12. J. Klein and M. Tribus, Forced Convection from Nonisothermal Surfaces, University of Michigan, Aug. 1952.
13. L. M. K. Boelter and M. Tribus, An Investigation of Aircraft Heaters II—Properties of Gases, NACA-ARR, Oct. 1942.
14. L. M. K. Boelter et al, An Investigation of Aircraft Heaters XXVII—Distribution of Heat Transfer Rate in the Entrance Section of a Circular Tube, NACA-TN-1451, July 1948.
15. A. Cholette, Chem. Eng. Prog. 44, No. 1, Jan. 1948, pp 81-88.
16. A. H. Shapiro and R. D. Smith, Friction Coefficients in the Inlet Length of Smooth Round Tubes, NACA-TN-1785, Nov. 1948.
17. L. V. Humble et al, Measurements of Average Heat Transfer and Friction Coefficients for Subsonic Flow of Air in Smooth Tubes at High Surface and Fluid Temperatures, NACA-1020, 1951.
18. R. N. Lyon, CE-501, Feb. 25, 1943 (classified).
19. W. H. McAdams, Heat Transmission, 2nd edition, McGraw-Hill Book Company, Inc., New York, 1942.
20. N. A. Hall, Thermodynamics of Fluid Flow, Prentice Hall Inc., New York, 1951, pp 26-29.
21. W. M. Kays, Loss Coefficients for Abrupt Changes in Flow Cross Section With Low Reynolds Number Flow in Single and Multiple Tube Systems, Stanford University, 1949.
22. W. H. McAdams et al, Heat-Transfer and Pressure Drop for Air Flowing in Small Tubes, NEPA-1688, Dec. 1950.
23. A.S.M.E. Trans. 67, 1945.
24. R. E. Drexel and W. H. McAdams, Heat Transfer Coefficients for Air Flowing in Round Tubes, in Rectangular Ducts, and Around Finned Cylinders, NACA-ARR-4F28, Feb. 1945.
25. W. M. Kays, A. L. London, and D. W. Johnson, Gas Turbine Plant Heat Exchangers, A.S.M.E. publication, April 1951.
26. W. G. Kennedy and P. E. Teets, NEPA-1758, Feb. 8, 1951 (classified).
27. L. M. K. Boelter et al, An Investigation of Aircraft Heaters XXXVIII—Determination of Thermal Performance of Rectangular- and Trapezoidal-Shaped Inner-Skin Passages for Anti-Icing Systems, NACA-TN-2524, Nov. 1951.
28. L. M. K. Boelter, An Investigation of Aircraft Heaters XXXIV—Experimental Determination of Thermal and Hydrodynamical Behavior of Air Flowing between a Flat and a Wave-Shaped Plate, NACA-TN-2426, Aug. 1951.
29. E. R. G. Eckert and G. M. Low, Temperature Distribution in Internally Heated Walls of Heat Exchangers Composed of Non-circular Flow Passages, NACA-TN-2257, Jan. 1951.
30. H. C. Claiborne, A Review of the Literature on Heat Transfer in Annuli and Non-circular Ducts for Ordinary Fluids and Liquid Metals, CF-52-8-166, n.d.
31. H. C. Claiborne, A Critical Review of the Literature on Pressure Drop in Non-circular Ducts and Annuli, ORNL-1248, May 22, 1952.
32. C. L. Segasser, ORNL-89, July 9, 1948 (classified).
33. H. B. Fairchild, ANL-OCS-29, July 19, 1946 (classified).
34. J. R. Henry, Design of Power Plant Installations—Pressure Loss Characteristics of Duct Components, NACA-LAP26, June 1944.
35. W. G. Kennedy and F. R. Scholhammer, NEPA-1824, April 13, 1951 (classified).
36. NEPA-1252 (classified).
37. NEPA-1825 (classified).
38. R. M. Armstrong, Pressure Loss in Piping Systems; A Comparison of Conventional Factors for Fluid Friction in Piping Components, AECU-454, n.d.
39. R. C. Alrich et al, Battelle R-111, Aug. 10, 1948 (classified).
40. L. R. Jackson et al, Battelle, R-128, Jan. 1949 (classified).
41. W. H. Denton et al, The Heat Transfer and Pressure Loss in Fluid Flow through Randomly Packed Spheres, HPC-35, June 28, 1949.
42. B. Gamson et al, Trans. A.L.Ch.E. 39, No. 1, 1943.
43. W. E. Ranz, Chem. Eng. Prog. 48, No. 5, May 1952.
44. O. P. Bergelin et al, Research on Tubular Heat Exchangers UD-H6, University of Delaware, Oct. 1, 1950.
45. J. H. Perry, Chemical Engineers' Handbook, McGraw-Hill Book Company, Inc., New York, 1950, p 392.
46. A.S.M.E. Trans. 59, p 583.

SELECTED READING LIST

EXPERIMENTAL INVESTIGATION OF AVERAGE HEAT TRANSFER AND FRICTION COEFFICIENTS FOR AIR FLOWING IN CIRCULAR TUBES HAVING SQUARE-THREAD-TYPE ROUGHNESS, National Advisory Committee for Aeronautics, E. W. Sams, NACA-RME52D17, June 27, 1952, 42 pp.

ANALYTICAL AND EXPERIMENTAL INVESTIGATION OF FULLY DEVELOPED TURBULENT FLOW OF AIR IN A SMOOTH TUBE WITH HEAT TRANSFER WITH VARIABLE FLUID PROPERTIES, National Advisory Committee for Aeronautics, R. G. Deissler and C. S. Eian, NACA-TN-2629, Feb., 1952, 43 pp.

MEASUREMENTS OF AVERAGE HEAT TRANSFER AND FRICTION COEFFICIENTS FOR SUBSONIC FLOW OF AIR IN SMOOTH TUBES AT HIGH SURFACE AND FLUID TEMPERATURE, National Advisory Committee for Aeronautics, L. V. Humble, W. H. Lowdermilk, and L. G. Desmon, NACA-1020, 1951, 15 pp.

THERMODYNAMICS OF FLUID FLOW, N. A. Hall, 1st ed., Prentice-Hall, Inc., New York, 1951.

AN INVESTIGATION OF AIRCRAFT HEATERS XXXIV-EXPERIMENTAL DETERMINATION OF THERMAL AND HYDRODYNAMICAL BEHAVIOR OF AIR FLOWING BETWEEN A FLAT AND WAVE-SHAPED PLATE, National Advisory Committee for Aeronautics, L. M. K. Boelter et al, NACA-TN-2426, Aug. 1951, 30 pp.

CHEMICAL ENGINEER'S HANDBOOK, edited by J. H. Perry, 3rd ed., McGraw-Hill Book Company, Inc., New York, 1950.

LOSS COEFFICIENTS FOR ABRUPT CHANGES IN FLOW CROSS SECTION WITH LOW REYNOLDS NUMBER FLOW IN SINGLE AND MULTIPLE TUBE SYSTEMS, Stanford University, W. M. Kays, NP-3901, Jan. 1, 1950, 21 pp.

CORRELATIONS OF HEAT TRANSFER DATA AND OF FRICTION DATA FOR INTERRUPTED PLANE FINS STAGGERED IN SUCCESSIVE ROWS, National Advisory Committee for Aeronautics, S. V. Manson, NACA-TN-2237, Dec. 1950, 14 pp.

HEAT TRANSFER AND PRESSURE DROP FOR AIR FLOWING IN SMALL TUBES, Massachusetts Institute of Technology, W. H. McAdams, J. N. Addoms, and C. L. Kroll, NEPA-1688, Dec. 1950, 298 pp.

HEAT TRANSFER FROM HIGH TEMPERATURE SURFACES TO FLUIDS III-CORRELATION OF HEAT TRANSFER DATA FOR AIR FLOWING IN SILICON CARBIDE TUBE WITH ROUNDED ENTRANCE, INSIDE DIAMETER OF $\frac{3}{4}$ INCH, AND EFFECTIVE LENGTH OF 12 INCHES, National Advisory Committee for Aeronautics, E. W. Sams and L. G. Desmon, NACA-RM-E9D12, June 23, 1949, 33 pp.

AN INVESTIGATION OF AIRCRAFT HEATERS XXVII-DISTRIBUTION OF HEAT TRANSFER RATE IN THE ENTRANCE SECTION OF A CIRCULAR TUBE, National Advisory Committee for Aeronautics, L. M. K. Boelter et al, NACA-TN-1451, July 1948, 53 pp.

FRICTION COEFFICIENTS IN THE INLET LENGTH OF SMOOTH ROUND TUBES, National Advisory Committee for Aeronautics, A. H. Shapiro and R. D. Smith, NACA-TN-1785, Nov. 1948, 44 pp.

HEAT TRANSFER COEFFICIENTS FOR AIR FLOWING IN ROUND TUBES, IN RECTANGULAR DUCTS, AND AROUND FINNED CYLINDERS, National Advisory Committee for Aeronautics, R. E. Drexel and W. H. McAdams, NACA-ARR-4F28, Feb. 1945, 36 pp.

MEASUREMENTS OF RECOVERY FACTORS AND COEFFICIENTS OF HEAT TRANSFER IN A TUBE FOR SUBSONIC FLOW OF AIR, National Advisory Committee for Aeronautics, W. H. McAdams et al, NACA-TN-985, June 1945, 30 pp.

HEAT TRANSMISSION, W. H. McAdams, 2nd ed., McGraw-Hill Book Company, Inc., New York, 1942.

HEAT TRANSFER AND FLUID FLOW HANDBOOK, Fairchild Engine and Airplane Corporation, NEPA-1767, 57 pp, n.d.

Fuel Elements

The gas-cooled reactors considered to date have utilized solid fuel elements for which the general requirements have been:

- (1) Resistance to chemical attack or erosion by the coolant stream.
- (2) Retention of fission-product activity within the fuel element.
- (3) Mechanical stability against thermal stresses resulting from heat generation. and for which the heat-transfer requirements have been:
- (4) Adequate surface-to-volume ratio for selected operating power level. (A practical limit is imposed by stability of the particular materials of fabrication.)

Requirement (4) is determined not only by the power desired but also by the allowable free gas-flow area and by the heat-transfer coefficient at the solid-gas interface. In power reactors, a high surface-to-volume ratio, consistent with the mechanical stability of the fuel element and the neutron economy of the reactor, is desirable to minimize both the pumping power and the reactor size. There is, however, an optimum amount of absorbing material that may be introduced in adding heat-transfer surface to a specific volume of fuel. Extended surfaces are utilized more efficiently if they can be designed as fuel-bearing members. In thermal power reactors, a substantial amount of moderator material must be closely associated with each fuel element, and a high surface-to-volume ratio is again required. Designs which incorporate fuel and moderator together in the same mass have the advantage that all surfaces exposed to the coolant gas can be very nearly equally effective in transferring heat. There is some improvement, too, in neutron economy if the uranium can be coated with a moderating metal such as beryllium to keep the fission products out of the coolant stream.

This chapter is concerned only with the confinement of reactor fuel in such a manner that fission products will be prevented from diffusing into the gas stream. In this regard the chapter outlines some practical designs for gas-cooled fuel. Chapter 3.6 describes practical fuel-element configurations and coolant-gas distribution in reactor cores.

In current designs of gas-cooled reactors, uranium or uranium oxide is enclosed in a thin casing of metal, such as aluminum or stainless steel, to prevent oxidation of the uranium and to confine fission products within the fuel element.

ROD-TYPE FUEL ELEMENTS

For unenriched graphite-moderated air-cooled reactors, neutron-economy requirements dictate the use of a low-cross-section cladding material, such as aluminum, zirconium, or beryllium, for uranium. Aluminum has been the most extensively developed. Gurinsky noted early in the Manhattan Project that uranium in contact with aluminum formed an intermetallic compound, now known to be UAl_3 , at temperatures as low as 200° - 300° C. With

a clean aluminum surface in contact with a clean uranium surface, this alloying reaction causes an increase in volume of about 17 percent. The uranium diffuses to the aluminum surface through the UAl_3 layer, and if the aluminum surface is that of a thin-walled container, the aluminum above the expanding alloy is forced up to form a blister which is visible on the outside of the can. The maximum penetration rate of the alloy into the aluminum is shown as a function of aluminum-uranium interface temperature in Table 3.5.1 and Fig. 3.5.1.

The alloying reaction can be prevented either with an anodic coating on the aluminum or by the presence of another diffusion barrier, such as $U(AlSi)_3$, formed on the uranium slug surface by immersion in a molten aluminum-silicon alloy prior to canning.

A second feature of the uranium canning operation is the elaborate weld-sealing process required to exclude oxygen which reacts with the uranium to cause swelling and rupture of the can. The rate of oxidation is strongly temperature dependent, being about 27 times as fast at 250°C as it is at 100°C.¹

Operating experience dictates that aluminum-jacketed, uranium fuel elements should not be operated at an interface temperature above 225°C. Above this temperature, there is a marked tendency toward instability of the fuel element owing to either or both of the above causes. For operating temperatures below 225°C, the following canning and testing procedure, developed at Oak Ridge, can be used:

UNBONDED, ALUMINUM-JACKETED, URANIUM FUEL ELEMENTS

(E. J. Boyle and C. D. Cagle, ORNL)

CANNING PROCEDURE

These elements are prepared by drawing the 2S-aluminum cans on the uranium slugs; i.e., the slug is inserted in the can, and the assembly is forced through a sizing die. Fuel elements with the following specifications have been employed:

Resistance-welded

Aluminum can

Material	2S, impact-extruded
Length, in.	4.375
ID, in.	1.116
Wall thickness, in.	0.017 to 0.020

Uranium

Material	gamma-extruded
Length, in.	4.000 ± 0.010
Diameter, in.	1.100 ± .002
Chamfer on bottom end, in. radius	0.010

Arc-welded

Aluminum can

Material	2S, impact-extruded
Length, in.	4.375
ID, in.	1.116
Wall thickness, in.	0.035

¹ References appear at end of chapter.

Uranium

Material	gamma-extruded
Length, in.	4.000 ± 0.010
Diameter, in.	$1.100 \pm .002$
Chamfer on bottom end, in. radius	0.010

The arc-welded slugs differ from the resistance-welded units in that a somewhat heavier cap (1.102 in. in diameter and 0.060 in. thick) is compositely forced through the die in the drawing operation. The excess wall metal is trimmed to the lip of the cap, and the cap and wall are then joined by argon arc-welding.

ALUMINUM-SILICON BONDING OF ALUMINUM-JACKETED, URANIUM FUEL ELEMENTS (E. J. Boyle and C. D. Cagle, ORNL)

Stabilization of aluminum-jacketed uranium fuel elements above 225°C has been achieved by coating the uranium with $U(AlSi)_3$ to prevent the alloying reaction and protect against oxidation resulting from leaks in the aluminum welds. The dimensional specifications for the slugs are:

Uranium slug	
Diameter, in.	$1.102 - 0.003 + 0.000$
Length, in.	$4.000 - .000 + .005$
Corner radius, in.	$0.060 - .000 + .040$
Material	alpha-rolled
Aluminum can	
ID, in.	$1.121 + 0.000$ $- 0.003$
Wall thickness, in.	$0.033 + 0.000$ $- 0.003$
Bottom thickness, in.	0.051 ± 0.005
Length, in.	$4-21/32 \pm 1/64$
Material	2S, deep-drawn
Canned slug	
Length, in.	4.120 ± 0.0065
Bond layer thickness, in.	0.004 to 0.0065

CANNING OF URANIUM IN ANODIZED ALUMINUM TUBING (D. H. Gurinsky, BNL)

The uranium-aluminum alloying reaction may be prevented by interposing a diffusion barrier, consisting of a coating of aluminum oxide, on the inside of the aluminum container tube. A fuel element with this feature is described below.

The BNL fuel element is an 11-ft element consisting of thirty-three 4-in., natural-uranium slugs encased in a six-finned aluminum tube. Physics calculations for this reactor established the aluminum-to-uranium volume ratio at 0.2. This rather low ratio resulted in a very-thin-walled tube (0.028 to 0.030 mils thick) and very slender, tapered fins (0.6 in. high, 0.025 in. at the base, and 0.018 in. at the tip). Four-in.-long uranium slugs were selected because little was known of the warping tendencies and the difficulties of machining and heat-treatment of long rods.

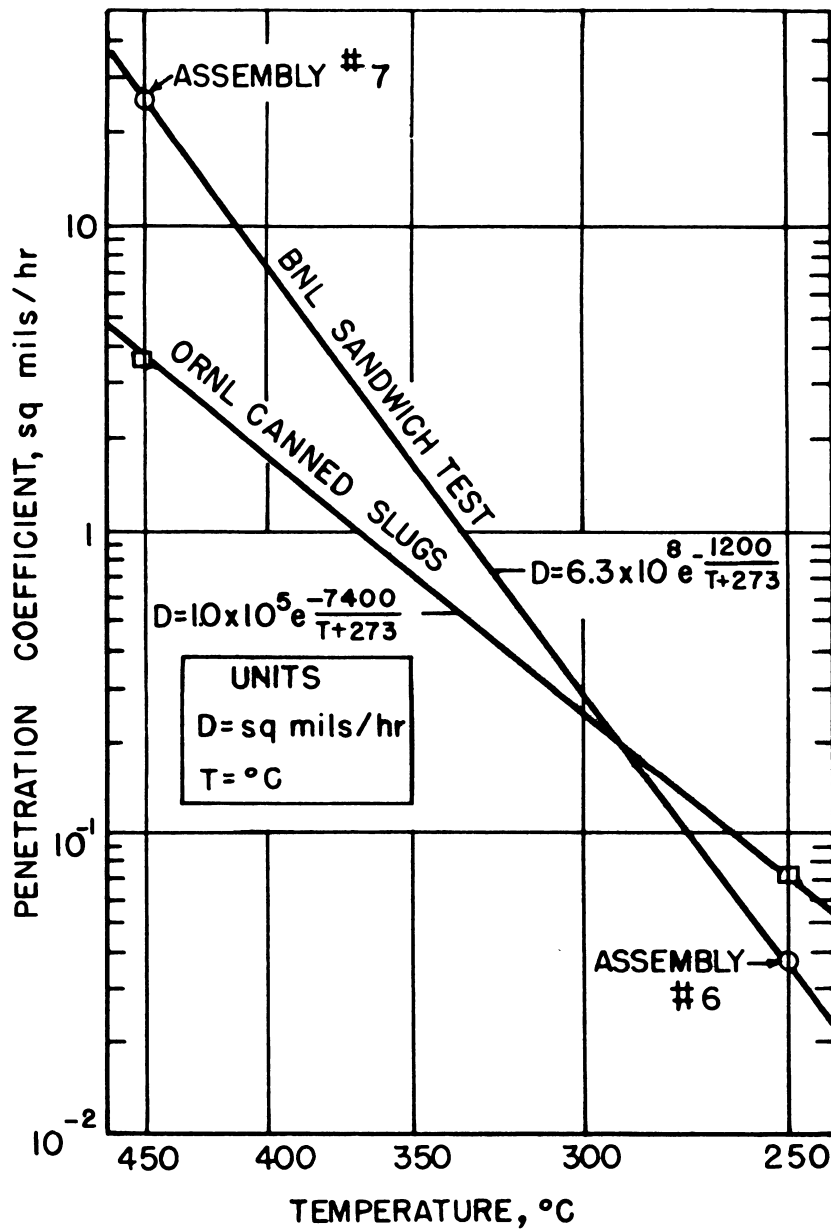


Fig. 3.5.1 — Variation of the Maximum Aluminum Penetration Rate with Temperature (BNL and ORNL Data). Reprinted from BNL-38, Dec. 15, 1949 (BNL Log No. D-2106).

Table 3.5.1—Minimum Time Required to Penetrate 30 Mils of Aluminum by the Uranium Alloying Reaction

(D. W. Bareis, Studies of the Aluminum-Uranium Alloying Reaction, BNL-38, Dec. 15, 1949)

Temperature, °C	Time for penetration	
	BNL sandwich assemblies	ORNL canned slugs
250	990 days	510 days
300	130 days	150 days
350	22 days	52 days
400	130 hr	21 days
450	35 hr	10 days

FABRICATION OF FINNED TUBING

The details of fabrication* of the finned tubing are described in Warner.² To summarize, the tubing was extruded from a 2S-aluminum billet $6\frac{1}{8}$ in. OD by 12 in. long; each billet resulted in approximately 95 ft of tubing. The extrusion temperature was 538°-540°C, the extrusion pressure 66,000 psi, and a so-called web-type die, in which the mandrel is stationary, was used. In this case, the metal was forced through six ports, the streams from these six ports joining in the mixing chamber and the tube forming around the mandrel which faces that part of the die in which the fins are formed.

This tubing represented shape and thickness requirements which had not been met in the industry before and therefore required a great deal of experimentation on the part of the fabricating company. The essence of the problem lay in equalizing the frictional forces existing at the land of the mandrel and at the faces along which the fins had to pass. Since the tubing could not be extruded to the tolerances required, the extruded shape was subjected to one drawing operation which resulted in a cold working of the order of 15 percent. Only the tubing itself was subjected to the drawing friction. Since the fins are attached to the tube, these are also worked because they must extend to the same degree as the tubing. The tubing was subjected to a pressure test of 90 psi prior to shipment by the company and had to pass an inspection based on the specifications listed for Fig. 3.5.2.

SELECTION AND MACHINING OF URANIUM

The uranium was cast into 9-in.-long by 4-in.-OD right cylinders and extruded at the Hanford Works into bars 1.24 in. in diameter. The extruded bars were shipped to the Chapman Valve Company for machining.³ The bars were first straightened, then machined on a six-spindled Conomatic lathe, where the average time per 4-in. slug was 30 sec. The slugs came out of this machine approximately 0.010 in. oversize in diameter and 0.020 in. oversize in length. They were then heat-treated for 12 hr at 600°C in an argon atmosphere to decrease the hydrogen content of the metal, to relieve the quenching, forming, and machining stresses, and to minimize the tendency to warp.

The slug diameter was brought to final dimensions in a centerless grinder. A button was machined on the end of the slugs and finished to length on a hand-operated turret lathe. After this operation, the slug was slotted along its full length. Then the slugs were again heat-treated (400°C) to remove traces of oil and water. The dimensions and tolerances are given in Fig. 3.5.3.

* Fabricated by Alcoa.

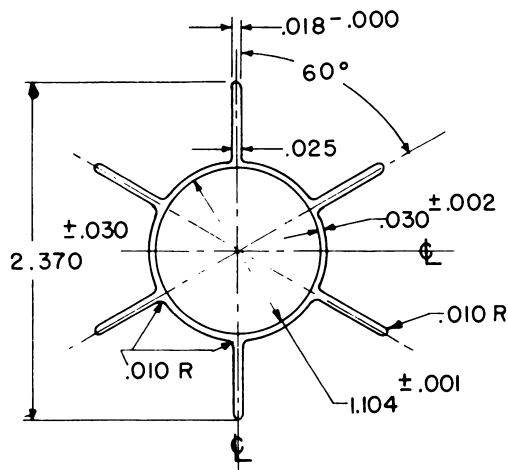


Fig. 3.5.2—Specifications for Finned Aluminum Tubing. Reprinted from BNL- 54, May, 1950 (BNL Log No. D-437).

Purity:

Standard specifications for 2S aluminum; impurities not to exceed 1%.

Dimensions:

- (1) Wall thickness: 0.030 in. \pm 0.002 in.
- (2) Internal diameter: 1.104 in. \pm 0.001 in., subject to specification No. 11.*
- (3) Distance from tip of one fin to tip of opposite fin: 2.370 in. \pm 0.030 in.
- (4) Fin dimensions at tip: 0.018 in. - 0.000 \pm .†
- (5) Spiral of fin: 1°/ft.

Special specifications:

- (6) Weight per foot: Not to exceed 0.230 lb/ft.
- (7) Bowing of tube: Not greater than 0.100 in. in 10 ft.
- (8) Plug test: The tube is acceptable if it shows no sign of rupture after a tapered steel plug has been driven into both ends so as to expand the inside diameter by $\frac{1}{8}$ in.
- (9) Pressure test: An air pressure of 90 psi shall be applied to the inside of each tube for a period of not less than 5 sec. Any tube which leaks, as indicated by the formation of air bubbles in the testing fluid, shall be rejected.
- (10) Surface inspection: The tubing and fin shall be clean, smooth, and free from seams, slivers, laminations, grooves, cracks, blisters, and other injurious defects.
- (11) Clearance: A 4.500 in. \times 1.101 in. O.D. Micarta rod with chamfered ends shall readily pass through each tube. This will be considered the "Go" gauge. The "No Go" gauge shall be 4.5 in. long by 1.105 in. O.D. and should not pass through the tube.
- (12) Finished length: 12 ft-6 in. \pm 0.5 in.
- (13) Packaging: Each tube should be encased in a $\frac{3}{16}$ -in.-wall mailing tube for its full length and then shipped in a substantial wooden crate, the latter to be so constructed that the material can be repacked in the same container, i.e., closure can be effected by means of screws or straps of metal.‡

Acceptance of material which does not meet with all of the above specifications will depend on special arrangements which shall be made between the Aluminum Specialties Co. and ALCOA's Inspection Department.

* This dimension is stated; however, acceptance will be based on specification No. 11.

† Subject to specification No. 6.

‡ This shape corresponds to ALCOA die No. 26873.

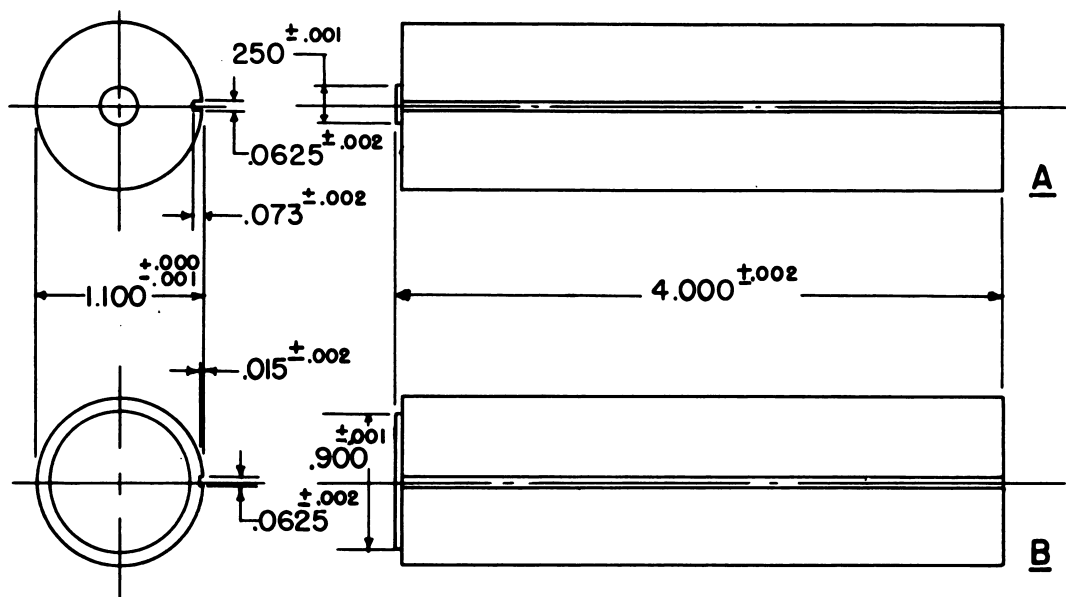


Fig. 3.5.3—Uranium Slug Specification. Reprinted from BNL-54, May 1, 1950 (BNL Log No. D-2054). End faces must be parallel within ± 0.001 in reference to slug axis; cylindrical section to be ground finished; tool marks not to exceed 0.003 in. on ends; remove all burrs. (A) Original slug; (B) Revised slug.

Final Handling

(1) Special precaution must be taken to ensure that the slugs after the second degassing operation shall not be permitted to come in contact with water or moisture, including possible moisture through accidental handling of slugs with bare hands or damp gloves.

(2) Cleaning and dusting of slugs after second degassing and prior to hermetically sealing in cans. Slugs shall be brushed and wiped after the second degassing operation to remove any loose or adherent dust and scale.

(3) Time limit of slug exposure to atmosphere after final degassing shall be limited to a maximum of 24 hr.

THE CANNING OPERATION

The actual canning consisted of 13 individual operations:

- (1) Chemically stripping anodized film
- (2) Trimming finned tube
- (3) Welding butt closure
- (4) Dehydrating anodized film
- (5) Leak test #1—welded closure and tube wall
- (6) Loading welded can
- (7) Trimming loaded can
- (8) Induction-brazing cartridge
- (9) Leak test #2—cartridge
- (10) Collapsing cartridge wall
- (11) Flame-brazing anchor
- (12) Flame-brazing helium tube
- (13) Leak test #3—completed assembly

Step (1) was required because it was found impossible to execute a good arc weld without it; steps (2) and (3) follow naturally. Step (4) was required as a result of some heat tests in which it was noted that the anodic coating absorbed up to 1 to 2 cc of water. This water reacted with uranium on heating to form hydride producing minor bumps which were considered undesirable. Steps (5), (6), and (7) again follow. Induction-brazing was selected over argon arc-welding because a good job of removing the anodic film was considered difficult. Once the details had been worked out, the brazing was very straightforward and yielded a high percentage of acceptable cartridges. Step (10), collapsing of the cartridge, was decided upon when it was realized that these cartridges might breathe unless a constant pressure could be maintained within the cartridge, even though the coefficients of expansion of the uranium and aluminum were different. For details of this calculation, see Warner.²

Since the cartridge temperature was to change from essentially room temperature to 350°C with an associated 1-in. elongation, the cartridge had to be anchored somehow to the graphite structure to prevent "walking" of the assembly under reactor operating conditions. These considerations resulted in step (11).

One of the advantages of a long cartridge is that it is possible to attach to it a conduit through which a constant gas-pressure may be maintained on the interior of the cartridge. It should thereby be possible, by proper manifolding and pressure-measuring devices, to determine a leaking cartridge before serious difficulties develop. For this reason, a 40-ft so-called "helium" tube was brazed to each of the cartridges. The final leak test, step (13), consisted of pressurizing with helium the interior of the finished assembly while it was in an evacuated tube. A leak in the cartridge would result in the escape of gas to the evacuated tube which was under constant surveillance by a helium mass spectrograph. This test was extremely sensitive in that the over-all pressure differential between the interior and exterior of the cartridges was of the order of 100 psi. Figure 3.5.4 is an assembly drawing of the completed cartridge.

DEVELOPMENT WORK

Final design of the unit elements was determined by a number of tests on the components, one of the most important of which was a study of the interaction of uranium and aluminum at elevated temperatures. Since this fuel element was to be operated at a 350°C uranium-aluminum interface temperature, some barrier had to be evolved. Experiments performed at Brookhaven and MIT indicated that if aluminum were anodized the reaction between ura-

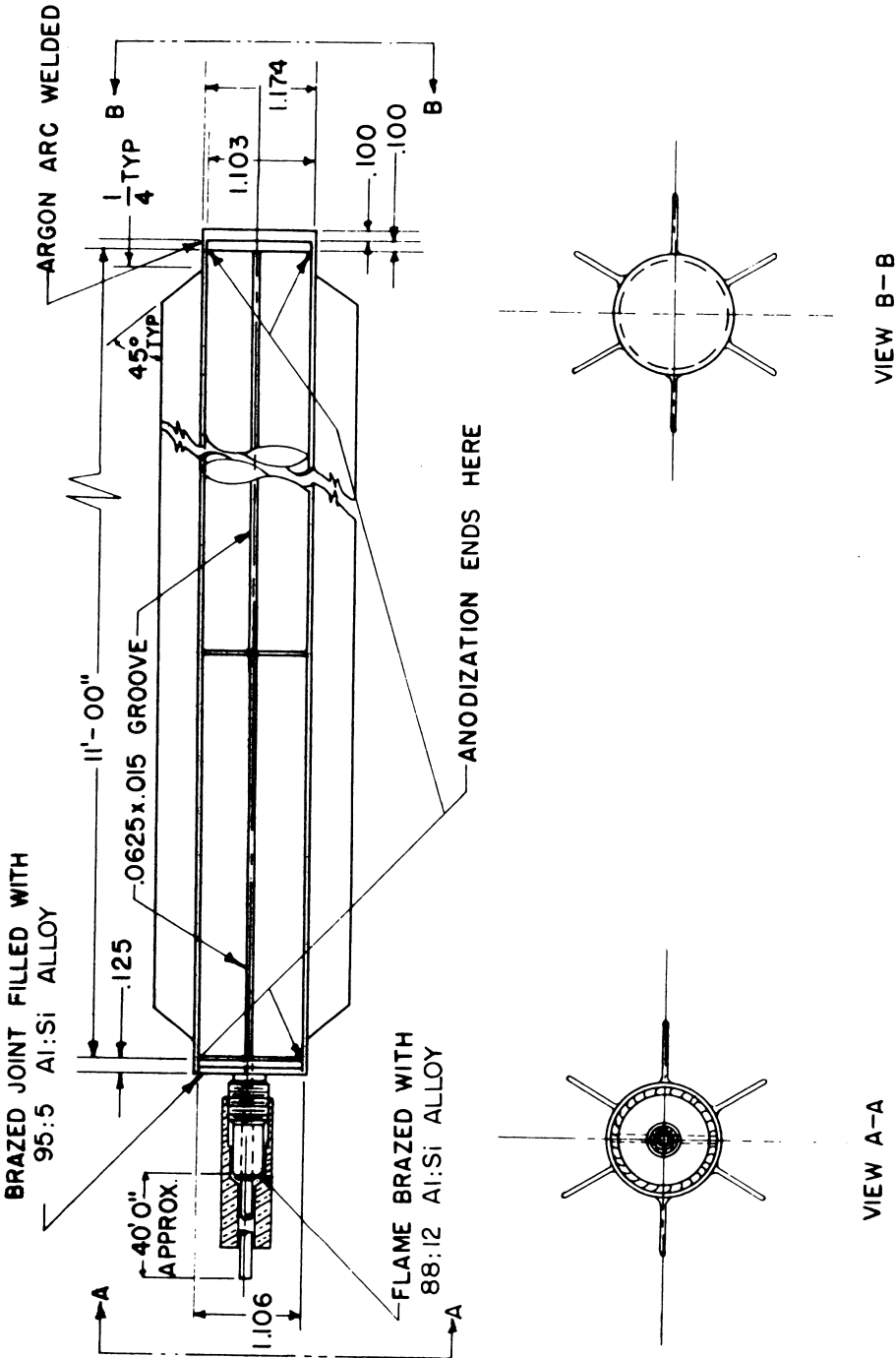


Fig. 3.5.4— Cross Section of Anodized, Aluminum-jacketed, Uranium Fuel Element. Reprinted from BNL-54, May 1, 1950 (BNL Log No. D-745).

nium and aluminum did not take place even over one month at temperatures as high as 550°C. The subsequent development of a method for anodizing the interior of a 12-ft-long tube to a thickness of 0.6 mil is described in detail by Warner.²

Since the weight of the uranium must be supported by the rather fragile fins, the factor of safety was determined by engineering tests⁴ using loads two, three, four, six, and eight times that expected at the operating temperature (350°C).

CORROSION OF ALUMINUM JACKET IN AIR

Since this element was to be cooled by air known to contain a small amount of salt, a number of corrosion tests were conducted at 350°C. In these tests, a mist of air and salt water, which was held above the dew point even though salt was being deposited, was passed over the finned cartridge. No corrosion was observed under these conditions.

The corrosion behavior of aluminum in air at 400°, 450°, and 500°C has also been determined. The weight gains to date are 0.5 mg/in.² for 6500 hr, 1.1 mg/in.² for 6500 hr, and 1.4 mg/in.² for 4828 hr of exposure. Weight-gain curves⁵ show that the weight gain has leveled off for the 400° test but is still rising for the 450° and 500° tests.

REFERENCES

1. E. J. Boyle and C. D. Cagle, Fuel Elements for ORNL Graphite Reactor, Oak Ridge Nat. Lab., CF-526-10.
2. W. T. Warner, Brookhaven Nat. Lab., BNL-54, May 1950 (classified).
3. HKF-4 (classified).
4. TID-5061 (classified).
5. BNL Log No. C-6032.

CHAPTER 3.6

Circulating Systems

DESIGN CONSIDERATIONS IN REACTOR CORE

RADIAL POWER DISTRIBUTION

For most design purposes, the radial flux distribution over the active core of a cylindrically loaded reactor can be assumed to follow the Bessel function $J_0(2.405 r/R)$, where r is the distance from the central axis and R is the augmented radius of the reactor. Because of the effect of neutrons from the reflector, there is a slight perturbation in flux near the edge of the loading as shown in Fig. 3.6.1. From a heat transfer and pressure drop point of view, the ideal power distribution would be where the heat released per unit volume equalled any radius of loading. This is probably not a realistic case because loading of fissionable material to obtain such an ideal power distribution would be exceedingly difficult. However, it is possible to flatten the radial power distribution significantly by nonuniform loading of the reactor with fissionable materials.

Two design methods devised for flattening the radial thermal flux are shown in Table 3.6.1.

AXIAL (LONGITUDINAL) POWER DISTRIBUTION

The shift in position of maximum flux owing to a separation of 2.75 in. between 25- × 25- × 12.5-ft halves of a typical unenriched reactor is shown in Table 3.6.2. The radial flux distribution is estimated to vary as a sine function between this point of maximum flux and a zero point 1.5 ft from the low-flux end of the fuel elements.

HEAT TRANSFER AND PHYSICS

Large heat-transfer area per unit volume of reactor is obtained with flow passages of small hydraulic radius. Because of the limited heat capacity of a gas, however, small fluid-flow passages necessitate a "pancake" reactor configuration (high ratio of diameter to flow passage length) which results in unfavorable geometry from a nuclear and shielding standpoint. Engineering problems are greatly decreased if relatively large passage diameters are employed. This, however, implies an increase in reactor dimensions. As the passage diameters are decreased, the length of the heated passages decreases for a fixed temperature rise of the fluid at fixed mass velocity and fixed pressure drop. The frontal area required for flow is not changed, however. The total frontal area of the reactor can be decreased by increasing the mass velocity (by increasing the linear velocity or increasing the gas density) or by increasing the fraction of the reactor frontal area which is utilized for fluid flow. From a heat-transfer standpoint, it is desirable to utilize all of the reactor frontal area for flow passages. From a nuclear standpoint, however, this is impossible, and a compromise must be achieved, but in the present state of the art, no "optimum" solution of the problem is apparent. The best approach is to set up several

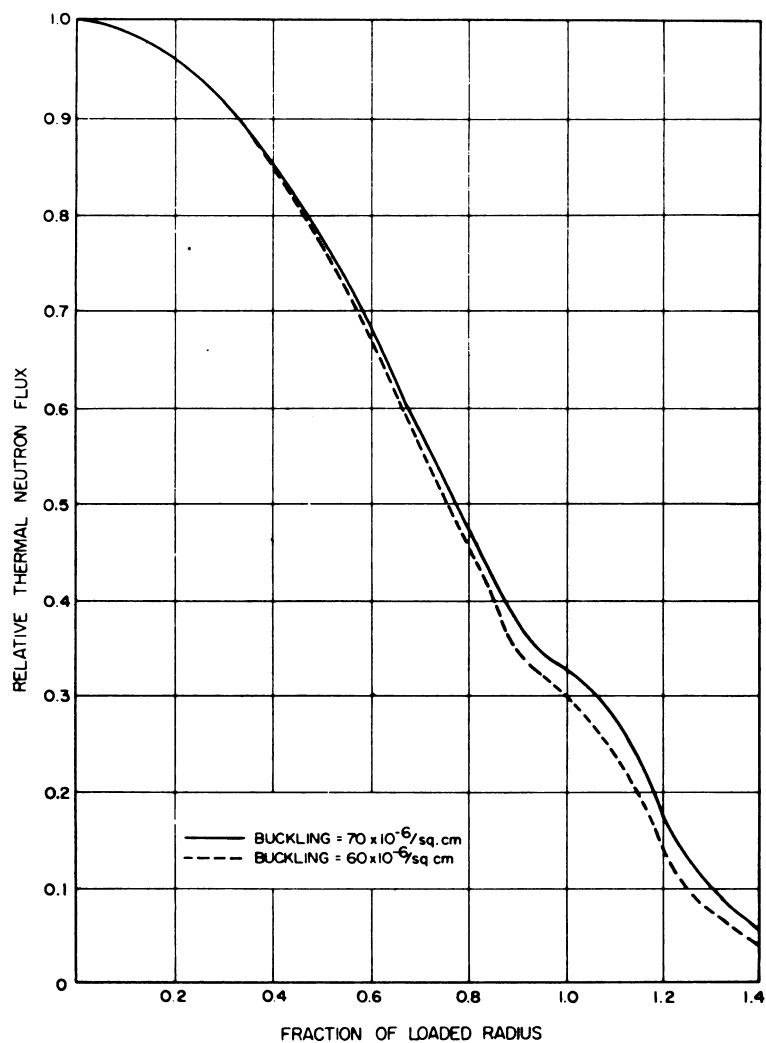


Fig. 3.6.1— Radial Thermal Flux Distribution for a Uniformly Loaded, Un-enriched, Cylindrical Reactor With Reflector. Reprinted from BNL-152, Jan. 1952.

Table 3.6.1—Methods of Flattening Radial Thermal Flux

Method	Where applied
"Bowling"; increasing the ratio of uranium to reactor volume as a function of loading radius	X-10 reactor (thermal), Oak Ridge
Poisoning central portion of reactor	Brookhaven reactor (thermal)

Table 3.6.2—Shift of Position of Maximum Axial Flux Caused by Gap at Center of Unenriched Uranium Reactor

(I. Kaplan and J. Chernick, The Brookhaven Nuclear Reactor: Theory and Nuclear Design Calculations, BNL-152, Jan. 1952)

Radius of loading, ft	Position of maximum axial flux (distance from central plane), ft
9.52	2.31
10.41	2.08
11.21	1.90
11.95	1.77
12.64	1.66

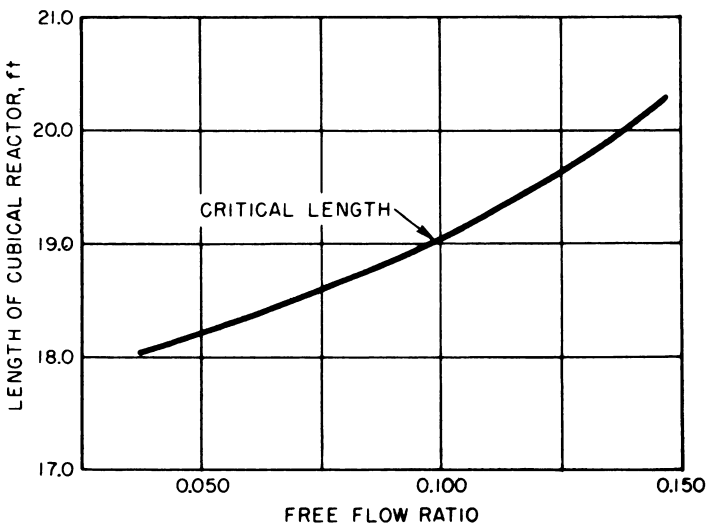


Fig. 3.6.2— Critical Length of a Bare, Cubic, Unenriched-uranium, Graphite-moderated Reactor as a Function of Channel Area. Reprinted from BNL-152, Jan. 1952. Lattice dimension, 8 in.; aluminum-uranium volume ratio, 0.2; radius of fuel rod in channel, 1.40 cm.

hypothetical designs on the basis of known requirements of gas flow, temperature rise, and pressure-drop range, make certain basic assumptions, and then study the effects of the introduction of the several variables in turn.

The effect of varying parameters is illustrated in Fig. 3.6.2 for an unenriched-uranium, graphite-moderated reactor. (For background information on the latter figure refer to BNL-152.)

STRAIGHT-THROUGH VS SPLIT-FLOW DESIGN

Because of the nature of the sinusoidal flux pattern in the axial direction in cylindrical reactors, considerable study has been given to designs that permit the coolant gas to enter a reactor at the center between halves of the cylinder. The gas then distributes itself from

the central header through the fuel-containing passages. Compared to a straight-through reactor, the cooling gas in such a "split-flow" design must travel only half as far (dis-counting the length of flow path down the central header). In addition, the coolest gas is supplied to the point where the heat generation per pound of uranium is greatest. Such an arrangement permits reactors of the same longitudinal length as the straight-through type to have smaller radii of loading (smaller uranium investment) for the same gas-pumping power because of the smaller free-flow area required. Thus, shield diameters and possibly shield weights are somewhat smaller with split-flow design than they are with straight-through design. Reactor designs with L/D ratios < 1 , so-called "pancake" reactors, have the same advantage of shortening the length required for gas flow and, when the proper L/D ratio is selected, have a smaller uranium investment than straight-through designs although the shielding diameter is greater than that of the split-flow type. The effect of varying the L/D parameter is illustrated in Table 3.6.3.

For the same pumping power and reactor loading in unenriched-uranium experimental reactors, a significantly greater flux level can be obtained with the split-flow design. One split-flow reactor now operating has a power level eight times higher than a similar type of reactor with straight-through design while the pumping power is only four times as high. The effect of the gas header in the center of the split-flow reactor is shown in Fig. 3.6.3 as a function of gap width for an enriched-uranium reactor in terms of U^{235} requirement. Figure 3.6.4 shows a similar effect for an unenriched, graphite-moderated reactor.

Two methods have been devised for reducing over-all pressure drop in straight-through reactors so that they can compete with the split-flow type. These are:

1. Use of lower volume ratios of fuel elements to coolant in the entrance region of the reactor where the coolant is at a lower temperature.
2. Use of variable-area flow channels with smaller area where a higher heat-transfer coefficient is desired.

FLAT-PLATE REACTOR

Another design flow configuration which takes advantage of shorter flow paths and higher temperature driving forces between fuel element and coolant is illustrated in Fig. 3.6.5. The gas enters along the central axis of the cylinder and fans out along the radii. A comparison of reactor diameter and solidity for this and the straight-through types of reactor is shown in Fig. 3.6.6 for a pressure drop of 2.97 atm and an initial pressure in each case of 10.97 atm.

FOLDED REACTOR

A fourth configuration, not as yet fully developed, for gas flow through reactors, uses very short heat-transfer passages of small diameter. The fuel elements of such a reactor would consist of layers of fine-mesh wire screening or other suitable mechanical arrangements for obtaining large surface-to-volume ratios and small diameter passages. The arrangement shown in Fig. 3.6.7 would allow the coolant to flow down a header of constantly decreasing width inside the reactor and to split off from the main stream as needed for fuel-element cooling.

Table 3.6.4 presents calculated comparisons¹ of through-drilled and folded configurations. The calculated pressure drop includes friction and turning losses for both power levels. The pressure drop owing to acceleration upon heating was negligible for the 60,000-kw reactor but was significant for the high mass-flow rate for the 750,000-kw reactor.

¹Reference appears at end of chapter.

Table 3.6.3—Uranium Inventories for “Pancake” and Split-flow Air-cooled Reactors with 5-in. Reflector

(NEPA Project quarterly Project Report for the Period July 1,—Sept. 30, 1950; NEPA-1587)

Free-flow area, ft ²	Core volume, ft ³	“Pancake” reactors				Split-core reactors			
		Ratio length to diameter	Core diameter, ft	Free-flow ratio	U ²³⁵ , lb	Ratio of length to diameter	Core diameter, ft	Free-flow ratio	U ²³⁵ , lb
3	12.3	0.41	3.36	0.34	210	0.9	2.58	0.287	82
3	16.3	.49	3.48	.315	72	.9	2.85	.235	65
3	21.2	.56	3.64	.288	49	.9	3.1	.20	50
3	29.0	.68	3.78	.267	41	.9	3.45	.16	47
6.55	29.0	.325	4.83	.36	160	.9	3.45	.35	110
6.55	40	.45	4.84	.356	75	.9	3.83	.284	80
6.55	50	.55	4.87	.35	54	.9	4.13	.24	70
6.55	70	.65	5.16	.313	38	.9	4.63	.2	64
15	70	.275	6.87	.4	200	.9	4.63	.445	155
15	100	.33	7.28	.36	115	.9	5.21	.35	120
15	150	.48	7.36	.35	100	.9	5.96	.27	115

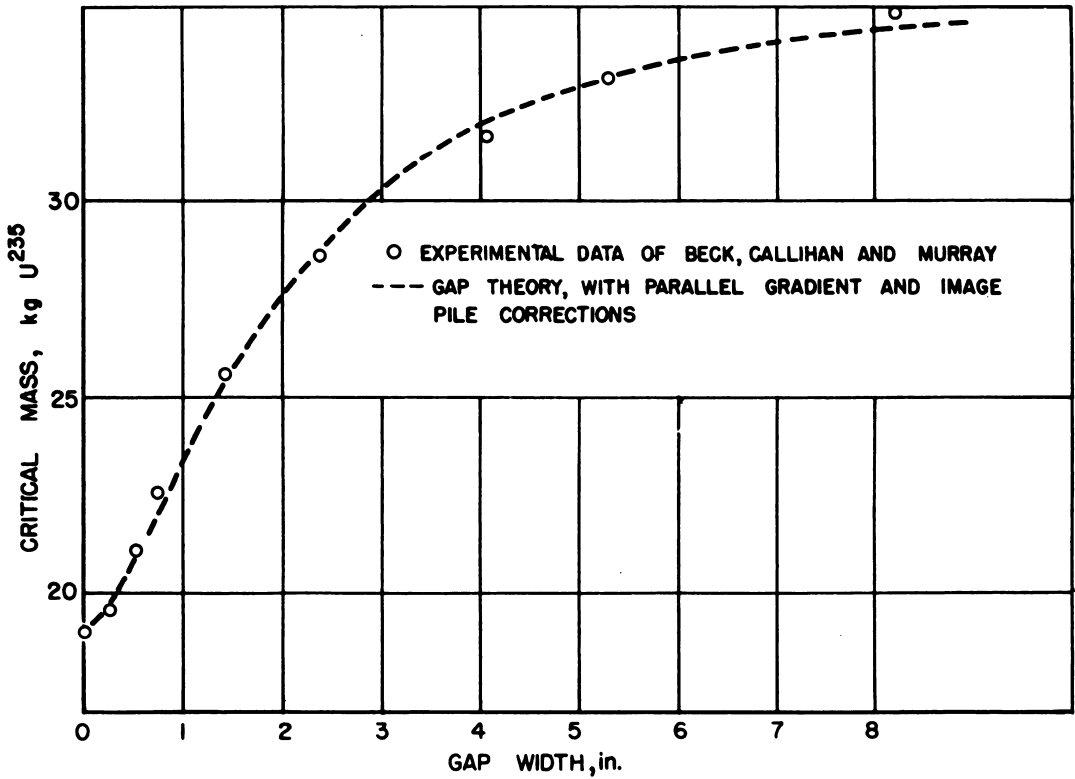


Fig. 3.6.3— Effect of Gap Width on Critical Size for an Enriched-uranium Re-actor.

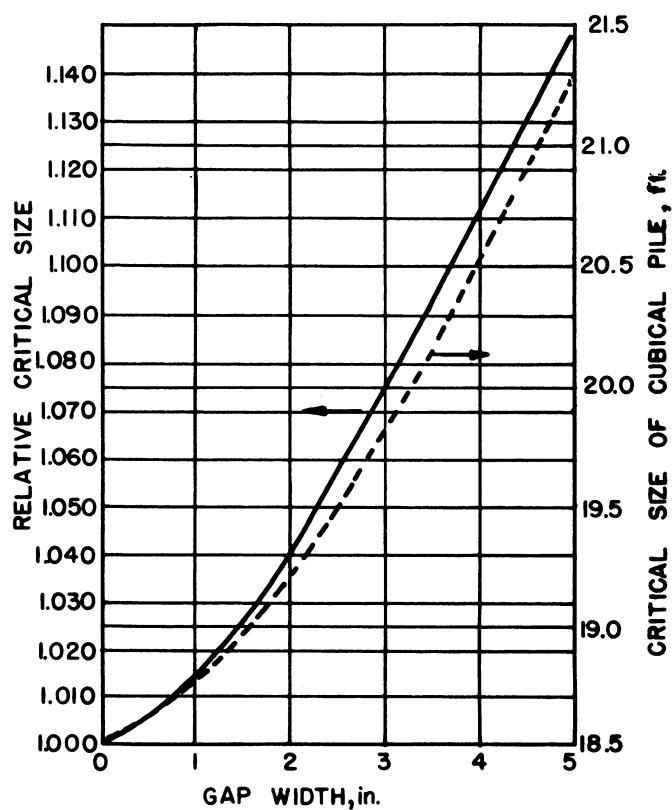


Fig. 3.6.4 — Effect of Central Transverse Gap Width on Critical Size for Cubical, Graphite-moderated, Natural-uranium Reactor. Submitted by BNL, Sept. 1952.

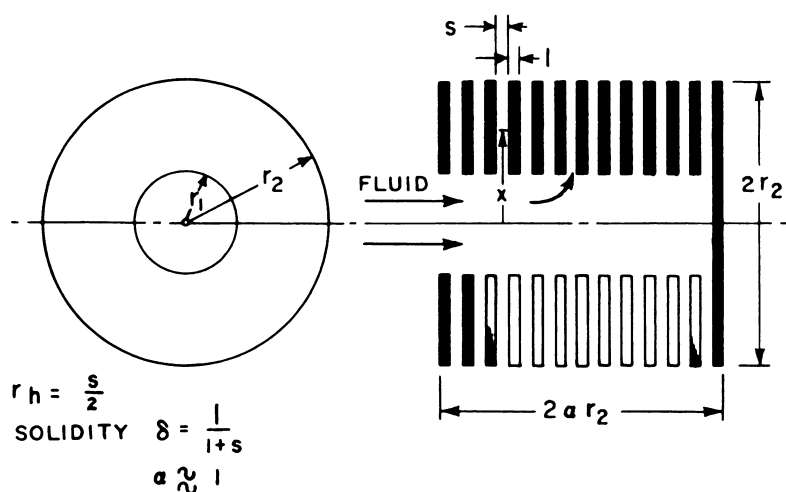


Fig. 3.6.5—Schematic Drawing of a Flat-plate Reactor. Reprinted from NAA-SR-5, May 7, 1948.

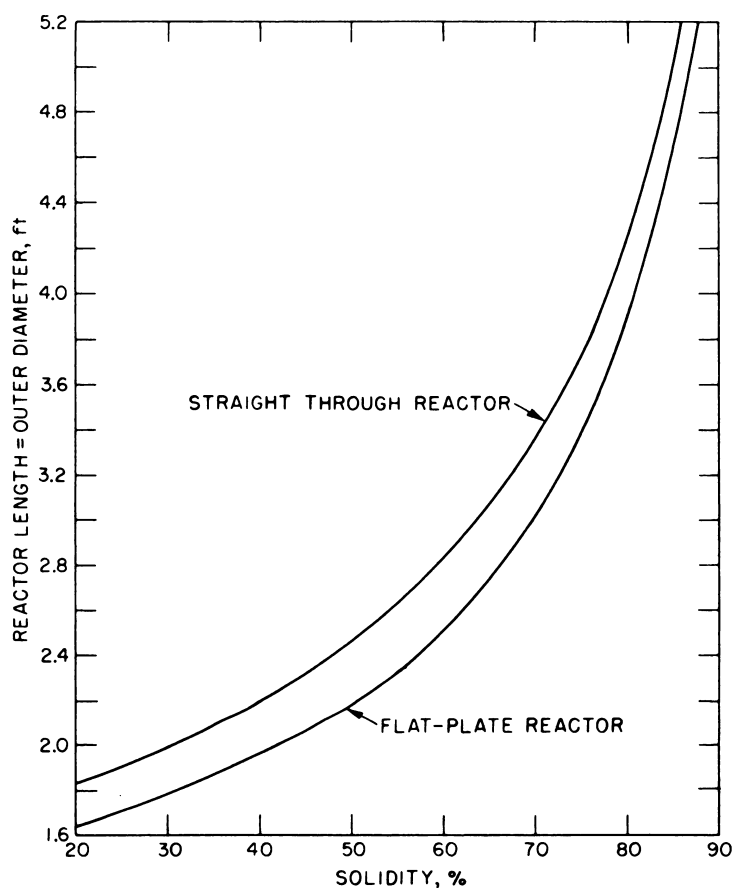


Fig. 3.6.6—Comparison of Reactor Diameter and Solidity Requirements for Straight-through and Flat-plate Designs. Reprinted from NAA-SR-5, May 7, 1948. Based on the following conditions: Heating—466 lb/sec air from 1216°R to 3073°R; entrance pressure—10.97 atm; exit pressure—8.0 atm; and reactor wall temp. = 4091°R.

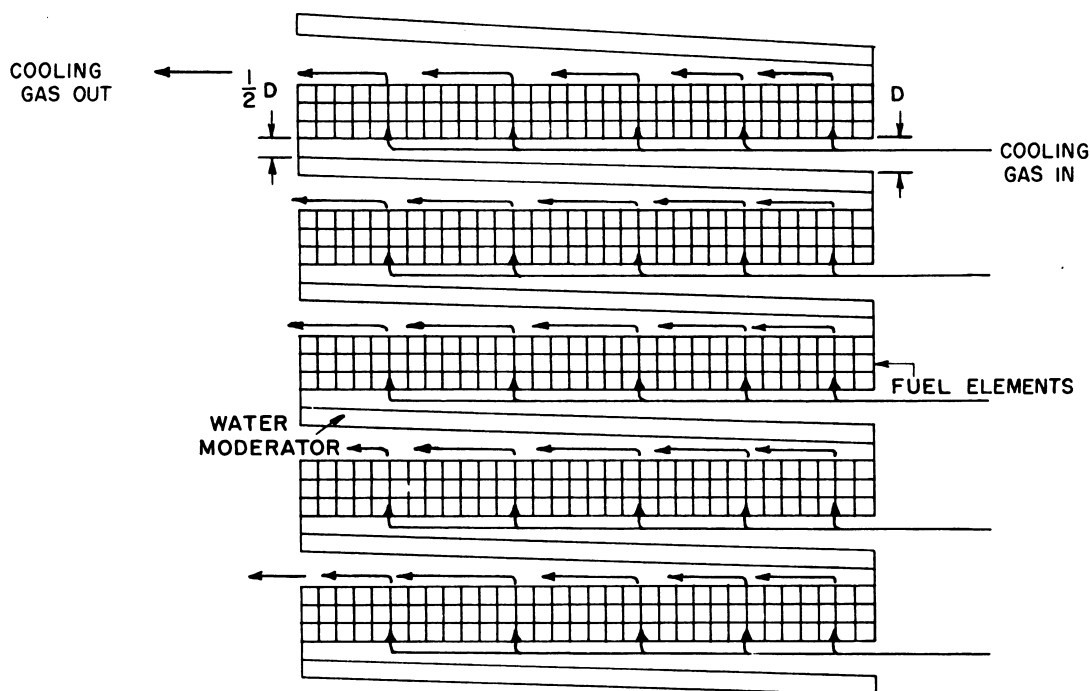


Fig. 3.6.7—Schematic of Folded Reactor. Submitted by BNL, Sept. 1952.

Table 3.6.4—Comparison of Through-drilled and Folded Configurations
 (R. W. Dayton et al, A High-Power-Density Gas-Cooled Reactor Core Configuration,
 BMI-T-27, May 15, 1950)

Characteristic	60,000-kw reactor (2-psia press. drop)				750,000-kw reactor (15-psia press. drop)		
	Straight	Folded			Straight	Folded	
Coolant passage length, in.	48	2	4	6	48	2	4
Approximate hole diameter, in.	0.12	0.0055	0.010	0.017	0.30	0.018	0.050
Approximate plate solidity, %	...	920	930	935	...	950	955
Convective temperature drop, °F	80	13	30	60	640	420	800
Conductive temperature drop, °F	60	1	1	1	700	15	120
Pressure, psia	1500				1500		
Reactor volume, cu ft	64				64		
Solidity, %	80				80		
Coolant	Helium				Helium		
Moderator	Beryllium				Beryllium		
Coolant exit temperature, °F	1,000				2,000		
Coolant entrance temperature, °F	400				400		
Coolant average temperature, °F	700				1200		
Coolant viscosity, lb/(ft)(sec)(°F)	22×10^{-6}				28×10^{-6}		
Coolant thermal conductivity, Btu/(ft)(sec)(°F)	41.5×10^{-6}				52.5×10^{-6}		
Moderator thermal conductivity, Btu/(ft)(sec)(°F)	0.0067				0.0032		
Coolant flow rate, lb/sec	75.5				355		

The convective temperature drop determines the surface temperature of the wall materials, while the conductive temperature drop is the cause of thermal stresses.

DESIGN CONSIDERATIONS IN EXTERNAL CIRCULATING SYSTEM

The use of high pressures and high temperatures, the desirability of small pressure losses in the system external to the reactor, and the potential hazard of radioactivity in the circulating gas call for special designs for several of the components of the system external to the reactor. These special design features are described below.

COMPRESSORS AND GAS TURBINES (ALLIS-CHALMERS MANUFACTURING CO.)

As discussed in Chap. 3.2 on thermal cycles, the gas turbine represents a highly efficient method of utilizing power from a gas-cooled reactor when pressures of the order of 2000 psi and exit gas temperatures (from the reactor) in excess of 1100°F are used. Figures 3.6.8 and 3.6.9 are sectional drawings of the turbines and compressors illustrating the general construction of the casings and rotors.

The entire gas-turbine unit, consisting of both turbines, both compressors, and starting motors, is contained in a continuous casing which seals the unit against leakage of gas into the machinery space. This casing is of the barrel type, with no longitudinal joint because of the high internal pressure involved, and is built in sections with circumferential flanges for assembly. An inner case, split longitudinally, carries the stationary blades, stationary-shaft seal members, bearings, and the like and is assembled with the rotor before it is inserted in the outer or pressure casing.

The high-pressure and low-pressure compressor rotor is a three-bearing unit, the center bearing being a combination thrust and journal bearing to take the thrust of the compressors and the high-pressure turbine. The high-pressure turbine rotor is a two-bearing unit and is connected to the compressors by a thrust-transmitting type of flexible coupling. This consists of a gear-tooth coupling to transmit the torque and a long, ball-end rod to transmit thrust and provide the required flexibility. To facilitate assembling, the thrust rod extends through the high-pressure compressor rotor and is connected to it at the low-pressure end. The starting motor is a two-bearing unit connected to the low-pressure compressor by an over-running clutch. The low-pressure turbine rotor is overhung, has one bearing, and is connected between the rotors of the low-pressure and high-pressure turbines.

Stepped labyrinth glands are used to reduce leakage along the shaft between elements. Adjacent glands of the compressors are in series, the gas leaking from one gland through passages in the bearing housing and back into the system through the other gland. This leakage is very small, owing to the small total pressure difference (about 14 psi) across the two glands. The series arrangement of glands is also used between the high-pressure compressor and high-pressure turbine and between the two turbines. The starting motor is totally enclosed and operates at the same pressure as the low-pressure compressor inlet; therefore, the gland at this point will pass only the gas required to seal the bearing.

SHAFT SEALS

Two types of shaft bearings have been considered, an oil-lubricated bearing and a gas-operated bearing. The oil-lubricated type requires an effective seal to prevent contamination of the gas by the lubricant, whereas the gas type, using helium from the system as

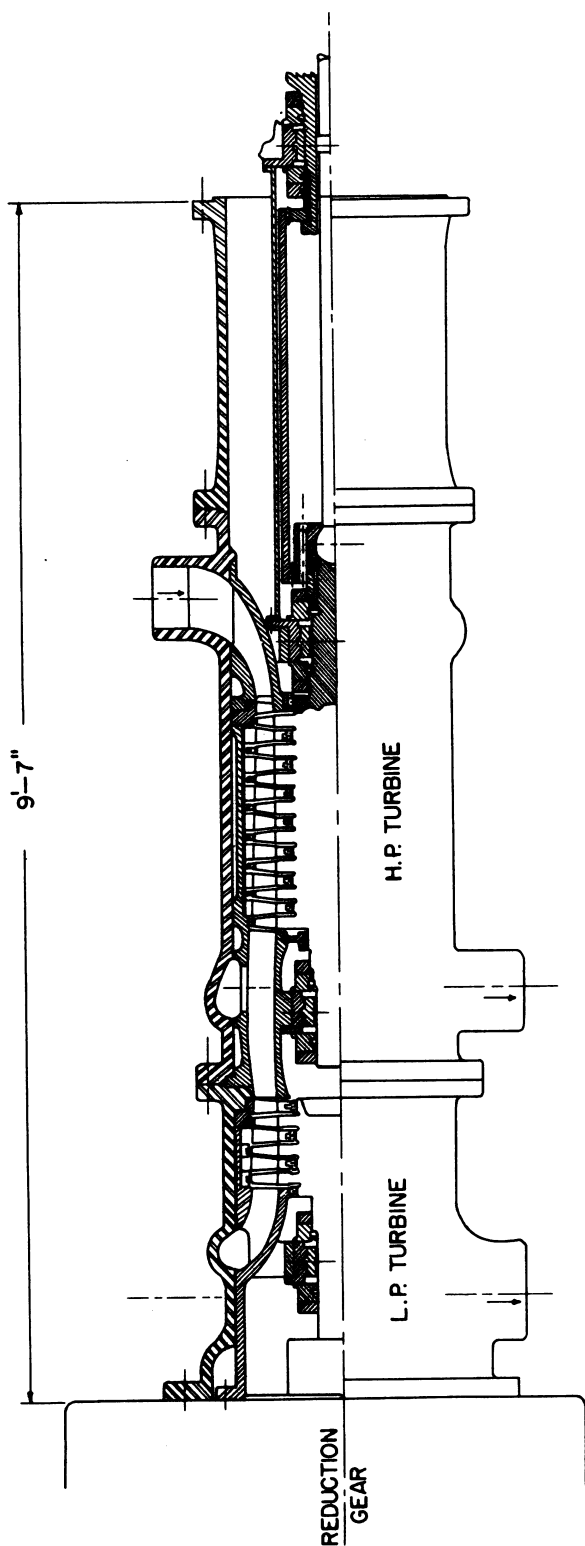


Fig. 3.6.8 — High-pressure and Low-pressure Marine Gas Turbine for Operation at 2000 psi Maximum Helium Pressure. Reprinted from NP-3683, Feb. 15, 1952.

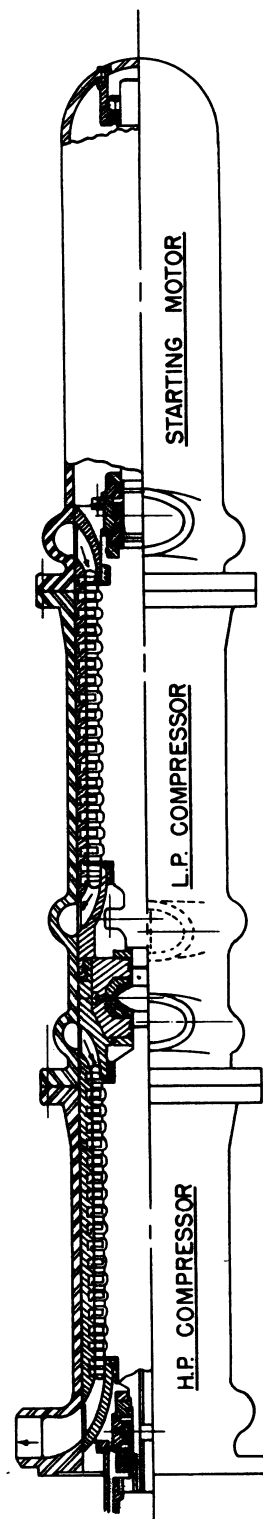


Fig. 3.6.9 — High-pressure and Low-pressure Marine Gas Compressors for Operation at 2000 psi Helium Pressure. Reprinted from NP-3683, Feb. 15, 1952.

the actuating gas, eliminates the contamination problem entirely. An oil-lubricated journal is shown in Fig. 3.6.10. It consists essentially of the bearing with an oil seal and a gas baffle on each side. It is provided with a separate oil tank, oil cooler, and contaminated-gas discharge pump, all sealed into the system. Since the shaft bearings operate in areas

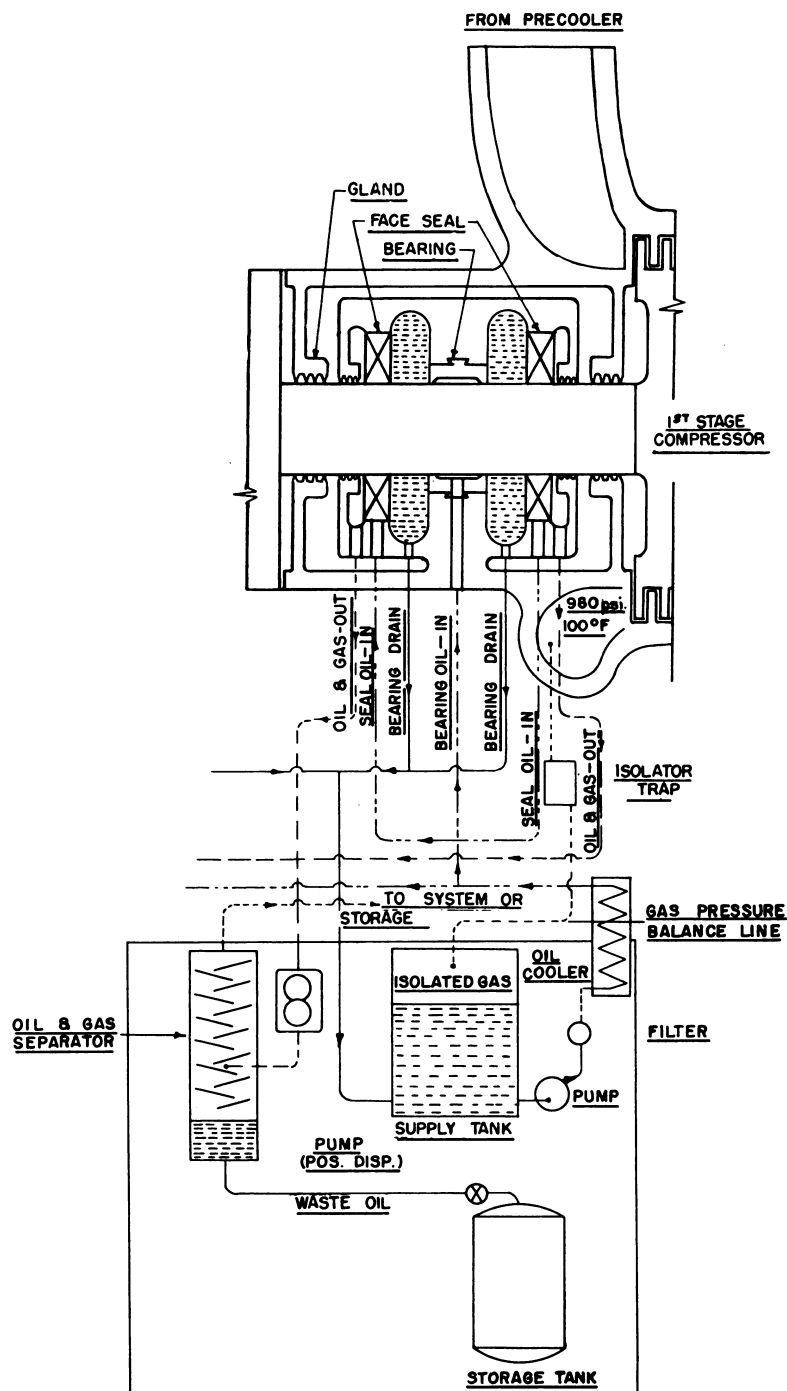


Fig. 3.6.10—Oil-lubricated Journal-bearing System for High-pressure Helium Gas Turbine. Reprinted from NP-1522, May 1, 1950.

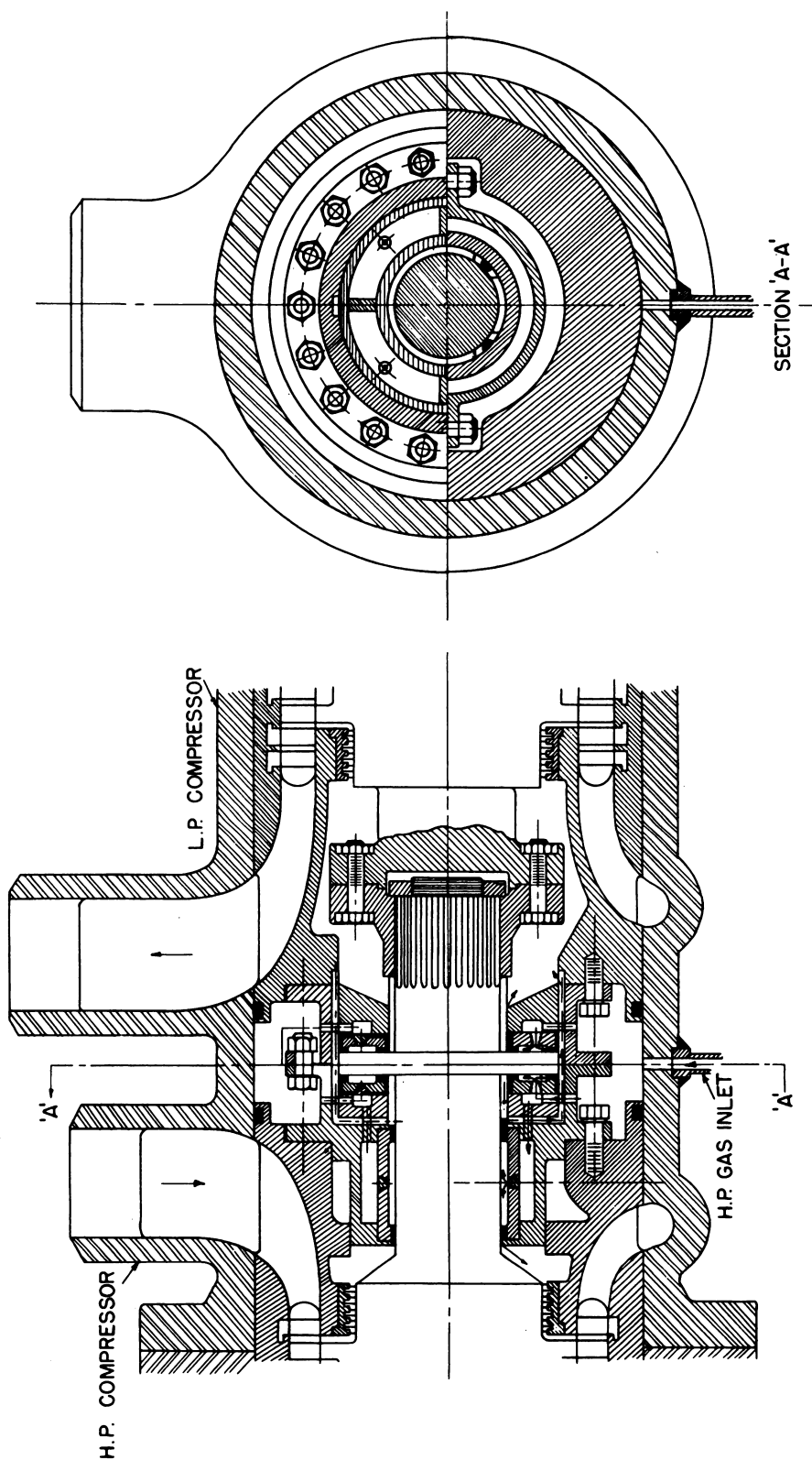


Fig. 3.6.11 — Gas Bearing for High-pressure Helium Turbine. Reprinted from NP-3683, Feb. 15, 1952.

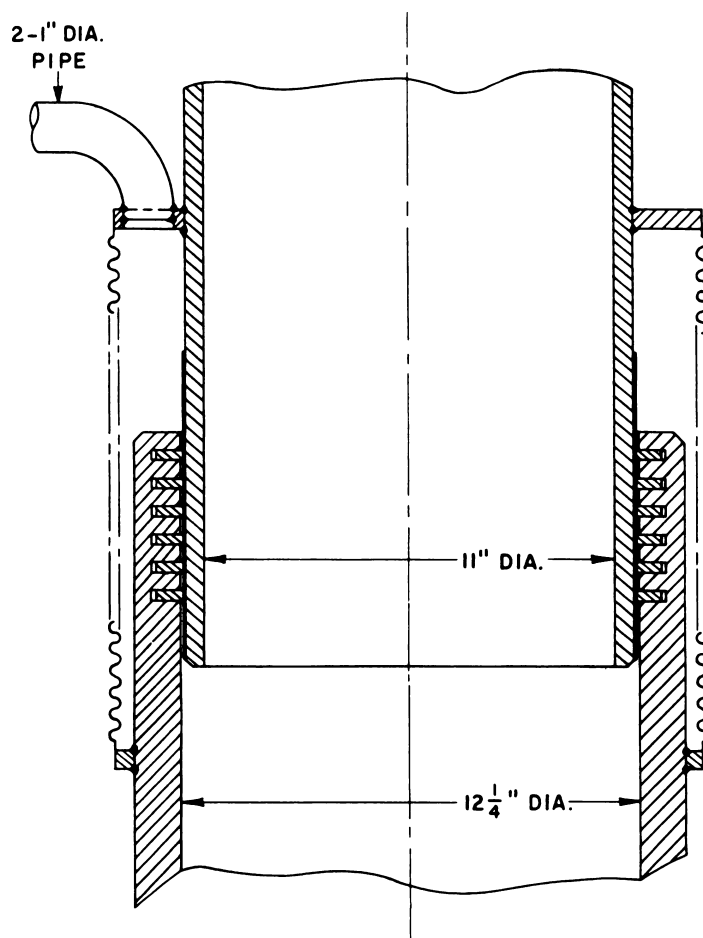


Fig. 3.6.12—Piston-ring-type Slip-expansion Joint. Reprinted from NP-3683, Feb. 15, 1952.

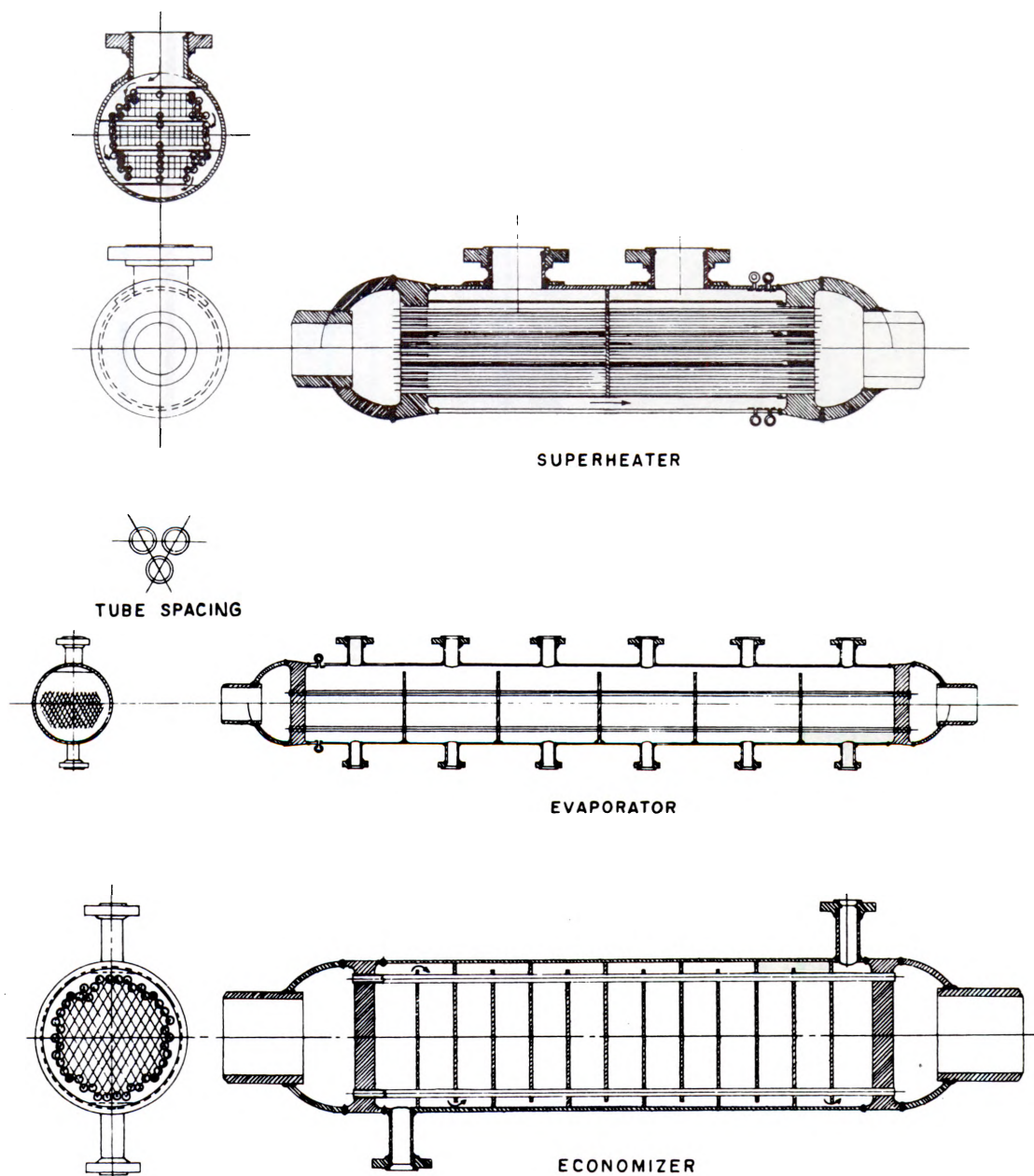


Fig. 3.6.13—Heat-exchange System for High-pressure Gas to Steam. Reprinted from NP-3683, Feb. 15, 1952.

of different pressures, a complete oiling system is provided for each bearing or pressure level. Oil is supplied to the bearing by the pump and discharged into an annular space around the bearing; thence, it goes back to the tank and cooler. A small positive-displacement pump on the same shaft as the oil pump is used to meter a small quantity of gas through the gas baffles. This gas picks up any slight oil leakage by the seal rings and delivers it to a purifying system where the gas is purified and returned to the system at a lower-pressure point. Because of the low pressure differentials involved and the metering characteristics of the displacement pump, the quantities of oil and gas thus removed are very small. It is estimated that the oil loss is about 40 cc/hr per seal, which can be replaced by means of a hand pump.

A gas bearing (as well as a combination thrust and journal bearing) is shown in Fig. 3.6.11. The journal bearing consists of four pockets, as shown in section "AA," to which high-pressure gas is admitted through individual orifices, and from which the gas is discharged through the annular clearance space between the sides of the pockets and the shaft. Since the leakage area from each pocket depends upon shaft position, any transverse shift of the shaft will alter the gas pressure in the pocket and provide a restoring force to re-center the shaft. The thrust bearing operates on the same principle, except that the annular pockets are continuous and the gas is discharged through the clearance areas at the inner and outer diameters of the bearing.

BLOWERS FOR HIGH-PRESSURE COOLANT GAS

A totally enclosed induction-motor-driven blower circumvents the helium leakage problem. A shaft seal similar to that used on the gas turbine can be used to seal the motor enclosure from the main helium stream inside the blower. Some consideration has also been given to the use of a turbomagnetic drive operating in a balanced-pressure system and to the use of a unipolar design.

PIPING EXPANSION JOINTS

A preliminary design of a piston-ring-type slip-expansion joint is illustrated in Fig. 3.6.12.

HEAT EXCHANGERS

For high-pressure helium in the gas-turbine-cycle design, the precooler, intercooler, and regenerator units may all be two-pass, counter-flow, tubular heat exchangers provided with "U" tubes to eliminate floating tube-sheets or expansion problems. For the precooler and intercooler under conditions where the fouling characteristics of water are a potential problem, the gas should be in the shell and the water in the tubes. If, however, the fouling possibilities are negligible, the coolers can be made smaller and lighter by having the water in the shell and the gas in the tubes. To transfer heat from high-pressure gas to steam, heat exchangers such as those illustrated in Fig. 3.6.13 may be used.

REFERENCE

1. R. W. Dayton, et al, BMI-T-27, May 15, 1950 (classified).

CHAPTER 3.7

Economic Comparison of Gas Coolants

The evaluation of various coolants from only a heat-transfer consideration can be made by considering the relationships involving:

1. Pressure drop in coolant flowing through the system.
2. Work required to pump coolant through the system.
3. Heat balance (rate of heat removal by the coolant = rate of heat transfer to the coolant).
4. Empirical correlations of the heat-transfer coefficient to the physical properties of the fluid.
5. Empirical and theoretical correlations between physical properties.

The above basic considerations lead to equations that express the relationship between reactor output, heat generated in reactor, physical properties of the coolant, and design and operating variables of the system. Examples of such equations are given in Table 3.7.1, and the nomenclature is defined in Table 3.7.2.

Table 3.7.1 — Typical Equations Involving Coolant Properties

Equation	Source	Eq. No.
$\frac{kw_0}{A_g} = 428 P \sqrt{R\theta} \sqrt{\frac{\eta b}{F_X^2 F_Y F_L F_C}} \sqrt{\frac{\Delta T^2}{T_p T_b}} \left(\frac{\gamma}{\gamma-1} \sqrt{\frac{9\gamma-5}{2(\gamma-1)mw}} \right)$	MonN-299	(1)
$\frac{W}{Q} = \frac{1}{J_g} \left[\frac{Q^2 L^2}{V_n^2 \Delta T^2 \Delta t} \right] \left[\frac{\eta}{C_p^2 d^3 k Pr^{0.4}} \right]$	NP-155	(2)
$E = \frac{R_0^2 d^2 C_p^3}{Q^2} \left[A + B \left(\frac{C_p \eta}{k} \right)^{0.6} (1/\eta^{0.2})^{-2} \right]$	MonN-157	(3)

Equation (1) has the term $\gamma/(\gamma-1) \sqrt{(9\gamma-5)/[2(\gamma-1)mw]}$ which is the only term dependent on the coolant used. Table 3.7.3 shows by means of Eq. (1) the ratio of reactor thermal output obtainable with various gases compared to that obtainable with air as 1.0 for a fixed reactor size and cross-sectional flow area. The tabulation is based on the same operating pressures, temperatures, and percentage of blower power using room-temperature values of γ .

In Eq. (2), the term $(\eta/C_p^2 d^3 k Pr^{0.4} = X)$ depends on the properties of the coolant. In Table 3.7.4 this physical-property group is evaluated for various coolants at 0°C and 1 atm and compared with hydrogen. A low value is desirable for this group to keep the pump-

Table 3.7.2—Table of Nomenclature

Symbol	Meaning	Dimension
A	Constant not dependent on properties of gas	
A_g	Total gas passage area	sq ft
B	Constant not dependent on properties of gas	
C_p, C_v	Heat capacity at constant pressure or volume	Btu/(lb)(°F)
E	Heat removed per unit of energy removed	
F_C	Ratio of pressure drop of system to pressure drop in reactor	
F_L	Factor that takes into account pressure drop in reflector, end losses, acceleration, and eddy-current effects	
F_X	Ratio of maximum rate to average rate of power generation at control plane of reactor perpendicular to gas flow	
F_Y	Ratio of maximum rate to average rate of power generation along central channel	
g	Acceleration of gravity	ft/sec ²
J	Conversion constant	ft-lb/Btu
k	Thermal conductivity	Btu/(hr)(ft)(°F)
kw_0	Rated output of the reactor	kw
L	Length of heat-transfer passage	ft
mw	Molecular weight of coolant	lb/lb-mole
P	Operating pressure of reactor	atm
Pr	Prandtl number ($C_p \eta / K$)	
Q	Rate of heat removal	Btu/hr
R	Ratio of thermal power required for blower to thermal output of reactor	
R_0	Permissible uranium surface temperature rise above entering gas temperature	°F
Δt	Average temperature difference between wall of heat-transfer passage and bulk temperature of coolant	
ΔT	Temperature rise of coolant in passing through reactor	°F
T_b	Temperature of coolant going to boiler	°R
T_p	Average temperature of gas at center of reactor	°R
V_n	Volume of reactor occupied by coolant	cu ft
W	Work required to pump the coolant	Btu/hr
γ	Ratio of C_p to C_v	
η_b	Efficiency of conversion of thermal energy required to drive blower to gas-pressure energy produced by blower	
η	Viscosity of gas film	lb-hr/ft
d	Density of gas	lb/cu ft
θ	Temperature difference between reactor material and gas at center of reactor	°F

Table 3.7.3—Effect of Type of Gas Coolant on Specific Power of a Reactor

(A. Amorosi, Heat Transfer in Gas-cooled Piles, MonN-299, May 29, 1947)

Gas	Molecular weight	Specific power					
		$\gamma^* = 1.67$ (monatomic)	$\gamma^* = 1.40$ (diatomic)	$\gamma^* = 1.33$ (triatomic)	$\gamma^* = 1.31$	$\gamma^* = 1.23$	$\gamma^* = 1.17$
Hypothetical gas	2	2.4	3.8				
H ₂	2		3.8				
He	4	1.7					
Hypothetical gas	10	1.1	1.7	2.2			
CH ₄	16				1.8		
H ₂ O	18			1.4			
HF	20		1.2				
N ₂	28		1.0				
Air	29		1.0				
C ₂ H ₆	30					1.8	
O ₂	32		1.0				
Hypothetical gas	100	0.3	0.5	0.6			
P ₄	124						1.2
Hg	200	0.24					

* γ = specific-heat ratio

Table 3.7.4—Values of the Physical-properties Group for Gas Coolants

(E. R. Gilliland, D. Bareis, and G. Feick, Heat Removal from Nuclear Reactors, NP-155, Feb. 9, 1949)

Gas	$\eta/C_p^2 d^2 k Pr^{0.4} = X^*$	X/X_{H_2}
H ₂	652	1.0
D ₂	1,313	2.0
C ₂ H ₆	1,850	2.8
C ₂ H ₂	2,325	3.6
CCl ₃ F (Freon-11)	2,680	4.1
CH ₄	2,770	4.25
NH ₃	2,880	4.4
He	3,315	5.1
H ₂ O	5,040	7.7
CO ₂	6,560	10.0
H ₂ S	6,635	10.0
HF	6,700	10.0
SO ₂	7,570	11.6
Air	8,150	12.5
N ₂	8,740	13.4
CO	9,030	13.8
NO	9,550	14.6
O ₂	9,600	14.7
HCl	11,540	17.7
F ₂	13,000	20.0
Cl ₂	13,670	21.0
Xe	106,000	162.6
Hg	161,700	248.0

* Turbulent flow

ing power and the volume of the heat-transfer passages at a minimum. Since the temperatures and pressures in both the reactor and pump would be above 0°C and 1 atm, the values should be corrected for actual operating conditions.

Equation (3) contains the term ($d^2C_p^3$), the cooling-efficiency index, which depends on the properties of the gas; the term ($C_p\eta/k$) is nearly the same for all gases. The cooling-efficiency index is evaluated in Table 3.7.5 for various gases.

Table 3.7.5— Cooling-efficiency Index of Gases at 100°C and 1 Atm.

(M. C. Leverett, Gas-cooled Piles, Chap. 3 in "Graphite Uranium Production Piles," edited by L. B. Borst, National Nuclear Energy Series, Division IV, Volume 5, U. S. Atomic Energy Commission, Technical Information Service, Oak Ridge, Tenn., 1951)

Gas	d, gm/l	C_p , cal/gm	$d^2C_p^3$
H ₂	0.066	3.43	0.18
He	.131	1.25	.030
CO ₂	1.45	0.20	.017
Air	0.95	.24	.013
SO ₂	2.14	.14	.013
CH ₄	0.53	.59	.0058
H ₂ O	.598	.48	.0040

Table 3.7.6— Thermal-neutron-absorption Cross Section for Gas Coolants

Element	σ_{thermal}
Helium	0.000
Deuterium	.001
Oxygen	.001
Carbon	.004
Fluorine	.01
Hydrogen	.32
Sulfur	.49
Argon	1.2
Nitrogen	1.7
Chlorine	35
Mercury	430

These three methods of evaluating heat-transfer properties lead to certain inconsistencies (e.g., methane compared with air). This may result from evaluation of the parameters at different temperatures and from various assumptions as to the "ideality" of the properties of the gas. Equation (2) would seem to be the most reliable, since it is based on fundamental thermodynamic and heat-transfer principles. It contains no approximations, such as correlations between physical properties, except for the heat-transfer coefficient. The foregoing calculations based on Eqs. (1) to (3) are order-of-magnitude calculations and as such should not be applied to design work without modification.

The selection of the most desirable gas coolant for a particular reactor depends not only on the pumping power required but also on the nuclear characteristics of the coolant, its thermal and chemical stability, and the reactor application. The thermal-neutron cross sections of some of the elements, compounds, and mixtures considered in Table 3.7.4 are given in Table 3.7.6. Decomposition under irradiation and lack of chemical and thermal

stability rule out many of the coolants listed in Table 3.7.4. For the general case, the choice narrows down to four coolants: helium, carbon dioxide, steam, or air. Although air requires about twice the pumping power used for the other coolants, the fact that recycling is not necessary with air makes it the preferred coolant in many cases. However, because of the high cross section of nitrogen (1.7 barns), air can absorb a considerable fraction of excess k and is not a satisfactory coolant at high pressures for any but enriched reactors. The air in a typical unenriched graphite-moderated reactor at a pressure slightly below 1 atm absorbs approximately $\frac{1}{2}$ percent in k (see Table 3.8.2). Figure 3.7.1 indicates that, for a given reactor, the power per unit of fissionable material is higher with helium than with air. This plot applies for the following conditions:*

Outlet temperature = 3000°K

Outlet pressure = 10 atm

Outlet mach number = 0.5

Tube length = 36 in.

Void space = 25%

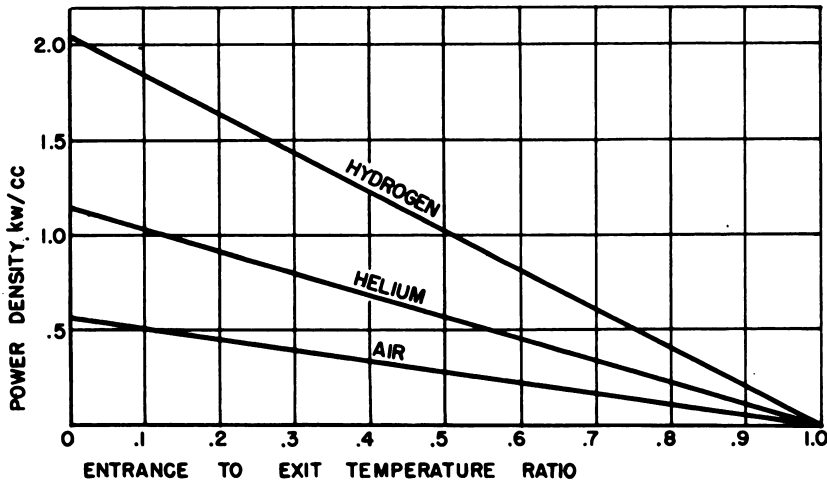


Fig. 3.7.1— Power Density vs Entrance-to-Exit Temperature Ratio. Submitted by North American Aviation, Inc., June 11, 1948.

* A. S. Thomson, NAA-SR-11, June 11, 1948 (classified).

CHAPTER 3.8

Radioactivity in Coolants

Activity in a reactor coolant varies directly with the reactor power level, directly with the volume of coolant in the reactor, and inversely with the U^{235} concentration in the reactor. The chief sources of induced radioactivity are (1) reactions of neutrons with the coolant or with impurities in the coolant and (2) diffusion of fission products into the coolant stream.

INDUCED ACTIVITY IN COOLING AIR (M. E. Smith)

Of the gaseous coolants that might be used in a reactor, only air is likely to be deliberately discharged continuously in an open-cycle system. Elements in the air which become radioactive may thus constitute a routine problem that must be solved by the design of the installation and/or the operating program.

RADIOACTIVE GASES IN REACTOR COOLING AIR

Radioargon is the most abundant radioactive product in the air discharged from an air-cooled reactor. Formed from the A^{40} that comprises about 1 percent of the normal atmosphere, A^{41} is a beta-gamma emitter with a half-life of 110 min. Because of the rapid natural decay of radioargon, however, the area receiving significant radiation from radioargon is relatively small, and since argon is chemically inert, assimilation of the radioactive gas by biological processes is not possible.

Carbon-14, although less abundant than A^{41} by a factor of about 10^4 , presents a greater potential hazard because of its long half-life (5000 yr) and the role of CO_2 in biological processes. In the design of most reactors, however, C^{14} emission would not constitute a serious problem.

A^{41} EMISSION AS A FUNCTION OF REACTOR PARAMETERS

The rate of radioargon production is dependent on the volume of air exposed to the neutron flux. In practice, it is usually necessary to calculate the A^{41} production rate for two or more different sections of the reactor based on both the volume and mean flux of each section. The sum of these production rates multiplied by the decay constant is the A^{41} emission rate (Q).

The A^{41} emission rate (Q) is nearly constant for a given power level since the half-life is long compared with the time of passage through the reactor. The stack concentration (χ_s), however, varies with the air flow.

SAMPLE CALCULATION OF A^{41} EMISSION RATE

The following calculation was made for the Brookhaven reactor. The rate of activation (R) is given by:

$$R = f V N \sigma_a \quad (1)$$

where V = volume of the section

f = average neutron flux over V

N = number of A^{40} atoms/cu ft

σ_a = activation cross section (0.6 barn)

In the case of the Brookhaven reactor, it was necessary to consider three separate volumes (see Table 3.8.1) to obtain the total activation rate of $24.2 \times 10^{12} A^{41}$ atoms/sec. Using a value of $1.07 \times 10^{-4} \text{ sec}^{-1}$ for the decay constant, calculation of the A^{41} emission rate (Q) yields a value of $6.94 \times 10^{-2} \text{ c/sec}$, or $6 \times 10^3 \text{ c/day}$, at the full power of 30 mw. The air flow at full power is 300,000 cfm, which gives a specific activity in the stack of $13.9 \times 10^{-6} \text{ c/cu ft}$ ($4.9 \times 10^{-10} \text{ c/cm}^3$).

Table 3.8.1 — Rate of Activation (A^{41}) in Brookhaven Reactor

	Channels	Plenum chambers	Graphite voids
$f, n/(\text{cm}^2)(\text{sec})$	2.1×10^{12}	1×10^{11}	2.1×10^{12}
V, cm^3	1.44×10^7	3.14×10^8	8.98×10^7
$R, A^{41} \text{ atoms/sec}$	2.92×10^{12}	3.04×10^{12}	18.2×10^{12}

ATMOSPHERIC DISPERSION OF RADIOACTIVE GASES AND PARTICULATES

The release of radioactive effluent to the atmosphere often provides a convenient means for disposing of one of the many wastes associated with the operation of a nuclear reactor. Atmospheric turbulence will normally accomplish a sufficiently rapid reduction in concentrations to render even a very "hot" effluent harmless at a short distance. However, in planning an air-cooled reactor, it must be noted that the rate of dilution in the atmosphere varies tremendously, both in magnitude and character, and that the size and shape of the building complex and the stack parameters will influence the behavior of the effluent stream close to the source. These two aspects of the dispersion problem, called¹ "aerodynamic" and "meteorological," respectively, provide a convenient breakdown and will be treated separately.

AERODYNAMIC FACTORS

In the vicinity of the installation, the effectiveness of a stack in reducing ground-level radiation will be determined by many factors that are under at least partial control of the design engineer. The aerodynamic factors discussed here should be applicable to identical installations in different locations subject to differences in local climatological distributions of wind, temperature, and stability.

Effluent Temperature and Speed

The stream of cooling air ascending vertically from a stack into a horizontal wind field generally may be expected to rise to some level above the stack top before assuming horizontal motion. This results from the upward momentum of the effluent and from the buoyancy of the warm gases ejected into cooler ambient air. This rise of stack effluent is

¹References appear at end of chapter.

limited, however, by the increase in turbulence with increasing stack speed and the decrease in effluent density with increasing temperature. The horizontal wind flow also reduces the effectiveness of momentum and buoyancy.

These effects have been investigated by a number of researchers, and a wide variety of theoretical and empirical formulas has been developed. Unfortunately, most of these studies have been performed in wind tunnels, and corollary field investigations either have been lacking or have not been sufficient to establish the unquestioned superiority of a particular approach.

Of the many possible choices, it is believed that the formulas presented by Bosanquet, Carey, and Halton² offer the most promise. They have been found to agree reasonably well with a number of independent results. Their formula for "effective stack height" (the height above ground at which the plume levels off) is:

$$H = H_S + \frac{4.77}{1 + 0.43 v/u} \frac{\sqrt{Qu}}{v} + 6.37g \frac{Q\Delta}{v^3 T_1} \left(\ln J^2 + \frac{2}{J} - 2 \right) \quad (2)$$

where H = height of plume, ft

H_S = stack height, ft

v = wind speed, ft/sec

u = gas velocity at exit, ft/sec

Q = gas rate (at T_1), cu ft/sec

g = acceleration of gravity, ft/sec²

T_1 = temperature at which density of flue gas equals that of the atmosphere, °C abs.

Δ = temperature difference between flue gas and T_1 , °C

$$J = \frac{v^2}{\sqrt{Qu}} \left(0.43 \frac{v}{u} \frac{\sqrt{T_1}}{gG} - 0.28 \frac{u}{g} \frac{T_1}{\Delta} \right) + 1$$

G = gradient of atmospheric potential temperature, °C/ft

It should be noted that the third term of Eq. (2), which is associated with the buoyancy effect, will give a maximum value only when the atmosphere is stable and the potential temperature increases with height. In unstable cases, the warm effluent would theoretically remain warmer than the surrounding air, and the plume would continue to ascend. Thus, H_S is theoretically greater in unstable cases than in stable cases.

Buildings and Local Terrain

The presence of obstacles in a horizontal wind flow results in localized eddy patterns which must be considered in the design of cooling-air disposal systems. These eddies may be generated by either buildings or terrain in the immediate vicinity of the stack. The most common feature of such artificial turbulence is the presence of one or more "standing eddies" which may cause considerable down-wash in the lee of the obstacle.

The height and horizontal position of a stack in relation to the buildings must be such that the effluent plume will not be entrained in the localized eddy pattern. This problem has been recognized for many years, and the "rule of thumb" that a stack must extend to a height two and one-half times that of the building structure has often served to eliminate the difficulty. Recent evidence obtained from wind-tunnel and field tests indicates that even this ratio may be inadequate in some cases. No reliable rules are available to specify the correct relation of stack height to building dimensions and shape. Wind-tunnel tests are the only means of investigating the flow around a particular building and terrain complex.

It is advisable to locate a reactor in an area in which no additional construction is contemplated to avoid the possibility of undesirable changes in flow resulting from new structures.

Stack Design

Relatively little attention has been devoted to the shape and flow characteristics of stack tops. The eddies produced by the stack itself have been known to cause down-wash with high wind speeds, in some cases resulting in an effective stack height significantly lower than the stack itself.³

The effective stack height can be increased significantly by proper design of the stack top.⁴ In a series of wind-tunnel tests conducted jointly by the Consolidated Edison Company of New York and the College of Engineering, New York University, the uniformity of the gas velocity across the stack orifice was found to be the most important factor; the more uniform the velocity profile, the greater the effective stack height. Davidson also reports that, although shaping the stack to hide an internal nozzle was detrimental, a stack top having a semielliptic nozzle facing into the wind increased the effective stack height about 25 percent.

METEOROLOGICAL FACTORS

At some distance from the source, the initial parameters related to emission become unimportant, and subsequent dispersion of a gaseous effluent becomes entirely a function of natural meteorological processes. Despite the fact that the engineer has little control over the latter, an installation can be designed and located to take the best advantage of these processes. Although precise estimates of ground-level concentrations are not yet possible even over level terrain, the qualitative aspects of dispersion are well understood.

It should be noted that there is evidence showing that the condition of the vegetation and soil has an effect on convective eddies, and the engineer may find it possible to control the meteorological conditions slightly.

Atmospheric turbulence is generated by both frictional and thermal processes and is thus related to the roughness of the terrain, the horizontal wind flow, and the vertical temperature structure near the ground surface. The effects of variations in these factors on the behavior of an effluent have received detailed attention in other publications. Most of the following discussion is based on experience with the 355-ft test-stack at Brookhaven National Laboratory; although minor differences in stack behavior may be expected in other locations, the general principles that follow are applicable to all stacks.

Lapse Conditions

On almost all sunny days a rapid decrease of temperature with height is found in the lower air layers, usually at a rate associated with instability (-1.0° to $-2.0^{\circ}\text{C}/100\text{ m}$). Large, thermal eddies are present, causing portions of the effluent trail to be carried alternately to the ground and to levels above the stack at intervals of about 5 to 15 min (Fig. 3.8.1). Wide horizontal oscillations are also present. With light winds (2 to 6 mph), these convective eddies predominate. Winds greater than 6 mph cause an increase in high-frequency frictional turbulence which is superimposed on the longer-period fluctuations. The dispersion is such that effluent is seldom present continuously at any point on the ground, at least within the first 50 stack-heights. Instead, puffs are carried over a given point on the ground at distinct intervals, the concentrations varying from high values to zero.

Neutral Conditions

During cloudy weather with winds equal to or greater than 10 mph, the air temperature generally decreases with height in the first 400 ft above ground at a rate of 0.0° to $-0.7^{\circ}\text{C}/100\text{ m}$. Turbulence is almost entirely frictional, high-frequency eddies predominating. The effluent is dispersed in a gradually widening cone that first reaches the ground at a distance of 10 to 30 stack-heights and is often present continuously at sampling points with much smaller variations in concentration than are found in lapse conditions.

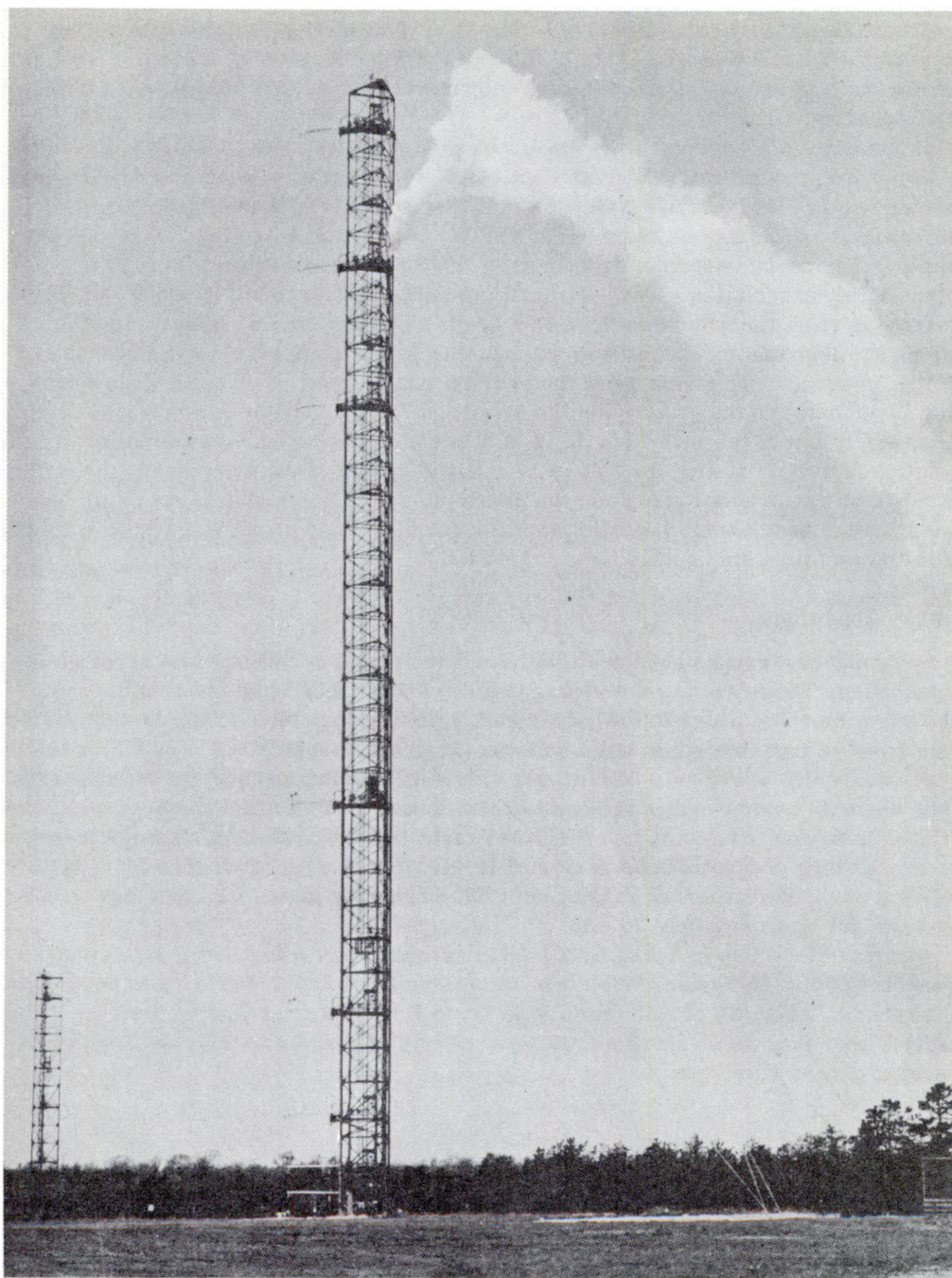


Fig. 3.8.1— Dispersion in Unstable Air. Submitted by Brookhaven National Laboratory, May 1952. The oil-fog trail shows the effect of large convective eddies; a portion of the plume was brought to the ground 250 ft from the tower base. The wind speed was 3 mph, and the vertical temperature difference ($T_{410'} - T_{37'}$) was -1.0°C .

Inversion Conditions

The character of dispersion alters markedly when the air temperature increases with height. The effluent trail spreads out in a thin sheet that widens horizontally, but not vertically, down-wind of the source (Figs. 3.8.2 and 3.8.3). With a stack extending well above the terrain, no concentrations are detected at ground level, even at distances of several hundred stack-heights.

The importance of the temperature inversion in stack dispersion is difficult to overestimate. Under these conditions, the rate of diffusion of the effluent is so small that high concentrations within the plume are found at great distances. It is thus of great importance that the stack and buildings be designed so that the plume will extend above ground for a considerable horizontal distance, depending on the initial rate of emission.

The preceding description refers primarily to surface inversions, in which the temperature increases from the ground surface to a height of approximately 500 to 1500 ft. Similar inversions are found aloft, usually with an unstable layer of air between the ground and the base of the inversion. This results in the vertical confinement of effluent ejected into the unstable layer between the ground and the inversion, with a measurable increase in ground-level concentrations if the inversion lid is at a low level. In some areas, this meteorological situation is very common, the city of Los Angeles being the classic example. A definite relationship between radiation fog and the development of an unstable layer of air under an inversion lid has been found⁵ indicating that the condition may occur frequently in localities where radiation fog is common.

Transitory Conditions

The foregoing paragraphs have dealt with meteorological conditions that predominate in many localities. There are at least two transitory effects worthy of mention.

In the early morning hours following a clear, calm night, heating of the ground surface causes a layer of unstable air to build up from the ground surface and replace the temperature inversion which previously existed and which still remains above the unstable layer. When the unstable layer reaches the level of the plume, a rapid overturning occurs in which the effluent is thoroughly mixed into the lower layer but not upward through the inversion. This produces high concentrations at ground level, often at great distances from the source. The effluent normally disperses rapidly with the increasing instability, and high concentrations remain for approximately 30 min.

The reverse effect may be found in the early evening when a daytime lapse condition is being replaced by an inversion. The turbulence is much reduced just prior to the formation of the inversion, and puffs of effluent may be trapped locally at ground level in the developing stable layer. Such concentrations will generally dissipate or be carried away by the light wind at a very slow rate.

Topography

The above generalized description of the behavior of an effluent plume applies over flat terrain, but local topography will alter the patterns to a varying degree. Some of these factors are discussed below without attempting to cover more than a small portion of the many possibilities. Plans for an installation in rough terrain should include a meteorological survey to establish the significance of local anomalies.

Rugged landforms affect the local meteorology in many ways. One of the most obvious is the creation by hills and ridges of standing vertical and horizontal perturbations in the wind flow. The scale of these variations is a function of the scale of the landforms, but it is common to find wide variations in wind direction and speed over very short distances. For example, parallel ridges and valleys, such as those found in sections of the Appalachian Mountains, tend to restrict the valley wind flow to the long axis of the landforms, and the

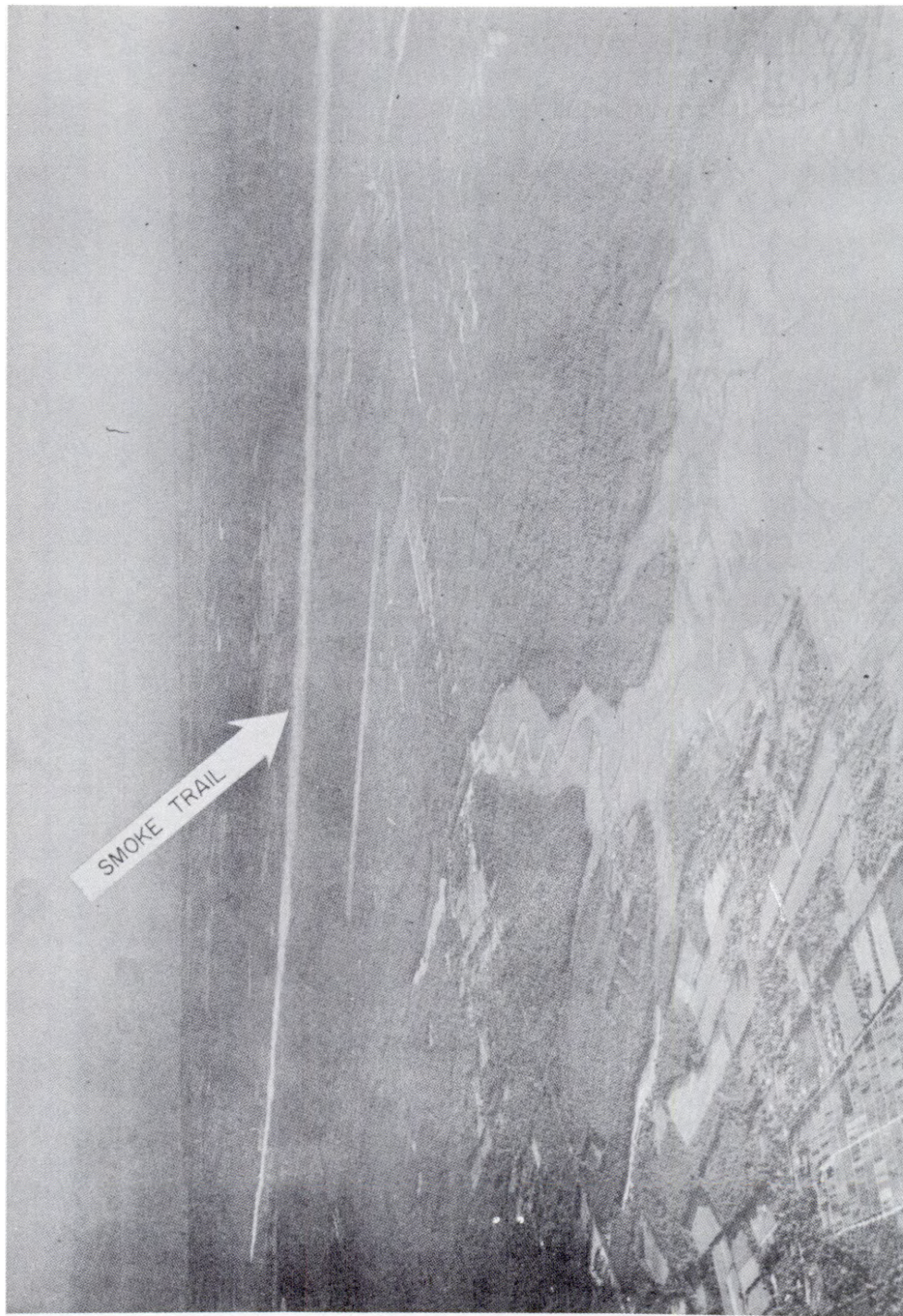


Fig. 3.8.2—Dispersion in Stable Air. Submitted by Brookhaven National Laboratory, May 1952. The aerial view of the oil-fog plume shows the marked suppression of vertical motion with a surface temperature inversion. Six miles of the trail can be seen in the photograph. The wind speed was 4 mph, and the temperature difference ($T_{40'} - T_{37'}$) was $+10^{\circ}\text{C}$.



Fig. 3.8.3— Dispersion in Stable Air. Submitted by Brookhaven National Laboratory, May 1952. The photograph was taken shortly after that shown in Fig. 3.8.2. In this view, the effects of the weak horizontal eddies are evident.

frequency distributions of wind velocity obtained from ridge top and valley floor, respectively, may be remarkably different.

The vertical wind distribution also shows sharp variations, particularly when inversions are present. Shifts of 180° in wind direction with small changes in altitude are common. Figure 3.8.4 shows such a case at Brookhaven, where the terrain is relatively flat.

Temperature inversions are more common in valleys than over flat terrain. The dispersion of effluent emitted in or under such inversions may be restricted in virtually all directions so that very little reduction in concentrations can occur until the temperature structure becomes unstable to levels several thousand feet above ground. In fact, concentrations may increase as the first layers above ground become unstable but before the inversion aloft disappears. An effect of this type almost certainly contributed to the Donora disaster.

The presence of nearby water surfaces has a strong influence on the wind and stability structure. The fact that 24 percent of the winds at Brookhaven are southwesterly during the summer months is partly a result of the "sea-breeze" effect that is present on most summer days. Similarly, the persistent temperature inversions that are so important in the Los Angeles smog may be partly attributed to the advection of warm air over the cold coastal waters.

PARTICULATES

The presence of particulate matter in a stack effluent adds a complicating factor to the process of dispersion and may necessitate the use of a different standard for the allowable concentration of radioactivity. In most installations, it is reasonable to assume that the vast majority of large particles ($>10\mu$) will have been filtered out within the cooling system. The settling rate of the remaining particles will therefore be so small that the effluent may be treated as a gas for practical purposes.

The dispersion of particulates differs from that of gases in two ways: (1) Settling of the particles causes them to have a net downward motion resulting in maximum concentrations closer to the source, and (2) a portion of the effluent is continuously deposited on the ground, reducing the total amount of effluent with increasing distance from the source.

The settling rate of an aerosol of fairly homogeneous particle size may be approximated by assuming that the X-axis of the plume is tilted downward at an angle depending on the ratio of settling rate to wind speed. The deposition rate is difficult to determine, especially for small particles, since effluent distribution and atmospheric motion very close to the ground have not yet been defined with sufficient accuracy and since forces other than gravity may be important. Both problems have been considered in some detail by Baron, Gerhard, and Johnstone⁶ as well as others. It should be noted that, although the deposition of radioactive particulates will have the effect of reducing the amount of effluent in the atmosphere, the radiation at ground level may increase with continued emission until an equilibrium value depending on decay, atmospheric concentration, and deposition has been reached.

ESTIMATION OF GROUND-LEVEL DOSE RATES FROM A^{41}

Estimation of A^{41} dose rates is carried out in two phases: (1) The three-dimensional distribution of effluent is first described mathematically for the meteorological conditions encountered, and (2) the dose rate values are then derived from these distributions.

EFFLUENT CONCENTRATIONS

At present there is no completely acceptable theory to explain atmospheric dispersion, but a thorough summary of the current status has been presented.⁷ The salient features of one treatment that has produced operational results are considered below. Improvements or simplifications in component steps of this treatment can be made in accordance with the

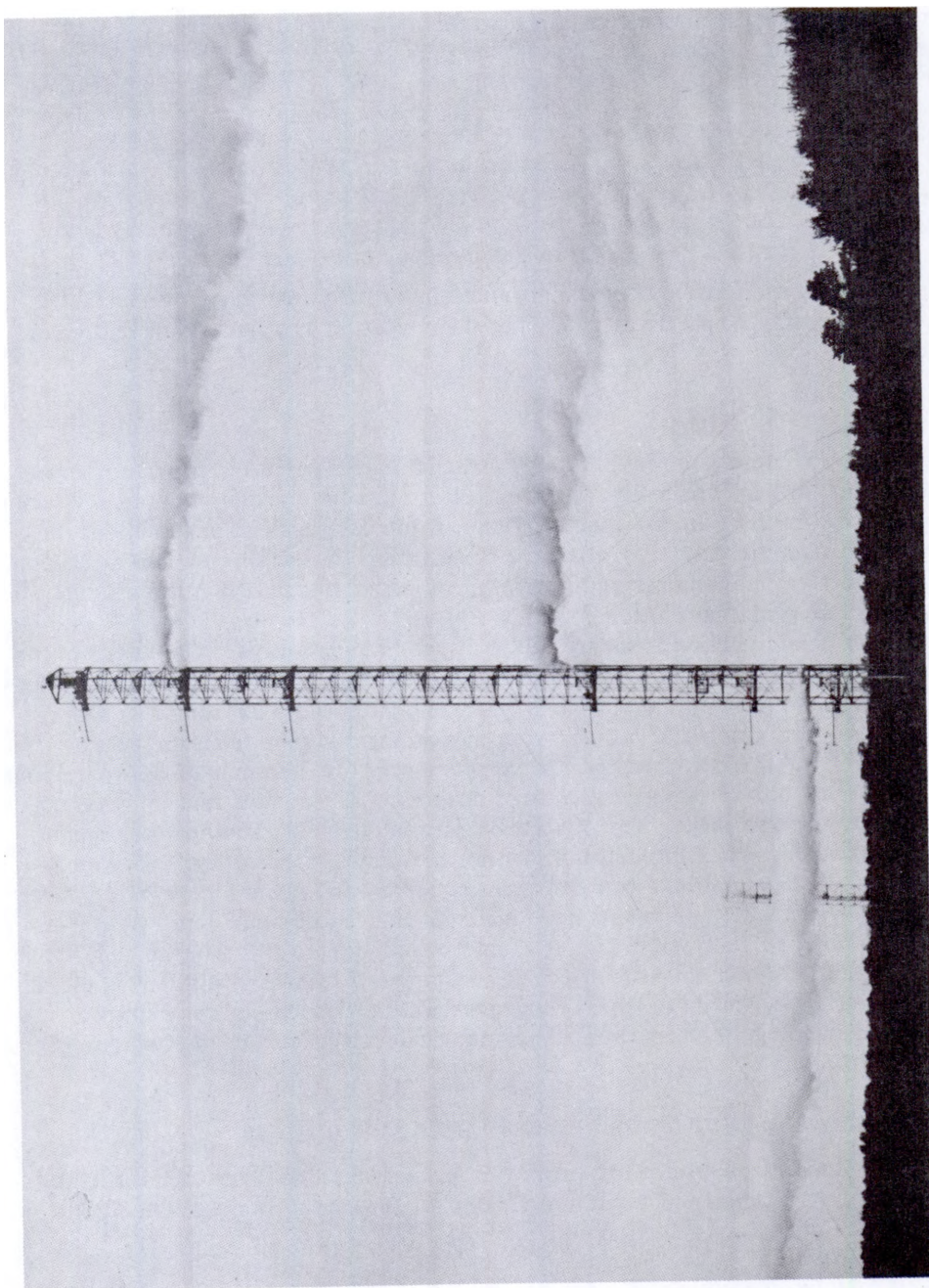


Fig. 3.8.4— Marked Variation of Wind in the Vertical. Submitted by Brookhaven National Laboratory, May 1952. Three oil-fog trails at 50, 150, and 355 ft are visible, each moving away from the source in a different direction. This photograph was taken during a temperature inversion ($T_{40}' - T_{30}' + 5^{\circ}\text{C}$), and the odd wind pattern persisted for approximately 3 hr.

individual problem and with advances in meteorological treatment of atmospheric diffusion. The Brookhaven approach⁸ has been chosen as a model.

The Brookhaven meteorological staff adopted the formula developed by Sutton⁹ as the mathematical model for dispersion under lapse and neutral conditions. This formula expresses the diffusion of an effluent cloud from a point source in the following form:

$$\chi_{(x,y,z)} = \frac{Q}{\pi \mu C_y C_z x^{2-n}} e^{-\frac{y^2}{C_y^2 x^{2-n}}} \left[e^{-\frac{(z-h)^2}{C_z^2 x^{2-n}}} + e^{-\frac{(z+h)^2}{C_z^2 x^{2-n}}} \right] \quad (3)$$

where χ = concentration, mg/m³

Q = rate of emission, mg/sec

u = wind speed, m/sec

n = a pure number

C_y = virtual crosswind diffusion coefficient, m^{n/2}

C_z = virtual vertical diffusion coefficient, m^{n/2}

This equation describes an effluent plume with boundaries in a form lying between a cone and a paraboloid. The concentration along the X-axis decreases at a rate proportional to x^{2-n} , where n lies between 0 and 1. When applied to a source located above the ground surface, the maximum ground-level concentration is found to be inversely proportional to the square of the stack height although this does not apply to concentrations at fixed points. The nomographs presented in Figs. 3.8.5 and 3.8.6 provide a convenient means of obtaining the maximum concentrations and their distance from the source as predicted by the Sutton formulas.

Brookhaven oil-fog tests under unstable conditions showed mean hourly maximum concentrations which were less than those predicted by the Sutton equations by a factor varying between 2 and 10. However, it is felt that the diffusion of individual clouds of effluent are predicted by the equation with reasonable accuracy and that appropriate hourly mean values can be obtained by weighing the basic results in accordance with the hourly frequency distribution of wind direction.

The numerical values for n , C_z , and C_y for various degrees of wind gustiness must be determined by appropriate instrumentation or estimated from results in other locations.

The Sutton equation does not accurately describe the dispersion found with temperature inversions, which exist 40 percent of the time at Brookhaven. However, the narrow trail of effluent from a high stack can be approximated by the mathematical forms of the line and plane source for estimating radiation dose rates at ground level. It is clear that a more accurate representation of the cloud would be necessary with low stacks.¹⁰

RADIATION DOSE RATES

A⁴¹ is a beta-gamma emitter, decaying to K⁴¹ with a half-life of 110 min. It is necessary to consider each type of radiation separately in calculating ground-level dose rates.

Beta Radiation

The beta radiation from A⁴¹ has a maximum energy of 1.2 mev and an average energy of 0.46 mev, for which the respective ranges in air at sea level are approximately 4.2 and 1.1 m. Large volumes need not be considered in the calculation of beta dose rates, and point concentrations of the effluent, obtained from the Sutton formula and weighted in accordance with the wind frequency distribution, can be used to obtain mean hourly distributions of the beta contribution in lapse and neutral conditions. With a sufficiently elevated source, no effluent is present at ground level under inversions, and the beta dose rate is effectively zero.

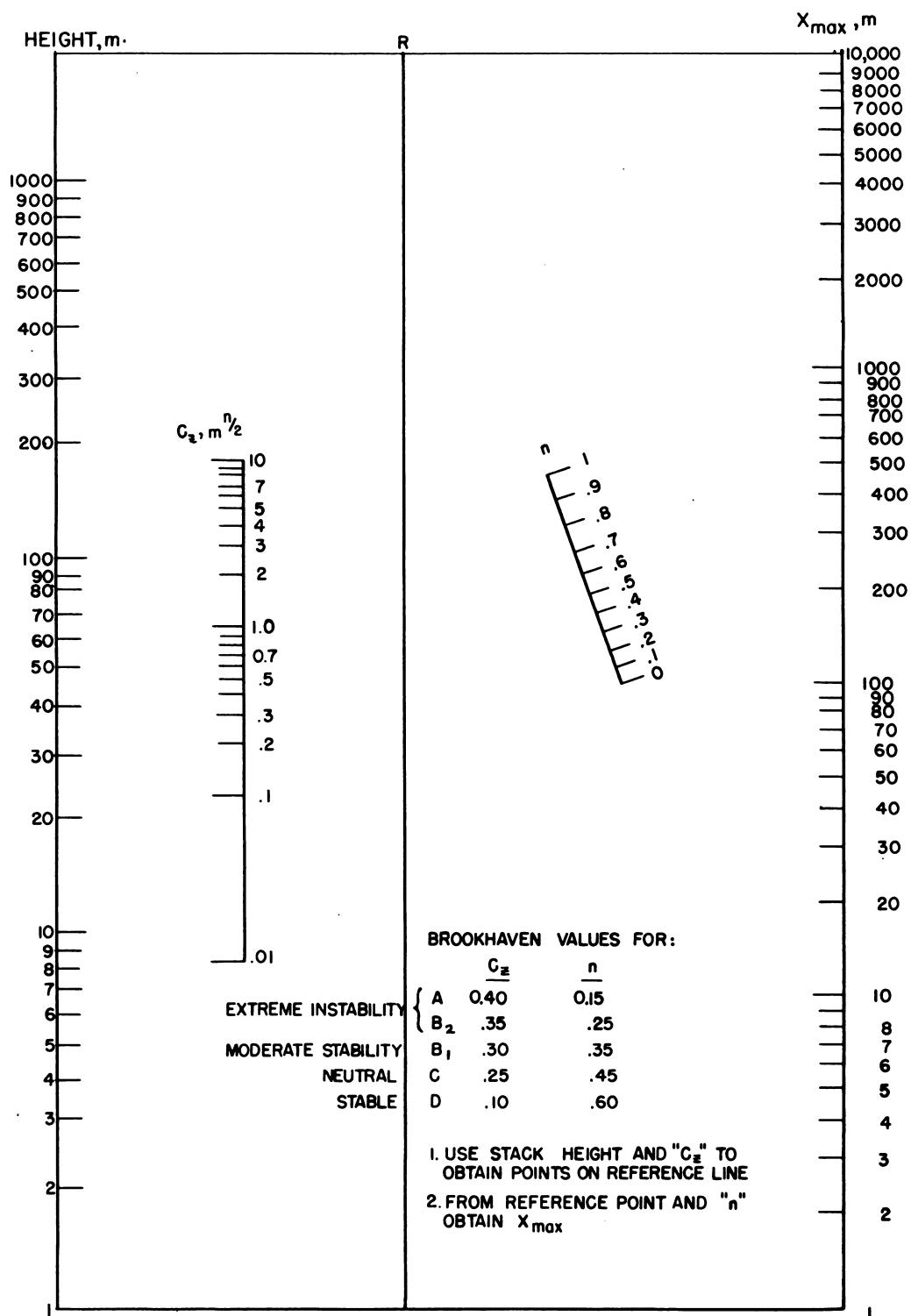


Fig. 3.8.5 — Nomogram for Solving the Sutton Equation $\left[X_{max} = \left(\frac{h^2}{C_z^2} \right)^{\frac{1}{2-n}} \right]$ for the Distance of Maximum Ground Concentration. Prepared by I. A. Singer; submitted by Brookhaven National Laboratory, May 1952.

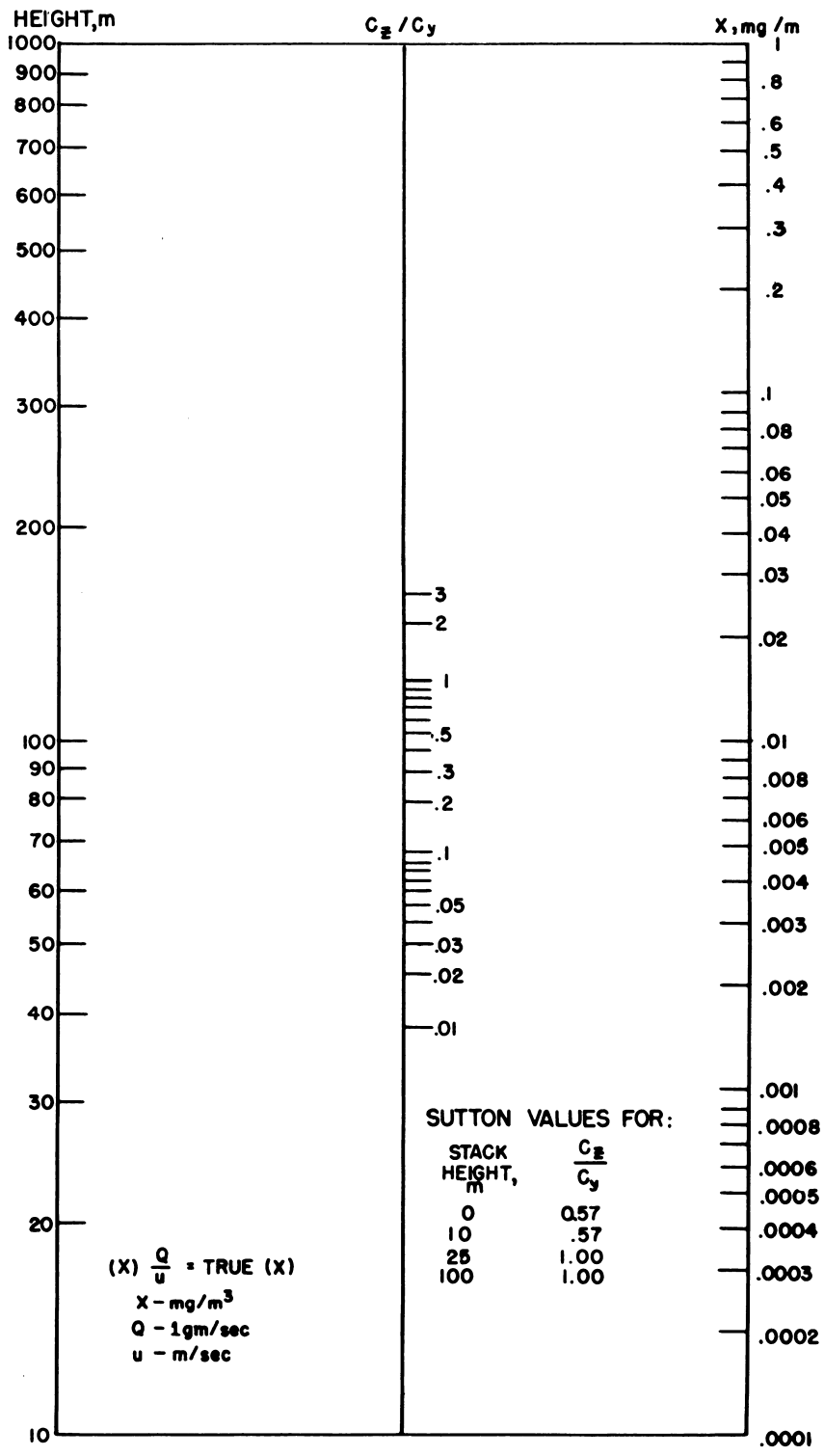


Fig. 3.8.6— Nomogram for Solving the Sutton Equation $\left[X_{\text{max}} = \frac{2Q}{e\pi u h^2} \left(\frac{C_z}{C_y} \right) \right]$ for the Maximum Ground Concentration. Prepared by I. A. Singer; submitted by Brookhaven National Laboratory, May 1952.

Gamma Radiation

A very different problem is encountered in the treatment of gamma radiation, which has a mean free path of about 300 m. The spatial distribution of the effluent must be considered, for the assumption of a semi-infinite cloud of uniform concentration cannot be expected to apply except, perhaps, at very great distances from the source. Under inversions, the effluent from a high stack may be approximated by a plane source extending from the stack to infinity, widening uniformly at a half-angle of 1.5° . To obtain the dose rate for a specific point at ground level, the assumption of a plane of infinite length having a finite width depending on the 1.5° half-angle and the radial distance from the stack may be used. The integration is simplified by the further assumption that the entire plume has the concentration calculated on the basis of the decay over the point of observation.

Close to the stack, the assumption of a line source gives results of good accuracy. Values within 10 percent of those obtained from a plane source will be achieved if the vertical half-angle subtended by the edges of the plume above the observer does not exceed 30° . If the inversion plume is close to the ground, more sophisticated models of the dispersion become necessary. These may be selected on the basis of empirical test data or from the available theoretical formulas.

The ground-level dose rate distribution obtained in this manner applies to an invariant mean wind. A distribution representing a typical hour may be obtained by utilizing the hourly frequency distribution of stack-height wind direction.

Dose rates under unstable conditions may be derived in basically similar fashion. The Sutton formulas can be assumed to describe the three-dimensional distribution of the effluent plume and the corresponding dose rates obtained. The mathematics is rendered more tractable if the simplifying assumptions are made that the concentration in the X-direction is constant and that the effluent extends to + and - infinity in the X-direction. The latter is clearly valid only if the point of observation is further from the stack than one mean free path (300 m). It is also helpful to treat the decay factor as a constant, as is done in the inversion case.

It is clear from the foregoing that estimates of dose rates under varying meteorological conditions can be achieved, although the approach is not as yet sufficiently general to warrant routine application of the method to a wide variety of sites. In practice, the meteorology of each site should be carefully considered to determine what observational data are needed to supplement generalized knowledge of the problem. In some cases, engineering estimates will be relatively simple; in others, especially where rugged terrain is involved, a complete meteorological survey will be required.

INDUCED ACTIVITY IN HELIUM

Neutron reactions involving helium itself are negligible, as shown in Table 3.8.2. The helium isotope with a relatively large thermal-neutron absorption cross section is He^3 , but its abundance¹¹ is of the order of 10^{-7} to 10^{-6} . The extent of neutron reactions with impurities in the helium are approximated in Table 3.8.3, which presents the activity calculated on the basis of 100 ppm argon in the helium. Argon was chosen as typical of an impurity that would give rise to a substantial quantity of activity. Actual impurity concentrations in high-grade helium are shown in Table 3.3.14.

Table 3.8.4 presents estimates of activity in the helium stream resulting from the diffusion of fission products into the helium. The maximum activity is based on a complete transfer of all the fission products from the fuel rods into the gas stream. The minimum value results from considering the transfer of only those fission products from the slug surface film whose thickness is equal to the recoil range of the fission fragments. Further work¹²

Table 3.8.2—Approximate Loss in k Owing to Gases Used for Cooling

(M. C. Leverett, Gas-cooled Piles, Chap. 3 in "Graphite Uranium Production Piles," edited by L. B. Borst, National Nuclear Energy Series, Division IV, Volume 5, U. S. Atomic Energy Commission, Technical Information Service, Oak Ridge, Tenn., 1951)

Gas	Δk^*	Gas	Δk^*
Hydrogen	0.0007	Sulfur dioxide	0.0005
Helium	0	Methane	.0014
Carbon dioxide	0	Water	.0007
Air	0.003		

*Based on ratio of free space to metal existing in the Clinton reactor at a pressure of approximately 1 atm

Table 3.8.3—Activity from Argon Impurity in Helium*

(B. T. Feld, The Activity of the Coolant in Closed-cycle Systems, LP-157, Sept. 7, 1948)

Power level, mw	100
Gas pressure, psia	1000
Gas temperature, °F	1800
Fraction coolant in reactor	0.10
Weight of U^{235} , kg	10
Thermal-neutron flux, per sq cm-sec	2.4×10^{14}
Gamma energy, mev	1.3
Gamma rays, per day	3×10^{16}
Gamma flux, per sq cm-day (at 10 m)	2×10^{-9}
Gamma flux, per sq cm-day (at 1000 m)	2×10^{-14}

*Reactor assumed to be a cylinder 2 sq ft in cross section having a volume of 6.3 cu ft. The concentration of the argon impurity is taken as 100 ppm

Table 3.8.4—Calculation of Helium Activity

(C. R. McCullough and J. A. Swartout, Calculation of Levels of Radioactivity to be expected in the Coolant of the Power Pile, Oak Ridge National Laboratory, CF-47-1-41, Jan. 15, 1947.)

Power level,* mw	40
Coolant volume, cu ft	4100
Beta activity, c/cu ft	20 to 5×10^4
Gamma activity, c/cu ft	10 to 2.5×10^4
Long-lived activity,† c/cu ft	8

*Based on reactor containing 5600 hollow cylindrical fuel rods 6 in. by 1.5 in. OD and $\frac{1}{8}$ in. ID

†Activity induced in He by complete diffusion with half-lives greater than 1 hr

gives a comparable figure of 6.76 c/cu ft* for this minimum value, and it is noted that at high temperatures diffusion may be more important than the stoppage of recoil fragments.

Table 3.8.5 presents the results of a calculation scaling up the activity induced in helium based on small-scale experimental work. This calculation is of value as an order-of-magnitude estimate and indicates the possibility of undue pessimism in the values given in Table 3.8.4.

Table 3.8.5—Experimental Data and Calculated Scale-up of Activity Induced in Helium
(N. Sugarman, Collection of Activity in a Circulating Helium System, CC-418, Jan. 15, 1943)

Experimental data	
Gas velocity, l/sec	0.49
Neutron intensity, neutrons/(cm ²)(sec)	11.9×10^7
Fission rate, fissions/(gm)(sec)	1.35×10^6
Surface area, cm ²	86.4
Gas activity, disintegrations/(cc)(sec)	
Fluid	4.7
Solid	2.8
Calculated scale-up*	
Power level, mw	100
Weight of metal, tons (metric)	50
Surface area, cm ²	1.64×10^7
Fission rate, fissions/(gm)(sec)	6×10^{10}
Helium volume, cu ft	46,520
Cycle time, sec	20.8
Gas velocity, l/sec	6.3×10^5
Gas activity,† c/cu ft	
Fluid	0.283
Solid	.142
Fraction of reactor activity in gas	3×10^{-5}

*Reactor is assumed to consist of units of three concentric cylinders of inner radii 0.5, 1.2, and 1.9 in. and outer radii 0.7, 1.4, and 2.0 in.

†Experiments indicate that the total activity can be lowered 45 percent by filtering through charcoal. Activity indicated is at 2 sec from reactor center

A fuel-rod coating that would keep the fission products from diffusing into the helium stream would simplify the purification process considerably. Filtration of the helium through activated charcoal has been suggested as a method of decontaminating the helium coolant. Other suggested methods are the use of a diffusion cascade, storage for the decay of short-lived activity, and absorption into fats.¹³

A purification method incorporating cooling and filtration has also been suggested.¹⁴ This process consists of cooling the helium to the temperature of liquid air at a pressure of 500 psia. The contaminants are removed as liquid, and the remaining impurities are removed in an absorbent charcoal filter.

*The original figure is 34 c induced by one fuel rod 1.4 cm in radius and 11 ft long operating at a 25-mw power level. The figure of 6.76 c/cu ft is derived from this value in order to make a comparison with the value in Table 3.8.4.

FILTER SYSTEMS FOR RADIOACTIVE PARTICLES

Filters are placed in the coolant gas streams from reactors to remove radioactive particles introduced usually from one or more of three main sources:

- (1) Particles, such as salt and dust, entering with the cooling air for an open-cycle reactor and remaining in the reactor for a time sufficient to acquire radioactivity.
- (2) Particles, such as graphite, beryllium oxide, and other dusts, from the moderator, the fuel elements, or parts of the reactor structure.
- (3) High-activity particles of uranium or uranium oxide from ruptured fuel elements.

The first source of particles is important only when stagnant air pockets or low air-velocity regions are present in or close to the reactor so that particles settle out, become radioactive, and are subsequently picked up by the air stream again. This condition can be prevented successfully by installing high-efficiency filters in the inlet air stream. Most particles not retained by the filters are no larger than $0.5\ \mu$ in diameter; these remain air-borne and have no chance to become radioactive.

To catch radioactive particulate matter that enters the gas stream inside the reactor, an efficient filter must be used in the exhaust stream (see Fig. 3.8.7). The primary source of such particles in existing air-cooled reactors has been oxidized uranium from aluminum-can ruptures. Maximum safety, therefore, depends upon designing the fuel element so that the possibility of release of uranium particles is minimized. Such procedures are described in Chapter 3.5. The use of filters in the inlet and/or outlet coolant streams depends on the reactor characteristics.

For air-cooled experimental reactors at air temperatures of 215°F or lower, special types of glass fiber filters with the characteristics shown in Table 3.8.6 give satisfactory service. When the filters were used in series with the larger fiber material preceding the smaller, good results were achieved for two and more years depending on the location. The combination of the FG-25 backed by FG-50 appears to be just as efficient as two $\frac{1}{2}$ -in. layers of FG-50 and has an estimated useful life 3.54 times the latter based on a pressure-drop consideration of 4 in. H_2O at 25 ft/min.¹⁵

Table 3.8.7 presents operating data for a typical installation using these two types of filters in series in the same frame. If necessary, the total atmospheric dust removed may be increased from 99.3 to about 99.7 weight percent by the use of back-up filters containing either Chemical Warfare Service No. 6 paper or AEC No. 1 paper. The characteristics of these papers are shown in Table 3.8.8. As an indication of dust load on location, an installation similar to that on which Table 3.8.7 is based showed a pressure-drop build-up of less than $\frac{1}{4}$ -in. $\text{H}_2\text{O}/\text{yr}$ for the same linear velocities through the mediums.

The efficiency of a particular filter installation depends largely, especially with these highly efficient mediums, on the sealing at the periphery of the frames. The above efficiencies on the FG-25, FG-50 combination are for a carefully gasketed installation where calking compound was used between the frames and the supporting structure and where $\frac{1}{4}$ -in. felt gaskets were used between frames. In the case of the CWS No. 6 and AEC No. 1 paper installation, a positive pressure of air with respect to the coolant air existed around the frames, and any leakage was into the system rather than around the filters.

Any particles that get through either the Filterdown combination or the CWS No. 6 paper are so small that they are dispersed over an extremely wide area when discharged through a 200- to 300-ft stack. If these small particles did not originate in the reactor, their short transit time through the reactor would preclude their acquiring any significant radioactivity.

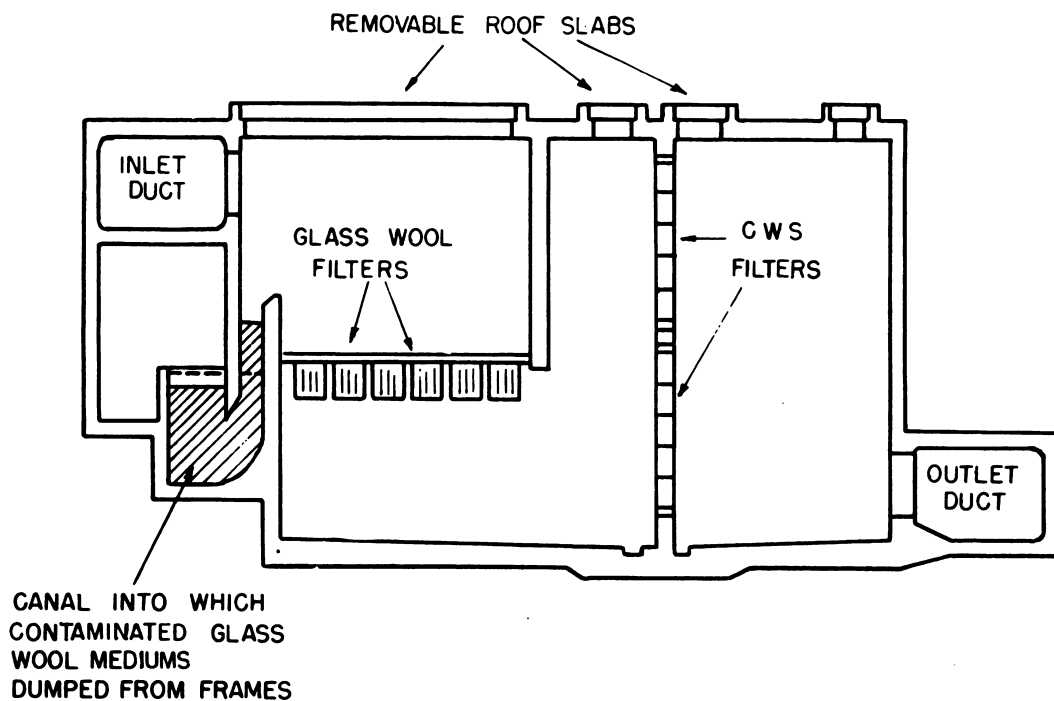


Fig. 3.8.7— Cross Section of Filter House on Downstream Side of Reactor.
Submitted by Oak Ridge National Laboratory, May 1952.

Table 3.8.6— Characteristics of Glass-fiber Filters Used in Air Streams of Experimental Reactors*

	Fine fiber (FG-50)†	Medium-fine fiber (FG-25)†
Thickness of filter bed, in.	0.5	0.5
Density of medium, oz/sq ft	.8	.7
Fiber diameter, μ	1.25	2.75
Discoloration efficiency (atmospheric dust), %	85+	70
Medium velocity, ft/min	20	20
Initial resistance at 20 ft/min, in. H_2O	0.32	0.11
Initial resistance at 35 ft/min, in. H_2O	.56	.35

*F. M. Tench and M. E. Ramsey, Oak Ridge National Laboratory, personal communication, 1952

†American Air Filter Company "Filterdown"

Table 3.8.7—Operating Information for Typical Filterdown Filter Installation*

Size of installation	
No. of 2- by 3-ft frames	600
Filter medium	$\frac{1}{2}$ in. FG-50
	$\frac{1}{2}$ in. FG-25
Total air flow at 215°F and 360 in. H ₂ O abs, cfm	120,000
Average linear velocity through medium, ft/min	33
Operating data	
Dust load,† gm/(sq ft)(yr)	23.6
ΔP , in. H ₂ O (clean filter)	0.9
ΔP build-up, in. H ₂ O/yr	~2
Average filter-use time, yr	2
Approximate cost, 600-frame filter change	
Materials	\$3800
Labor and equipment	3400
	\$7200
Total atmospheric dust removed, wt-%	~99.3

*F. M. Tench and M. E. Ramsey, Oak Ridge National Laboratory, personal communication, 1952

†Uranium was not a significant part of the dust load

Table 3.8.8—Characteristics of CWS No. 6 and AEC No. 1 Filter Papers*

CWS No. 6:

Composition: Bolivian asbestos, strengthened with cellulose fibers

Thickness, in.: 0.035 to 0.045

Resistance at 28 ft/min: 110 mm H₂O or less

Penetration of 0.3- μ dioctyl phthalate smoke at 28 ft/min: 0.12% or less for 0.035-in. thickness

AEC No. 1:

Composition: Kraft pulp and asbestos fibers

Thickness, in.: 0.033 to 0.045

Resistance at 28 ft/min: 110–115 mm H₂O or less

Penetration of 0.3- μ dioctyl phthalate smoke at 28 ft/min: 0.10 to 0.15% or less

CWS No. 6 and AEC No. 1 frame characteristics:

Amount of filter medium per frame, sq ft: 257

Size of frame: 2 ft by 2 ft by 11½ in. thick

Length of filter-medium pleats, in.: 11

Resistance to air flow of 1000 cfm at 65° to 100°F: 1.25 in. H₂O or less

Penetration of 0.3- μ dioctyl phthalate smoke at 1000 cfm: 0.05% or less

Maximum ΔP across filter without visible sagging, buckling, shifting, or vibration: 7 in. H₂O

Operating data on filters when preceded by FG-25, FG-50 combination:

Average linear velocity through paper, ft/min: 2.34

Dust load, gm per square foot of filter paper per year: <0.007 and ~0.007

ΔP , in. H₂O (clean filter): 1.10

ΔP build-up, in. H₂O/yr.: 1.6

Average filter-use time, yr: 2½

Approximate cost, 200-frame filter change:

Materials	\$10,000
Labor and equipment	4,500
	\$14,500

*F. M. Tench and M. E. Ramsey, Oak Ridge National Laboratory, personal communication, 1952

REFERENCES

1. W. F. Davidson, *Stack Meteorology as Related to Power Plants*, Chap. 93 in "Air Pollution," edited by L. C. McCabe, McGraw-Hill Book Company, Inc., New York, 1952.
2. C. H. Bosanquet, W. F. Carey, and E. M. Halton, *Dust Deposition from Chimney Stacks*, Inst. Mech. Engrs. London, Proc. 162, 1950, pp 355-367.
3. R. H. Sherlock and E. A. Stalker, *A Study of Flow Phenomena in the Wake of Smokestacks*, Univ. Mich. Dept. Eng. Res. Bull. No. 29, 1941, 49 pp.
4. W. F. Davidson, personal communication.
5. R. G. Fleagle, W. H. Parrott, and M. L. Barad, *Theory and Effects of Vertical Temperature Distribution in Turbid Air*, Jour. Meteorology 9, 1952, pp 53-60.
6. T. Baron, E. R. Gerhard, and H. F. Johnstone, *Dissemination of Aerosol Particles Dispersed from Stacks*, Ind. Eng. Chem. 41, 1949, pp 2403-2408.
7. T. F. Malone, editor, *Compendium of Meteorology*, Waverly Press, Inc., Baltimore, 1951, pp 1139-1157.
8. P. H. Lowry, *The Theoretical Ground-level Dose Rate from the Radioargon Emitted by the Brookhaven Reactor Stack*, BNL-81, July 1950, pp 426-436.
9. O. G. Sutton, *The Theoretical Distribution of Airborne Pollution from Factory Chimneys*, Quart. Jour. Roy. Meteorological Soc. 73, 1947, pp 426-436.
10. M. L. Barad, *Diffusion of Stack Gases in Very Stable Atmospheres*, Meteorological Monographs 1, No. 4, 1951, pp 9-14.
11. J. H. Coon, LAMS-654, Dec. 8, 1947, 3 pp (classified).
12. J. Chernick and I. Kaplan, BNL-20, Nov. 3, 1948, 25 pp (classified).
13. C. R. McCullough et al, MonN-383, Sept. 15, 1947, 422 pp (classified).
14. L. B. Borst et al, CEPS-1100, Jan. 1, 1952 (classified).
15. H. C. Savage, ORNL-500, Dec. 1, 1949, 19 pp (classified).

SELECTED READING LIST

Aerodynamic Factors

DUST DEPOSITION FROM CHIMNEY STACKS, C. H. Bosanquet, W. F. Carey, and E. M. Halton, Inst. Mech. Engrs. London, Proc. 162, 1950, pp 355-367.

INVESTIGATION OF THE PENETRATION OF AN AIR JET DIRECTED PERPENDICULARLY TO AN AIR STREAM, E. E. Callaghan and R. S. Ruggeri, NACA-TN-1615, June 1948, 13 pp.

A STUDY OF FLOW PHENOMENA IN THE WAKE OF SMOKESTACKS, R. H. Sherlock and E. A. Stalker, Univ. Mich. Dept. Eng. Res., Bull. No. 29, 1941, 49 pp.

Meteorological Factors

AIR POLLUTION, edited by L. C. McCabe, McGraw-Hill Book Company, Inc., New York, 1952, pp 775-839.

THEORY AND EFFECTS OF VERTICAL TEMPERATURE DISTRIBUTION IN TURBID AIR, R. G. Fleagle, W. H. Parrott, and M. L. Barad, Jour. Meteorology 9, 1952, pp 53-60.

COMPENDIUM OF METEOROLOGY, edited by Thomas F. Malone, Waverly Press, Inc., Baltimore, 1951, pp 1139-1157.

METEOROLOGICAL FACTORS IN ATMOSPHERIC POLLUTION PROBLEMS, M. E. Smith, Am. Ind. Hyg. Assoc. Quart. 12, No. 4, Dec. 1951, pp 151-154.

ON ATMOSPHERIC POLLUTION, A Group of Contributions by J. H. Carter, C. A. Gosline, E. W. Hewson, H. Landsberg, M. L. Barad, G. W. Brier, P. H. Lowry, D. A. Mazzarella, H. F. Poppendiek, H. Rouse, R. H. Sherlock, and M. E. Smith, Meteorological Monographs 1, No. 4, 1951, 55 pp.

THE THEORETICAL GROUND-LEVEL DOSE RATE FROM THE RADIOARGON EMITTED BY THE BROOKHAVEN REACTOR STACK, Brookhaven National Laboratory, P. H. Lowry, BNL-81, July 1950, 33 pp.

STACK METEOROLOGY AND ATMOSPHERIC DISPOSAL OF RADIOACTIVE WASTE, N. R. Beers, Nucleonics 4, No. 4, 1949, pp 28-38.

DISSEMINATION OF AEROSOL PARTICLES DISPERSED FROM STACKS, T. Baron, E. R. Gerhard, and H. F. Johnstone, Ind. Eng. Chem. 41, 1949, pp 2403-2408.

THE THEORETICAL DISTRIBUTION OF AIRBORNE POLLUTION FROM FACTORY CHIMNEYS, O. G. Sutton, Quart. Jour. Roy. Meteorological Soc. 73, 1947, pp 426-436.

Section 4

AQUEOUS FUEL SYSTEMS

Prepared under the direction of
J. A. LANE AND N. F. LANSING
OAK RIDGE NATIONAL LABORATORY

AUTHORS' PREFACE

The advantages of circulating-fuel reactors, particularly those using aqueous solutions or slurries of uranium salts, have been well recognized since the early days of the Manhattan Project. A considerable development effort aimed at applying these systems to the problem of producing plutonium was undertaken in the period from 1943 to 1944 at the University of Chicago and elsewhere. However, the project was terminated because adequate quantities of heavy water and/or slightly enriched uranium could not be obtained within the assigned time. The subsequent small-scale development program was principally devoted to studying the properties of uranium solutions and slurries and to work on reactor components for handling these materials.

Interest in aqueous, homogeneous reactors was renewed in 1946 at Oak Ridge National Laboratory in connection with the design and construction of a high-neutron-flux, research facility. After due consideration, the circulating-fuel system was again dropped in favor of a solid-fuel reactor because of difficulties encountered in the handling and pumping of radioactive slurries and the serious question concerning possible nuclear instability arising from the presence of large numbers of bubbles.

The third major attempt to solve the technical problems associated with aqueous solution reactors was initiated at Oak Ridge in 1949. The extent of this effort is indicated from the wealth of data accumulated and reported in the following chapters, with results to date culminating in the operation of the Homogeneous Reactor Experiment at conditions suitable for the production of electricity. Operation of this reactor, known as the HRE, has served chiefly to demonstrate the feasibility of equipment for circulating active fuel solutions and the inherent nuclear stability of the system. The major problems remaining to be solved are the effect of radiation on corrosion and the development of components for a full-scale reactor. The applications of the various solution or slurry systems for U-233 production and central-station power plants remain an attractive possibility, and the development effort is being continued at an undiminished rate.

The objectives of the various portions of this Section have depended on the particular subject at hand. Where appropriate, basic data bearing on a given topic have been assembled and analyzed. In other cases, current developments and applications of established theories to problems of particular relevance to aqueous homogeneous reactors have been described.

Generally, the data compilations have been inclined toward material which has not been compiled elsewhere but which is of special pertinence to aqueous homogeneous reactors. This approach tended to avoid duplication of certain non-project compilations and placed the major effort on previously unorganized material.

The portions of the Section devoted to specific problems are of a somewhat more transitory nature than the data compilations. They include the results of calculations for particular systems and experience acquired in the design, development, and operation of specific equipment. This material may be regarded as somewhat more indicative of the state of the art rather than definitive.

With a few exceptions, the cut-off date of the Section is July 1, 1952. Some of the experience resulting from operation of the Homogeneous Reactor Experiment has been included during final preparation of the manuscript, but these portions are readily identi-

AUTHORS' PREFACE

able by the context. The cut-off date is perhaps of most significance to the material on aqueous slurries (Chapter 4.4) as research results are rapidly unfolding within that area.

Certain contributions to the preparation of the Section have not been sufficiently delineated by the author credits. The preparation of most of Chapter 4.3 was guided by C. H. Secoy, while A. S. Kitzes assumed general responsibility for assembling Chapter 4.4. In addition, the entire Author Group wishes to acknowledge the contributions of the many who have assisted in the preparation of the manuscript. Mrs. Lou Gunnels contributed much to the assembling of the references. Special thanks are due to Mrs. Jo Millsaps who assumed responsibility for preparation of all charts and figures. Many helpful editorial revisions were introduced by Mrs. Mary Jenks.

J. A. Lane
N. F. Lansing

CHAPTER 4.1

General Reactor Characteristics

J. A. Lane

ADVANTAGES OF AQUEOUS SYSTEMS

Aqueous fuel systems possess certain advantages which make them particularly attractive for numerous nuclear-reactor applications ranging from small reactors for mobile units or packaged power plants to large, high-power reactors for large-scale production of plutonium, uranium-233, and/or power. These advantages stem partly from the fluid nature of the fuel and partly from the homogeneous mixture of the fuel and moderator; i.e., an aqueous homogeneous reactor combines the attributes of liquid-fuel heterogeneous reactors with those of water-moderated heterogeneous reactors.

If practical methods for handling an active aqueous fuel system can be developed, the inherent simplicity of this type of reactor should result in considerable economic gains in the production of fissionable material and power.

The principal advantages of aqueous fuel systems are:

HIGH SPECIFIC POWER

Since there is no heat-transfer barrier between fuel and coolant, the power density in a liquid-fuel reactor is limited only by the pumping rate and by the temperature rise of the fuel solution, itself. Thus, power densities of 50 to 200 kw are possible.

HIGH BURN-UP OF FUEL

In heterogeneous reactors, burn-up is limited by radiation damage to fuel elements or loss of reactivity. In liquid-fuel reactors, continual removal of poisons is possible as well as continual addition of new fuel, thereby permitting unlimited burn-up.

CONTINUOUS PLUTONIUM RECOVERY

Continuous removal of neptunium or plutonium is possible in a liquid-fuel reactor. This yields a product with a low plutonium-240 content and increases the value of the plutonium.

SIMPLE FUEL PREPARATION AND REPROCESSING

The use of aqueous fuel solutions or slurries eliminates the expensive fuel-element fabrication step and simplifies the reprocessing of depleted fuel.

EASY FUEL HANDLING

Charging and discharging fuel can be accomplished without shutting down the reactor or providing extensive fuel handling facilities.

HIGH NEUTRON ECONOMY

Neutron economy is improved by eliminating absorption of neutrons by cladding material and structural material within the reactor core. In addition, an aqueous fuel system lends itself more readily to a spherical core geometry which minimizes neutron leakage.

SIMPLE CONTROL SYSTEM

Density changes in the moderator create a sensitive, negative, temperature coefficient of reactivity which makes this system self-stabilizing. This eliminates the need for mechanically driven regulating rods. In addition, shim control can be achieved by changing the fuel concentration.

WIDE RANGE OF CORE SIZES

Depending on concentration and enrichment, critical H_2O and D_2O homogeneous reactors range from $1\frac{1}{2}$ ft to more than 30 ft in diameter. Correspondingly, there is a wide range of application for these reactor systems.

PROBLEMS OF AQUEOUS SYSTEMS

Many apparently formidable practical problems are associated with continued operation and maintenance of systems of active fuel solutions. It is believed, therefore, that extensive experience in adequately scaled reactor installations will be necessary to demonstrate the reliability of aqueous homogeneous reactors; this will necessitate a long-range development program. In addition, the choice of water as the fuel-bearing medium limits both the fuel concentration and operating temperature to values which may be less than optimum for production of plutonium and power. The principal problem of aqueous fuel systems are:

CORROSION OR EROSION OF EQUIPMENT

Circulation of fuel solutions or slurries at high rates creates corrosion and erosion problems in the reactor and its associated heat-removal equipment. Special provisions must therefore be made for decontaminating and maintaining equipment.

EXTERNAL CIRCULATION OF FUEL SOLUTION

To achieve the high specific powers mentioned previously, heat is removed by circulating the fuel solutions through external heat exchangers. This increases the inventory of fuel and D_2O , gives rise to a loss of delayed neutrons, and causes induced activity in the external equipment which results in additional shielding and maintenance problems. By permitting the core contents to boil and by removing heat from the vapor, these problems may be eliminated, probably however, with considerable sacrifice in specific power and possibly greater nuclear instability.

NUCLEAR STABILITY

The nuclear stability of the reactor depends on both bubble formation and the hydrodynamics of the system. In aqueous reactors, excessive gas formation resulting from decomposition may occur at higher power densities and give rise to serious fluctuations in reactivity. Solution of these problems may require an extensive development effort for each reactor modification.

LIMITED URANIUM CONCENTRATION

In solution reactors, uranium concentration is limited by solubility or corrosion effects, and in slurries, by the viscosity. In H_2O -moderated reactors in particular, a high uranium concentration is necessary for a large conversion ratio. Because of their limited uranium concentration, slightly enriched H_2O homogeneous reactors are not economical for plutonium production.

LIMITED OPERATING TEMPERATURE

Either excessive pressure or the phase stability of aqueous systems limits the operating temperature range to 250° to 300°C . This results in lower thermal efficiencies than those realized in liquid-metal-cooled systems.

Assuming that the investment cost of power-recovery equipment is comparable for both liquid-metal and aqueous systems, the lower thermal efficiencies of the latter may result in less economical power production.

EXPLOSIVE DECOMPOSITION PRODUCT

Radiation-induced decomposition of the moderator can produce an explosive mixture of hydrogen and oxygen in the reactor system. This hazard means that special precautionary design measures must be taken.

COMPOSITION OF AQUEOUS FUELS

The proper choice of fuel solution for an aqueous homogeneous reactor depends on considerations of chemical and nuclear stability, corrosion or erosion, and fuel handling and reprocessing. These are balanced against neutron absorption properties, which determine the required enrichment and rate of production of fissionable material, in order to find the optimum system. Unfortunately, existing information on the behavior of aqueous systems under actual reactor operating conditions is too meager for a realistic appraisal of their relative worth. At best, one can predict in only a general way the advantages of each fuel type.

The physical properties of aqueous solutions of the three most promising uranium salts— UO_2SO_4 , UO_2F_2 , and $\text{UO}_2(\text{NO}_3)_2$ —are fairly well known, at least under static conditions and in the absence of reactor radiation. In general, these solutions have comparable corrosion characteristics with type 347 stainless steel. More detailed data on corrosion are given in Chapter 4.3. The chemical stability of $\text{UO}_2(\text{NO}_3)_2$ may be somewhat less than that of solutions of UO_2SO_4 and UO_2F_2 but is satisfactory at low temperatures.

From a nuclear standpoint, the UO_2F_2 - D_2O system is more desirable than the UO_2SO_4 - D_2O system because the fluoride neutron cross section is considerably lower than that of sulfur. Similarly, the high absorption cross section of nitrogen makes the nitrate system even less desirable, unless one considers the use of nitrogen-15, which can be obtained only by isotope-separation methods.

The chemical processing of aqueous fluoride solutions is believed to be considerably more difficult than that of sulfate or nitrate systems.

On the basis of the existing information on corrosion, chemical stability, and chemical processing, the UO_2SO_4 - D_2O system appears to be the preferable fuel solution, although its use results in a minor compromise in neutron economy.

The relative merits of an oxide slurry and an aqueous solution are more difficult to assess. A slurry system has the advantage of high neutron economy, high chemical stability, and less corrosion difficulty but presents a more difficult fuel-handling problem. Moreover, the nuclear stability of the system, depends on the physical stability of the

suspension. This accentuates problems of reactor start-up and shutdown and continued maintenance of equipment which can only be solved through an extensive development program and experience with actual reactor operation.

CHAPTER 4.2

Neutron Chain Reactions in Aqueous Homogeneous Systems

CRITICAL CALCULATIONS

(S. Visner)

The statics of chain reactions in aqueous homogeneous reactors are of interest primarily in connection with the estimation of the inventory of fuel for a critical reactor and the rate of production of fissionable isotopes. The most important factors determining criticality are geometry; nature, concentration, and enrichment of the fuel; nature and distribution of other components in the reactor; and operating temperature. The production of fissionable isotopes depends principally on the neutron economy resulting from the competition for neutrons between the fertile material and the various other absorbers. The latter include materials of construction, moderator, fuel compound, fission products, and various nonfissionable nuclides formed by parasitic neutron capture in the fuel or other heavy nuclei in the system. In designing a reactor for the production of fissionable isotopes, it is therefore important to choose materials, other than fuel, for the core, which have a low neutron capture cross section. This in turn leads to the almost universal selection of D_2O as the moderator. The constituents of the fuel compound must also be selected on this basis.

The fuel element usually considered is uranium. In general, the highest enrichment available is desired for conversion of thorium-232 to uranium-233, since uranium-235 is required to minimize neutron capture by uranium-238. The thermal breeder considered here contains uranium-233 as both the fuel and the product.

It is shown later that appreciable quantities of the higher isotopes of uranium are built up as a result of parasitic capture of neutrons by the fuel.

METHODS OF CALCULATION

For simplicity, this discussion is restricted to spherical reactors. Since both heavy and light water are excellent moderators, the energy of fission neutrons is rapidly degraded to the thermal region, with the result that most of the fissions are produced by thermal neutrons. Both the one-group and two-group diffusion equations are therefore applicable for criticality calculations on aqueous homogeneous reactors.

For a large, bare, spherical reactor of radius R , the one-group equation for criticality is:

$$B^2 = \frac{k - 1}{L^2 + k\tau} \quad (1)$$

where:

$$B = \pi/R \quad (2)$$

and:

$$k = \eta \epsilon p f \quad (3)$$

with ϵ , the fast-fission effect, taken as unity, and:

$$\eta = \frac{\nu \Sigma_f(U)}{\Sigma_a(U)} \quad (4)$$

The thermal utilization, f , is given by:

$$f = \frac{\Sigma_a(U)}{\Sigma_a(U) + \Sigma_a(\text{mod}) + \Sigma_a(\text{other})} \quad (5)$$

and the resonance escape probability, p , is given by:

$$p = \exp \left[- \frac{N_x \left[\int \sigma \frac{dE}{E} \right] \text{eff}}{\Sigma_i (N \sigma_s \xi)_i} \right] \quad (6)$$

with N_x the number of atoms per cc which exhibit resonance absorption of neutrons and $(N \sigma_s \xi)_i$ the slowing down power of the i 'th constituent. Also:

$$L^2 = \frac{L^2(\text{mod}) \theta \sigma_a(\text{mod}) f}{F^2 \Sigma_a(U)} \quad (7)$$

where F is the fraction of the volume occupied by the moderator and θ is the ratio of moderating atoms to uranium atoms.

Thus, for an aqueous solution of UO_2SO_4 with a uranium-235 enrichment of α , and a ratio of moderating atoms to uranium atom of θ :

$$\eta_f = \frac{\alpha \nu \sigma_f(25)}{\alpha \sigma_a(25) + (1 - \alpha) \sigma_a(28) + \theta \sigma_a(\text{mod}) + \sigma_a(\text{UO}_2\text{SO}_4)} \quad (8)$$

where:

$$\alpha = N_{25}/N_{28} + N_{25}$$

The two-group critical equation for this type of reactor is:

$$k = (1 + L^2 B^2) (1 + \tau B^2) \quad (9)$$

The ratio of neutron absorptions in the fertile isotope to absorptions in the fuel isotope is the quantity:

$$\frac{\Sigma_a(\text{fertile isotope})}{\Sigma_a(\text{fuel isotope})} + \frac{(1 - p)}{1 + B^2 \tau} \quad (10)$$

where the second term is the contribution from resonance absorption.

TWO-REGION REACTORS

The two-group diffusion equations have been used for criticality calculations for two-region reactors consisting of two concentric spheres. The effect of a thin shell of thickness

t separating the two regions can be taken into account by including its absorption of thermal neutrons in the boundary condition for the slow-neutron current. For a reactor containing essentially a low concentration (~ 1 gm/l) of uranium-233 or uranium-235 in the core and containing fertile material dispersed in a moderator in the blanket, the equations are:

Core fast flux:

$$D_{FC} \nabla^2 \phi_{FC} - \Sigma_{FC} \phi_{FC} + (k_C/p_C) \Sigma_{SC} \phi_{SC} = 0 \quad (11)$$

Core slow flux:

$$D_{SC} \nabla^2 \phi_{SC} - \Sigma_{SC} \phi_{SC} + \Sigma_{FC} \phi_{FC} = 0 \quad (12)$$

Blanket fast flux:

$$D_{FB} \nabla^2 \phi_{FB} - \Sigma_{FB} \phi_{FB} - \Sigma_{RB} \phi_{FB} + (k_B/p_B) \Sigma_{SB} \phi_{SB} = 0 \quad (13)$$

Blanket slow flux:

$$D_{SB} \nabla^2 \phi_{SB} - \Sigma_{SB} \phi_{SB} + \Sigma_{FB} \phi_{FB} = 0 \quad (14)$$

The first letter of the subscript indicates the neutron group (F for fast and S for slow); the second letter indicates the reactor region (C for core and B for blanket). Thus, ϕ_{FC} is the fast-neutron flux in the core, and D_{SB} is the diffusion coefficient for slow neutrons in the blanket. Σ_{FC} and Σ_{FB} are "slowing-down" cross sections,* and Σ_{RB} is the true macroscopic absorption cross section for the fast group.

The boundary conditions at the shell, where $r = a_1$, are:

$$(\phi_{FC})_{r=a_1} = (\phi_{FB})_{r=a_1} \quad (15)$$

$$-D_{FC}(\nabla \phi_{FC})_{r=a_1} = -D_{FB}(\nabla \phi_{FB})_{r=a_1} \quad (16)$$

$$(\phi_{SC})_{r=a_1} = (\phi_{SB})_{r=a_1} \quad (17)$$

$$-D_{SC}(\nabla \phi_{SC})_{r=a_1} + D_{SB}(\nabla \phi_{SB})_{r=a_1} = \Sigma_a(\text{shell}) t (\phi_{SC})_{r=a_1} \quad (18)$$

Furthermore:

$$(\phi_{FB})_{r=a_2+E_F} = (\phi_{FB})_{r=a_2+E_F} = (\phi_{SB})_{r=a_2+E_S} = 0 \quad (19)$$

where E_F and E_S are the extrapolation distances for the fast- and thermal-neutron flux, respectively, and a_2 is the outer radius of the blanket.

Solution of the above system of equations yields the critical fuel concentration and the neutron fluxes, thereby permitting calculation of the conversion ratio or breeding gain. The conversion ratio is the ratio of the quantity:

$\{[\Sigma_a(\text{fissionable isotope}) - \Sigma_a(\text{higher isotopes in chain})]\phi + \Sigma_{RB} \phi_{RB}\}$ to $\Sigma_a(25) \phi_{SC}$ whereas the breeding gain is the difference between unity and a similar ratio where $\Sigma_a(25)$ is replaced by $\Sigma_a(23)$.

* $\Sigma_{FB} = D_{FB}/\tau_B$. The quantity $\Sigma_{FB} \phi_{FB}$ is the rate of loss per unit volume of fast neutrons which have entered the slow-neutron group.

BUILD-UP OF HIGHER ISOTOPES

The higher isotopes built up by neutron capture influence the neutron economy in the reactor and therefore the conversion ratio and breeding gain. This build-up occurs in accordance with the chain shown in Fig. 4.2.1. Only the more important reactions are indicated. Fast neutron reactions of the type (n,2n) are not included since their contribution is small.

BUILD-UP FROM THORIUM IN BLANKET

In predicting the quantities of higher isotopes in the blanket, the assumption is usually made, with negligible error, that thorium-233 decays to protactinium-233 immediately upon formation. It is also postulated that thorium-232 is continually replenished and is thus maintained at a constant concentration. After the desired concentrations are reached in the blanket, the contents are assumed to be processed continually to remove protactinium, uranium, and fission products at a rate proportional to the quantity present, corresponding to a "chemical decay" constant C . For example, $C N_{23}$ is the chemical removal rate of uranium-233 in unit time from unit volume. The steady-state concentrations are given by:

$$\frac{N_{13}}{N_{02}} = \frac{\sigma_c(02) \phi_{SB}^*}{\sigma_c(13) \bar{\phi}_{SB} + \lambda_{13} + C} \quad (20)$$

$$\frac{N_{23}}{N_{02}} = \frac{\sigma_c(02) \bar{\phi}_{SB}^* \lambda_{13}}{[\sigma_c(13) \bar{\phi}_{SB} + \lambda_{13} + C] [\sigma_a(23) \bar{\phi}_{SB} + C]} \quad (21)$$

$$\frac{N_{24}}{N_{23}} = \frac{\sigma_c(23)}{\sigma_a(24) + C/\bar{\phi}_{SB}} \quad (22)$$

$$\frac{N_{25}}{N_{24}} = \frac{\sigma_c(24)}{\sigma_a(25) + C/\bar{\phi}_{SB}} \quad (23)$$

$$\frac{N_{26}}{N_{25}} = \frac{\sigma_c(25)}{\sigma_a(26) + C/\bar{\phi}_{SB}} \quad (24)$$

where $\bar{\phi}_{SB}$ is the average slow-neutron flux in the blanket, averaged over the external system as well (including, for example, heat exchangers), and λ_{13} is the natural radioactive disintegration constant for protactinium-233. A correction for the resonance absorption in thorium-232 is applied to ϕ_{SB} to yield ϕ_{SB}^* .

BUILD-UP FROM URANIUM-233 FUEL

Utilization of uranium-233 as a fuel gives rise to a sequence of higher uranium isotopes as shown in Fig. 4.2.1. Since uranium-237 has a half-life of only 6.9 days, it and the remainder of the uranium chain will be present in only very small quantities, and in most calculations they are usually ignored. The neptunium chain is also usually ignored on the basis that it is removed chemically from the reactor.

PURE URANIUM-233 FUEL

The concentrations of higher isotopes at equilibrium are given by:

$$\alpha_{43} \equiv \frac{N_{24}}{N_{23}} = \frac{\sigma_c(23)}{\sigma_a(24)} \quad (25)$$

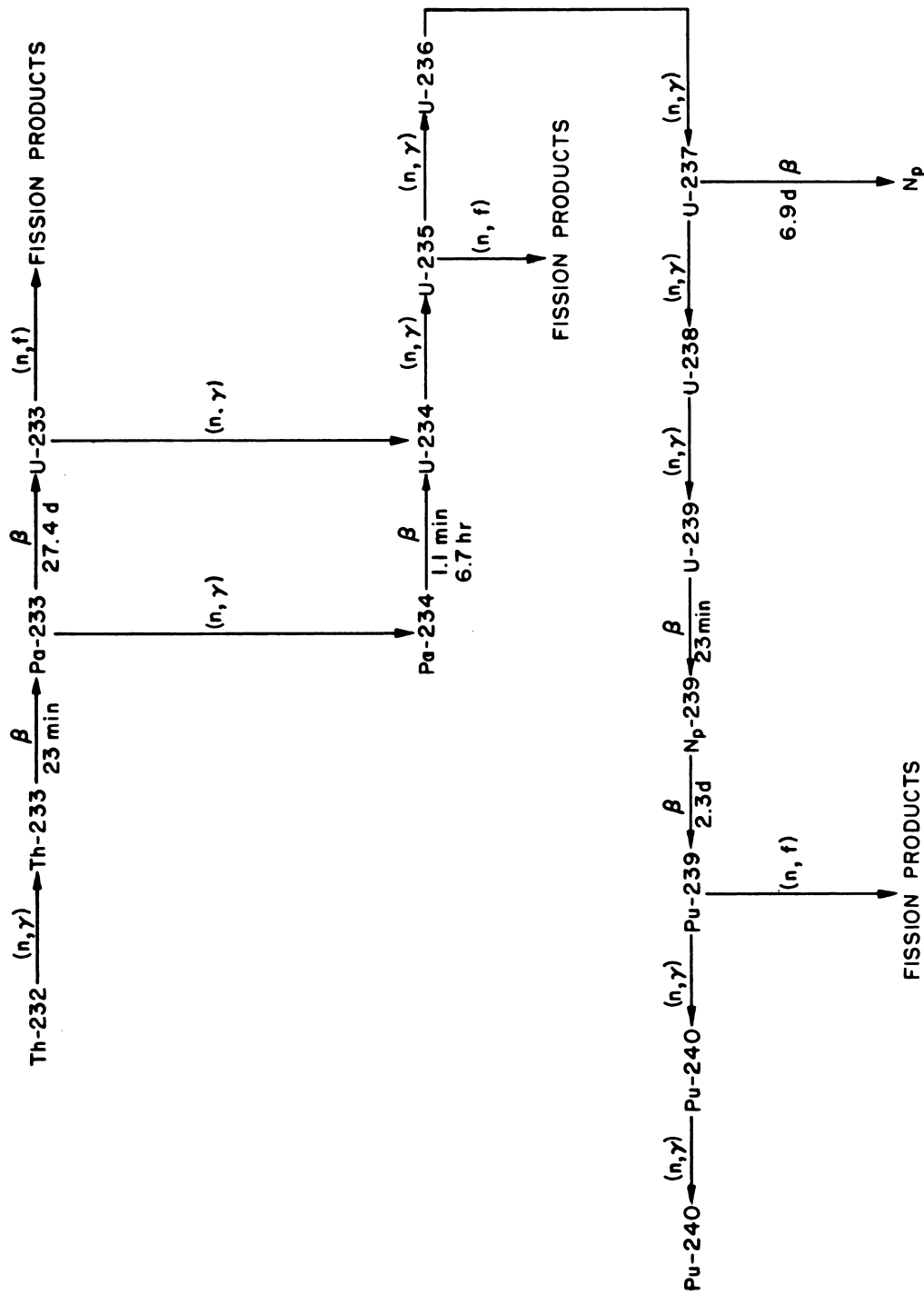


Fig. 4.2.1—Chain Showing Build-up of Higher Isotopes. Submitted by Oak Ridge National Laboratory, Nov. 25, 1952.

$$\alpha_{53} \equiv \frac{N_{25}}{N_{23}} = \frac{\sigma_c(23)}{\sigma_a(25)} \quad (26)$$

$$\alpha_{63} \equiv \frac{N_{26}}{N_{23}} = \frac{\sigma_c(23)}{\sigma_a(25)} \frac{\sigma_c(25)}{\sigma_a(26)} \quad (27)$$

Further, the ratios of macroscopic absorption cross sections are:

$$\Sigma_a(24)/\Sigma_a(23) = 0.0928$$

$$\Sigma_a(25)/\Sigma_a(23) = 0.0928$$

$$\Sigma_a(26)/\Sigma_a(23) = 0.0142$$

for the particular values of cross sections given in Table 4.2.1. The time dependence of the concentrations is given by:

$$\frac{N_{24}}{N_{23}} = \frac{\sigma_c(23)}{\sigma_a(24)} [1 - e^{-\bar{\phi}\sigma_a(24)t}] \quad (28)$$

$$\frac{N_{25}}{N_{23}} = \frac{\sigma_c(23)}{[\sigma_a(25) - \sigma_a(24)]} [1 - e^{-\sigma_c(24)\bar{\phi}t}] + \frac{\sigma_c(23) \sigma_a(24)}{[\sigma_a(25) - \sigma_a(24)] \sigma_a(25)} [1 - e^{-\sigma_c(25)\bar{\phi}t}] \quad (29)$$

and:

$$\frac{N_{26}}{N_{23}} = \frac{\sigma_a(23)\sigma_c(25)}{\sigma_a(25)\sigma_a(26)} [1 - e^{-\sigma_a(24)\bar{\phi}t}] + [1 - e^{-\sigma_a(25)\bar{\phi}t}] [1 - e^{-\sigma_a(26)\bar{\phi}t}] \quad (30)$$

where ϕ_{SC} is the thermal flux, averaged over both the core and the external system.

Table 4.2.1—Constants for Uranium at 20°C

(BNL-170)

Isotope	σ_f	σ_a	ν	η	σ_s
U-233	514	564	2.60	2.37	
U-234		89			
U-235	549	650	2.51	2.12	
U-236		21.3			
U-238		2.8			9.3

The presence of uranium-234 and uranium-236 leads to a loss of neutrons, but the absorption of one neutron by uranium-235 yields η_{25} neutrons. The net loss of neutrons to the higher isotopes is shown in Fig. 4.2.2 as a function of the product of neutron flux and time. The fraction of neutrons produced by uranium-233 which is lost to the higher isotopes reaches a maximum value of 0.0029, then decreases to -0.0008, and finally levels off at 0.0013.

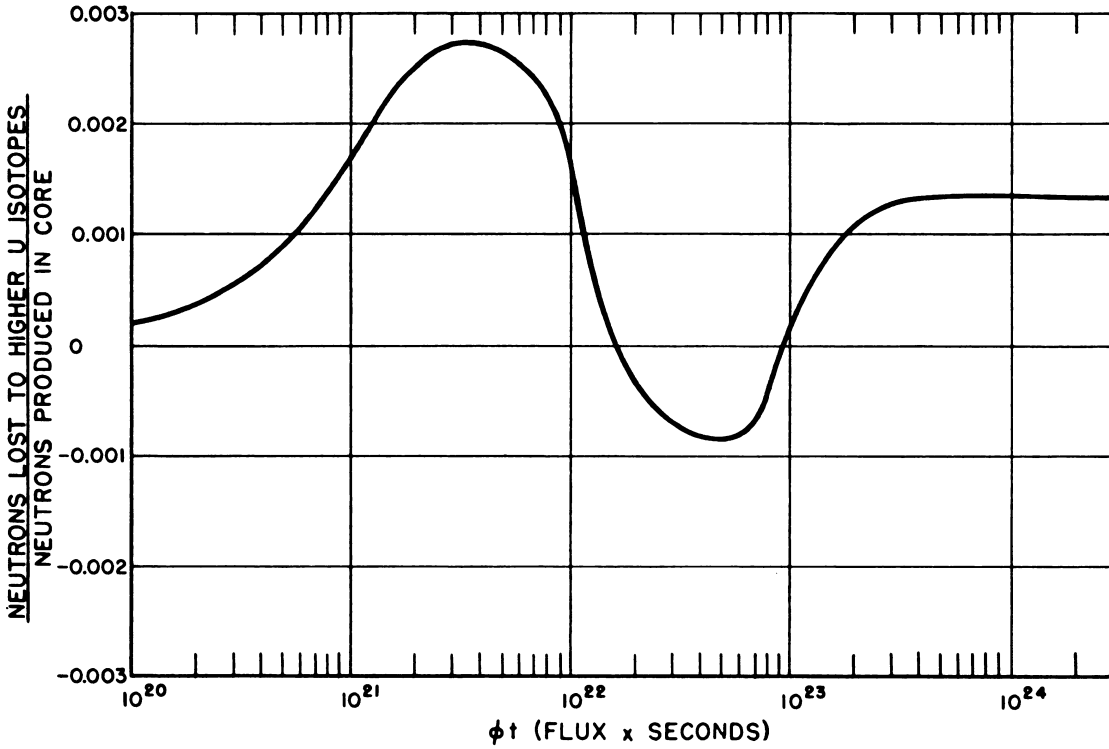


Fig. 4.2.2— Neutron Losses to Higher Isotopes in Breeder Core. Submitted by Oak Ridge National Laboratory, Nov. 25, 1952. Reprinted from ORNL-51-10-110.

CORE FED WITH URANIUM-233 PRODUCED IN BLANKET

In a two-region reactor for breeding, the fuel derived from the blanket and fed to the core is primarily uranium-233 containing quantities of uranium-234, uranium-235, and uranium-236 built up by (n, γ) reactions in the blanket. At equilibrium, the concentrations of the higher isotopes in the core are:

$$\frac{N_{24}}{N_{23}} = \frac{\sigma_c(23) + \alpha_{43}\sigma_a(23)}{\sigma_a(24)} \quad (31)$$

$$\frac{N_{25}}{N_{23}} = \frac{\sigma_a(23) + \sigma_a(23)\{\alpha_{43} + \alpha_{53}\}}{\sigma_a(25)} \quad (32)$$

$$\frac{N_{26}}{N_{23}} = \left[\frac{\sigma_a(23) + \sigma_a(23)\{\alpha_{43} + \alpha_{53}\}}{\sigma_a(25)} \right] \frac{\sigma_c(25)}{\sigma_a(26)} + \alpha_{63} \frac{\sigma_c(23)}{\sigma_a(26)} \quad (33)$$

where the α 's have already been defined.

BUILD-UP FROM URANIUM-235 FUEL

The build-up of isotopes higher than uranium-236 is here considered to be negligible. Variation of the uranium-236 concentration with time is given by:

$$\frac{N_{26}}{N_{25}} = \frac{\sigma_c(25)}{\sigma_a(26)} [1 - e^{-\sigma_a(26)\bar{\phi}t}] \quad (34)$$

In a reactor producing uranium-233, the fuel is uranium of high uranium-235 enrichment, in which case the uranium-238 diluent is constantly fed into the reactor at a rate $(1-\gamma)P$, where γ is the ratio of N_{25} to N_{28} in the feed material and P is the rate of fuel burn-up. If it is postulated that the uranium is continually reprocessed to remove fission products and that there is a resulting loss of uranium at a rate μN_U , the build-up of uranium-238 is then given by:

$$\frac{N_{28}}{N_{25}} = \frac{(1-\gamma)[\sigma_a(25) + \mu/\bar{\phi}_{SC}]}{\sigma_a(28) + \mu/\bar{\phi}_{SC}} \left[1 - e^{-(\mu + \sigma_a(28)\bar{\phi}_{sc})t} \right] \quad (35)$$

EXAMPLE OF BUILD-UP OF HIGHER ISOTOPES IN A TWO-REGION URANIUM-233 CONVERTER

Figure 4.2.3 shows the rate of build-up of neutron absorption cross section for uranium-236 and uranium-238 in the core of a two-region converter with the following characteristics:

Core Properties

$\phi = 1.1 \times 10^{15}$
 Diameter: 10 ft
 Content: UO_2SO_4 in D_2O
 Temperature: 250°C
 Power: 630×10^6 watts
 Isotopic ratio of uranium-235: ~90 percent
 $\mu = 5.8 \times 10^{-9}$ (corresponding to a uranium loss of 0.1 percent for a chemical processing cycle of two days)

Blanket Properties

$\phi = 0.06 \times 10^{15}$ (initially)
 Thickness: 2 ft
 Content: ThO_2 in D_2O
 Temperature: 250°C
 No processing

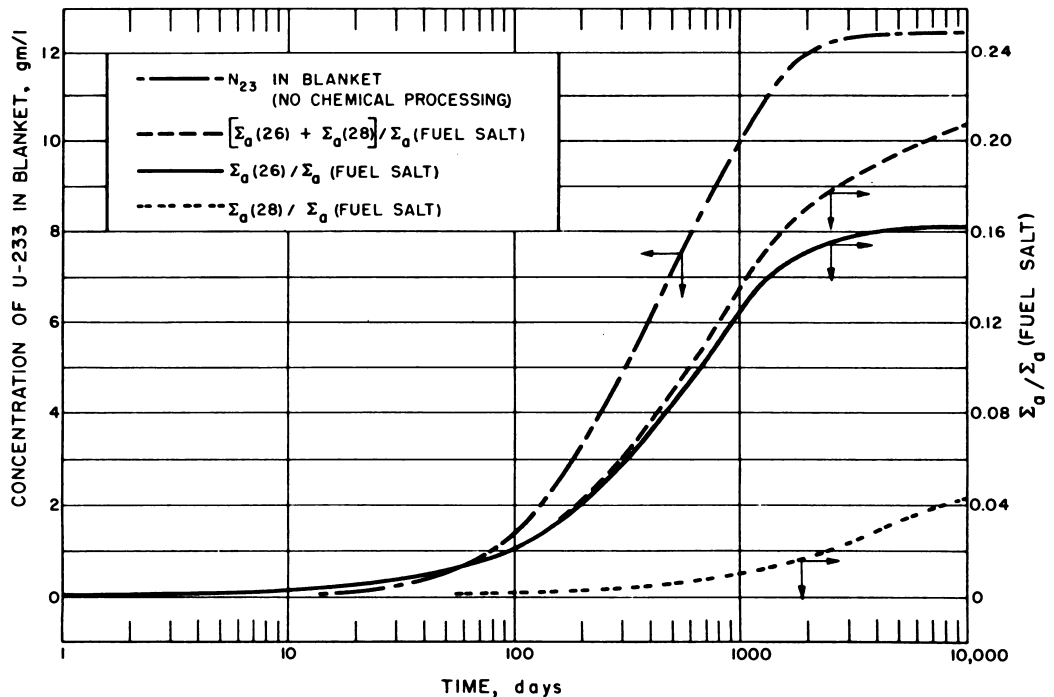


Fig. 4.2.3 — U-233 Two-region Converter Reactor. Build-up of Heavy Isotopes for 10-ft-diameter Core, 2-ft-thick Blanket of 1000 gm-Th/l; Power, 630 mw. Submitted by Oak Ridge National Laboratory, Nov. 25, 1952. Reprinted from ORNL-51-10-110.

The increase in uranium-233 content in the blanket is also shown. The average value for the slow-neutron flux in the blanket varies with time owing to variations of the fission rate in the blanket and changes in the hold-up volume in heat exchangers. For example, when a uranium-233 concentration of 7 gm/l is reached in the blanket, the fission power level in the blanket is approximately 300×10^6 watts.

NUCLEAR CONSTANTS

The nuclear constants for aqueous homogeneous systems which generally enter into calculations of criticality and isotope production are presented in Tables 4.2.1 thru 4.2.4.

Table 4.2.2—Constants for Heavy Water (99.84% D₂O and 0.16% H₂O)

Property	20°C	250°C
L^2 , cm ²	15,130	35,440
τ , cm ²	120	197
D_{thermal} , cm	0.91	125
σ_s (resonance), barns	9.97	9.97
$D_{\text{resonance}}$, cm	1.30	1.66
σ_a (thermal), barns	0.001824	0.001366
$\xi\sigma_s$, barns	5.009	5.009

Table 4.2.3—Constants for Uranium-233 Producers

Nuclide	Property	Magnitude at 20°C
Th-232	σ_a , barns	7
	σ_s (thermal), barns	12.8
	σ_s (resonance), barns	14.6
ThO	σ_s , barns	1.002
Pa-233	σ_a , barns	37
	Half-life, days	27.4
O	σ_a , barns	$<10^{-4}$
	σ_s (thermal), barns	4.1
	σ_s (resonance), barns	3.7
S	σ_a , barns	0.49
N	σ_a , barns	1.78
H	σ_a , barns	0.32

Table 4.2.4—Constants for ThO₂-D₂O Slurry

Th concentration, gm/l	1000	1000	500	500
Temperature, °C	20	250	20	250
D_{thermal} , cm	0.885	1.152	0.897	1.198
$D_{\text{resonance}}$, cm	1.180	1.429	1.236	1.537
Macroscopic resonance abs. cross section, cm ⁻¹ × 10 ³	4.86	4.62	2.87	2.72
τ (Fermi age), cm ²	121	187	120	191

The Fermi age, τ_B , in the slurry is obtained from the value of the age for heavy water, $\tau(D_2O)$ by the following relationship:

$$\tau_B = \frac{[\Sigma_{\text{trans}}(D_2O)] [\xi \Sigma_{\text{scatt}}(D_2O)]}{[\Sigma_{\text{trans}}(ThO_2 + D_2O)] [\xi \Sigma_{\text{scatt}}(ThO_2 + D_2O)]} \tau(D_2O) \quad (36)$$

The diffusion constants for the slurry are obtained as follows:

$$D(ThO_2 + D_2O) = \frac{1}{3\Sigma_{\text{trans}}(ThO_2 + D_2O)}$$

with:

$$\Sigma_{\text{trans}}(ThO + D_2O) = \Sigma_{\text{trans}}(ThO_2) + \Sigma_{\text{trans}}(D_2O)$$

and:

$$\Sigma_{\text{trans}}(D_2O) = \frac{F}{3D(D_2O)}$$

where F is the volume fraction occupied by the D_2O .

The macroscopic absorption cross section for thorium in the fast region, Σ_{RB} , is obtained as follows:

$$\Sigma_{RB} = \frac{D_{FB} N_{th}}{\tau_B \xi \Sigma_{\text{scatt}}} \int_{\text{thermal}}^{\text{fission}} \sigma_a(Th) \frac{dE}{E} \quad (37)$$

The value¹ of the resonance absorption integral, $\int_{\text{thermal}}^{\text{fission}} \sigma_a(Th) \frac{dE}{E}$, is $8.33 (\sigma_s)^{0.253}$,

where σ_s is the total macroscopic scattering cross section in the resonance region per thorium atom. For the limiting case of infinite dilution, the value of the integral is 81.3.

The resonance escape probability, p , is obtained by means of:

$$p = \exp \frac{\int_{\text{thermal}}^{\text{fission}} \sigma_a \frac{dE}{E}}{\sigma_s} \quad (38)$$

where σ_s is again the total macroscopic scattering cross section for resonance energies per atom exhibiting resonance absorption. For uranium, the resonance integral can be approximated analytically by $3.05 (\sigma_s)^{0.471}$. Values of p as a function of the ratio of uranium to D_2O atoms are presented graphically in Fig. 4.2.4. The corresponding curve for uranium in H_2O is shown in Fig. 4.2.5.

RESULTS

Many of the calculations for aqueous homogeneous systems have been made for UO_2SO_4 as the fuel compound. The nature of the fuel compound does affect to some extent the critical concentration and to a greater extent the conversion ratio through the neutron economy. Results for several fuel compounds will be given for comparison.

¹References appear at end of chapter.

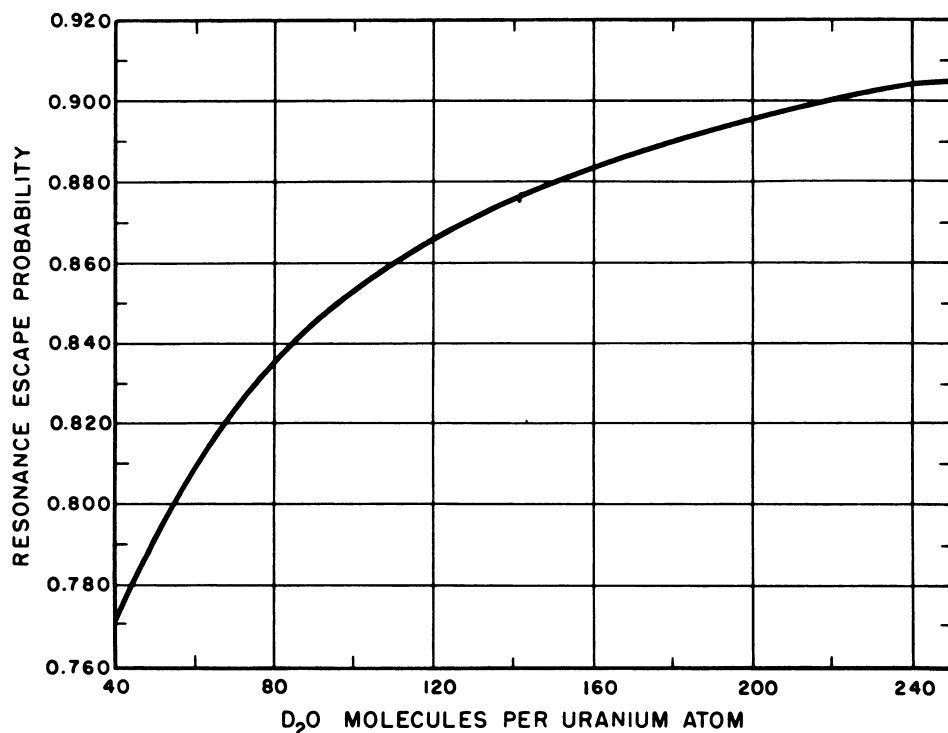


Fig. 4.2.4 — Resonance Escape Probability in Systems with Natural Uranium as UO_2SO_4 in Heavy Water. Submitted by Oak Ridge National Laboratory, Nov. 25, 1952. Reprinted from ORNL-51-11-41. Basis: 99.84% D_2O , 0.16% H_2O ; $\sigma = 9$ barns.

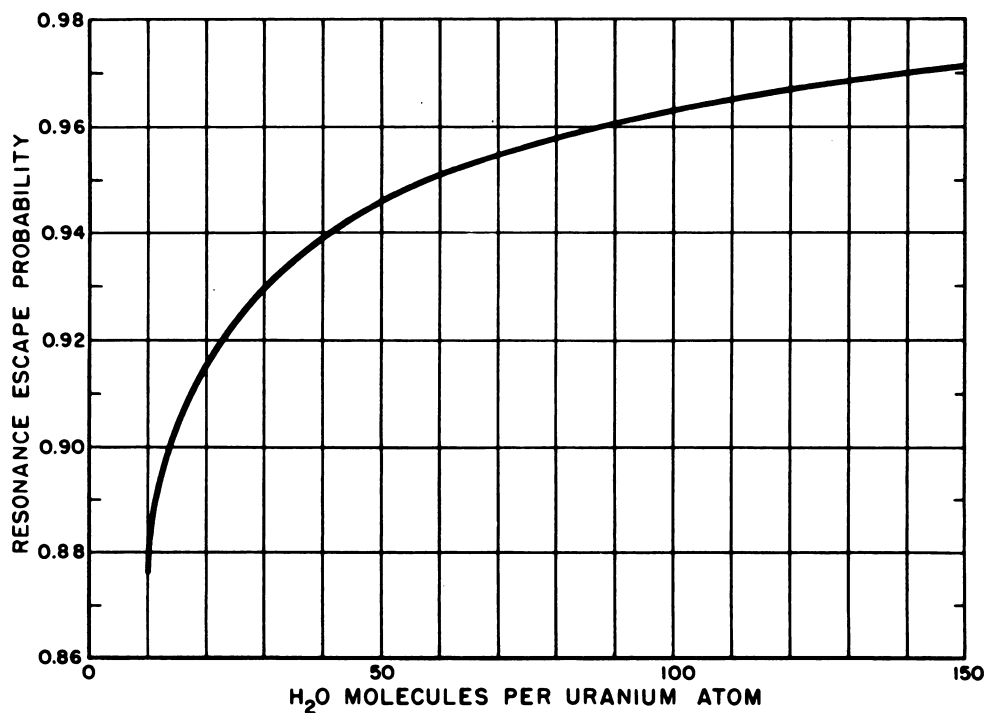


Fig. 4.2.5 — Resonance Escape Probability in Systems with Natural Uranium as UO_2SO_4 in Ordinary Water. Submitted by Oak Ridge National Laboratory, Nov. 25, 1952. Reprinted from ORNL-51-11-91.

Table 4.2.5—Maximum Powers for Spherical Reactors

Core diameter, ft	Power, megawatts ($\times 10^{-3}$)
5	0.090
8	.34
10	.63
15	2.0
20	4.9
25	9.5
30	16.2

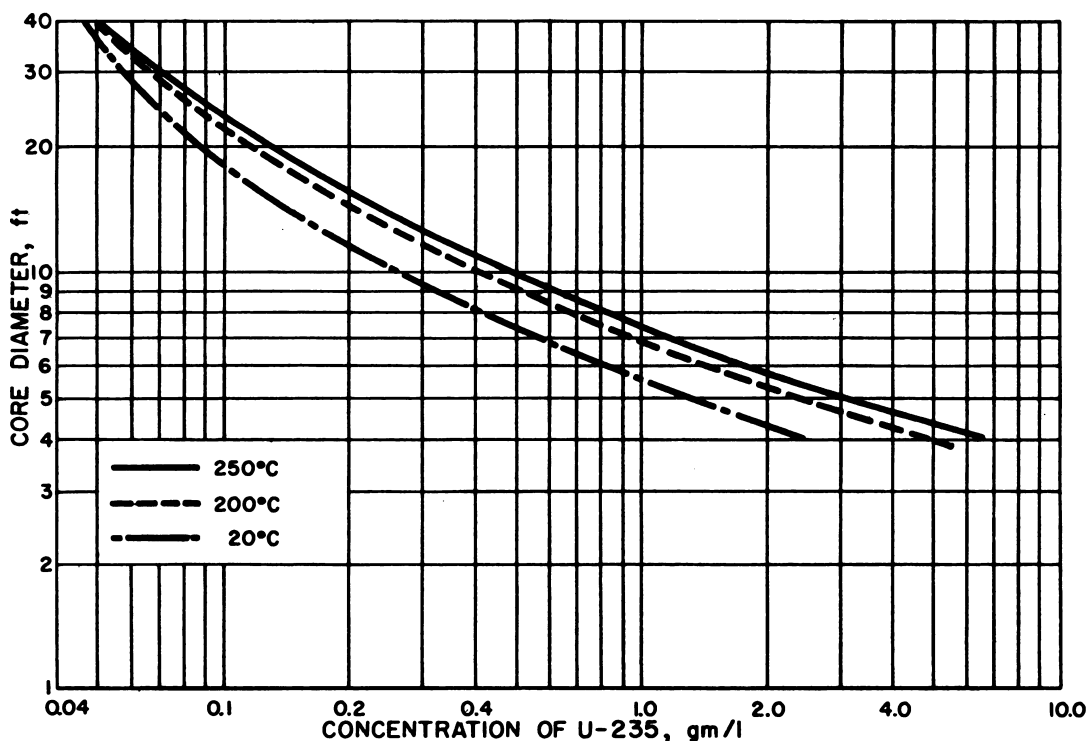


Fig. 4.2.6—Concentration of U-235 Required for Criticality of Bare UO_2SO_4 - D_2O Homogeneous Spherical Reactors. Submitted by Oak Ridge National Laboratory, Nov. 25, 1952. Reprinted from ORNL-51-10-110.

PERMISSIBLE REACTOR POWER

The maximum powers for spherical reactors of various diameters have been deduced from considerations of heat removal and reactor stability in the presence of gas formation and are listed in Table 4.2.5 for spherical reactors. The criteria used are: The power density should not exceed 40 kw/l, and the decomposition gases from the water in the core should not exceed the delayed neutron fraction in reactivity value.

BARE REACTORS

In Fig. 4.2.6, the critical core diameter of spherical reactors is plotted as a function of uranium-235 concentration at 20°, 200°, and 250°C. The reactor contains only highly en-

riched (90 percent) uranium-235 as UO_2SO_4 in D_2O . At 250°C , the critical concentration varies from 4.0 gm/l of uranium-235 for a 5-ft radius to 0.47 gm/l for a 10-ft radius.

Similar results at 250°C are available for bare spherical reactors using uranium-235 of low enrichment. In Fig. 4.2.7, the isotopic ratio of uranium-235 (as UO_2SO_4) is plotted as a function of the ratio of moderating molecules to uranium atoms, for spheres 4-, 6-, 8-, and 10-ft in diameter. Allowance is made for poisons to the extent of 2 percent in k_{eff} . Values are presented both for H_2O and for D_2O moderators.

The minimum critical radius of an unpoisoned, bare, spherical reactor utilizing UO_2SO_4 in D_2O is shown in Fig. 4.2.8 as a function of the isotopic concentration of uranium-235. Curves are given at 20° , 100° , and 250°C for uranium-235 enrichment between 0.7 and 5.0 percent. At 250°C , a comparison is made of the results based on a value of η for natural uranium of 1.350 and a value of 1.335. The critical radius for isotopic ratios from 0.7 to 5.0 percent is plotted in Figs. 4.2.9, 4.2.10, and 4.2.11 for reactor temperatures of 20° , 100° , and 250°C , respectively. The effect on the critical radius of changing η from 1.335 to 1.350 decreases with enrichment; thus, at 0.71 percent isotopic concentration of uranium-235, the difference in radius is about 10 percent, whereas at 1.0 percent enrichment the difference is only 5 percent.

Further results on uranium-235 enrichment and reactor diameter are available where an allowance of 2 percent excess k_{eff} is made for parasitic poisons. In Fig. 4.2.12, the isotopic concentrations of uranium-235 concentration in the fuel is plotted against the ratio of moderating atoms to uranium atoms for diameters of 15, 20, and 30 ft, with UO_2SO_4 as the fuel salt. Similar results for $\text{UO}_3\text{-D}_2\text{O}$ and $\text{UO}_2(\text{NO}_3)_2\text{-D}_2\text{O}$ systems are shown in Figs. 4.2.13 and 4.2.14, respectively. It is found that the required isotopic ratio increases absorption by the fuel compound. UO_3 has the most favorable properties in a reactor, and $\text{UO}_2(\text{NO}_3)_2$ has the least desirable of the three compared. The performance of the nitrate can be improved by the use of nitrogen enriched in N^{15} which has a thermal absorption cross section of only 2×10^{-5} barns.

The effect of the reactor operating temperature on required uranium-235 enrichment is shown in Fig. 4.2.15 for the $\text{UO}_2\text{SO}_4\text{-D}_2\text{O}$ system. The increased neutron leakage from the reactor with temperature requires that enrichment also be increased.

ONE-REGION REACTOR FOR URANIUM-233 CONVERSION

Calculated results are available for bare, spherical reactors intended to convert thorium to uranium-233 at an operating temperature of 250°C . The reactor contents are ThO_2 , UO_2SO_4 (with a uranium-235 concentration of 90 percent), D_2O , and poisons to the extent of 2 percent in k_{eff} . The critical fuel concentrations and conversion ratios are given in Table 4.2.6 for reactors of 10-, 15-, and 20-ft diameter and thorium concentrations from 100 to 1000 gm/l. The conversion ratio increases with both diameter and thorium concentration, whereas the uranium-235 concentration decreases with increasing diameter but increases with thorium concentration.

ONE-REGION REACTOR FOR URANIUM-233 BREEDING

Results similar to those in Table 4.2.6 are presented in Table 4.2.7 for reactors intended to utilize uranium-233 as the fuel for breeding at 250°C . Allowance for poisoning has been included to the extent of 2 percent in k_{eff} . The trends of critical concentration and breeding gain with thorium concentration and reactor diameter are similar to those described for the uranium-233 converter.

TWO-REGION SPHERICAL REACTORS

As an alternative to the one-region reactors described previously, consideration can also be given to reactors containing a central core of fuel and a blanket containing mainly fertile

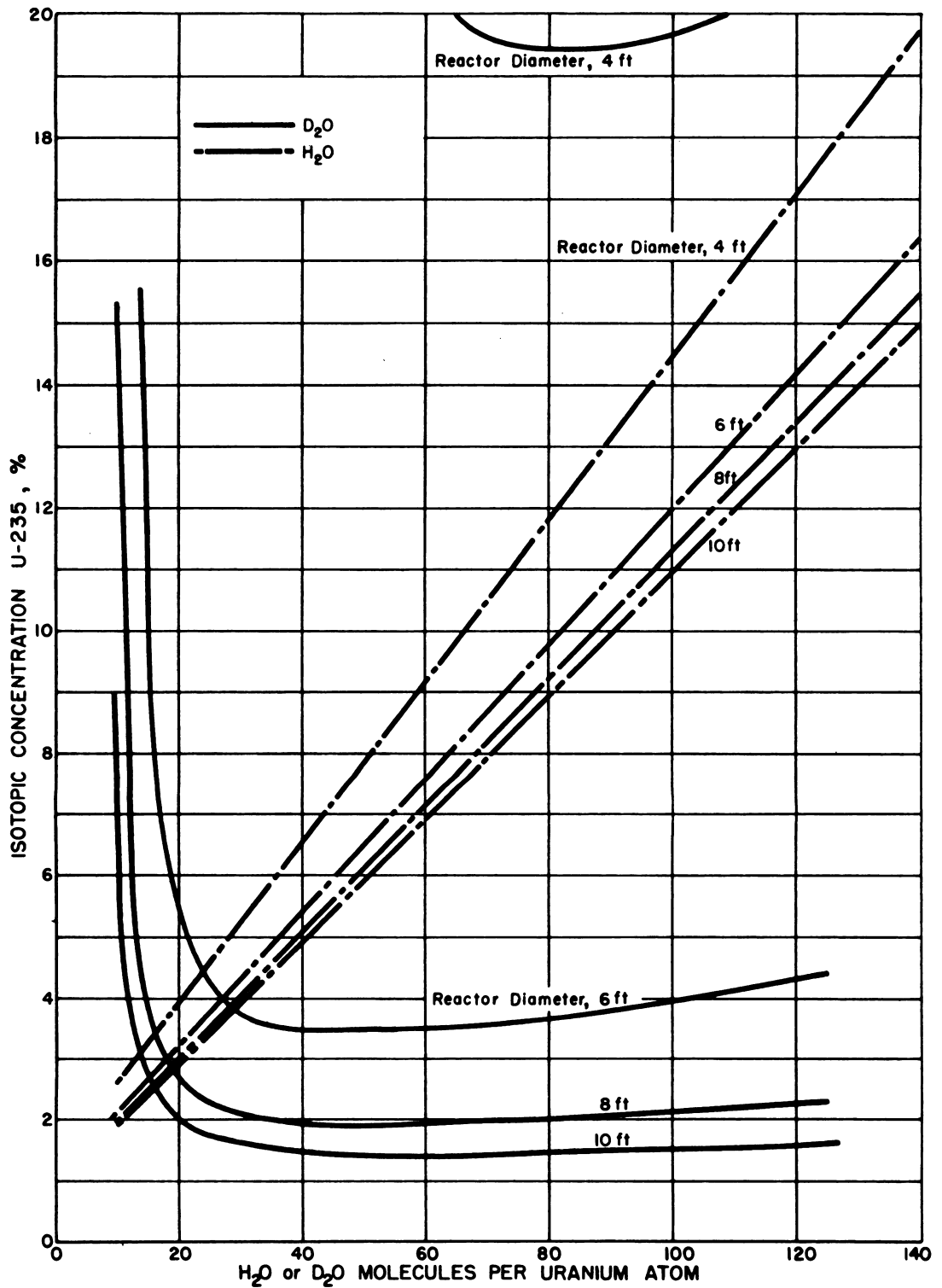


Fig. 4.2.7 — Isotopic Concentration of U-235 Required for Criticality of Aqueous UO_2SO_4 Solutions. Submitted by Oak Ridge National Laboratory, Nov. 25, 1952. Reprinted from ORNL-51-11-91. Calculated for bare spherical homogeneous reactors with $k_{\text{eff}} = 1.02$.

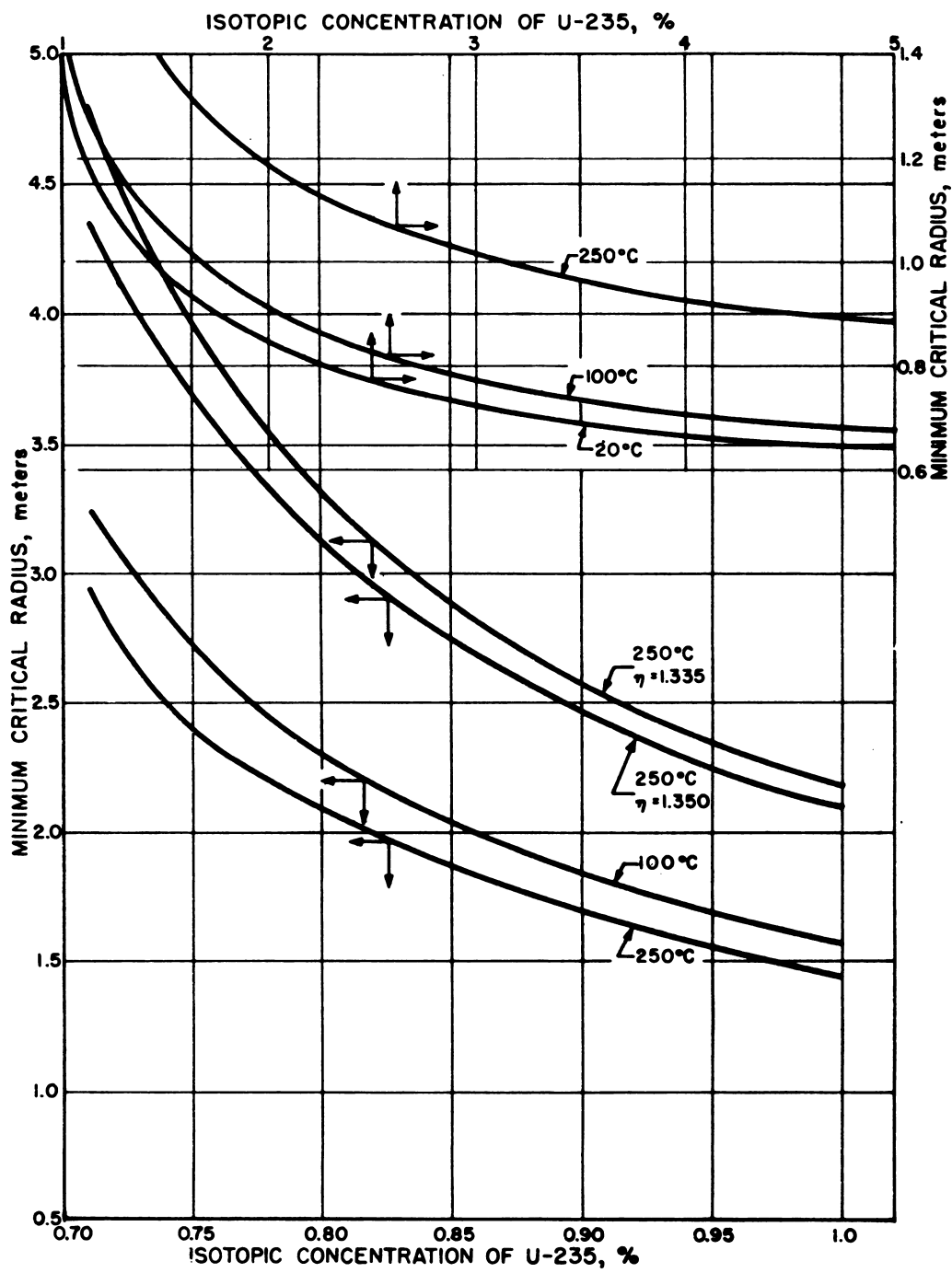


Fig. 4.2.8 — Minimum Critical Radii of Bare, Spherical Homogeneous $\text{UO}_2\text{SO}_4\text{-D}_2\text{O}$ Reactors. Submitted by Oak Ridge National Laboratory, Nov. 25, 1952. Reprinted from ORNL-51-11-41. Basis: heavy water contains 0.16% H_2O ; unpoisoned system.

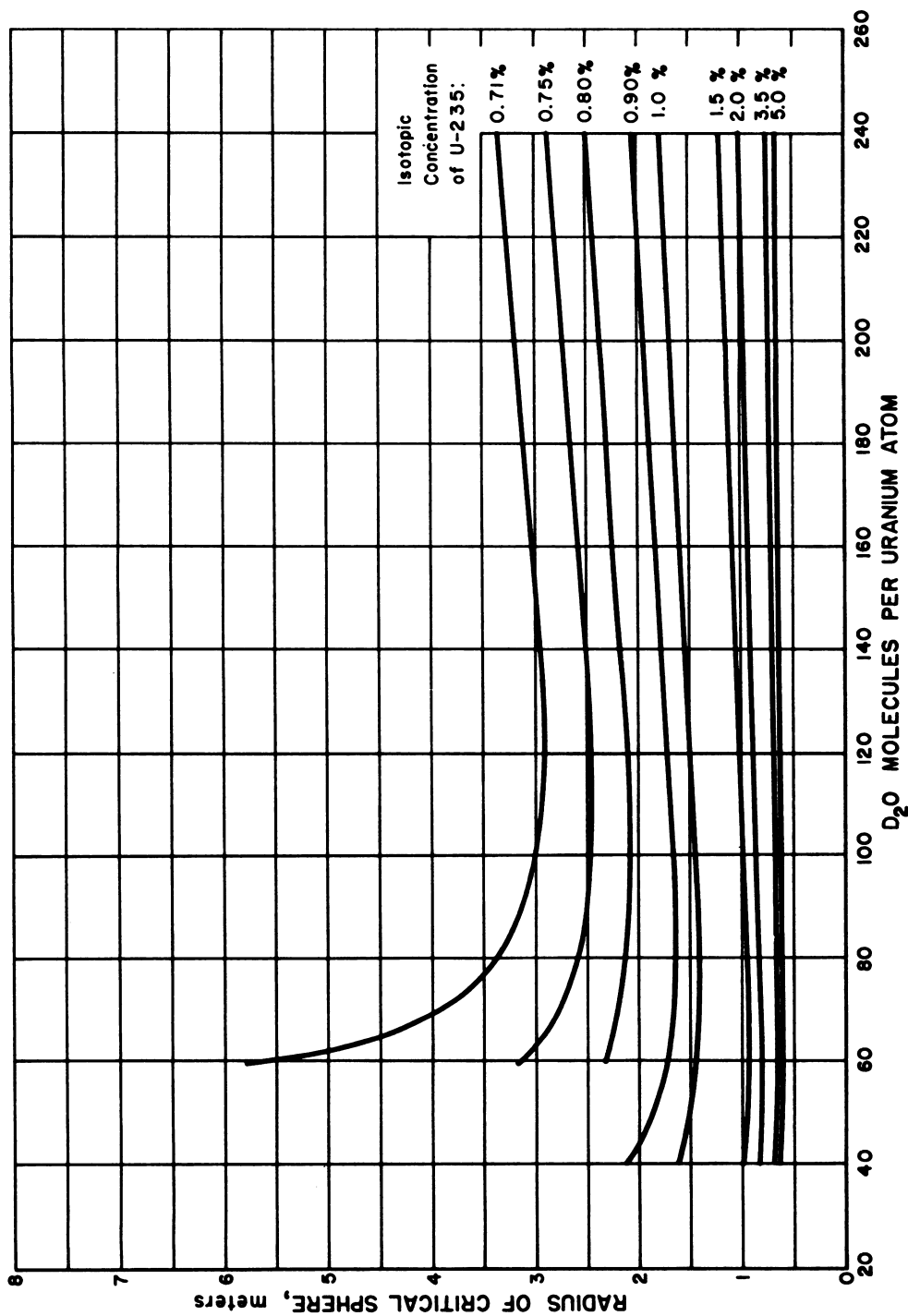


Fig. 4.2.9 — Critical Radii of Bare, Spherical, Homogeneous, $\text{UO}_2\text{SO}_4\text{-D}_2\text{O}$ Reactors at 20°C . Submitted by Oak Ridge National Laboratory, Nov. 25, 1952. Reprinted from ORNL-50-11-41. Basis: heavy water contains 0.16% H_2O ; $\sigma_a(\text{U-238}) = 2.59\text{b}$; $\eta = 1.35$ for natural uranium; unpoisoned system.

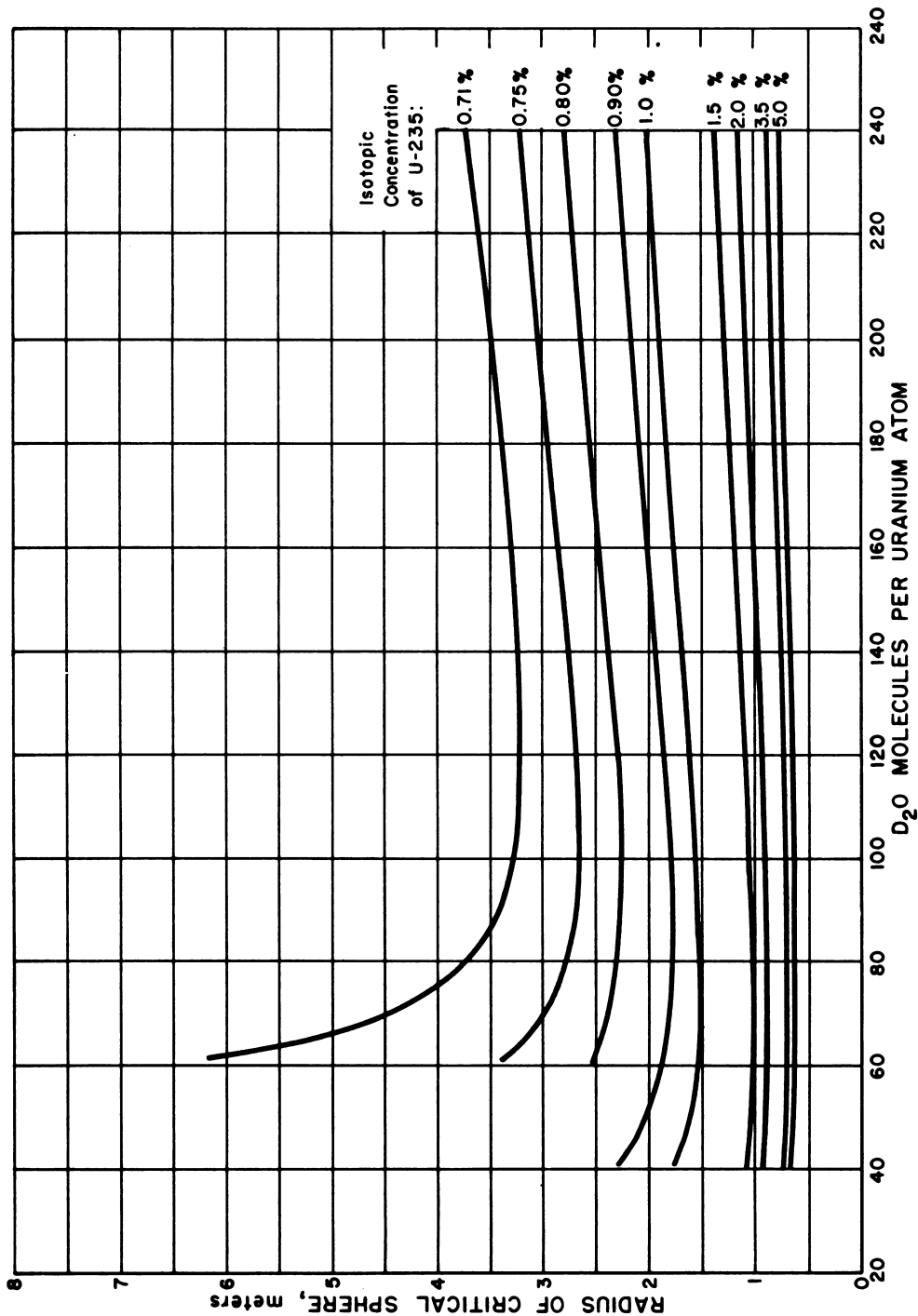


Fig. 4.2.10—Critical Radii of Bare, Spherical, Homogeneous, $\text{UO}_2\text{SO}_4\text{-D}_2\text{O}$ Reactors at 100°C . Submitted by Oak Ridge National Laboratory, Nov. 25, 1952. Reprinted from ORNL-50-11-41. Basis: heavy water contains 0.16% H_2O ; $\sigma_a(\text{U-238}) = 2.59\text{b}$; $\eta = 1.35$ for natural uranium; unpoisoned system.

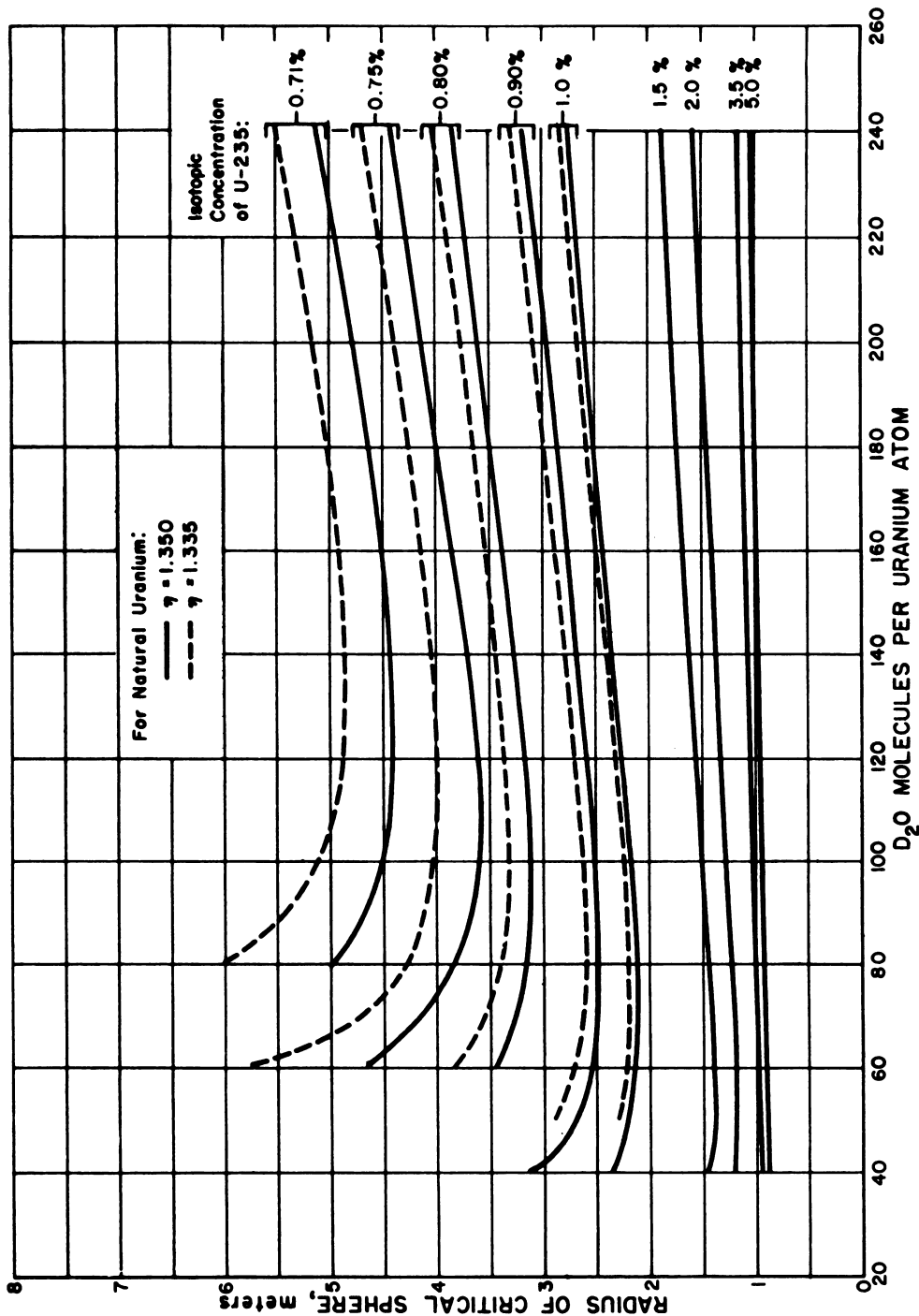


Fig. 4.2.11—Critical Radii of Bare, Spherical, Homogeneous, $\text{UO}_2\text{SO}_4\text{-D}_2\text{O}$ Reactors at 250°C . Submitted by Oak Ridge National Laboratory, Nov. 25, 1952. Reprinted from ORNL-50-11-41. Basis: heavy water contains 0.16% H_2O ; $\sigma_a(\text{U-238}) = 2.59\text{b}$; $\eta = 1.35$ for natural uranium, unpoisoned system.

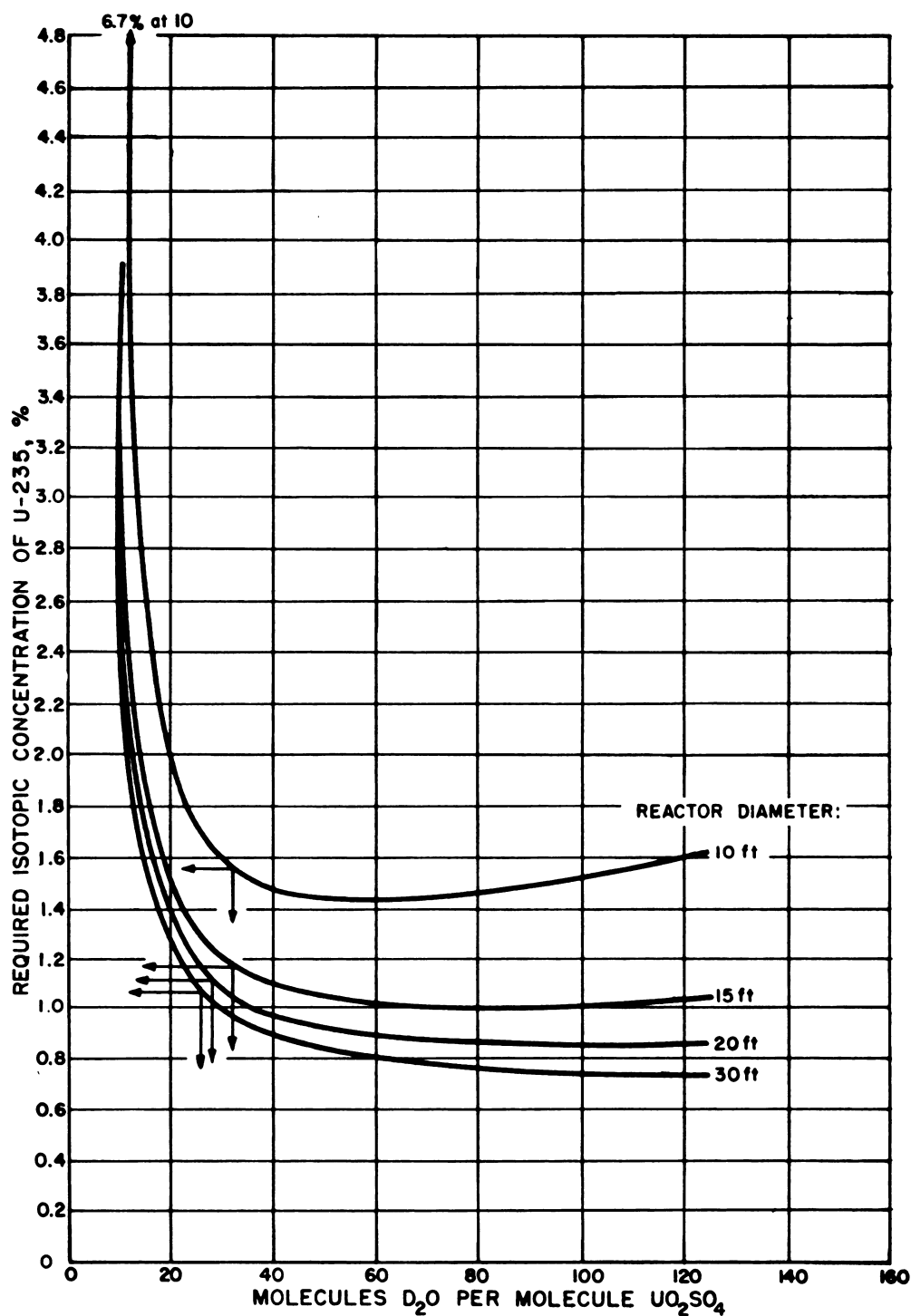


Fig. 4.2.12—Isotopic Concentration of U-235 Required for Criticality in Bare, Spherical $\text{UO}_2\text{SO}_4\text{-D}_2\text{O}$ Reactors at 250°C. Submitted by Oak Ridge National Laboratory, November 25, 1952. Reprinted from ORNL-1096.

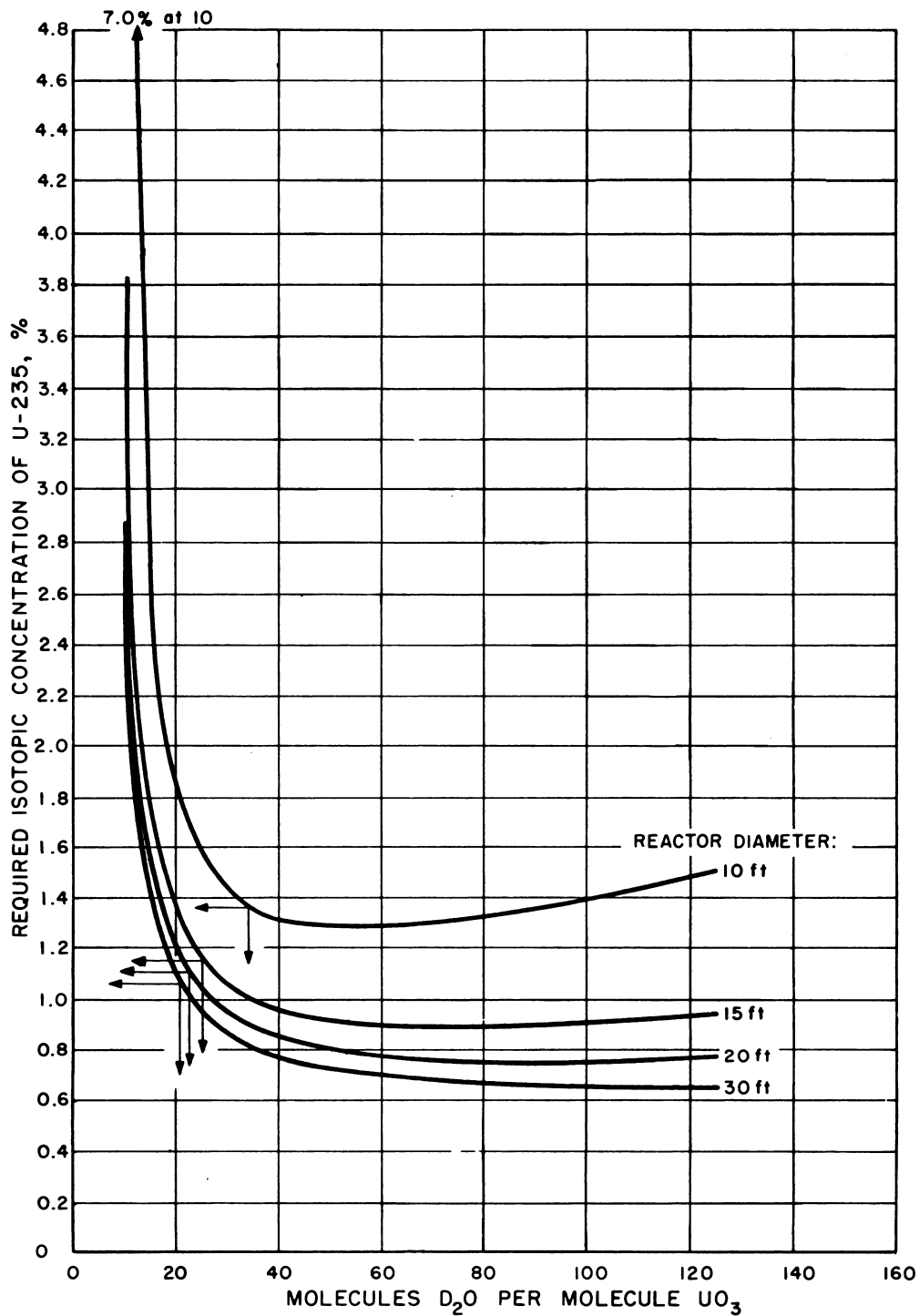


Fig. 4.2.13—Isotopic Concentration of U-235 Required for Criticality in Bare, Spherical UO₃-D₂O Reactors at 250°C. Submitted by Oak Ridge National Laboratory, Nov. 25, 1952. Reprinted from ORNL-1096.

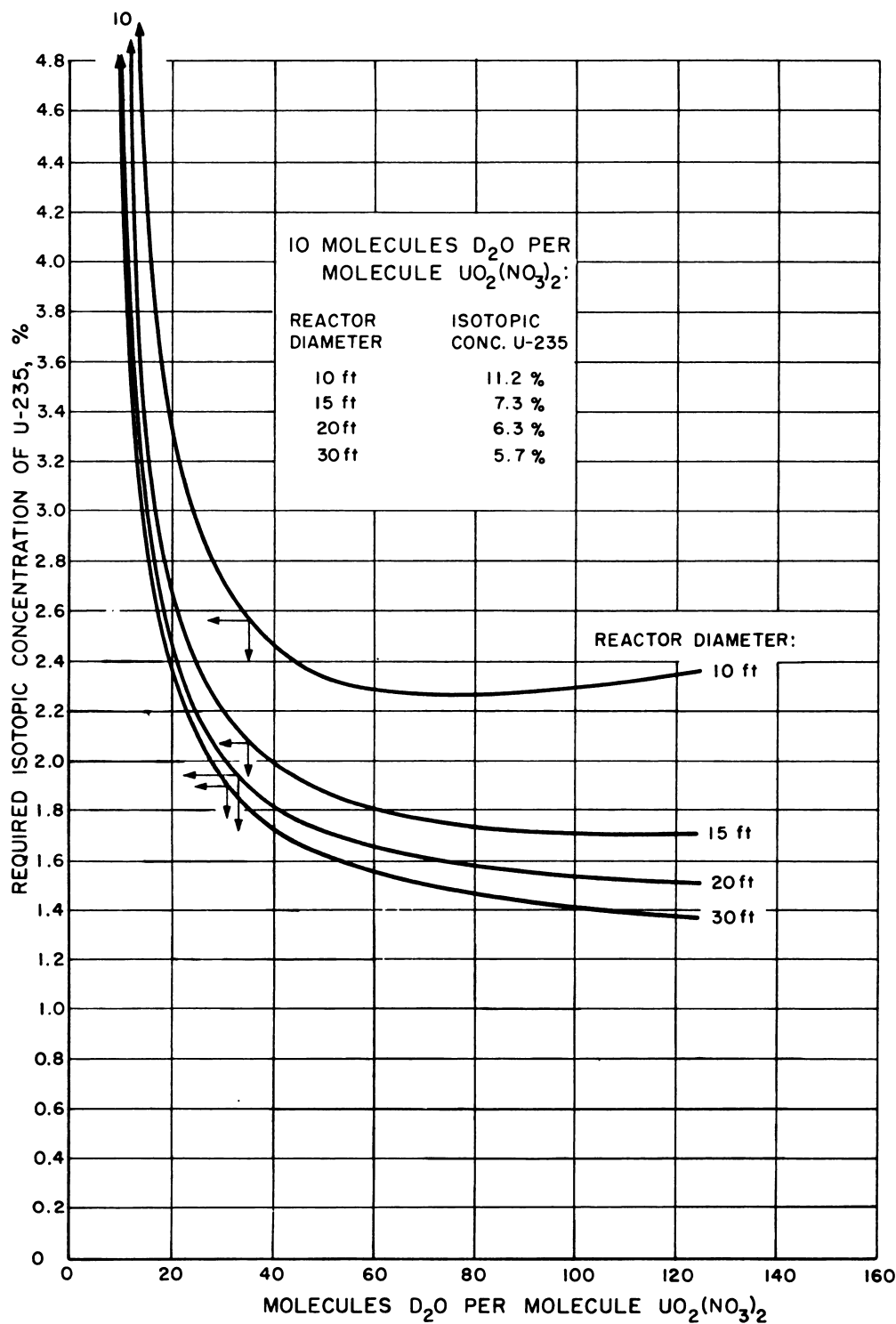


Fig. 4.2.14 — Isotopic Concentration of U-235 Required for Criticality in Bare, Spherical $UO_2(NO_3)_2$ - D_2O Reactors at 250°C. Submitted by Oak Ridge National Laboratory, Nov. 25, 1952. Reprinted from ORNL-1096.

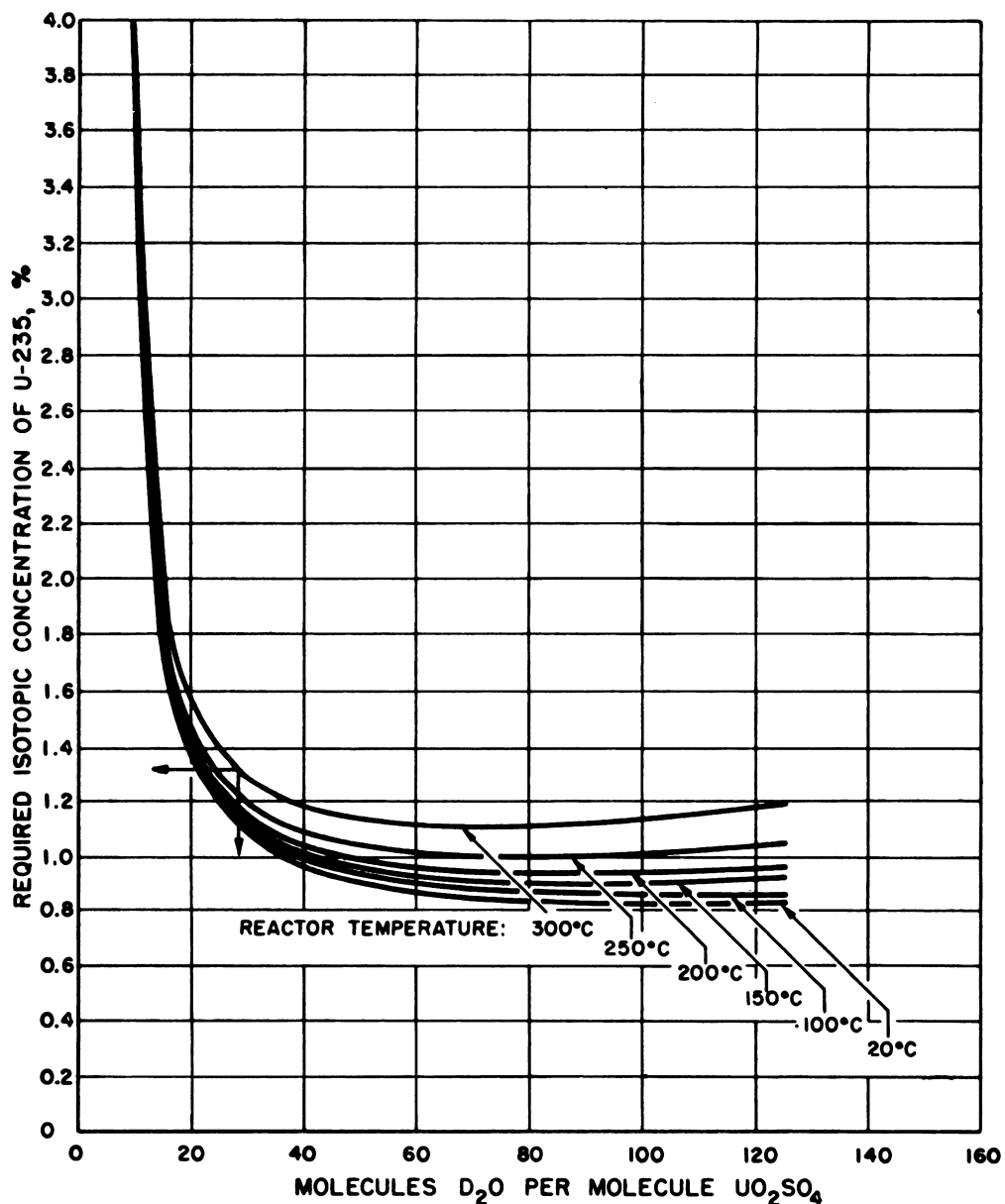


Fig. 4.2.15 — Isotopic Concentration of U-235 Required for Criticality in Bare, 15-ft-diameter, Spherical, $\text{UO}_2\text{SO}_4\text{-D}_2\text{O}$ Reactors at Various Temperatures. Submitted by Oak Ridge National Laboratory, Nov. 25, 1952. Reprinted from ORNL-1096.

Table 4.2.6—Critical Fuel Concentrations and Conversion Ratios

Th conc., gm/l	10-ft-diameter reactor		15-ft-diameter reactor		20-ft-diameter reactor	
	Conc. U-235, gm/l	Conversion ratio	Conc. U-235, gm/l	Conversion ratio	Conc. U-235, gm/l	Conversion ratio
100	2.105	0.687	1.588	0.865	1.433	0.942
200	4.313	.805	3.466	.944	3.214	.999
300	7.305	.853	5.962	.974	5.571	1.020
500	16.45	.895	13.32	.998	12.45	1.037
1000	253.05	.931	117.19	1.022	98.24	1.052

Table 4.2.7—Critical Fuel Concentrations and Breeding Gains

Th conc., gm/l	10-ft-diameter reactor		15-ft-diameter reactor		20-ft-diameter reactor	
	Conc. U-233, gm/l	Breeding gain	Conc. U-233, gm/l	Breeding gain	Conc. U-233, gm/l	Breeding gain
100	1.944	-0.174	1.485	0.034	1.346	0.124
200	3.899	-.031	3.182	.129	2.964	.192
300	6.441	.026	5.362	.164	5.039	.216
500	13.65	.075	11.42	.193	10.76	.237
1000	87.5	.119	62.52	.221	56.71	.250

material in a moderator. Separating the two regions is a shell which significantly affects the nuclear constants of the system. Zirconium has been considered as the shell material on the basis of maximum tensile strength per unit macroscopic absorption cross section. Two alternative designs are considered: One provides for a shell sufficiently thick to sustain the full operating pressure; the other utilizes a shell of minimum thickness to separate the two regions but not sufficient to sustain the full pressure. In the latter case, the pressure in the two regions must be equalized.

TWO-REGION REACTORS FOR URANIUM-233 CONVERSION

Calculations are available for two-region reactors having highly enriched uranium-235, in the form of UO_2SO_4 in D_2O , in a central core 5-, 8-, and 10-ft in diameter surrounded by $\text{ThO}_2\text{-D}_2\text{O}$ slurry in a blanket 2 ft thick. Separating the two regions is a zirconium shell whose thickness enters conveniently as a parameter. Among the factors which influence the critical concentration and conversion ratio and which have been considered in the calculations are: power level in the blanket owing to build-up of uranium-233, temperature of core and blanket, thickness of the core shell, concentration of thorium in the blanket, and thickness of the blanket. Results are also available on the behavior of the reactors as a function of operating time in order to take into account the build-up in both the core and blanket of heavy isotopes by neutron capture.

The critical concentration of uranium-235 as a function of shell absorption, $\Sigma_a t$ (where t is the shell thickness), is displayed in Fig. 4.2.16 for core diameters of 5, 8, and 10 ft. The corresponding conversion ratios are presented in Fig. 4.2.17. For a given shell thickness, the conversion ratio increases with decreasing core diameter owing to increasing neutron

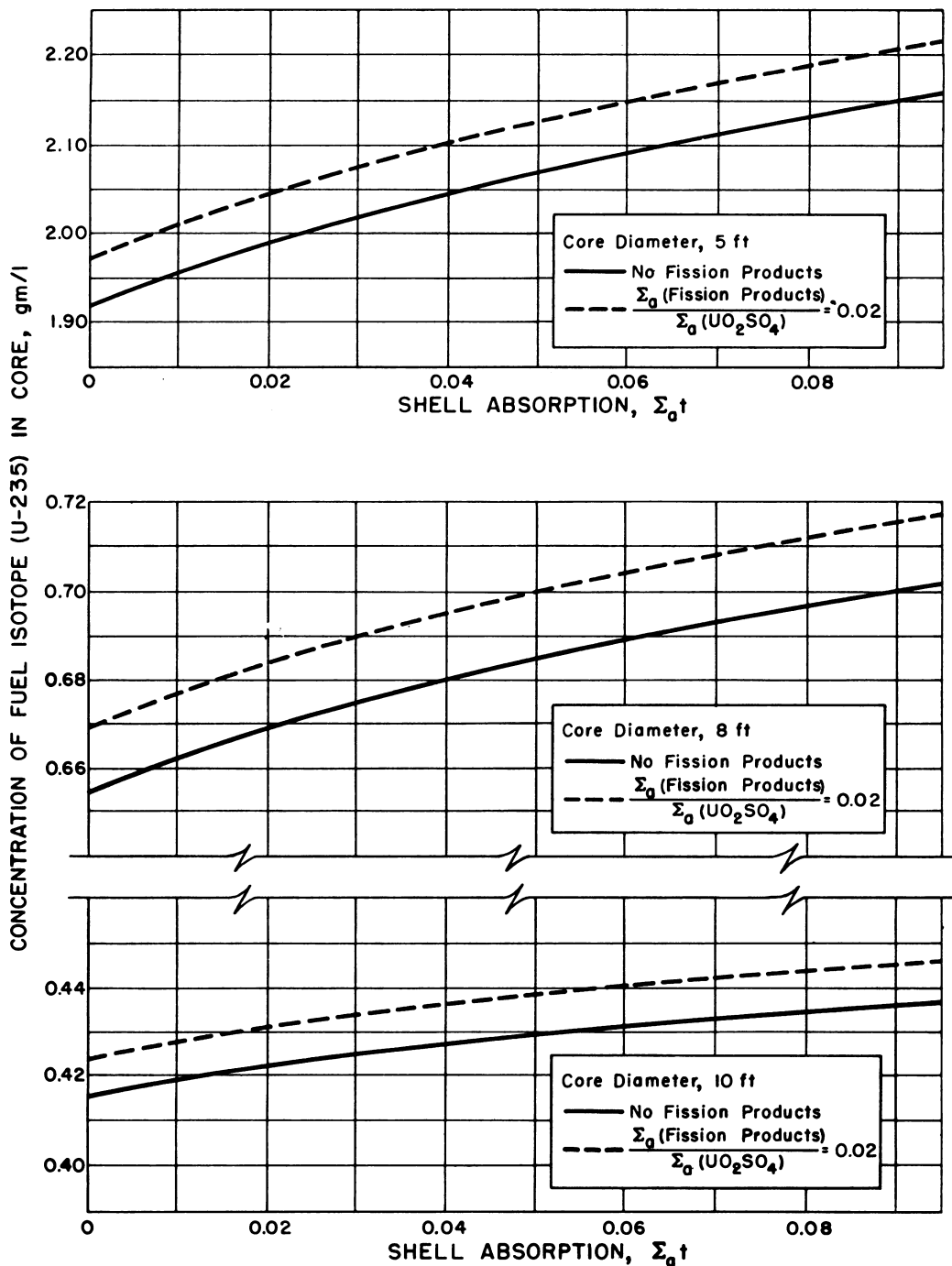


Fig. 4.2.16—U-233 Two-region Converter Reactor; U-233 Concentration in Core as Function of Shell Absorption with 2-ft-thick Blanket of 1000 gm Th/l. Submitted by Oak Ridge National Laboratory, Nov. 25, 1952. Reprinted from ORNL-51-10-110. System at 250°C; no build-up of heavy elements.

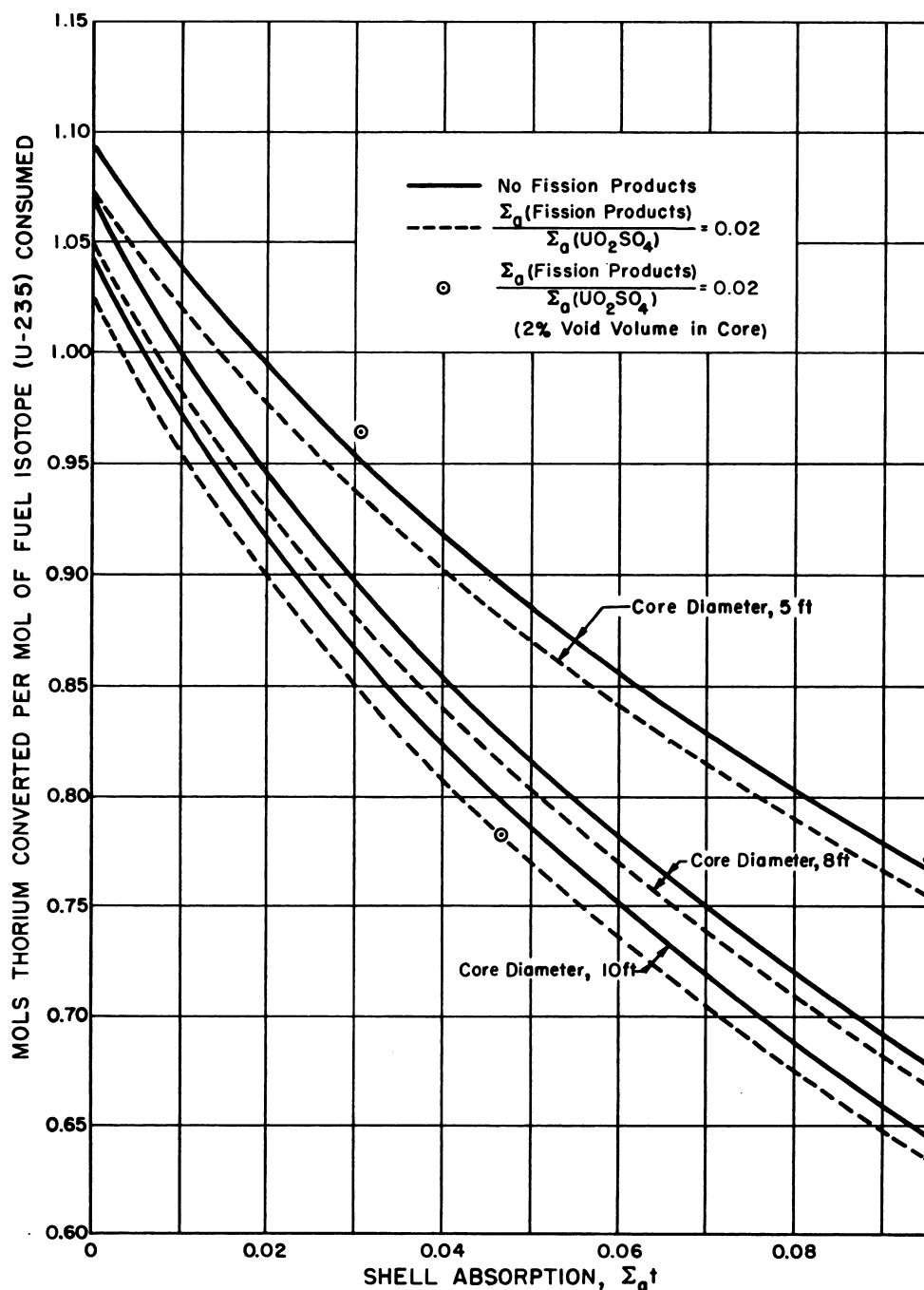


Fig. 4.2.17—U-233 Two-region Converter Reactor; Dependence of Conversion Ratio on Shell Absorption for 2-ft Blanket of 1000 gm Th/l. Submitted by Oak Ridge National Laboratory, Nov. 25, 1952. Reprinted from ORNL-51-10-110. System at 250°C; no build-up of heavy elements.

leakage from the core to the blanket. The increase in conversion ratio is even more pronounced if the shell is required to be of sufficient strength to withstand the full reactor pressure, since the smaller core requires a thinner shell.

The effects of (1) thorium concentration in the blanket and (2) blanket thickness on uranium-235 concentration and conversion ratio are shown in Fig. 4.2.18 and Fig. 4.2.19. The conversion ratio increases with thorium concentration since the relative absorption of neutrons by the shell and the moderator decreases. Very little gain is realized in utilizing blankets thicker than 2 ft.

Reactor Temperature

Figures 4.2.20 and 4.2.21 show the effects of varying the core and blanket temperatures; the conversion ratio increases with both core and the blanket temperatures.

Higher Isotopes and Blanket Power Time

Results are given in Figs. 4.2.22 and 4.2.23 for various concentrations of higher isotopes and fission-product poisons in both regions of a spherical reactor with a 10-ft-diameter core and a 2-ft-thick blanket. The uranium isotope concentrations correspond to various operating times for the reactor whereas the macroscopic absorption cross section for the fission products in the core is set at 2 percent of the value for the fuel salt. It is postulated that the gaseous fission products are purged very rapidly and the remaining fission products are continually removed by chemical means at a rate appropriate to the above 2 percent value. The required fuel concentration increases and the conversion ratio decreases with increasing poison content in the core. The poison may be either fission products or heavy isotopes resulting from neutron capture. The decrease in conversion ratio is numerically equal to the percentage of poison in the core. Increasing the ratio of blanket to core power tends to increase the conversion ratio. Increased fissioning in the blanket corresponds to higher uranium-233 content, reduced processing rate for the blanket, and consequently increased uranium-234 content and fission-product poisoning.

TWO-REGION REACTORS FOR URANIUM-233 BREEDING

Similar calculations have been performed for reactors containing uranium-233 in the core as UO_2SO_4 in D_2O and a 2-ft blanket of ThO_2 in D_2O . The effects of temperature, blanket thickness, and blanket concentration are similar to the effects already discussed in the case of the converter. Therefore, for all the breeding reactors to be discussed, the following conditions were postulated: Temperatures of core and blanket of 250°C , and a thorium concentration of 1000 gm/l in the blanket, whose thickness is 2 ft.

A convenient parameter for expressing the performance of a breeder is the "breeding gain," g , defined as the net gain in fissile material produced in the reactor per unit quantity of fuel burned:

$$g \equiv \frac{\text{net U-233 produced}}{\text{U-233 burned in core}} - 1$$

where the net uranium-233 produced is the difference between the quantity of thorium converted and the quantities of protactinium and uranium-233 lost by neutron absorption in the blanket.

CORE DIAMETER

In Fig. 4.2.24, the breeding gain is plotted against the shell absorption for core diameters of 5, 8, and 10 ft. The critical concentrations of uranium-233 in the core are shown

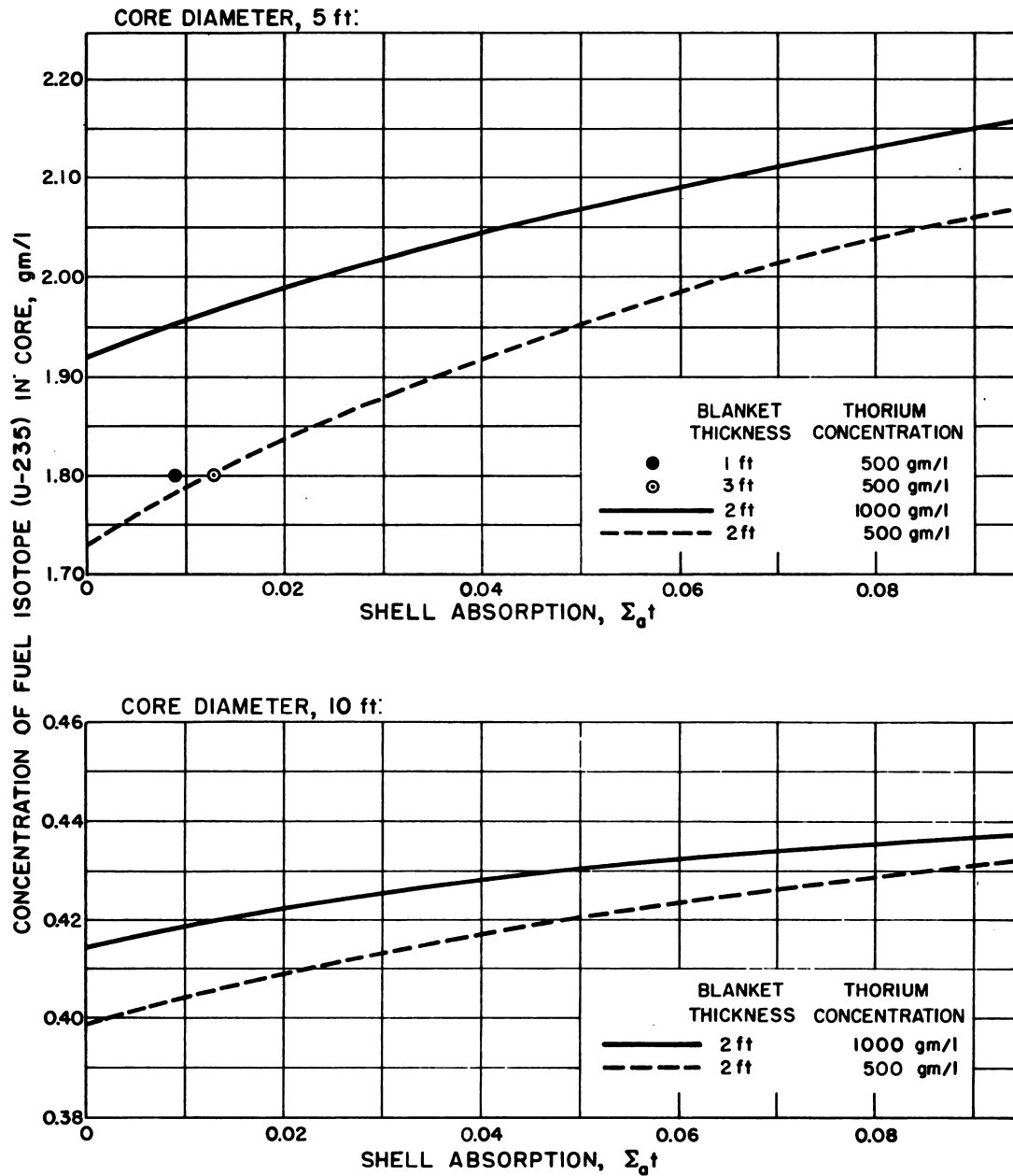


Fig. 4.2.18—U-233 Two-region Converter Reactor; Effect of Blanket Concentration and Thickness on Core Concentration. Submitted by Oak Ridge National Laboratory, Nov. 25, 1952. Reprinted from ORNL-51-10-110. System at 250°C.

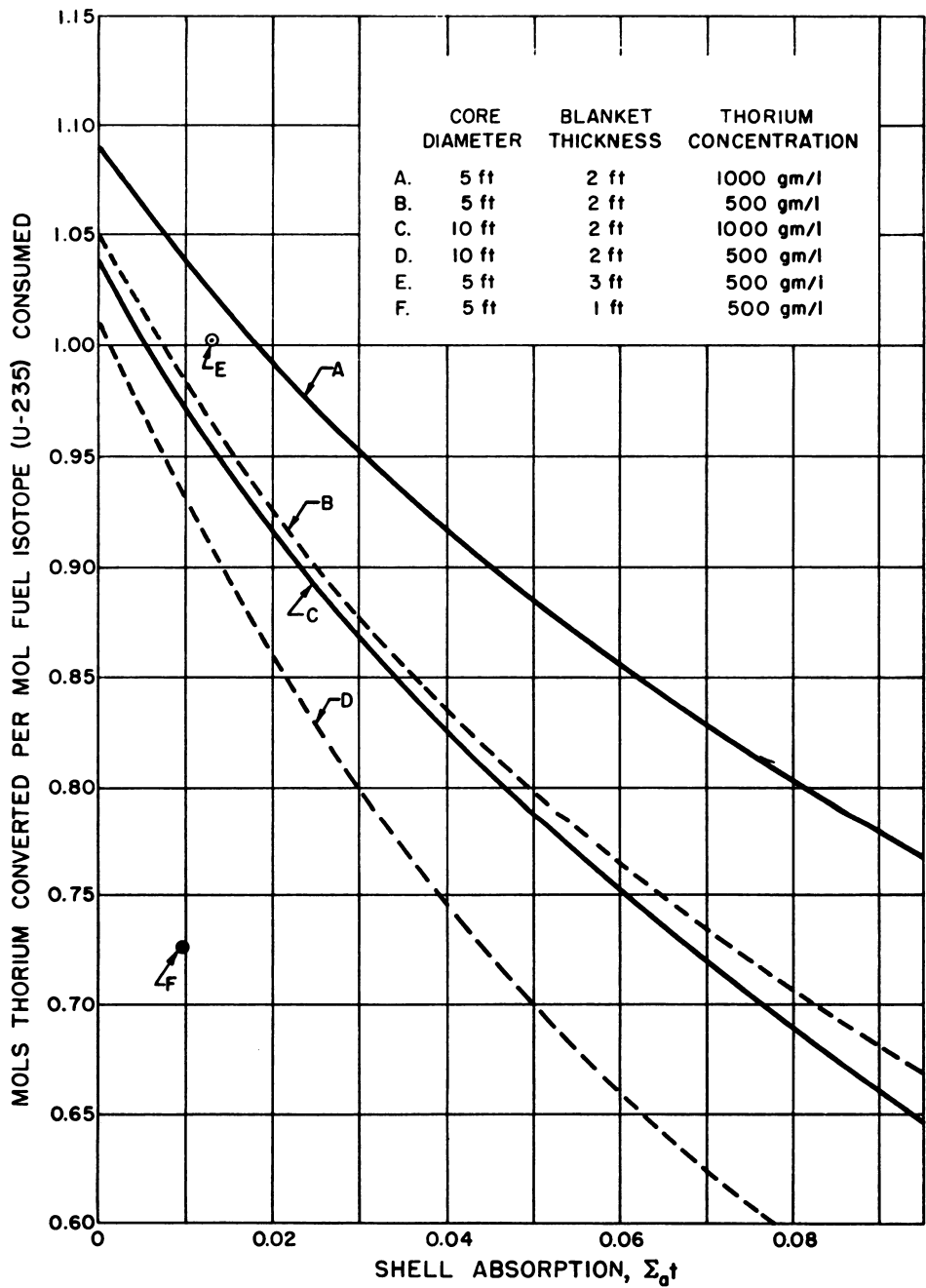


Fig. 4.2.19—U-233 Two-region Converter Reactor; Effect of Blanket Concentration and Thickness on Conversion Ratio for an Unpoisoned Reactor Operating at 250°C. Submitted by Oak Ridge National Laboratory, Nov. 25, 1952. Reprinted from ORNL-51-10-110.

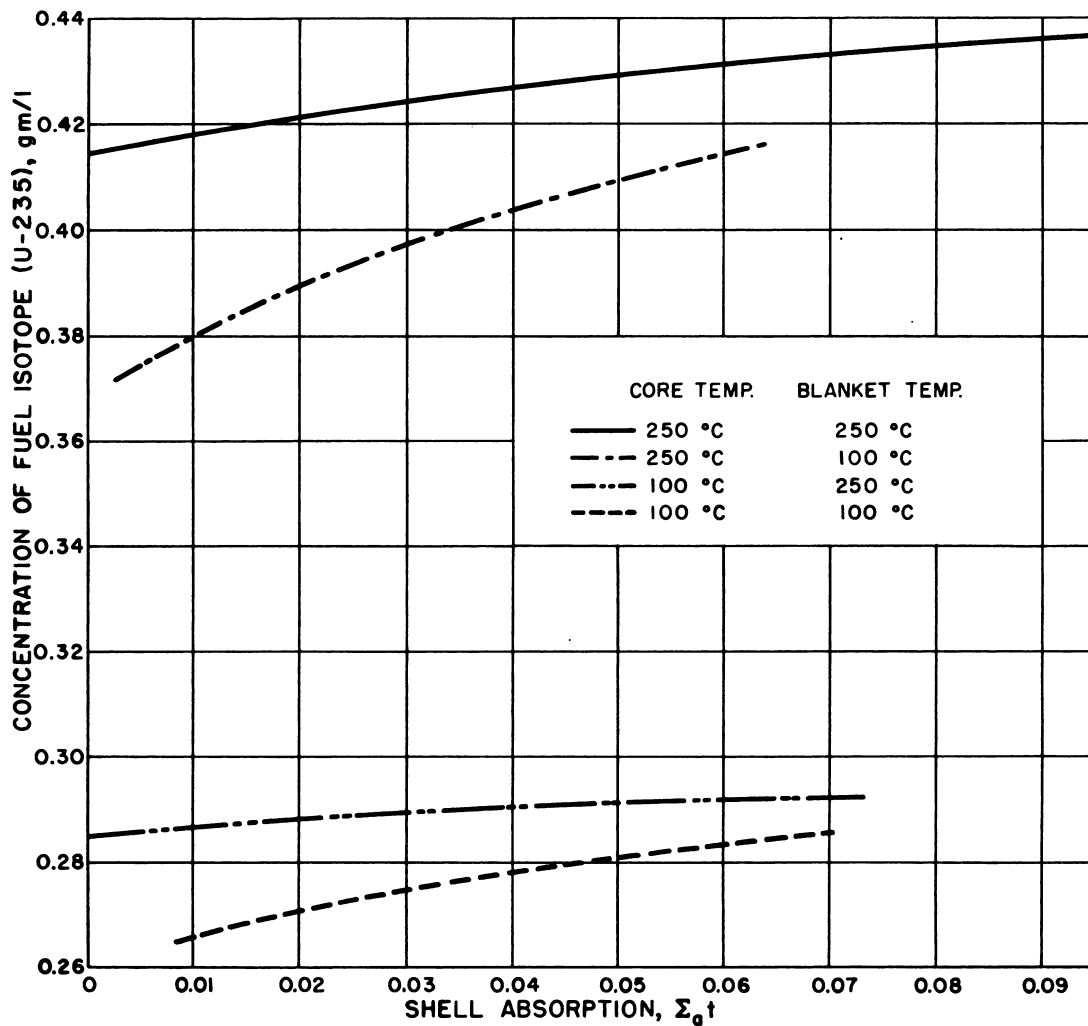


Fig. 4.2.20 — U-233 Two-region Converter Reactor; Dependence of Fuel Concentration on Shell Absorption at Various Temperatures. Submitted by Oak Ridge National Laboratory, Nov. 25, 1952. Reprinted from ORNL-51-10-110. Core diameter, 10 ft; 2-ft-thick blanket of 1000 gm Th/l.

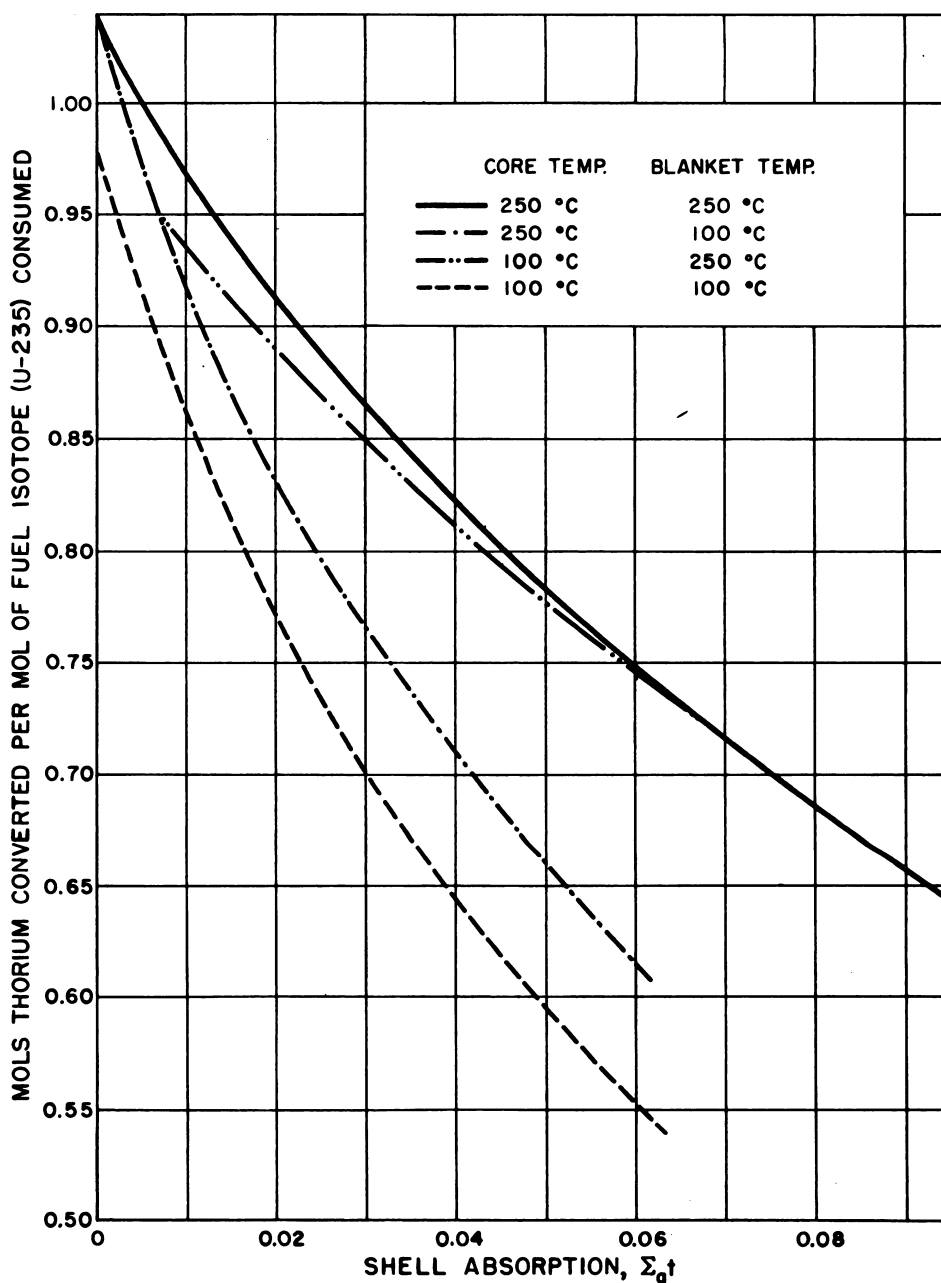


Fig. 4.2.21 — U-233 Two-region Converter Reactor; Effect of Temperature on Conversion Ratio for a 10-ft diameter Core, 2-ft-thick Blanket of 1000 gm Th/l. Submitted by Oak Ridge National Laboratory, Nov. 25, 1952. Reprinted from ORNL-51-10-110. Initial Operation: unpoisoned, no build-up of heavy elements.

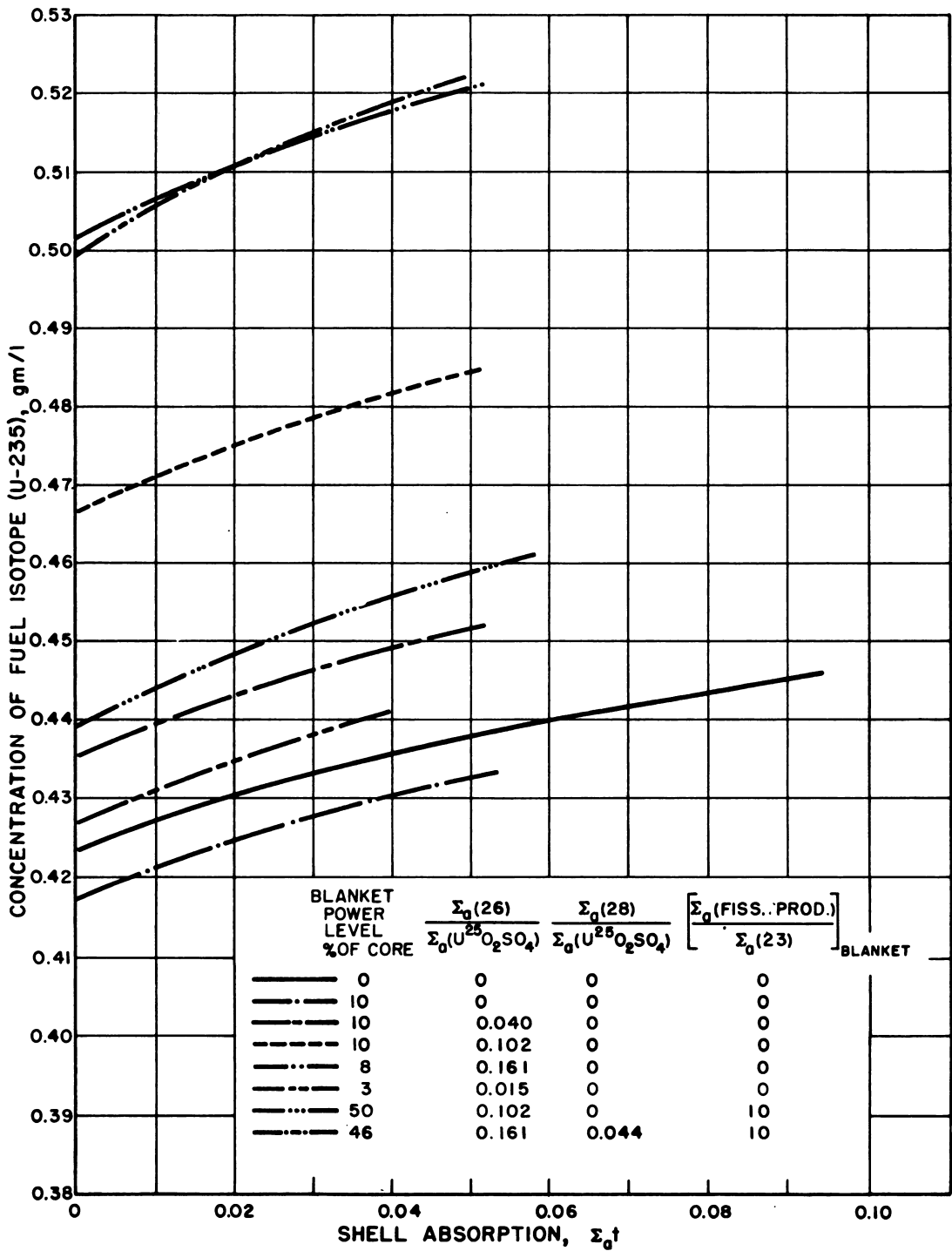


Fig. 4.2.22 — U-233 Two-region Converter Reactor; Dependence of U-235 Concentration Required for Criticality on Shell Thickness at Various Power Levels for System with 10-ft-diameter Core and 2-ft-thick Blanket of 1000 gm Th/l. Submitted by Oak Ridge National Laboratory, Nov. 25, 1952. Reprinted from ORNL-51-10-110. System at 250°C with $\Sigma_a(\text{fission products})/\Sigma_a(UO_2SO_4) = 0.02$ in core.

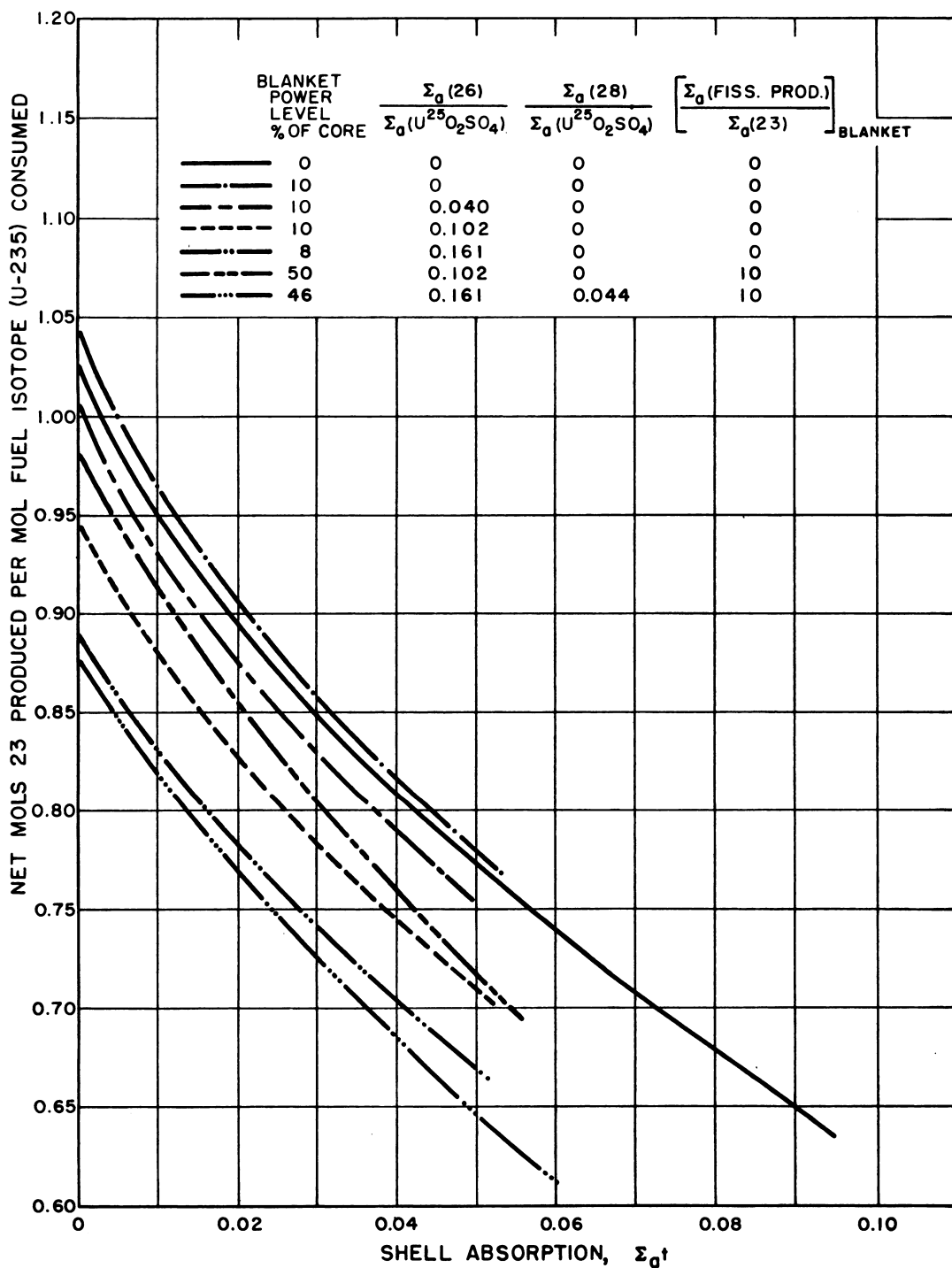


Fig. 4.2.23—U-233 Two-region Converter Reactor; Dependence of U-233 Production on Shell Absorption at Various Power Levels for System with 10-ft-diameter Core with 2-ft-thick Blanket of 1000 gm Th/1. Submitted by Oak Ridge National Laboratory, Nov. 25, 1952. Reprinted from ORNL-51-10-110. System at 250°C with $\Sigma_a(\text{fission products})/\Sigma_a(UO_2SO_4) = 0.02$ in core.

in Fig. 4.2.25. For a given shell absorption, the larger breeding gains are obtained with the smaller cores. To realize a positive breeding gain, Σ_{at} must be less than 0.035, 0.043, and 0.061 for core diameters of 10, 8, and 5 ft, respectively. The presence of fission-product macroscopic cross sections to the extent of 2 percent of the value for the fuel reduces the breeding gain by approximately 0.02.

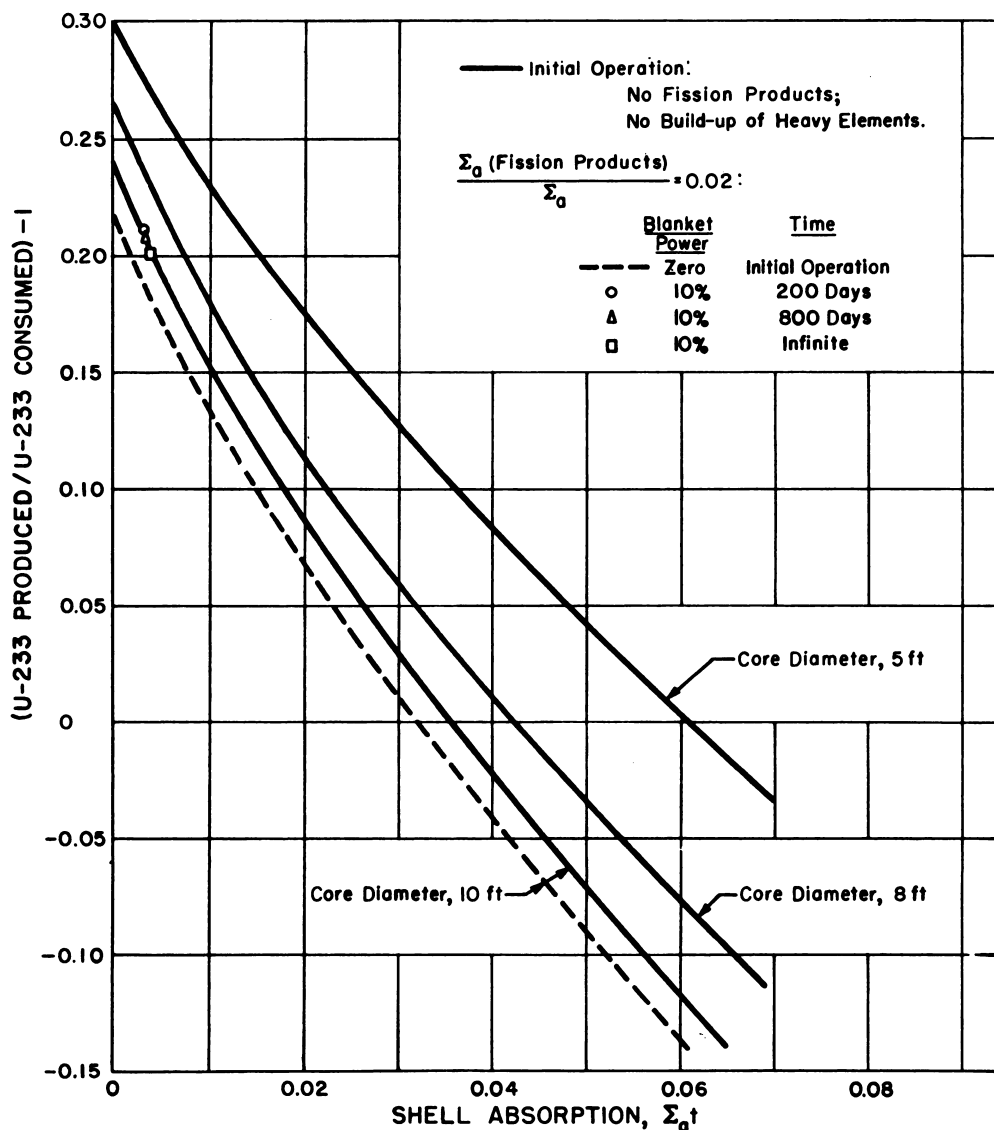


Fig. 4.2.24—U-233 Two-region Breeder Reactor; Dependence of Breeding Gain on Shell Absorption for a 2-ft Blanket of 1000 gm Th/l. Submitted by Oak Ridge National Laboratory, Nov. 25, 1952. Reprinted from ORNL-51-10-110. System at 250°C.

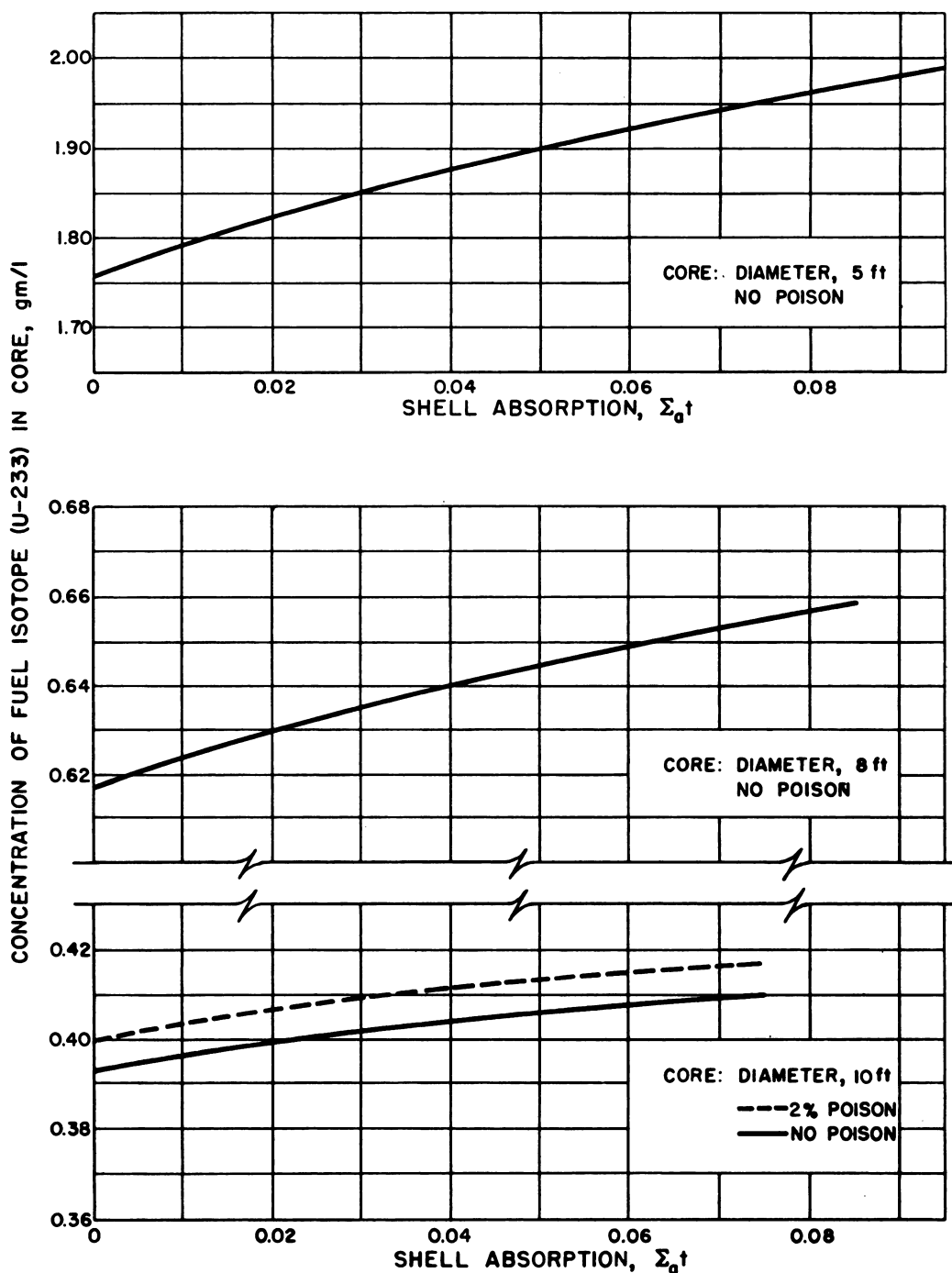


Fig. 4.2.25—U-233 Two-region Breeder Reactor. U-233 Concentration in Core as a Function of Shell Absorption. Submitted by Oak Ridge National Laboratory, Nov. 25, 1952. Reprinted from ORNL-51-10-110. Two-ft-thick blanket of 1000 gm Th/l; system at 250°C; no blanket power.

HIGHER ISOTOPES

In Fig. 4.2.24, results are presented for a breeder with a 10-ft-diameter core, ratio of blanket to core power of 0.1, and periods of operation corresponding to 200 days, 800 days, and infinite time. The cross-section ratios of the various uranium isotopes are given in Table 4.2.8. The values of the breeding gain for these three cases fall on the curve corresponding to zero blanket power level and no core poison, the initial condition of operation.

Table 4.2.8—Cross-section Ratios of Uranium Isotopes

Days' operation	$\frac{\Sigma_a(24)}{\Sigma_a(23)}$	$\frac{\Sigma_a(25)}{\Sigma_a(23)}$	$\frac{\Sigma_a(26)}{\Sigma_a(23)}$
200	0.059	0.059	0.0022
800	.091	.091	.0095
∞	.093	.093	.0142

Although the breeding gain remains fairly constant with operating time, the net quantity of uranium-233 produced will decrease if the reactor is operated at a constant power level. This is brought about by the build-up of uranium-235 which contributes to the fission rate. To maintain a constant power level, the neutron flux must be reduced, decreasing the burn-up of uranium-233 in the core, and, since the breeding gain remains constant, the output of uranium-233 must also be reduced.

BLANKET POWER LEVEL

The desired ratio of blanket power to core power determines the common rate of chemical processing for the removal of uranium, protactinium, and fission products from the blanket, the removal rate decreasing with increasing power level ratio. As noted previously, build-up of the higher uranium isotopes as well as fission products is determined by the processing rate.

The characteristics of breeder reactors with a 10-ft-diameter core and 2-ft-thick blanket of ThO₂ in D₂O are listed in Table 4.2.9, for a range of blanket power levels, with thick and thin zirconium shells, and with the corresponding equilibrium concentrations of higher isotopes and fission products in both the core and blanket. The breeding ratio for a given shell thickness reaches a maximum for a ratio of blanket power to core power of 0.5. For higher values of this ratio, the increase in concentration of fission products in the blanket with decreasing chemical processing rates required to attain the higher power-level ratios begins to offset appreciably the benefits of the blanket fissions. No breeding gain is realized in any case where the thickness separating the core and blanket is sufficient to withstand the entire core pressure.

NEUTRON CHAIN REACTOR KINETICS IN AQUEOUS HOMOGENEOUS SYSTEMS

(P. R. Kasten)

A study of the kinetics of a reactor leads to a determination of the stability or instability of any given over-all reactor design. By stability is meant the ability of a reactor to operate in a steady-state and to return to a steady-state condition when certain disturbances are introduced into the system. Kinetic studies will also give a measure of the degree of stability or safety of any given system as determined by the extremes encountered in operating

Table 4.2.9 — U-233 Two-region Breeder Reactor*

Blanket power ratio	Core at equilibrium, 0 (initial operation)	Core at equilibrium, 0 (initial operation)	0.10	0.10	0.50	0.50	0.80	0.80	0.95	0.95
Core shell thickness (Zr), cm	1.0	4.5	1.0	4.5	1.0	4.5	1.0	4.5	1.0	4.5
Concentration U-233 in core, gm/l	0.4036	0.4130	0.4048	0.4144	0.3868	0.3958	0.3762	0.3863	0.3700	0.3852
N_{24}/N_{23} in core	0	0	.818	.860	1.08	1.21	1.31	1.45	1.53	2.00
N_{25}/N_{23} in core	0	0	.0890	.0936	0.118	0.135	0.145	0.162	0.172	0.228
N_{26}/N_{23}	0	0	.4363	.459	.58	.69	.73	.82	.88	1.23
Chemical process cycle, days	1	1	1	1	1	1	1	1	1	1
For core	59.7	88.4	278	460	514	842	840	1970
For blanket	0	0	0.819	0.740	1.14	1.00	1.17	1.06	1.01	0.846
N_{23} in blanket, gm/l	0	0	1.08	1.44	5.41	7.20	8.11	10.83	9.76	14.1
N_{24}/N_{23} in blanket	0	0	0.0094	0.0146	0.0424	0.0589	0.0705	0.0886	0.0981	0.157
N_{25}/N_{23} in blanket	0	0	.000108	.000247	.00165	.00283	.00376	.00534	.00622	.0121
N_{26}/N_{23} in blanket	0	0	1.9×10^{-4}	6.9×10^{-6}	.000138	.000138	.00053	.000975	.00127	.00422
Z_{24} (fiss. prod.)/ Z_{26}	0	0	0.033	0.035	.083	.104	.145	.181	.20	.33
(U-233) in blanket	0.138	-0.054	.154	-.041	.202	-.016	.188	-.065	.142	-.163
Breeding ratio										
Breeding ratio referred to initial										
burn-up rate	.135	-.054	.141	-.038	.162	-.015	.162	-.058	.122	-.142

* Z_{24} (fission product)/ Z_{26} (fuel salt), 10-ft-diameter core = 0.02 in core, 2-ft-blanket 1000 gm Th/l, power = 630 megawatts

variables (e.g., nuclear power, reactor core temperature, and pressure) for a given disturbance. The mathematical system describing the kinetics of the reactor is a function of the specific reactor design, and in general, for mathematical simplicity, the variables refer to average or bulk values; hence, the results obtained should be applied only in discriminating between first- and second-order effects. More general equations of motion have been discussed only briefly (see pp 98-102, Ref 2).

CIRCULATING NONBOILING SYSTEMS

The kinetic behavior of homogeneous reactors²⁻⁷ and particularly that of the HRE^{2,8-14} has been analyzed in detail. Hence, a circulating, nonboiling reactor system of the HRE type will be considered. Figure 4.2.26 is a schematic diagram of such a system. The soup passes out of the reactor core through the pressurizer pipe, into the outside piping, and thence through the heat exchanger and pump back to the core.

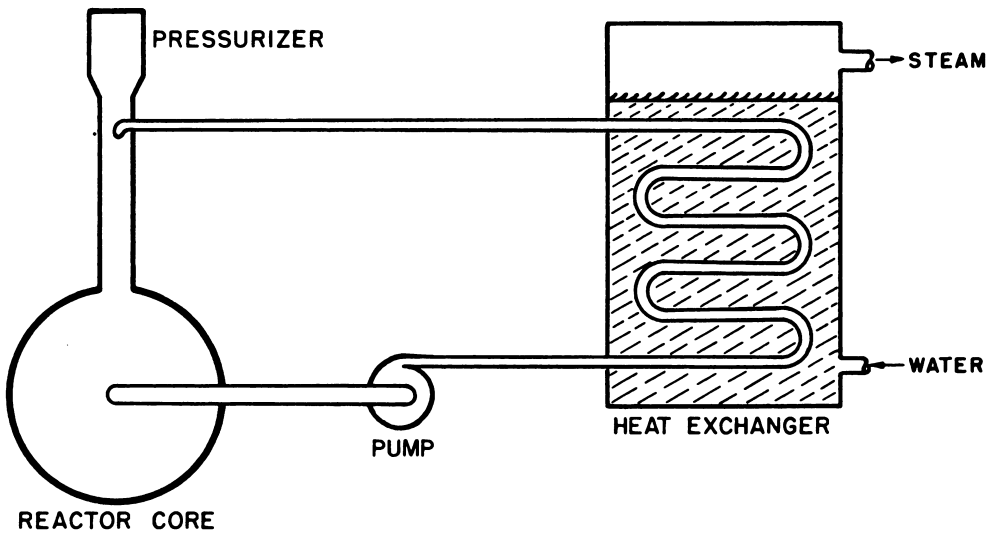


Fig. 4.2.26—Schematic Diagram of a Circulating, Nonboiling Reactor System.
Submitted by Oak Ridge National Laboratory, Nov. 25, 1952.

POWER EQUATIONS

The nuclear power equations^{6,15} can be written as:

$$\frac{dP}{dt} = \lambda_0 [k(1-\beta) - k_c] P + \sum_i \lambda_i c_i \quad (39)$$

$$\frac{dc_i}{dt} + \lambda_i c_i = \lambda_0 \beta_i k_{co} P \quad (40)$$

where: P = nuclear power generated within reactor

$$\lambda_0 = 1/\tau \quad k_c \approx 1/\tau_0 \quad k_{co}$$

k = material multiplication constant = $\eta \xi \text{ pf}$

$\beta = \sum_i \beta_i$ = fraction of fission neutrons which are delayed

$k_0 = k$ required for criticality

- $k_{co} = k_c$ evaluated under initial conditions
 λ_i = decay constant associated with the i 'th group of delayed-neutron emitters
 c_i = a measure of the concentration of the i 'th group of delayed-neutron emitters
 τ = average lifetime of a neutron
 $\tau_0 = \tau$ evaluated under initial conditions

It has been found^{8,16,17} that Eqs. (39) and (40) are approximated rather closely by considering a constant source of delayed neutrons. This approximation yields:

$$\frac{dP}{dt} = \lambda_0 [k(1-\beta) - k_c] P + \lambda_0 \beta k_{co} P_0 \quad (41)$$

where: $P_0 = P$ evaluated under initial conditions.

In evaluating β , the delayed neutrons lost while the soup is outside the reactor must be considered¹⁸ although it has been shown^{19,20} that under certain operating conditions, the effect of losing a portion of the delayed neutrons is small.

REACTIVITY CONSIDERATIONS

A common method of studying the stability and safety of a reactor is to note its behavior following an increase in the reactivity. This is easily done by considering an instantaneous increase in k and the behavior of the reactor dependent upon the resultant variation in k_0 . In general, k_c will be a function of the temperature, pressure, and fraction gas plus vapor in the core:

$$k_c = k_{co} + \alpha_1(T - T_0) + \alpha_2(p - p_0) + \alpha_3(f_g - f_{g0}) \quad (42)$$

where: T = average temperature of the core

p = average pressure of the core

f_g = average fraction of gas plus vapor in the core

$\alpha_1, \alpha_2, \alpha_3 = \frac{\partial k_c}{\partial x}$, where x is the variable in question averaged over the specific range covered

x_0 = variable x evaluated under initial conditions

Under appreciable power operation, the effect of temperature on criticality arises mainly through density variations of the core material²¹ although in general the scattering cross sections are functions of temperature which will influence $\partial k_c / \partial T$ to some degree.^{22,23} The effect of pressure on k_c arises through its influence on core density, and although this effect is not great under certain operating conditions, large power surges may result in undesirable stable-pressure oscillations^{24,25} unless certain restrictions are imposed upon the pressurizer and core dump line designs.²⁶⁻²⁹ Gas in the core will also lower density and thus change k_c . Therefore, with density as the determining influence on k_c , Eq. (42) can be written in the form:

$$k_c = f(\rho) \quad (43)$$

where ρ is the core average density. ρ can be expressed as:

$$\rho = \rho_1(1 - f_g) + \rho_g f_g \quad (44)$$

where: ρ_1 = average density of liquid phase = $f_1(p, T)$

ρ_g = average density of gaseous phase = $f_2(p, T)$

f_g = average fraction of core which is gas plus vapor = $f_{g0} f_3(p, T) F(P)$

Under most conditions, the last term in Eq. (44) can be neglected. Functions f_1 , f_2 , and f_3 are evaluated from thermodynamic relations.

CONNECTING RELATIONS BETWEEN NUCLEAR AND PHYSICAL SYSTEMS

The presence of gas and vapor will effect stability in a manner dependent upon the form of the function describing the gas generation within the core. This functional relation between f_g and P is complex, although some plausible relations have been presented.^{30,31}

To obtain the pressure surges arising from power pulses, negligible error is introduced by considering the density of the liquid ejected into the pressurizer pipe as constant^{8,32} or:

$$\frac{d\rho}{dt} = -\frac{Av}{V} \rho_{10} \quad (45)$$

where: A = average cross-sectional area of pressurizer pipe

v = deviation from steady state value of fluid velocity in pressurizer pipe

V = volume of reactor core

Pressure surges can then be obtained from the force equation:

$$a_0 \frac{dv}{dt} = \Delta p - a_1 v - a_2 v |v| \quad (46)$$

where: a_0 , a_1 , a_2 = constants

Δp = pressure deviation from normal value

To complete the mathematical system, the relation between T and P is required. The core temperature will depend on the power generation and rate of cooling. For safety calculations, times of interest are so short that the temperature of the soup entering the reactor can be considered constant³³ and under this condition:

$$\frac{dT}{dt} = \epsilon (P - P_0) \quad (47)$$

where: ϵ = reciprocal heat capacity of core

For stability calculations, relations describing the functioning of the heat exchanger-boiler system are required, and for the HRE, some specific cases have been analyzed.³⁴

TECHNIQUES FOR SOLUTION OF THE EQUATIONS

The solution of the above nonlinear system of equations appears to be best solved for individual cases by high-speed digital machines, although useful approximate formulas have been developed which are valid for short time intervals.⁸

Certain of the variables have proved to be relatively unimportant insofar as peak powers obtained for a step increase in reactivity. By assuming instantaneous fuel ejection from the core with decreasing soup density, and neglecting the gas effects, the mathematical system is:

$$\begin{aligned} \frac{d\sigma}{dt} &= \lambda_0 [k(1-\beta) - k_c] \sigma + \lambda_0 \beta k_{co} \\ k &= k_{co} + \Delta k \\ k_c &= k_{co} + \alpha_1 (T - T_0) \\ \frac{dT}{dt} &= \epsilon' (\sigma - 1) \end{aligned} \quad (48)$$

where: $\sigma = \frac{P}{P_0}$ and $\epsilon' = \epsilon P_0$

The above is a nonlinear system of differential equations, but it can be solved graphically in the phase plane by the method of isoclines as follows: Let:

$w = k(1-\beta) - k_c$ = a measure of the excess reactivity of reactor

Differentiating:

$$\frac{dw}{dt} = -\frac{dk_c}{dt} = -\alpha\epsilon'(\sigma-1) \quad (49)$$

On combining the above with the power equation, time is eliminated and the phase plane relation is:

$$\frac{dw}{d\sigma} = \frac{-\alpha\epsilon'(\sigma-1)}{\lambda_0(w\sigma + \beta k_{c0})} \quad (50)$$

By assuming various values for $dw/d\sigma$, curves of w vs σ called "isoclines" can be drawn which give the positions at which the final desired curve can have the assumed slope. Given initial conditions, the desired curve can be approximated closely by considering a sufficient number of isoclines. With the phase-plane plot, the time relations of the variables can be obtained by graphical integration of the initial equations. Results of such analyses show that the delayed neutrons have an extreme dampening effect on any power oscillations arising from reactivity addition. Some typical plots of the variables considered are given in Fig. 4.2.27. The curves indicate that the reactor system being considered exhibits a highly dampened behavior to reactivity disturbances and is therefore self-stabilizing. Specific cases for the system and cases in which the pressurizer effects have been included are presented elsewhere.⁸

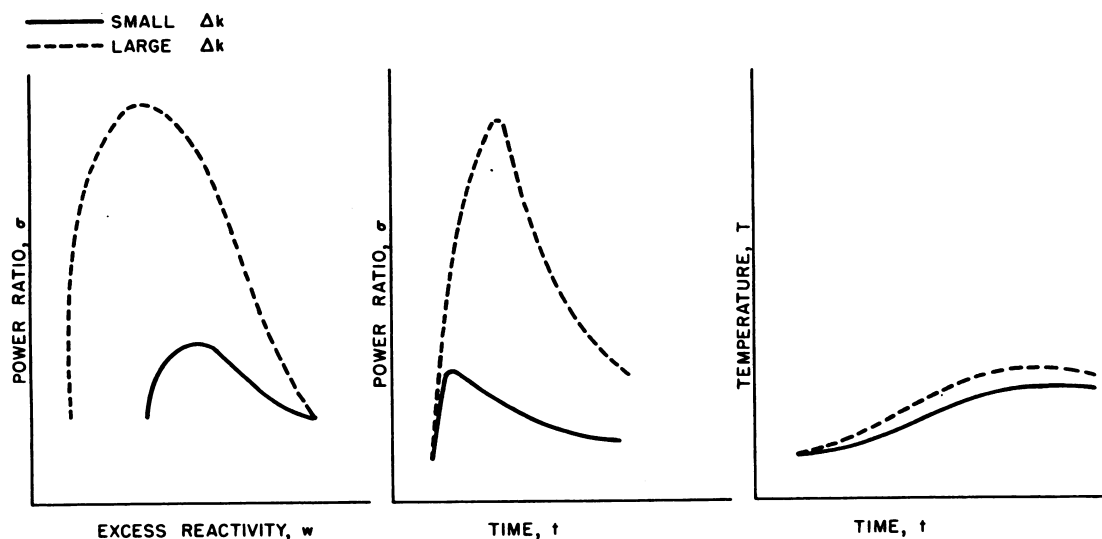


Fig. 4.2.27 — Typical Plots for Temperature and Power Ratio Behavior as a Function of Impressed Δk . Submitted by Oak Ridge National Laboratory, Nov. 25, 1952.

BOILING REACTOR KINETICS

Another possible aqueous fuel reactor is the boiling-type reactor illustrated in Fig. 4.2.28. In this reactor, the fission energy vaporizes the liquid, the rising steam condenses on the heat exchanger and then drops back into the core. The kinetics of this reactor type are similar to the one previously discussed, except the relation between f_g and P now assumes great importance, and the reactor has in effect a large pressurizer chest. Material pertaining to boiling reactor kinetics has appeared in reports concerning homogeneous reactors in general³⁵ and more recently has been presented specifically.^{3,4,36-39}

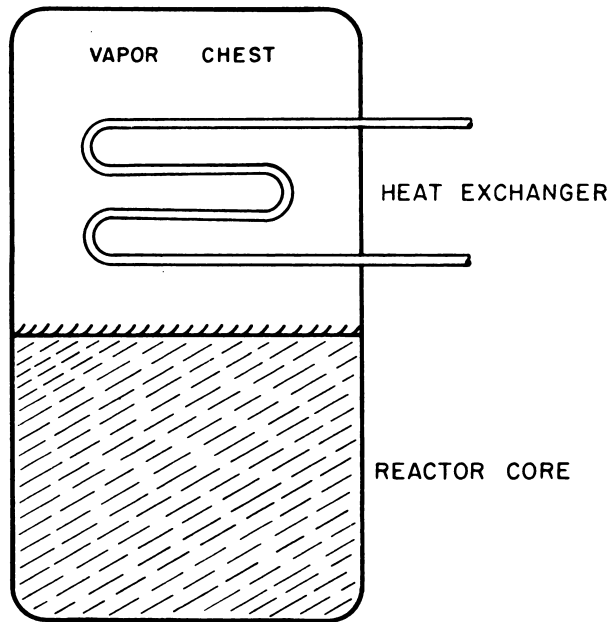


Fig. 4.2.28—Schematic Diagram of a Boiling-type Reactor. Submitted by Oak Ridge National Laboratory, Nov. 25, 1952.

Any lag in the formation of vapor with respect to nuclear power will be detrimental to stability. This can be easily seen by considering the formation of vapor to lag power by some discrete amount ξ . The mathematical system is then:

$$\begin{aligned}\frac{d\sigma}{dt} &= \lambda_0(w\sigma + \beta k_{co}) \\ k &= k_{co} + \Delta k \\ k_c &= k_{co} + \alpha_3(f_g - f_{go}) \\ \frac{df_g}{dt} &= b[\sigma(t - \xi) - 1]\end{aligned}\tag{51}$$

Linearizing the above:

$$\frac{d^2\sigma}{dt^2} + \lambda_0 [\beta k_{co} - \alpha_3 b \xi] \frac{d\sigma}{dt} + \lambda_0 \alpha_3 b (\sigma - 1) = 0\tag{52}$$

In this equation, $(\beta k_{co} - \alpha_3 b \xi)$ is the dampening coefficient. The delayed neutrons, β , thus have a positive damping action, whereas ξ acts in opposition to β and has a deleterious action on reactor stability.

SAFETY CONSIDERATIONS

INHERENT STABILITY

In any reactor, it is desirable that an inherent power coefficient of reactivity exist, so that, as the nuclear power rises during a power surge, the reactivity will decrease at such a rate as to prevent the power from rising excessively. In aqueous systems, this property can exist either as a temperature coefficient (as in an HRE-type circulating reactor) or as a bubble coefficient (as in a boiling-type reactor). The size of the coefficient along with the response of the variable to power changes will determine the inherent safety of the reactor. Thus, although the temperature coefficient is not so large as the bubble coefficient,⁴⁰ the response of temperature to power is instantaneous, but the response of gas and vapor bubble formation to power is not immediate.^{38,41}

REFERENCES

1. Hughes and Eggler, Resonance Absorption of Thorium, Univ. Chicago, CP-3093, July 1945.
2. C. E. Winters and C. H. Secoy, ORNL-925, Jan. 30, 1951 (classified).
3. J. M. Stein and P. R. Kasten, ORNL-1062, Nov. 23, 1951 (classified).
4. T. A. Welton, ORNL-CF-51-11-163, Nov. 27, 1951 (classified).
5. K. Cohen, H. K. Ferguson Company, HKF-109, Dec. 15, 1950, pp 3.15-3.29 (classified).
6. H. Hurwitz, Jr., On the Derivation and Integration of the Pile-Kinetic Equations, Knolls Atomic Power Laboratory, AECD-2438, Apr. 5, 1948 (Declassified Jan. 4, 1949).
7. F. de Hoffman, Criticality of the Water Boiler and Effectiveness of Delayed Neutrons, Los Alamos Scientific Laboratory, AECD-3051, Dec. 8, 1944 (Declassified Jan. 30, 1951).
8. W. C. Sangren, ORNL-1205, Apr. 1, 1952 (classified).
9. J. A. Swartout, C. H. Secoy, T. A. Welton, and C. E. Winters, ORNL-1221, Mar. 13, 1952 (classified).
10. J. A. Swartout, C. H. Secoy, and C. E. Winters, ORNL-1121, Dec. 27, 1951 (classified).
11. C. E. Winters and C. H. Secoy, ORNL-990, May 18, 1951 (classified).
12. C. E. Winters and A. M. Weinberg, ORNL-730, July 6, 1950 (classified).
13. C. E. Winters, ORNL-630, Apr. 21, 1950 (classified).
14. C. B. Graham, C. H. Secoy, I. Spiewak, E. H. Taylor, A. M. Weinberg, C. E. Winters, and J. L. English ORNL-527, Aug. 28, 1949 (classified).
15. Winters and Secoy, ORNL-925, p 78 (classified).
16. Stein and Kasten, ORNL-1062 (classified).
17. Winters and Secoy, ORNL-925, pp 80 ff (classified).
18. Swartout, Secoy, Welton, and Winters, ORNL-1221, pp 82-88 (classified).
19. Winters and Secoy, ORNL-925, p 48 (classified).
20. Winters and Secoy, ORNL-990, pp 34-39 (classified).
21. Winters and Weinberg, ORNL-730, p 54 (classified).
22. S. Glasstone and M. C. Edlund, ORNL-CF-51-9-128, Oct. 31, 1951, pp XI 31-50 (classified).
23. E. Greuling and G. Goertzel, Atomic Energy Commission, TAB-84, Aug. 3, 1950 (classified).
24. Swartout, Secoy, and Winters, ORNL-1121, pp 88-102 (classified).
25. T. A. Welton, ORNL-CF-51-8-53, Aug. 7, 1951 (classified).
26. Swartout, Secoy, Welton, and Winters, ORNL-1221, pp 79-81.
27. R. E. Aven, ORNL-CF-52-1-77, Jan. 11, 1952 (classified).
28. R. E. Aven and G. T. Trammell, ORNL-CF-51-10-21, Oct. 2, 1951 (classified).
29. T. A. Welton, ORNL-CF-51-8-31, Aug. 6, 1951 (classified).
30. Swartout, Secoy, Welton, and Winters, ORNL-1221, pp 62-64 (classified).
31. Winters and Weinberg, ORNL-730, pp 67 ff (classified).
32. Swartout, Secoy, Welton, and Winters, ORNL-1221, p 89 (classified).
33. Winters and Weinberg, ORNL-730, pp 66 and 70 (classified).
34. Swartout, Secoy, Welton, and Winters, ORNL-1221, pp 64-68 (classified).
35. J. E. Wilkins, Clinton Laboratories, CP-3068, June 26, 1945 (classified); CP-3088, 1945 (classified); CP-2709, Feb. 10, 1945 (classified); CF-3067, June 25, 1945 (classified).
36. J. A. Swartout, C. H. Secoy, T. A. Welton, and C. E. Winters, ORNL-1280, June 25, 1952, pp 90-94 (classified).
37. L. C. Widdoes, G. H. Cohen, K. W. Downes, F. R. Grisak, J. H. Hill, V. P. Kovacic, and D. G. Ott, ORNL-CF-51-8-84, Aug. 6, 1951, pp 35-47 (classified).

38. W. H. Bowman and G. T. Parish, Carbide and Carbon Chemicals Division, Oak Ridge, Tennessee, K-25 Area, KT-95, Nov. 15, 1950 (classified).
39. R. Bakal and D. L. James, Carbide and Carbon Chemicals Division, Oak Ridge, Tennessee, K-25 Area, KT-97, Oct. 23, 1950 (classified).
40. Winters and Weinberg, ORNL-730, pp 56, 60, 69, 70 (classified).
41. W. M. Breazeale, Oak Ridge National Laboratory, June 11, 1952 (classified).

CHAPTER 4.3

Properties of Aqueous Solution Systems

URANIUM SALT SOLUTIONS

THE SYSTEMS $\text{UO}_2\text{SO}_4\text{-H}_2\text{O}$ AND $\text{UO}_2\text{SO}_4\text{-D}_2\text{O}$

CHEMICAL PROPERTIES

Chemical Stability (C. H. Secoy)

Solubility

The utility of an aqueous solution in a homogeneous reactor depends on its physical and chemical stability over the range of desired reactor conditions. Of prime importance is the preservation of homogeneity over the desired concentration and temperature range.

The solubility of uranyl sulfate in H_2O has been determined by Secoy^{1,2} from the ice — $\text{UO}_2\text{SO}_4 \cdot 3\text{H}_2\text{O}$ eutectic at -38.5° to 370°C . The data are given in Table 4.3.1 along with points determined by Helmholtz and Friedlander³ at 30° , 35° , and 40°C and by Dittrich⁴ for the freezing points of very dilute solutions. Other data appearing in the early literature⁵ are not in good agreement and are not included in the table. Figure 4.3.1 shows the phase diagram for the system. From Fig. 4.3.1 it is apparent that, insofar as solid-liquid equilibria are involved, the solubility of uranyl sulfate in H_2O is higher at all temperatures from room temperature to 370°C than that required for any proposed homogeneous reactor.

The analogous study of the solubility of uranyl sulfate in D_2O has not been made, but it is assumed that the values would not be sufficiently different from those in light water to affect the feasibility of a uranyl sulfate- D_2O solution.

Solutions of uranyl sulfate in H_2O not saturated with respect to the solid display a two-liquid phase region (miscibility gap) with a minimum critical solution temperature of 284.5°C . The upper limit of the region is the critical temperature of H_2O (374.0°C), at which temperature the water-rich liquid phase and the vapor phase become identical. This region has been studied extensively by Secoy¹ and by Jones and Marshall,⁶ and their data are given in Table 4.3.2. A graph of the region plotted from the data of Jones and Marshall is included in Figs. 4.3.1 and 4.3.2. The data of the latter are believed more nearly correct than the earlier values in that there was a likelihood that the salt used by Secoy was contaminated with traces of acid. Table 4.3.3 and Fig. 4.3.2 give analogous data for the $\text{UO}_2\text{SO}_4\text{-D}_2\text{O}$ system as determined by Jones and Marshall.⁶ The upper temperature limit of homogeneous-reactor operation is determined by these curves.

¹References appear at end of chapter.

Table 4.3.1 — Solubility of Uranyl Sulfate in Water
(Solid-liquid equilibria)

Temp., °C	m, moles UO_2SO_4 per 1000 gm H_2O	Solid phase	Reference
-0.0705	0.03	Ice	4
-.1100	.05	Ice	4
-.200	.10	Ice	4
-.516	.30	Ice	4
-.948	.60	Ice	4
-17.7	2.87	Ice	2
-22.9	3.33	Ice	2
-38.5	3.82	Eutectic	2
-27.0	3.84	$\text{UO}_2\text{SO}_4 \cdot 3\text{H}_2\text{O}$	2
30.0	4.135	$\text{UO}_2\text{SO}_4 \cdot 3\text{H}_2\text{O}$	3
35.0	4.171	$\text{UO}_2\text{SO}_4 \cdot 3\text{H}_2\text{O}$	3
40.0	4.225	$\text{UO}_2\text{SO}_4 \cdot 3\text{H}_2\text{O}$	3
46.8	4.31	$\text{UO}_2\text{SO}_4 \cdot 3\text{H}_2\text{O}$	2
57.3	4.50	$\text{UO}_2\text{SO}_4 \cdot 3\text{H}_2\text{O}$	2
71.7	4.73	$\text{UO}_2\text{SO}_4 \cdot 3\text{H}_2\text{O}$	2
80.8	4.70	$\text{UO}_2\text{SO}_4 \cdot 3\text{H}_2\text{O}$	2
90.1	5.02	$\text{UO}_2\text{SO}_4 \cdot 3\text{H}_2\text{O}$	2
93.5	5.06	$\text{UO}_2\text{SO}_4 \cdot 3\text{H}_2\text{O}$	2
106.2	5.26	$\text{UO}_2\text{SO}_4 \cdot 3\text{H}_2\text{O}$	2
116.8	5.59	$\text{UO}_2\text{SO}_4 \cdot 3\text{H}_2\text{O}$	2
118.4	5.73	$\text{UO}_2\text{SO}_4 \cdot 3\text{H}_2\text{O}$	2
119.9	5.66	$\text{UO}_2\text{SO}_4 \cdot 3\text{H}_2\text{O}$	2
125.2	5.90	$\text{UO}_2\text{SO}_4 \cdot 3\text{H}_2\text{O}$	2
134.9	6.25	$\text{UO}_2\text{SO}_4 \cdot 3\text{H}_2\text{O}$	2
139.0	6.51	$\text{UO}_2\text{SO}_4 \cdot 3\text{H}_2\text{O}$	2
140.7	6.55	$\text{UO}_2\text{SO}_4 \cdot 3\text{H}_2\text{O}$	2
145.1	6.72	$\text{UO}_2\text{SO}_4 \cdot 3\text{H}_2\text{O}$	2
149.6	6.89	$\text{UO}_2\text{SO}_4 \cdot 3\text{H}_2\text{O}$	2
153.6	7.14	$\text{UO}_2\text{SO}_4 \cdot 3\text{H}_2\text{O}$	2
168.6	7.75	$\text{UO}_2\text{SO}_4 \cdot 3\text{H}_2\text{O}$	2
181	8.66	Transition	2
152	8.97	$\text{UO}_2\text{SO}_4 \cdot \text{H}_2\text{O}(\text{m})$	2
287	7.75	$\text{UO}_2\text{SO}_4 \cdot \text{H}_2\text{O}$	2
311	7.57	$\text{UO}_2\text{SO}_4 \cdot \text{H}_2\text{O}$	1
347	7.33	$\text{UO}_2\text{SO}_4 \cdot \text{H}_2\text{O}$	1
365	7.24	$\text{UO}_2\text{SO}_4 \cdot \text{H}_2\text{O}$	1
49.2	4.70	$\text{UO}_2\text{SO}_4 \cdot 2\text{H}_2\text{O}(\text{m})$	2
53.2	4.73	$\text{UO}_2\text{SO}_4 \cdot 2\text{H}_2\text{O}(\text{m})$	2
75.5	5.06	$\text{UO}_2\text{SO}_4 \cdot 2\text{H}_2\text{O}(\text{m})$	2

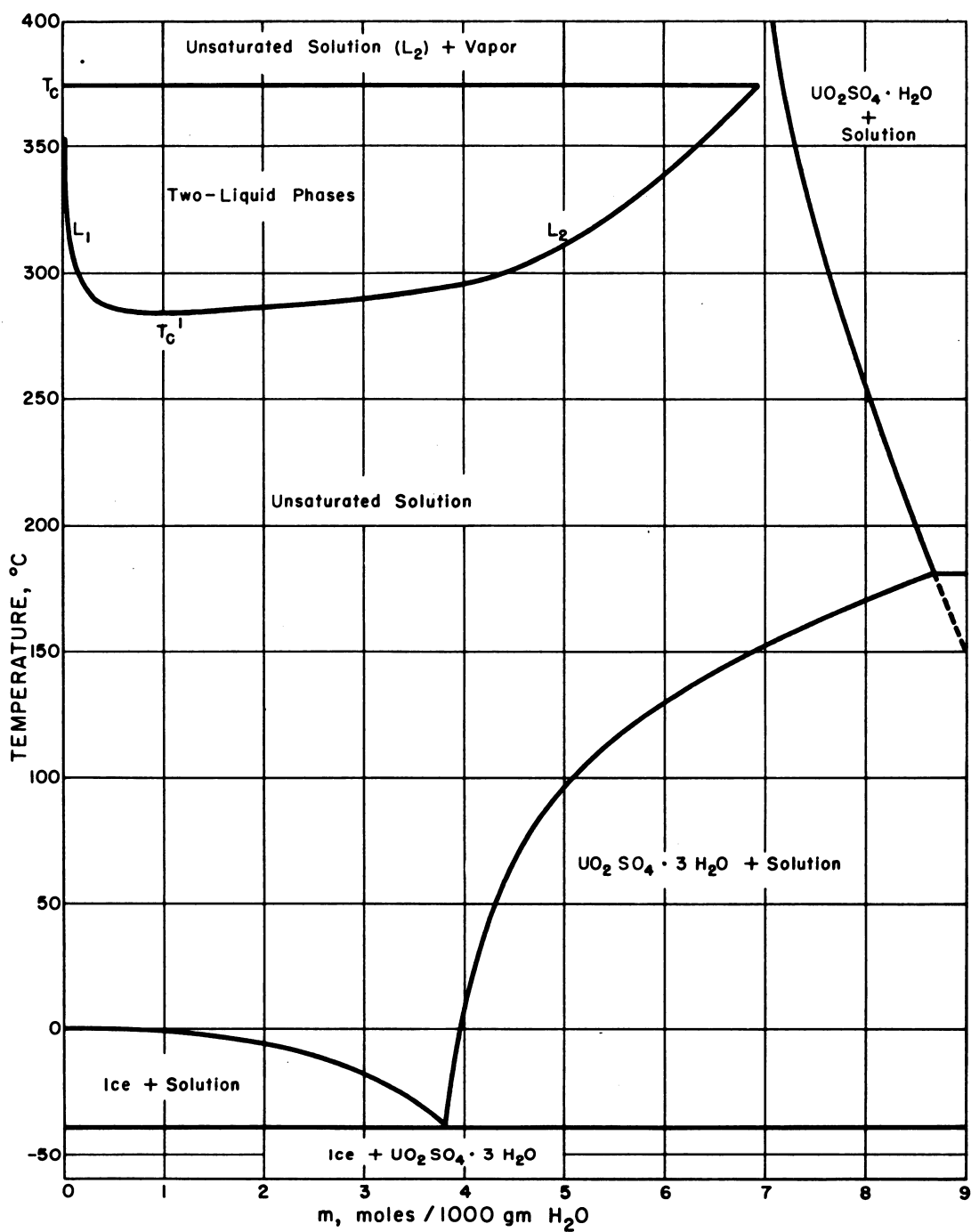


Fig. 4.3.1 — Phase Diagram for the System $\text{UO}_2\text{SO}_4\text{-H}_2\text{O}$. Submitted by Oak Ridge National Laboratory, Nov. 25, 1952.

Table 4.3.2—Solubility of Uranyl Sulfate in Water
(Liquid-liquid equilibrium)

Temp., °C	m, moles UO_2SO_4 per 1000 gm H_2O	Phase appearing or disappearing*	Critical temp. of L_1
Data from Secoy			
335.1	0.021	L_2	...
319.4	.089	L_2	...
310.1	.170	L_2	...
299.9	.383	L_2	374.3
295.8	.700	L_2	...
295.5	1.265	L_1	374.0
297.5	1.876	L_1	374.2
302.3	2.527	L_1	374.2
308.2	3.399	L_1	...
312.5	3.872	L_1	374.4
316.2	4.201	L_1	...
320.5	4.517	L_1	...
339.6	5.655	L_1	...
363.0	6.687	L_1	...
Data from Jones and Marshall			
304.7	0.107	L_2	...
303.7	.110	L_2	...
300.8	.114	L_2	...
287.6	.357	L_2	...
284.7	.683	L_2	...
284.7	1.294	L_1	...
285.0	1.464	L_1	...
288.1	2.550	L_1	...
294.5	3.986	L_1	...

* L_1 = water-rich liquid; L_2 = UO_2SO_4 -rich liquid

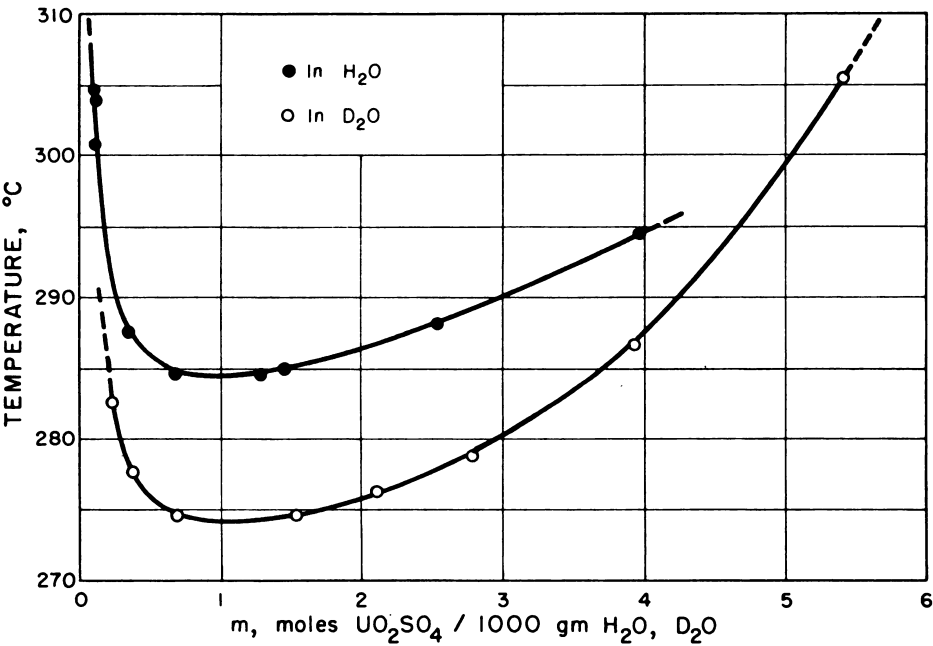


Fig. 4.3.2 — Two-liquid Phase Region of Uranyl Sulfate in Ordinary and Heavy Water. Submitted by Oak Ridge National Laboratory, Nov. 25, 1952.

Table 4.3.3 — Liquid-Liquid Equilibrium in the System UO₂SO₄-D₂O⁶

Temp., °C	m, moles UO ₂ SO ₄ per 1000 gm D ₂ O
282.7	0.231
277.7	.375
274.7	.684
274.7	1.540
276.3	2.105
278.8	2.791
286.6	3.934
305.5	5.412

Since it is conceivable to operate a homogeneous reactor with a solution in which the mole ratio of UO_3 to SO_3 is other than unity, studies of the miscibility gap in the three-component system $\text{UO}_3\text{-SO}_3\text{-H}_2\text{O}$ have been made by Secoy and co-workers.⁷⁻¹⁰ Their data are given in Tables 4.3.4, 4.3.5, and 4.3.6 and are presented graphically in Figs. 4.3.3 and 4.3.4. The marked elevation of the miscibility gap by the addition of sulfuric acid makes possible much higher temperatures of operation, provided a suitable container material for the more acid solution is available and provided the increased pressure which accompanies the increase in temperature is not excessive.

Hydrolysis

Uranyl sulfate solutions are quite acidic because of hydrolysis. No extensive study of the hydrolytic equilibrium and its temperature dependence has been made, but the pH as a function of concentration has been measured by McInnes and Longworth,¹¹ Helmholtz and Friedlander,³ and Lietzke, Wright, and Marshall.¹² Their data are shown graphically in Figs. 4.3.5 and 4.3.6.

Also of interest in connection with the hydrolytic stability is the solubility of UO_3 in uranyl sulfate solutions as a function of temperature and concentration. Although a complete study has not been made, some data are available. These are presented in Tables 4.3.7, 4.3.8, 4.3.9, and 4.3.10. The acidity of the UO_3 -rich solutions has also been studied, and some of the data are included in Tables 4.3.9 and 4.3.10. Additional pH data are given in Tables 4.3.11 and 4.3.12.

The general trends indicated by the data are (1) that the solubility of UO_3 in uranyl sulfate solutions decreases markedly with increasing temperature and (2) that the solubility is nearly independent of the uranium concentration except in very dilute solutions where it also decreases sharply.

Reduction of the Uranyl Ion

At elevated temperatures, the uranyl ion is subject to reduction if reducing species are present either in the solution or as constituents of the containing vessel. The products are either black insoluble UO_2 or U_3O_8 or both.

Radiation Stability (H. F. McDuffie)

When fissioning takes place in aqueous fuel solutions of uranyl sulfate, the observable effects are those which follow upon the decomposition of water to hydrogen, oxygen, and peroxide. Except for the precipitation of uranyl peroxide as discussed below, it has not been possible to demonstrate any radiation instability of the uranyl sulfate. The leading reference for the decomposition of water by fissioning solutions¹⁷ presents initial yields of hydrogen gas production for aqueous solutions of uranyl sulfate, fluoride, nitrate, and uranous sulfate, determined as functions of uranium concentration, isotopic enrichment, temperature, hydrogen ion concentration, and the presence or absence of various anions and added solutes. Values for G_{H_2} (molecules of hydrogen produced per 100 electron volts of energy absorbed by the solution) are presented in Table 4.3.13 and Figs. 4.3.7 and 4.3.8. For calculations in connection with aqueous reactor systems, it may sometimes be convenient to use the derived formula relating reactor power density to gas production:

$$K = 0.0052 \times G \times \text{PD moles hydrogen}/(l)(\text{min}) \quad (1)$$

where PD = the reactor power density in kw/l, and G = value appropriate for the solution being considered. This formula assumes that all the fission energy is absorbed by the

Table 4.3.4—Two-liquid Phase Coexistence Curve for Acid-rich Solutions in the System $\text{UO}_3\text{-SO}_3\text{-H}_2\text{O}$

H_2SO_4 , M	UO_2SO_4 , m*	Temp., °C	Phase separating	Temp., °C	Reference
0.099	0.118	346.3	L_2	381.5	10
	.296	323.9	L_2		10
	.900	305.5	L_2	381.6	10
	1.405	304.1	L_2		10
	2.618	307.8	L_1		10
	3.971	318.0	L_1		10
0.248	0.112	383.9	L_2	393.0	10
	.300	347.5	L_2		10
	.308	349.8	L_2		9
	.755	327.5	L_2		9
	.877	326.4	L_2	392.9	10
	1.406	322.2	L_2		10
	2.581	323.8	L_1		10
	2.730	323.9	L_1		9
	3.901	331.2	L_1		10
0.365	0.722	340.2	L_2		9
	.750	338.9	L_2		9
	1.187	333.9	L_2		9
	1.892	331.2	L_2		9
	2.641	331.7	L_1		9
	3.466	333.7	L_1		9
0.480	1.189	353.2	L_2		9
	1.858	342.7	L_2		9
	2.695	343.1	L_1		9
	3.244	344.8	L_1		9
0.624	2.940	355.8	L_1		9

 * m = moles/1000 gm H_2O

Table 4.3.5 — Two-liquid Phase Coexistence Curve^a for UO_3 -rich Solutions in the System UO_3 - SO_3 - H_2O

(Work of E. V. Jones and W. L. Marshall)

Mole ratio, UO_3/SO_3	m, moles/1000 gm H_2O		Temp., °C
	UO_3	SO_3	
1.1	0.333	0.303	291.3
1.1	.451	.410	282.3
1.1	.572	.520	281.3
1.1	.872	.793	279.3
1.1	1.168	1.062	279.3
1.1	1.803	1.639	279.3
1.1	2.498	2.271	279.3
1.1	3.190	2.900	279.3
1.1	3.902	3.547	283.3
1.1	4.413	4.012	290.3
1.2	0.06	0.05	>338
1.2	.12	.10	>322
1.2	.30	.25	290.3
1.2	.62	.52	280.8
1.2	.95	.79	277.3
1.2	1.62	1.35	278.0
1.2	2.34	1.95	276.6
1.2	3.11	2.59	277.3
1.2	3.86	3.22	279.3
1.2	4.66	3.88	286.3

Table 4.3.6 — Two-liquid Phase Coexistence Curve⁷ for Acid-rich Solutions in the System $\text{UO}_3\text{-SO}_3\text{-H}_2\text{O}$

(Work of A. W. Wright, W. L. Marshall, and C. H. Secoy)

Mole ratio, UO_3/SO_3	m, moles/1000 gm H_2O		Temp., °C
	UO_3	SO_3	
0.893	0.0197	0.0220	338
	.0441	.0495	327
	.0956	.1074	317
	.1903	.2128	308
	.3173	.3551	301
	.5567	.6237	299
	.9000	1.008	300
	1.375	1.540	303
	2.341	2.622	312
0.701	0.0358	0.0507	340
	.1509	.2159	324
	.2403	.3437	321
	.3485	.4967	320
	.5224	.7461	322
	.7942	1.132	326
	1.313	1.873	337
	2.201	3.141	355
0.531	0.0229	0.0429	351
	.0651	.1233	342
	.1153	.2164	342
	.2061	.3880	339
	.3766	.7098	348
	.6504	1.224	353
	1.146	2.187	379
	2.240	4.156	>525
0.404	0.0141	0.0346	364
	.0319	.0793	358
	.0623	.1544	355
	.1058	.2626	356
	.1847	.4586	360
	.3673	.9091	370
	.6536	1.622	387
	1.133	2.816	>530
0.339	0.0072	0.0209	370
	.0182	.0536	364
	.0532	.1572	366
	.1267	.3742	363
	.2418	.7147	372
	.5367	1.585	>525
	1.116	3.043	>530

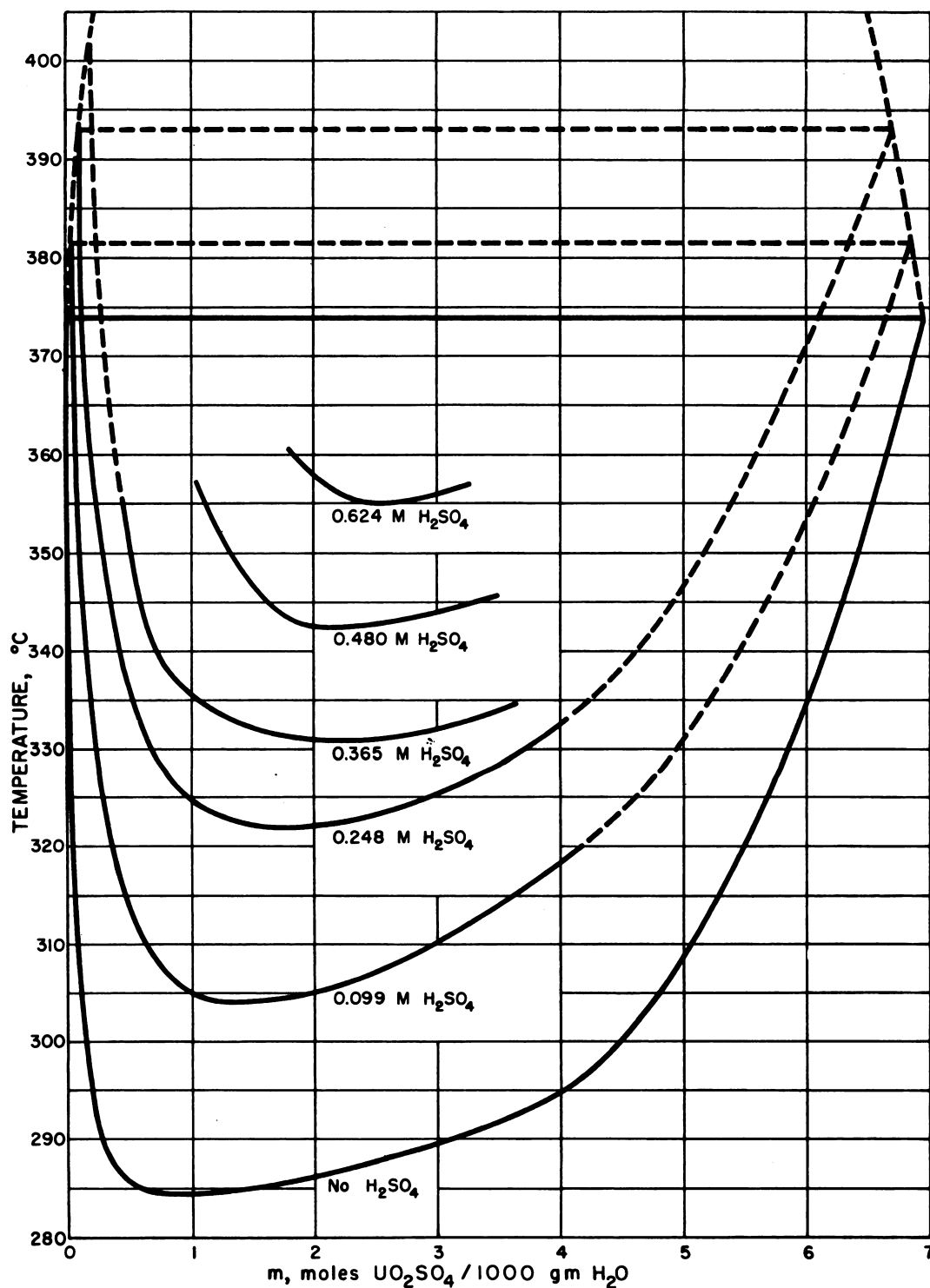


Fig. 4.3.3—Two-liquid Phase Region in the System $\text{UO}_2\text{SO}_4\text{-H}_2\text{SO}_4\text{-H}_2\text{O}$. Submitted by Oak Ridge National Laboratory, Nov. 25, 1952.

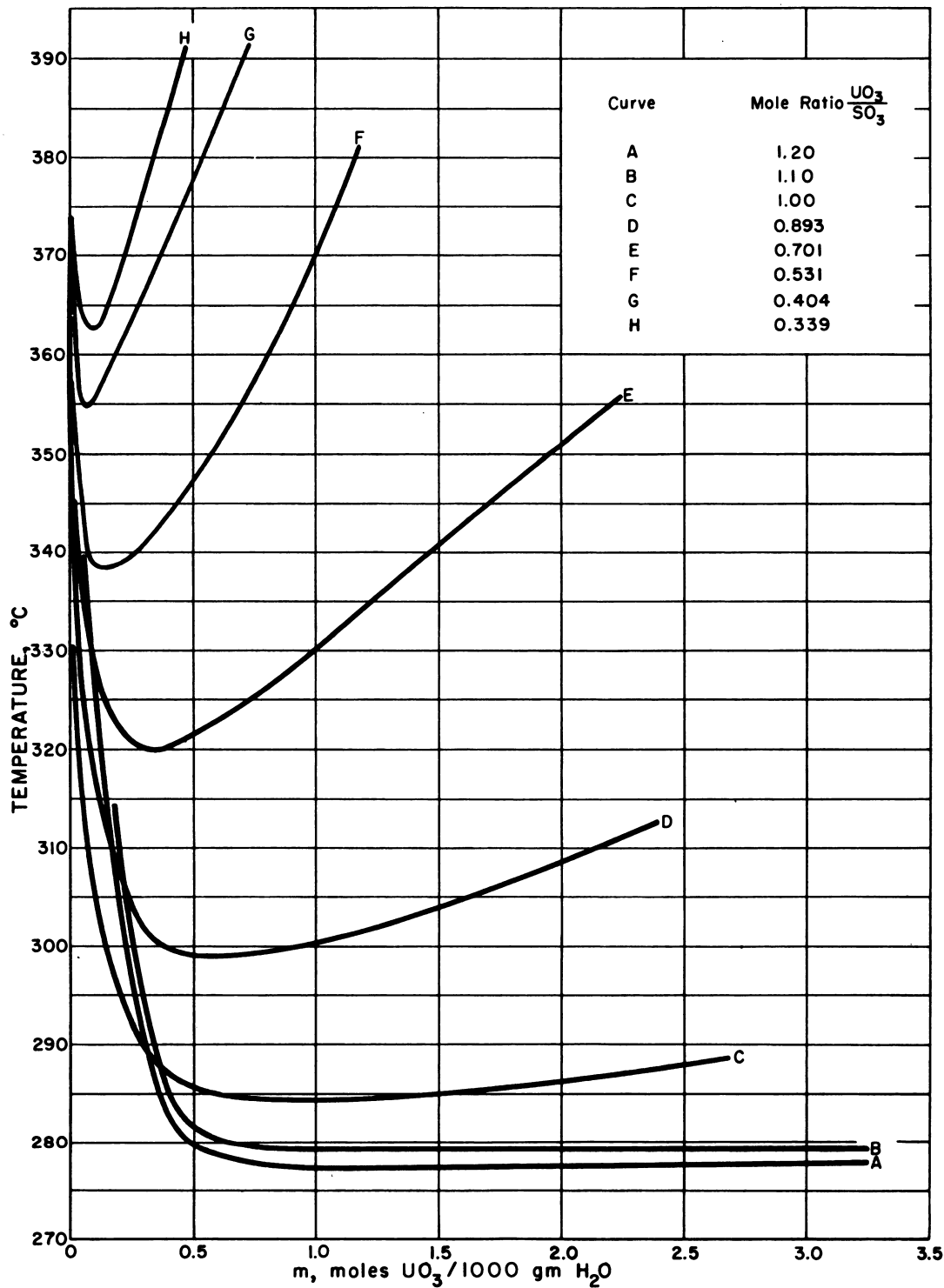


Fig. 4.3.4 — Two-liquid Phase Region in the System, $UO_3-SO_3-H_2O$. Submitted by Oak Ridge National Laboratory, Nov. 25, 1952.

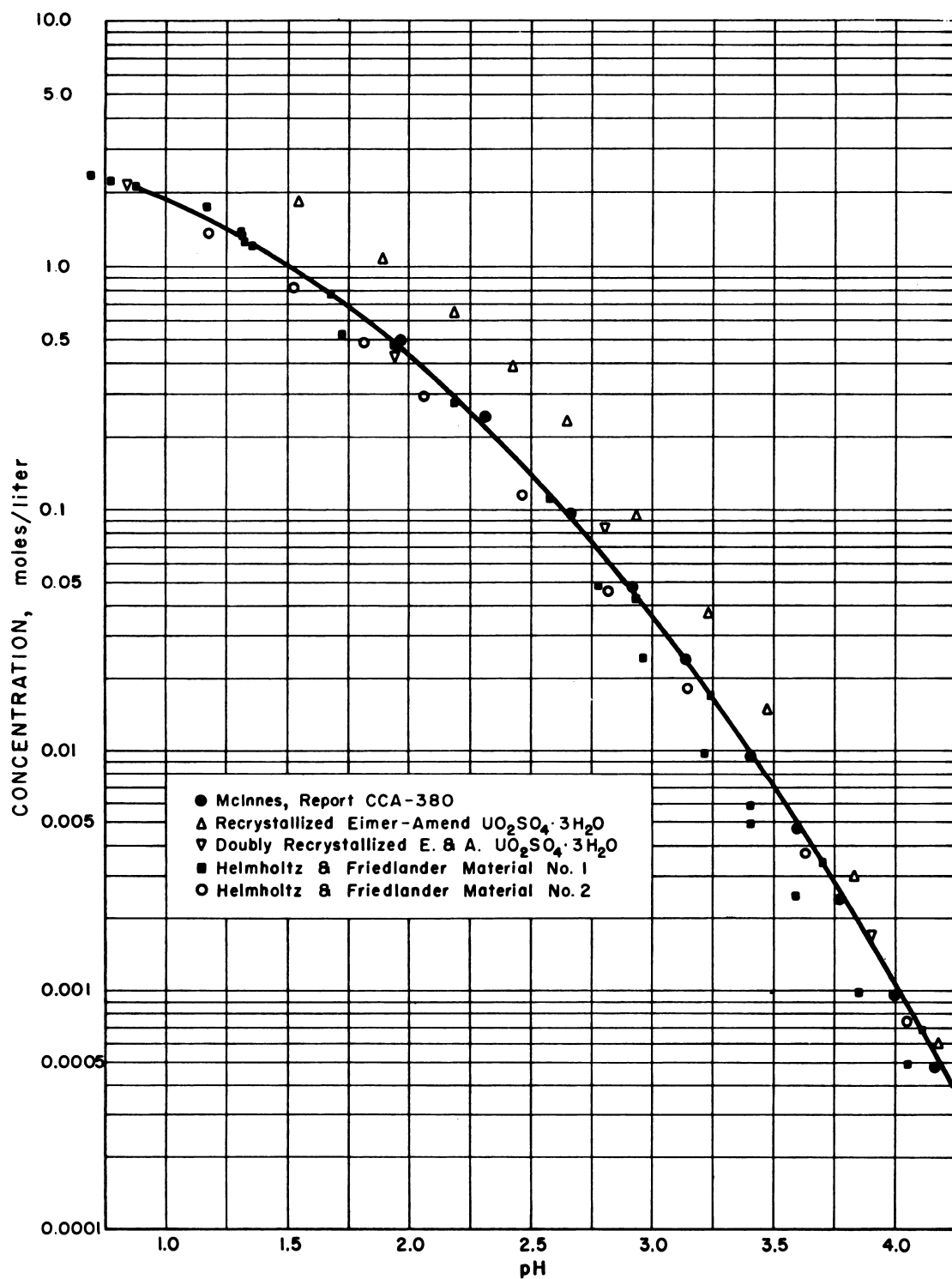


Fig. 4.3.5 — The Effect of Material Preparation on the pH of Uranyl Sulfate Solutions of Various Concentrations at 22°C. Reprinted from MDDC-808. Submitted by Oak Ridge National Laboratory, Nov. 25, 1952.

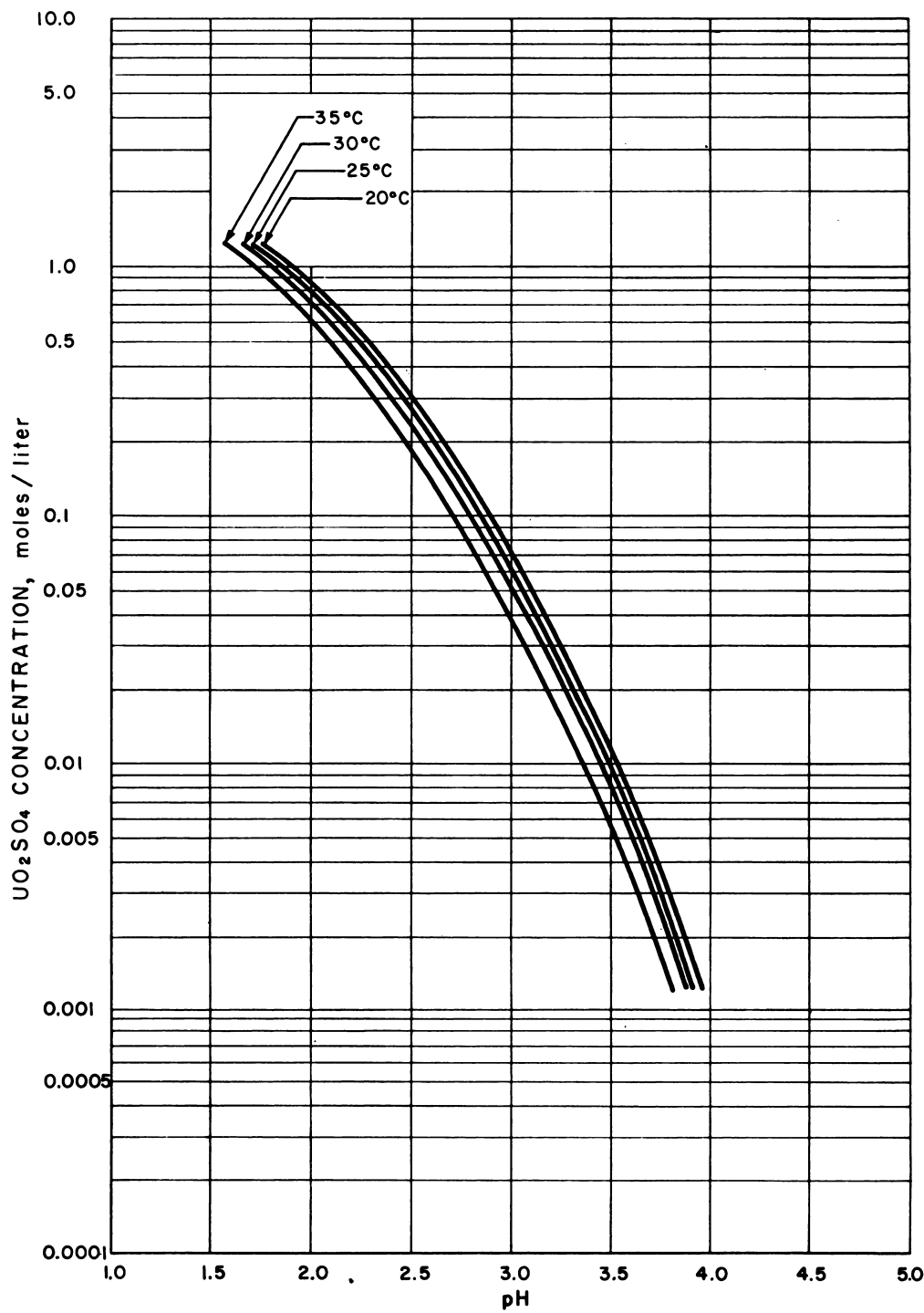


Fig. 4.3.6 — The Relationship of Concentration to the pH in Aqueous Uranyl Sulfate Solutions at Various Temperatures. Submitted by Oak Ridge National Laboratory, Nov. 25, 1952.

Table 4.3.7—Solubility of UO_3 in Uranyl Sulfate Solutions¹³

25°C			100°C		
UO_3 , moles per 1000 gm H_2O	SO_3 , moles per 1000 gm H_2O	Mole ratio, UO_3/SO_3	UO_3 , moles per 1000 gm H_2O	SO_3 , moles per 1000 gm H_2O	Mole ratio, UO_3/SO_3
0.264	0.171	1.54	0.204	0.160	1.28
.647	.418	1.55	.470	.361	1.30
.790	.545	1.45	.708	.533	1.33
1.164	.843	1.38	.989	.785	1.26
1.513	1.029	1.47	1.335	.989	1.35
1.875	1.302	1.44	1.712	1.268	1.35
2.224	1.600	1.39	2.111	1.552	1.36
2.716	1.968	1.38	2.615	1.937	1.35
3.877	2.937	1.32	3.832	2.797	1.37

Table 4.3.8—Solubility of UO_3 in Uranyl Sulfate Solutions^{14,15}

Temp., °C	Total U, moles/liter	Sulfate, moles/liter	Mole ratio, UO_3/SO_3
25	0.168	0.105	1.600
50	.084	.056	1.500
50	.126	.083	1.518
50	.168	.113	1.487
100	.084	.062	1.355
100	.126	.093	1.355
100	.168	.124	1.355
150	.084	.068	1.235
150	.126	.102	1.235
150	.168	.136	1.235
200	.084	.075	1.120
200	.126	.111	1.135
200	.168	.147	1.143
250	.084	.080	1.050
250	.126	.120	1.050
250	.168	.157	1.070

Table 4.3.9 — Solubility of UO_3 in Uranyl Sulfate Solutions^b at 250°C

(Work of J. S. Gill, E. V. Jones, and W. L. Marshall)

Total U, moles/liter	Sulfate, moles/liter	Mole ratio, UO_3/SO_3	pH (25°C)
0.0134	0.0127	1.06	3.80
.0228	.0220	1.04	3.40
.0323	.0298	1.08	3.50
.0525	.0518	1.01	3.31
.0869	.079	1.10	3.52
.1458	.1251	1.17	3.32
.2472	.2059	1.20	3.41
.6529	.5317	1.23	3.20
1.381	1.106	1.25	2.90
1.506	1.185	1.27	2.91
1.657	1.308	1.27	2.84
2.352	1.812	1.30	2.66
2.542	1.970	1.29	2.65
3.002	2.341	1.28	2.52
3.805	3.096	1.23	1.91

 Table 4.3.10 — Solubility of UO_3 in Uranyl Sulfate Solutions^c at 175°C

(Work of E. V. Jones, J. S. Gill, and W. L. Marshall)

Total U, moles/liter	Sulfate, moles/liter	Mole ratio, UO_3/SO_3	pH (25°C)
0.119	0.100	1.19	3.25
.292	.239	1.22	3.30
.594	.471	1.26	3.25
.890	.680	1.31	3.20
1.217	.948	1.28	3.20
1.528	1.178	1.30	2.73
1.790	1.360	1.31	2.80
2.508	1.934	1.30	...
2.986	2.397	1.25	2.30
4.020	2.964	1.36	2.20
4.370	3.370	1.30	1.70
4.440	3.380	1.31	1.90

Table 4.3.11 — Acidity of UO_3 -rich Uranyl Sulfate Solutions^{14,15} at 25°C

Total U, moles/liter	Sulfate, moles/liter	Mole ratio, UO_3/SO_3	pH
0.084	0.0840	1.000	2.71
	.0798	1.053	3.11
	.0714	1.176	3.58
	.0672	1.250	3.72
	.0630	1.333	3.83
	.0588	1.429	3.92
0.126	0.1260	1.000	2.54
	.1220	1.033	2.89
	.1180	1.068	3.15
	.1130	1.115	3.32
	.1090	1.156	3.46
	.1050	1.200	3.55
	.1010	1.247	3.64
	.0966	1.304	3.75
	.0924	1.364	3.81
0.168	0.1680	1.000	2.43
	.1575	1.067	2.79
	.1523	1.103	3.11
	.1470	1.143	3.23
	.1418	1.185	3.30
	.1391	1.208	3.40
	.1365	1.231	3.45
	.1260	1.333	3.68
	.1050	1.600	3.93

Table 4.3.12 — Acidity of Uranyl Sulfate Solutions¹⁶ with Excess UO_3

U, moles per 1000 gm H_2O	SO_4^{--} , moles per 1000 gm H_2O	SO_4^{--} , moles per liter (25°C)	Mole ratio, UO_3/SO_3	pH			
				25.0°C	35.0°C	44.8°C	59.8°C
1.344	0.954	0.914	1.41	3.29	3.12	2.89	2.40
0.333	.236	.233	1.41	3.72	3.52	3.42	2.69
.0331	.0235	.0235	1.41	4.08	3.92	3.82	3.69
.00329	.00233	.00233	1.41	4.32	4.19	4.12	3.99
2.234	1.738	1.576	1.29	2.82	2.68	2.35	1.94
0.536	0.417	0.405	1.29	3.35	3.18	2.91	2.59
.0509	.0394	.0394	1.29	3.90	3.72	3.60	3.18
.00507	.00392	.00392	1.29	4.21	4.08	3.89	3.74
2.069	1.730	1.579	1.19	2.54	2.38	2.09	1.78
0.497	0.416	0.405	1.19	3.19	3.08	2.71	2.41
.0490	.0411	.0411	1.19	3.78	3.59	3.46	3.08
.00487	.00409	.00409	1.19	4.09	3.96	3.88	3.75
1.904	1.738	1.606	1.10	2.10	1.96	1.72	1.36
0.460	0.420	0.410	1.10	2.89	2.76	2.42	2.13
.0455	.0415	.0415	1.10	3.54	3.38	3.17	2.83
.00453	.00413	.00413	1.10	3.95	3.83	3.68	3.53
...	...	1.593	1.00	1.24	1.18	0.98	0.93

Table 4.3.13 — Initial Rates of H₂ Gas Production from Reactor-irradiated Uranium Solutions

Solute	Concentration, gm U/l	Enrichment, gm U ²³⁵ /l	Fission energy: total energy	pH	G _{H₂}
UO ₂ SO ₄	0.399	0.372	0.688		1.61
	4.03	3.76	.957	3.26	1.66
	18.6	1.63	.906	2.90	1.48
	38.1	0.274	.619		0.95
	40.7	37.9	.995	2.42	1.53
	102.1	37.4	.995	2.00	1.35
	105.2	38.9	.995	0.10*	1.20
	108.4	40.1	.995		1.35
	202.3	0.063	.273		0.69
	202.5	37.6	.995	1.61	1.11
	203.4	189.6	.999		1.11
	227.0	1.63	.906		0.98
	310.4	0.096	.364		.62
	386.0	1.63	.906		.80
	431.3	37.8	.995	1.32	.77
	436.8	3.10	.949		.73
	477.2	0.148	.467		.56
	713.5	33.5	.995		.56
	796.0	37.4	.995	1.03	.49
UO ₂ F ₂	4.25	3.96	0.959	4.25	1.63
	40.1	37.3	.995	3.32	1.58
	118.8	37.1	.995	2.98	1.36
	272.0	37.2	.995	2.64	1.11
	377.0	39.3	.996	1.35*	0.84
	405.7	42.3	.996	2.41	.95
UO ₂ (NO ₃) ₂	4.24	3.95	0.960		1.63
	42.3	39.4	.995	2.05	1.5
	318.0	2.29	.932	1.03	0.6
	420.1	36.9	.994	0.60	.55
U(SO ₄) ₂	42.2	39.3	0.995	1.95	1.45
	92.5	35.1	.996	0.1	1.25
	350.0	32.0	.995	.1	0.75

*pH adjusted by adding acid

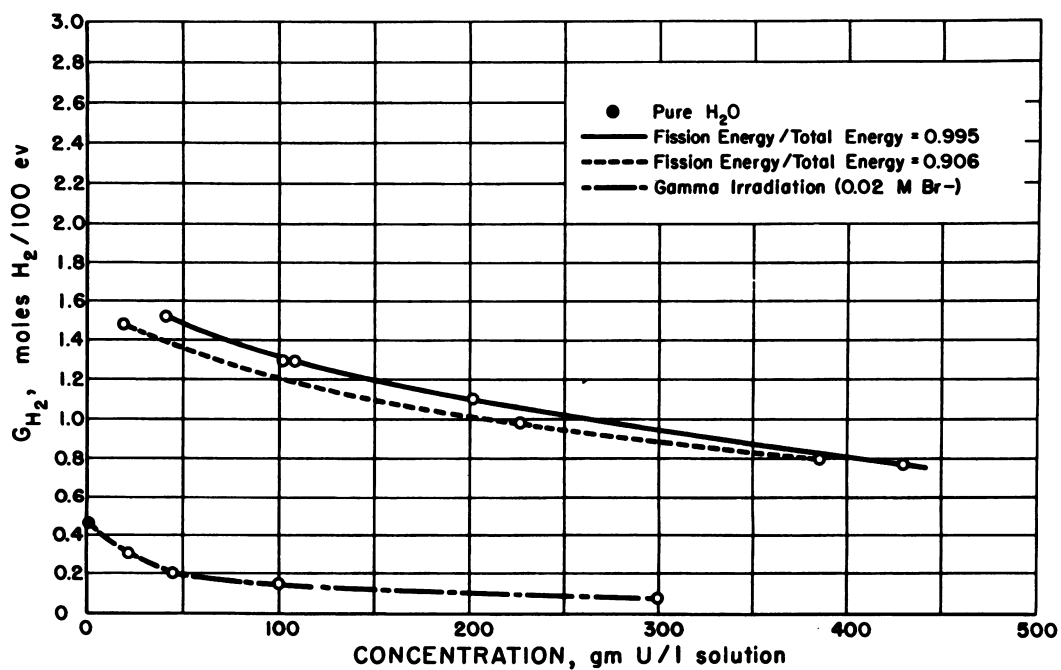


Fig. 4.3.7 — Effect of Uranium Concentration on Hydrogen Gas Yields from Irradiated Uranyl Sulfate Solutions. Reprinted from CF-52-8-103. Submitted by Oak Ridge National Laboratory, Nov. 25, 1952.

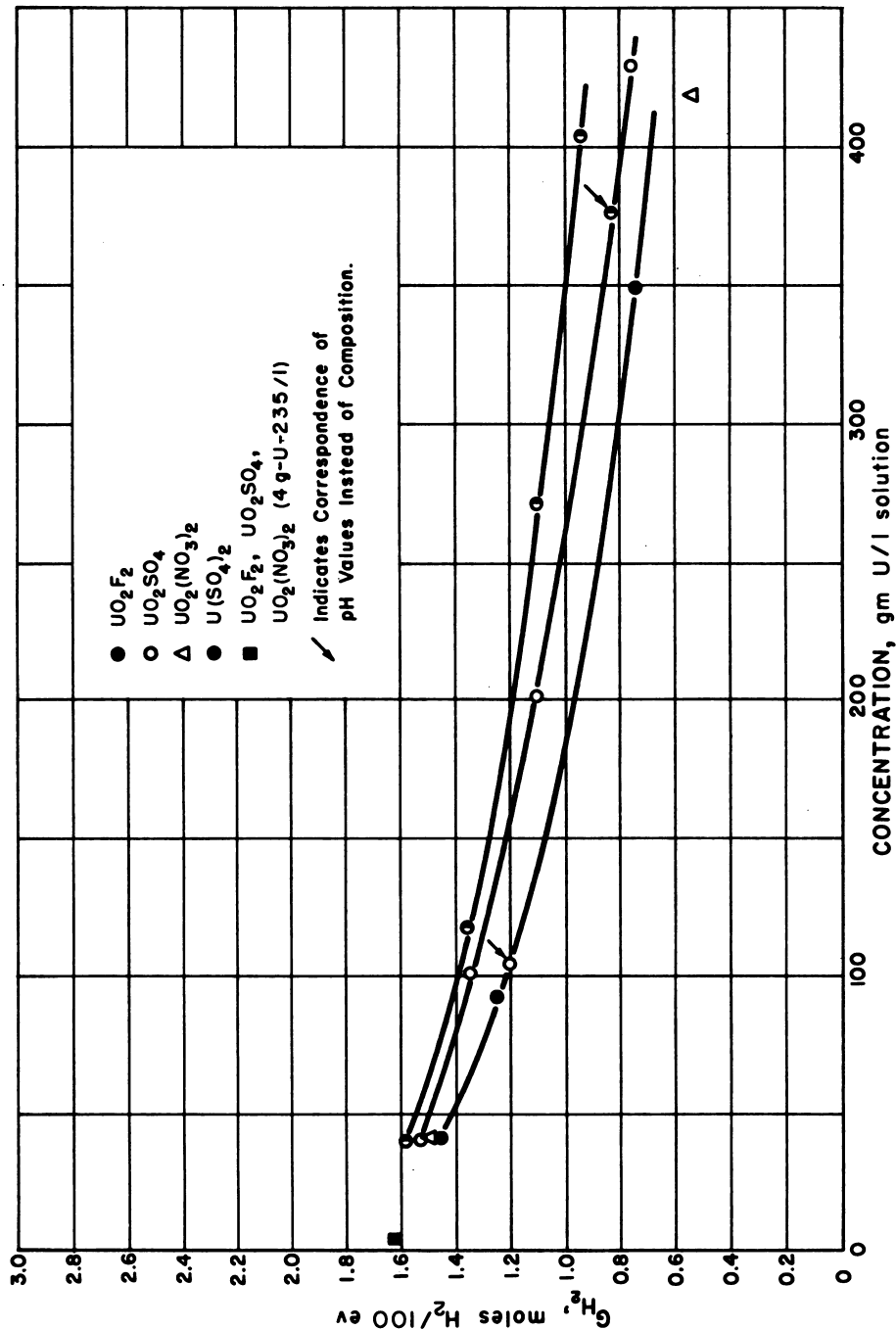


Fig. 4.3.8 — Hydrogen Gas Yields for Uranium Solutions Containing 38 gm of U^{235} per Liter. Reprinted from CF-52-8-103. Submitted by Oak Ridge National Laboratory, Nov. 25, 1952.

solution, whereas actually some gamma and some fast-neutron energy will escape. These reported yields all relate to solutions in light water. No reported yields for heavy-water solutions are known to the reviewer. Research on this problem is presently under way at ORNL.

A secondary effect of radiation upon uranyl solutions is the formation and precipitation of uranium peroxide. In discussing the products of irradiation, Boyle et al.¹⁷ present considerable additional support for the assumption that peroxide is an intermediate in the formation of oxygen. Thus, for every molecule of hydrogen formed by radiation decomposition of water, one may assume that one molecule of peroxide is also formed; i.e., $G_{H_2} = G_{H_2O_2}$. If environmental conditions are such that this peroxide is not destroyed, its concentration will rise until the associated equilibrium concentration of uranium peroxide exceeds its solubility limits. Studies of the kinetics of the decomposition of hydrogen peroxide in uranyl sulfate solutions at temperatures up to 100°C have been carried out by McDuffie et al.¹⁸ The tolerable peroxide concentration, if precipitation is to be avoided is related to a reactor power level, in the case of fissioning solution, by the expression:

$$PD = \frac{C_{ss}}{0.0052 \times G} K_1 \quad (2)$$

where C_{ss} = the allowable steady-state molar concentration of peroxide

PD = reactor power density, kw/l

K_1 = first-order rate constant for peroxide decomposition in the solution under consideration, min^{-1}

A brief study¹⁹ of the thermal decomposition of hydrated uranium peroxide in the presence of excess liquid water was made by sealing water slurries of this compound into pyrex glass capsules which were then heated for measured lengths of time at various temperatures. Subsequent analyses for total uranium and peroxide uranium were used to measure the extent of decomposition. The half-life for decomposition at 100°C was reported as about 400 hr, whereas the reaction was said to be essentially complete in one hour at 185°C.

Recent experiments at ORNL²⁰ have raised the possibility of the existence of precipitated uranium peroxide in uranyl sulfate solutions undergoing fission at high temperatures. From this work, it appears that the temperature dependence of the decomposition of peroxide, the tolerable concentration of peroxide to avoid precipitation, and/or the rates of decomposition of crystalline uranium peroxide once formed must be more carefully evaluated at elevated temperatures.

PHYSICAL PROPERTIES (R. B. BRIGGS)

Density

Several investigators have measured the density of $\text{UO}_2\text{SO}_4\text{-H}_2\text{O}$ solutions at temperatures between 0° and 100°C. Data have been obtained by Orban at the Mound Laboratory for 0.174 to 2.473 molar solutions at temperatures of 20° and 30°C.²¹ Densities were measured at 30°C for solutions containing 25 to 60 wt-% of anhydrous uranyl sulfate and at temperatures from 0° to 93°C for 51-, 39.9-, and 29.9-percent solutions by Helmholtz and Friedlander at Los Alamos.³ Lietzke, Wright, and Marshall²² at ORNL measured the density of 0- to 3.33-molar solutions at 25°C.

Two series of measurements of solution densities at temperatures above 100°C have been reported by ORNL. Secoy determined the volume expansion of a 34.9-percent uranyl

sulfate solution at temperatures from 22° to 372°C. W. H. Davenport and R. H. Powell obtained data for several concentrations at 50°C and for 4.6-percent solution at 184° to 232°C. These data are reported in convenient form by Marshall.²³

Marshall has derived equations based on these data which relate the density of uranyl solution to that of water at the same temperature:

$$d_{\text{soln}} = \frac{1}{\frac{78.65}{U} - 1.046} + d_{\text{H}_2\text{O}} \quad (3)$$

$$= \frac{1}{\frac{120.9}{S} - 1.046} + d_{\text{H}_2\text{O}} \quad (4)$$

where d_{soln} and $d_{\text{H}_2\text{O}}$ = densities of solution and pure water, respectively, at the saturated vapor pressure and the temperature of interest

U = concentration of uranium in wt-%

S = concentration of sulfate in wt-%

The equations agree with the experimental data to ± 0.5 percent at temperatures from 25° to 300°C with solutions containing less than 10 wt-% uranyl sulfate. Agreement to ± 1.0 percent in the temperature range 120° to 250°C and to ± 2.0 percent in the ranges 25° to 120°C and 250° to 280°C are obtained with concentrations from 10 to 50 percent.

Van Winkle²⁴ presents curves and formulas relating solution densities to temperature and concentration based on a theoretical analysis. Agreement with the experiments is reasonable but not as good as that obtained with the empirical formulas of Marshall.

Density data obtained by the investigators are presented in Tables 4.3.14 and 4.3.15. A curve of the density of water at the saturation pressure as a function of temperature is plotted in Fig. 4.3.9 for use with Eqs. (3) and (4).

The data are in good agreement with curves and formulas of Van Winkle and with the following equation of Marshall obtained by substituting the density of D_2O for that of H_2O in deriving Eqs. (3) and (4):

$$d_{\text{soln}} = \frac{1}{\frac{71.0}{U} - 0.944} + d_{\text{D}_2\text{O}} \quad (5)$$

$$= \frac{1}{\frac{109}{S} - 0.944} + d_{\text{D}_2\text{O}} \quad (6)$$

A curve for the density of D_2O at the saturation pressure as a function of temperature is also plotted in Fig. 4.3.9.

Viscosity

Viscosity data for the $\text{UO}_2\text{SO}_4\text{-H}_2\text{O}$ system at 20° and 30°C as reported by Orban of the Mound Laboratory are reproduced in Table 4.3.16. Van Winkle²⁴ has compared the data of Roarty et al with published data for H_2O and D_2O to obtain the curves shown in Figs. 4.3.10 and 4.3.11. These curves are based upon extrapolation of low-temperature data to high temperatures and are not expected to be accurate.

Heat Capacity

Van Winkle has estimated the heat capacity of dehydrated uranyl sulfate by comparison

Table 4.3.14 — Density of Uranyl Sulfate Solutions at 20°–30°C

Conc., moles/liter	Conc., wt-% UO_2SO_4	ρ_{20}^{21}	ρ_{25}^{12}	ρ_{30}^{21}	ρ_{30}^3
0.0	0.0 ¹		0.9970		
.174		1.0543		1.0521	
.4196			1.1295		
.436		1.1381		1.1341	
.644		1.2028		1.1986	
.827		1.2614		1.2567	
.8455			1.2668		
.880	25.3				1.273
.986		1.3127		1.3068	
1.10	30.0				1.349
1.233		1.3911		1.3839	
1.2597			1.4002		
1.36	34.9				1.420
1.406		1.4440		1.4383	
1.53	38.0				1.476
1.604		1.5072		1.5026	
1.6755			1.5298		
1.70	40.8				1.526
1.792		1.5658		1.5610	
1.90	44.0				1.585
2.0939			1.6610		
2.11	46.8				1.652
2.3249			1.7260		
2.43	50.6				1.758
2.473		1.7789		1.7727	
2.5635			1.7994		
2.7244			1.8573		
2.8718			1.9076		
3.3309			2.0484		
3.42	60.2				2.080

Table 4.3.15—Effect of Temperature on Density of Uranyl Sulfate Solutions

Temp., °C	Density					
	4.4% ²⁵	4.6% ²⁵	29.9% ³	34.9% ⁶	39.9% ³	51% ³
0.0			1.3547		1.5350	
15.0			1.3499		1.5283	1.7959
20.0			1.3479		1.5257	1.7926
22.3						
25.0			1.3455	1.432	1.5228	1.7891
30.0			1.3430		1.5199	1.7854
35.0			1.3403		1.5166	1.7816
40.0			1.3376		1.5133	1.7777
45.0					1.5099	1.7736
48.8				1.410		
50.0	1.028		1.3314		1.5064	1.7696
55.0					1.5028	1.7655
60.0			1.3249		1.4992	1.7612
65.0						1.7569
70.0				1.393	1.4913	1.7526
70.2			1.3178			
75.0						1.7472
79.4			1.3106			
79.9					1.4829	
80.0						1.7427
88.0				1.380		
93.2			1.2998			
93.4					1.4713	
93.6						1.7300
108.8				1.360		
129.2				1.340		
152.6				1.317		
175.7				1.294		
184		0.925				
187				1.282		
203		0.902				
231.7				1.227		
232		0.863				
249.4				1.199		
274				1.153		
303.8				1.081		
325.8				1.004		
345.8				0.911		
356.3				.861		
366.5				.787		
371.5				.753		

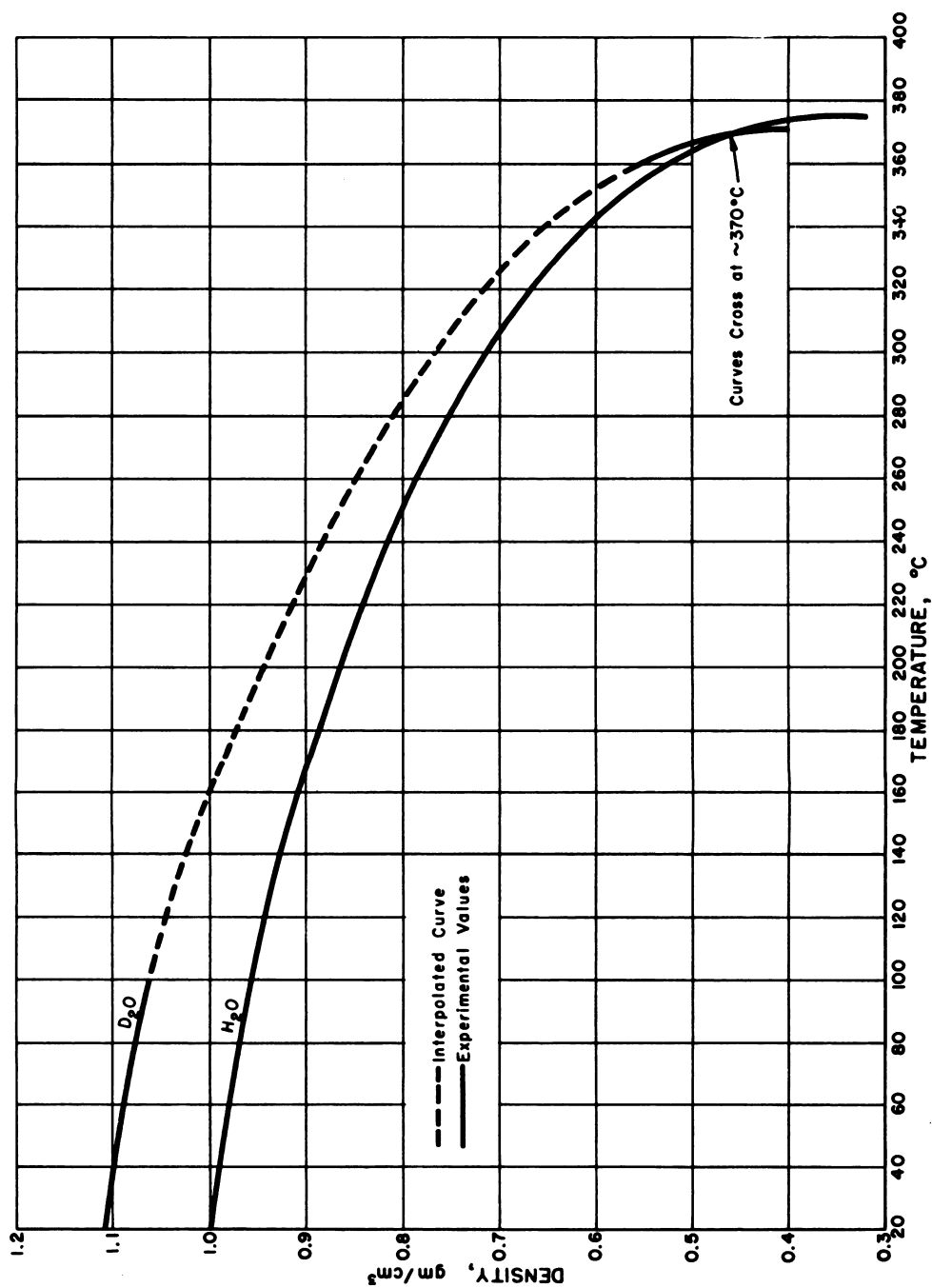


Fig. 4.3.9 — Density—Temperature Relation for Ordinary and Heavy Water. Submitted by Oak Ridge National Laboratory, Nov. 25, 1952. Pressure: one atmosphere to boiling point; saturation above boiling point.

Table 4.3.16—Viscosity of Uranyl Sulfate Solutions at 20° and 30°C

Concentration, moles/liter	Viscosity, cp	
	20°	30°
0.174	1.128	0.8901
.436	1.359	1.063
.644	1.573	1.231
.827	1.809	1.403
.986	2.047	1.572
1.233	2.509	1.921
1.406	2.912	2.218
1.604	3.501	2.641
1.792	4.178	3.145
2.473	8.541	6.256

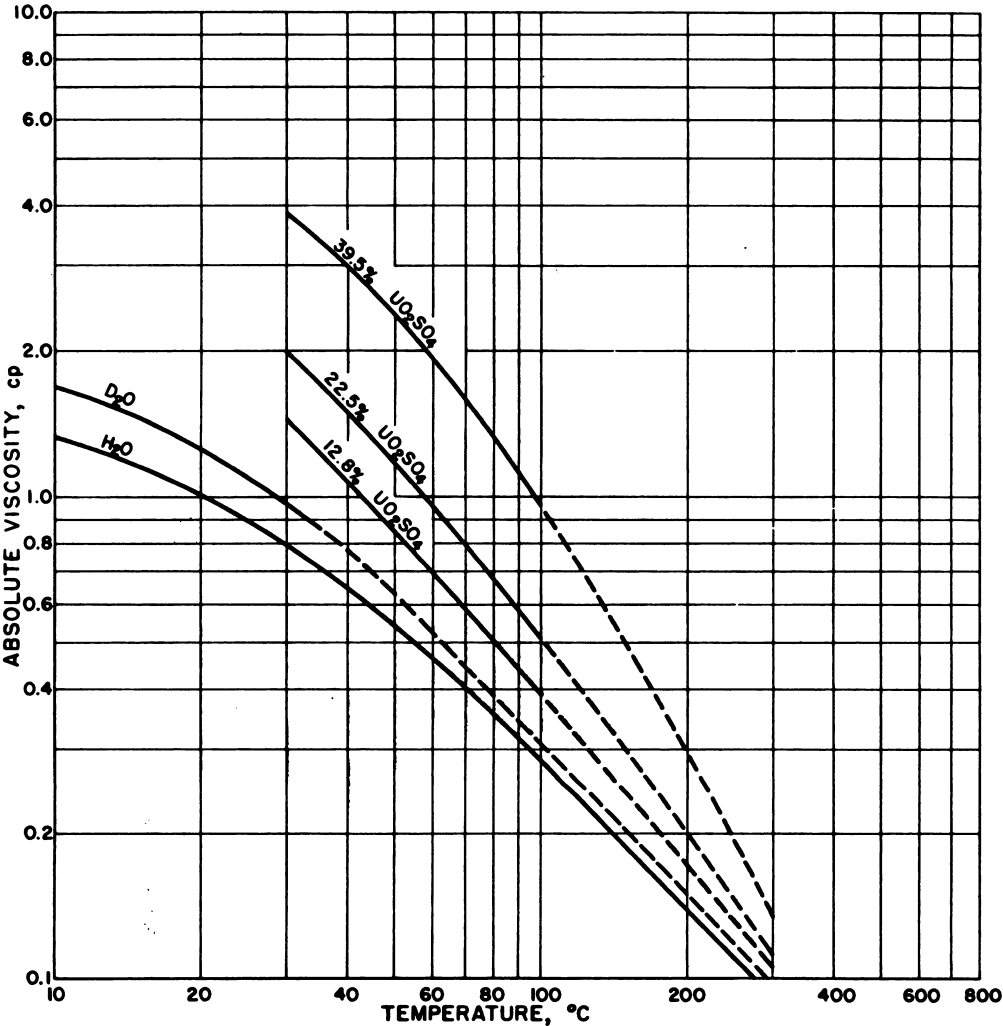


Fig. 4.3.10—Absolute Viscosity vs Temperature for H_2O , D_2O , and Aqueous UO_2SO_4 Solutions. Submitted by Oak Ridge National Laboratory, Nov. 25, 1952.

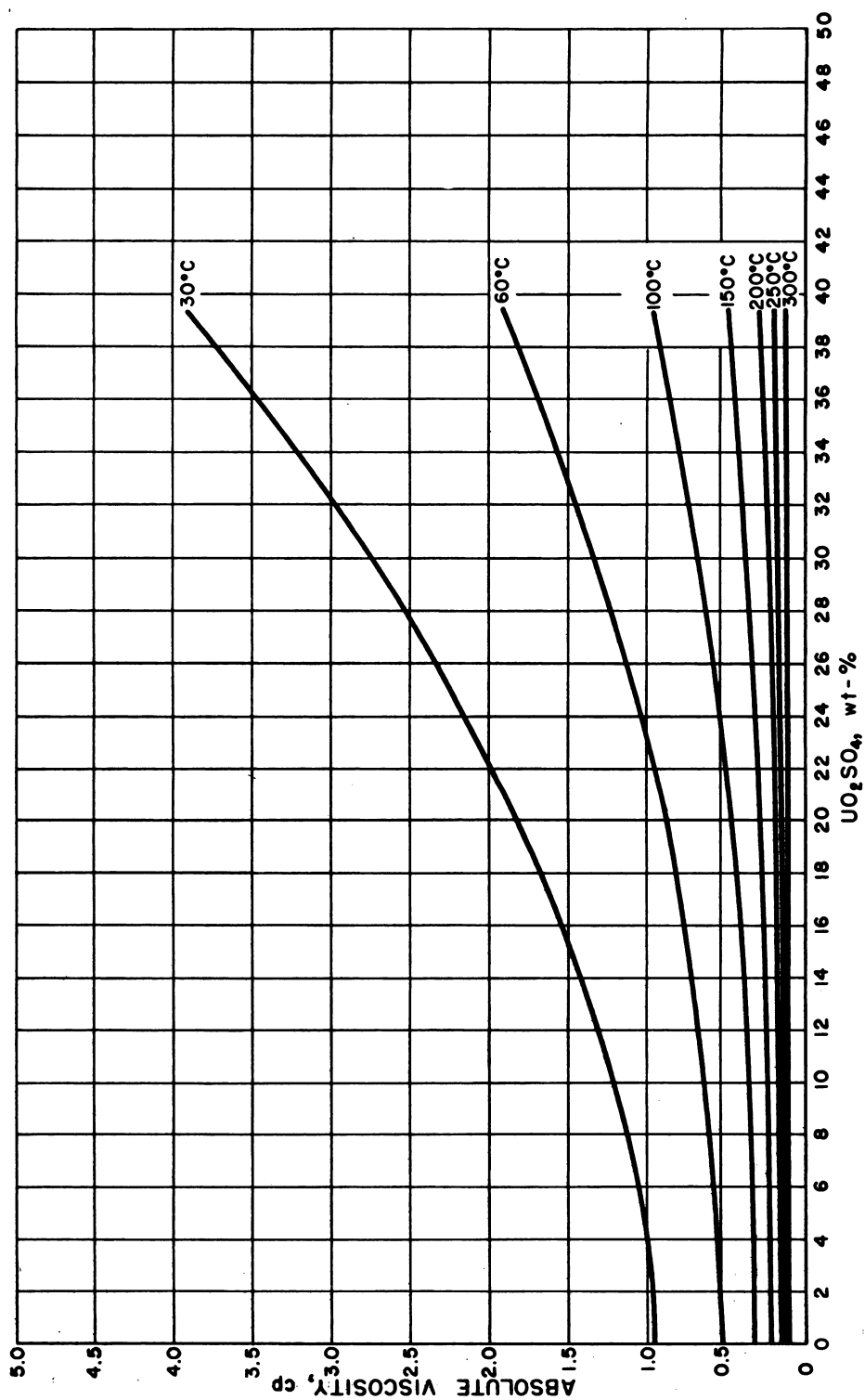


Fig. 4.3.11—Viscosity vs Concentration for Uranyl Sulfate Solutions at Various Temperatures. Submitted by Oak Ridge National Laboratory, Nov. 25, 1952.

with uranyl nitrate and with salts of other metals and has estimated the heat capacity of solutions of uranyl sulfate in D_2O . His estimated heat capacities of solutions at $25^\circ C$ are given²⁴ in Table 4.3.17 and plotted in Fig. 4.3.12.

The heat capacity of UO_2SO_4 - D_2O solutions at other temperatures is estimated by the equation:

$$(C_p)_T = (C_p)_{25} \frac{[C_p(D_2O)]_T}{[C_p(D_2O)]_{25}} \quad (7)$$

where the subscripts T and 25 refer to temperatures on the Centigrade scale at which the respective values for C_p are to be obtained.

The heat capacity of H_2O as a function of temperature is presented in Fig. 4.3.13. Values plotted are those estimated by Van Winkle.²⁴

Included in Table 4.3.17 and Fig. 4.3.12 are estimated heat capacities for the UO_2SO_4 - H_2O system at 25° and $250^\circ C$ based upon data given by Van Winkle.²⁴ A curve of heat capacity of H_2O vs temperature obtained from Harrison's report²⁶ is presented in Fig. 4.3.13. The formula:

$$(C_p)_T = (C_p)_{25} \frac{[C_p(H_2O)]_T}{[C_p(H_2O)]_{25}} \quad (8)$$

where the symbols are defined as are those in Eq. (7), may be used to estimate the heat capacities of UO_2SO_4 - H_2O solutions at elevated temperatures.

Surface Tension

The surface tension of UO_2SO_4 - H_2O solutions has been measured by Orban²¹ at the Mound Laboratory. These data are given in Table 4.3.18.

Van Winkle²⁴ presents curves (Fig. 4.3.14) relating the surface tensions of several uranyl sulfate solutions to temperature. They are based upon surface-tension data from Dorsey,²⁷ Kirshenbaum's measurements²⁸ indicating that there is essentially no difference between the surface tension of H_2O and D_2O at $25^\circ C$, and on measurements of UO_2SO_4 - D_2O solutions obtained by Roarty et al²⁹ at temperatures between 30° and $80^\circ C$.

Refractive Index

The index of refraction of UO_2SO_4 - H_2O solutions at $25^\circ C$ has been reported by Marshall.¹² Data are presented in Table 4.3.19.

THE SYSTEM UO_2F_2 - H_2O AND RELATED SYSTEMS

CHEMICAL PROPERTIES

Chemical Stability (C. H. Secoy)

Uranyl fluoride, like uranyl sulfate, is strongly hydrolyzed in solution, and as a consequence, excess UO_3 is readily soluble in uranyl fluoride solutions. The solubility behavior of the system is dependent on the stoichiometry of the salt. The system can be studied as a simple two-component system, stoichiometric UO_2F_2 - H_2O , or it can be treated more adequately as a three-component system, UO_3 -HF- H_2O . In fact, at high temperatures where the vapor phase contains HF as well as H_2O , it must be treated as a three-component system.

Table 4.3.17 — Heat Capacities of Uranyl Sulfate Solutions

UO ₂ SO ₄ , wt-%	Estimated heat capacity at 25°C, cal/(gm)(°C)	
	D ₂ O solutions	H ₂ O solutions
0	1.005	0.9983
10	0.916	.905
20	.830	.809
30	.745	.714
40	.658	.619
50	.568	.523
60	.474	.428
70	.370	.333
80	.252	.238
85.9 (UO ₂ SO ₄ ·3D ₂ O)	.174	
87.2 (UO ₂ SO ₄ ·3H ₂ O)		.170

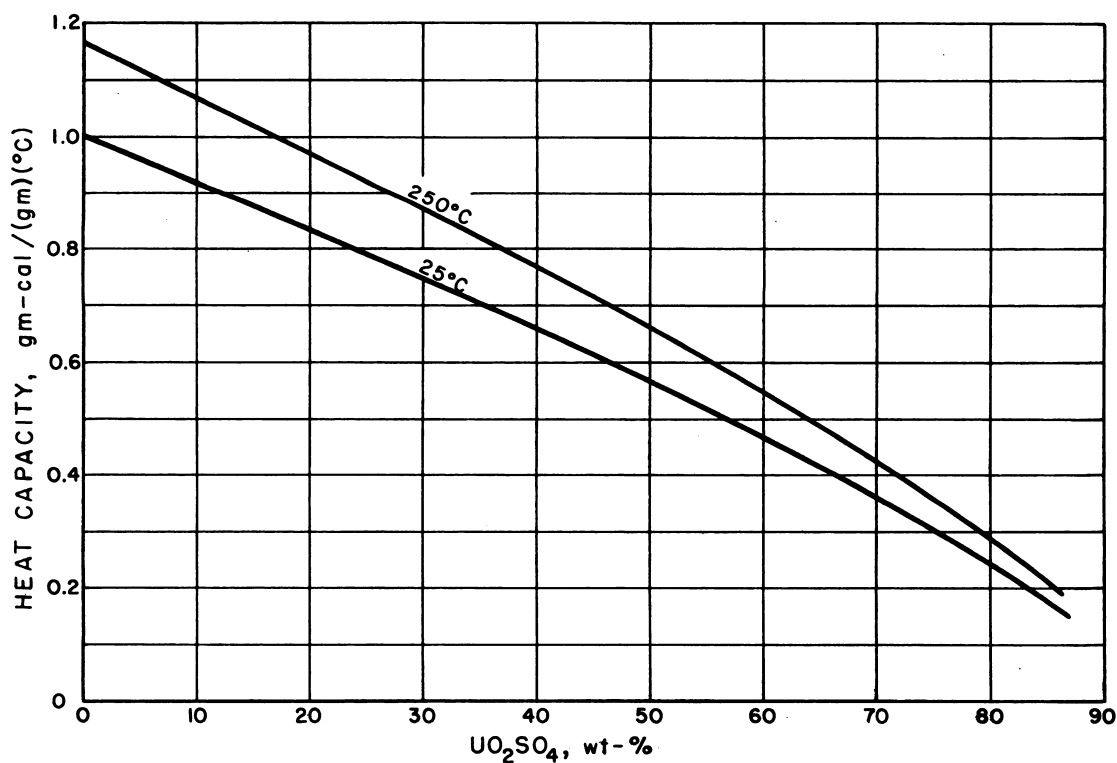


Fig. 4.3.12 — Heat Capacity of Aqueous Uranyl Sulfate Solutions. Submitted by Oak Ridge National Laboratory, Nov. 25, 1952.

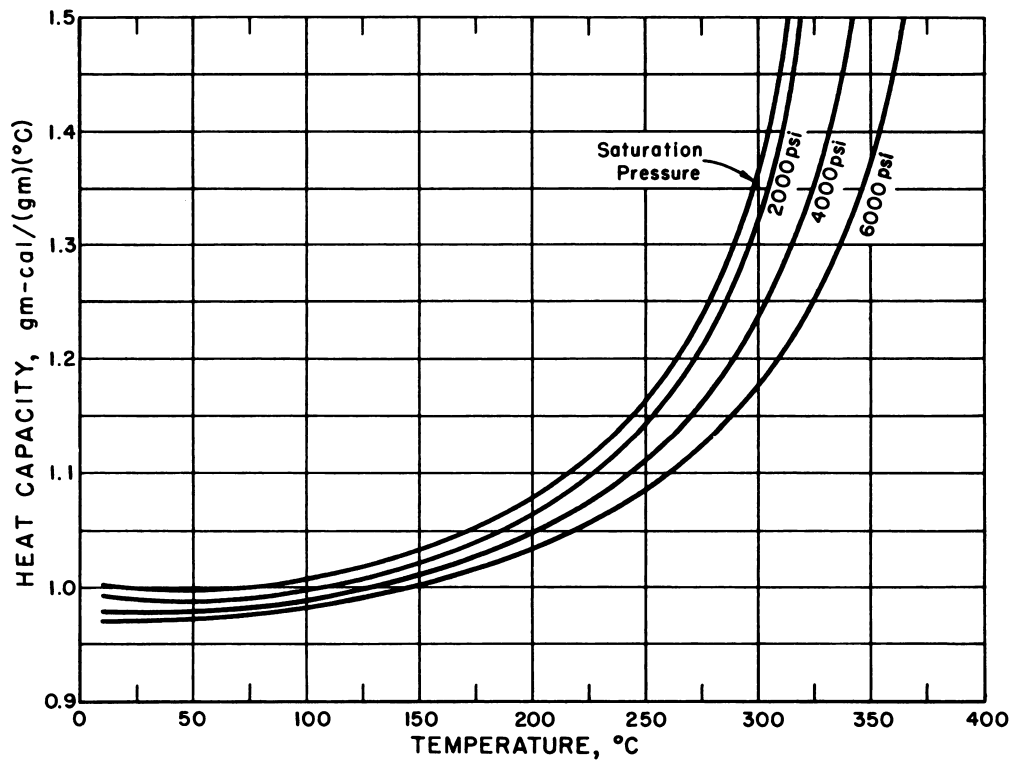


Fig. 4.3.13 — Heat Capacity vs Temperature for Ordinary Water. Submitted by Oak Ridge National Laboratory, Nov. 25, 1952.

Table 4.3.18 — Surface Tension of $\text{UO}_2\text{SO}_4\text{-H}_2\text{O}$ Solutions at 20°C

Conc., moles/liter	Surface tension, dynes/cm ²
0.174	72.90
.436	73.03
.644	73.46
.827	73.88
.986	74.26
1.406	75.23

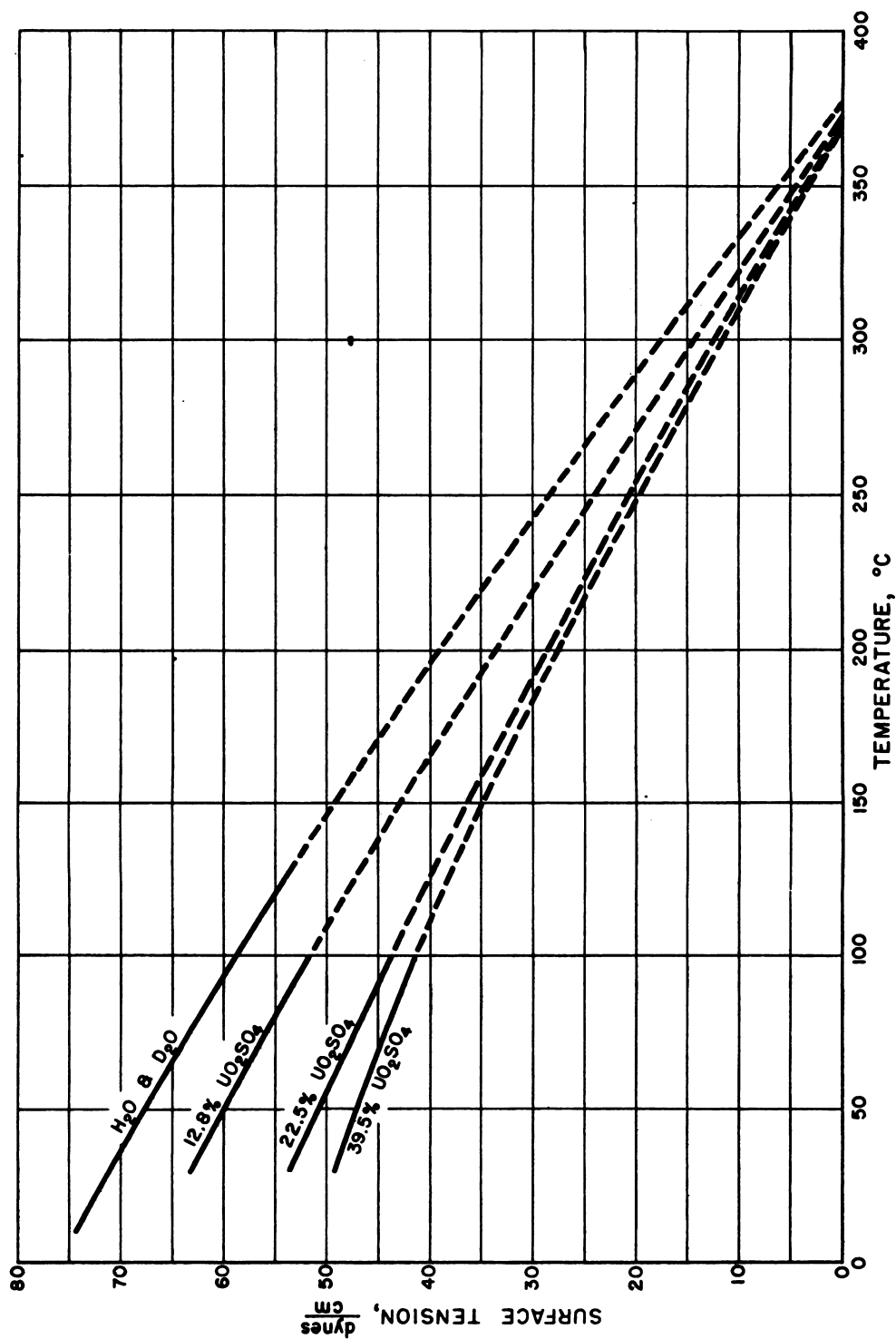


Fig. 4.3.14—Surface Tension vs Temperature for Ordinary and Heavy Water and for Uranyl Sulfate Solutions. Submitted by Oak Ridge National Laboratory, Nov. 25, 1952.

Table 4.3.19 — Refractive Indices of $\text{UO}_2\text{SO}_4\text{-H}_2\text{O}$ Solutions at 25°C

Conc., moles/liter	Refractive index
0.0	1.3320
.4196	1.3452
.8455	1.3583
1.2597	1.3705
1.6755	1.3844
2.0939	1.3973
2.3249	1.4024
2.5635	1.4089
2.7244	1.4145
2.8718	1.4189
3.3309	1.4312

The solubility of stoichiometric UO_2F_2 in water has been reported by Katz,³⁰ by Kunin,³¹ and in a much more complete manner by W. L. Marshall, J. S. Gill, and C. H. Secoy.³² Their data are presented in Tables 4.3.20, 4.3.21, and 4.3.22, respectively, and are shown graphically in Fig. 4.3.15. This system, like the uranyl sulfate system, displays a two-liquid phase region which, however, differs in that its upper temperature limit is an invariant system (Solid - Liquid I - Liquid II - Vapor) rather than the critical vanishing of one of the liquid phases.

The minimum in the two-liquid phase co-existence curve has been studied by Jones and Marshall⁶ in both H_2O and in D_2O . Their data⁷ appear in Table 4.3.23. As in the case of uranyl sulfate, the minimum is approximately 10° lower in D_2O than in H_2O .

A portion of the acid-rich system, $\text{UO}_2\text{F}_2\text{-HF-H}_2\text{O}$, has been studied at 25°C by Kunin.³¹ His data are given in Table 4.3.24 and Fig. 4.3.16. The solubility of UO_3 in uranyl fluoride solutions has been reported by Jones, Gill, Marshall, and Secoy⁷ at 175° and 250°C and is reported in Table 4.3.25. This study is being extended to other temperatures.

The effect of excess HF or UO_3 on the two-liquid phase region has not been studied quantitatively.

The acidity of stoichiometric uranyl fluoride solutions as reported by Marshall, Gill, and Secoy³² is given in Table 4.3.26. The pH of the high-temperature UO_3 -saturated solutions as measured after cooling to 25°C is included in Table 4.3.25.

Radiation Stability

See discussion of this subject under Properties of Uranyl Sulfate Solutions.

PHYSICAL PROPERTIES (H. O. DAY)

Densities in the $\text{UO}_2\text{F}_2\text{-H}_2\text{O}$ and $\text{UO}_3\text{-HF-H}_2\text{O}$ Systems³⁰

Densities for these systems are shown in Tables 4.3.27 through 4.3.31.

Viscosity and Thermal Conductivity

No data on these properties were found for the $\text{UO}_3\text{-HF-H}_2\text{O}$ system.

Heat Capacity³⁷ of Solid UO_2F_2

Heat capacity is given for solid anhydrous UO_2F_2 (no more than 0.07 wt-% impurity) from 13° to 418°K (−260° to +145°C).

Table 4.3.20 — Solubility of Uranyl Fluoride in Water

Temp., °C	UO ₂ F ₂ , wt-%
25.0	67.3
75.0	69.6
99.9	72.4

Table 4.3.21 — Solubility of Uranyl Fluoride in Water

Temp., °C	UO ₂ F ₂ , wt-%
1	61.4
25	65.6
60	71.0
100	74.1

Table 4.3.22—The System Uranyl Fluoride-water

UO ₂ F ₂ , wt-%	Temp., °C	Equilibrium phases*	Invariant temp., °C (S _α -L ₁ -L ₂ -V)	Critical temp., °C (L ₁ -V)
44.23	-4.2	S _I -L-V		
47.72	-5.0	S _I -L-V		
50.76	-5.9	S _I -L-V		
55.49	-7.8	S _I -L-V		
57.28	-8.1	S _I -L-V		
58.54	-9.2	S _I -L-V		
61.20	-10.9	S _I -L-V		
62.58	-11.9	S _I -L-V		
64.25†	-13.2†	S _I -S _α -L-V		
64.28	-10.7	S _α -L-V		
64.30	0.0	S _α -L-V		
64.40	10.1	S _α -L-V		
66.09	19.7	S _α -L-V		
66.50	30.5	S _α -L-V		
67.78	39.8	S _α -L-V		
67.25	51.2	S _α -L-V		
68.45	54.3	S _α -L-V		
68.42	60.1	S _α -L-V		
69.37	65.8	S _α -L-V		
71.73	75.0	S _α -L-V		
73.02	89.8	S _α -L-V		
76.98	125	S _α -L-V		
81.72	150	S _α -S _β -L-V		
81.40	195	S _β -L-V		
82.61	219	S _β -L-V		
83.0†	240†	S _β -S _A -L-V		
82.53	243	S _α -L-V		
81.22	252	S _α -L-V		
77.05	283	S _α -L-V		
72.31	322	S _α -L-V		
70.5†	347†	S _α -L ₁ -L ₂ -V		
66.46	324	L ₁ -L ₂ -V	344	
61.98	320	L ₁ -L ₂ -V		
55.13	314	L ₁ -L ₂ -V	347	
49.24	314	L ₁ -L ₂ -V	347	
40.98	313	L ₁ -L ₂ -V	347	
36.1				376
34.76	313	L ₁ -L ₂ -V	347	
26.75	313	L ₁ -L ₂ -V	344	
23.0				378
19.36	314	L ₁ -L ₂ -V		
13.86	313	L ₁ -L ₂ -V		
10.85				377

* S_I = solid ice; S_α = solid α·UO₂F₂·2H₂O; S_β = solid βUO₂F₂·2H₂O; S_A = solid αUO₂F₂·XH₂O;
 L = saturated solution; L₁ = H₂O-rich liquid; L₂ = UO₂F₂-rich liquid; V = vapor

† Extrapolated values

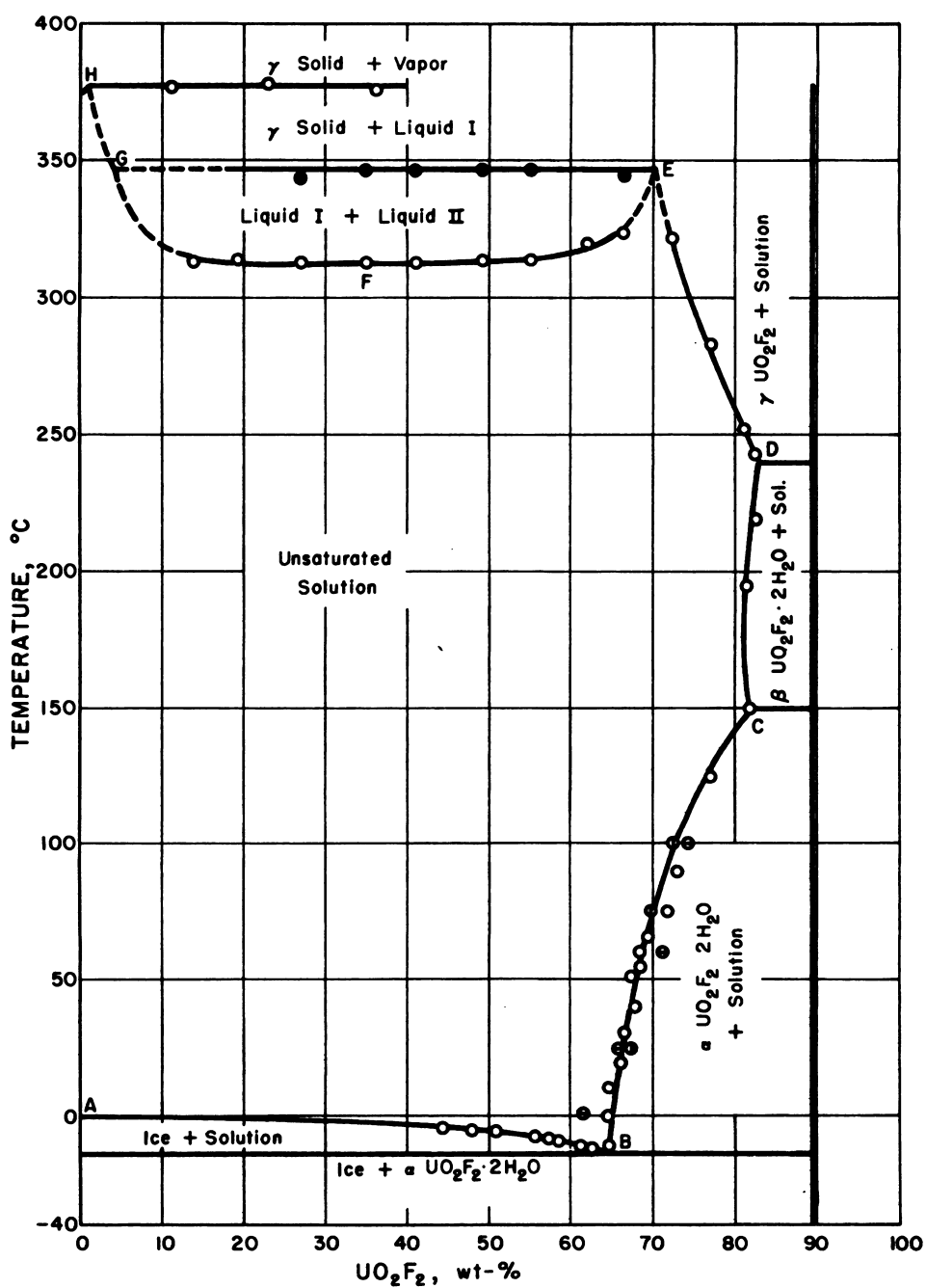


Fig. 4.3.15—The System Uranyl Fluoride-Water. Submitted by Oak Ridge National Laboratory, Nov. 25, 1952.

Table 4.3.23 — Two-liquid Phase Temperatures for Uranyl Fluoride in H₂O and D₂O

In H ₂ O		In D ₂ O	
Temp., °C	UO ₂ F ₂ , wt-%	Temp., °C	UO ₂ F ₂ , wt-%
350	4.42	340	5.24
326.2	14.73	340	16.12
315.8	24.77	308.4	18.67
315.8	36.99	310.4	20.85
315.3	51.90	307.4	26.01
322.2	65.15	307.4	36.25
		308.7	52.43
		312.6	59.86
		313.1	62.80

 Table 4.3.24 — The System UO₂F₂-HF-H₂O at 25°

Liquid phase			Specific gravity	Wet solid		
HF, %	UO ₂ F ₂ , %	H ₂ O, %		HF, %	UO ₂ F ₂ , %	H ₂ O, %
0.0	65.55	34.45	2.224
1.28	47.58	51.14
3.59	39.78	56.63
9.78	32.25	57.97	1.430
11.88	31.88	56.24	1.440	8.52	51.95	39.53
20.70	22.29	57.01	...	18.20	32.50	49.30
25.75	18.19	56.01	...	14.51	51.25	34.24
32.51	11.35	56.14	1.231	{ 12.06	64.47	23.47
41.70	6.10	52.20	...	{ 3.50	83.76	12.74
				8.77	75.2	16.03

 Table 4.3.25 — The Solubility of UO₃ in Uranyl Fluoride Solutions at 175° and 250°C

175°C				250°C			
U, wt-%	F, wt-%	Mole ratio U/2F	pH 25°C	U, wt-%	F, wt-%	Mole ratio U/2F	pH 25°C
1.14	0.18	1.012	4.65	3.89	0.672	0.924	2.92
3.99	.60	1.033	4.40	14.64	2.38	.982	3.50
5.23	.81	1.022	4.30	19.68	2.95	1.07	3.90
18.11	2.63	1.100	3.90	26.54	3.75	1.13	3.60
30.78	4.23	1.161	3.57	29.99	4.33	1.11	3.49
35.62	4.93	1.153	3.37	39.84	5.67	1.12	3.90
41.45	5.20	1.273	3.20	42.07	5.77	1.16	3.25
47.13	6.24	1.206	2.70	42.93	5.91	1.16	3.10
50.17	6.32	1.267	2.60	46.51	6.78	1.09	2.85
55.95	7.24	1.240	1.60				

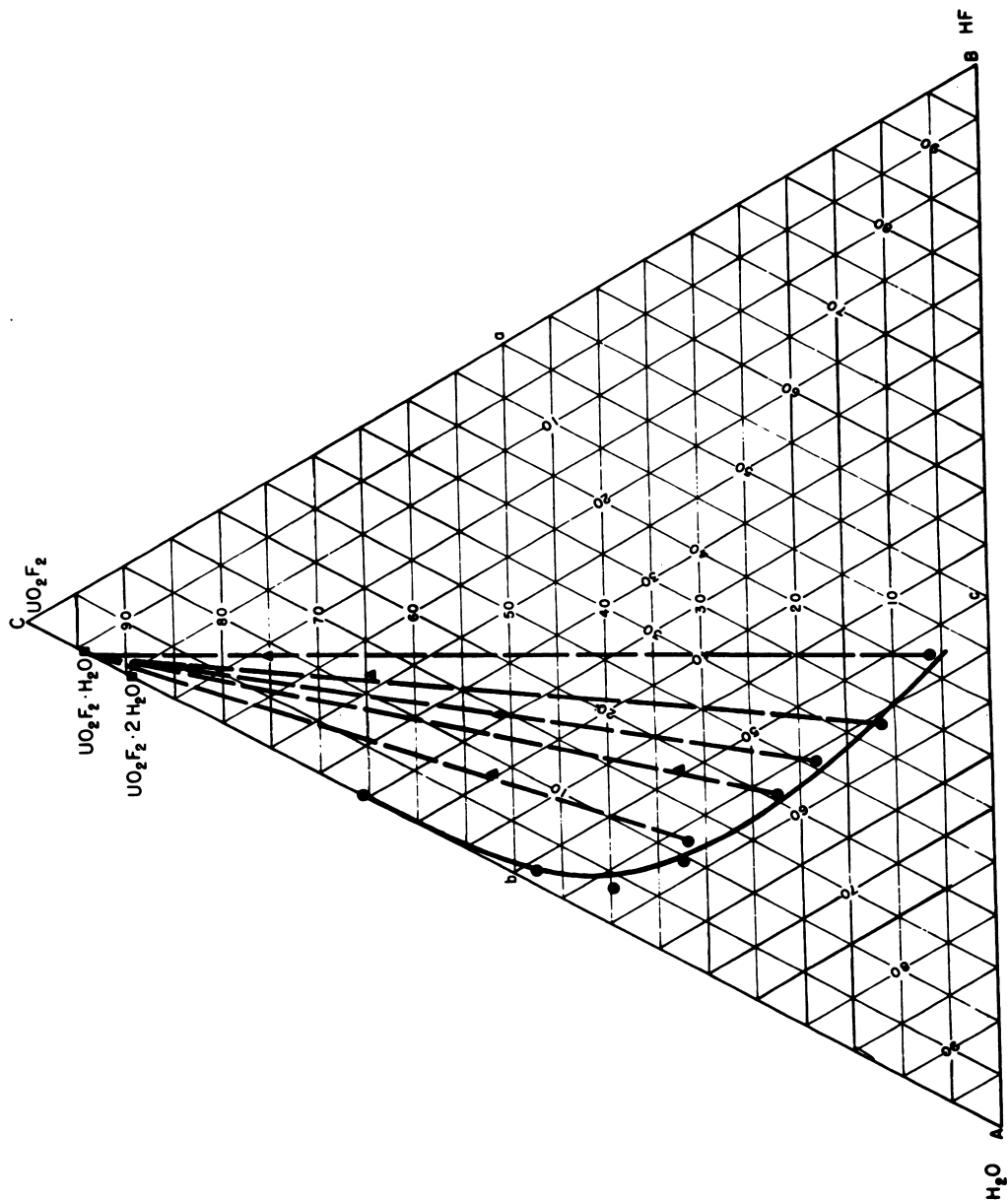


Fig. 4.3.16 — The System UO_2F_2 -HF- H_2O at 25°C. Submitted by Oak Ridge National Laboratory, Nov. 25, 1952.

Table 4.3.26 — The pH of Uranyl Fluoride Solutions at 25°C

UO ₂ F ₂ , wt-%	Density	pH, 25°C
2.112	1.0136	3.70
7.565	1.0699	3.18
13.86	1.1349	2.86
19.39	1.2005	2.69
26.75	1.3016	2.50
34.76	1.4411	2.25
40.98	1.5754	2.13
49.24	1.7511	2.05
55.13	1.9212	1.76
61.98	2.1764	1.52

 Table 4.3.27 — Solubility of UO₂F₂ in Water

Temp., °C	Wt-%	Moles/liter	Density, gm/ml
25.0	67.3	5.18 ± 0.02 M	2.405
75.0	69.6	5.59	2.472
99.9	72.4	6.08	2.588

 Table 4.3.28 — Specific Gravity of UO₂F₂ Solutions³³ at 25°C

Concentration, * molar	Concentration ³⁴		Sp. ³⁴ grav. ₄ †
	Molar	Wt-%	
0.50	0.502	13.62	1.136
1.00	1.004	24.29	1.274
2.00	2.004	39.99	1.544
3.00	3.009	51.17	1.812
4.00	4.012	59.45	2.079
5.00	5.030	65.98	2.349
	5.180 (Sat'd)	66.40	2.400

* From 0 to 4M the data are represented by the equation:

$$D = 0.997 + 0.277M - 0.0015M^2 \quad (9)$$

where M = molarity

† Accuracy = ±0.001 gm/ml

Table 4.3.29 — Densities in the UO_2F_2 -HF- H_2O System³¹

Density (D_{25}^{25})	Composition liquid, wt-%		Wet solid	
	UO_2F_2	HF	HF	UO_2F_2
2.224	65.55	0
1.430	32.25	9.78
1.440	31.88	11.88	8.52	51.95
1.231	1.35	32.51	12.06	64.47
			3.50*	83.76*

* Partially dried

Table 4.3.30 — Densities of Uranyl Fluoride Solutions³² at 25°C

UO_2F_2 conc., wt-%	Density*	Density ³⁵
2.112	1.014	1.0136
7.565	1.070	1.0699
13.86	1.135	1.1349
19.39	1.200	1.2005
26.75	1.302	1.3016
34.76	1.441	1.4412
40.98	1.575	1.5754
49.24	1.751	1.7511
55.13	1.921	1.9212
61.98	2.176	2.1764

* Listed in paper submitted for publication in Jour. Am. Chem. Soc.

Table 4.3.31 — Density of Uranyl Fluoride Solutions³⁶

UO ₂ F ₂ conc., wt-%		Density, gm/cc		
Analytical	Averaged analytical, dilutions*	25°C		30°C (exp.)
		Exp.	Cal.†	
	2.495	1.0202‡	1.0203	
4.999	4.985	1.0443	1.0444	1.0429
	5.025	1.0448	1.0448	
10.20	10.20	1.0983	1.0984	1.0967
20.08	20.09	1.2164	1.2167	1.2146
20.46	20.48	1.2219‡	1.2219	
30.09	30.10	1.3632	1.3635	
30.14	30.18	1.3632	1.3646	1.3607
	40.30	1.5509	1.5516	1.5481
50.27	50.27	1.7893	1.7899	1.7859
61.50	61.63	2.1627	2.1622	2.1589

* These values were obtained by considering all analyses in a series of quantitative dilutions. Calculated values based on these concentrations. Concentration is principal uncertainty.

† Calculated by equation:

$$\frac{1}{d} = 1.0029 - 0.9126 F_2 + 0.0578 F_2^2 \quad (10)$$

where d is density and F_2 is weight fraction of UO₂F₂

‡ These values were determined by gradient tube method. All others by pycnometer of about 25 cc capacity

THE SYSTEM UO₂(NO₃)₂-H₂O AND RELATED SYSTEMS (E. V. JONES)

CHEMICAL PROPERTIES

The monohydrate UO₂(NO₃)₂ · H₂O is prepared by heating the dihydrate to 165°C in a stream of HNO₃ vapor and CO₂ for 3 hr;³⁸ anhydrous UO₂(NO₃)₂ is prepared from UO₂(NO₃)₂ · 3H₂O by dehydrating below 130°C under HNO₃ vapor and CO₂ for more than 60 hr.

Thermal decomposition pressures are as follows:

Temp., °C	87	131	141	150	160 ^{39,40}
Press., mm	95	157	219	340	540



The heat of decomposition by the Nernst approximation formula is 39.442 kcal. The dissociation in solution is $\text{UO}_2(\text{NO}_3)_2 \rightleftharpoons \text{UO}_2\text{NO}_3^+ + \text{NO}_3^-$. Alpha values are:

Eq./1	1.000	0.500	0.250	0.125	0.0625
α	0.78	0.80	0.82	0.88	0.94

At concentrations less than 0.01 molar, a second dissociation occurs;³⁹ i.e., $\text{UO}_2\text{NO}_3^+ \rightleftharpoons \text{UO}_2^{++} + \text{NO}_3^-$.

The boiling points of the hydrates of $\text{UO}_2(\text{NO}_3)_2$ are as follows⁴¹ (vapor pressure of water equals one atmosphere):

Monohydrate	292°C	Trihydrate	176°C
Dihydrate	281°C	Hexahydrate	128°C

A saturated solution of $\text{UO}_2(\text{NO}_3)_2$ at 22°C gave a yellow cloudy solid on a quartz tube at 264°C, more at 290°C with yellow vapor, and yellow precipitate at 335°C. Vapors deepened to wine red at 380°C. As the temperature dropped, the color changes reversed. The solution was a clear yellow at all temperatures.⁴²

Solubility

Solubility data for the uranyl nitrate–water system from 60° to 184°C are given in Tables 4.3.32 and 4.3.33. The melting point of the dihydrate is 184°C; decomposition occurs above 184°C. The incongruent melting point of the trihydrate is 113°C.⁴³

There is evidence that $\text{UO}_2(\text{NO}_3)_2 \cdot 6\text{H}_2\text{O}$ changes to $\text{UO}_2(\text{NO}_3)_2 \cdot 24\text{H}_2\text{O}$ between –25° and –35°C.⁴⁴

At temperatures above 250°C, uranyl nitrate solutions are found to hydrolyze,⁴⁵ precipitating anhydrous or hydrated UO_3 . Table 4.3.34 gives the highest temperatures at which the solutions are stable. Stability data for $\text{UO}_2(\text{NO}_3)_2$ solutions for periods greater than 200 hr, during which no significant decomposition occurs, are given in Table 4.3.35. All runs were made with oxygen of not less than 200 psi when reduced to room temperature. The solid phase appearing in this study was thought to be one of the two polymorphic forms of $\text{UO}_3 \cdot \text{H}_2\text{O}$.

Further data showing the lowest temperatures at which $\text{UO}_2(\text{NO}_3)_2\text{--HNO}_3$ solutions begin to hydrolyze to UO_3 are summarized in Table 4.3.36. The results of a study of the thermal decomposition of aqueous uranyl nitrate solutions are summarized in Tables 4.3.37 and 4.3.38.

Radiation Stability

See previous discussion given for uranyl sulfate systems.

PHYSICAL PROPERTIES OF URANYL NITRATE - WATER SYSTEMS (H. O. DAY, JR. AND C. H. SECOY)

Density

$\text{UO}_2(\text{NO}_3)_2$ in H_2O

The densities of aqueous solutions of uranyl nitrate over a wide range of concentrations and at temperatures up to 100°C have been reported by a number of workers (references 48–51, 40, 44, and 52–55). In addition, such references as the International Critical Tables,⁵⁷ Gmelin's Handbuch,³⁹ the Landolt-Bornstein Tabellen,⁵⁸ and Mellor's Treatise⁵⁹ quote values from the original literature or present smoothed values derived therefrom. In view of the ready accessibility of these data, they are not reproduced here.

A graphic inspection of all the values for the density at 25°C as a function of concentration discloses that all data obtained prior to 1940 lie on a smooth curve, whereas all values reported since 1940 agree well with another smooth curve but are not in agreement with the earlier data. The more recent data are consistently about 1.2 percent higher. The reason for this increase is not obvious, and whether it reflects improved techniques in density determinations or greater purity of materials is not known. In view of the care

Table 4.3.32 — The Solubility of Uranyl Nitrate in Water,⁴³ 60°–184°C

Temp., °C	UO ₂ (NO ₃) ₂ , liquid, %	Solid phase	
		UO ₂ (NO ₃) ₂ , %	Composition
70	77.25	87.08 (theoret. 87.95)	UO ₂ (NO ₃) ₂ ·3H ₂ O
77			UO ₂ (NO ₃) ₂ ·3H ₂ O
77.2	78.49		UO ₂ (NO ₃) ₂ ·3H ₂ O
85	79.92		UO ₂ (NO ₃) ₂ ·3H ₂ O
90.5	80.98		UO ₂ (NO ₃) ₂ ·3H ₂ O
92	81.37	87.05	UO ₂ (NO ₃) ₂ ·3H ₂ O
100	82.57		UO ₂ (NO ₃) ₂ ·3H ₂ O
110	84.14		UO ₂ (NO ₃) ₂ ·3H ₂ O
113*	84.67		UO ₂ (NO ₃) ₂ ·3H ₂ O + UO ₂ (NO ₃) ₂ ·2H ₂ O
120	85.25		UO ₂ (NO ₃) ₂ ·2H ₂ O
130	86.13	90.58 (theoret. 91.63)	UO ₂ (NO ₃) ₂ ·2H ₂ O
133	86.54		UO ₂ (NO ₃) ₂ ·2H ₂ O
137	87.07		UO ₂ (NO ₃) ₂ ·2H ₂ O
141.2	87.02		UO ₂ (NO ₃) ₂ ·2H ₂ O
141.5			UO ₂ (NO ₃) ₂ ·2H ₂ O
147	87.75		UO ₂ (NO ₃) ₂ ·2H ₂ O
154.5	88.23		UO ₂ (NO ₃) ₂ ·2H ₂ O
159	88.74		UO ₂ (NO ₃) ₂ ·2H ₂ O
160	88.94		UO ₂ (NO ₃) ₂ ·2H ₂ O
165.5	89.22		UO ₂ (NO ₃) ₂ ·2H ₂ O
172	89.92		UO ₂ (NO ₃) ₂ ·2H ₂ O
180	90.78		UO ₂ (NO ₃) ₂ ·2H ₂ O
181	91.01		UO ₂ (NO ₃) ₂ ·2H ₂ O
184†	91.63		UO ₂ (NO ₃) ₂ ·2H ₂ O

* Intersection point for incongruent melting point, trihydrate

† True melting point, dihydrate

 Table 4.3.33 — Melting Point Determinations⁴³

UO ₂ (NO ₃) ₂ , wt-%	87.2	87.5	89.1	89.9	91.63
First observed melting, °C	113	113	113	112	184

Table 4.3.34—High-temperature Stability Limits of $\text{UO}_2(\text{NO}_3)_2$ Solutions⁴⁵ with Excess HNO_3

$\text{UO}_2(\text{NO}_3)_2$ conc., M	Excess HNO_3 conc., M	Temp., °C
0.055	None	265 ± 7
.322	None	265 ± 9
.280	0.09	$\leq 271 \pm 3$
.241	.16	281 ± 3
.349	.70	301 ± 11
.350	.90	$\geq 279 \pm 3$
.322	2.00	≥ 298
1.000	None	$> 288 \pm 2$

Table 4.3.35—Long-term Stabilities of $\text{UO}_2(\text{NO}_3)_2$ at High Temperatures⁴⁵

$\text{UO}_2(\text{NO}_3)_2$, M	HNO_3 , M	Temp., °C	Total time, hr
0.055	None	250 – 260	397
.322	None	260 ± 4	213
.349	0.7	295 ± 5	193
.340	.9	250 – 281	573
1.00	None	249 – 291	880

Table 4.3.36—Data on $\text{UO}_3\text{--HNO}_3\text{--H}_2\text{O}$ System⁴⁶

Temp., °C	Analytical molarities			Molalities		
	U	Total NO_3^-	Excess NO_3^- (by dif.)	U	Total NO_3^-	Excess NO_3^- (by dif.)
$265 \pm 5^*$	0.055	0.110	0.000	0.055	0.110	0.000
$265 \pm 5^*$.322	.644	.000	.331	.662	.000
$313 \pm 5^*$.945	1.89	.00	1.025	2.05	.00
$269 \pm 2^*$.015	0.10	.09	0.015	0.10	.09
$281 \pm 2^*$.241	.56	.08	.247	.57	.08
329 ± 2	.951	2.00	.10	1.037	2.18	.11
315 ± 5	.358	1.10	.38	0.374	1.15	.40
341 ± 2	.892	2.08	.30	.973	2.27	.32
350 ± 2	.984	2.35	.38	1.085	2.59	.42

* Taken from previous data

Table 4.3.37 — Thermal Stability Characteristics of Uranyl Nitrate—Water and Uranyl Nitrate—Nitric Acid—Water Solutions
 (W. L. Marshall and J. S. Gill, Aqueous Uranyl Nitrate and Uranyl Nitrate—Nitric Acid—Water Solutions above 100°C,
 ORNL-990, Feb. 28, 1951)

Run No.	UO ₂ (NO ₃) ₂ , M	HNO ₃ , M	Temperature of "dry" solid formation, °C	Temp. of vapor phase coloration, °C	Temp. of direct precipitation from solution, °C	Highest temperature, * °C	Observations after run
1	0.171	0	290	None observed	None observed	344 (explosion)	
2	.90	0	300	305	None observed	366 (explosion)	
3	.90	0.05	310	310	None observed	325	Est. 1 to 3 mg of yellow precipitate
4	.90	.10	305	300	None observed	325	Est. 1 to 3 mg of yellow precipitate
5	.90	.20	None observed	300	None observed	325	No observable change
6	.90	.20	None observed	300	None observed	371 (explosion)	
7	1.90 (sat'd at 22°C)	0	270	290	340	376	Est. 1 to 3 mg of yellow precipitate
8	1.80	0.03	330	290	None observed	378	Est. 1 to 3 mg of yellow precipitate
9	1.80	.42	None observed	280	None observed	350 (explosion)	
10	1.80	.42	None observed	290	None observed	351	No observable change

* These temperatures reached in 5 to 6 hr by slowly increasing the heat

Table 4.3.38—Thermal Decomposition of Aqueous Uranyl Nitrate Solutions⁴⁷

UO ₂ (NO ₃) ₂ ·6H ₂ O, wt-%	Run No.	Temp., °C	Mixing time, hr	Observations	
				Solution	Vapor
3.24	1	250	18	Clear	Colorless
		260	4	Clear	Colorless
		270	4	Yellow solid appeared	Colorless
12.52	2	280	18	Clear	Colorless
		288–295	2	Clear	Slight yellow-brown
		295	2	Yellow solid appeared	Yellow-brown
30.53	3	285	3	Clear	Slight yellow-brown
		300	4	Clear	Yellow-brown
		314	18	Yellow solid appeared	Red-brown
54.78	4	250	18	Clear	Colorless
		260	2	Clear	Slight yellow-brown
		270	18	Clear	Yellow-brown
		320	64	Clear	Red-brown
		338	4	Clear	Intense red-brown (tube explosion)
54.78	5	350	2	Yellow solid precipitated	Intense red-brown
72.48	6	240	3	Clear	Slight yellow-brown
		275–300	42	Clear	Red-brown
		312	18	Clear	Intense red-brown
		328	6	Yellow solid appeared	Intense red-brown
72.48	7	330	18	Yellow solid appeared	Intense red-brown
85.83	8	208	2	Clear	Slight yellow-brown
		215	5	Clear	Red-brown
		222	8	Yellow solid appeared	Red-brown
		280	4	No increase in precipitation (?)	
91.62	9	184		Melting point of UO ₂ (NO ₃) ₂ ·2H ₂ O	Red-brown above 184°C

required to obtain uranyl nitrate free of excess nitrate ion, it may be that the material used in the earlier work was always contaminated with excess HNO_3 .

The curve for the more recent data can be described by the empirical equation:

$$D_4^{25} = x_1(a + b x_1) + 0.99704 x_2$$

where x_1 = the mole fraction of $\text{UO}_2(\text{NO}_3)_2$, x_2 = the mole fraction of water, and a and b are constants ($a = 18.95$; $b = -59$). This equation reproduces all data obtained since 1940 with a mean error of less than 0.2 percent.

The earlier data can be described by the same equation, but in order to secure equally good agreement, it is necessary to select different values of the constants a and b for different concentration ranges, as follows:

$10^3 x_1$	a	b
0–1.5	15.43	–113.3
1.5–12.6	15.00	+175.5
12.6–32.0	17.75	–43.0
32.0–saturation	18.64	–71.25

For purpose of calculation, the equation can be put in the form:

$$D_4^{25} = x_1(a - 1 + b x_1) + 0.99704$$

The temperature dependence is not so easily amenable to a simple empirical expression. The data of Grant et al.,⁴⁹ are more complete than those of any other and, insofar as one can judge, are as reliable. They are reproduced in Table 4.3.39. For convenience, the data on surface tension and viscosity taken from this reference are included in the table.

Three-component Systems: $\text{UO}_2(\text{NO}_3)_2\text{-H}_2\text{O-X}$

Densities for the system $\text{UO}_2(\text{NO}_3)_2\text{-HNO}_3\text{-H}_2\text{O}$ are available in graphic form⁴⁰ and are not reproduced here. Additional data appear in Table 4.3.40.

$\text{UO}_2(\text{NO}_3)_2$ Solutions Containing H_2SO_4 and HNO_3

Densities of solutions of uranyl nitrate containing both sulfuric acid and nitric acid have been reported by Turk and Olson.⁶⁰ Their values are given in Table 4.3.41.

Viscosity of Uranyl Nitrate Solutions

For the data of W. E. Grant et al., see Table 4.3.49. Further viscosity data are given by Clagett⁶³ and are presented in Table 4.3.42.

Thermal Conductivity

No thermal conductivity data could be found for the $\text{UO}_3\text{-HNO}_3\text{-H}_2\text{O}$ system.

Heat Capacities of Uranyl Nitrate Solutions

The Project Handbook, Report CL-697, reports the heat capacities of some uranyl nitrate solutions. These heat capacities are shown in Tables 4.3.43 and 4.3.44. The values were obtained by interpolation between the heat capacity of pure water and the heat capacity of solid $\text{UO}_2(\text{NO}_3)_2 \cdot 6\text{H}_2\text{O}$ as determined by Coulter et al.⁶⁴ and reproduced in Table 4.3.45.

Table 4.3.39 — Density, Surface Tension, and Viscosity of Uranyl Nitrate Solutions

Temp., °C	UO ₂ (NO ₃) ₂ ·6H ₂ O conc., moles/liter	Density, gm/cc	Surface tension, dynes/cm	Absolute viscosity, cp
0	0.1529	1.0509		1.90
25	.1523	1.0473		0.943
30	.1521	1.0459		.844
40	.1515	1.0420		.691
50	.1507	1.0365		.580
60	.1501	1.0324		.492
0	0.2291	1.0740	76.4	1.98
20	.2286	1.0714	73.3	1.11
25	.2283	1.0703	72.4	0.989
30	.2280	1.0687	71.6	.884
35	.2277	1.0671	70.6	.796
40	.2273	1.0651	69.8	.726
50	.2262	1.0609	68.5	.603
60	.2253	1.0559	66.9	.514
80	.2230	1.0457	63.2	
100	.2201	1.0315	59.9	
0	0.4127	1.1328	76.6	2.19
20	.4112	1.1291	73.4	1.22
25	.4107	1.1275	72.7	1.09
30	.4102	1.1260	72.0	0.974
35	.4094	1.1240	71.3	.880
40	.4088	1.1219	70.4	.794
50	.4071	1.1175	69.0	.668
60	.4053	1.1124	67.5	.568
80	.4019	1.1026	63.6	
100	.3966	1.0889	60.6	
0	0.4842	1.1575		2.26
20	.4828	1.1540		1.28
25	.4821	1.1522		1.14
30	.4815	1.1506		1.02
35	.4804	1.1488		0.195
40	.4800	1.1477		.832
50	.4777	1.1423		.696
60	.4755	1.1369		.587
0	0.6250	1.1985	76.8	2.43
20	.6219	1.1920	73.7	1.33
25	.6210	1.1903	73.0	1.22
30	.6201	1.1886	72.2	1.09
35	.6191	1.1867	71.5	0.978
40	.6181	1.1847	70.6	.892
50	.6158	1.1800	69.2	.745
60	.6131	1.1748	67.8	.632
80	.6074	1.1642	64.2	
100	.5995	1.1492	61.0	
0	0.8316	1.2701	77.6	
20	.8271	1.2634	74.6	
25	.8260	1.2615	73.9	
30	.8247	1.2596	73.4	
35	.8231	1.2570	72.7	
40	.8215	1.2546	71.8	
50	.8181	1.2495	70.3	
60	.8145	1.2440	69.0	
80	.8063	1.2314	65.0	
100	.7980	1.2187	61.9	

Table 4.3.40 — Densities of $\text{UO}_3\text{--HNO}_3\text{--H}_2\text{O}$ Solutions

Temp., °C	Density	UO_3 , %	HNO_3 , %	Solid phase	Reference
25	1.012	1.52	0.36	$\text{UO}_3 \cdot \text{XH}_2\text{O}$	61
25	1.033	3.28	.82	$\text{UO}_3 \cdot \text{XH}_2\text{O}$	61
25	1.073	6.71	1.81	$\text{UO}_3 \cdot \text{XH}_2\text{O}$	61
25	1.114	9.95	2.74	$\text{UO}_3 \cdot \text{XH}_2\text{O}$	61
25	1.214	17.0	4.65	$\text{UO}_3 \cdot \text{XH}_2\text{O}$	61
25	1.213	17.2	4.70	$\text{UO}_3 \cdot \text{XH}_2\text{O}$	61
25	1.241	18.5	5.11	$\text{UO}_3 \cdot \text{YH}_2\text{O}$	61
25	1.419	28.2	8.07	$\text{UO}_3 \cdot \text{YH}_2\text{O}$	61
25	1.752	40.4	13.0	$\text{UO}_3 \cdot \text{YH}_2\text{O}$	61
25	2.088	49.4	15.9	$\text{UO}_3 \cdot \text{YH}_2\text{O}$	61
25	2.101	49.8	16.0	$\text{UO}_3 \cdot \text{YH}_2\text{O}$	61
25	1.900	43.7	17.2	$\text{UO}_2(\text{NO}_3)_2 \cdot 6\text{H}_2\text{O}$	61
25	1.821	40.9	18.2	$\text{UO}_2(\text{NO}_3)_2 \cdot 6\text{H}_2\text{O}$	62
25	1.681	25.3	39.8	$\text{UO}_2(\text{NO}_3)_2 \cdot 6\text{H}_2\text{O}$	62
40	1.338	22.79	10.04		60
40	1.354	22.79	12.04		60
40	1.372	22.79	14.04		60
40	1.462	28.48	12.55		60
40	1.482	28.48	14.55		60
40	1.501	28.48	16.55		60
42.5	(2.17)*	36.8	32.1		63
48.1	(2.07)*	44.9	25.5		63
50.5	(2.17)*	46.5	28.5		63
53.8	2.26	50.4	26.6		63
59.9	2.19	53.2	28.8		63
62.9	2.18	(52.4)*	31.7		63
93.5	2.50	58.0	27.6		63
96.0	2.55	58.7	26.3		63
96.0	2.54	(61.5)*	26.9		63
104.0	2.77	(59.0)*	29.6		63
106.0	2.92	62.4	26.4		63
106.0	3.11	62.8	26.9		63
106.0	2.84	62.8	31.3		63
110.2	2.92	62.9	23.9		63
111.0	3.34	(60.8)*	25.3		63
160†	2.95	64.2	28.6		63
130.0	3.17	64.5	26.2		63

* Values in parentheses are doubtful. Density units are undefined, but probably are D_4^{25}

† The value is uncertain in that the report is not clear here

Table 4.3.41 — Density of Uranyl Nitrate Solutions Containing Sulfuric Acid and Nitric Acid

UHN, %	H ₂ SO ₄ , %	HNO ₃ , %	Density		
			20°C	30°C	50°C
16.5	3.0	0.8	1.144	1.138	1.130
21.8	4.0	1.1	1.204	1.197	1.188
27.2	5.1	1.3	1.268	1.260	1.250
35.0	7.1	1.9	1.374	1.364	1.354
37.7	7.1	1.9	1.423	1.418	1.406
40.0	8.1	2.1	1.447	1.436	1.424
43.0	8.1	2.1	1.523	1.511	1.498
48.3	9.0	2.4	1.630	1.617	1.602

Table 4.3.42 — Viscosity of Uranyl Nitrate Solutions*

Temp., °C	No. 1 spindle		No. 2 spindle		Solution composition		
	100 rpm	50 rpm	100 rpm	50 rpm	UO ₃ , %	HNO ₃ , %	H ₂ O, %
100	25	18	25	24	50.4	26.6	23.0
100	42	30	42	34	58.7	26.3	14.9
120	45	33	53	41	62.4	26.4	11.2
125	60	50	67	50	(60.8)†	25.3	14.0

* These viscosities were determined with a Brookfield Synchro-Lectric Viscometer, Multi-Speed Model RVF

† Value in parenthesis is doubtful

Table 4.3.43 — Heat Capacity of Uranyl Nitrate Solutions at 25°C

Anhydrous UO ₂ (NO ₃) ₂ , %	Specific heat relative to H ₂ O at 15°C; C _p at 25°C, cal/(gm)(°C)
0	0.997
5	.97
10	.94
15	.91
20	.87
25	.84
30	.79
35	.75
40	.70
43 (eutectic)	.68
45	.65
50	.59
55	.53

Table 4.3.44 — Heat Capacities of Uranyl Nitrate Solutions in Terms of Uranyl Nitrate Hexahydrate

$\text{UO}_2(\text{NO}_3)_2 \cdot 6\text{H}_2\text{O}, \%$	$C_p, \text{ cal}/(\text{gm})(^\circ\text{C})$
0	0.997
5	.975
10	.95
15	.925
20	.90
25	.875
30	.84
35	.81
40	.78
45	.74
50	.70
55	.66
60	.62
65	.57
70	.525

Table 4.3.45 — Heat Capacities of Solid Uranyl Nitrate Hexahydrate

Temp., $^\circ\text{K}$	$C_p, \text{ cal}/(\text{deg})(\text{mole})$
273.08*	103.2
274.73*	102.6
275.53	102.8
282.13*	105.3
283.09*	106.1
283.36	105.7
285.31*	107.1
287.63	106.6
290.65*	109.1
296.17	110.9
298.68*	112.2

* Considered the better values. 0°C is taken as 273.10°K

Heat capacities of uranyl nitrate solutions are given on page 114 in Gmelin's Handbuch.³⁹ This work quotes Dittrich.⁶⁵ It is stated that the average heat capacity in cal/(gm)(°C) in the temperature range 20° to 55°C for a 0.5N $\text{UO}_2(\text{NO}_3)_2$ solution is 0.892, and that of a 0.25N solution is 0.957. Gmelin also quotes W. Oechsner de Coninck⁶⁶ to the effect that the specific heat of a 10-percent aqueous solution of $\text{UO}_2(\text{NO}_3)_2 \cdot 6\text{H}_2\text{O}$ is 0.946. No temperature range is given.

More recent experimental heat capacities as reported by M. Lister⁶⁷ are given in Table 4.3.46. The report by Lister also gives heat capacities for NH_4NO_3 , $\text{UO}_2(\text{NO}_3)_2 + \text{NH}_4\text{NO}_3$, and $\text{UO}_2(\text{NO}_3)_2 + \text{NH}_4\text{NO}_3 + \text{HNO}_3$ solutions.

Table 4.3.46—Heat Capacities of Uranyl Nitrate Solutions

Conc. of $\text{UO}_2(\text{NO}_3)_2$, wt-%	C_p of solution, cal/(gm)(°C)	Conc. of $\text{UO}_2(\text{NO}_3)_2$, wt-%	C_p of solution, cal/(gm)(°C)
11.8	0.894	47.4	.583
25.9	.759	52.4	.530
26.2	.757	52.7	.542
39.3	.646	55.5	.493
39.3	.641	55.6	.521
46.75	.573	56.0	.513
47.2	.574		

Heat capacity data for uranyl nitrate solutions in butex and HNO_3 are given by Jenkins et al.⁴⁸ For pure $\text{UO}_2(\text{NO}_3)_2$ solution at a concentration of 300 gm U/liter, the heat capacity at 25°C is given as 0.93 cal/(gm)(°C).

In a paper by Katzin, Simon, and Ferrara⁶⁸ it is stated that a heat-capacity plot of $\text{UO}_2(\text{NO}_3)_2$ solution shows that composition vs heat capacity is linear from 0.770 cal/(gm)(°C) at 25 wt-% $\text{UO}_2(\text{NO}_3)_2$ to the heat capacity value for pure water. This conclusion is obtained from a combination of their own data with that of Lister's data just given.

Heats of Solution and Dilution of Uranyl Nitrate Solutions

J. Aloy⁶⁹ states that addition of the heat of solution for $\text{UO}_2(\text{NO}_3)_2 \cdot 3\text{H}_2\text{O}$ is -3.7 kcal/mole of salt. The experimental conditions are solution of one mole of the salt in 1000 to 2500 moles of water between 18° and 20°C.

Gmelin (page 113, reference 40) quotes heats of dilution from a paper by C. Dittrich.⁶⁵ Heat of dilution of a 0.5N $\text{UO}_2(\text{NO}_3)_2$ solution is 4 cal when the solution is diluted from 200 to 400 cm³ at 19°C. For a 0.25N solution at 15°C and for the same dilution, the heat of dilution is 11 cal.

W. Oechsner de Coninck⁵³ gives the heat of solution of $\text{UO}_2(\text{NO}_3)_2 \cdot 3\text{H}_2\text{O}$ at -3.8 kcal.

Marketos⁷⁰ gives some heats of solution for $\text{UO}_2(\text{NO}_3)_2$ and a number of its hydrates as follows (the dilution factors are not given):

Salt	Heat of solution, kcal	Salt	Heat of solution, kcal
$\text{UO}_2(\text{NO}_3)_2$	+16	$\text{UO}_2(\text{NO}_3)_2 \cdot 3\text{H}_2\text{O}$	+2.00
$\text{UO}_2(\text{NO}_3)_2 \cdot 2\text{H}_2\text{O}$	+5.42	$\text{UO}_2(\text{NO}_3)_2 \cdot 6\text{H}_2\text{O}$	-4.76

de Forcrand (p. 1207, reference 38; p. 24, reference 41) is quoted by Gmelin (p. 113, reference 39). It is stated that the heats of solution of one mole of anhydrous uranyl nitrate and its hydrates in 1000 to 1100 moles H_2O at 11° to 13°C are as follows:

Salt	Heat of solution, kcal
$\text{UO}_2(\text{NO}_3)_2$	+19.00
$\text{UO}_2(\text{NO}_3)_2 \cdot \text{H}_2\text{O} (?)$	11.87
$\text{UO}_2(\text{NO}_3)_2 \cdot 2\text{H}_2\text{O}$	5.05
$\text{UO}_2(\text{NO}_3)_2 \cdot 3\text{H}_2\text{O}$	1.35
$\text{UO}_2(\text{NO}_3)_2 \cdot 6\text{H}_2\text{O}$	-5.45

It might be noted at this point that Colani⁶² and Germann and Frey⁷¹ deny the existence of a monohydrate, and a heat of solution for such a species is reported only by de Forcrand (except in other reference works in which de Forcrand is the original source). It should also be noted that heat lost to the surroundings has been given the plus sign, a convention which is not used at the present time.

The widely used reference work on thermochemistry by Bichousky and Rossini⁷² gives the following:

Compound	Heat of solution (12°; 220 moles H_2O), kcal
$\text{UO}_2(\text{NO}_3)_2$	+19.0
$\text{UO}_2(\text{NO}_3)_2 \cdot \text{H}_2\text{O}$	11.87
$\text{UO}_2(\text{NO}_3)_2 \cdot 2\text{H}_2\text{O}$	5.05
$\text{UO}_2(\text{NO}_3)_2 \cdot 3\text{H}_2\text{O}$	1.85
$\text{UO}_2(\text{NO}_3)_2 \cdot 6\text{H}_2\text{O}$	-5.45

It will be noted that almost all the heat-of-solution values given are taken from the work of de Forcrand. An exception is the value given for the trihydrate. This could be a typographical error (8 instead of 3), or else Bichousky and Rossini made some unknown weighing between other sources and that of de Forcrand.

de Forcrand (p. 24, reference 41) distinctly writes that 1000 to 1100 moles of water were used. This makes the value of 220 moles quoted by Bichousky and Rossini a definite error.

Coulter, Pitzer, and Latimer⁶⁴ give the value of the heat of solution of uranyl nitrate hexahydrate as:

$$\Delta H_{\text{soln}} = 5.25 \text{ kcal/mole}$$

The dilution factor was the addition of 1 mole of the UNH to 929 and 911 moles of water, or an average of 920 moles of H_2O . Here, heat lost to the surroundings is given the minus sign.

Values for the heats of solution of uranyl nitrate and its hydrates as given on p. 52 of the Project Handbook⁴⁰ are as follows:

Compound	Heat of solution kcal/mole	Btu/lb
$\text{UO}_2(\text{NO}_3)_2$	19.00	86.8
$\text{UO}_2(\text{NO}_3)_2 \cdot \text{H}_2\text{O}$	11.87	51.9
$\text{UO}_2(\text{NO}_3)_2 \cdot 2\text{H}_2\text{O}$	5.05	21.1
$\text{UO}_2(\text{NO}_3)_2 \cdot 3\text{H}_2\text{O}$	1.35	5.43
$\text{UO}_2(\text{NO}_3)_2 \cdot 6\text{H}_2\text{O}$	-5.25	-18.8

It is stated that the final concentration is 1 mole of the compound in 220 moles of water. This is a repetition of the statement by Bichousky and Rossini which has shown to be in

error. The numerical values are taken from the work of de Forcrand except for UNH. Here the value of ΔH found by Coutler et al is used.

Report CL-697 gives Gmelin (pp. 113-116, reference 39), Bichousky and Rossini,⁷² and Borst (private communication) as the references for the values reported.

Figure 3 II C. 4 of Report CL-697 is a plot of heat of solution of uranyl nitrate hexahydrate vs weight-percent of UNH in the solution. The origin of this plot is not discussed, and exactly which data were used to formulate the curve are not known.

Heats of solution and dilution of $\text{UO}_2(\text{NO}_3)_2 \cdot 6\text{H}_2\text{O}$ are given by Lister.⁶⁷ The results of two runs are as follows:

Run No. 1, 22.5°C		Run No. 2, 24.35°C	
Q, cal	Conc. of UNH, %	Q, cal	Conc. of UNH, %
5315	12.5	5260	17.65
5180	26.3	5340	30.0
5260	36.4	5455	39.1
5560	44.0	5630	46.1
5650	50.0	5835	51.7
5845	54.8	6130	57.6
6020	58.8	6420	62.2
6225	62.2	6690	65.9
6490	65.9		

Q is the number of calories which must be added to a solution to bring it back to its original temperature when 1 mole of solid $\text{UO}_2(\text{NO}_3)_2 \cdot 6\text{H}_2\text{O}$ is dissolved in water to give a solution of the given concentration.

The most recent and perhaps the most accurate heat-of-solution data are found in a paper by Katzin, Simon, and Ferrara.⁶⁸ Although the data can be found in various ANL reports of a previous date, all pertinent data are included in their paper, from which the following information is taken:

Compound	Heat of solution, kcal/mole of solid
$\text{UO}_2(\text{NO}_3)_2 \cdot 2\text{H}_2\text{O}$	-5.37 ± 0.06
$\text{UO}_2(\text{NO}_3)_2 \cdot 3\text{H}_2\text{O}$	$-1.66 \pm .05$
$\text{UO}_2(\text{NO}_3)_2 \cdot 6\text{H}_2\text{O}$	$5.48 \pm .03$

The dilution ratio is 1 mole of solid to 180 moles of water. Heat lost to the surroundings is given the minus sign. For the dihydrate the data agrees with Marketos⁷⁰ but not with deForcrand.

The value for the trihydrate is almost equal to the average between the values of Marketos and de Forcrand. The value for the hexahydrate agrees with de Forcrand but not with the data of Coulter et al.⁶⁴ The terminal concentration of the uranyl nitrate in the experiments of Coulter et al and de Forcrand were about five times as dilute as the solutions used by Katzin et al.

The paper by Katzin et al includes heats of solution of uranyl nitrate in various organic liquids.

URANYL CARBONATE SYSTEMS (E. V. JONES)

CHEMICAL PROPERTIES

Uranyl carbonate, UO_2CO_3 , may be prepared by the action of UO_3 slurry and CO_2 in an autoclave at high temperature.⁷³ It forms a cream-colored crystal of density about 5.7.

Solubility at 30°C is 0.0028 gm/100 gm H₂O and at 60°C is 0.0083 gm/100 gm H₂O. It forms unidentified complexes with Na₂CO₃.

The results of detailed studies on the UO₂CO₃-Na₂CO₃-H₂O system are presented in Tables 4.3.47 and 4.3.48. The data in Table 4.3.47 are for solutions in contact with solid UO₂CO₃ (U/CO₃ = 1.01 to 1.03); data in Table 4.3.48 are for solutions in contact with solid Na₄UO₂(CO₃)₃. In experiment 1030, both solids were present.

A plot of data for the 3-component system shows that the region of solubility for this system is small. It has a sharp eutectic between the solution in contact with solid tricarboxonate and that in contact with solid uranyl carbonate.

The data for the UO₃-Na₂CO₃-H₂O system are summarized in Table 4.3.49; data for the Na₄UO₂(CO₃)₃-NaHCO₃-H₂O system⁷⁴ are summarized in Table 4.3.50.

Sodium uranyl carbonate, 2Na₂CO₃-UO₂CO₃, was obtained⁷⁷ by slow evaporation of UO₂SO₄ solution containing an excess of Na₂CO₃ while CO₂ bubbled through it. Its solubilities in various solvents at 30°, 60° and 90°C are summarized in Tables 4.3.51, 4.3.52, and 4.3.53.

Evidence for the existence of the tricarbonate ion, UO₂(CO₃)₃⁴⁻, was obtained by spectrophotometric methods,⁷⁸ and an approximate value of its dissociation constant was calculated for the following mechanism:



The approximate value of $K_3 = 4.5 \times 10^{-7}$.

The following metal salts were found to give complex uranyl-metal-carbonates: Ag, Hg⁺, Hg²⁺, Cu, Pb, Cd, Zn, Fe²⁺, Ni, Co, Ba, and Sr. Mg, Ca, Al, and Mn did not give such complexes.⁷⁹

Two new complex sodium-uranyl-carbonates, Na₆[(UO₂)₂(CO₃)₅] and Na₆[(UO₃)₃(UO₂)₂(CO₃)₅], have been prepared and their principal reactions studied.⁸⁰ The approximate decomposition temperatures for the complex sodium uranyl carbonates are as follows:

Na ₆ [(UO ₃) ₃ (UO ₂) ₂ (CO ₃) ₅]	400°C
Na ₆ [(UO ₂) ₂ (CO ₃) ₅]	410°
Na ₄ [UO ₂ (CO ₃) ₃]	420°

Compounds having the general formulas [UO₂(CO₃)₃] M₂ and [(UO₂)₂(CO₃)₅] M₃, where M represents Mg, Ca, Sr, or Ba, have been prepared and, in most cases, isolated.⁸⁰ They are readily hydrolyzed. No similar Be salts could be obtained. The solubility of K₄UO₂(CO₃)₃ in K₂CO₃ solutions at 25°C is summarized by Blake and Lowrie in Table 4.3.54 (p. 36, reference 81), and a comparison of the solubility of UO₂CO₃ in K₂CO₃ and Na₂CO₃ solutions at 25°C is given (p. 7, reference 82) in Table 4.3.55.

A study was made of the effect of carbon dioxide pressure on the stability of saturated (0.24M) Na₄UO₂(CO₃)₃ solutions (at 25°C) when heated to 250°C in silica tubes by H. W. Wright and J. S. Gill (The Effect of Carbon Dioxide on the Sodium Uranyl Carbonate-Water System. ORNL-1121, Aug. 1951). The presence of carbon dioxide retarded and decreased the amount of yellow precipitate but did not prevent its formation at 200°C.

Radiation Stability (J. W. Boyle)

A few radiation experiments were made on uranium solutions in alkali media in 1945. It was found⁸³ that, as the uranium concentration was changed (by adding UO₃) from 0.01-0.02M and the concentration of Na₂CO₃ was varied from 0.1-0.2M, the amount of hydrogen gas liberated per fission differed by only 5 percent in three experiments. In an experiment⁸⁴ in which the uranium concentration was "varied over a wide range" in 0.3M NaHCO₃, a deviation of about 10 percent from the value at 3 gm U/l was observed. At 70°C, there was an indication that hydrogen production was 15 percent lower than at

Table 4.3.47—The UO_2CO_3 , Na_2CO_3 , H_2O System⁷⁴
(UO_2CO_3 Solid Phase)

Test No.	Method of preparation	Solution analysis, gm./liter			d ₂₅ °C	Weight-percent based on									
		U	Na	CO ₃		4-component system				3-component system					
						UO ₃	Na ₂ O	CO ₂	H ₂ O	UO ₂ CO ₃	Na ₂ CO ₃	H ₂ O			
1003	UO ₂ CO ₃ + 1% Na ₂ CO ₃	20.7	4.5	10.5	1.029	2.4	0.5	0.8	96.2	2.8	0.9	96.3			
1005	UO ₂ CO ₃ + 2% Na ₂ CO ₃	41.4	8.2	21.2	1.061	4.7	1.0	1.4	92.9	5.5	1.8	92.8			
1034	UO ₂ CO ₃ + 4% Na ₂ CO ₃	80.5	16.4	40.4	1.121	8.6	2.0	2.7	86.7	10.0	3.4	86.6			
1000	UO ₂ CO ₃ + tricarb.	88.0	16.9	42.2	1.132	9.4	2.1	2.7	85.8	10.8	3.3	85.9			
1004	UO ₂ CO ₃ + 6% Na ₂ CO ₃	124.0	26.2	61.4	1.188	12.6	3.0	3.8	80.6	14.5	4.6	80.9			
1008	UO ₂ CO ₃ + 8% Na ₂ CO ₃	176.6	35.6	81.2	1.257	17.1	4.0	4.7	74.2	19.4	6.5	74.1			
1041	UO ₂ CO ₃ + 10% Na ₂ CO ₃	211.0	39.8	98.3	1.314	19.3	4.1	5.5	71.1	22.2	7.0	70.8			
1010	UO ₂ CO ₃ + 12% Na ₂ CO ₃	259.0	45.4	113.4	1.373	22.6	4.5	6.1	66.8	26.2	7.6	66.2			
1043	UO ₂ CO ₃ + 15% Na ₂ CO ₃	278.0	59.6	141.0	1.421	23.5	5.7	7.3	63.5	27.1	8.8	64.1			
1030	UO ₂ CO ₃ + tricarb.*	309.0	62.8	144.0	1.470	25.2	5.8	7.2	61.8	29.2	9.9	60.9			
1031	UO ₂ CO ₃ + 15% Na ₂ CO ₃	321.0	61.0	144.0	1.474	26.2	5.6	7.2	61.1	30.2	9.6	60.3			
1048	UO ₂ CO ₃ + 18% Na ₂ CO ₃	335.0	71.8	172.0	1.490	27.0	6.5	8.5	58.0	31.2	10.8	58.0			
403	UO ₂ CO ₃ + NaHCO ₃	12.9	2.9	6.9	1.019	1.5	0.4	0.5	97.6	1.8	0.6	97.6			
404	UO ₂ CO ₃ + NaHCO ₃	53.0	10.1	27.2	1.079	5.9	1.3	1.9	90.9	6.8	2.2	91.0			
405	UO ₂ CO ₃ + NaHCO ₃	106.0	19.8	53.6	1.160	11.0	2.3	3.4	83.3	12.7	3.9	83.4			

* Solid residue shows presence of $\text{Na}_4\text{UO}_2(\text{CO}_3)_3$

Table 4.3.48—The UO_2CO_3 , Na_2CO_3 , H_2O System*
[$\text{Na}_4\text{UO}_2(\text{CO}_3)_3$, Solid Phase]

Test No.	Method of preparation	Solution analysis, gm./liter			d _{25°C}	Weight-percent based on							
		U	Na	CO ₃		4-component system			3-component system				
						UO ₃	Na ₂ O	CO ₂	H ₂ O	UO ₃ CO ₃	Na ₂ CO ₃	H ₂ O	
†	Tricarb. + Na ₂ CO ₃	1.45	149.6	195.9	1.278	0.1	15.8	11.2	72.9	0.2	27.0	72.8	
†	Tricarb. + Na ₂ CO ₃	5.4	99.1	130.6	1.202	.5	11.1	8.0	80.4	.6	19.0	80.4	
†	Tricarb. + Na ₂ CO ₃	16.3	53.7	74.2	1.128	1.7	6.4	4.8	87.1	2.0	11.0	87.0	
†	Tricarb. + Na ₂ CO ₃	32.4	35.9	55.1	1.106	3.5	4.4	3.7	88.4	4.1	7.5	88.4	
†	Tricarb. + H ₂ O	63.2	24.5	47.7	1.118	6.8	3.0	3.1	87.1	7.9	5.0	87.1	
145†	Tricarb. + H ₂ O	65.6	26.1	51.6	1.128	7.0	3.1	3.4	86.5	8.1	5.3	86.6	
146†	Tricarb. + H ₂ O	68.6	27.7	54.8	1.128	7.3	3.3	3.6	85.8	8.5	5.7	85.8	
1018†	Tricarb. + dicarb.‡	95.8	29.1	61.7	1.164	9.9	3.4	3.9	82.8	11.4	5.8	82.8	
1017†	UO ₃ CO ₃ + tricarb.	226.0	46.9	115.0	1.349	20.2	4.7	6.3	68.8	23.2	8.0	68.8	
1052†	Tricarb. + dicarb.‡	306.0	59.0	151.0	1.451	25.3	5.5	7.6	61.6	29.2	9.3	61.5	

* All measurements made in constant temperature room at $26^\circ \pm 2^\circ\text{C}$

† See reference 75

‡ See reference 74

§ Solution

Table 4.3.49—The UO_3 , Na_2CO_3 , H_2O System
(UO_3 Solid Phase)

Test No.	Method of preparation	Solution analysis, gm./liter			d 25°C	Weight-percent based on									
		U	Na	CO ₃		4-component system					3-component system				
						UO ₃	Na ₂ O	CO ₂	H ₂ O	UO ₃	Na ₂ CO ₃	H ₂ O			
*	UO ₃ + H ₂ O	0.064	0	0	1.00	0.008	0	0	99.99	0.008	0	99.99	0	99.99	
*	UO ₃ + Na ₂ CO ₃	2.25	2.30	3.00	1.00	.27	0.31	0.22	99.2	.27	0.53	99.2	0.53	99.2	
*	UO ₃ + Na ₂ CO ₃	2.27	2.76	3.60	1.00	.27	.37	.26	99.10	.27	.63	99.10	.63	99.10	
*	UO ₃ + Na ₂ CO ₃	2.48	3.68	4.80	1.01	.30	.49	.35	99.86	.30	.84	99.86	.84	99.86	
*	UO ₃ + Na ₂ CO ₃	2.52	4.04	5.28	1.01	.30	.54	.38	98.78	.30	.92	98.78	.92	98.78	
*	UO ₃ + Na ₂ CO ₃	2.82	4.60	6.00	1.02	.33	.61	.43	98.63	.33	1.04	98.63	1.04	98.63	
*	UO ₃ + Na ₂ CO ₃	2.87	6.90	9.0	1.03	.34	.90	.64	98.12	.34	1.54	98.12	1.54	98.12	
*	UO ₃ + Na ₂ CO ₃	3.07	9.20	12.0	1.04	.35	1.19	.85	97.61	.35	2.04	97.61	2.04	97.61	
*	UO ₃ + Na ₂ CO ₃	3.18	13.8	18.0	1.05	.36	1.77	1.26	96.61	.36	3.03	96.61	3.03	96.61	
*	UO ₃ + Na ₂ CO ₃	3.72	18.4	24.0	1.06	.42	2.34	1.66	95.58	.42	4.00	95.58	4.00	95.58	
427†	UO ₃ CO ₃ + Na ₂ CO ₃ + NaOH	14.0	79.0	110.0	1.1	1.6	9.7	7.4	81.3	1.6	17.0	81.3	17.0	81.4	
427-L†	UO ₂ CO ₃ + Na ₂ CO ₃ + NaOH	18.2	93.3	125.2	1.2	1.8	10.5	7.7	80.0	1.8	18.2	80.0	18.2	80.0	

* See reference 76

† See reference 74

Table 4.3.50 — The $\text{Na}_4\text{UO}_2(\text{CO}_3)_3$, NaHCO_3 , H_2O System⁷⁴

Test No.	Method of preparation	Solution analysis, gm./liter			d ₂₅ °C	Weight-percent based on							
		U	Na	CO ₃		4-component system				3-component system			
						UO ₃	Na ₂ O	CO ₂	H ₂ O	Tri*	NaHCO ₃	H ₂ O	
†	Tricarb. + NaHCO ₃ †	18.15	31.2	76.7	1.100	2.00	3.82	5.12	89.06	3.76	8.0	88.3	
†	Tricarb. + NaHCO ₃ †	22.3	27.7	66.7	1.092	2.46	3.42	4.48	89.64	4.65	6.38	89.0	
†	Tricarb. + NaHCO ₃ †	38.8	24.4	54.0	1.098	4.25	3.00	3.61	89.14	8.06	3.14	88.8	
315	Tricarb. + NaHCO ₃ §	11.3	31.0	77.5	1.112	1.22	3.75	5.11	89.8	2.3	9.6	88.8	
314	Tricarb. + NaHCO ₃ §	22.8	37.5	84.2	1.140	2.41	4.43	5.42	87.8				

* $\text{Na}_4\text{UO}_2(\text{CO}_3)_3$
† See reference 75
‡ Solid phase tricarb. only
§ Solid phase NaHCO_3 only

Table 4.3.51 — Solubility of Sodium Uranyl Carbonate at 30°C

Solvent	Solubility expressed as grams of $2\text{Na}_2\text{CO}_3 \cdot \text{UO}_2\text{CO}_3$ contained in 100 ml of solvent	Solubility expressed as grams of U_3O_8 contained in 100 ml of solvent	Density of saturated solution	pH of satu- rated solution
Water	14.38	7.45	1.118	8.78
0.51M Na_2CO_3	7.36	3.81	1.106	10.99
1.03M Na_2CO_3	3.72	1.93	1.128	11.28
2.11M Na_2CO_3	1.23	0.64	1.202	11.40
3.24M Na_2CO_3	0.33	.17	1.278	11.60
0.41M NaHCO_3	8.83	4.57	1.098	8.72
0.83M NaHCO_3	5.08	2.63	1.092	8.25
0.05M NaHCO_3	4.13	2.14	1.100	8.32
0.50M Na_2SO_4	6.45	3.34	1.110	8.78
0.50M Na_2SO_4	3.98	2.06	1.138	11.00
0.51M Na_2CO_3	4.53	2.35	1.120	8.17
0.42M NaHCO_3	4.09	2.12	1.094	8.78
0.51M K_2SO_4	2.82	1.46	1.111	8.18
0.41M NaHCO_3	20.01	10.36	1.201	8.47
0.48M $(\text{NH}_4)_2\text{CO}_3$	17.20	8.91	1.197	8.05
0.35M NaHCO_3	15.20	7.87	1.123	6.85
Water saturated with CO_2				

Table 4.3.52 — Solubility of Sodium Uranyl Carbonate at 60°C

Solvent	Solubility expressed as grams of $2\text{Na}_2\text{CO}_3 \cdot \text{UO}_2\text{CO}_3$ contained in 100 ml of solvent	Solubility expressed as grams of U_3O_8 contained in 100 ml of solvent	Density of saturated solution	pH of satu- rated solution
Water*	12.31	6.38	1.094	8.72
0.52M Na_2CO_3	4.81	2.49	1.079	11.22
1.05M Na_2CO_3	2.15	1.11	1.106	11.31
2.12M Na_2CO_3	0.66	0.34	1.187	11.58
3.31M Na_2CO_3	.19	.10	1.278	11.68
0.43M NaHCO_3	6.56	3.40	1.070	8.32
0.05M Na_2CO_3	3.46	1.79	1.062	8.38
0.68M NaHCO_3	1.86	0.96	1.076	8.32
1.47M NaHCO_3	1.38	0.71	1.099	8.50
1.64M NaHCO_3	1.38	0.71	1.099	8.50
0.18M Na_2CO_3	5.02	2.60	1.092	8.50
0.51M Na_2SO_4	2.34	1.21	1.113	11.12
0.50M Na_2SO_4	2.34	1.21	1.113	11.12
0.51M Na_2CO_3	2.80	1.45	1.098	8.32
0.50M Na_2SO_4	4.58	2.37	1.091	8.86
0.48M NaHCO_3	2.90	1.50	1.124	11.27
0.52M NaCO_3	0.49M K_2SO_4	1.71	1.106	8.38
0.48M NaHCO_3	3.30	1.71	1.106	8.38
Water saturated with CO_2	12.85	6.65

* 0.02M Na_2CO_3 and 0.02M NaHCO_3 present because of decomposition

Table 4.3.53 — Solubility of Sodium Uranyl Carbonate at 90°C

Solvent	Solubility expressed as grams of $2\text{Na}_2\text{CO}_3 \cdot \text{UO}_2\text{CO}_3$ contained in 100 ml of solvent	Solubility expressed as grams of U_3O_8 contained in 100 ml of solvent	Density of saturated solution	pH of satu- rated solution
Water*	10.17	5.26	1.074	8.78
0.53M Na_2CO_3	3.56	1.84	1.059	10.82
1.02M Na_2CO_3	2.11	1.09	1.095	10.99
2.13M Na_2CO_3	0.47	0.24	1.175	11.28
3.37M Na_2CO_3	.17	.09	1.259	11.32
0.52M Na_2SO_4	3.44	1.78	1.047	9.10
0.51M Na_2SO_4	1.51	0.78	1.096	10.72
0.53M Na_2CO_3				
Water saturated with CO_2	11.56	5.99	1.081	7.12

* 0.02M Na_2CO_3 and 0.04M NaHCO_3 present because of decomposition

Table 4.3.54 — Solubility of $\text{K}_4\text{UO}_2(\text{CO}_3)_3$ in K_2CO_3 Solutions at 25°C

Solvent	U, gm/liter	Density	pH
Water	36.7	1.070	9.0
Water	35.6	1.068	8.8
0.07M K_2CO_3	30.0	1.063	10.4
0.14M K_2CO_3	23.3	1.055	10.7
0.28M K_2CO_3	14.3	1.056	...
0.28M K_2CO_3	13.6	1.056	11.0
0.43M K_2CO_3	9.1	1.062	11.3
0.56M K_2CO_3	6.4	1.071	11.4
0.71M K_2CO_3	4.5	1.083	11.5

Table 4.3.55 — Solubility of UO_2CO_3 in K_2CO_3 and Na_2CO_3 at 25°C

Test No.	Solvent	U, gm/liter	Wt-% of 4-component system			
			UO_3	M_2O	CO_2	H_2O
B-119	1% K_2CO_3	8.0	1.0	0.5	0.4	98.1
1003	1% Na_2CO_3	20.7	2.4	0.5	0.8	96.2
B-123	6% K_2CO_3	46.1	5.1	3.3	2.4	89.6
1004	6% Na_2CO_3	124.0	12.6	3.0	3.8	80.6

lower temperatures (presumably 20°C). More recent experiments with uranyl solutions other than carbonates cast some doubt on this temperature effect. It should be checked before being accepted. It was also found⁸³ that the gas liberated per U^{235} fission in 0.1 to 0.2M Na_2CO_3 solution was the same as that liberated per Pu^{239} fission in 0.5M H_2SO_4 . This is probably true only in dilute solutions.

The concentration of H_2O_2 was determined in six samples together with the total amount of gas.^{84,85} These data are presented in Table 4.3.56.

Table 4.3.57 gives the yield of hydrogen gas at 100°C in eight ampoules⁸⁶ containing 4 gm U^{235} /l (about 83-percent enriched). The net yield of hydrogen gas per 100 ev absorbed in the solution is presented in the last column and is to be compared with the pressure column to show the effect of pressure on the net yield of decomposition.

Chemical analyses were not carried out on any of the solutions in Table 4.3.57, but in the longer irradiation, 2.2 percent of the H_2O present in the samples was decomposed to its elements without any visible deterioration of the solution. No precipitates were noted. The gas analyses were all about the same and averaged 67.1 percent H_2 , 31.8 percent O_2 , and 1.1 percent CO_2 . No peroxide determinations were made. The value of G_{max} is about 2.0.⁸⁷ The greatest error in calculating this value is in estimating the energy absorbed in the solution. About 96 percent of the energy comes from the fissioning uranium in the samples and 4 percent from reactor fast neutrons and γ -rays. On an absolute energy basis, the G value of 2 is probably not better than ± 20 percent. Experiments with other uranyl solutions indicate that it may be about 20 percent too high. (See discussion of radiation stability given for uranyl sulfate systems.)

The data indicate that no peculiar radiation effects would be encountered with carbonate or bicarbonate systems. If the system can be thermally tolerated without radiation, apparently the only effect of radiation would be to decompose the solvent water.

PHYSICAL PROPERTIES (H. O. DAY, JR.)

No density, viscosity, or thermal conductivity data exist for the system $UO_3-CO_2-H_2O$ as far as can be determined. However, for the system potassium uranyl tricarbonate in solutions of potassium carbonate at 25°C a small amount of data exists (see p. 36, reference 81). These data are presented in Table 4.3.58.

Density data for $Na_2CO_3-UO_2CO_3-H_2O$ system are given (p. 6, reference 88) in Table 4.3.59. It is assumed that the temperature is 25°C. Density units are not specified.

URANYL PHOSPHATE SYSTEMS (E. V. JONES)

CHEMICAL PROPERTIES

Uranyl phosphate, $UO_2(HPO_4) \cdot 4H_2O$, forms yellow tetragonal crystals which are soluble in aqueous Na_2CO_3 and insoluble in acetic acid.

Uranyl acetate added to solutions of mono-, di-, or tri-orthophosphates of Na, K, NH_4 , or Ca gives a neutral double orthophosphate of the type UO_2MPO_4 ; with H_3PO_4 , UO_2HPO_4 is formed. An excess of $UO_2(AcO)_2$ gives $(UO_2)_3(PO_4)_2$. All uranyl phosphates, single or double, are soluble in H_3PO_4 with the formation of complex ions. On dilution, a precipitate of UO_2HPO_4 forms. All precipitates are hydrated.⁸⁹

The following dialkali-uranyl-sec.-phosphites have been prepared from saturated alkali phosphite solutions and solutions of UO_2SO_4 or $UO_2(NO_3)_2$: $K_2[UO_2(HPO_3)_2]$, $(NH_4)_2[UO_2(HPO_3)_2]$, and $Na_2[UO_2(HPO_3)_2]$. All are yellow; the color intensity and solubility in water decrease in the order listed.

The di-alkali-uranyl pyrophosphates of Li and Na, $Li_2(UO_2P_2O_7)$, and $Na(UO_2P_2O_7)$, have been prepared by adding saturated solutions of the corresponding alkali pyrophosphates to

Table 4.3.56—Concentration of H_2O_2 in Reactor-irradiated Aqueous Uranium Trioxide-Sodium Carbonate Samples(Uranium conc., 4.9 gm/l; U^{235} conc., 4 gm/l; volume of sample, 0.5 ml; temp., 20°C)

Sodium carbonate molarity	Reactor power, kw*	Irradiation time, min	H_2O_2 , N	Total gas, cc (STP)
0.5M Na_2CO_3	3650	10	0.0061	0.284
0.5M Na_2CO_3	4000	60	.016	...
0.5M Na_2CO_3	4000	60	...	2.05
0.5M Na_2CO_3	2000	60	0.011	1.06
0.5M Na_2CO_3	2000	60	.01	1.1
0.3M NaHCO_3	3800	60	...	4.1†

* It is estimated that the thermal neutron flux is approximately 8.2×10^{11} at 4000 kw

† This value is apparently too high

Table 4.3.57—Yield of Hydrogen Gas in Reactor-irradiated Uranium Carbonate Samples(U^{235} conc., 4 gm/l; temp., 100°C)

Wt of soln., gm*	MWH†	H_2 pressure, atm	cc H_2 (STP)	G‡
0.1934	12.8	>1	1.29	2.01
.2107	12.8	>1	1.38	1.98
.0448	12.8	57	0.270	1.82
.0434	12.8	70	.254	1.76
.0418	53.9	187	.93	1.59
.0406	53.9	194	.89	1.57
.0448	68.2	302	1.24	1.57
.0446	68.2	323	1.26	1.60

* Density at 22°C = 1.017

† It is estimated that the thermal flux is approximately 8.2×10^{11} at 4000 kw

‡ Molecules of hydrogen gas produced per 100 ev

Table 4.3.58—Properties of UO_3 - CO_2 - H_2O System

Density (25°C)	Solvent	Solubility, gm/l
1.070	Water	36.7
1.068	Water	35.6
1.063	0.07M K_2CO_3	30.0
1.055	0.14M K_2CO_3	23.3
1.056	0.28M K_2CO_3	14.3
1.056	0.28M K_2CO_3	13.6
1.062	0.43M K_2CO_3	9.1
1.071	0.56M K_2CO_3	6.4
1.083	0.71M K_2CO_3	4.5

Table 4.3.59—Density of $\text{Na}_2\text{CO}_3\text{--}\text{UO}_2\text{CO}_3\text{--}\text{H}_2\text{O}$ System

Solution	Solubility of $2\text{Na}_2\text{CO}_3\cdot\text{UO}_2\text{CO}_3$, gm/100 ml solvent	Molar solubility	Density of solution
H_2O	14.38	0.265	1.118
0.5M Na_2CO_3	7.36	.136	1.106
1.03M Na_2CO_3	3.72	.069	1.128
2.11M Na_2CO_3	1.23	.023	1.202
3.24M Na_2CO_3	0.33	.006	1.278

solutions of UO_2SO_4 or $\text{UO}_2(\text{NO}_3)_2$. The K and NH_4 salts could not thus be obtained.⁹⁰

Data from a study⁹¹ of the thermal stability of the $\text{UO}_3\text{--}\text{H}_3\text{PO}_4\text{--}\text{H}_2\text{O}$ system are given in Tables 4.3.60, 4.3.61, and 4.3.62. Only one solid phase was identified, $(\text{UO}_2)_3(\text{PO}_4)_2\cdot 4\text{H}_2\text{O}$, in one or the other of its two polymorphic forms, tetragonal and orthorhombic—the former being far more prevalent.

Uranyl nitrate and Na_2HPO_3 give UO_2HPO_3 , which is readily soluble in dilute mineral acids. When heated in air, it gives a grayish residue which hydrolyzes readily and gives a phosphate test when dissolved in HNO_3 . When heated with concentrated KOH solution, UO_2HPO_3 gives uranyl phosphate. It is easily hydrolyzed to give H_3PO_3 and hydrated uranyl hydroxide; the H_3PO_3 is then oxidized to H_3PO_4 , and uranyl phosphate is obtained.⁹²

The solubility of UO_3 in varying concentrations of H_3PO_4 at 250°C , is given in Table 4.3.63 (J. S. Gill, W. L. Marshall, and H. W. Wright, The Uranium Trioxide–Phosphoric Acid–Water System. ORNL-1121, Aug. 15, 1951). The results of exploratory studies of the solubility of UO_3 in 1, 2, and 3M H_3PO_4 at temperatures ranging up to 340°C are given in Table 4.3.64.

URANYL PHOSPHATE- $\text{H}_3\text{PO}_4\text{--}\text{H}_2\text{O}$ SYSTEMS (H. O. DAY, JR.)

No density, viscosity, or thermal conductivity data were found for this system.

PROPERTIES OF PLUTONIUM SALT SOLUTIONS (K. S. Warren)

CHEMICAL PROPERTIES

SOLUBILITIES OF PLUTONIUM SALTS

The solubilities of plutonium salts are listed in Tables 4.3.65 to 4.3.67.

Table 4.3.60 — Thermal Stability of $\text{UO}_2\text{-H}_3\text{PO}_4\text{-H}_2\text{O}$ Systems⁴⁶
(Data on 0.3M U in 2M total H_3PO_4 ; solutions of UO_3 in excess H_3PO_4)

Temp., °C	Analytical molarities		Molarities		P/U
	U	Total phosphate	U	Total phosphate	
Initial, 25°C	0.308	1.98	0.343	2.21	6.44
161	.257	1.90	.284	2.10	7.40
199	.224	1.91	.247	2.11	8.54
256	.201	1.76	.220	1.93	8.78
267	.203	1.88	.223	2.07	9.28
274	.195	1.91	.215	2.10	9.77
298	.198	1.95	.218	2.15	9.86
330	.258	2.24	.290	2.52	8.69
355.5	.229	2.12	.255	2.36	9.26
380	.592	2.97	.706	3.54	5.02

Table 4.3.61 — Solubility Data⁴⁶ Obtained upon Equilibrating Excess $(\text{UO}_3)_3(\text{PO}_4)_2 \cdot 4\text{H}_2\text{O}$ with Initially 0.3–0.5M UO_3 Dissolved in 2.9–3.2M H_3PO_4

Temp., °C	Analytical molarities		Molalities		P/U
	U	Total phosphate	U	Total phosphate	
25	>0.45	3.18	>0.51	3.62	<7.1
200	.559	3.12	.670	3.74	5.58
250	.601	3.40	.734	4.15	5.66
291	.561	3.29	.678	3.98	5.87
400	(Solid at room temperature)		75.6	13.7	<2.4

Table 4.3.62 — Thermal Stability of $\text{UO}_3\text{-H}_2\text{PO}_4\text{-H}_2\text{O}$ System⁴⁶
(Data on 0.3M UO_3 dissolved in 1.7M H_3PO_4 + 0.3M NaH_2PO_4)

Temp., °C	Analytical molarities		Molalities		P/U
	U	Total phosphate	U	Total phosphate	
Initial, 25°C	0.16 < 0.30	1.90	<0.333	2.11	>6.34
200	.216	1.885	.238	2.08	8.73
295	.171	1.86	.188	2.04	10.9
333	.136	1.99	.150	2.19	14.6
335	.217	2.14	.242	2.39	9.99
350	.157	1.97	.173	2.17	12.5

Table 4.3.63 — Solubility of Uranium Trioxide in Orthophosphoric Acid Solutions at 250°C

Sample No.	Molarity of H_3PO_4	Molarity of UO_3	Mole solubility ratio, PO_4/U
1	2.77	0.23	12
2	3.57	.42	8.5
3	4.86	.78	6.2
4	5.05	.84	6.0
5	5.95	1.26(?)	...
6	6.05	1.13	5.35
7	6.69	1.30	5.15
8	6.95	1.43	4.86

Table 4.3.64 — Solubility of Uranium Trioxide in Orthophosphoric Acid Solutions*

Investigator	H_3PO_4 , M	Uranium, M	Temperature of precipitation, °C
Morse†	1	0.17	65–85 (dissolved)
Ryon and Kuhn‡	1	.17	96 (analytical method)
Our data	1.017	.192	102
Our data	1.017	.0616	240
Our data	1.017	.0616	250
Our data	1.017	.0278	290
Ryon and Kuhn	2	.8	96 (analytical method)
Our data	2.075	.414	163
Our data	2.075	.373	176
Our data	2.075	.366	183
Our data	2.075	.271	228
Our data	2.075	.26	266'
Our data	2.075	.224	316
Los Alamos§	3	.9	250 (precipitated)
Los Alamos	3	.9	340 (dissolved)
Our data	3.113	.546	242 (precipitated)
Our data	3.113	.617	273 (precipitated)

* W. L. Marshall, J. S. Gill, and H. W. Wright, The Uranium Trioxide–Phosphoric Acid–Water System, ORNL-1057, Oct. 1951

† Morse, Chemical Technology Division, Oak Ridge Nat. Lab., unpublished data

‡ A. D. Ryon and D. W. Kuhn, Solubility of Uranyl Ammonium Sulfate, Y-381, Apr. 1, 1949

§ R. P. Hammond, Los Alamos Scientific Lab., private communication

Table 4.3.65—Solubilities of Plutonium-III Compounds⁸³

Solid phase	Aqueous phase	Temp., °C	Solubility, mg Pu/liter
Fluoride, $\text{PuF}_3 \cdot x\text{H}_2\text{O}$	1M HF 0.25M HCl	25	69
	1M HF 0.50M HCl	25	49
	1M HF 1.0M HCl	25	37
Phosphate, PuPO_4	.6M H_3PO_4 0.15M HNO_3	25	7
	.6M H_3PO_4 0.25M HNO_3	25	8
	.6M H_3PO_4 0.53M HNO_3	25	20
	.6M H_3PO_4 1.0M HNO_3	25	28
	.8M H_3PO_4 0.1M HCl	25	20
	.8M H_3PO_4 0.25M HCl	25	66
	.8M H_3PO_4 0.50M HCl	25	210
	.8M H_3PO_4 0.90M HCl	25	3890
	.8M H_3PO_4 0.08M H_2SO_4	25	32
	.8M H_3PO_4 0.23M H_2SO_4	25	37
	.8M H_3PO_4 0.49M H_2SO_4	25	199
	.8M H_3PO_4 0.98M H_2SO_4	25	545
	.8M H_3PO_4 0.1M H_2SO_4	75	23
	.8M H_3PO_4 0.3M H_2SO_4	75	120
	.8M H_3PO_4 0.4M H_2SO_4	75	900

Table 4.3.66—Solubilities of Plutonium-IV Compounds⁹³

Solid phase	Aqueous phase	Temp., °C	Solubility, mg Pu/liter
Fluoride, $\text{PuF}_4 \cdot x\text{H}_2\text{O}$	0.1–2.0M HNO_3 plus	25	300 – 700
	0.5–2.0M HF		
Nitrate, $\text{Pu}(\text{NO}_3)_4 \cdot x\text{H}_2\text{O}$	2M HNO_3	25	500×10^3
	.1M H_3PO_4 0.1M HNO_3	25	0.13
Phosphate, $\text{Pu}_3(\text{PO}_4)_4 \cdot x\text{H}_2\text{O}$.1M H_3PO_4 0.5M HNO_3	25	1.7
	.1M H_3PO_4 1.0M HNO_3	25	4.5
	.1M H_3PO_4 2.0M HNO_3	25	23.0
	.6M H_3PO_4 0.1M HNO_3	25	3.7
	.6M H_3PO_4 0.5M HNO_3	25	7.9
	.6M H_3PO_4 1.0M HNO_3	25	19.0
	.6M H_3PO_4 2.0M HNO_3	25	77.0
	.1M H_3PO_4 0.1M H_2SO_4	25	4
	.1M H_3PO_4 0.5M H_2SO_4	25	63
	.0M H_3PO_4 1.0M H_2SO_4	25	550
	.8M H_3PO_4 0.1M H_2SO_4	25	18
	.8M H_3PO_4 0.5M H_2SO_4	25	81
	.8M H_3PO_4 1.0M H_2SO_4	25	120
	.8M H_3PO_4 2.0M H_2SO_4	25	563
	.8M H_3PO_4 0.1M H_2SO_4	75	24
	.8M H_3PO_4 0.25M H_2SO_4	75	36
	.8M H_3PO_4 0.50M H_2SO_4	75	80
	.8M H_3PO_4 1.0M H_2SO_4	75	290
	.6M H_3PO_4 0.1M HCl	25	4
	.6M H_3PO_4 1.0M HCl	25	12
	.8M H_3PO_4 0.1M HCl	25	12
	.8M H_3PO_4 0.5M HCl	25	16
	.8M H_3PO_4 1.0M HCl	25	29
	.8M H_3PO_4 2.0M HCl	25	72

 Table 4.3.67—Solubilities of Plutonium-VI Compounds⁹³

Solid phase	Aqueous phase	Temp., °C	Solubility, mg Pu/liter
Chloride, $\text{PuO}_2\text{Cl}_2 \cdot x\text{H}_2\text{O}$	Approx. 5M HCl	25	350×10^3
Nitrate, $\text{PuO}_2(\text{NO}_3)_2 \cdot x\text{H}_2\text{O}$	Approx. 0.5M HCl	25	500×10^3

AQUEOUS FISSION-PRODUCT SYSTEMS (W. L. Marshall)

CHEMICAL PROPERTIES

SOLUBILITIES OF FISSION PRODUCTS

Systems of fission-product sulfates in water alone are included for comparison with studies in fuel media and for those in which the investigations were made above 100°C (see Tables 4.3.68 to 4.3.76). Additional studies of sulfate salts in water up to 100°C are compiled by Seidell.^{94,95}

Molybdenum Oxide

Molybdenum oxide is appreciably soluble in 1.26M UO_2SO_4 at room temperature. At 250°C, 1 percent or more of MoO_3 is completely soluble in 1.26M UO_2SO_4 .⁹⁸

Zirconium Sulfate

Zirconium sulfate appeared to be at least 6.53 to 11.15 wt-% soluble in 1.26M UO_2SO_4 when heated to about 280°C, but at that temperature an irreversible change began which yielded a considerable mass of white precipitate.⁹⁸

Multiple Fission-product Solubilities

A few exploratory experiments have been made on multiple fission-product solubilities in 0.125 and 1.25M UO_2SO_4 solutions at 250°C. Of the elements studied (Ce, Zr, Cs, Mo, Ru, Ba, Sr, La, Nb, and Y), it was concluded that Ce, Zr, Ru, Ba, and Nb would be the first elements to precipitate because of fission-product buildup.¹⁰²

Heats of Solution

An attempt has been made to interpret solubility data for $\text{Y}_2(\text{SO}_4)_3$, $\text{La}_2(\text{SO}_4)_3$, Cs_2SO_4 , CdSO_4 , Ag_2SO_4 , and $\text{Ce}(\text{SO}_4)_2$ in water, 0.126M UO_2SO_4 , and 1.26M UO_2SO_4 .¹⁰² The data have been plotted using the van't Hoff isochore. The results for ΔH solution are given in Table 4.3.77.

PHYSICAL PROPERTIES

GROWTH OF FISSION PRODUCTS (W. L. MARSHALL)

Calculated values are given in Table 4.3.78 for solid fission-product growths in a homogeneous reactor operating continuously at 50 kw/liter.¹¹¹

Calculations of the growth and behavior of barium and xenon in a homogeneous reactor operating with 0.13 molar UO_2SO_4 solution at 14.3 kw/liter are presented. It is also concluded that BaSO_4 will precipitate in from 30 min to 25 days, depending on the rate of xenon gas removal from solution.¹¹²

The following paragraphs pertain to fission-product growth in uranium solid but can be applied to a uranium fuel solution if fission-gas removal is neglected:

The estimated weights of fission products (in grams of element per 100 gm of ^{235}U destroyed) are listed^{113,114} for various times of operation and cooling. Some of the results are given in Table 4.3.79.

Compiled data on fission-product growth and decay of both a general and a specific nature (but not applying directly to an aqueous homogeneous reactor) may be found in various sources.¹¹⁵⁻¹²² The bulk of this work applies to decay schemes.

Table 4.3.68—The Solubility of Yttrium Sulfate in Water and in Uranyl Sulfate Solutions*

Temp., °C	Y ₂ (SO ₄) ₃ , wt-%	Reference
In water		
108	4.76	96
150	2.38	96
155	1.59	96
160	1.19	96
161	0.95	96
163	.64	96
176	.48	96
186	.23	96
195	.12	96
190	.010	97
200	.0009	97
218	.00001	97
230	.00175	97
240	.00028	97
In 0.126M UO ₂ SO ₄		
153	4.47	96
162	2.23	96
189	0.81	96
229	.22	96
210	.144	97
235	.084	97
270	.033	97
315	.007	97
340	.001	97
In 1.08M UO ₂ SO ₄		
208	4.32	98
215	3.41	98
217	3.44	98
230	2.78	98
245	2.12	98
†	1.43	98
†	1.08	98
In 1.26M UO ₂ SO ₄		
212	4.31	98
221	3.62	98
224	3.43	98
231	2.99	98
237	2.74	98
†	2.34	98
†	2.14	98

* The data in this table are illustrated in Fig. 4.3.17

† Two liquid layers at about 277°C. No crystals up to 320°C. Held at 320°C for 2 hr

‡ Two liquid layers at about 270°C. No crystals after several hours above 280° to 310°C for 2.14 wt-% Y₂(SO₄)₃ solution

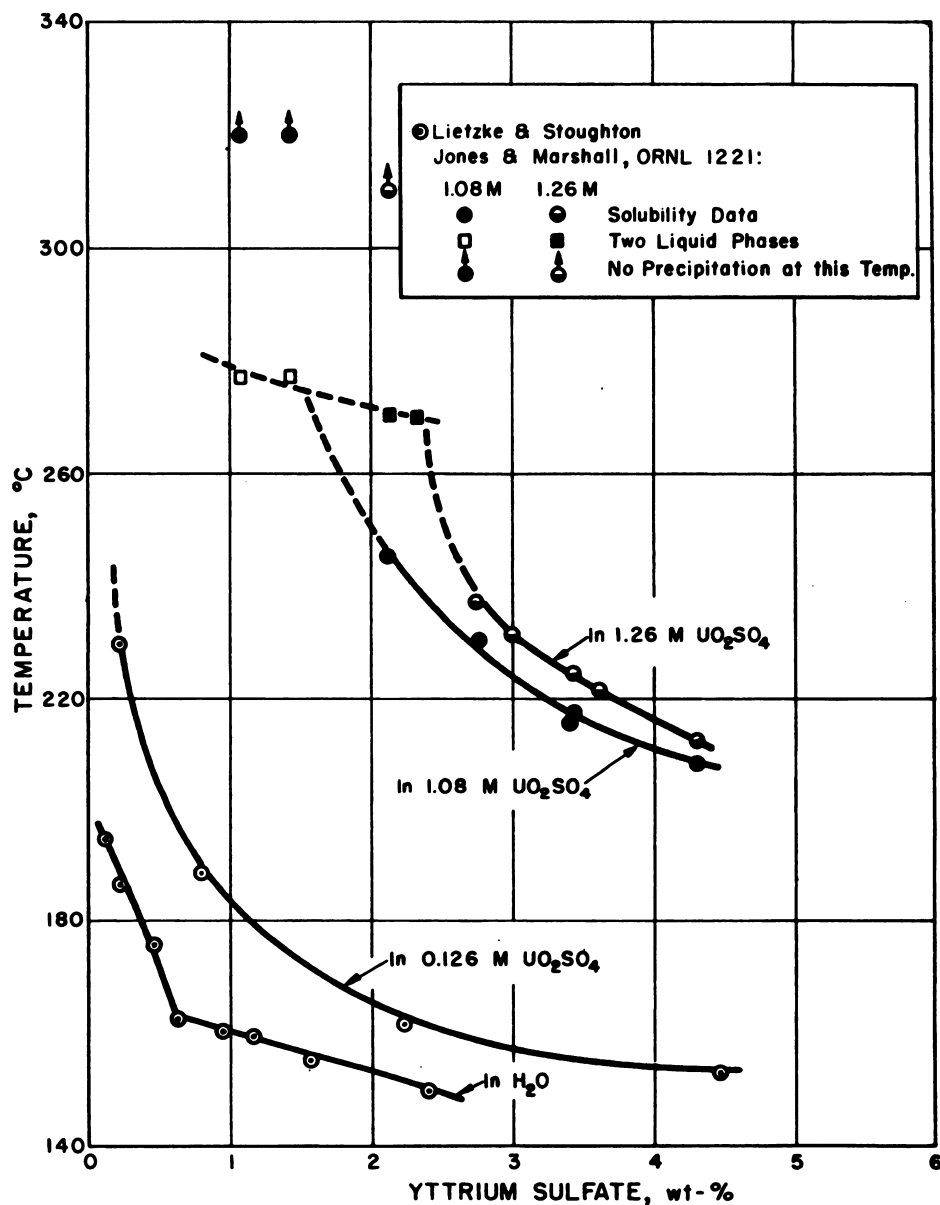


Fig. 4.3.17—Solubility of Yttrium Sulfate in Aqueous Uranyl Sulfate. Reprinted from ORNL-1221. Submitted by Oak Ridge National Laboratory, Nov. 25, 1952.

Table 4.3.69—The Solubility of Lanthanum Sulfate in Water and in Uranyl Sulfate Solutions*

Temp., °C	La ₂ (SO ₄) ₃ , wt-%	Reference
In water		
0	2.91	99
14	2.53	99
26	2.04	100
30	1.86	99
50	1.47	99
75	0.95	99
100	.68	99
108	.61	96
113	.46	96
115	.37	96
117	.31	96
106	.598	101
155	.142	101
180	.041	101
200	.024	101
216	.012	101
278	.0062	101
350	.0061	101
In 0.126M UO ₂ SO ₄		
97	2.04	96
105	1.74	96
120	0.87	96
145	.29	96
169	.15	96
199	.083	96
215	.042	96
In 1.26M UO ₂ SO ₄		
78	4.39	98
91 and 149 (double point)	3.97	98
148	3.80	98
150	3.75	98
150.5	3.70	98
151	3.60	98
152	3.46	98
154	3.25	98
160	2.69	98
168	2.30	98
178	1.85	98
202	1.22	98
222	0.88	98
Two liquid layers at 291°C	.57	98

* The data in this table are illustrated in Figs. 4.3.18 and 4.3.19

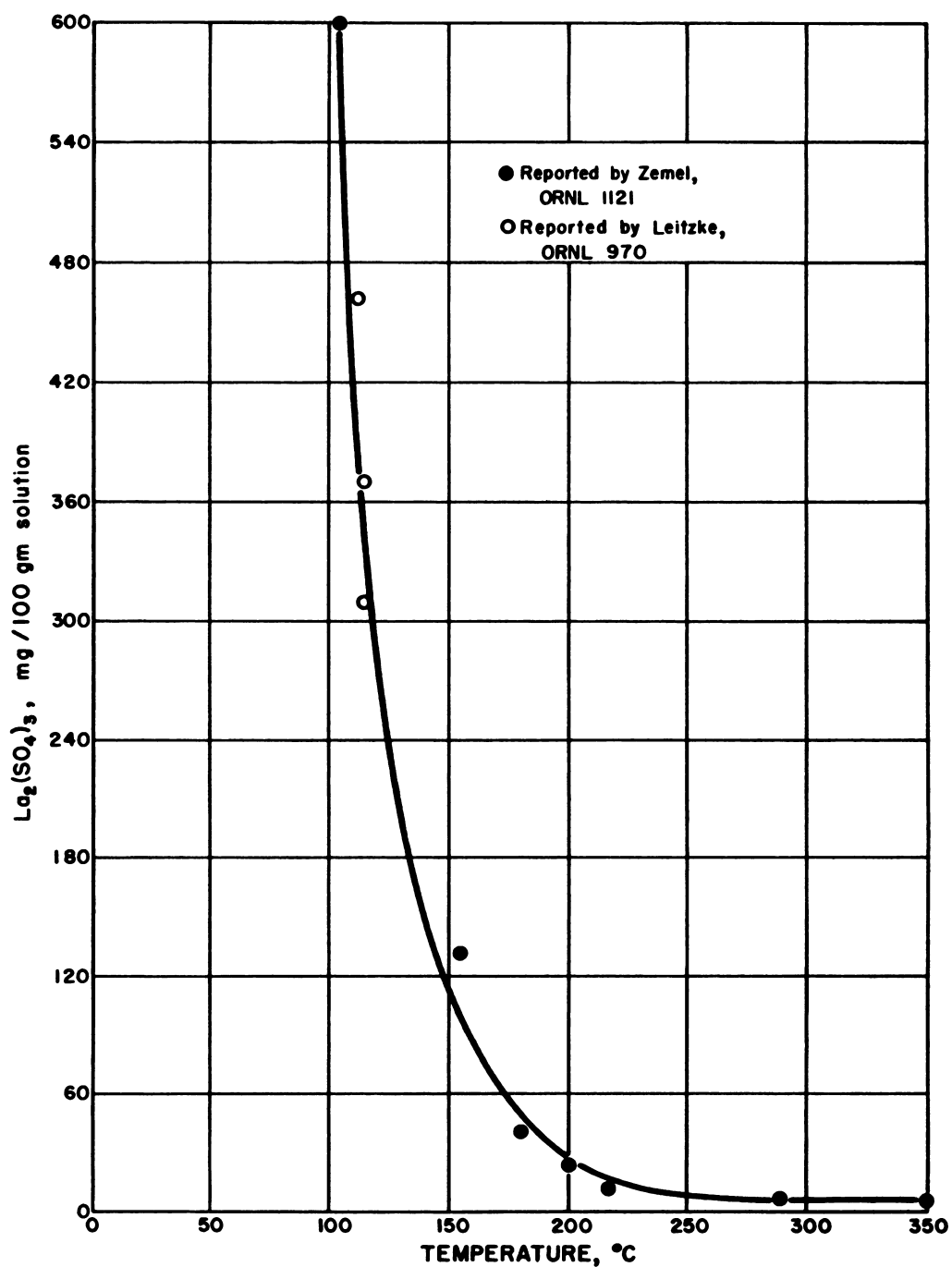


Fig. 4.3.18—Solubility of Lanthanum Sulfate in Ordinary Water from 100° to 350°C. Reprinted from ORNL-1121. Submitted by Oak Ridge National Laboratory, Nov. 25, 1952.

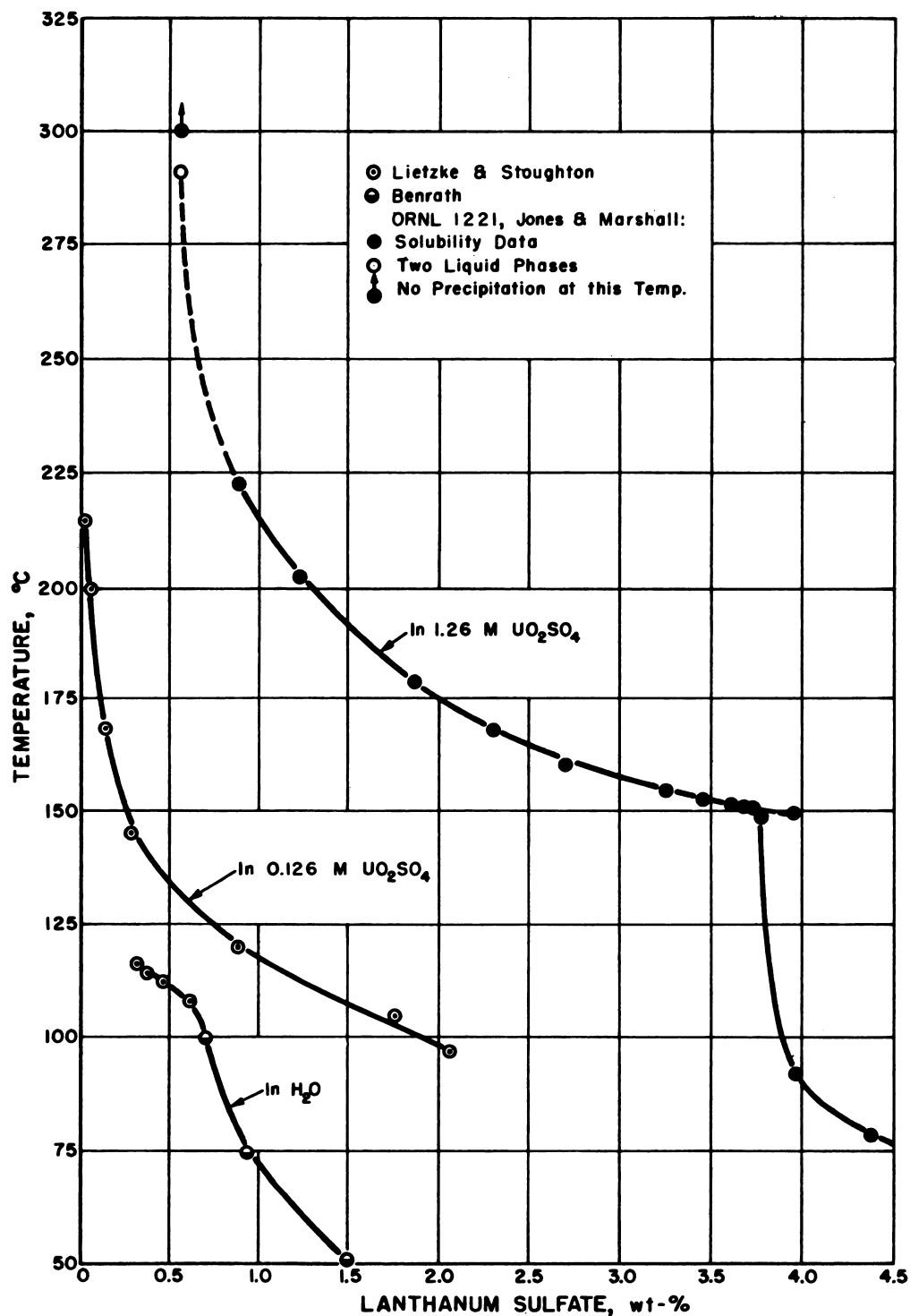


Fig. 4.3.19 — Solubility of Lanthanum Sulfate in Aqueous Uranyl Sulfate. Reprinted from ORNL-1221. Submitted by Oak Ridge National Laboratory, Nov. 25, 1952.

Table 4.3.70—The Solubility of Cesium Sulfate in Water and in Uranyl Sulfate Solutions*

Temp., °C	Cs ₂ SO ₄ , wt-%	Reference
In water		
0	62.6	100
10	63.4	100
20	64.1	100
23	63.5	96
30	64.8	100
40	65.5	100
50	66.1	100
60	66.7	100
70	67.2	100
80	67.8	100
90	68.3	100
100	68.8	100
108.6	69.2	100
175	71.8	96
211	73.5	96
270	75.0	96
292	75.5	96
In 0.126M UO ₂ SO ₄		
53.8	64.19	102
61.6	66.00	102
77.3	67.12	102
84.2	67.55	102
104.8	68.58	102
140.2	70.07	102
177.5	71.66	102
228.6	73.48	102
In 1.26M UO ₂ SO ₄		
167.7	0.30	102
178.5	.33	102
187.3	.37	102
214.8	.44	102
245.3	.49	102
285.6	.54	102
288.6	.78	102
293	†	

* The data in this table are illustrated in Fig. 4.3.20

† Two liquid layers at 293°C much undissolved

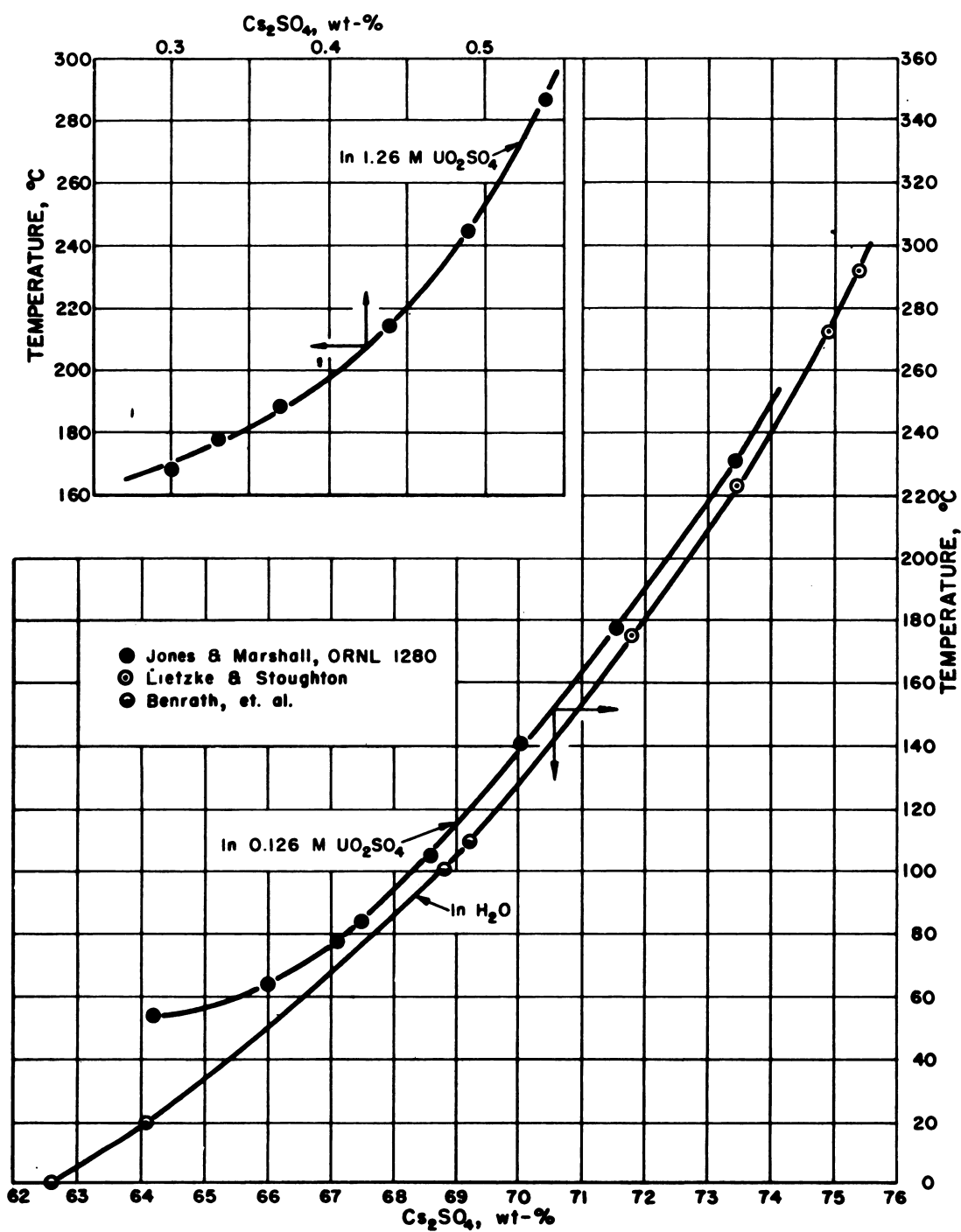


Fig. 4.3.20—Solubility of Cesium Sulfate in Uranyl Sulfate Solutions. Reprinted from ORNL-1280. Submitted by Oak Ridge National Laboratory, Nov. 25, 1952.

Table 4.3.71—The Solubility of Ceric Sulfate in Water and in Uranyl Sulfate Solutions*

Temp., °C	Ce(SO ₄) ₂ , wt-%	Reference
In water		
35	7.8	103
40	5.71	103
50	3.31	103
65	1.85	103
82	0.98	103
100.5	.42	103
105	.300	101
139	.113	101
169	.050	101
199	.019	101
211	.017	101
220	.013	101
244	.0029	101
269	.0022	101
284	.00049	101
325	.00094	101
350	.00083	101
In 0.126M UO ₂ SO ₄		
137	0.290	101
200	.113	101
220	.0805	101
242	.0437	101
267	.0233	101
338	.00182	101

* Some of the data in this table are illustrated in Fig. 4.3.21. Ceric sulfate exhibits a solubility of less than 0.014 percent at room temperature in 1.26M UO₂SO₄-H₂O solution⁸⁸

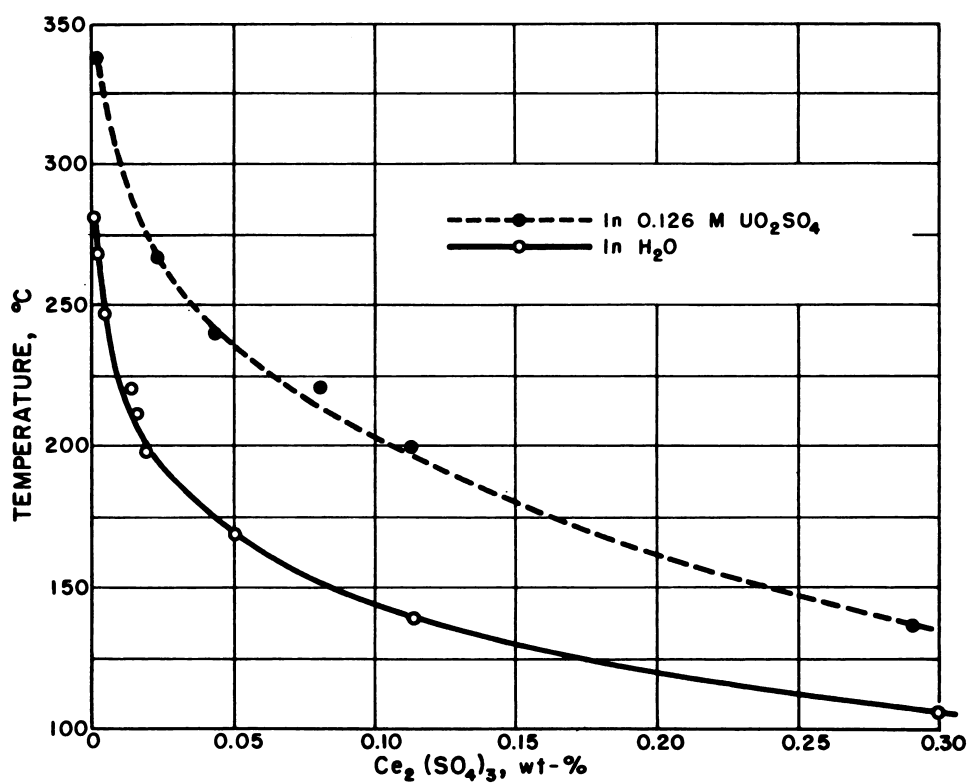


Fig. 4.3.21—The Solubility of Ceric Sulfate in Ordinary Water and in Uranyl Sulfate Solution. Submitted by Oak Ridge National Laboratory, Nov. 25, 1952.

Table 4.3.72—The Solubility of Strontium Sulfate in Water

Temp., °C	SrSO ₄ , gm/100 gm H ₂ O	Reference
124	0.00261	104
127	.00264	104
163	0.00125, 0.00135	104
168	.00129, .00137	104
186	0.00066	104
199	.0008	104
220	.00063	104
250	.000248	104
260	0.0001, 0.000096	104
273	0.000124	104
280	.000123	104
319	.00005	104
194 ± 2	.0032	105
203 ± 1	.0025	105
208 ± 1	.0031	105
259 ± 2	.0026	105
284 ± 5	.0029	105
293 ± 4	.0017	105
307 ± 4	.0022	105
333 ± 2	.0013	105
339 ± 2	.0018	105
348 ± 1	.0016	105
381 ± 2	.0009	105
401 ± 3	.0003	105
426 ± 2	.0005	105

Table 4.3.73 —The Solubility of Barium Sulfate in Water and in Uranyl Sulfate Solutions

Temp., °C	BaSO ₄ , wt-%	Reference
In water		
150	60.4×10^{-6}	97
180	26.5×10^{-6}	97
220	11.25×10^{-6}	97
250	5.25×10^{-6}	97
250	6.2×10^{-6}	97
262	4.6×10^{-6}	97
290	2.3×10^{-6}	97
291	1.4×10^{-6}	97
In 0.12M UO ₂ SO ₄		
185	15×10^{-6}	101
200	11×10^{-6}	101
250	9×10^{-6}	101
270	10×10^{-6}	101
296	6×10^{-6}	101
At 250°C as a function of UO ₂ SO ₄ concentration*		
UO ₂ SO ₄ , M	Molar solubility of BaSO ₄	Reference
0.000	0.53×10^{-5}	106
.125	1.46×10^{-5}	106
.313	3.32×10^{-5}	106
.625	8.95×10^{-5}	106
.775	10.34×10^{-5}	106
1.00	17.40×10^{-5}	106
1.15	22.42×10^{-5}	106
1.25	37.35×10^{-5}	106

* Barium sulfate solubility as a function of UO₂SO₄ concentration is illustrated in Fig. 4.3.22

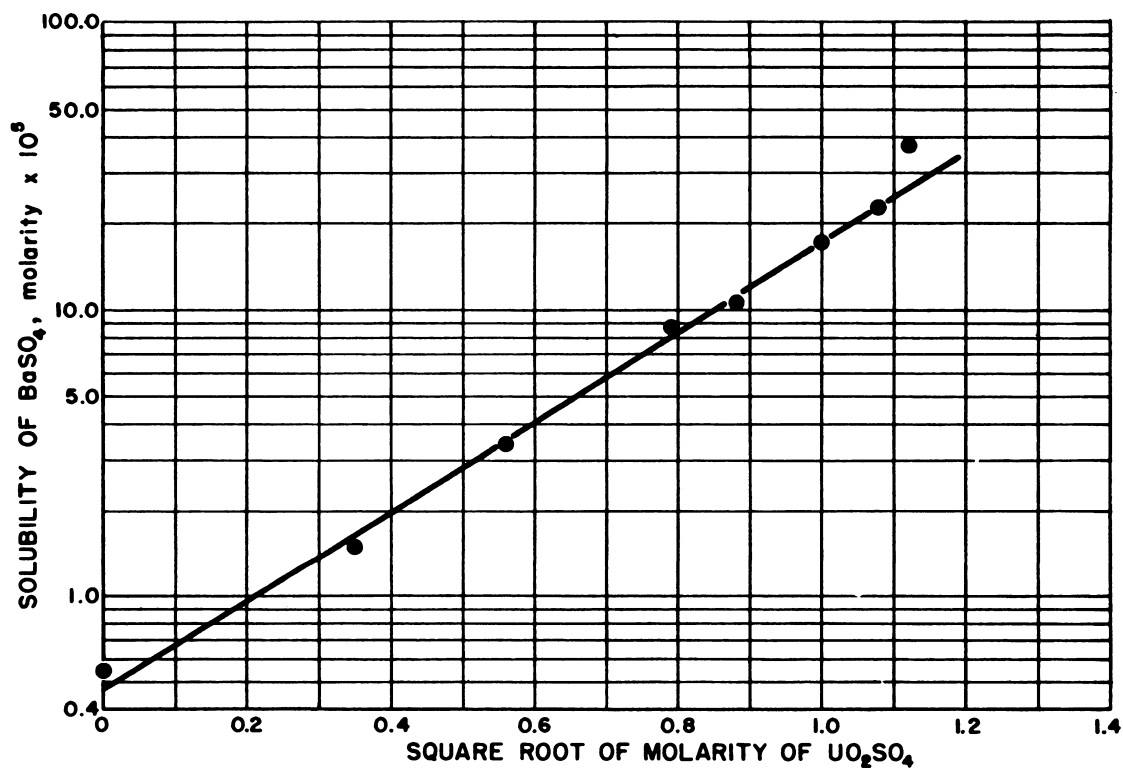


Fig. 4.3.22 — Solubility of Barium Sulfate in Aqueous Uranyl Sulfate at 250°C. Reprinted from ORNL-1318. Submitted by Oak Ridge National Laboratory, Nov. 25, 1952.

Table 4.3.74—The Solubility of Silver Sulfate in Water and in Uranyl Sulfate Solutions*

Temp., °C	Ag ₂ SO ₄ , wt-%	Reference
In water		
145	0.894	107
157	.65	107
199	.45	107
199	.376	107
250	.40	107
250	.35	107
305	.329	107
305	.295	107
330	.28	107
In 0.126M UO ₂ SO ₄		
36.0	1.04	106
54.0	1.46	106
83.3	2.18	106
107.8	2.72	106
127.4	3.01	106
140.0	A red product formed	106
In 1.26M UO ₂ SO ₄		
42.5	1.54	106
52.0	2.36	106
84.6	3.63	106
106.5	5.38	106
131.4	7.43	106
161.6	9.89	106
174.3	11.01	106
197.1	12.82	106
214.9	14.14	106
237.5	15.75	106
259.1	17.25	106

* The data in this table are illustrated in Fig. 4.3.23

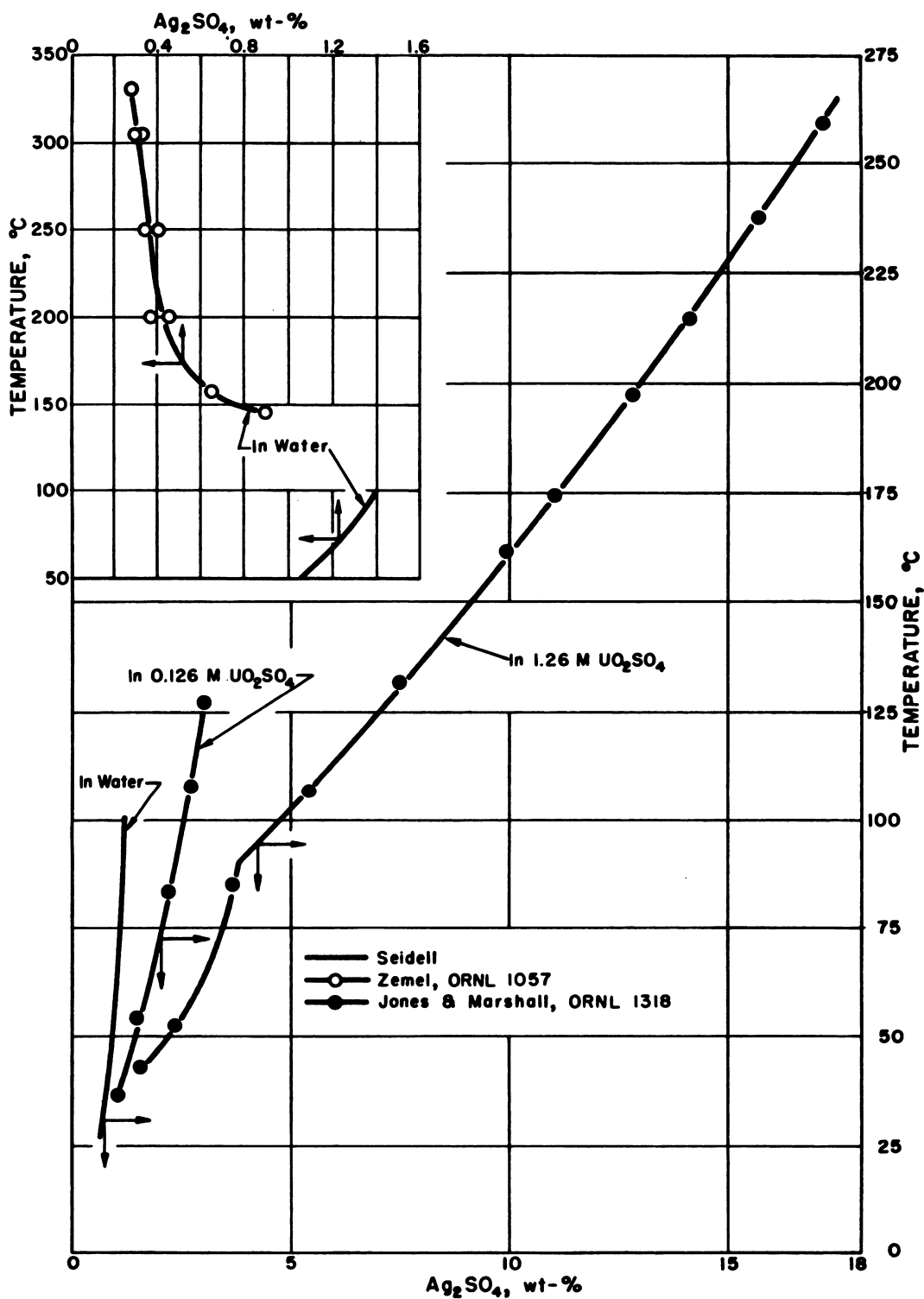


Fig. 4.3.23—Solubility of Silver Sulfate in Water and Aqueous Uranyl Sulfate. Reprinted from ORNL-1318. Submitted by Oak Ridge National Laboratory, Nov. 25, 1952.

Table 4.3.75—The Solubility of Cadmium Sulfate in Water and in Uranyl Sulfate Solutions*

Temp., °C	CdSO ₄ , wt-%	Reference
In water		
25	43.73	108
50	43.53	108
75	40.97	108
99	36.85	108
119	32.3	109
124	29.6	96
131	26.9	109
159	15.6	109
160	14.8	96
161	14.8	109
166	12.3	109
172	9.8	109
182	7.4	96
187	4.9	109
190	3.0	96
In 0.126M UO ₂ SO ₄		
175	28.5	96
200	14.2	96
219	7.1	96
251	2.8	96
In 1.26M UO ₂ SO ₄		
21	31.62	102
47.8(209)†	31.33	102
84.2	30.50	102
102.9(215.8)†	30.12	102
215.8	29.37	102
216.8	29.69	102
220.8	28.68	102
228.7	26.54	102
230.6	25.83	102
244.3	22.51	102

* The data in this table are illustrated in Fig. 4.3.24

† Double solubility points

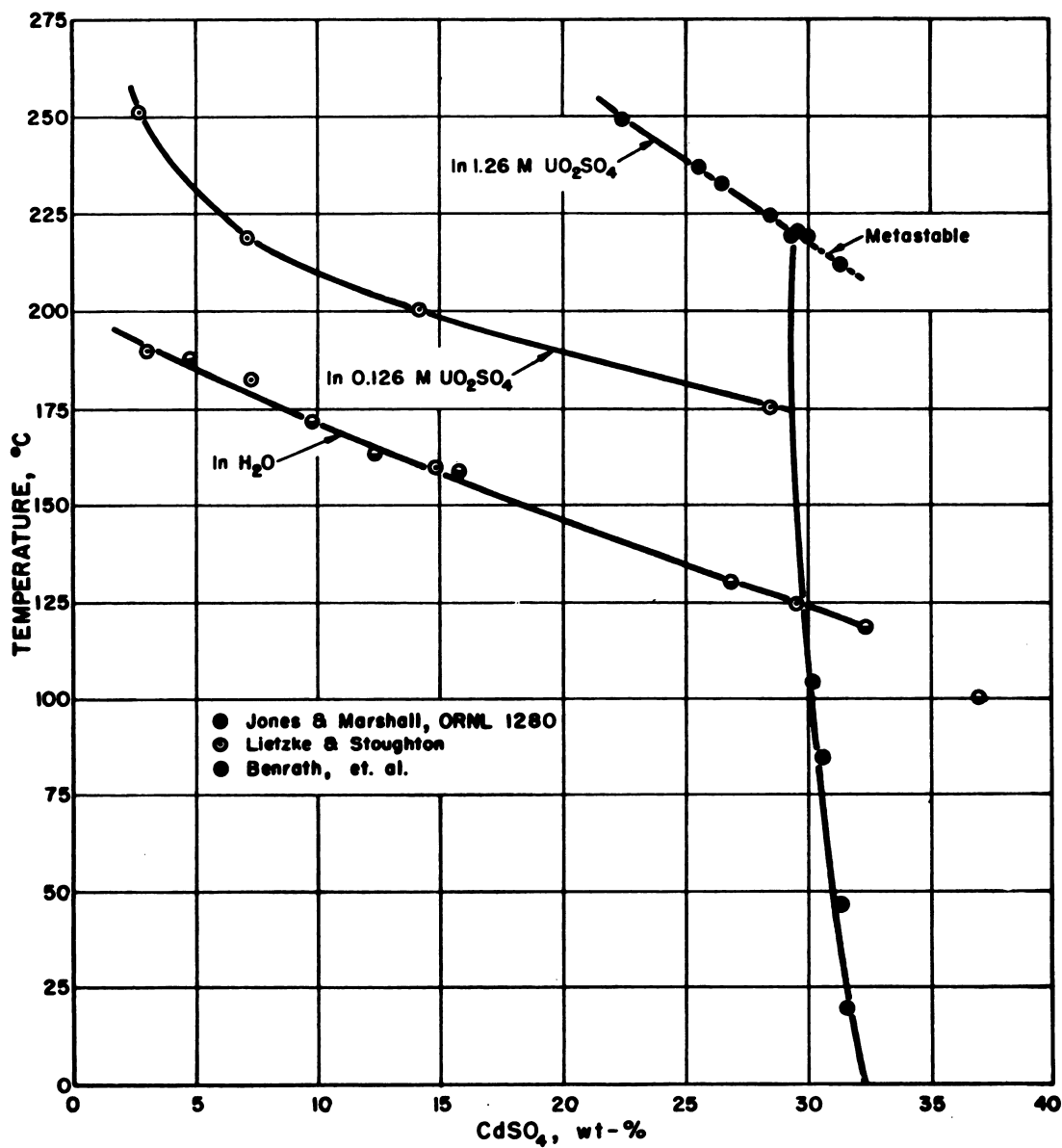


Fig. 4.3.24 — Solubility of Cadmium Sulfate in Aqueous Uranyl Sulfate Solution. Reprinted from ORNL-1280. Submitted by Oak Ridge National Laboratory, Nov. 25, 1952.

Table 4.3.76—The Solubility of Zinc Sulfate in Water

Temp., °C	ZnSO ₄ , wt-%	Reference
178	34.0	96
203	25.5	96
219	22.7	96
238	17.0	96
248	11.3	96
253	8.5	96
255	5.1	96
257	2.1	96
90	50	110
115	45	110
145	40	110
175	35	110
205	25	110
230	20	110
255	15	110
250	10	110
255	5	110

 Table 4.3.77—Some Differential Heats of Solution of Fission-product Sulfates in Water and Uranyl Sulfate Solutions¹⁰²

Salt	ΔH_{soln} , kcal/mole		
	In H ₂ O	In 0.126M UO ₂ SO ₄	In 1.26M UO ₂ SO ₄
Y ₂ (SO ₄) ₃	-27	-16	-9
La ₂ (SO ₄) ₃	-23	-12	-8
CdSO ₄	-17	-14	-5.4
Ce(SO ₄) ₂	-10	-6.9	...
Ag ₂ SO ₄	+1.1	+2.3	+3.7
Cs ₂ SO ₄	+0.20	+0.20	+1.5

Table 4.3.78—Growth of Solid Fission Products

Element	Fission-product buildup in operation for one month, gm/l		Fission-product buildup in operation for one year, gm/l	
	With no gas removal	With 100% gas removal	With no gas removal	With 100% gas removal
Ce	0.2	0.06	2	0.7
Nd	.2	.07	2	.8
Zr	.2	.08	2	.6
Cs	.1	.0	2	.0
Mo	.1	.1	1	1.
Ru	.1	.1	1	1.
Ba	.09	.0001	0.8	0.001
Sr	.08	.007	.8	.1
La	.07	.0	.7	.0
Pr	.04	.0	.6	.0
Nb	.04	.004	.5	.1
Y	.04	.0	.3	.0
Tc	.03	.03	.5	.5
Rb	.03	.007	.3	.01
Pm	.02	.02	.2	.2
Rh	.006	.006	.3	.3

Table 4.3.79—Estimated Weights of Fission Products for Various Times of Operation and Cooling

 (In grams of element per 100 grams of ${}_{92}\text{U}^{235}$ destroyed)

Element	40*				100*			
	0†	3†	30†	100†	0†	3†	30†	100†
Se	0.1	0.1	0.1	0.1	0.1	0.1	0.1	0.1
Br	.06	.06	.06	.06	.06	.06	.06	.06
Kr	1.5	1.5	1.5	1.5	1.5	1.5	1.5	1.5
Rb	1.8	1.8	1.8	1.8	1.8	1.8	1.8	1.8
Sr	5.3	5.3	4.8	4.2	4.9	4.9	4.6	4.1
Y	4.5	4.4	3.8	2.8	3.9	3.8	3.4	2.5
Zr	11.0	10.9	10.5	10.6	10.7	10.6	10.5	10.8
Cb	3.8	3.9	4.3	5.1	4.2	4.3	4.6	5.3
Mo	7.2	7.2	8.1	8.7	7.9	7.9	8.5	8.8
43	2.6	2.8	2.9	2.9	2.8	2.9	2.9	2.9
Ru	6.4	6.3	6.0	5.6	6.0	6.0	5.8	5.5
Rh	0.4	0.5	0.7	1.1	0.7	0.7	0.9	1.1
Pd	.5	.5	.5	0.6	.5	.5	.5	0.6
Ag	.03	.03	.06	.09	.06	.06	.08	.10
Sb	.04	.04	.03	.02	.03	.03	.02	.02
Te	1.8	1.6	1.4	1.3	1.5	1.4	1.3	1.3
I	0.9	0.8	0.6	0.7	0.7	0.7	0.6	0.7
Xe	11.9	11.9	11.9	11.9	11.9	11.9	11.9	11.9
Cs	11.0	11.2	11.6	11.4	11.4	11.4	11.6	11.6
Ba	6.1	5.9	4.7	4.4	5.1	5.0	4.5	4.4
La	3.6	3.6	3.4	3.4	4.5	4.5	4.4	4.4
Ce	12.6	12.7	12.6	11.5	12.4	12.4	12.1	11.2
Pr	5.5	5.4	5.2	5.2	5.3	5.3	5.2	5.1
Nd	8.2	8.4	10.0	11.5	9.6	9.8	10.7	11.9
61
Sm	3.3	3.3	3.3	3.3	3.3	3.3	3.3	3.3
Eu	0.4	0.4	0.5	0.5	0.4	0.4	0.5	0.5
Gd	.02	.02	.02	.02	.02	.02	.02	.02
Np	9.1	4.2	1.0	1.0	4.2	2.3	1.0	1.0
Pu	91.7	96.6	100.0	100.0	96.7	98.6	100.0	100.0

* Time of operation in days

† Time of cooling in days

THORIUM SOLUTIONS (W. L. Marshall)

THE SYSTEM THORIUM NITRATE – WATER

CHEMICAL PROPERTIES

Chemical and Phase Stability

These stabilities are shown in Tables 4.3.80 to 4.3.82, and Figs. 4.3.25 and 4.3.26.

Corrosion

No data available.

Radiation Damage

No data available.

Acidity

Schaal and Faucherre¹²⁷ give graphic data on variation of pH as a function of the dilution which may be applied in the study of soluble basic salts.

Neish and Burns¹²⁸ present one approximate graphic pH of 2 to 3 for a 0.001N $\text{Th}(\text{NO}_3)_4$ - H_2O solution.

PHYSICAL PROPERTIES

Density

The densities are shown in Tables 4.3.83 to 4.3.85 and Fig. 4.3.27.

Vapor Pressure

Vapor pressures are shown in Tables 4.3.86 to 4.3.89 and Fig. 4.3.28.

Refractive Index

The refractive indices are shown in Table 4.3.90.

Heat and Free Energy (Work) of Dilution and Solution

The heats of dilution and solution are given in Tables 4.3.91 and 4.3.92 and Fig. 4.3.29. The heats and free energies of dilution are given in Table 4.3.93.

Table 4.3.80—Solubility of $\text{Th}(\text{NO}_3)_4$ in H_2O

Temp., °C	Solubility of $\text{Th}(\text{NO}_3)_4$, wt-%	Solid $\text{Th}(\text{NO}_3)_4$, wt-%	Solid phase
Part A ¹²³			
-0.2	1.0		Ice
-1.5	9.0		Ice
-4.0	20.0		Ice
-6.0	33.0		Ice
-9.0	41.0		Ice
-15.0	47.7		Ice
-25.0	55.7		Ice
-35	60.6		Ice
-40.6	62.0		Ice
-43.5	64.0		Ice
-22	64.2		$\text{Th}(\text{NO}_3)_4 \cdot 6\text{H}_2\text{O}$
0	65.0		$\text{Th}(\text{NO}_3)_4 \cdot 6\text{H}_2\text{O}$
+10	65.2		$\text{Th}(\text{NO}_3)_4 \cdot 6\text{H}_2\text{O}$
+20	65.6		$\text{Th}(\text{NO}_3)_4 \cdot 6\text{H}_2\text{O}$
Part B ¹²⁴			
29.8 ± 0.2	66.2		Bipyramidal crystals*
40.1 ± 0.2	67.5		Bipyramidal crystals*
50.0 ± 0.2	69.1		Bipyramidal crystals*
58.8 ± 0.2	70.2		Bipyramidal crystals*
60.5 ± 0.2	70.6		Bipyramidal crystals*
77.6 ± 0.5	73.5		Bipyramidal crystals*
82.4 ± 0.5	74.6		Bipyramidal crystals*
99.2 ± 0.5	77.3		Bipyramidal crystals*
109.4 ± 0.5	79.5		Bipyramidal crystals*
121.5 ± 0.5	81.6		Bipyramidal crystals*
142.0 ± 0.5	83.9		$\text{Th}(\text{NO}_3)_4 \cdot 4\text{H}_2\text{O}$
158.0 ± 0.5	85.5		$\text{Th}(\text{NO}_3)_4 \cdot 4\text{H}_2\text{O}$
Part C ¹²⁵			
37.3	67.07	81.18 (theor. 81.62)	$\text{Th}(\text{NO}_3)_4 \cdot 6\text{H}_2\text{O}$
54.5	69.78		$\text{Th}(\text{NO}_3)_4 \cdot 6\text{H}_2\text{O}$
72.0	73.39		$\text{Th}(\text{NO}_3)_4 \cdot 6\text{H}_2\text{O}$
90.2	76.39	80.82 (theor. 81.62)	$\text{Th}(\text{NO}_3)_4 \cdot 6\text{H}_2\text{O}$
99.7	78.56		$\text{Th}(\text{NO}_3)_4 \cdot 6\text{H}_2\text{O}$
110.4	81.11		$\text{Th}(\text{NO}_3)_4 \cdot 6\text{H}_2\text{O}$
110.9	81.50		$\text{Th}(\text{NO}_3)_4 \cdot 6\text{H}_2\text{O}$
111(a)	...		$\text{Th}(\text{NO}_3)_4 \cdot 6\text{H}_2\text{O} + \text{Th}(\text{NO}_3)_4 \cdot 4\text{H}_2\text{O}$
120.6	82.01		$\text{Th}(\text{NO}_3)_4 \cdot 4\text{H}_2\text{O}$
128	82.41		$\text{Th}(\text{NO}_3)_4 \cdot 4\text{H}_2\text{O}$
129.5	...	85.84 (theor. 86.95)	$\text{Th}(\text{NO}_3)_4 \cdot 4\text{H}_2\text{O}$
130.5	82.85		$\text{Th}(\text{NO}_3)_4 \cdot 4\text{H}_2\text{O}$
139.5	84.27		$\text{Th}(\text{NO}_3)_4 \cdot 4\text{H}_2\text{O}$
146.0	85.30		$\text{Th}(\text{NO}_3)_4 \cdot 4\text{H}_2\text{O}$
149.0	85.81		$\text{Th}(\text{NO}_3)_4 \cdot 4\text{H}_2\text{O}$
151(b)	...		$\text{Th}(\text{NO}_3)_4 \cdot 4\text{H}_2\text{O} + \text{Th}(\text{NO}_3)_4 \cdot \text{XH}_2\text{O}$
159	87.41		$\text{Th}(\text{NO}_3)_4 \cdot \text{XH}_2\text{O}$
211	91.82		$\text{Th}(\text{NO}_3)_4 \cdot \text{XH}_2\text{O}$

 * Bipyramidal crystals $\text{Th}(\text{NO}_3)_4 \cdot 6\text{H}_2\text{O}$ (Fuhse and Misciatelli) or $\text{Th}(\text{NO}_3)_4 \cdot 51/2\text{H}_2\text{O}$ (Templeton)

Table 4.3.81—Hydrolytic and Phase Stability¹²⁸ Above 50°C
 (Decomposition-precipitation temperatures of thorium nitrate–water solutions)

Th(NO ₃) ₄ , wt-%	Upper temp. limit before hydrolytic pptn, °C
87.41	229
55.23	217
32.94	~176
7.41	~113

Table 4.3.82—Boundary Curve Data¹²⁸ for Th(NO₃)₄–H₂O
 (Calculated from density–temperature–solubility–precipitation data)

Temp., °C	Solubility of Th(NO ₃) ₄ , gm Th/cc	Conc. of solution at decomposition- precipitation temperature
50	0.704	...
60	.735	...
70	.779	...
80	.825	...
90	.872	...
100	.922	...
110	.979	...
120	1.007	...
130	1.026	0.040
140	1.059	.060
150	1.099	.084
160	1.144	.115
180	1.195	.200
200	1.240	.335
210	1.281	.440
220	1.302	.600
225	1.32	.715
230	1.34	1.14
232	1.35	1.35

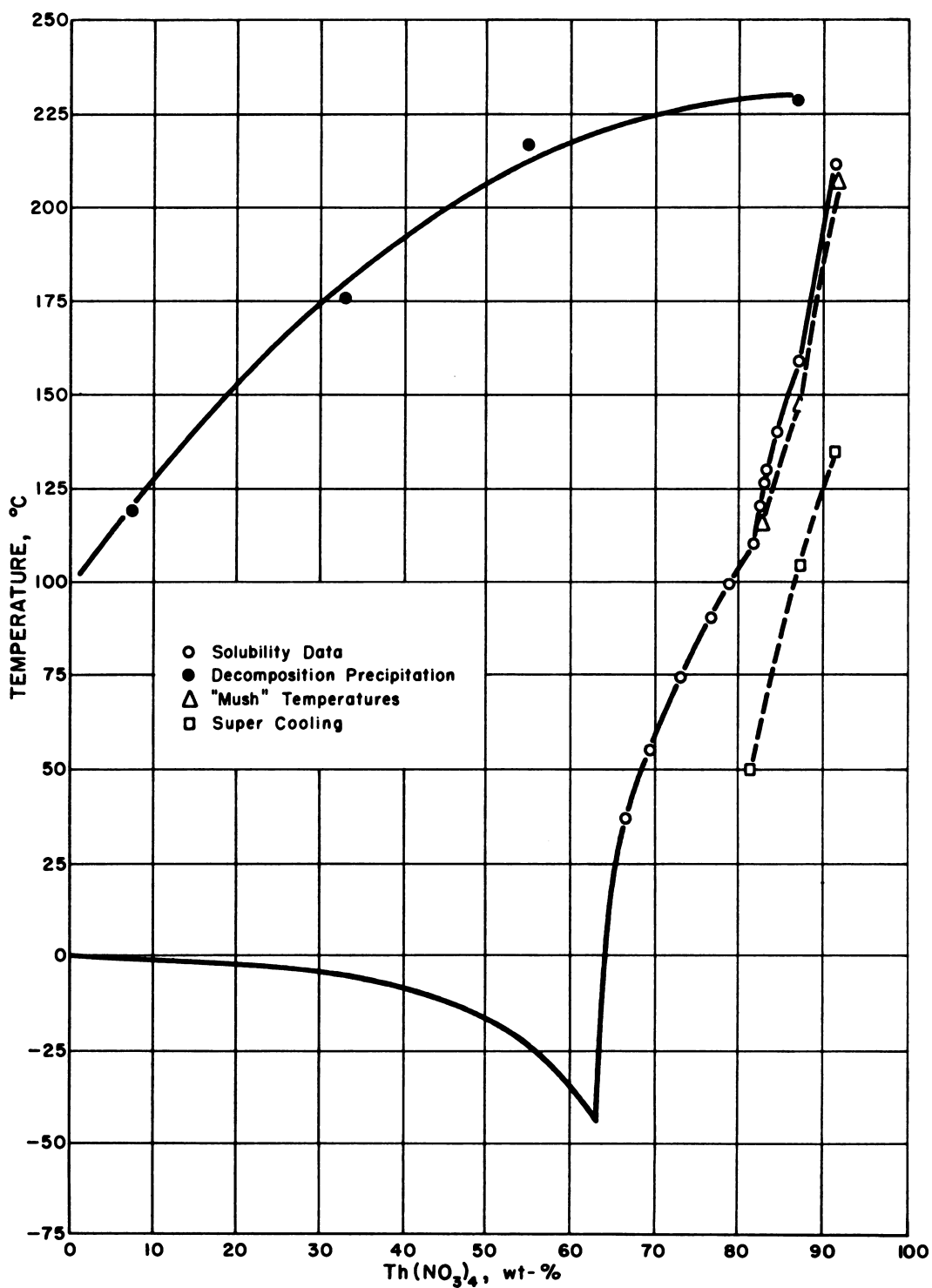


Fig. 4.3.25—The Thorium Nitrate-Water System. Reprinted from ORNL-925. Submitted by Oak Ridge National Laboratory, Nov. 25, 1952.

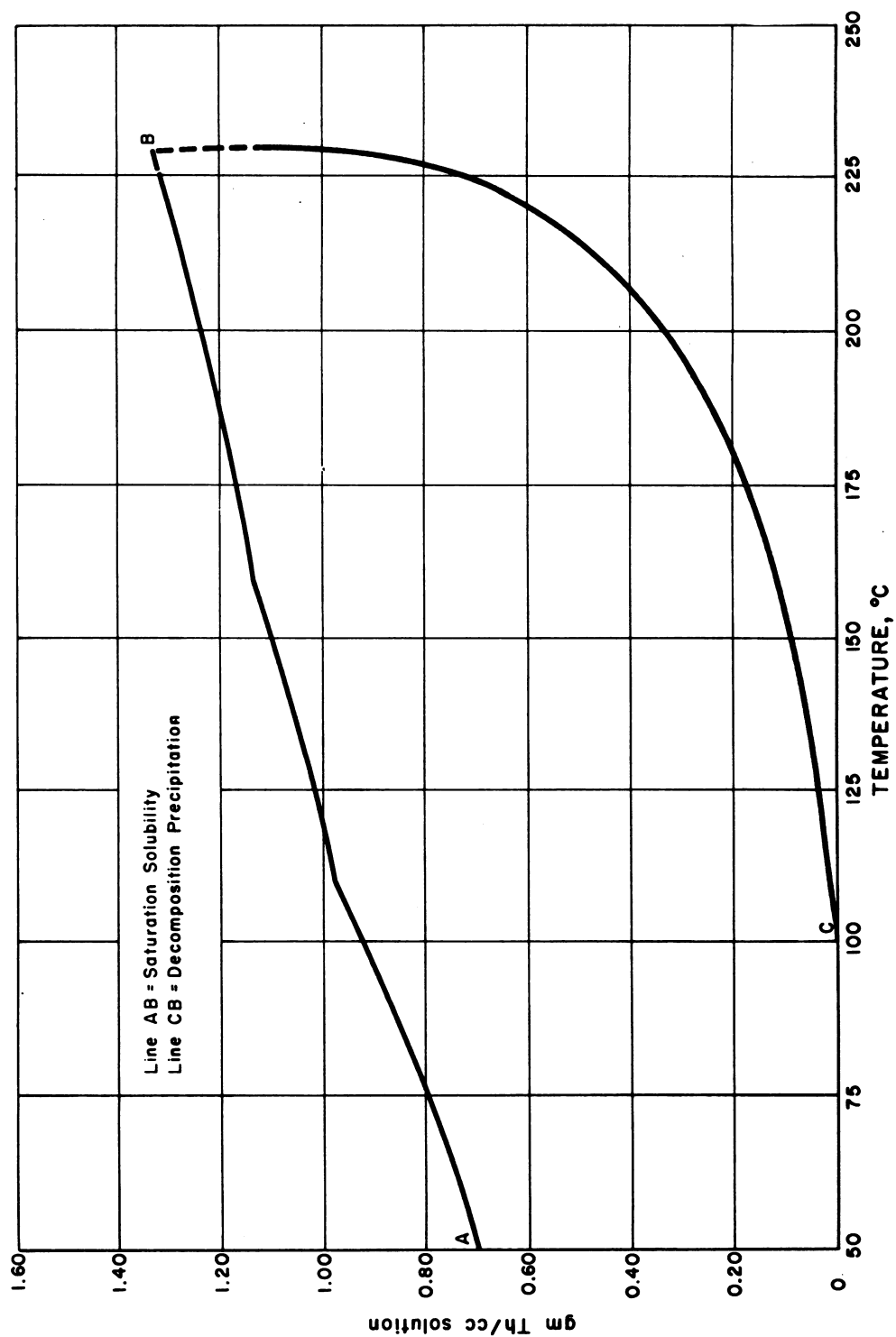


Fig. 4.3.26 —Grams Thorium per cc of Solution as a Function of Temperature. Reprinted from ORNL-925. Submitted by Oak Ridge National Laboratory, Nov. 25, 1952. Boundary Region for complete solution, $\text{Th}(\text{NO}_3)_4\text{-H}_2\text{O}$ closed system.

Table 4.3.83—Density of $\text{Th}(\text{NO}_3)_4$ – H_2O Solution¹²⁹

$\text{Th}(\text{NO}_3)_4$, wt-%	$\text{Th}(\text{NO}_3)_4$ concentration, gm/100 cc soln.	Density (15°/15°)
0.7228	0.73	1.0061
1.7928	1.8	1.0140
3.5204	3.6	1.0327
5.205	5.4	1.0483
6.835	7.3	1.0639
8.419	9.1	1.0796
9.949	11	1.0962
12.87	14	1.1297
15.66	18	1.1609
18.29	22	1.1926

Table 4.3.84—Density of $\text{Th}(\text{NO}_3)_4$ – H_2O Solution at Room Temperature¹²⁸

(Density Data of J. L. Bamberg)

$\text{Th}(\text{NO}_3)_4$, wt-%	Density at room temperature, gm/cc
16.54	1.161
34.30	1.400
41.39	1.508
45.41	1.586
51.02	1.694
54.41	1.765
57.63	1.833
60.84	1.894
61.94	1.938
63.34	1.971
66.06	2.035
68.26	2.110

Table 4.3.85—Density of $\text{Th}(\text{NO}_3)_4$ – H_2O Solution at Saturation Temperature¹²⁸

$\text{Th}(\text{NO}_3)_4$, wt-%	Density at saturation temperature, gm/cc
67.07	2.09
69.78	2.17
73.39	2.23
76.39	2.37
78.56	2.41
81.11	2.44
81.50	2.45
82.01	2.54
82.85	2.53
84.27	2.70
87.27	2.70
97.41	2.75
91.82	2.82

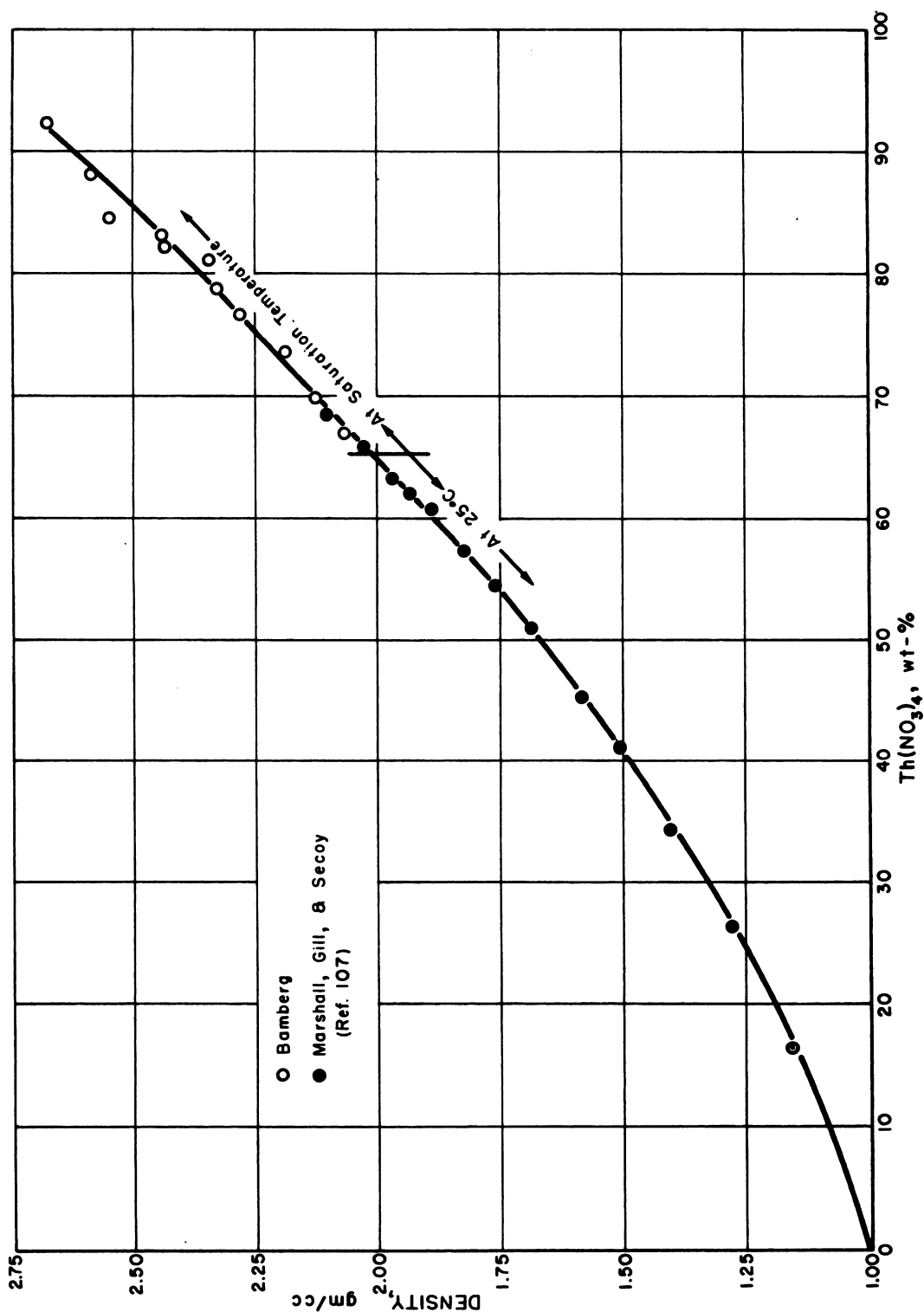


Fig. 4.3.27—The Density of Aqueous Thorium Nitrate Solutions. Reprinted from ORNL-925. Submitted by Oak Ridge National Laboratory, Nov. 25, 1952.

Table 4.3.86—Vapor Pressure of $\text{Th}(\text{NO}_3)_4$ – H_2O Solution¹³⁰

Moles H_2O /mole $\text{Th}(\text{NO}_3)_4$	P, mm Hg	
	0°C	15°C
16.48	2.69 ₈	7.72 ₄
18.18	2.88 ₂	8.21 ₀
20.31	3.08 ₅	8.73 ₈
29.29	3.26 ₅	9.16 ₅
24.46	3.40 ₈	9.53 ₃

 Table 4.3.87—Vapor Pressure of $\text{Th}(\text{NO}_3)_4$ – H_2O Solution^{*131}

Moles H_2O /mole $\text{Th}(\text{NO}_3)_4$	P, mm Hg	
	0°C	15°C
14.87	2.45 ₇	7.13 ₉
16.71	2.64 ₁	7.63 ₂
18.74	2.86 ₂	8.21 ₄
21.87	3.14 ₁	8.91 ₂
25.24	3.37 ₅	9.54 ₆
28.16	3.56 ₈	10.02 ₆

* These data are superseded by the later results in Table 4.3.86

 Table 4.3.88—Boiling Points of Aqueous Thorium Nitrate Solutions¹²⁸

(At 760 mm Hg pressure)

$\text{Th}(\text{NO}_3)_4$, wt-%	Temp., °C
22.3	101
58.0	110
72.3	130
85.3	147

Table 4.3.89—Osmotic Pressure, Vapor Pressure, and Activity Coefficient of
 $\text{Th}(\text{NO}_3)_4\text{--H}_2\text{O}$ Solution^{132,133}

(Osmotic coefficients at 25°C, $\text{Th}(\text{NO}_3)_4\text{--H}_2\text{O}$ solution)*

m	Osmotic coefficient	Activity coefficient
0.1	0.675	(0.279)
.2	.685	0.225
.3	.705	.203
.4	.734	.192
.5	.770	.189
.6	.807	.188
.7	.846	.191
.8	.885	.195
.9	.925	.201
1.0	.965	.207
1.2	1.044	.224
1.4	1.120	.246
1.6	1.192	.269
1.8	1.259	.296
2.0	1.325	.326
2.5	1.455	.405
3.0	1.546	.486
3.5	1.616	.568
4.0	1.659	.647
4.5	1.688	.722
5.0	1.706	.791

* By use of the equation, osmotic coefficient = $-55.51/\mu$ molality $\ln P/P^0$, vapor pressures may be calculated

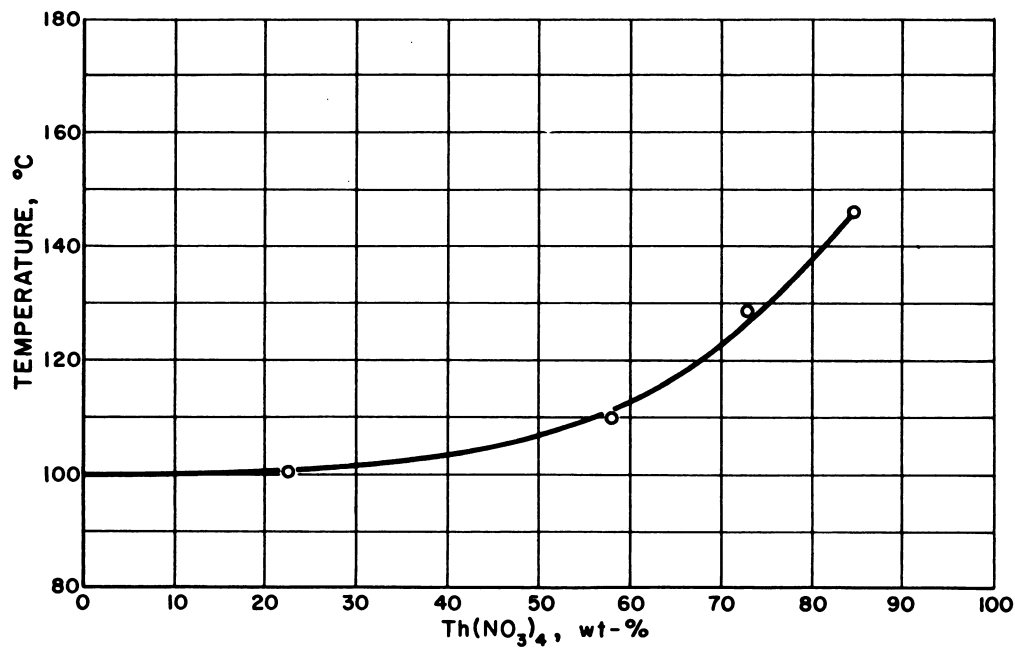


Fig. 4.3.28 — The Boiling Points of Aqueous Thorium Nitrate Solutions at 760 mm Hg Pressure. Reprinted from ORNL-925. Submitted by Oak Ridge National Laboratory, Nov. 25, 1952.

Table 4.3.90 — Refractive Index of Th(NO₃)₄–H₂O Solution¹²⁹

Th(NO ₃) ₄ , wt-%	Th(NO ₃) ₄ concentration, gm/100 cc soln.	Refractive index (15°C)
0.7228	0.73	1.33478
1.7928	1.8	1.33582
3.5204	3.6	1.33804
5.205	5.4	1.34025
6.835	7.3	1.34283
8.419	9.1	1.34489
9.949	11	1.34724
12.87	14	1.35235
15.66	18	1.35732
18.29	22	1.36188

Table 4.3.91 — Molar Integral Heat of Solution of $\text{Th}(\text{NO}_3)_4$ – H_2O System¹³⁰
(From calorimetric data)

Moles H_2O /mole $\text{Th}(\text{NO}_3)_4$		ΔH_{soln} /mole $\text{Th}(\text{NO}_3)_4$, cal
Initial	Final	
15.65	510	3477
15.92	497	2912
17.65	543	2113
22.37	545	1242
24.68	553	888
28.18	562	513

Table 4.3.92 — Molar Differential Heat of Solution¹³⁰
(From calorimetric data)*

Moles H_2O /mole $\text{Th}(\text{NO}_3)_4$	ΔH_{soln} /mole $\text{Th}(\text{NO}_3)_4$, cal
16.00	1100
16.50	550
17.00	375
20.00	175
22.00	155
26.00	132

* The data in this table are shown in Fig. 4.3.29

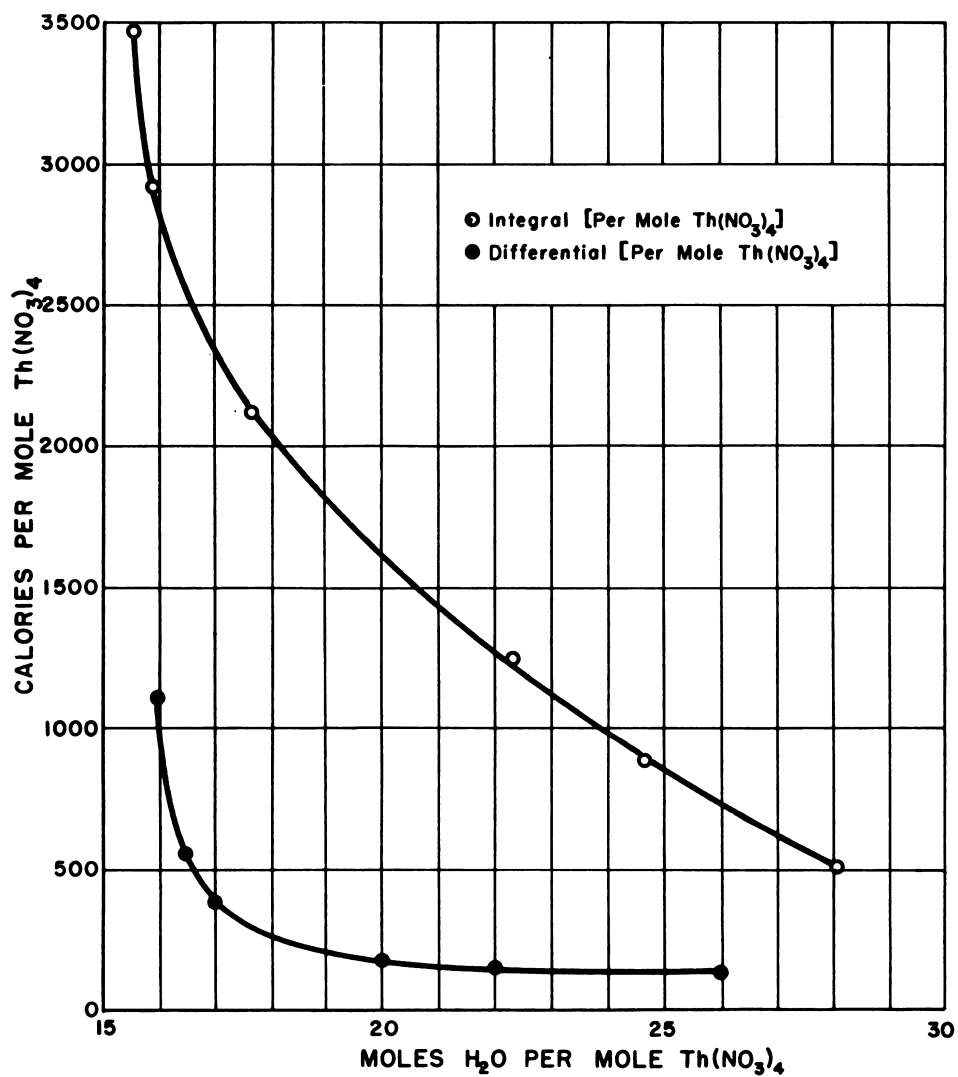


Fig. 4.3.29—Integral and Differential Heats of Dilution for Thorium Nitrate. Data taken from reference 136. Submitted by Oak Ridge National Laboratory, Nov. 25, 1952.

Table 4.3.93—Calculated Molar Differential Heat and Work (Free Energy) of Dilution of $\text{Th}(\text{NO}_3)_4$ – H_2O Solutions
(From vapor-pressure data)

Moles H_2O /mole $\text{Th}(\text{NO}_3)_4$	Work of dilution cal/mole		Heat of dilution, cal/mole	Reference
	$A_{0^\circ\text{C}}$	$A_{15^\circ\text{C}}$	$U_{0^\circ-15^\circ\text{C}}$	
16.48	287	288	258	130
18.18	251	253	206	130
20.31	214	218	146	130
22.29	183	190	54	130
24.46	160	168	15	130

The following data are superseded by the previous results:

14.87	328	334	414	131
16.71	298	295	357	131
18.74	255	253	285	131
21.87	204	207	167	131
25.24	165	167	132	131
28.16	135	139	65	131

REFERENCES

URANYL SULFATE SYSTEMS

1. C. H. Secoy, *Jour. Am. Chem. Soc.* 72, 1950, p 3343.
2. C. H. Secoy, *Jour. Am. Chem. Soc.* 70, 1948, p 3450.
3. I. Helmholtz and G. Friedlander, *Physical Properties of Uranyl Sulfate Solutions*, Los Alamos Scientific Lab., MDDC-808, 1943.
4. C. Dittrich, *Z. physik Chem.* 29, 1899, p 449.
5. J. Mellor, *A Comprehensive Treatise on Inorganic and Physical Chemistry*, Vol. 12, Longmans, Green & Co., Inc., New York, 1932, pp 103-105.
6. J. A. Swartout et al, Oak Ridge Nat. Lab., ORNL-1280, June 25, 1952, pp 180-183, 190 (classified).
7. J. A. Swartout et al, Oak Ridge Nat. Lab., ORNL-1424, Dec. 17, 1952 (classified).
8. J. S. Gill, E. V. Jones, and W. L. Marshall, Oak Ridge Nat. Lab., ORNL-1318, Sept. 2, 1952, pp 143-146 (classified).
9. R. E. Leeds and C. H. Secoy, Oak Ridge Nat. Lab., ORNL-870, Sept. 30, 1950, pp 29-30 (classified).
10. C. H. Secoy, Oak Ridge Nat. Lab., ORNL-607, Dec. 31, 1949, pp 33-38 (classified).
11. D. A. McInnes and L. G. Longworth, *The Measurement and Interpretation of pH and Conductance Values of Aqueous Solutions of Uranyl Salts*, Rockefeller Institute for Medical Research, University of Chicago, MDDC-911, Nov. 24, 1942.
12. M. H. Lietzke, H. W. Wright, and W. L. Marshall, Oak Ridge Nat. Lab., ORNL-1121, Dec. 27, 1951, p 124 (classified).
13. W. L. Marshall and J. S. Gill, Oak Ridge Nat. Lab., ORNL-990, Feb. 28, 1951, pp 134-136 (classified).
14. W. L. Marshall and J. S. Gill, Oak Ridge Nat. Lab., ORNL-630, Feb. 28, 1950, pp 49-53 (classified).
15. W. L. Marshall and J. S. Gill, Oak Ridge Nat. Lab., ORNL-1036, Dec. 31, 1950, pp 13-19 (classified).
16. E. Orban, Mound Laboratory Central Files Number 52-8-84, Aug. 19, 1952 (classified).
17. J. W. Boyle, J. A. Ghormley, C. J. Hochanadel, W. F. Kieffer, and T. J. Sworski, *Reactor Sci. Technol.*, ORNL-52-8-103, 3, No. 1, Mar. 1953, pp 32-49 (classified).
18. H. F. McDuffie et al, Oak Ridge Nat. Lab., ORNL-1318, pp 59-65 (classified).
19. D. M. Gillics, *Some Studies of the Reactions of Uranium Oxides with Hydrogen, Oxygen and Water*, Columbia University, MDDC-647, June 1946.
20. H. F. McDuffie and J. W. Boyle, Oak Ridge Nat. Lab., 1952 (classified).
21. E. Orban, Mound Laboratory, MLM-659, Feb. 15, 1952 (classified).
22. J. A. Swartout et al, Oak Ridge Nat. Lab., ORNL-1121, Dec. 27, 1951 (classified).
23. W. L. Marshall, Oak Ridge Nat. Lab., ORNL-CF-52-1-93, Jan. 15, 1952 (classified).
24. R. Van Winkle, Oak Ridge Nat. Lab., ORNL-CF-52-1-124, Jan. 18, 1952 (classified).
25. W. H. Davenport and R. H. Powell, ORNL-CF-52-1-93, Jan. 15, 1952 (classified).
26. W. B. Harrison, Oak Ridge Nat. Lab., ORNL-156, Part 12, pp 7, 8, Oct 1, 1948 (classified).
27. N. E. Dorsey, *Properties of Ordinary Water Substances*, Reinhold Publishing Company, New York, 1940, p 577.

28. I. Kirshenbaum, Physical Properties of Heavy Water, Columbia University, AECD-1991.
29. J. D. Roarty, S. I. Kaplan, W. D. Powers, and R. F. Redmond, Oak Ridge Nat. Lab., ORNL-52-3-253, Mar. 10, 1952 (classified).
30. M. S. Katz, Metallurgical Lab., University of Chicago, CC-1744, June 17, 1944 (classified).
31. R. Kunin, Carbide and Carbon Chemicals Company, A-3255, May 8, 1945 (classified).
32. W. L. Marshall, J. S. Gill, and C. H. Secoy, Oak Ridge Nat. Lab., ORNL-795, Oct. 30, 1950, pp 22-28 (classified).
33. G. R. Dean, Metallurgical Lab., University of Chicago, CC-1536 (A-2211), Apr. 15, 1944, p 10 (classified).
34. G. R. Dean, Metallurgical Lab., University of Chicago, CC-2092, Sept. 23, 1944, p 5 (classified).
35. C. E. Winters, Oak Ridge Nat. Lab., ORNL-826 (classified).
36. J. S. Johnson and K. A. Kraus, private communication; to appear in future ORNL Chemistry Division Quarterly Progress Report (classified).
37. Wacker and Cheney, Jour. Res. Nat. Bur. Standards 39, 1947, pp 317-320.

URANYL NITRATE SYSTEMS

38. M. de Forcrand, The Dehydration and Decomposition of the Hydrates and Uranyl Nitrate, the Formation of the Monohydrate Compt. rend. 156, 1913, pp 1044-1048 and 1207.
39. Gmelin, Handbuch der Anorganische Chemie, Vol. 55, 8th ed., Berlin, Verlag Chemie, J.M.B.H., 1936.
40. Project Handbook, CL-697, Vol. I, Chap. II C, Metallurgical Project, University of Chicago, May 1945, pp 47-52 (classified).
41. M. de Forcrand, Am. chim. 3, No. 9, 1915, pp 5-48.
42. W. L. Marshall, Oak Ridge Nat. Lab., ORNL-499, Dec. 6, 1949 (classified).
43. W. L. Marshall, J. S. Gill, and C. H. Secoy, The Uranyl Nitrate-Water System Above 60°C, Jour. Am. Chem. Soc. 73, 1950, p 1867.
44. F. E. E. Germann, A. New Hydrate of Uranyl Nitrate, Jour. Am. Chem. Soc. 44, 1922, p 1466.
45. R. M. Bidwell et al, Los Alamos Scientific Lab., CMR-10-210, Dec. 1951 (classified).
46. R. M. Bidwell, B. J. Thamer, and R. P. Hammond, private communication, Los Alamos Scientific Lab., 1952 (classified).
47. W. L. Marshall, J. S. Gill, and C. H. Secoy, Oak Ridge Nat. Lab., ORNL-1053, 1951 (classified).
48. R. Jenkins, H. A. C. McKay, and A. R. Mathieson, Atomic Energy Research Establishment, AERE C/R 364, June 1949 (classified).
49. W. E. Grant, W. J. Darch, S. T. Bowden, and W. J. Jones, Jour. Phys. & Colloid Chem. 52, 1948, p 1227.
50. A. F. Kapustinskii and L. I. Liplina, Doklady Akad. Nauk. S. S. R. 62, 1948, pp 485-488 (see C. A. 43, 1242g).
51. W. L. Kay and B. F. Faris, Specific Gravity of Certain $\text{UO}_2(\text{NO}_3)_2 \cdot 6\text{H}_2\text{O}$ Solutions, Hanford Works, (H) CN-3181 S-C (SE-PC-34), May 18, 1945.
52. L. Gomez, An. Espanol 17, 1919, p 45.
53. W. Oechsmier de Coninck, Compt rend. 131, 1900, p 1219; Bull. soc. Chim. France, 4, No. 17, 1915, p 422.
54. A. Vasiliev, Jour. Russ. Phys. Chem. Soc. 42, 1910, p 570; Jour. Russ. Ges. [Chem.] 43, 1911, p 1184.
55. A. Bromer, Ber. Wien Akad. 110, 11a, 1901, p 943.
56. Becquerel, Ann. chim. et phys. 12, No. 5, 1877.
57. International Critical Tables, McGraw-Hill Book Company, Inc., 1923-1936.
58. Landolt-Bornstein, Physikalisch-Chemische Tabellen, 5th ed., Julius Springer, Berlin, 1923; 2nd part of 3rd Supplement, 1936.
59. J. W. Mellor, A Comprehensive Treatise on Inorganic and Theoretical Chemistry, Vol. XII, Longmans, Green & Co., Inc., New York, 1932.
60. E. H. Turk and C. M. Olson, Hanford Works, CN-3170 (SE-PC-14), Apr. 10, 1945 (classified).
61. C. A. Kraus, Brown University, A-360, NRCC-L, May 26, 1942 (classified).
62. A. Colani, Bull. soc. chim. France, 4, 39, 1926, p 1243.
63. F. Clagget, Hanford Works, HW-18406, July 24, 1950 (classified).
64. Coulter, Pitzer, and Latimer, Jour. Am. Chem. Soc. 62, 1940, pp 2845-2851.
65. C. Dittrich, Z. physik. Chem. 29, 1899, p 487.
66. W. Oechsmier de Coninck, Bl. Acad. Belg., 1901, p 222.
67. M. Lister, Canadian Atomic Energy Project Report No. MX-234, 1946.
68. L. I. Katzin, D. M. Simon, and J. R. Ferraro, Jour. Am. Chem. Soc. 74, 1952, pp 1191-1194.
69. J. Aloy, Compt. rend. 122, 1896, p 1541.
70. M. Markatos, Compt. rend. 155, 1912, p 210.
71. Germann and Frey, Jour. Coll. Wyo. Acad. Sci., 1(1), 1929, p 54.
72. F. R. Bichowsky and F. D. Rossini, Thermochemistry of Chemical Substances, Reinhold Publishing Corp., New York, 1936, p 99.

URANYL CARBONATE SYSTEMS

73. P. D. Miller, H. A. Pray, and H. P. Munger, The Preparation and Properties of Uranyl Carbonate, Battelle Memorial Institute, AECD-2740, Aug. 1949.
74. C. A. Blake, R. S. Lowrie, D. G. Hill, and K. B. Brown, Studies in the Carbonate-Uranium System, Oak Ridge Nat. Lab., Y-673, AECD-3280, Dec. 1950.
75. W. E. Bunce, N. H. Furman, and R. J. Mundy, The Solubility of Sodium Uranyl Carbonate in Water and in Solutions of Various Salts, Princeton University, M-4238, Revised May 1947.
76. R. Bersohn and E. L. Brady, A Chemical Study of Hexavalent Uranium Compounds in Sodium Hydroxide, Sodium Carbonate, and Sodium Bicarbonate Solutions, Monsanto Chemical Works, MonC-109, Mar. 1, 1946.
77. R. J. Mundy and W. E. Bunce, Madison Square Area, Princeton Analytical Lab., A-2904, June 1945 (classified).
78. C. A. Blake, R. S. Lowrie, K. B. Brown, and D. G. Hill, Oak Ridge Nat. Lab., Y-794, Aug. 1951 (classified).
79. J. A. Hedvall, Contribution to the Knowledge of Complex Uranyl Carbonates, Z. anorg. u. allgem. Chem. 146, 1925, pp 225-229.
80. M. Bachelet et al, The Preparation and Properties of Uranyl Carbonates, Bull. soc. chim., France, 19, 1952, pp 55-60, 565-569.

81. K. B. Brown et al, Oak Ridge Nat. Lab., ORNL-1220, Jan. 25, 1952 (classified).
82. C. A. Blake and R. S. Lowrie, Oak Ridge Nat. Lab., Y-823, 1951 (classified).
83. Warren C. Johnson, Clinton Lab., MonN-2 (classified).
84. Warren C. Johnson, Clinton Lab., MonN-26 (classified).
85. Warren C. Johnson, Clinton Lab., MonN-15 (classified).
86. J. W. Boyle, TID-272 (classified).
87. J. R. Coe and E. H. Taylor, Clinton Lab., MonN-311 (classified).
88. Joseph Kennedy, Los Alamos Scientific Lab., La-1017, June 1947 (classified).

URANYL PHOSPHATE SYSTEMS

89. André Chretien and Jean Kraft, Uranyl Orthophosphates, *Bull. soc. chim.*, [5]5, 1938, pp 372-385.
90. Heinrich Glasner, Alkali Uranyl Phosphites and Pyrophosphates, *Z. anorg. u. allgem. Chem.* 153, 1926, pp 130-134.
91. R. M. Bidwell, B. J. Thamer, and R. P. Hammond, private communication, Los Alamos Scientific Lab., 1952 (classified).
92. E. Montignie, Uranyl Phosphates, *Bull. soc. chim.*, [5]4, 1937, pp 112-114.

PLUTONIUM SALT SOLUTIONS

93. Charles Allen Thomas, editor, MUC-JCW-223, Dec. 1944 (classified).

AQUEOUS FISSION-PRODUCT SYSTEMS

94. A. Seidell, Solubilities of Inorganic and Metal Organic Compounds, Vol. I, Third Edition, D. Van Nostrand Company, Inc., 1940.
95. A. Seidell and W. F. Linke, Solubilities of Inorganic and Organic Compounds, Supplement to the Third Edition, D. Van Nostrand Company, 1952.
96. M. H. Lietzke and R. W. Stoughton, Oak Ridge Nat. Lab., ORNL-970, Mar. 13, 1951 (classified).
97. B. Zemel, Oak Ridge Nat. Lab., ORNL-990, May 18, 1951, pp 105-106 (classified).
98. E. V. Jones and W. L. Marshall, Oak Ridge Nat. Lab., ORNL-1221, Mar. 13, 1952, pp 99-103 (classified).
99. W. Muthmann and H. R8lig, *Ber.* 31, 1898, p 1728.
100. Earl of Berkeley, *Trans. Roy. Soc.*, (London) 203A, 1904, p 210.
101. B. Zemel, Oak Ridge Nat. Lab., ORNL-1121, Dec. 27, 1951, pp 166-170 (classified).
102. E. V. Jones and W. L. Marshall, Oak Ridge Nat. Lab., ORNL-1280, June 27, 1952, pp 177-180 (classified).
103. J. Koppel, *Z. anorg. Chem.* 41, 1904, p 377.
104. M. H. Lietzke and B. Zemel, Oak Ridge Nat. Lab., ORNL-990, Jan. 30, 1951, pp 251-260 (classified).
105. H. S. Booth and R. M. Bidwell, *Jour. Am. Chem. Soc.* 72, 1950, pp 2567-2575.
106. E. V. Jones and W. L. Marshall, Oak Ridge Nat. Lab., ORNL-1318, Sept. 3, 1952, pp 142-143 (classified).
107. B. Zemel, Oak Ridge Nat. Lab., ORNL-1057, Oct. 10, 1951, pp 117-118 (classified).
108. A. Benrath and C. Thonnesen, *Z. anorg. u. allgem. Chem.* 203, 1932, 405-416.
109. A. Benrath, F. Gjedebø, B. Schiffrs, and H. Wunderlich, Solubility of Salts and Salt Mixtures in Water at Temperatures Above 100°, *Z. anorg. u. allgem. Chem.* 231, 1937, p 285.
110. A. Benrath, *Z. anorg. u. allgem. Chem.* 247, 1941, pp 147-160.
111. J. S. Gill and W. L. Marshall, Oak Ridge Nat. Lab., ORNL-1280, June 27, 1952, pp 175-176 (classified).
112. O. E. Myers and M. H. Lietzke, Oak Ridge Nat. Lab., ORNL-990, May 18, 1951, pp 108-115 (classified).
113. T. P. Kohman, University of Chicago, Metallurgical Project, CN-522 (classified).
114. T. P. Kohman and A. Turkevich, Weights of Fission Products in Pile Material, Report for Month Ending November 10, 1943, Metallurgical Project, University of Chicago, CN-1044.
115. E. L. Brady and A. Turkevich, Project Handbook, CL-697, Vol. II, Chap. III, Sect. D (classified).
116. M. A. Greenfield, North American Aviation, Inc., NAA-SR-6, Nov. 1, 1947 (classified).
117. H. F. Hunter and N. E. Ballou, Simultaneous Slow Neutron Fission of U-235 Atoms. I. Individual and Total Rates of Decay of the Fission Products, Naval Radiological Defense Lab., ADC-65, Feb. 24, 1949.
118. J. Halperin and R. W. Stoughton, Oak Ridge Nat. Lab., ORNL-1368, Sept. 29, 1952 (classified).
119. F. J. Keneshea, Jr. and A. M. Saul, Contribution by Chemical Element to the Total Beta Activity of Fission Products, North American Aviation, Inc., NAA-SR-187, June 13, 1952 (classified).
120. J. K. Thornton and W. J. Houghton, North American Aviation, Inc., NAA-SR-45, Sept. 1, 1950 (classified).
121. K. Way and E. P. Wigner, The Rate of Decay of Fission Products, *Phys. Rev.* 73, 1948, p 1318.
122. Radiochemical Studies: The Fission Products, Books I, II, III, C. D. Coryell and N. Sugarman, editors, National Nuclear Energy Series Vol. IV, 9, McGraw-Hill Book Co., Inc., New York, 1951, p 229 Parts I-VIII.

THORIUM SOLUTIONS

123. P. Misciatelli, *Gazz chim. ital.* 60, 1930, p 833.
124. Charles C. Templeton, The System Thorium Nitrate-Water, 20° to 160°C, Michigan University, AECU-1721, Report Number 1, Aug. 1, 1950.
125. W. L. Marshall, J. S. Gill, and C. H. Secoy, The $\text{Th}(\text{NO}_3)_4\text{-H}_2\text{O}$ System Above 20°C, *Jour. Am. Chem. Soc.* 73, 1951, p 4991.
126. W. L. Marshall, J. S. Gill, and C. H. Secoy, Oak Ridge Nat. Lab., ORNL-925, Jan. 30, 1951, pp 279-290 (classified).
127. R. Schaal and J. Faucherre, *Bull. soc. chim. France*, 14, 1947, pp 927-932.
128. A. C. Neish and J. W. Burns, *Can. Chem. Met.* 5, 1921, p 69.
129. L. Koppel and H. Holtkamp, *Zeit anorg. Chem.* 67, 1910, p 290.
130. R. Fricke, *Z. Elektrochem.* 35, 1929, pp 631-640.
131. R. Fricke and L. Havestadt, *Z. Elektrochem.* 33, 1927, pp 441-455.

132. R. A. Robinson and B. J. Levien, *Trans. Proc. Roy. Soc., New Zealand* 76, 1947, pp 295-299.
133. R. A. Robinson and R. H. Stokes, *Trans. Faraday Soc.* 45, 1949, pp 612-624.

SELECTED READING LIST

DENSITY OF HEAVY WATER, Tsing-lein Chang and Lu-Ho Tung, *Nature* 163, (D_2O : 0° – 100°) 1949, p 737.

DIE KRITISCHEN DATEN VON LEICHTEM UND SCHWEREM WASSER UND IHR DICHT-TEMPERATUR-DIAGRAMM, Riesenfeld und Chang, *Zeitschrift für Physikalische Chemie*, B30:61 (D_2O —near critical), 1935.

THERMODYNAMIC PROPERTIES OF STEAM, Keenan and Keyes, John Wiley and Sons, 1st ed. (H_2O : 0° – $374^{\circ}C$), 1936.

CHAPTER 4.4

Properties of Aqueous Slurry Systems

URANIUM SLURRIES ($\text{UO}_3\text{-H}_2\text{O}$, $\text{U}_3\text{O}_8\text{-H}_2\text{O}$, $\text{UO}_2\text{-H}_2\text{O}$ - $\text{U}_2\text{O}_5\text{-H}_2\text{O}$)

INTRODUCTION (A. S. Kitzes)

The selection of a fuel for a slurry reactor depends upon such factors as thermal and radiation stability, corrosion and erosion characteristics, neutron economy, pumping characteristics, and stability to the products of reactor operation.

Uranium oxide slurry reactors are being considered because they offer better neutron economy¹ than solutions of most uranium salts and because the fuel is more stable chemically and less corrosive than most uranium salts. However, processing of the fuel and control of the reactor are two factors which may, in the long run, outweigh the advantages gained by the use of slurries.

The great amount of experimental work performed with uranium oxide slurries, especially in the early days of the Manhattan Project, prohibits a comprehensive review of the subject. However, reference is made to the early investigations to help those about to start an experimental study on slurries. An excellent review of early project work is given by Kirshenbaum.²

OXIDE STABILITY

As aqueous slurries, the oxides of uranium (UO_3 , U_3O_8 , U_2O_5 , and UO_2) appear to possess to an appreciable extent most of the characteristics required of a reactor fuel. Many experiments have been performed to determine which of these oxides would be the most stable under simulated reactor conditions.^{3,4} Heating UO_2 and U_3O_8 slurries in a stainless-steel bomb under approximately equal pressures of hydrogen and oxygen at 250°C resulted in almost complete oxidation to the hexavalent state.⁵ In the case of uranium trioxide, however, only slight reduction occurred when the slurry was heated in the presence of a large excess of hydrogen. Data are reported in Tables 4.4.1, 4.4.2, and 4.4.3.

No data are available which indicate the stability of U_2O_5 slurries to oxidation and reduction at elevated temperatures. As a first approximation, it would be safe to assume that these slurries behave as U_3O_8 suspensions. Since it was concluded that uranium trioxide was the most stable at elevated temperatures in aqueous reactor systems, most work to date has been carried out with uranium trioxide.

STABILITY OF OXIDE UNDER DYNAMIC CONDITIONS (A. S. KITZES)

Uranium trioxide, so far the only oxide that has been circulated at elevated temperatures, is chemically stable as the monohydrate when circulated in water at 250°C .⁶ How-

¹References appear at end of chapter.

Table 4.4.1 — Oxidation of UO_2 Slurries when Heated under Varying Partial Pressures of Hydrogen and Oxygen

Heating conditions		Gas pressure		Uranium oxidized, %
Temp., °C	Time, hr	H_2 , psi	O_2 , psi	
200	48	63.5	31.8	64.9
250	16		202	74.5
	16		378	82.2
	24	70	61.5	78.4
	24	70	175	91.4

Table 4.4.2 — Oxidation of U_3O_8 Slurries when Heated for 24 Hr under Varying Partial Pressures of Hydrogen and Oxygen

Temp., °C	Gas pressure		Uranium oxidized, %
	H_2 , psi	O_2 , psi	
150	51.8	25.9	63.2
170	59.5	29.8	71.7
200	63.5	31.8	90.1
225	67	33.5	92.6
250	...	35	88.0
	175	35	85.1
	70	17.5	75.2
	70	175	96.8

Table 4.4.3 — Reduction of UO_3 Slurries at 250°C under Varying Partial Pressures of Hydrogen and Oxygen

Heating time, hr	Gas pressure		Uranium reduced, %
	H_2 , psi	O_2 , psi	
20	263	26.3	0.5
	378	...	1.39
24	70	35	0
68	527	26.3	0.4

ever, the rod-type $\text{UO}_3 \cdot \text{H}_2\text{O}$ when circulated at 20 ft/sec at 250°C does undergo allotropic modification and abrasion of the rods. The rods, which are originally 2 to $3\ \mu$ in diameter and 15 to $20\ \mu$ long, become either spherical or ellipsoidal with essentially no change in diameter. The fragments which are abraded from the rods also become spherical.

When uranium trioxide rods are pulverized and digested at 250°C , they are converted to platelets (delta form). A partial conversion, probably resulting from increased solubility of the extremely fine oxide particles, was observed when the rods were circulated at 250°C for at least 100 hr. No conversion occurs at 150°C although the rods are abraded into oval shapes at this temperature.

CRYSTALLOGRAPHY (J. O. BLOMEKE AND A. S. KITZES)

Uranium trioxide is stable in water at 250°C as the monohydrate, which was found to exist in three allotropic modifications depending on its mode of preparation and treatment.⁷ Uranium peroxide on heating at 300°C in air yields anhydrous uranium trioxide, which when heated in water at 185° to 300°C is converted to uranium trioxide monohydrate in the form of rods.^{3,7} Decomposition of uranyl nitrate at 300° to 400°C yields uranium trioxide, which on hydration at 185° to 300°C produces crystals having the form of platelets. Pulverized uranium trioxide rods digested at 200° to 250°C are converted to the platelet form, whereas pulverized uranium trioxide platelets digested at 150° to 200°C are transformed into rods. In the presence of several hundred ppm of uranyl ion, both the rods and the platelets are converted to a third modification, crystals resembling truncated bipyramids.

The rods are normally 1 to $5\ \mu$ in diameter and 10 to $30\ \mu$ long. The platelets are 6 to $50\ \mu$ along each edge and about $1\ \mu$ thick, while the bipyramids are several microns along each edge. X-ray diffraction studies show the rods, platelets, and bipyramids to have an orthorhombic structure. Since the platelets are formed by digestion of pulverized or fragmented rods, it has been concluded that the UO_3 monohydrate most likely to be stable in an aqueous reactor fuel at 250°C will be that in the form of the small platelet crystals.

U_2O_5 , which has been surface treated with $0.5\text{M NaH}_2\text{PO}_4$,⁸ does not react with water or undergo allomorphic changes when digested at 250°C in pyrex glass capsules. U_2O_5 slurries are discussed later under "Stable Slurries."

UO_3 SLURRY CHARACTERISTICS (J. O. BLOMEKE)

Very encouraging slurries have been prepared of both the rods and the platelets. On the other hand, the bipyramids, because of their size, require rather violent agitation to keep them in suspension and are regarded as too large to be of much interest as a reactor fuel.

The characteristics of a typical uranium trioxide slurry which has been heated at 250°C in stainless steel for several days are presented in Table 4.4.4. The viscosity at 30°C (1.2 cp) is about 50 percent greater than that of water at the same temperature. The significance of the impurities in the indicated concentration range has not been completely investigated; however, it is believed that they might play an important part in such factors as chemical stability, dispersibility, and corrosion. The settling rate represented essentially complete settling. The soluble uranium was present in a concentration (4 ppm) which is about the solubility of pure $\text{UO}_3 \cdot \text{H}_2\text{O}$ in water at room temperature.

PARTICLE-SIZE GROWTH (L. E. MORSE)

Particle-size growth studies on $\text{UO}_3 \cdot \text{H}_2\text{O}$ rods and platelets heated in water at 250°C were made⁹ using a concentration of 250 gm U/liter. Particle-size analyses were made by gravitational and centrifugal sedimentation. The experimental details and results are given in Tables 4.4.5 and 4.4.6. The particle size of both species of oxide increased very rapidly in the first 2 hr of heating, but growth decreased markedly when the heating was extended to 24 hr. After heating for 24 hr, the average particle size was $3.9\ \mu$ for rods and $7.8\ \mu$ for platelets.

Table 4.4.4—Characteristics of Typical Uranium Trioxide Slurry
(250 gm U/l as UO_3 - H_2O Platelets)

Surface area* of solids	0.5 sq m/gm
Viscosity† at 30°C	1.2 cp
Impurities	
Fe	30 ppm
Ni	15 ppm
Cr	10 ppm
NO_3	30 ppm
pH	6.5
Settling rate, vol. settled solid/total vol.	0.56 in 60 min
Soluble uranium	4 ppm

* Measured by nitrogen adsorption

† Measured with capillary tube viscosimeter

Specifically, the values given in Tables 4.4.5 and 4.4.6 should be considered as applying to the actual oxides used in the experiment. Generally, the growth process can be broken down into two parts. When small particles are present, the growth process is very rapid, since combinations of particles are possible by a collision process leading to the dissipation of the high surface energies of the small particles. However, as the particles grow, this factor becomes less important, and the rate of growth is governed by such factors as solubility and the rates of diffusion and deposition of solute. These latter processes govern the ultimate sizes attained by the particles. Tables 4.4.5 and 4.4.6 show the range of particle size as well as the soluble uranium.

STABLE SLURRIES

The criterion for stability of a solid-liquid system is difficult to establish, since the required conditions for satisfactory reactor operation are not known. What is desired is a suspension that is sufficiently homogeneous within the reactor core to ensure adequate control and that can be pumped or otherwise handled like a true solution. There are two divergent approaches to this problem: (1) a solid-liquid system that will not settle out on standing for an arbitrary length of time, and (2) a slurry that is homogeneous only under dynamic flow conditions but capable of being readily redispersed if it once settles.

Bentonite-stabilized Slurries (L. E. Morse and A. S. Kitzes)

Preparation of stable slurries has been directed mainly toward those suitable for use in reactors operated at 250°C. Such a slurry is considered satisfactory if it does not settle to less than 50 percent of its original volume in 24 to 28 hr and if it can readily be resuspended after being heated at 250°C and allowed to cool.

UO_3 slurries containing 250 gm of uranium per liter of slurry cannot be stabilized with bentonite, because the viscosity increases so rapidly that it is impossible to incorporate the required amount of oxide.

Anhydrous UO_3 , prepared by the thermal decomposition of uranyl peroxide at 250°C, forms stable thixotropic slurries at room temperatures when suspended in water at concentrations of 40 gm of uranium per liter of slurry.¹⁰ However, autoclaving at 250°C for 1 hr makes the suspension unstable; the oxide settles very rapidly at room temperatures. The ratio of settled-solids volume to total volume is found to be 0.2.

Table 4.4.5 — Particle-size Growth in $\text{UO}_3 \cdot \text{H}_2\text{O}$ Rods on Heating*

Heating conditions	Particle size, μ			Soluble uranium in supernate, mg/ml
	Average	2.5 wt-% less than	10 wt-% greater than	
Unheated slurry	0.5	0.3	1.3	...
Heated to 160°C and allowed to cool	2.6	1.0	3.9	0.134
Heated to 250°C and allowed to cool	2.3	1.6	2.7	.096
Heated at 250°C for 1 hr	3.0	1.6	6.1	.135
2 hr	3.1	1.9	4.9	.210
4 hr	3.2	1.5	5.3	.240
24 hr	3.9	1.8	5.5	.200

* Conditions: 250 gm U/l; heated in sealed quartz tubes; all particle sizes are equivalent spherical diameters

Table 4.4.6 — Particle-size Growth in Slurries of $\text{UO}_3 \cdot \text{H}_2\text{O}$ (Platelets)*

Heating conditions	Particle size, μ			Soluble uranium in supernate, mg/ml
	Average	2.5 wt-% less than	10 wt-% greater than	
Unheated slurry	1.8	0.4
Heated to 160°C and allowed to cool	2.8	.7	7.4	0.250
Heated to 250°C and allowed to cool	4.2	1.6	10.3	.310
Heated at 250°C for 1 hr	4.8	1.3	10.4	.280
2 hr	6.2	2.2	13.8	...
4 hr	6.0	2.5	13.3	0.468
24 hr	7.8	5.0	14.6	.625

* Conditions: 250 gm U/l; heated in sealed quartz tubes; all particle sizes are equivalent spherical diameters

Bentonite, an aluminosilicate clay having cation exchange properties and an acceptably low neutron cross section, can be used to enhance the stability of uranium oxide slurries at 250°C. By converting the bentonite to the hydrogen form by electrodialysis, acid elution, or ion-exchange resins and by using only those particles which are less than 25 μ , the stabilizing power of bentonite is increased many fold. When this fractionated hydrogen bentonite is used, slurries containing 40 gm of uranium (as anhydrous UO_3) and 13 gm of stabilizer per liter are stable after heating for 330 hr at 250°C.¹ The pH of these slurries is approximately 4.

Room temperature stability of material heated at 250°C for time T can be represented by the following empirical expression:

$$\frac{V_s}{V_t} = 0.97 - 0.019 T \quad (1)$$

where: V_s = volume occupied by solids after settling 24 hr
 V_t = total volume of slurry
 T = days autoclaving at 250°C

Reactor radiations do not affect the sedimentation characteristics of uranium oxide slurries stabilized by fractionated hydrogen bentonite. Slurries containing 40 gm of uranium (as UO_3) and 13 gm of stabilizer per liter have been irradiated in the ORNL graphite reactor for one week at 250°C in a thermal-neutron flux of 5×10^{11} neutrons/(cm²)(sec) with no apparent damage.

Stable U_2O_5 Slurries

Although a series of stable binary uranium oxide slurries containing no stabilizing agent has been prepared, the U_2O_5 slurries present the best possibility as a reactor fuel. U_2O_5 particles approximately 60 mμ in diameter, prepared by spray-burning uranyl nitrate dissolved in acetone, form stable slurries when treated with 0.5M NaH_2PO_4 .⁸ Samples heated at 250°C in pyrex glass tubing for 5 hr showed a slight settling; however, the solids are easily redispersed by mild shaking, and there is no clear supernatant liquid. Properties of this slurry are shown in Table 4.4.7.

Table 4.4.7 — Characteristics of Typical U_2O_5 Slurry

Surface area of solids	13.2 m ² /gm
Viscosity* at 25°C	1.0 cp
pH	10.0
Color	Gray-black
Specific conductance at 25°C	2.6×10^{-5} ohm/cm
Stability of slurry after heating at 250°C	Slight settling

* Viscosity determined with Brookfield Synchroelectric viscometer.

RADIATION STABILITY (J. P. McBRIDE)

Both chemical and physical changes may be expected in a uranium oxide slurry during its use as a reactor fuel. The purpose of radiation stability studies is to determine the extent of any such effects.

At present, information on this subject is essentially limited to three in-reactor studies using $UO_3 \cdot H_2O$ rods at a concentration of 250 gm/l.^{11,12} These experiments have demonstrated that under reactor irradiation some reduction of the uranium occurs along with considerable fragmentation but without significant growth of the slurry particles. The ultimate fate of the slurry or the final crystal form resulting from these processes has not yet been determined. No valid conclusions can yet be drawn with regard to the effect of radiation on the dispersibility or caking characteristics of the slurry. Gas production, while significant, was considerably less than in a solution of the same uranium concentration. Details of the irradiation experiments are summarized in Table 4.4.8. It should be

noted that the slurries used in these studies contained small amounts of nitrogen impurity (approximately 50 to 100 ppm), presumably as $\text{UO}_2(\text{NO}_3)_2$. To what extent the observed effects are influenced by the presence of this impurity is of course unknown. Presumably, its release from the slurry particles accounts for the increase in soluble uranium whose presence in the solution may influence some of the phenomena which occur under irradiation, such as gas recombination or the conversion of rods to platelets.

 Table 4.4.8 — Summary of the Effects of Reactor Irradiation on $\text{UO}_3 \cdot \text{H}_2\text{O}$ Slurries

Observation	Typical slurry properties	Irradiation conditions and effects		
		Natural uranium	90% enriched uranium	90% enriched uranium
Neutron flux, $n/(\text{cm}^2)(\text{sec})$...	7×10^{11}	$2-3 \times 10^{11}$	$4-5 \times 10^{11}$
Irradiation time, hr	...	136	250	144
Temperature, °C	...	250	250	300
Soluble uranium in supernate, mg/ml	<0.020	0.080	0.445	0.180
U^{+4} in slurry, %	<0.1	11	3	5
Fluid pH	6.7	5.6	5.9	5.3
Crystal habit	Rods	Rods (fragments)	Rods (fragments), platelets	Rods (fragments), platelets
Steady-state gas pressure excluding steam, psia	...	330	3000	1550
Gas composition, %		
H_2			64.8	65
O_2			32.4	30
CO_2			1.3	1
Inerts			1.5	4
Approximate G value*	0.5
Fission products in supernate, %	...	1	1	1

* G = molecules H_2O decomposed/100 ev energy absorbed

THERMAL PROPERTIES (A. S. KITZES)

Convective heat transfer involving turbulent uranium trioxide slurries can be predicted by the relations appropriate to normal fluids, since the turbulent viscosity of these slurries appears to be independent of the Reynolds modulus.

Slurries containing as much as 200 gm of uranium as trioxide per liter have been pumped through a stainless-steel loop at a velocity of 10.5 ft/sec with a centrifugal pump.¹³ Results of periodic heat-transfer measurements at 150°C indicate that the over-all heat-transfer coefficient is independent of the oxide concentration in the slurry and approximates within the experimental error the value obtained when pumping distilled water through the loop. The heat-transfer coefficient did not vary with time, indicating that film did not form on the heat-transfer surfaces.

VISCOSITY AND DENSITY

For proper engineering design of systems requiring the pumping of slurries, the viscosity, density, and other related physical properties of the slurries must be known as a function not only of the concentration of uranium but also of particle size.

Viscosity

The viscosity of slurries of $\text{UO}_3 \cdot \text{H}_2\text{O}$ and H_2O can be ascertained over a wide range of temperatures by measuring the pressure drop required to give a desired flow rate of slurry through a given length of small-diameter tubing.¹⁴ The plasticity parameters shown for amorphous $\text{UO}_3 \cdot 2\text{H}_2\text{O}$ - H_2O in Table 4.4.9, can then be determined from a plot of the shear diagrams. The coefficient of rigidity may be defined by the equation:

$$\frac{\Delta P \times D \times X}{4L} = n \frac{8V}{gD} \quad (2)$$

Table 4.4.9 — Plasticity Parameters of Amorphous $\text{UO}_3 \cdot 2\text{H}_2\text{O}$ - H_2O Slurries

	Temperature, °C					
	40	70	80	100	120	140
Concentration, 290 gm/l						
Coefficient of rigidity (n), lb/(ft)(sec)		0.0023		0.0021	0.0018	0.0016
Yield stress (τ_y), lb/ft ²		.175		.146	.065	.065
Concentration, 190 gm/l						
Coefficient of rigidity (n), lb/(ft)(sec)	0.0021		0.0018	0.0015	0.0011	
Yield stress (τ_y), lb/ft ²	.131		.101	.069	.030	

where: ΔP = pressure drop for given flow rate, lb/ft²

D = diameter of tube, ft

L = length of tube, ft

V = velocity of slurry, ft/sec

g = 32.2 (lb/lb force) (ft/sec²)

n = coefficient of rigidity = slope of curves

Apparent viscosities for $\text{UO}_3 \cdot \text{H}_2\text{O}$ - H_2O slurries can be calculated by using the parameters listed in Table 4.4.5 in the following equation:

$$\mu_c = n + \frac{D\tau_y}{6V} \quad (3)$$

where: μ_c = apparent viscosity

n = coefficient of rigidity, lb/(ft)(sec)

τ_y = yield stress, lb/ft²

D = diameter of pipe, ft

V = velocity, ft/sec

The viscosity of $\text{UO}_3 \cdot \text{H}_2\text{O}$ slurries as a function of temperature is shown in Fig. 4.4.1. The data indicate no difference in viscosity between slurries of gamma oxide (rods) and delta oxide (platelets) containing 250 gm U/l.

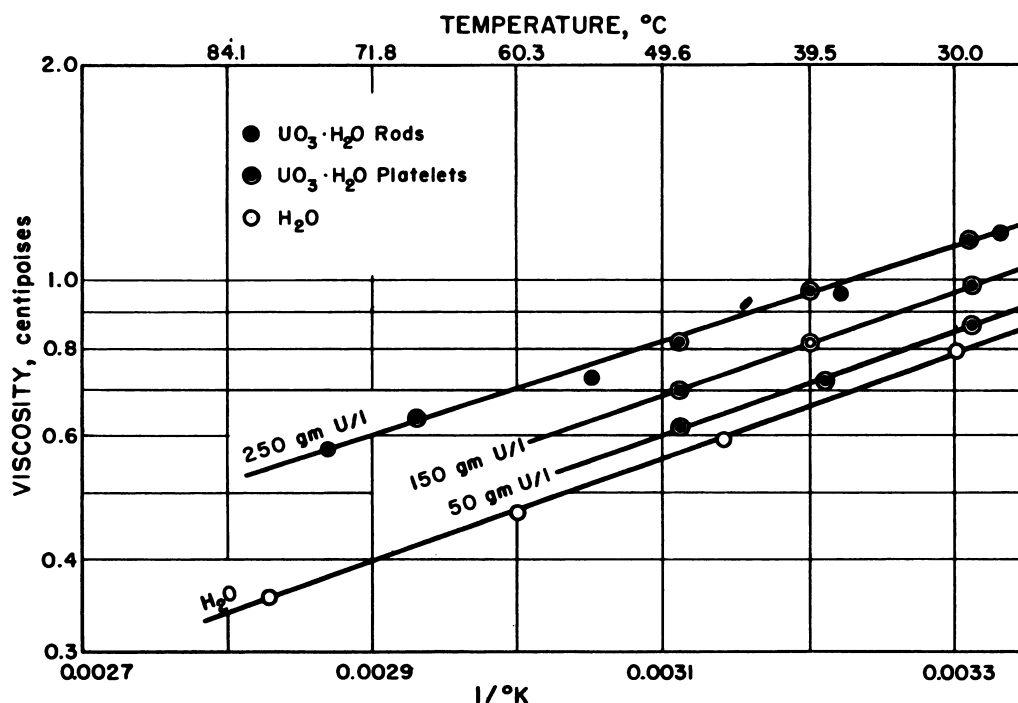


Fig. 4.4.1 — Viscosity of $\text{UO}_3 \cdot \text{H}_2\text{O}$ Slurries as a Function of Temperature.
Submitted by Oak Ridge National Laboratory, Nov. 25, 1952.

Plots of the fluidity (reciprocal of viscosity) vs concentration for fixed temperatures are shown in Fig. 4.4.2. The resulting isotherms when extrapolated to zero fluidity converge at a concentration of 890 gm U/l. This result is of interest since it appears to be related to the volume occupied by the solid phase of a settled slurry that has been heated at 250°C for 24 hr. Viscosity determinations⁹ were made by measuring the time required for a known volume of slurry to flow through a vertical tube of the proper dimensions. The pressure was fixed by the head of the suspension within the viscosimeter so that only the temperature and concentration could be varied for a given tube.

With stable suspensions, a Stoermer viscosimeter using a modified Babbitt and Caldwell cup can also be used to determine the plasticity parameters for slurries.¹⁵ A literature review on this subject as applied to uranium oxide slurries is given by Kirshenbaum.²

Values for the turbulent viscosity of uranium trioxide slurries can also be determined from pressure-drop data. This is done by finding the Reynolds number which corresponds to the measured friction factor for water and solving for viscosity, for given tube-diameter, and for density and velocity of the slurry. For slurries containing as much as 300 gm of uranium (as $\text{UO}_3 \cdot \text{H}_2\text{O}$) per liter, the turbulent viscosity appears to be independent of the Reynolds number as long as the slurry is in turbulent flow.

Density

The density of oxide slurries can be calculated using the following relation and assuming the density of dry oxide to be constant up to 250°C :

$$d_1 = V(d_2 - d_3) + d_3 \quad (4)$$

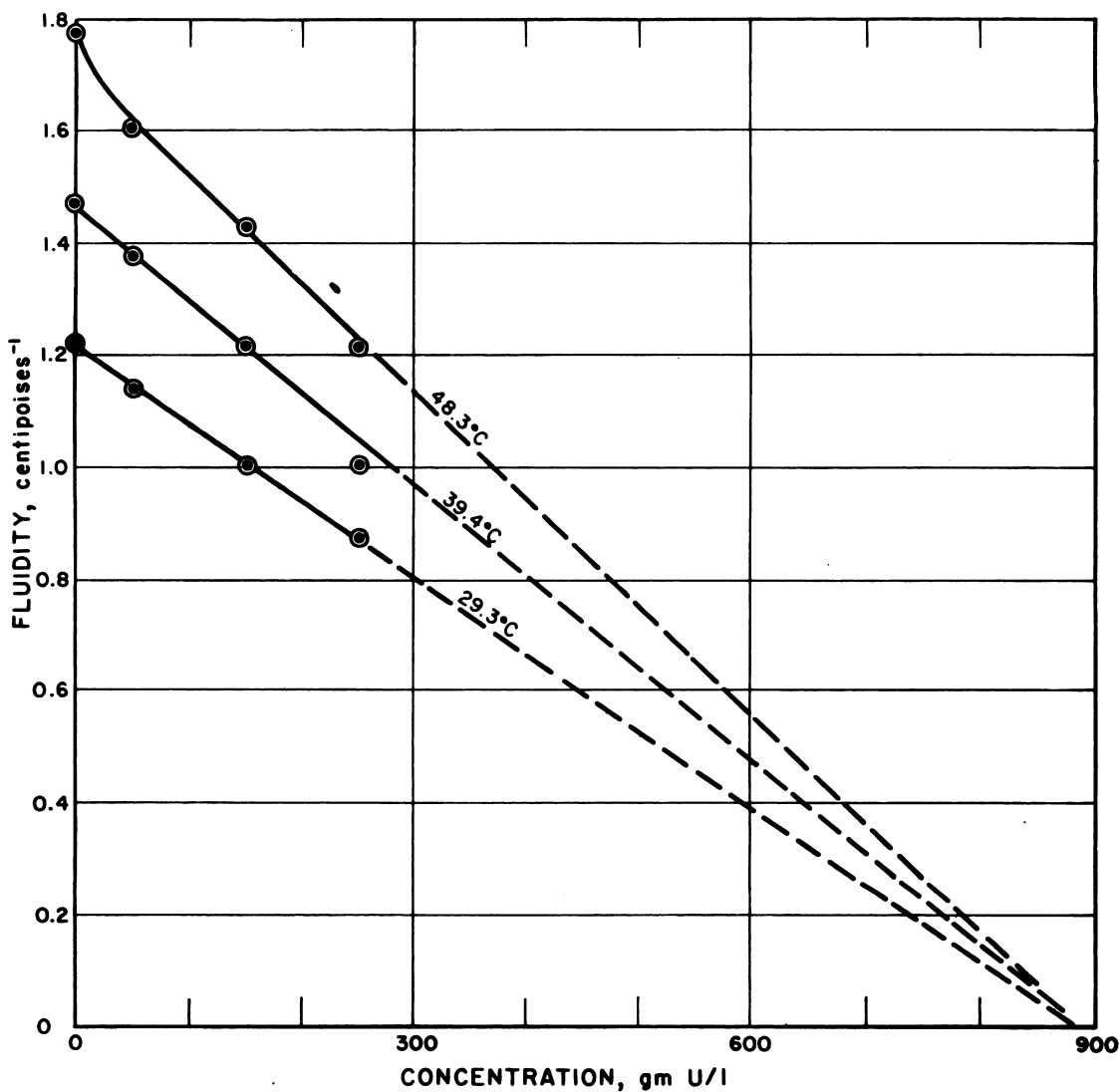


Fig. 4.4.2 — Fluidity of $\text{UO}_3 \cdot \text{H}_2\text{O}$ (Platelet) Slurries as a Function of Concentration. Submitted by Oak Ridge National Laboratory, Nov. 25, 1952.

where: d_1 = density of slurry, gm/cm^3
 d_2 = density of solids, gm/cm^3
 d_3 = density of water at temperature T , gm/cm^3
 V = volume fraction of solids in slurry

EROSION BEHAVIOR (A. S. KITZES)

The erosion of system components by circulating uranium trioxide slurries is not as serious as first believed. Results of many tests in which uranium trioxide slurries have been circulated under a variety of conditions indicate that (1) 18-8 stainless steels are not abraded (eroded) by these slurries and (2) the trioxides are much softer than the stainless steels.

Amorphous uranium trioxide monohydrate slurries have been circulated continuously by means of a fluid-bearing canned-rotor pump* (0.010-in. clearance between motor rotors and motor cans) at room temperature for approximately 1000 hr without detectable wear.¹⁶ Examination of the pump parts after disassembly showed no visible or measurable wear or corrosion. The oxide particles were, however, reduced in size.

Slurries, containing as much as 200 gm U/liter of water have been cycled between 150° and 110°C while being pumped with a centrifugal pump for more than 1000 hr at a maximum velocity of 26 ft/sec, which occurred in the throat of a venturi. Inspection of impeller, venturi, and various bends showed no visible signs of erosion or corrosion, although the particles were comminuted.

Examination of the pump impeller, orifice, and test samples of a loop in which $\text{UO}_3 \cdot \text{H}_2\text{O}$ was circulated at 250°C for 100 hr showed no apparent signs of corrosion or abrasion other than a shiny film.⁵ Maximum velocity in the loop was 70 ft/sec which occurred at the throat of a venturi. The particles, originally rods 2 to 3 μ in diameter by 15 to 30 μ long, were abraded into spheres or ovals 2 to 3 μ in diameter.

No erosion or wear was observed when a Stellite bearing and journal were lubricated with a 100-gm/l rod-type UO_3 slurry supplied by a small pump. The Stellite journal, 1.4995 in. in diameter, was rotated in a 1.502 in.-diameter bearing for 100 hr at 1750 rpm with a radial load of 20 psi.

Additional erosion data for various oxides against a variety of metals, including aluminum, stainless steel, cold-rolled steel, beryllium oxide, and lead, are given by Kirshenbaum.² The data were obtained essentially from laboratory testing units in which test specimens were rotated at varying speeds from 1750 to 3500 rpm in a slurry of UO_2 or U_3O_8 . According to the data, the rate of erosion depends markedly on:

- (1) Particle size of the oxide
- (2) Time
- (3) Concentration of solids in the slurry
- (4) Linear velocity at the eroding surface
- (5) Physical properties of the materials

Qualitatively, the rate of erosion of the materials tested decreased in the following order: Lead, aluminum, aluminum alloys, cold-rolled steel, stainless steel, and beryllium oxide. This order is in agreement with the one expected from a consideration of scratch hardness.

THORIUM SLURRIES (ThO_2 - H_2O)

(T. C. Runion and J. O. Blomeke)

Only a very limited amount of experimental work has been devoted to the development of aqueous thorium oxide slurries for use as breeding blankets. Contributions to this subject have been made by Hellman¹⁷ of the Manhattan Project and, more recently, by Runion¹⁸ of the Homogeneous Reactor Experiment at ORNL. The over-all objective of both programs was the development of an aqueous ThO_2 slurry containing 1000 gm Th/l. The principal requirements considered for these slurries were that they possess high fluidity concomitant with low pumping requirements and good heat transfer, low corrosivity and erosivity in the stainless steels, stability to heat and radiation, and low settling rates with easy dispersability. Hellman studied only unstable slurries using commercially available ThO_2 of questionable purity. Runion, using ThO_2 obtained by laboratory calcination of purified thorium salts, also prepared slurries stabilized with small amounts of bentonite (Montmorillonite clay).

*Described in ANP-65, p 170.

UNSTABLE ThO_2 SLURRIES

A theoretical consideration of the fluidity and settling rates of 1000-gm/l ThO_2 - H_2O suspensions indicates that particles approximately $1\ \mu$ in size should give a slurry which could be pumped easily without excessive erosion and yet possess very favorable settling characteristics. Starting with material covering a broad range of particle sizes, particles were fractionated by sedimentation and centrifugation into the following size ranges: 1 to $10\ \mu$, 0.1 to $1\ \mu$, 0.1 to $0.5\ \mu$, and $<0.1\ \mu$. Slurries of these fractions had the properties indicated in Table 4.4.10. Some agglomeration was observed in the slurries containing particles less than $1\ \mu$ in size, and slurries of particles of less than $0.5\ \mu$ exhibited thixotropy. Slurry No. 3 of Table 4.4.10 was reported to have been easily dispersible after having been allowed to stand at room temperature for one month.

Table 4.4.10— Properties of Unstable ThO_2 - H_2O Slurries
(Concentration, 1000 gm Th/l)

Slurry No.	Particle size range, μ	Settling rate	Viscosity	Dispersibility
1	1–10	10 cm/min	2 cp	Poor
2	0.1–1	1 cm/hr	2 cp	Good
3	0.1–0.5	0.5 cm/hr	Slightly thixotropic	Good
4	0.1	0	Thixotropic	...

Using 0.75 to 1.0 wt-% of fractionated bentonite, stable thorium slurries were prepared along the lines suggested by the preparation of uranium slurries. The amount of bentonite required for slurry stabilization varied directly with bentonite particle size. If bentonite particles less than $25\ \text{m}\mu$ in diameter were used, stable slurries containing 1000 gm of thorium per liter were obtained; nearly three times as much naturally occurring bentonite was required to produce the same stabilization. However, no appreciable advantage was realized by the use of particles of less than $1\ \mu$. By using a Brookfield Model LVF viscosimeter, a typical range of viscosities (10,000–2,000 cp) with varying shear rates was obtained. At lower viscosities, the slurries settled rapidly, and at higher values, stiff gels resulted.

The thermal stability of ThO_2 slurries was tested by heating the slurries at 250°C in quartz tubes for periods up to two weeks. Although no appreciable change in properties was observed in these tests, similar tests in stainless-steel autoclaves under gentle agitation resulted in deposition of bentonite on the walls of the container and failure of the slurry.

RADIATION STABILITY

No evidence of caking or instability was observed when a slurry was heated at 100°C for one week in the ORNL reactor at a neutron flux of 5×10^{11} .

CORROSION AND EROSION

To determine the corrosive-erosive behavior of circulating thorium oxide slurries, a preliminary experiment was made using a slurry containing 88 gm of thorium per liter cycled between 150° and 110°C for 100 hr. Results of this one run indicate that (1) thorium oxide slurries are erosive, and (2) the over-all heat-transfer coefficient decreases because thorium oxide is deposited on the heat-transfer surfaces. A need for further study of thorium oxide slurries flowing under a variety of conditions is therefore indicated.

REFERENCES

1. J. A. Lane et al, Oak Ridge Nat. Lab., ORNL-1096, Dec. 10, 1951, pp 26-46 (classified).
2. I. Kirshenbaum, United States Atomic Energy Commission, Tech. Inf. Serv., Oak Ridge, Tenn., NNES, III-4B, 1951 (classified).
3. D. Vier, Columbia University, A-1277, May 26, 1944 (classified).
4. D. M. Gillies, Some Studies of the Reaction of Uranium Oxides with Hydrogen, Oxygen, and Water, Columbia University, MDDC-64C, June 1946.
5. F. R. Bruce et al, Oak Ridge Nat. Lab., ORNL-1280, Mar. 15, 1952, pp 101-109 (classified).
6. A. S. Kitzes et al, Oak Ridge Nat. Lab., ORNL-1318, Mar. 15, 1952, pp 84-86 (classified).
7. F. R. Bruce et al, Oak Ridge Nat. Lab., ORNL-1221, Nov. 15, 1951, pp -128-132 (classified).
8. R. S. Hansen et al, Reactor Sci. Tech. 2, No. 1, Apr. 1952, pp 86-88 (classified).
9. F. R. Bruce et al, Oak Ridge Nat. Lab., ORNL-1318, July 1, 1952, pp 76-88 (classified).
10. L. E. Morse et al, Oak Ridge Nat. Lab., ORNL-1057, May 15, 1951, pp 131-133 (classified).
11. F. R. Bruce and J. O. Biomeke, Oak Ridge Nat. Lab., ORNL-CF No. 52-3-217 (classified).
12. F. R. Bruce and J. P. McBride, Oak Ridge Nat. Lab., ORNL-CF No. 52-7-111 (classified).
13. A. S. Kitzes et al, Oak Ridge Nat. Lab., ORNL-1221, Nov. 15, 1951, pp 133-134 (classified).
14. C. E. Lapple, Fluid and Particle Mechanics, University of Delaware Press, Newark, Dec. 1951, pp 115-133.
15. J. H. Perry, Chemical Engineer's Handbook, 3rd ed., p 387, McGraw-Hill Publishing Company, New York, 1950, p 387.
16. A. S. Kitzes et al, Oak Ridge Nat. Lab., ORNL-1280, Mar. 15, 1952, pp 84-86 (classified).
17. N. N. Hellman, United States Atomic Energy Commission, Tech. Inf. Serv., Oak Ridge, Tenn., NNES IV-17B, paper 3.20, 1952, CC-3056 (classified).
18. T. C. Runion, Thorium, Oak Ridge Nat. Lab., ORNL-925, pp 295-296 (classified); ORNL-990, pp 140-143 (classified); ORNL-1057, pp 123-127 (classified).

SELECTED READING LIST

THE CHEMISTRY OF URANIUM, Part I, J. J. Katz and E. Rabinowitch, NNES, VIII-5, McGraw-Hill Book Company, Inc., New York, 1951,

CHAPTER 4.5

Properties of Aqueous Moderators

J. W. Boyle

RADIATION INDUCED DECOMPOSITION

The interaction of radiation with matter is discussed in a number of texts,¹⁻⁴ and recent advances in radiation chemistry, particularly with respect to aqueous solutions, have been summarized in several excellent articles.⁵⁻⁹ A brief outline of the present concepts, however, involving the formation and reaction of free atoms and radicals, is given here as an aid in understanding the discussion that follows.

Water may be considered to decompose by two separate processes: the forward reaction, Eq. (1), in which molecular products are formed, and the radical reaction, Eq. (2), in which free radicals are formed.



The symbol \rightsquigarrow may be read "under high-energy irradiation yields." Some of the hydrogen peroxide formed in the forward reaction may decompose into oxygen and water:



The products observed after irradiation are the molecular products H_2 , O_2 , and H_2O_2 . If the water is pure, a low steady-state concentration of these products is reached—a condition in which the decomposition products, both molecular and free radical, are reacting with each other to re-form water at a rate equivalent to the decomposition rate. Two important reactions in this back reaction process are:



This back reaction chain, Eqs. (4) and (5), is the chief method by which the molecular decomposition products are used up. If oxygen is present, e.g., as in Eq. (3), it can also be used in the following way:



¹References appear at end of chapter.



Impure water may contain solutes¹⁰ which react with or cause recombination of the free radicals, thereby inhibiting the back reaction, Eqs. (4) and (5), so that the molecular products, Eqs. (1) and (3), accumulate. The reader is referred to Hochanadel¹¹ and to some of the preceding references for a more detailed discussion of the mechanisms involved.

The rate of the forward reaction, Eq. (1), depends on the intensity and type of radiation and is independent of temperature. The rate of the back reaction, Eqs. (4) and (5), depends on the temperature, concentration of dissolved products (pressure), and type and intensity of radiation.

EFFECT OF TYPE OF RADIATION

The decomposition of water by radiation can be conveniently expressed as the molecules of hydrogen gas produced per 100 ev of energy absorbed in the water. This number, when no back reaction of decomposition products to re-form water is present, gives the maximum rate of decomposition which can occur and is called G_{H_2} for hydrogen production. G_{H_2} may vary as much as six to eight fold depending on the type of radiation. In Table 4.5.1, G_{H_2} is given for three different types of radiation.

Table 4.5.1 — G_{H_2} , Maximum Rate of Decomposition per 100 ev of Various Radiations Absorbed in Water*

Radiation	G_{H_2}
γ -ray	0.3 – 0.7
Fast neutrons ¹²	
(proton recoils)	1.5
Fission fragments ¹²	1.8

* Various reliable investigators cited by Allen⁹ obtained the spread of values shown in this table. Hochanadel¹¹ obtained a value near the average of 0.46 for degassed solutions using a calorimetric measurement of the energy input

Only γ -rays and fast neutrons cause decomposition in pure moderator water, as fission fragments do not get into the water. See Chap. 4.3 of this section for the effects of fission fragments on water.

By assuming that the yields for the various types of radiation are additive, the rate of decomposition under mixed radiations can be approximated in a reactor. (The value for fast neutrons in Table 4.5.1 was obtained by making this assumption.) For example, if 60 percent of the energy absorbed by water is derived from the proton recoils of the fast neutrons and 40 percent of the energy from γ -rays, then $0.60 \times 1.5 + 0.40 \times 0.46 = 1.08 = G_{\text{H}_2}$.

Thermal neutrons cause no decomposition in pure water except by a secondary process:



This process has a cross section of 0.31 barn and may add an appreciable contribution to the γ -ray component of the energy. For example, in the reflector of a reactor such as the HRE, it may amount to as much as 20 percent of the γ -ray component.

The type of radiation also has a marked effect on the radiation back reaction and thus on the steady-state pressure which is reached.¹⁰ Gamma-rays, x-rays, and fast electrons decompose water only to a small extent, the concentration of decomposition products amounting to only a few micro-moles per liter at the steady state.¹³ In heavy-particle radiations, such as α -rays or proton recoils from fast neutrons, a higher concentration of decomposition products is necessary before the steady state is reached.¹⁴ The radiations in a reactor are mixed γ -rays and fast neutrons, so one would expect a steady-state pressure between the steady-state pressures of pure γ -rays and fast neutrons.

The effect of the type of radiation on the steady-state pressure has been well illustrated by the Radiation Chemistry Group^{9,10} at ORNL by the following experiment which is plotted in Fig. 4.5.1A and B.

A typical sample of pure water (Fig. 4.5.1A) was irradiated in a silica ampoule in a graphite reactor until a steady-state pressure was reached; then it was re-irradiated while surrounded with paraffin, thereby altering the γ -ray component only a little while greatly reducing the number of fast neutrons getting into the water. The steady-state pressure dropped to a much lower value. Another typical sample (Fig. 4.5.1B) was also irradiated until a steady-state pressure was reached, then re-irradiated while surrounded with lead. The steady-state pressure was raised since very few of the fast neutrons were slowed down or absorbed by the lead whereas many of the γ -rays were absorbed. Different samples gave different steady-state values because the nature of the impurities produced during radiation varied with the different samples of silica tubing; steady-state pressure varied from 51 to 147 cm in a series of ampoules upon the first irradiation. This experiment demonstrates that the steady-state pressure can be lowered by increasing the γ -ray/fast neutron ratio in a reactor. The time necessary to reach equilibrium depends upon the geometry of the sample, a nearly filled ampoule reaching equilibrium much quicker than a half-filled ampoule. The degree of filling (gas/liquid ratio) also will affect the magnitude of the steady-state pressure (see below).

EFFECT OF PRESSURE

Pressure does not affect the radiation decomposition of water, Eq. (1), but does have an influence on the reactions between the decomposition products. The rate of the back reaction, Eqs. (4) and (5), is thermally sensitive; it is accelerated by increasing the concentration of hydrogen but is decelerated by increasing the concentration of either hydrogen peroxide or oxygen.^{9,11,15} The concentration of dissolved gases is governed by Henry's Law and has been measured for hydrogen and oxygen over a wide range of temperature at Battelle Memorial Institute.¹⁶

If the pressure of the system is below the steady-state pressure, the rate of the decomposition reaction is greater than the rate of the recombination reaction, and the pressure builds up until the steady-state pressure is reached, at which point both rates are equal and no further net decomposition occurs. If the system has a pressure greater than the steady-state pressure, the recombination rate is greater than the decomposition rate, and the pressure decreases until the steady-state pressure is reached.

The ratio of the molecular decomposition product concentrations in solution is of importance.^{10,11} If hydrogen is added to water prior to irradiation or if a solution of oxygen and hydrogen peroxide contains a large excess of hydrogen, the decomposition of water may be almost completely repressed. The kinetics of the back reaction in the presence of a large excess of hydrogen is reproducible and is proportional to the concentration of hydrogen, inversely proportional to the hydrogen peroxide concentration, and independent of radiation intensity:

$$\frac{-d(\text{H}_2)}{d(\text{dose})} = \frac{-d(\text{H}_2\text{O}_2)}{d(\text{dose})} = -G_F + K \frac{(\text{H}_2)}{(\text{H}_2\text{O}_2)} \quad (9)$$

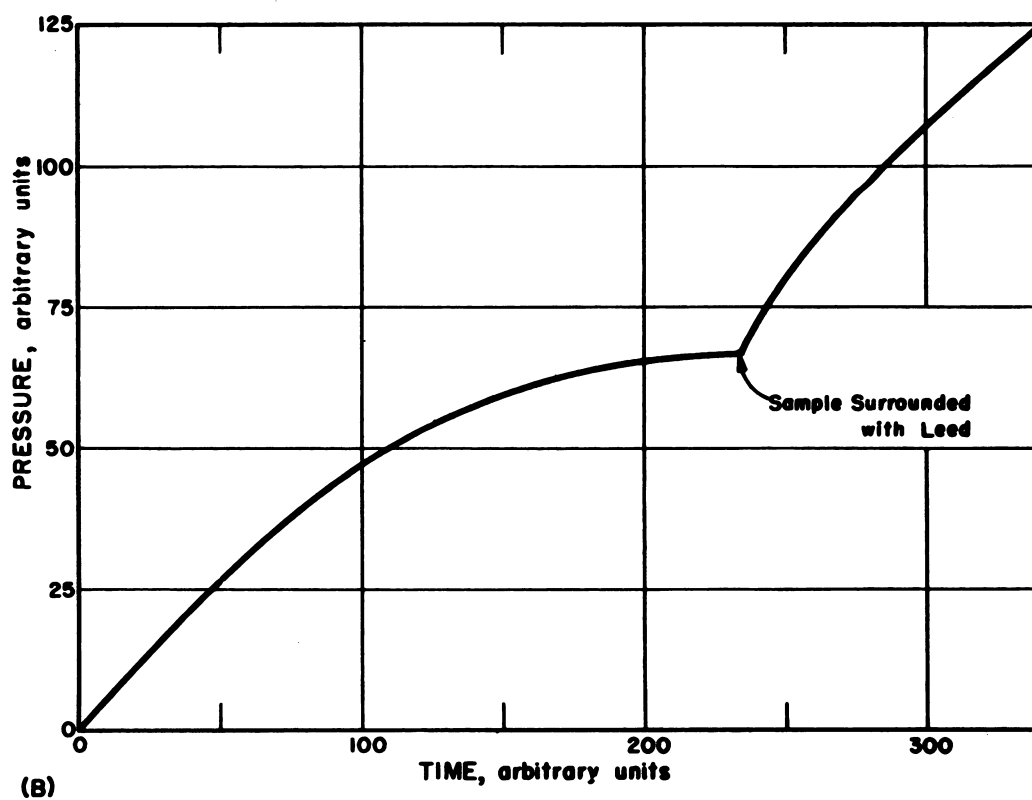
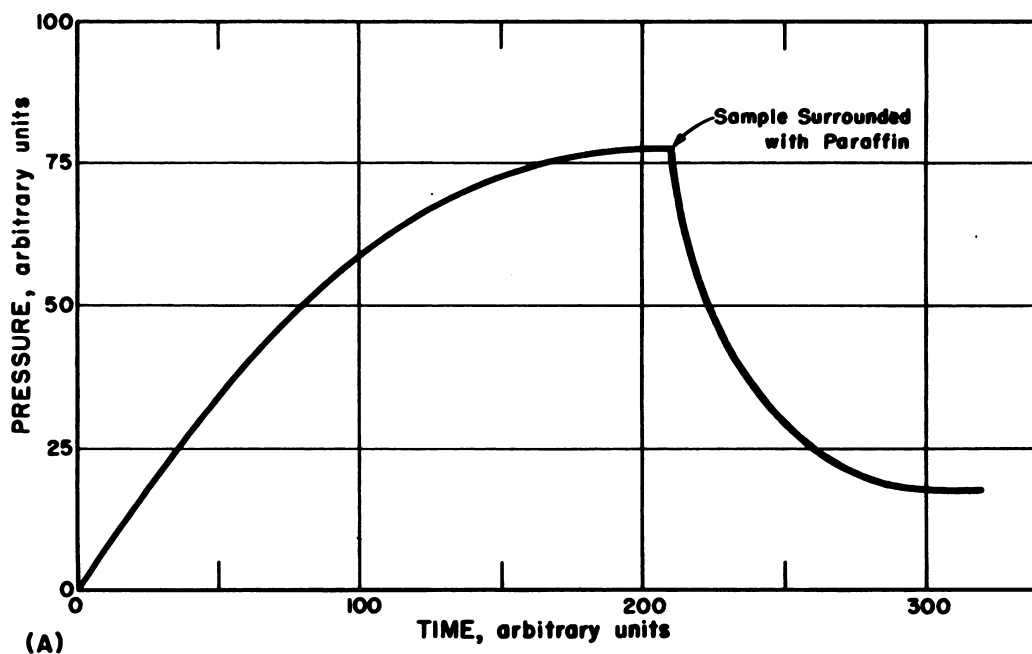


Fig. 4.5.1 — Effect of Radiation Type on Water Decomposition. Submitted by Oak Ridge National Laboratory, Jan. 13, 1953.

G_F is the yield of formation of hydrogen for the radiation involved and may be obtained from Table 4.5.1.

If oxygen or hydrogen peroxide is added initially (aerated water), the rates are not reproducible, and decomposition may continue to high levels with much hydrogen and oxygen being produced.

It follows from the preceding discussion that the gas phase/liquid phase ratio has an influence on the steady-state pressure attained. If no gas phase is present, all decomposition products remain in solution, a steady state is reached sooner, and the steady-state concentration is lower. In the latter case, much of the hydrogen and oxygen escape into the gas phase, leaving an excess of hydrogen peroxide in solution. In the X-10 graphite reactor where about two thirds of the energy absorbed by the water is from fast neutrons and one third from γ -rays,¹⁷ the steady-state concentration of hydrogen at 250°C is about 20 micro-moles/liter which is equivalent to a hydrogen pressure over the water of 20 mm of Hg.¹⁸ The energy input in this case amounts to about 2×10^{18} ev/(gm)(min).

If high steady-state pressures are attained, then explosive gases accumulate in the gas phase. If neither high pressures nor the presence of explosive gases can be tolerated, the decomposition gases have to be bled off or recombined by some external means.

EFFECT OF TEMPERATURE

The rate of radiation-induced water decomposition is probably independent of temperature, but the rate of the back reaction between the decomposition products is temperature dependent; therefore the steady-state pressure is also dependent on temperature. The production of hydrogen (under constant radiation dose) as a function of temperature between 30° and 250°C has been studied for UO_2^{++} solutions.¹² No detectable change in the rate of hydrogen production was observed within this temperature range. The steady-state pressure is markedly reduced by an increase in temperature.¹⁸ The pronounced effect of temperature on the radiation-induced back-reaction is shown in Fig. 4.5.2, which is

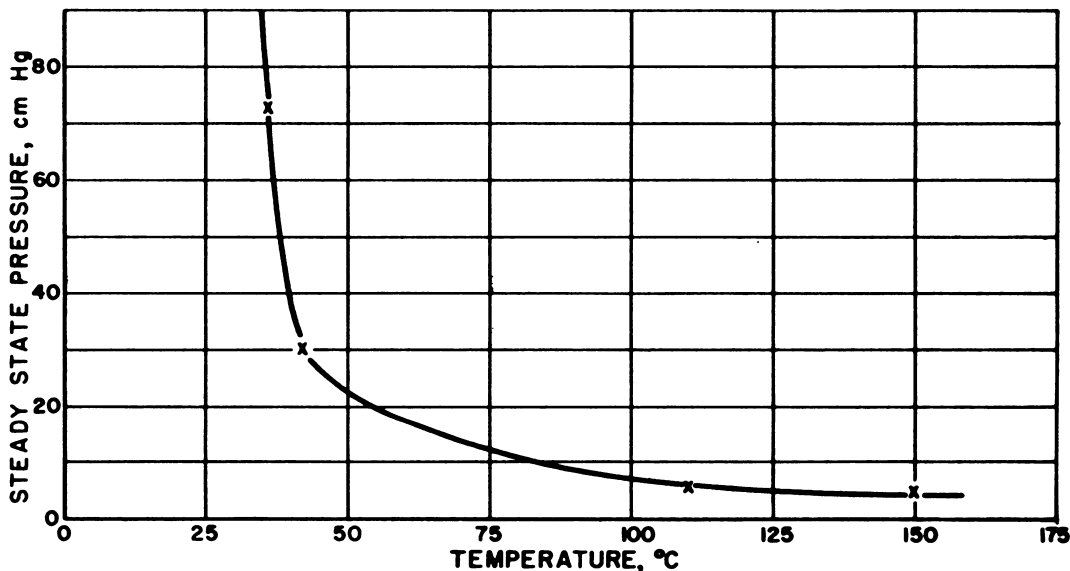


Fig. 4.5.2 — Effect of Temperature on Water Decomposition by Reactor Radiation.
Submitted by Oak Ridge National Laboratory, Jan. 13, 1953.

a plot of an experiment carried out in the X-10 graphite reactor by members of the Radiation Chemistry Group at ORNL. The energy input amounted to about 2×10^{18} ev/(gm)(min) of which approximately two thirds was from fast neutrons and one third from γ -rays. A duplicate sample differed somewhat because of trace impurities but showed the same strong temperature dependence. Work at ORNL and elsewhere has shown that the purer the water, the lower the steady-state pressure over the water.^{10,18} It seems fair to infer from two seemingly duplicate samples that the one showing the lower steady state is the purer.

In a reactor where it is possible to purify the water continuously by some means such as passing through a mixed cation-anion resin, a lower steady-state level should be encountered than in a small container where impurities from the container wall are continually accumulating in the water. It has been shown that impurities entering from the walls of a container gradually but steadily raise the steady-state pressure.

The CP-3 Argonne heavy-water reactor has a somewhat similar history. The accumulation of impurities from the start-up in 1944 until 1950 lowered the pH of the water, increased water decomposition, and resulted in loss of reactor reactivity. In the spring of 1951, the reactor D₂O was distilled in a bypass stream which reduced the impurities considerably. In May 1951, a mixed-bed resin column was placed in a bypass stream; since then, net decomposition has decreased to practically zero, and excess reactivity has been greatly increased.

THERMAL PROPERTIES

The thermal properties of both light and heavy water are given in many standard references. See also Section 1 of this volume.

REFERENCES

1. F. Rasetti, *Elements of Nuclear Physics*, Prentice-Hall, Inc., New York, 1936.
2. E. Rutherford, J. Chadwick, and C. D. Ellis, *Radiations from Radioactive Substances*, Cambridge University Press, London, 1930.
3. R. D. Evans, *Fundamentals of Nuclear Physics, The Science and Engineering of Nuclear Power*, Vol. I, Addison-Wesley Press, Inc., Cambridge, Mass., 1947.
4. S. C. Lind, *The Chemical Effects of Alpha Particles and Electrons*, 2nd ed., The Chemical Catalog Company, New York, 1928.
5. M. Burton, *Radiation Chemistry*, Annual Reviews of Physical Chemistry, Vol. I, Annual Reviews, Inc., Stanford Calif., 1950.
6. F. S. Dainton and E. Collinson, *Radiation Chemistry*, Annual Reviews of Physical Chemistry, Vol. II, Annual Reviews, Inc., Stanford, Calif., 1951.
7. A. O. Allen, *Radiation Chemistry*, Annual Reviews of Physical Chemistry, Vol. III, Annual Reviews, Inc., Stanford, Calif., 1952.
8. M. Burton, *An Introduction to Radiation Chemistry*, Jour. Chem. Ed. 28, 1951, p 404.
9. A. O. Allen, *Mechanism of Decomposition of Water by Ionizing Radiations*, Discussions of the Faraday Society 12, 1952, p 79.
10. A. O. Allen, T. W. Davis, G. V. Elmore, J. A. Ghormley, B. M. Haines, and C. J. Hochanadel, Oak Ridge Nat. Lab., ORNL-130, 1949. See also Jour. Phys. Chem. 56, 1952, p 575.
11. C. J. Hochanadel, *Effects of Cobalt Gamma Radiation on Water and Aqueous Solution*, Jour. Phys. Chem. 56, 1952, pp 587-594.
12. J. W. Boyle, W. F. Kieffer, C. J. Hochanadel, T. J. Sworski, and J. A. Ghormley, Reactor Sci. Tech. 3, No. 1, 1953, p 32 (classified).
13. A. O. Allen, Jour. Phys. Colloid Chem. 52, No. 3, 1948, p 479.
14. F. C. Lanning and S. C. Lind, Jour. Phys. Chem. 42, 1938, p 1229.
15. A. O. Allen et al, Jour. Phys. Chem. 56, 1952, p. 575.
16. H. A. Pray, C. H. Scheibelhut, and B. M. Minnich, Battelle Memorial Institute, BMI-T-25, 1950.
17. D. M. Richardson, Oak Ridge Nat. Lab., ORNL-129, 1949 (classified).
18. M. Sivetz and C. H. Scheibelhut, Reactor Sci. Tech. 2, No. 2, 1952, p 121 (classified).

CHAPTER 4.6

Nuclear Design Data

CONTROL OF HOMOGENEOUS AQUEOUS REACTORS

INTRODUCTION (R. B. Briggs)

Control requirements for aqueous homogeneous reactors are similar to those for other types. It must be possible (1) to start the reactor and bring it to a prescribed operating power and temperature, (2) to make changes in operating power and temperature while the reactor is operating, (3) to control reactivity disturbances which might cause damage to the equipment, and (4) to shut down the reactor at will. The fluid nature of both the fuel and moderator make several methods of control possible in addition to the method using conventional mechanical control rods.

Calculations for the Homogeneous Reactor Experiment (HRE) at ORNL indicate that the negative temperature coefficient of reactivity is large enough to control any foreseeable disturbances in the reactivity, item (3) above, before the equipment can be damaged. If the power level and temperature are permitted to vary about prescribed mean values, the negative temperature coefficient makes the reactor self-regulating.

Other means are required to accomplish items (1), (2), and (4) above. Some of these which have been considered are control of fuel concentration, control of fuel enrichment, control of rate of heat removal, control of reflector level in D_2O -reflected reactors, and dumping the fuel solution.

NONMECHANICAL CONTROL METHODS (R. B. Briggs)

CONCENTRATION CONTROL

Using an aqueous solution fuel permits changing the reactivity of the reactor by adjusting the fuel concentration. A typical curve of critical concentration vs temperature is shown in Fig. 4.6.1. The reactor may be started at 100°C or below by filling the circulating system with D_2O and gradually adding fuel until the reactor becomes critical. With the reactor operating at lower power, the fuel concentration is increased which increases the temperature correspondingly; this is continued until the desired fuel concentration and operating temperature are reached. During operation, slow changes in operating temperature can be achieved by adjusting the fuel concentration. Evaporators are provided to separate excess fuel solution into D_2O and a fuel concentrate.

The effectiveness of concentration control during operation depends on the slope of the temperature-concentration curve at the operating point. In the case of the HRE, where the reactor is operated with ~ 90 percent uranium-235 in 25 to 40 gm/l solution, $\delta k/\delta c = 1.3 \times 10^{-2}$ per gm uranium-235 per kg of H_2O at 100°C and 1.0×10^{-2} per gm uranium-235 per kg of H_2O at 200°C .

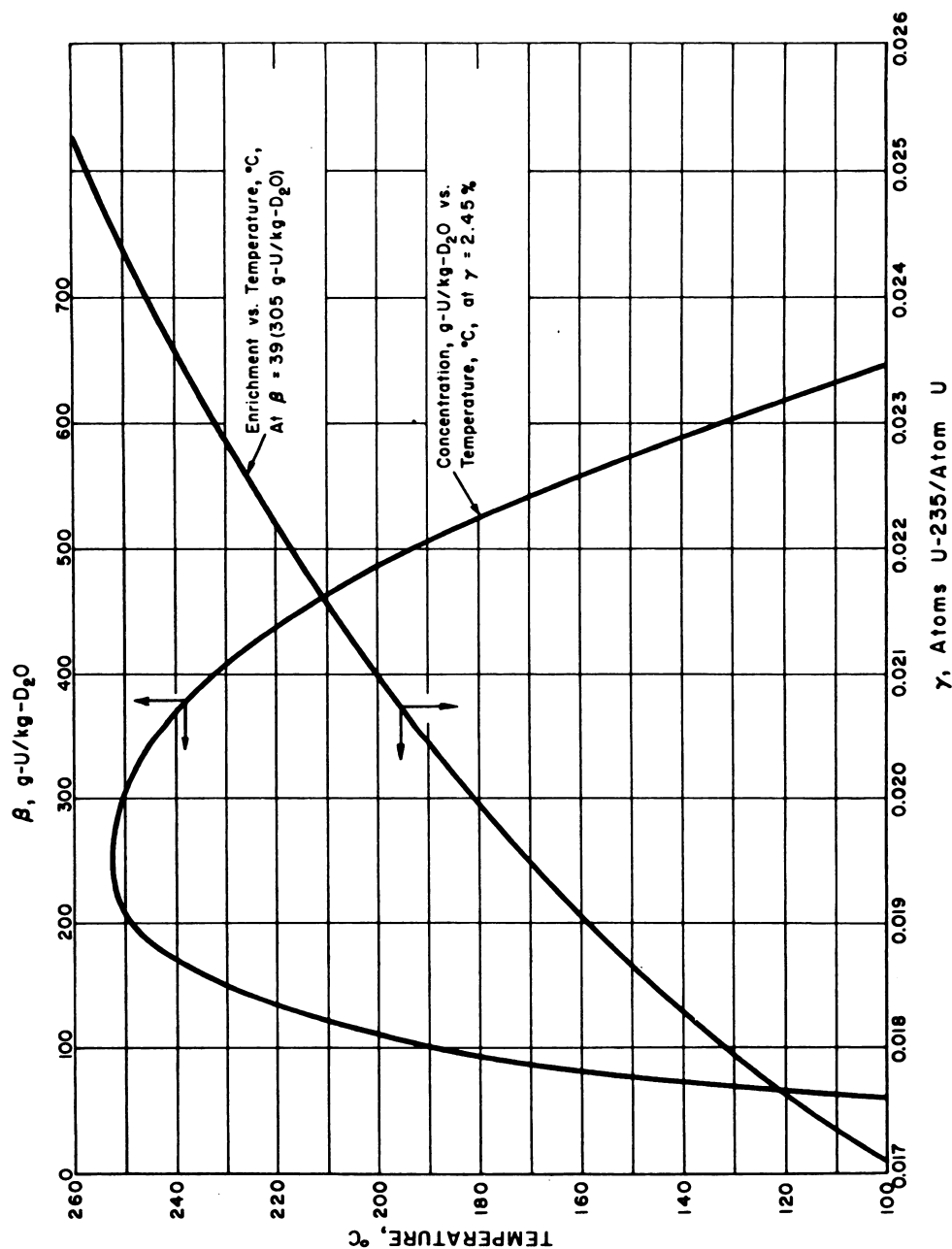


Fig. 4.6.1 — Critical Conditions in 6-ft-diameter Core Sphere for Proposed Homogeneous Reactor. Submitted by Oak Ridge National Laboratory, Nov. 25, 1952.

ENRICHMENT CONTROL

As an alternative to varying the concentration in order to change the reactivity of an aqueous homogeneous reactor, it is possible to vary the fuel enrichment. A typical curve of critical enrichment vs temperature is shown in Fig. 4.6.1. In starting the reactor, the circulating system can be filled at 100°C with fuel solution of less than the desired operating concentration and less than the critical enrichment for operation at 100°C. Enriched fuel can be added to the reactor as it becomes critical and as the temperature rises until the desired operating temperature and fuel concentration are reached. Changes in operating temperature can be achieved by adjusting the enrichment of the fuel added continuously or at frequent intervals.

CONTROLLED RATE OF HEAT REMOVAL

Aqueous homogeneous reactors are designed and fueled to operate at a specified average temperature. The operating power can be controlled by the rate at which the fuel solution is pumped through the reactor and by the difference in temperature between the average reactor temperature and the inlet fluid temperature. The operating power of a given system can be increased by removing more heat in the external system, i.e., by decreasing the reactor inlet temperature. It can be decreased by removing less power in the external system which results in a higher reactor inlet temperature. If the heat-removal equipment is operated to maintain a constant temperature of fluid entering the core, the power can be varied by varying the flow of fluid.

DUMPING FUEL

Fluid-fueled reactors can be shut down by dumping a part of the fuel from the core. Valves are provided which open upon a signal from the operator or the control instruments to dump the fuel into external storage tanks.

REFLECTOR-LEVEL CONTROL

The reactivity of the HRE can be controlled by regulating the level of the D₂O reflector which surrounds the core. Measurements made during the critical experiments showed the reflector to be worth 6.6 percent in Δk_{eff} at 20°C.

MECHANICAL RODS OR PLATES (C. L. Segaser and R. B. Briggs)

In addition to means for varying the fuel-solution concentration and the reflector level, the HRE was provided with three sets of mechanical control plates in the reflector surrounding the core tank. These are shown in Fig. 4.6.2.

Figures 4.6.3 and 4.6.4 show the mechanism devised for raising and lowering the safety plates and the regulating plate, respectively.¹ All mechanisms pertaining to the control-plate drives are contained within thimbles attached mechanically to the top flange closure. The pressure within these thimbles is maintained at the same value (1000 psi) as in the reflector pressure vessel, but the temperature is reduced by running coolant through jackets surrounding the thimbles. The portions of the drive mechanism (electrical insulation and the like) which are likely to be damaged by radiation are located at the maximum practical distance from the core tank and are partially shielded by the 10-in.-thick steel top flange closure.

Pressure is maintained in the control mechanism thimbles and in the reflector vessel by introducing helium at 1000 psi near the top of each thimble. This helium, as it flows downward through thimbles, prevents diffusion of dissociation gases (D₂ and O₂), thus reducing the possibility of an explosion.

¹References appear at end of chapter.

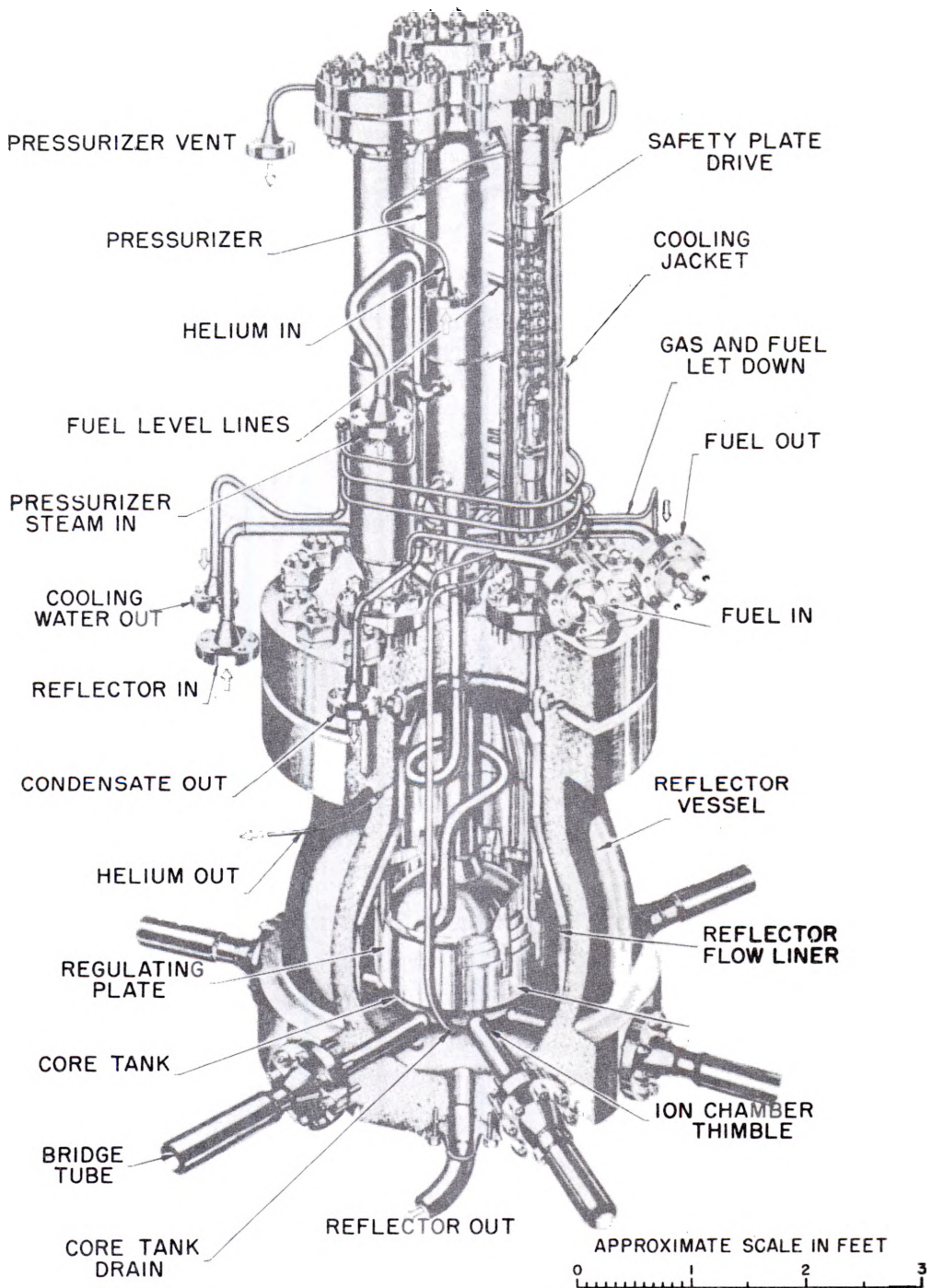


Fig. 4.6.2— Homogeneous Reactor Experiment Reactor Tank Assembly
 Reprinted from ORNL-1318, Sept. 9, 1952; submitted by Oak Ridge National Laboratory, Nov. 25, 1952.

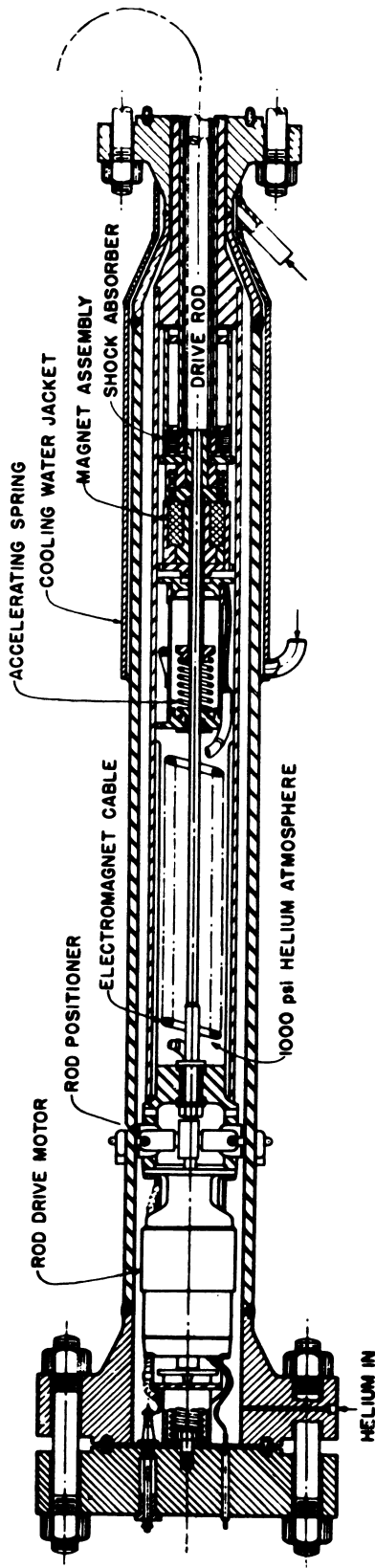
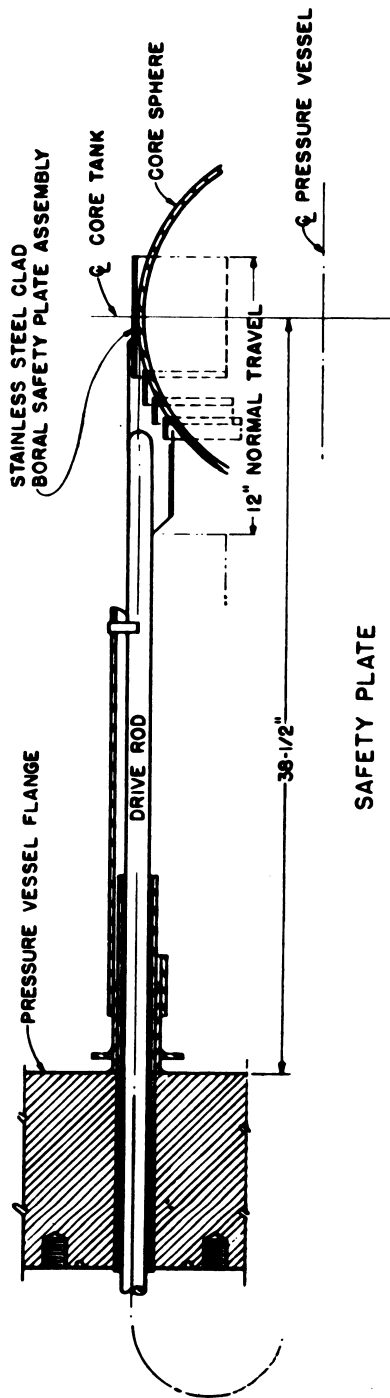
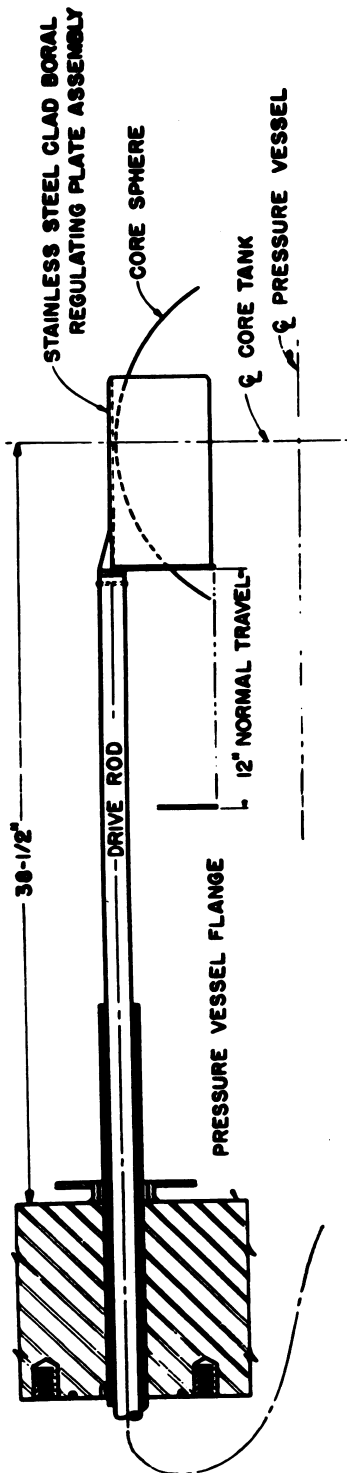


Fig. 4.6.3— Safety Rod Assembly for Homogeneous Reactor Experiment. Submitted by Oak Ridge National Laboratory, Nov. 25, 1952.



REGULATING PLATE

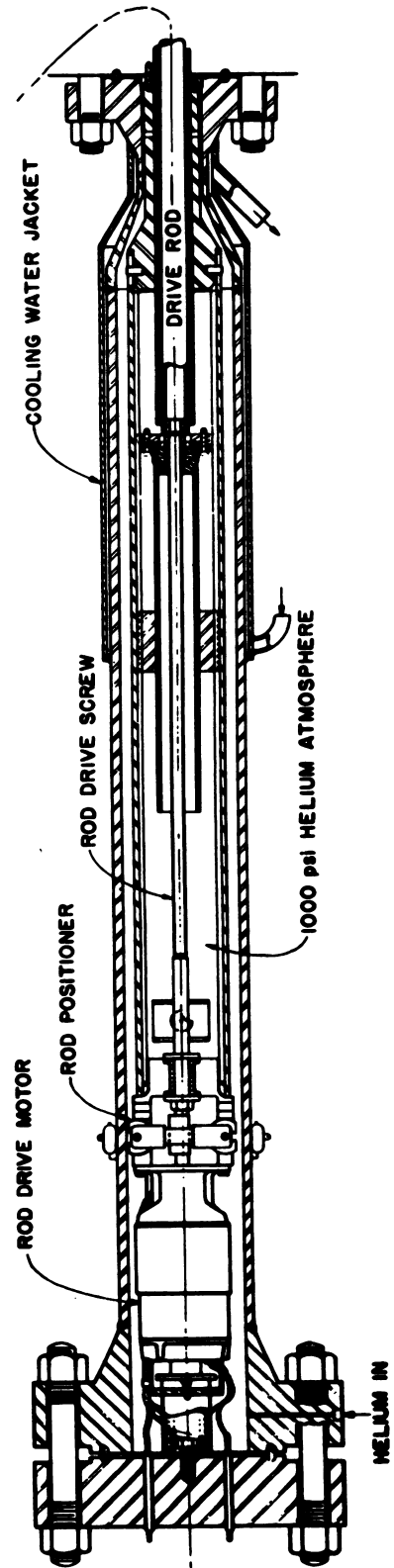


Fig. 4.6.4—Regulating Rod Assembly for Homogeneous Reactor Experiment.
Submitted by Oak Ridge National Laboratory, Nov. 25, 1952.

The safety plates are connected by a rod through a hole in the top flange closure to an armature in the safety-rod thimble. An electromagnet, above the armature, is driven by a power screw connected to a vertically mounted gear-motor. The magnet may be lowered to engage and magnetically connect the armature, and by reversing the motor, it will lift the rod and connected plate from around the core tank. By de-energizing the magnet, the rod will fall by gravity plus an initial acceleration imparted by the force of a compressed spring. A shock absorber stops the rod at the termination of its drop by absorbing a portion of its kinetic energy. The safety plates can be withdrawn at a rate of 4 in./min. They drop into place around the core in 0.15 sec.

The regulating plate is connected by a rod through a hole in the top closure to a guided nut in the regulating-rod thimble. A power-driven screw varies the position of the regulating plate relative to the core tank as demanded by small changes in reactivity. The three holes through the top closure for the control-plate drive-rods are limited in size and are located as far from the center of the closure as possible to avoid weakening the flange. The regulating plate can be withdrawn or inserted at a rate of 4 in./min. Rapid fluctuations in reactivity are controlled by the power or temperature coefficient.

The control plates were made by enclosing boron sheet (a mixture of boron carbide and aluminum) in a stainless-steel envelope. An improvement in this technique consists of cladding a boron carbide copper compact with stainless steel. Measurements obtained in critical experiments show each of the safety plates to be worth 0.48 percent in Δk_{eff} at 100°C and 0.64 percent at 200°C. The regulating plate controls 0.33 percent in Δk_{eff} at 100°C and 0.44 percent at 200°C.

SAFETY CONSIDERATIONS

INHERENT STABILITY

See "Neutron Chain Reactor Kinetics" in Chapter 4.1.

GAS EXPLOSIONS (P. N. Haubenreich)

The generation of hydrogen and oxygen from the decomposition of water in aqueous homogeneous reactors presents a possible explosion hazard. Gas bubbles will form, and if the system pressure is sufficiently high, these bubbles will contain an explosive mixture of hydrogen, oxygen, and water vapor. Explosions might occur in the core, gas separator, recombiner system, and connecting piping.

A chemical explosion may occur by one of two distinct processes:

- (1) Deflagration, or smooth burning, which is controlled by chemical reaction rate and mixing processes and is characterized by a relatively low velocity of flame propagation.
- (2) Detonation, which is largely a hydrodynamic phenomenon and is characterized by a shock wave which travels through the unburned gas at a velocity greater than that of sound.

The measured explosion (deflagration) limits of mixtures of hydrogen, oxygen, and water vapor indicate that when the concentration of hydrogen and oxygen in stoichiometric ratio is less than 25 percent, the mixture is generally nonexplosive, and the mixture is definitely nonexplosive when the concentration is less than about 17 percent. The explosive limits vary little over the pressure range of 1 to 68 atm.

Pressures from constant-volume deflagrations can be calculated quite accurately as confirmed by experimental data. A more realistic approach is to consider the effect of changes in gas volume resulting from compression of the surrounding liquid and the expansion of the vessel as the gas burns. In this case, unlike the constant volume process, the explosion pressure is a function of both gas and liquid volumes and vessel design. If the explosion occurs in a large vessel, a shock wave may build up in the medium surrounding the explosion and reach the wall of the vessel. The peak pressure would then be

approximately twice the calculated equilibrium explosion pressure.* If the pressure wave striking the wall is reflected without appreciable energy loss, the peak pressure may be fourfold greater than the equilibrium pressure.

Figure 4.6.5 shows the equilibrium explosion pressures and resultant shell stresses for the deflagration of various amounts of gas in the core of the ISHR when operating at 250°C and 1000 psia. The volume of the core is 113.1 cu ft, and in this case, the spherical shell is assumed to be 2.5 in. thick. Compression of the liquid and expansion of the shell were taken into account, but the effect of the pressurizer was not considered, assuming instead that no liquid escapes from the core during the explosion. Since the change in gas volume owing to shell expansion is quite small compared with that from compression of the liquid, the pressures shown for a particular gas-to-liquid ratio should apply in any part of the system where the initial pressure and temperature are approximately the same as in the core. In the gas separator, the gas-to-liquid ratio will be much higher than in the core, with resultant higher explosion pressures. In the lines carrying only gas, the explosion pressure will approach that for constant-volume deflagration, which is 4710 psia for initial conditions of 250°C and 1000 psia.

Composition limits of detonability are not well defined, since a detonation may begin in a more combustible mixture and progress into a mixture of poor detonability. However, in such a case the detonation wave becomes unstable and degenerates to a normal compression wave.

The occurrence of a stable detonation wave is a strong function of the geometry of the system, in general existing only in channels not widely diverging in cross-sectional area. A fully formed detonation wave can be degenerated by allowing it to encounter obstacles such as a wire helix, baffles, numerous bends and elbows, or a series of expanding and diverging sections to bring about irreversible energy losses. A combustible mixture in a large sphere will not detonate even if the source of ignition is a detonation wave that has progressed through a tube that terminates in the center of the sphere. Hence, there is little likelihood of a detonation occurring in the core vessel unless there is a vortex through which the detonation could progress in unidirectional flow. In any component of the reactor equipment where the combustible gas mixture exists as a continuous gas phase in a relatively long, straight tube, there is a possibility of detonation and high impact pressures. If the gas is a stoichiometric mixture of hydrogen and oxygen in equilibrium with water at 250°C and 1000 psia, the stable detonation wave velocity would be about 6920 ft/sec with a resulting impact pressure of 14,400 psia. Since the detonation wave, once formed, travels so rapidly, there is little chance of pressure relief by means of surge capacities in the system. If reflection occurs, the peak pressure may be two fold greater than the calculated impact pressure.

INDUCED ACTIVITY IN EXTERNAL EQUIPMENT

(P. N. Haubenreich)

A problem of special importance in circulating-fuel reactors is the difficulty of maintenance because of induced radioactivity. Even when pumps, valves, and heat exchangers are separated from the reactor compartment by shielding, they will become radioactive because of the capture of delayed neutrons emitted by the circulating fuel. The level of activity depends on the density of neutron emission in the fuel, the size and shape of the liquid volume, and the nature of the materials exposed to the neutrons.

The density of delayed-neutron emission is fixed by the reactor power level, the system volume and flow rate, and the location of the point being considered. The total number of

* The pressure which would be measured after the pressure transients have died out and before cooling of the combustion products.

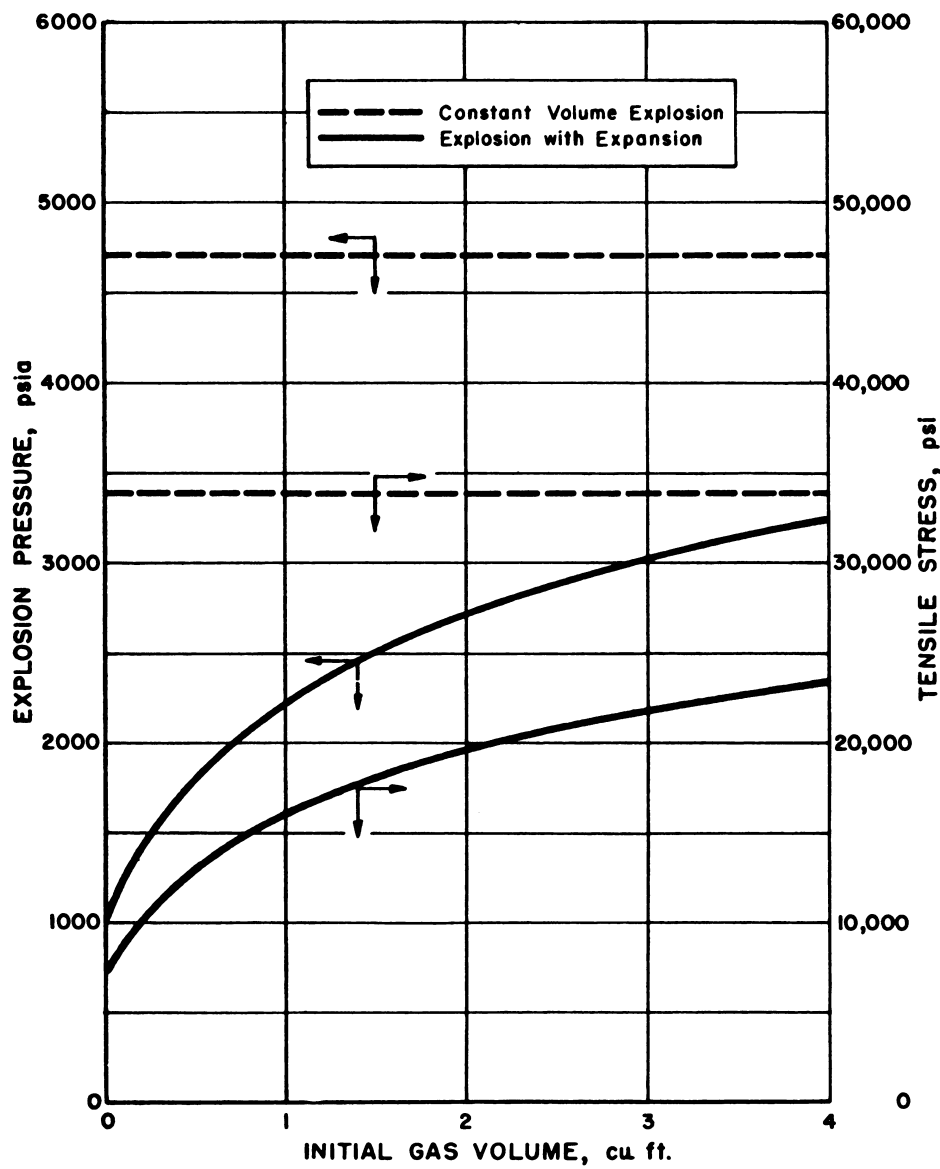


Fig. 4.6.5—Calculated Pressures and Stresses Resulting From an Explosion in the Core of the Proposed Homogeneous Reactor. Submitted by Oak Ridge National Laboratory, Nov. 25, 1952.

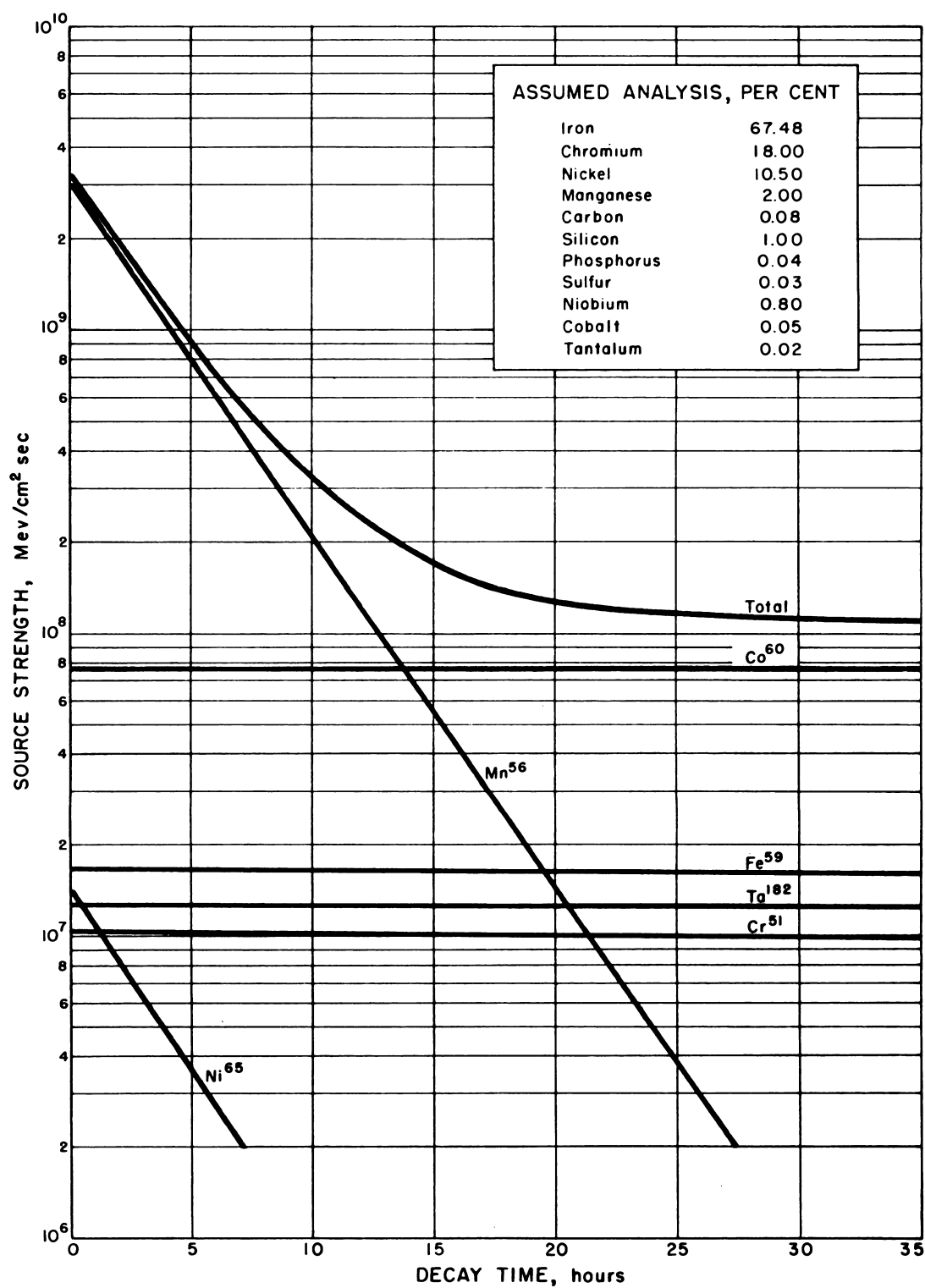


Fig. 4.6.6— Decay of Induced Radioactivity in Type 347 Stainless Steel. Submitted by Oak Ridge National Laboratory, Nov. 25, 1952. Predicated on 2-yr irradiation with 2.3×10^{10} absorptions/(cm²)(sec).

delayed neutrons being emitted is determined by the reactor power, whereas the flow rate and relative volumes of reactor and external circulatory system fix the fraction emitted outside the core. As the ratio of external volume to core volume becomes larger, the fraction of delayed neutrons emitted in the external system also increases, but because of a longer decay time per cycle which reduces the concentration of delayed neutron precursors, the emission density becomes smaller.

The size and shape of the liquid volume affect the leakage probability and the multiplication, which in the case of larger volumes appreciably increases the number of neutrons. Calculation of the actual number of absorptions in equipment is sometimes difficult because of complicated geometry. A convenient assumption is the upper limit in which all neutrons emitted in a piece of equipment are absorbed in the walls. For simple shapes, a closer approximation can be had by taking into account flux distributions and absorption cross sections.

To predict accurately the induced activities in equipment, the energy distribution of the leakage neutrons should be considered, since some reactions which lead to radioactive isotopes [such as $\text{Ni}^{60}(\text{n,p})\text{Co}^{60}$] take place only at higher energies. Other necessary information includes the analysis of the material, and the abundances, absorption cross sections, and decay schemes of the isotopes. A careful analysis is necessary since elements which appear in only trace amounts may be major sources of activity. Notable examples are cobalt, which appears to some extent in almost all alloys, and tantalum, which shows up in stainless steel containing niobium. Both these elements are troublesome because of a large cross section, high yield of penetrating gamma rays, and a long half-life.

Figure 4.6.6 shows the calculated upper limit of induced activity in the walls of a 20-in. pipe in a Homogeneous Reactor after operation at 48,000 kw for two years. The figures are for a flow rate of 20,000 gpm, a core volume of 113 cu ft, and an external system volume of 272 cu ft. For these conditions, 0.6 of the delayed neutrons are emitted in the external system, giving an average delayed-neutron emission density of 2.2×10^9 neutrons/(cm³)(sec). Taking into account leakage probabilities and multiplication in a 20-in. pipe, the leakage is 2.3×10^{10} neutrons/(sec)(cm²) of external surface. If all these are absorbed in the pipe walls, the source strength will be shown. After a 24-hr decay, the activity will be 0.0033 curies/cm² of surface with an average photon energy of about 1 mev.

REFERENCE

1. A. Zulliger, Design Report on Control Rods for the HRE, Oak Ridge Nat. Lab., ORNL-CF-52-3-36, Mar. 10, 1952 (classified).

SELECTED READING LIST

GAMMA ACTIVITY INDUCED IN ENGINEERING MATERIALS, C. D. Bopp, Oak Ridge Nat. Lab., ORNL-1371, Dec. 22, 1952.

CHAPTER 4.7

Engineering Design Information

REACTOR CONFIGURATION (R. B. Briggs)

GENERAL CHARACTERISTICS

Two basic configurations have been considered for aqueous homogeneous reactors, namely the single-region reactor, which is essentially a bare reactor, and the two-region reactor, which consists of a core surrounded by a reflector or by a blanket of fertile material. Both types of reactors can be used for breeding uranium-233 or for producing power (Figs. 4.7.1 and 4.7.2).

Two-region reactors have been suggested primarily as thorium-uranium-233 breeder reactors. They consist of a core of fissile material and moderator surrounded by a blanket of fertile material and moderator. D_2O is the moderator required for thermal breeding or economical conversion. The core is made as small as possible consistent with the power to be removed and the criticality requirements. The concentration of thorium in the blanket is made as great as possible to obtain a thin blanket and a minimum over-all diameter. A two-region reactor can thus be small with essentially no leakage but at the expense of parasitic absorption of neutrons in the wall of the tank which separates the core from the blanket. When the core is small, the critical concentration can be 1 to 5 gm U/l; the inventory of fissile material in the core can thus be less than 15 kg while that in the external system can be half or less than half of that required in a single-region reactor.

There is little difference between one- and two-region reactors that produce power by consuming highly enriched fissile material without producing additional fissile atoms. In either case, the reactor can be small and moderated by either H_2O or by D_2O . When H_2O is used, the uranium-235 concentration must be greater than 10 gm/l; by using D_2O , the uranium-235 concentration can be reduced to 1 to 5 gm/l, and the cost of the fuel solution is usually less in this case. A reflector surrounds the core of a two-region power producer of this type. The reflector reduces the critical concentration required in the core, and if a fluid reflector is used, it provides a control method through adjustment of the reflector level.

DESIGN PROBLEMS OF ONE- AND TWO-CORE REACTOR VESSELS

The problems encountered in designing pressure vessels for one- and two-region reactors (the outer vessel in the two-region reactor) are similar in most respects. Both are designed on the basis of the same maximum permissible stress for a given material of construction. The construction material can be chosen on the basis of corrosion resistance and structural and thermal properties with little regard for nuclear properties.

Two principal types of stresses must be considered in designing the pressure vessels: (1) stresses resulting from the confined pressure and (2) thermal stresses resulting from heat production, and consequent temperature differences, in the metal.

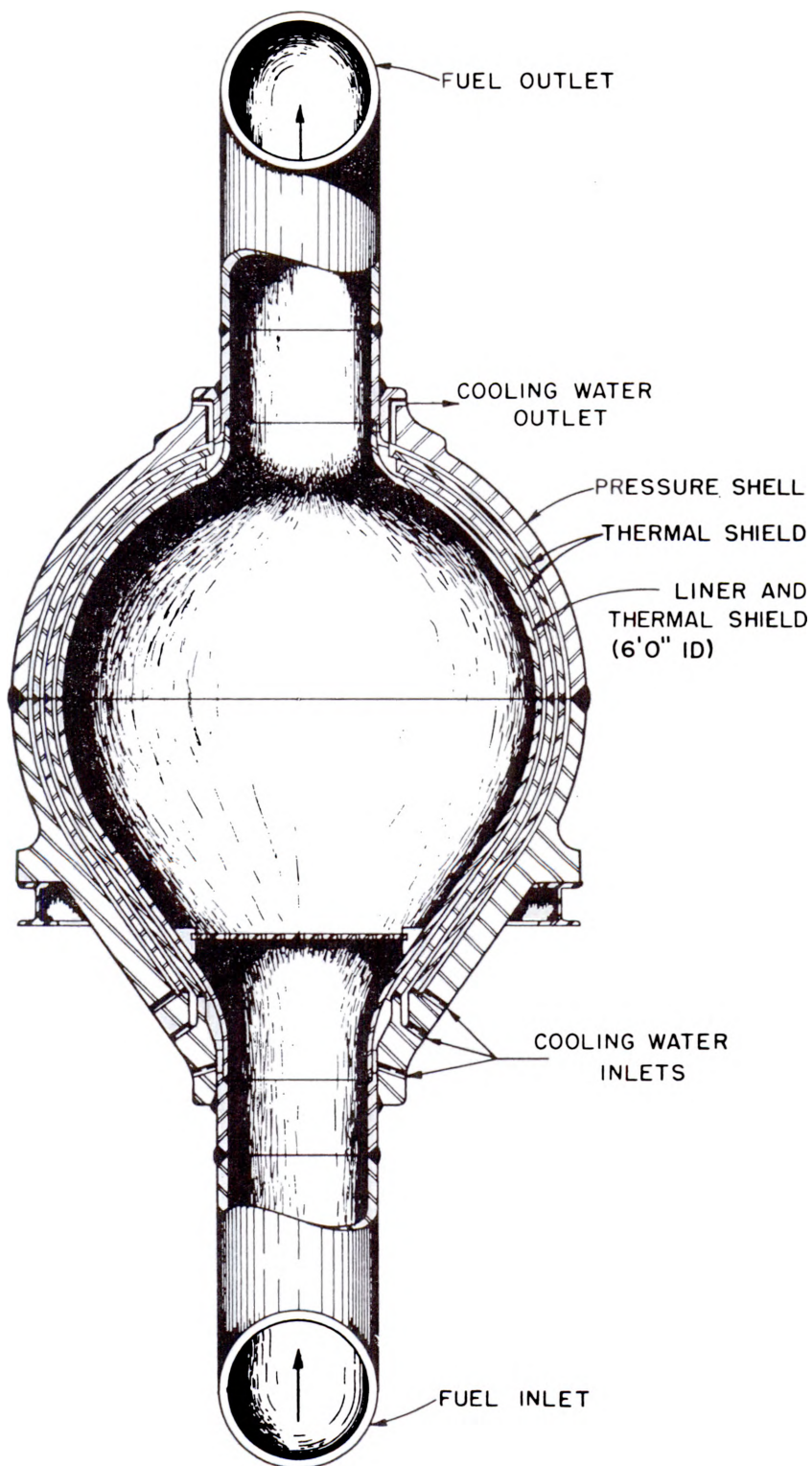


Fig. 4.7.1 — Typical Arrangement for Single-region Reactor. Submitted by Oak Ridge National Laboratory, Nov. 25, 1952.

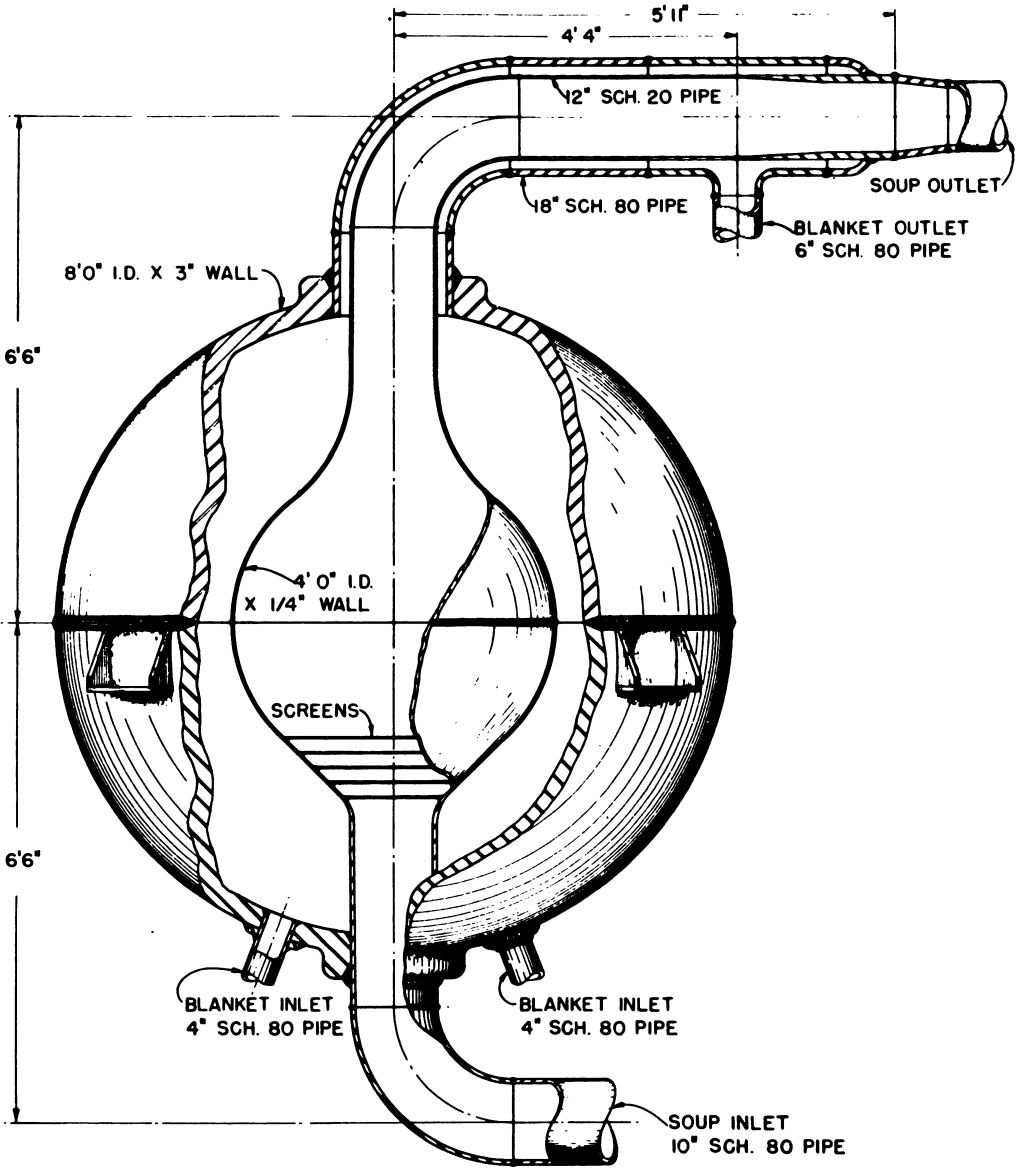


Fig. 4.7.2— Typical Arrangement for Two-region Reactor. Submitted by Oak Ridge National Laboratory, Nov. 25, 1952.

Usually the pressure-vessel wall is thin in comparison with the inner radius of the vessel; the "thin-wall" formulas for calculating pressure stresses are then applicable. They are:

$$\sigma_{\theta} = \frac{Pa}{b-a} \quad (\text{for cylinders}) \quad (1)$$

and:

$$\sigma_{\theta} = \frac{Pa^2}{b^2-a^2} \quad (\text{for spheres}) \quad (2)$$

where: σ_{θ} = tangential stress, lb/in.²
 P = internal pressure, lb/in.²
 a = inside radius, in.
 b = outside radius, in.

Thermal stresses are superposed on the pressure stresses and can be approximated by the following formulas for hollow cylinders:¹

$$\sigma_r = \frac{\alpha E}{(1-\gamma) r^2} \left(\frac{r^2 - a^2}{b^2 - a^2} \int_a^b Tr \, dr - \int_a^r Tr \, dr \right) \quad (3)$$

$$\sigma_{\theta} = \frac{\alpha E}{(1-\gamma) r^2} \left(\frac{r^2 + a^2}{b^2 - a^2} \int_a^b Tr \, dr + \int_a^r Tr \, dr - Tr^2 \right) \quad (4)$$

$$\sigma_z = E \epsilon_z - \frac{\alpha ET}{1-\gamma} + \frac{2\gamma \alpha E}{(1-\gamma)(b^2 - a^2)} \int_a^b Tr \, dr \quad (5)$$

and by the following formulas for hollow spheres:²

$$\sigma_r = \frac{2\alpha E}{1-\gamma} \left(\frac{r^3 - a^3}{(b^3 - a^3) r^3} \int_a^b Tr^2 dr - \frac{1}{r^3} \int_a^r Tr^2 dr \right) \quad (6)$$

$$\sigma_{\theta} = \frac{2\alpha E}{1-\gamma} \left(\frac{2r^3 + a^3}{2(b^3 - a^3) r^3} \int_a^b Tr^2 dr + \frac{1}{2r^3} \int_a^r Tr^2 dr - \frac{1}{2} T \right) \quad (7)$$

where: σ_r = radial stress, lb/in.²
 σ_{θ} = tangential stress, lb/in.²
 σ_z = axial stress, lb/in.²
 α = linear coefficient of expansion, in./in. °F
 E = Young's modulus, lb/in.²
 γ = Poisson's ratio
 r = radius, in.
 a = inner radius, in.
 b = outer radius, in.
 T = temperature at radius, r , °F
 ϵ_z = the constant axial strain, in./in., which makes the resultant of normal forces distributed over the cross-sectional area of the cylinder equal to zero.

Equations (3), (4), and (5) apply directly to a cylinder with no mechanical constraints, with only radial temperature gradients, and at sections distant from the ends. Maximum

¹References appear at end of chapter.

tangential and axial stresses are equal and occur at the inner and outer radii. Equations (6) and (7) apply where there are no constraints and where the temperature is a function of radius only. Solution of the stress equations depends upon a knowledge of the radial temperature distribution which in turn depends upon the manner in which heat is generated in the metal wall and/or upon the temperatures at the inner and outer surfaces. Heat is produced in the metal by the following processes:

- (1) The absorption of gamma rays arising from neutron capture, from fission products, and from fission within the vessel.
- (2) The recoil energy from the scattering of fast neutrons in the shell.
- (3) The absorption of gamma rays produced by the inelastic scattering of fast neutrons in the shell.
- (4) The absorption of capture gamma rays produced as neutrons are captured in the shell.

Although it may be possible to obtain the heat production function for the desired cylindrical or spherical geometry, it is simpler and usually sufficiently accurate to obtain the leakage fluxes of gamma rays and neutrons into the pressure shell for the desired geometry and then to calculate the heat production for a slab geometry with the same leakage fluxes into the slab. Methods for obtaining the heat production function have been described by Grotenhuis,³ Segaser,⁴ Enlund,⁵ and Spiewak.⁶ The function can usually be described by the sum and difference of several exponentials. For most purposes, a single exponential can be used as a satisfactory approximation, and a uniform volumetric heat production rate may often be assumed.

Carter⁷ has reported temperature distributions and stresses for spheres, rods, tubes, and plates for uniform heat generation. Where the heat production is defined by exponential functions, the temperature distribution is usually calculated for a slab using the relation:

$$\frac{d^2T}{dx^2} = -\frac{H}{k} \quad (8)$$

where H is the heat production function and k is the thermal conductivity. The thermal stresses can be estimated by substituting the equation for temperature distribution for T in the stress equations. The total stress is obtained by combining the pressure stresses with the thermal stresses as shown in Fig. 4.7.3. Pressure stresses decrease and thermal stresses increase with increasing shell thickness such as results in a minimum combined stress. Often this stress is greater than the permissible design stress; thermal shielding must then be provided between the core and pressure vessel to reduce heat production and obtain a reasonable stress. Use of a thermal shield is illustrated in Fig. 4.7.1. Segaser⁴ and Spiewak⁶ report stresses and temperature distributions in spherical steel shells for various boundary conditions.

Designing the core tank in a two-region reactor presents special problems. Compared to the pressure vessel, the core tank may be made of a different material and may operate at a different temperature leading to problems of differential expansion. Bellows expansion joints in the piping or a piping design, as shown in Fig. 4.7.2, that will permit bending of the piping may be required to compensate for differential expansion. Absorption of neutrons by the core tank constitutes an important loss, and the core tank must be made as thin as is consistent with the strength requirements dictated by the pressure differences which can exist between the core and the blanket. The selection of materials must be based on a compromise between mechanical and nuclear properties of the construction materials.

Some properties of four possible core tank materials are tabulated in Table 4.7.1. The ranges listed should not be taken as authoritative but only as representative of the values. The factor $\alpha E/k$ is directly proportional to the thermal stresses, and the product $\Sigma_a t$ is a measure of the number of neutrons absorbed in passing through vessel walls of the same strength.

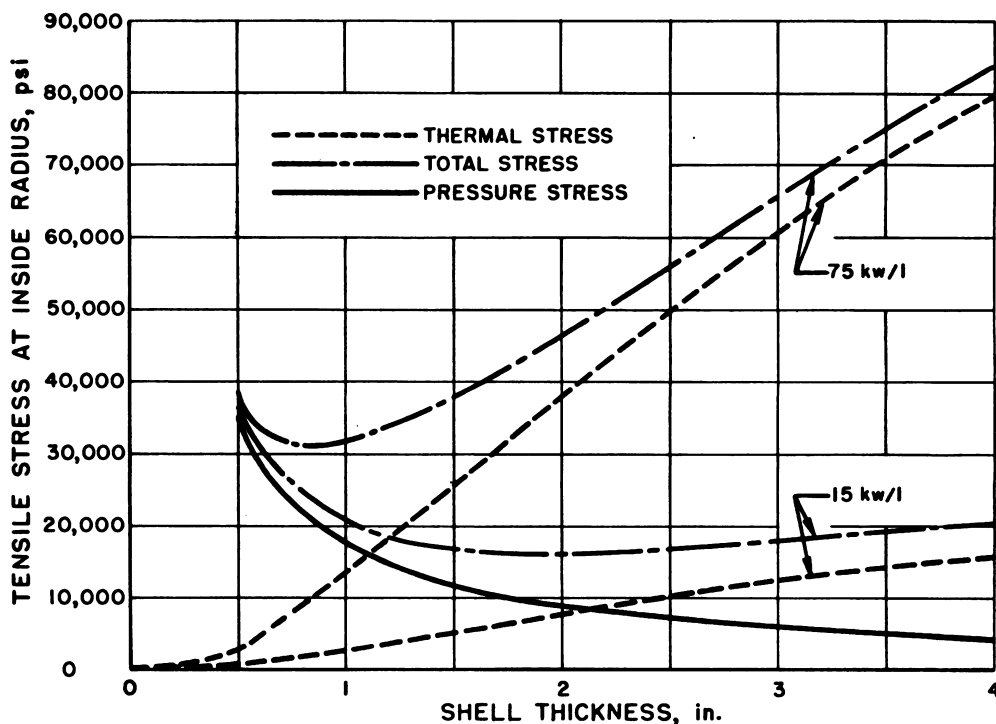


Fig. 4.7.3—Tensile Stress at Inner Surface of 6-ft-ID Spherical Reactor Core Vessel. Submitted by Oak Ridge National Laboratory, Nov. 25, 1952.

Table 4.7.1—Properties of Core-tank Materials

Property	Carbon steel	Austenitic stainless steel	Titanium	Zirconium
$\alpha \times 10^6$, in./in.(°F)	5.6–6.3 (32°–212°F)	8–11.2 (32°–1200°F)	4.95–5.12 (80°–1350°F)	2.9–4.9 (300°–700°F)
$E \times 10^{-6}$, lb/in. ²	31–26.7 (70°–752°F)	29–24 (212°–752°F)	14 (70°F)	10 (70°F)
k , Btu/(hr)(ft)(°F)	30–25 (70°–700°F)	8–12.8 (212°–932°F)	7.5–10 (32°F)	11.3–10.7 (32°–500°F)
$\frac{\alpha E}{k} \sim$	5.8–6.7	29–21	9.3–7	2.5–4.5
Ultimate strength, lb/in. ²	~65,000	80–100,000	70–80,000	20–30,000
Yield strength, lb/in. ²	~35,000	35–60,000	45–55,000	~11,000
Thickness (t), in.*	1	1–0.58	0.78–0.64	3.2
Σ_a , cm ⁻¹	0.202†	0.244†	0.316†	0.0072†
$\Sigma_a t$ } thermal } neutrons	0.202	0.244–0.142	0.246–0.202	0.021

*t is relative thickness based on yield strength of carbon steel as unity

† Calculated from values of σ_a obtained from H. Pomerance, ORNL

FORCED-CONVECTION COOLING (R. B. Briggs and C. L. Segaser)

Cooling by forced convection is the method commonly proposed for removing heat from aqueous homogeneous reactors. The term "forced convection" is used in the sense that the water solution or slurry of fuel is pumped through a circuit consisting of the reactor core, heat exchangers, and connecting piping. A mechanical pump is usually proposed, although gas and vapor lifts have often been considered. The power that can be removed from a reactor cooled by forced convection depends upon the rate at which the fluid can be pumped through the core, the heat capacity of the fluid, and the permissible temperature rise. The volume of voids present in the core is minimized by pressurizing the system.

In high-temperature systems where steam is generated in the heat exchanger and passed through a turbogenerator to produce power, the steam temperature is significantly below the minimum fuel-solution temperature. The increased thermodynamic efficiency of the steam cycle with increasing temperature is an incentive to reduce the difference between the maximum and minimum fuel-solution temperatures in a system of fixed maximum temperature. This reduction can be accomplished by increasing the circulation rate; this, in turn, requires larger pumps, piping, and heat exchangers, increases the holdup of reactor fluid in the external system, and increases pumping costs. Optimizing such a reactor-power-plant system entails balancing the costs of equipment, fuel solution, and pumping against the increased power-plant efficiency and the value of the electricity produced. An optimization of this type was made in ORNL-1096.⁸ For an aqueous homogeneous reactor operating with a maximum temperature of 250°C, an optimum steam temperature near 200°C was indicated.

The net efficiency of large nuclear power plants operating at 250°C to produce steam at 200°C and using forced-convection cooling should be approximately 22 percent. A boiling reactor operating with the same maximum temperature but producing steam at a temperature of 240°C should have a net efficiency near 25 percent. In systems cooled by flash vaporization, the pumps would consume essentially all the electricity produced.

Although the boiling reactor has a higher efficiency than a reactor cooled by forced convection for the same maximum temperature, it appears likely that more heat can be extracted from a given reactor volume or from the total volume of fuel solution in a circulating-fuel reactor. The maximum specific power that can be achieved in a large boiling reactor may be 5 kw/l or less. An over-all specific power of 15 kw/l (and perhaps as high as 25 kw/l) appears possible in a forced-convection system.

To achieve a specific power as great as 25 kw/l, the volume of the circulating system must be reduced to a minimum, and the equipment arrangement must be compact. Fluid velocities through the piping should be in the range of 20 to 30 ft/sec. The effectiveness of the heat exchangers must be high. Examples of such exchangers are the Homogeneous Reactor Experiment (HRE) exchanger (shown in Fig. 4.7.23) and the 50-mw exchanger (shown in Fig. 4.7.4) which is one of several proposals for installation in the proposed Homogeneous Reactor at Oak Ridge National Laboratory. In both exchangers, the fuel solution flows through the tubes, and steam is produced in the shell. Small tubes are used to minimize holdup. The maximum tube diameter considered is $\frac{1}{2}$ in. OD, and significant savings in the required amount of fuel solution may be achieved by reducing the tube diameter to $\frac{3}{8}$ or $\frac{1}{4}$ in.

Calculation methods for heat transfer in the 50-mw exchanger have been reported by Segaser.⁹ The over-all heat-transfer coefficient for such an exchanger is about 750 Btu/(ft²)(hr)(°F), neglecting scaling of the tubes. This may be subdivided into an inside convective heat-transfer coefficient of 3000 Btu/(ft²)(hr)(°F), a tube-wall coefficient of 2000 Btu/(ft²)(hr)(°F) for 16-gauge tubes, and an average boiling heat-transfer coefficient of 2000 Btu/(ft²)(hr)(°F). Scaling of the tubes could be expected to reduce the over-all coefficient to 500 or less, although short-term tests on single tubes have failed to show any important reduction in heat-transfer coefficient.

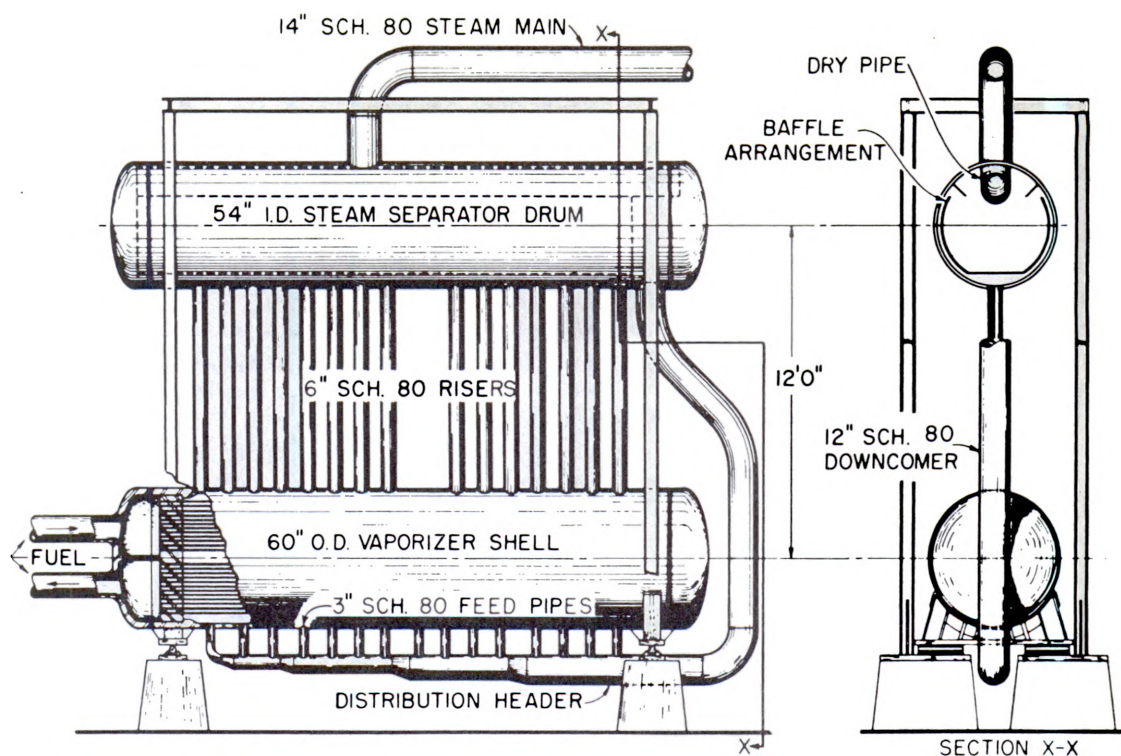


Fig. 4.7.4— Proposed Heat Exchanger for Proposed Homogeneous Reactor. Submitted by Oak Ridge National Laboratory, Nov. 25, 1952.

REMOVAL OF POWER FROM BOILING REACTORS (P. C. Zmola)

From the power-removal standpoint, the design objective is to permit the greatest vapor disengagement from the boiling aqueous solution for a given mean density.

Vapor disengagement can be accomplished by utilizing the natural rise of the bubbles or by providing centrifugal separators. Although natural bubble rise can be conveniently employed in small units (high free surface-to-volume ratio), this scheme in large units severely restricts the permissible specific power for a given mean density, and separators must be provided to obtain a specific power as large as that which appears possible in a small reactor. The process-solution holdup in the separator must be a small fraction of the total inventory. Centrifugal separators in modern steam generators can produce steam of $\frac{1}{4}$ to $\frac{1}{2}$ percent moisture at rates corresponding to 1500 kw of heat per square foot of horizontal projected drum area at an operating pressure of 1000 to 2400 psia. The severity of the vapor disengagement problem increases if foaming occurs.

The operating mean density in small units is determined by the natural rise velocity of the bubbles. In larger units, the radial density difference can establish a convective pattern which reduces the mean density for a given total power provided that a large fraction of the vapor formed can be removed in every circulation pass. Estimates of circulation velocities as a function of density decrement from saturated liquid values have been made on the basis of a simplified model.¹⁰

At present the only aqueous homogeneous reactor which has operated under boiling conditions (Los Alamos Water Boiler) has possessed an unfavorable geometry for steam release. Specific power of 0.5 kw/l was attained at atmospheric pressure, but this should not be construed as any general sort of limit.

FLASH VAPORIZATION (P. N. Haubenreich)

The flash-vaporization system shown in Fig. 4.7.5 has been suggested as a means of removing heat and preventing the formation of gas bubbles and explosive mixtures in homogeneous reactors. In this scheme the pressure on the reactor fuel solution is suddenly reduced by an orifice (or some other device) to such an extent that a portion of the fluid

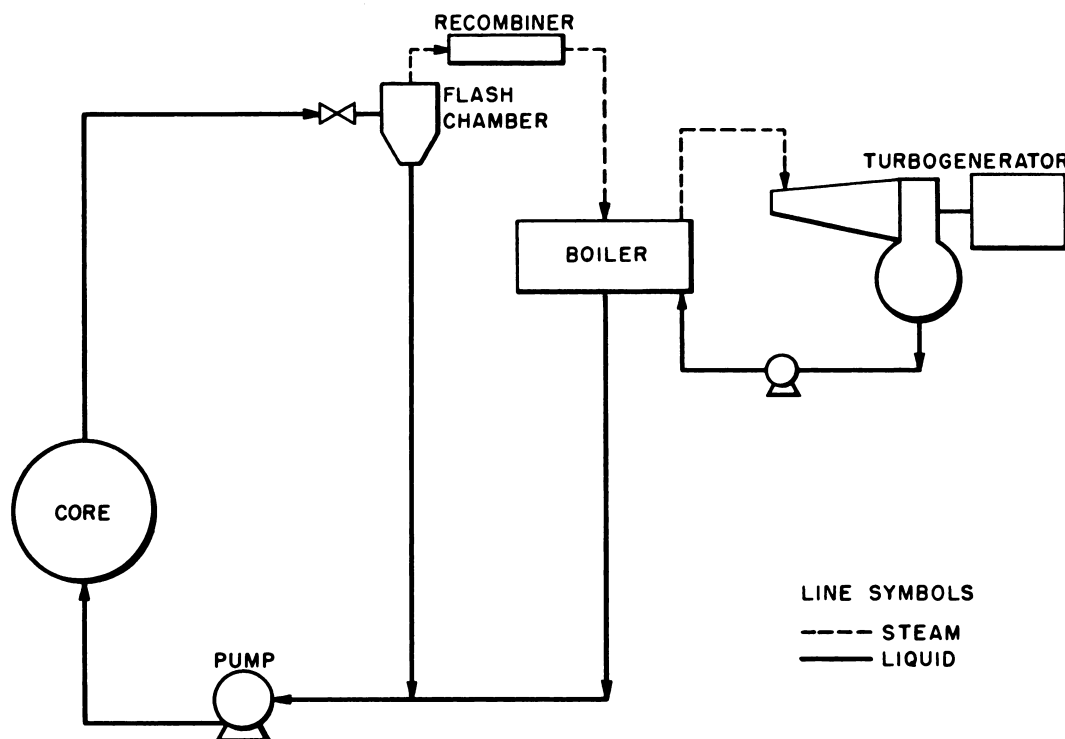


Fig. 4.7.5—Proposed Cycle for Power Generation from Steam Derived by Flash Vaporization. Submitted by Oak Ridge National Laboratory, Nov. 25, 1952.

flashes into steam. This steam is removed, carrying with it essentially all the decomposition gases. After passing through a recombiner, the steam is condensed in a heat exchanger which serves as a boiler to provide steam for a turbogenerator through a secondary circuit. The fuel solution entering the core is free of gas. The pressure and flow rate in the reactors are maintained high enough so that the gas concentration is kept below saturation there.

Among the advantages of such a system are the absence of gas bubbles in the core, the nonexplosive character of the mixture supplied to the recombiners, and a high heat-transfer coefficient in the heat exchanger. Its major disadvantage is the large amount of pump power required because of the available energy lost in flashing. The design of a device for reducing the pressure would also be difficult.

The results of some calculations for such a system are shown in Figs. 4.7.6 and 4.7.7. These results are based on the following conditions:

- (1) Heat release in core, 50,000 kw
- (2) Gas evolution rate, 1 molecule/100 ev
- (3) Gas concentration at core outlet, 80 percent of saturation
- (4) Core outlet temperature, 482°F
- (5) Temperature difference in heat exchanger, 20°F

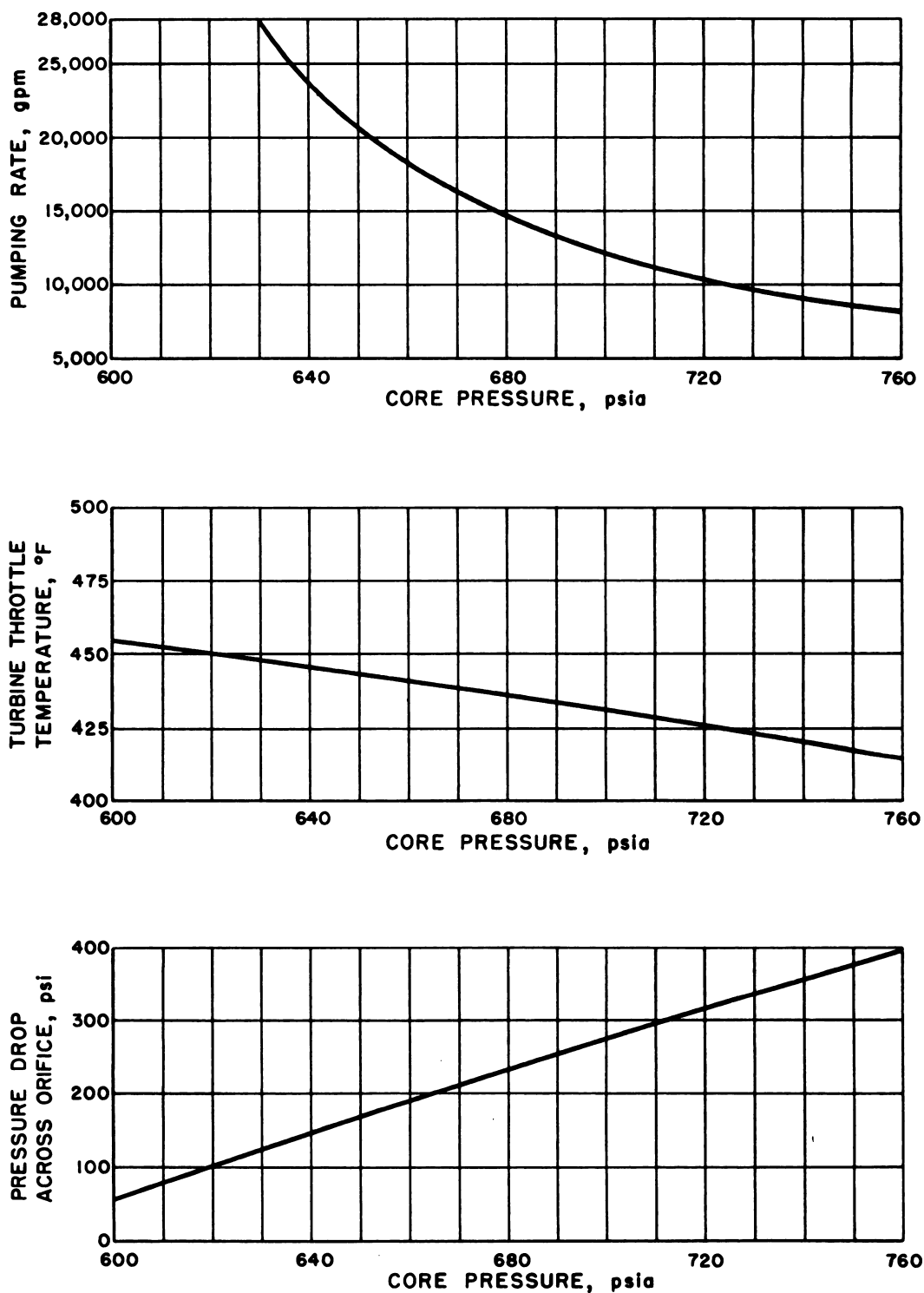


Fig. 4.7.6—Pumping Rate, Pressure Drop, and Throttle Temperature vs Core Pressure for Flash-vaporization Cycle. Submitted by Oak Ridge National Laboratory, Nov. 25, 1952. Reprinted from ORNL CF-51-11-28.

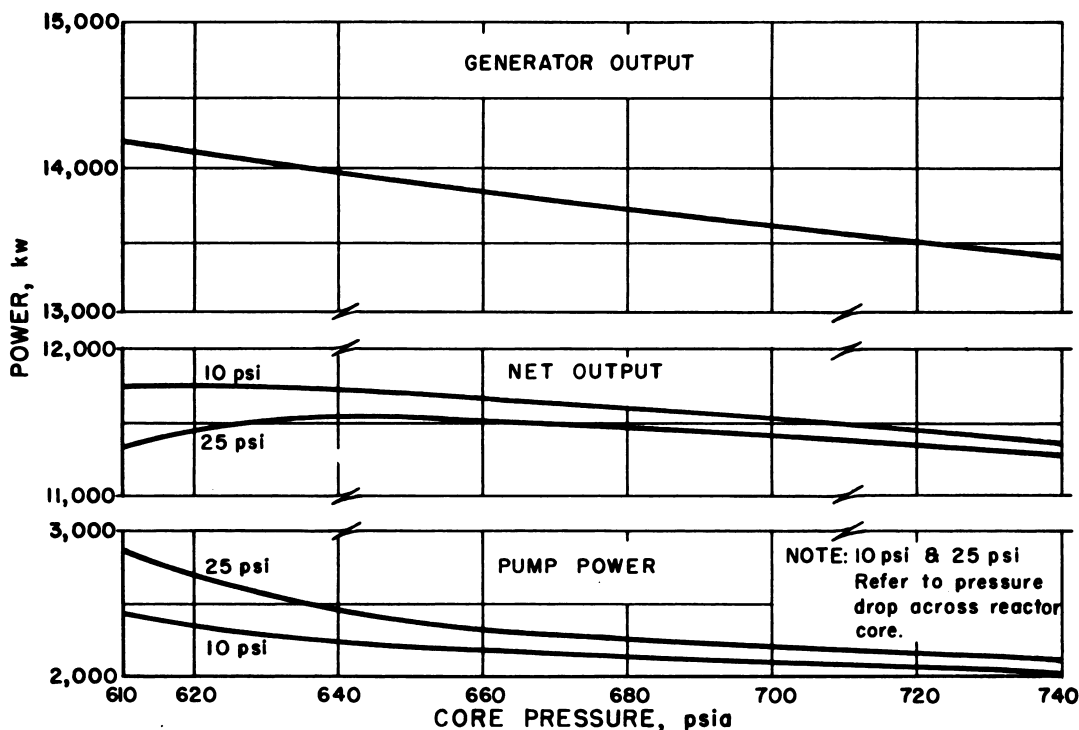


Fig. 4.7.7—Power vs Core Pressure for Typical Flash-vaporization Cycle. Submitted by Oak Ridge National Laboratory, Nov. 25, 1952. Reprinted from ORNL CF-51-11-28.

The vapor pressure of the solution is assumed to be the same as that of pure water. Solubility data are based on those in BMI-T-25 and steam-cycle efficiencies on those in ORNL CF-51-7-66. Pump-power requirements are calculated on the basis of 10- and 25-psi pressure drops across the reactor core.

GAS HANDLING SYSTEMS

EXTERNAL RECOMBINERS (J. A. Ransohoff and C. B. Graham)

The operation of a reactor in which the fuel is an aqueous solution or slurry will result in the evolution of gas from two sources. Gaseous fission fragments or their descendants contribute a small volume, but a much greater volume is evolved as hydrogen and oxygen from the radiolytic dissociation of water in the reactor. The fission products are produced in small enough quantities to be adsorbed in a shielded charcoal bed, but to stabilize the solution concentration and reduce the total volume of reactor gases, the H_2 and O_2 should be recombined and the water returned to the system.

Two aqueous-solution reactors have been built and operated: the Los Alamos water boiler and the ORNL Homogeneous Reactor Experiment (HRE). The gas handling problem of the latter includes most of the difficulties anticipated in disposing of gaseous products of aqueous-solution reactors, and the following discussion is devoted primarily to the disposal of gas in that reactor.

HRE OFF-GAS SYSTEM

The HRE is expected to produce 2H_2^+ to O_2 at a rate of about 12 cu ft* (STP)/min when the reactor is operating at 1000 kw. The gas formed in the fuel solution at pressures up to 1000 psi and temperatures up to 250°C is removed from the solution, reduced to atmospheric pressure, recombined to water, and returned as such to the fuel solution. Since the operating level may be set at any fraction of design power for prolonged periods, the gas-handling system must accommodate any quantity of gas between 0 and 15 cu ft/min.

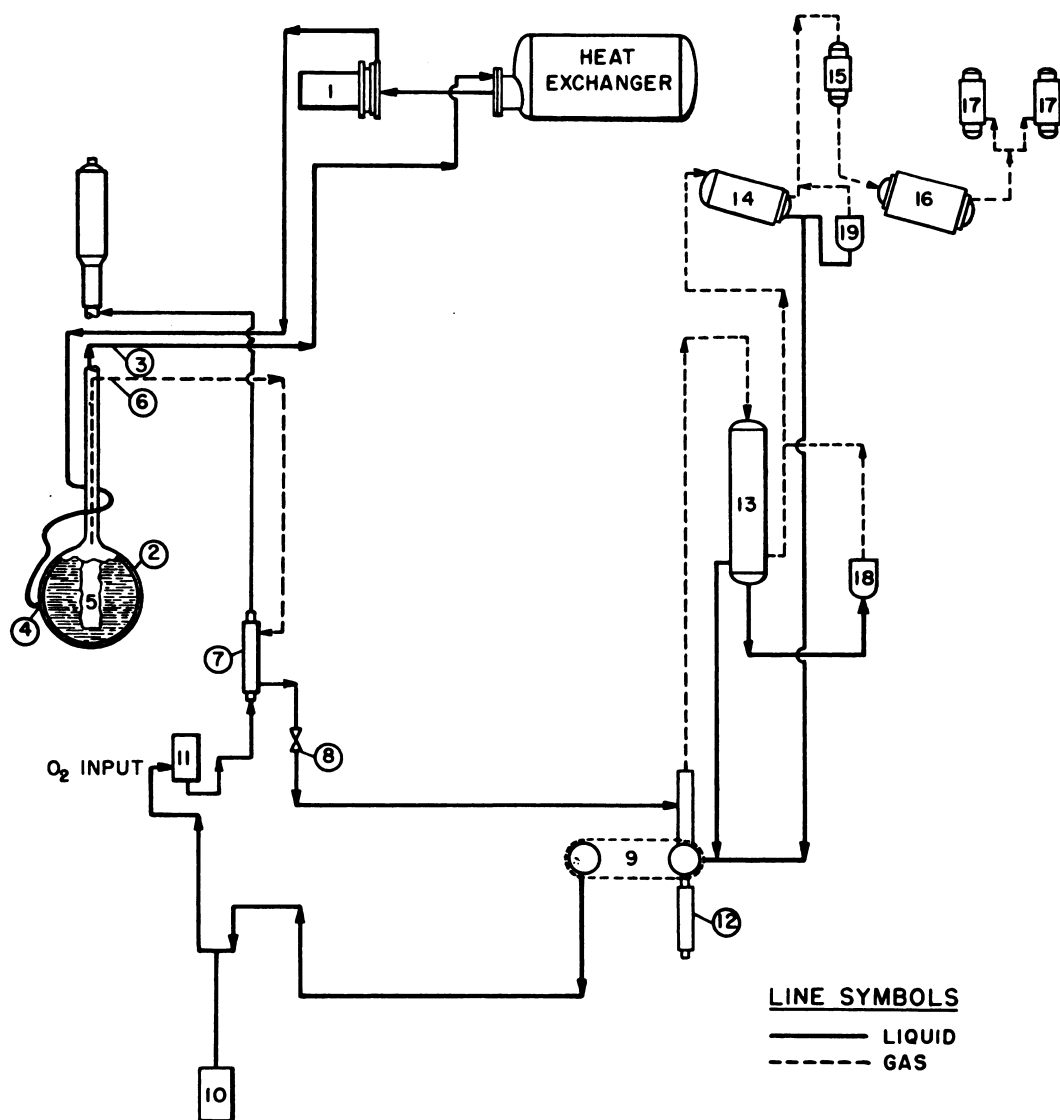
The removal of gas from the fuel solution is facilitated by creating a gas vortex along the vertical diameter of the core. A simplified diagram of the HRE off-gas system is shown in Fig. 4.7.8. The 75 liters of fuel solution in the high-pressure system are circulated at a rate of 100 gal/min by a canned-rotor centrifugal pump (1). The liquid flows from the core (2) through the second of three concentric pipes stemming from the top (3) and is pumped through a heat exchanger back into the core tangentially at (4). The fluid in the core therefore rotates rapidly. The gas-liquid density difference causes the gas to separate from the liquid and establish a vortex along the axis of the resulting centrifugal force field (5). The gas in the vortex, along with a considerable quantity of liquid, flows through the innermost of the three concentric pipes (6), through a double-pipe heat exchanger (7) to a valve (8) which throttles the stream to atmospheric pressure. Fuel solution is continually pumped by a pulsafeeder (10) from the dump tanks (9) through the inner pipe of the double-pipe heat exchanger (7) into the core to replace the gas-liquid mixture which is let down from the high-pressure system into the dump tanks.

The line from the let-down valve connects into the vapor space at the top of the dump tanks. Most of the liquid in the stream drops into the dump tanks, but some is flashed with the gas which goes to the recombiner system. The amount of steam flashed at this point varies from 5 to 50 percent of the total gas flow, depending on the gas-liquid ratio in the let-down stream, the core temperature, the pumping rate, and other factors. An evaporator (12) in the dump tanks adds up to 40 scfm of steam to the gas to make the mixture flowing from the dump tanks to the recombiner system nonexplosive.^{11,12} The steam is condensed from the gas in a large fore condenser (13); this returns the mixture to combustible form. The condensate is either returned by gravity to the dump tanks or is collected in condensate weigh tanks if it is desirable to concentrate the fuel solution.

Flame Recombiner

The gas flows from the condenser to the flame recombiner (14) where the H_2 and O_2 are burned to water. The flame is established at a many-holed nozzle upon which a spark impinges from one of two spark plugs located along the periphery of the nozzle, Fig. 4.7.9. The spark impluse is produced by a magneto with an ignition transformer on standby. The combustion chamber is a $3\frac{1}{2}$ -ft length of 10-in. pipe, jacketed by a 12-in. pipe through which cooling water is circulated. The cooling water removes 70 to 80 percent of the heat of combustion even at high gas flows.¹³ With combustible gas flows of 15 scfm, for instance, the temperature at the downstream end of the flame recombiner did not exceed 600°C , and 70 percent of the heat of combustion was recovered in the jacket of the flame recombiner. The additional heat was recovered in the after condenser (16). The gases remaining after combustion [fission products plus the 1200 cc/min of excess O_2 which is continuously added to the system at (11)] are adsorbed in a charcoal bed after being stripped of all

* Operation of the HRE at the design power of 1000 kw yielded 10 scfm of $2\text{H}_2 + \text{O}_2$ per megawatt of reactor power. On March 18, 1953, the reactor was operated at 1500 kw long enough to observe the recombiner system in operation at its rated load. It was able to handle the 15 cfm of $2\text{H}_2 + \text{O}_2$ produced at that power; however, the temperature at the bottom of the flame recombiner reached 620°C during the operation, and it is questionable whether the system should be submitted to higher loads.



1. CANNED ROTOR CENTRIFUGAL PUMP
2. CORE
3. SECOND OF 3 CONCENTRIC PIPES
4. INLET FROM HEAT EXCHANGER TO CORE
5. VORTEX
6. THIRD OF 3 CONCENTRIC PIPES
7. DOUBLE-PIPE HEAT EXCHANGER
8. LETDOWN VALVE
9. DUMP TANKS
10. PULSAFEEDER

11. OXYGEN ABSORBER
12. FUEL EVAPORATOR
13. FORE CONDENSER
14. FLAME RECOMBINER
15. CATALYTIC RECOMBINER
16. AFTER CONDENSER
17. COLD TRAPS
18. STEAMER POT
19. STEAMER POT

Fig. 4.7.8—Simplified Flow Diagram for HRE Off-gas System. Submitted by Oak Ridge National Laboratory, Nov. 25, 1952.

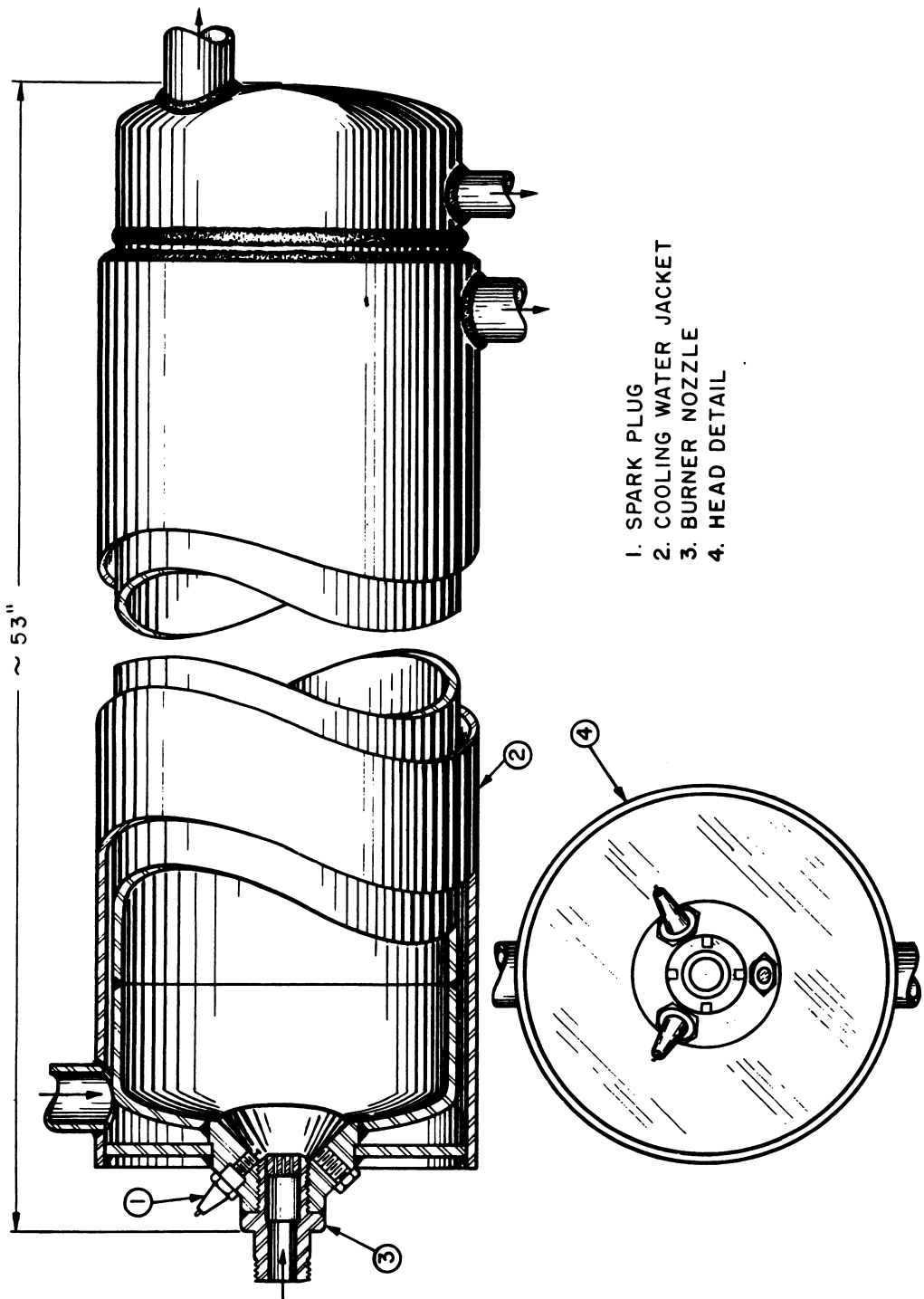


Fig. 4.7.9— Primary Flame Recombiner for Fuel Circuit in Homogeneous Reactor Experiment. Submitted by Oak Ridge National Laboratory, Nov. 25, 1952.

their water vapor in cold traps (17); the condensed products of combustion are returned to the dump tanks by gravity.

The flow area of the nozzle consists of 147 holes $\frac{1}{32}$ in. in diameter, the total cross section of which is 0.112 sq. in. When the flow rate is 30 cu ft/min, the velocity through the nozzle is 640 ft/sec, and the pressure drop through the nozzle approaches the 11-ft (water) head by which water is returned from the recombiner to the dump tanks. At flows of less than 3 scfm, the pressure drop through the nozzle is so low that the flame burns too closely to the tip, the nozzle overheats, and flashbacks result.

Flashbacks

To prevent flashbacks, a steamer pot (18) adds 2 to 3 scfm of steam to the gas stream flowing from the fore condenser to the flame recombiner. This serves both to cool the flame by diluting it and to provide the minimum flow necessary to keep the flame from burning directly on the nozzle. At extremely low flows (less than $\frac{3}{4}$ scfm), the spark must operate at all times to ensure constant burning of the extremely dilute gas.

Flashbacks originating in the recombiner system create peak pressures of from 100 to 400 psi, depending on the starting pressure and the mechanism of the reaction.¹⁴ Such reactions will be quenched in the gas line between the dump tanks and the fore condenser if the gas in the line contains more than 70 percent steam. There is, of course, a possibility that the process-solution evaporator (12) may fail or be shut off for some reason, or that gas flows greater than those expected will have to be handled. It was feared that if the mixture in the off-gas line were combustible, an explosion originating in one of the recombiners might travel back through the off-gas line to the dump tanks and thence through the let-down valve into the high-pressure system. Tests of the recombiner while installed in the HRE indicate that this will not occur with the reactor operating at 1000 psi and 250°C and a pulsafeder pumping rate of 1 gpm.

Following a flashback, a flame could be established in the fore-condenser where the gas is combustible. In such a situation, if the cooling water to the condenser is turned off for a few moments, the noncombustible front will move forward and should force the flame back to the nozzle where it may become reestablished in the presence of a spark. To protect the condenser, however, it is advisable to reduce the power level of the reactor to a point where less than one scfm of gas is being produced.

Catalytic Recombiner

At extremely low power levels (less than 20 kw), operation of the flame recombiner is inconsistent, and over-all recombiner operations are usually improved if the spark is shut off and the gas-steam mixture is allowed to flow into the catalytic recombiner (15) where the reaction of hydrogen and oxygen is catalysed by platinum. The catalytic recombiner is shown in Fig. 4.7.10. The thin layer of platinum metal used as catalyst is supported by $\frac{1}{8}$ -in. alumina pellets which offer extremely high surface area per unit volume. The permissible space velocity for 99.9 percent conversion through a bed of $\frac{1}{8}$ -in. alumina pellets is more than 3×10^5 hr⁻¹; the $5\frac{1}{2}$ -in. length of 3-in. pipe used in the HRE is thus only partially used in recombining the $\frac{1}{2}$ scfm of gas, the maximum load anticipated during operation of the reactor.¹⁵ Local overheating will occur in the catalyst bed, and unless the gases are diluted below the explosive limit, backflashes will result.¹¹ Since most of the steam that flows with the combustible gas through the flame recombiner nozzle is condensed on the cold walls of the recombiner chamber, another steamer pot (19) was placed between the flame recombiner and catalytic recombiner to dilute the combustible gas. This pot operates continuously, and at full load (about 3 scfm), it produces enough diluent to prevent flashbacks from the catalyst for all combustible-gas flows up to $\frac{1}{2}$ scfm.

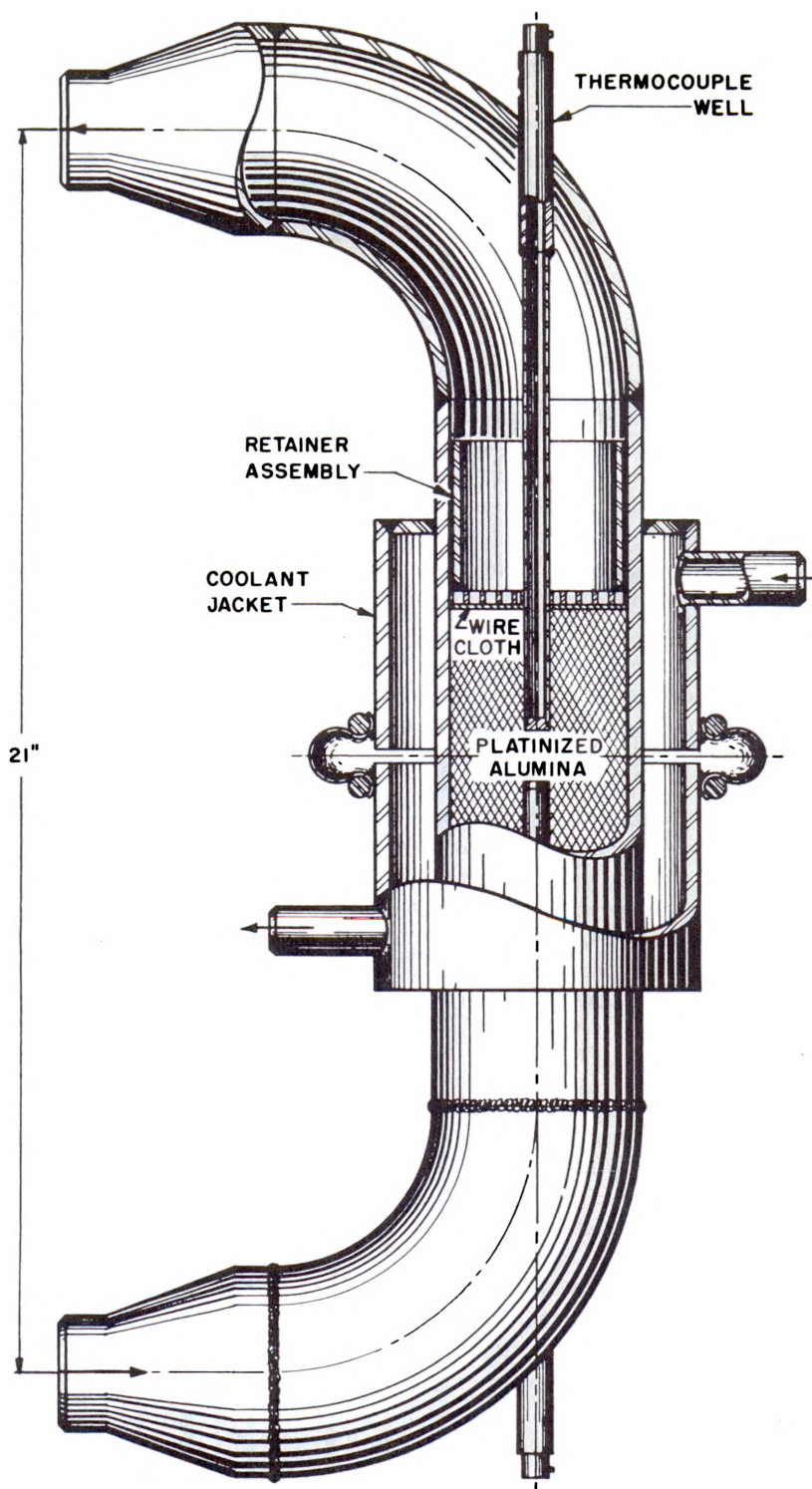


Fig. 4.7.10—Low-pressure Catalytic Recombiner for Fuel Circuit in Homogeneous Reactor Experiment. Submitted by Oak Ridge National Laboratory, Nov. 25, 1952.

The catalyst may be poisoned by films of either water or iodine. Water poisoning is avoided by jacketing the recombiner with steam, which serves to keep the catalyst dry at all times. Since iodine is one of the more predominant fission products, iodine poisoning is possible unless the recombiner is heated occasionally to 400°C to volatilize the iodine.¹⁵ This can be done either by the heat from the catalytic reaction of the combustible gases or by the heat produced in burning the gases, which is carried over into the catalyst bed at high gas-flow rates.

Plans for future reactors indicate that it might be desirable to recombine the gases at high pressure rather than either at atmospheric pressure, as is now done in the HRE, or at reduced pressure as is done in the water boiler.¹⁶ At high pressures, however, the consequences of an explosion would be quite severe, and it is highly desirable that a noncombustible mixture exist at all times. Since a flame recombiner can of course not operate with a non-combustible gas mixture, a high-pressure flame recombiner can not be considered, and accordingly, all development work after satisfactory operation of the HRE flame recombiner was achieved has been directed toward determining the reaction controlling mechanism on platinum as the first step toward designing a high-pressure catalytic recombiner.^{17,18}

One high-pressure catalytic recombiner has already been operated satisfactorily. In the reflector system of the HRE, the formation of approximately $\frac{1}{4}$ scfm of gas is expected as a result of radiation when the reactor is operating at 1000 kw. The gas space of the reflector vessel is filled with He gas which is circulated through a high-pressure catalytic recombiner that is similar to the low-pressure recombiner described above. The He serves as a diluent for the decomposed gas, and the gas mixture is pulled through the catalyst bed by a liquid jet at a rate of more than 5 scfm; this ensures a combustible-gas composition of less than 5 percent in the gas stream. The recombiner has been operated several times with a reflector pressure of 600 psi and a temperature of 200°C while approximately $\frac{1}{4}$ scfm of stoichiometric gas was added to the system. The recombiner is heated with 220-psi steam to keep the catalyst dry, since the partial pressure of water vapor at 200°C (reflector temperature) is about 200 psi.

A similar catalytic recombiner is also used in the low-pressure reflector system of the HRE to recombine any dissociated gas admitted to that part of the system when the reflector is dumped.

GAS PRODUCTION

Chapter 4.3 has described the effects of fission fragments upon the decomposition of water to hydrogen and oxygen. Values of G (the molecules of hydrogen produced per 100 ev of energy absorbed by the solution) have been presented for a variety of fissionable species at different concentrations, temperatures, enrichments, and the like. For convenience, the gas production in a reactor solution may be calculated from the simple equation:

$$K = 0.312 \times G \times PD \quad (9)$$

where K = moles hydrogen per liter per hour

PD = the power density of the reactor in kilowatts per liter

This equation may easily be derived from a more comprehensive expression given in ORNL-1280.¹⁹

SPECIAL EQUIPMENT DESIGN

PUMPS

*ROTARY PUMPS (W. L. Ross, R. J. Kedl, and C. B. Graham)***Five-gpm Allis-Chalmers Pump**

A small, canned-rotor, 3600-rpm, 60-cycle, 110-v pump has been developed by the Allis-Chalmers Mfg. Co. for applications where leakage cannot be tolerated. The unit, shown in Figs. 4.7.11 and 4.7.12. can be produced at a relatively low cost.

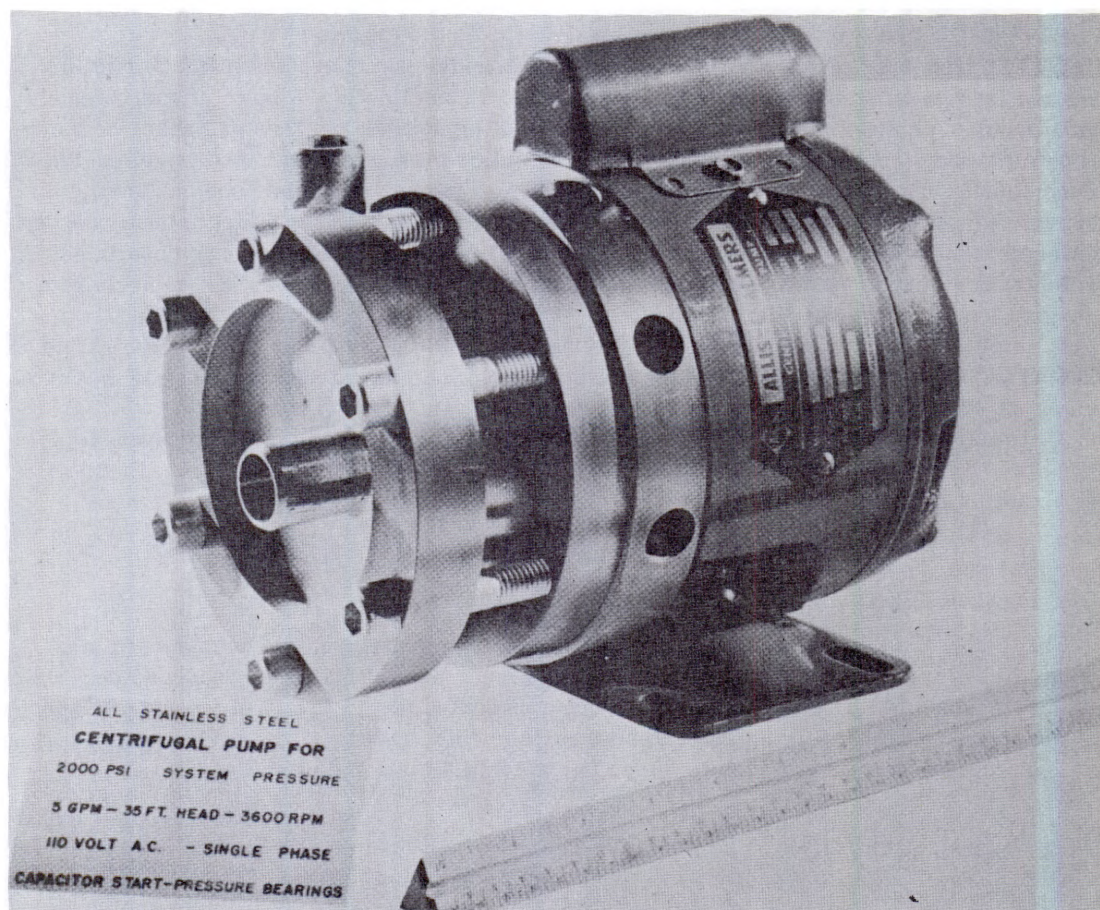


Fig. 4.7.11—Allis-Chalmers 5-gpm Enclosed-rotor Pump. Submitted by Oak Ridge National Laboratory, Nov. 25, 1952. Allis-Chalmers Photo No. 164399.

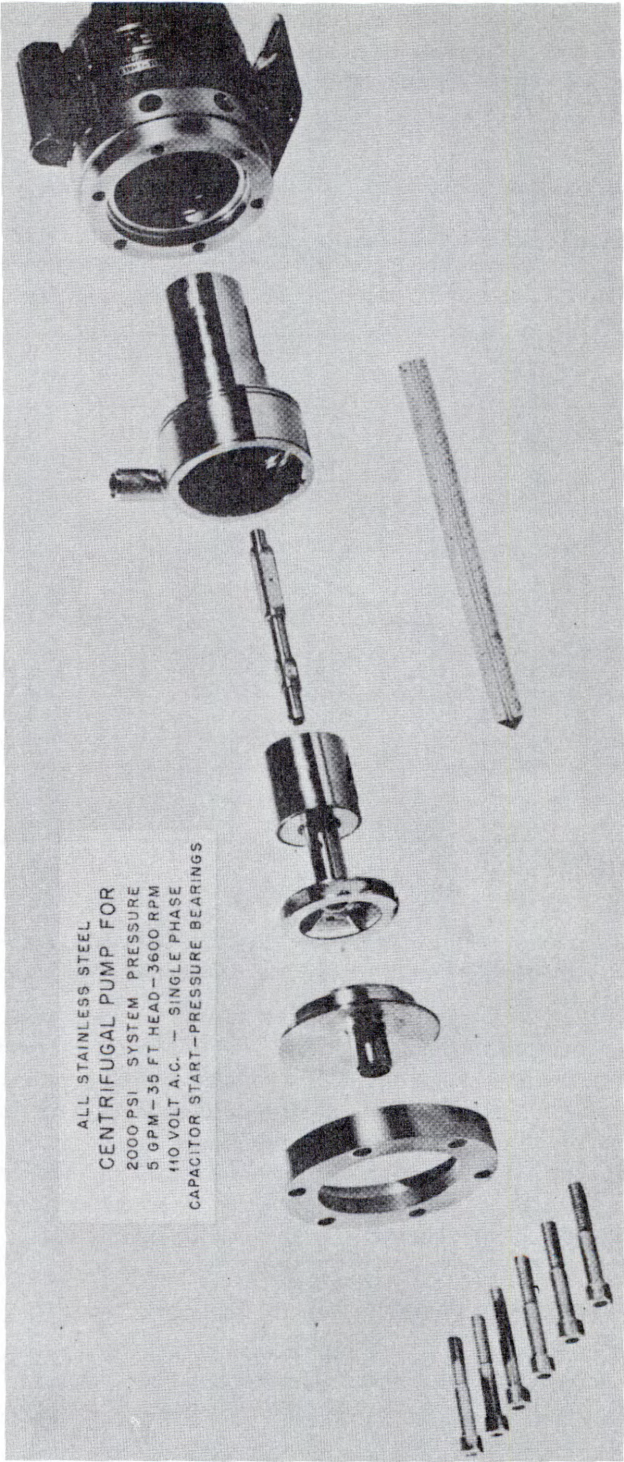


Fig. 4.7.12—5-gpm Allis-Chalmers Enclosed-rotor Pump. Submitted by Oak Ridge National Laboratory, Nov. 25, 1952. Allis-Chalmers Photo No. 164400.

The pump is rated at 5 gpm of water against a 35-ft head, but higher flows and heads can be obtained (up to 18 gpm \times 40) as shown in the characteristic curves, Fig. 4.7.13. Suction pressures up to 2000 psi and temperatures up to 500°F may be used; special stator windings would permit higher temperatures. All wetted parts of the pump are made of type 347 stainless steel, and provisions have been made to permit a welded closure, if one is desired. Some of the wearing parts have been chrome-plated, but this is believed to be unnecessary.

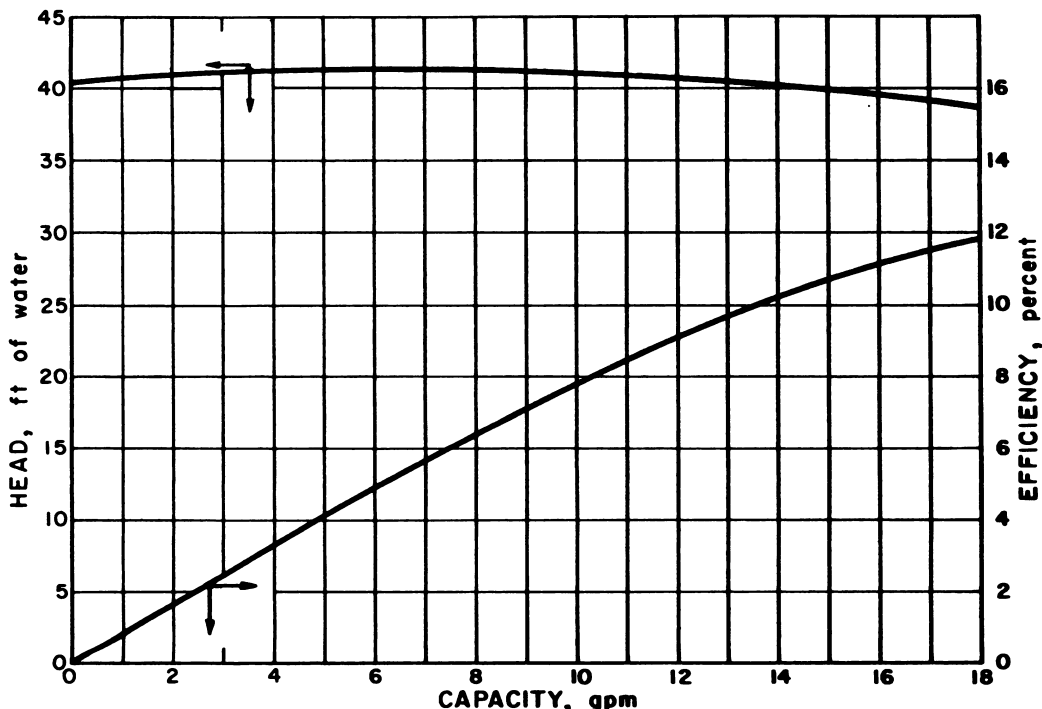


Fig. 4.7.13—Characteristic Curves for Allis-Chalmers 5-gpm Enclosed-rotor Pump. Submitted by Oak Ridge National Laboratory, Nov. 25, 1952.

Figure 4.7.14 shows a section through the pump. The hydrostatic-type bearings are supplied with liquid from the discharge chamber as shown by the arrows. This liquid flows through the hollow, stationary, bearing shaft and then through orifices into the radial bearing cavities. As the liquid leaves the bearings it flows through various passages back to the pump suction. Thrust loads are carried by hydrostatic bearings which are incorporated into the impeller shrouds, as shown. Thus the rotating, rotor-impeller assembly "floats" on a liquid pad, without mechanical contact, during operation.

Model 100 and 100A Westinghouse Pumps

This pump was initially developed by the Westinghouse Electric Corporation. As shown in Fig. 4.7.15, it is a totally enclosed type in which the oil-cooled stator is jacketed with a 0.040-in. sheet of Inconel and the rotor is jacketed with a 0.014-in. sheet of stainless steel. This design eliminates packing and thus avoids the leakage problem. It also permits water to be injected into the motor and bearing chamber; by continuously flushing water through the labyrinth, all abrasives or corrosive material in the fluid being pumped will be kept out of this chamber. The maximum operating pressure-temperature combination of this

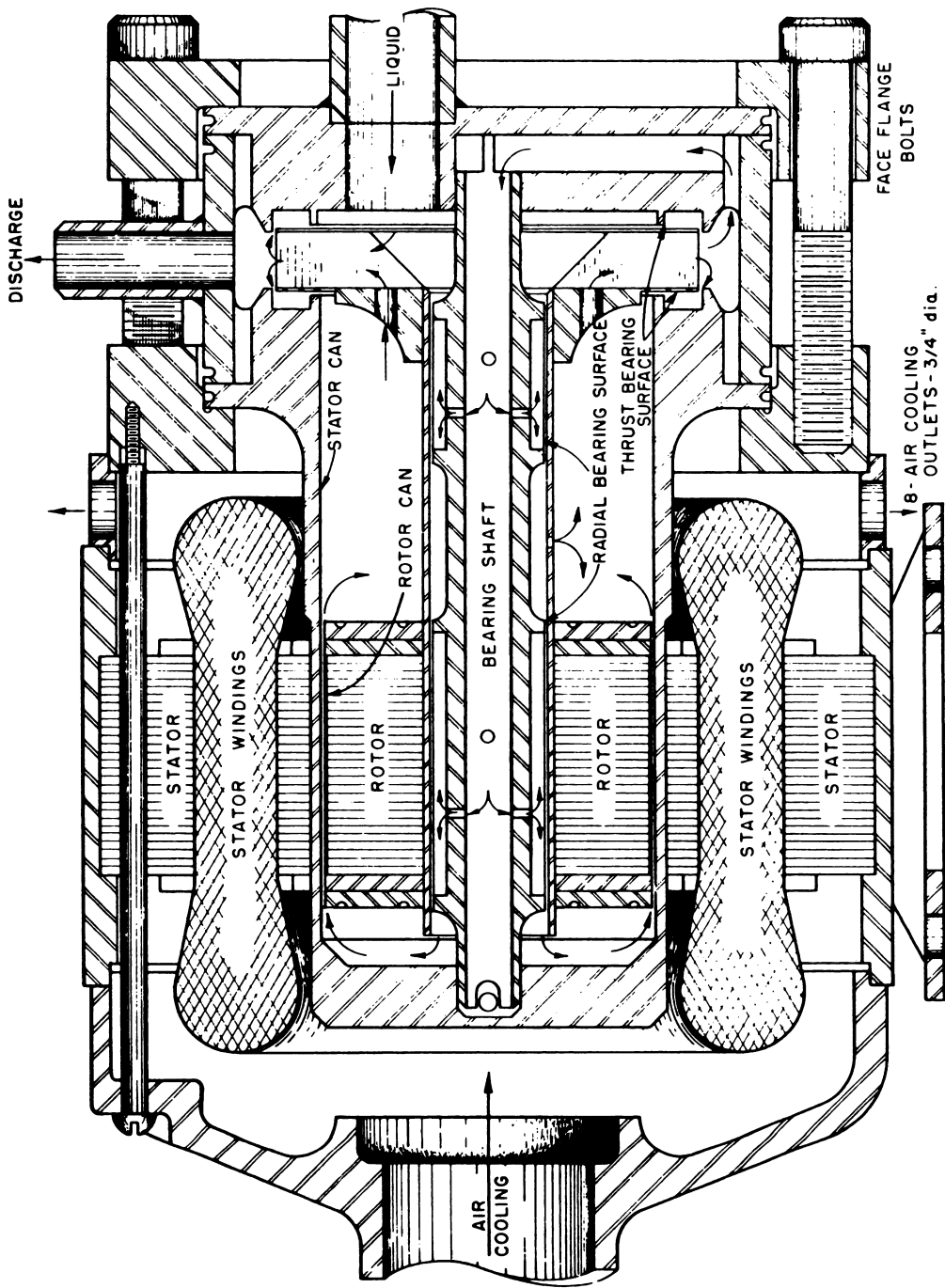


Fig. 4.7.14 —Simplified Section Through Allis-Chalmers 5-gpm Enclosed-rotor Pump. Submitted by Oak Ridge National Laboratory, Nov. 25, 1952.

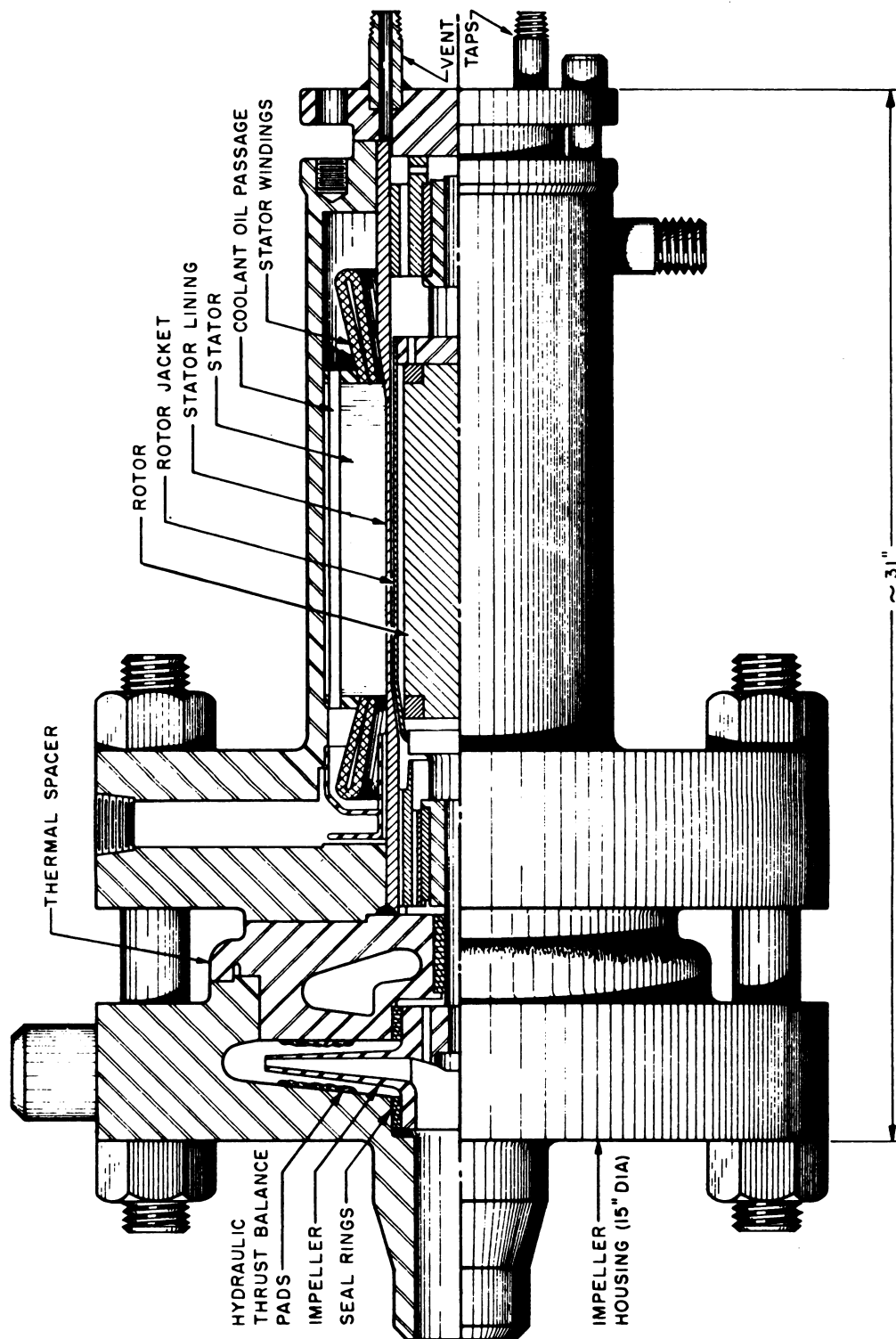


Fig. 4.7.15—100-gpm Westinghouse Model 100-A Enclosed-rotor Pump. Submitted by Oak Ridge National Laboratory, Nov. 25, 1952.

pump is 2000 psi at 600°F. Figure 4.7.16 shows a plot of the discharge pressure vs capacity for this pump. The materials of construction in the standard pump which are in contact with the fluid circuit are:

Casing and impeller	Type 347 stainless steel
Shaft	Squirrel-cage type; copper bars in a soft iron core with a can of 347 stainless steel welded over the assembly
Stator jacket	Inconel, wrought
Bearings	Carbon graphite
Journal bushings	Titanium carbide, Model 100A Chrome-plated, Model 100
Labyrinth disks	Nickel

There are two models of this pump, Model 100 and Model 100A, differing principally in bearing design. The former has a chrome-plated journal 1 by $1\frac{1}{8}$ in. with the rear bearing

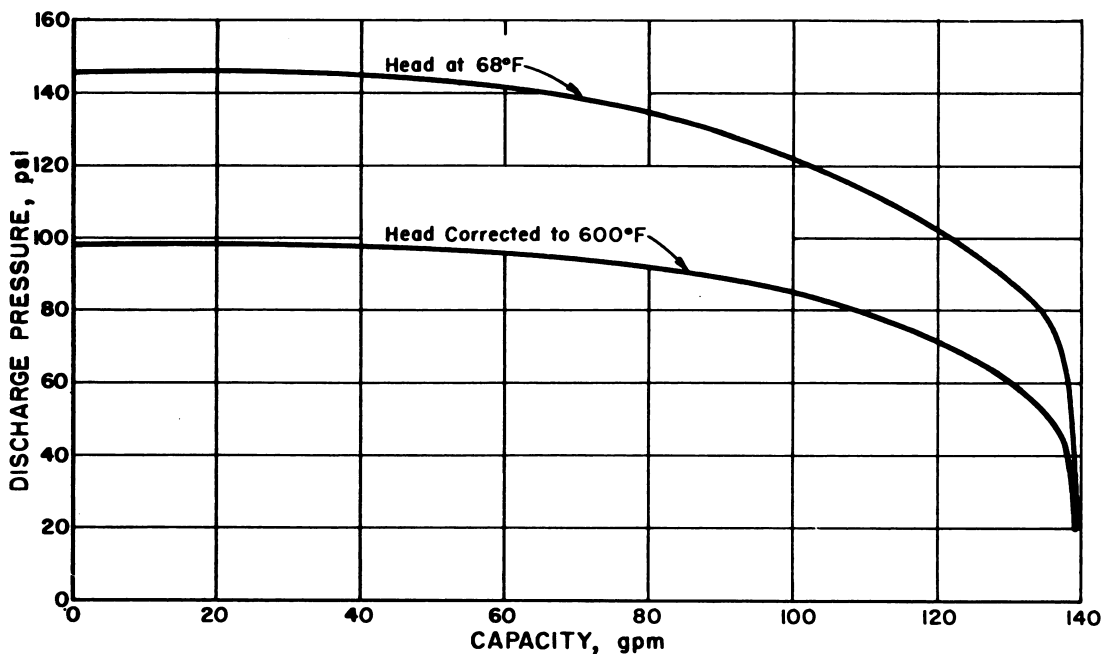


Fig. 4.7.16 — Discharge Pressure-capacity Relation for Westinghouse Model 100-A Enclosed-rotor Pump. Submitted by Oak Ridge National Laboratory, Nov. 25, 1952.

mounted on the motor end plate; the latter has a titanium carbide journal $1\frac{1}{2}$ by 2 in., with a removable rear bearing mount. Several smaller (approximately 30-gpm) pumps have been built.

20,000-gpm Allis-Chalmers Pump

This pump is to be designed and built by the Allis-Chalmers company. Although construction has not yet started, the design is far enough along so that no major changes are anticipated. Specifications call for 20,000 gpm, 160-ft head, 1000-psi suction pressure, and stainless-steel construction.

The pump is a canned-rotor, totally enclosed type which employs a metallic diaphragm to seal the motor stator from the high-pressure fluid. The canned rotor, which includes a metal sealed armature, rotates submerged in the high-pressure fluid. The fluid fills the space between the rotor and stator in what would normally be the air-gap in a standard motor. Pump bearings to support and align the rotating parts are of a hydraulic-pressurized, fluid-piston (hydrostatic) type which utilizes either an auxiliary impeller attached to the rotating shaft (Fig. 4.7.17) or an external source to supply pressurized water to two radial bearings and one thrust bearing, the thrust bearing being able to take loads in two directions.

The pump will be mounted in a vertical position with the impeller at the bottom. The fluid-filled motor-bearing chamber will be separated from the impeller and volute by means of a close-clearance labyrinth. By injecting uncontaminated water into the motor-bearing chamber and continuously flushing it through the labyrinth into the volute, the corrosion on the motor and bearing parts should be reduced considerably. This auxiliary flow also keeps radioactive material from getting into the motor-bearing chamber, thus reducing irradiation of the electrical insulation. The flush volume is small enough to make dilution of the pumped fluid insignificant (in the order of 1 gpm flowing into a 20,000-gpm stream). The present design for the pump provides a cooler to keep the bearing water and motor-chamber water at less than 150°F.

The pump power will be supplied by a 440-volt, 6-pole (1200-rpm synchronous speed) induction motor. The stator, which is sealed from the high-pressure fluid by a metal diaphragm, has hollow conductors. Motor cooling water will flow through the hollow channels in the conductors and remove the heat developed in them. In the stator, the conductors are the major source of heat, and the motor cooling water will remove the heat close to its source; therefore, the conductor insulation will not be subjected to high temperatures.

The pump is so constructed that when the top flange is unbolted, the entire inside of the pump can be lifted out, leaving only the high-pressure casing in the pipe line. The stator or upper bearing may be replaced separately if desired. The induced radioactivity is low at the upper end of the pumps, and this replacement of the parts is expected to be relatively easy.

The principal characteristics of the pump are listed in Table 4.7.2.

POSITIVE DISPLACEMENT PUMPS (J. S. Culver, C. B. Graham)

The pulsafeeder pump, manufactured by the Lapp Insulator Co., Inc., consists essentially of a diaphragm and check valves actuated by a reciprocating oil pump. It is used for pumping small volumes (1 or 2 gpm) against high pressure (1000 psi). Its design offers several advantages to the HRE:

- (1) It is relatively simple and inexpensive.
- (2) The diaphragms are within the shield, thereby isolating the radioactive fuel. As there are two diaphragms, a rupture would not allow any radioactive material to escape from the shield.
- (3) The operating mechanism is outside the shield and easily accessible. There are no mechanical parts within the shield other than the diaphragms and check valves.

Each diaphragm is contained in a head assembly consisting of two machined flanges, between which the diaphragm is seal-welded, and a hoop into which the diaphragm and flanges are strength-welded. The faces of the flanges are contoured so that stress throughout a diaphragm will be essentially uniform when it is flush against the flange face. The maximum calculated stress in the diaphragm is 20,000 psi, permitting long-term operation without fatigue failure. The present design will withstand static pressures up to 5000 psi.

As shown in Fig. 4.7.18, the pump operates in the following manner: on the suction stroke of the oil pump, the intake ball-check valve opens, allowing the liquid being pumped to enter the pumping head at atmospheric pressure. As the oil piston reverses, the intake check

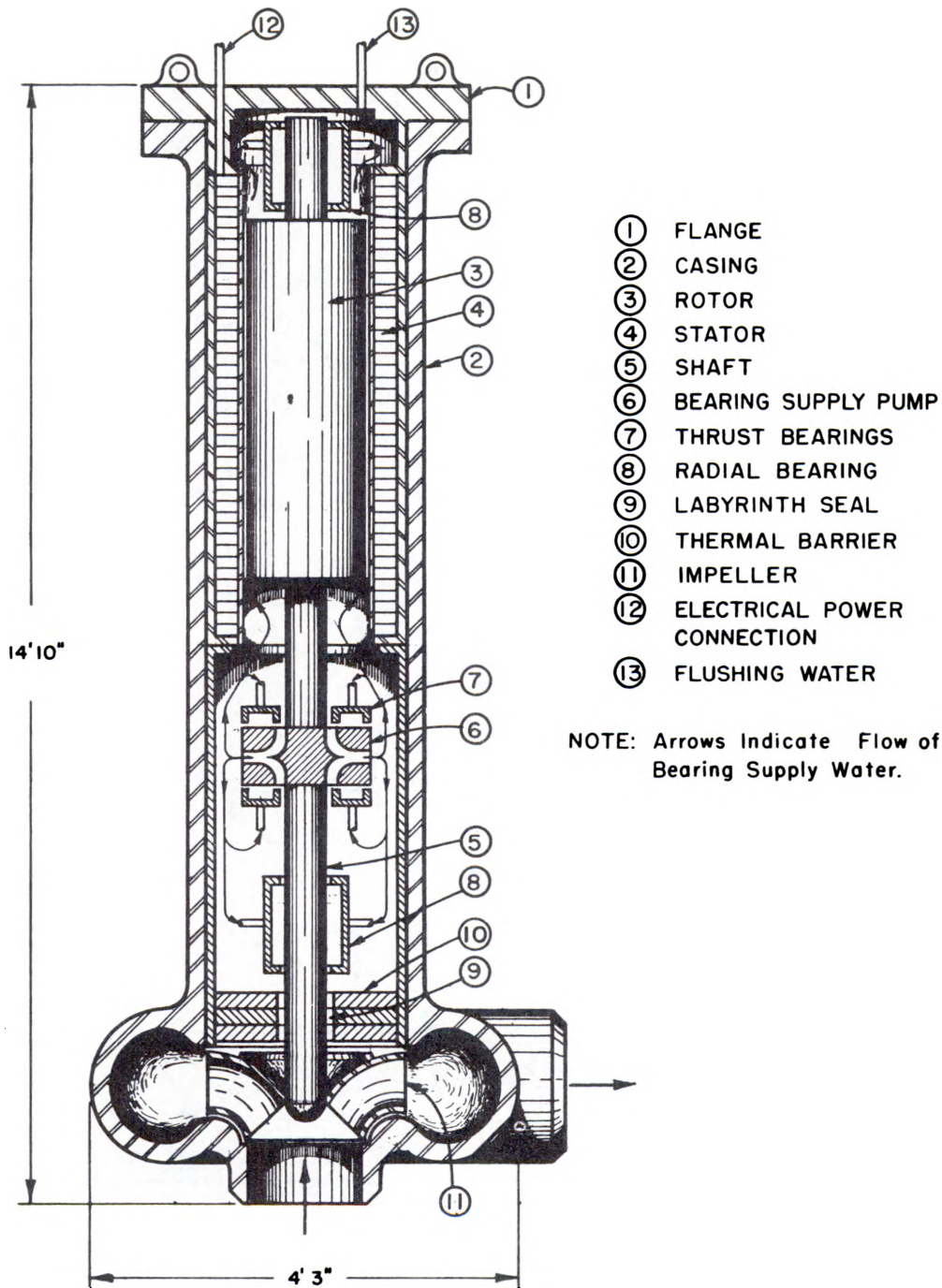


Fig. 4.7.17 — Proposed Allis-Chalmers 20,000-gpm Enclosed-rotor Pump. Submitted by Oak Ridge National Laboratory, Nov. 25, 1952.

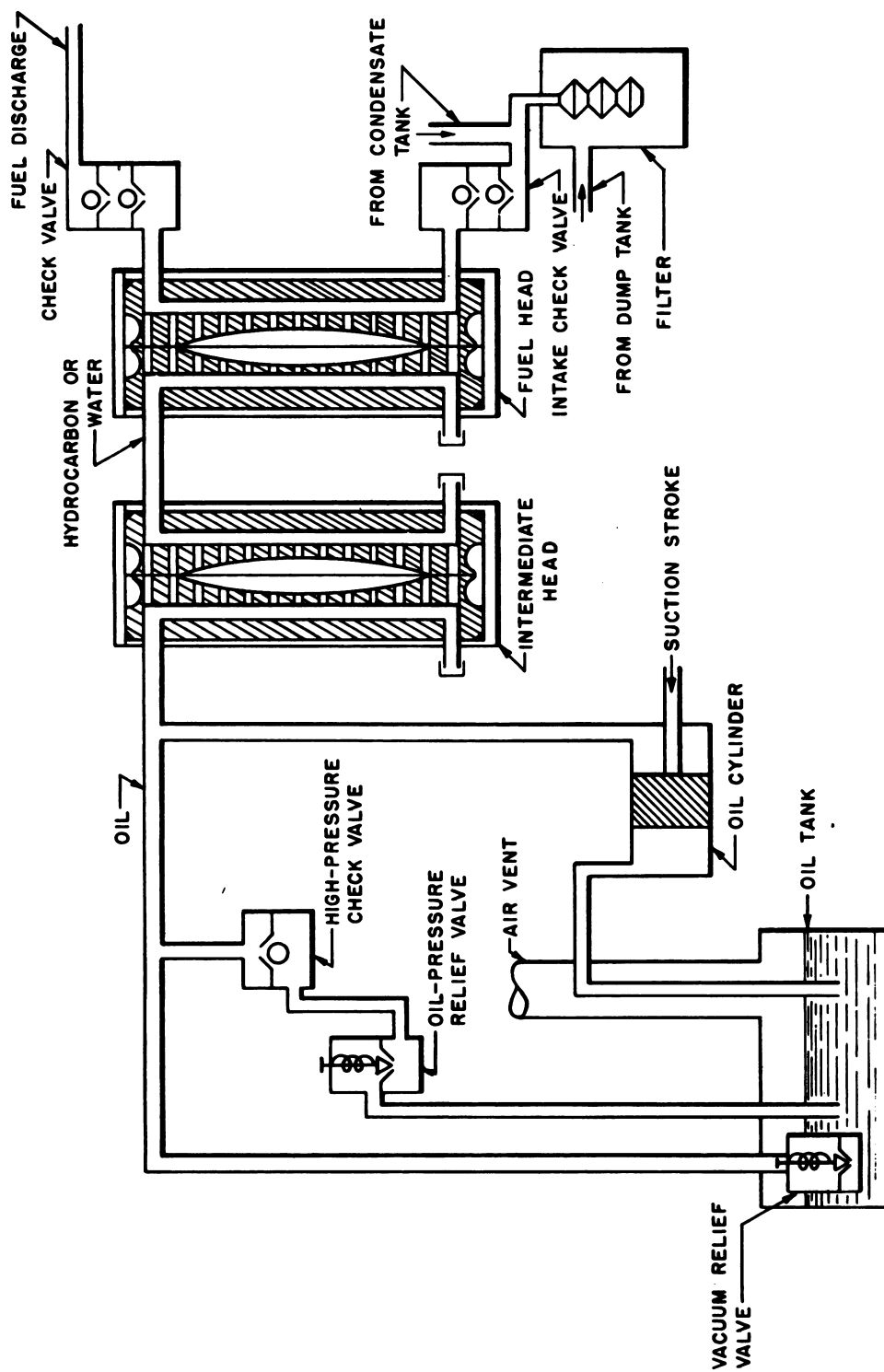


Fig. 4.7.18—Flow Diagram for Pulsafeeders. Submitted by Oak Ridge National Laboratory, Nov. 25, 1952. Reprinted from ORNL-1280.

Table 4.7.2—Characteristics of Allis-Chalmers 20,000-gpm Pump

Pumps liquid at 250°C
Specific gravity, 1.1–1.5
Static pressure, 1000 psi
Head, 160 ft
Power, 1200 hp (900 kw)
Net eff., ~78%
Weight, ~8 tons
Speed, 1200 rpm

valve seats, and the liquids in the connecting lines are compressed until the pressure in the system exceeds the pressure above the discharge ball-check valve, opening it and allowing the fluid to flow out.

The vacuum relief valve and pressure relief valve on the oil pump are essential to the operation of the pulsafeeder. If the pressure in the system exceeds the setting on the pressure relief valve, which happens when either of the diaphragms “bottoms” against the flange before the piston reverses, this valve opens, and oil flows out of the oil leg of the system until the piston reverses. If either of the diaphragms bottoms before the piston completes its suction stroke, the vacuum relief valve opens, allowing oil to re-enter the oil leg of the pulsafeeder system.

Pulsafeeders are used for supply pumps in both the fuel and reflector systems of the HRE. The intermediate fluid in the fuel system is water, but an insoluble fluorocarbon is used in the reflector system, since water would be too difficult to separate from D_2O in the event of a diaphragm rupture. Suction pressure is approximately atmospheric and discharge pressure is 1000 psi. The pressure relief setting is maintained at 1200 psi, and the vacuum relief setting is 10 in. of Hg below atmospheric. The normal output is 1 gpm at 50 rpm, but this may be varied as much as 50 percent of normal by varying the speed of the oil pump. The parts of the system coming in contact with corrosive liquid are constructed from type 347 stainless steel, and the ball-check valves are fabricated from Stellite, which is resistant to both physical wear and corrosion.

VALVES (W. L. Ross, C. D. Zerby, P. N. Stevens, and C. B. Graham)

Several corrosion- and radiation-resistant valves were required for the HRE. Trouble-free, leakproof construction was essential because of the value and radioactivity of the fluids. Most of the valves used were of $\frac{1}{2}$ in. nominal size purchased from the Fulton Sylphon Company (Fig. 4.7.19). Larger valves and valves for throttling service were purchased from Belfield (Figs. 4.7.20 and 4.7.21).

All valves were sealed by a welded-in, 1000-psi, stainless-steel bellows which was backed up by a packing gland. They were mounted in the system with the bellows on the low-pressure side of the seat so that under normal operating conditions the bellows is exposed only to essentially atmospheric pressure. The back-up gland was packed with hydrocarbon-free, graphited asbestos because this material is known to stand up well under radiation.

Pneumatic operators were used on all valves, and in regions of high radiation, all-metal construction was used (Fig. 4.7.19). Large valves were operated by neoprene diaphragms located several feet from the valve body and connected to it by a long stem extension.

Stellite plugs and seats were used throughout, and these were lapped to an essentially leakfree closure. A maximum leakage rate of 1 cc of water per day was achieved with

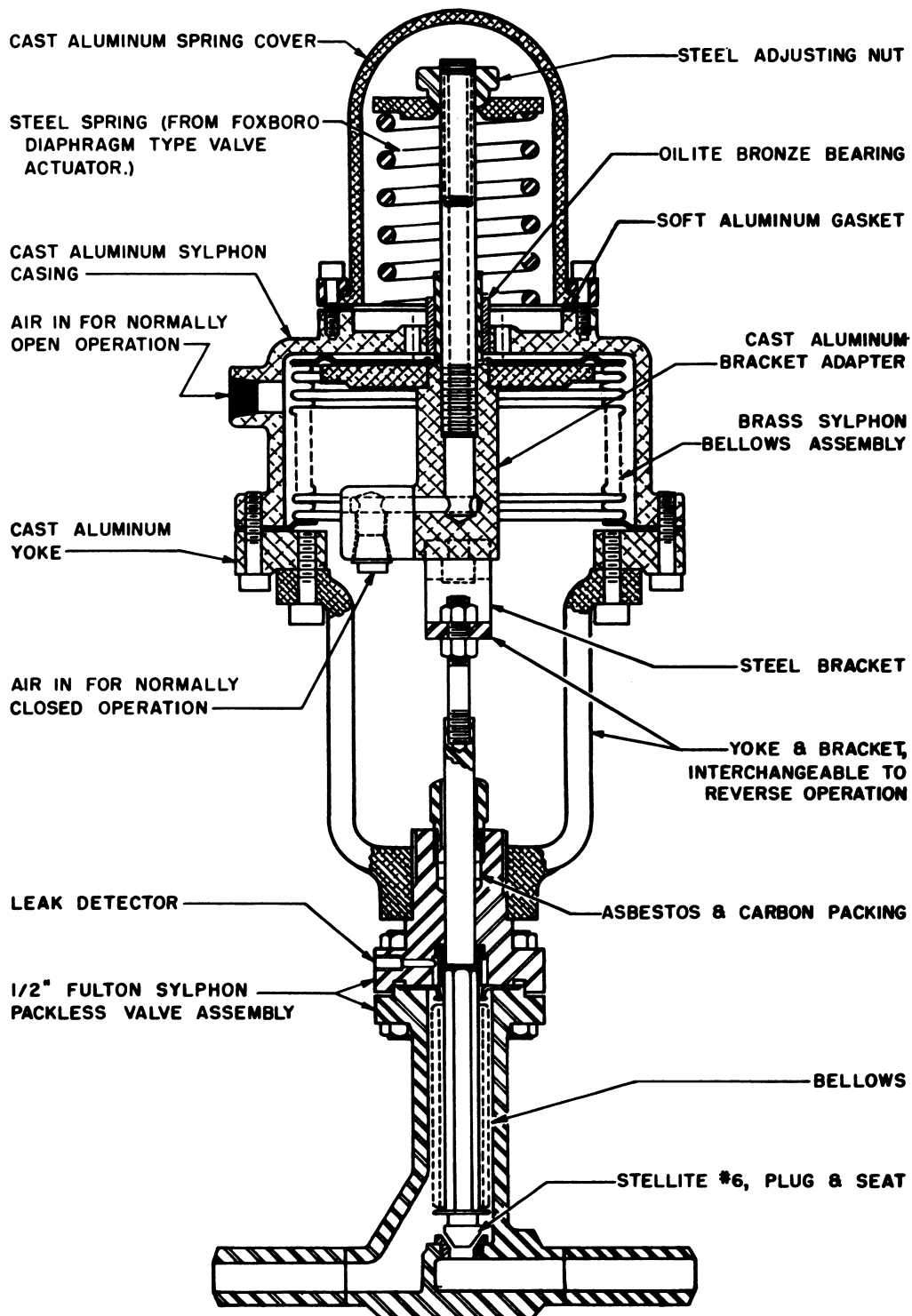


Fig. 4.7.19—Fulton-Sylphon One-half-inch Valve with Bellows Valve Operator.
Submitted by Oak Ridge National Laboratory, Nov. 25, 1952.

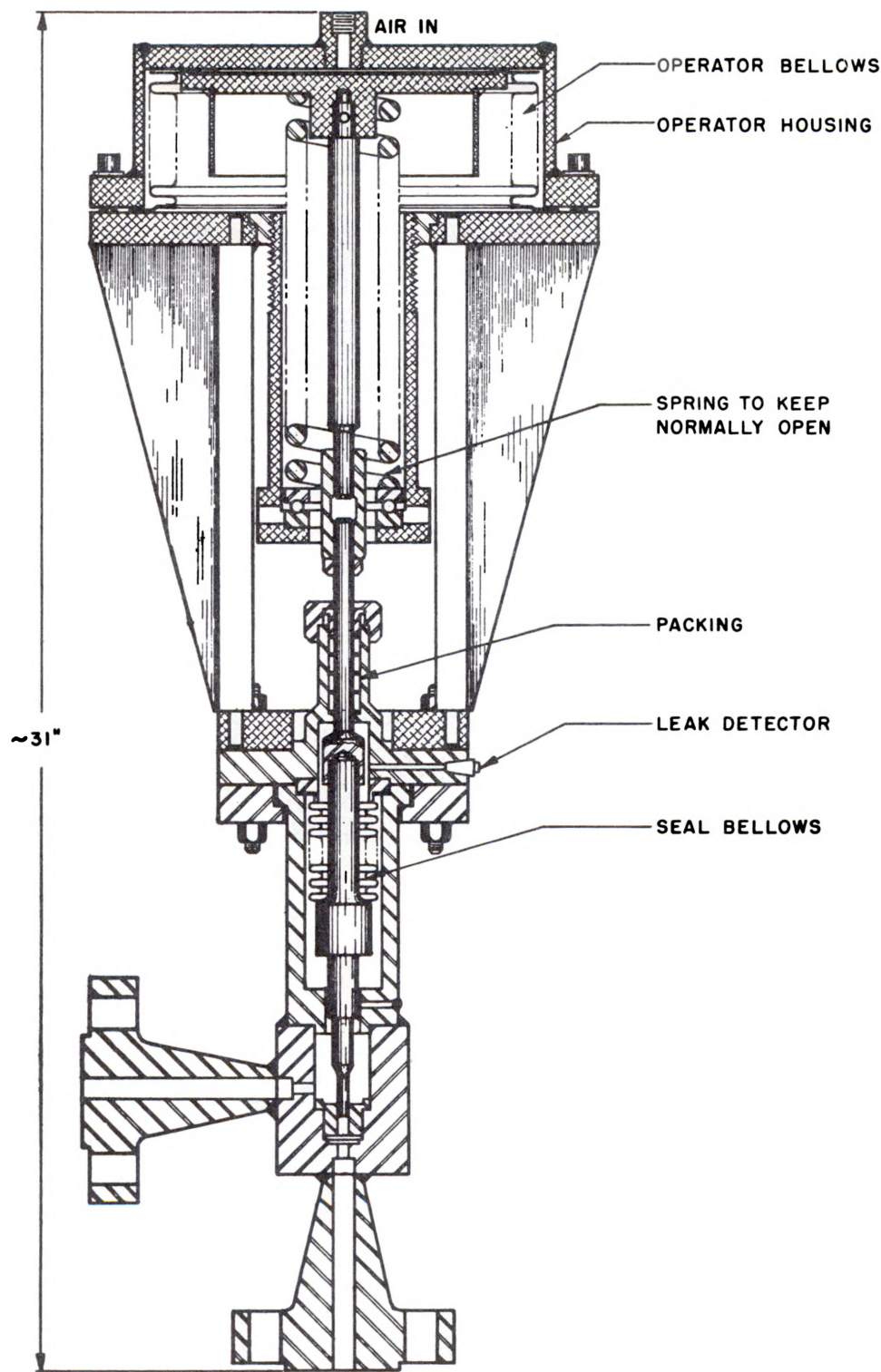


Fig. 4.7.20 —Modified Belfield Valve with Bellows Valve Operator. Submitted by Oak Ridge National Laboratory, Nov..25, 1952.

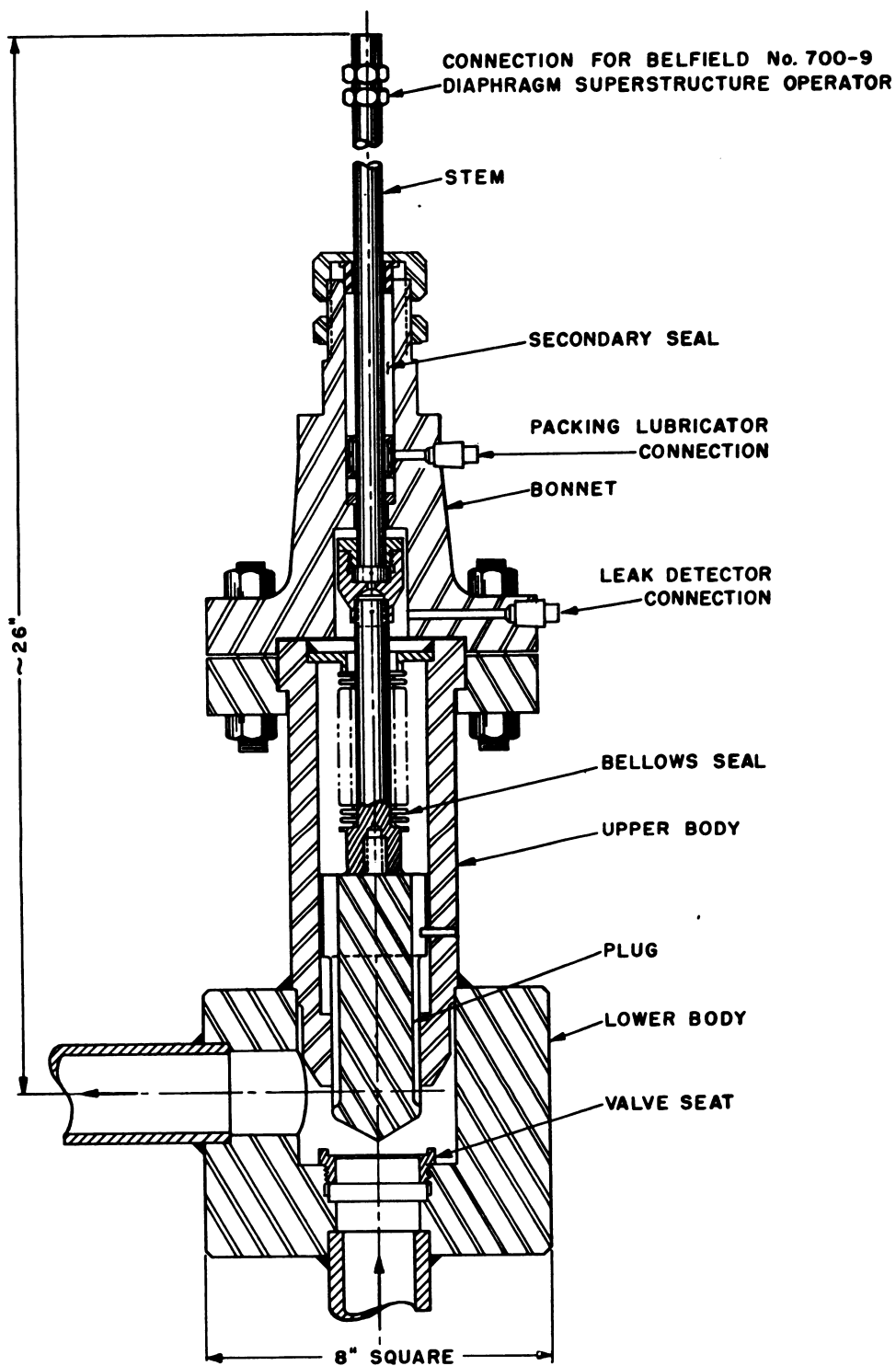


Fig. 4.7.21—Belfield Two-inch, Single-seat Angle Valve. Submitted by Oak Ridge National Laboratory, Nov. 25, 1952.

1000-psi pressure drop across the valve. The valve design shown in Fig. 4.7.19 allows the plug to align itself with the seat and avoids distortion of the parts when welding in the bellows and when welding the valve into the piping system.

HEAT EXCHANGERS (L. F. Goode)

The main heat exchanger of the HRE provides heat-transfer surface for removing the energy released in the reactor core. The heat is then used to generate steam which in turn is utilized to drive a turbogenerator set. The exchanger is a shell- and U-tube-type steam generator (Fig. 4.7.22) designed to produce 3025 lb/hr of 200-psia saturated steam at a heat load of 1000 kw. The reactor solution is passed through $\frac{1}{4}$ -in. tubes at an average velocity of 15.8 ft/sec in order to provide high heat flux with minimum liquid holdup.

The rate of heat exchange is regulated by varying the steam flow; the steam pressure at a reactor power of 200 kw is 315 psia, whereas at 1000 kw, the pressure is reduced to 200 psia.

An all-welded construction is used on components exposed to the reactor solution. Special low-holdup headers are provided, and pockets have been avoided in order to facilitate decontamination. The heat exchanger has been provided with a double tube-sheet, the tubes being rolled to the inner sheet and welded to the outer sheet. The space between the sheets serves as a leak detection device.

The feedwater heater is contained in the space above the tube bundle, the feedwater being distributed by means of a $\frac{1}{2}$ -in.-OD perforated pipe placed in the bottom of the exchanger and connected to the feedwater heater. Design information for the exchanger is summarized in Table 4.7.3.

REMOTE HANDLING OF EQUIPMENT IN HOMOGENEOUS REACTORS (S. E. Beall)

The problem of remote maintenance in homogeneous reactor systems is more difficult than in heterogeneous reactors because the fission-product activity of liquid fuels is not confined to a package. In a homogeneous system, one is faced with the contamination problem of chemical purification systems in addition to the induced activity problems of solid-fuel reactors. It is logical, then, in planning remote operations on homogeneous reactor equipment to borrow from the experience accumulated in maintaining chemical separations plants and reactors.

EQUIPMENT DESIGN CONSIDERATIONS

The major problem in maintaining and repairing any highly radioactive equipment, of course, is that of preventing excessive radiation exposure to personnel. In order to accomplish this, it is often necessary that extreme measures be taken to (1) reduce neutron activations by shielding the equipment, (2) thoroughly decontaminate fuel containers, and (3) provide adequate shielding for operating personnel.

Reduction of Neutron Activations

The activation of construction materials in homogeneous reactor systems is a result of (a) neutron emission inside the fuel container (prompt neutrons in the reactor vessel and delayed neutrons in attached equipment) and (b) neutron leakage from the reactor to external equipment.

It is unlikely that much can be done to prevent emission from fuel and fission gases being circulated in equipment attached to the reactor, although the resultant activities can be kept to a minimum by the proper selection of low-cross-section materials. It is not impossible that an element such as boron, which has both a large cross section for neutron capture and relatively weak radiation following capture, could be incorporated into the material of construction to compete for the delayed neutrons in external equipment. In the

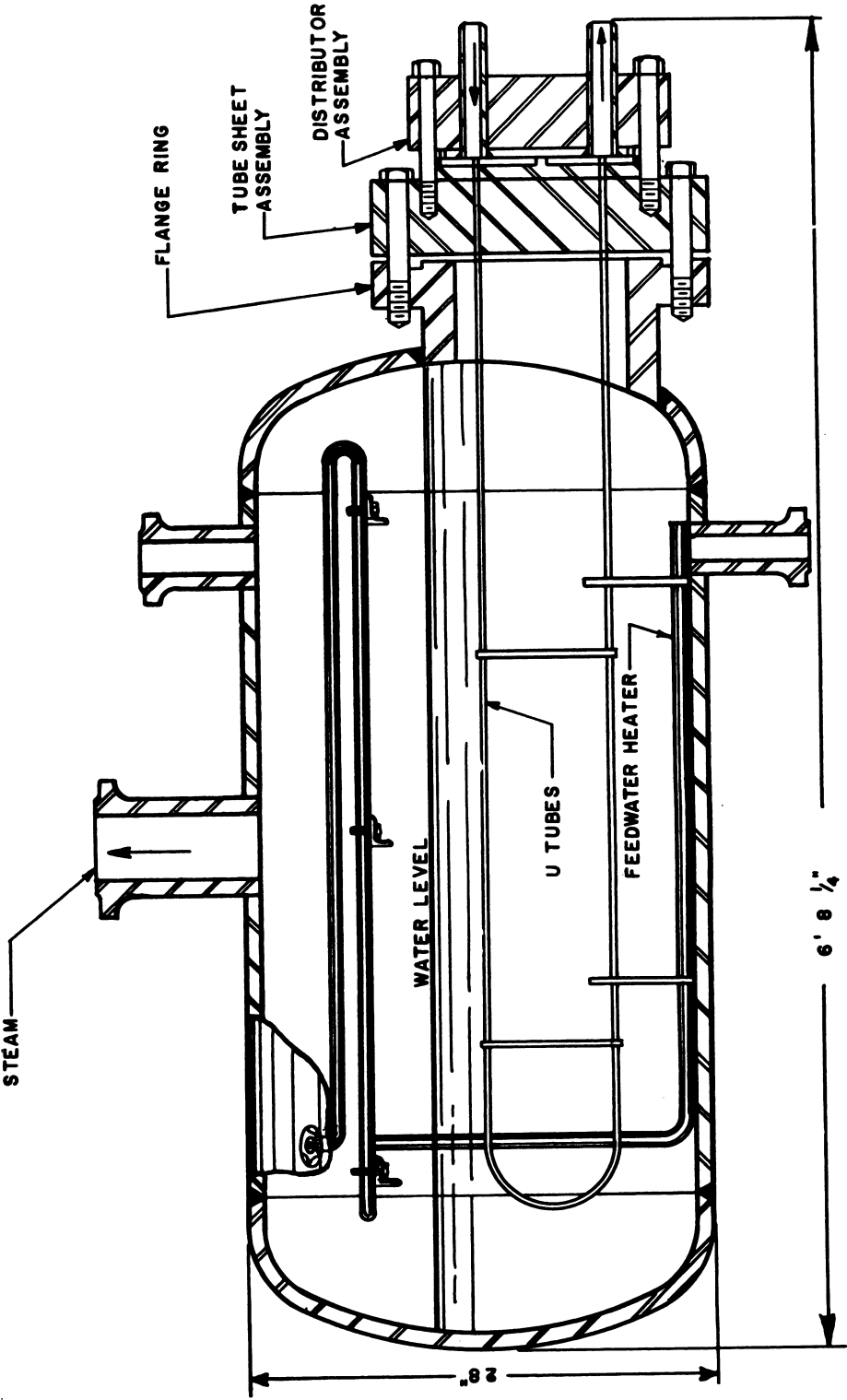


Fig. 4.7.22—Steam Generator for Homogeneous Reactor Experiment. Submitted by Oak Ridge National Laboratory, Nov. 25, 1952.

Table 4.7.3—Design Data for HRE Main Heat Exchanger*

Full load conditions	
Heat load	1000 kw
Over-all heat-transfer coefficient (U)	635 Btu/(hr)(ft ²)(°F)
Total process-solution holdup	5.5 l
Average process-solution velocity through tubes	15.8 ft/sec
Process-solution flow through tubes	100 gpm
Operating steam	200 psia (sat)
Process-solution conditions† T _{in} = 482°F	P _{in} = 1000 psi
T _{out} = 407°F	P _{out} = 975 psi
Tubes	
Number of U-tubes	112
Tube OD	1/4 in.
Tube thickness	18 BWG
Tube length, ave.	123.8 in.
Total heat-transfer area based on tube OD	75.5 ft ²
Tube material	347 stainless-steel seamless tubing, as per ASTM A-213-46
Shell	
Material	ASTM-A212 Gr B
Over-all length	~6 ft 11 1/4 in.
Shell diameter	28 in.
Shell thickness, radial	7/8 in.
Shell thickness, end	0.9 in. min.
Design pressures	
Tube side	2000 psig
Shell side	600 psig
Test pressures	
Tube side	4000 psig
Shell side	1200 psig

* The heat exchanger was fabricated by the A. O. Smith Corporation of Milwaukee as per their following drawings: Steam generator—MV-7304 (1 of 3 sheets)—ORNL-E-9584; steam generator—MV-7314 (2 of 3 sheets)—ORNL-E-9585; steam generator—MV-7314 (3 of 3 sheets)—ORNL-E-9586

case of double-walled vessels, e.g., heat exchangers, a neutron absorber between the walls would reduce the activity of the outer wall.

Decontamination of Equipment

The fission-product activity of a 40 gm/l enriched uranium solution will approach 30 curies/ml after long operation in 10^{13} neutron flux. It is obviously desirable that surfaces contacted by such solutions be cleaned before attempting repairs. Where the inner surfaces of piping and equipment are smooth and without scale, ordinary decontamination treatment with citric, nitric, or other acids is satisfactory for decontamination factors of 10^4 or 10^5 . In systems such as the HRE, in which corrosion resistance depends on the existence of a protective oxide coating on the metal surface, it is very difficult to remove activity held by the film. Decontamination factors of 10^2 or 10^3 can be achieved with normal agents. Solutions such as 4-percent HCl, 10-percent H_2SO_4 by volume at 150°F give better decontamination at the risk of high corrosion rates. No completely satisfactory agent has yet been reported. Another possible difficulty in welded systems is incomplete penetration of welds, leaving cracks which are difficult to clean. All joints in any liquid fuel system should be carefully inspected to be certain of smooth surfaces.

Shielding for Operating Personnel

Assuming that all reasonable steps have been taken to prevent neutron activation of materials and to remove contamination, if the β , γ activity of equipment is still intolerable, personnel shielding must be provided. Such shielding may be constructed as high-density solid materials, or the equipment may be so designed that it can be flooded with water. In either case it is necessary that remote handling devices penetrate the shield to perform the necessary operations; the advantages of a liquid shield for equipment in compartments are numerous.

One has the choice of either shielding the equipment pieces or providing a mobile shield for the operator. For large equipment groupings, a shielded crane cab for the operator, with electrically-driven wrenches and lifting devices, proved satisfactory in the original Hanford chemical separations plants. With smaller and less equipment in such an installation as the HRE, it is more economical to erect temporary shields for a particular job and to provide hand-operated tools.

TOOLS FOR REMOTE MAINTENANCE

In the design of any equipment for remote maintenance, much can be done to simplify the tools and procedures required to effect a repair. Proper spacing and arrangement of equipment is extremely important. Crowded cells and insufficient working space make a simple operation difficult. Bolts on flanges and joints should be large (not less than 1 in.), of the same size throughout if possible, and placed so that they can be easily reached. For instance, if the work is to be done from above, all bolts should be vertical. Electrical and instrument lines should be provided with easily detachable connectors. All removable pieces should be equipped with lifting eyes or yokes, properly located with respect to the center of gravity.

The types of equipment in the homogeneous reactor which are expected to require remote maintenance are the 100 gal/min fuel-circulating pump, the 1 gal/min feed pump, control-rod mechanisms, and valves. Each of these items is provided with bolted flanges. A typical procedure for replacement of an item would be as follows:

- (1) Drain fuel solution to storage tanks; rinse and decontaminate fuel system.
- (2) Arrange shielding plugs to provide an opening through which tools can be handled.
- (3) Erect temporary shielding of concrete block.
- (4) Install periscope in shielding plug close to equipment to be handled.
- (5) Disconnect flange with hand- or air-operated wrench with handles extended through shield.

- (6) Attach lifting device to equipment.
 - (7) With building hoist, lift equipment piece into a separate shield. Provide a "shadow" shield for the hoist operator if necessary.
 - (8) Lower new part into position and reconnect flanges with extension handle wrenches.
- A group of simple tools which might be needed for such an operation is pictured in Fig. 4.7.23. Tools A, B, and G are for lifting. Tool C is a knife for removing insulation. A long-handled socket wrench is shown at D. Items E and I are special tools for removing small parts of the control-rod mechanisms. The tool shown at F is a guide pin to aid in aligning flanges. A right-angle drive for starting nuts on horizontal flanges is pictured in position H, and the large air-operated wrench for tightening nuts is shown in position J.

SAMPLING EQUIPMENT (C. L. Segaser)

Operation of an aqueous homogeneous reactor, like the operation of any chemical process, requires that numerous samples be taken in maintaining control of the chemical system. In the case of the HRE at ORNL, equipment is provided for sampling the high-pressure reactor fluid, the D₂O reflector, and the off gases from the reactor and reflector. Because of the radioactivity associated with the fluids, standard sampling equipment must be modified, or entirely new apparatus must be devised for taking the samples. Examples of sampling equipment presented here were designed for use on the HRE.

HIGH-PRESSURE FUEL SOLUTION SAMPLING APPARATUS

It is necessary to take an 0.5 to 1.0 ml sample of fuel solution from the HRE for determination of total uranium, tetravalent uranium, pH, nickel, suspended solids, and fission-product contents.²⁰ The solution to be sampled is at a temperature of 250°C and a pressure of 1000 psi, and contains 40 gm U/l of UO₂SO₄-H₂O solution. The β and γ activity level of the solution is estimated to be 30 curies/ml, and delayed neutrons are emitted at a rate of 3.3×10^9 neutrons/(ml)(sec).

Figure 4.7.24 shows the sampling apparatus. It consists of a 30-ml isolation chamber (Item 4) connected into the main circulating stream through several valves in series (Items 1 to 6), equipment to remove the top from the isolation chamber and to pipet a sample. Lights, a mirror, and other auxiliaries required in carrying out the sampling operation are also provided as shown in Fig. 4.7.24. The equipment is housed in a stainless-steel box suspended within the concrete shielding structure. A 12-in.-thick plug, filled with lead and water, protects the operator. During some parts of the operation, the box can be flooded with water to reduce the neutron dosage to a tolerable level.

The procedure for extracting a sample of fuel solution is described briefly as follows:

A new ball, for sealing the isolation chamber, and a new pipet are placed in the sampler chuck, and the assembly is installed in the sample carrier. The sample carrier is then lowered through a hole in the inner carrier shield and into the sampler through the charging port in the shielding plug.

By opening valves 1 to 6, process solution is circulated through the isolation chamber. The valves are closed to isolate the sample, the sample is thermally cooled, and the non-condensable gases are vented through the line to the dump tanks.

The cover on the isolation chamber is removed, and the sample extracted in the pipet using the manipulator. Because the manipulator operates only in a vertical position directly above the isolation chamber, an indexing table is provided which rotates under the manipulator and charging port to hold the cover from the isolation chamber and to deliver the pipet.

The pipet is returned to the sample carrier. The new ball is inserted in the cover of the isolation chamber, and the cover is screwed onto the chamber to reseal the system. The sample carrier is removed from the sampler through the charging port and transported to the analytical laboratory in a shielded container.

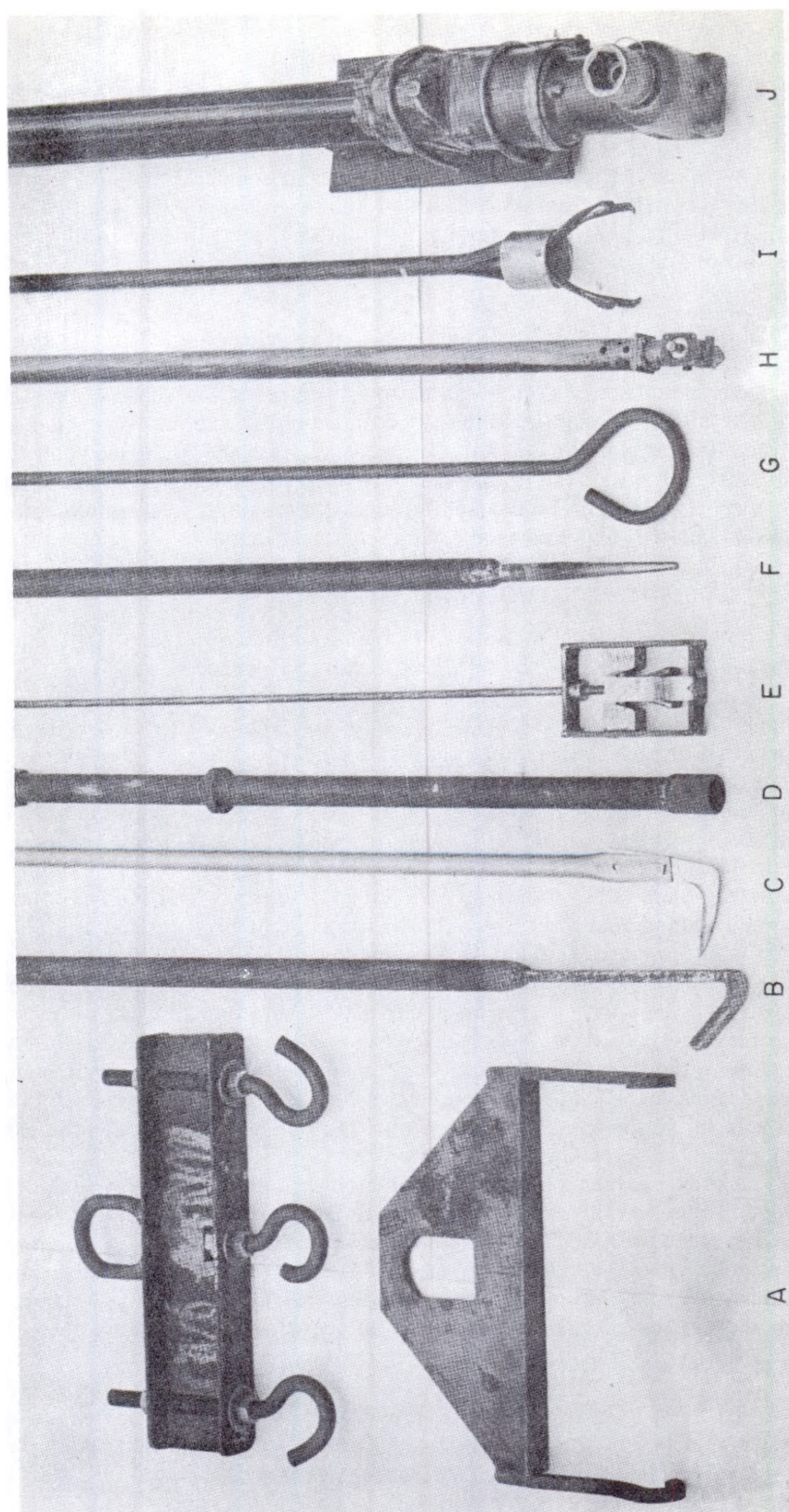


Fig. 4.7.23—HRE Remote Handling Tools. Submitted by Oak Ridge National Laboratory, Nov. 25, 1952. Reprinted from ORNL 52-6-160.

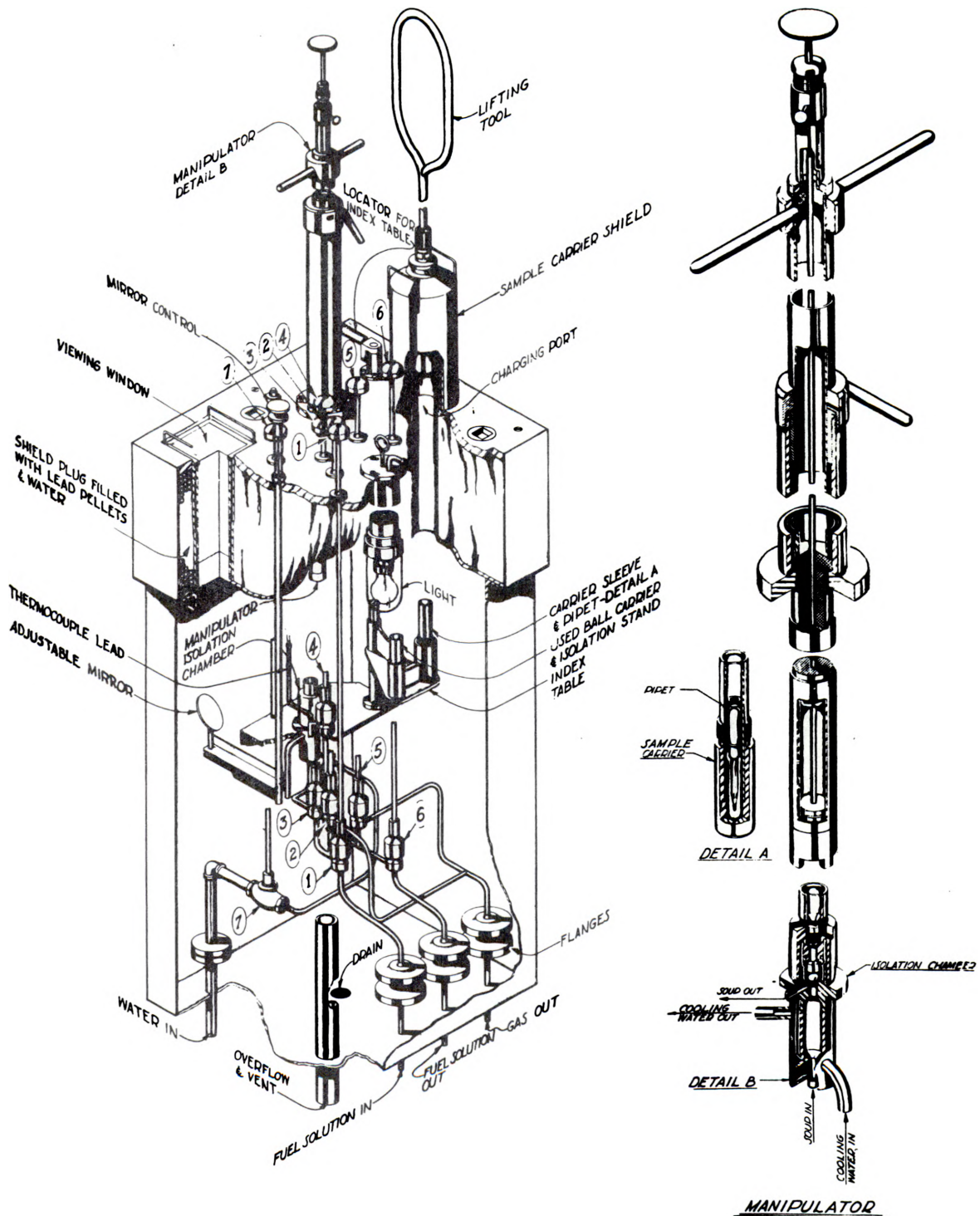


Fig. 4.7.24—HRE Fuel Sampler and Manipulator. Submitted by Oak Ridge National Laboratory, Nov. 25, 1952. Reprinted from ORNL 52-6-160.

ANALYTICAL LABORATORY HANDLING APPARATUS

An apparatus (Fig. 4.7.25) similar to the sampler has been developed for handling the radioactive fuel-solution samples in the analytical laboratory. Solutions are transported into the laboratory in a shielded carrier on a standard lift dolly. The carrier is placed under the bench shield in line with the unloading port. A handling tool is inserted through the upper loading tube, the auxiliary shielding block is removed, and connection is made to the exposed upper end of the sample carrier. The lead brick is then replaced, and the sample carrier is drawn up into the shielded cavity where it is transferred to the appropriate

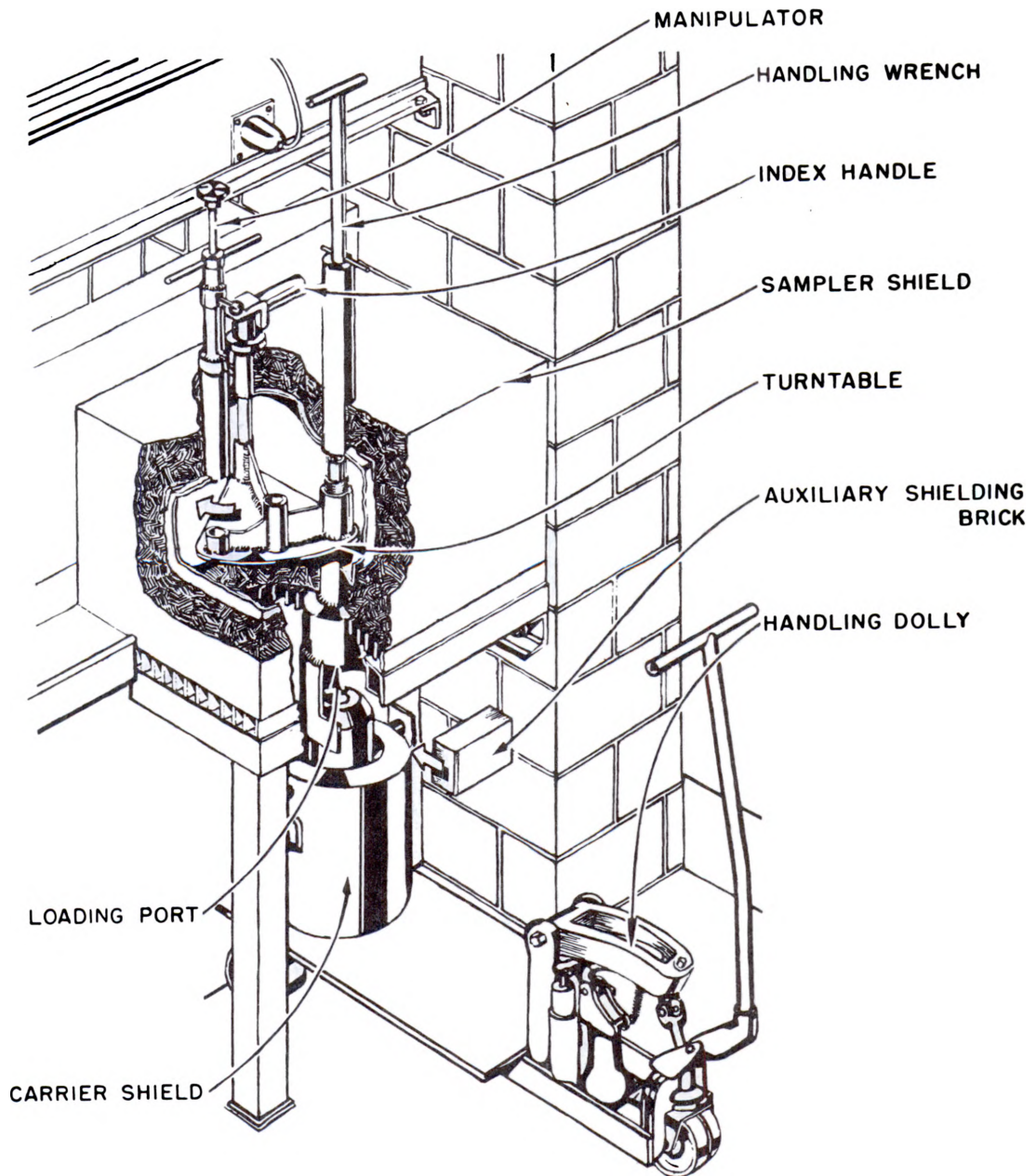


Fig. 4.7.25—Fuel Sampler for Use in Chemical Laboratory. Submitted by Oak Ridge National Laboratory, Nov. 25, 1952. Reprinted from ORNL-1318.

receptacle in the turntable. The sample carrier may then be manipulated by the devices provided for this purpose, the sample removed, and aliquots taken for analysis.

REFLECTOR SAMPLING APPARATUS

Sampling of the D_2O reflector of the HRE is required for determination of pH, D_2O -to- H_2O ratio, corrosion inhibitor and corrosion product content, and possible uranium content resulting from leakage into the reflector. The reflector contains some radioactivity, but the level is low compared with that in the fuel solution; so the equipment is less complicated.

Figure 4.7.26 is a flow diagram which shows how the sampler is installed in a bypass line in the reflector pumping system. A sample carrier having a capacity of 10 ml is shown in Fig. 4.7.27. The carrier is installed in the bypass line using Hansen quick-disconnect couplings with integral check valves which close to prevent atmospheric contamination of the reflector and sample when the coupling halves are separated.

An alternate sampling device is shown in Fig. 4.7.28. D_2O would be circulated through the chamber and a sample would be taken by inserting the needle into the bottle and pushing the needle assembly down to open the valve.

GAS-SAMPLING APPARATUS

Stations are provided on the HRE to obtain samples of gas from the fuel-solution system, the waste evaporator system, and the helium pressurizing system. The proposed apparatus and procedures for obtaining a sample from any of these systems are similar. Figure 4.7.29 is a schematic diagram of the method whereby a sample of gas from the high-pressure helium system is obtained. Two possible types of sample carriers are shown in Fig. 4.7.30.

The connection of the sampler with the helium system is made through Hansen couplings similar to those in the D_2O sampling system. The valved socket provides an additional block against leakage. After the sampler is coupled into the system, it is purged by opening the isolation valves and allowing the helium to flow through the sample carrier into the dump tanks. Upon completion of the purge, the downstream side of the carrier is valved off and the sample brought up to the required pressure. All valves are then closed, and the carrier is removed.

INSTRUMENTATION (W. M. Breazeale)

Instrumentation of aqueous homogeneous reactors is strongly affected by the fact that the reactivities of these reactors have a large negative temperature coefficient. This coefficient acts to stabilize the reactor and is also an inherent safety feature. As a result, the requirements which the safety circuits must meet are less stringent than those for heterogeneous, fixed fuel reactors. On the other hand, because a highly corrosive and radioactive liquid must be handled, the process instrumentation is somewhat more complex. This discussion can perhaps proceed best by outlining the main features of instrumentation of the Los Alamos "Water Boiler" and the Oak Ridge HRE.

INSTRUMENTATION OF THE WATER BOILER

The Water Boiler²¹ is used as a source of neutrons for experimental work, and hence the flux variation with time should preferably be as small as possible. To this end, a standard automatic servo system is used to regulate the flux level to ± 0.1 percent. The process solution normally remains in the core at all times, and the reactor is shut down by dropping the absorbing rods. Electronic tube amplifiers and circuits are used as sparingly as possible; wherever practical, Weston Sensitrols, operated directly by the

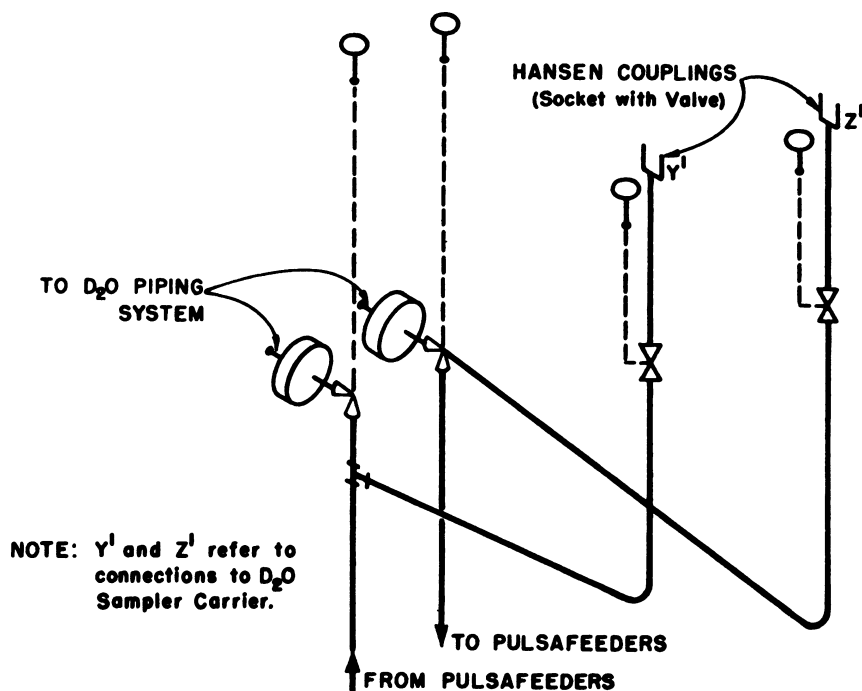


Fig. 4.7.26—D₂O Sampler in HRE Reflector System. Submitted by Oak Ridge National Laboratory, Nov. 25, 1952. Reprinted from ORNL 52-6-160.

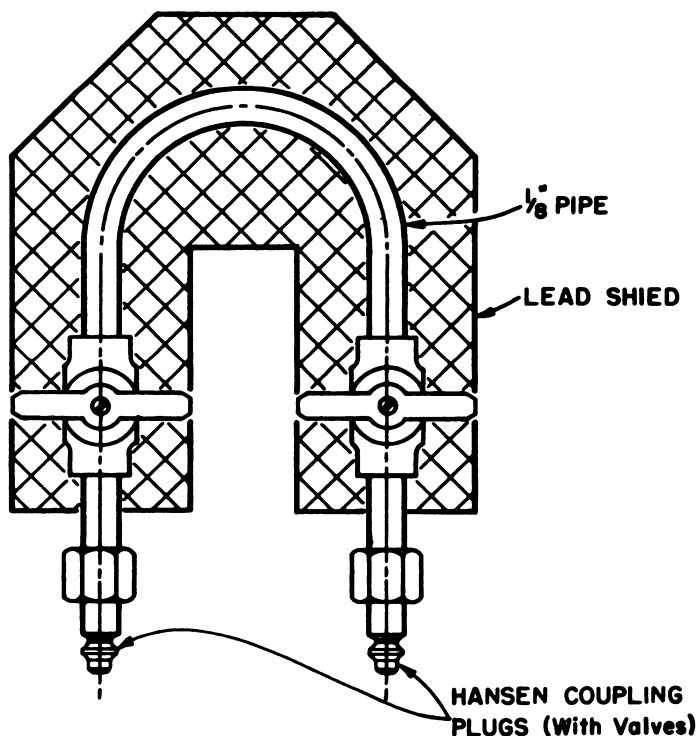


Fig. 4.7.27—D₂O Sample Carrier for HRE Reflector Sampling Apparatus. Submitted by Oak Ridge National Laboratory, Nov. 25, 1952. Reprinted from ORNL 52-6-160.

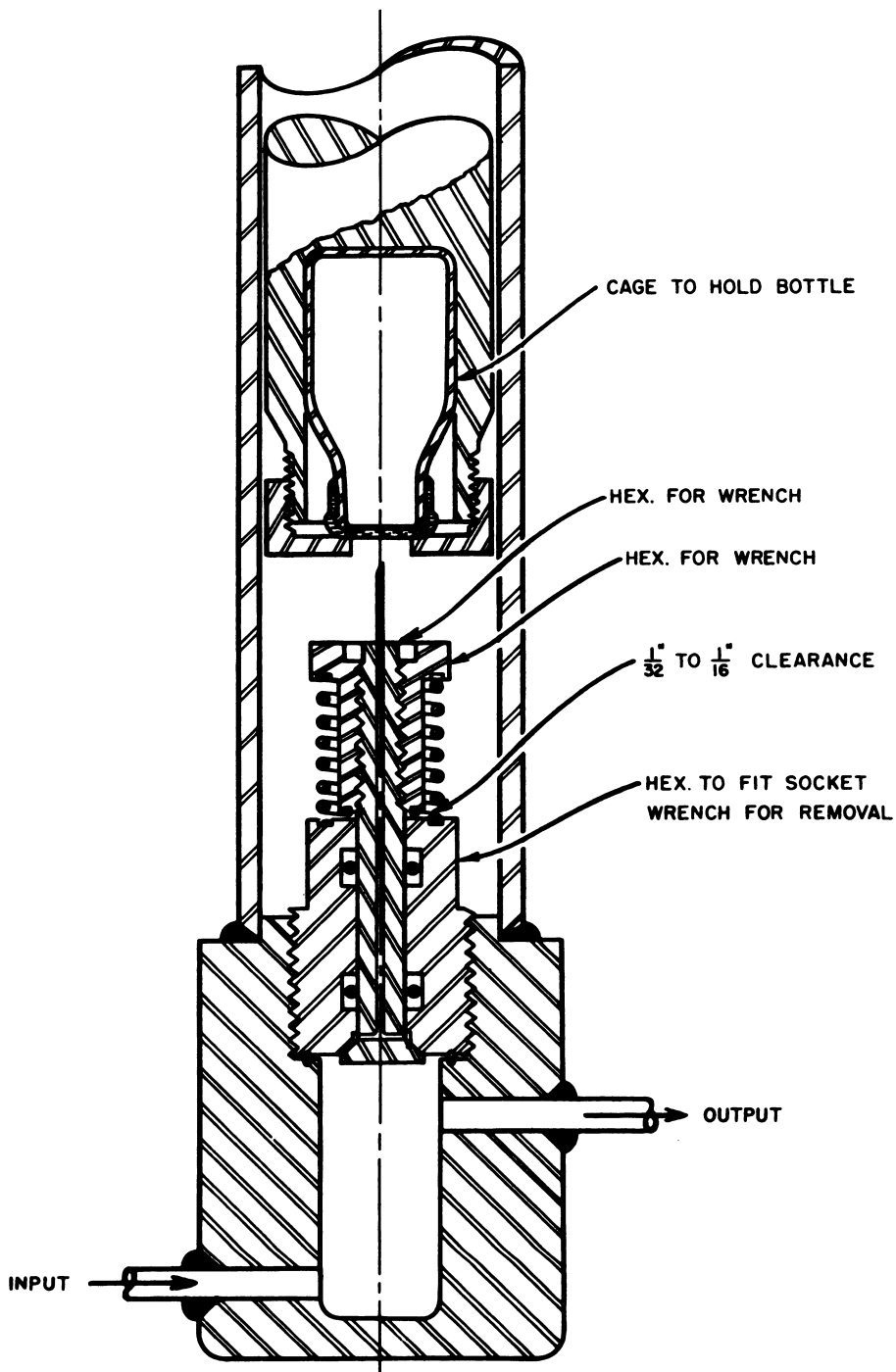


Fig. 4.7.28—Alternate Sampling Device for D_2O Sampling Apparatus. Submitted by Oak Ridge National Laboratory, Nov. 25, 1952. Reprinted from ORNL 52-6-160.

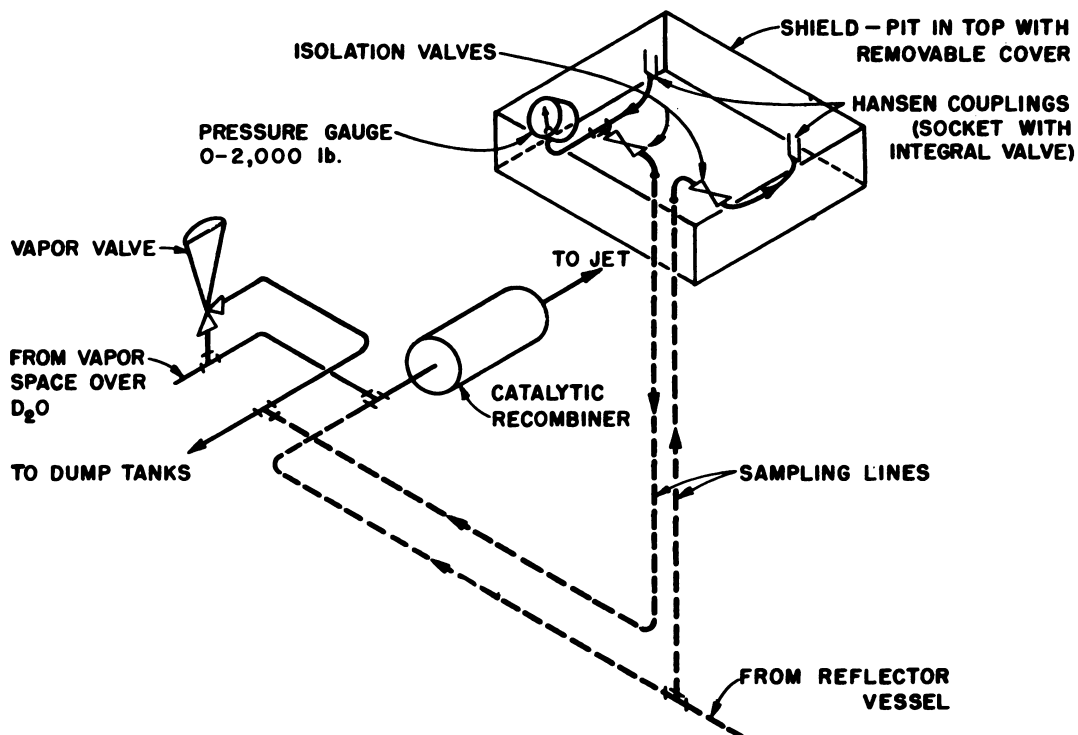


Fig. 4.7.29—Sampler for High-pressure Helium in HRE Pressurizing System. Submitted by Oak Ridge National Laboratory, Nov. 25, 1952. Reprinted from ORNL 52-6-160.

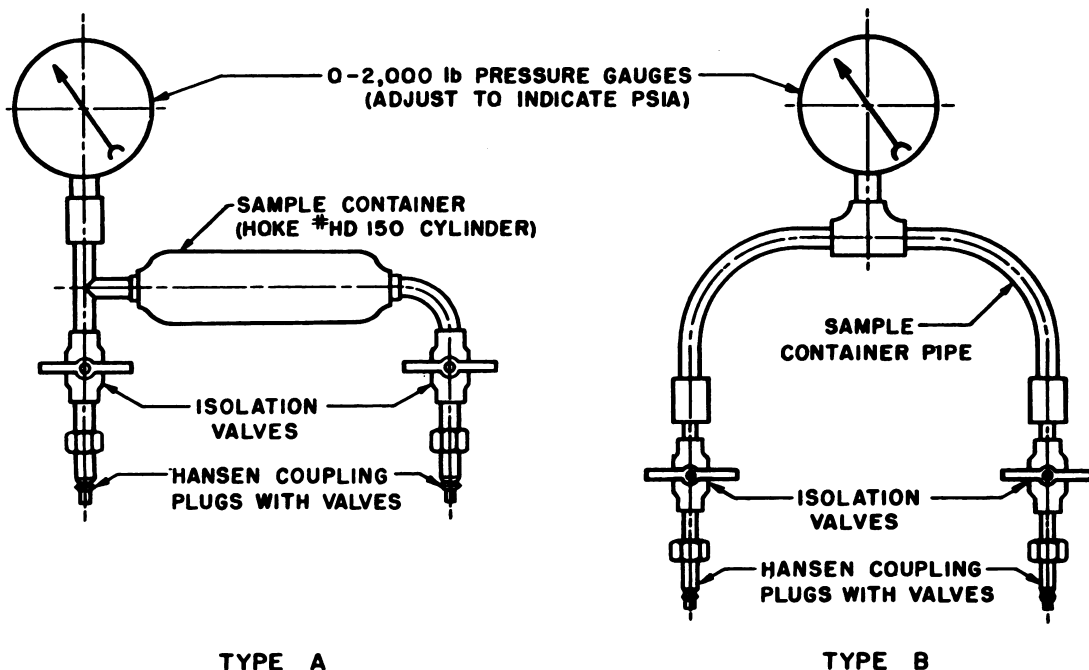


Fig. 4.7.30—Carriers for Samples from High-pressure Helium System of HRE. Submitted by Oak Ridge National Laboratory, Nov. 25, 1952. Reprinted from ORNL 52-6-160.

current from ion chambers, are used as safeties. However, for fast safeties, a hard vacuum tube circuit is necessary.

Nuclear control is accomplished with the aid of five vertical absorbing rods. Three of these are cadmium strips $2\frac{1}{2}$ by 30 by $\frac{1}{32}$ in. which move tangentially to the outside of the core and are worth 0.9 percent each in reactivity. The other two are internal rods cadmium-plated and filled with boron-10; these are worth 2.7 percent each in reactivity. Either of the internal rods can be controlled by the automatic servo system and serves as a regulating rod. The other four are used as shim-safety rods or can be hand controlled.

Nuclear Instrumentation

The standard chambers listed below are used to sense neutron level and supply information to various circuits.

(1) One B^{10} -coated chamber (Fig. 4.7.31) placed in a graphite reflector 16 in. from the core is connected directly in series with a high-voltage supply and a Leeds and Northrup galvanometer which has a sensitivity of 10^{-5} μ amp/mm at 1 meter. The range (with shunts) is from about 10^{-3} w to full reactor power. This galvanometer is used primarily to follow the neutron level during start-up.

(2) One B^{10} -coated graphite chamber is connected to a logarithmic amplifier and period circuit. The range is from 0.01 w to full power. For routine operation, the period circuit will shut down the reactor when periods of less than 8 sec are attained, and hence will ensure careful start-up. The location of this chamber is the same as (1) above.

(3) One small U-235 fission chamber is located so that it is in a flux of 10^8 neutrons/(cm^2)(sec) when the reactor is at full power. It is connected to an integrating counter and determines the total energy during a given period of time. It also supplies an audible signal (counts) to personnel at the control position.

(4) One U-235, $4\frac{1}{2}$ -in. safety chamber is connected to the high-voltage supply and the safety chassis. It initiates shutdown when the neutron flux rises above a predetermined level. It is located so that the chamber current is a little greater than 1 μ amp/kw of reactor power.

(5) One B^{10} -coated graphite chamber jacketed in lead and located under a bismuth curtain for isolation is used to indicate neutron flux level and to act as a second safety chamber. It is connected to the electronic safety chassis also.

(6) Another chamber, the same as above, is used to control the servo system. Both these chambers supply currents in excess of 1 μ amp/kw of reactor power.

All the high-voltage supplies in the nuclear and safety systems are monitored by Weston Sensitrol relays. If the voltage output of the supply deviates by ± 5 percent, the relay initiates reactor shutdown and indicates the trouble.

Process Instrumentation

The process instrumentation employs mostly standard sensing devices to indicate the condition of the process-solution system, off-gas system, and the like. The principal process instruments which act to protect the facility are:

(1) A thermocouple monitors the solution temperature and initiates reactor shutdown if the temperature rises above a predetermined value.

(2) A special set of pressure-sensitive devices shuts down the reactor if (a) the reactor system to exhaust stack pressure builds up, or (b) the stack exhaust blower is off, as indicated by the absence of a slight vacuum in the reactor system.

(3) If the solution level rises too high, a probe will make contact with the electrolyte and shut down the reactor.

(4) Three thermocouples in the catalytic recombination bed warn if temperature inversion takes place, thus indicating that the catalyst is not functioning properly.

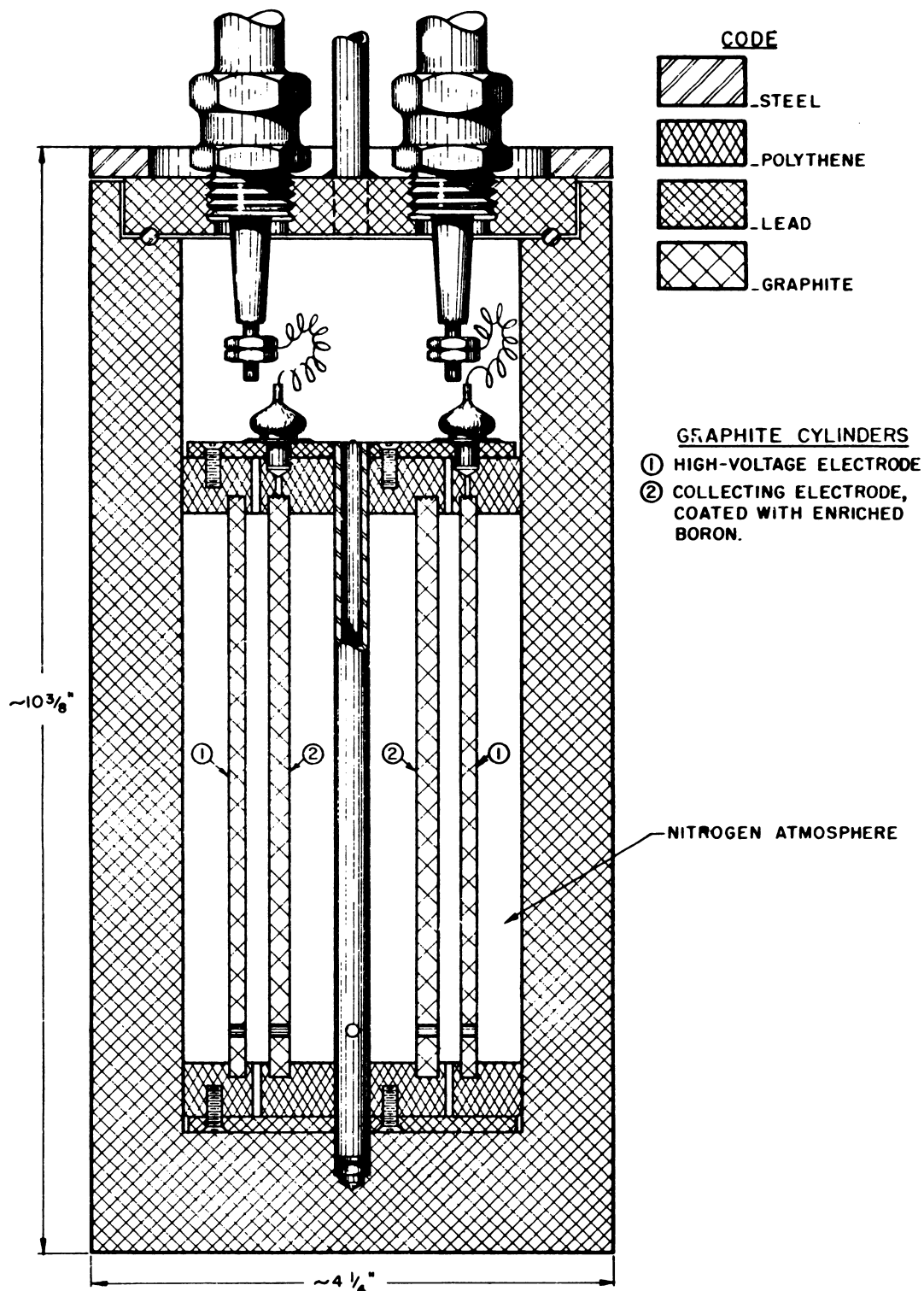


Fig. 4.7.31—Boron-10 Ionization Chamber used in Supo Model Water Boiler.
Submitted by Oak Ridge National Laboratory, Nov. 25, 1952.

(5) An air-circulation safety shuts down the reactor if air flow across the surface of the process solution is not maintained in sufficient volume to keep the H_2 concentration below that required for an explosive mixture.

INSTRUMENTATION OF HRE

The HRE at ORNL was designed to be a power producer rather than a source of neutrons for experiments, and it is not necessary that the flux level be particularly smooth. The reactivity, i.e., the operating temperature, is controlled by adjusting the D_2O reflector level and the concentration. When the reactor is shut down in the normal fashion, the process solution is diluted and drained into dump tanks.

Nuclear Instrumentation

The nuclear instrumentation is quite simple and is used mainly to aid in start-up and to determine the neutron flux levels as a cross check on power. The instruments are the same as those used on the MTR (q.v.). Excessive neutron flux scrams the reactor by dumping the reflector and the process solution as quickly as the pneumatically operated dump valves will function (2 to 4 sec). Rupture disks protect the core and the pressure vessel containing the D_2O from large pressure surges.

Process Instrumentation

The following discussion of the process control instruments and their functions is taken from ORNL-1094. The essentials of the fuel system are shown in Fig. 4.7.32. The main flow is through the heat exchanger and the 100-gpm circulating pump. The other fuel circuit permits adjustment of the concentration. Process solution from the dump tank is pumped into the core by the pulsafeeder (a diaphragm pump) and let down through the valve operated by a level controller on the pressurizer. Thus, there is a continuous circulation at approximately 1.5 gpm between core and dump tanks. The steam evaporator on the dump tank operates continuously, evaporating water from the process solution in the tank. The resulting steam is condensed, and if the concentrate valve is open, the condensate returns to the dump tank. There is no net change of concentration in the system under this condition. If both the concentrate and dilute valves are closed, the condensate is collected in the condensate tanks, and the process solution in the dump tanks becomes more concentrated. This in turn results in the core process solution becoming more concentrated since there is continuous circulation. To lower the concentration, the dilute valve is opened, dumping the condensate into the pulsafeeder intake line and hence giving almost pure water into the core. Both concentrate and dilute valves are throttling valves controlled from the console by the operator, so the rate of concentration or dilution may be adjusted by the operator.

The pressure in the reactor core is determined by the vapor pressure at the free surface in the pressurizer. The temperature of the solution here, and hence the pressure, is maintained by a steam jacket supplied from a 10-kw electrically heated boiler. The level of this free surface is sensed by a level indicator employing a restrained float (Fig. 4.7.33). This instrument provides proportional control to the pneumatically operated letdown valve. Through this valve flows a mixture of gases and wet steam to the condenser and the H_2 and O_2 recombiner.

Liquid flow rates are now measured by connecting a Foxboro differential cell across an orifice. A sketch of one such arrangement is shown in Fig. 4.7.34. Such a cell placed in a side arm can be used to measure liquid levels.

Unequal temperature coefficients of expansion of the two metals make the space between them a function of the heater current.

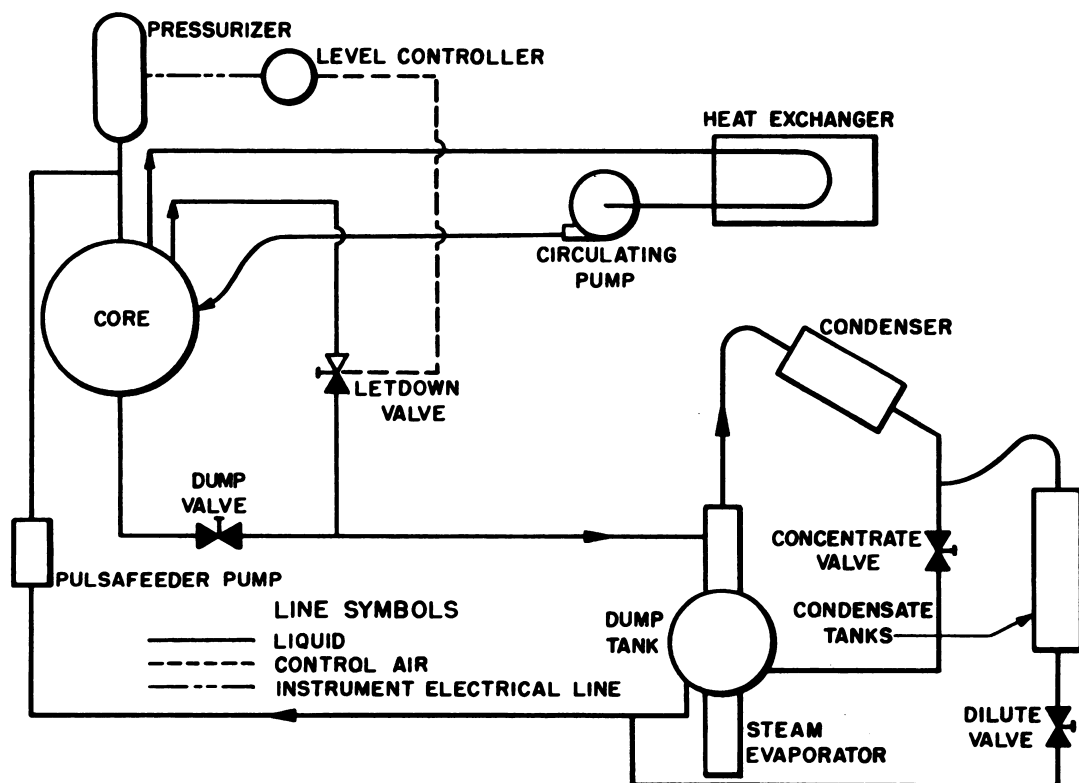


Fig. 4.7.32—Simplified Fuel Flow Diagram for HRE. Submitted by Oak Ridge National Laboratory, Nov. 25, 1952. Reprinted from ORNL-1094.

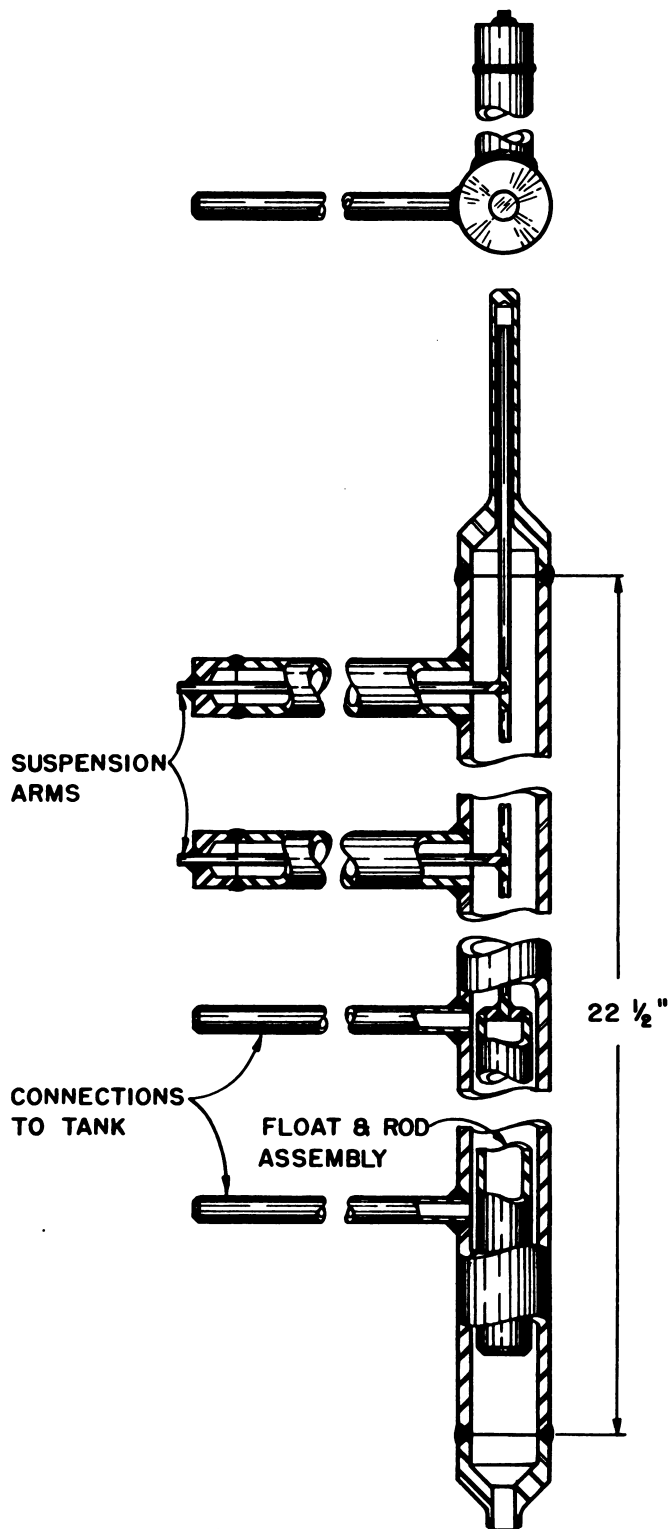


Fig. 4.7.33—Level Control Float for HRE Pressurizer. Submitted by Oak Ridge National Laboratory, Nov. 25, 1952.

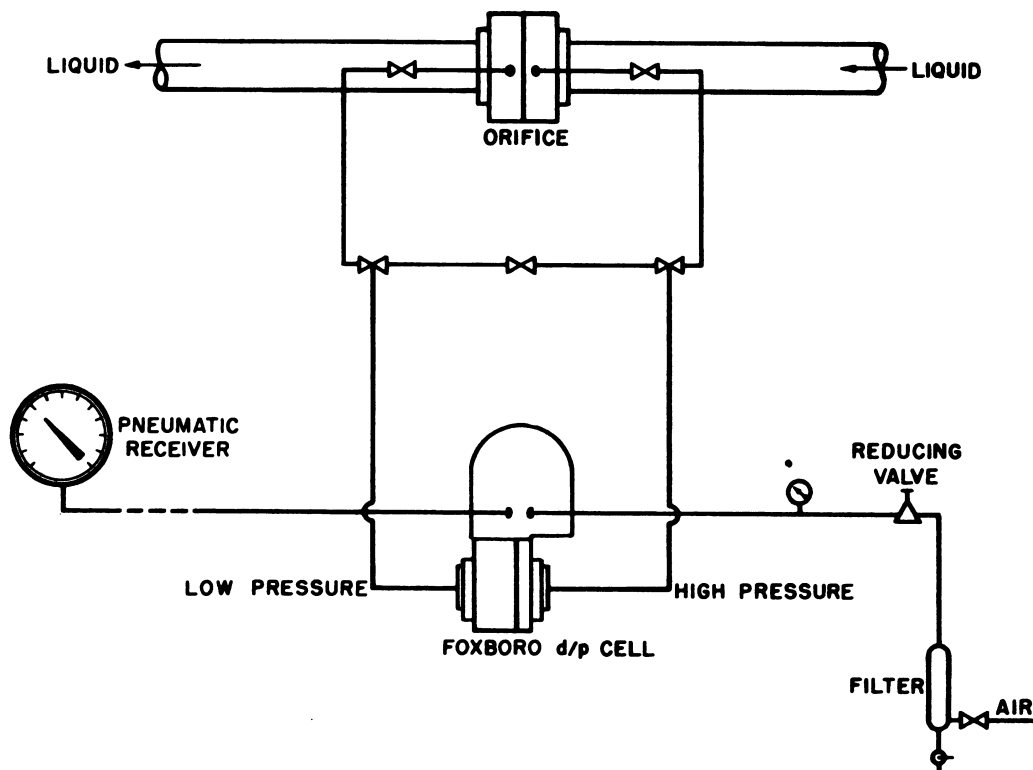


Fig. 4.7.34—Typical Installation of Flow Metering Instrument on Homogeneous Reactor Experiment. Submitted by Oak Ridge National Laboratory, Nov. 25, 1952.

Concentration is measured indirectly by weighing the water in the condensate tanks, which are suspended from a Baldwin weigh cell. Knowing the initial charge of water and uranyl sulfate, the concentration is determined from the water hold-up; so the weigh instrument may be calibrated in terms of concentration. As a check on the entire process-solution system, as well as the concentration instrument, the process solution in the dump tanks is also weighed. This method of determining concentration is not an absolute one since it cannot take into account any partial precipitation and hold-up of fuel in the system, nor is it capable of giving rapid measurements of concentration in the core itself.

Monitrons (large boron-lined chambers sensitive to neutrons) are located in strategic places and warn of leaks in the fuel system, either into the air or into the steam system through the heat exchanger, when the fuel solution is radioactive. They also initiate operation of equipment to isolate the defective section.

Besides concentration control, the reactivity can be varied by adjusting the level of the D_2O reflector. An outline of the reflector system is shown in Fig. 4.7.35, and the normal operation should be apparent from the figure. The reflector is pressurized by helium to a value slightly above the core pressure and held there by a differential pressure controller. The reflector level is raised by the pulsafeeder and lowered by opening the let-down valve. In an emergency, the reflector can be dumped through the dump valve and, if the reflector is full, the reactivity can be reduced some 6 percent in two or three seconds.

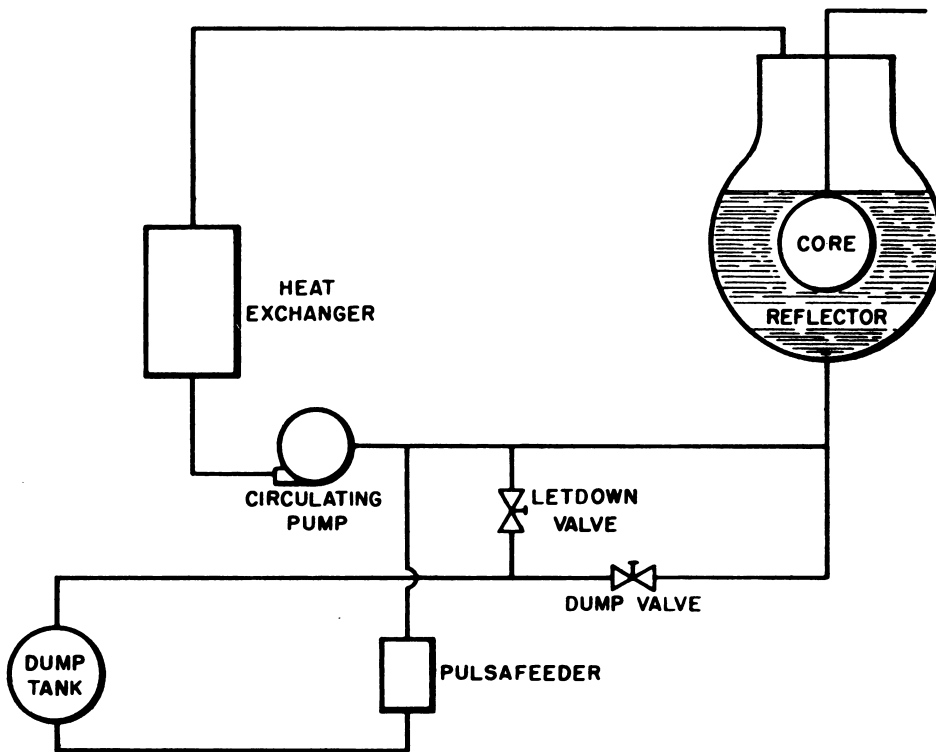


Fig. 4.7.35—Simplified Diagram of HRE Reflector System. Submitted by Oak Ridge National Laboratory, Nov. 25, 1952. Reprinted from ORNL-1094.

REFERENCES

1. S. Timoshenko, *Theory of Elasticity*, 1st ed., McGraw-Hill Book Company, Inc., New York, 1934, p 371.
2. Ibid., p 379.
3. H. Etherington et al, Argonne Nat. Lab., ANL-4379, Nov. 1949 (classified).
4. C. L. Segaser, *Thermal Shield and Pressure Shell Design for 15-ft Homogeneous Reactor Tank*, Oak Ridge Nat. Lab., ORNL-CF-51-6-42, June 12, 1951.
5. H. L. F. Enlund, *Energy Absorption of Capture Gammas*, Oak Ridge Nat. Lab., ORNL-CF-52-6-99, June 11, 1952.
6. L. Spiewak, Oak Ridge Nat. Lab., ORNL-CF-52-10-81, Oct. 9, 1952 (classified).
7. J. C. Carter, Argonne Nat. Lab., ANL-4690, Sept. 7, 1951 (classified).
8. J. A. Lane, Oak Ridge Nat. Lab., ORNL-1096, Dec. 10, 1951 (classified).
9. C. L. Segaser, Oak Ridge Nat. Lab., ORNL-CF-52-10-195, Oct. 20, 1952 (classified).
10. W. E. Thompson, Oak Ridge Nat. Lab., ORNL-1280, pp 86-89 (classified).
11. D. W. Kuhn et al, Oak Ridge Nat. Lab., Y-731, 1951 (classified).
12. H. M. McLeod et al, Oak Ridge Nat. Lab., Y-706, 1951 (classified).
13. R. Van Winkle, Oak Ridge Nat. Lab. (Memo to C. B. Graham (classified)).
14. T. H. Pigford, Oak Ridge Nat. Lab., ORNL-1322, 1952 (classified).
15. D. W. Kuhn, A. D. Ryon, and A. A. Palko, Oak Ridge Nat. Lab., ORNL-1209, 1952 (classified).
16. M. E. Bunker et al, *Gas Recombination System of the Los Alamos Homogeneous Reactor*, Los Alamos, LA-1337, 1952.
17. T. W. Costikyan, C. B. Hanford, and D. L. Johnson, *Massachusetts Institute of Technology Practice School*, Oak Ridge, KT-130, 1952 (classified).
18. J. V. Gaven, R. B. Bacostow, and A. C. Herrington, *Massachusetts Institute of Technology Practice School*, Oak Ridge, KT-134, 1952 (classified).
19. H. F. McDuffie et al, Oak Ridge Nat. Lab., ORNL-1280 pp 69-71, 155-172 (classified).
20. C. H. Secoy, Oak Ridge Nat. Lab., ORNL-CF 51-7-177, July 18, 1951 (classified).
21. L. D. P. King, *Los Alamos Scientific Lab.*, LA-1034, Dec. 1947 (classified).

Section 5

LIQUID-METAL-FUEL SYSTEMS

Prepared by
F. T. MILES
BROOKHAVEN NATIONAL LABORATORY

AUTHOR'S PREFACE

The authors wish to acknowledge the great help received from Dennis Puleston, Mary Jane Sears, and Elizabeth Motz in editing and proofreading the manuscript. George Cox prepared many of the figures, and Paul Hogroian did the heat-transfer calculations.

This Section is based upon data available up to about April 1952. For more recent information on the LMFR, the reader is referred to Nucleonics Vol. 12, No. 7, pp. 11-42, July 1954.

F. T. Miles

General Reactor Characteristics

F. T. Miles

Although reactors with liquid metal fuels were suggested as early as 1941,¹ they have received relatively little research and development, and the reactor characteristics have not been demonstrated in practice. It is possible, however, to list the potential advantages of such systems and their disadvantages. Here, we must distinguish between the features of fluid fuels in general and those of liquid metal fuels in particular. A reactor using any fluid fuel may have the following advantages over one with solid-fuel elements:

(1) Simple structure. A fluid fuel can be cooled in an external heat exchanger separate from the reactor core. Thus, the nuclear requirements (of the core) and the heat-flow requirements (of the exchanger) need not both be satisfied at the same place. This may allow design for very high specific power. For example, material of high cross section, such as tungsten or tantalum, which could not be used in the core, could be used in the heat exchanger.

(2) Easy fuel transport.

(3) Simplified reprocessing. The reduction to metal, fabrication, canning, and dissolving steps are eliminated. Because of this, decontamination need not be complete. The cooling time could be made much shorter resulting in a smaller holdup of fissionable material.

(4) Simplified waste disposal.

(5) Continuous removal of fission products. The removal of poisons would improve neutron economy and might permit higher burn-up. With a lower inventory of radioactive material, the potential hazard would be decreased; this might reduce the size of the exclusion area required for safety.

(6) Inherent safety and ease of control. Any liquid fuel which expands on heating gives an immediate negative temperature coefficient of reactivity. This effect is not delayed by any heat-transfer process; the rate of expansion is limited only by the speed of sound in the liquid. This instantaneous effect tends to make the reactor self-regulating. Adjustment of fuel concentration can be used as a shim control.

In a system which combines these advantages, the total investment and operating costs might be considerably lower than at present. The desirability of developing fluid-fuel reactors is therefore primarily economic.

Among the disadvantages of fluid fuels listed below, the first two would tend to make the control more uncertain.

(1) Possible fluctuations of reactivity caused by density or concentration changes in the fuel, e.g., bubbling.

(2) Loss of delayed neutrons in the fuel leaving the core.

¹References appear at end of chapter.

(3) External hold-up of fissionable material.

(4) Induced activity in pumps and heat exchangers and possible deposition of fuel and fission products.

(5) Corrosion problems. Each fuel system has its particular corrosion problems. These differ greatly from one system to another, but in every case, corrosion is the critical problem which must be solved.

(6) Special limitations of particular fluid fuels.

Among the fluid-fuel systems which have been considered are:

(1) Aqueous systems.

(2) Liquid metals.

(3) Fused salts.

(4) Other liquids (e.g., UF_6 and solutions containing it).

(5) Gases (again UF_6).

(6) Powders, "pebbles," or any divided solids which can be handled as fluids.

(7) Fluidized powders.

In some of these systems, both truly homogeneous systems (solutions) and mixtures (dispersions) must be considered. The last four systems have not been developed far enough to warrant discussing them at this time; the first three, treated in Sections 4, 5, and 6 of this volume, all show the potential advantages listed above, which are inherent in fluid fuels.

Comparing one system with another involves relative advantages and disadvantages. Liquid-metal-solution systems (in particular, solutions of uranium in bismuth) have the following advantages over aqueous systems:

(1) Metals can be operated at high temperatures without high pressures.

(2) Metal solutions are free from radiation damage and do not give off bubbles (except for fission-product gases). By using liquid metals, therefore, two factors which may limit the specific power of aqueous systems are avoided.

(3) Liquid metals have better heat-transfer properties than water [but water can carry more heat, cf. disadvantage (1) below].

(4) Metal systems do not have inherent moderating properties and can be used for fast and intermediate reactors as well as for thermal reactors provided the critical mass requirements are not excessive [cf. disadvantage (5) below].

(5) Liquid metals can be circulated by electromagnetic pumps if desired, though the efficiency may be poor, as with bismuth.

(6) Some suitable metals, e.g., bismuth, are cheaper than D_2O .

(7) Polonium, formed from bismuth by neutron capture, may be a valuable by-product [cf. disadvantage (7) below].

Liquid-metal systems have the following disadvantages in comparison with aqueous systems:

(1) The heat capacity is less than water. (On the basis of $\text{cal}/(\text{cm}^3)(^\circ)$, this is partially offset by the higher density of metals.)

(2) The higher density may be a disadvantage.

(3) Liquid metals are more difficult to pump.

(4) The absorption cross sections of the best metals (e.g., bismuth, $\sigma = 0.032$ barns) are inferior to D_2O , though better than H_2O . The cross section of bismuth may be low enough, however, to allow breeding of U^{233} from thorium by means of thermal neutrons.

(5) For a thermal reactor, moderator must be supplied [cf. advantage (4) above].

(6) The limited solubility of uranium in bismuth necessitates the use of enriched U^{235} or U^{233} as fuel. Uranium-238 or thorium cannot be held in solution in sufficient concentration to give internal breeding.

(7) Because of (4) and (5), liquid-metal-fuel reactors (LMFR) are at least 4 ft in diameter and cannot be scaled down as far as aqueous reactors can.

- (8) The high melting point of most metals makes the start-up of a reactor difficult.
- (9) Polonium may represent an additional hazard as well as a by-product [see advantage (7) above]. However, if the polonium remains with the fission products, it should not add to the problems already present. If it is separated, its value should pay for the additional precautions which would be taken.

The concentration of fissionable material in solution is limited by its solubility at the lowest temperature in the system. This limitation can be avoided by using a dispersion of a solid in the liquid metal. A dispersion might show the following advantages over a solution:

(1) The increased concentration of fissionable material might be necessary for a fast reactor or might allow increased neutron economy, smaller core dimensions, or the introduction of fertile material in the core. Disadvantages (4), (6), and (7), above, might thus be avoided.

(2) The liquid phase of the dispersion might be a low-melting eutectic, a situation that would eliminate objection (8).

(3) With the fissionable material in a solid form, contamination of pumps and heat exchangers might be reduced.

On the other hand, a liquid-metal dispersion might have these disadvantages:

(1) The solids might settle out and thereby cause concentration changes which would result in fluctuations of reactivity. Even if this did not occur with a fresh slurry, radiation damage and thermal cycling might result in changes in the particle size or shape that would increase the settling rate. Extra equipment, e.g., stirrers, might be required to keep the solids in suspension.

(2) The viscosity of the slurry might make circulation difficult. In this connection, there is the possible use of viscous liquid-metal mixtures, e.g., pastes, which would not be circulated to remove heat but rather would be used in a stationary fuel element. Such an element might retain some of the advantages of a liquid metal fuel, e.g., freedom from radiation damage, ease of handling and processing, and good heat transfer.

(3) With the fissionable material in a solid form, the removal of fission products and reprocessing would be more complicated.

(4) Finally, the presence of solids might cause erosion in addition to corrosion.

POSSIBLE APPLICATIONS OF LIQUID METAL FUELS

Of the many possible reactors using liquid metal fuels, only a very few have received even a preliminary design. One possibility, LMFR^{2,3}, would use a dilute solution of U²³³ or enriched U²³⁵ in bismuth in a core of the reactor. The core would consist of a tank through which the fuel would flow and in which beryllium rods would moderate the neutrons to thermal energy. The heat would be removed from the fuel externally. (Several types of external heat exchangers are discussed in Chapter 5.3.) The heat would be delivered at a suitably high temperature to produce electrical power. A large fraction of the neutrons would escape from the core and would be caught in a blanket to produce fissionable material. Thus, the LMFR could be either a power-breeder on the Th-U²³³ cycle or a power-converter consuming U²³⁵ and producing U²³³.

In LMFR, reprocessing of both the core and the blanket would be integrated with the reactor. This might lead to a considerable reduction in operating costs. The U-Bi solution in the core would be processed in the following ways:

(1) Rare gases (especially Xe¹³⁵) would be removed by gas sparging or pumping on every cycle of the fuel (approximately every 15 sec).

(2) Rare-earth fission products would be removed by extracting the metal with a fused salt, the eutectic mixture of LiCl and KCl. The blanket would consist of ThF₄ through which would circulate a gas containing F₂. This gas would cool the blanket and would re-

move the product U^{233} as UF_6 . Chemical processing is described in detail in Volume 4. This brief description is included here because integration of the chemical processing with reactor operation is one of the important economic justifications of LMFR.

REFERENCES

1. H. Halban and L. Kowarski, BR-7, Oct. 1941 (classified).
2. D. H. Gurinsky et al, BNL-111 (LFR-2 Revised), June 5, 1951 (classified).
3. F. T. Miles et al, Reactor Sci. Tech. 2, No. 1, April 1952, p 7 (classified).

Composition and Properties of Liquid Metal Fuels

R. J. Teitel

The range of compositions of interest as reactor fuels is limited by nuclear requirements. Semiquantitative limits on the amount of carrier material, C, which can be added to the fuel, F, are set by the calculation:

$$(N_C/N_F) (\sigma_C/\sigma_F)$$

where the first factor is the atomic ratio and the second is the ratio of absorption cross sections. The product represents the number of neutrons lost to capture by the carrier material per neutron captured by the fissionable material. To achieve a chain reaction, k_∞ must be greater than 1, and $N_C\sigma_C/N_F\sigma_F$ must be less than $(\eta - 1)$. Similarly, to produce more fissionable material than is consumed, $g > 1$, the product must not exceed $(\eta - 2)$.

Table 5.2.1 — Maximum Allowable Values of $\left[\frac{N_C}{N_F} \sigma_C\right]^*$

Fuel	Thermal neutrons	
	$(\eta - 1)\sigma_F$	$(\eta - 2)\sigma_F$
	for chain reaction ($k_\infty > 1$), barns	for breeding gain ($g > 1$), barns
U ²³³	767	203
U ²³⁵	721	(77)†
Pu ²³⁹	1035	0

* (Dilution of fuel) \times (cross section of carrier)

† U²³⁵ is not part of a breeding cycle

The values for $(\eta - 1) \sigma_F$ and $(\eta - 2) \sigma_F$ are given in Table 5.2.1 for different fuels and for thermal neutrons. These numbers represent the maximum values of $(N_C/N_F) \sigma_C$ which could be tolerated to achieve a chain reaction or a breeding gain. For example, bismuth has an absorption cross section for thermal neutrons of 0.032 barn. Therefore, to achieve a chain reaction with a U²³⁵-Bi solution, the dilution cannot exceed:

$$N_{\text{Bi}}/N_{25} < 721/0.032 = 2.25 \times 10^4$$

The atomic concentration of uranium would have to be at least 44 ppm. Neutron losses to the moderator and leakage would raise the required concentration.

This very rough rule is good enough to indicate the concentration ranges of interest for thermal reactors, but the situation is more complicated for fast reactors. The energy spectrum of the neutrons must be determined in this case, and this depends on various competing processes, the cross sections for which are not well known. Inelastic scattering may also be very important. For these reasons, the above rule, based on capture cross sections only, should be used with caution. In general, fast reactors require more concentrated fuels than do thermal reactors.

The capture cross sections¹⁻³ of possible components of liquid metal fuels are listed in Table 5.2.2 in order of increasing melting point. Where capture cross sections for fast neutrons are not known they can be estimated.⁴

Table 5.2.2—Capture Cross Sections of Liquid-metal-fuel Components

Component	Melting point, °C	Absorption cross section	
		Thermal, barns	Fast, barns
Hg	-39	380	...
Hg ²⁰⁰	-39	60	...
Hg ²⁰¹	-39	60	...
Cs	28	29.0	...
Ga	30	2.71	...
Rb	39	0.70	0.017
K	63	1.97	...
Na	97	0.49	0.00026
In	156	190	...
Li	186	67	...
Li ⁷	186	0.033	...
Sn	232	.65	...
Bi	271	.032	0.0034
Tl	300	3.3	...
Cd	321	2400	...
Pb	327	0.17	...
Zn	419	1.06	...
Te	450	4.5	...
Ce	600	0.70	0.005
Sb	631	6.4	...
Mg	650	0.059	...
Al	660	.215	0.00037
Ba	704	1.17	...
Sr	770	1.16	...
Nd	840	44	0.041
Ca	850	0.43	...

¹References appear at end of chapter.

LIQUID-METAL-SOLUTION FUELS

The data in this field are scanty, and extrapolation is therefore usually necessary. For instance, most of the liquid and solid densities are not well established, but by assuming that the atomic volumes of the constituent atoms in the alloy do not change, a simple calculation gives an estimated density which is usually within 10 to 15 percent of the true value. This approximation cannot be used for ionic compounds.

Many of the data have been taken from only a few sources. All the known data on uranium phase diagrams, for example, are summarized by Buzzard and Cleaves;⁵ another source is the unpublished information of Teitel.⁶

URANIUM SOLUTIONS IN LIQUID METALS

The solubility of uranium in various liquid metals at different temperatures has been reported,⁶⁻⁸ and the results appear in Table 5.2.3 and Figs. 5.2.1 and 5.2.2. No specific data on the physical properties or the stability to radiation damage appear in the literature. The properties should be very similar to those of the pure liquids, however, and radiation damage in liquid metals is believed to be negligible.

URANIUM-BISMUTH SOLUTIONS

The properties of pure bismuth, given in Table 5.2.4, provide a rough approximation of the properties of a dilute bismuth solution. The static corrosion of container materials by uranium-bismuth solutions has been studied in detail,^{9,10} and the results indicate that these solutions behave like bismuth. It seems likely, therefore, that those materials that cannot be used with bismuth cannot be used with its uranium solution but that the materials which have a good corrosion resistance with bismuth will be suitable for bismuth-uranium solutions. Containers that have been suggested are Cr-Mo steels, Cr-Mo-Si steels, silicon steels, plain carbon steels, beryllium, molybdenum, tungsten, and many ceramics. Dynamic corrosion properties are not known, and it is not possible to extrapolate from experience with pure bismuth since slight additions to liquid metals¹⁰ have been known to have large effects on dynamic corrosion behavior.

THORIUM SOLUTIONS IN LIQUID METALS

Solubility data for thorium⁷ in liquid metals are shown in Table 5.2.5. No data for the physical properties of these solutions appear in the literature. However, since the concentration of thorium is low, the properties of these solutions should follow closely those of the pure metals (refer to Section 2 "Liquid-metal-cooled Systems").

PLUTONIUM SOLUTIONS

Only a few solutions of Pu in low melting alloys have been found. The solubility of Pu in Bi is shown in Fig. 5.2.3. Other systems show low melting eutectics at the temperature and concentrations given in Table 5.2.6.

LIQUID-METAL-DISPERSION FUELS

To utilize higher concentrations of a fissionable component in liquid metals, dispersions in which the solid contains the fissionable component must be considered. This field is new, and the data are therefore meager. However, some properties can be extrapolated from the characteristics of pure liquid metals and solids.

The properties of muds and dispersions have been studied in the field of soil mechanics,¹¹ and certain of these principles can be carried over to liquid-metal-fuel dispersions. In

Table 5.2.3 — Solubility of Uranium in Liquid Metals and Alloys
(TID-65, July 1948)

Metal or alloy	Uranium solubility, atomic-%									
	900°C	850°C	800°C	750°C	700°C	650°C	600°C	550°C	500°C	450°C
Al	4.2	3.7	3.3	2.8	2.3	1.7				
62 Al : 38 Mg				0.29	.21	.17				
28 Al : 72 Mg					0.020	.016				
94.7 Al : 5.3 Si	1.4	0.9	.5	.3	.2	.2				
91.6 Al : 8.4 Si		0.6	.4	.2	.1	.08	0.05			
61 Al : 39 Ag	1.5	1.2	1.0	0.8	.6	.5	.4			
88 Al : 12 Zn			3.0	2.8	2.2	1.8	1.4			
70 Al : 30 Zn			3.1	2.7	2.3	1.9	1.3			
47 Al : 53 Zn						1.4	1.1	0.7		
Zn									0.32	
1.1 Al : 98.9 Bi		6.9								
Bi	12.3	9.3	7.1	5.3	4.2	3.1	2.2	1.6	0.9	
46 Bi : 54 Sn	3.1	2.2	1.2	0.8	.4	.2	.07	.06	.04	
Sn		0.2		0.03		*				
45 Bi : 55 Cd						0.40	0.23	.06		
78 Bi : 22 Na			2.3	1.6	1.2	1.0	0.9			
68 Bi : 32 Na				1.7	1.2	0.9	.6	.4	.2	
Sb	1.5	0.9	.4	.3	.2	.1				
Pb	0.52				0.05				0.02	
In	0.51	.34	.22	.12	.07	.05	.04			
Tl	0.13		0.10							*
Ga					<0.9					†

*Not detected

†Less than 0.03 at 40°C

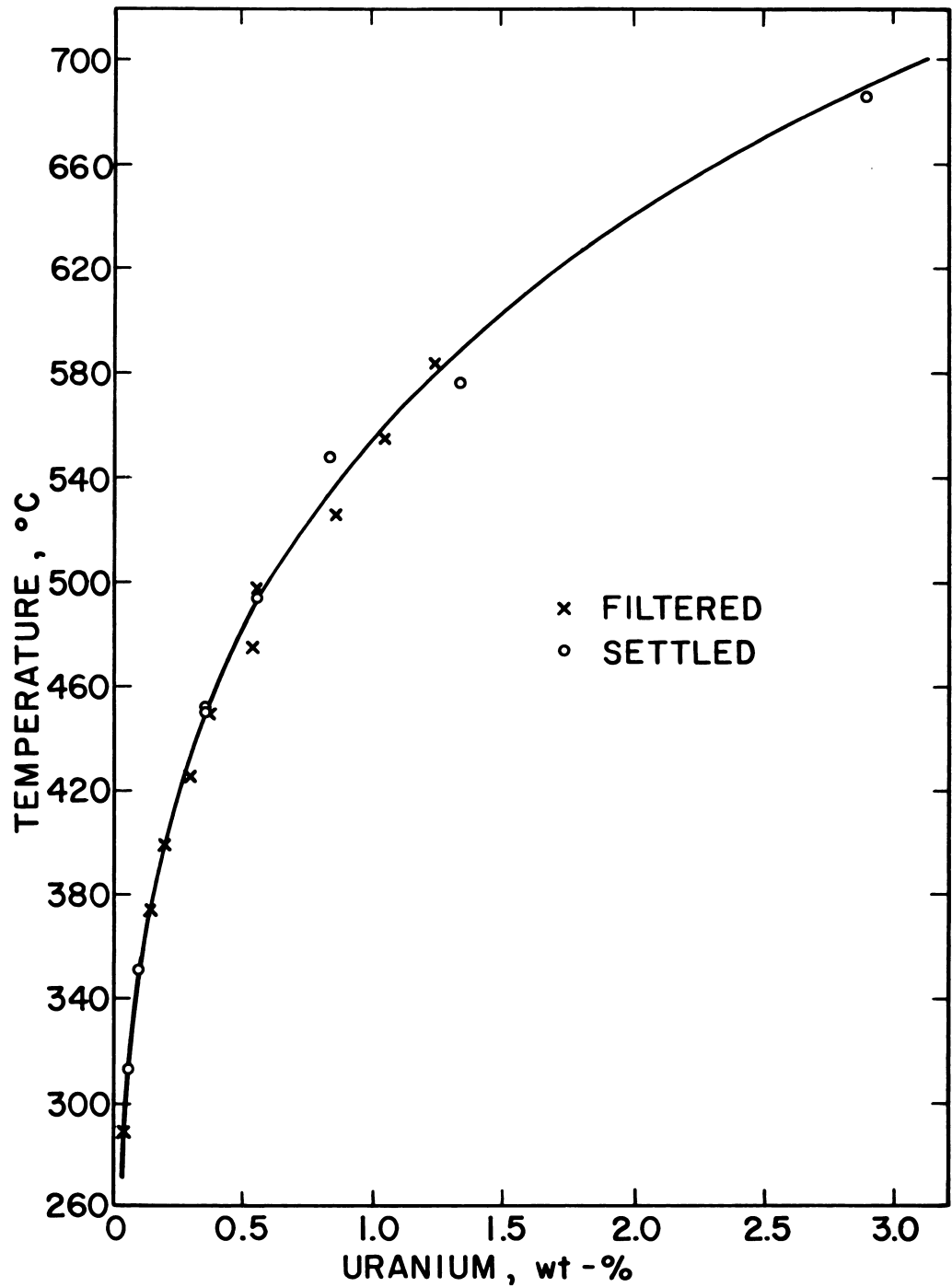


Fig. 5.2.1 — The Solubility of Uranium in Liquid Bismuth. Reprinted from BNL-75, Sept. 15, 1952. (BNL Log No. D-1558)

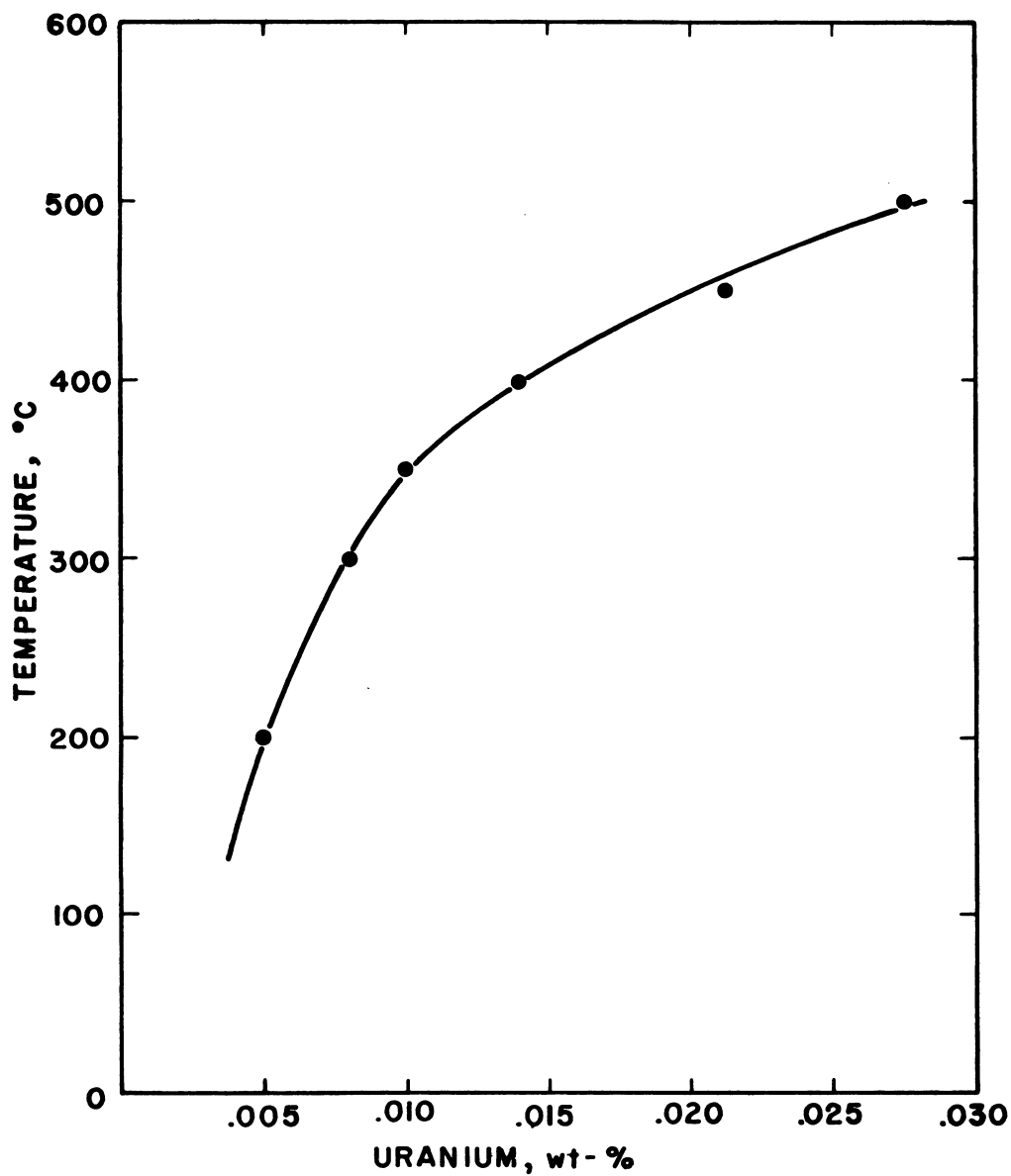


Fig. 5.2.2— The Solubility of Uranium in Liquid 47 Bi: 53 Pb Alloy.
Submitted by BNL, Aug. 21, 1952. (BNL Log No. D-2351)

Table 5.2.4—Properties of Pure Bismuth

(Liquid Metals Handbook, NAVEXOS P-733, June 1, 1950)

Melting point, °C	271	
Latent heat of fusion, cal/gm	13	
Boiling point, °C	1477	
Heat of vaporization, cal/gm	204.3	
Vapor pressure, mm Hg		
917 °C 1683 °F	1.0	
1067 °C 1953 °F	10.0	
1257 °C 2295 °F	100.0	
1325 °C 2417 °F	200	
1400 °C 2552 °F	400	
Density, gm/cc		
300 °C	10.03	
400 °C	9.91	
600 °C	9.66	
802 °C	9.40	
962 °C	9.20	
Specific heat, cal/(gm)(°C)		
271 °C	0.0340	
400 °C	.0354	
600 °C	.0376	
800 °C	.0397	
1000 °C	.0419	
Viscosity, poises × 10 ²		
304 °C	1.662	
451 °C	1.280	
600 °C	0.996	
Thermal conductivity, °C/cm		
300 °C	0.041	
400 °C	.037	
500 °C	.037	
600 °C	.037	
700 °C	.037	
Electrical resistance, μ ohms/cm		
300 °C	128.9	
400 °C	134.2	
600 °C	145.25	
750 °C	153.53	
Surface tension, dynes/cm ²		
300 °C	376	
350 °C	373	
400 °C	370	
450 °C	367	
500 °C	363	
Volume change on fusion, % of solid volume	3.32	
Isotopic composition of bismuth	100 ⁵ Bi ²⁰⁹	
Nuclear properties of bismuth	Thermal	Fast
Absorption cross section, barns	0.032	0.003
Scattering cross section, barns	1.35	...
Radiation products	Po ²¹⁰	...

Table 5.2.5—Solubility of Thorium in Liquid Metals and Alloys
(TID-65, July 1948)

		Thorium solubility, atomic -%															
T, °C	Al	63% Al 37% Mg	86% Al 14% Si	71% Al 29% Zn	61% Al 39% Ag	Bi	Sn	45% Bi 55% Cd	76% Bi 24% Na	Sb	Pb	In	Tl	Na	83% Sn 17% Na		
900						3.2	2.2			0.53	1.07	0.47	0.29	Trace of thorium only at 300°C			
850	6.4				3.0	2.3				.26							
800	5.3			3.1	2.5	1.5	1.4		1.0	.16	0.39	0.12	0.24				
750	4.6	0.8	2.5	2.4	2.0	1.1		N D*		.05							
700	4.1	.6	1.9	1.7	1.3	0.7	0.1		0.4	<.03	<0.1					0.09	
650	3.7	.4	1.4	1.1	0.5	.5				<.03		*					
600		.3	0.9	0.5		.3	<0.03		<0.07							<0.04	
550						.2											
500						.1											
450													<0.04				
*Not detected																	

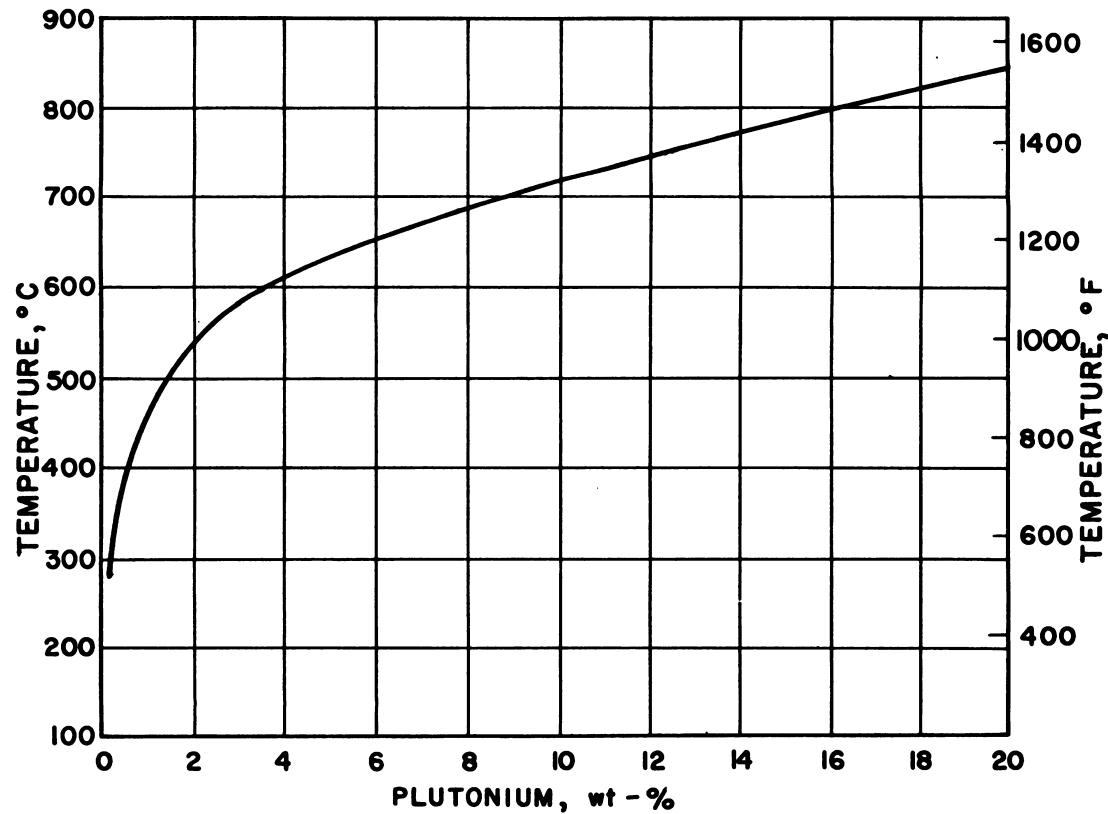


Fig. 5.2.3—Solubility of Pu in Bi. Submitted by Los Alamos Scientific Laboratory, Mar. 1953. (BNL Log. No. D-2350)

Table 5.2.6—Plutonium Liquid-metal Solutions
[References (12) and (13)]

Composition, wt-%	Freezing point, °C
36.7 Pu: 63.3 Ni	465
86.8 Al: 13.2 Pu	647
Pure Pu	635
35.5 Mg: 64.5 Pu	552

particular, it is known that the viscosity of a dispersion depends on the volume-percent solids, the particle size, and the particle shape. For a particular particle size, the volume concentration can be increased to a point beyond which the viscosity increases rapidly. This threshold volume-concentration of solid is diminished with finer particle size. For fuel dispersions, therefore, the maximum concentration of fissionable component decreases with particle size. This property is particularly important if the fuel is to be moved.

Another important property of dispersion is the density difference between the solid and the liquid. This factor affects settling and the erosive action of moving streams. These effects are insignificant for muds or pastes, however, because they are not likely to settle or to be moved fast enough to cause an appreciable amount of erosion.

Liquid-metal-dispersion fuels can be classified into two general groups, according to the nature of the dispersed phase: (1) intermetallic compound dispersions, in which the solid is either a pure metal or an intermetallic compound of the fissionable component with the liquid-metal components and (2) ionic compound dispersions, in which an ionic compound is dispersed in the liquid phase. Phase equilibria, phase diagrams, and properties of the phases are needed for Group (1), while Group (2) requires additional information about wettability.

METHOD OF PRODUCING DISPERSIONS

The method used by Teitel¹⁴ for making intermetallic compound dispersions of uranium has been to add uranium powder, produced from the reduction of the hydride, to the liquid metal at approximately 400°C. This technique has produced dispersions of U(Sn,Pb)₃ in Pb-Sn liquid having a particle size of 3 μ . Sub-microscopic sizes were produced by adding the hydride to the metal directly. Similarly, dispersions of ThBi₃ in Bi have been produced. It is believed that dispersions of plutonium can be produced by this procedure also.

Ionic compound dispersions are produced simply by adding the ionic compound to the clean liquid-metal surfaces.

RADIATION EFFECTS ON DISPERSIONS

No data appear in the literature on this subject.

THERMAL EFFECTS ON DISPERSIONS

An appreciable effect of temperature on a Pb-Sn-U dispersion is reported (see Pb-Sn-U system) in the following. Thermal effects on ionic compound dispersions are expected to be negligible.

URANIUM DISPERSIONS

Bi-U SYSTEM

The phase diagram of U-Bi is uncertain at present. Some time ago Ahman and Baldwin¹⁵ published the diagram shown in Fig. 5.2.4. However, more recent unpublished data by Teitel seem to indicate that the phase diagram is really that shown in Fig. 5.2.5. The solubility of uranium in bismuth at different temperatures has already been discussed above with regard to bismuth-solution fuels. The dispersion that is likely to be the most interesting is that of UBi_2 or U_3Bi_5 (depending upon which diagram is correct) in liquid Bi. General data on this dispersion are summarized in Table 5.2.7.

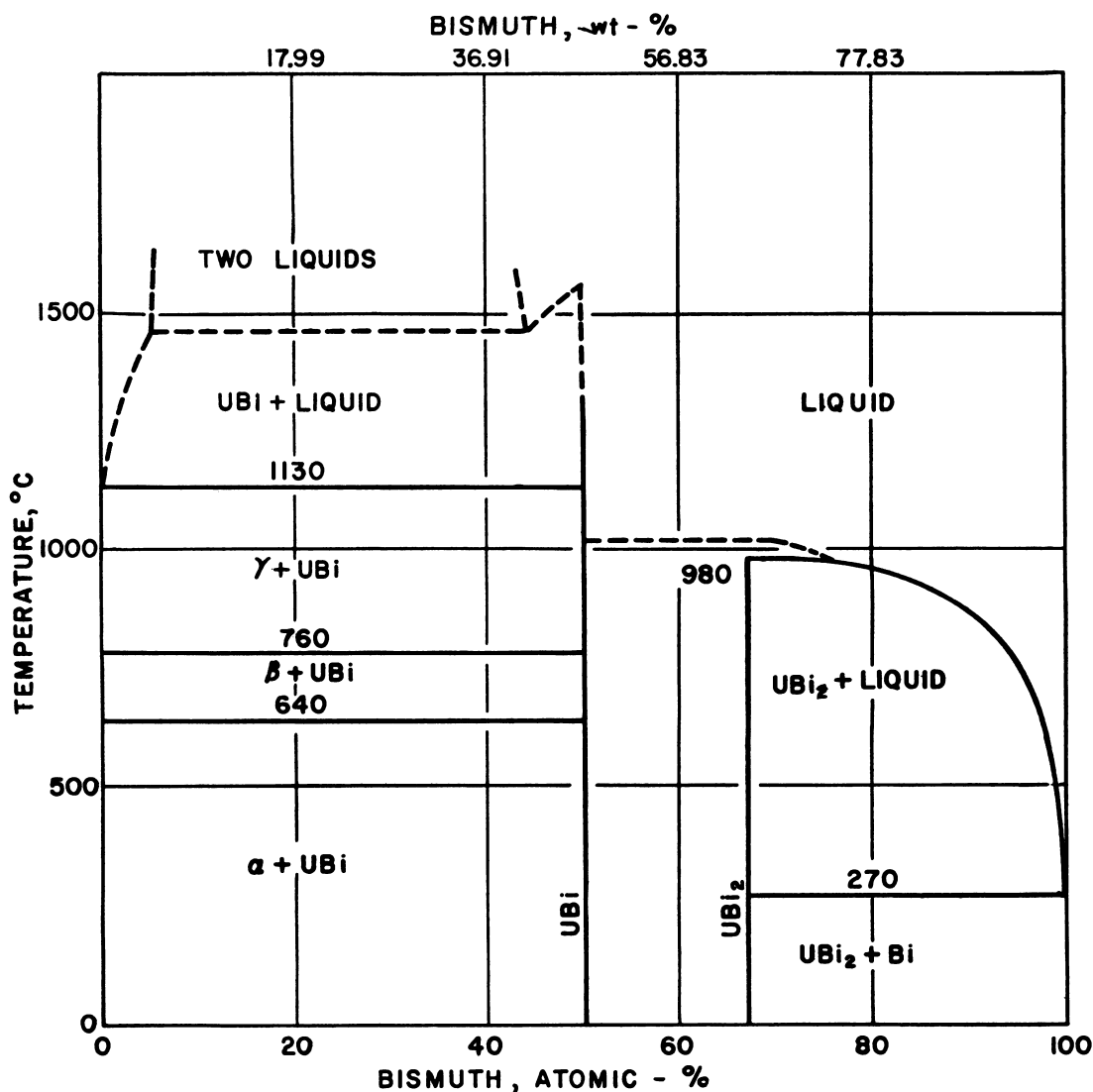


Fig. 5.2.4— The Bismuth-Uranium System. Reprinted from CT-2961. Nov. 12, 1945. (BNL Log No. D-1992)

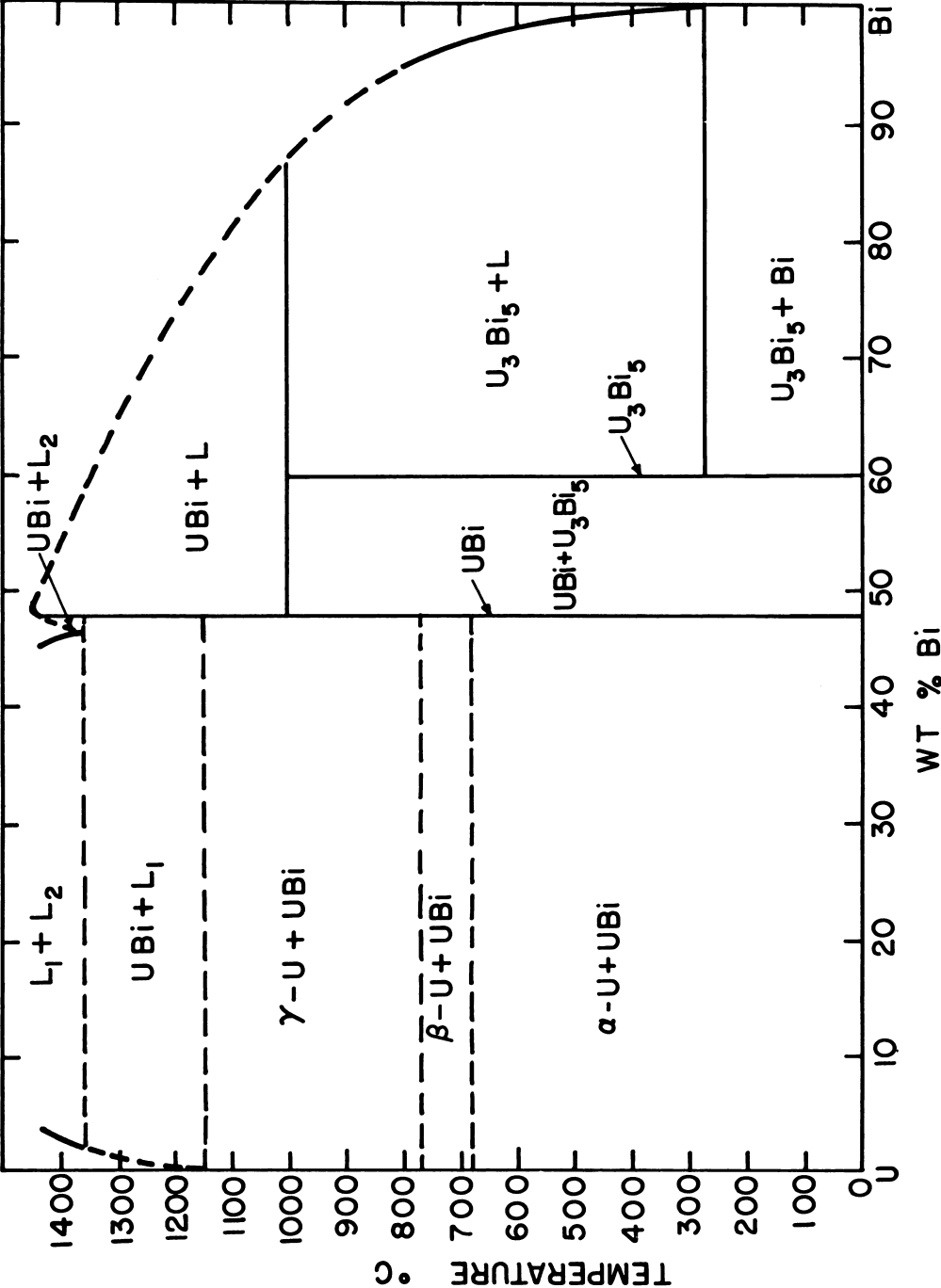


Fig. 5.2.5—The Bismuth-Uranium System. Submitted by BNL, Aug. 21, 1952. (BNL Log No. D-2292)

Table 5.2.7 — Uranium Intermetallic-compound Dispersions

Dispersion system	Solid			Liquid		
	Composition (formula)	Density, gm/cc	Melting temp., °C	Composition, wt-%	Temp., °C	Density, gm/cc
Bi-U	U ₃ Bi ₅ ^{d,e}	12	1000 (dissociates)	Bi	350	10.0
Pb-U	UPb ₃ ^{h,i}	12.98	~1250	Pb	350	10.6
Sn-U	USn ₃ ^{i,k}	10.0	~1350	Sn	400	6.8
Pb-Bi-U	U ₃ Bi ₅ ^{d,n}	(12)	1000 (dissociates)	OPb-81Bi	350	(10.1-10.5)
	UBi ₃ ^{d,n}	(11.5)	>1300	81Pb-95Bi	350	10.5
	UPb ₃ ^{h,i}	12.98	~1250	95Pb-100Bi	350	10.5-10.6
Sn-Bi-U	U ₃ Bi ₅ ^{d,e}	12	1000 (dissociates)	OSn-11Bi	350	10.0-9.5
	U ₃ Sn ₅ ^{d,m}	...	~1375	11Sn-12Bi	350	(9.5)
	USn ₃ ^{i,k}	10.0	~1350	12Sn-100Bi	350	(9.5-6.8)
Sn-Pb-U	UPb ₃ ^{k,i}	12.98	~1250	OSn-2Bi	350	(10.5-10.3)
	U(Sn,Pb) ₃ ^{i,k}	(10.0-10.5)	~1350	2Sn-100Pb	350	(10.3-6.8)
Sn-Pb-Bi-U	U(Sn,Pb) ₃ ^{i,k}	(10.0-10.5)	~1350	52Bi-16Sn-32Pb	350	(9.7)
Bi-Na-U	UBi ₃ ^{d,e}	(11.5)	1000 (dissociates)	4Na-96Bi	350	(7.0)
Hg-U	UHG ₄ ^d	14.6	360 (dissociates)	Hg	100	13.3
Al-U	UAl ₃	...	730 (dissociates)	Al	700	2.36
Ce-U	U ^d	19.8	1130	Ce	...	6.9
Ca-U	U ^d	19.8	1130	Ca	...	1.54

^a Densities in parentheses have been estimated on the assumption that the atomic volume is the same as that of the pure element

^b Melting temperature of compound alone

^c Freezing points were taken from the alloy exclusive of uranium

^d Pyrophoric

^e Plates

^f D. H. Ahman and R. R. Baldwin, The Uranium-Bismuth System, CT-2901, Nov. 12, 1945

^g R. J. Teitel, unpublished results

^h Slightly pyrophoric

ⁱ Cubes

^j R. J. Teitel, The Uranium-Lead System, Journal of Metals 4, No. 4, April 1952

^k Non-pyrophoric

^l D. A. Treick, J. H. Carter, A. I. Snow, R. R. Baldwin, and A. S. Wilson, The Uranium-Tin System, M-3107

^m Limiting composition decreases at higher temperatures

ⁿ Irregular shapes

^o Limiting composition increases at higher temperatures

^p Close density match with high-lead liquids

^q Extremely low melting point

^r W. Latimer, Progress Reports, UCRL-1054, Sept., Oct., Nov. 1950

^s R. W. Buzzard and H. E. Cleaves, The Binary Alloys of Uranium, TID-65, July 1948

Pb-U SYSTEM

This system (Fig. 5.2.6) has been reported by Teitel.¹⁶ The solubility of uranium in liquid lead is 0.005 at temperatures up to 700°C. A dispersion of UPb₃ in essentially pure lead would have the properties summarized in Table 5.2.7.

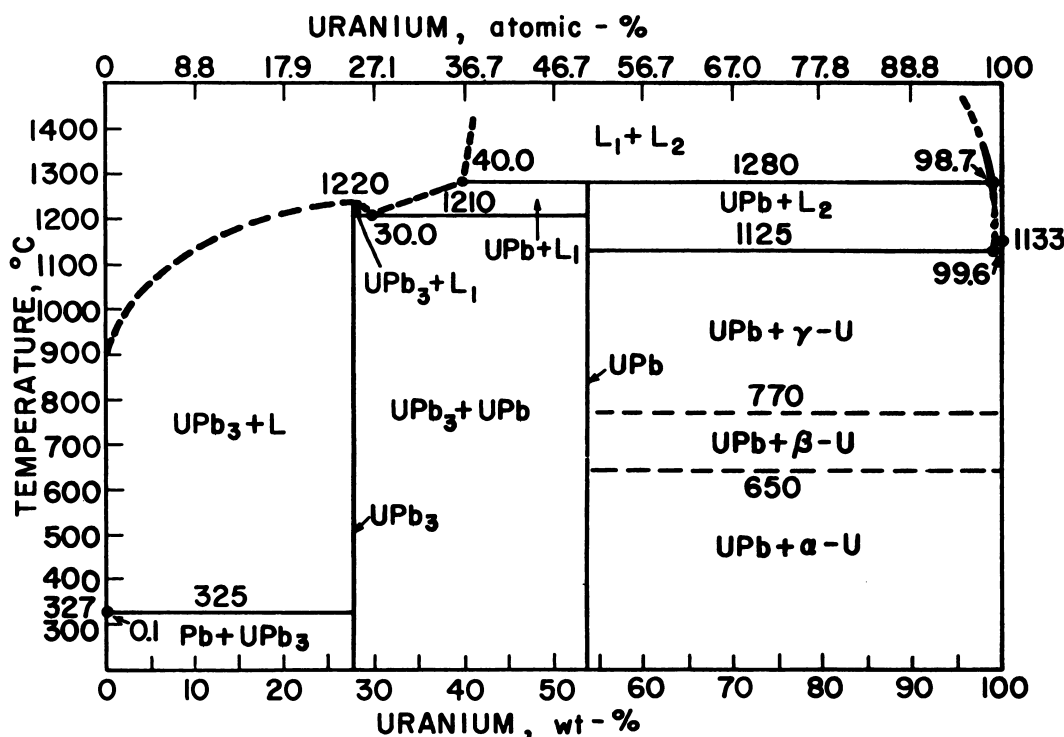


Fig. 5.2.6 — The Lead-Uranium System. Reprinted from the Journal of Metals, April 1952.

Sn-U SYSTEM

Treick et al.¹⁷ investigated this system, and their phase diagram is shown in Fig. 5.2.7. Uranium is less soluble in tin than it is in lead. USn₃ in liquid tin is a possible dispersion, and its properties are listed in Table 5.2.7.

Bi-Pb-U SYSTEM

By adding lead to uranium-bismuth alloys, the phase equilibria can be changed and the high uranium-bismuth compounds dispersed. This permits higher uranium concentrations for equivalent solid/lead volume ratios, i.e., viscosity change sets in at higher uranium concentrations. An isothermal (350°C) portion of the phase diagrams⁶ appears in Fig. 5.2.8, and some possible dispersions for use as either a fuel or plutonium converter system are given in Table 5.2.7. The solubility of uranium in lead-bismuth liquids (Fig. 5.2.2) is very low compared to that in pure bismuth. Phase equilibria at higher temperatures have not been completed.

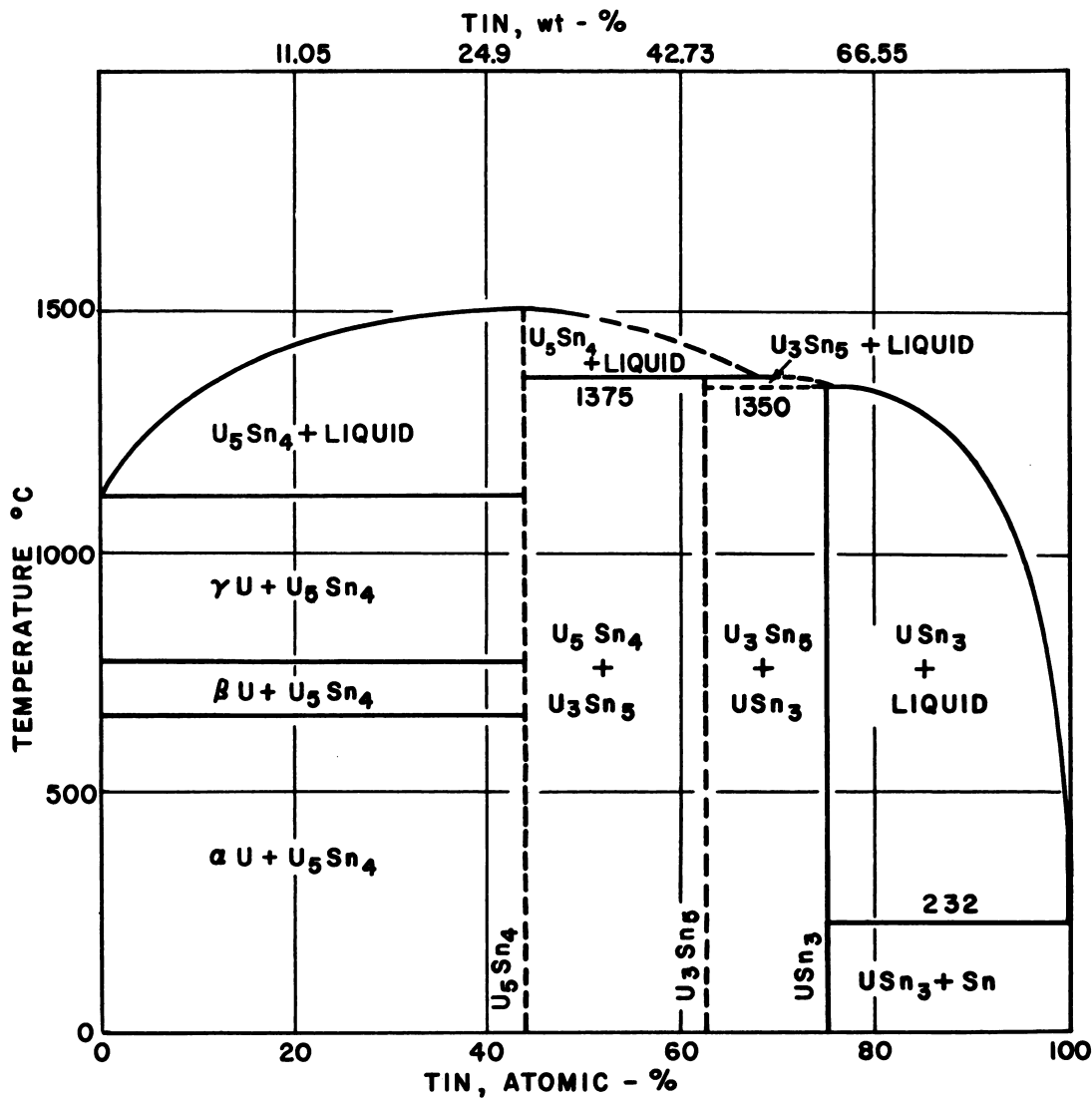


Fig. 5.2.7— The Tin-Uranium System. Reprinted from M-3107. (BNL Log No. D-1993)

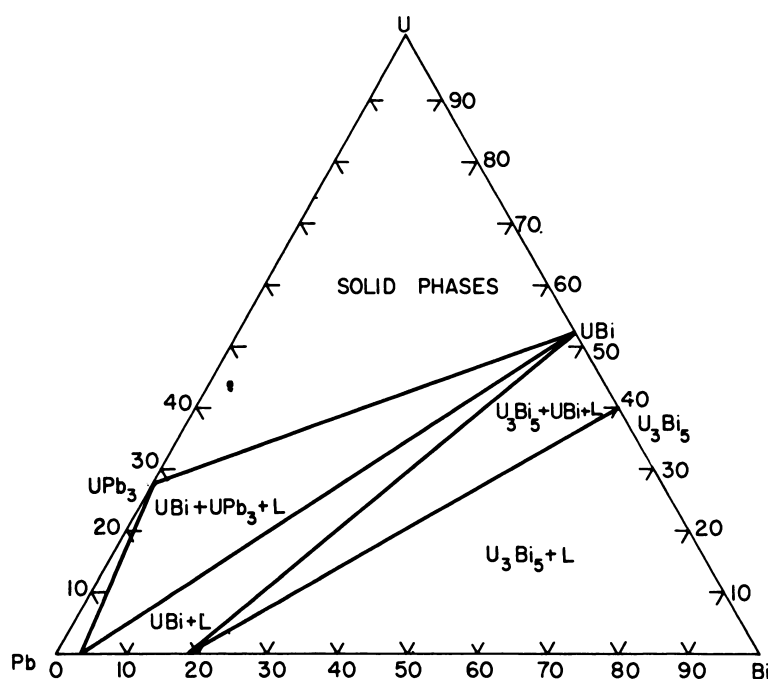


Fig. 5.2.8—An Isothermal (350°C) Section of the Bismuth-Lead-Uranium System. Submitted by BNL, Aug. 21, 1952. (BNL Log No. D-2304)

Bi-Sn-U SYSTEM

Additions of tin to uranium-bismuth alloys lower the solubility of uranium in the liquid phase, and tin compounds appear in equilibrium with liquids containing above 11 weight-percent tin. An isothermal section at 350°C is shown in Fig. 5.2.9. Some possible dispersions are reported in Table 5.2.7.

Pb-Sn-U SYSTEM

Lead and tin form compounds with uranium that have similar structures. Therefore it is not surprising that lead is soluble in solid USn_3 as shown in Fig. 5.2.10. This makes a very interesting group of dispersions because the density between solid and liquid (listed in Table 5.2.7) is very close to zero. This compound is not very pyrophoric.

Tests have been made to determine the effect of thermal cycling and isothermal treatment on the particle size. The isothermal growth at 500° and 600°C is 0.003 μ /hr. Cycling the dispersion between 300° and 600°C caused the particles to grow an additional 0.0007 μ /cycle. The total growth for any cycling speed can be calculated by the following formula:

$$G = G_T + G_C \cdot \frac{1}{t}$$

where G is total growth, G_T is growth owing to mean temperature, G_C is cycling growth, and t is the time for one cycle.

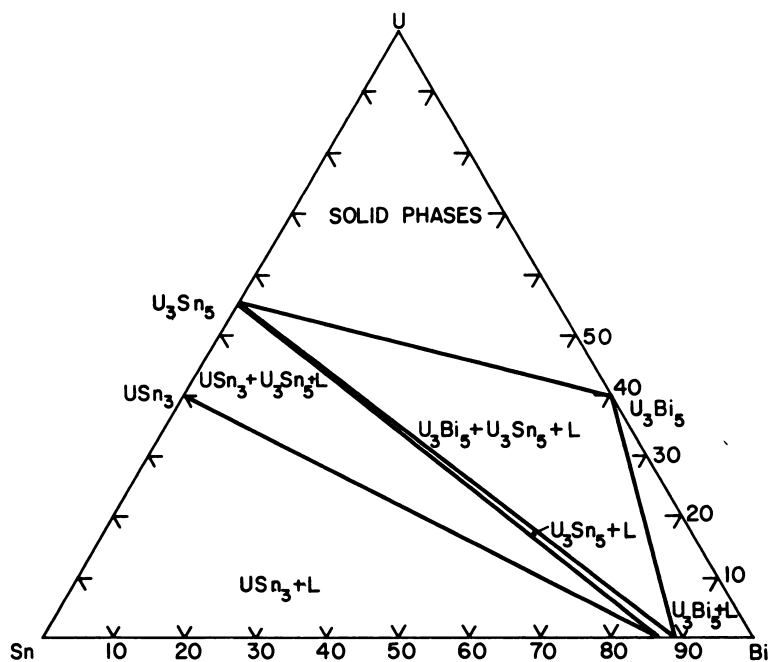


Fig. 5.2.9—An Isothermal (350°C) Section of the Bismuth-Tin-Uranium System. Submitted by BNL, Aug. 21, 1952. (BNL Log No. D-2303)

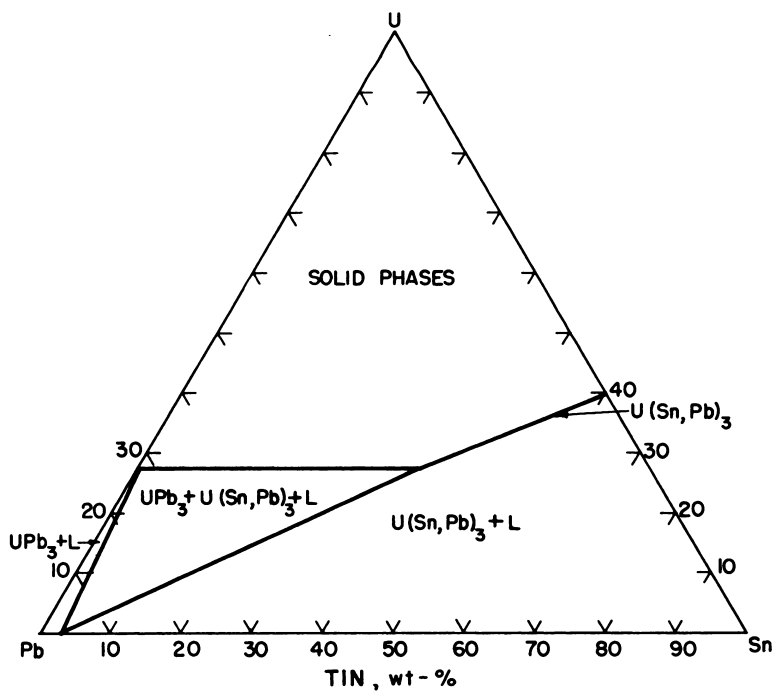


Fig. 5.2.10—An Isothermal (350°C) Section of the Lead-Tin-Uranium System. Submitted by BNL, Aug. 21, 1952. (BNL) Log No. D-2111)

Pb-Bi-Sn-U SYSTEM

Figure 5.2.11 shows a plot of the liquidus of the isothermal section of quaternary system at 350°C. This section neglects the slight solubility of uranium in representing the liquid composition. The lines in the figure separate the two-phase fields indicating the composition of the equilibrium solid phase. This system contributes an additional dispersion to those reported in Table 5.2.7.

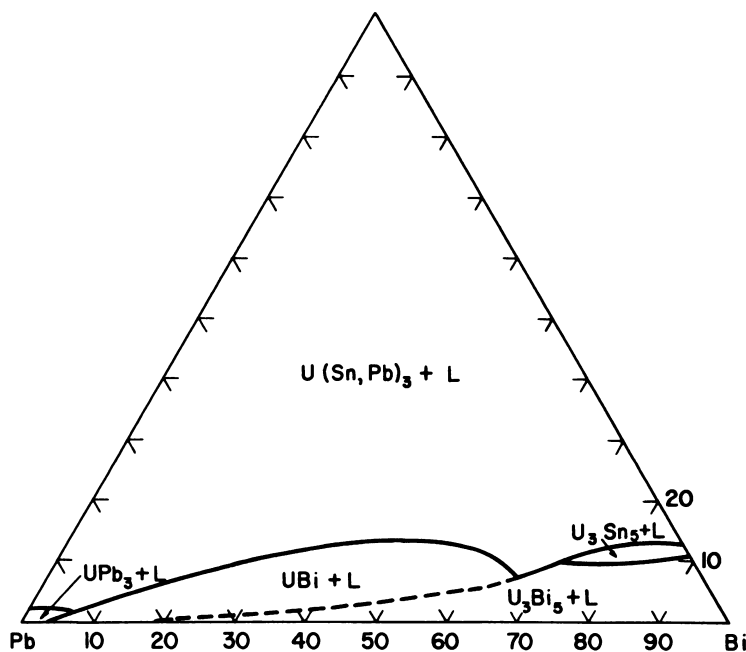


Fig. 5.2.11—A Plot of the Liquidus of an Isothermal (350°C) Section of the Bismuth-Lead-Tin-Uranium System. Submitted by BNL, Aug. 21, 1952. (BNL Log No. D-2302)

Bi-Na-U SYSTEM

It has been reported¹⁸ that UBi_2 is stable in some bismuth-sodium liquids. A possible dispersion for this system is given in Table 5.2.7.

Hg-U

The phase diagram for the U-Hg system appears in Fig. 5.2.12, and a possible dispersion from this system is given in Table 5.2.7.

U-Al

The phase diagram for this system is shown in Fig. 5.2.13, and a possible dispersion is given in Table 5.2.7.

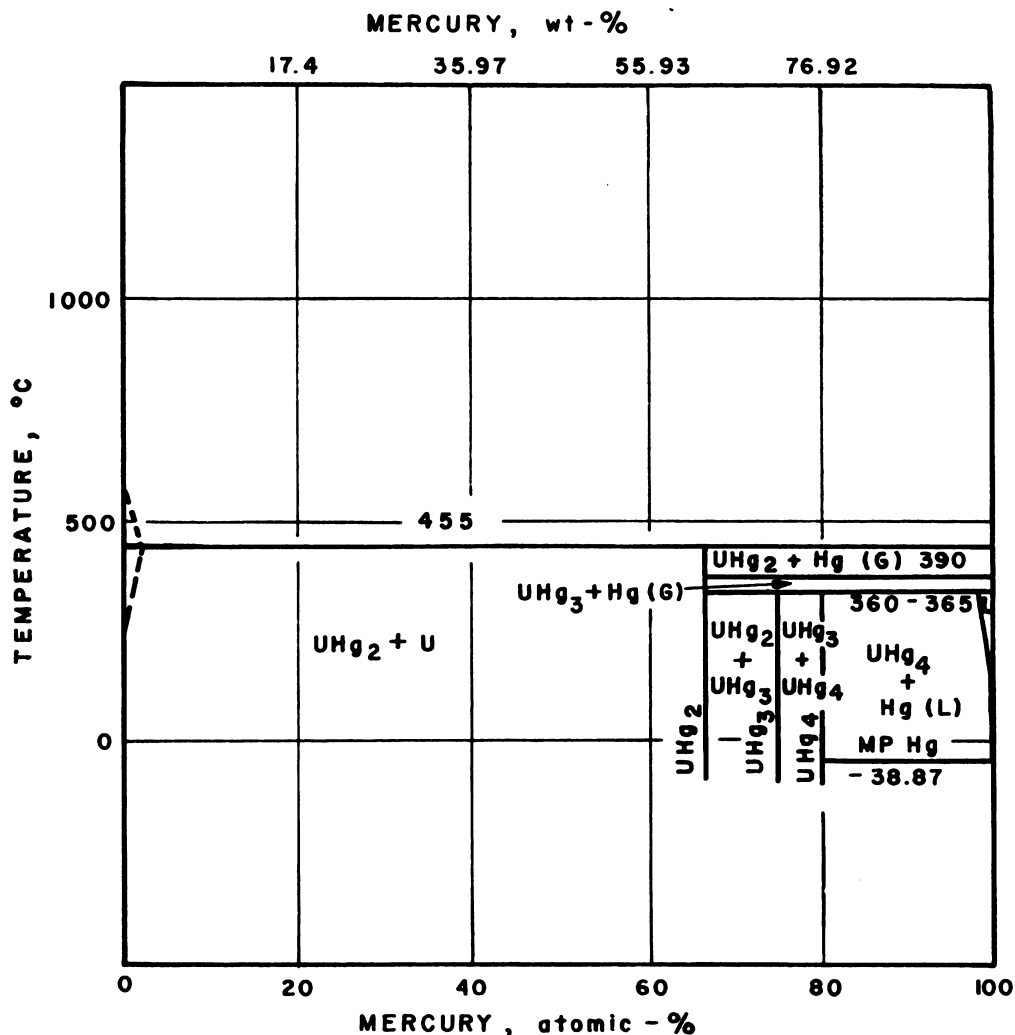


Fig. 5.2.12—The Mercury-Uranium System. Reprinted from TID-65, July 1948. (BNL Loe No. D-2153)

U-Ce

Reports have indicated that uranium is immiscible with Ce,⁵ and therefore, it might be possible to disperse particles of uranium in cerium. This dispersion would have the properties indicated in Table 5.2.7.

U-Cd

Cd does not seem to alloy with uranium.⁵ Consequently, a dispersion listed in Table 5.2.7 is possible.

U-Ca

Apparently calcium and uranium do not alloy.⁵ A possible dispersion is given in Table 5.2.7.

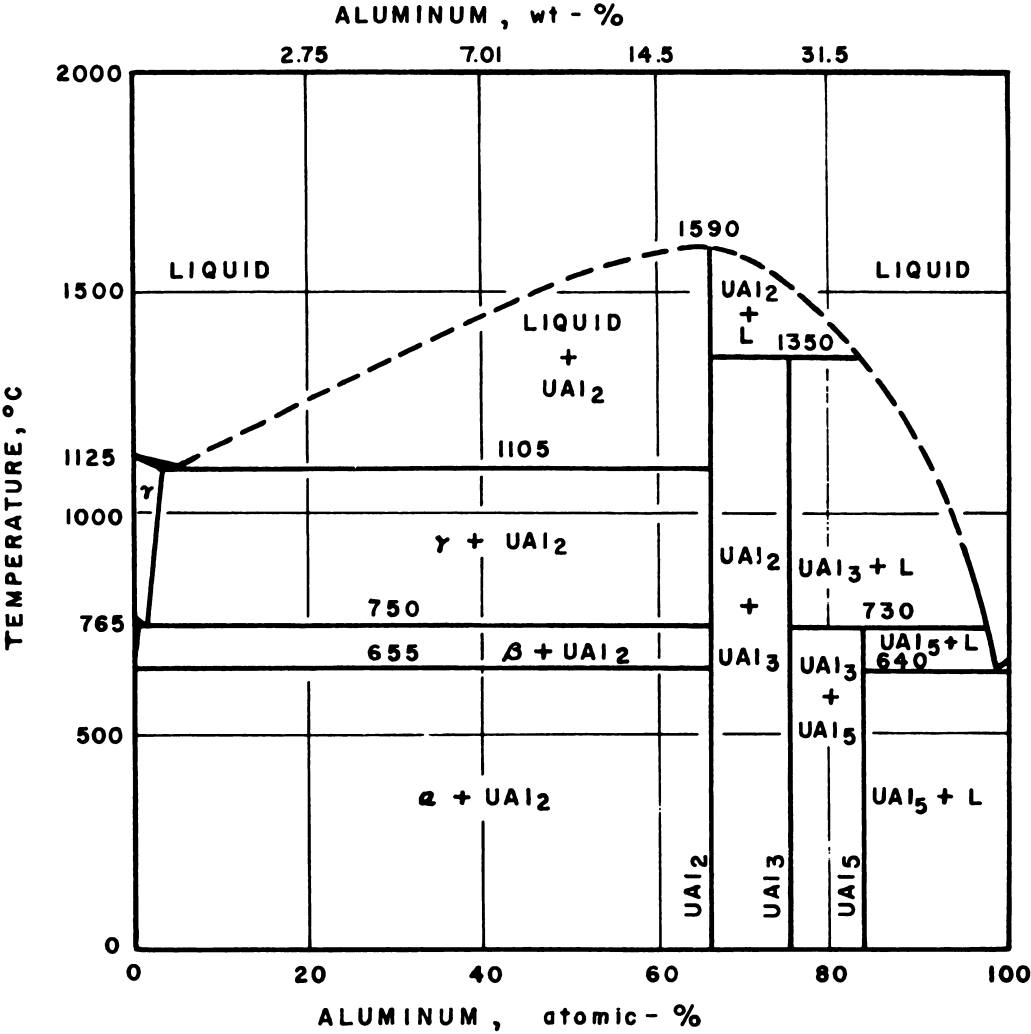


Fig. 5.2.13—The Aluminum-Uranium System. Reprinted from TID-65, July 1948. (BNL Log No. D-2152)

Table 5.2.8 — Compilation of Data on Uranium Ionic Compound Dispersions

Liquid	Cross section, barns	Melting point, °C	Density (ρ), gm/cc	Liquid-solid contact angle, degrees					
				U ₃ O ₈ (ρ = 8.41)	UO ₂ (ρ = 10.97)	UF ₄	USi ₂ (ρ = 9.98)	UAl ₃ (ρ = 7.80)	UH ₃ (ρ = 10.95)
Bi	0.032	271	10.03(300°C)	80(450°C) 87*(430°C)	110†(300°C)	>90†	>90†	>90†	Reacts
Pb	.18	327.4	10.68(327.4°C)	>110*(450°C)	>90†	>90†		>90†	Reacts
Sn	.65	231.9	6.83(409°C)	130*(300°C)	>90†	~90†		>90†	Reacts
Na	.45	97.9	0.928(100°C)	...	0 or reacted†	0 or reacted†		~90†	Reacts
55Pb-(?)Bi	.11	125	10.16(305°C)	...					Reacts
52Bi-32Pb-16Sn	.22	95	~9.5(300°C)	150*(200°C)					Reacts
Hg	430	-38.9	13.35(100°C)	...					0 in vac >0 in gas†

*R. J. Teitel, BNL-113

†R. J. Teitel, unpublished data

‡R. J. Teitel, BNL-142

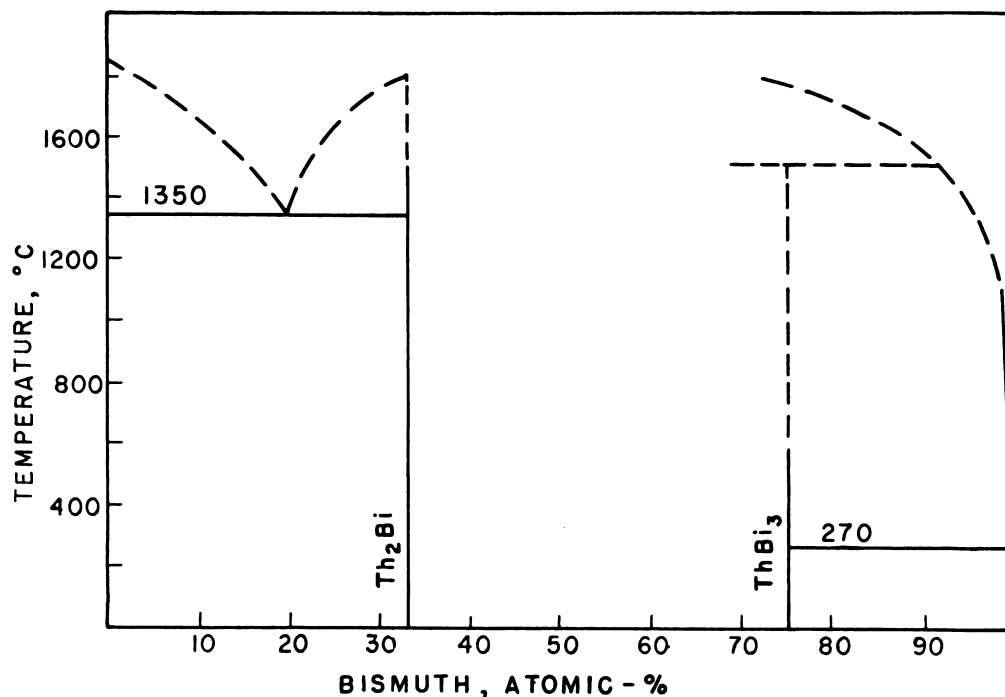


Fig. 5.2.14—The Bismuth-Thorium System. Reprinted from ISC-48, July 12, 1950. (BNL Log No. D-2154)

IONIC COMPOUND DISPERSIONS OF URANIUM

The stability of a dispersion depends upon whether the solid is wetted by the liquid. Usually, this means that the contact angle for the liquid phase is 0° . Indeed, this is the best condition. The available data on contact angles for the various solids and liquids as well as the properties of the solid and liquid are given in Table 5.2.8.

THORIUM DISPERSIONS

Very few of the phase diagrams for thorium have been given in the literature for low-thorium alloys. The only intermetallic compound dispersion that can be reported¹⁹ is that of ThBi_3 in Bi. The incomplete phase diagram appears in Fig. 5.2.14. The density of ThBi_3 (which is pyrophoric) is not known, but it is estimated to be close to that of bismuth. A dispersion of this type has been produced by means of the technique of adding uranium powder to bismuth. Bryner²⁰ has started to study intermetallic dispersions of thorium in lead-bismuth alloys, and a tentative isothermal section of this system is shown in Fig. 5.2.15.

Nothing has been reported on the contact angles of ionic thorium compounds versus various liquid metals.

PLUTONIUM DISPERSIONS

A few phase diagrams have appeared but none for the low-melting elements. It is known* that PuSn_3 and PuPb_3 exist, and it can be guessed that there might be a similar set of dispersions to that of uranium. No data are available on possible ionic compound dispersions.

*Submitted by Los Alamos Scientific Laboratory, March, 1953.

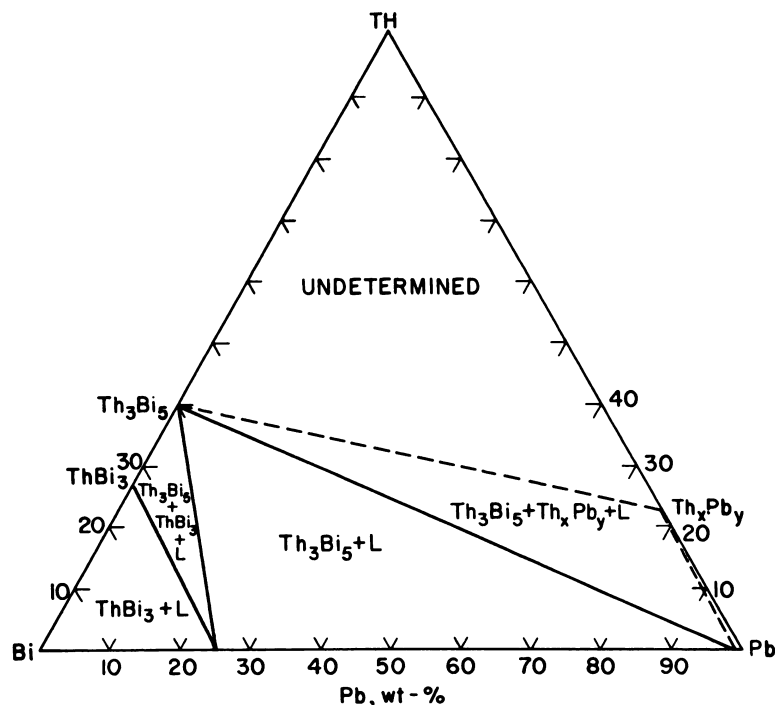


Fig. 5.2.15—Tentative Isothermal Section at 450°C of Th-Bi-Pb System. Submitted by BNL March 16, 1953. (BNL Log No. D-2349)

REFERENCES

1. D. J. Hughes, R. C. Garth, and C. Egger, Neutron Cross Sections, AEC Neutron Cross-section Advisory Group, AECU-2040, May 15, 1952.
2. D. J. Hughes, R. C. Garth, and C. Egger, Fast-neutron Cross Sections and Nuclear Level Density, loc. cit., to be published; abstracted Phys. Rev. 83, 1951, p 234.
3. R. C. Garth, D. J. Hughes, and J. S. Levin, Level Densities from Fast-neutron Capture, presented before Amer. Phys. Soc., May 3, 1952; abstracted Phys. Rev. 87, July 1, 1952, p 222.
4. D. J. Hughes, W. D. B. Spatz, and N. Goldstein, Capture Cross Sections for Fast Neutrons, Phys. Rev. 75, 1949, p 1781.
5. R. W. Buzzard and H. E. Cleaves, TID-65, July 1948, pp 25-53 (classified).
6. R. J. Teitel, unpublished work.
7. E. E. Hayes and P. Gorden, TID-65, July 1948, pp 130-141 (classified).
8. D. W. Bareis, BNL-75, Sept. 15, 1950 (classified).
9. M. A. Cordovi, BNL-179, Mar. 1, 1952 (classified).
10. Liquid Metals Handbook, edited by R. N. Lyons, Department of the Navy and U. S. Atomic Energy Commission, NAVEXOS p. 733, 1st ed., June 1, 1950; 2nd ed., June 1952.
11. J. M. Dallavalle, Micromeritics, Pitman Publishing Corp., N. Y.
12. G. W. Wensch and D. D. Whyte, LA-1304, Mar. 1951 (classified).
13. R. D. Moeller and F. W. Schonfeld, LA-1000, Feb. 1950 (classified).
14. R. J. Teitel, BNL-88, p 12 (classified).
15. D. H. Ahman and R. R. Baldwin, CT-2961, Nov. 12, 1945 (classified).
16. R. J. Teitel, The Uranium-Lead System, Jour. Metals 4, No. 4, April 1952, pp 397-400.
17. D. A. Treick, J. H. Carter, A. L. Snow, R. R. Baldwin, and A. S. Wilson, M-3107 (classified).
18. W. Latimer, UCRL-1054, Sept., Oct., Nov. 1950 (classified).
19. H. B. Johnson, ISC-48, July 12, 1950 (classified).
20. J. Bryner, BNL-142, p 8 (classified).

Engineering Design

HEAT TRANSFER (Orrington E. Dwyer)

The following is essentially a topical discussion of the characterizing factors and the underlying principles of heat transfer as related to liquid-metal-fuel reactors and is based primarily on heat-transfer studies conducted at the Brookhaven National Laboratory in conjunction with liquid-metal-fuel-reactor (LMFR) component investigations. Information pertaining to heat transfer with liquid metals can be found in the *Liquid Metals Handbook*,¹ and liquid-metal heat transfer is discussed in Section 2 of this volume.

Whereas nuclear reactors utilizing solid fuel elements must be cooled internally by a coolant flowing through the reactor, fluid-fuel reactors may be cooled either internally or externally. In external cooling, the fuel is continuously circulated in a closed circuit consisting of the reactor core and external heat-exchange units. A liquid-metal-fuel reactor, particularly the generic design visualized by the Brookhaven reactor group, is essentially a power-breeder or power-converter reactor with the emphasis on power. Heat transfer is thus of considerable importance: first, because of the high temperature involved and, second, because of the number of heat-exchange operations.

Ideally in the case of internal cooling, the structural material separating the liquid metal fuel from the coolant (probably another liquid metal) should have: (1) a geometry that will provide a large heat-transfer area without being excessively massive; (2) a low thermal-neutron absorption cross section; (3) a reasonably high thermal conductivity, and (4) sufficient structural strength and other physical properties to prevent cracks and ruptures. At present, no such ideal material exists. Graphite is the best from most stand-points but is presumably deficient with regard to point (4). Graphite coils to contain either the fuel or the coolant appear impractical, and the two liquid-metal streams must therefore circulate through a single mass of graphite.

The apparent advantages of internal cooling are:

- (1) Lower fuel inventory is possible.
- (2) Primary heat exchangers and associated piping and pumps can be eliminated without getting radioactive steam.
- (3) A secondary coolant would be non-radioactive.
- (4) Breeding can be accomplished in the coolant stream.

The advantages of external cooling are:

- (1) A smaller reactor core is possible in the absence of both coolant and, possibly, a separator material of relatively high neutron absorptivity.
- (2) Simpler reactor construction.
- (3) Less serious thermal stress problems.

¹References appear at end of chapter.

- (4) Better heat-transfer coefficients.
- (5) Less critical leak problem. External heat exchange can be accomplished in several parallel exchangers, providing greater flexibility and reliability of operation. Thus, if a leak should develop in a particular heat exchanger, it could be isolated from the system and replaced with another.
- (6) Prompt circulation of fuel permits rapid removal of gaseous fission products.
- (7) Rapid circulation of fuel permits better control of reactivity. The fuel concentration can be changed quickly by the addition or removal of fissile material as the fuel mixture is being circulated.

While both internal and external heat removal are being considered by the Brookhaven workers for liquid-metal-fuel reactors, most effort to date has been spent on external cooling. This type of cooling system is therefore the chief subject of the remainder of this discussion.

IMPORTANT PROPERTIES OF COOLANTS

For external cooling, the fuel-bearing liquid should meet as far as possible the same rigid specifications as the primary coolant for a solid-fuel reactor, in addition to the requirement that it satisfactorily dissolve or otherwise carry the uranium fuel. The important properties of a fuel-bearing liquid metal are:

- (1) Density—affects pumping power, heat-transfer-area requirements, and shielding requirements since gamma-absorption capacity depends on density.
- (2) Thermal conductivity—affects heat-transfer-area requirement and therefore fuel inventory.
- (3) Heat capacity and viscosity—affects pumping power and heat-transfer area.
- (4) Melting point—increases start-up problem if liquid melts above room temperature. At shutdown, presumably, there would be a sufficiently high concentration of fission products to prevent freezing.
- (5) Vapor pressure—determines pressure on reactor system.
- (6) Coefficient of volumetric expansion—the greater the value of this property, the easier to promote natural circulation and reactor stability.
- (7) Electrical resistivity—affects applicability of electromagnetic pumps.

In general, the density, thermal conductivity, heat capacity, and coefficient of volumetric expansion should be high; conversely, the viscosity, melting point, vapor pressure, and electrical resistivity should be as low as possible. Obviously, vapor pressures of liquid metals are relatively very low. Degree of "wetting" of the heat-transfer surfaces by a liquid metal is also an important characteristic of this type of coolant.

The properties of the ideal secondary coolant are essentially the same as those of the primary coolant (fuel stream). The one property of no importance in the case of the primary coolant but of appreciable importance for the secondary coolant is the density change on freezing. This property has considerable bearing on equipment shut-down and start-up. Another property which has greater significance for a secondary coolant is toxicity.

The Brookhaven liquid-metal-reactor system employs a fuel mixture consisting of uranium dissolved in molten bismuth. The concentration of the uranium is around 600 ppm, which is so low that for heat-transfer and fluid-mechanical considerations, the fuel mixture can be assumed to be liquid bismuth. Most of the proposals for power production thus far considered involve the production of steam through the use of a secondary coolant. Mercury, sodium, and the eutectic mixture of potassium chloride and lithium chloride have been considered as secondary coolants in some detail. Some of their physical and thermal properties at 450°C, along with those of bismuth, are shown in Table 5.3.1. A satisfactory operating temperature range for coolants in a reactor system similar to LMFR may be 350° to 500°C.

COMPARISON OF COOLANTS ON BASIS OF PUMPING-POWER REQUIREMENTS

One valuable criterion for judging the merits of a coolant is the amount of pumping power required for a given rate of heat removal. The three main pressure drops in the coolant system—those in the piping, the reactor, and the heat exchangers may be roughly of the same order of magnitude. The pumping power required to circulate the coolant through the piping system per unit rate of heat transfer for a fixed temperature rise in the coolant is:

$$\phi_p = \frac{\text{pumping energy required}}{\text{heat removed}} \approx \frac{(\Delta p)}{C_p \rho} \quad (1)$$

The symbols used in this and subsequent equations in this chapter are defined in Table 5.3.2.

Table 5.3.1 — Physical Properties of Coolants at 450°C (842°F)

Property	Bismuth	Mercury	Sodium	KCl-LiCl eutectic
Melting point, °F	520	-38	208	664
Boiling point, °F	2691	675	1621	...
Density, lb/cu ft	613	785	52.5	103
Specific heat, Btu/(lb)(°F)	0.036	0.035	0.30	0.27*
Heat capacity, Btu/(ft) ³ (°F)	22.1	25.9	15.75	27.8*
Thermal conductivity, Btu/(hr)(ft)(°F)	8.95	14.6	39.4	0.75*
Viscosity, cp	1.28	0.92	0.245	1.6*
Prandtl number, $C_p \mu / k$	0.0125	.00525	.00451	1.39*

* Owing to the absence of specific data for this mixture at 450°C, the values listed are only estimates

Table 5.3.2 — Nomenclature

A = Heat-transfer area
 cp = Centipoises
 C_p = Specific heat
 D = Diameter
 f = Friction factor, defined by Eq. (3)
 g = Acceleration due to gravity
 G = $v\rho$ = Mass velocity
 h = Film heat-transfer coefficient
 k = Thermal conductivity

m = Hydraulic radius = $\frac{\text{Cross-sectional area}}{\text{Total wetted perimeter}}$

n = Number of tubes in parallel
 N = Length of tubes
 p = Pressure

Δp = Pressure drop

q = Heat flow rate
 t = temperature

Δt = Over-all temperature drop across tube wall and films

U = Over-all heat-transfer coefficient

v = Linear velocity

V = Volumetric rate of flow

$$X = \frac{\mu^{0.2}}{\rho^2 C_p^{2.8}}$$

$$Y = \frac{\mu^{0.2}}{\rho^2 C_p^{0.8} U} = \frac{X}{U}$$

$$Z = \frac{\mu^{0.2} \rho^{0.8}}{U}$$

Greek Symbols

μ = viscosity

ρ = density

ϕ = $\frac{\text{pumping power}}{\text{heat removal rate}}$

Subscripts

H refers to heat exchanger

n means number of tubes is held constant

p refers to piping

o refers to outside diameter

v means linear velocity is held constant

1 means initial

2 means final

Available data indicate that the fluid-mechanical behavior of liquid metals is the same as that of ordinary liquids. Therefore, combining the friction factor equation:

$$f = 0.046(\mu/Dv\rho)^{0.2} \quad (2)$$

with the Fanning equation:

$$\Delta p = \frac{2fv^2\rho N}{gD} \quad (3)$$

yields:

$$\Delta p = \frac{0.092v^{1.8}\rho^{0.8}\mu^{0.2}N}{gD^{1.2}} \quad (4)$$

Combining Eqs. (1) and (4) and assuming constant pipe sizes and lengths results in:

$$\phi_p = (\text{a constant}) \frac{v^{1.8}\mu^{0.2}}{\rho^{0.2}\phi_p} \quad (5)$$

Since v is inversely proportional to C_p , Eq. (5) becomes:

$$\phi_p = (\text{a constant}) \frac{\mu^{0.2}}{\rho^{1/2}C_p^{2.8}} \quad (6)$$

The ratio $\mu^{0.2}/\rho^{1/2}C_p^{2.8}$, called "X," for a fixed heat-removal rate, temperature rise, and tube size, is a direct measure of the pumping power required for a given heat-transfer fluid. Table 5.3.3 gives values of X for the four fluids discussed above. The units of the physical properties used in evaluating X were the same as those presented in Table 5.3.1. The pumping power required for a given rate of heat removal in the heat exchanger system is:

$$\phi_H = \frac{\text{pumping energy required}}{\text{heat removed}} \approx \frac{(\Delta P)}{C_p\rho} \quad (1a)$$

Table 5.3.3 — Values of $\mu^{0.2}/\rho^{1/2}C_p^{2.8}$ for Various Coolants at 450°C

Coolant	X
Bismuth	0.0305
Mercury	.0224
Sodium	.00793
KCl-LiCl eutectic	.0041

If the pressure drop across the heat exchanger is assumed to result mainly from friction drop in the tubes (an assumption that is not necessarily always true), ΔP can be evaluated by Eq. (4). Assuming that:

- (1) Total heat removal is fixed, as before
- (2) Number of tubes in parallel is held constant
- (3) Inside diameter of tubes is held constant
- (4) Inlet and outlet temperatures are the same for all coolants
- (5) Over-all temperature drop from the fluid being cooled to the fluid being heated is the same in all cases
- (6) Average bulk temperature of the fluid is 450°C
- (7) Combined resistance of the tube wall and the other fluid is 0.00105 (hr)(ft)²/Btu (a typical value for 1-in.-ID tubes with 1/8-in. alloy-steel wall)

and combining these assumptions with Eqs. (1a) and (4) and remembering that v varies inversely as $C_p \rho$:

$$[\phi_H]_n = (\text{a constant}) \frac{\mu^{0.2} N}{C_p^{2.8} \rho^2} \quad (7)$$

Since N varies inversely as U :

$$[\phi_H]_n = (\text{a constant}) \frac{\mu^{0.2}}{C_p^{2.8} \rho^2 U} \quad (8)$$

The ratio, $\mu^{0.2}/C_p^{2.8} \rho^2 U$, which is a direct measure of the pumping power required to pass a given coolant through a tubular heat exchanger, is called "Y." Table 5.3.4 gives values of Y for the four fluids previously mentioned based on the conditions and assumptions stated above and the listed flow rates. General values of Y similar to those of X shown in Table 5.3.3 are not conveniently derived because U cannot be expressed as a simple function of the coolant properties. The film heat-transfer coefficients were calculated from Eqs. (14), (15), and (17).

In deriving Eq. (8), the number of tubes in parallel was kept constant, and the linear velocity of the coolant through the tubes was allowed to vary depending upon the required volumetric flow rate of the coolant. A similar analysis can be made keeping the linear velocity constant and allowing the number of tubes to vary. Combining Eqs. (1a) and (4) and remembering that v and D are constant:

$$[\phi_H]_v = (\text{a constant}) \frac{\mu^{0.2} N}{C_p \rho^{0.2}} \quad (9)$$

but:

$$N = A/(\pi D n) \quad (10)$$

Table 5.3.4—Values of Y for Various Coolants

Coolant	v , ft/sec	v , lb/(sec)(ft) ²	h , Btu/(hr)(ft) ² (°F)	U , Btu/(hr)(ft) ² (°F)	$Y \times 10^5$
Bismuth	9.9	6000	2840	671	4.55
Mercury	8.4	6550	3500	711	2.67
Sodium	13.9	730	7750	826	0.965
LiCl-KCl eutectic	7.85	800	1700	560	.725

$$A = q/U(\Delta t) \quad (11)$$

and:

$$n = \frac{V}{0.785D^2v} = \frac{q}{0.785D^2v C_p(t_2 - t_1)} \quad (12)$$

Combining the above four equations:

$$[\phi_H]_v = (\text{a constant}) \frac{\mu^{0.2} \rho^{0.8}}{U} \quad (13)$$

Here again, the over-all coefficient, U , appears in the equation, and since it is not a one-term function of the physical properties of the fluid, a typical case must be chosen to evaluate the ratio $\mu^{0.2} \rho^{0.8}/U$ which is called Z . By using the same case as before, except that the linear velocity is held constant at 10 ft/sec for all coolants, which means that the number of tubes in parallel varies, the results shown in Table 5.3.5 were calculated.

From the X , Y , and Z ratios shown in Tables 5.3.3, 5.3.4, and 5.3.5, it is clear that the power requirements differ widely for the four coolants under similar operating conditions

Table 5.3.5—Values of Z for Various Coolants

Coolant	Relative No. of tubes in parallel	v , lb/(hr)(ft ²)	h , Btu/(hr)(ft ²)(°F)	Btu/(hr)(ft ²)(°F)	Z
Bismuth	n	6130	2860	715	25.0
Mercury	$0.86n$	7850	3920	767	26.6
Sodium	$1.43n$	5250	6770	836	2.15
LiCl-KCl eutectic	$0.80n$	1030	2060	652	6.9

and for the same rate of heat removal. Since a heat-transfer fluid usually flows through two heat exchangers in series, one where it receives heat and the other where it releases heat, and since the combined pressure drop through the heat exchangers is much greater than that through the conduits, the Y and Z ratios have more significance than the X ratio. Of course, Y and Z were derived on the basis that kinetic losses were small, which may not always be the case. If the kinetic losses are not small, Y and Z should be given less consideration. Pressure drops resulting from kinetic effects are essentially proportional to the density of the coolant. The above calculated results may be summarized as follows:

(1) For the same size of conduit, same length of conduit, same rate of heat removal, and same inlet and outlet temperatures, the relative power requirements of the four fluids are:

Bismuth	7.50
Mercury	5.50
Sodium	1.95
KCl-LiCl eutectic	1.00

(2) For a typical geometry, identical heat-transfer conditions, and the same rate of heat removal, the relative pumping power required to circulate the four fluids through a heat exchanger is:

	n fixed	v fixed
Bismuth	6.27	11.6
Mercury	3.68	12.4
Sodium	1.33	1.00
KCl-LiCl eutectic	1.00	3.21

Although the above analysis is much simplified, it shows clearly that pumping-power requirements can vary greatly for different heat-transfer fluids and that even though the total pumping power actually delivered to the fluid may not be great in a given situation, the electrical power consumption may be appreciable owing to low pump efficiency.

COMPARISON OF COOLANTS ON BASIS OF HEAT-TRANSFER CHARACTERISTICS

For the same duty, geometry, and temperature, the size of a heat exchanger depends on the fluids passing through it, since the area required for heat transfer is inversely proportional to the over-all heat-transfer coefficient, itself a function of the physical properties of the fluids. Table 5.2.4 gives values of U for a typical situation where the number of tubes in parallel is constant, and Table 5.2.5 shows the effect of keeping the linear velocity constant. The relative sizes (i.e., heat-transfer areas) of heat exchangers using one of the following fluids are:

Relative sizes of exchangers

	n is fixed	v is fixed
LiCl-KCl eutectic	1.00	1.00
Bismuth	0.835	0.912
Mercury	.788	.85
Sodium	.678	.78

For a fixed geometry, the holdup volume increases with the heat-transfer area of a heat exchanger, but the increase is not proportional owing to the header volumes.

In the above discussion, the same tube-wall thickness has been assumed for all coolants. Because of corrosion considerations, however, this assumption may not be valid since it is possible for the good heat-transfer characteristics of a particular coolant to be nullified by a thicker or less conductive tube wall, necessitated by the coolant's greater corrosiveness.

ARGUMENTS FOR AND AGAINST THE USE OF A SECONDARY COOLANT

Heat can be transferred directly from the liquid fuel (primary coolant) to steam, or a second coolant may be interposed between these two fluids. The main advantages of the direct-transfer scheme are:

- (1) Elimination of primary heat exchangers.
- (2) Elimination of secondary coolant.
- (3) Elimination of piping and pumps for secondary-coolant circuits.

The disadvantages are:

- (1) Probably greater opportunity for leaks in the fuel circuit because the fuel will have to flow through two or maybe three units in series, such as a superheater, reheater, and boiler.
- (2) Heavy reactor construction to withstand full steam pressures in case a leak developed in any of the steam generating equipment.

(3) Assuming that the fuel flows inside the tubes and the water and steam outside to minimize fuel inventory, thick-shelled heat exchangers and costly steam-generating equipment must be provided. If the fuel flowed outside the tubes, this disadvantage would not exist.

(4) Greater heat-transfer area and therefore greater fuel hold-up, since the steam generating equipment would have lower over-all heat-transfer coefficients than a liquid metal-to-metal heat exchanger.

(5) Difficulty in reducing temperature gradients to avoid high thermal stresses. It is often desirable to produce steam at a temperature appreciably below the average temperature of the liquid metal, and an intermediate heat exchanger is convenient to step down the temperature of the fuel stream at the high-temperature end. An intermediate coolant can provide greater flexibility of operation.

(6) Radioactive steam. This aggravates steam-plant maintenance and presents a shielding problem.

(7) Inferior heat-transfer characteristics and therefore larger steam-generating equipment than that conceivable with a secondary coolant.

HEAT-TRANSFER EQUIPMENT

Several types of heat exchangers can be used to transfer heat from the molten-metal fuel mixture in nuclear power systems depending on the nature of the heat-transfer process and the coolant. If a liquid metal is used as a secondary coolant, the heat exchanger may be of the shell-and-tube variety equipped with double-wall tubes with two or more passes on the tube side and baffled on the shell side. Since a high degree of reliability is demanded of these heat exchangers, they must be expertly designed and the thermal stresses held at safe maxima. Liquid metal-liquid metal heat exchangers are discussed in Section 2 of this volume.

HEAT TRANSFER THROUGH PHASE CHANGE

Another way of delivering heat from a molten-metal fuel to steam is to boil mercury with the heat released from the primary coolant, then to condense the mercury in and thereby supply heat to the steam-generating equipment. Good heat-transfer film coefficients for both boiling and condensation are realizable, but the vapor lines required are prohibitively large, even at vapor velocities approaching 100 ft/sec. In fact, it appears that for nuclear power purposes heat transmission using the vaporization-condensation of mercury is out of the question because of the difficult problem of transporting the vapor. Even when the steam boiler is placed directly above the mercury boiler and the cross-sectional area of the vapor duct is as large as the boilers themselves, the scheme does not look promising.

SPRAY-TYPE HEAT EXCHANGERS

If the secondary coolant is a fused salt, it is possible to transfer heat from liquid bismuth by spraying the metal in fine droplets through the salt, thereby bringing the two fluids into intimate contact. With this type of heat exchanger, the chief problem is that of achieving good phase separation at desirable flow rates. Two versions of spray-type heat exchangers are shown in Fig. 5.3.1, one employing gravity separation and the other centrifugal separation. This type of heat exchanger, particularly the gravity-separation version, has been given some consideration by the Brookhaven Reactor Group, for it has features that make it peculiarly adaptable to LMFR. The high heat-transfer coefficients of spray-type heat exchangers mean low metal holdups. In addition, this system eliminates tubes and circumvents the thermal-stress problem.

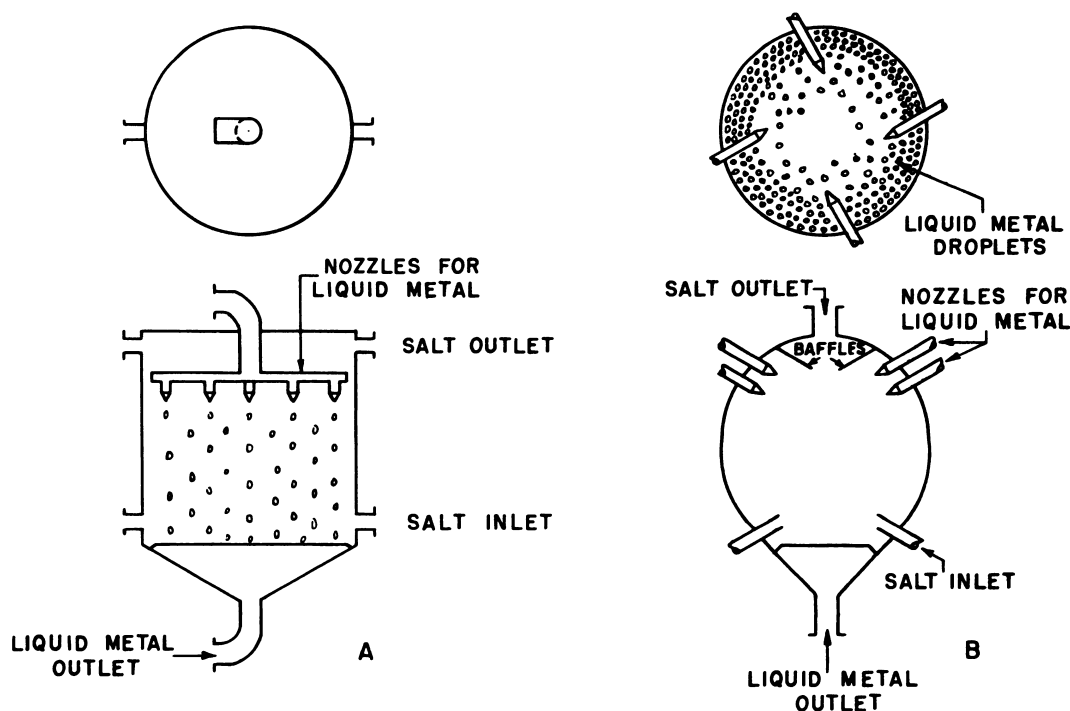


Fig. 5.3.1 — Direct-contact, Liquid-metal Salt Heat Exchangers. Submitted by BNL, Sept. 1952.

The presence of the salt along with the liquid metal probably amplifies the corrosion problem and would be a serious drawback. Another conceivable disadvantage is the possibility of carry-over of liquid metal by the salt and/or salt by the liquid metal. The latter phenomenon is more probable. Carry-over of salt by the bismuth in the case of LMFR would be almost intolerable because of reactor poisoning. However, the bismuth/salt density ratio is about six and the other pertinent properties are sufficiently favorable so that satisfactory separation of the two phases by centrifugation may be possible. Such separation could probably be incorporated in the centrifugal pumps located in the exit metal and salt lines from the heat exchanger. There is a strong possibility that the Brookhaven Reactor Group will investigate experimentally the feasibility of the spray-type heat exchanger for application to LMFR if preliminary work on the hydrodynamics of droplet formation, phase separation, and salt creep on metal surfaces looks promising.

STEAM-GENERATING EQUIPMENT

In the direct heat-transfer system (no secondary coolant), the metal-fuel mixture releases its heat directly to boiling water and steam in steam-generating units. Under these conditions, the liquid-metal fuel should flow inside the tubes to conserve fuel. When a secondary coolant, such as sodium, is employed, however, the liquid metal may be on the outside of the tubes, particularly in the superheaters. With liquid metal on the outside of the tubes, the required shell thickness is small, and the steam-generating units themselves are usually smaller because of greater heat-transfer capacity. Where the steam-generating equipment is heated with the metal-fuel mixture or with an alkali metal, the

tubes should be double-walled. Possible exceptions would be the tubes in the superheater and re-heater when such units are "fired" with an alkali metal. To minimize thermal stresses, the number of passes on the tube side should be two or some multiple thereof, unless curved tubes are employed.

If the secondary coolant is a heavy metal like lead, mercury, or bismuth, or a fused salt, the design of the steam generating equipment would be similar to that using alkali metals, except that the tubes need not be double-walled.

CALCULATION OF HEAT-TRANSFER FILM COEFFICIENTS

In this chapter, heat-transfer film coefficients were obtained from the following relationships:

(1) Fused salts, inside tubes:²

$$\frac{hD}{k} = 0.023 (DG/\mu)^{0.8} (C_p \mu/k)^{0.4} \quad (14)$$

(2) Sodium, inside tubes:³

$$\frac{hD}{k} = 7.0 + 0.025 (DGC_p/\mu)^{0.8} \quad (15)$$

(3) Sodium, in-line flow outside tube banks: Same as for case (2) where:

$$D = 4m$$

(4) Sodium, cross-flow in tube banks: Film heat-transfer coefficients were obtained by making the simple assumption that the Colburn⁴ equation, when used to determine outside film coefficients for an alkali metal flowing normal to tube banks, gave results which were as much too high as Eq. (14) above for the same metal flowing inside tubes. This has not been checked experimentally. The Colburn equation is used in the form:

$$\frac{hD_0}{h} = 0.33 \left(\frac{D_0 G_{\max}}{\mu} \right)^{0.6} \left(\frac{C_p \mu}{k} \right)^{0.333} \quad (16)$$

(5) Bismuth, inside tubes:*

$$\frac{hD}{k} = 4.9 + 0.018 (DGC_p/\mu)^{0.8} \quad (17)$$

(6) Mercury, cross-flow in tube banks: Film heat-transfer coefficients were obtained similarly to case (4) above.

(7) Mercury, in-line flow outside tube banks: By Eq. (17) above, where:

$$D = 4m$$

LMFR PLANT DESIGNS

In general, the design of a nuclear power plant must be predicated upon high degree of plant reliability, minimized costs, and severe safety requirements. The Brookhaven Reactor Group has considered the problem of heat transfer in power-plant design for

* This equation is obtained by multiplying the right-hand side of Eq. (15), the Lyon-Martinelli equation, by 0.7. In general, the experimental data which have thus far been obtained on the heavy metals indicate values of h about 30% lower than those predicted by the Lyon-Martinelli equation.

LMFR, and although no experimental work has yet been undertaken, several schemes have been studied, three of which are discussed below. One of the more difficult problems in the design of heat-transfer equipment for handling liquid metals, viz., that of minimizing thermal stresses, is accentuated in LMFR because the temperature drop across tube walls in the boiler may vary greatly from one end to the other as a result of sensible heat being converted to latent heat.

SCHEME A—MERCURY AS SECONDARY COOLANT

For a liquid-metal-fuel reactor system like LMFR, mercury has certain real advantages, chief among which is that it does not react violently with water. Also, it has a reasonably low vapor pressure and is a liquid at room temperature. Its nuclear properties are satisfactory, although considerable shielding is required. The relative pumping-power requirements for mercury are about the same as those for bismuth for a given heat-removal rate and similar heat-transfer conditions. In this regard, mercury compares quite unfavorably with an alkali metal like sodium, which may require only $\frac{1}{10}$ to $\frac{1}{5}$ the pumping power. The container problem with mercury is not serious but does exist. Like all heavy, weakly-reducing metals, mercury has a high electrical resistivity which makes it unsuitable for electromagnetic pumping. In addition, it is a fairly toxic material and is very expensive on a volume basis.

The flow diagram of a hypothetical LMFR power plant using mercury as a secondary coolant is shown in Fig. 5.3.2. The uranium-bismuth fuel mixture leaves the reactor at 950°F and is pumped through a number of heat exchangers operating in parallel (although three heat exchangers are shown, more would probably be used in a full-scale plant, i.e., one of 500 megawatts total heat rate). From the heat exchangers, the fuel mixture (at 644°F) returns to the reactor. Gaseous fission products are removed in a vacuum de-

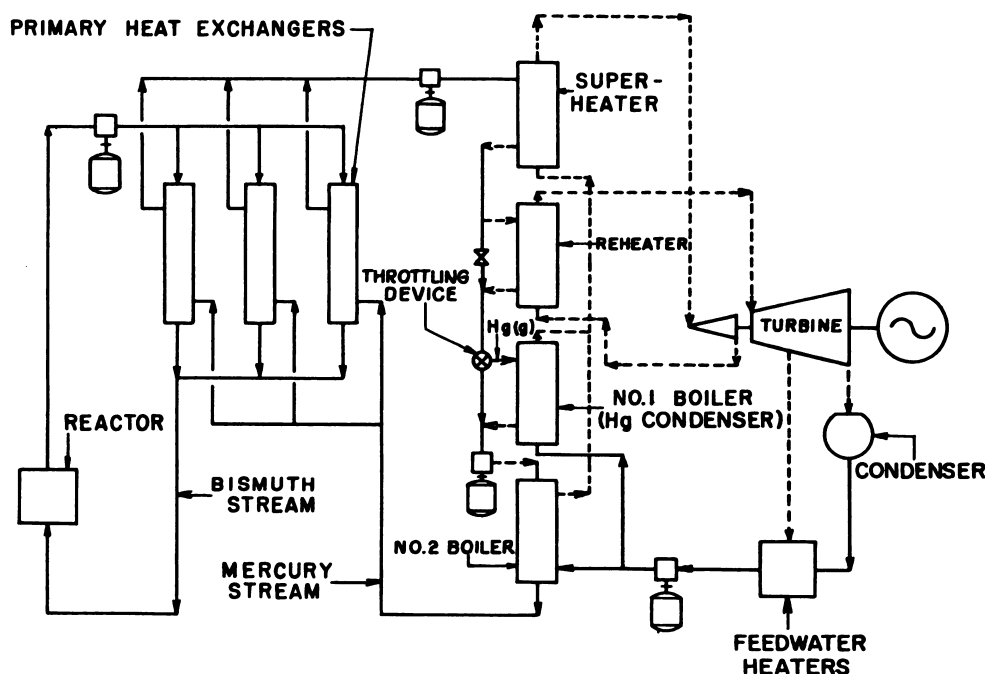


Fig. 5.3.2—LMFR Power Plant Employing Mercury as the Secondary Coolant. Submitted by BNL, Sept. 1952. Fuel processing equipment not shown.

gassing chamber, and most of the remaining fission products are removed by extraction with a KCl-LiCl salt mixture (fuel processing is discussed in Volume 4). (Equipment for these operations is not shown in Fig. 5.3.2.)

In the heat exchangers, mercury at about 80 psia is heated from 553° to 860°F. It then flows through a steam superheater in which it is cooled to 811°F; after leaving the superheater, a portion of the stream flows through a steam reheater. The two mercury streams then unite and flow through a throttling valve which reduces the pressure to about 20 psia. As a result of throttling, a portion of the mercury is vaporized at 700°F. This vapor is then condensed in Boiler No. 1, the condensate from which is united with the unvaporized mercury, and the combined stream is pumped through Boiler No. 2 where it is cooled to 560°F. The mercury is then pumped back to the primary heat exchangers to complete the cycle. In practice, the steam-generating equipment would consist of multiple units, operated in parallel.

In this scheme, tube stresses are minimized by (1) using a reheater, (2) throttling the mercury, and (3) using double-walled tubes in the boilers. The annuli between the tubes are filled with mercury.

The steam cycle in Fig. 5.3.2 calls for 600 psig steam with 390°F superheat at the turbine throttle, a reheat at 115 psia to 700°F, an exhaust to 1½ in. Hg pressure, and regenerative feed heating with the condensate entering the boilers at 400°F. The chief purpose of the steam reheater is to transfer heat from the mercury to the steam at a high temperature under conditions where the temperature drop across the tube walls does not vary much from one end of the heat exchanger to the other. If the high-temperature mercury were fed to a 600 psig steam boiler, the temperature drops across the tube walls would be prohibitively high. There is no tube-stress problem in the first boiler because of the uniform over-all temperature drop. Thus, of the five heat-transfer units in Scheme A, only the No. 2 boiler has a large variation in over-all temperature drop from 70°F at the mercury exit to 210°F at the mercury inlet. If necessary, to lower the thermal stress, the pressure in one or both of the boilers may be raised. If the high-pressure steam is above the optimum pressure for most economic operation, it could be throttled to the desired pressure before expansion in the turbines. As a satisfactory compromise between economic and engineering considerations, the Brookhaven group decided to work with 600-psig, 800°F (390° superheat) steam.

It is obviously essential to keep the fuel inventory as low as possible. The U-Bi holdup in the reactor is determined by nuclear considerations, but the holdups in the conduits and heat exchangers are determined by engineering design. The holdup in the conduits may be determined by two factors: the maximum velocity permissible from pumping and/or erosion standpoints and the possible need for incorporating thermal pumping. In the primary heat exchangers, holdup is essentially a question of manifold, header, and exchanger geometry. Theoretically, the optimum conduit size would be determined by an economic balance between fixed charges on the U-Bi holdup and piping on the one hand and pumping costs on the other, but in all probability, the velocity in the conduits would be determined by corrosion-erosion considerations. A similar situation exists for heat-exchanger design. From economic and shielding standpoints, it is also desirable to keep the mercury inventory as low as possible.

Typical shell-and-tube heat-exchanger design conditions are given in Table 5.3.6, and a typical set of design conditions for the bismuth circuit is given in Table 5.3.7.

SCHEME B—SODIUM AS SECONDARY COOLANT

Compared to mercury, sodium has one outstanding disadvantage as a secondary coolant for LMFR and that is its violent reactivity with water; another disadvantage is that it is a solid at room temperature. Its physical properties, however, are such that it has excellent heat-transfer characteristics with low pumping-power requirements; it also has

Table 5.3.6 — Design Conditions and Calculated Results of Shell-and-tube Heat Exchangers for LMFR

Secondary coolant	Mercury
Number of passes on tube side	One
Heat rate	300 Mw
Temperatures	
Bismuth, inlet	510°C, 950°F
Bismuth, outlet	340°C, 644°F
Mercury, inlet	290°C, 553°F
Mercury, outlet	460°C, 860°F
Velocities	
Bismuth, in tubes	5 ft/sec
Mercury, max. normal to tubes	2.5 ft/sec
Mercury, in-line with tubes	2.5 ft/sec
Tube data	
ID	0.500 in.
OD	0.875 in.
Spacing on triangular lattice	0.250 in.
Material of construction	Croloy 5-Si
Thermal conductivity	15 Btu/(hr)(ft)(°F)
Maximum thermal stress	4000 lb/sq in.
Pressure drop across heat exchanger on Bi side	18 lb/sq in.
Number of heat exchangers in parallel	3
Length of tubes	16 ft
Diameter of heat exchangers	5 ft
Bismuth holdup	58 tons
Mercury holdup	160 tons

Table 5.3.7 — Typical Set of Design Conditions for U-Bi Circuit in LMFR

Heat rate	300 Mw
Velocity in conduit and manifold	10 ft/sec
Diameter of conduit	2.31 ft
Effective height of convective loop	8 ft
Over-all height of total assembly	33 ft
Total length of piping, exclusive of heat exchanger manifold	52 ft
Pressure drops	
Across reactor	4 lb/sq in.
Across main conduits and heat exchanger manifolds	6 lb/sq in.
Across heat exchanger	19 lb/sq in.
Total	29 lb/sq in.
Pumping power input to bismuth	320 hp
Holdups	
Reactor	44 tons
Conduit	67 tons
Manifolds	24 tons
Heat exchanger (mercury)	58 tons
Total	193 tons

low cost. Two other advantages are that sodium can be efficiently pumped with electro-magnetic pumps and that it can be contained in 18-8 stainless steel. A disadvantage is the fairly high level of gamma radiation induced when sodium is exposed to high neutron fluxes, but in this respect it may not be much worse than mercury. Although this calls for appreciable shielding, this usually is not a determining factor. While sodium is a solid at room temperature, NaK, which has heat-transfer characteristics similar to those of sodium, melts at 12°F. Possibly, NaK would require more shielding. Although this discussion pertains to sodium it applies in principle to NaK also.

As a result of the work of the General Electric group at KAPL, firing steam-generating equipment with molten sodium is no longer considered to present serious difficulties. The problem is solved by using double-walled tubes and filling the annulus between the two walls with a third fluid, such as mercury or the lead-bismuth eutectic, at a pressure between that of the sodium and that of the water. In the event of a break in a tube wall, leakage would thus be from the water to the annulus and from the annulus to sodium and would be readily detected by sensitive instruments. Compared to the hazard in the steam boilers, that in the superheating equipment is far less serious because of the relatively small masses of water vapor contained therein. The effect on the design of the heat exchanger described in Table 5.3.6 when the secondary coolant is changed from mercury to sodium is shown in Table 5.3.8. From the standpoint of the primary exchanger, sodium is highly advantageous.

A typical power-plant layout for a liquid-metal-fuel reactor employing sodium as the secondary coolant would be identical, in most respects, with that shown for mercury in Fig. 5.3.2, the only major changes being in the steam-generating equipment. The exit sodium from the heat exchangers would flow consecutively through the superheater, reheater, and boiler units, all identical units being connected in parallel. Steam conditions and over-all total coolant temperature drop are the same as those for the mercury scheme. All steam-generating equipment would be of double-walled tube construction with an even number of passes on the tube side. The radioactivity of the sodium and its explosive chemical reactivity with water call for very careful design and arrangement of the steam generating equipment, especially the boilers.

SCHEME C—COMPROMISE DESIGN TO MINIMIZE FUEL INVENTORY

For the nuclear-power-plant design described in Fig. 5.3.2 and Table 5.3.7, it is at once apparent that the U-Bi inventory is quite large. It is further evident that nearly half of this inventory can be attributed to the hold-up in conduit and manifolds. Figure 5.3.3 illustrates a nuclear-power-plant system which nearly eliminates this type of fuel holdup

Table 5.3.8—Effects of Changing from Mercury to Sodium as Secondary Coolant on Primary Heat Exchanger* Characteristics

Characteristics	Mercury (scheme A)	Sodium (scheme B)
Heat rate, Mw	300	300
Coolant film heat-transfer coefficient, Btu/(hr)(ft) ² (°F)	3000	7700
Over-all heat-transfer coefficient, Btu/(hr)(ft) ² (°F)	430	470
Length of tubes, ft	18.6	17.0
Bismuth holdup in tubes, tons	48	44
Secondary coolant holdup, tons	160	9.75
Secondary coolant cost, \$/lb	2.75	0.17
Power necessary to pump coolant, hp	36	11

*Design of the heat exchanger is described in Table 5.3.6

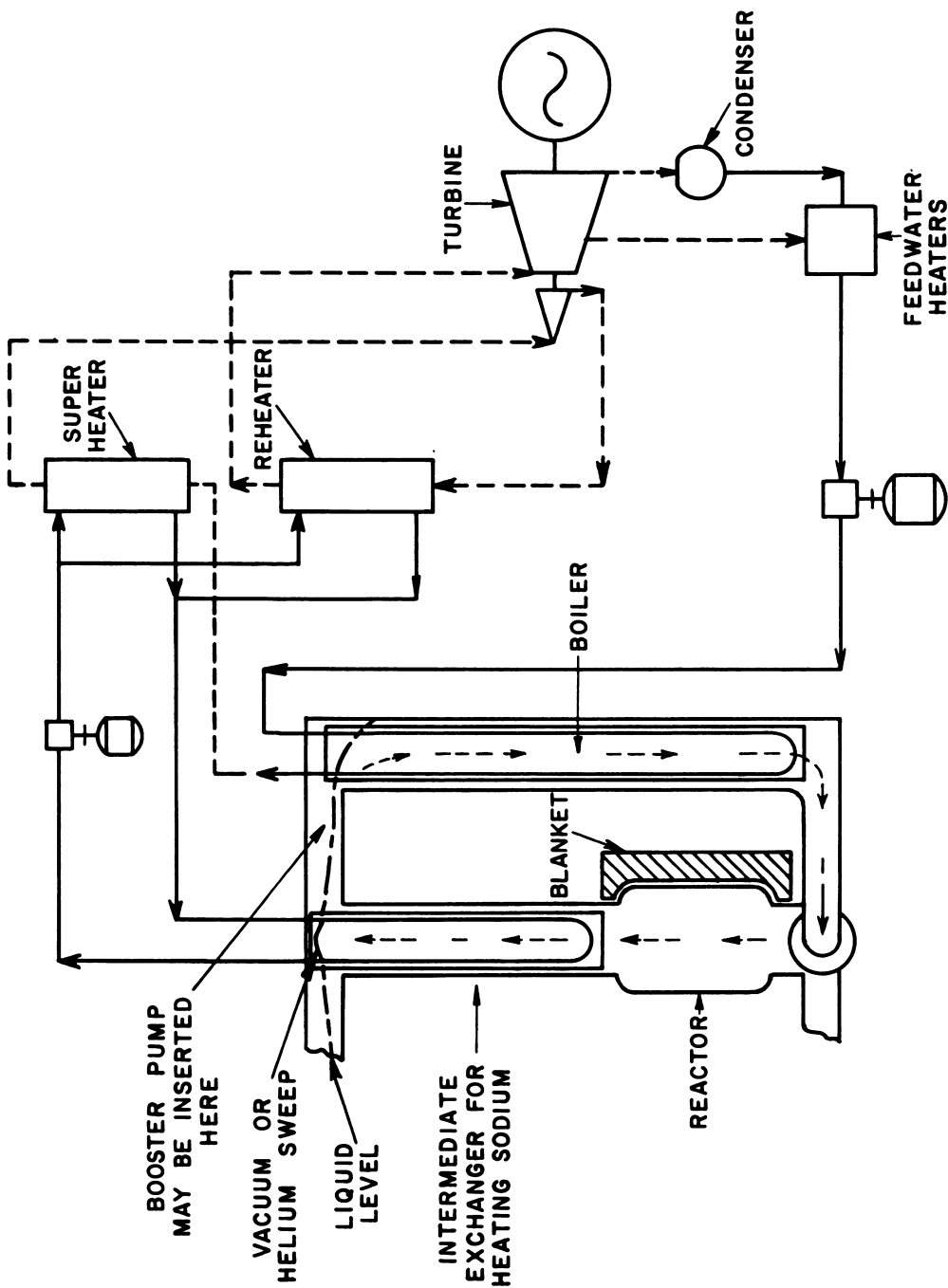


Fig. 5.3.3 — LMFR Power Plant Employing Sodium as Secondary Coolant for Steam Superheating and Reheating but with Direct Heat Transfer from Fuel to Steam Boiler. Submitted by BNL, Sept. 1952. Fuel processing equipment not shown.

and thereby achieves a very great reduction in U-Bi inventory. In this scheme, the liquid-metal-fuel mixture flows vertically through the reactor, leaving it at a temperature of 510°C to enter a tubular heat exchanger located directly above the reactor. In this exchanger, heat is transferred to liquid sodium, which then becomes the heat source for steam superheating and reheating units. Half of the fuel stream, now at about 470°C, flows through each of two side loops in which saturated steam is generated by direct heat transfer from the fuel to the steam. From the side loops, the fuel mixture (at 350°C) is returned to the bottom of the reactor core by means of centrifugal pumps. Typical values describing the design and performance of such a reactor system are given in Table 5.3.9.

Table 5.3.9—Typical Set of Design and Operating Conditions for Reactor Heat-transfer System Described Under Scheme C

Heat rate	300 Mw
Linear velocity of U-Bi fuel mixture outside tubes	10 ft/sec
Linear velocity of sodium in tubes	20 ft/sec
Tube data	
ID	0.250 in.
OD	.500 in.
Spacing on triangular lattice	.250 in.
Material of construction	"Croloy" 5-Si
Thermal conductivity	15 Btu/(hr)(ft)(°F)
Temperatures	
Bismuth, outlet reactor core	510°C, 950°F
Bismuth, inlet reactor core	340°C, 644°F
Sodium, inlet	371°C, 700°F
Sodium, outlet	448°C, 840°F
Saturated steam	252°C, 486°F
Approximate height of fuel-sodium heat exchanger	12.0 feet
Approximate diameter of fuel-sodium heat exchanger	3.0 feet
Approximate height of boilers	18.5 feet
Approximate diameter of boilers	2.2 feet
Approximate bismuth inventory	100 tons
Number of tubes in parallel	2080

The chief objective of this design is to minimize fuel inventory and plant investment at some expense of plant flexibility and reliability compared to the design shown in Fig. 5.3.2. The distinguishing features of Scheme-C design are summarized briefly as follows:

- (1) The heat exchangers are essentially suspended tube bundles, which can be lifted out of the reactor system without dumping the fuel and replaced with minimum difficulty.
- (2) The tubes in the heat exchangers are either U-shaped or multipass to minimize thermal stresses, and all welds are located in the gas space above the liquid metal.
- (3) The fuel flows outside of the tubes. By using a fuel flow inside the tubes, the inventory would be reduced still further, but this would mean more complicated construction, welded tube-sheets submerged in the fuel, and greater possibility of plugging.
- (4) Pressure drops through the heat exchangers are minimized by having the fuel flow chiefly parallel to the heat-exchanger tubes.
- (5) The heat used to superheat and reheat the steam is first transferred to sodium and then to the steam. Direct heat transfer from the fuel to dry steam would require somewhat larger heat exchangers because of the low heat-transfer coefficients on the steam side. This is not true of the boiler, where the steam-side coefficients are of the same order of magnitude as those for liquid metals. While direct heat transfer from fuel to steam eliminates an appreciable investment, it has the disadvantages discussed earlier in this chapter.

(6) The basic heat-transfer scheme illustrated in Fig. 5.3.3 is presumably suitable for either a solution-type or slurry-type fuel, i.e., for breeding only in the blanket, only in the core, or partly in each.

(7) In the figure, the pumps are shown located at the bottom of the reactor system, which means that the fuel must be dumped before they can be removed. It is also possible to locate additional pumps at the tops of the loops. This would provide added reliability and flexibility of operation. Bottom pumps are desirable, however, for filling the reactor and helping to prevent settling of particulates.

(8) Although the flow of the metal fuel mixture will realize a certain amount of thermal pumping power, this power is not sufficient to circulate the metal at the necessary rate in the event of a power failure. This means that standby power must be provided by batteries.

SCHEME D—HEAT EXCHANGE WITH IMMISCIBLE FLUIDS

All schemes for carrying out this type of heat transfer consist of first dispersing the metal in a fused salt and then separating the two phases. Dispersion can be achieved by high-velocity flow through spray nozzles in a pipe or chamber, and phase separation can be effected by either gravity or centrifugal action. Figure 5.3.4 shows a flow diagram of a nuclear-reactor power plant using KCl-LiCl eutectic as the secondary coolant and a simple spray, gravity-separation type of heat exchanger. The centrifugal pumps in the salt and metal streams leaving the exchanger can be so designed that final phase separation of both streams is accomplished by centrifugation. Aside from the primary heat exchanger, the plant layout in Fig. 5.3.4 is similar to that where sodium is the secondary coolant.

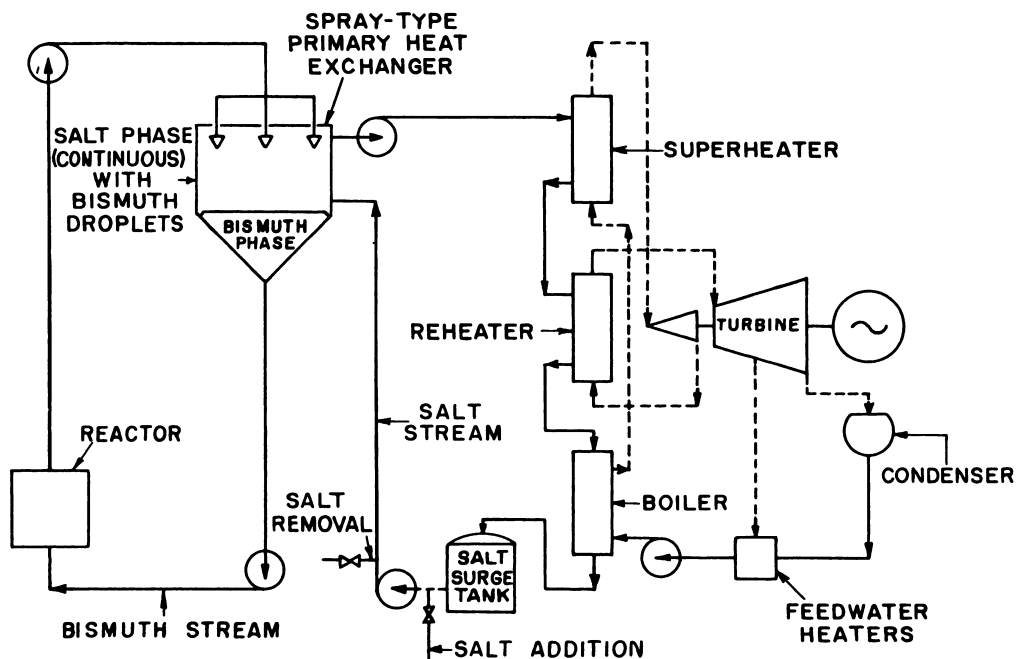


Fig. 5.3.4 — LMFR Power Plant Employing Spray-type Heat Exchanger with Salt. Submitted by BNL, Sept. 1952. Removal of fission-product gases not shown.

The outstanding advantages of the liquid metal-salt type of intimate-contact heat exchanger as applied to LMFR are:

- (1) Considerably reduced fuel inventory because of high heat-transfer coefficients. The metal-to-salt heat-transfer coefficients may be as high as five times those for conventional shell-and-tube heat exchangers.
- (2) Removal by the salt of most of the fission products from U-Bi fuel mixture. There is no need to remove a side-stream of metal for fuel-processing purposes.
- (3) Less opportunity for leaks in fuel circuit because there are no heat-exchanger tubes or troublesome tube-sheet welds.
- (4) Higher steam pressure and thermal efficiencies because the temperature of the heated salt can conceivably be very close to the highest fuel temperature.
- (5) The possibility of maintaining the fission-product concentration in the U-Bi mixture so low that shut-down temperature rise will not require any auxiliary cooling equipment.
- (6) No thermal stress problem, since tubes are eliminated.

The disadvantages are:

- (1) High level of radioactivity in secondary coolant system because of a large holdup of fission products in the salt stream. This means appreciable shielding requirements.
- (2) Carryover of salt with the metal and metal with the salt. It is presumed that final phase separation can be achieved by centrifugal action or other means. If this should not turn out to be the case, this type of heat exchanger would be eliminated from consideration.
- (3) Possibility of salt "creep" on metal surfaces. This problem may be more apparent than real and solved without undue difficulty.
- (4) A definite corrosion problem. In addition to corrosion by the individual liquids, the metal-salt mixture may possibly be even more corrosive.

A few other factors are pertinent but not determining. There is a slight possibility that the presence of delayed neutrons in the salt in the steam-generating equipment would induce some radioactivity in the steam. Such radioactivity is expected to be very minor, however, because of the long holdup time of the neutron-emitting fission products from the time they are produced in the reactor to the time they appear in the steam boiler.

Because it must be very pure, the salt is expensive, somewhere between \$1.00 and \$1.50/lb. The salt would remove a certain amount of uranium from the metal-fuel mixture, but the total amount of uranium so removed would be the same as for side-stream processing when the total salt used would equal the salt holdup in the salt-spray system. This assumes that the concentration of fission products in the salt is the same in both cases. In the salt heat-exchange system, the concentration of fission products in the salt might be lower because of the much greater quantity of salt involved.

SPECIAL EQUIPMENT FOR LIQUID METAL FUELS

(Chad J. Raseman)

PUMPS

A list of references⁵ pertaining to pumps for liquids has been compiled by the Atomic Energy Commission. This compilation has been organized by headings which indicate anticipated applications, namely, "Hot" Solution Pumps, Liquid Metal Pumps, Slurry Pumps, Water Pumps, and Miscellaneous. The majority of the references pertain to work conducted at AEC laboratories. In the case of liquid-metal pumps, which can be classified as mechanical or electromagnetic, a good deal of development work has been done by the Fairchild Engine and Airplane Corporation-NEPA Division, the Allis-Chalmers Company, and the Babcock and Wilcox Company.

MECHANICAL PUMPS

Most pump development work has been aimed at pumping sodium or sodium-potassium alloys. The most serious problem relative to the design of a mechanical, liquid-metal pump appears to be that of suitable bearings and seals.

Bismuth was pumped by NEPA in 1950.⁶ The system was operated for 37 hr; the maximum flow rate measured was 2 gpm; the maximum head developed was 66 psi; and the maximum bismuth temperature reached was 1765°F. The pump was a modified Browne and Sharpe No. 206, machine-tool-coolant pump.

In another experiment,⁷ NEPA circulated bismuth with a 50-gpm centrifugal pump for 100 hr at a mean temperature of 1500°F with a temperature differential of 500°F. An accumulation in the sump of a residue high in oxide content and dissolved elements reduced the flow and forced suspension of operation. This residue probably resulted from an impure inert atmosphere above the liquid metal. The containing material selected was type-347 stainless steel which had shown some promise in bismuth solubility tests at temperatures up to 1800°F.

The California Research Corporation made a survey of the various types of pumps that might be used for liquid bismuth and came to the conclusion that a centrifugal pump would best fit the need. A test unit was built that operated for 1037 hr, and a report⁸ stated that the centrifugal pump proved to be a very satisfactory means for circulating bismuth in an isothermal system at 700°–750°F. The pump, designed and built by the Byron Jackson Company, is shown in Fig. 5.3.5. The pump and driver are on a common shaft, the shaft being top-suspended with all bearings in the motor chamber. Space was provided for a labyrinth to separate the pump chamber from the motor chamber, although no seal was used during operation. Table 5.3.10 lists the design conditions. Typical characteristic curves for the pump are shown in Fig. 5.3.6. The head-capacity curve had a shut-off head slightly lower than the maximum head in the performance test conducted by Byron Jackson with water as the fluid.

CANNED-ROTOR PUMPS

The Allis-Chalmers Manufacturing Company believes it has a canned-rotor-pump design suitable for pumping bismuth or molten salt at temperatures as high as 1000°F. Allis-Chalmers has built a leakless, canned-rotor pump that is rated at 3800 gpm against a 165-ft head of sodium. The canned-rotor pump has also been discussed in the Homogeneous Reactor Project Quarterly Progress Reports. In the long-range homogeneous reactor program, emphasis is shifting from 4000-gpm circulating pumps to those of larger capacity (20,000 gpm).

ELECTROMAGNETIC PUMPS

In the early days of the project, a magnetic pump for bismuth was described by B. Feld and L. Szilard.⁹ Design calculations were also made for a cylindrical electromagnetic pump (6-coil, 3-phase, 12.5 cycles/sec) with a bismuth flow of 3200 gpm and efficiency of 22 percent.¹⁰ These calculations were only preliminary and not to be taken as a practical working design. They merely indicate the methods used for, and the variables introduced into, the design of an actual pump.

The poor electrical characteristics of bismuth compared to those of sodium or NaK have generally ruled out the use of large electromagnetic pumps for this material. The uncertainty of "wetting" between bismuth and container walls also made the choice of large electromagnetic pumps questionable.

The Fuel Processing Group of Brookhaven National Laboratory required a pilot-plant pump that would circulate uranium-bismuth fuel with absolutely no leaks. The U-Bi fuel

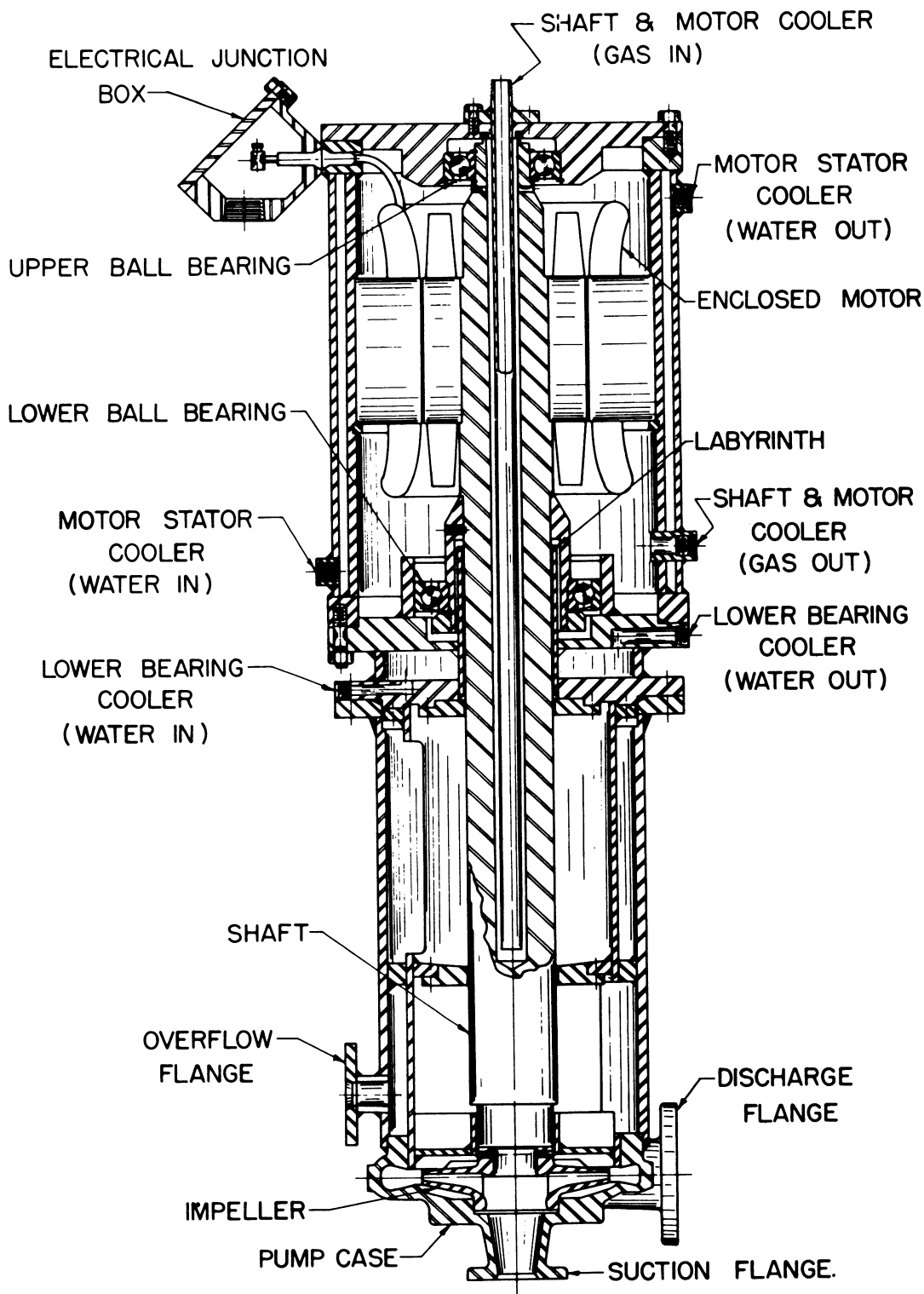


Fig. 5.3.5 — Molten-metal Pump; Canned-motor, Direct-drive, Centrifugal, 2-in. Pipe Size. Design by Byron Jackson Co. Submitted by BNL, Sept. 1952.

Table 5.3.10— Pump Design Conditions

(J. E. Walkey, Design, Construction, and Operation of Molten Bismuth Test Pump, Calif. Res. Corp., SPL-51 : 28, Oct. 9, 1951)

Liquid temperature	800°F
Liquid specific gravity	10
Liquid viscosity	1.7 cp
Flow rate	50 gpm
Suction pressure	15 psia
Differential	100 psi
Differential head	22 ft of liquid
Discharge pressure	115 psia

was eventually to be circulated through an experimental hole in the Brookhaven reactor where fission products and polonium would be generated. Since a small flow rate of approximately 1 gpm was desired and efficiency was of little regard, it was decided to try an electromagnetic pump.

An experimental loop¹¹ was set up to circulate "cold" U-Bi by means of a General Electric Model G-4 AC electromagnetic pump. This loop ran continuously for 2400 hr. During the first 160 hr, the rig was operated isothermally at a temperature of 340°C; during the remainder of the time, the loop was run isothermally at 450°C. The U-Bi solution was circulated for most of this period at a rate of 1 gpm by means of the electromagnetic pump. There were no signs of plugging or flow restriction.

VALVES

The standard-stem, packed, gate valves used in early NEPA bismuth tests⁶ proved that special valves would be required for successful liquid-bismuth operation. High leakage rates through the packing caused maintenance difficulties throughout the tests.

A 1½-in., Fulton-Sylphon, bellows-type, stainless-steel valve was cycled 1000 times at the rate of 77 times/min against bismuth at a temperature of 1000°F and a pressure of 25 psig. No failure of the bellows or other valve parts occurred.

NEPA also checked valves for metal-to-metal self-welding effects.¹² Tests of valve operation reached 1500°F with liquid bismuth on standard Stellite-faced poppets and seats without indication of self-welding effects.

The use of bellows-sealed valve stems is probably the solution to most liquid-metal valve applications. Two or more bellows in series is one method of guarding against bellows failures, and special pickup devices are used to indicate a leak in either bellows.¹³ Bellows tests at Argonne National Laboratory¹⁴ have shown the following facts:

(1) In nearly all cases, failures occurred at a weld; therefore, bellows with the least number of welds are favored. However, mechanically formed bellows should be examined for cracks and other flaws that may be introduced in the forming.

(2) There was no evidence that corrosion played a part in the failure of any bellows.

(3) The predominant factor determining bellows life is the relative amount of travel.

(4) Other factors affecting bellows life are temperature and the relative distribution between compression and extension. It was found that the outer bellows failed before the inner bellows which operated at a higher temperature.

(5) Some bellows designs had not failed up to 10⁶ cycles, at which point the test was stopped.

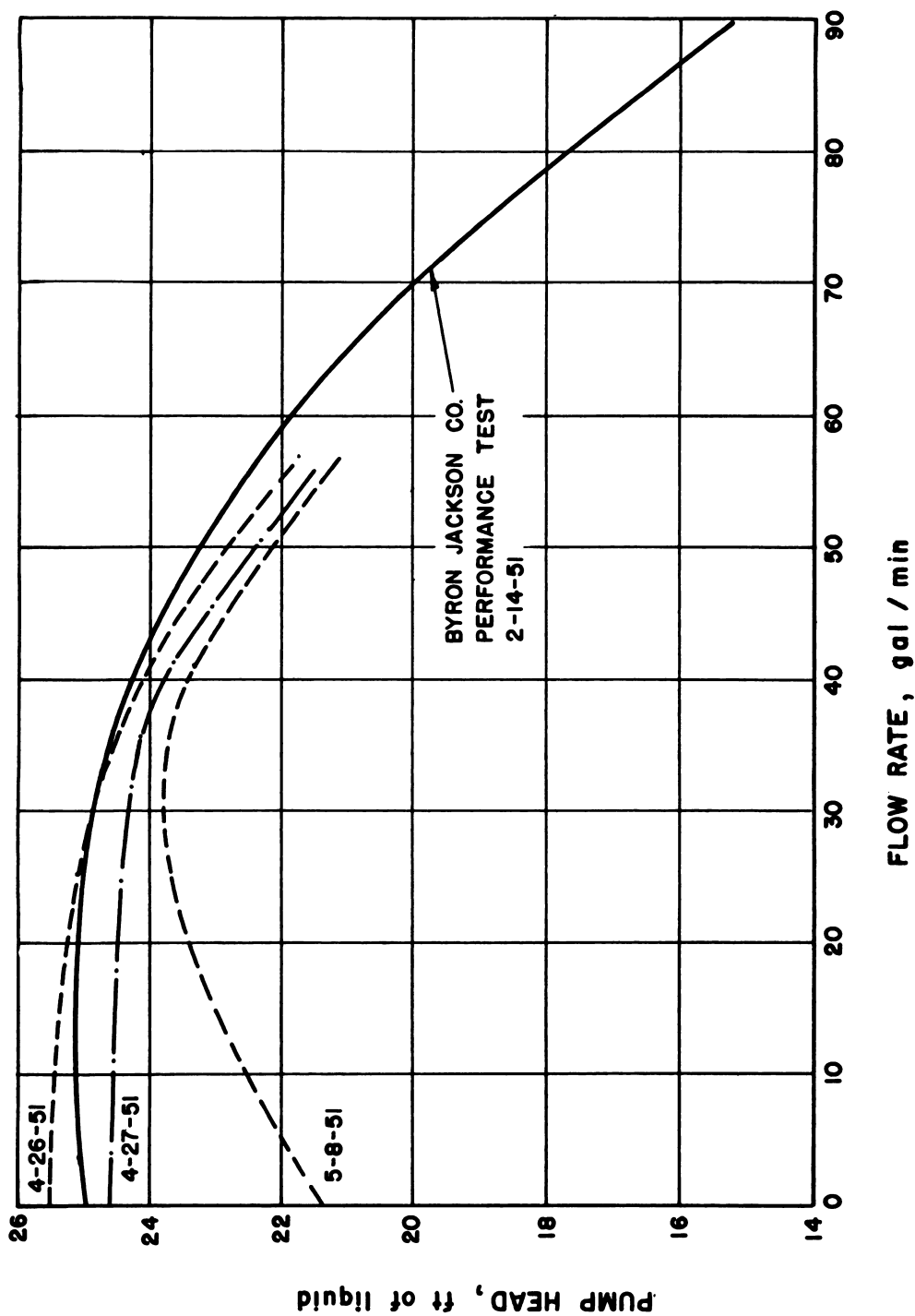


Fig. 5.3.6 — Head vs Capacity Curves for Molten-metal Pump. Reprinted from SPL-51:28, Oct. 9, 1951.

Oak Ridge National Laboratory has reported on the use of special high-temperature packing¹⁵ for valve stems. This packing consists of successive layers of Inconel braid, graphite, nickel powder, and another layer of Inconel braid.

It has been shown at practically all AEC activities that two sections of a circulation system can be isolated from each other by freezing a short section of connecting pipe. This plug can be remelted and flow resumed after a short wait. If mass-transfer corrosion or other solubility limits are approached, the use of freeze plugs should be carefully examined.

PIPING

Complete procedure specifications have been prepared by Brookhaven National Laboratory for special heliarc welding of A.I.S.I., type-347, stainless steel pipe, fittings, and vessels for use with liquid metals and liquid salts. This procedure was developed through cooperation with the Metallurgy Division of ORNL.

Liquid-metal and liquid-salt systems should be of all-welded construction. Experimental and operating procedures, however, often make it advantageous to have removable joints. An oval cross-section ring for a flanged joint was used by NEPA¹⁶ in a bismuth system between 520° and 660°F and at 300 psig. There were no leaks, and the flange was easily disassembled.

Flanged joints were also used successfully by the California Research Corporation⁸ on 1½-in. piping containing bismuth at 700°–750°F.

The ability of liquid metals and liquid salts to leak through extremely small openings has made the use of helium, mass-spectrometer, leak testers or halogen-type leak detectors practically a specified test step.

North American Aviation¹⁷ successfully circulated molten bismuth in an all-graphite thermal loop for two weeks with the hot leg at 1500°C and the cold leg at 1000°C. No serious attack on the graphite was noted. Graphite sections were joined with MoSi₂ cement. A larger dynamic all-graphite system is under construction.

HEATING EQUIPMENT AND INSULATION

Keeping the entire piping system above the melting point of its contents is another requirement and is most easily done by winding the pipes and vessels with resistance heating wire designed for this purpose. For ease in handling, the insulation of this resistance wire is armored with a woven wire sheath. Where high-intensity heat is required, special strip or tubular type heaters can be used. Induction heating has been used with good results on bismuth.⁷

Samples of twenty-six Johns-Manville insulating materials were tested for possible reaction with molten bismuth.¹⁸ In general, the results indicated that little or no reaction, particularly of an explosive nature, occurred when molten bismuth at 1832°F came into contact with the unheated materials but that none of the materials would withstand contact with the bismuth when both were at 1832°F for more than a few hours. Greatest resistance to bismuth attack was shown by three types of asbestos millboards.

CLEANING OF EQUIPMENT

Owing to the corrosive nature of most liquid metals, the type of container employed and the condition of the container-liquid interface is of great importance. The presence of oxygen in a liquid-metal system, either in a dissolved form or as the oxide, can accelerate the attack upon the container material to varying degrees. Other impurities, soluble and insoluble, can have similar effects in catalyzing the reaction between molten metal and adjacent container walls. As a result, it is desirable to remove all foreign material from a liquid-metal system before charging.

The Committee of Stainless Steel Producers of the A.I.S.I. reported¹⁹ several recommended procedures for cleaning stainless steels. They place impurities and methods of removing them into five categories. The more important groups include:

(1) Ordinary dirt, grease, soot and product residue from stainless equipment that operates at low temperatures. Agents—ordinary soap and water (with or without detergent) applied with sponge, fiber brush, or cloth. To hasten action, add either soda ash, baking soda, sodium perborate, TSP, or any of several non-abrasive commercial cleansing agents. For non-water-soluble substances, try CCl_4 , acetone, gasoline, ether, alcohol, and the like.

(2) Splatter or condensed vapor that has “baked” onto equipment. Agents—sometimes, above methods may be used. Also suggested is a polish made with water and NH_3 as liquid, and either Bon Ami, MgO , finely powdered pumice or French chalk as solid. For more resistant deposits, use either stainless-steel scouring sponge or stainless-steel wool of the finest texture available. Do not use common-steel wool, scouring pads, scrapers; wire brushes, files or other steel tools. They may mar the surface or leave small particles of iron embedded in the stainless steel. Rusting of these particles will cause stains. Marred surfaces collect dirt more rapidly, become progressively more difficult to clean, and open the way to corrosive attack.

(3) Grease, oil and foreign matter in drains, vats and piping, where it is difficult to scrub by hand. Agents—use of a strong cleaning solution, followed by thorough rinsing, is suggested. With water-soluble materials, 4- to 6-percent solutions of Na metasilicate, TSP, Na metaphosphate or Na pyrophosphate produce excellent results. For non-water-soluble materials, try CCl_4 , naphtha, trichlorethylene, acetone, kerosene, gasoline, ether, alcohol, or benzene. For truly stubborn deposits of organic or carbonaceous deposits, use 10- to 20-percent HNO_3 . After using any strong solution, flush thoroughly with plenty of water.

The Oak Ridge technique²⁰ for decontaminating stainless steel or removing stains, is in general, somewhat more severe since it is more essential to remove radioactive material than to be concerned about subsequent extensive corrosion. Their methods are:

- (1) Free high-pressure steam and water wash.
- (2) Oxalic acid—5-percent and 2-percent solutions at 100°C .
- (3) Citric acid—3-percent and 1-percent solutions at 100°C .
- (4) Ammonium bifluoride—1 to 2 percent at 60°C for $\frac{1}{2}$ hr.
- (5) Ammonium fluorosilicate—4-percent or 5-percent HNO_3 at 100°C for 1 hr.
- (6) NaOH —30-percent or 10-percent citric acid at 100°C .

The use of 0.5- to 1-percent HCl for less than 15 min as light pickling bath and hydrogen passed through very hot evacuated pipes as a reducing agent have also been suggested.

In application, some of the above methods are too harsh or difficult to apply. The Oak Ridge procedures and others²¹ would probably etch most stainless steels. This could conceivably result in preferential corrosion attack by the molten metal. The same may be said for the HCl wash. If it is necessary to remove the passivating coat of oxide that is frequently associated with stainless steels, it may be necessary to employ the hydrogen reduction technique at elevated temperatures. The dilution of hydrogen with helium or argon would probably be a desirable safety feature.

The BNL procedure has been:

- (1) Thorough trichlorethylene washing to remove non-water-soluble material.
- (2) Detergent wash to remove all other soluble material. These washes are physically removed, rather than evaporated away.
- (3) Water rinse.
- (4) Acetone rinse.
- (5) If possible, rinse system with liquid metal or salt to be used.

HANDLING

Liquid-metal systems should be designed so that they can be completely drained and vented. This makes precleaning, loading, and unloading operations easier to perform.

Bismuth should be added by means of a charging tank and inert-gas pressure. A sintered, stainless-steel filter in the charging tank discharge line will remove insoluble impurities.

If possible, gravity-dumping designs should be used as pressure-dumping has on several occasions caused excessive loss of liquid metals through leaks that were the cause of the shutdown.

After the system has been drained and, if necessary, decontaminated, inert gas is maintained at a slight pressure in the system. Repairs may then be made with a minimum of harm to the interior of the rig.

SAMPLING EQUIPMENT

Nonradioactive sampling has been accomplished by use of evacuated, glass tubes that have a fragile tip at one end. The samples are taken by immersing the sealed tube in the molten metal or salt and then breaking the glass tip against the side or bottom of the vessel. Because most metals and salts attack glass to varying degrees at high temperatures, use of this technique is limited.

A molten-fuel sampler¹⁵ which has been used successfully during the filling of a convection loop consists of a heavy-walled, 100-cc, graphite crucible held between two metal flanges with the required transfer and gas-pressuring line attached. A spark-plug-type level device is used to indicate when the required quantity of sample has been taken.

Another sampler has been designed by the same group that will permit repeated sampling of an operating system. In this design, molten fuel drips continuously through the sampler and a vial is shifted to catch the drops when desired.

A sampler for radioactive liquid metals has been designed at KAPL.²² This device will have sufficient shielding to allow 1-gm samples to be taken at an activity level of 50 mc/gm.

INSTRUMENTATION

Successful operation of high-temperature systems circulating molten metals or salts depends to a large extent on new instruments developed for the unique operating conditions encountered.

Pressure can be measured by conventional pressure gauges in conjunction with seal pots that transmit the pressure from the liquid to trapped inert gas. Each seal pot can be equipped with one or more liquid-level indicators. Differential pressure can be indicated by the null-balance-type of pressure gauge connected to the molten liquid by means of a seal pot.

Another pressure instrument uses a sealed-pressure transmitter which maintains a pressure balance across a diaphragm, and the balancing pressure is measured.

An electromagnetic pressure gauge has been designed by L. B. Vandenburg at the Knolls Atomic Power Laboratory.²³ A small DC electromagnetic pump produces high-pressure liquid metals to oppose the pressures to be measured. Pump pressures greater than the opposing pressure cause liquid metal evacuation of a vacuum-tight inlet tube which also serves as a pump armature circuit inlet lead. The additional electrical resistance in the armature circuit caused by the evacuating tube restricts the armature current. The armature current is proportional to, and controls, the pump pressure output. An equilibrium condition results where the pump pressure automatically balances the pressure to be measured, and the armature current indicates the pressure to which it is proportional.

FLOWMETERS FOR LIQUID METALS

Three general techniques are employed for the measurement of liquid-metal flow rates. These include:

- (1) Conventional orifice-plate meters.
- (2) Rotameters with electrical transmitter and remote dial indicator.
- (3) Electromagnetic flowmeters.

The pressure taps associated with the orifice plate are not readily adaptable to a pressure-sensitive indicator. Because of the danger of contacting the instrument with molten metal, some intermediate container is required as a holdup and catch tank. Seal pots, in which the levels are kept more or less constant by bleeding inert gas into or out of the pot, can be used for this purpose. The gas pressure required to maintain these levels can be conveniently read on a conventional pressure gauge.

A type of rotameter has been employed by KAPL and NEPA, presumably for liquid sodium and bismuth, respectively. The device, designed by Fischer and Porter Co., permits the impulse to be electrically transmitted to a remote dial indicator.

An electromagnetic flowmeter has been designed and analyzed theoretically by General Electric Company Laboratory and by Babcock and Wilcox on a NEPA contract. A permanent magnet is mounted around the pipe through which molten metal is flowing, with the faces of the magnet creating a field perpendicular to the pipe. Two leads are welded to the pipe wall, mutually perpendicular to both the pipe and magnetic flux. The electromotive force generated by the molten metal when cutting the lines of flux is picked up by the leads and can be transmitted to any potential-sensitive instrument. The theoretical analysis of this type of flowmeter agrees within 6 percent of experimental results.

LIQUID-LEVEL INDICATORS

Determination of liquid levels in a closed, metallic system, such as that generally encountered in liquid-metal work, can be approached either as a single-level problem or as a continuously indicating level problem. The requirements for the former are:

- (1) A metallic probe, preferably of the same material as the metallic container.
- (2) High-temperature insulation between the probe and the vessel whose liquid level is to be found.
- (3) A gas-tight seal between insulation and both adjacent metallic parts.
- (4) An appropriate external circuit to note the attainment of the particular level.

Experience at Brookhaven has shown that the most successful manner for providing both good insulation and a satisfactory high-temperature seal is the use of automotive spark plugs, specifically, the Firestone "Chromalox" type. It is suggested that the seal be removed from direct contact with the heat source by means of an appropriate pipe extension. A stainless-steel probe can be welded to the spark plug after removal of the bent side electrode. The external circuit consists of a transformer, relay, and indicating lights. By the use of two probes and interlocked relays, it is possible to indicate a level beneath the lower probe, between probes, or above the upper probe.

The continuous level indicators are of three general types:

- (1) A manually adjustable probe with appropriate gasket seal.
- (2) A type depending upon the change of electrical resistance of a probe as more of it is short-circuited from the electrical path by the rising molten metal.
- (3) An electromagnetic type, which is in essence a transformer whose secondary current changes as the liquid level rises.

At Brookhaven, these techniques are currently being tested. At the present time, the electromagnetic type looks most promising, since it affords an opportunity for recording the output (millivolts) continuously.

RADIATION MEASUREMENT

A neutron detector that operates at high temperatures has been built by the General Electric Company.²⁴ Hanford tests of the neutron chamber were successful.²⁵

Other tests²⁶ on ion chambers have established that they will withstand temperatures of 700°C without damage and will operate satisfactorily in the range of 350° to 400°C depending on the current drawn.

Bremsstrahlung activity associated with a molten-lithium experiment has been measured by ionization chambers.²⁷ The chambers operated adjacent to lines that were conducting the molten lithium at a temperature of 1000°F.

OPERATIONAL PROBLEMS

The findings of an evaluation survey of operational problems associated with the use of bismuth and lithium as reactor coolants have been presented in a NEPA report.²⁸ This report lists references which pertain to items such as the polonium hazards resulting from neutron irradiation of bismuth. Polonium, a short half-life alpha emitter, is one of the most poisonous substances known and, therefore, constitutes a grave handling problem when present in the slightest quantity.

REFERENCES

1. Liquid Metals Handbook; published jointly by the Atomic Energy Commission and the Department of the Navy, June 1952.
2. W. H. McAdams, Heat Transmission, 2nd edition, McGraw Hill, New York, 1942.
3. Liquid Metals Handbook, R. N. Lyon, editor-in-chief, published jointly by U. S. Atomic Energy Commission and the Department of the Navy, June 1950.
4. A. P. Colburn, Trans. Amer. Inst. Chem. Eng. 29, 1933, pp 174-210.
5. R. L. Morgan, AEC Tech. Inf. Service, TID-3015 (Rev.), Jan. 11, 1952, 10 pp (classified).
6. R. S. Wingard, Jr., Fairchild Engine and Airplane Corp., NEPA Division, NEPA-1621, Oct. 5, 1950, 58 pp (classified).
7. J. F. Collins, Fairchild Engine and Airplane Corp., NEPA Division, NEPA-1675, Dec. 15, 1950 (classified).
8. J. E. Walkey, Calif. Res. Corp., SPL-51:28, Oct. 9, 1951, 41 pp (classified).
9. B. Feld and L. Szilard, Argonne Nat. Lab., CE-279, July 14, 1942, 7 pp.
10. B. T. Feld, Argonne Nat. Lab., CP-326, Oct. 17, 1942 (classified).
11. C. Williams, BNL-176, Jan. 1-Mar. 31, 1952, 37 pp (classified).
12. NEPA-1587, Sept. 1950, 153 pp (classified).
13. A. H. Barnes, Argonne Nat. Lab., ANL-4138, Dec. 1947-Feb. 1948, p 14 (classified).
14. Argonne National Laboratory Report, ANL-4481, Mar. 1-May 31, 1950 (classified).
15. ORNL-1227, May 7, 1952, 200 pp (classified).
16. NEPA-1482, June 2, 1950, 30 pp (classified).
17. D. W. Lillie, Div. of Res., AEC, Wash-89, April 16, 1952, 7 pp (classified).
18. The Effect of Molten Bismuth on Insulating Materials, Fairchild Engine and Airplane Corp., NEPA Division, NEPA-1306-SCR-56, Feb. 9, 1950, 16 pp.
19. American Machinist, Nov. 12, 1951.
20. D. G. Reid, Oak Ridge Nat. Lab., ORNL-490, Dec. 27, 1949, 20 pp (classified).
21. ORNL-1033, Oct. 23, 1951, 82 pp (classified).
22. KAPL-640, Dec. 1951 (classified).
23. KAPL-824, Nov. 25, 1952, 74 pp (classified).
24. D. H. Morley, High-temperature Ionization Chamber Mark I, General Electric Co., General Engineering Consulting Lab., R-50GL126, May 15, 1950, 11 pp.
25. I. M. Jacobs, General Electric Co., Nucleonics Division, HW-23694, Mar. 4, 1952, 10 pp (classified).
26. General Electric Co., Knolls Atomic Power Lab., KAPL-577, June 1951, 147 pp (classified).
27. Oak Ridge Nat. Lab., ORNL-1128, July 31, 1951, 77 pp (classified).
28. Varge Cornett, Fairchild Engine and Airplane Corp., NEPA-1232, Dec. 7, 1949, 33 pp (classified).

Section 6

FUSED-SALT SYSTEMS

Prepared by
W. R. GRIMES
D. R. CUNEO
F. F. BLANKENSHIP
MATERIALS CHEMISTRY DIVISION
OAK RIDGE NATIONAL LABORATORY

AUTHOR'S PREFACE

While the use of fused salts in industrial applications is not uncommon, most of the familiar salt systems are of little interest from the standpoint of nuclear reactor applications. Considerable attention has, however, been given to molten chlorides, fluorides, and hydroxides as possible reactor fluids and for use in certain chemical processing applications at temperatures in the vicinity of 800°C. The results indicate a promising future for fused salts.

This section reviews and tabulates the best measurements on fused salts as compiled from the project literature available at the beginning of 1953. Particular emphasis has been placed on salt mixtures under consideration as solvents or carriers of fissionable materials, as moderating fluids, and as high-temperature heat-transfer fluids.

Many of the investigations pertaining to the behavior of fused salts have been of an exploratory nature; much of the available information provides only preliminary indications. As in any new field, this has made the task of sorting and evaluating data for inclusion in a handbook very difficult. Various qualitative conclusions and tentative deductions can be drawn from much of the early work, but because of the complexity of the phenomena, the results cannot be reduced to quantitative values of any significance.

W. R. Grimes

General Reactor Characteristics

As far as it is known, no reactor which utilizes molten salts has yet been placed in operation. During the past few years, however, the favorable properties of liquids as reactor materials have been widely recognized and amply demonstrated. Fused salts have been proposed as fuels and as moderators in thermal power producers and as fuels for fast converters. In addition, fused salts may be used as dissolvants for heterogeneous reactor fuel elements, such as zirconium, titanium, and stainless steel, which are only difficultly soluble in aqueous systems.

The state of the art has progressed to a point where it is obvious that use of fused salts is not a panacea for reactor problems. The use of fused salts as fuels, for example, disposes of problems of fuel-element fabrication and stability, promises to simplify recovery problems, and simplifies the difficulties in reactor control; however, their use as fuels poses a different, and difficult, set of problems in compatibility of materials and in the virtually unknown technology of high-temperature liquids.

Firm statements are risky regarding the feasibility of general application of fused salts, since much information on their fundamental properties and, especially, on details of their technology is fragmentary or completely lacking. Nevertheless, at the present stage of development, no unsurmountable obstacles have been encountered, and the available information encourages continued and extended study in this field.

GENERAL CONSIDERATIONS

In common with other liquid systems, fused salts offer, at least in principle, several advantages as reactor fuels. As spent fuel, they can be easily removed and processed; difficult problems of fuel-element fabrication are avoided; to the extent that fission products are removed automatically or through side-stream processing, they afford improved neutron economy; because they can be circulated to heat exchangers, they simplify the problem of heat removal and effect additional neutron economy by decreasing parasitic capture by structural metals in the core; in addition, the high thermal-expansion coefficient of the liquids furnishes a negative component to the temperature coefficient of reactivity and thus simplifies the control problem.

Fused-salt systems may also claim a few advantages not shared by other liquid systems known at this time. They are capable of operating with low vapor pressures at very high temperatures. By proper choice of component salts, the concentration of fissionable and fertile material may be varied over wide limits, and for reactors of moderate size, the fuel may be made self-moderating. Their radiation stability, on the basis of incomplete experiments, seems likely to prove adequate for many if not all applications.

The most outstanding disadvantage of those fused-salt systems studied to date is the generally high melting points of the salts, which are inconvenient for reactor startup. Also, fused-salt fuel systems containing considerable concentrations of fissionable material have moderately high viscosities in the operating-temperature range and have heat-transfer

properties that are considerably inferior to those of liquid metals. Perhaps the most serious disadvantage of these systems is the vast lack of knowledge concerning them.

POSSIBLE REACTOR APPLICATIONS

Nuclear reactors now in operation or contemplated are intended to produce either fissionable isotopes or power alone. Each category is capable of considerable subdivision with regard to both nuclear considerations and physical configuration. The application of currently known or anticipated fused-salt systems appears feasible in virtually all these classifications. Considerable experimental effort will, however, be necessary before successful application can be assumed.

THERMAL REACTORS

BREEDERS

The extremely low parasitic capture losses tolerable in breeder reactors seriously limit the number of fused salts which can be considered for these units; such compounds are listed in Table 6.1.1. Of these, only Li^7OD , Li^7F , Li^7D , BeF_2 , BiF_3 , and $\text{B}_2^{10}\text{O}_3$ appear to be useful; from these compounds and the fissionable and fertile materials as fluorides, however, some practicable systems may be demonstrated.

A reactor containing U^{233} as fuel and using Th^{232} as fertile material is generally considered to be the most promising of the thermal breeders. Fuel for an internal breeder would need a low concentration of U^{233} and a high concentration of Th^{232} , and an external breeder would require the two materials in separate fluids. In principle, a mixed type in which the core contains sufficient fertile isotopes to replenish the fuel is attractive.

Hydrogenous Fuels

The most attractive combination for an internal breeder (a solution of acceptable uranium and thorium compounds dissolved in molten Li^7OD) can probably be eliminated at once from the standpoint of the solubility of thorium compounds. As the alternative case, an external breeder might possibly be fueled with a dilute solution of U^{233}O_3 in this vehicle. As little as 0.4 percent of U^{233} by weight in this solvent may be adequate,¹ and solubilities of this magnitude might possibly be achieved at $1100^\circ\text{--}1200^\circ\text{F}$. If metallic zirconium (or zirconium-tin alloy) has sufficient strength and can contain the $\text{UO}_3\text{--LiOD}$ solution at $1100^\circ\text{--}1200^\circ\text{F}$, which is possible but not likely, then a useful external breeder with low critical mass may be available.

Fluoride Fuels

Mixtures of $\text{LiF--BeF}_2\text{--ThF}_4$ would seem to be quite suitable blankets, and similar but dilute UF_4 solutions could serve as fuels for thermal breeders.² With these materials, however, operation of the reactor would be restricted to temperatures where molybdenum or iron-chrome-nickel alloys would be required. These are hardly permissible in an external breeder. However, substituting a small quantity of UF_4 for ThF_4 in the fuel should not seriously affect the properties of the mixture, and a good internal-breeder fuel should be possible.

To remove heat from the core, it may prove necessary to circulate the fuel and cool it externally, even at the expense of increasing the inventory of fissionable material and losing

¹ References appear at end of chapter.

Table 6.1.1 — Possible Moderators and Fuel Diluents for Thermal Breeders

(R. P. Schuman and A. D. Tevebaugh, Knolls Atomic Power Laboratory in Oak Ridge National Laboratory. Report CF-52-4-197 (classified)).

	Melting point, °C	Boiling point, °C
DF	-83	19.4
D ₂ O	3.82	101.4
Li ⁷	186	1336
Li ⁷ N ¹⁵ O ₃	261	*
Bi	271	1450
Li ⁷ B ¹¹ D ₄	275	275*
Li ⁷ N ¹⁵ O ₂	...	*
Li ⁷ DF ₂	*	...
BiF ₃
Li ⁷ N ¹⁵ D ₂	290	430
Li ⁷ OD	445	925*
B ₂ ¹¹ O ₃	577	1500
Li ₂ ⁷ CO ₃	618	1200d
Li ⁷ D	680	*
BeF ₂	800	...
Li ₂ ⁷ C ₂
Bi ₂ O ₃	820	1900
Li ₂ ⁷ B ¹¹ D ₂	843	...
Li ₃ ⁷ N ¹⁵	845	...
Li ⁷ F	870	1670
Li ₂ ⁷ O	Sublimes	1000

*Materials decomposed

a considerable fraction of the delayed neutrons. Cooling the reactor by circulating the Li⁷OD would probably (since both fluids have only fair heat-transfer properties) increase the parasitic capture unduly by introducing metal into the core, even if the corrosion problem for LiOD were solved. From the standpoint of the metal introduced in the core heat-exchanger, cooling with Li⁷ or Bi would be preferable, but neither of these metals can yet be contained easily at these temperatures.

At the present state of development, fused salts as breeders seem best suited for internal breeding with a Li⁷F-BeF₂-U²³³F₄-ThF₄ fuel mixture in a reactor several feet in diameter operating in the 1350°-1100°F range with the fuel circulated to an exchanger for heat removal. While such a reactor would involve several novel features, no unsurmountable engineering problems appear to be involved.

FAST REACTORS

Since the generation time in a fast reactor is much smaller than that in a thermal reactor, fast reactors are inherently more difficult to control. The high thermal-expansion coefficient of fused salts should be of distinct advantage in this connection. The nuclear requirements of fast breeders and converters, however, seriously limit the choice of components for fused-salt fuel systems. Fuel materials, in addition to having a low capture cross section for fast neutrons, must not moderate the neutrons excessively either by elastic or inelastic scattering. Thus, bromine and iodine have prohibitively high capture cross sections and hydrogen, boron, carbon, nitrogen, oxygen and fluorine may be present only in

Table 6.1.2—Elements Which May Be Useful as Moderators or Diluents in Thermal Reactors

Elements	Absorption cross-section, σ_a^*	Average number of collisions to thermalize neutrons	Moderating ratio, $\frac{\sigma_s}{\sigma_a} E$
Natural elements			
H	0.330 ± 0.007	19.8	115
He	0.008	46.1	43
Be	0.009 ± 0.0005	95.1	162
C	0.0045	124	169
O	<.0002	163	> 2710
F	<.010	193	> 42
Na	0.49 ± 0.02	232	0.695
Mg	0.059 ± 0.004	238	.493
Al	$.215 \pm 0.008$	272	.475
Si	0.13 ± 0.03	282	.92
P	$.19 \pm 0.03$	311	3.35
S	$.49 \pm 0.02$	321	0.138
K	1.97 ± 0.06	391	.0384
Rb	0.6	845	.47
Sr	1.16 ± 0.06	868	.197
Zr	0.18 ± 0.02	900	.978
Ba	1.17 ± 0.10	1355	.100
Pb	0.17 ± 0.01	2045	.637
Bi	0.032 ± 0.0003	2065	2.70
Separated isotopes			
D	0.00046 ± 0.0001	27.3	
Li ⁷	0.033	75.5	
B ¹¹	<.05	115	
N ¹⁵	<.00002	150	
Cl ³⁷	.61	374	

* K. Way and G. Haines, Thermal neutron cross sections for elements and isotopes, CNL-33, Feb. 29, 1948

E. Melkonian, L. J. Rainwater, and W. W. Havens, Neutron-beam spectrometer studies of oxygen, M-2554

R. G. Nucholls, The total scattering cross sections of deuterium and oxygen for fast neutrons, MDDC-37, June 17, 1946

K. Way and G. Haines, Tables of neutron cross sections, MonP-405, Oct. 28, 1947 (supplement issued April 20, 1948)

H. H. Goldsmith and H. W. Ibser, Neutron cross sections of the elements, MUC-HHG-7, Dec. 5, 1945

Chart of the Nuclides, General Electric Res. Lab., Knolls Atomic Power Lab., third edition, Oct. 1950

Nuclear Cross Sections, AEC Neutron Cross Section Advisory Group, Brookhaven National Laboratory, Classified Cross Sections, BNL-170, May 15, 1952; supplement, BNL-170A, Nov. 1, 1952

Nuclear Cross Sections, AEC Neutron Cross Section Advisory Group, Brookhaven National Laboratory, Unclassified Cross Sections, AECU-2040, Mar. 15, 1952. Supplement 1, AECU-2040, Nov. 15, 1952

traces because of their moderating properties. These restrictions seriously limit the choice of anions. Silicon, phosphorus, arsenic, sulfur, selenium, and tellurium may be permissible, and the latter three might be useful. To a first approximation, however, the only anion available for fast reactors is chlorine.

Fortunately, low-melting fused-salt systems containing UCl_4 appear to be feasible. Although no ternary systems containing this compound have yet been described, analogy with the fluoride systems suggests that melting points below 400°C (perhaps even below 300°C) should be possible at moderately high uranium concentrations. A recent study has indicated melting points of about 315°C in the system $\text{NaCl-PbCl}_2\text{-UCl}_4$.³ No studies of phase equilibria involving the chlorides of plutonium have been reported.

The corrosion problems associated with fused chlorides are likely to prove more difficult than those of the analogous fluoride mixtures since, although some improvement would normally be expected by virtue of the somewhat lower temperatures, thermodynamic considerations indicate that reaction of UCl_4 with structural metals to yield UCl_3 and the structural-metal chloride is more likely than the analogous reactions of UF_4 .³

The relatively low capture cross sections of fission products for fast neutrons and the possibility of removing these materials easily from the fluid permits large fractional burn-up of fuel in fast reactors. Fused salts have proved reasonably stable to radiation, but as yet, no data are available on their response to appreciable fuel burnup.

REFERENCES

1. R. W. Dayton and J. W. Chastain, Jr., Battelle Memorial Institute, BMI-746, May 26, 1952, 30 pp (classified).
2. R. P. Schuman, Knolls Atomic Power Lab., KAPL-634, Aug. 24, 1951, 63 pp (classified).
3. G. Scatchard et al, Mass. Inst. Tech., MIT-5001, Oct. 15, 1952 (classified).

Composition of Fused-salt Systems

HYDROGENOUS FUELS

Deuterium is by far the most desirable moderator for a power-breeder, and hydrogen is probably the most desirable moderator for a power producer. Such compounds as the normal and the deuterium-substituted hydroxides, bifluorides, bisulfates, and hydrides are, accordingly, all worthy of consideration as solvents for fissionable materials. Of these materials, only the alkali and alkaline-earth hydroxides and lithium and calcium hydride are thermally stable above 500°C.

Decomposition pressures of bifluorides and bisulfates could certainly be lowered, with possible gain in melting temperature and certain loss in hydrogen content per unit volume, by addition of normal fluoride or sulfate, respectively.

From a nuclear viewpoint, the only hydrogenous compound likely to be useful as a fuel vehicle for a thermal power-breeder is Li^7OD , although Li^7OH and NaOH could probably be used in thermal power-converters and RbOH , KOH , and the alkaline-earth hydroxides are probably admissible in enriched power producers.

The only studies reported to date with regard to the solubility of fissionable materials in high-temperature hydrogenous melts are concerned with the solubility of uranium compounds in fused hydroxides. These studies, which do not appear encouraging, are reviewed in Chapter 6.3.

Phosphoric acid, which might otherwise be considered as a fuel solvent at relatively low temperatures, shows extensive radiation damage at relatively low power levels.

FUSED SALTS AS REACTOR FUELS

From the viewpoint of physical and chemical properties as well as from that of anticipated radiation stability, mixtures of halides of the fissionable materials with halides of low-cross-section elements seem to offer the most promise as fuels. Nuclear considerations indicate that bromides and iodides are not suitable because of the high capture cross section of the anions, that fluorides are the best choice for thermal reactors, both because of the low cross section of fluorine and because moderation by fluorine could be useful in large reactors, and that chlorides are probably the best choice for fast-reactor fuels.

There is no reason to doubt that fluoride and chloride fuels containing plutonium could be developed.

PHASE EQUILIBRIA IN FUSED FLUORIDES

Uranium-bearing fused salts have so far been studied largely as an exploratory program. Many possible systems had to be examined to select those which exist in the liquid phase over proper ranges of uranium concentration. The studies have been conducted by

the method of thermal analysis which was unsupported, in many cases, by evidence from other techniques. Diagrams for representative systems are given in Figs. 6.2.1 through 6.2.4.

PHASE EQUILIBRIA IN FUSED CHLORIDES

Comparison of Figs. 6.2.5 to 6.2.9 with the preceding figures shows that the systems containing UCl_4 as a component have lower melting points than the corresponding systems containing UF_4 . This advantage, however, is probably more than offset for high-temperature thermal reactors by the capture cross section of chloride ion and the relatively high vapor pressure of UCl_4 . The vapor pressure can probably be lowered by substituting UCl_3 as the fissionable material, and it is likely that the corrosion problem would be considerably simplified at the same time.

While such materials would seem to be of considerable interest as fast-reactor fuels, no experimental studies of three-component systems containing either UCl_4 or UCl_3 have been published. The immiscibility of liquid UCl_4 and UCl_3 is still uncertain^{1,2}, and the allowable concentration ranges when both compounds are used in fuel mixtures are therefore questionable. The miscibility of PuCl_3 with UCl_4 must also be determined by experiment.

A systematic study of chloride systems would be very desirable.

HEAT-TRANSFER AGENTS

HYDROGENOUS MATERIALS

While the ideal use of hydrogenous high-temperature liquids would be as fuel solvents so that truly homogeneous reactors could be developed, important advantages could also be gained if these materials could be used as moderator-coolants with stationary liquid- or solid-fuel reactors.³

Of the high-temperature hydrogenous liquids available, the alkali and possibly the alkali-earth hydroxides seem to offer a number of advantages. From rather limited data, their radiation stability (see Chapter 6.3) and their corrosivity at temperatures below 1000°F (Chapter 6.3) appear to be acceptable. As moderator-heat-transfer agents for fuels having good heat-transfer properties, they are almost certainly adequate; for use with fuels having relatively poor heat-transfer properties, such as fused-salt mixtures, their practicability is questionable.

Figures 6.2.9 through 6.2.13 show melting-point-composition diagrams for five binary hydroxide systems. The system NaOH-LiOH (Fig. 6.2.9) is of special interest since certain mixtures of these compounds show unusual solvent action for uranium compounds (Chapter 6.3).

FUSED SALTS

While certain mixtures of fluorides (notably LiF-BeF_2) may be of value as heat-transfer materials for special applications, the phase-equilibrium diagrams of typical fluoride systems are presented in Figs. 6.2.14 through 6.2.17 primarily for their possible value as solvents for fissionable materials.

Since relatively few diagrams of chloride systems containing fissionable-material components are currently available and since interest in these systems is increasing, the melting points and eutectic compositions of various binary and ternary chloride systems are listed in Tables 6.2.1 and 6.2.2.

¹References appear at end of chapter.

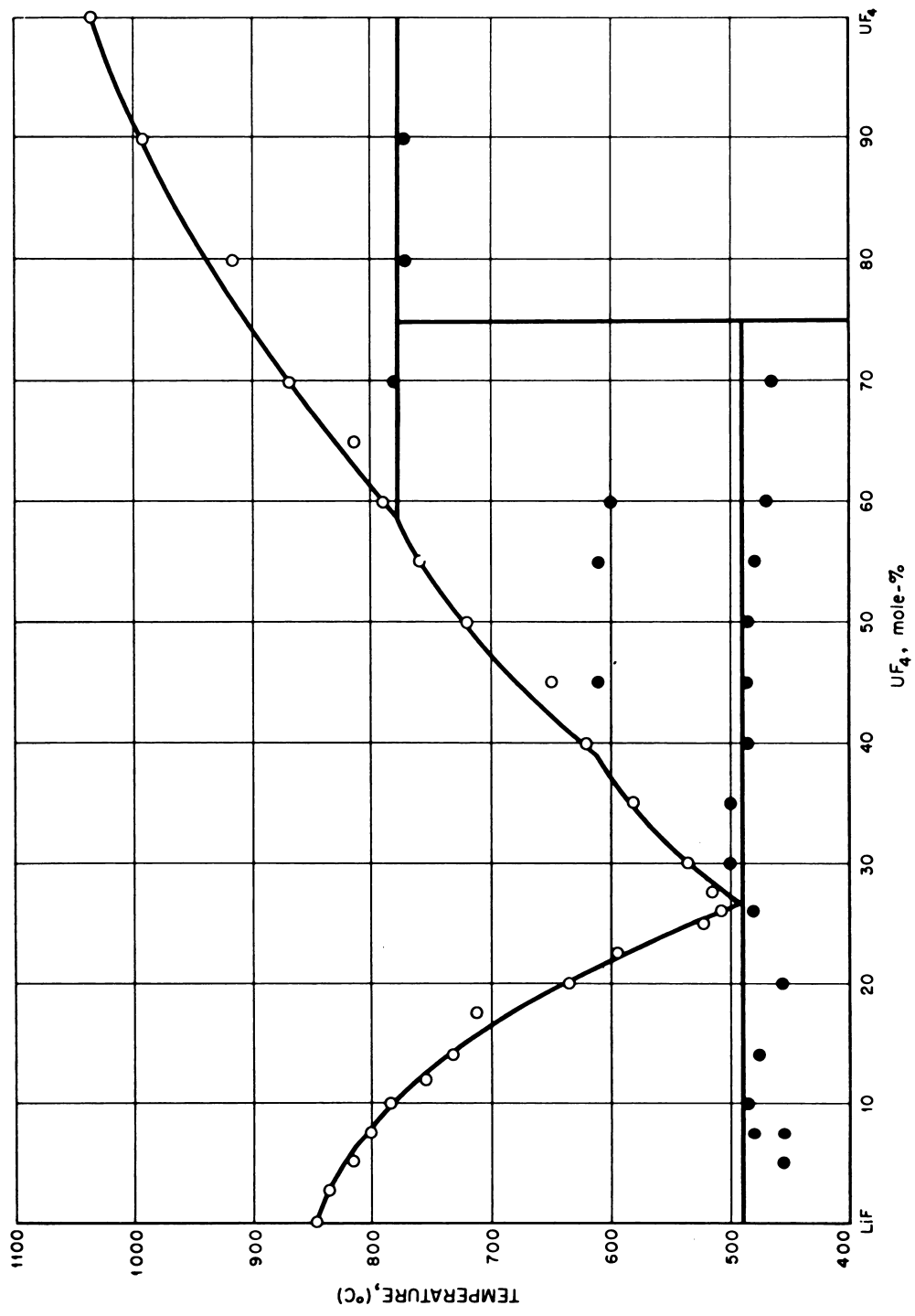


Fig. 6.2.1 — The System $\text{LiF}-\text{UF}_4$. Reprinted from ORNL-919, Dec. 10, 1950.

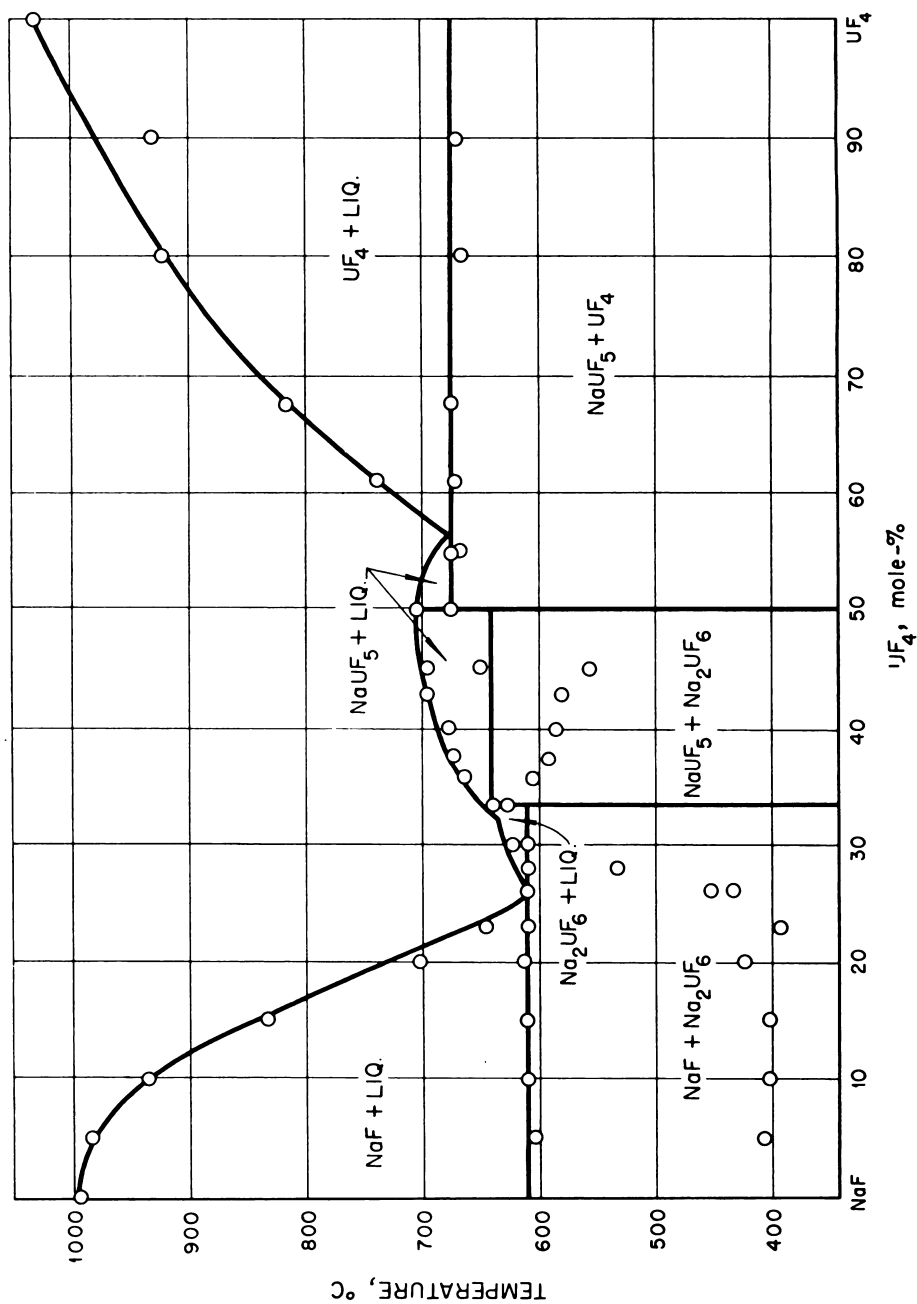


Fig. 6.2.2 — The System NaF-UF₄. Unpublished work, ORNL.

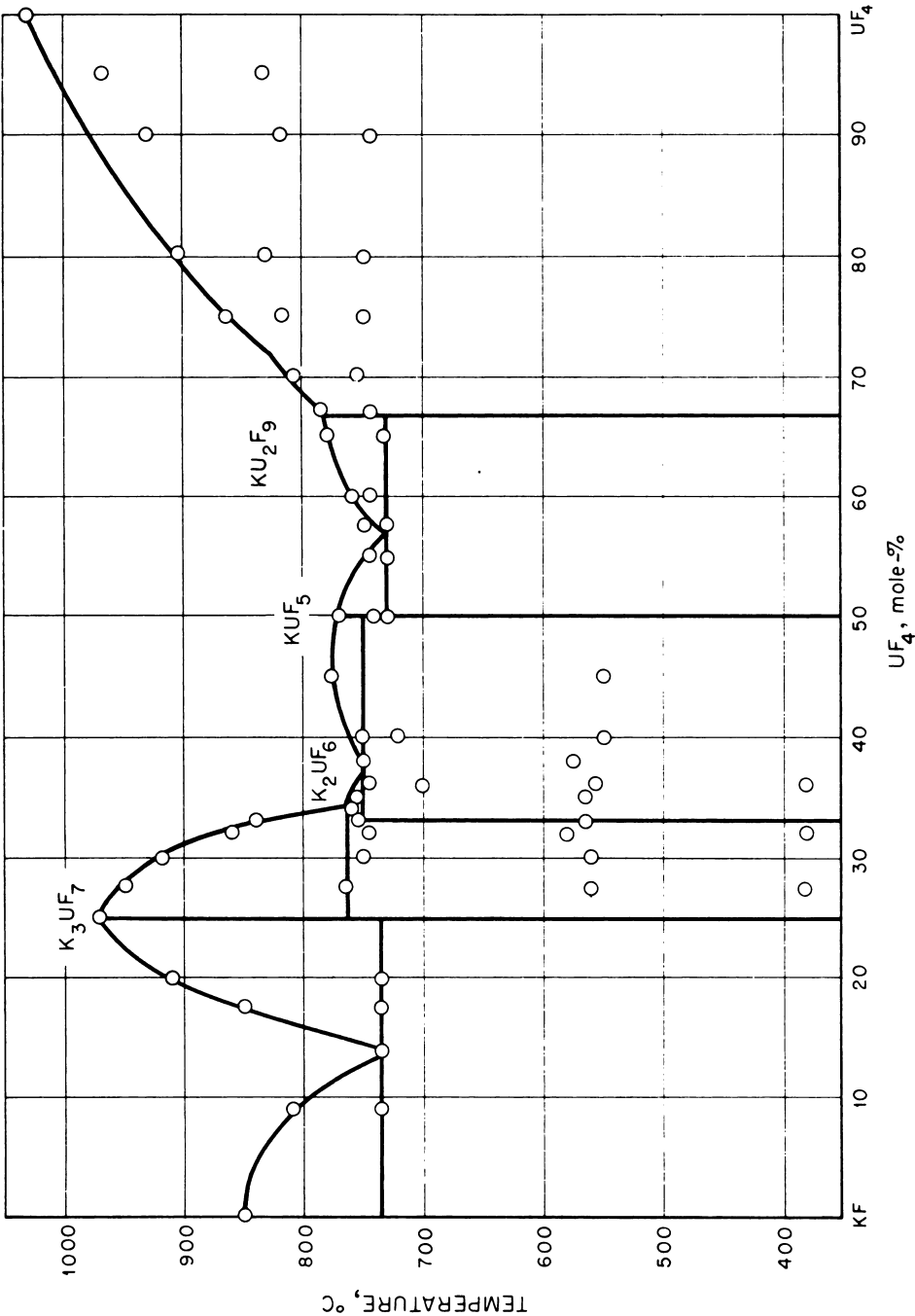


Fig. 6.2.3 — The System KF-UF₄. Unpublished work, ORNL.

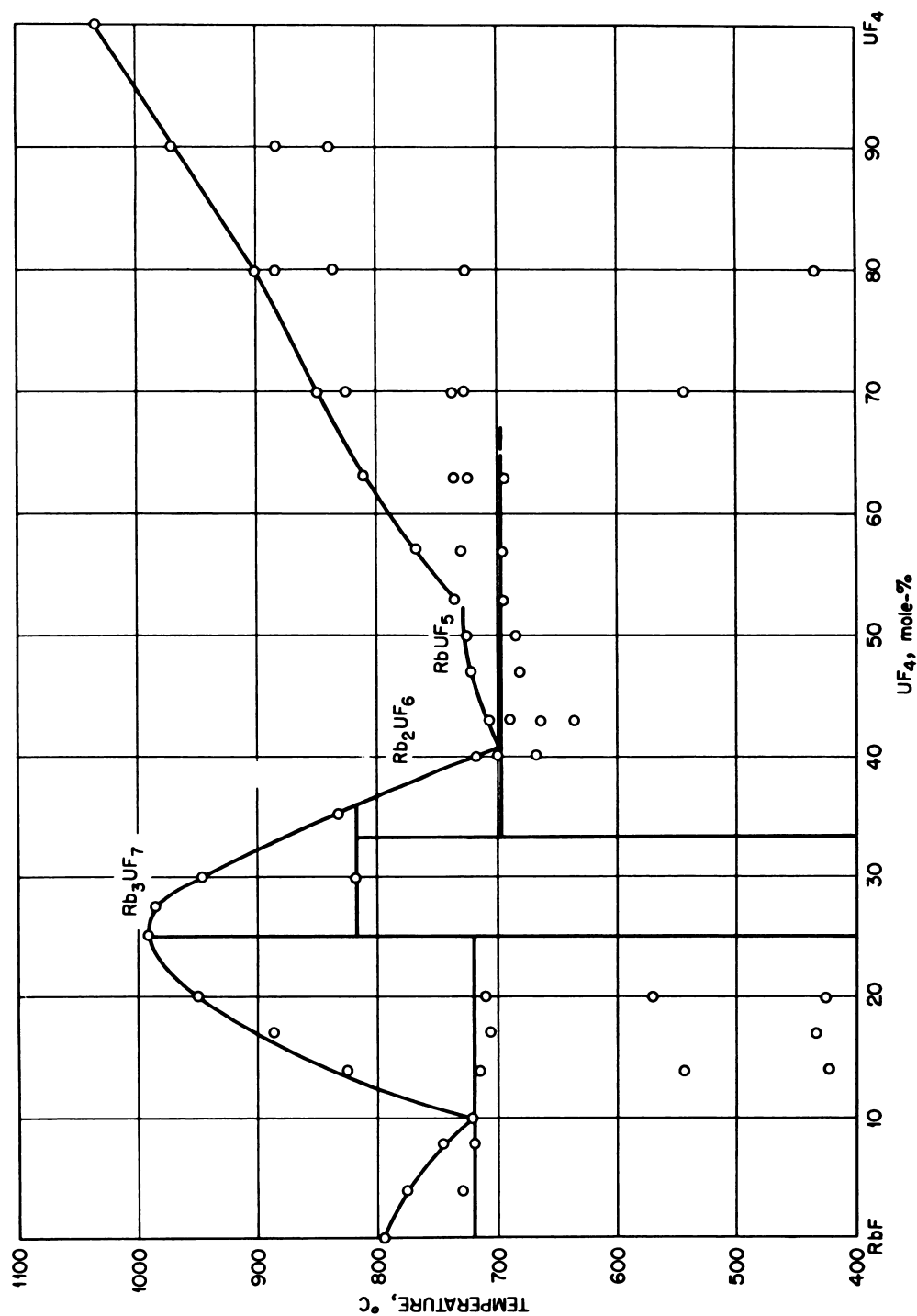


Fig. 6.2.4 — The System RbF-UF₄. Unpublished work, ORNL.

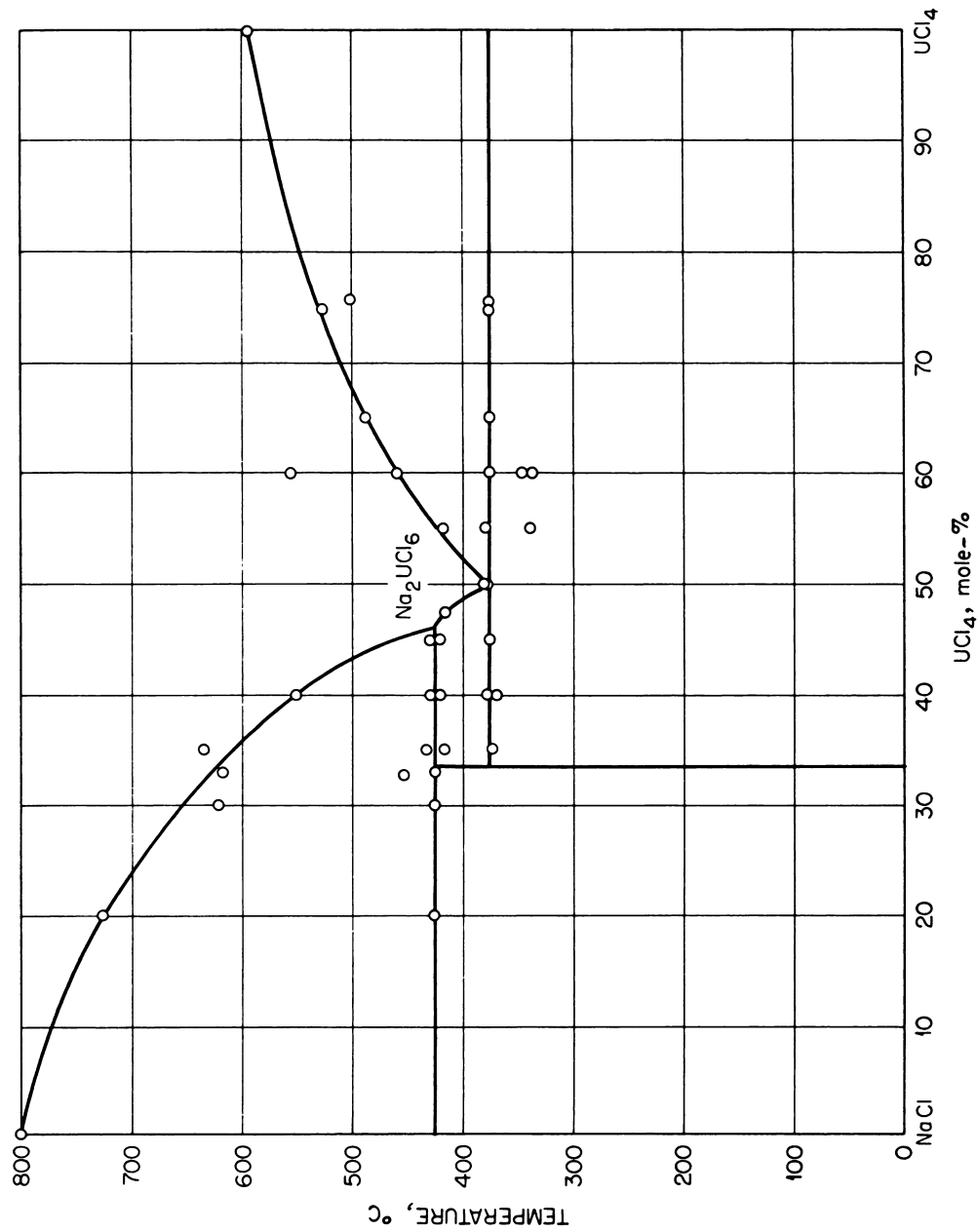


Fig. 6.2.5 — The System NaCl-UCl₄. Copied from M-251, July 1, 1943.

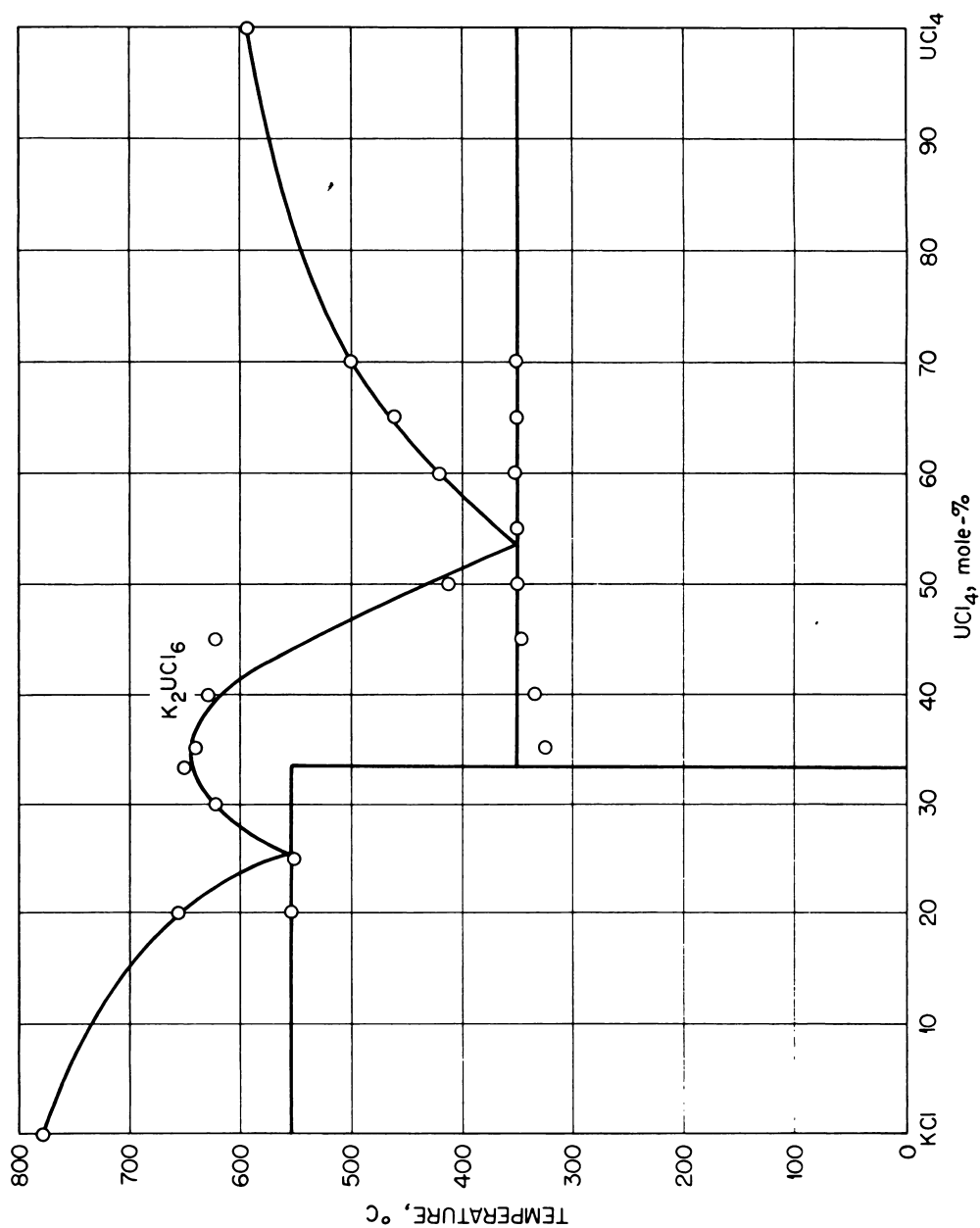


Fig. 6.2.6 — The System $\text{KCl}-\text{UCl}_4$. Copied from M-251, July 1, 1943.

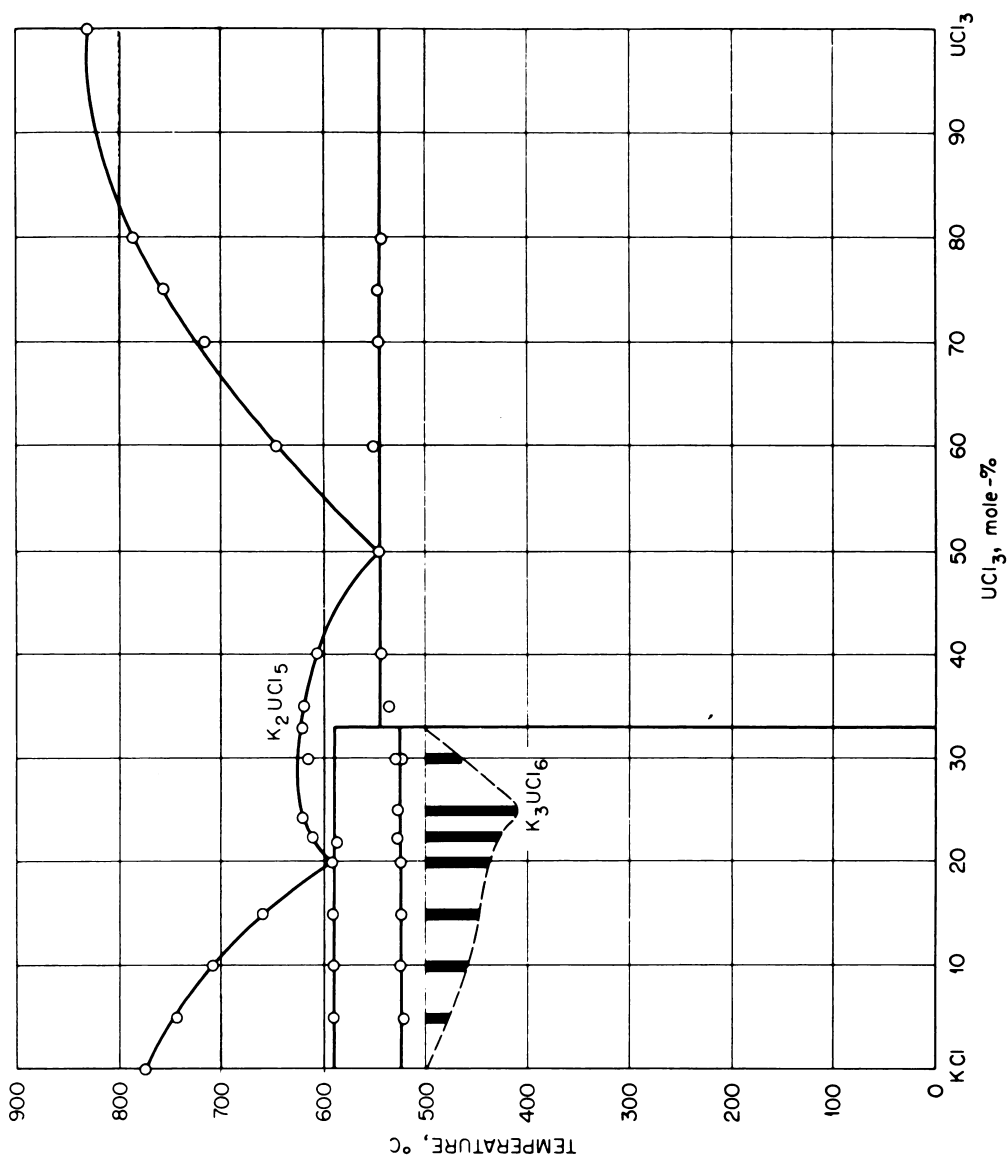


Fig. 6.2.7 — The System KCl-UCl₃. Copied from M-251, July 1, 1943.

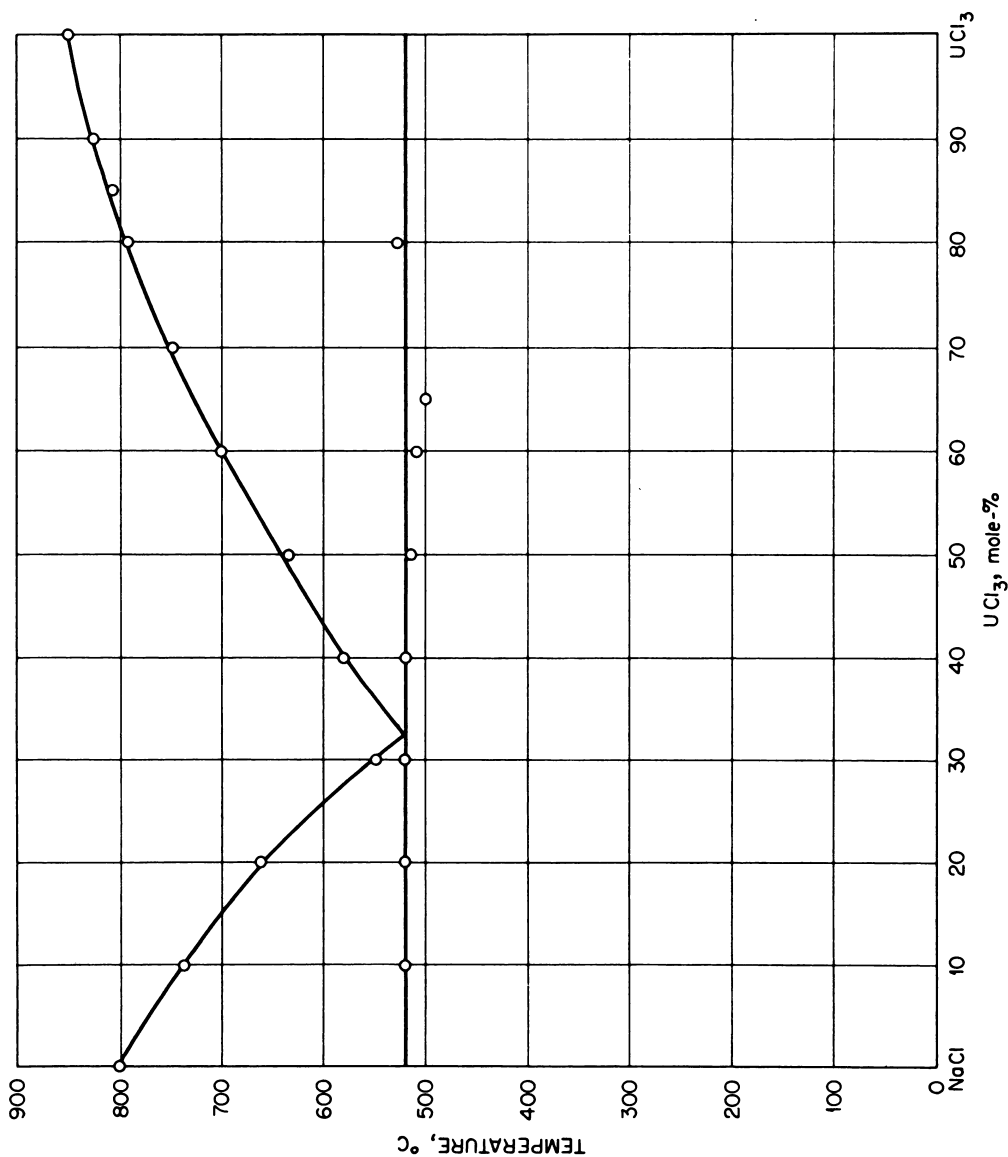


Fig. 6.2.8—The System NaCl-UCl₃. Copied from M-251, July 1, 1943.

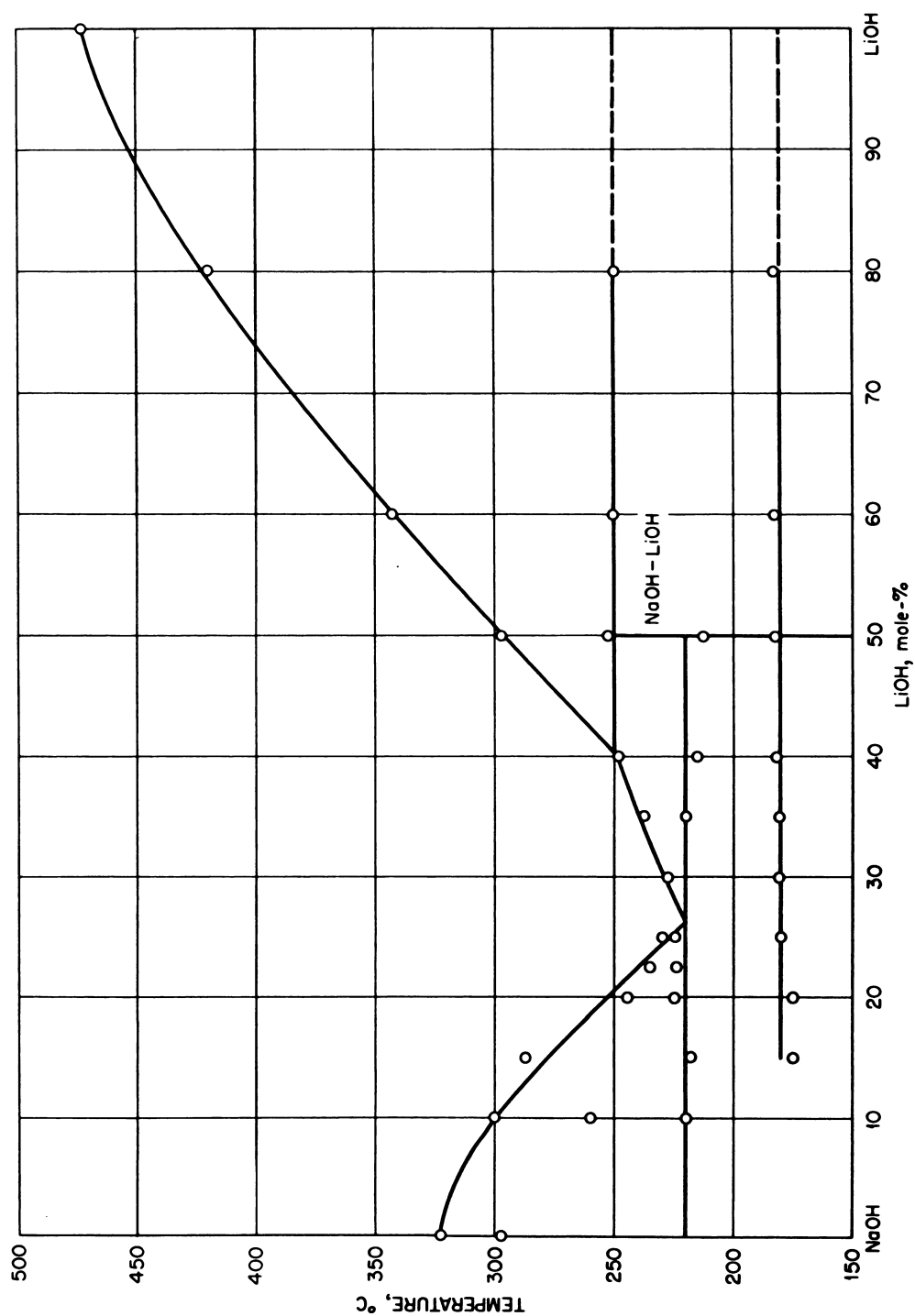


Fig. 6.2.9 —The System NaOH-LiOH. Reprinted from ORNL-1154, Sept. 10, 1951.

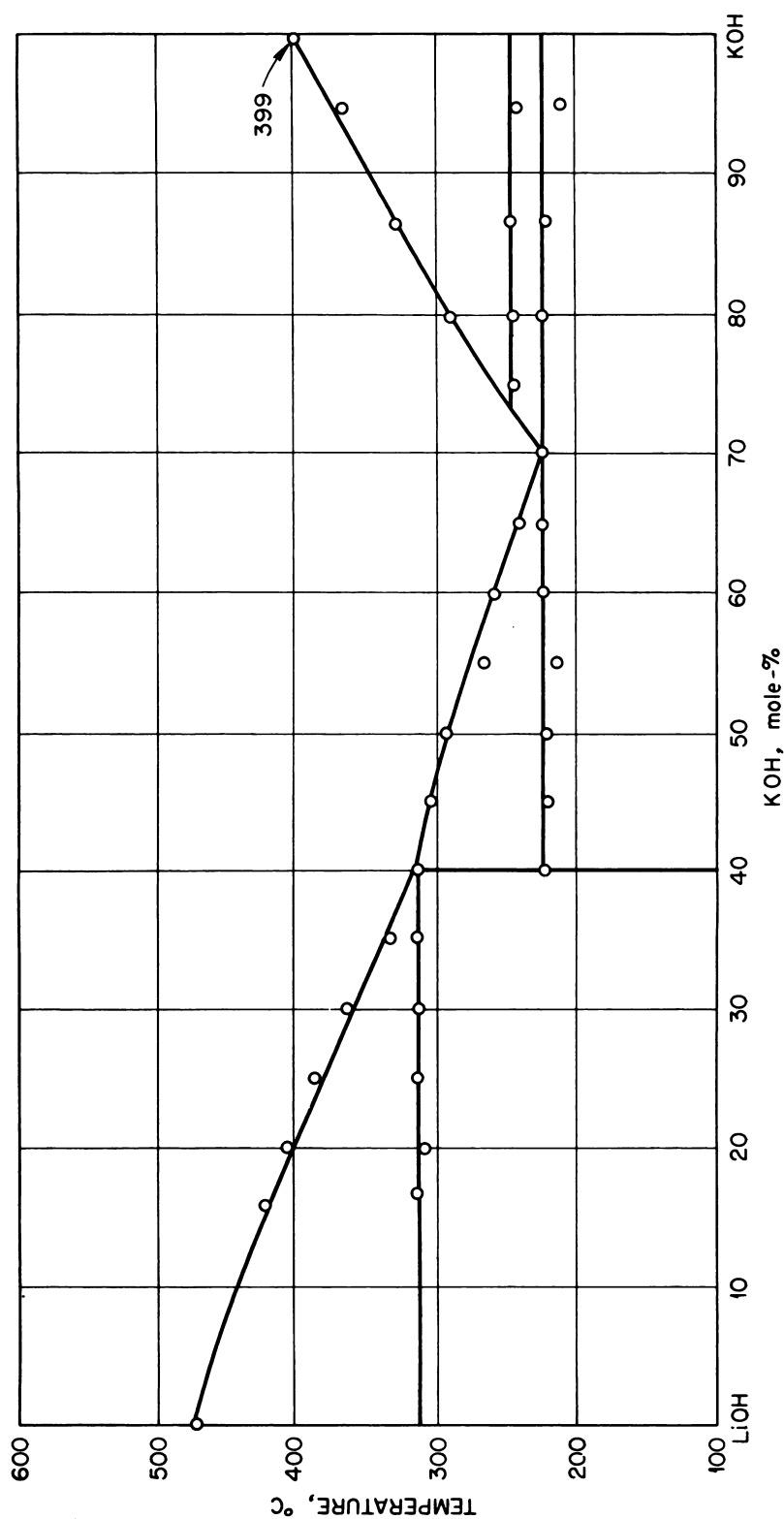


Fig. 6.2.10 — The System LiOH-KOH. Reprinted from ORNL-1170, Dec. 10, 1951.

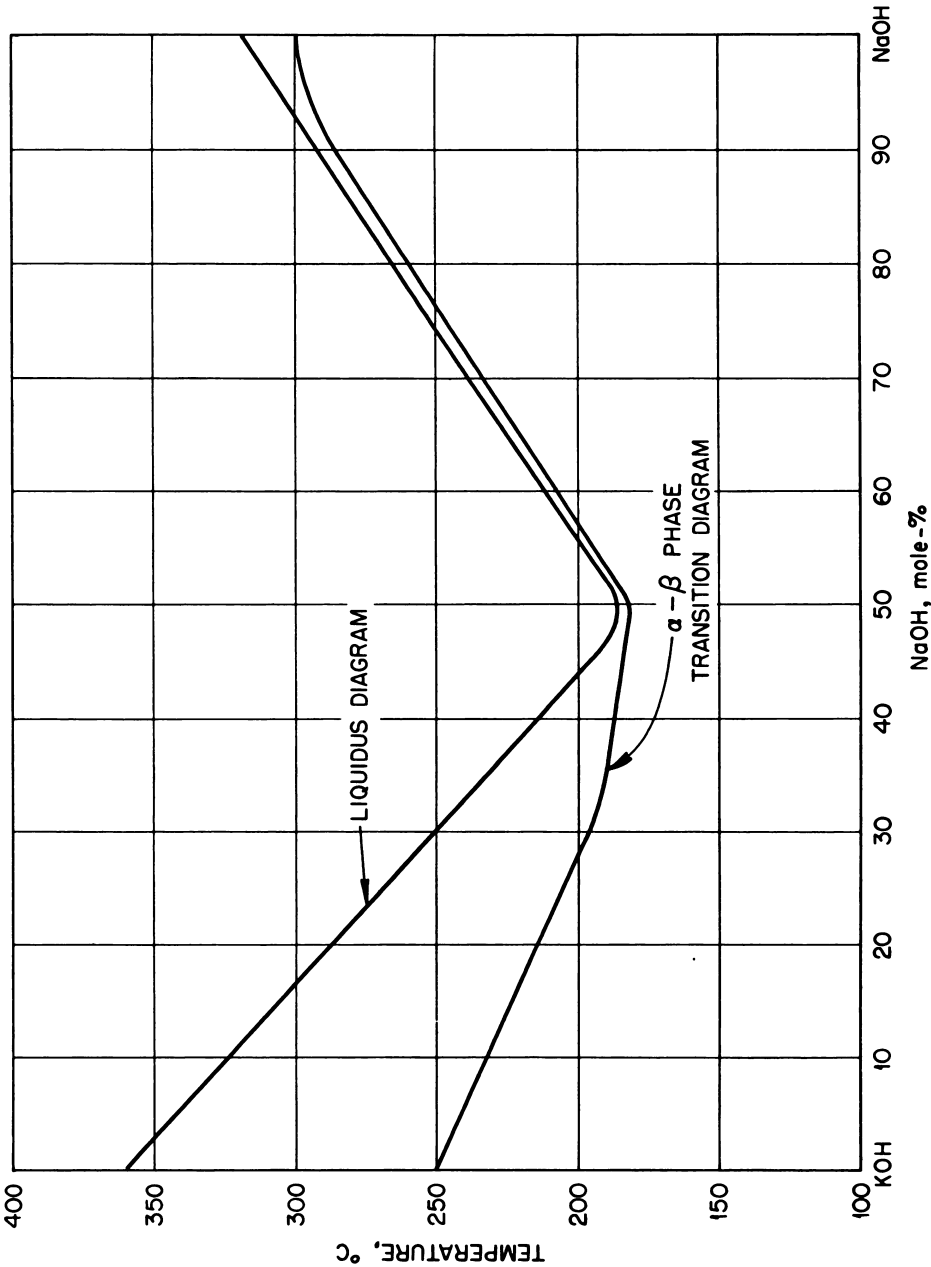


Fig. 6.2.11 — The System NaOH-KOH. Copied from Z. Physik. Chem. 73, 1910.

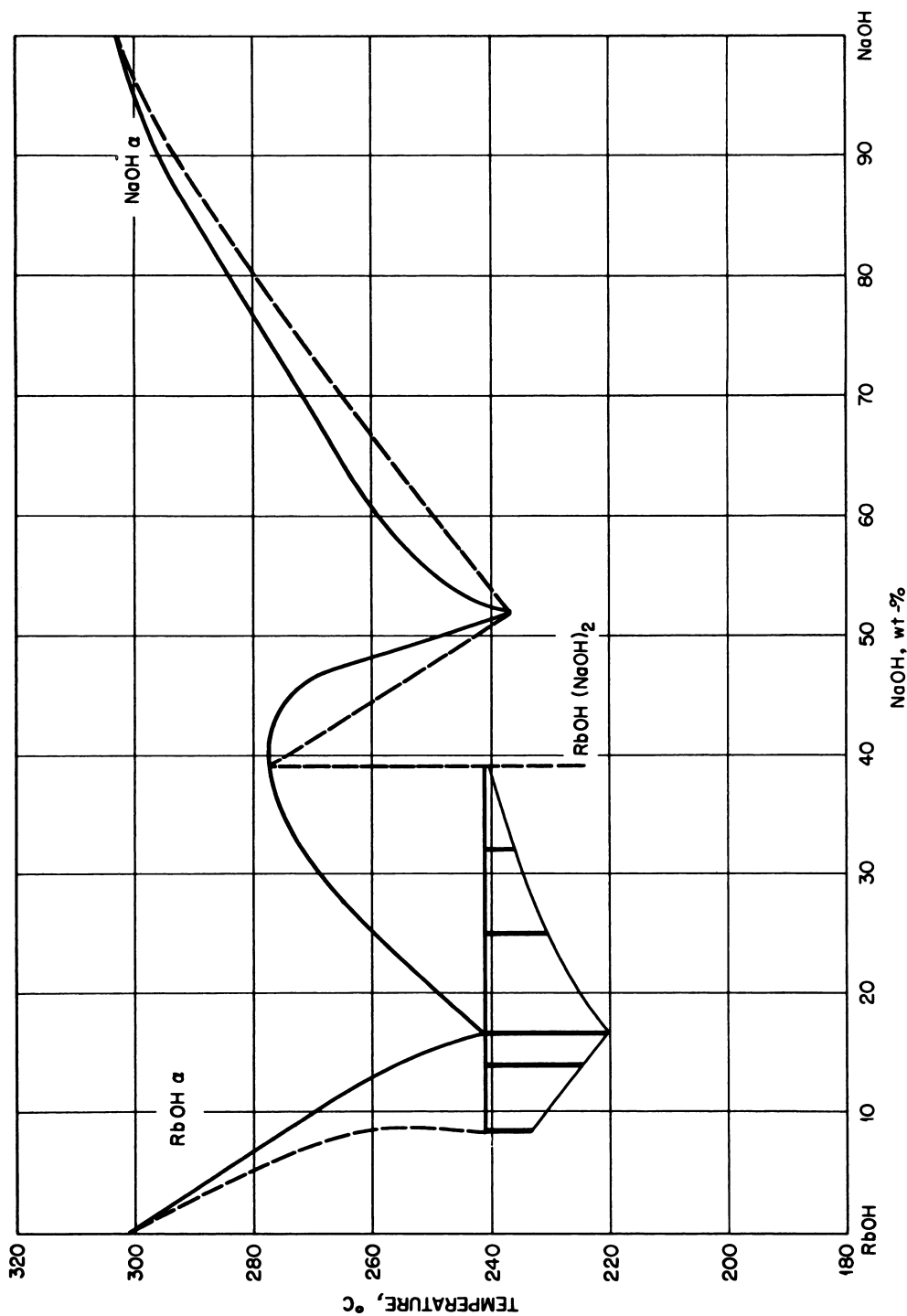


Fig. 6.2.12—The System NaOH-RbOH. Copied from Z. Physik. Chem. 73, 1910.

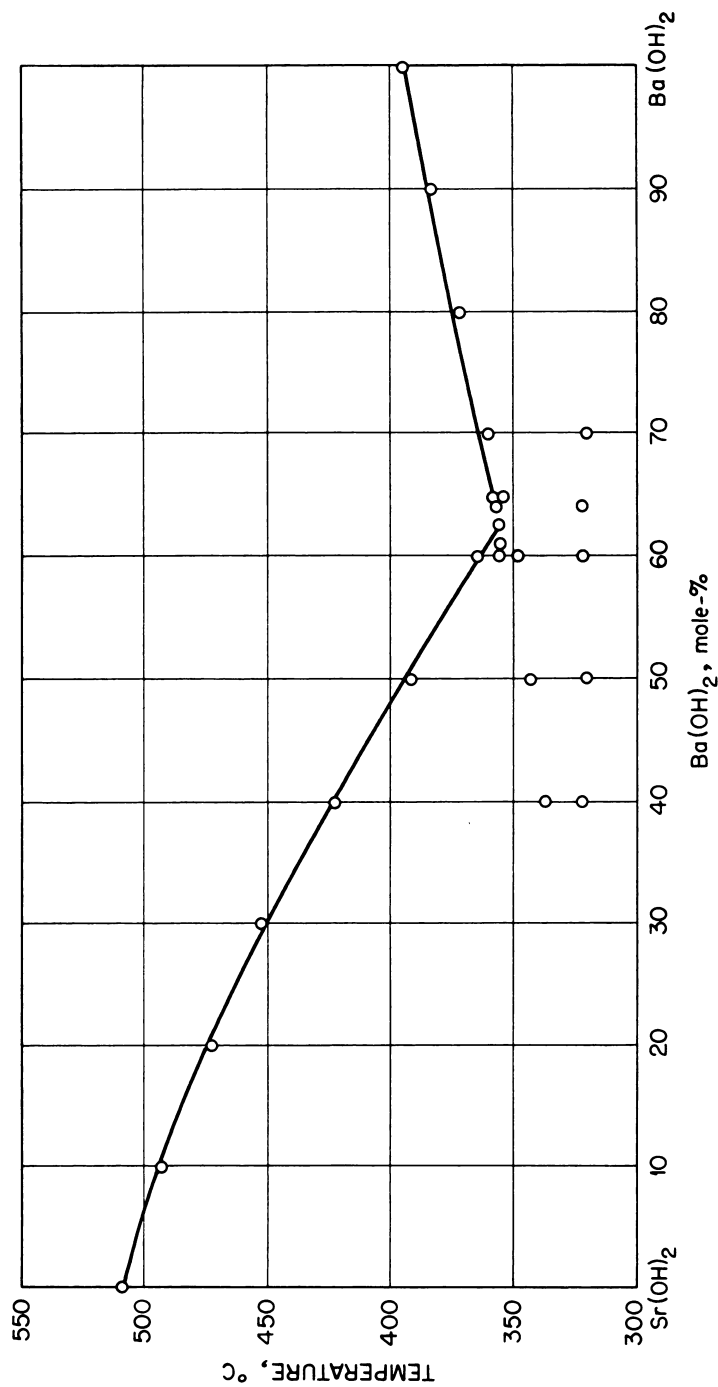


Fig. 6.2.13 — The System Ba(OH)₂-Sr(OH)₂. Reprinted from ORNL-1154, Sept. 10, 1951.

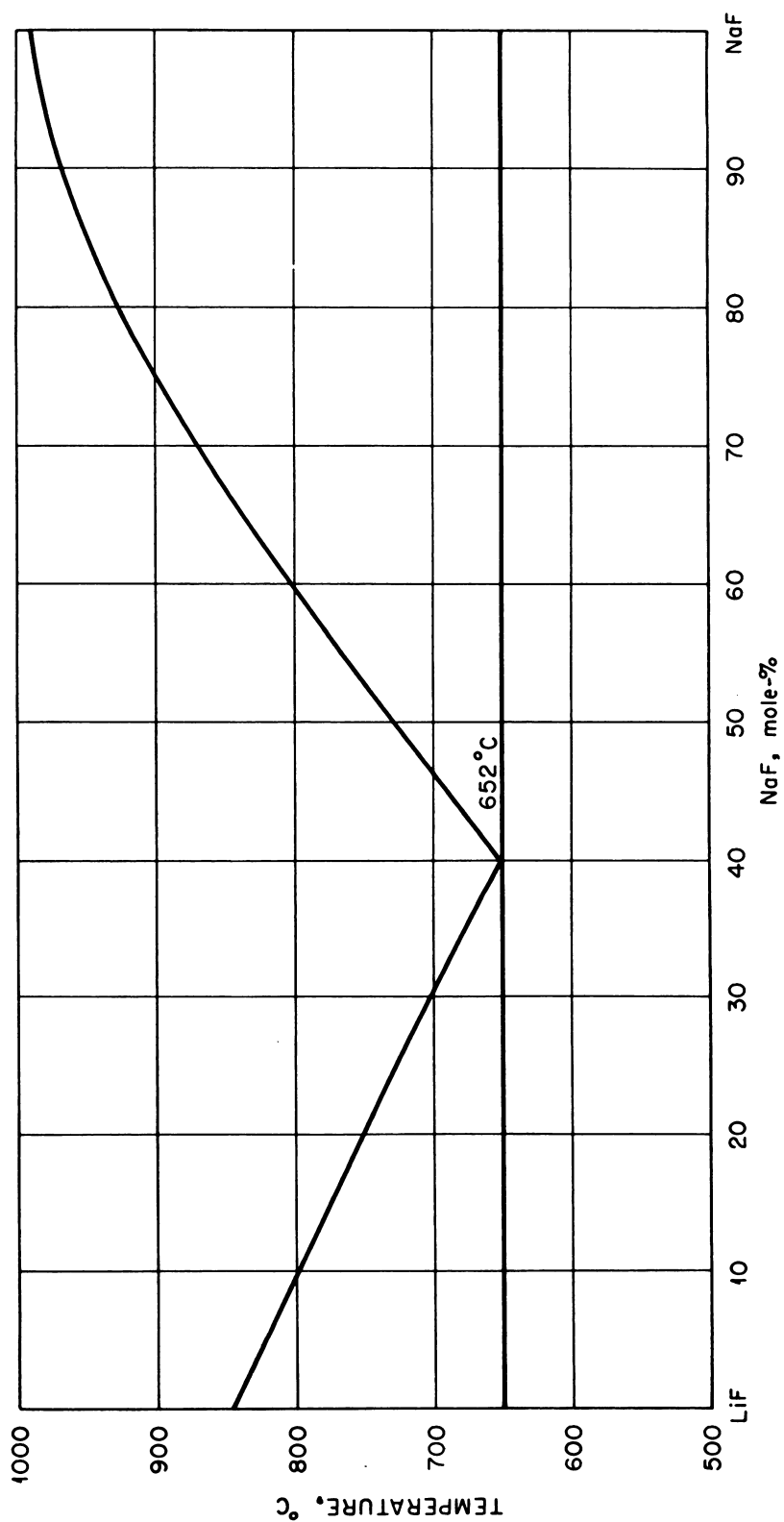


Fig. 6.2.14 — The System NaF-LiF. Copied from Compt. rend. acad. sci., U.R.S.S. 31, 1941.

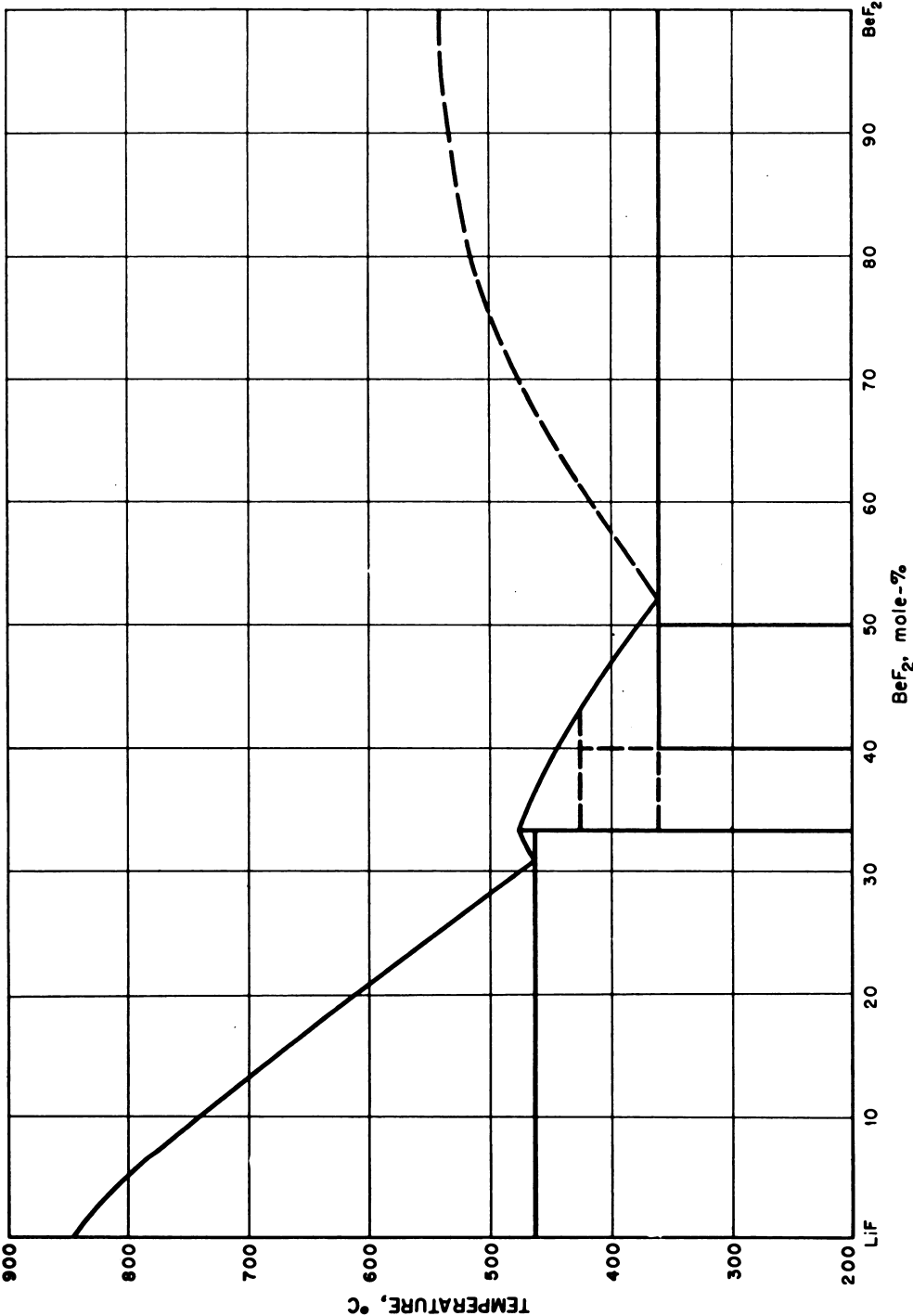


Fig. 6.2.15 —The System $\text{LiF}-\text{BeF}_2$. Copied from Zeit. f. anorg. chemie 258, 1949, and Jour. Am. Ceram. Soc. 33, 1950.

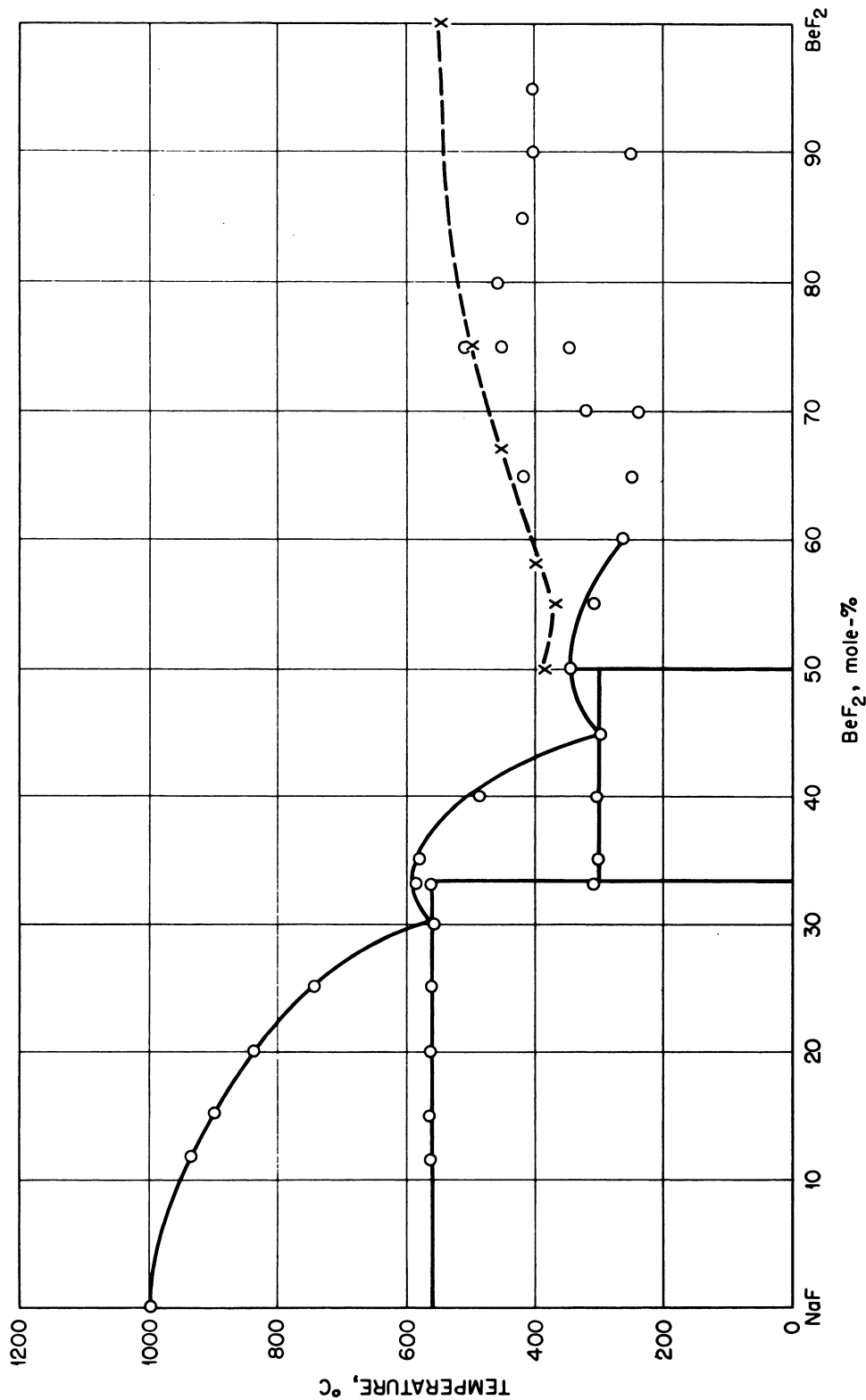


Fig. 6.2.16—The System NaF-BeF₂. Copied from Jour. Gen. Chem. (U.S.S.R.) 14, 1944, and Jour. Am. Ceram. Soc. 33, 1950.

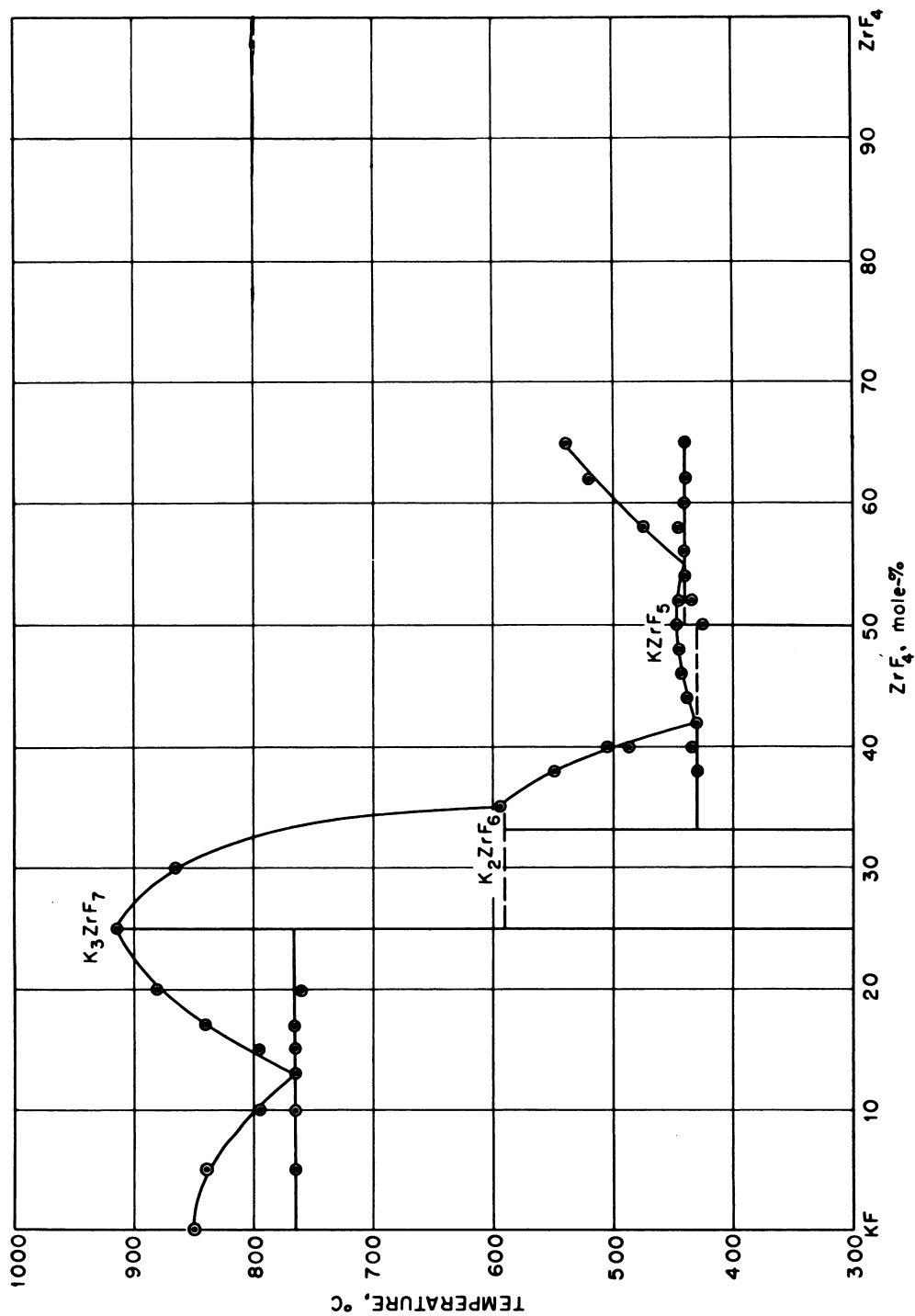


Fig. 6.2.17 — The System $\text{KF}-\text{ZrF}_4$. Reprinted from ORNL-1294, June 10, 1952.

Table 6.2.1—Binary Chloride Systems with Low Melting Points

(W. R. Grimes and D. G. Hill, Oak Ridge National Laboratory, Y-657, July 20, 1950)

Eutectic temperature, °C	Components	Conc. of 2d component, mole-%	Boiling points, °C	
			1st component	2d component
122	TlCl-CuCl	60	720	1366
150	RbCl-CuCl	60	1390	1366
150	KCl-CuCl	65	1500	1366
171	ZnCl ₂ -SnCl ₂	36	732	623
172	CuCl-SnCl ₂	66	1366	623
178	TlCl-SnCl ₂	72	720	623
180	KCl-SnCl ₂	62	1500	623
183	NaCl-SnCl ₂	68	1413	623
193	TlCl-ZnCl ₂	52	720	732
210	TlCl-AgCl	60	720	1550
214	CsCl-CuCl	75	1290	1366
215	NaCl-BeCl ₂	50	1413	520
215	SnCl ₂ -LiCl	15	623	1353
228	ZnCl ₂ -KCl	46	1500	732
233	SnCl ₂ -MnCl ₂	5	623	1190
235	AgCl-BeCl ₂	40	1550	520
240	SnCl ₂ -CoCl ₂	4	623	1049
242	CuCl-ZnCl ₂	88	1366	732
253	RbCl-AgCl	60	1390	1550
258	CsCl-AgCl	72	1290	1550
260	CuCl-AgCl	54	1366	1550
262	TlCl-PbCl ₂	14	720	950
262	KCl-ZnCl ₂	71	1500	732
262	NaCl-ZnCl ₂	59.5	1413	732
276	InCl ₃ -ZnCl ₂	96	vol. 600	732
280	CuCl-PbCl ₂	42	1366	950
292	PbCl ₂ -BeCl ₂	53	950	520
300	LiCl-BeCl ₂	56	1353	520
300	TlCl-BeCl ₂	56	720	520
306	KCl-AgCl	70	1500	1550
310	AgCl-PbCl ₂	41	1550	950
311	CoCl ₂ -ZnCl ₂	93	1049	732
314(325)	NaCl-CuCl	75(77)	1413	1366
316	NaCl-InCl ₃	39	1413	vol. 600
318	RbCl-LiCl	58.3	1390	1353
323	CaCl-LiCl	59.3	subl. 1290	1353
327	CdCl ₂ -BeCl ₂	80	960	520
340	LiCl-TlCl	62	1353	720
361	LiCl-KCl	41.5	1353	subl. 1500
362	TlCl-MgCl ₂	26	720	1412
368	CdCl ₂ -PbCl ₂	62	960	950
369	InCl ₃ -AgCl	77	vol. 600	1550
372	BaCl ₂ -BeCl ₂	87	1560	520
378	TlCl-PbCl ₂	42	720	950
382	CdCl ₂ -KCl	18	960	1500
388	CdCl ₂ -KCl	47	960	1500
390	CaCl-TlCl	75	1290	720
400	CuCl-CaCl ₂	20 (wt-%)	1366	1600*

Table 6.2.1 — (Continued)

Eutectic temperature, °C	Components	Conc. of 2d component, mole-%	Boiling points, °C	
			1st component	2d component
406	KCl-PbCl ₂	52	1500	950
406	MgCl ₂ -CuCl	90	1412	1366
408	PbCl ₂ -MnCl ₂	30	950	1190
408	LiCl-CuCl	80	1353	1366
410	LiCl-PbCl ₂	54	1353	950
411	PbCl ₂ -KCl	33	950	1500
411	NaCl-PbCl ₂	72	1413	950
412	NaCl-TlCl	82	1413	720
419	TlCl-CaCl ₂	7	720	1600*
424	CoCl ₂ -PbCl ₂	76.5	950	950
426	KCl-MgCl ₂	33	1500	1412
428	KCl-PbCl ₂	88	1500	950
432	ZnCl ₂ -KCl	68.5	732	1500
438	PbCl ₂ -PbO	22	950	...
450	AgCl-CaCl ₂	18	1550	1600*
450	NaCl-MgCl ₂	48	1550	1412
450	LiCl-KCl	40	1353	subl. 1500
451	RbCl-CdCl ₂	40	1390	960
455	AgCl-MgCl ₂	9	1550	1412
459	MgCl ₂ -PbCl ₂	93.5 (wt-%)	1412	950
468	CaCl ₂ -PbCl ₂	83	1600*	950
470	MgCl ₂ -KCl	42	1412	1500
473	LiCl-SrCl ₂	48	1353	...
476	InCl ₃ -CdCl ₂	51	600	vol. 960
496	LiCl-CaCl ₂	62	1353	1600*
500	SrCl ₂ -MnCl ₂	46	...	1190
500	NaCl-CaCl ₂	52	1413	1600*

*Greater than

Table 6.2.2 — Ternary Chloride Systems with Low Melting Points

(W. R. Grimes and D. G. Hill, Oak Ridge National Laboratory, Y-657, July 20, 1950)

Eutectic temperature, °C	Components	Composition, mole-%
188	KCl-TlCl-AgCl	7-37-56
203	ZnCl ₂ -NaCl-KCl	60-20-20
318	RbCl-LiCl-NaCl	41.0-56.6-2.4
320	CdCl ₂ -PbCl ₂ -KCl	44.0-41.5-14.5
320	CsCl-LiCl-NaCl	40.3-58.0-1.7
357	KCl-LiCl-NaCl	24-43-33
383	PbCl ₂ -KCl-NaCl	71-11-18
386	NaCl-KCl-CdCl ₂	24-43-33
396	MgCl ₂ -KCl-NaCl	60-20-20
415	KCl-NaCl-TlCl	6.3-6.3-87.4
440	BaCl ₂ -MgCl ₂ -KCl	20-60-20
450	CaCl ₂ -NaCl-BaCl ₂	47.0-38.5-14.5

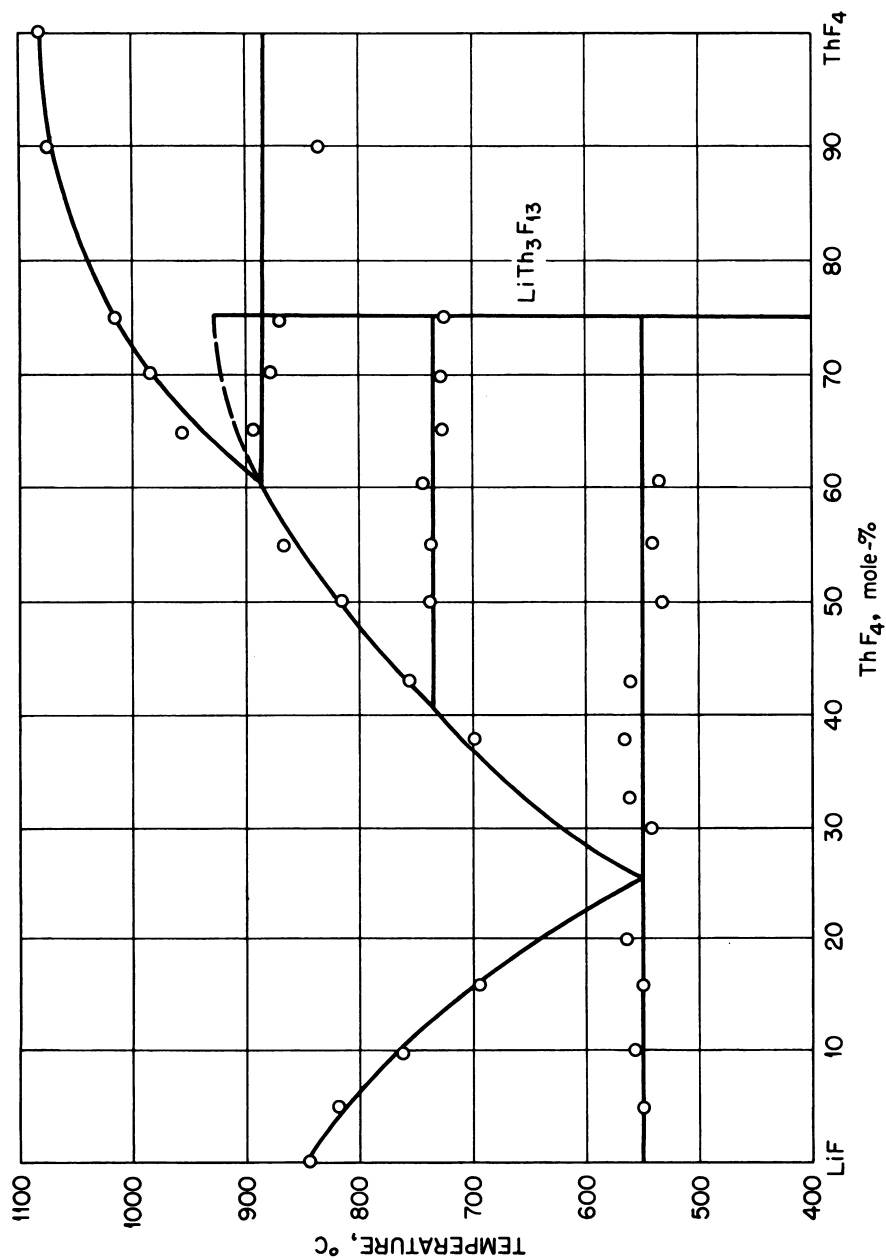


Fig. 6.2.18—The System $\text{LiF}-\text{ThF}_4$. Reprinted from ORNL-1030, June 19, 1951.

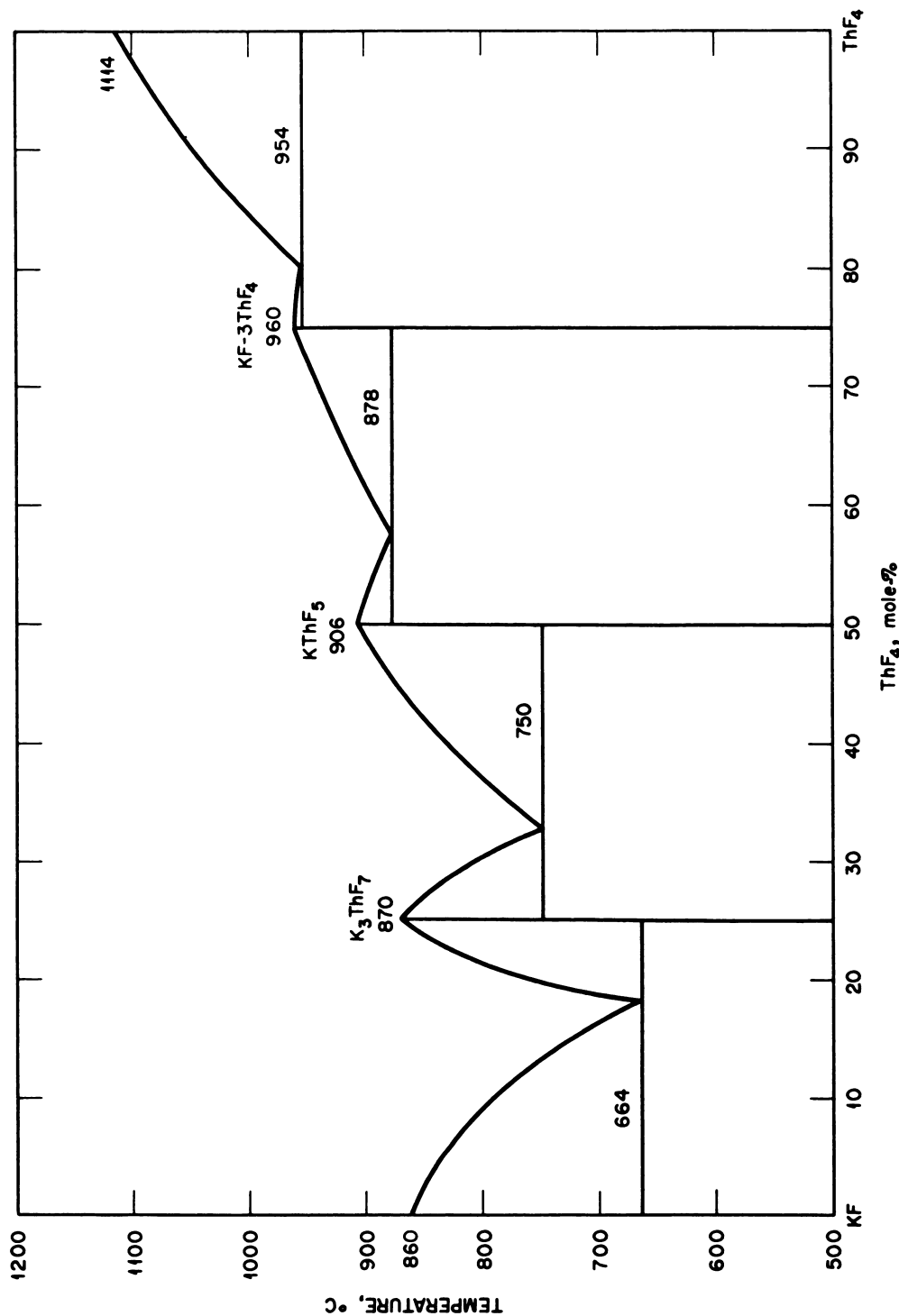


Fig. 6.2.19 — The System KF-ThF₄. Copied from Doklady Akad. Nauk S.S.S.R 60, 1948.

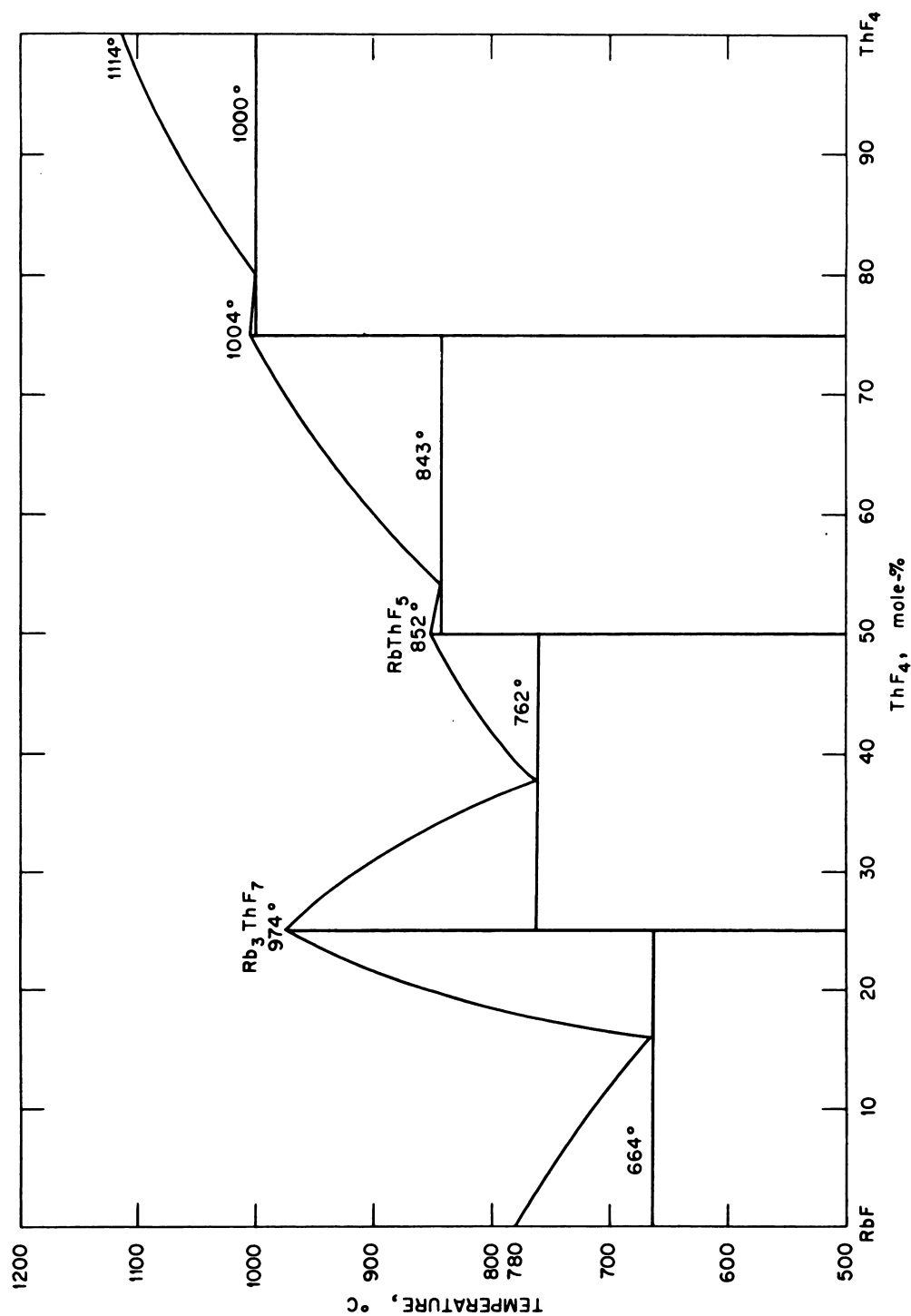


Fig. 6.2.20—The System $\text{RbF}-\text{ThF}_4$. Copied from Doklady Akad. Nauk S.S.S.R. 60, 1948.

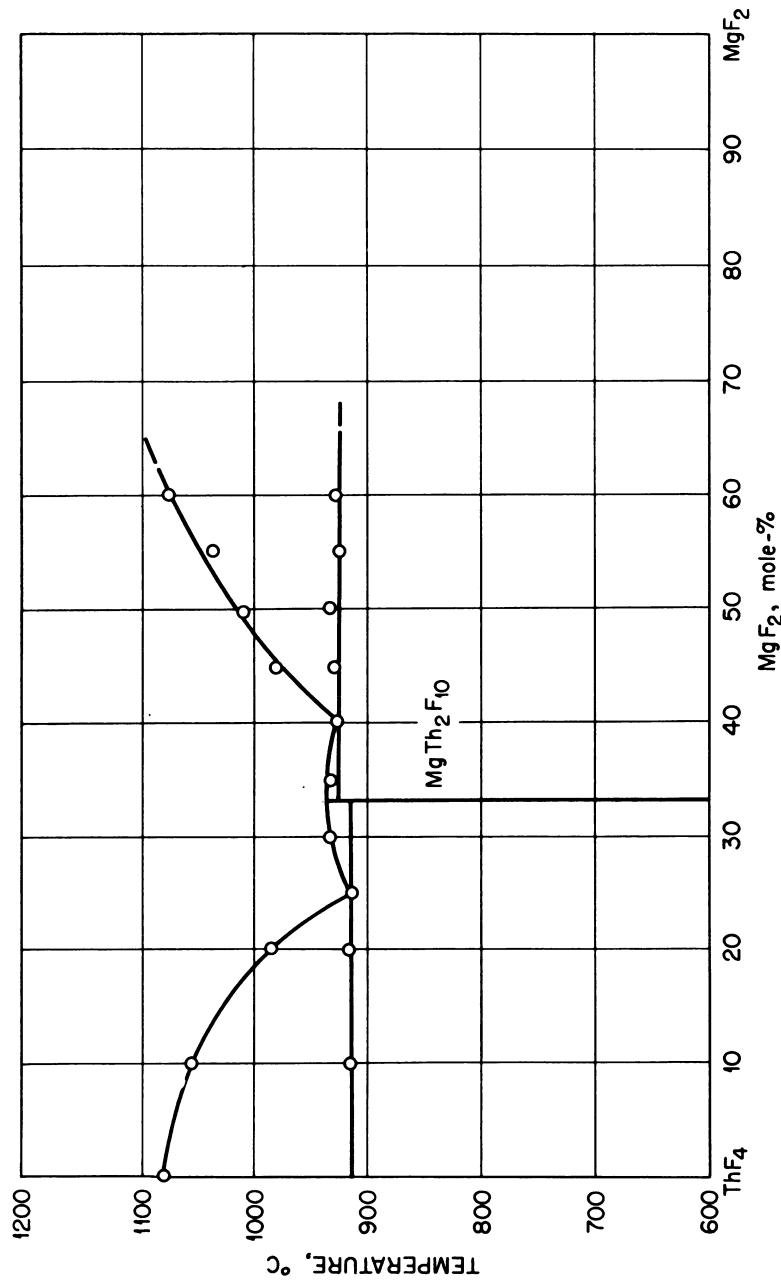


Fig. 6.2.21 — The System MgF_2 - ThF_4 . Reprinted from ORNL-1030, June 19, 1951.

BREEDER BLANKETS

From the standpoint of nuclear properties alone, certain fluoride mixtures would seem to be applicable as thermal-breeder blankets. While no data on systems containing both uranium and thorium are available, it is very likely that replacement of a small fraction of the ThF_4 with UF_4 would affect the melting temperatures only slightly; there is some prospect, therefore, of an internal breeder utilizing $\text{Li}^7\text{F}-\text{UF}_4-\text{ThF}_4$. Relatively easy product recovery from the external breeder-blanket should be feasible by stripping UF_6 from the melt with diluted fluorine or halogen fluorides.

Phase-equilibrium data for four binary systems including ThF_4 as one component are shown in Figs. 6.2.18 through 6.2.21. The melting temperatures obtainable are higher than those in the corresponding UF_4 system.

REFERENCES

1. C. A. Kraus, Brown Univ., M-251, July 1, 1943, 20 pp (classified).
2. V. P. Calkins and R. W. Nottorf, Iowa State Univ., CC-1975 (A-2889), Oct. 7, 1944, 15 pp (classified).
3. R. W. Dayton et al, Battelle Memorial Institute, BMI-T-51, Jan. 2, 1951, 60 pp (classified).

Properties of Fused-salt Systems

HYDROGEN-BEARING FUEL SYSTEMS

SOLUBILITY OF URANIUM IN HYDROXIDES

Attempts that were made to dissolve uranium compounds in molten hydroxides under neutral or oxidizing atmospheres resulted in oxidation of the uranium to the hexavalent state; complete reaction of the resulting compound with the hydroxide and consequent formation of alkali or alkaline-earth uranates proceeds very rapidly.

If reducing atmospheres are maintained, the high-temperature reaction apparently results in the formation of UO_2 ; this material appears quite insoluble in the molten hydroxide at any readily attainable temperature.

The solubility of UO_3 , or its reaction products, in alkali and alkaline-earth hydroxides is shown in Table 6.3.1. The solubility of this compound in NaOH-LiOH mixtures appears sufficiently high — 4 wt-% U at 750°F — to be of interest if the corrosion problems could be readily solved.

The solubility of UO_3 can be improved by adding large quantities of B_2O_3 to the hydroxide, as shown in Table 6.3.2. However, the melting point and the viscosity of the mixture appear to be adversely affected. The addition of alkali fluorides and alkali carbonates does not seem to improve the solubility of uranium compounds in fused caustic.

In early Project work attempts were made to dissolve various uranium compounds, such as uranium dioxide, uranium trioxide, uranium tetrafluoride, and sodium diuranate, in sodium hydroxide using both silver and nickel crucibles, under both oxidizing and reducing atmospheres, and with and without prior addition of small amounts of various classes of compounds to the caustic. No comparative data or details of the technique are given, but it is stated that most of the systems tested exhibited very little uranium solubility.

Prior addition of tellurium chloride, elemental boron and boron compounds, and elemental phosphorus and phosphates to molten sodium hydroxide in silver crucibles in air each tended to increase the solubility of uranium when the uranium was subsequently added in the form of either uranium trioxide or sodium diuranate. Preliminary fusion of the additives with either uranium trioxide or sodium diuranate and addition of this melt to molten sodium hydroxide also increased the solubility of uranium. However, no solubility greater than 0.1–0.2 percent (by weight) resulted. Although an increased solubility (up to 1 weight-percent or uranium) of UO_3 in NaOH with additions of K_2CO_3 is reported, the UO_3 could not be kept in solution.

The early work suggested that both silver and nickel act as precipitants for uranium from sodium hydroxide, as analysis of the precipitate in each case showed the presence of nickel. An adequate uranium solubility might therefore be achieved in sodium hydroxide if the corrosion and container problem can be sufficiently resolved. There are, at present, no known solutions of uranium compounds in molten hydroxides which are useful at temperatures such that the corrosion could be tolerated.

Table 6.3.1—Solubility of UO_3 in Various Hydroxides¹⁻⁴

Solvent composition, wt-%*					Solubility of UO_3 , wt-% U		
NaOH	KOH	LiOH	$\text{Ba}(\text{OH})_2$	RbOH	650°C	700°C	750°C
100					0.03		
		100			0.5		2.0
	100				0.1		0.3
75		25				0.2	
50		50			2.0		4.0
25		75				1.0	
				100	0.1		
25	75						0.1
		25	75		0.1		0.2
		50	50		0.1		0.3
		75	25		0.4		
50			50				0.1
45		45		10	1.2		
40		40		20	0.8		

* Purity of hydroxides used:

NaOH - Less than 0.1% Na_2CO_3 ; less than 0.1% H_2O KOH - Less than 0.5% K_2CO_3 LiOH - Less than 0.2% Li_2CO_3 $\text{Ba}(\text{OH})_2$ - Less than 0.4% BaCO_3 or BaORbOH - Contained about 5% Rb_2CO_3 Table 6.3.2—Solubility of UO_3 in Various Hydroxides with Added Boron Compounds⁵

Hydroxide matrix, wt-%*			Material added, wt-%		UO_3 dissolved, wt-%	
LiOH	NaOH	KOH	B_2O_3	$\text{Na}_2\text{B}_4\text{O}_7$	650°C	800°C
100	0.5	>2.0
92	83	
84	169	
80	208	
...	10003	
...	85	...	153	
...	70	...	30	...	1.3	
...	95	5	0.1	0.1
...	85	15		.4
...	80	20		.5
...	55	45		5.0
...	70	...	15	15	0.9	2.7
...	60	...	15	25		4.7
...	...	100	0.1	>0.3
...	...	95	53	
...	...	90	107	
...	...	85	15	...	1.6	
...	...	80	20	...	1.5	
...	...	75	25	...	†	
50	50	2.0	>4
47	48	...	5	...	1.0	
43	42	...	15	...	1.7	...

* For hydroxide specifications, see Table 6.3.1

† Mixture melted above 700°C

¹ References appear at end of chapter.

SUSPENSIONS OF URANIUM IN HYDROXIDES

A very limited study of suspensions of uranium compounds in molten hydroxides has been made. Addition of UO_3 to molten hydroxides results in an unstable suspension of a material which appears to be Na_2UO_4 . The stability of such a suspension is almost independent of the initial UO_3 particle size but, as the data in Table 6.3.3 indicate, the stability is very poor at 600°C or higher. Apparently stirring of the material for a few days causes particle growth. A considerable increase in the stability of similar suspensions and a greatly decreased particle growth at low temperatures are shown by the data of Table 6.3.4. It is interesting to note that these systems may be readily resuspended after settling for several days, no tendency for the settled particles to cake having been observed.

Attempts to create suspensions of quadrivalent uranium compounds of comparable stability have not been successful.

RADIATION STABILITY OF HYDROGENOUS FUELS

Hydroxides have been shown to possess considerable stability to neutrons and ionizing radiations at lower levels up to 30 watts/cc (see "Radiation Stability of Hydroxides," discussed later in the chapter). However, no studies in which fission products were present in the hydroxide mixtures have been made.

Table 6.3.3—Settling Rate for Suspensions of UO_3 in NaOH
As Functions of Temperature and Age¹⁻⁴

Settling time, min	Uranium remaining in suspension*, % of original					
	600°C		700°C		800°C	
	Stirred 18 hr	Stirred 42 hr	Stirred 20 hr	Stirred 95 hr	Stirred 2 hr	Stirred 20 hr
1	98	61	85	37	83	2
2	86	44	66	17	71	2
3	83	34	61	2	47	1
4	61	21	51	2	51	1
5	58	21	39	2	27	2

* In upper 25% of the liquid

Table 6.3.4—Stability of Suspensions of UO_3 in NaOH-KOH at 250°C^{1-4}
(61% NaOH - 39% KOH by weight; 5 wt-% UO_3 added)

Settling time, min	Uranium remaining in suspension, % of original		
	Stirred 24 hr	Stirred 48 hr	Stirred 120 hr
120	95	95	95
240	75	85	85
360	55	65	
960		0.2	

CORROSION BY HYDROGENEOUS FUELS

Studies of container materials for alkali hydroxides at elevated temperatures have shown this problem to be very difficult (see "Corrosion by Hydroxides," discussed later in this chapter). Apparently, no corrosion tests have been reported in which dissolved or suspended uranium compounds were present. It is likely that the presence of hexavalent uranium compounds in the caustic would markedly increase the corrosion rates.

FUSED-SALT FUEL SYSTEMS

RADIATION STABILITY OF FUSED SALTS

Pioneer experiments on radiation stability of fused salts were apparently confined to possible gross changes in the molten materials. Subsequent experimental work in this field has been restricted almost entirely to reactor irradiation and cyclotron bombardment of uranium-bearing fluoride mixtures. These experiments are not sufficiently diverse or extensive to permit general evaluation of fused salts. It appears, however, that while no gross changes in composition or properties of the fused salts studied have been observed at high power levels, the rate of attack on the container vessel is in some cases significantly increased at levels above 1000 watts/cc. It has been definitely established whether this radiation-induced increase is a function of impurities in the fluoride mixture or the temperature control of the irradiated specimen.

STABILITY UNDER REACTOR IRRADIATION

Stability of Chlorides⁷

In the only recorded irradiation of molten chlorides, a sample of LiCl-KCl eutectic was maintained at 1200°F for 14 days in an evacuated quartz capsule at a position in the ORNL graphite reactor where the thermal flux was 7×10^{11} neutrons/(cm²)(sec). No change in the cooling curve could be detected during or after irradiation, and there is no reason to believe that molten chloride mixtures are unstable to this relatively light dosage. No studies under fission-fragment bombardment have been reported, however.

STABILITY UNDER ELECTRON BOMBARDMENT⁷

The only recorded study of behavior of fused salts under electron bombardment is an irradiation for 1 hr by 50 μ amps of 2-mev electrons of a small sample of 3NaF-UF₄ in a nickel container. The ionization density measured calorimetrically was 120 watts/cc. Helium gas from the blanket in the target chamber was analyzed for fluorine, and although decomposition of as little as 0.05 percent of the irradiated portion of the sample could have been detected, no appreciable decomposition of the specimen was observed.

VOLATILITY OF FISSION PRODUCTS

One of the advantages claimed for high-temperature liquid fuels is that low-boiling poisons, especially Xe¹³⁵, will be continually removed from the fuel by volatilization. Qualitative observations during reactor irradiations (described above) showed that considerable activity was transmitted through the vapor lines to the reactor face by this mechanism. Only one experiment dealing directly with this subject has, however, been reported.⁸

PHYSICAL AND THERMAL PROPERTIES

Data on the physical and thermal properties of fused-salt mixtures which are of interest as reactor fuels are meager. It is noteworthy that the thermal conductivity of fused fluo-

rides is decreased markedly as the UF_4 concentration is increased, but insufficient data are available to ascertain whether other quadrivalent fluorides, such as ThF_4 , show this effect.

Vapor pressure equations for pure fluorides are presented in Table 6.3.5.

Table 6.3.5 — Vapor Pressures of Various Fluorides*

Substance	Temp. range, °C	$A \times 10^{-13}$	B
Uranium tetrafluoride†	1037–1185	9.171	7.792
Sodium fluoride‡	1396–1557	12.385	9.180
Potassium fluoride‡	1351–1503	9.168	8.019
Lithium fluoride‡	1353–1547	12.057	9.071
Rubidium fluoride‡	1163–1410	8.753	8.124
Beryllium fluoride†	920–1019	8.609	8.614
Zirconium tetrafluoride†	722–825	10.926	12.113
Aluminum fluoride‡	1094–1251	16.934	13.927
Magnesium fluoride‡	1661–1856	15.154	8.864
Zinc fluoride‡	1156–1465	9.922	8.477
Lead fluoride§	1078–1289	8.625	8.391

* Constants listed for equation $\log_{10} P(\text{mm Hg}) = -A/T(^{\circ}\text{K}) + B$

† H. von Wartenberg and H. Schulz, Z. fur Elektrochemie 27, 1921

‡ O. Ruff and L. LeBoucher, Z. anorg. Chem. 219, 1934

§ H. von Wartenberg and O. Bosse, Z. fur Elektrochemie 28, 1922

† R. E. More, Oak Ridge Nat. Lab., ORNL-1294, -1375, and -1439; K. O. Johnson, Y-F-42, Oct. 20, 1949

MODERATOR-COOLANTS

RADIATION STABILITY OF HYDROXIDES

Data on the radiation stability of pure sodium and potassium hydroxides at elevated temperatures are promising but relatively meager. No irradiations of alkaline-earth hydroxides, lithium hydroxide, or mixtures of hydroxides at elevated temperatures have been reported.

STABILITY UNDER REACTOR IRRADIATION

Sodium hydroxide at reactor ambient temperature has been shown to be unstable in the ORNL graphite reactor⁹ by irradiation as 0.5-gm samples contained in glass ampoules in a thermal flux of 3×10^{11} neutrons/(cm²)(sec).

The fast flux was estimated to be about 10 percent of the thermal value. After irradiation for one week, no volatile decomposition products could be observed; after one month, however, considerable gaseous products were evident.

Tests performed at higher temperature, where virtually complete recombination of volatile products would be expected, have been more satisfactory. A sample of sodium hydroxide, dehydrated in vacuo at 850°C, was exposed in an A-nickel container in the ORNL

graphite reactor for one week at 400°C and for an additional week at 700°C. The thermal flux available was 8.5×10^{11} neutrons/(cm²)(sec) with the fast flux estimated at 10 percent of the thermal value. Cooling curves taken at 48-hr intervals revealed no detectible change in composition during this interval.

Molten potassium hydroxide (containing less than 0.3 percent K₂CO₃ and 0.2 percent H₂O) showed no pressure rise when irradiated for 16 hr in a stainless-steel capsule at 450°C in the ORNL graphite reactor at a thermal flux level of 8×10^{11} neutrons/(cm²)(sec).¹⁰ A similar sample¹⁰ when exposed to a thermal flux of 1.2×10^{13} neutrons/(cm²)(sec) for about 60 hr at 425° to 450°C in the LITR showed a pressure rise of 3 psi. This same pressure rise was shown, however, in a similar test without irradiation.

STABILITY UNDER ELECTRON BOMBARDMENT

Molten sodium hydroxide has been shown to be stable when irradiated for several hours in continuously evacuated platinum containers with a 100-amp beam of 1-mev electrons from Van de Graaff equipment. Irradiations were performed at 700°, 815°, and 980°C with a calorimetrically determined ionization density of 30 watts/cc. A comparison of hydrogen and water vapor yields before, during, and after irradiation revealed that less than 1 percent of the material had decomposed as a result of irradiation. The material was similar in appearance in all respects to unirradiated caustic.

CONCLUSIONS

For use as moderator-coolants, molten hydroxide need not be stable to fission-product recoils, and the reactor could presumably be designed so that power dissipation in the caustic would not exceed 50 watts/cc. While radiation studies are badly needed over longer times and with more sensitive means for detection of damage, alkali hydroxides appear to be sufficiently stable to radiation to be applicable as reactor moderators.

CORROSION BY HYDROXIDES

Virtually all the conclusions regarding corrosion by hydroxides have been drawn from experiments with sodium hydroxide. The relatively small amount of data obtained from other hydroxides suggests that the same general principles apply and that the corrosion rates are quantitatively similar.

CORROSION OF STRUCTURAL METALS BY NaOH

For each metal, there appears to be a temperature above which it reacts with sodium hydroxide to liberate hydrogen. In the case of more noble metals, such as gold, silver, platinum, copper and nickel, this temperature is above 1000°F; in the case of more active metals, such as iron and aluminum, hydrogen evolution begins at 600° to 700°F. As a result of this reaction, the metal is oxidized to a variety of dark-colored complex oxides which often form surface layers and which are generally observable in the solid melt.

A large increase in corrosive action is evident when neutral or oxidizing atmospheres are maintained over the molten mixture. Maintenance of reducing conditions over the melt during the test is beneficial and prevents attack entirely on a number of noble metals at 1000°F. No metals tested have proved to be completely unattacked at 1500°F even under atmospheres of pure hydrogen.

Tables 6.3.6 and 6.3.7 list the results obtained when various alloys are tested for 24 hr under static conditions in an atmosphere of 90% N₂-10% H₂ at 1000°F and 1500°F, respectively.

Attempts to obtain quantitative data in support of an electromotive series for metals in molten hydroxides have not been successful. However, it is generally recognized that, of the common structural metals, only nickel resists corrosion to a satisfactory degree

Table 6.3.6—Behavior of Metals and Alloys in Sodium Hydroxide for 24 Hours at 1000°F

(BMI-706, Nov. 6, 1951)

Material	Condition	Area of specimen, sq cm	Weight change, mg/sq cm	Results of visual or metallographic examinations
Materials Showing Little or No Attack				
L-nickel	Sheet	11.28	+ 0.115	No attack
Silver, 999.5 fine	Sheet	12.87	+ .015	No attack
Electrolytic copper	Cold rolled	11.90	+ 1.54	0.0004-in. deposit of nickel
Copper, OFHC	Wrought	8.73	- 0.137	Bright; very slight nickel deposit
Chromium	Hot-rolled plate	6.95	- .115	Brown discoloration; fine trans-granular cracks, possibly from specimen preparation
Gold	Sheet	6.91	- .332	Brown discoloration; shallow pitting, < 0.0002-in.
Platinum	Sheet	7.11	+ .323	Brown discoloration; no attack
Monel	Sheet	12.04	- .157	Brown discoloration; no attack
Inconel	Sheet	11.15	+ .116	Brown discoloration; scale adherent on one end; slight low intergranular attack, 0.0009 in.
Zirconium	Sheet	10.02	+ .558	Oxide film; scale < 0.001 in.; no other attack
70 Au-30 Pt	Sheet	7.03	+ .355	Oxide film; altered surface structure, 0.0002-in. thick; no attack
90 Pt-10 Ir	Sheet	6.78	+ .530	Oxide film; no attack
Graphite	E.C.A. grade	7.25	+ .854	Caustic not completely removed
Aluminum	2S sheet	17.19	- .337	Caustic not completely removed; slight pitting
High-purity French aluminum	Sheet	9.76	- 1.680	No attack
Hastelloy B	Sheet	6.49	+ 0.030	No visible attack
Hastelloy C	Sheet	7.86	- .496	Scale = 0.00153-in.; no other attack
Palladium	Wire	0.553	+ 6.59	Very slight pitting
Colmonoy No. 6	Rod, weld	8.674	- 0.484	Etched; change in structure, 0.0046-in. deep
Colmonoy No. 5	Rod, weld	6.057	+ .627	No attack; surface layer of different structure, 0.002-in. deep
Chromel P	Wire	3.523	+ .085	Possible intergranular corrosion
Colmonoy No. 9	Rod, weld	5.239	+ .229	Brown scale, 0.0030-in. thick
Nickel-plated cold-rolled steel	Plate, 0.005 in.	15.449	+ .323	Good nonporous plate is 0.006 in. thick
Ni-Resist (Type III)	Cast	14.918	+ .060	Scale 0.0007 in. thick
Nickel-plated cold-rolled steel	Plate, 0.010 in.	15.999	+ .118	Nonporous plate 0.009 in. thick
Nickel-plated cold-rolled steel	Plate, 0.030 in.	20.662	- .150	Nonporous plate 0.024 in. thick
Elgiloy	Solution-annealed sheet	10.784	- .639	Black scale 0.0046-in. thick. Few shallow pits
Materials Showing Intermediate Attack or Oxidation (Scale Formation)				
Cast iron	Ground surface	11.27	- 2.13	Loose rust
Cast iron	Electropolished	12.00	- 3.02	Loose rust
Armco iron	Sheet	8.96	- 8.77	Loose rust; pitting more pronounced at grain boundaries - 0.0008 in. depth
304 stainless steel	Sheet	10.32	+ 5.35	Scale, 0.0003-in.; pitting attack and general intergranular precipitation
Vitallium	Plate	10.50	+ 12.95	Scale, 0.006 in.; pitting attack
347 stainless steel	Sheet	9.31	+ 13.38	Scale, 0.007 in.; no other attack
Beryllium	Sheet	9.60	- 5.67	Pitting and exfoliation attack
Inconel X	Sheet	12.34	- 7.80	Nonadherent scale, 0.001 in.
Cobalt	As-cast	9.18	- 4.238	No apparent attack
Cobalt	Hot-rolled	7.10	- 4.888	Pitting, max. depth 0.001 in.
446 stainless steel	Sheet	6.99	- 2.803	Heavy black scale

Table 6.3.6—(Continued)

Material	Condition	Area of specimen, sq cm	Weight change, mg/sq cm	Results of or metallographic examination
Hastelloy A	Sheet	6.97	-3.157	Shallow pitting, max. 0.0015 in. irregular deposition of nickel
Worthite	Cast bar stock	7.65	+2.798	Discontinuous tan scale; general intergranular corrosion
317 stainless steel	Sheet	7.82	-3.887	Heavy black scale; intergranular corrosion
80-20 brass	Sheet	10.08	-4.335	Dezincification, 0.003 in. deep
430 stainless steel	Sheet	10.94	+0.746	Dark, rusty scale, 0.0015 in. thick
Phosphur bronze (Grade C)	Sheet	10.11	+0.038	Nickel deposited
Al-Si bronze	Sheet	8.746	+15.28	Blistered; heavy zone of altered structure
410 stainless steel	Sheet	8.341	-4.75	Dark-brown scale, 0.0007 in. thick
Ni-Hard	Rod, weld	5.468	-3.639	Etched; dark band, 0.0046 in. thick
Stellite No. 6	Rod, weld	5.035	-11.142	Black scale, 0.0002 in. thick
Alumel	Wire	3.656	+0.355	Blue-black scale and intergranular corrosion, 0.0046 in. deep
Ni-Resist (Type I)	Cast bar	15.862	-2.664	Scale, 0.0015 in. thick
Ni-Resist (Type II)	Cast bar	15.938	-2.014	Scale, 0.0007 in. thick
Haynes alloy multimet	Sheet	6.000	+7.850	Black scale, 0.0075 in. thick
Haynes alloy No. 25	Forged plate	11.109	+9.172	Black scale, 0.0046 in. thick; surface structure change
Haynes alloy No. 25	Cast	12.389	+9.968	Black scale, 0.0061 in. thick
Haynes Stellite No. 31	Rod, weld	14.913	+6.765	Black scale, 0.0076 in. thick
Constantan	Sheet	9.140	+2.221	Bright
Nimonic 80 A	Hot-rolled	7.898	+11.509	Black scale, 0.0006 in. thick
Nimonic 90	Hot-rolled	8.348	+6.971	Black scale, 0.0030 in. thick
Graphitar	Grade 20	12.775	+14.13	No dimensional change
Graphitar	Grade 2	10.746	+16.61	No dimensional change
Graphitar	Grade 10	8.659	+31.08	No dimensional change
Graphitar	Grade 49	14.721	-13.409	NaOH retained by sample
Materials Severely Attacked or Dissolved				
Molybdenum	Sheet	9.867	-306.8	Severely attacked
Duriron	Cast	27.93	...	Exfoliation type of attack
Tungstun	Plate	22.13	-30.93	Exfoliation type of attack
Tantalum	Sheet	10.41	...	Completely dissolved
Titanium	Sheet	14.59	-23.7	Rapidly attacked
Manganese	Electrolytic	Completely dissolved
25-20 stainless steel	Sheet	9.35	-107.9	General uniform solution
Silicon	Cast	Rapid exothermic reaction
Nickel-plated cast iron	0.015-in. thick plate	12.36	...	Nickel plate ruptured
Nickel-plated cast iron	0.004-in. thick plate	12.33	...	Nickel plate ruptured
Invar	Bar stock	10.22	-27.7	Fine precipitation or edge attack
Columbium	Sheet	3.48	-52.8	Rapid attack
Vanadium	Cast button	Completely dissolved
Boron	Vapor-deposited rod	Completely dissolved
Cerium	97 percent	Completely dissolved
Illium	Sheet	9.68	-16.87	Exfoliation, intergranular attack, and cracking
Cartridge brass	Bar stock	19.31	-27.81	Complete dezincification
Magnesium	Extruded rod	10.55	...	Completely dissolved
Manganal	Rod, weld	5.012	-22.605	Gray scale
Hastelloy F	Sheet	9.887	+27.8	Black and gray scale, total depth 0.0145 in.
Ni-Resist (Type II, ductile)	Cast	11.879	-83.84	Thin brown scale
Elgiloy	Rolled sheet	7.842	+5.547	Thick gray scale
Elgiloy	Age hardened	9.778	...	Very brittle; some pieces lost
60Cr, 25Fe, 25Mo, 0.04C	Cast	8.032	-112.4	Thick black scale

Table 6.3.7 — Behavior of Metal and Alloys in Sodium Hydroxide for 24 Hours at 1500°F

(BMI-706, Nov. 6, 1951)

Material	Condition	Area of specimen, sq cm	Weight change, mg/sq cm	Remarks	
				Visual examination	Metallographic examination
Materials Showing the Least Attack					
L-nickel	Sheet	7.700	+ 1.662	Gray scale in spots	Intergranular attack, 0.0031 in. deep
Copper, OFHC	Wrought	10.781	-2.161	Black scale plus nickel deposit	Shallow pitting; nickel deposit, 0.0003 in. thick
Zirconium	Sheet	8.828	+ 0.872	Grayish scale	Scale, 0.00015 in. thick; nitride layer, 0.00045 in. thick; slight pitting
Silver	Sheet	8.987	+ 2.894	No change	Zone of altered structure, 0.006 in. deep; intergranular corrosion, 0.02 in. deep
Monel	Sheet	14.492	-4.574	General solution	Zone of altered structure, 0.0075 in. deep
Materials Severely Attacked or Dissolved					
Colmonoy No. 5	Rod, weld	5.834	+ 70.46	Thick gray scale	Pitting; change in structure, 0.062 in. deep
Colmonoy No. 6	Rod, weld	7.994	-71.85	Thick gray scale	Pitting; change in structure, 0.062 in. deep
Colmonoy No. 9	Rod, weld	5.534	...	Completely dissolved	No examination made
Inconel	Sheet	6.879	...	Completely dissolved	No examination made
Gold	Sheet	5.706	...	Specimen broke	Pitting; altered structure; no gold color
Platinum	Sheet	5.442	...	Specimen broke	Pitting and altered structure, 0.003 in. deep
Palladium	Rod	2.865	+ 175.3	Etched	Zone of altered structure, 0.014 in. deep; possibly from nickel diffusion
Chromium	Hot-rolled plate	8.057	-40.37	Black scale; surface cracks	Black scale, 0.0015 in. thick; cracks from surface
70 Au-30 Pt	Sheet	5.676	...	Heavy scale; broke into pieces	Blistered; pitting attack
90 Pt-10 Ir	Sheet	5.294	+ 27.18	Blistered	Irregular deposition or blistering; pitting
Hastelloy B	Sheet	5.564	-53.0	Loose powdery deposit	Rounded corners; pitting; longitudinal crack and change in structure
Chromel P	Wire	3.441	...	Completely dissolved	No examination made
Ni-Resist (Type III)	Cast	11.682	-84.09	Etched	Change in structure, 0.107 in. deep
Graphite	E.C.A. grade	10.400	...	Completely dissolved	No examination made
Nimonic 80A	Hot-rolled	9.859	...	Completely dissolved	No examination made
Nimonic 90	Hot-rolled	9.002	...	Completely dissolved	No examination made
Elgiloy	Solution-annealed sheet	7.934	...	Completely dissolved	No examination made
Haynes Stellite No. 31	Rod, weld	12.947	...	Completely dissolved	No examination made
Inconel	Sheet	9.310	...	Completely dissolved	No examination made

at temperatures above 1000°F. The low tensile and creep strength of nickel at such temperatures impose very difficult design problems insofar as reactors are concerned.

As the data in Table 6.3.8 indicate, the rate of attack of L-nickel by sodium hydroxide increases rapidly with increasing temperature, considerably with decrease in partial pressure of H₂ from 760 mm to 76 mm, and slowly with contact time. The rate of attack appears to be nearly independent of the extent of cold working of the nickel.

Effect of NaOH on Mechanical Properties of L-Nickel

Mechanical properties of L-nickel initially in an annealed and a 50-percent cold-worked condition have been examined after annealing at 1000°F and 1250°F in argon and after dynamic exposure to caustic at these temperatures under various dry atmospheres. Comparison of the data shown in Tables 6.3.9 and 6.3.10 reveals that, while L-nickel does not anneal to the same extent in the two media, these mechanical properties are not adversely affected and that there is no evidence for caustic embrittlement even in the cold-worked specimens.

Table 6.3.8 — Dynamic* Corrosion of L-Nickel in Sodium Hydroxide† As Function of Atmosphere and Temperature

(BMI-794, Dec. 18, 1952)

Condition of material	Atmosphere above caustic	Temperature, °F	Change in weight, mg/sq cm ‡					
			Scale not removed					Scale removed§
			24 hr	48 hr	96 hr	120 hr	168 hr	168 hr
Annealed	Forming gas	1000	-0.242	-1.27	-1.27	-1.30	-1.27	-4.79
50% cold work	Forming gas	1000	-.19	-1.09	-1.11	-1.13	-1.13	-5.04
Annealed	Hydrogen	1000	-.125	-0.100	-0.108	-0.162	-0.181	-2.26
50% cold work	Hydrogen	1000	-.073	-.049	-.078	-.140	-.151	-2.42
Annealed	Nitrogen	1250¶	-3.2	-10.7	-21.7	-26.6	-42.3	-45.9
50% cold work	Nitrogen	1250¶	-2.5	-9.7	-20.5	-25.0	-39.4	-42.3
Annealed	Forming gas	1250¶	-5.0	-5.4	-6.3	-6.6	-7.1	...
50% cold work	Forming gas	1250¶	-4.8	-5.1	-6.0	-6.3	-6.7	...
Annealed	Hydrogen	1250¶	-0.62	-1.08	-1.77	-1.06	-1.55	-6.24
50% cold work	Hydrogen	1250¶	-.62	-1.27	-1.95	-1.24	-1.66	-5.62
Annealed	Hydrogen**	1250¶	-.93	-16.3	-18.7	-18.8	-19.1	-21.5
50% cold work	Hydrogen**	1250¶	-.40	-14.7	-16.6	-16.7	-17.0	-19.0
Annealed	Forming gas	1500¶	-111.3	-141.5
50% cold work	Forming gas	1500¶	-68.5	-94.9
Annealed	Hydrogen	1500¶	-1.8	-2.7	-3.6	-8.5	-12.6	-15.0
50% cold work	Hydrogen	1500¶	-1.6	-2.4	-3.2	-7.8	-11.6	-14.6

*Specimens immersed in caustic and rotated 30 ft/min

†Bakers Special stick sodium hydroxide used

‡Each value reported is averaged of 3 independent determinations

§Scale removed by treatment at 210°F with 10% HNO₃ solution containing 1 teaspoonful NaCl per liter

¶Caustic cooled to 1000°F before samples were removed

**Sodium hydroxide used contained 5% by weight of metallic sodium

Table 6.3.9—Mechanical Properties of L-Nickel After Argon Annealing
(BMI-794, Dec. 18, 1952)

Condition of material	Mechanical properties*			
	Tensile strength, psi	0.2% offset yield strength, psi	Elongation, % in 1 in.	VHN
Initial properties				
Annealed	57,800	35,400	45	122
50% cold work	94,300	93,300	3.3	209
After anneal in argon at 1000°F†				
Annealed	57,300	25,000	46	100
50% cold work	58,800	16,900	40	90
After anneal in argon at 1250°F†				
Annealed	56,100	23,400	46.5	91.4
50% cold work	58,800	13,600	42	76

*Average of values from 3 specimens

†Annealed for 360 hr at 1000°F or 168 hr at 1250°F

Table 6.3.10—Effect of Exposure* to Sodium Hydroxide† on Mechanical Properties of L-Nickel
(BMI-794, Dec. 18, 1952)

Condition of material	Atmosphere above caustic	Temperature, °F	Change in weight, mg/cm ²	Mechanical properties‡			
				Tensile strength, psi	0.2% offset yield strength, psi	Elongation, % in 1 in.	VHN
Annealed	Argon	1000	-0.03	57,900	28,400	44	106
50% cold work	Argon	1000	-.08	78,900	66,300	12	182
Annealed	Argon	1250	-86	53,700	20,400	42	80
50% cold work	Argon	1250	-80	50,400	12,800	39	77
Annealed	Forming gas	1250	-1.0	55,100	21,500	46	84
50% cold work	Forming gas	1250	-3.9	55,300	15,400	44	75
Annealed	Air	1250	-155	50,700	19,200	41	83
50% cold work	Air	1250	-116	50,800	15,000	40	76

*Specimens rotated at 30 ft/min while immersed in caustic for 360 hr at 1000°F or 168 hr at 1250°F

†Bakers Special stick hydroxide: 98% NaOH, 0.0002% PO₄, 0.000% SO₄, 1.5% Na₂CO₃, 0.007% SiO₂, 0.000% heavy metals as Ag, 0.001% Cl, 0.006% Fe, 0.0003% nitrogen

‡Average of values from 4 specimens

Mechanism of Attack of Ni by NaOH

In molten sodium hydroxide above 1000°F, metallic nickel, as well as most other noble metals, is removed in a uniform fashion from the hottest portion of the test specimen. When the hydrogen produced is removed—for example, by sweeping with inert gas or by evacuation—deposits of nickel oxide are observed. When the hydrogen is retained in the system or when a reducing atmosphere is supplied, crystals of nickel are formed on cooler portions of the apparatus; at 1500°F, these deposits are quite copious unless a pure hydrogen atmosphere is maintained or thermal gradients are carefully avoided. This “mass-transfer” phenomenon is not well understood but almost certainly does not result from “physical” solubility of Ni^0 in the caustic.

Effect of Added Materials

The most harmful impurity in sodium hydroxide, assuming the absence of sodium peroxide, is generally believed to be Na_2O . Perhaps because of this, traces of water in the caustic appear beneficial although larger amounts appear to cause increased attack.

The presence of carbonate in the amounts found in C.P. sodium hydroxide appears to have little effect.

Additions of metallic sodium and of sodium hydride apparently result in increased corrosion.

In a few tests, addition of sodium aluminate to sodium hydroxide appeared beneficial; under most conditions this improvement is not observed.

CORROSION OF CERAMICS BY NaOH

The data in Table 6.3.11 show the behavior of a number of ceramic materials in static systems of nickel containing sodium hydroxide at 1000°F. Aluminum oxide and zirconium oxide are most resistant, although graphite and $\text{MgO-Al}_2\text{O}_3$ mixtures approaching the composition of spinel are also satisfactory. No ceramic which lasts more than a few hours at 1500°F has been found.

CORROSION BY OTHER HYDROXIDES

As the data in Table 6.3.12 indicate, the behavior of $\text{Ba}(\text{OH})_2$, $\text{Sr}(\text{OH})_2$ and LiOH in static tests at 1500°F is similar to that of NaOH , described above. Although some evidence suggests that KOH may be contained for 1000 hr in Inconel under an inert atmosphere at temperatures as high as 1250°F without destructive attack, “caustic embrittlement” of this alloy has been reported at 800°C. No experiments on corrosion by mixtures of hydroxides have been reported.

PHYSICAL AND THERMAL PROPERTIES OF HYDROXIDES

Melting points and heat capacities of various pure hydroxides are listed in Table 6.3.13 and the densities and viscosities of sodium and potassium hydroxides are listed in Table 6.3.14. Except for melting points (see Chapter 6.2), physical or thermal properties of hydroxide mixtures have been reported. The thermal conductivity of sodium hydroxide is $0.81 \text{ Btu}/(\text{hr})(\text{ft})(^\circ\text{F})$.¹¹ Values for other hydroxides are lacking.

COOLANTS

RADIATION STABILITY

Only one fused-salt specimen of possible interest as a reactor coolant (see “Stability of Chlorides,” above) has been studied under irradiation. However, since coolants would

Table 6.3.11 — Behavior of Ceramic Materials in Sodium Hydroxide at 1000°F for 24 Hours*

(BMI-794, Dec. 18, 1952)

Material	Treatment	Apparent porosity, %	Bulk density	Initial weight, gm	Change in weight, %	Visual observations
Materials Showing the Least Attack						
Alundum, Al_2O_3	Hot pressed	8.3510	-0.06	No change
Single-crystal Al_2O_3	0.4807	-.40	Surface etched
Alundum, Al_2O_3	Sintered	12.0325	-.16	No change
Stabilized ZrO_2 , tan	Fired, 3090°F, air	<0.5	...	2.4453	-.14	No change
Stabilized ZrO_2 , dark	Fired 3090°F, argon	< .5	...	2.9676	-1.35	No change
71.7% Al_2O_3 :28.3% MgO	Fired 3100°F	4.5	3.24	3.6022	-0.09	No observable change
74.5% Al_2O_3 :25.5% MgO	Fired 3100°F	0.047	3.33	3.3533	-.48	No observable change
75.9% Al_2O_3 :24.1% MgO	Fired 3100°F	.13	3.36	3.9972	-.29	No observable change
77.3% Al_2O_3 :22.7% MgO	Fired 3100°F	1.9	3.33	4.1000	-.26	No observable change
71.7% Al_2O_3 :28.3% MgO	Fired 3000°F	8.91	3.15	3.9389	...	Broke into three pieces
74.5% Al_2O_3 :25.5% MgO	Fired 3000°F	5.59	3.21	4.6970	-0.52	No observable change
77.3% Al_2O_3 :22.7% MgO	Fired 3000°F	7.48	3.25	4.6146	-.41	No observable change
Materials Appreciably Attacked or Dissolved						
75.9% Al_2O_3 :24.1% MgO	Fired 3000°F	6.19	3.24	4.9458	-13.2	No observable change
BeO crucible	0.9921	-39.1	General solution
90% Al_2O_3 :10% Al	Fired 1800°F	36.6	2.00	4.1943	...	Decomposed on contact with water
80% Al_2O_3 :20% Al	Fired 1800°F	22.3	2.08	3.6049	...	Decomposed on contact with water
79.08% Al_2O_3 :20.9% Al	Fired 1000°F	35.52	2.32	3.6457	...	Decomposed on contact with water
71.2% Al_2O_3 :28.8% Al	Fired 2400°F	30.52	2.62	3.3507	...	Decomposed on contact with water
CaO	Fired 3450°F	3.0	...	2.9407	-46.3	Severely attacked
TiN	...	4.0	...	3.4704	-100	Completely dissolved
TiC	...	0.5	...	3.5662	-100	Completely dissolved
ZrC	...	15.0	...	3.6962	-100	Completely dissolved
70% Fe_2O_3 :20% ZnO:10% NiO	Compressed and sintered	15.1392	...	Badly cracked; pieces fell out
70% Fe_2O_3 :20% ZnO:10% NiO	Fired 4 hr 2450°F, air	11.5007	...	Cracked into pieces
Tungsten carbide	97% WC, 3% Co	34.0609	-3.32	Matte-gray surface
TiC mix (65% TiC: 15% CbC + TaC:20%Ni)	21.9519	-3.32	Bright-appearing specimen
ZnO	Compressed and sintered	4.0868	-8.00	...
Cu_2O	Compressed and sintered	9.7112	-100	Changed to a sponge-like mass
$NaSbO_3$	Compressed and sintered	5.0413	-100	Completely dissolved
TiO_2 , Batch 1	Vacuum-sintered, 3 hr 1400°F	15.9163	-100	Completely dissolved
TiO_2 , Batch 2	Vacuum-sintered, 2 hr 1400°F	18.9496	...	Thick white scale; specimen heavily attacked
B_4C , Norbide	Hot pressed	7.2145	-32.9	...
Mixed borides ($B_4C + TiB_2$)	Hot pressed	5.442	-100	Completely dissolved
Bonded Al_2O_3	AXF 2616	5.8060	-100	Completely dissolved
SiC, Cystalon	2.0971	-1000	Completely dissolved
MgO	Sintered 4100°F, argon	8.2838	-4.11	Surface glasslike

* Forming-gas atmosphere (90% $N_2 + 10\% H_2$) above caustic; specimens suspended on nickel wires; caustic contained in individual nickel crucibles; Eimer and Amend sodium hydroxide pellets of the following analysis used:

Assay (NaOH)	97.6%	Phosphate (PO_4)	0.000%
Chloride (Cl)	0.005%	Silica + NH_4OH ppt.	.000%
Iron (Fe)	.001%	Total nitrogen (as $NH_3 \cdot NO_3$)	.001%
Other heavy metals (as Ag)	.000%	Sulfate (SO_4)	.000%
Carbonate (Na_2CO_3)	.32%		

Table 6.3.12 — Corrosion of Structural Metals* by Various Hydroxides†
(ORNL-1170, Dec. 10, 1951)

Hydroxide used	Structural metal	Weight change, g/in. ²	Depth of specimen affected, mils	Metallographic observations
Ba(OH) ₂	304 stainless steel	...	5.5	0.010-in. oxide layer
	316 stainless steel	...	9.0	0.010-in. oxide layer
	347 stainless steel	-0.083	4.7	0.006-in. oxide layer
	446 stainless steel	...	5.0	0.008-in. oxide layer
	Iron (Globe)	-0.994	8.5	Heavy oxide formed
	Zirconium†	-.221	9.0	0.001-in. gray oxide layer
	Hastelloy-B	-1.109	9.5	Heavy oxide formed
	Inconel-X	...	6.5	0.020-in. oxide layer
	Nickel-Z	...	6.0	Erratic attack, 0.002 in average
	Monel	-0.005	0.0	No evidence of attack
	Copper (O.F.H.C.)	-.003	.5	No evidence of attack
Sr(OH) ₂	304 stainless steel	...	12.0	Heavy oxide layer
	316 stainless steel	...	3.0	0.003-in. oxide layer
	347 stainless steel	...	7.0	0.020-in. oxide layer
	446 stainless steel	...	4.0	0.011-in. oxide layer
	Iron (Globe)	...	2.0	Heavy oxide layer, 0.017 in. deep
	Zirconium†	...	7.0	0.001-in. oxide layer
	Inconel X	...	3.0	0.007-in. oxide layer
	Hastelloy B	...	9.0	Specimen heavily oxidized
	Copper (O.F.H.C.)	...	0.0	No evidence of attack
	Nickel A0	No evidence of attack
	Nickel Z	...	1.5	0.002-in. oxide layer
LiOH	304 stainless steel	-0.185	4.5	0.014-in. oxide layer
	Inconel	+.043	4.0	0.006-in. oxide
	Nickel-A	-.001	0.0	No evidence of attack

* Test specimens were exposed in sealed, evacuated capsules of the same metal except as specified

† Exposed for 100 hr at 1500°F under static conditions

‡ Samples exposed in capsules of nickel

Table 6.3.13 — Melting Points and Heat Capacities of Pure Hydroxides¹¹

Compound	Melting point, °C	Heat Capacity	
		Cal/(gm)(°C)	Temperature interval, °C
LiOH	473	0.85 ± 0.06	500 - 900
NaOH	323	.49 ± .02	340 - 990
KOH	380	.35 ± .02	400 - 950
Sr(OH) ₂	510	.32 ± .03	570 - 900
Ba(OH) ₂	395	.20 ± .01	470 - 900

Table 6.3.14 — Density, Viscosity, and Vapor Pressure of Sodium and Potassium Hydroxides

	Sodium hydroxide	Potassium hydroxide
Density, gm/cc	$\left\{ \begin{array}{l} 320^{\circ}\text{C} - 1.786^{*} \\ 400^{\circ}\text{C} - 1.746^{*} \\ 450^{\circ}\text{C} - 1.722^{*} \end{array} \right.$ $\left\{ \begin{array}{l} 320^{\circ}\text{C} - 1.90^{\dagger} \\ 360^{\circ}\text{C} - 1.88^{\dagger} \\ 400^{\circ}\text{C} - 1.86^{\dagger} \\ 440^{\circ}\text{C} - 1.84^{\dagger} \end{array} \right.$	$\left\{ \begin{array}{l} 400^{\circ}\text{C} - 1.77^{*} \\ 500^{\circ}\text{C} - 1.673^{*} \\ 550^{\circ}\text{C} - 1.651^{*} \\ 600^{\circ}\text{C} - 1.629^{*} \end{array} \right.$ $\left\{ \begin{array}{l} 400^{\circ}\text{C} - 1.85^{\dagger} \\ 440^{\circ}\text{C} - 1.81^{\dagger} \end{array} \right.$
Viscosity*, cp	$\left\{ \begin{array}{l} 350^{\circ}\text{C} - 4.0 \\ 450^{\circ}\text{C} - 2.2 \\ 550^{\circ}\text{C} - 1.5 \end{array} \right.$	$\left\{ \begin{array}{l} 400^{\circ}\text{C} - 2.3 \\ 450^{\circ}\text{C} - 1.7 \\ 500^{\circ}\text{C} - 1.3 \end{array} \right.$ $\left\{ \begin{array}{l} 550^{\circ}\text{C} - 1.0 \\ 600^{\circ}\text{C} - 0.8 \end{array} \right.$
Vapor pressure \ddagger	$\log_{10}P_{\text{mm}} = \frac{-6,894}{T^{\circ}\text{K}} + 7.030$ (1010° - 1402°C)	$\log_{10}P_{\text{mm}} = \frac{-7,103}{T^{\circ}\text{K}} + 7.330$ (1170° - 1327°C)

* Arndt and Ploetz, Z. physik. Chem. 121, 1926

\dagger Meyer and Heck, Z. physik. Chem. 100, 1922

\ddagger von Wartenberg and Albrecht, Z. Electrochem. 27, 1921

probably receive a radiation dosage of less than 100 watts/cc, it is likely, in view of the radiation stability of uranium-bearing fluoride systems, that non-uranium bearing fused salts would prove satisfactory in this regard.

PHYSICAL AND THERMAL PROPERTIES

Physical properties of commonly considered coolants are listed in Table 6.3.15. Thermal-conductivity values for fused salts compare favorably with those for water and sodium hydroxide but are much less than that of sodium and three to four times less than those of heavy metals. The absolute viscosities of these salt mixtures are 10-fold higher than those of heavy metals.

The system $\text{Li}^{\dagger}\text{F}-\text{BeF}_2$, with its resultant low induced activity, would seem to be a promising coolant mixture.

BREEDER BLANKETS

No experiments other than phase equilibrium studies have been reported for systems containing thorium fluoride. Since radiation stability of fluoride fuel systems has been established at low power levels, it is likely that fused-salt breeder blankets would be satisfactory in this respect.

Corrosion by fluoride mixtures containing ThF_4 should be no worse than that exhibited by systems containing UF_4 ; it is likely that the ThF_4 systems would resemble the uranium-free ZrF_4 mixtures in this respect.

Physical and thermal properties of concentrated ThF_4 solutions are probably similar to those of similar concentrated UF_4 systems. The relatively high viscosities and low thermal conductivities, as well as the generally high melting points, of these mixtures will probably be major disadvantages.

Table 6.3.15 — Heat-transfer Properties of Various Coolants

(R. C. Briant. Oak Ridge Nat. Lab., CF-52-19-9, Dec. 1, 1952)

Coolant	Melting point, °c	Thermal conductivity, Btu/(hr)(°F)(ft)	Viscosity, cp	C _p , cal/(gm)(°C)	Density, g/cc	C _p × D, cal/(°C)(cc)
Air	...	0.04	0.04	0.29	0.00032	0.60008
H ₂ O*	0	.35	.7	1.0	1.0	1.0
NaOH	323	.7	1	0.49	1.7	0.83
Hg†	...	7.5	1	.032	13	0.42
Pb	327	8.6	1.2	.037	10	.37
Na	98	34.5	0.2	.30	0.78	.23

*At 100°F

†At 500°F

REFERENCES

1. J. D. Redman, L. G. Overholser et al, ORNL-858, Nov. 29, 1950, p 107 (classified).
2. J. D. Redman, L. G. Overholser et al, ORNL-919, Feb. 26, 1951, p 235 (classified).
3. J. D. Redman, L. G. Overholser et al, Unpublished Work, ORNL (classified).
4. J. D. Redman, L. G. Overholser et al, Unpublished Work, ORNL (classified).
5. J. D. Redman, L. G. Overholser et al, ORNL-1170, Feb. 18, 1952, p 83 (classified).
6. W. E. Browning, Chemical Radiation Damage to Molten Compounds, Fairchild Engine and Airplane Corp., TID-5021, Mar. 6, 1951, p 44.
7. W. E. Browning, op. cit., p 45.
8. M. T. Robinson and D. D. Davies, Oak Ridge Nat. Lab., ORNL-1359, Jan. 15, 1953 (classified).
9. O. Sisman and C. D. Bopp, Oak Ridge Nat. Lab., ORNL-528, Dec. 10, 1950, 41 pp (classified).
10. G. W. Keilholtz et al, Oak Ridge Nat. Lab., ORNL-1261, Sept. 25, 1952, 44 pp (classified).
11. H. F. Poppendiek et al, Oak Ridge Nat. Lab., CF-52-8-212, Aug. 28, 1952, 9 pp (classified).

Section 7

HANDLING AND CONTROL

Prepared by
REMOTE CONTROL ENGINEERING DIVISION
ARGONNE NATIONAL LABORATORY

AUTHORS' PREFACE

The development of suitable means for process operation or control, at a distance or from behind a shield, is prerequisite to the solution of many problems in nuclear reactor technology. The four chapters of this section cover (1) viewing equipment for safely observing them in process, (2) the handling of materials which are highly radioactive, (3) integrated "hot laboratories," and (4) nuclear reactor control equipment, methods, and systems. The material of these topics constitutes an infant technology rather than an established science, and its application at the various laboratories and reactor sites depends on the particular requirements and a proper weighing of cost and performance factors.

The chapter material was prepared by several authors under the general direction of H. I. Hull, with D. F. Uecker assisting in coordination and scheduling.

Chapter 7.1, "Remote Handling," is believed to be the first published attempt at correlating the various manipulator designs that are in existence and in use. A nearly complete catalog of manipulators developed during the past five years is included. The authors are indebted to the many designers and operators who supplied the information on construction and performance necessary to such a listing.

Chapter 7.2, "Remote Viewing," examines five basic viewing methods that have found wide application in this field. Advantages and limitations for each are given, especially for use in conjunction with various shielding materials and manipulators. The authors used material on periscopes published by J. M. Holeman of Hanford Works as background, and are indebted to W. B. Doe and L. M. Safranski of Argonne National Laboratory for data on zinc bromide and radiation-resistant glass.

Chapter 7.3, "Hot Laboratories," attempts to show the range in end-product that has resulted at the various sites when the building-blocks of viewing, manipulation, and shielding are combined in various ways. The five installations described are the first modern, high-level experimental facilities constructed at their several sites, and the operating experience which is accumulating may allow the future designer to narrow the field of choice. The author wishes to thank R. T. Jones of Westinghouse Atomic Power Division, T. J. E. Glasson of Knolls Atomic Power Laboratory, and J. S. Gifford of Hanford Works who reviewed the chapter and supplied detailed information on their respective installations.

Chapter 7.4, "Nuclear Reactor Instrumentation and Control," is believed to be a first attempt to assemble this type of design data, and the author hopes that his colleagues in the field will take the initiative in checking these design values so that better ones will be available in the future.

The author thanks R. K. Swank, L. E. Johnson, A. C. Lapsley, H. Bryant, S. G. Kaufmann, and W. C. Redman for helping him assemble data on instruments; J. R. Dietrich for assistance on the reactor physics; T. Brill, J. S. DeShong, and W. C. Lipinski for helping with the other phases of control. All of these men on the Argonne National Laboratory staff gave generously of their time in both editing and consultation.

Invaluable advice and assistance was also obtained from M. A. Schultz at Westinghouse Atomic Power Division and E. P. Epler at Oak Ridge National Laboratory. The author re-

AUTHORS' PREFACE

grets that, owing to lack of time, he was unable to lean more heavily upon these control specialists for assistance and ideas.

In all of the above, an attempt has been made to include developments through late 1952. Where a field has been recognized as being especially in a state of flux, or where development work still in progress was included, the several authors have generally so qualified their remarks.

For the Remote Control Engineering Group

H. L. Hull*

D. F. Uecker

*Present address, Farnsworth Electronics Company, Ft. Wayne, Ind.

Remote Handling

R. C. Goertz and F. Bevilacqua

A continuing need exists for equipment with which to handle the radioactive specimens and assemblies encountered in reactor development and operation. Obviously, any human participation in such handling operations must occur behind a barrier or at a considerable distance. Two alternatives are open to the person faced with a remote handling operation: He may design a special-purpose machine to accomplish only the specific task at hand, or he may use one of the general-purpose manipulators which are, however crude, mechanical arms capable of many of the operations that the man could perform.

The advantage may lie with the special-purpose machine if the handling task is: (1) beyond the ability, in precision or speed, of the operator or (2) sufficiently repetitive to justify the time and cost of construction. These requirements are characteristic of many of the AEC's production operations. Of the many possible examples, however, only selected reactor-refueling equipment is illustrated in this chapter since that handling task is common to the design of all heterogeneous reactors.

If, as is usual in reactor development, the handling task is not well known in advance or if it varies widely and frequently and is so complex that construction of a special-purpose machine would be prohibitively expensive, the more versatile general-purpose manipulator is indicated. The illustrations given here comprise a nearly complete catalog of those general-purpose manipulator designs completed during the last five years. It is possible that some of these may be useful in future applications with little or no modification.

REACTOR REFUELING SYSTEMS

The complexity of a refueling system can vary over a wide range. The basic refueling techniques, however, can be grouped into four major categories: (1) "Through-hole refueling" in which fuel is charged into holes on the cool side of the reactor, simultaneously discharging spent fuel from the hot side; (2) "single-end refueling" in which a shielding coffin is used to protect personnel; (3) "single-end refueling" in which the refueling operation takes place in a shielded room from which personnel are excluded; (4) "single-end refueling" in which refueling takes place beneath a light-water shield. An example of the last category has been selected for detailed description below. The design details, which are included to indicate the general complexity of the system are not typical beyond that extent but are, instead, completely dependent on the requirements of the reactor and the fuel elements with which it operates.

SINGLE-END REFUELING USING A LIGHT-WATER SHIELDING TANK

Representative of this system is that of the MTR reactor described in detail in the Oak Ridge National Laboratory Manual ORNL-963 entitled *Materials Testing Reactor Project*

Handbook and shown schematically in Figs. 7.1.1 and 7.1.2. Although this particular reactor is a 30,000-kw unit designed specifically for materials testing, a similar fuel-handling technique could be applied to large production reactors which use light-water moderation and cooling.

The basic advantage of this type of system is the economy resulting from the use of light-water shielding through which personnel above the reactor can work safely. Such a system allows the use of locally controlled apparatus for unloading with direct observation of the procedure through the shielding water.

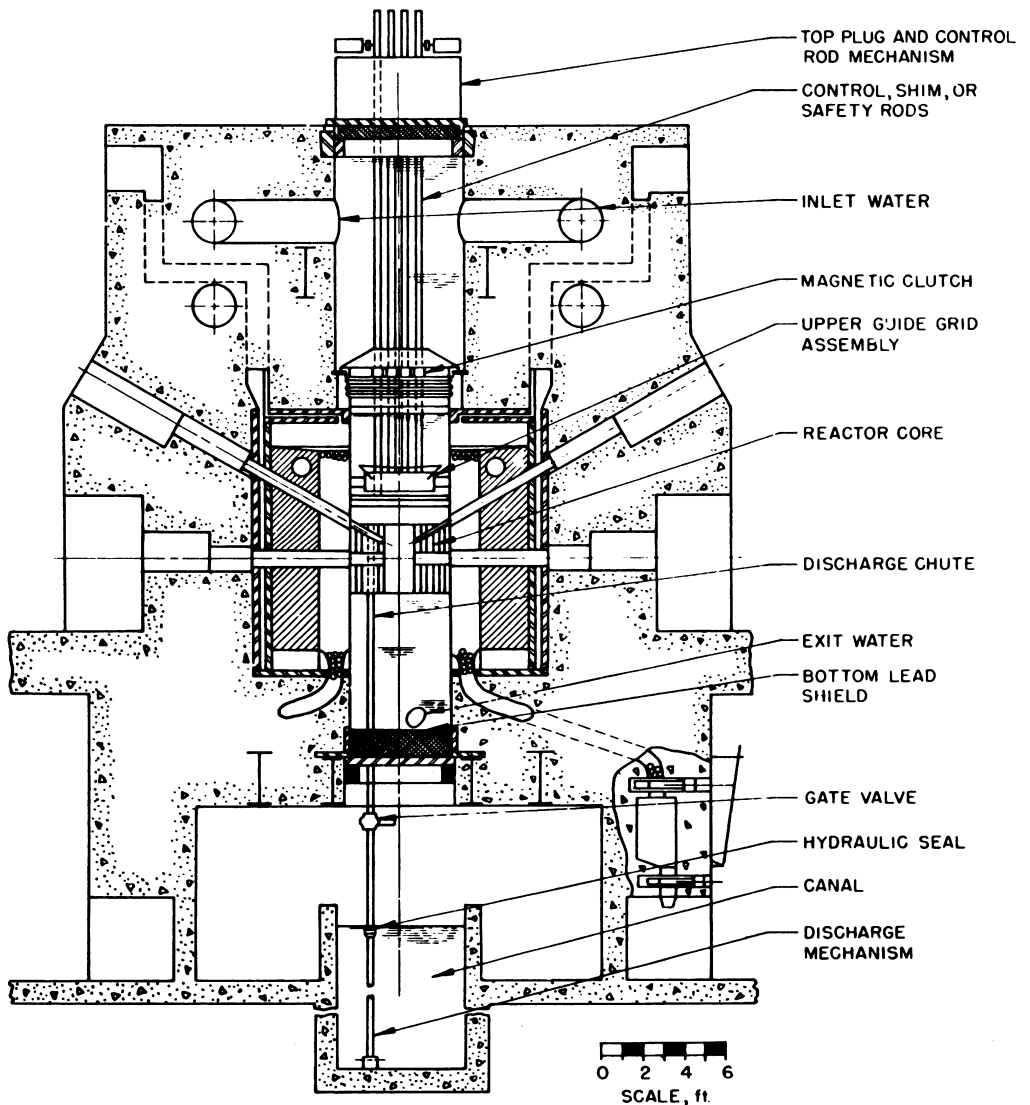


Fig. 7.1.1 — MTR Schematic.

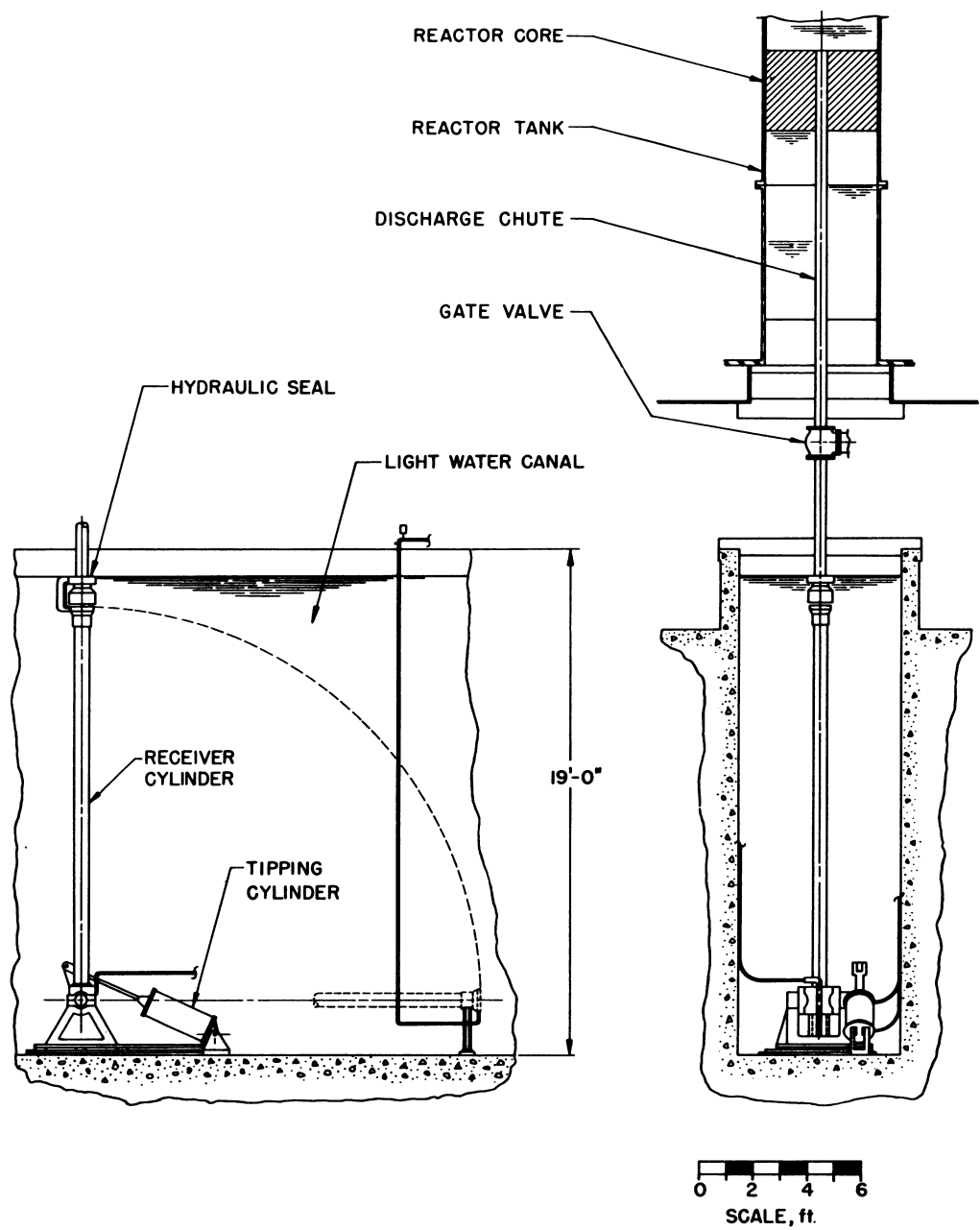


Fig. 7.1.2 — Discharge Mechanism.

TYPE OF REACTOR

Light-water moderated and cooled, single-end, vertical fuel-loading reactor.

TYPE OF ELEMENTS HANDLED

1. Fuel assemblies consisting essentially of 18 aluminum-clad enriched-uranium plates, approximately 0.060 in. thick, spaced 0.118 in. apart, and brazed into aluminum side plates to form a fuel element approximately 3 in. \times 3 in. \times 48 in. long.

2. Shim rods approximately 3 in. \times 3 in. \times 13 ft long.

3. Safety rods approximately 3 in. \times 3 in. \times 13 ft long.

EQUIPMENT REQUIRED

1. A large crane to remove the top plug.

2. A small crane to aid in handling fuel and other reactor elements.

3. A variety of long-handled tools for grappling the fuel elements under 17 ft of water.

4. An underwater light assembly to provide adequate illumination.

5. A special discharging mechanism for transferring the reactor elements from the reactor discharge hole to the canal. This mechanism consists essentially of an assembly receiver cylinder which can be rotated from a vertical to a horizontal position; within the cylinder is a hydraulically operated piston

SHIELDING REQUIREMENTS

A biological shield of steel and concrete surrounds the reactor to absorb the neutron and gamma fluxes escaping through the reflector during operation. The shield reduces these radiations to a level safe for personnel and at which sensitive instruments can be operated outside the shield.

The top of the reactor is shielded by approximately 17 ft of light water and a 12-in.-thick lead-shot-filled stainless-steel plug used to support the control rods and their drive mechanisms. With the reactor shut down the water alone provides adequate shielding for personnel working on top of the reactor. The bottom of the reactor is shielded by approximately 6 ft of light water and an 18-in.-thick lead-shot-filled stainless-steel plug.

Under the reactor runs a canal which is sufficiently deep so that personnel can handle submerged fuel elements safely. The top of the canal is approximately 7 ft below the bottom of the reactor.

CONTROL SYSTEM

All operations are performed manually or with small power tools except for the element transfer in the sub-reactor room. This operation is controlled from a station adjacent to the reactor and the canal. Pushbuttons on the panel control the following:

(1) Elevating or lowering the receiver cylinder.

(2) Opening or closing of the seal at the discharge chute and receiver junction.

(3) "Raising" or "lowering" the piston in the receiver cylinder.

(4) Purging the discharge-chute.

(5) Opening or closing the discharge-chute gate valve.

The position of the piston in the receiver cylinder is indicated on a dial mounted on the control board. Indicator lights on the control board provide information about the other operations. Interlocks are provided to ensure proper sequence of operations. Indicator lights and telephones provide additional communication between the operators at the top of the reactor and those at the control panel.

TYPICAL OPERATING SEQUENCE

The reactor is shut down and allowed to cool. During this time, water pressure is relieved, and the shim rods and regulator rods are de-clutched, allowing them to rest in their lowest position. The top plug with the control mechanism is unbolted, lifted, and carried by the main crane to a storage area. The upper guide-grid assembly is lifted from its support casting and placed on a support rack within the reactor tank. Before any fuel elements are lifted, two pieces of the beryllium reflector and the discharge-chute shielding plug are lifted and stored within the tank. With long-handled tools, men working on top of the reactor through the light-water shielding grapple a fuel assembly, raise it clear of the lattice, move it sideways to the discharge chute, and lower it into the discharge-chute. The discharge mechanism is raised to the vertical position just beneath the discharge tube. A remotely operated hydraulic seal at the lower end of the discharge tube is actuated, joining the cylinder and the discharge tube. The piston in the cylinder is raised or lowered to a position depending on the type of assembly to be received. A purging line attached to the upper end of the hydraulic seal supplies demineralized water at a pressure greater than the head pressure in the reactor tank, ensuring a steady flow of inactive water up the discharge tube when the gate valve is opened. With the gate valve opened, the fuel element is lowered manually into the receptacle in the piston. The gate valve is closed, the purge stopped, the seal opened, the discharge cylinder rotated to the horizontal position, and the fuel assembly ejected onto the receiving table. The assembly may then be picked up with long tongs and transferred manually to the canal storage area. The discharge cylinder is returned to the vertical position, and the cycle is repeated.

Charging of the reactor can be accomplished by either of two methods. New and inactive elements can be manually loaded from the top of the reactor. Fuel and other elements can also be loaded into the reactor by reversing the unloading procedure. This permits introducing elements which have become active and were temporarily stored in the canal.

EXTRAORDINARY OPERATING CONDITIONS

During transfer of the fuel element into the discharge cylinder all personnel must be excluded from the sub-reactor room. All other operations are carried on beneath a sufficient depth of light water to protect the personnel.

GENERAL-PURPOSE MANIPULATORS

A general-purpose manipulator is considered to be a remotely-controlled mechanical arm capable of gripping diverse objects and having sufficient degrees of freedom to manipulate an object to almost any orientation and position in a working volume. All movements of the manipulator arm are controlled by a human operator who is outside the working volume and separated from it by a shielding barrier or distance.

The general-purpose manipulator may also be considered to be a remotely-controlled mechanical arm capable of performing the same general type of handling and manipulations as are ordinarily done manually. Of course, the manipulator may have a lower or higher load capacity than the human arm.

It may also be considered to be a mechanical arm remotely-controlled to follow the demands or actions of a human operator and to assume some of his skills of manipulation.

Manipulators which fall within one or more of the above definitions have been designed and built in many different shapes and sizes and with different functional characteristics. Features that may be desirable for some uses may not be desirable in others or may not be justifiable from an economic point of view. Since the manipulator is a mechanical arm with many degrees of freedom of motion and since all these motions are under the direct control of an operator, the design of the manipulator system must be considered from two

different points of view. In the first place, it is necessary to build a mechanical arm capable of performing the work expected of it; that is, it must have enough degrees of freedom, power capacity, and the like. Secondly, it is necessary to design the control system and some additional features of the manipulator arm itself so that the operator can control it with reliability and dexterity.

TYPES OF MANIPULATIONS AND CORRESPONDING REQUIREMENTS

In order to establish some of the fundamental requirements in the design of a remote, general-purpose manipulator, the three most common types of manipulations will be examined.

FIRST TYPE OF MANIPULATION

The first type involves the handling and orientation of solid objects without bringing them into precise contact with fixed equipment, e.g., picking up a container from a surface, transporting and tipping it to pour out a specimen, or picking up a solid specimen and placing it into a loose-fitting chuck or vise. Requirements for this type of manipulation are listed below.

Degrees of Freedom

The mechanical arm must have a minimum of three independent degrees of freedom of translation and three independent degrees of rotation to position and orient its tongs and the grasped object. The tongs must have another independent motion for opening and closing their jaws. Either a rectilinear or polar system can be used to provide effectively translational motion. Additional degrees of freedom are often needed to change the shape of the arm, extend the working volume, add gripping motions, or to eliminate "zenith" effects when two axes become parallel.

Shape of Arm

The arm should have a long slender shape with a wrist joint at the end. The tongs are attached to the wrist joint. For any given load capacity, it should be as small as possible to avoid visual and physical interference with other equipment in the shielded space.

Mounting

Some part of the arm must be mounted on a "rigid" structure and have the seven principal degrees of freedom with respect to this reference. This mounting is needed so that the arm may exert a force in any direction or a couple about any of its axes. The "rigid" reference may be adjustable so as to move the manipulator to a new location or change its orientation. These arms, mounted on a suitable remote-controlled vehicle, would form a general-purpose robot.

Load Limits

Force and torque limits are needed to protect the object, equipment contacted by the manipulator, and the arm itself.

Controls

This type of manipulation may use relatively simple controls such as "on-off-on" electric switches. More complicated controls may be desirable to increase speed, accuracy, and ease of operation.

Power Drives

Any power system may be used that is remotely controllable. The efficiency of the prime mover, mechanical gearing, and linkages may be low.

SECOND TYPE OF MANIPULATION

This type involves the handling of precision parts or specimens and manipulating them into place on a snug-fitting mating part of a fixed piece of apparatus. An example is to pick up a precision cylinder from a table top, move it through space, and place it into a close-fitting collet chuck. The operator can control the motions of the manipulator required to bring the cylinder to the chuck, orient it approximately, but cannot control the small final orientation and exact final position. The final small alignment of the cylinder is determined by the chuck and not by the manipulator. To avoid high forces and to allow for the alignment, the manipulator must yield a small amount.

Compliance

Some form of compliance, or effective compliance, must be included into the manipulator arm to accomodate the final alignment. This could be in the form of elasticity, yield by clutch slippage or, as indicated below, the drives could be bilateral.

THIRD TYPE OF MANIPULATION

This is the condition where a control part or handle on a fixed apparatus is operated by the general-purpose manipulator. The control part is generally free to move in only one degree of freedom. The total path of the part and the manipulator tongs gripping it is determined by the apparatus. Turning a crank is an example. The operator cannot control the manipulator to follow this path exactly. Since the control on the apparatus is probably not capable of withstanding the maximum forces that the manipulator could exert in any direction, the manipulator must, through forces on its tongs, accommodate this path without exerting high forces except in the direction of the path. The path may not be easy to follow by direct control of the manipulator and the positional and orientational errors may be fairly large.

Bilateral Drive and Force Reflection

Although it is possible to perform some of these manipulations if the manipulator arm has enough compliance, the more complicated control motions where forces must be carefully limited, can better be controlled with bilateral force-reflecting drives in all of the principal degrees of freedom. This will allow the manipulator to be driven backwards to follow the prescribed path but at the same time to exert a force in approximately the right direction. Efficient mechanical linkages, such as those used in "master-slave" manipulators, are examples of this kind of bilateral drive. Another bilateral system is an electrically connected force reflecting positional servomechanism. Several laboratory models have been reduced to practice at Argonne National Laboratory.

Human Engineering and Additional Requirements

In order for the operator to control the general-purpose manipulator, it is necessary that the over-all system be compatible with his capabilities; a brief review of these capabilities will be helpful.

Direct manual manipulation is one of the highly developed skills of the human being. The steps in manual manipulation are usually to visually observe a situation, plan the changes desired, move the hand to grasp the object, and then apply a force to move it in the de-

sired direction. This very complicated process takes place so fluently and quickly that it is generally taken for granted. Internal stimuli are sent from the brain causing the muscles to respond. The brain continually receives four general types of stimuli: visual, kinesthetic, tactual, and auditory. Kinesthetic stimuli are sent from muscles, ligaments, and the like to the brain to give the approximate position, speed, force, etc., of the arm and hand. Another important characteristic of the human arm and hand is that all of its motions are bilateral; i.e., they can be motivated by their own power drives (muscles) or can be caused to move backwards by an external mechanical force.

In the design of a manipulative system, it is desirable to take advantage of these characteristics so that the operator can control the manipulator with greater accuracy and speed.

Quite often it is desirable for the operator to control all seven principal degrees of freedom at one time and at the same time devote most of his intelligence and attention to the effects or results of the manipulation instead of on the manipulator controls.

Vision

Good visual means must be provided. The system should provide a natural three-dimensional view.

MASTER-SLAVE MANIPULATORS

In an attempt to capitalize on the natural characteristics of the human operator, master-slave manipulators (Figs. 7.1.9 to 7.1.13) were developed. All seven motions of the slave tong are driven synchronously in orientation and position by a single master handle. All motions have high mechanical efficiency, low inertia, low friction, and are bilateral. Therefore, the position and force on the tongs are reflected back to the control handle so that the forces and torques are approximately the same as if the operator had the tongs and its grasped object in his hand.

The manipulators are easy to operate and require only a small amount of operator training. All three types of manipulation, described above, can be carried out with good dexterity.

The present designs have mechanical connection for all motions and consequently have limitations of load capacities and installation. Loads are limited by the strength of the operator's hand as applied to the control handle (5 to 10 lb maximum). The use of bilateral servos can extend this load capacity to much higher (or much lower) values and retain natural movement of control handle and reflected force "feel" proportional to the load.

OTHER MANIPULATORS

Many manipulators have been designed that do not include many of the features of the master-slave type but gain other features (Figs. 7.1.3 to 7.1.10). Generally, these manipulators are powered with unilateral on-off or variable-speed drives and are driven by electrical motors or electrically-controlled hydraulic systems. They can be designed for almost any load capacity, require only electric wires between the controls and the mechanical arm, and can be constructed out of standard commercial components for the most part.

A certain amount of human engineering is included in the design of these manipulators. For example, the controls are generally arranged in an orderly fashion and are often arranged to move in a direction corresponding to the motion they control. Force indication is often provided on the "squeeze" motion.

The operating speed and dexterity of these manipulators is much lower than those of master-slave manipulators. Extreme care is required when working in the vicinity of delicate equipment and apparatus. They are suitable for the first type and, to a limited extent, the second type of manipulation described above. They are not generally suitable for the third type of manipulation.

SPECIFIC MANIPULATORS

Figures 7.1.3 through 7.1.18 illustrate the over-all dimensions and brief functional characteristics of 11 manipulators in use or well along in design or construction. This list includes most of the general-purpose manipulators in use within the AEC and one for use by the Army Chemical Center (Bridge Hydraulic).

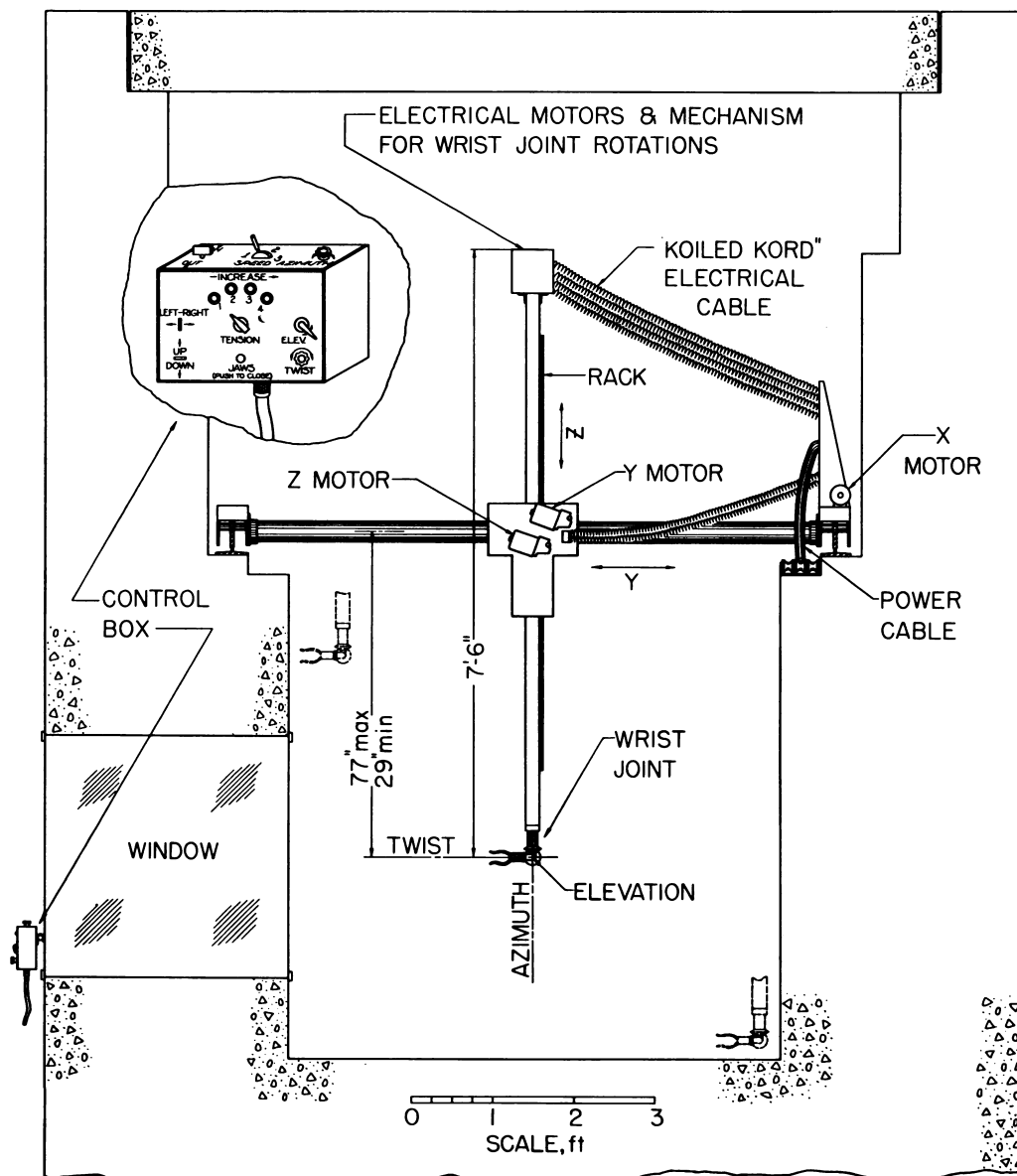


Fig. 7.1.3—Argonne Rectilinear Manipulator. This light-duty manipulator was designed to operate in confined spaces. The wrist-joint drive motors and gripping drive are mounted at the top of the column to conserve space at the wrist-joint. The motions are driven by DC motors whose speed and direction are switch-controlled at the control box shown. One of four degrees of gripping force can be selected, the highest of which generally limits the use of the manipulator to objects weighing 1 lb or less. The installation shown has a working volume of $60 \times 6 \times 4$ ft high.

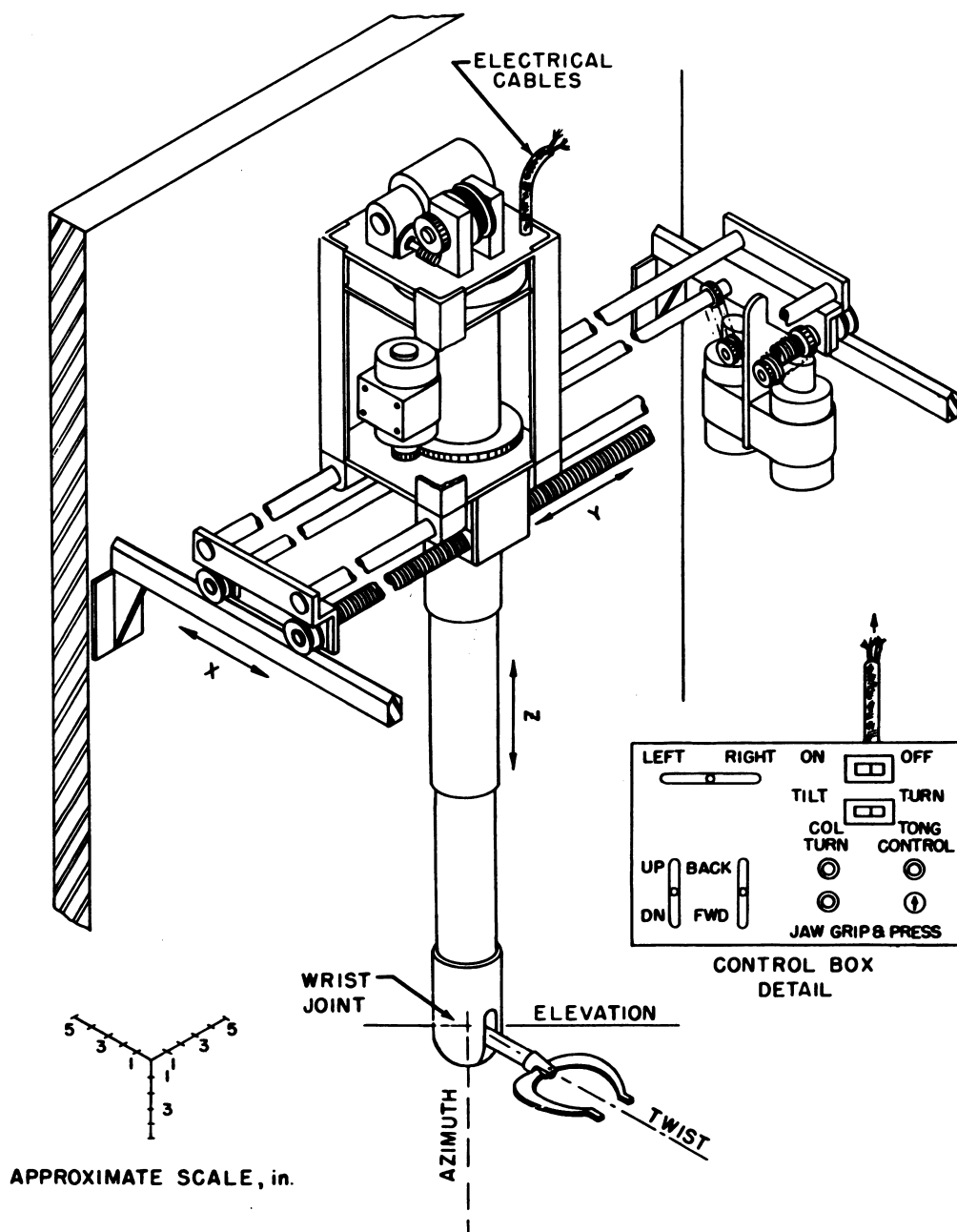


Fig. 7.1.4— Brookhaven Electric Manipulator. A pneumatic cylinder with controllable air pressure is used to develop gripping forces up to 175 lb. The tongs are capable of handling objects weighing up to 15 lb, but the Z motion is capable of a 200-lb lift. This manipulator is installed in a "benchtop" cave having a working volume of $10 \times 2 \times 4.5$ ft high.

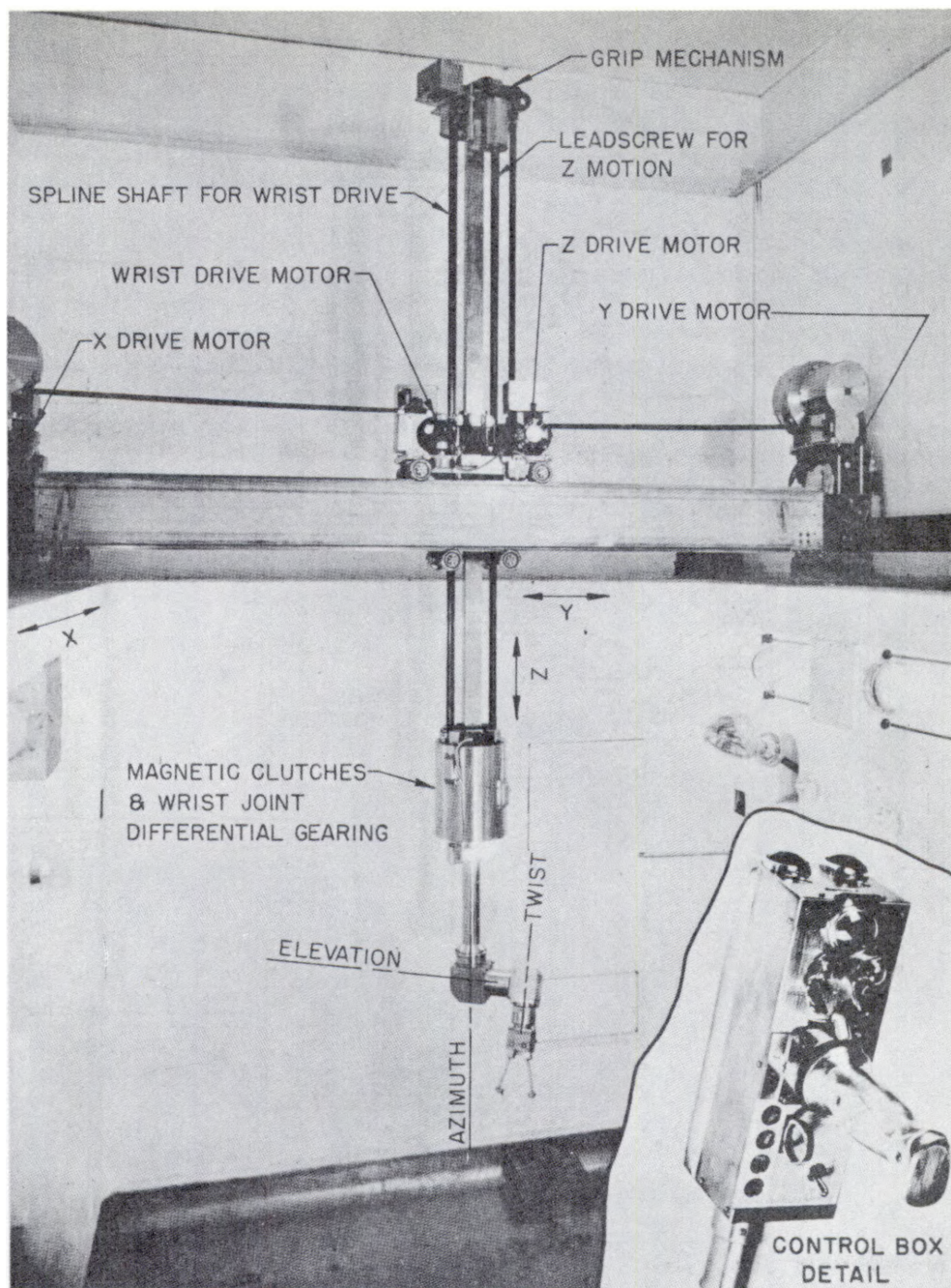


Fig. 7.1.5—Oak Ridge Electric Manipulator. All of the wrist motions of this manipulator are capable of unlimited rotation as a result of the offset wrist construction. A single motor drives the three rotations, the desired one being selected by magnetic clutches and a planetary gearset. The motor-driven tongs, which are interchangeable, stop automatically when a preselected gripping force is reached. The manipulator is generally capable of handling objects up to 20 lb. The translational motions have deliberate compliance, with electrical limit switches in case the compliance is exceeded. The installation shown has a working volume of $38 \times 5.5 \times 4$ ft high.

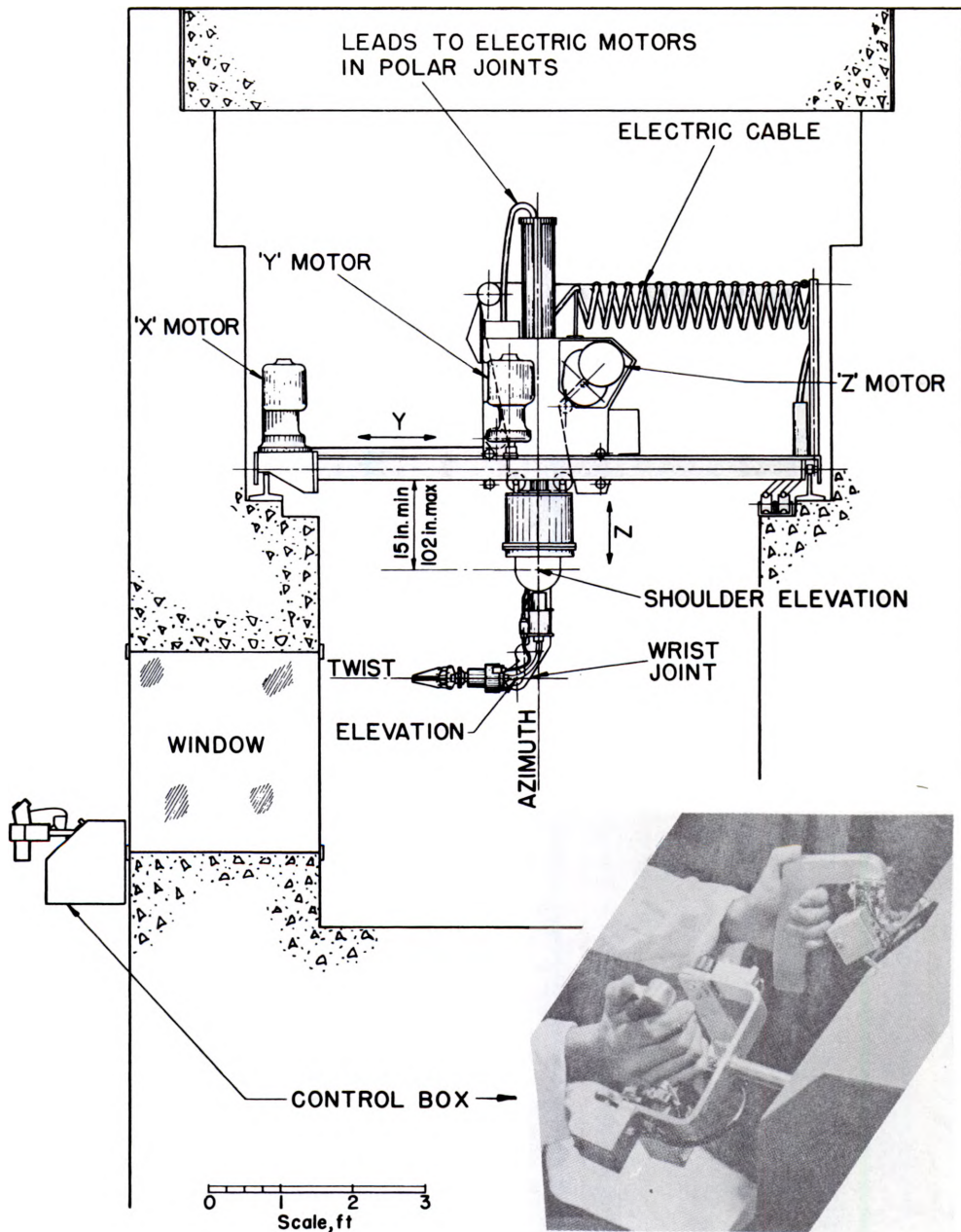


Fig. 7.1.6 — Mechanical Arm, Model C (General Mills, Inc.). The tongs of this manipulator can be remotely replaced with a hook which is capable of greater force exertion and which can operate specially designed "hand tools," such as tin snips and an impact hammer. Meter indication is provided of the gripping force, which is sufficient to handle objects weighing up to 75 lb. All motions are driven with d-c motors, variable voltage being supplied from the two-handed control console shown. The installation shown has a working volume of $60 \times 6 \times 7$ ft high.

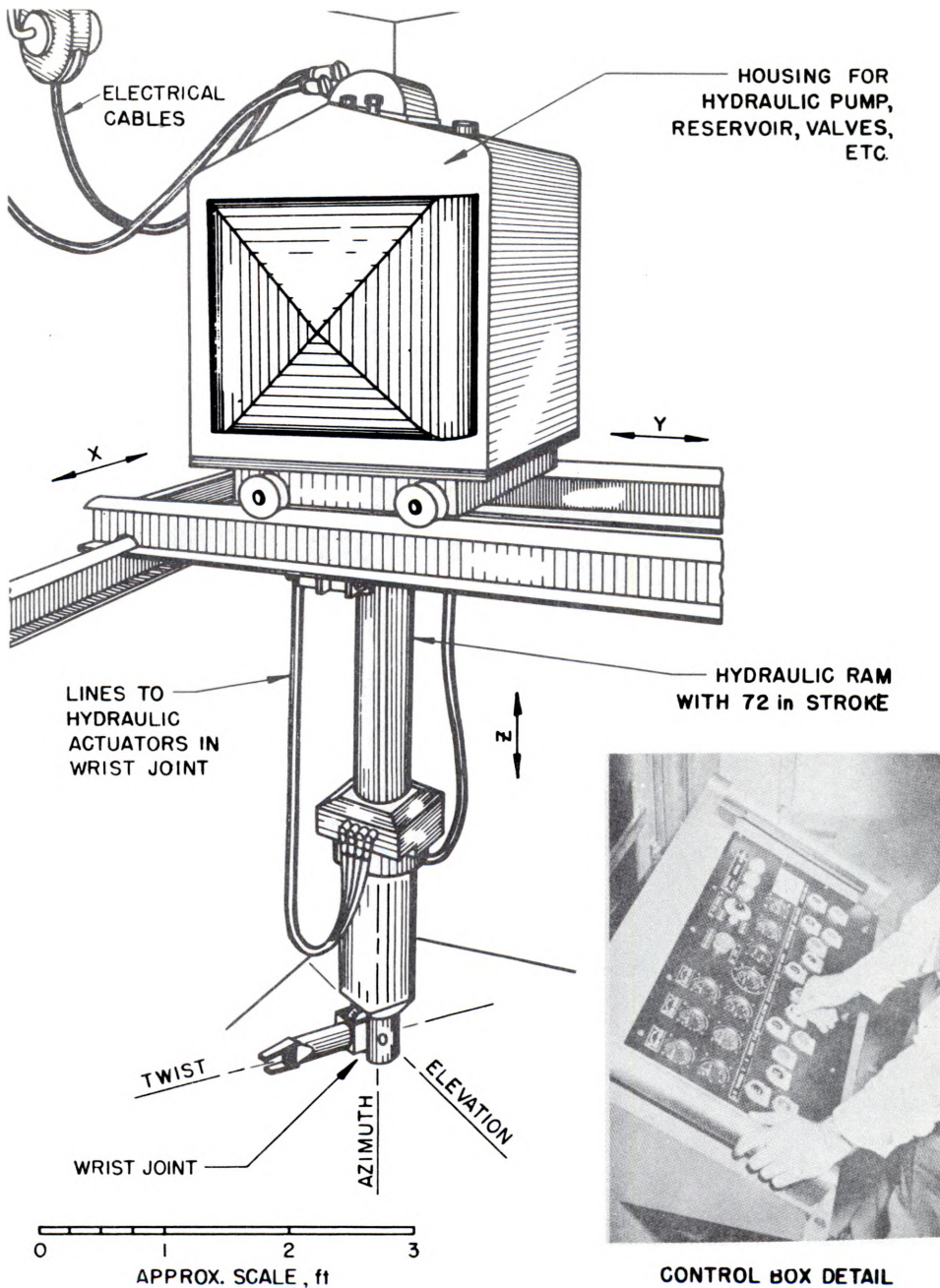


Fig. 7.1.7 — Bridge Hydraulic (Greer Hydraulics, Inc.). All motions of this manipulator are hydraulically driven from a single pump. The variable pump output is directed to the several motions by solenoid valves operated from the console shown. Visible are the forward and reverse pushbuttons for each motion, the common speed control, and the position indicators. The tongs, which are remotely interchangeable with a variety of special-purpose tools, are capable of handling objects weighing up to 100 lb. The installation shown has a working volume of $18 \times 8.5 \times 6$ ft high.

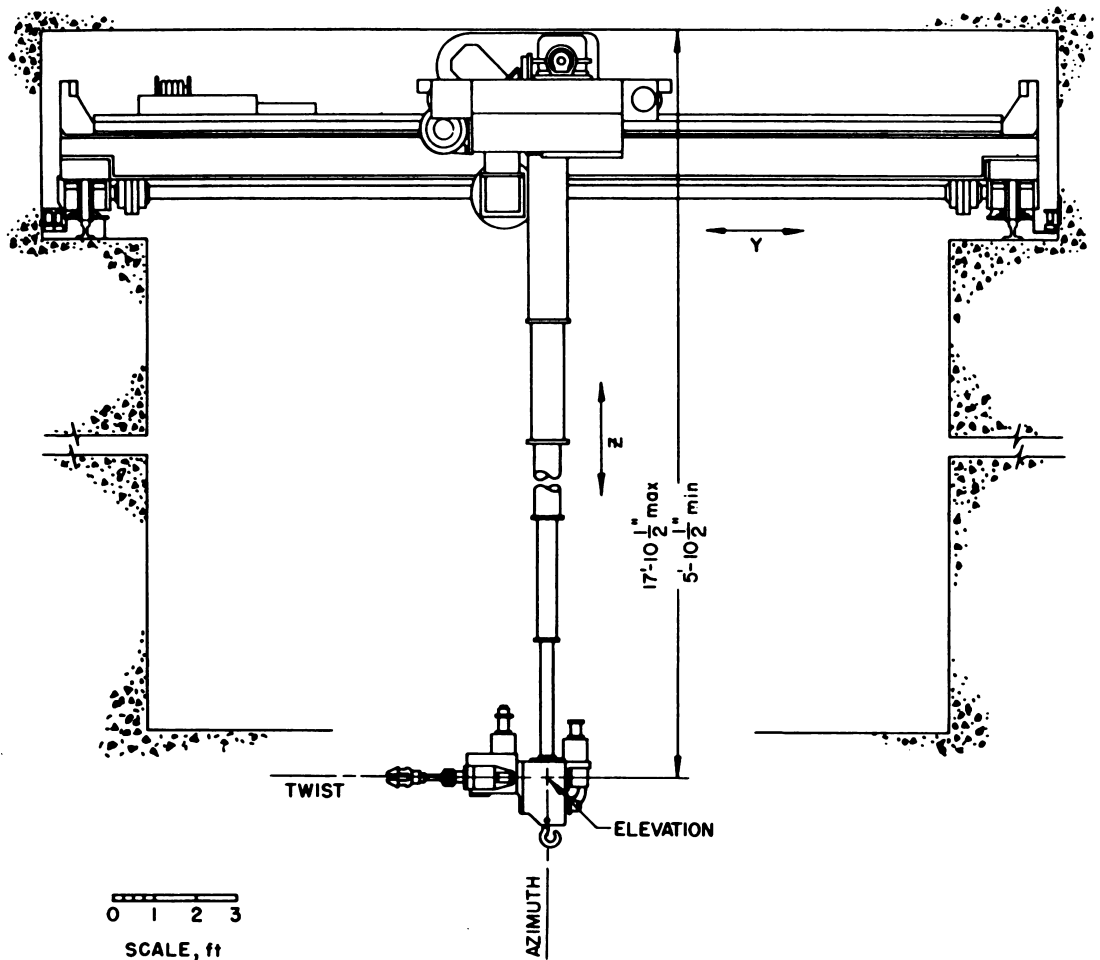
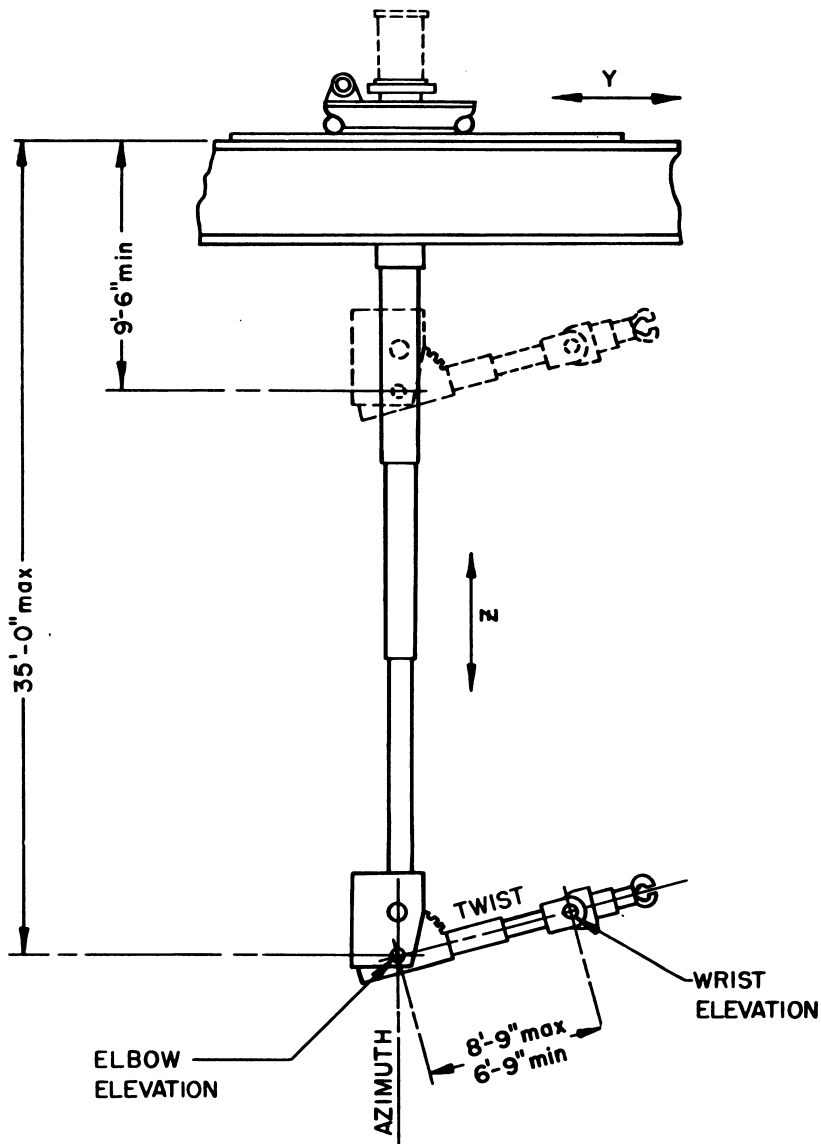


Fig. 7.1.8—General-purpose Manipulator (Farrel-Birmingham Co., Inc.). The entire wrist-joint assembly of this manipulator can unscrew itself from the column and be remotely replaced. A two-handed control console is provided on which the right hand controls wrist rotations and the left hand controls translational motions. The manipulator is capable of a 100-lb force in any direction and a normal gripping force of 50 lb. The tongs are remotely replaceable with others having grips of up to 300 lb.



DO NOT SCALE

Fig. 7.1.9 — Heavy Manipulator (General Electric Co.). Most of the motions of this manipulator will be powered with amplidyne sets individually controlled at the console. It is to be capable of a 500-lb force in any direction with a gripping force of 2500 lb and a straight lifting capacity of 5000 lb. The proposed working volume is $150 \times 51 \times 26.5$ ft high.

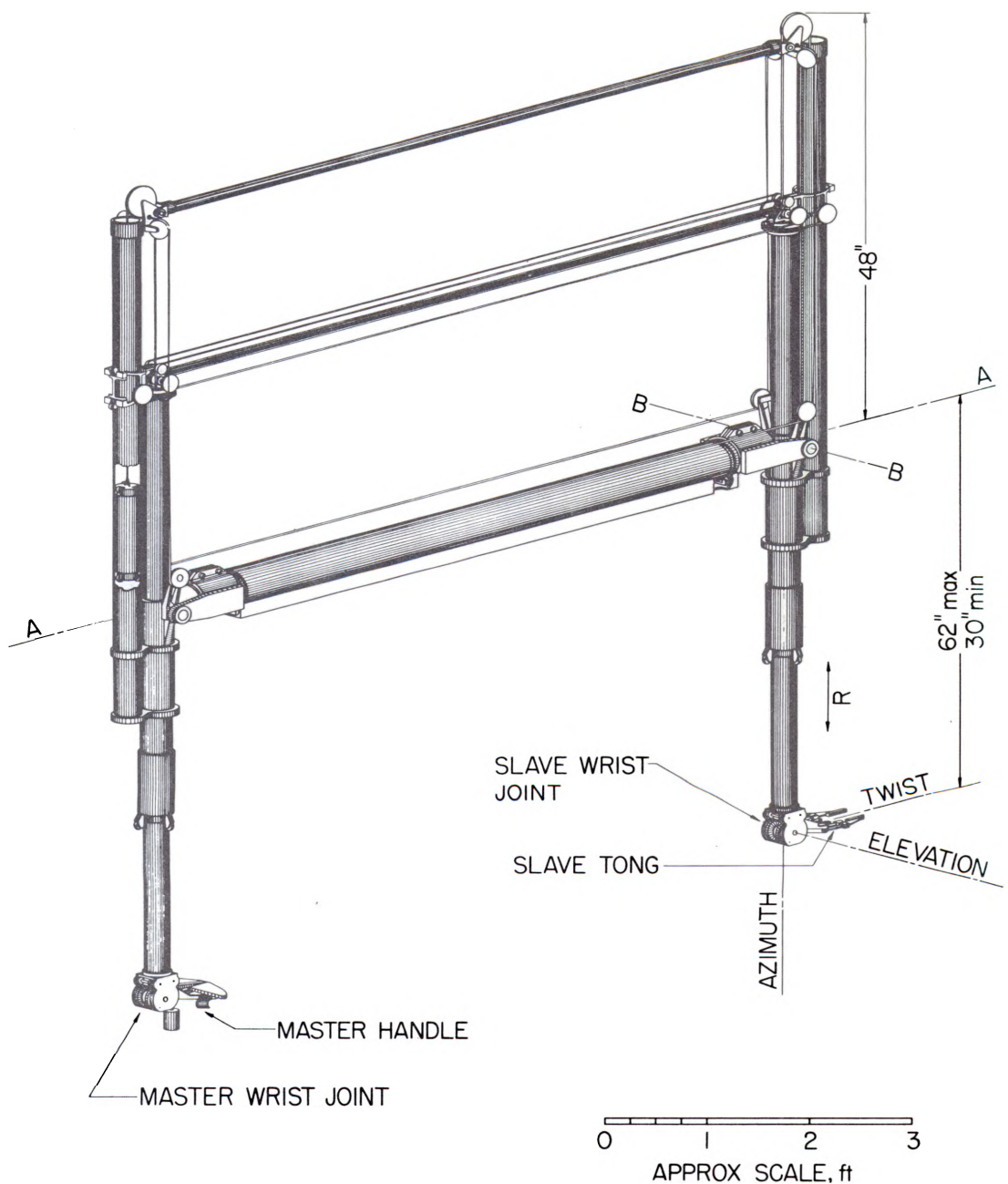


Fig. 7.1.10 — Argonne Master-Slave, Mod. 4. This fully master-slave manipulator is in use in a number of installations. The slave arm normally enters the shield through an oversize hole in the roof; the resulting scattered radiation limits use to activities of about 500 curies, unless the roof is extended to also cover the operator. The design has been highly refined to achieve minimum mass, friction, and resilience and has been declassified for manufacture outside of the AEC. It is capable of handling objects of up to 10 lb, but it is especially applicable where fragile specimens or delicate equipment require sensitive manipulation.

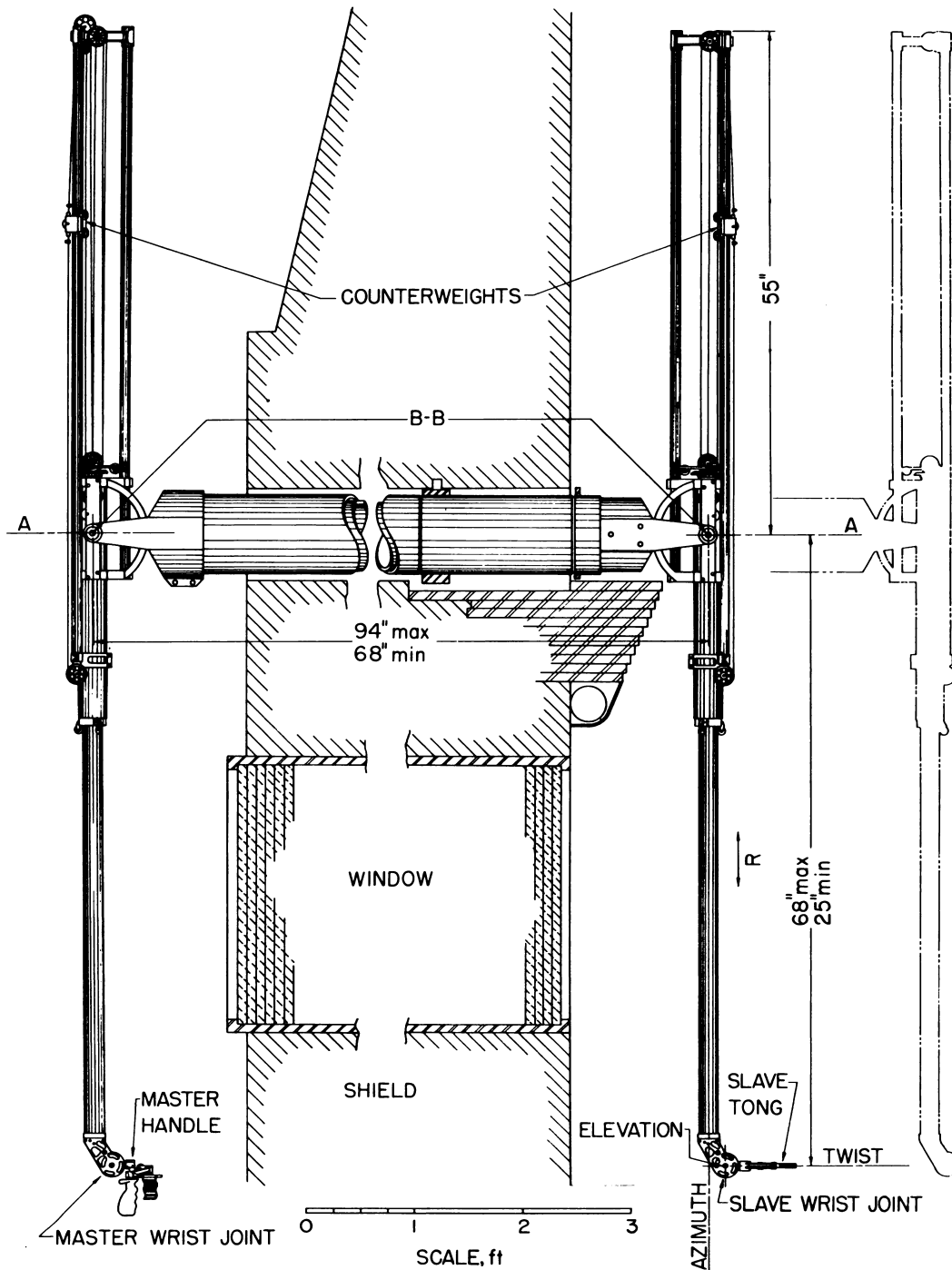


Fig. 7.1.11—Argonne Master-Slave Mod. 6. These manipulators work through a slot in the cave wall and are mounted on a carriage which traverses the length of the slot. The static coverage is further increased by a motor-driven telescoping of the horizontal tube. The later Mod. 6B achieves a similar result with a fixed tube by translating the entire manipulator. The itinery of the Elgiloy tapes which connect the master and slave ends is considerably complicated by having to pass through the horizontal tube, and there is a noticeable increase in friction by comparison with the Mod. 4 design. The Mod. 6 and 6B designs have been declassified for manufacture outside of the AEC.

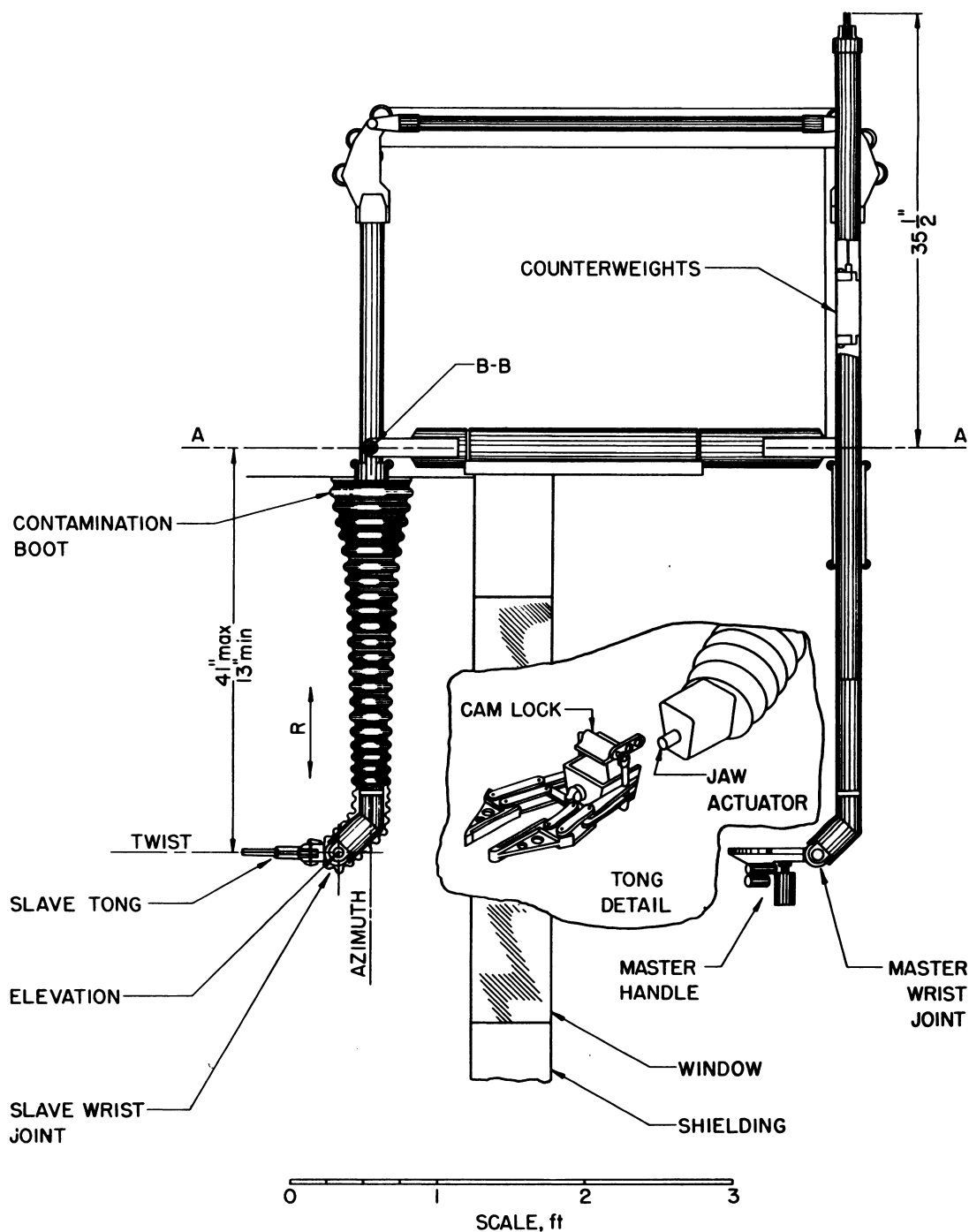


Fig. 7.1.12 — Argonne Master-Slave, Mod. 7. A contamination boot has been provided on this manipulator, being sealed to the roof of the cell and covering the wrist joint so that only the tongs are exposed. The manipulator is therefore useful for performing "open" chemistry in a shielded dry box and other situations where a serious contamination hazard exists. The manipulator was designed to be a permanent part of a mobile shielding wall. The counter-weight tubes can be easily lowered and the manipulator set at its lowest position for clearance through normal-sized doors. It has a load capacity of about 4 lb.

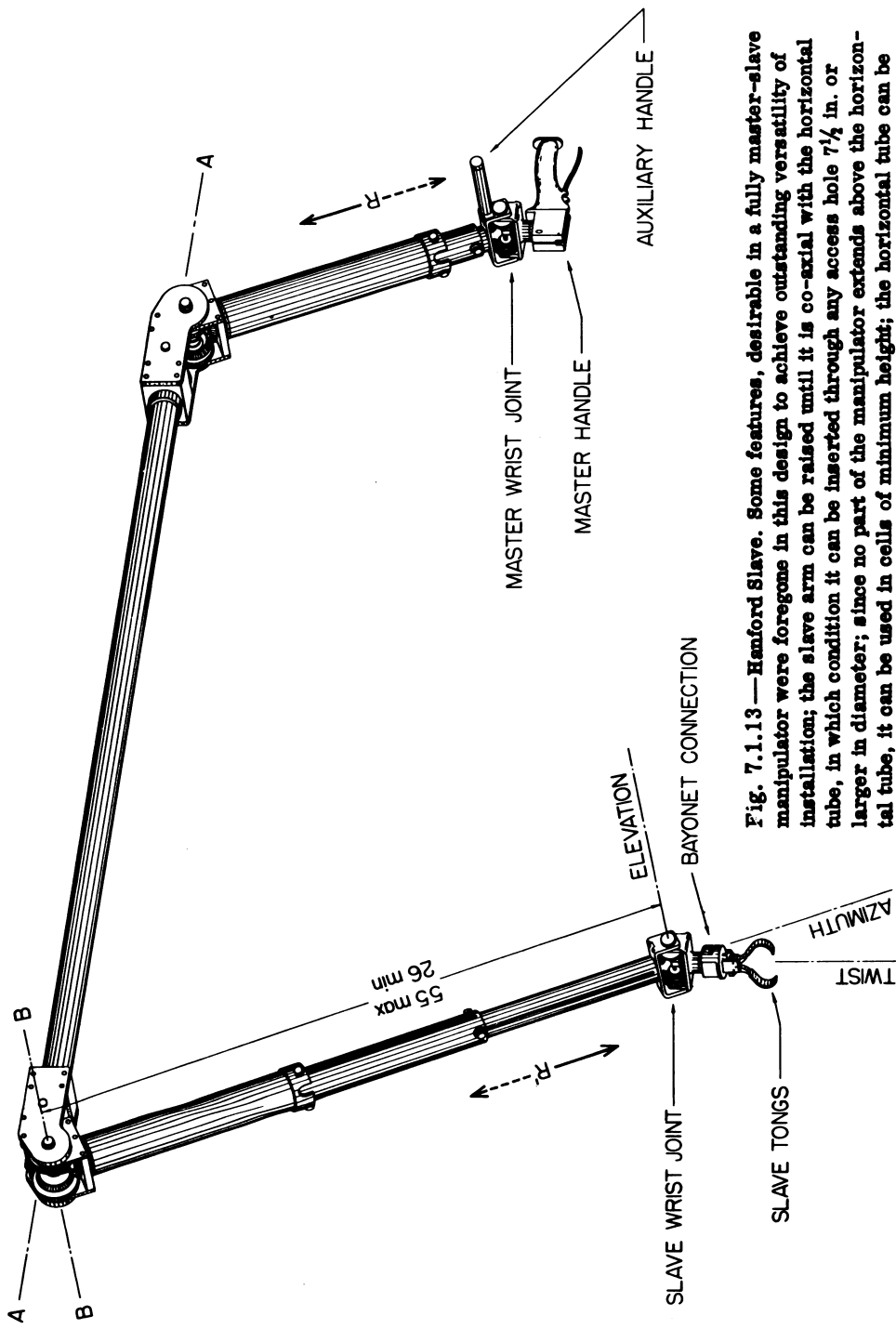


Fig. 7.1.13—Hanford Slave. Some features, desirable in a fully master-slave manipulator were foregone in this design to achieve outstanding versatility of installation; the slave arm can be raised until it is co-axial with the horizontal tube, in which condition it can be inserted through any access hole $7\frac{1}{4}$ in. or larger in diameter; since no part of the manipulator extends above the horizontal tube, it can be used in cells of minimum height; the horizontal tube can be quickly replaced with longer or shorter ones to work through shields of various thickness. Vertical telescopic motion of the control-handle side and slave side are reversed, however, and friction and resilience are high compared to master-slave designs. The manipulator is designed generally to handle objects of up to 10 lb.

CHAPTER 7.2

Remote Viewing

G. S. Monk, K. R. Ferguson, and D. F. Uecker

REQUIREMENTS OF VIEWING SYSTEMS

The observation of a procedure involving radioactive material is complicated by the necessity of seeing through or around the required biological shield. "Seeing" here denotes receiving the same visual impressions as those of an observer moving around inside the shield. These visual impressions depend upon: (1) a wide angle of view and the ability to scan to provide an impression of over-all size and spatial relationships in two dimensions; (2) depth perception to "round out" the view, a powerful aid if manipulation is contemplated; (3) the ability to view from various vantage points and distances; (4) color perception; and (5) the ability to use optical aids for special purposes such as macro- and micro-examinations. In addition, the image should be sufficiently free of distortion and other optical defects to allow its prompt interpretation and of sufficient resolution to permit perception of fine detail.

No single viewing method has been devised which satisfies all of these requirements. Complementary viewing methods have been provided, therefore, to satisfy the needs of a particular installation.

BASIC TECHNIQUES

Viewing methods which are all-optical depend on the difference in degree of transmission, reflection, and refraction between visible light and high-energy radiation; i.e., visible light may be preferentially passed through a filter of glass or liquid or propagated by means of mirrors or lenses through a labyrinth which is essentially opaque to atomic radiation. Methods which depend upon transparent shielding material to filter out high-energy radiation include observation of submerged operations and observation through windows. Methods which depend upon a labyrinth effect for shielding include observation by means of reflecting systems, periscopes, or borescopes. Television, not being all-optical, constitutes a third basic technique. The passage of the camera cable through the shield creates little radiation hazard, but low resolution and other difficulties have prevented its widespread use.

SUBMERGED OPERATION

Where the nature of the radioactive material and equipment allows, the entire process may simply be submerged to a sufficient depth in water. The method has the following advantages:

- (1) It is inexpensive and reliable, both as a shield and a means for viewing.
- (2) It is the only satisfactory method known for very high activity levels.
- (3) The open top of the tank allows freedom for more than one operator to see and work from various angles.
- (4) It allows the use of simple, longhandled tools and grapples to accomplish rudimentary manipulations.

An important disadvantage is that commercial machinery and equipment is not suitable for underwater operation, and adaptation may be expensive.

The method is widely used, primarily to receive reactor fuel for cooling and for preliminary operations such as sorting, weighing, and gross inspection. A few installations for experimental work are known, including a versatile machine tool which was custom built for underwater service.

A simple and useful optical aid is a glass-bottomed box floating on the surface which eliminates ripples. Unaided vision is thereby greatly improved, and the use of a telescope or binoculars is made possible. For considerably magnified views, waterproofed periscopes have been built that dip down to the vicinity of the operation. Their optical design is generally not complicated by the necessity for underwater operation.

Cloudiness or contamination can be controlled by replacing the water periodically, but facilities for handling large volumes of liquid waste are therefore necessary. An alternative is the use of a recirculating filter.

WINDOWS

DESCRIPTION

A shielding window is an opening in a biological shield which is filled with a transparent material having the same protecting properties as the surrounding shield. Water, concentrated aqueous solutions, other dense liquids, and glasses of various compositions have all been used. An economical and popular form of window is a simple rectangular solid, although a frustum of a pyramid conserves window material. In either case, the optical faces are parallel, and the resulting effects are those of a thick parallel plate.

APPLICATIONS

Some of the capabilities and limitations of windows are:

- (1) They can be used to provide the gamma-shielding equivalent of up to 4 ft of concrete (more if the exposure is intermittent).
- (2) The stability of materials other than water is not as well known for neutron activity as it is for gamma irradiation.
- (3) Apertures up to 5-ft square are feasible, so that the operator has considerable bodily freedom while observing. In the case of a small shielded enclosure, this freedom can be used to achieve a variety of vantage points.
- (4) In a large enclosure, gross changes of vantage points require multiple windows and operator mobility. This may require multiple control stations for manipulative equipment or preclude the use of mechanically connected manipulators.
- (5) More of the elements of normal vision are retained than with any other single viewing method, e.g.:
 - (a) The field of view can approach 180° , over which the eye can rapidly scan.
 - (b) Unimpaired binocular vision is retained with a minimum optical distance.*

*The optical thickness of the window for small angles of incidence is $1/n$ of the actual thickness, where n is the index of refraction of the window material. For objects close to the inner surface of the window, image size and depth discrimination are perceptibly increased.

(6) For experimental work, standard commercial apparatus may be used with nearly normal operator-equipment orientation.

PERFORMANCE

A shielding window tends to reduce the acuity of vision by its effect on the following optical factors: (1) resolution; (2) discrimination of color and contrast, and (3) freedom from distortion.

RESOLUTION

A window introduces chromatic aberration, spherical aberration, and localized optical imperfections, all of which contribute to a slight loss of resolution.

In viewing with the unaided eye, most of the loss of resolution can be attributed to chromatic aberration which occurs only for viewing distances shorter than a few multiples of the window thickness. In the case of a 3-ft-thick window with a sight line having a 60° angle of incidence, the loss of resolution is just measurable at an observer-to-object distance of 8 ft, though color fringes are definitely observable at greater distances.

For magnified vision through a window, tests indicate that local imperfections are of minor importance compared with spherical and chromatic aberrations.¹ Resolution can be increased by optimizing the aperture, i.e., objective-lens diameter, of the telescope as the viewing distance is varied. For smaller apertures the resolution of the telescope-window system is reduced by the telescope, and for larger apertures by the window aberrations. Table 7.2.1 lists the range of optimum apertures and magnification for various distances.

Table 7.2.1—Optimum Telescope Apertures and Magnification for Vision Through Windows

Viewing distance, ft	Aperture, in.*	Total aberrations, seconds of arc	Magnification
100	1.5 – 3.5	4	15
60	1.2 – 3.3	5	12
30	0.8 – 2.4	8	8
20	.8 – 1.8	9	7
10	.5 – 1.2	14	4

*At the limits of the range of apertures indicated, the aberrations are increased by 1 second of arc. The data were obtained by measurements on a 3-ft-thick glass-filled window with white light illumination

The tabulated values of optimum magnification may be increased to allow for imperfections in the telescope and the eye and to relieve eyestrain, but no increase in resolution will be achieved, and excess power will limit the angle of view. When viewing at other than zero incidence angle through a window with object distances under 100 ft and with white light illumination, the usable magnification decreases rapidly with increasing incidence angle and approaches unity at an incidence angle of 60° . This magnification may be increased by a small amount by the use of monochromatic lighting.

DISCRIMINATION OF COLOR AND CONTRAST

Color is important in most viewing and can be preserved by using colorless window materials and white light illumination. As pointed out previously, the use of monochromatic lighting will increase the resolution that can be achieved in some cases. However, be-

¹References appear at end of chapter.

cause of the resulting loss of color discrimination, monochromatic lighting is desirable only where the white light would actually interfere with observation.

Object and lighting contrast is a paramount optical factor in the discrimination of detail. With good window materials and designs, the existing contrast will not be perceptibly altered. Haze in liquid windows, incomplete polish on glass surfaces, and multiple surface reflections are some of the factors that must be controlled to preserve contrast.

DISTORTION

A window introduces a distortion which curves plane surfaces, since the apparent distance is a function of the window thickness along the line-of-sight. This curvature is severe only when the viewing distance approximates the window thickness or when viewing at an angle of incidence greater than about 60°.

TRANSPARENT SHIELDING MATERIALS

It is usually desirable that the window material have approximately the same shielding effectiveness per unit of thickness as the rest of the biological shield. Interest has been concentrated, therefore, on materials with half-value layers* comparable to those of concrete, steel, and other common shielding materials.

A second requirement is that the window material have such desirable optical qualities as: a high transmission of at least a portion of the visible spectrum; freedom from imperfections, such as local variations of index of refraction (striae); a minimum of haze or turbidity; and a high index of refraction to permit a large angle of view through a small window aperture.

A third requirement is stability of color and clarity against both time and intense radiation.

The installed cost of a window and the radiation hazard and possible toxicity of the window material in case of breakage are further factors for consideration.

The materials discussed below satisfy various weightings of the above requirements.

WATER

Water is the logical choice for economy and radiation stability. Distilled water or freshly filtered water is sufficiently clear to permit excellent vision through 10 ft or more, cheap enough to be attractive in spite of the larger size required by its low density and index of refraction, literally water-white, and virtually unaffected by gamma or neutron absorption.

Its low density does require a window which is 2.5 to 8 times as thick as an equivalent glass or dense liquid window, however. Detail perception for objects near the window is correspondingly impaired. For machinery installations and the like which cannot be brought close to the window for examination the lower density is of less disadvantage. For a given angle of view, a water-filled window requires a greater aperture through the shield. This in turn will require larger and thicker cover plates and, in the extreme case, multiple panes strengthened by mullions.

The deposits and cloudiness observed in some windows filled with filtered water are not well understood. The need to replace the water and remove the cover plates for periodic cleaning should be anticipated.

ZINC BROMIDE SOLUTION

A water solution of zinc bromide is in current widespread use as a window material.² The requirements of the "optical grade" solution are covered by a general specification.³

*A half-value layer is the thickness of any given substance required to attenuate the incident radiation by one half, commonly abbreviated HVL.

The density range of the zinc bromide solution has been chosen to give a freezing point just above that of water. (This allows the solution to be shipped by common carrier with ordinary precautions against freezing.) The solution density is 2.50 to 2.54, corresponding to 77.0 to 78.3 percent dry weight of zinc bromide (16.0 to 16.6 lb of dry zinc bromide per gallon of solution). At the current dry-weight price of zinc bromide, \$0.60/lb, the average price of the solution is \$10/gal. Table 7.2.3 lists some properties of zinc bromide solution. With material of the quality currently being produced, it is no longer necessary to provide for periodic filtering of the solution. The light transmission of the solution is initially excellent, and the thickness of window that may be used is limited only by the radiation stability of the solution.

Hazes

Occasional difficulty has occurred with haze formed by the slow precipitation of alkaline-earth sulphates (barium, strontium, and calcium have been identified) thought to result from mixing different production batches. Metallurgical experimentation was continued without interruption through a 3-ft window while such a haze formed and settled out after 9 to 12 months.

Oxidation

Oxidation can result either by contact with the air or by exposure to radiation. In either case the solution will be deeply colored by the oxidation of only a few parts per million of iron. In the absence of any other reducing agent, exposure to radiation will liberate free bromine from the solution. To prevent these effects, a reducing agent is added whose oxidation products introduce neither color nor haze to the solution. Hydroxylamine hydrochloride, $\text{H}_2\text{NOH}\cdot\text{HCL}$, is satisfactory in this respect. The addition of 4 oz per 100 gal of zinc bromide solution will protect a thin layer of the solution from a 10^6r exposure. In a thick window, relatively unexposed solution on the operator's side will be thermally mixed with exposed solution from which the reducing agent has been exhausted. On this basis, an exposure to Co^{60} radiation of about 10^7r will be required to consume the reducing agent in a 3-ft-thick window. With radiation having a range of energies, the low-energy component will be absorbed in the first few layers and cause a more localized exhaustion of the reducing agent.

The gaseous oxidation products of hydroxylamine are somewhat soluble in the zinc bromide solution, but incident exposures of 10^5 to 10^6r within 24 hr will certainly cause gas evolution. If the bubbles rise rapidly the effect may not be serious, but operating experience is lacking.

The sulfide-ion concentration in the zinc bromide solution can be kept below a few tenths part per million by completely oxidizing the solution during its preparation, as required by the specification. Unless this is done, a haze of free sulfur, which will not be reduced by the stabilizer, will form upon irradiation.

Contamination

Contamination can be eliminated by allowing only materials to come in contact with the solution which have been so tested for a year or more. Nickel and cobalt are soluble in and impart color to zinc bromide solution. Chromium from dissolved stainless steel will precipitate slowly and form a haze. Many organic materials will impart strong color to the solution and produce dense hazes. The following materials are suitable for equipment coming in contact with the solution for very limited periods, preferably less than 1 day: Polythene, Tygon, Koroseal (all types), and hard rubber. Table 7.2.2 indicates the rating of container-lining materials.

Table 7.2.2—Container Materials for Zinc Bromide Solution

Type	Excellent	Limited life	Not usable
Paint	Amercoat 31		Amercoat 55
Baked finished	Lithcote		
Plastic linings	Teflon [*]	Koroseal 9234	Amerplate Saran Polythene
Metals	Silver	Copper S. S. 347 Brass	Nickel and other common metals

Wherever feasible, a seven-coat application of Amercoat 31 over hot-rolled steel is highly recommended because of its superior resistance to zinc bromide, ease of application, and economy.

OTHER DENSE LIQUIDS

A number of dense liquids and aqueous solutions other than zinc bromide solution have been considered as prospective window materials. The list includes: lead acetate, zinc chloride, methylene bromide, acetylene tetrabromide, a mixture of stannic bromide and stannic chloride, barium and mercuric bromide, and cadmium borotungstate.² Though development work might improve the competitive position of some of these materials, most have been ruled out for reasons of low density, high cost, instability, or toxicity.

SHIELDING GLASSES

Table 7.2.3 presents the pertinent properties of some commercial glasses and of some in the development stage. The properties of nonbrowning lime glass are described in a general specification.⁴

Table 7.2.3—Physical Properties of Transparent Shielding Materials

Type	Density	Index of refraction	Optical transmittance*		Color	Radiation stability index†	Fading index‡	Price per pound
			Tungsten†	Sodium				
Commercial lime‡	2.52	1.52	94.6	94.3	Green	2.6×10^2	2-5	\$0.50
Water-white lime‡	2.52	1.52	99.0	99.0	Colorless	2.6×10^2	2-5	1.25
Nonbrowning lime‡	2.68	1.53	96.8	97.0	Light yellow	1.6×10^3	1-3	2.25
Corning 8362	3.27	1.59	97.6	98.2	Yellow	0.8×10^3	1-3	...
X-ray lead‡**	4.88	1.76	90.0	92.0	Deep yellow	2.0×10^2	2-5	2.50
Dense lead††	6.20	1.98	94.1	95.2	Yellow-orange	1.5×10^2	10-50	4.00
Zinc bromide solution‡‡	2.52	1.56	98.5	99.0	Colorless	0.47

*Optical transmittance in percent for 1-in.-thickness and average specimens, less surface reflection

†Light of the quality of I.C.I. Illuminant A

‡The exposure in r required to produce a change in optical density of 0.01, for white light and a thickness of one HVL. Optical density is the common logarithm of the reciprocal of the transmittance. The exposure rate was 100 a 700 r/min

§The ratio by which the exposure in (c) must be increased in order that the change in optical density is 0.01, 2 weeks after the termination of the exposure

‡Commercial samples from the Pittsburgh Plate Glass Company

**Transmittance and price are for laminated sections

††Commercial samples from the Penberthy Instrument Company. A similar glass has been prepared experimentally by the Corning Glass Works

‡‡Commercial samples from Dow Chemical Company

Glass may be manufactured for windows in the form of polished plate or as cast sections. Experience has shown that 1-in.-thick plate glass can be produced with an optical quality suitable for windows in a maximum practicable sheet size about 5 ft square. X-ray lead glass is manufactured in $\frac{1}{4}$ -in. thickness only, but it can be laminated with plastic sheet to a 3-in. thickness. Castings of dense lead glass with good optical quality have been made with a maximum volume of 400 cu in. Large glass castings are still in the preproduction stage. It is believed that castings as large as 36 in. square and 4- to 6-in. thick will be feasible.

Radiation Tests on Shielding Glasses

The factors that influence the change in light transmission of glass exposed to gamma radiation include: (1) exposure rate and total exposure; (2) continuity of exposure; (3) time elapsed between exposure and transmittance measurement; (4) temperature during and following exposure, and (5) for some glasses, the amount of visible light incident on the glass during and following exposure.⁵

Figure 7.2.1 shows the change in optical density of commercial lime glass when exposed to gamma radiation. From this figure it can be seen that 4 days after exposure at a rate of 600 r/min, samples have about the same change in optical density as those measured only 1 hr after the same exposure received at the rate of 20 r/min. All samples were kept at room temperature and in the dark during and after exposure.

Figure 7.2.2 shows the change in optical density for nonbrowning lime glass with gamma irradiation. If it is assumed that the coloration of the glass is a function of the total energy absorbed per unit volume, the data presented in Figs. 7.2.1 and 7.2.2 can be applied to gamma energies different from those emitted by Co^{60} . The gamma-energy flux per roentgen is about constant for gamma energies from 0.1 to 2.0 mev. Hence, gamma exposures of different energies should produce the same change in optical density for glass thicknesses corresponding to their respective half-value layers.

The increase in optical density with varying window thickness is shown in Fig. 7.2.3. Of course, to obtain the final optical density of a window, it is necessary to add the initial optical density (produced by the intrinsic color of the glass) and the increase in optical density produced by a given irradiation. No correction was made for the change in exposure rate through the window. It was assumed that the radiation would follow a simple exponential absorption, and an average value for a HVL was chosen to account for 'build-up' effects.⁶ For a nonbrowning glass window and 1-mev gamma radiation, the density values for a window thickness greater than 50 in. represents an extrapolation of the experimental data. The curves are intended to be demonstrative and should be given only qualitative significance.

DESIGN CONSIDERATIONS

RADIATION EFFECTS

The controlling consideration is the effect of radiation on all of a window's components, including tank lining materials, gaskets, and laminating liquids, as well as the transparent shielding material. The performance of complete window assemblies in gamma-ray shields with thickness equivalents of up to 4 ft of concrete has been well tested in operation. Additional laboratory testing is required to predict their performance under continuous exposure in thicker shields.

THICKNESS

Bulk shielding tests made on hot laboratory installations indicate that the gamma-shielding properties of ordinary concrete, magnetite concrete, zinc bromide, lime glass, and steel may be compared approximately on the basis of specific gravity alone.⁶

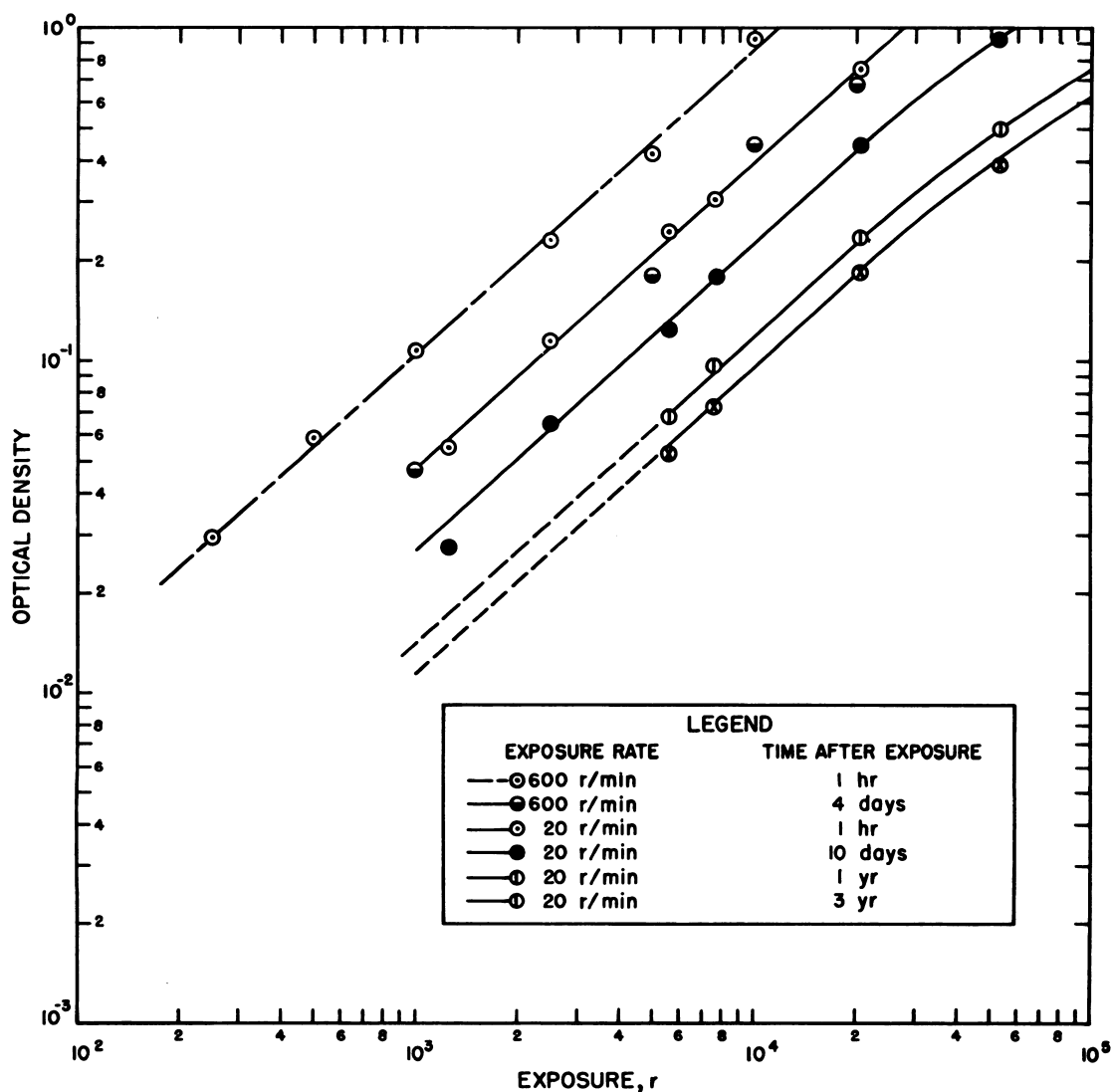


Fig. 7.2.1 — The Increase in Optical Density of Commercial Lime Glass with Gamma Irradiation. Submitted by Argonne National Laboratory, May 28, 1952. Optical density is the common logarithm of the reciprocal of the light transmittance. Values of density are for sodium light and a thickness of one HVL. This thickness was taken to be 3 in. for Co^{60} radiation and the geometry of the test. The exposure is the average received by a volume of air occupying the same position as the glass sample.

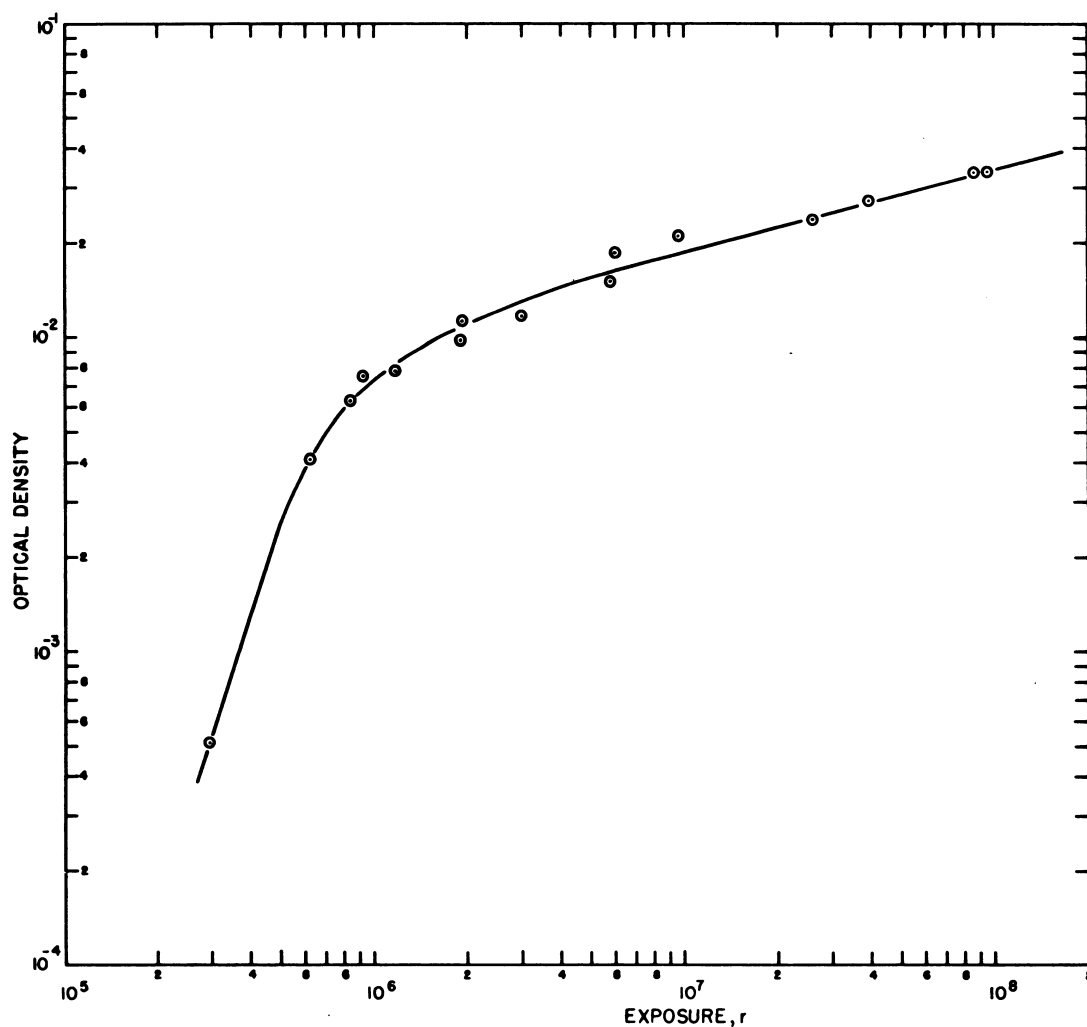


Fig. 7.2.2—The Increase in Optical Density of Nonbrowning Lime Glass with Gamma Irradiation. Submitted by Argonne National Laboratory, May 28, 1952. Values of density are for tungsten light, a thickness of one HVL, and an exposure rate of 4×10^4 r/hr. The HVL thickness was taken to be 2.88 in. for Co^{60} radiation and the geometry of the test.

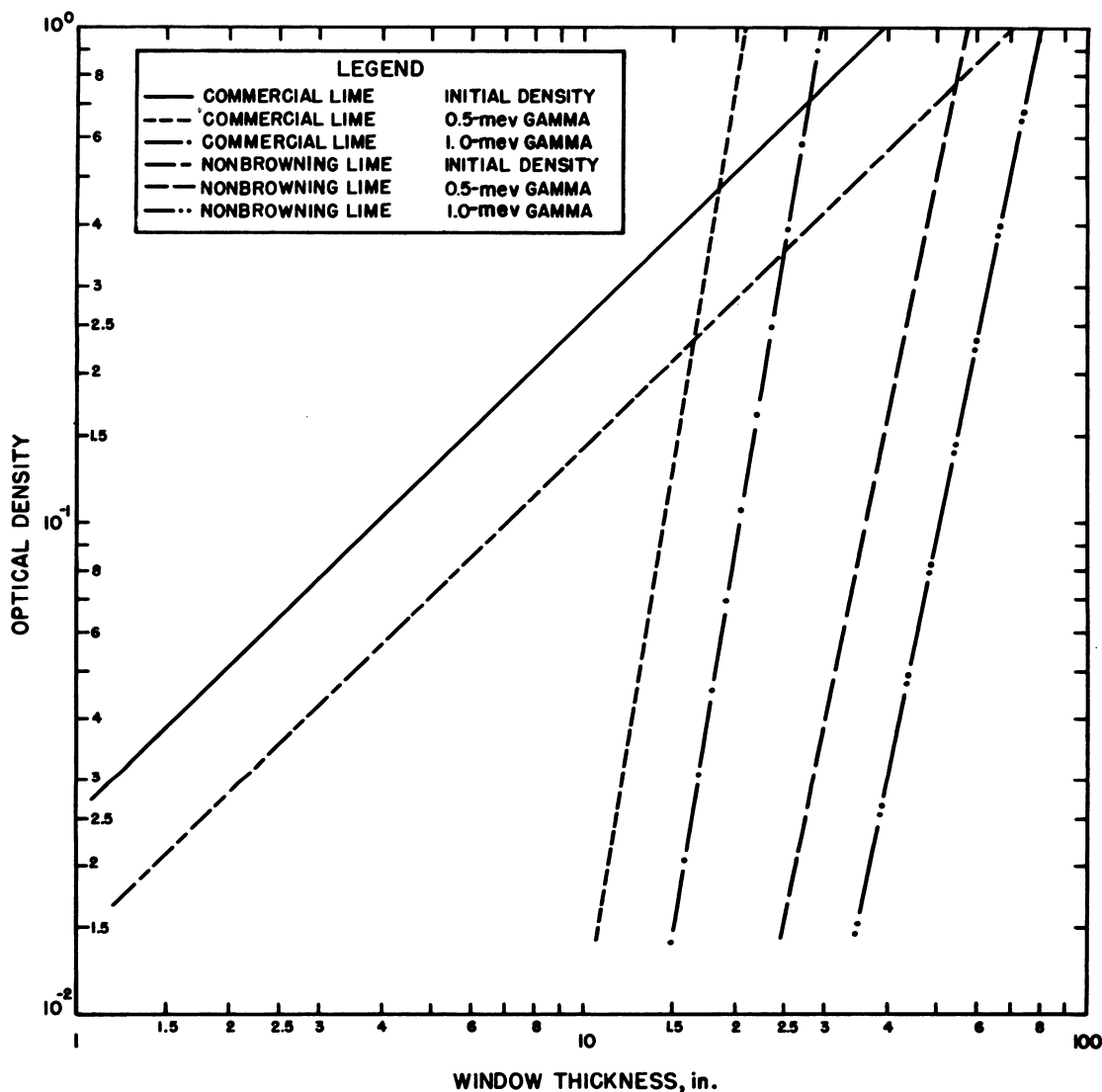


Fig. 7.2.3 — Increase in Optical Density of Glass Windows of Varying Thickness with Gamma Irradiation. Submitted by Argonne National Laboratory, May 28, 1952. Densities for commercial lime glass based on sodium light and for nonbrowning lime glass on tungsten light. All densities based on 1000 hr continuous exposure with an intensity of 10 mr/hr at the observer. It is assumed that the radiation beam is parallel. For commercial lime glass, the average HVL through the window was assumed to be 2.4 in. for 1-mev gammas and 1.67 in. for 0.5-mev gammas.

Lead glasses, however, are better shields than indicated by their specific gravities; a glass with a lead oxide content of 80 percent and a specific gravity of 6.2 is equivalent to steel for 1-mev radiation.

LIGHTING

The same considerations are involved in lighting a shielded enclosure as those for any other room. Proper weight must be given such factors as brightness, diffusion, and elimination of objectionable shadows, as well as lighting level.

Once a satisfactory level of illumination is determined, it is only necessary to increase the level to allow for the absorption of the window. The initial transmittance values should be reduced to correct for radiation darkening of the glass sections of the window.

AREA

The minimum area of a window depends on the degree of freedom desired in observer mobility or equipment position. For a small piece of fixed equipment, the narrow cone of vision through a small window will suffice. If the observer is free to move from side to side and up and down to "scan" a larger area, the next smallest aperture, whose frontal dimensions are easily calculated from the index of refraction, will result. If the same area must be scanned from a more fixed vantage point (limited mobility of the operator), the aperture at the inside face of the shield will be twice as large; the window in this case may be pyramidal, however, with a volume about equal to that for the second case. If the operator must have freedom to move about coupled with wide visual coverage of the interior, as with a fully master-slave manipulator, the aperture must approach the size of the working area.

CONSTRUCTION DETAILS

The following typical window constructions have been developed over the past several years and represent the best current practice for their respective types.

ZINC BROMIDE WINDOW

Figure 7.2.4 shows a zinc bromide window, $30 \times 36 \times 36$ in. thick, sealed in a concrete wall by means of a liner, G, which is cast directly into the wall. The use of a removable window allows it to be assembled in a room with special facilities and to be installed in the shield without interruption of other construction activities. The crack between the window tank and the liner is shielded by a step, H, made of lead which is held in place by strips of steel over the lead. When neutron radiation is present, cracks must be not only stepped but also calked tight with suitable material. The window tank is fabricated from hot-rolled steel plates with minimum of welding (intermittent structural welds on the outside and light seal welds on the inside) to decrease the possibility of warping the frame. Major machining is required only on the ends of the tank to form the gasket seats. The type of clamping arrangement illustrated here requires a minimum thickness ($1\frac{1}{4}$ in.) of tank wall at point M. The clamping bars B are not joined together at the corners so that each may seat individually. The gaskets, L, which will come in contact with zinc bromide should be fabricated from Koroseal (grade 116, B. F. Goodrich Company); the inside gasket should be continuous and cut from sheet stock.

The inside of the tank, K, is covered with seven coats of Amercoat 31 paint. The last coat should be black to minimize glare. All weld splatter should be removed and the welds smoothed by grinding before the paint is applied. Pits and irregularities may be filled with Amercoat 58 putty. All corners on the tank in contact with zinc bromide should be rounded to prevent thinning of the paint film.

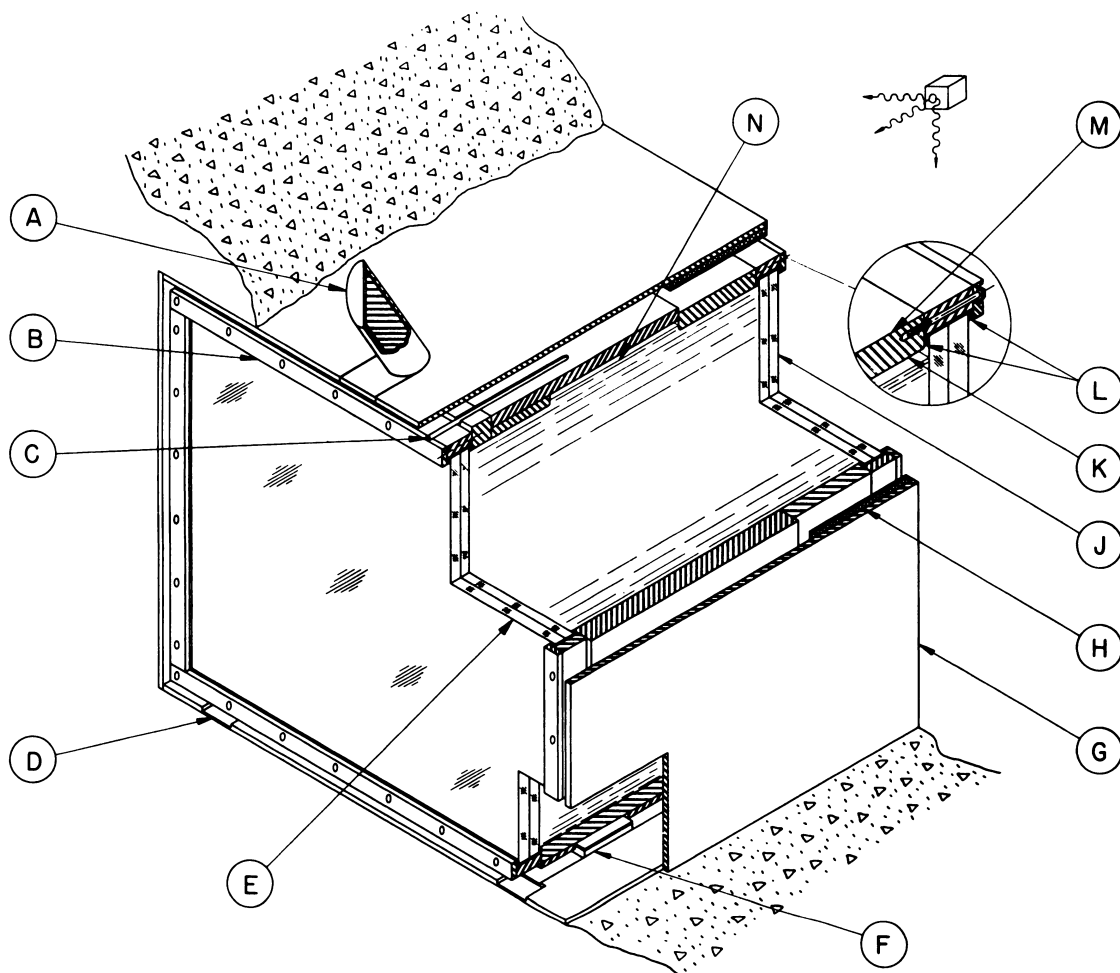


Fig. 7.2.4 — Construction Details of a Zinc Bromide Window. Submitted by Argonne National Laboratory, May 28, 1952. A, stirring port; B, clamping bars; C, air vent; D, transfer rail guides; E, laminated commercial glass; F, window tank supports; G, wall liner; H, lead step; J, laminated nonbrowning glass; K, window tank lining; L, gaskets; M, window tank wall; N, expansion chamber.

It is desirable to laminate the glass cover plates. In large windows it is required for strength, but it is always desirable as a safeguard in case one plate is damaged. The glass may be tempered if still greater strength is required. A load safety factor of 10, as recommended by the glass manufacturers, should always be used. The cover plate, J, on the active side must be made from nonbrowning glass. The cover plate, E, on the operator's side can be made from commercial plate glass selected for the same optical quality as the nonbrowning glass.

Provisions should be made to allow for the thermal expansion of the liquid. The coefficient of cubical expansion for zinc bromide is about $0.6 \times 10^{-3}/^{\circ}\text{C}$. For a temperature change of 20°C , a volume change of 1.2 percent results. If an external expansion tank is used, it should be located directly above the window tank and should be of minimum height so as not to increase excessively the hydrostatic pressure on the glass cover plates. An internal expansion space, as shown at N, is a satisfactory arrangement. The air vent at C or the vent on an external tank should be kept free at all times.

Striations will be encountered in the zinc bromide solution when originally filling the window tank or when making adjustments to the liquid level. These striations can be removed by stirring the solution for a short time. A stirring port, as shown at A, is convenient. A 1.5- to 2-in. pipe is lined with copper tubing which is silver-soldered to the main tank wall. The Amercoat paint is lapped well up on the copper to cover the joint. A steel plug is shown in the stirring port to cover the slot in the wall required to accommodate the port. The tank is slipped into the wall liner with the cover glasses installed. Notches in the liner at D aid in holding the rails used during the transfer from a transport cart. The tank is supported on cast-iron pads mounted on rubber, shown at F, which slide on runners machined in the liner, G. Only moderate pressures are thus required to jack the tank into place.

GLASS WINDOW

Figure 7.2.5 illustrates a glass window 30 × 36 × 36 in. thick. The glass used here is 1-in.-thick plate glass. Surface reflections from the many plates are almost completely

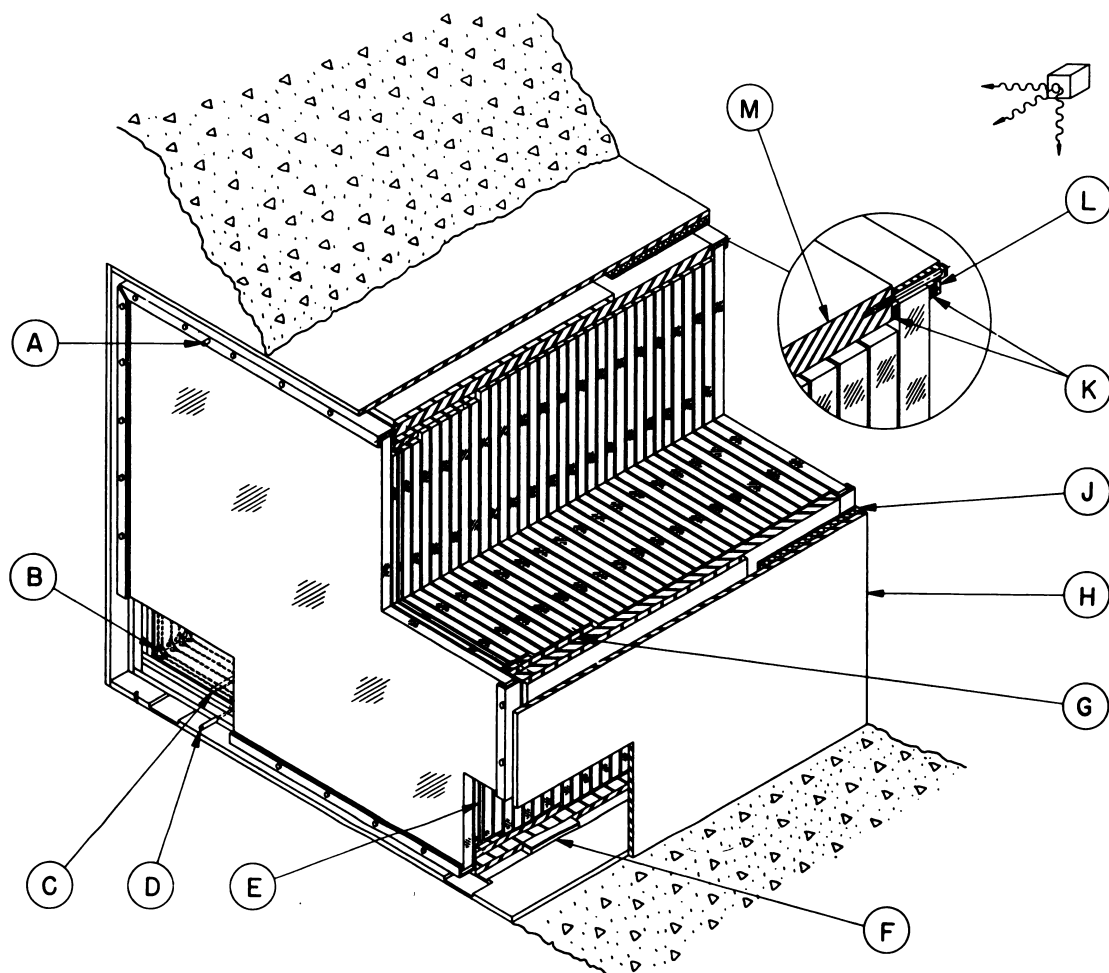


Fig. 7.2.5 — Construction Details of a Glass Window. Submitted by Argonne National Laboratory, May 28, 1952. A, air vent; B, spacers; C, glass plate supports; D, filling tube; E, fractional thickness plates; F, window tank support; G, radiation step; H, wall liner; J, lead step; K, gaskets; L, clamping bars; M, window tank wall.

removed by filling the space between the plates with a mineral oil with an index of refraction about equal to that of the glass. This space between the plates is maintained by soft copper spacers at the four corners, as shown at B. The thickness of the spacer is 0.025 to 0.035 in. Since the oil is of lower density than the glass, the crack between the glass and tank wall must be stepped as shown at G. The glass plates are supported on $\frac{1}{4}$ -in.-thick strips of Koroseal, grade 116, as shown at C. Koroseal also can be used for the gaskets at K. The clamping arrangement, shown at L, utilizes standard angle stock and can be accommodated by a plate thickness at M of as little as 1 in. It is satisfactory for sealing glass cover plates up to 1 in. thick. The diameter of bolts should be chosen carefully since bending stresses are developed in the bolts. The inside of the hot-rolled-steel tank can be smoothed by hand grinding and coated with a thin coat of clear Glyptal to facilitate thorough cleaning.

The glass plates are handled vertically in the washing and loading operation. Each plate is thoroughly washed, rinsed, and dried; it is then picked up by the edges with a mechanical device which supports the plate as it is inserted into the window frame. Because of the variation in thickness of the glass plates, the window might not be filled with an integral number of plates. Any remaining space should be filled with $\frac{1}{2}$ - or $\frac{3}{4}$ -in. plates or a combination of both, as shown at E. If they are installed on the operator's side of the window, these fractional-thickness plates may be commercial plate glass.

After the tank is sealed, the oil is introduced slowly through the lower filling tube at D. A slight space is left at the top of the tank for thermal expansion of the oil. The air vent at A must be kept open at all times.

COMPOSITE WINDOW

Combinations of transparent materials may be used to achieve a window with properties not possible with any single material. In some high-level applications it will be necessary to use nonbrowning glass instead of zinc bromide on the active side of the window to prevent bubbling of the solution. The use of dense lead glass on the operator's side will reduce the window thickness and the size of the window required to view a given area. In addition, these glass sections afford some protection to personnel in case of sudden loss of the liquid shielding. The window of Fig. 7.2.6 consists basically of zinc bromide solution, which is used for its optical quality and economy, supplemented by nonbrowning glass for radiation stability, and dense lead glass for reduced size.

SIMPLE REFLECTING SYSTEMS

One can see around a corner or through a labyrinth by reflection from one or more mirrors. The method is simple and reliable for applications where its optical characteristics suffice.

The angle of view is that subtended by the shield opening at the observer's point of view. Though direct radiation is avoided by a single reflection outside of the shield, air scattering at even moderate activity levels encourages that the shield opening be a minimum and some distance above the observer. The latter distance can be reduced by making additional turns in a shielded labyrinth. In either case, a static angle of view of 20° would be considered exceptionally large and many installations have 10° or less.

The static angle of view can easily be supplemented by a scanning mirror inside the shield. The scanned angle can approach 90° , but the scanning mirror becomes quite large beyond 60° , especially if coupled with a large static angle of view. One or both of the usual mirrors inside the shield can readily be made translatable to achieve a variety of view-points. The orientation of the view varies during scanning or translation, which may be confusing to the inexperienced observer at his fixed viewing station. An other-than-normal

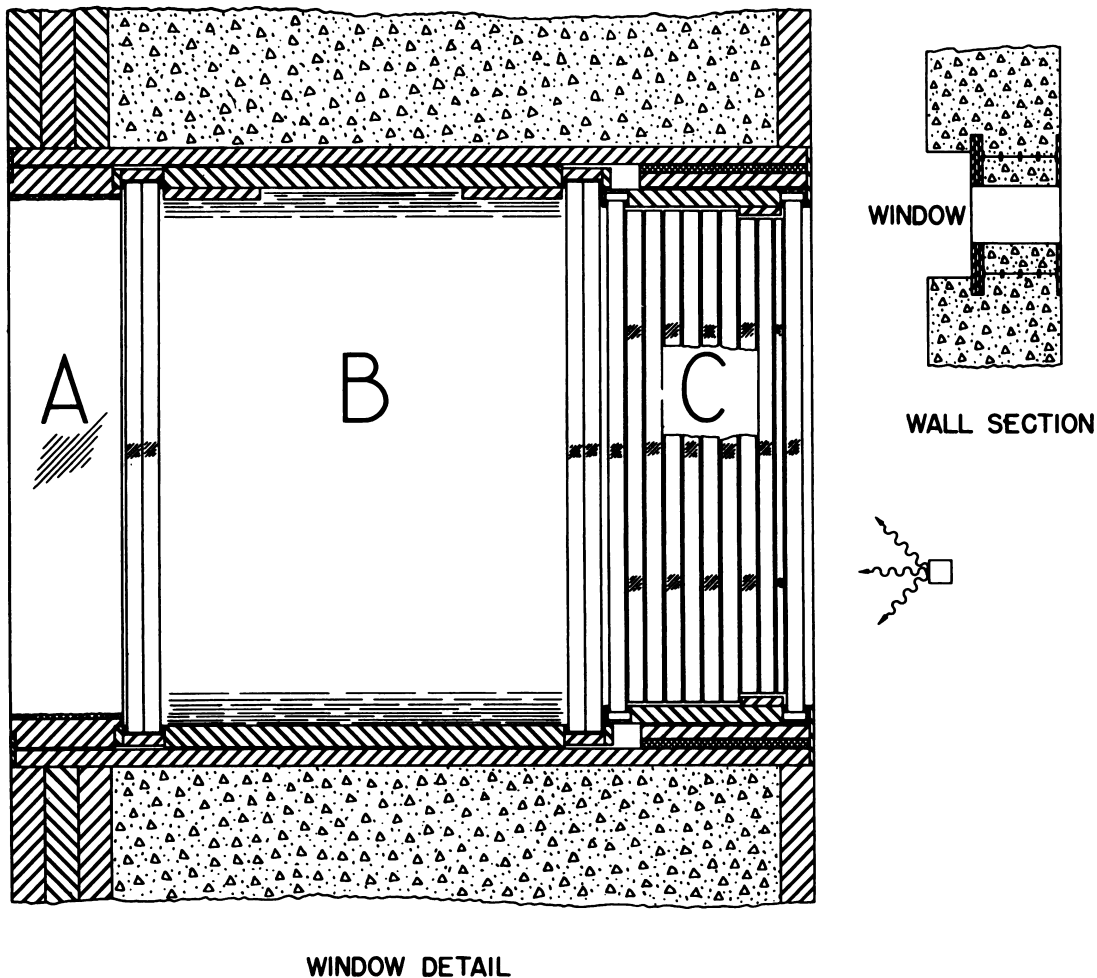


Fig. 7.2.6 — A Composite Window for High-level Applications. Submitted by Argonne National Laboratory, May 28, 1952. A, dense lead glass (two or more sections may be liquid-laminated with monochlorobenzene, currently used at HW, or the surfaces may be low-reflection coated); B, zinc bromide; C, non-browning glass and liquid laminant.

orientation is intolerable to the user of a master-slave type of manipulator but is satisfactory for switch-controlled equipment.

The image is perceived at a distance equal to the developed optical length. In practical designs, this length is two to five times the straight line distance; detail and depth perception are correspondingly impaired. Detail perception can be restored by the use of binoculars if the mirrors are front-silvered and of high quality. Such mirrors of large size are expensive and easily damaged. A larger angle of view and a shortened optical path are made possible by combining a mirror system with a semi-shielding window placed to intercept only scattered radiation from the cell interior.

PERISCOPES

DESCRIPTION

By definition, a periscope may consist of a simple reflection system as described above. Much improvement in performance is achieved, however, by adding a suitable lens train. A simple and much used form of periscope consists of a pair of telescopes facing each other as shown in Fig. 7.2.7 at (A). Military instruments of this type are often called "sights." An important optical result is the formation of an image of the observer's eye at the entrance pupil, from which point of vantage it can cover a much larger field than would be possible through the empty periscope tube.

If the hole through which the periscope must be used is long or of small diameter, additional lenses may be added to lengthen the instrument without increasing its diameter, as shown in Fig. 7.2.7 at (B). Extreme examples of this type are the gastroscope and the cystoscope for medical use and the borescope for industrial use.

In any region where the rays from each object point are parallel, there is some latitude in lens separation, allowing an extensible instrument. The periscope may be bent at any point with the aid of mirrors, or, in the parallel-ray regions mentioned above, with prisms. Some added protection against radiation may be obtained by filling the optical path with liquid or glass of the highest optical quality.

ADVANTAGES AND DISADVANTAGES

A periscope has the following unique advantages:

(1) For close examination of details, a large image of excellent quality can be achieved through even a thick shield.

(2) A periscope can be used in conjunction with instruments requiring eye-presence, such as a microscope or micro-hardness apparatus.

Its disadvantages are:

(1) The observer is closely confined to the eyepiece, which is apt to be tiring and certainly impedes any simultaneous work such as manipulation. This is particularly true of binocular or stereoscopic instruments.

(2) The usual field of 50° or less is insufficient for over-all observation. Mechanical scanning helps but is slow and unnatural.

(3) With a basic instrument, only one person at a time may see.

(4) Increasing the versatility of a periscope to overcome the shortcomings of the basic instrument also increases its complexity and cost.

DESIGN CONSIDERATIONS

The design of a high-performance periscope is not simple, and for a large, complex, or expensive instrument it is strongly urged that the services of a skilled optical designer be obtained.

OPTICAL COMPONENTS

Several standard periscope or "sight" designs employ lenses which may be adapted to most needs. "Surplus" lenses may sometimes be used but must be selected for compatibility if the image is to have good quality. Quite often, certain lenses must be specially designed, and it is then usually wiser to have the entire periscope designed as a unit.

Periscope components made of standard optical glasses are not resistant to darkening by gamma and other high-energy radiations. This shortcoming can be mitigated by placing

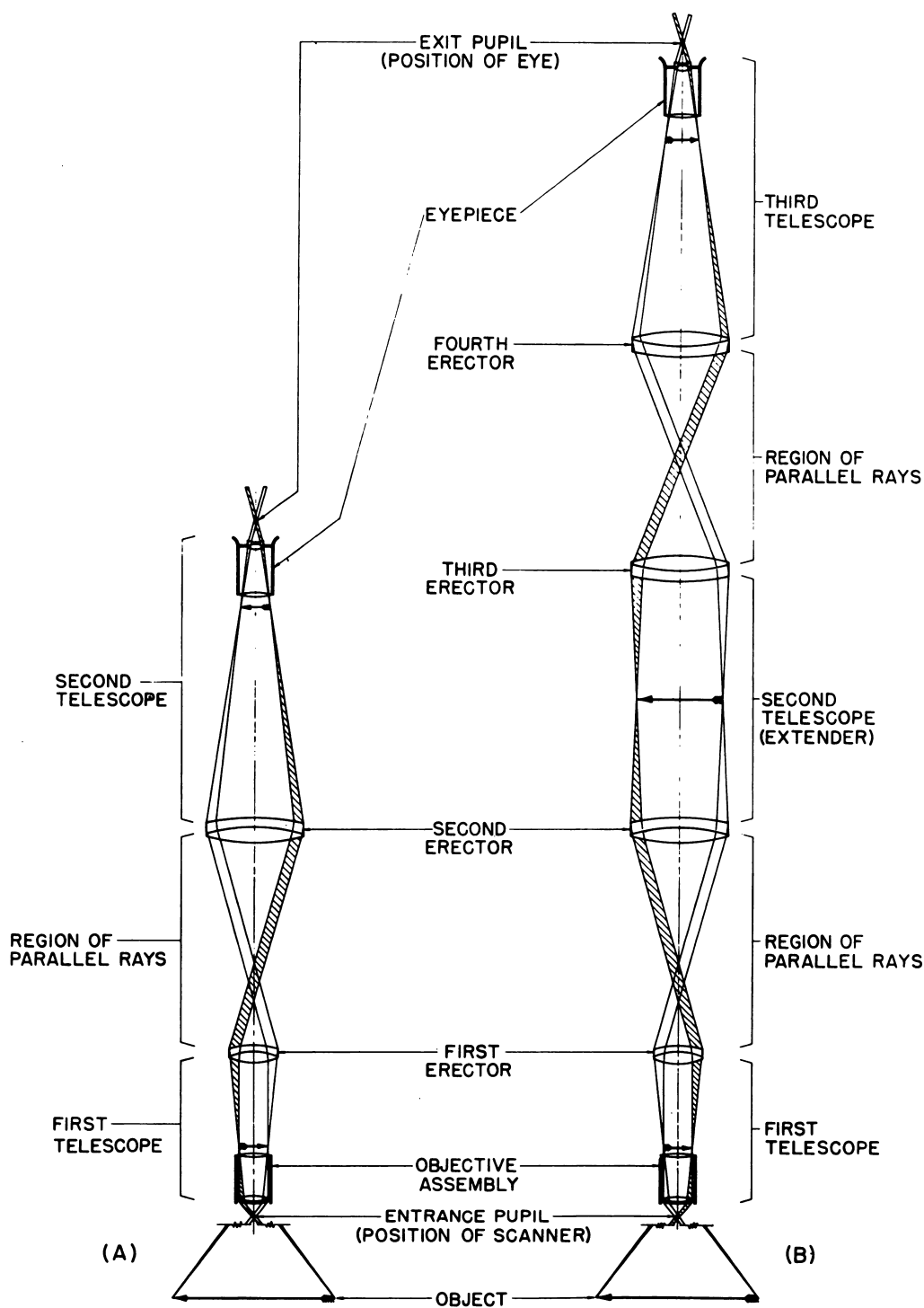


Fig. 7.2.7 — (A) A Simple Periscopic Sight. (B) Same with Extender Lenses.
Submitted by Argonne National Laboratory, May 28, 1952.

shielding around the optical glass parts which are closest to the source of radiation. Two alternatives are available: (1) Cerium-stabilized radiation-resistant optical glasses are known, but lenses made of them are not commercially available at this writing; (2) achromatic lenses that withstand intense radiation with minor effects can be made from styrene and acrylic resins. The best of the resin lenses are polymerized in a mold, and if the quantity involved is sufficient, they may be molded at a cost comparable to that of glass lenses.

DIMENSIONS

The relationship of the length of a periscope to its diameter has an important bearing on its performance. "Real" field of view (defined below), magnification, eye relief, and image quality usually require a length:diameter ratio of 30:1 or less. The diverging bundles of parallel rays between the erectors of Fig. 7.2.7 require either that the separation of the erectors be small or that the size of the second one be large.

EXTENSIBILITY

An extensible periscope can be made by providing for variable extension in any region where the image-forming rays are parallel. For a simple instrument having an aspect ratio of 25:1, the practical limit of the maximum length:minimum length is about 3:2. Consideration of Fig. 7.2.7 will show that if the separation is made too great some rays will fail to pass through the second erector, and the field will be curtailed. Eye relief will also decrease unless special designs are used.

ANGULAR FIELD OF VIEW

The "apparent" angle of view of a periscope is that subtended by the field which the observer sees from the exit pupil. An upper limit to this angle is set by the problems of eyepiece design. Conventional eyepieces allow an apparent angle of up to 40° or 50° before aberrations become intolerable. The "real" angle of view is that subtended at the entrance pupil by the field which the periscope covers without scanning. This real angle equals, by definition, the apparent angle of view divided by the angular magnification of the instrument. It has a normal upper limit of 40° to 50° for the same reasons that influence eyepiece design. It can, however, be made as large as 90° by accepting fractional magnification, some curvature of field, and other distortion. Limitations encountered elsewhere in the periscope design may further limit the angles of view.

MAGNIFICATION

Instrument magnification is the ratio of the apparent angle to the real angle of view. Usual values for this ratio are between unity and 2. It can be made much larger but at the expense of light intensity, image quality, or simplicity of design; in addition, the field of view may become so narrow that the observer may lose orientation and his concept of spatial relationship. If high magnification is required only intermittently, a turret of objective or eyepiece lenses or, at greater expense, a "zoom" arrangement can be provided. The apparent magnification increases considerably as the object is brought quite close to the objective lens. Although a system designed for viewing distant objects will not work as well for very close objects, a surprisingly large latitude in object-objective distance is possible with a low-power periscope, and where occasion demands, quite high magnifications may be obtained in this way.

EYE RELIEF

In general, the greater the eye relief, i.e., the distance between the eye lens of an eyepiece and the exit pupil, the larger the exit pupil will be, although its actual size depends

upon the elements of the periscope. In celestial telescopes and other instruments where high resolution is important, best results are achieved by design which results in a small exit pupil and small eye relief. For persons engaged in manipulation and manual control, it is desirable to have both large enough to allow considerable freedom of motion of the head and body. This is usually, though not necessarily, achieved by low magnification.

SCANNING

The usefulness of a periscope is greatly increased if the line of sight emerging from the objective lens can be deflected through a variable angle. Such provision enables the observer to scan the interior of a cell and view a larger area than the static angle of view permits. The simplest means for achieving this is a small prism or mirror arranged to pivot in front of the objective lens. By rotating the prism or mirror around two axes, an entire hemisphere is easily covered. With either of these simple provisions, however, the orientation of the view is altered. Reflection causes an inversion of field, and rotation causes the field to revolve in the eyepiece, either of which can be compensated by additional optical elements.

DEPTH PERCEPTION (BINOCULAR DESIGNS)

Although some depth perception is possible with a monocular instrument because of eye accommodation and perspective effects, true stereopsis and eye convergence depend upon the use of a dual instrument, which might be termed a "binocular periscope." The optical and mechanical problems attending a versatile binocular periscope are formidable, and the need for stereovision should be clearly established before a design is attempted.

BORESCOPIES

Often it is necessary to inspect the inside surface of a slender tube or similar configuration or to pass the whole length of a long periscope through a small opening. The name "borescope" is given to this type of periscope. For use in an unlighted tube, the head may be provided with a small lamp near the objective lens. Scanning is usually done by rotating the whole instrument which is provided with a fixed mirror and by moving it back and forth along the tube. Variable power and similar features common to other periscopes are usually omitted.

An inherent optical defect of the borescope is curvature of the field, the center seeming to be much nearer than the edge. This is an additive effect requiring special compensation in a train of erectors. Although it is often tolerable to the eye, it is troublesome when a camera is to be used to record the image.

In periscopes of this slender construction with a multiplicity of lenses in train, resolution is not as good as in an instrument of the same length but which is not so restricted in diameter.

REPRESENTATIVE INSTALLATIONS

The following descriptions and illustrations indicate the size, complexity, and cost of a wide range of instruments. In general, mechanical construction costs account for 80 to 90 percent of the prices given, which are based on current production in small lots by one of the lower bidders; commercial bids may range up to 10 times the given figure.

SHORT SCANNING PERISCOPE, FIG. 7.2.8

This simple instrument was inserted at an angle of 45° through a 24-in. concrete wall to enter the enclosure near an inside corner. The enclosure was scanned by rotating the entire tube and pivoting the scanning mirror. Mirror reversal and rotation of the field

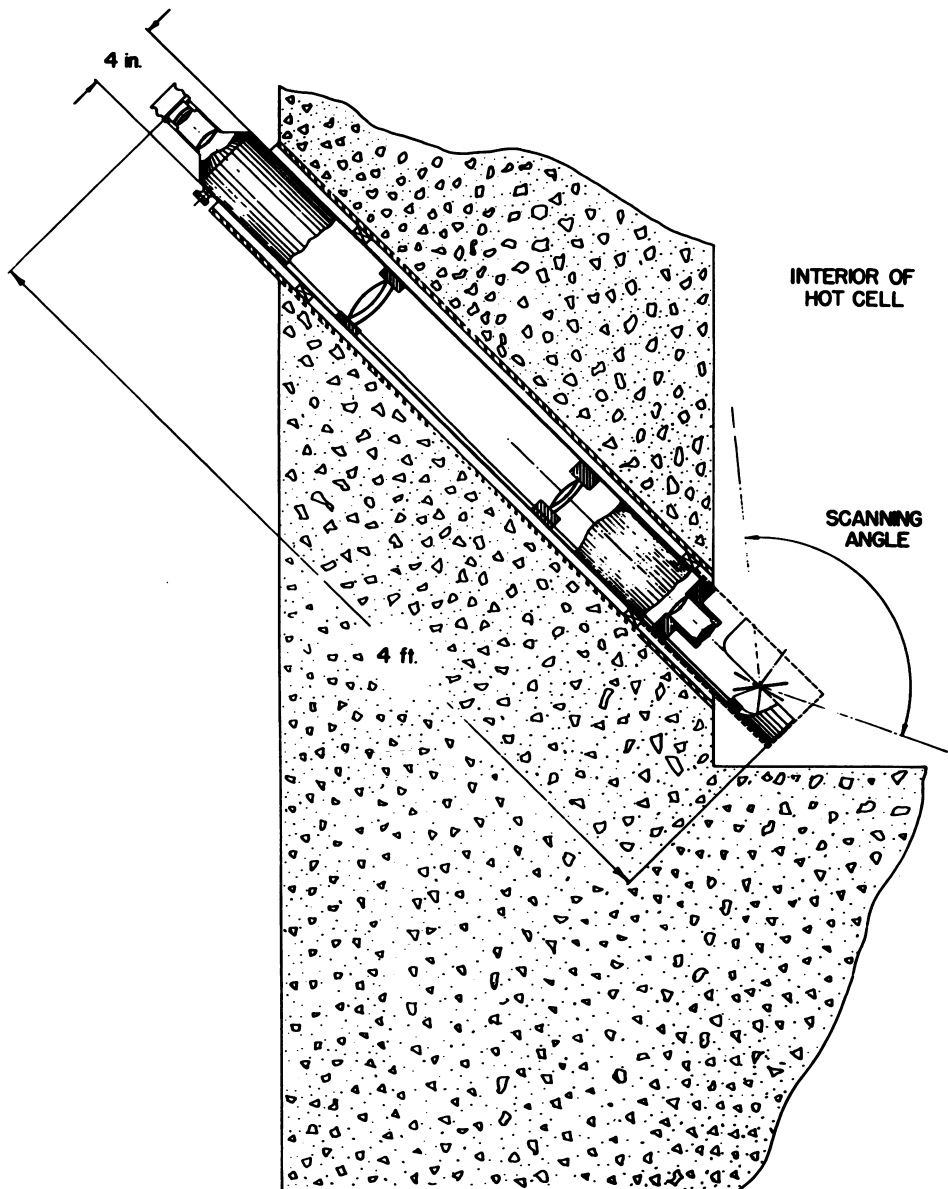


Fig. 7.2.8—Short Scanning Periscope. Submitted by Argonne National Laboratory, May 28, 1952.

during scanning were not objectionable since the contents of the cell were well known. The real field is about 25° and the power unity, except for very near objects. \$800 to \$1200.

CORNER PERISCOPE, FIG. 7.2.9

This instrument is optically similar to that shown in Fig. 7.2.8 but utilizes four bends to baffle out the radiation. Two mirrors are used at the objective to yield uninverted images. Scanning is accomplished by pivoting the first mirror and by motorized rotation of the head. The real field is about 25° and the power unity, except for close objects. \$2000 to \$2500.

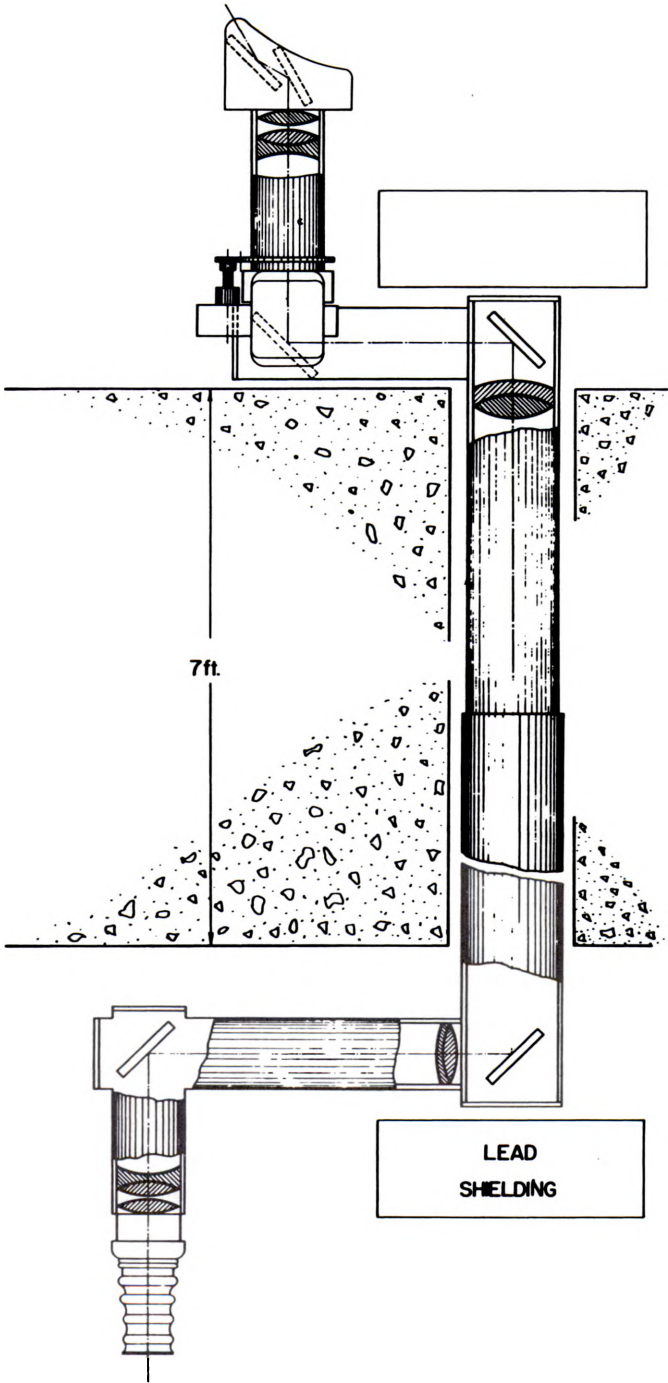


Fig. 7.2.9 — Corner Periscope. Submitted by Argonne National Laboratory, May 28, 1952.

SADDLE PERISCOPE, FIG. 7.2.10

This instrument is similar in optical design to those shown in Figs. 7.2.8 and 7.2.9, except that it also contains unit power extenders to keep the tube diameter small. It is designed to rest on or ride along the top of a lead wall. Scanning is done by manually turning the head and mirror. The scanning end, comprising the objective and first erector, may be raised or lowered. The eye end is also extensible to accommodate persons of different heights. Real field is about 25° and power, unity. \$2000 to \$2500.

SPOT MAGNIFIER, FIG. 7.2.11

This low-cost magnifier will serve where a $2\times$ to $5\times$ magnification of only a small area is required. It should be made of noncoloring glasses. A pair of achromats a few inches from the sample provides the prime magnification. The image thus formed at infinity is focused at normal reading distance by a large simple lens. The image is inverted, but if necessary a 4-mirror erector system may be added. \$100 to \$200.

OVER-ALL VIEWER, FIG. 7.2.12

The short-focus objective of this periscope forms a reduced image in or near the rear surface of the third element. Using a Bausch and Lomb No. 28 aspheric condenser followed by a Cinephor No. 20 aspheric condenser, selected for quality and properly spaced, the image is rectilinear. As shown in the figure, a bi-convex spherical element may be added to increase the field angle. A transfer system of two achromats forms a final erect image near the large (8- to 10-in.-diameter) field lens. No eye lens is used. Since the rays from any object point proceed beyond the field lens in an expanding cone, binocular observation with the unaided eyes is possible if the head is placed at an appropriate distance. Field curvature must be corrected for photographic use. Chromatic and spherical aberration, which are both considerable, are limited in effect since the aperture-stop of the system is the pupil of the eye. The instrument is not a substitute for a conventional periscope but can fulfill the occasional need for a very wide (90°) real angle of view. \$750 to \$2000.

HIGH-POWER MICROSCOPE-PERISCOPE COMBINATION, FIG. 7.2.13

Where high magnification is required, the microscope should be inside the irradiated area; the image so formed can then be transferred through the shield by a conventional periscope. To put the periscope first and the microscope outside the shield would require that the former be capable of good resolution with powers equivalent to those of the latter. One obvious disadvantage is that standard microscope objective lenses color rapidly under the intense radiation. Another is the complexity of focusing and other manipulations. An advantage is that the conventional periscope through the shield may serve other purposes when not used with the microscope.

LOW-POWER PERISCOPE COMBINATION, FIG. 7.2.14

This binocular arrangement consists of two identical trains of lenses, with mirrors so arranged that the divergent beams from the image duplicate those from the object. Both object and image are at the principal foci of the lenses closest to them. The chief limitation of this instrument is the relative apertures of these lenses. If their diameters are too small in relation to their focal lengths, the field of view in the microscope will be diminished, especially for higher powers. A stereoscopic camera arrangement may be substituted for the binocular microscope, but field curvature is encountered. Powers up to $30\times$ are feasible. \$1000 to \$2500.

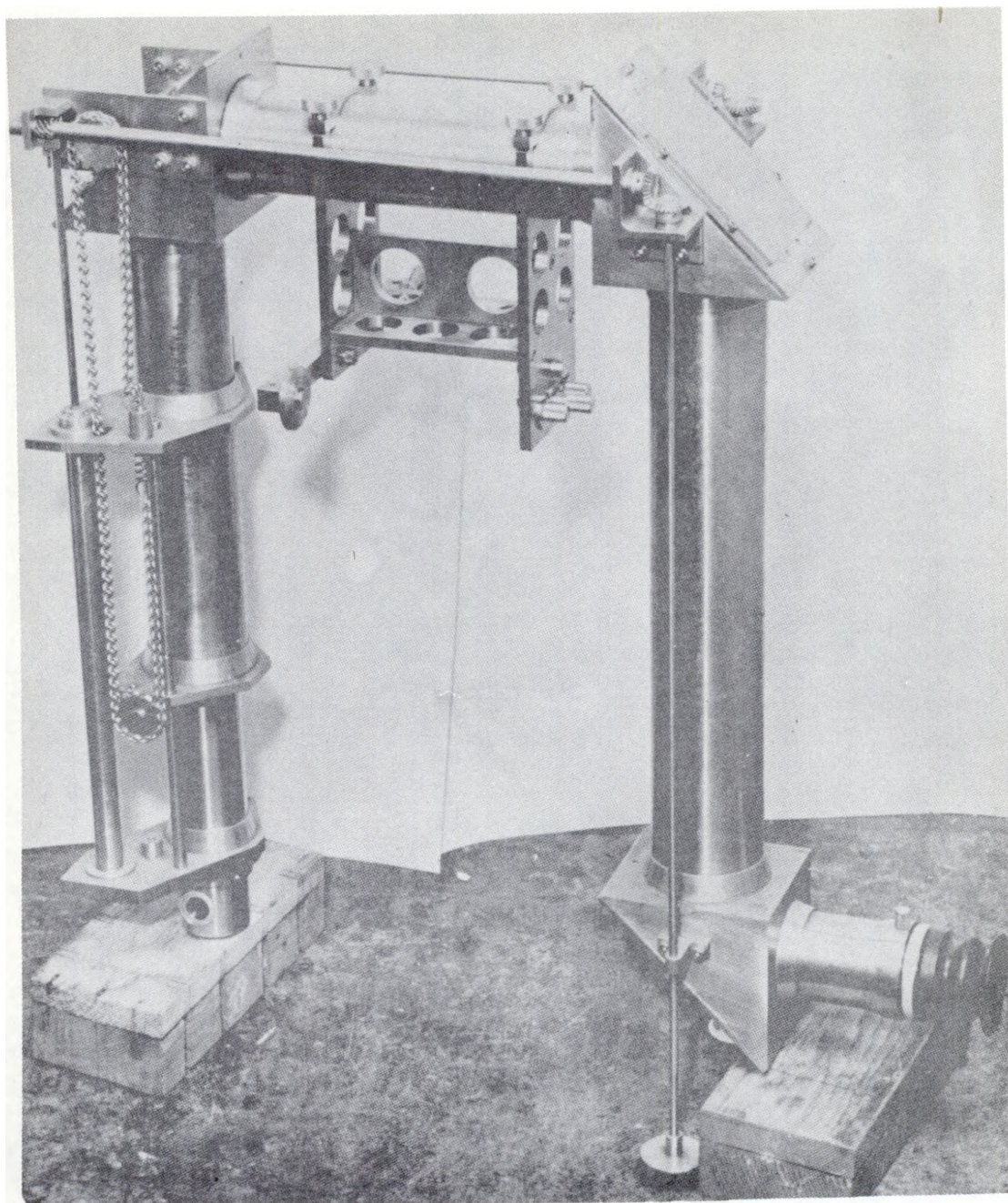


Fig. 7.2.10 —Saddle Periscope. Submitted by Argonne National Laboratory, May 28, 1952.

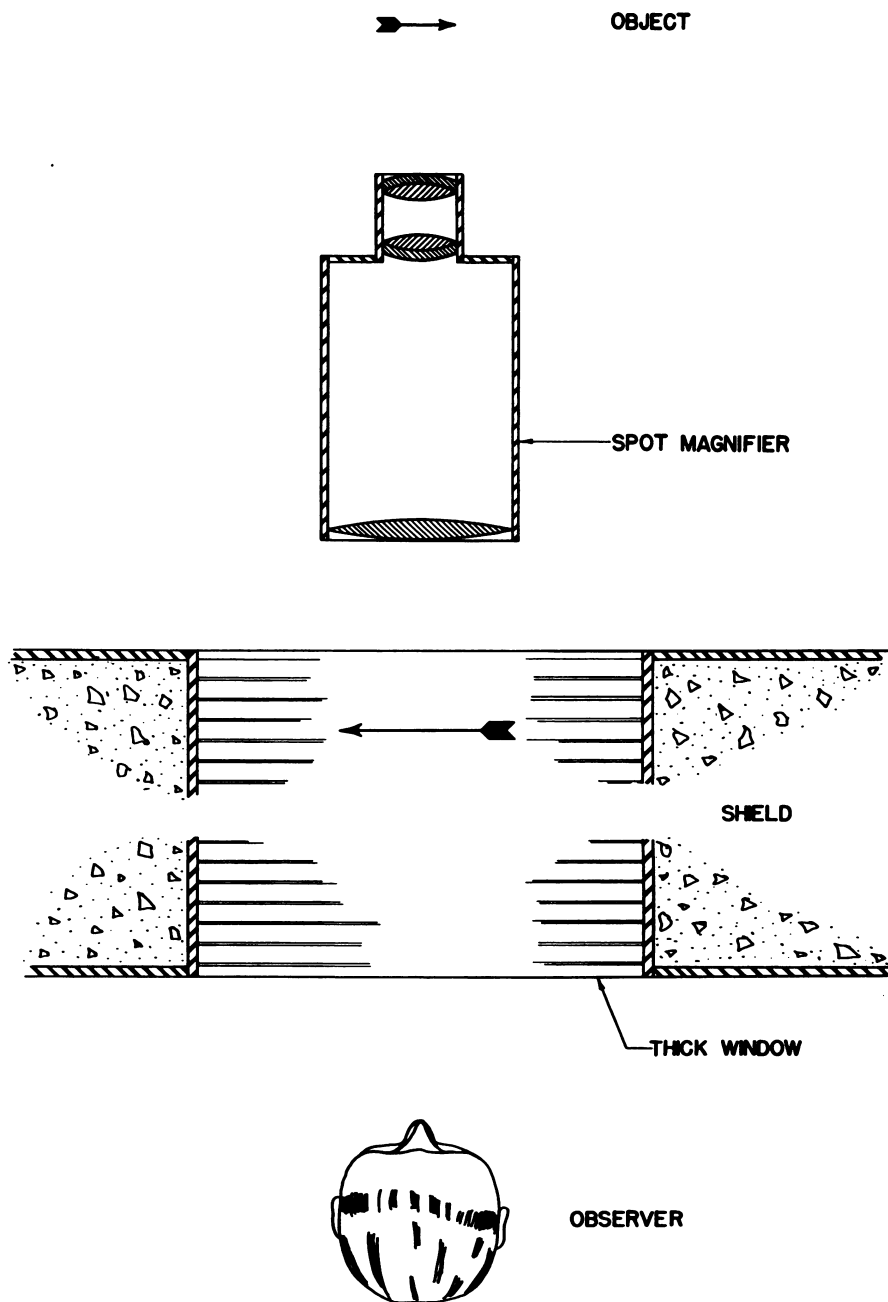


Fig. 7.2.11 — Spot Magnifier. Submitted by Argonne National Laboratory, May 28, 1952.

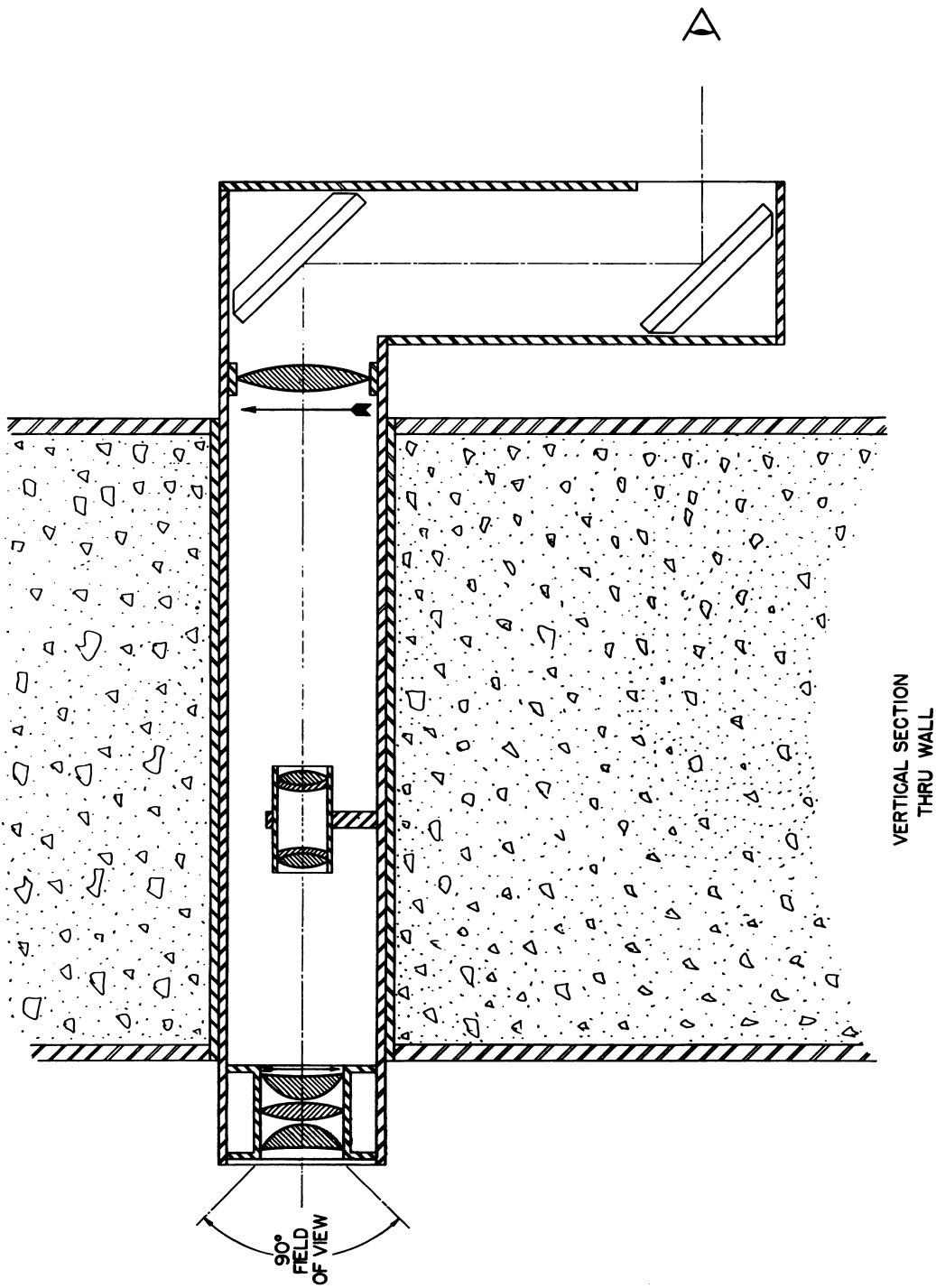


Fig. 7.2.12 —Over-all Viewer. Submitted by Argonne National Laboratory, May 28, 1952.

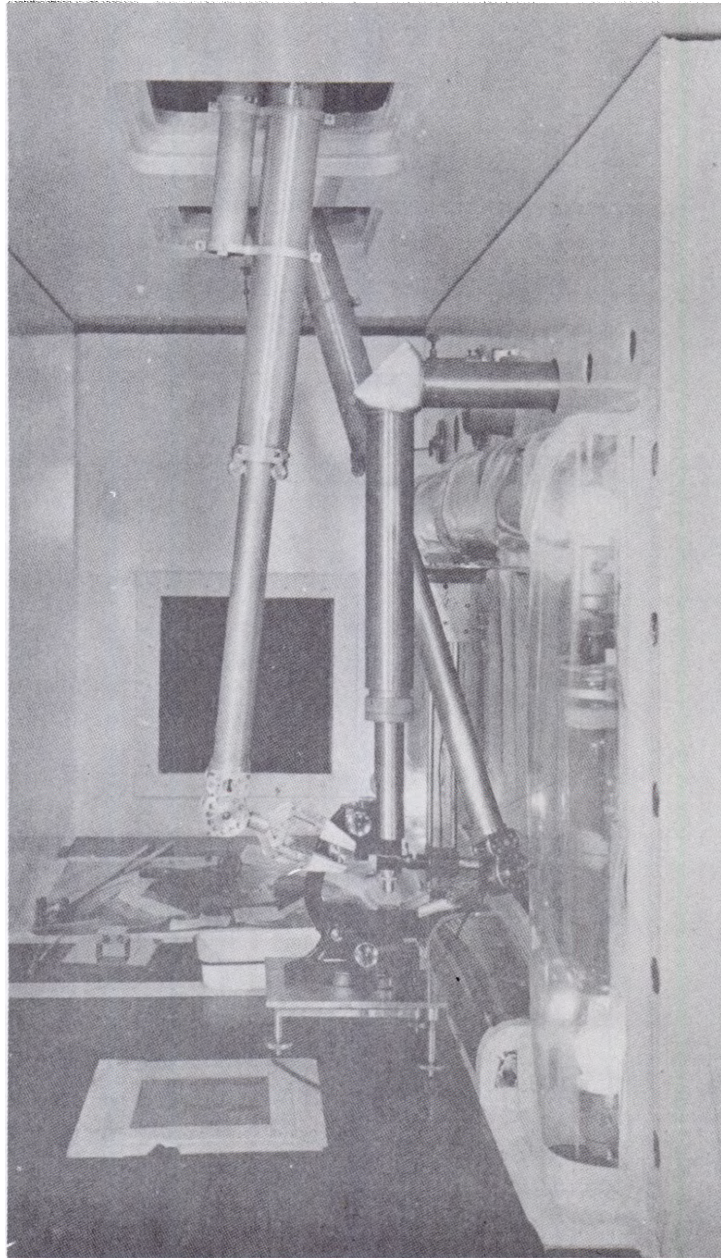


Fig. 7.2.13 — See facing page for legend.

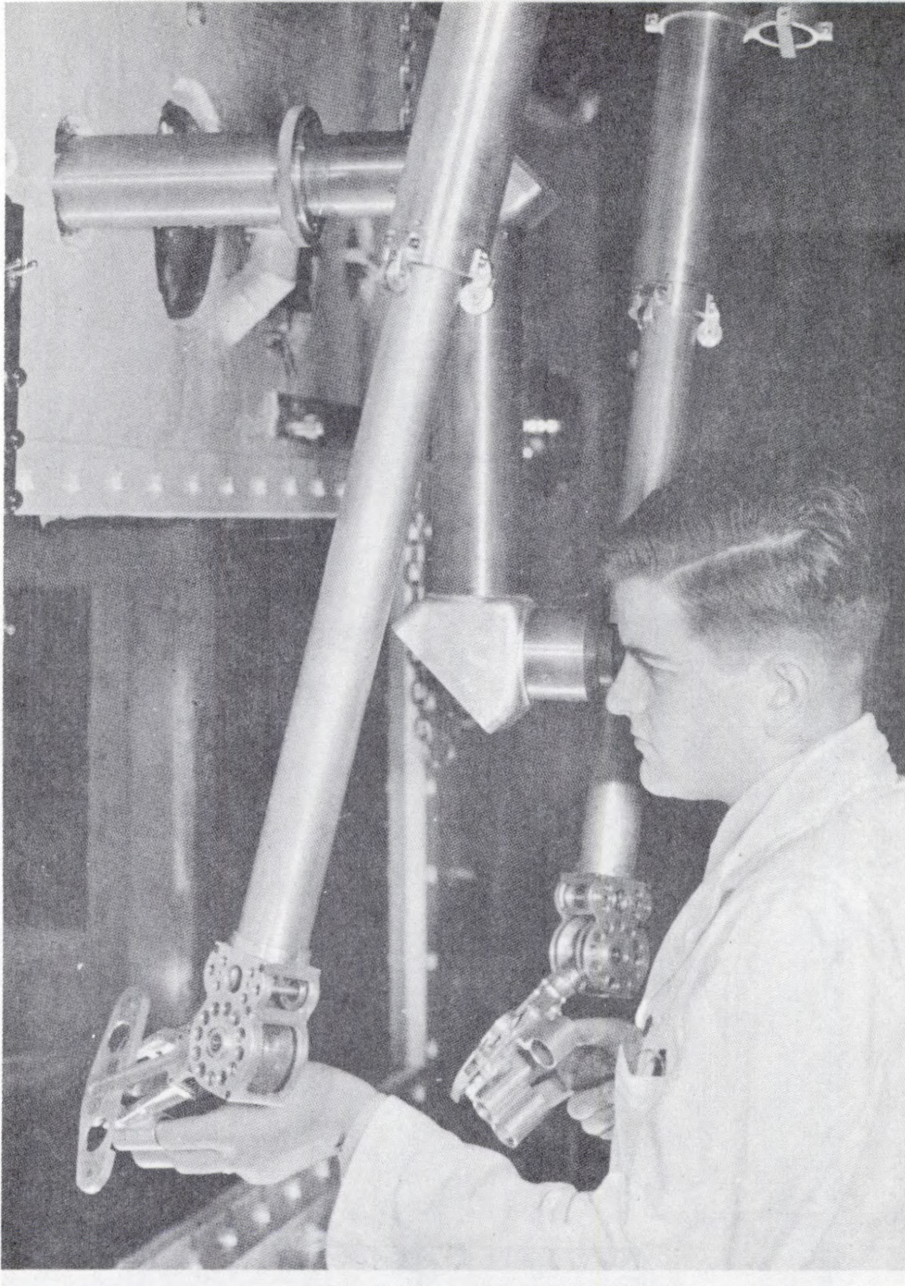


Fig. 7.2.13 — High-power Microscope-periscope Combination. Submitted by Argonne National Laboratory, May 28, 1952.

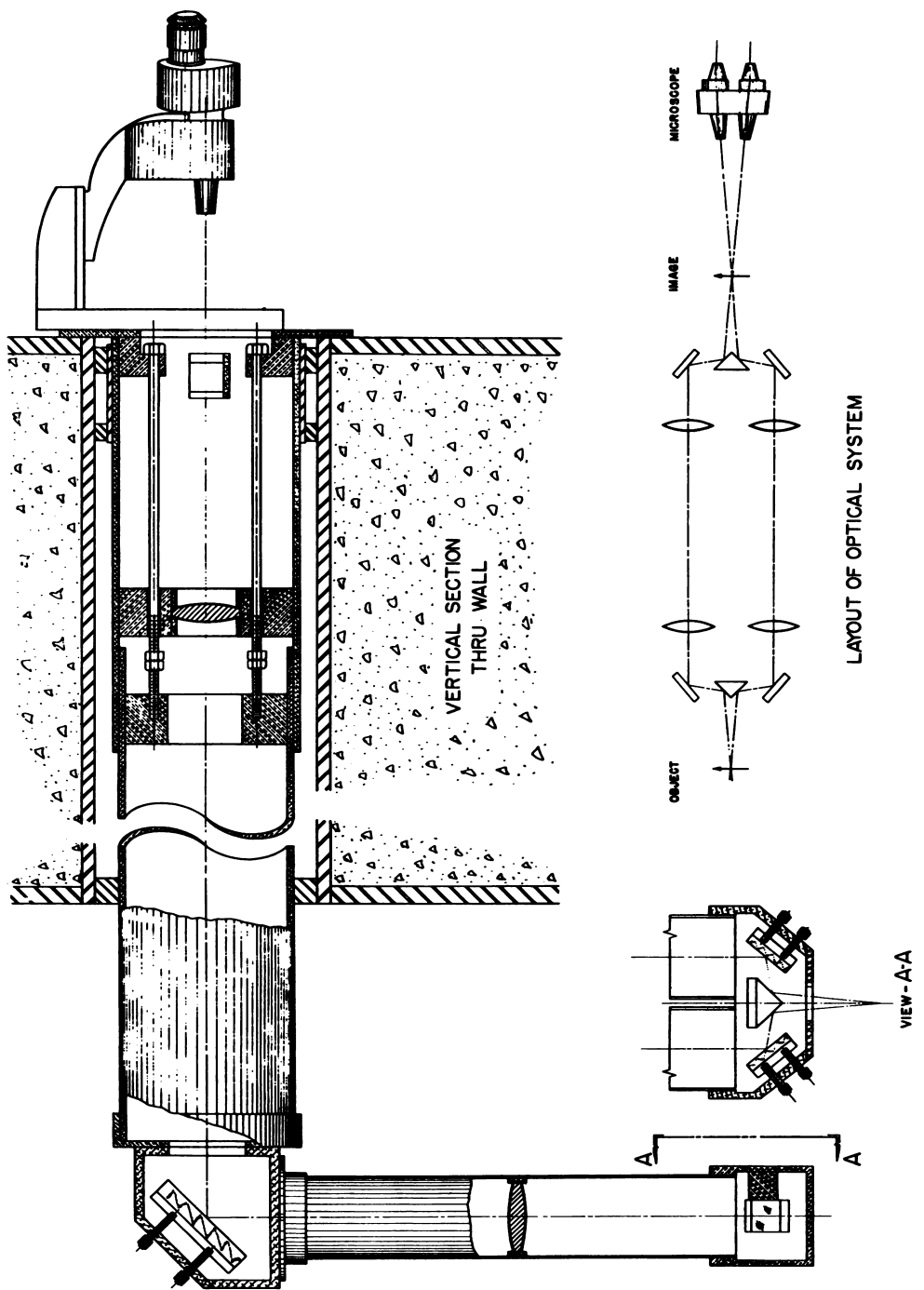


Fig. 7.2.14 — Low-power Periscope Combination. Submitted by Argonne National Laboratory, May 28, 1952.

BORESCOPE, FIG. 7.2.15

This instrument was built to provide inspection of process tubes in a reactor. The design illustrated was $1\frac{3}{8}$ in. in diameter and capable of extension to 50 ft or more by the addition of successive 8-ft or 4-ft sections. A 4-ft section contained two identical erector lenses with parallel rays between them and their principal foci near the ends of the tube, optically arranged as in Fig. 7.2.7 at (A). An 8-ft section contained four such lenses, optically arranged as in Fig. 7.2.7 at (B). All sections of equal length were completely interchangeable. Price with terminal sections and 48 ft of extenders, \$4500 to \$15,000.

ELEVATOR PERISCOPE, FIGS. 7.2.16, 17, 18

The objective and first erector are set horizontally with scanner and other optical parts. Scanning is horizontal only. This assembly moves vertically from top to bottom of the hot cell. The light-beam from it is reflected down to a tilting mirror from the upper portion of the cell and up from the lower portion. As in Fig. 7.2.8, the receiving portion of the periscope is horizontal and inclined at an angle to provide maximum baffling of high-energy radiations from the interior of the hot cell.

Figure 7.2.17 shows the moving portion of the periscope, exposed by rolling the steel door aside, and a viewing tube through another door to a second system. Fig. 7.2.18 shows the exterior with both doors closed and the entire unit in operation. \$5000 to \$7500.

TELEVISION

Television may be useful when:

- (1) The operation is so hazardous or inaccessible as to require viewing from a distance or more than about 100 ft.
- (2) Simultaneous observation of widely separated points, by one operator or at one control station, is required.
- (3) The view must be brought out around numerous bends or obstructions.
- (4) Viewing equipment must be provided in a minimum of time, as in case of catastrophe.

As of this writing, the view possible with the best of commercially available television equipment is inferior to that of even a moderately good periscope if an all-optical method is possible. Table 7.2.4 lists some characteristics of the major wired TV systems.

If the best of these pictures is viewed from a distance such that it subtends the usual camera field of 40° , the resolution is about 5' compared with the 1' of which the human eye is capable. The image is further degraded by limited contrast ratio and linearity.

Since the image has no depth, television cannot provide eye-accommodation effects to aid depth perception. Several varieties of stereotelevision have been demonstrated, however. In each, the eyes are provided with displaced viewpoints, an important factor in depth perception.

Available commercial wired-television chains have been considerably improved in simplicity and reliability over earlier models. In mockups and installations, however, they require frequent service and adjustment, and skilled technicians are a practical necessity. At least one complete stand-by unit should be provided if reasonably uninterrupted service is expected.

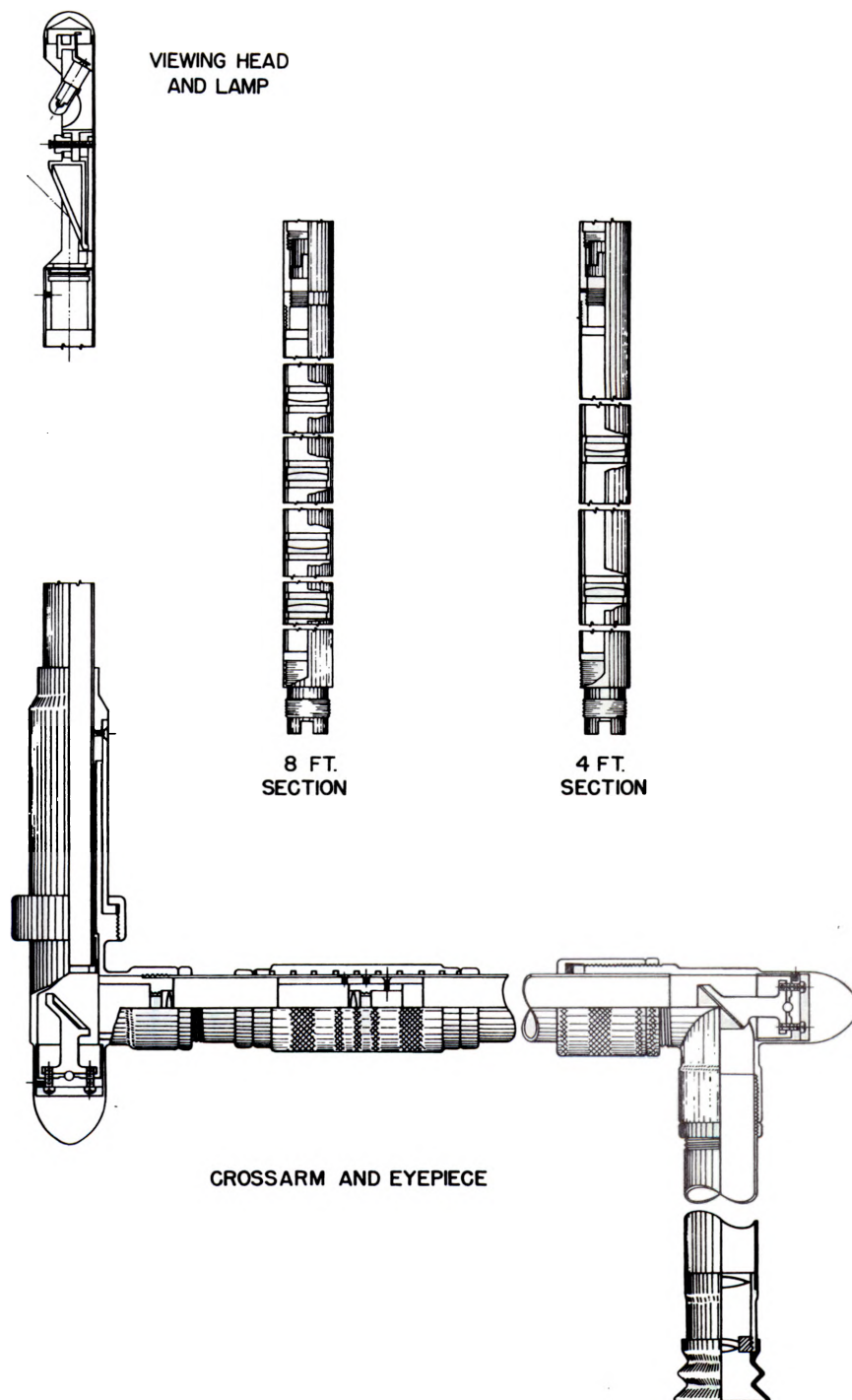


Fig. 7.2.15 — Borescope. Submitted by Argonne National Laboratory, May 28, 1952.

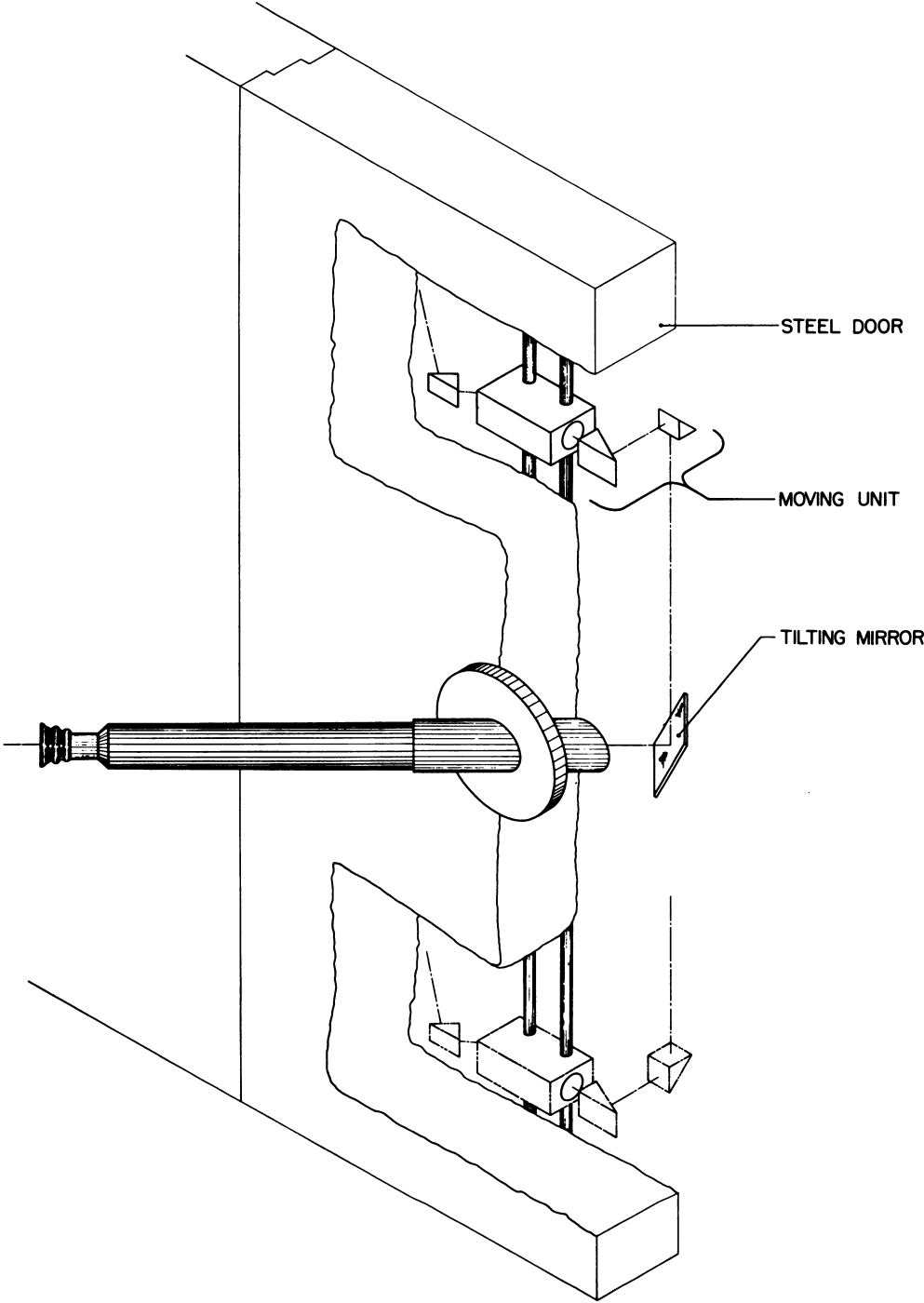


Fig. 7.2.16—Elevator Periscope Schematic. Submitted by Argonne National Laboratory, May 28, 1952.

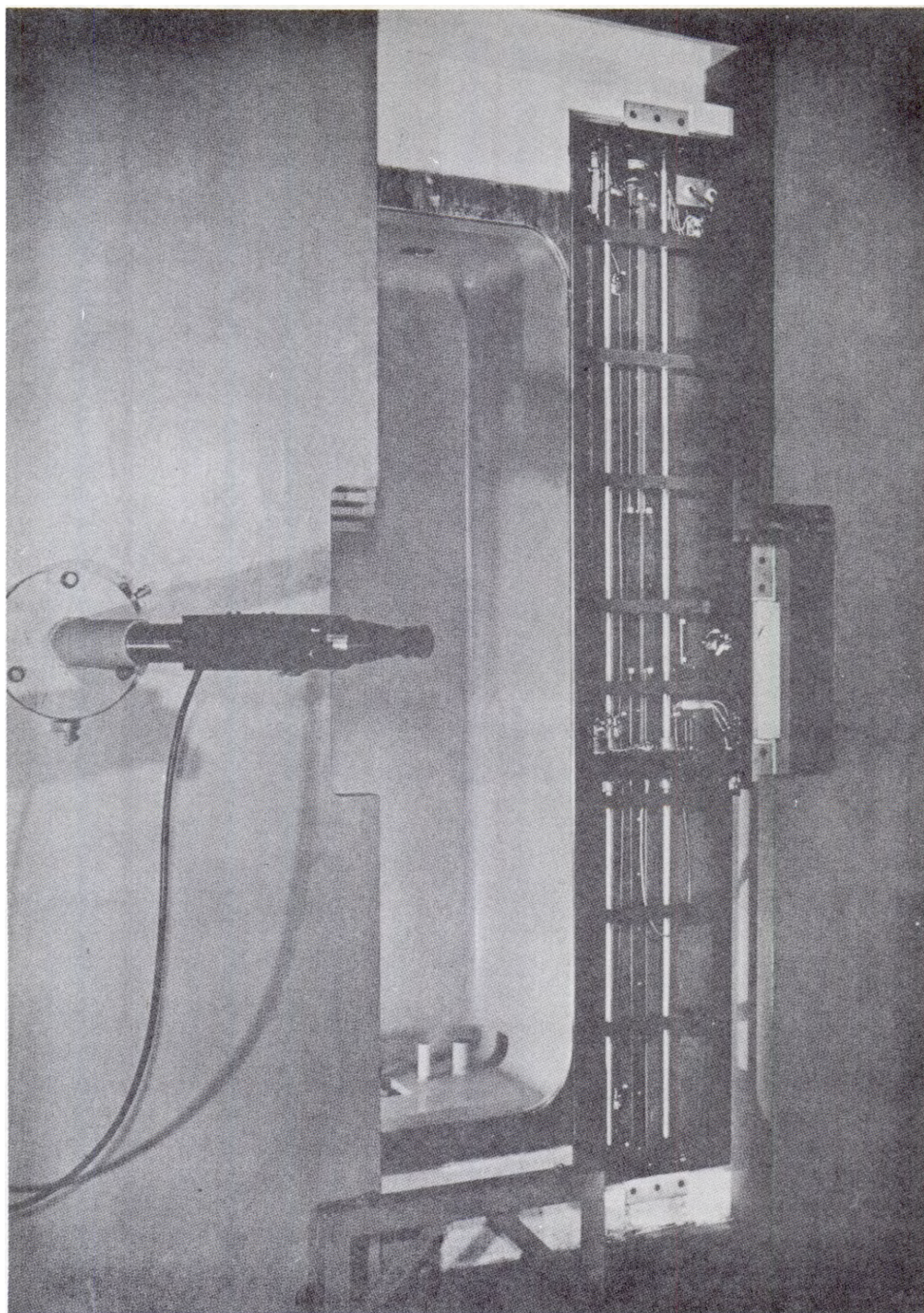


Fig. 7.2.17 — Moving Unit with Door Open. Submitted by Argonne National Laboratory, May 28, 1952.

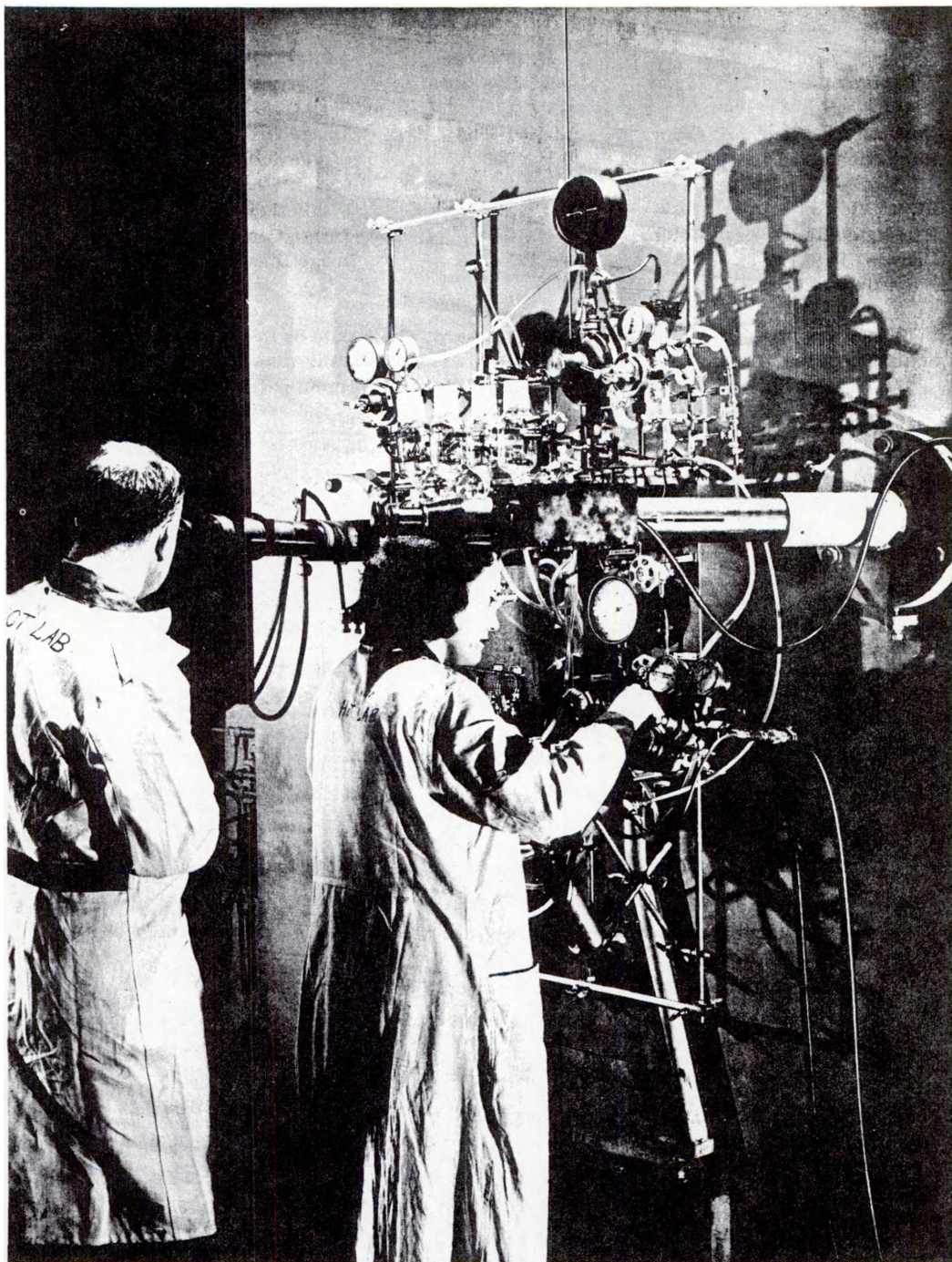


Fig. 7.2.18—Elevator Periscope with Cell in Operation. Submitted by Argonne National Laboratory, May 28, 1952.

Table 7.2.4 — Commercial* Wired TV Chains

Designation	Type	Resolution, effective lines	Pickup tube type	Light level required†
DuMont	Color	450–500	Image Orthicon	Medium
Remington-Rand “Vericon”	B&W	300	Vericon	High
RCA “Vidicon”	B&W	300	Vidicon	High
Remington Rand	Color	350	Image Orthicon	Medium
Diamond Power Specialties Corp.	B&W	250–300	Image Dissector	Very high

*There are many other suppliers, not listed here, who should be investigated at the time of actual purchase. Their products are generally not as standardized as those shown

†An image orthicon, without filters, would require “low” lighting level

REFERENCES

1. W. B. Doe, ANL Memo Report, Aug. 22, 1951 (classified).
2. W. B. Doe, ANL report, to be published.
3. Specifications and Requirements for Optical Grade Zinc Bromide Solution, ANL, July 8, 1952.
4. Nonbrowning Lime Glass for Shielding Windows, ANL, Aug. 15, 1950.
5. R. H. Kernohan and G. M. McCammon, Fading Characteristics of Gamma Induced Coloration in High Density Glass, ORNL-975, 19 pp, Mar. 20, 1951.
6. Paper 31, ANL-4670, 368 pp, May 16-18, 1951 (classified).

SELECTED READING LIST

NATIONAL NUCLEAR ENERGY SERIES, Div. IV, Vol. 8, McGraw-Hill Book Company, Inc., New York, 1954.

FUNDAMENTALS OF OPTICAL ENGINEERING, D. H. Jacobs, McGraw-Hill Book Company, Inc., New York, 1943.

THE PRINCIPLES OF OPTICS, A. C. Hardy and F. H. Perrin, McGraw-Hill Book Company, Inc., New York, 1932.

CHAPTER 7.3

Hot Laboratories

D. F. Uecker

Shielding, handling, and viewing means are necessary in most experiments involving radioactivity. For a single-purpose facility accommodating a production or routine analytical process, the treatment of these topics elsewhere* in this handbook may suffice. In the case of an experimental facility or hot laboratory, the design problems are more complex. The nature of future experiments and the equipment to be employed may vary widely and may be quite unpredictable at the time the facility is constructed. If the activity to be handled is on the order of many curies of fission-product activity, a hot laboratory will represent a major investment.

The need for versatility has been generally recognized, but different approaches to it have been made. A choice may be made between the following extremes: (1) initially providing a permanent shield with general-purpose manipulators and viewing means adequate for any experiment or (2) initially providing only a shield having many access ports or easily altered sections for viewing and remote-handling equipment devised specifically for each experiment.

The high-level gamma laboratories described below† represent various compromises of these viewpoints. The descriptions are arranged in approximately descending order of the emphasis placed on achieving versatility with original equipment, and the number of examples has been held to the minimum necessary to illustrate this range of choice. The approach for any such installation should be essentially an economic one, in which the cost of the original facilities, experimental equipment, operating time, and decontamination time are duly weighted.

ANL PHYSICS AND METALLURGY FACILITIES

DESCRIPTION

Two caves of the type illustrated in Figs. 7.3.1, 7.3.2, and 7.3.3 have been in operation for two years. The floor area is 6×10 ft surrounded on three sides by a three-foot thickness of magnetite concrete. The fourth side consists of two steel doors, 14 in. thick, which

*See: "Radiation Shielding," Vol. 1, Sect. 2; "Remote Handling," Vol. 2, Chap. 7.1; "Remote Viewing," Vol. 2, Chap. 7.2.

† Only facilities for solid-state work are included. The chemistry of radioactive materials, fortunately, can often be carried out by fluid flow in closed systems, with little need for remote handling. The contamination hazard attending the handling of liquids and powdered materials in beakers and the like encourages the former approach wherever possible.

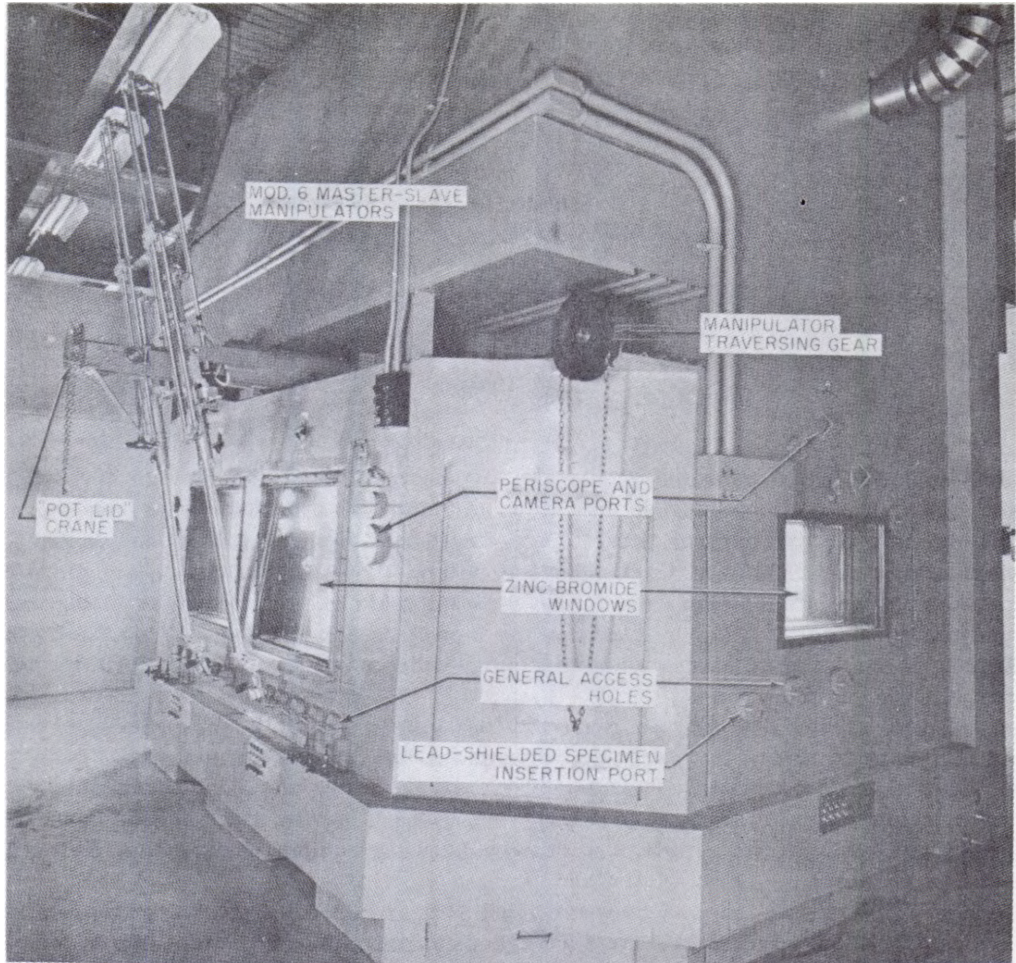


Fig. 7.3.1—Operating Side of ANL Cave. Photo submitted by Argonne.

roll apart on overhead trolleys to uncover an opening 6 ft wide by 7 ft high. There is no stepped threshold so that experimental apparatus mounted on castored dollies can easily be rolled into and out of the cave. Two 30- × 36-in. zinc bromide windows are installed in the front wall with a single, smaller window in each end wall. Sodium-vapor lights are distributed around all of the edges of the front-wall windows to furnish diffuse, shadowless lighting of any apparatus viewed through these windows. Two Mod. 6* master-slave manipulators are mounted on a single carriage which can be moved across the width of the cave in a horizontal slot in the front wall. A 1000 lb-capacity crane is situated between the manipulators to perform heavy lifting. Movable blocks of steel close up that part of the slot not occupied by the carriage. The working volume of the manipulators is the 36-in. by 48-in. by 10-ft space just inside the front wall windows. A row of general-purpose access holes is provided under each window, and other holes specifically designed for periscope observation, photography, and specimen introduction are situated at planned positions. No portion of the shield is capable of easy alteration for additional access.

* For a description of this manipulator see Fig. 7.1.16 of this section.

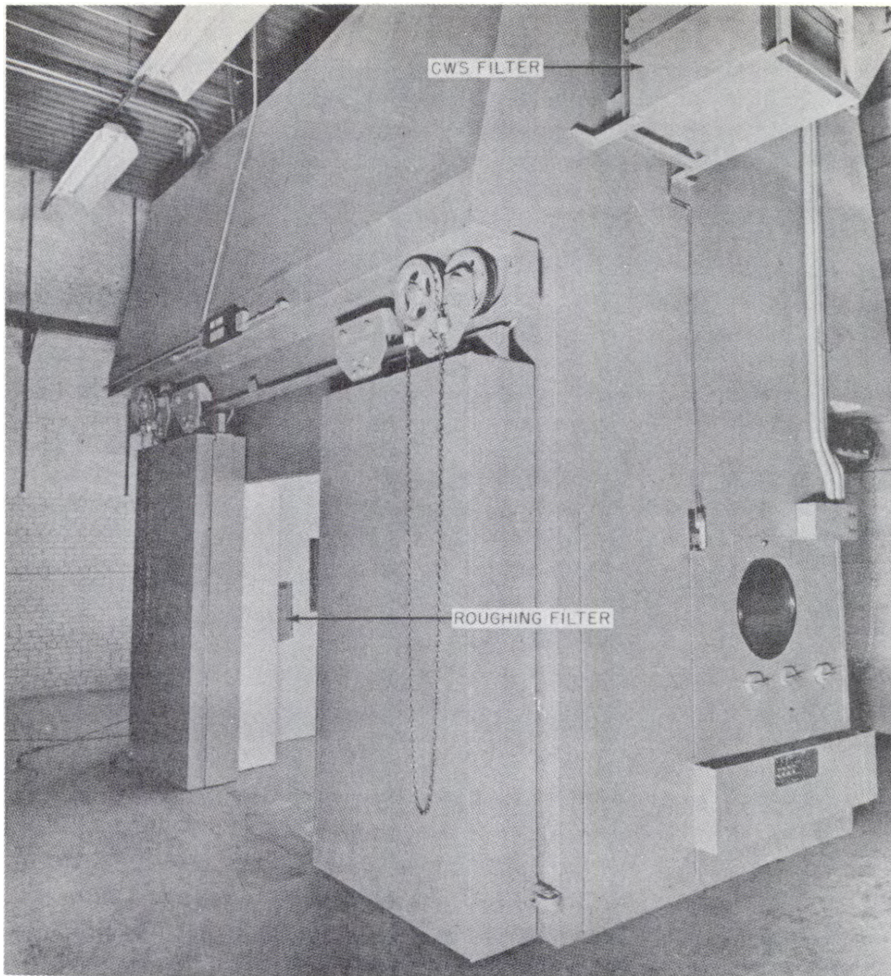


Fig. 7.3.2 — ANL Cave; Rear Side with Access Doors Open. Photo submitted by Argonne.

OPERATION

Equipment for such standard metallurgical procedures as determination of specific gravity, hardness, electrical resistivity, and surface roughness has been developed and successfully used. Less usual operations, such as the removal of tightly driven and corroded screwed fastenings and the machining of non-fissionable materials, have also been accomplished. In these operations, the manipulators have been used not only to transport and position the specimen but also to operate the equipment wherever their capabilities in strength, stiffness, or dexterity were not exceeded. Specifically: a standard Rockwell hardness tester is completely operated by the manipulators with no alteration other than an extension of the cocking lever; the table screws of a small milling machine are turned by the manipulators with crank handles substituted for the handwheels; the coarse focus of a microscope is adjusted with the manipulators, but the fine focus is electrically motorized; an impact wrench is spring-supported from the 1000-lb crane but directed and operated with the manipulators; the knee and table motions of a large milling machine are brought out by chain drives and shafts through access holes for manual operation; the manipulators are

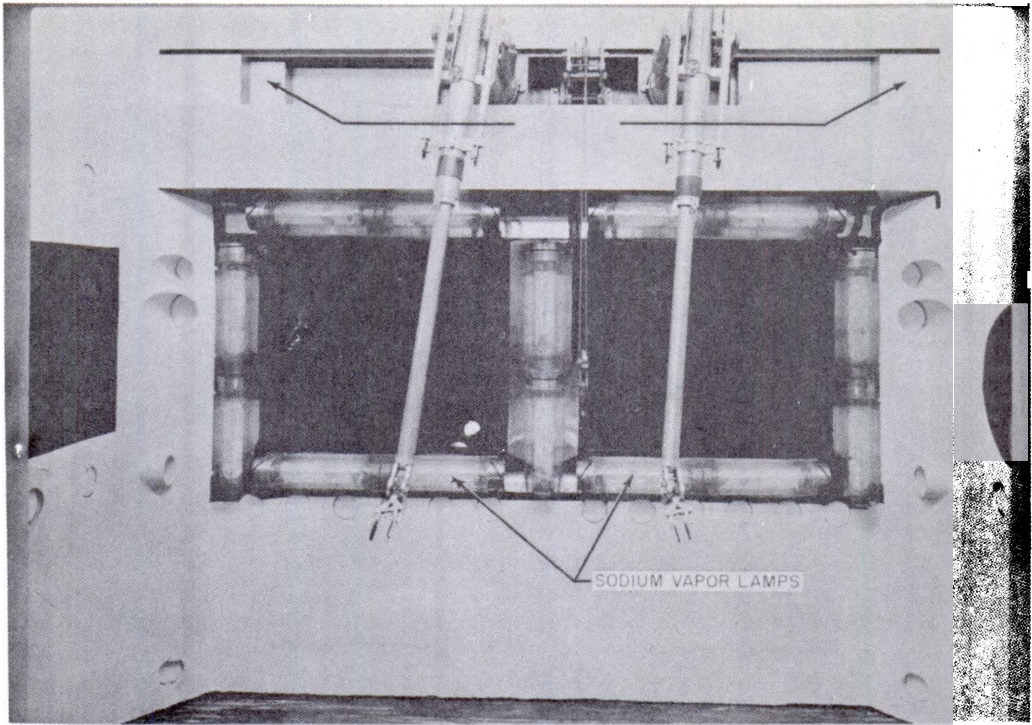


Fig. 7.3.3 — Interior of ANL Cave. Photo submitted by Argonne.

used to insert the crane hook and steady the load during heavy lifting.

Unaided vision through the front windows, sometimes supplemented by low-powered binoculars and views through the end windows, has been adequate for the above operations. Dial gauges, micrometer graduations, and the illuminated scale of an analytical balance are regularly read through the windows with binoculars. Magnified surface examinations and photographs have been made by periscope, but no periscopes have been built or used to supplement the windows for general viewing.

DECONTAMINATION

Experimental set-ups are frequently replaced since the cave space is too small to permit leaving idle equipment in place. The dollies on which experimental equipment is mounted are equipped with table-like tops which extend a foot or so beyond the apparatus. Polythene sheeting is used to cover the table top and mask off as much of the apparatus as can be done without interfering with manipulation. For the usual measurements of physical properties, the apparatus is not enclosed in a hood as this would seriously hinder manipulator operation.

After experiments involving clean, corrosion-free specimens, the apparatus is manually wiped to remove loose particles, usually leaving a fixed contamination of less than 10–15 mr/hr. With corroded specimens or containers, particles of which flake off, or after machining non-fissionable materials, the apparatus and table top are first brushed and wiped down using the manipulators. An operator wearing an assault mask completes the cleanup of loose particles. The apparatus is not removed from the cave until a fixed-contamination level of 10–50 mr/hr is achieved. The average time required for such a procedure is four hours.

WAPD PHYSICS AND METALLURGY FACILITIES

DESCRIPTION

The cave shown in Figs. 7.3.4, 7.3.5, and 7.3.6 has been in operation for two years. A floor area of 6×60 ft is shielded by magnetite concrete walls three feet thick. This area is divided by 8-in.-thick steel barriers into five cells of equal size. The top of the cave is covered with one-foot-thick concrete slabs laid crosswise; these slabs can be removed by an overhead crane to install or remove large or heavy equipment. Vertically sliding, 10-in.-thick steel doors in the back wall provide access into each cell for personnel and light equipment. The threshold of these doors is about 3 ft above outside floor level. Two 35×31 -in. windows in the front wall permit vision into each cell. Six of the windows are glass-filled; the remaining four are water-filled since certain experiments do not require the full shielding ability of the cave walls. Sodium-vapor lights are distributed along the top and sides of each window, and fluorescent lighting is provided for standby use. Three types of handling equipment operate on rails running the entire length of the cave: a one-ton crane for heavy lifting; two General Mills manipulators* for intermediate hoisting and manipulation, and two Argonne-built light-duty manipulators* for operation in restricted spaces. The barriers between cells terminate just below rail level and consist partly of a door which opens to allow the manipulators to pass from cell to cell. The spaces between the top of the barriers and the ceiling of the cave are closed by vertically sliding gates of 1-in. boiler plate. Vertical rows of 3-in.-diameter access holes are provided between windows for electrical and fluid conduits; 6-in.-diameter holes are provided over each window for general-purpose periscopes and transfer-type optical systems.

OPERATION

Sufficient cells and work stations are available so that some equipment has been permanently installed. Equipment for many of the metallurgical and metallographic tests and procedures has been modified and successfully used in the cells; a listing to date would include a small milling machine, power hack-saw, punch press, analytical balances, hardness testers, impact tester, profilometer, specimen mounting press, polishing equipment, and macro- and microphotographic equipment. The manipulators are used mainly to transport and position specimens in the various pieces of apparatus, most of which are power driven so that they can be operated independently of the manipulators. Control boxes for the manipulators and some of the apparatus are visible in the photographs.

DECONTAMINATION

The operating side of the cave is separated from the access side by a wall in which the only door leads through a clothing-change and wash room; this arrangement tends to confine contamination to the access side. Loose contamination is usually cleaned up by operators who enter the cells at the completion of an experiment. Ventilation and filtration equipment of sufficient capacity has been installed to exhaust 500 cfm continuously from each cell and maintain an air velocity of 180 fpm through any open cell door.

HW METALLURGY CELLS

DESCRIPTION

Four cells, as illustrated in Fig. 7.3.7 (A), are scheduled for early construction. Operating experience with these is lacking, excepting that similar cells built of lead brick have

* For a description of these manipulators, see Figs. 7.1.8 and 7.1.11 of this section.

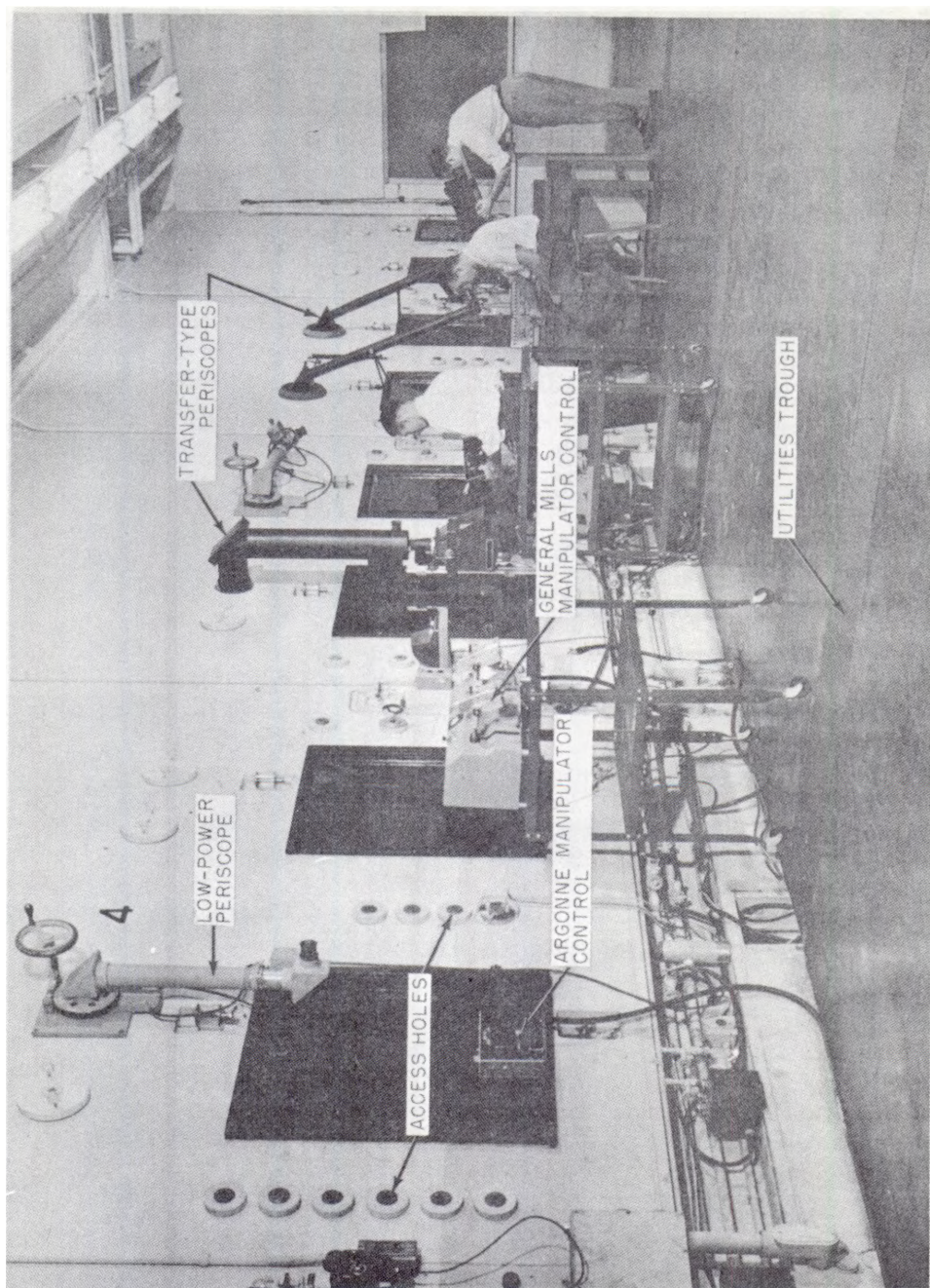


Fig. 7.3.4 — Operating Wall of WAPD Cave. Photo submitted by WAPD.

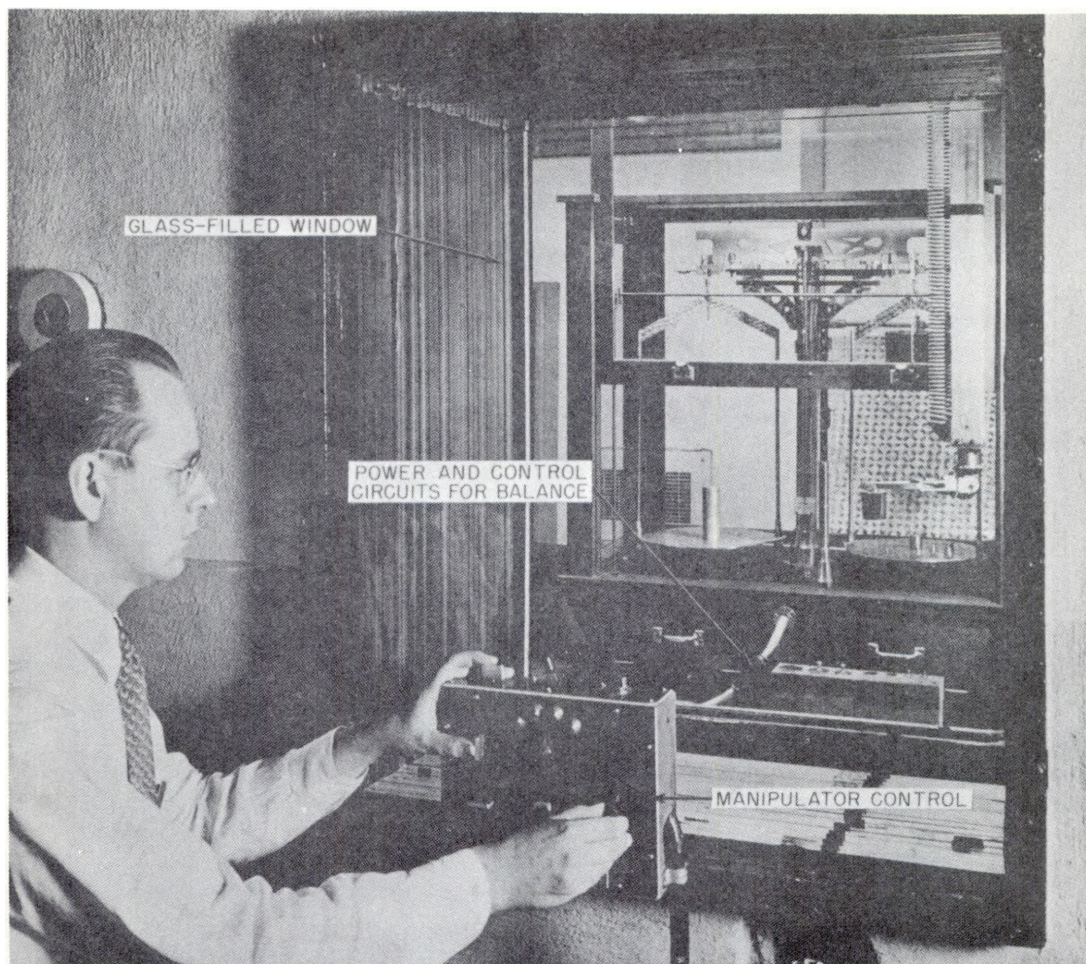


Fig. 7.3.5 — WAPD Cave; Typical Equipment Installation. Photo submitted by WAPD.

been used for several years. The cells have an interior volume of $52 \times 52 \times 72$ in. with steel walls either $10\frac{1}{2}$ or 15 in. thick. The end walls are contained in guides and may be raised by means of an overhead crane to insert or remove equipment. One hundred and forty holes of $7\frac{1}{4}$ in. diameter are provided in the sides and top of each cell; these holes can be stopped against radiation with any of the plugs shown at (B).

OPERATION

Apparatus will be mounted on pallets which will be lifted into position by a fork truck. Each experiment will be planned so that much of the specimen handling and all control or operation of the equipment can be accomplished by electrical motorization or by mechanical connection through access plugs. Careful location of the pallet will ensure that the apparatus will line up with the planned access holes. The Hanford slave manipulator* is designed so that it can be inserted through an access hole at any time and by working only

* For a description of this manipulator see Fig. 7.1.18 of this section.

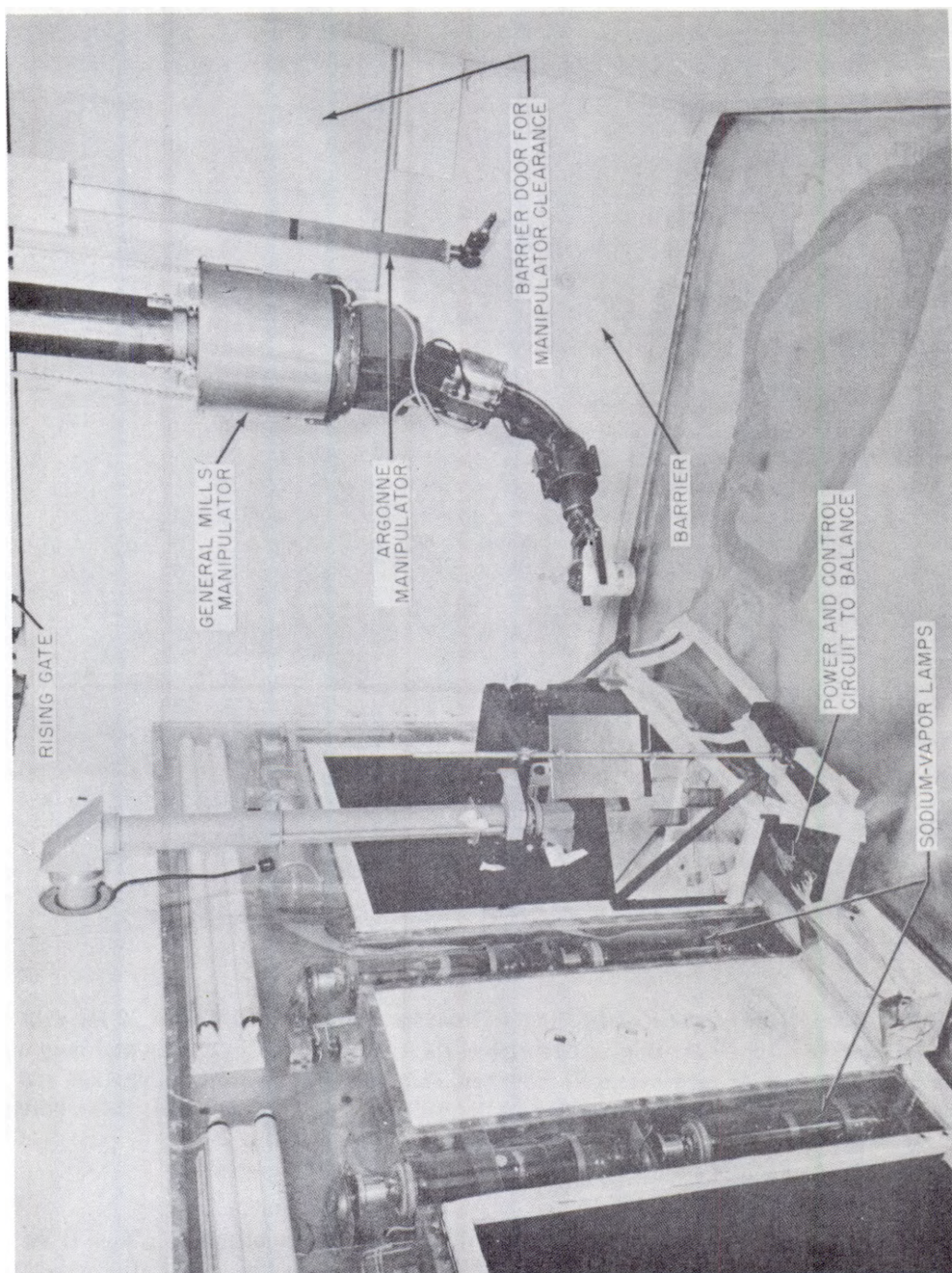
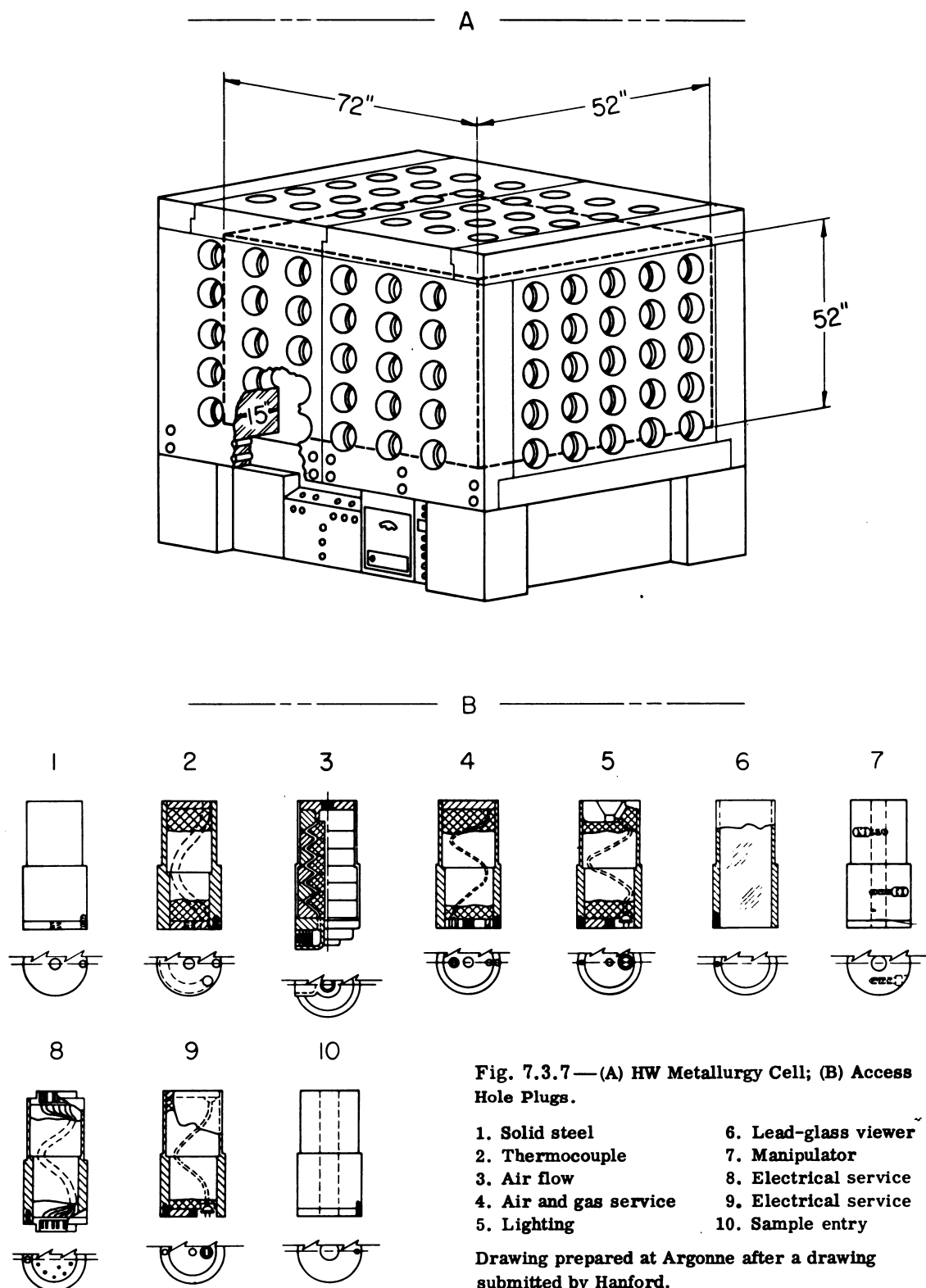


Fig. 7.3.6 — Interior of WAPD Cell. Photo submitted by WAPD.



from the outside. It will be used to receive the specimen at the "sample entry" plug and transfer it to the special handling devices. It will also be used, probably, to cope with any handling emergency that might arise from a shortcoming or malfunction of the special-purpose equipment.

DECONTAMINATION

The base of each cell contains the blowers and filters necessary to decontaminate the air leaking through cracks and through the "air flow" plugs that will be deliberately provided to control air flow in the cell. Contamination-collecting funnels or other anti-contamination means to be developed for each apparatus will accumulate heavier chips and particles for removal in cardboard cartons. At the completion of an experiment, radiation probes will be introduced through access holes to survey the apparatus, which will not be removed from the cell until the level is 50 mr/hr or less at 2 ft. Special decontamination cells will be provided in the building for more complete treatment.

KAPL RADIOACTIVE MATERIALS LABORATORY

DESCRIPTION

Two caves, illustrated in Figs. 7.3.8, 7.3.9, and 7.3.10 have recently been placed in service. The two caves are built back-to-back to utilize a common wall. The floor area of each is 6.5×25.5 ft. A 12-in.-thick steel door can be closed to separate the 6.5×19 -ft working area from the remainder of the cave, constituting a radiation lock. The outer ends of the locks are closed by 15-in.-thick steel doors. The walls are of magnetite concrete, 3 ft thick.

The operating wall of each cave is divided into 3 modules 5 ft wide. Each module has three removable rectangular plugs set into the wall, each having many access holes of a standard size on a standard spacing. The plugs are steel boxes filled with loose iron ore so that special openings can be provided without great difficulty as the occasion demands. Additional access holes pass through the permanent concrete.

The first viewing system provided is a mirrored labyrinth passing through a slot at the top of each module. The slot is partially shielded by a 6-in.-thick glass window. The middle removable plug in each module is being replaced with a zinc bromide and lead-glass window.

A carriage having vertical and horizontal degrees of freedom runs along rails on the rear wall of each cell. To the carriage can be mounted one of the various attachments including a mirror to supplement viewing a wrist joint for general-purpose manipulation, a standard specimen-can handler, and a television camera.

Rails are provided on the inside of the operating wall so that experimental equipment can be rolled into working position in the cell.

OPERATION

Many of the features of this installation were designed to accommodate experiments with a high contamination potential. It was planned that such experiments would be set up in dust-tight isolation boxes, access to which would be through a double-doored contamination lock. The radioactive specimen would be placed in the lock by means of the rear-wall manipulator, and the outer door would be closed. All subsequent manipulation of the specimen and operation of the equipment would be carried out with a small manipulator* contained wholly within the box and with special-purpose devices prepared as a part of each particular apparatus.

*Details were not available, since the manipulator had not been completely developed at this writing.

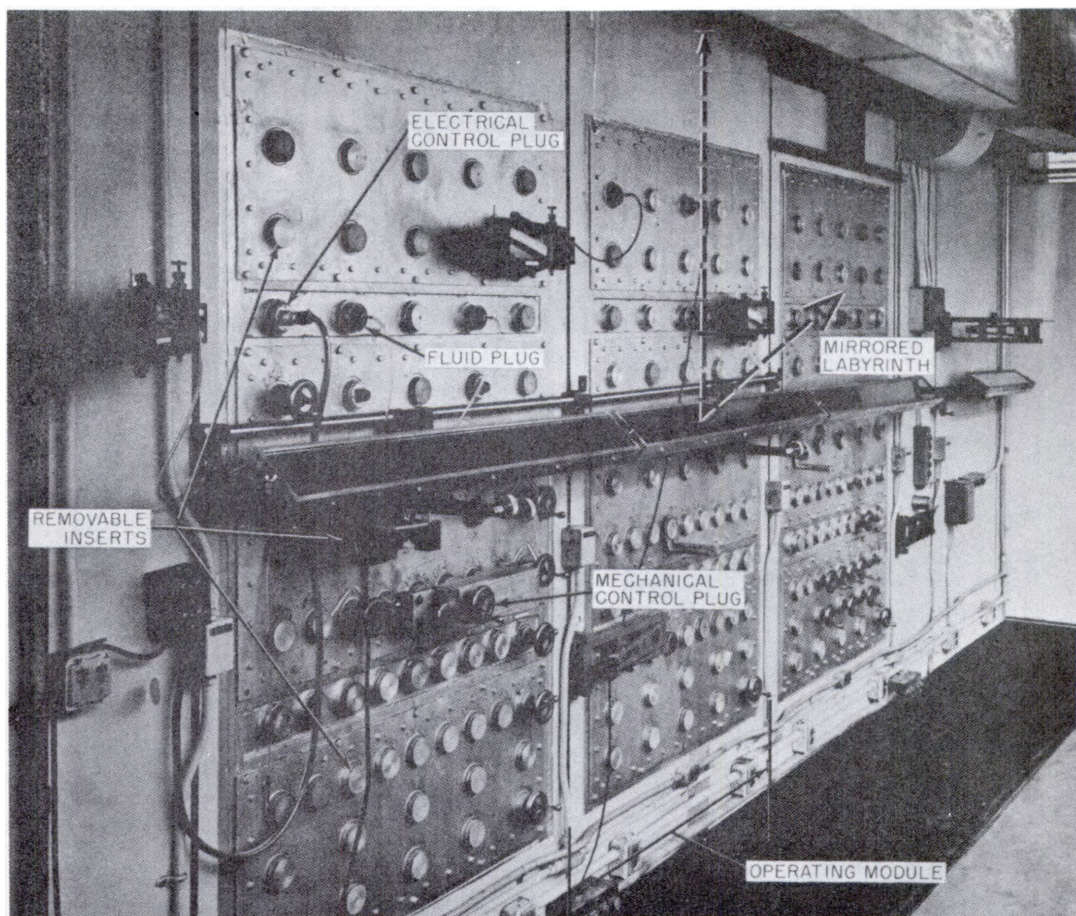


Fig. 7.3.8—KAPL Cell; Outside of Operating Wall. Photo submitted by KAPL.

Experience has indicated that the contamination potential attending many experiments is sufficiently low so that operation need not be limited to the above technique. In such cases, one or more walls of the isolation box may be omitted, allowing participation by a manipulator mounted outside of the box. The back-wall manipulator, with its general-purpose wrist-joint attachment, is being so used, and a master-slave manipulator capable of easy insertion through the front wall is to be added in the near future.

DECONTAMINATION

Each isolation box is equipped with a small blower and filters with which the interior is held at a slight negative pressure. At the conclusion of an experiment involving little contamination hazard, it should be possible to remove the box directly to "cold" storage. If the apparatus is slightly contaminated, it will be moved to a decontamination cell where the back of the isolation box may be removed and replaced with a glove panel. At higher levels, the back may be removed in the cave and a preliminary cleanup made with the manipulator. In the worst case, the box can be removed from the cave in a shielded dolly for hot storage or burial.

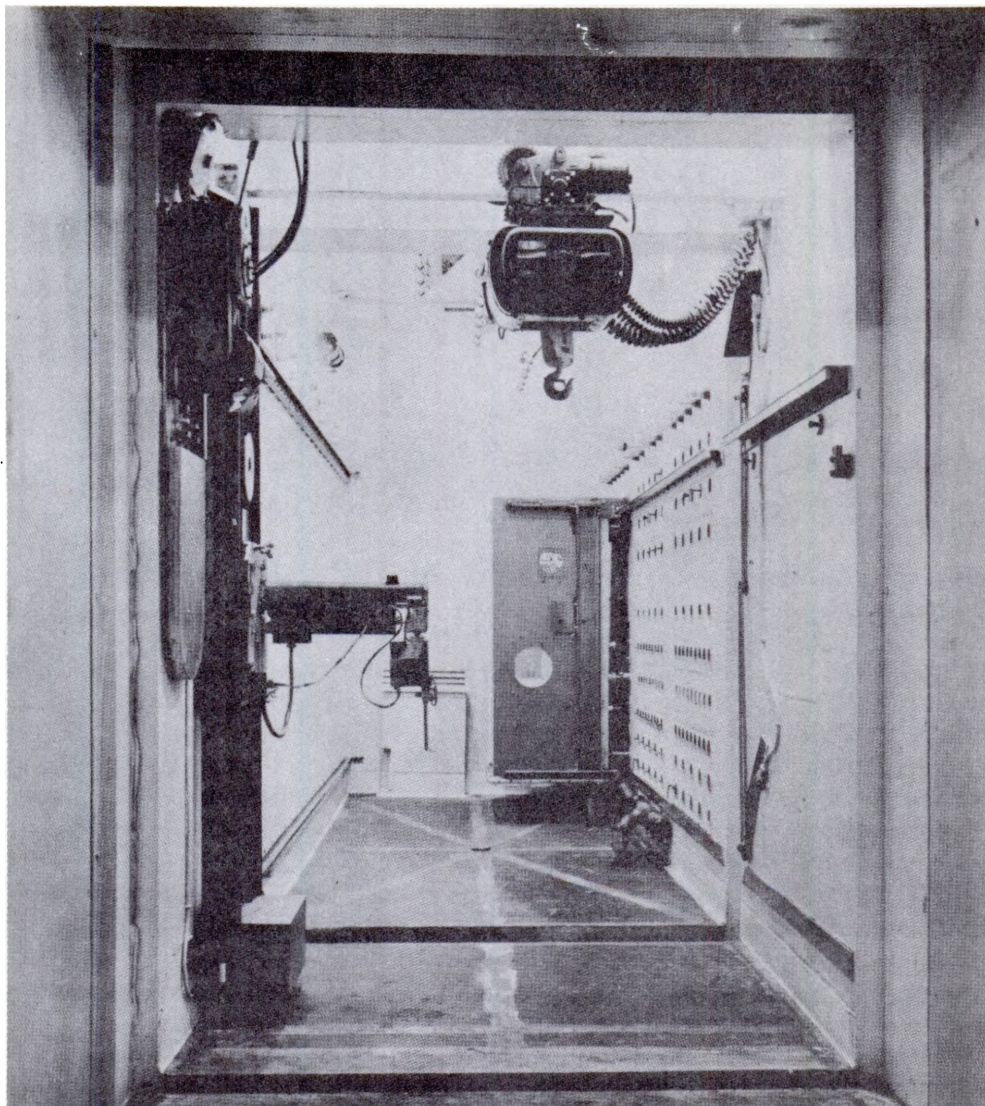


Fig. 7.3.9—Interior of KAPL Cell. Photo submitted by KAPL.

HW MULTICURIE CELLS

This group of cells was recently placed in service and is especially noteworthy because of its unusual wall construction.*

As seen in Figs. 7.3.11 and 7.3.12, the operating walls consist of 9-in.-thick steel blocks bolted to a row of vertical stepped-steel columns. The blocks are also stepped in the vertical direction, the larger ones increasing in height. The smaller blocks are used to chink the gap and do not extend to the inner face. A variety of the larger blocks is available to provide windows of dense lead-glass, thimbles for fluid and electrical conduit, and access

* A more complete description will be found in the report on the second Information Meeting on Hot Laboratories and Equipment, held at ORNL on October 7, 8, and 9, 1952, to be published.

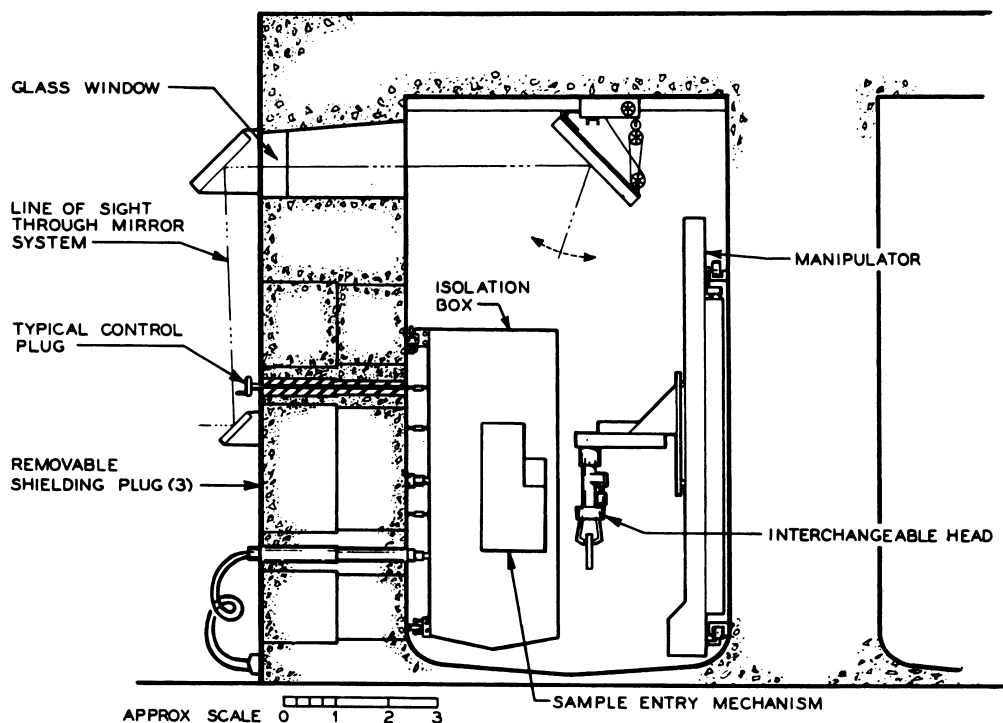


Fig. 7.3.10—Cross Section of KAPL Cave. Drawing prepared at Argonne from sketches and photos from KAPL.

holes through which larger apparatus, including the Hanford slave* manipulator, may be passed.

The utilities blocks have their central portion of cast lead which can be easily melted out and re-poured to accommodate a new thimble pattern. Handling equipment is available with which these blocks may be readily rearranged. Such construction, which is reportedly competitive costwise with cast dense concrete, approaches the ultimate in its capability of being remodelled to accommodate a particular experiment.

* For a full description of this manipulator, see Fig. 7.1.18 of this section.

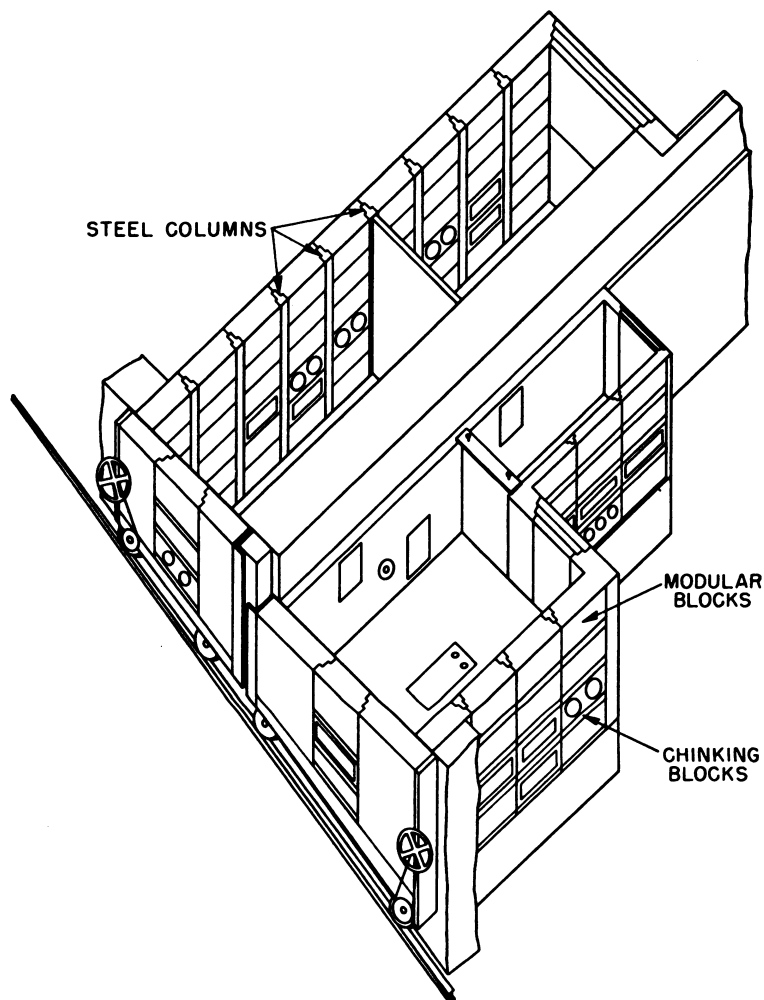


Fig. 7.3.11—HW Multicurie Cells with Roofs Removed. Drawing submitted by Hanford, legend added by Argonne.

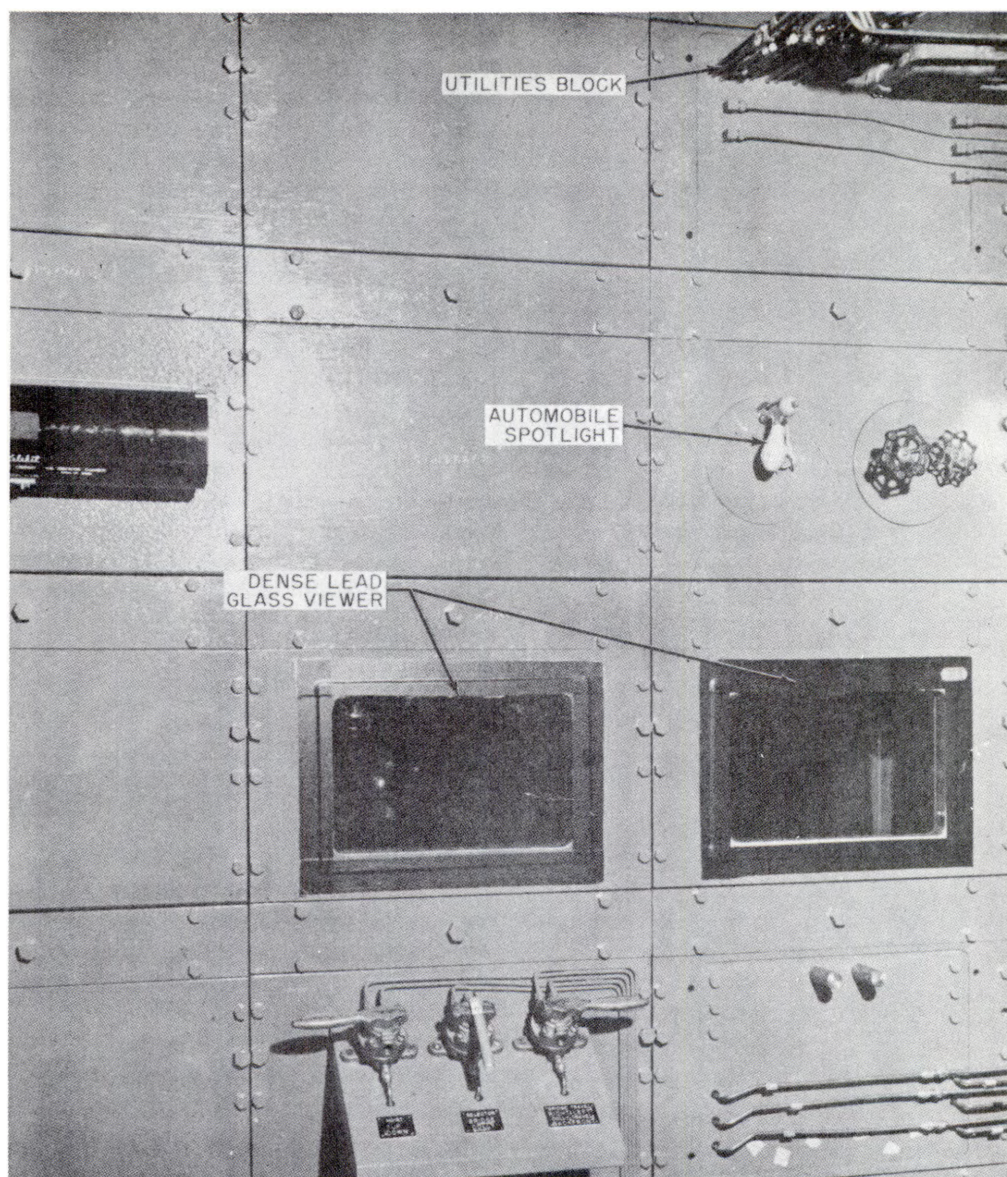


Fig. 7.3.12—HW Cell; Section of Operating Wall Showing Modular Construction.
Photo submitted by Hanford.

CHAPTER 7.4

Nuclear Reactor Instrumentation and Control

J. M. Harrer

The term "control," as it is applied to a nuclear reactor, refers to devices for changing reactivity and regulating reactor neutron density or power. Control feasibility is first considered when a reactor is planned. Simpler control methods are being stressed. The reactor control picture is changing rapidly, and a basic set of rules or practices valid for future reactor designs cannot be formulated at this time. It is assumed that the user of the following data is familiar with mechanical and electrical design practice, including the basic principles of automatic control and protective interlock system design; therefore, only values, quantities, or numbers useful for the design of components are given. References to complete designs and some qualifying statements are given to illustrate points in selecting or designing components, but appraisal of a particular design is not intended. Discussion of what is loosely referred to as "philosophy of reactor control" is avoided because this chapter deals with generalized design.

"Reactor instrumentation" is the term generally applied to neutron-sensitive instruments. This field of design is well advanced in many respects since, necessarily, it preceded the reactors themselves. In reactor work, information is channeled from each sensing instrument through counters, amplifiers, and the like to the operator's panel; these assemblies are referred to as "instrument channels." Many ways of assembling channels are in use—the selection of any particular method depends upon the reactor design. To present an over-all picture in the following, many typical sensing elements are catalogued along with some of their operating characteristics. No attempt was made to evaluate these instrument designs, all of which have been used on reactors or were tested for use on proposed reactors. The objective is to show a wide variety of possible assemblies which are in themselves practical units. The balance of an instrument channel is made up of electrical circuits of which only a few have not already received detailed treatment in published works. Very few circuits have been included, and the listed references should be consulted for information about channel components other than the sensitive element itself.

Automatic neutron-density regulation has received much attention from designers of control systems. The chief difficulty in evaluating these designs is the lack of performance data obtained when the systems were used to control full-scale reactors. Some data are included here to permit evaluating the performance of proposed control systems; some important factors to be considered when designing a system are brought out; and successful design values are given. All details are omitted, however, except those considered necessary additions to the general knowledge.

The possibilities of reactor self-regulation through the inherent reactivity stabilizing effect of temperature is being studied with much interest at present with a view toward planning safe and mechanically simple reactors. Very few factual data are as yet available, however.

A discussion of reactor time-dependent behavior is included to make available certain data taken from electrical analogue studies and frequently used to predict control-system performance.

CONTROL SYSTEM

A generalized nuclear-reactor control system is shown on Fig. 7.4.1.

The controlled variable is average neutron density. This quantity, designated as n (neutrons per cubic centimeter), is a direct measure of reactor power production. The product of n and the neutron velocity (v) in centimeters per second is called the average neutron flux and designated as nv . This is the quantity measured by a neutron-sensitive instrument near the reactor core, in the reflector, or in the shield. The absolute value of flux at the instrument determines the electrical current from the instrument and is a measure of average neutron density when the element is calibrated against the average reactor power (shown by coolant temperature rise and flow rate). The power calibration of a neutron-sensitive instrument sometimes changes as a result of variation in neutron distribution in the reactor.¹ Instruments used with power reactors in which xenon is a large effective poison may require frequent calibration because of changes in flux distribution, especially when the reactor power output is changed. Fast changes in power are measured with flux-sensitive instruments in fractions of a second. In contrast, the coolant power measurement is accomplished relatively slowly; measuring time is in the order of minutes.

The control variable is k or δk ; k and its effect on neutron density are discussed under "Reactor Time Dependent Behavior." The operator determines the position for the control element by observing the changes in average neutron density indicated by the neutron-sensitive instruments. When starting a reactor or maintaining a power level, he observes both the rate of change and the magnitude of neutron density. Automatic protective electrical circuits supervise his operation and limit the rate of change of flux and its magnitude to present safe values. These circuits shut the reactor down either slowly or rapidly as determined by the observed maloperation; this operation is discussed more fully under "Automatic Protective System." Accurate position measurement of the control means for k is most helpful in this operation; the accuracy of measurement is discussed under "Position Measurement." Mechanical and electrical interlocks are used to prevent damage to the control-means drive motors and to prevent improper operating sequences. Tedious prolonged operation at a fixed power or in a fixed-power range is sometimes assigned to an automatic flux, power, or temperature controller; this operation is covered under "Automatic Power Regulation."

REACTOR TIME DEPENDENT BEHAVIOR

REACTOR EQUATIONS

The important parameters affecting the variation of reactor neutron density as a function of time are k , δk , β_i , λ_i , c_i and l^* (see Table 7.4.1). $l^* = 1/v\Sigma_a$ for a large (infinite) reactor. The value of l^* varies from 2.3×10^{-3} sec for a large thermal heavy-water-moderated reactor, to as low as 10^{-4} for a natural-water-moderated thermal reactor. For

¹References appear at end of chapter.

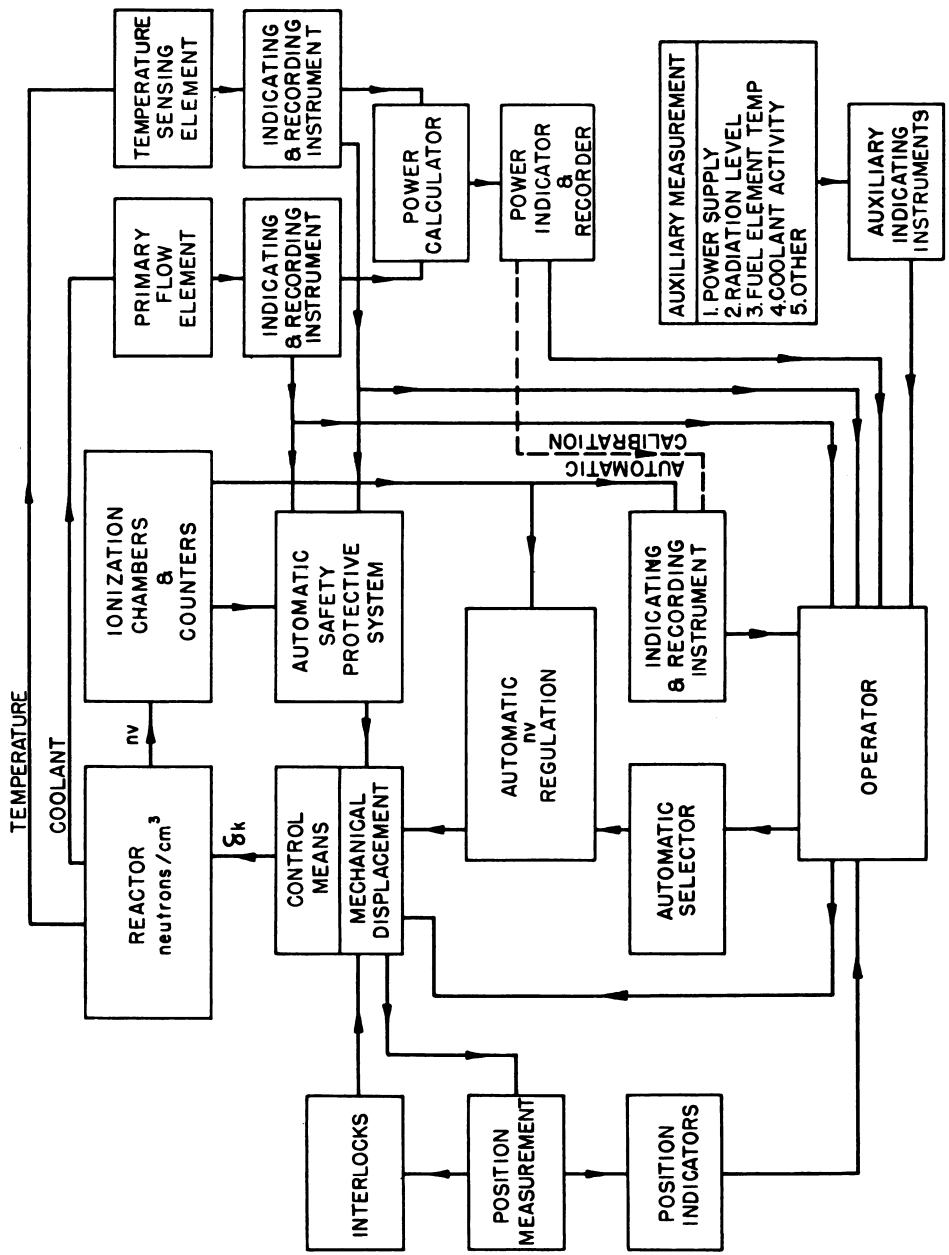


Fig. 7.4.1—Generalized Reactor Control Block Diagram. Submitted by Argonne National Laboratory, Sept. 1952.

Table 7.4.1 — Instrumentation Control Nomenclature

Symbol	Definition	Units
n	Neutron density	Neutrons/cu cm
n'	Variation in neutron density from a specified density	Neutrons/cu cm
n_0	Minimum reactor neutron density in the regulated range	Neutrons/cu cm
n_d	Demand neutron density for regulation	Neutrons/cu cm
ν	Neutron flux	Neutrons/(sq cm)(sec)
k	Thermal-energy neutrons produced per thermal neutron absorbed in a particular finite reactor	Neutrons/neutron
δk	Thermal-energy neutrons produced per thermal neutron absorbed in a particular finite reactor, minus one ($k-1$)	Neutrons/neutron
l^*	Mean effective neutron lifetime or the mean time which elapses from when neutrons are produced until they return to fission again or are lost to the reaction	Seconds
β	Total fraction of delayed neutrons	Neutrons/neutron
β_i	Fraction of delayed neutrons of group i	Neutrons/neutron
λ	Decay constant for delayed-neutron emitter	Seconds ⁻¹
λ_i	Decay constant for delayed-neutron emitter of group i	Seconds ⁻¹
c	Concentration of delayed-neutron emitter	Neutrons/cu cm ³
c_i	Concentration of delayed-neutron emitter of group i	Neutrons/cu cm ³
I	Electrical current	Amperes
ΔI	Change in electrical current	Amperes
E	Electrical potential	Volts
ΔE	Change in electrical potential	Volts

high-energy-neutron reactors, l^* is 10^{-5} sec or less. These parameters are related to neutron density (n) by the following simplified equations:

$$\frac{dn}{dt} = \frac{\delta k - \beta}{l^*} n + \sum_{i=1}^5 \lambda_i c_i$$

$$\frac{dc_i}{dt} = \frac{\beta_i}{l^*} n - \lambda_i c_i$$

The most useful solutions for these equations are obtained from an analogue computer,² but a useful, very close approximation³ is obtained if:

$$c = \sum_{i=1}^5 c_i; \delta k \ll \beta$$

and an average value of $\lambda = 0.1 \text{ sec}^{-1}$ are used:

$$\frac{n(t)}{n(0)} = \frac{b-c}{b-a} e^{at} + \frac{c-a}{b-a} e^{bt} \quad (1)$$

where t = time in seconds:

$$c = \frac{\delta k}{l^*} \quad (2)$$

$$b = \frac{\delta k - 7.6 \times 10^{-3}}{l^*} \quad (3)$$

$$a = \frac{\delta k \times 10^{-1}}{l^* \times 10^{-1} + 7.6 \times 10^{-3} - \delta k} \quad (4)$$

when the values $l^* = 10^{-3}$ sec and $\delta k = 2.57 \times 10^{-5}$ are used in Eq. (1):

$$\frac{n(t)}{n(0)} \approx e^{t/3600}$$

A δk of 2.57×10^{-5} is, therefore, frequently referred to as an "inhour" for a reactor with $l^* = 10^{-3}$ sec. An inhour is calculated from exact formulas; refer to Vol. 1, Chapter 1.5. For a reactor with $l^* = 10^{-4}$ sec or less, $\delta k = 2.54 \times 10^{-5}$ times the reactivity in "inhours." δk is also given in dollars and cents. The δk in dollars equals $\delta k/\beta$.

Subcritical reactors where k is less than 1 behave according to Eq. (5) which gives the equilibrium neutron density approached after infinite time has elapsed. When:

$$n = \frac{\text{source } n}{1 - k} \quad (5)$$

the absolute value of $1 - k$ is $< \beta$ this value of n is closely approached in about 1 sec.

INVERSE REACTOR PERIOD

The value $1/n \, dn/dt$ is called "inverse reactor period." It is measured with a period meter circuit, discussed more fully under "Indicating and Recording Instruments," and is used as a guide for the reactor operator. For a supercritical reactor, the inverse period is a measure of δk , a short positive period indicating a large positive δk .

A subcritical reactor having a neutron source will exhibit an apparent period if k is changed. Figure 7.4.2 shows the reactor power as a function of time for a uniform k rate of change from 0.667 to above prompt critical where $\delta k = \beta = 7.6 \times 10^{-3}$.

REACTOR TRANSFER FUNCTION

The transfer-function concept of reactor neutron-density response to δk variation is shown on Figs. 7.4.3 and 7.4.4. δk must be less than β and vary harmonically.^{4,5} The reactor gain at 0 decibel is set at $n'/n\delta k = 136$. These curves are used in the synthesis of the regulating-rod control systems and in experimental work where the effect of an absorber is to be determined. Basic limitations are discussed in the references.

δk CONTROL MEANS

The reactor nv may be controlled by mechanically positioning absorber rods, reflector material, and fuel or by changing the concentration of neutron absorbers in the coolant or core. Only the mechanically controlled type is treated here. Important factors requiring control-rod movement are: fuel depletion, fission-product poisoning, and reactor temperature changes. Reactors are usually designed to have a negative temperature coefficient which, in principle, provides inherent nv -regulation since a negative δk is produced by a

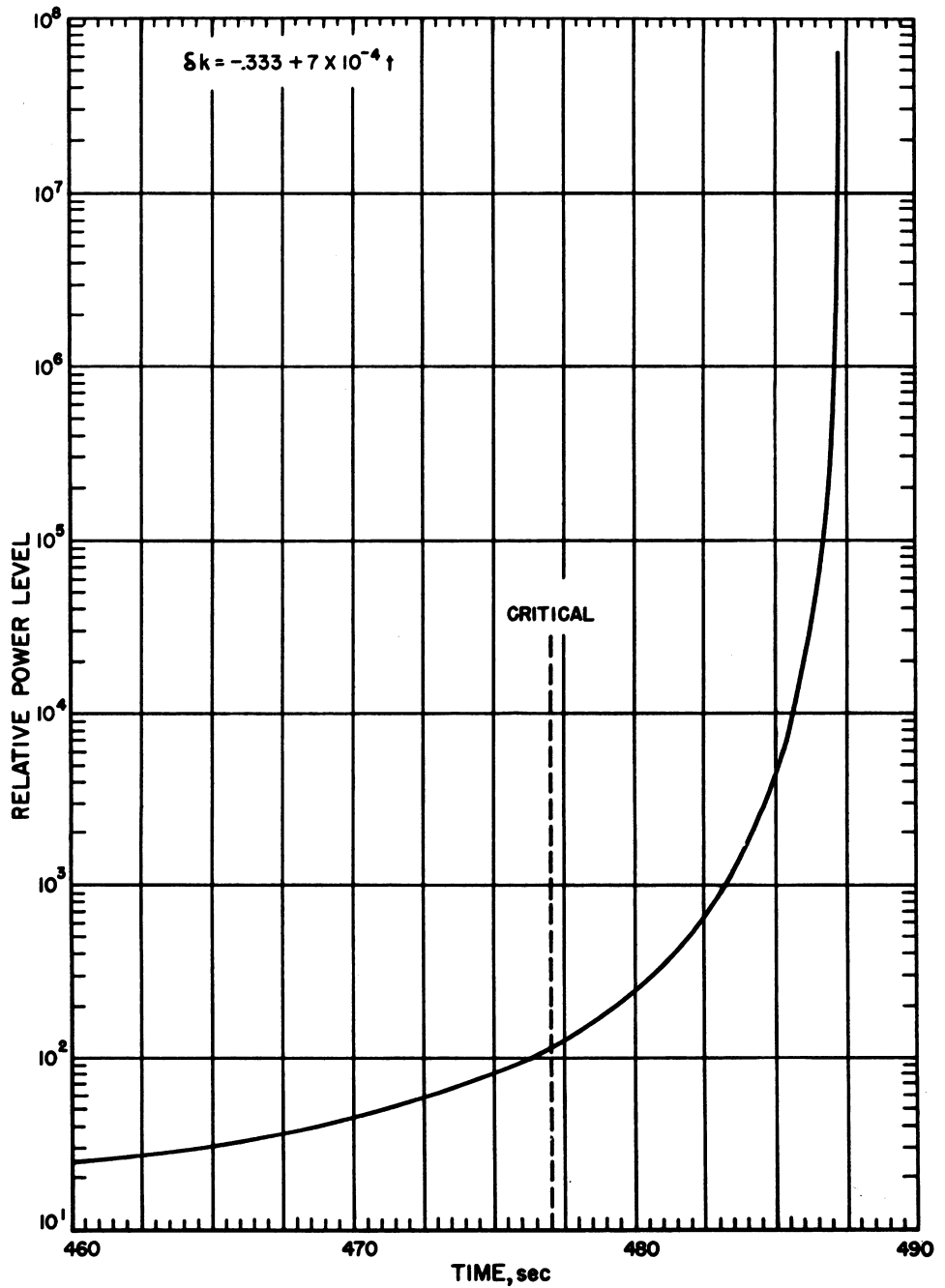


Fig. 7.4.2 — Relative Power Level as a Function of Time for a k Rate of Change of 7×10^{-4} Per Second. Redrawn from Figure 62-4, Robert G. Durnal, Reactor Kinetics, WAPD-RM-62, Aug. 1951.

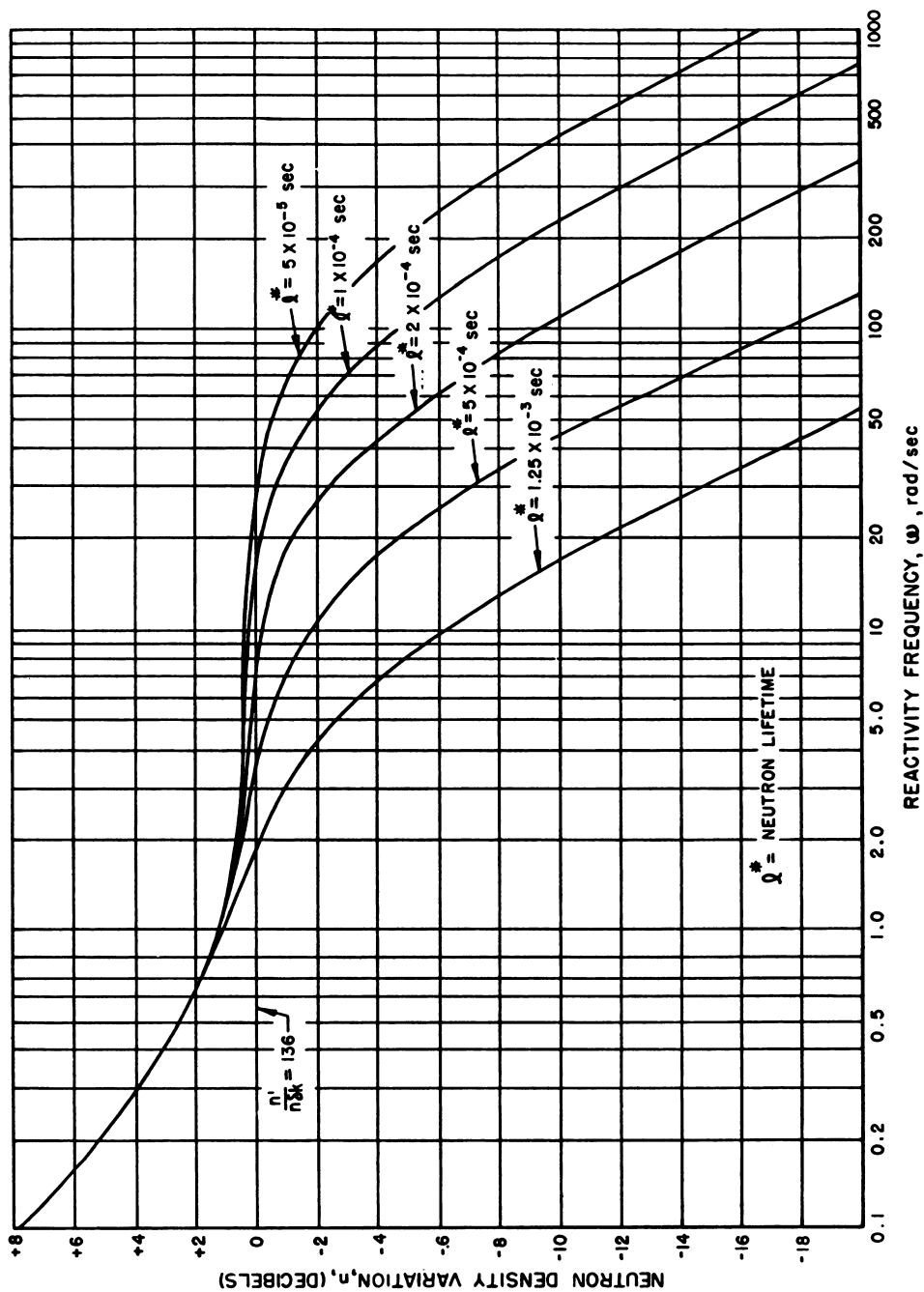


Fig. 7.4.3 — Relative Amplitude of Reactor Neutron Density Variation, n' as a Function of the Frequency for a Harmonic δk Variation of Small Amplitude. Submitted by Argonne National Laboratory, Sept. 10, 1952.

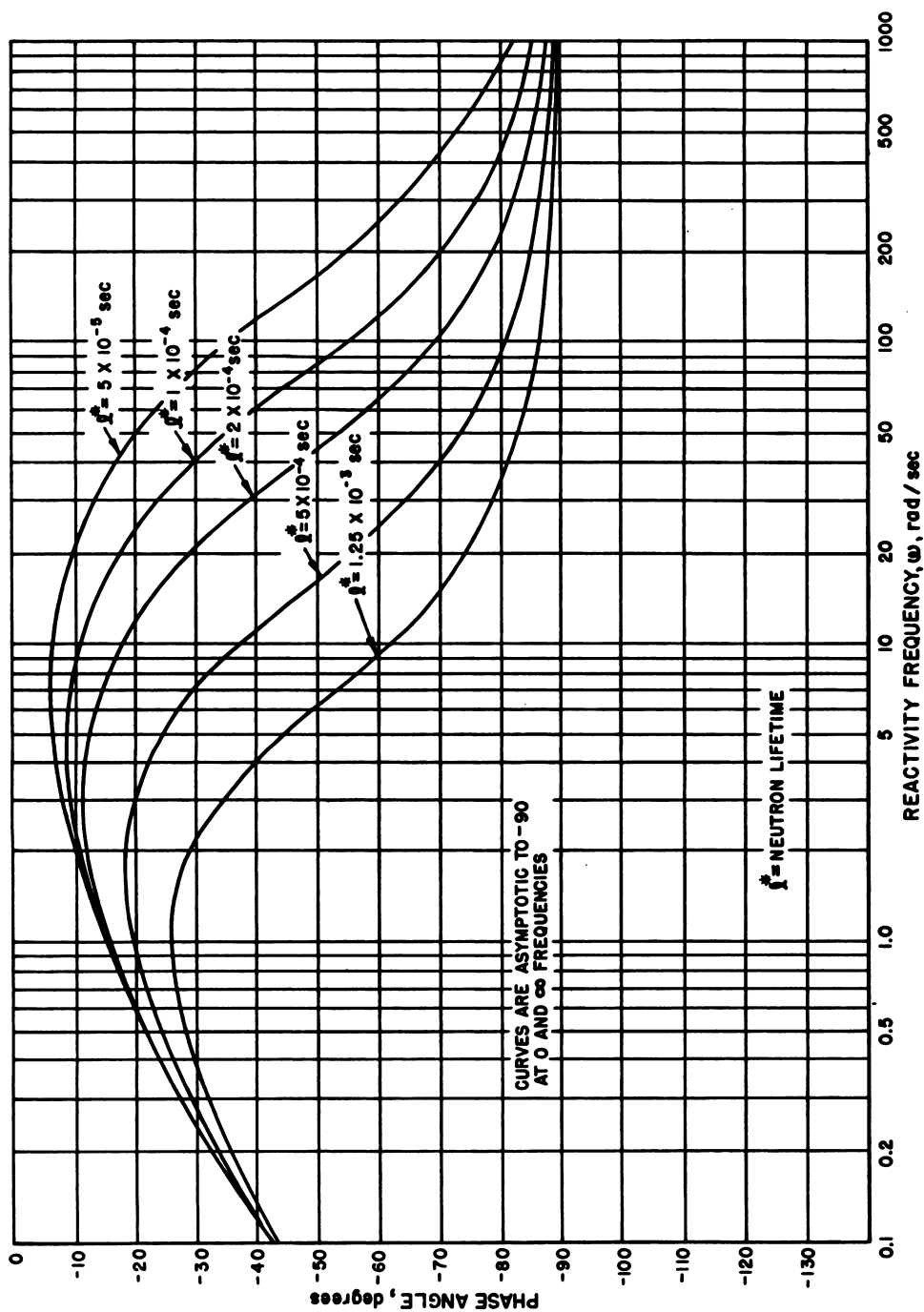


Fig. 7.4.4 — Phase Shift Between Reactor Neutron Density Variation, n' , and δk as a Function of Frequency for a Harmonic Variation in δk of Small Amplitude. Submitted by Argonne National Laboratory, Sept. 12, 1952.

power increase. This regulation will generally be stable in the normal sense (see "Temperature Coefficient Power Regulation") that no continued oscillations will occur if the combined heat capacity of the reactor, its coolant, and heat exchanger are large, as is the case with the Experimental Breeder Reactor (EBR). Temperature coefficient is a result of physical changes in the reactor element size with temperature changes, changes in average neutron energy, doppler broadening of resonance absorption lines and, if the coolant is a moderator, is largely a result of coolant density changes. Temperature control of the coolant by varying coolant flowrate is frequently employed to relieve the rods of some of their duty in offsetting temperature-induced changes in k . Temperature changes may occur rapidly and, if not controlled, must be considered in determining the speed with which rods are moved. Depletion and poisoning occur more slowly and are seldom factors influencing rod-speed design.

CONTROL-ROD DRIVE REQUIREMENTS

Mechanical design of the rod drives cannot be reduced to formula at present. A presentation of certain basic requirements is given here to guide the designer. The rod-system designs covered in references (6) and (7) are recommended as giving a better understanding of the requirements. Since a perfect design is sacrificed to certain engineering compromises, the basic requirements are not always fully met by these referenced designs.

SAFETY RODS

EFFECTIVENESS

Safety rods are designed with an effectiveness large enough to keep $k < 1$ by 0.1 to 0.2 under all operating conditions.

VELOCITY

Safety rods are generally moved at a uniform displacement rate through their entire stroke, but their effectiveness in δk per unit displacement is not uniform. Normally, a rate is selected which corresponds to about 0.001 at the point where they are changing k the largest amount per unit displacement. About 5 to 10 min is normally allowed for full stroke in the direction from maximum effect to the "ready" or minimum effectiveness position. For safety action (that is, high-speed k change toward the minimum reactor k position, called "scram"), the velocity is made as high as mechanically feasible. Providing a large negative δk for "scram" in the first 0.1 sec is important. A value of 0.01 δk in 0.1 sec sometimes is used as a target for design. Scram action should take place through stored energy sources, such as gravity or springs, with a slower but positive mechanical-drive follower to back up the primary scram method.

POSITIONING

Safety rods need not be positioned accurately along their stroke. In the "ready" position, they should be held securely by a quick-release, fail-safe device, such as a holding electromagnet or electromagnetically operated latch.

RELEASE

Release of the rods from the ready position should be accomplished rapidly and positively. A release time of 0.05 sec after a danger signal is received is usually adequate, but

faster release is desirable. At the end of the "scram" stroke, the rods must be stopped by shock absorbers. The effective distance through which these shock absorbers operate should be held to about 5 percent of the rod stroke or less, if possible.

SHIM RODS

EFFECTIVENESS

Several rods called "shims" are designed into a reactor, each rod with a large δk effectiveness. They may be designed to act in banks or singly, depending upon the purpose of the reactor. The total δk is greater than the sum of k changes owing to the temperature coefficient, the fission-product poisoning, and the fuel depletion between reloadings.

POSITIONING

The drive motor and mechanical linkages to a rod should be capable of positioning the rod anywhere in its total stroke so that a resolution corresponding to $0.00002 \delta k$ exists at the most effective rod position. When not being moved, the rods should be held absolutely still and not allowed to vibrate or move as the result of forces developed on them by the coolant or by gravity.

VELOCITY

The shim-rod velocity in a direction of positive or negative δk depends upon the type of control system being used. A wide velocity range, adjustable after installation on the reactor, is advisable with a minimum adjustable range of 10-to-1 recommended. The unit displacement per second is usually set at the point where the rods have the largest δk per unit displacement. This value varies widely over the stroke. A maximum δk per second of 5×10^{-4} and a minimum of 5×10^{-5} are used on existing reactors where the operator positions the shims. Sometimes the shims are positioned automatically by observing the position of the regulating rod (see "Automatic Regulation of Power"). A maximum δk per second equal to about $\frac{1}{6}$ of the regulating rod maximum speed may then be used but is usually fixed by general safety considerations. The speed is so dependent upon the control-system design in this case that a value cannot be selected independently.

A "scram" speed as high as possible, about 0.01 per second or more, is sometimes provided to back up the safety-rod system.

MECHANICAL DESIGN

Shim rods are positioned by means of racks and pinions, lead screws and nuts, cable hoists, and the like. The primary driving motor may be hydraulic or electrical. Electrical motors are used with differential gearing and brakes to provide reliable, very-wide-range speed adjustment.

REGULATING RODS

EFFECTIVENESS

The regulating rod is similar to a shim rod in most of its functions but is usually selected for a high effective δk per unit displacement. The duty of regulating ν in narrow ranges is assigned to this rod. Its stroke may be mechanically restricted to a region of linear effect on ν for control purposes.

POSITIONING

Continuous, accurate positioning is necessary. A resolution of $0.00001 \delta k$ is used for experimental reactors. The rod should be held stationary by a mechanical brake when not being moved and should be guided to prevent vibration. If proportional feed-back rod-positioning control is provided (see "Automatic Power Regulation"), the brake is not used.

VELOCITY

A speed of 10^{-5} to $5 \times 10^{-4} \delta k/\text{sec}$ is used for operator positioning of the rod. Speeds for automatic positioning are discussed under "Automatic Power Regulation."

SHIM-SAFETY RODS

A shim-safety rod^{6,7} is one which combines the functions of shim and safety rods. All values and requirements given for either a shim or a safety rod apply for this rod. It must position accurately for shim action and move rapidly for "scram" action.

POSITION MEASUREMENT

The position of the control means for δk is measured and displayed on the operator's control panel.

REMOTE-POSITION INDICATORS

These usually are operated by a standard synchrotransmitter and receiver pair having the torque required to drive the dial selected. An instrument servomechanism for accurate rod-position indication⁸ and an indicating system for a sealed reactor⁶ have been described.

ACCURACY OF MEASUREMENT

For experimental reactors, the rod-position measurement resolution should correspond to about a δk of 1×10^{-5} for at least one rod.

POSITION INDEXING

Accurate indexing should be provided where possible by exposing a mechanical link to the rod-drive mechanism. The remote indicators on the operator's panel are set to correspond to this positive indication. For sealed systems, magnetic detectors must be used. A special detecting device has been described.⁹

AUTOMATIC POWER REGULATION

Automatic power regulation is used to relieve the operator of the tedious duty of continually repositioning the rods and to provide more accurate average reactor n_v or average temperature regulation. In general, relatively rapid changes are offset by the designated regulating rod and slow changes by the shims. These rods are discussed under " δk Control Means." The principle followed is to provide a feed-back control system to set the regulating-rod position and then to set the shim positions to keep the regulating rod

close to an optimum regulating position. The duty of positioning the shim rods is frequently left to the operator; however, the usefulness of the automatic system is extended if a shim-regulating rod tie-in is provided.

REGULATING ROD CONTROL

RANGE

The designated range of maximum δk control assigned to the regulating rod has a decided bearing on the selection of feed-back control-system characteristics. A linear δk per unit displacement over the total range is desirable because the δk per unit displacement is part of the system gain and, if large changes are encountered, system tightness and stability will be affected. For regulating rods with a maximum speed between about 0.02 $\delta k/\text{sec}$ and 0.002 $\delta k/\text{sec}$, the δk total is limited to about 0.8 β to limit accidental short-reactor-period resulting from a rod control system malfunction. For slower rods, the total rod δk is limited only by the linear range available or the flux distribution distortion which may result from rod movement. For reasonably flexible control in a system where the shims are not positioned automatically, a desirable δk value is twice the temperature coefficient δk which results from a power change from 1 percent to 100 percent of operating power.

REGULATING-ROD CONTROL-LOOP

Figure 7.4.5 shows the regulating-rod control-loop. The purpose of the system is to establish automatically the value $\delta k = 0$ for the reactor at a desired reactor neutron density, n_d . The loop disturbance is designated as δk , which represents k change owing to insertion or removal of experiments, fuel depletion, temperature coefficient, or fission-product poisoning.

The actual error signal is designed as n'_d . This error is time dependent upon reactor δk or frequency dependent as shown in Figs. 7.4.3 and 7.4.4. However, the magnitude of n'_d is dependent upon the magnitude of n_d and so must be normalized with respect to n_d to present a fixed system gain at the input to the preamplifier. This normalized error is designated as n'_f .

The control-loop shown by solid lines can be stabilized by system gain adjustment, but the dotted internal feed-back loop is usually added to improve operation and system tightness.

The basic loop design is predicated upon control of δk which regulates neutron density n to the desired value n_d .

NORMALIZED ERROR n'_f

The normalized error n'_f is equal to n'_d divided by n_d . Several methods are available for obtaining the n'_f value. This operation adds to control system flexibility but also adds somewhat to design complexity. Where the range of control to be covered by a system is over 90 to 100 percent of design power, the change in gain and control accuracy owing to the use of n'_f instead of n' is 10 percent. Where the range control can be restricted, the calculation of n'_f can be eliminated from the system. This is the case with the regulation scheme of the EBR in which the deflection of a galvanometer, with about a 3-sec period, was used to determine the difference between the ion chamber current and a fixed bucking current proportional to the demand n'_d . Deflection of the galvanometer activates photocells which operate relays and start the regulating rod running in a direction to make $\delta k = 0$.

One useful method of obtaining n'_f is presented in Fig. 7.4.6. In this circuit, the load resistance CR_p decreases as reactor power rises. Chamber dynamic resistance $\Delta E/\Delta I$ also decreases as reactor power rises, and a ratio of 100 between the chamber $\Delta E/\Delta I$ and

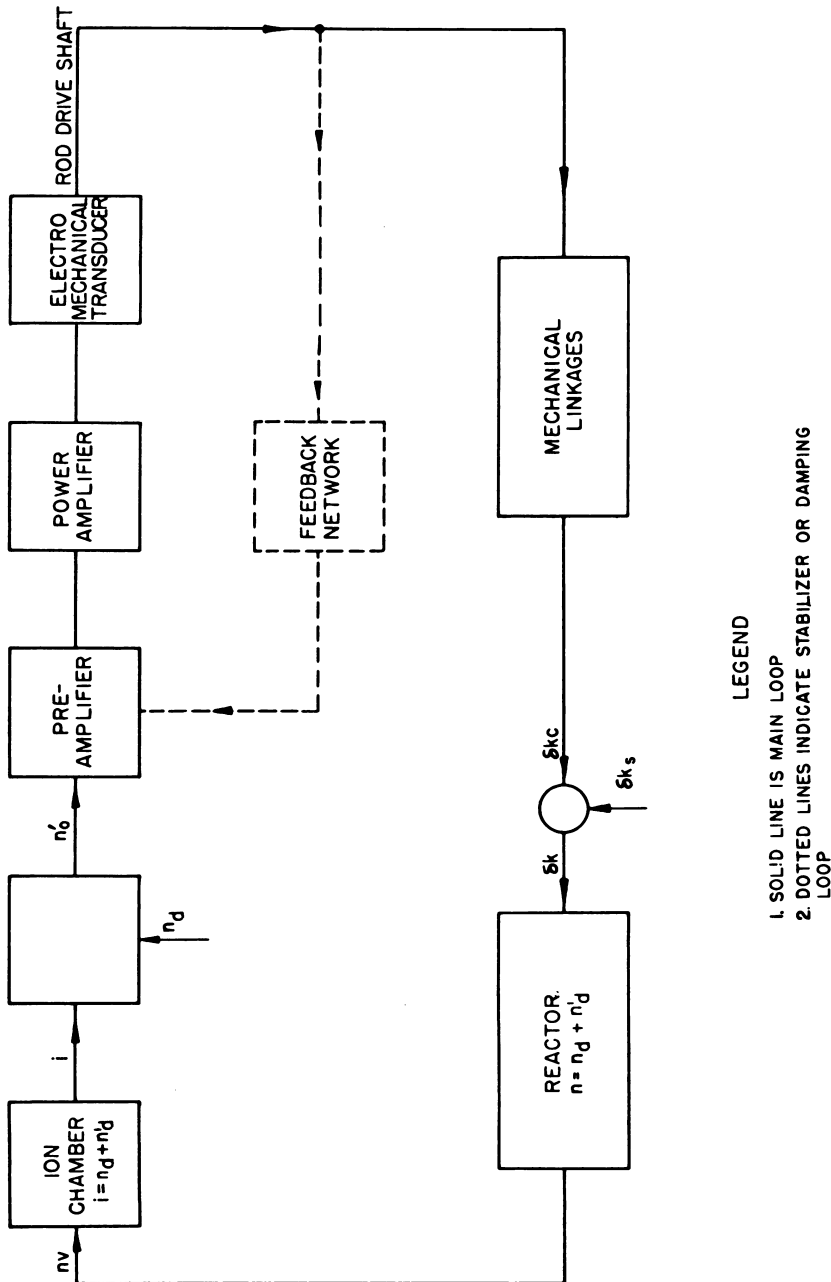


Fig. 7.4.5 — Regulating-rod Control Loop. Submitted by Argonne National Laboratory, Sept. 1952.

the load resistance is needed to ensure a linear relation between reactor n'_d and chamber current. With this circuit, the load resistance decreases as the dynamic chamber resistance decreases making the ratio more easily obtainable in power range. Another design is shown in reference (7), Fig. 5.3c, in which the chamber current is fed to the total fixed potentiometer resistance. For the circuit of Fig. 7.4.6, feedback can be employed at the input grid of the preamplifier because the grid resistance is constant.

If R_p on Fig. 7.4.6 is made logarithmic, a constant rate of displacement of the arm will correspond to a constant period of neutron density demand change. This type of potentiometer design is very special and costly for total resistance values above 0.5×10^6 ohms.

To reduce complication, the range of control n_{\max}/n_0 can be limited to 10: Power changes below n_0 are then made by lowering v_0 ; however, the gain reduces as v_0 , and the accuracy of control is not maintained in this lower range.

Figure 7.4.7 shows a method for obtaining n'_0 over a wide range of n control and providing an instrument calibration adjustment. This system requires an additional amplifier, but the resistance values are normally lower than those of Fig. 7.4.6.

CONTROL-LOOP CHARACTERISTICS

The control-loop for the regulating rod can be operated as either a proportional regulating system or a discontinuous regulating system.

A proportional regulating system is one in which the position of the regulating rod is changed in proportion to and in phase opposition to the error n'_0 . In this case, n'_0 develops either a torque or a velocity of the rod in proportion to n'_0 magnitude. Regulation of n to a value ± 0.1 percent of n_d can be obtained with this type of system.

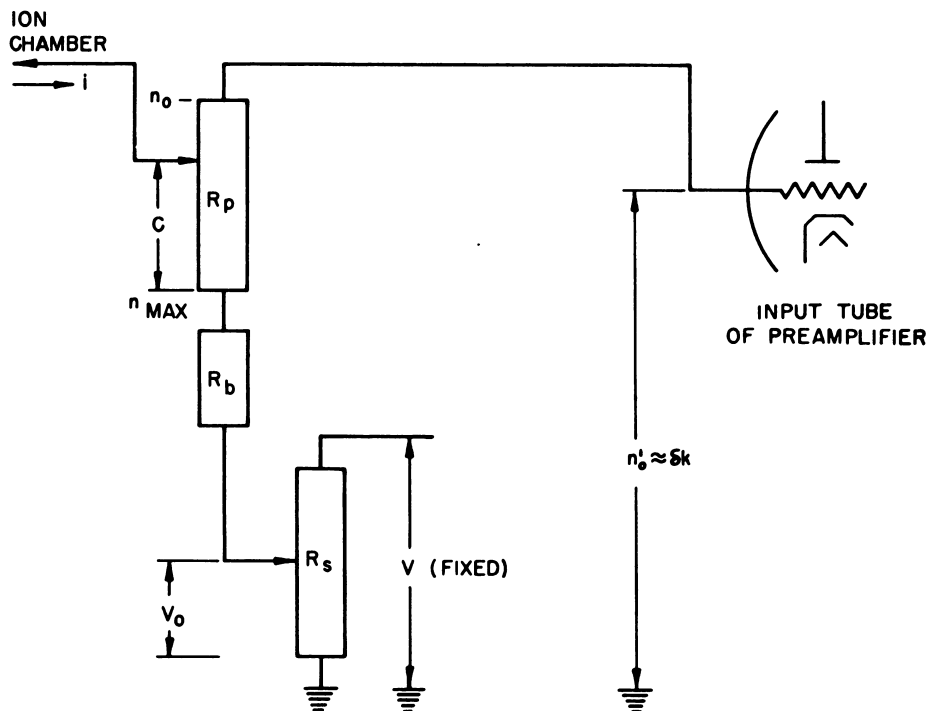
A discontinuous regulating system is one in which no control is obtained unless the n'_0 error represents a deviation in n of some fixed percentage away from n_d . When a sufficiently large error occurs, the rod is run at a set velocity. Regulation of n to ± 0.5 percent of n_d can be obtained with this type of regulating system.

Choice of type of system for a particular reactor should be made on the basis of desired control accuracy. However, if a discontinuous system is selected, it is important to note that when the error n'_0 is in the control "dead" zone between ± 0.5 percent the rod usually is held stationary by a mechanical brake or by friction in the rod guides to make operator rod-positioning simple. In a proportional system, any forces acting on the rod develop an error n'_0 large enough to hold the rod in place through the torque developed at the rod-drive motor. For operator control, the n'_0 error is not available and additional circuitry is usually necessary to hold the rod in position against disturbing forces. For this reason, discontinuous type of control offers an operating advantage over proportional control and should be used unless the better accuracy is necessary.

An example of a proportional system is described in reference (10). A discontinuous type system is described in reference (11).

SELECTION OF CONTROL-SYSTEM COMPONENTS

Control-system design is predicated on the selection of a drive motor for the regulating rod. The amplifiers for a proportional system or contactors for a discontinuous system can be selected or designed to meet requirements by using frequency analysis methods applied generally to regulating systems. The transfer function of the reactor has been presented in Figs. 7.4.3 and 7.4.4. A discontinuous system can be treated as shown in references (11) and (13) or by the method of reference (14). Selection of a regulating-rod drive-motor can be made from the standpoint of physical size and ambient conditions. However, when the motor is not fixed by these conditions, a choice can be made on the basis of system performance desired, fixing the maximum velocity torque, and acceleration needed by the motor as given under "System-Performance Evaluation."

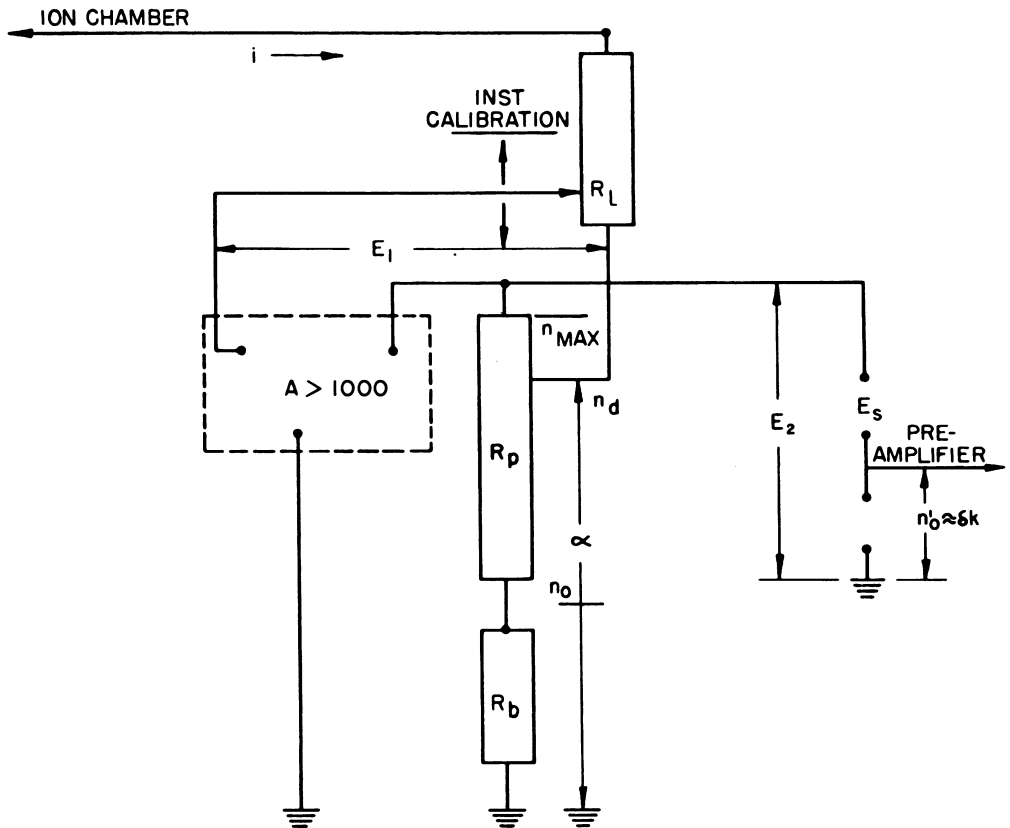


LEGEND

1. $C = \frac{n_0}{n_d} \left(\frac{n_{MAX} - n_d}{n_{MAX} - n_0} \right)$
- * 2. R_p = THE INPUT POTENTIOMETER RESISTANCE (5×10^6 TO 50×10^6 ohms)
3. n_0 = MINIMUM REACTOR FLUX.
4. $n_{MAX} = \frac{R_b + R_p}{R_b} n_0$
5. V_0 = MINIMUM FLUX SETTING ADJUSTMENT.
6. n_d = DEMAND FLUX OR CENTRAL POINT.
7. R_s = SOURCE OF V_0 (5×10^5 ohms)

* FOR LINEAR DISPLACEMENT OF C vs n, R_p MUST BE AN INVERSE POTENTIOMETER.

Fig. 7.4.6 — Circuit Used to Obtain Error from Ion Chamber Current. Submitted by Argonne National Laboratory, Sept. 1946.



LEGEND

1. $E_2 = \frac{E_1}{\alpha} = \frac{\text{amp PER FLUX} \times n R_L}{\alpha}$
2. $R_L \gg R_p$ $R_L \approx 5 \times 10^5$ ohms (SET BY TIME CONSTANT)
 $R_p \approx 5 \times 10^3$ ohms
 $R_b \approx 5 \times 10$ ohms
3. n_d = DEMAND FLUX
4. $E_s = \text{amps PER FLUX} \times n_{MAX}^{R_L}$
5. FOR UNIFORM α VS n , R_p IS NEARLY LINEAR
 WHEN $\frac{n_{MAX}}{n_0} \geq 100$

Fig. 7.4.7 — n'_0 Circuit with Instrument Calibration. Submitted by Argonne National Laboratory, Oct. 1952.

SYSTEM-PERFORMANCE EVALUATION

The performance of the regulating-rod control system can be evaluated as follows:

 δk Disturbance

Select a δk disturbance to be controlled by the regulating rod. This value must be less than or equal to the total δk of the regulating rod. Convert this δk to rod displacement, d , in feet. Select a time base, t , in seconds in which this value of δk is to be handled by the rod. Use Table 7.4.2 to convert t to the peak power ratio which indicates approximately

Table 7.4.2 — n_p/n_d = Peak Power Ratio = $1 + 300A \delta k$

t, sec	ω , radians	A		
		$1* = 10^{-3}$ sec	$1* = 10^{-4}$ sec	$1* = 10^{-5}$ sec
10.0	0.3	2.00	2.00	2.00
4.0	.75	1.50	1.50	1.5
2.0	1.5	1.00	1.25	1.25
1.0	3.0	1.00	1.00	1.00
0.4	7.5	0.75	0.85	1.00
.2	15.0	.50	.75	1.00
.1	30.0	.25	.65	1.00

how much the reactor power will deviate from the control n_d under the influence of a step δk of the magnitude selected. The value of ω shown in the table is used to obtain peak torque T_m , velocity v_m , and acceleration a for the drive motor from Eqs. (6), (7), and (8):

$$v_m = \omega d \text{ ft/sec} \quad (6)$$

$$a = \omega^2 d \text{ ft/sec}^2 \quad (7)$$

$$T_m = \text{system inertia} \times a \text{ ft-lb} \quad (8)$$

The velocity v_m converted to δk per second, at the point of minimum effectiveness must be no less than the δk per second resulting from the temperature-coefficient effect occurring as a result of an expected load change. v_m ranges from 2×10^{-2} $\delta k/\text{sec}$ to 10^{-3} $\delta k/\text{sec}$ for existing designs of proportional-type systems. For discontinuous-type systems, v_m ranges from 10^{-3} to 10^{-5} $\delta k/\text{sec}$. For the discontinuous system, the gearing between motor and rod is usually made a high ratio to make the load essentially only the motor itself. For the proportional type, a similar gear ratio may be taken for a high-speed motor, but a more direct approach has been described.¹⁴

Signal-to-Noise Ratio

Noise in the signal will dictate the gain designed into the preamplifier and power amplifier. Good values of signal-to-noise ratio for use in design are: 100:1 for a power reactor with flowing coolant and 1,000:1 for a reactor with no coolant flow measured at ion chamber output. The torque or velocity developed by the noise in the signal should not be more than 26 db less than the saturation torque or velocity of the drive motor for a proportional-type system. In a discontinuous system, there is the inactive zone where n_d

is less than the allowable power variation. The gain of the preamplifier should be low enough to keep the noise at less than 0.1 of this inactive zone.

Additional Design Notes

The effect of contactor lag upon the stability of a discontinuous-type system has been shown;¹³ for a reactor, wide range of stability has been obtained with an h/Δ of 0.03.

In a discontinuous-type system, the stalled-motor torque and the inertia at the motor shaft determine the motor time-constant. A time constant of 0.2 sec or less is satisfactory. The action of a brake to stop the rod adds greatly to stability by decreasing phase lag. A stopping time of 0.02 sec or less from full speed is recommended.

AUTOMATIC SHIM AND REGULATING ROD OPERATION

The shim rods may be used to extend the ability of an automatic system. If a point or range is designated as optimum in the regulating rod stroke, then the deviation of the rod from this position under automatic control-system operation is a measure of shim rod corrective δk desired in as much as the normal duty of the regulating rod has been exceeded. If the shim rods can change δk at a rate equivalent to the temperature-coefficient rate of change of δk , the shim rods can be used to effectively extend the regulating-rod range. Thus, the total regulating-rod δk can be restricted to a more linear region, and also a higher maximum velocity in δk per second can be assigned to the regulating rod. The optimum regulating-rod position for this condition is the center of its stroke.

Where the shims are too slow, the δk positive available in the rod is made at least 0.001 δk greater than the negative δk owing to power-range temperature change. For a water-cooled reactor, this may be as large as 0.006 so that a positive δk of 0.007 is required. A somewhat less negative value is required, making a total of about 0.01 δk for the rod. This places the optimum position at 30 percent of full stroke. Since possible maloperation is always anticipated for an automatic rod, the maximum rod speed should be limited to about 0.0005 $\delta k/\text{sec}$ for this case.

In general, the $\delta k/\text{sec}$ of the shims must be greater than the anticipated rate of δk change which must be offset by them. When the regulating rod deviates an amount equal to the total δk it is designed to offset, the shims are placed in motion. The physical distance of regulating-rod excursion away from the selected optimum point is set, and limit switches are used to start the shim rods running at a constant speed. This amounts to a discontinuous-type control system which can be designed as shown for the discontinuous regulating-rod systems. Proportional speed control is not used because of the additional complication it introduces into the shim-rod control-system design. Generally, a preferred method is to let the automatic system run the shim rods in a negative δk direction, reserving positive δk motion for operator control. Permissive switches are used to prevent shim movement toward positive δk unless the regulating rod has deviated from its optimum point by a fixed amount. In this way, the shim position is made to improve the usefulness of the regulating rod.

The factors given consideration here are amplified in reactor design reports given in the reference list at the end of this chapter.

AUTOMATIC PROTECTIVE SYSTEM

A nuclear reactor is protected from damage by a system of electrical interlocks, sensing elements, relays, and instruments, the complexity of which is a matter of engineering compromise based on the end purpose of the reactor, the fuel-element design, nature of the coolant, quality of the shield, and the like. Some important conditions considered dangerous to the nuclear reactors are listed below for use as a guide, but each

nuclear-reactor design brings up its individual array of conditions for protective system action.

In general, an effort should be made to design protective system elements to "fail safe;" that is, if an element fails to operate, it either deactivates a protective circuit and sets off an alarm or causes the control means to reduce k .

NUCLEAR REACTOR SHUTDOWN

Measurements which initiate fast rod motion are referred to as "scram signals."

A false scram is undesirable and failure of the "scram" system is dangerous; combination relaying methods are therefore used to improve "scram" system speed and reliability. For example, similar "scram" signals are read by sensing elements connected directly to sensitive relays, either electronic or magnetic or a combination of both. With at least three such assemblies provided, the relaying system may be designed so that if two of the three measure a dangerous condition, "scram" is initiated. Parallel systems are also used in which a fast-acting electronic relay is placed in parallel with a magnetic relay and, if failure of the electronic relay occurs, the magnetic relay backs it up. This is done to gain the advantage of high-speed electronic relay action in addition to the reliability of magnetic relays. To preclude the failure of one element or instrument in a measuring system, the readings of several elements are converted to voltages, and these voltages are compared by diode circuits arranged to send only the highest voltage to a scram circuit. This type of action is sometimes called "auctioneering." Particular "scram" signals are discussed further in the following paragraphs.

NEUTRON DENSITY 150% OF NORMAL DENSITY

Measuring is done with different types of primary elements, such as neutron-sensitive ion chambers, gamma chambers, pulse counters, scintillation counters, and neutron thermopiles. The trip settings are made adjustable because they must be set experimentally after installation on the reactor. Approximate settings are initially calculated to obtain a starting point setting for the protective circuits.

FLUX PERIOD LESS THAN 1 SECOND

Neutron-sensitive ion chambers and pulse counters are used as sensing elements. Positive and negative periods may be used to provide similar protective action. Basically, the positive period is considered the dangerous one, but negative-period protection is provided on the assumption that a short uncontrolled negative period may be followed by a short positive period.

EXCESSIVE COOLANT TEMPERATURE

This is measured with thermocouples, resistance thermometers, and gas or mercury bulbs in the coolant stream. Temperature indication is obtained with a 2- to 4-sec response period, depending upon the heat capacity of the element enclosure.

RAPID CHANGES IN COOLANT TEMPERATURE

These changes are indicated by attaching amplifiers and rate circuits to the coolant temperature instruments.

LOSS OF INSTRUMENT ELECTRICAL POWER SUPPLY

Under-voltage relays both time-delayed and instantaneous are used. For increased reliability, instruments are fed by battery-driven DC motors and AC generator sets. The battery is, in turn, "floated" on an AC motor and DC generator combination driven from the purchased power supply.

POWER REDUCTION

In some cases, signals similar to the shut-down signals are used to reduce reactor power rather than "scram" the reactor. The action may consist of driving selected rods toward the minimum reactor k position at a nominal speed, or in case automatic power control by a regulating-rod control system is installed, the demand n_d may be run to a minimum setting. Typical signals for this type of action are: neutron density = 120 percent design density; flux period less than 5 sec; coolant flow = 80 percent normal; temperature of coolant = 105 percent normal; and loss of purchased power supply.

OPERATING PROCEDURE INTERLOCKS

In addition to the preceding shut-down conditions, the operator's procedure in starting a reactor is supervised by a system of interlocks, annunciators, and signals. The following paragraphs discuss conditions in this category.

PERMISSIVE LOCKS

The main power supply should be key-locked "open" with one or more locks to be used for supervisory control or to enforce a routine area inspection before start-up.

SAFETY RODS READY

Ready-position limit switches are provided on the safety rods to indicate that they are ready to "scram" the reactor. These limit switches are inserted into the control system to prevent shim-rod removal when the safety rods are not ready. Where shim-safety rods are used, magnet current is sometimes used as an indication that the rods are held in position. Where latches are used, the latch position is sometimes detected directly by limit switches or can be detected through the magnet current magnitude.

REGULATING ROD READY

Limit-switch interlocking is sometimes used on the regulating-rod drive-mechanism or on an auxiliary program device to ensure that the rod is in an optimum or desired control position before the shim-rods are moved away from the minimum k position. Optimum rod position was discussed under "Automatic Shim and Regulating Rod Control."

COMPLETE SYSTEM DESIGNS

To describe the design of a protective interlock system requires a comprehensive discussion beyond the scope of this chapter. It is desirable to leave complex procedure interlocking out of the system and depend upon the intelligence of the operator for proper procedure in starting up a reactor or making a power change. A more involved system of interlocking is provided for MTR.⁷ Other experimental reactor systems have also been described.^{15,16}

TEMPERATURE-COEFFICIENT POWER REGULATION

The temperature coefficient of the reactor is important to control. Some aspects of the effect on control system design have been discussed under "δk Control Means" and "Automatic Power Regulation." This coefficient is referred to as negative if increasing power produces negative δk. Many reactors currently in operation have a net negative temperature coefficient, but the likelihood of there being a positive coefficient is always considered in proposed designs. From currently available information, it is very unlikely

that a water-moderated and water-cooled reactor could have a positive temperature coefficient, because the effect is produced by a combination of dimensional changes and moderator density change. These effects have been large enough to offset any nuclear cross-section change which might oppose them, and the net effect found in the completed reactor is a negative coefficient. The liquid-metal-cooled Experimental Breeder Reactor (EBR) also has a negative temperature coefficient. The usefulness of this effect has been demonstrated in the EBR system where, by simply changing the load or heat removal, the reactor power will self-regulate to a new value equal to the demand on the system, no rod-position changes being necessary. When more heat is removed by the external power system, the lowered temperature of the coolant lowers the fuel-element temperature providing a positive δk for increasing the power. The increase in temperature drop in the coolant across the reactor which results from higher power returns the δk to 0. Quantitative data for EBR are not yet in published form. The temperature coefficient is about 10^{-3} total δk for the temperature rise in the useful power range. For CP-3', the experimental heavy-water-moderated reactor at ANL, the total δk resulting from the power change in the operating range between 3 kw and 275 kw is about 5×10^{-3} . The factor of 5 difference is largely a result of moderator or density change.

APPROXIMATE ANALYSIS

The dynamic control effect of the negative temperature coefficient can be estimated for the simple case where a suitable single dominant time constant can be established.

Let the effect of the temperature coefficient on reactor k be δk_T ; then, the relation between power and δk_T for a power increase is given in Eq. (9):

$$\frac{\delta k_T}{P_0} = Z(1 - e^{-t/\tau_1}) \quad (9)$$

where: P_0 = fractional power change

Z = total δk owing to temperature effect in the operating range from 1 to 100 percent of design power divided by 99

τ_1 = the dominant time constant (in seconds) of the heat exchange in the reactor which produces the temperature effect

The description of Z given here limits consideration of temperature effect to that range where a significant rise in coolant temperature across the reactor is obtained, that is, above about 1 percent design power. Below this power, there still is a temperature effect on the reactor k , but the changes in temperature are not produced entirely by power changes in the reactor because heat must be added to the coolant system from another source to maintain its temperature.

A k change δk_c from control means or changes in other k effects will then cause the reactor power to rise or fall to a new power which is a function of Z and k_c as given in Eq. (10):

$$P = P_0 + \frac{k_0}{Z} \quad (10)$$

where P and P_0 are in fractions of full power.

Whether reactor power will approach the new value, P , either by overshooting or by not overshooting P , is a function of $1^*/\beta$, τ_1 , and the magnitude of Z . When τ_1 is much larger

than $1/\beta$ and Z is large, an overshoot can be expected. When Z is decreased or when τ_1 gets near $1/\beta$, no overshoot is to be expected.

To estimate the condition existing for a particular reactor, assume that a step change positive in k of a magnitude δk_c has taken place. Calculate P from Eq. (10). Then using Table 7.4.2, calculate the power ratio for δk_c positive with an ω equal to $1/\tau_1$. If the power indicated by the power ratio is less than P , there will be no overshoot. If it is greater than P , there will be no overshoot.

This method of analysis is only for estimating the effects of temperature and is presented here in lieu of more analyses, experimental work, and quantitative data.

The above considerations were based on the assumption that all heat supplied by the reactor was removed by the external heat exchanger or power system. When a δk disturbance takes place and it is assumed that no heat is removed from the coolant of a water-moderated reactor, an oscillating condition is found. The heat is stored in sections or slugs of the coolant, and when that slug returns to the reactor, the average temperature of the coolant is higher, injecting a negative δk which must again be stabilized by the temperature coefficient. On the next cycle, this process is reversed, and the resulting oscillations occur in periods corresponding to the period of coolant circulation. Heat losses in a practical system should prevent a long continuation of the oscillation and certainly prevent any instability. Some exploratory work¹⁷ was done on this effect. In a liquid-metal-cooled reactor, this effect would be minimized because the ratio of the fuel-element temperature to the coolant temperature is higher than in a water-cooled reactor.

REACTOR INSTRUMENTATION

GASEOUS COUNTERS AND CURRENT CHAMBERS

B¹⁰ TYPE

An electrical potential difference is applied between two electrodes enclosing a normally non-conducting gas. As ionizing agent enters the gas, positive and negative ions are formed and are collected at the electrodes. An electrical current between the electrodes results. The sensing element design is normally aimed at getting the current magnitude directly proportional to the radiation to be measured. Short-range alpha particles give the largest amount of specific ionization; gammas give the least amount of specific ionization owing to their very high range. Neutrons are detected by absorption in B^{10} which results in an n, α reaction; the α particles, in turn, cause gas ionization. The electrodes may be coated with B^{10} or the chamber may be filled with $B^{10} F_3$ gas.

When the gas is ionized, the electrons may gather energy from the electric field and cause further ionization. This effect, referred to as "gas multiplication," is enhanced by higher electric-field strength and is used in proportional counters. If a low $n\gamma$ is incident on the chamber, intermittent current pulses will result. These pulses are counted in scalers (combinations of electronic and mechanical counters) usually used in a range between 10 and about 100,000 counts/sec. Counters of this type are commercially available.

COUNTERS

A sensory element that operates with a circuit which accepts and registers pulses is called a "pulse chamber." If the observed pulse is amplified linearly by gas multiplication in the element, it is referred to as a "proportional counter." Figure 7.4.8 shows a typical pulse chamber used for general-purpose work at ANL with a maximum counting rate of 10^7 counts/min. This type of chamber operates with a wide-band, high-gain amplifier having a rise time of about 10^{-7} sec and a noise level of 10^{-4} volts with a chamber

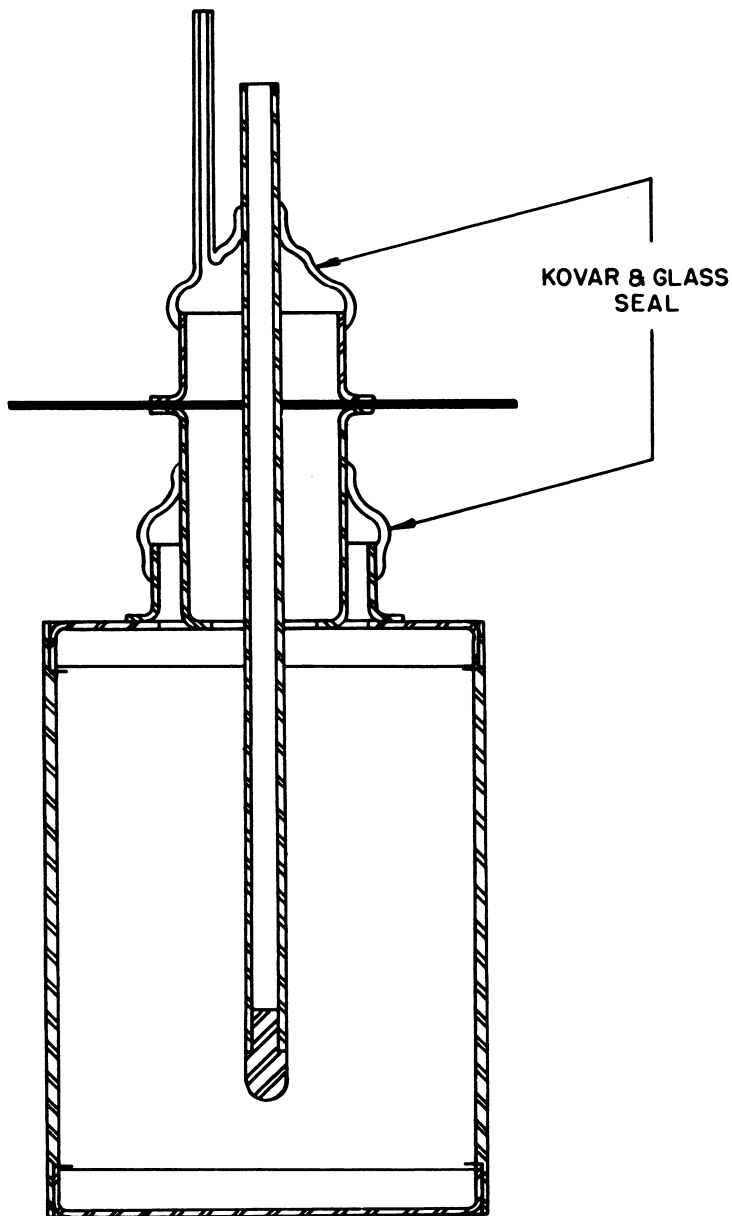


Fig. 7.4.8—Cross Section of a Typical Pulse Counter. Submitted by Argonne National Laboratory, Sept. 15, 1952. For dimensions, see Fig. 7.4.9.

capacity of $10\ \mu\text{f}$. The B^{10} disintegration will produce pulses of 2×10^{-4} to 5×10^{-4} volts. Electrode sizes are selected so that collection time will be 0.2×10^{-6} sec at 1 atm of BF_3 . Dimensions and characteristics of three typical counters are shown in Fig. 7.4.9.

A shock-resistant version of B^{10}F_3 proportional counter is shown in Fig. 7.4.10, and a B^{10} -lined proportional counter is shown in Fig. 7.4.11. The characteristic curve was taken with a combined amplifier and scaler with input sensitivity of 2×10^{-3} volt.

CURRENT CHAMBERS

When a continuous current is used for radiation measurement, the chamber is referred to as a "current ion chamber." Gas multiplication is not utilized for this type of neutron detection; thus, in general, the potentials applied to ion chambers are less than those applied to pulse chambers, and the electrodes have a relatively large area. The useful current range is from 10^{-12} to 10^{-4} amp from current ion chambers. A typical current ion chamber for measuring reactor nv is shown in Fig. 7.4.12. The plates are B^{10} -coated, and a spacing of $\frac{1}{8}$ in. is used to obtain a relatively low effect from gamma ionization in the gas between the plates. Electrolytic-iron electrodes are used.

A B^{10}F_3 -filled chamber is shown in Fig. 7.4.13, and its saturation curve is shown in Fig. 7.4.14. The drawing does not show the grounded outside shell necessary to protect and shield the chamber in use with a reactor.

FISSION CHAMBERS

Current ion chambers and pulse chambers can be built using U^{235} coatings on one or both electrodes. The neutrons are readily absorbed by uranium, and high ionization is produced as a result of fission. Pulse counters operating on this principle are called "fission counters." An advantage of this type of instrument is the very high current pulses produced by neutrons compared to the relatively small pulses produced by gammas. If U^{238} is used as the coating, the instrument can be used as a high-energy-neutron detector.

FISSION PULSE COUNTERS

A concentric cylinder type of construction is shown in Fig. 7.4.15; this is a comparatively simple method of building such an element.

Another type, called "spiral-wound fission counter,"¹⁸ the object of which is to provide a large, coated area in a small volume, is shown in Fig. 7.4.16.

FISSION-CURRENT ION CHAMBERS¹⁹

The fission counter of Fig. 7.4.15 was operated as a current ion chamber at 4×10^{-7} amp output and gave a sensitivity of 4×10^{-14} amp/flux with 300 volts on the electrodes.

A typical natural-uranium current ion chamber is shown on Fig. 7.4.17. The use of natural uranium precludes the danger of burn-up at high nv because the U^{238} is converted to plutonium. This chamber was designed for operation in 10^{12} nv or more. The characteristic curves are shown in Figs. 7.4.18 and 7.4.19.

GAMMA ION CHAMBERS

For wide-range reactor control, the quantity to be measured is the average neutron flux in the reactor. The average value of this flux may vary from 10^5 to 10^{15} . The gamma radiation resulting directly from fission (called "prompt gamma") is sometimes as good a measure of neutron density as the neutrons themselves, both being proportional to the neutron density.

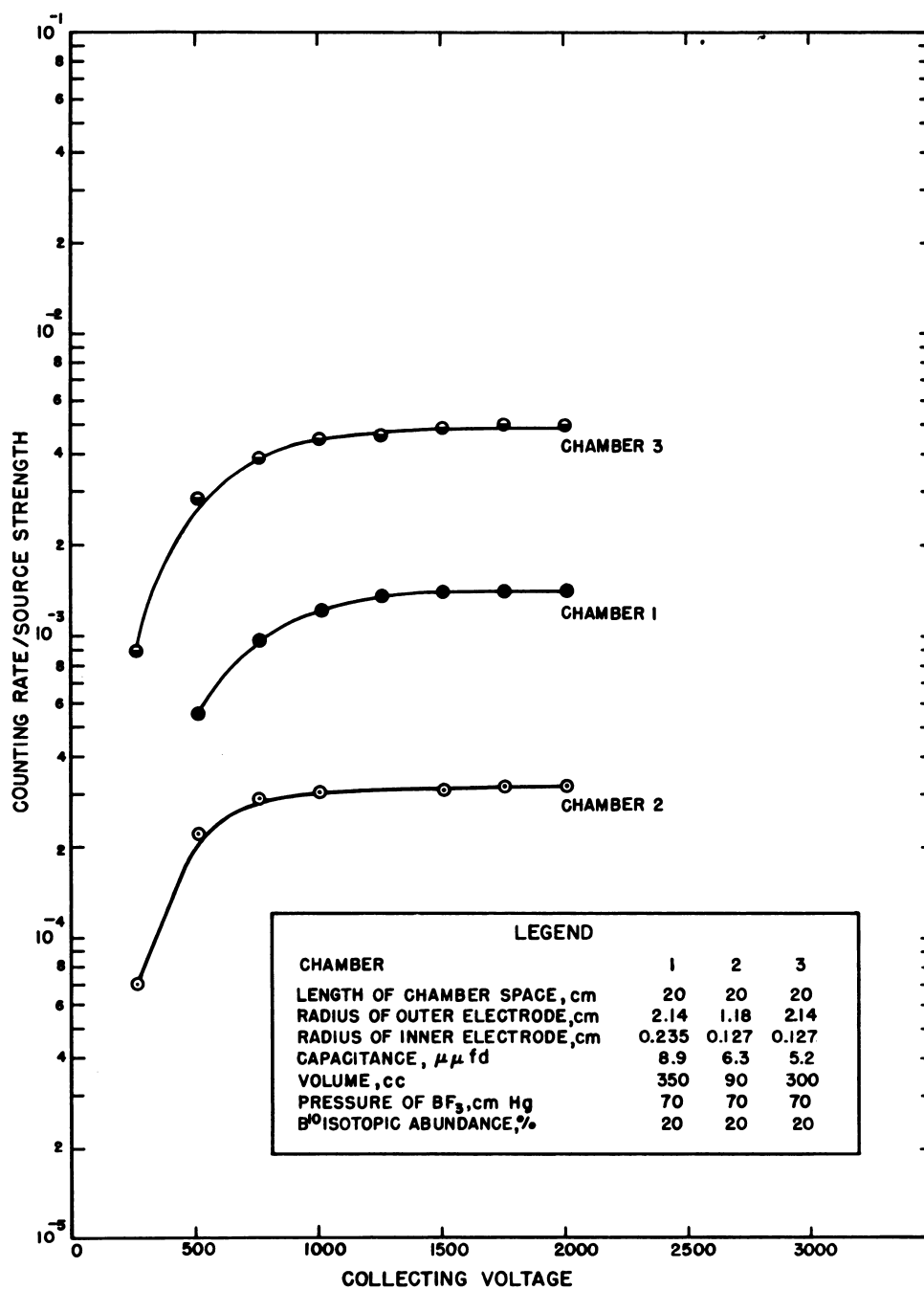
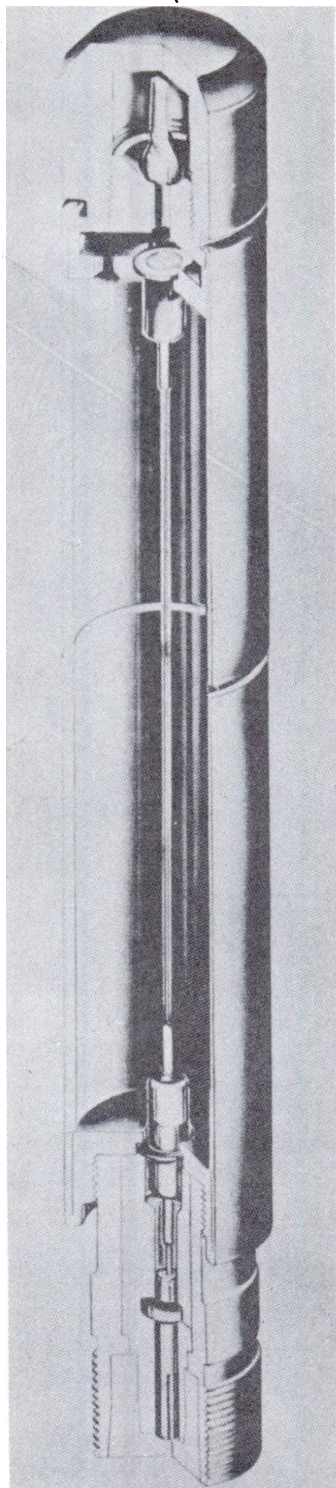


Fig. 7.4.9—Relative Counting-rate Response to a Standard Neutron Source as a Function of Electrode Voltage for Typical Pulse Counters. Submitted by Argonne National Laboratory, Sept. 12, 1952.



LEGEND

1. EXTERNAL CYLINDER, 10 x 1 in.
2. DIAMETER OF CENTER WIRE, .001 in.
3. GAS PRESSURE, 55 cm Hg
4. SENSITIVITY, 4 COUNTS/(sec)(nv)

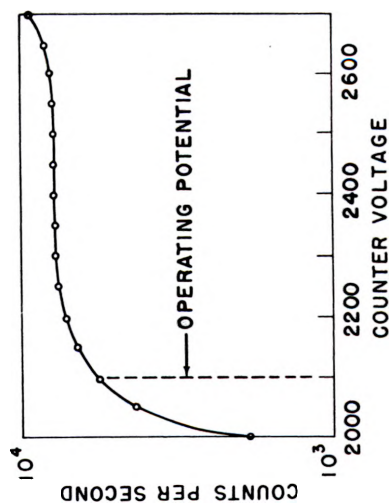


Fig. 7.4.10 — Shock-resistant Proportional Counter B¹⁰F₃-filled and the Saturation Curve for This Counter. Redrawn from R. R. Leonard, Radiation Detecting Instruments, WAPD-RM-68.

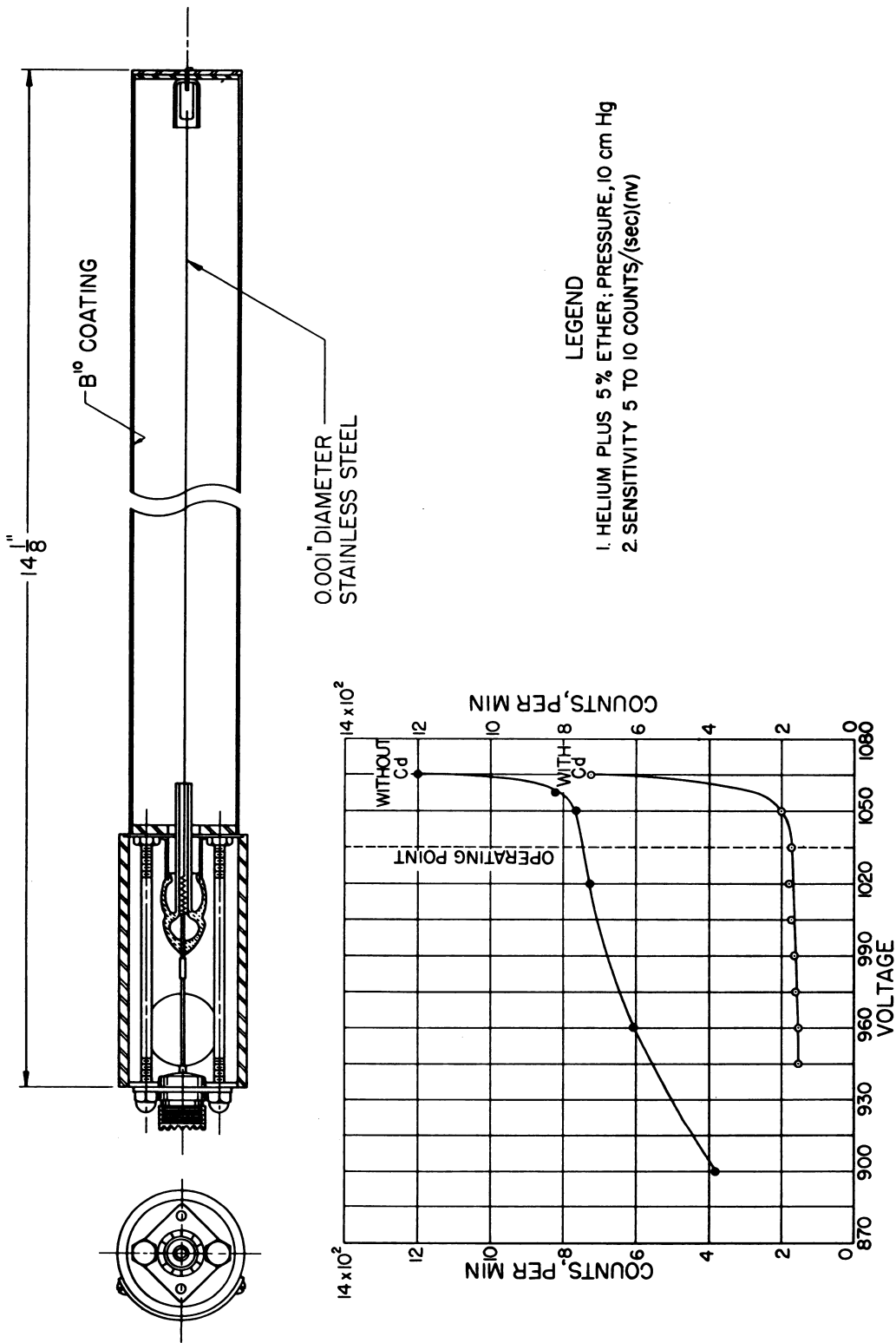
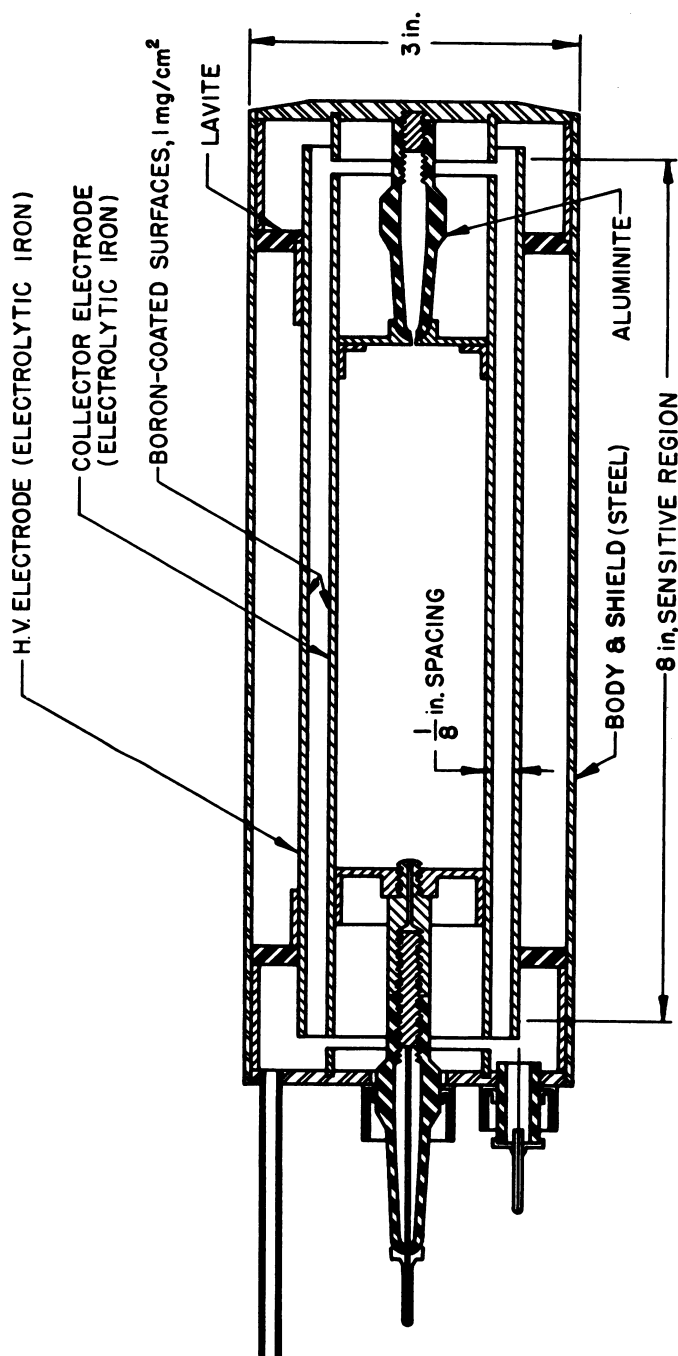


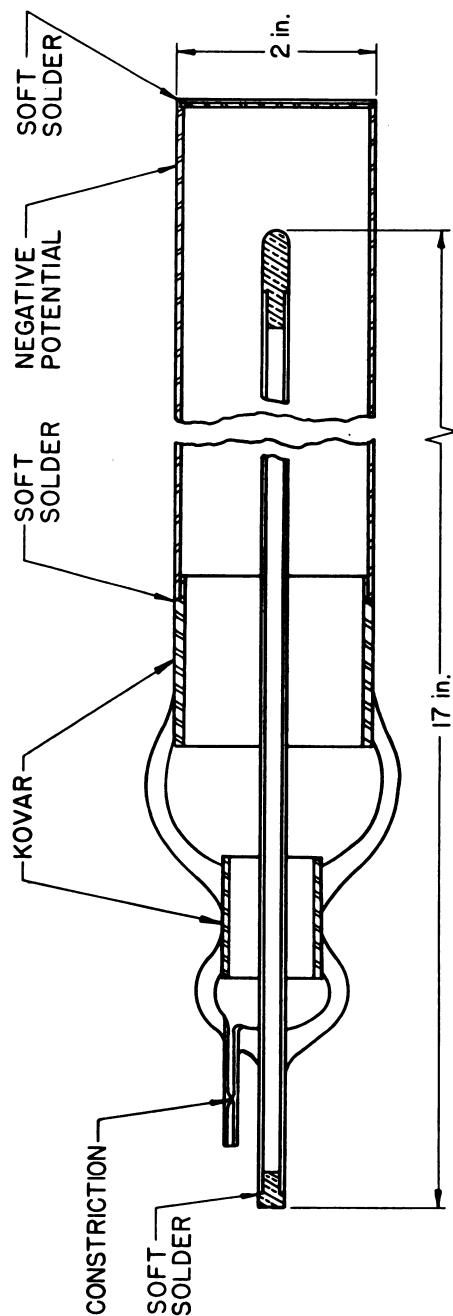
Fig. 7.4.11 — B¹⁰-coated Counter and Saturation Curves. Submitted by Argonne National Laboratory, Sept. 1952.



LEGEND

1. SENSITIVITY NATURAL BORON, 6×10^{-15} amp/nv.
2. SENSITIVITY B^{10} -COATED, 3×10^{-14} amp/nv.
3. CHAMBER OPERATES UP TO 350°C .
4. ALUMINITE INSULATORS HAVE 10^6 ohms RESISTANCE AT 250°C .
5. FILLING GAS DRY ARGON, 96.6 % PURE.

Fig. 7.4.12 — B^{10} -coated Current Ion Chamber. Redrawn from D. H. Morley, High-temperature Ionization Chamber, Knolls Atomic Power Laboratory Technical Information Series No. R-50GL126



LEGEND

1. FILLING $B^{10}F_3$ AT 120 cm Hg PRESSURE
2. ENCLOSING BODY AT GROUND POTENTIAL IS NOT SHOWN. STAND-OFF INSULATORS OF POLYSTYRENE ARE USED TO SUPPORT THE ASSEMBLY IN THE BODY.
3. SENSITIVITY, 3.5×10^{13} amp per flux.
4. SEE FIG. 7.4.17 FOR PLATEAU.

Fig. 7.4.13 — $B^{10}F_3$ -gas-filled Current Ion Chamber. Submitted by Argonne National Laboratory, Sept. 1952.

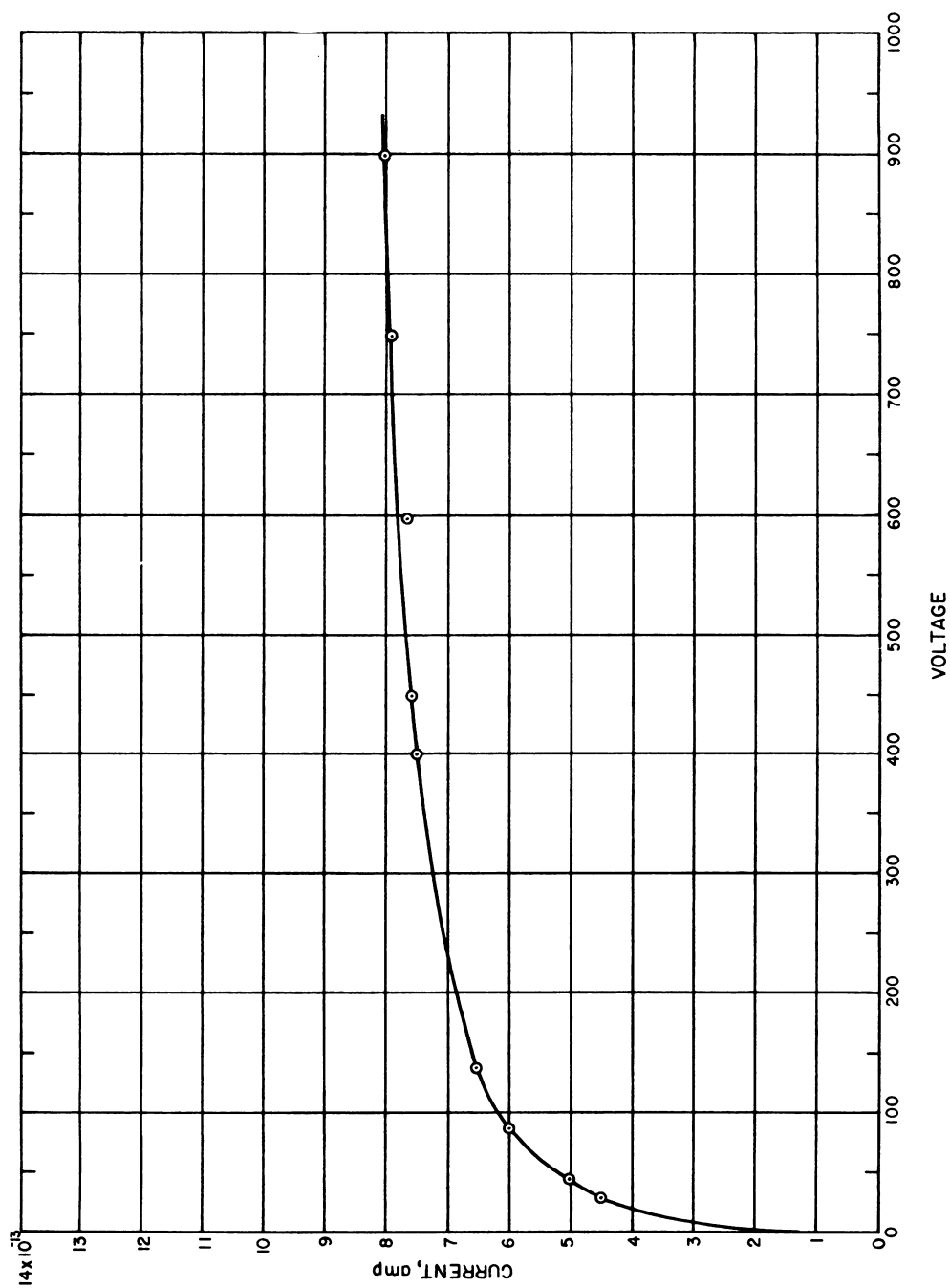
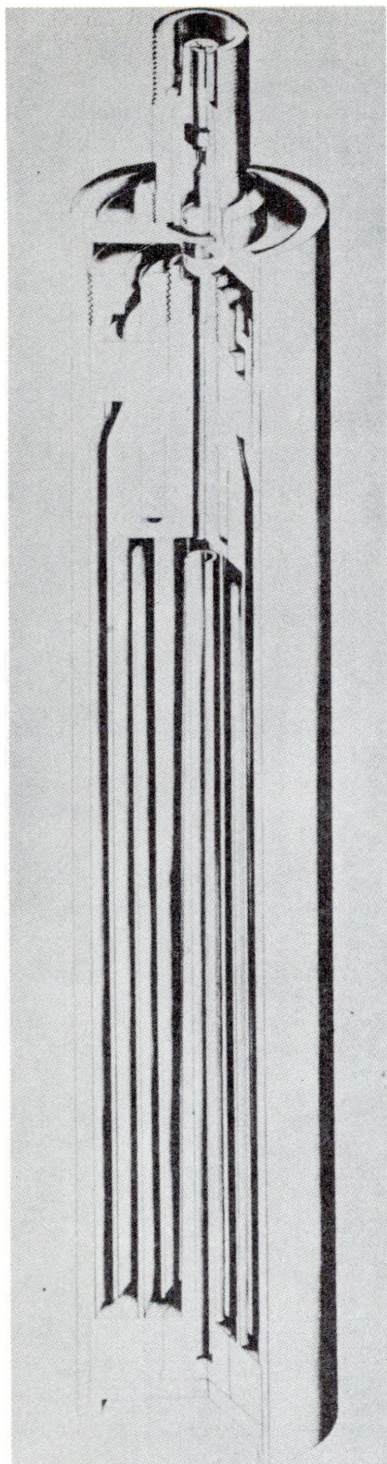


Fig. 7.4.14 — Saturation Curves for $B^{10}F_3$ -filled Ion Chamber of Fig. 7.4.13. Submitted by Argonne National Laboratory, Sept. 1952.



LEGEND

1. ELECTRODE SPACING .15 in.
2. OPERATING VOLTAGE, 300 volts
3. COATING, 2 mg/cm²
4. FILLING NITROGEN, 2 atm.
5. TOTAL OF 1.6 gm ENRICHED U²³⁵
6. SENSITIVITY, 0.7 counts per unit thermal flux

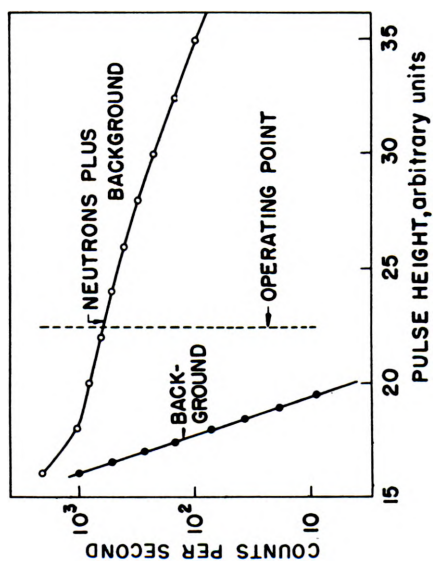
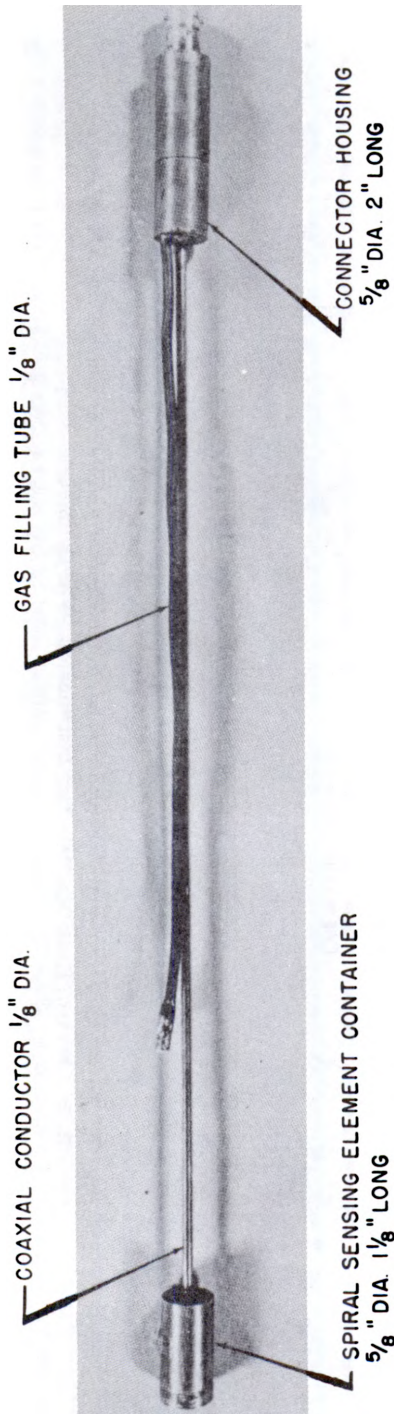
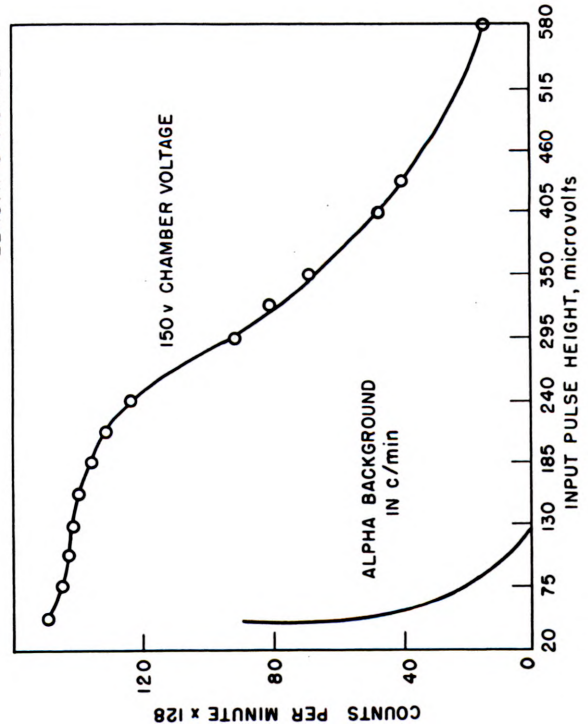
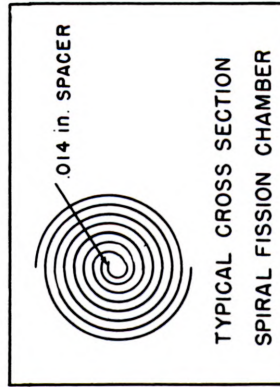


Fig. 7.4.15 — Concentric-cylinder-type Fission Pulse Counter and Performance Curve. Redrawn from R. R. Leonard, Radiation Detecting Instruments, WAPD-RM-68.



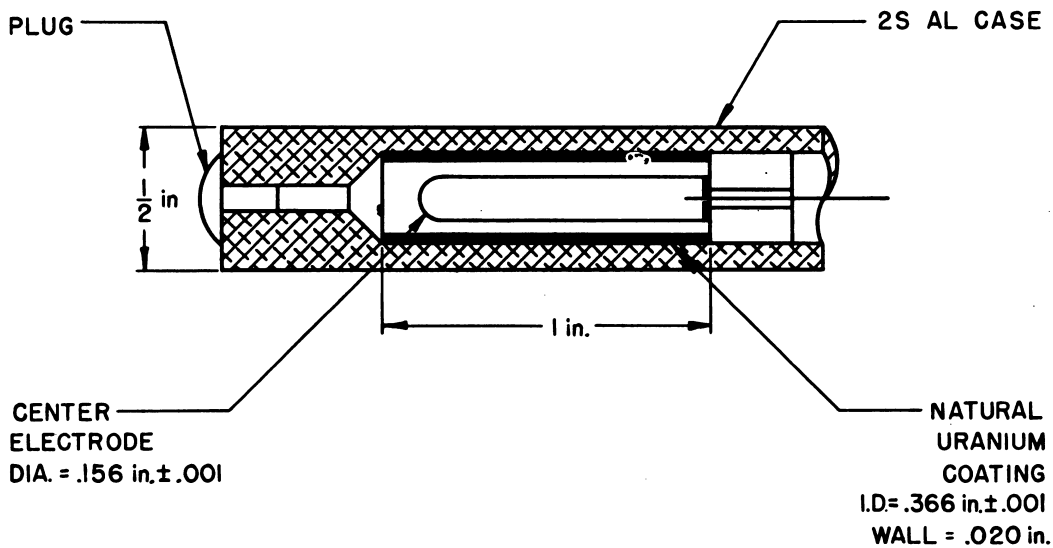
NOTE: OVER-ALL LENGTH 16",
LENGTH OPTIONAL.



LEGEND

1. OVER-ALL LENGTH 16", LENGTH OPTIONAL
2. $\frac{1}{2}$ " DIA. \times $\frac{1}{2}$ " LONG NATURAL URANIUM SPIRAL
3. FISSION CHAMBER
4. ARGON PRESSURE, 120 PSI
5. CHAMBER CAPACITY, 105 $\mu\mu\text{f}$
6. CABLE CAPACITY, 152 $\mu\mu\text{f}$
7. AMPLIFIER GAIN, 32,000
8. RISE TIME OF .25 μsec
9. DECAY TIME, 3 μsec
10. DISCRIMINATOR DEAD TIME, APPROX. 35 μsec
11. DATA TAKEN AT 10^7 nV

Fig. 7.4.16—Spiral-electrode-type Fission Chamber. Submitted by Argonne National Laboratory, Sept. 1952.



LEGEND

1. CHAMBER FILLED WITH ATMOSPHERIC AIR.
2. POLARITY OF ELECTRODE AFFECTS SENSITIVITY USE WITH, CENTER POSITIVE, OUTER NEGATIVE, COMPARE FIGS 7.4.21 & 7.4.22
3. A CHANGE IN OUTPUT CURRENT TAKES PLACE FOR SEVERAL MINUTES WHEN THIS CHAMBER IS FIRST EXPOSED TO A HIGH VALUE OF FLUX. CONTINUAL EXPOSURE RESULTS IN A STEADY OUTPUT CURRENT READING
4. THIS CHAMBER WAS EXPOSED TO 10^{13} nv. A CHANGE IN SENSITIVITY OF 10% WAS OBSERVED DURING THE FIRST 8 HOURS. NO CHANGE WAS OBSERVED AFTER THAT TIME.
5. CHAMBER IS TEMPERATURE-SENSITIVE.

Fig. 7.4.17 — Natural-uranium Fission-current Ion Chamber. Submitted by Argonne National Laboratory, Sept. 1952.

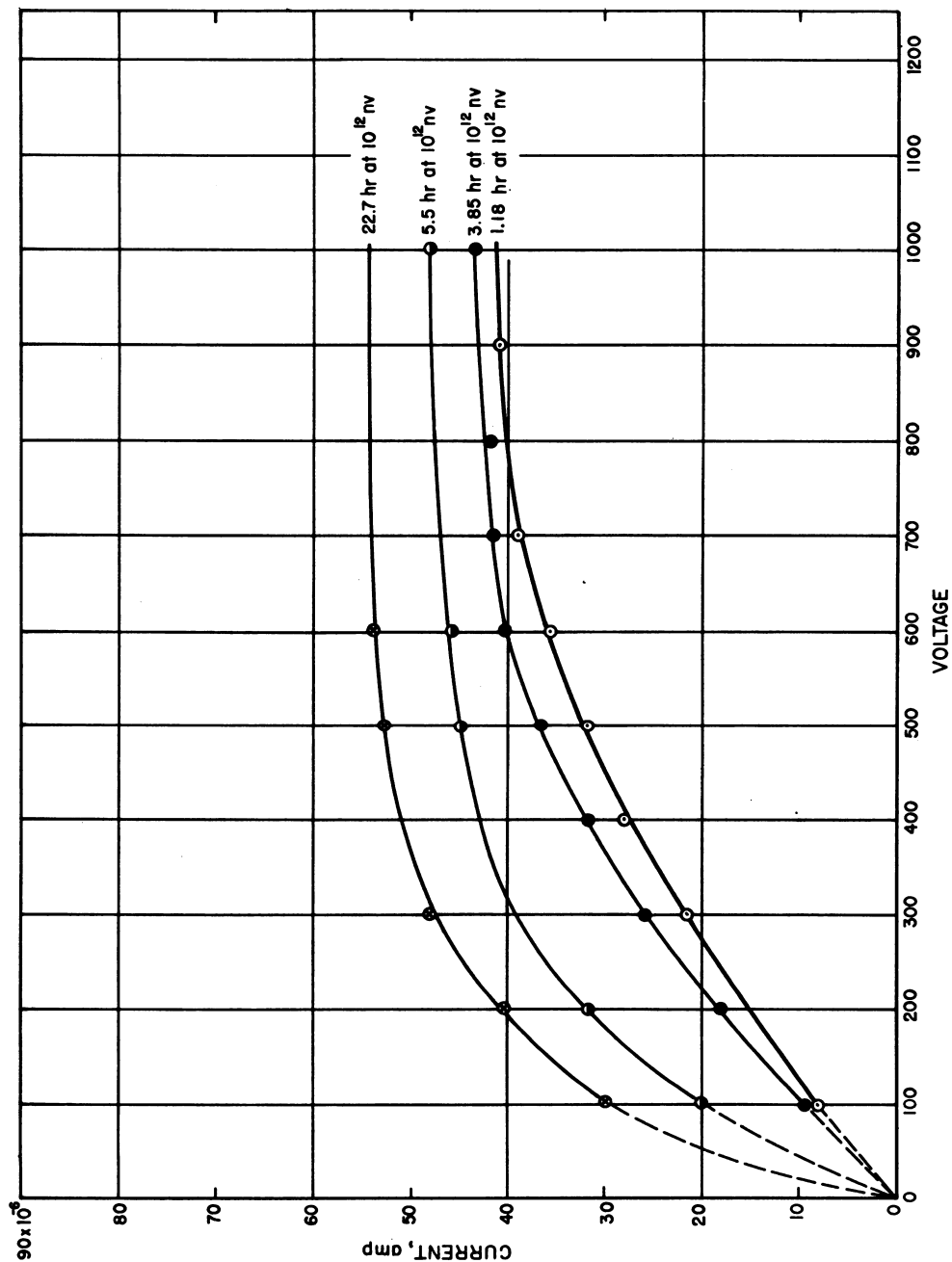


Fig. 7.4.18 — Characteristic Curves for Fission Ion Chamber of Fig. 7.4.17 with Positive Potential on the Center Electrode. Submitted by Argonne National Laboratory, Sept. 1952.

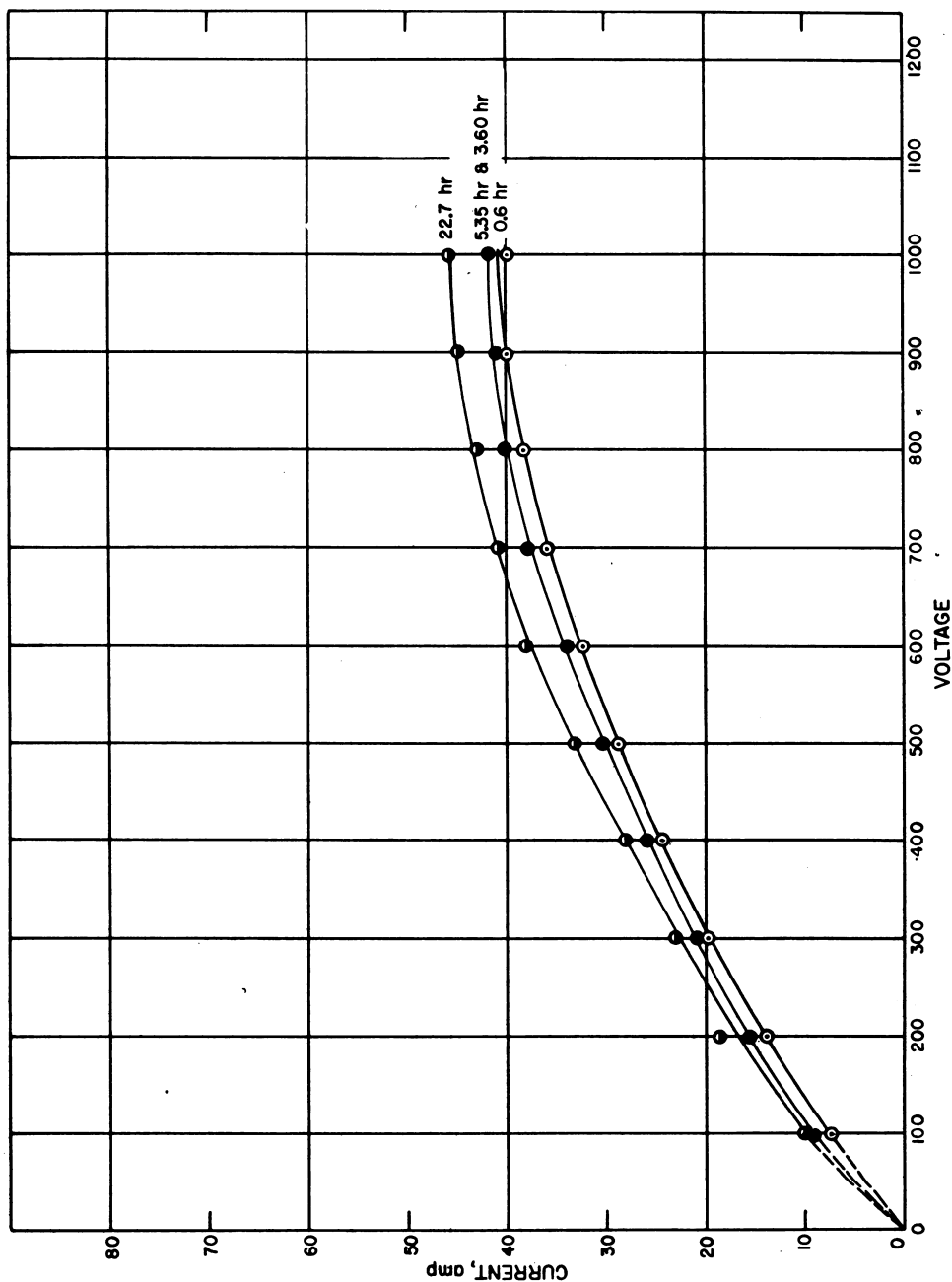


Fig. 7.4.19 — Characteristic Curves for Fission Ion Chamber of Fig. 7.4.14 with Negative Potential on the Center Electrode. Submitted by Argonne National Laboratory, Sept. 1952.

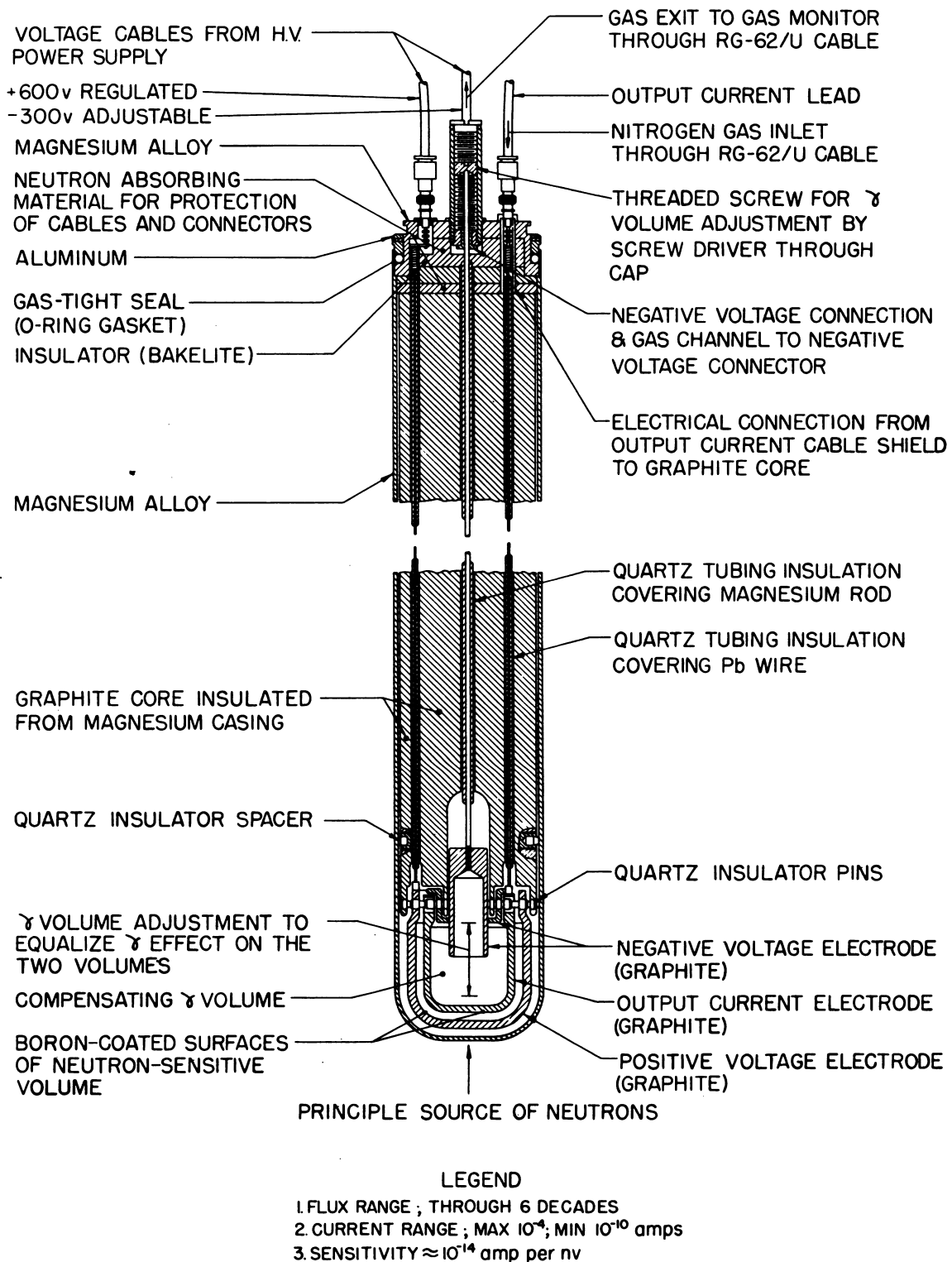


Fig. 7.4.20—Compensated Current Ion Chamber. Redrawn from Fig. 4, MTR Safety System and Its Components, ORNL 1193.

Gamma-current ion chambers are used to determine power in zero-power reactors and are useful as back-up or safety-type chambers on many reactor installations. A typical gamma-current ion chamber is similar in construction to neutron-sensitive chambers, but the filling-gas pressure must be high to provide reasonable sensitivity. A typical value is 600 lb/sq in. of argon.

COMPENSATED ION CHAMBERS

Gamma radiation present near a reactor may result from the combination of activated structural material, fission-product gammas, and prompt gammas, and the instrument current is therefore not always proportional to neutron density alone. The sensitivity of a sensory element to gamma radiation can be reduced by close spacing of the electrodes; $\frac{1}{8}$ in. to $\frac{1}{4}$ in. spacings are frequently used; optimum electrode spacing is discussed in reference (20). Gamma-compensated ion chambers are built with two nearly equal gas volumes located next to one another. One volume is made sensitive to neutrons plus gamma rays, the other to gamma rays only. By opposing the currents from these, the net chamber current becomes a measure of neutrons alone. This assembly is referred to as a "compensated ion chamber."

A typical compensated chamber is shown in Fig. 7.4.20. Nitrogen gas is circulated through the chamber along the leads. This serves to maintain known gas in the chamber and keep the leads dry. Chamber materials are selected to have a minimum of residual activity. Compensation is adjusted by changing the position of the inner electrode, which effectively changes the compensation volume, and by changing the voltage of the negative supply. Another compensated chamber is shown in Fig. 7.4.21. This chamber is compensated by changing the potential between the compensating electrodes. The center electrode is shaped to produce a weak-field region so that the ratio of ΔI to ΔE along the plateau of this section is larger than the same value for the neutron-sensitive section. Figure 7.4.22 shows the field in the compensating volume.

TEMPERATURE-TYPE ELEMENTS FOR NEUTRON DETECTION

Neutrons can be detected by absorption in boron-coated temperature-sensitive elements. The absorption of neutrons causes the temperature of the element to rise. Thermocouples have been assembled with several closely spaced junctions in series. Alternate junctions are coated with boron or uranium (a neutron absorber) and are connected electrically so that the potentials of the coated and uncoated junctions oppose. The net voltage output of this assembly is a measure of the neutron density at the junctions.²¹

These assemblies are called "neutron thermopiles." Their chief advantage is compactness and low impedance. They can be inserted into the reactor core where space is very limited. A typical unit assembly is shown in Figs. 7.4.23 and 7.4.24. The sensitive element is chromel P-constantan wire, 0.003 in. in diameter, and alternate junctions are coated with 15 mg of B^{10} powder applied with Sauereisen No. 1 cement or polystyrene-acetone dope. The active section is 0.04 in. thick. The thermocouple ends are soldered to copper terminals which are insulated from the 2S aluminum case by mica.

Sensitivity is 10^{-3} volts per 10^{11} nv. The response is linear up to 3×10^{12} nv. The time constant owing to heat capacity of the detecting element is about 4 sec. Such an element was exposed for 5 months at 5×10^{11} nv with no change in sensitivity or failure resulting from deterioration. Figure 7.4.25 shows a watertight version of the neutron thermopile sealed in a 2S aluminum can.

An alternate temperature method has been investigated by WAPD in which small-diameter platinum wires have been coated with boron. Using an uncoated unit and a coated unit together in a resistance bridge provides a rugged and accurate method of flux determination. The assembly was called a "Bolometer Flux Meter."

The disadvantage of both types of temperature elements is slow response to flux changes.

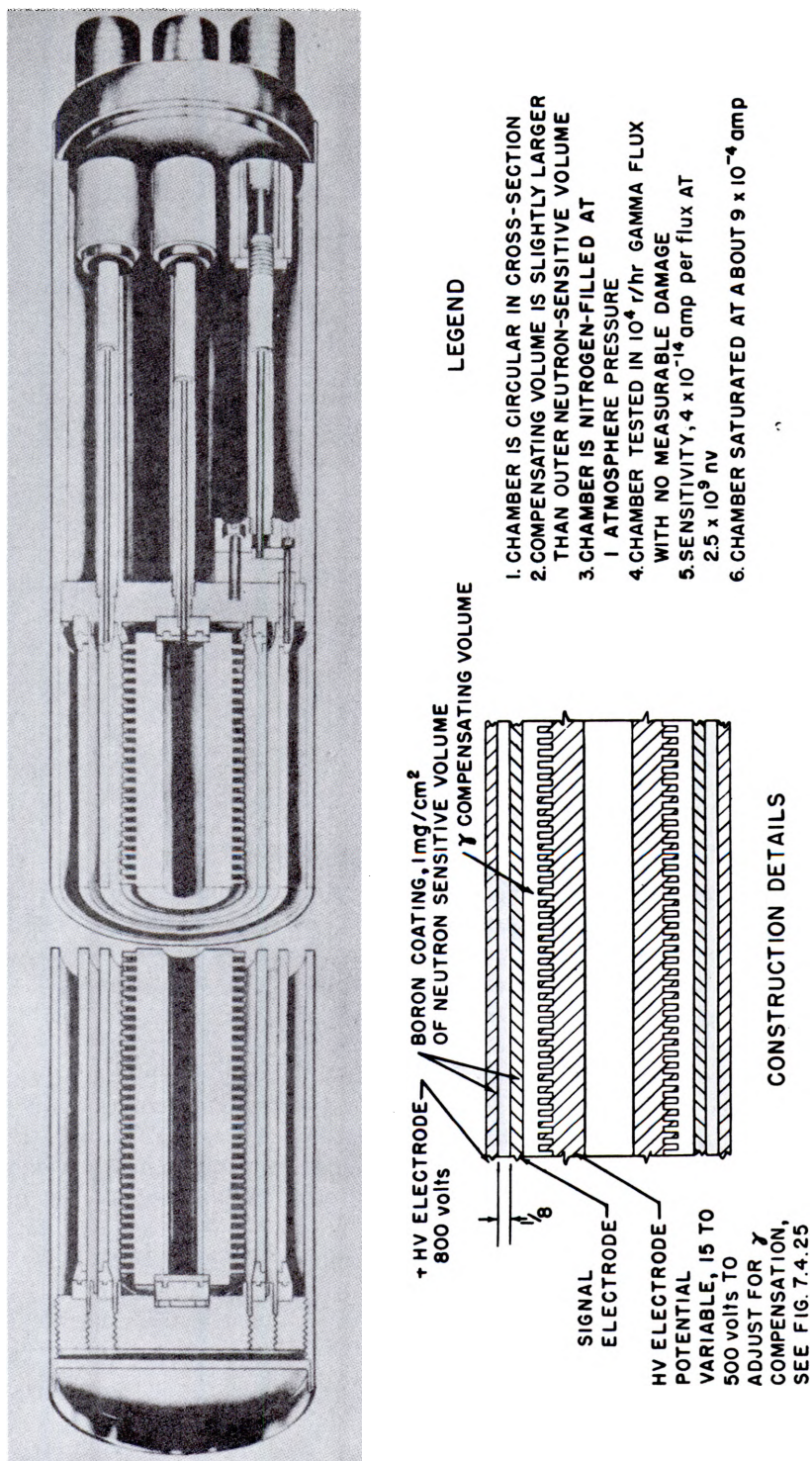
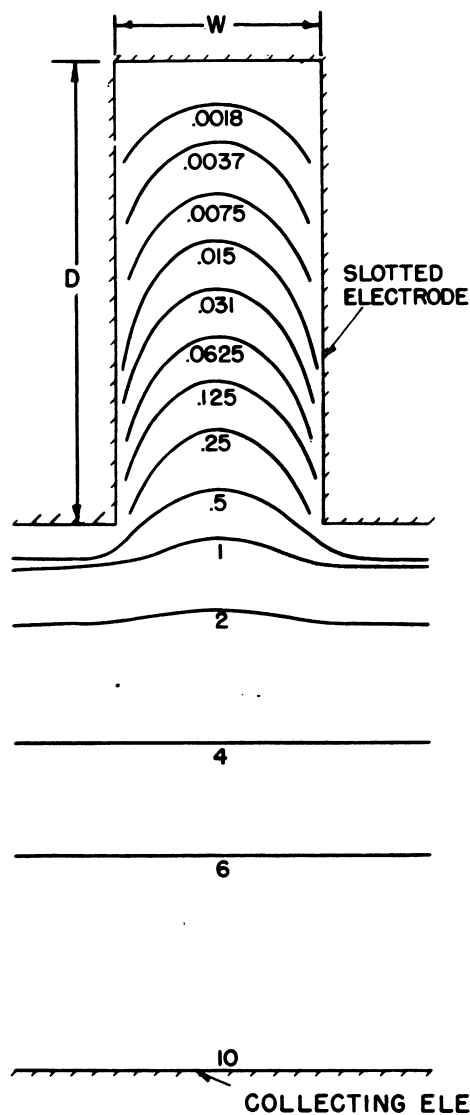


Fig. 7.4.21 — Compensated Current Ion Chamber. Redrawn from R. R. Leonard, WAPD-RM-68, Fig. 68-15.



LEGEND

1. THE NON UNIFORM FIELD PRODUCES A SATURATION CURVE FOR THE γ COMPENSATING VOLUME WHICH RISES STEEPLY THEN GRADUALLY AS THE VOLTAGE APPLIED IS CHANGED FROM 15 TO 500 VOLTS.

2. OPTIMUM $\frac{D}{W} = 2$

Fig. 7.4.22—Compensating Electrode Field for Chamber of Fig. 7.4.21. Submitted by Argonne National Laboratory from unpublished WAPD data.

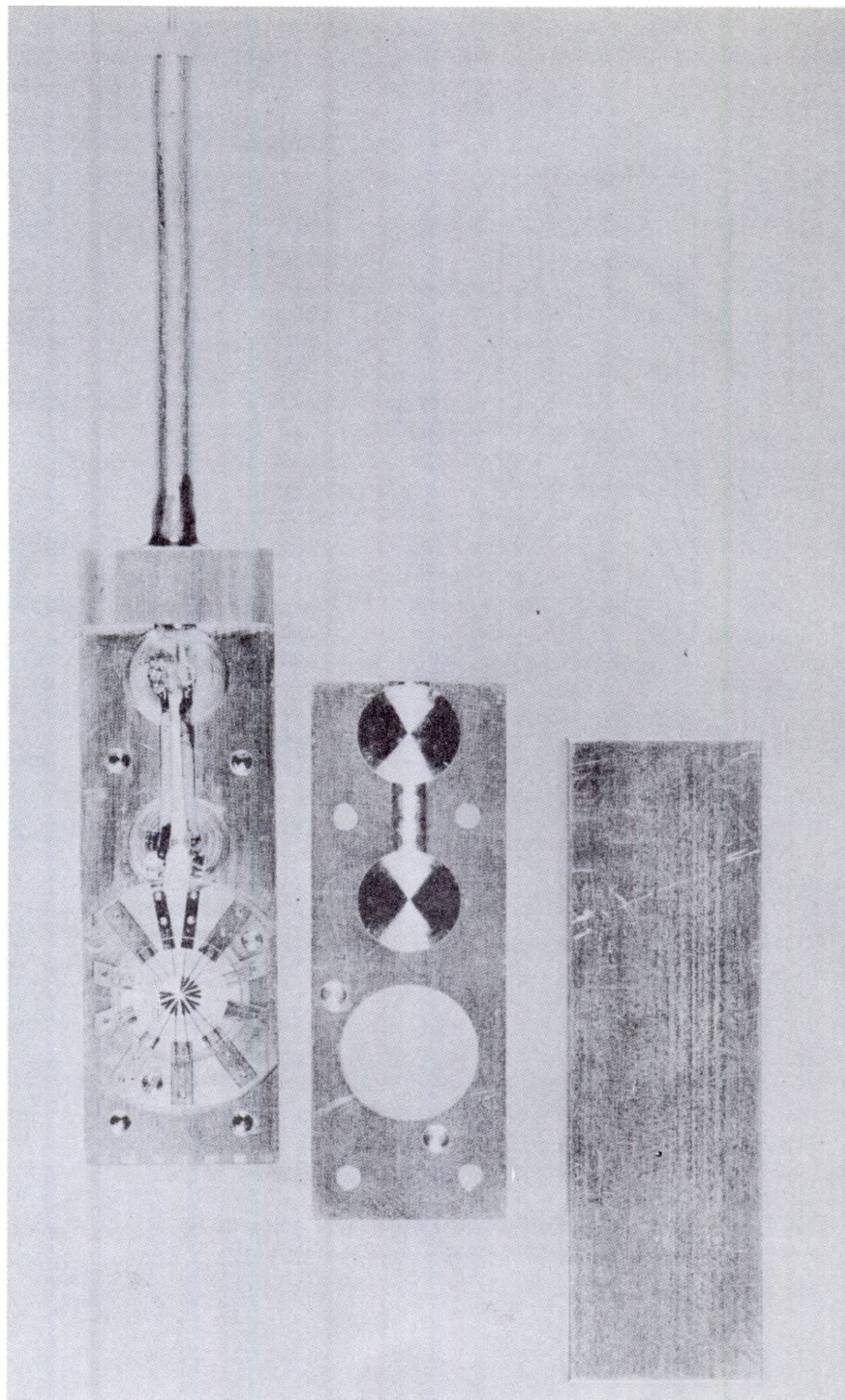


Fig. 7.4.23—Neutron Thermopile Unassembled. Submitted by Argonne National Laboratory, Sept. 1952.

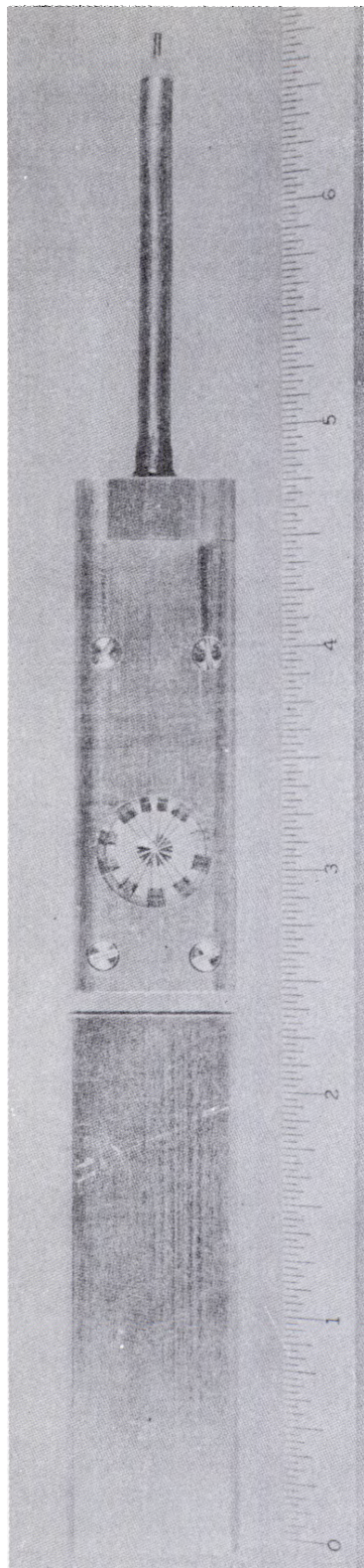


Fig. 7.4.24—Neutron Thermopile Assembly. Submitted by Argonne National Laboratory, Sept. 1952.

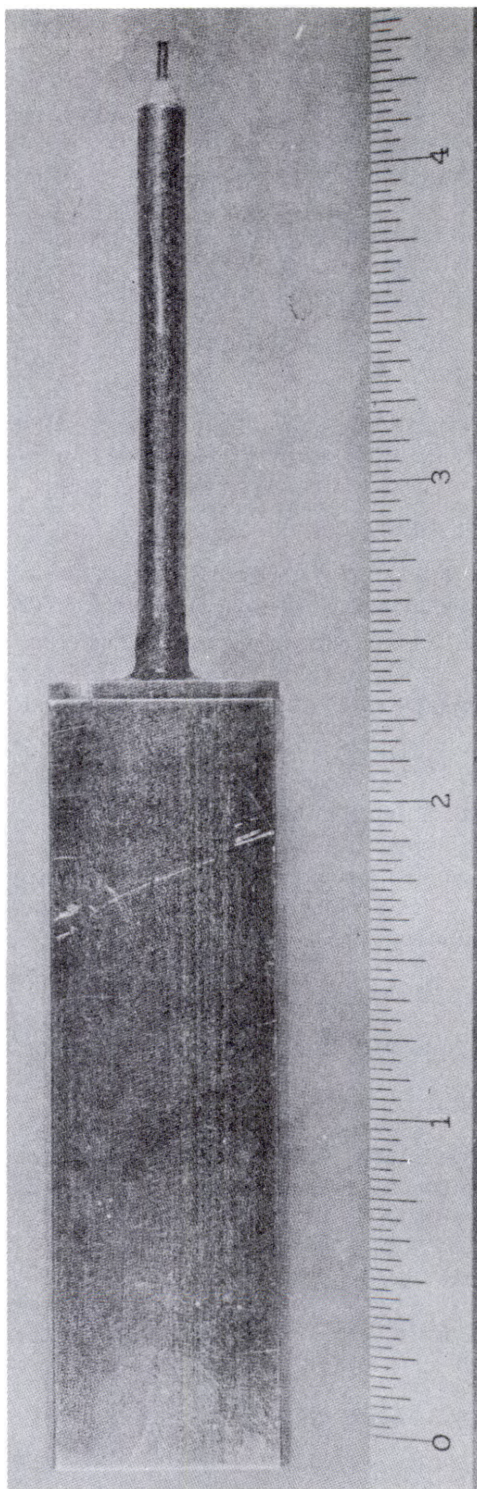


Fig. 7.4.25—Neutron Thermopile, Watertight Assembly. Submitted by Argonne National Laboratory, Sept. 1952.

SCINTILLATION COUNTERS

Solid-state counters have relatively high sensitivity and are therefore useful for low-power-reactor measurements. Radiation absorbed in the scintillating material gives off light which will produce free electrons in a photomultiplier where the signal is amplified through the medium of secondary electron multiplication. This overcomes the effect of noise in conventional thermionic amplifiers. The availability of a scintillator having the correct nuclear and physical properties determines the usefulness of this class of counters.

Table 7.4.3 lists the useful scintillators and some of their properties. Figure 7.4.26 shows the construction of a typical scintillation counter. The following are brief notes on the usefulness of the scintillators.

SODIUM IODIDE

This scintillator, with its light output and high atomic number, is most useful for gamma counting. A $1\frac{1}{2}$ -in. thickness is 40-percent efficient for gamma rays at 4.5 mev.

LITHIUM IODIDE

This scintillator is useful for neutron detection and neutron-energy discrimination. A 1-cm thickness is 65-percent efficient for thermal-energy neutrons, and the efficiency decreases as the neutron energy increases in a one/v relationship. Pulse size increases as $4.78 + E_n$ where E_n is the neutron energy in mev. The neutron energies must differ by 1 mev for good discrimination. The scintillator must be protected against moisture.

ZINC SULFIDE

This scintillator is useful as an α detector. It must be covered with a light-tight barrier of aluminum. A 20-micron grain size powder of ZnS mixed with lucite molding powder and molded into a pellet is a good detector of higher than 1-mev neutrons with an efficiency of 0.2 percent. Small particle size makes this a detector which will discriminate against gamma rays.

CALCIUM TUNGSTATE

This scintillator is a good gamma-detector. It resists attack by corrosive solutions.

ANTHRACENE

This scintillator has a high, light output and is used chiefly for beta-ray detection. Hydrogen content makes this a good fast-neutron detector, but it does not discriminate against gammas.

STILBENE

This scintillator is sometimes used in place of anthracene, its advantage being a shorter decay time.

PHOTOMULTIPLIERS

The most common is RCA type 5819, end-window construction, $1\frac{3}{4}$ -in. circular cathode. Spectral response is a peak at 4600\AA . It produces about 1 electron for every 10 photons. The gain is about 10^6 at 100 volts per stage. For fast coincidence work, the maximum peak current is about 60×10^{-3} amp. Collection efficiency is 70 percent with 200 volts between

Table 7.4.3—Scintillator Properties

Scintillator	Efficiency,* p.e./kev	Particle used	Particle energy	Decay time, μ sec	Formula	Density, gm/cm ³	Melting point, °C	Highest Z	Refractive index	Misc.
Sodium iodide	3.0	β	1 kev--00	0.25	NaI(Tl)	3.7	651	53	1.7	Hygroscopic
Lithium iodide	0.3	β	670 kev	.7	LiI(Sn)	4.1	446	53		Extremely
	.27	α	4.7 mev	.7						hygroscopic
Zinc sulfide	6.0	α	5 mev	10	ZnS(Ag)	4.1	1850 (150 atm)	30	2.4	Available only in powder form
Calcium tungstate	0.3	β	670 kev	6	CaWO ₄	6.1	1525	74	1.9	Excellent chemical stability
Anthracene	1.0	β	100 kev--00	0.03	C ₁₄ H ₁₀	1.25	216	6		
	0.1	α	5 mev							
	.25	H ⁺	1 mev							
Stilbene	.5	β	1 mev	.008	C ₁₄ H ₁₂	0.97	124	6		Extremely brittle
Xylene + 5 gm/l terphenyl	.3	β	1 mev	.002	C ₈ H ₁₀	.87	-53.6	6	1.50	Very sensitive to impurities
Polystyrene + 1.5% tetraphenyl butadiene	.3	β	1 mev	.008	(C ₈ H ₆) _M	1.05	Softens 75	6	1.58	Easily machinable

*The number of photoelectrons produced in a type 5819 photomultiplier of 40 micro-amp per lumen-sensitivity per kilovolt expended by the particle in the crystal

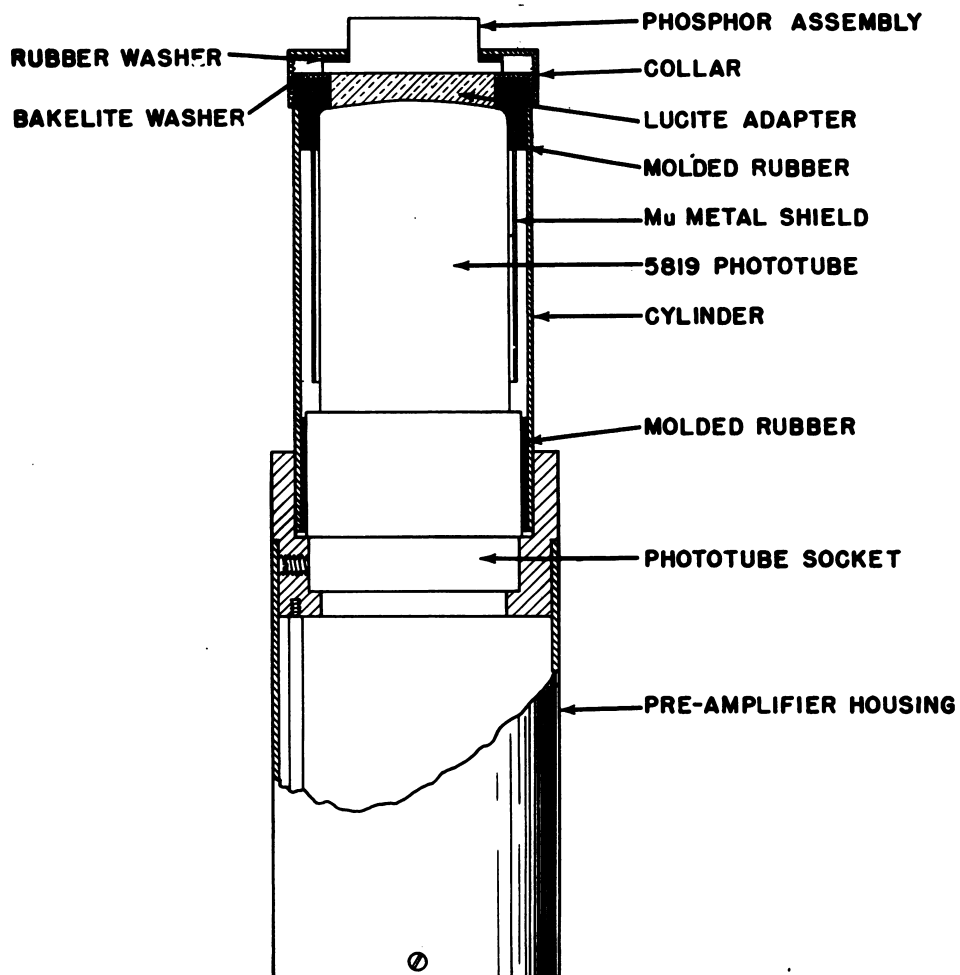


Fig. 7.4.26—Scintillation Counter Assembly. Submitted by Argonne National Laboratory, Sept. 1952.

cathode and first dynode. For a dark current counting rate of 1 count/min or less, a discriminator level corresponding to 50 cathode electrons is used. An assembly of a typical counter is shown in Fig. 7.4.26.

SCINTILLATION-COUNTER DESIGN

Scintillation-counter design is a rapidly developing field, and further information may be obtained from references (22) through (37).

INSTRUMENT INSTALLATION

The following notes on good practice for reactor instrument installation are to be used as a guide for selection and location of the sensory element and measuring instrument.

LOCATION AND RANGE

Ion chambers used for reactor control should be placed in a flux of 5×10^{10} nv or (preferably) less. The response and characteristics of counters is usually affected by 10^6 nv or a gamma of 10^2 r/hr. The counter should be protected with cadmium or removed if these radiation values will be encountered at its location.

Figure 7.4.27 summarizes the normal useful range of coverage of sensing elements for nuclear-reactor control instrumentation.

CABLES AND CHAMBER MOUNTINGS

The sensory element (especially an ion chamber) should be securely mounted and vibration-free. Ion chambers tend to be microphonic. This should be considered if fast-response circuits are to be attached to the chamber. If a slow-response instrument like a galvanometer is used with the chamber, this effect is relatively unimportant. If possible, the chamber position should be readily adjustable, as with a nut and a lead screw drive, for range adjustment and power calibration.

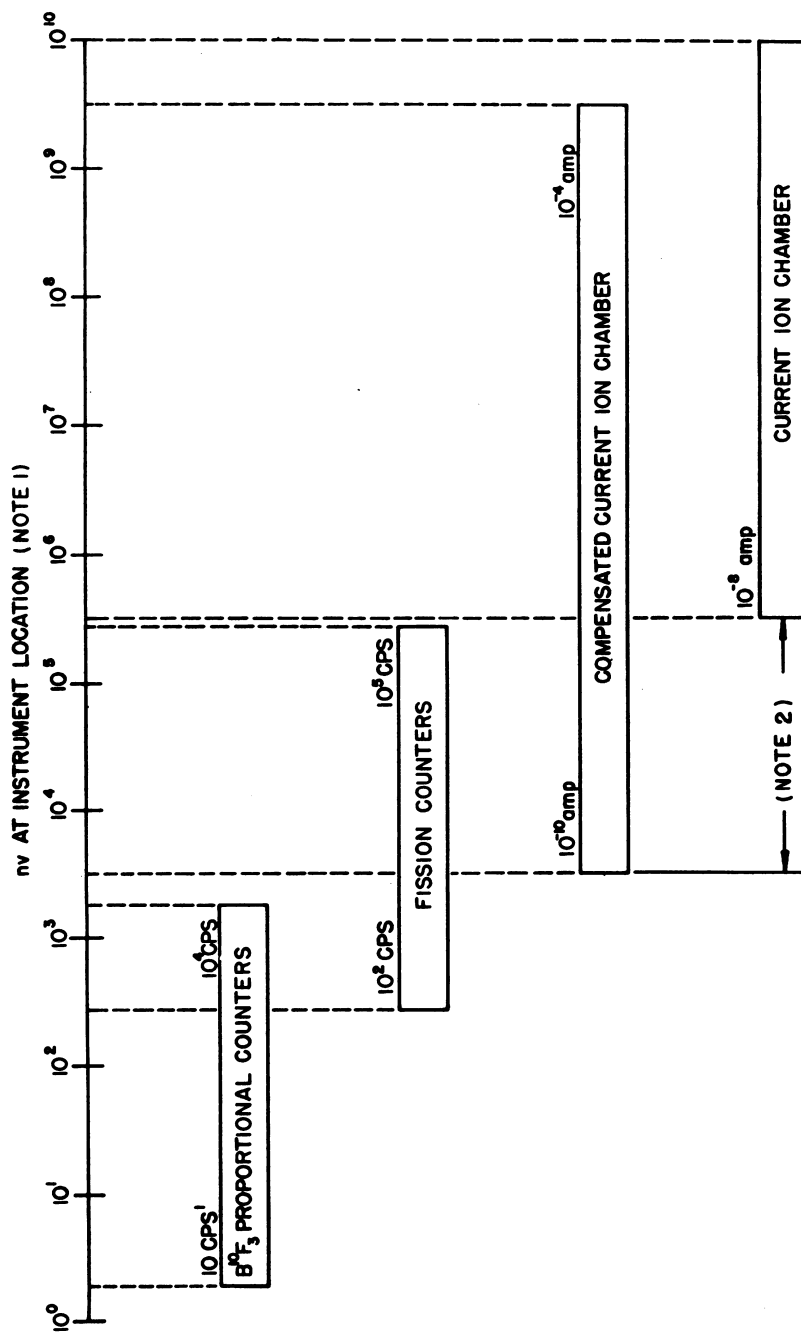
The leads which run between high-impedance devices, such as the sensory element and measuring circuit, should preferably be of anti-static and anti-microphonic construction. Cables that provide for continuous electrical conduction between both surfaces of the dielectric and the metallic members³⁸ are available for this purpose. The leads should be mechanically protected.

Ion chambers are constructed with a protective shield which is to be grounded. For small current measurements, this shield should be insulated from the reactor structure and connected to the cable shield which connects to the amplifier chassis. This system should be connected at only one point to a building ground to eliminate ground-current pickup.

The instruments selected for indicating control readings should be panel-mounted so that maintenance can be performed on one indicator without obstructing the operator's view of the other instruments.

CIRCUIT CONSIDERATIONS

To all chambers and counters, a range of voltage can be applied over which very little change in current or counting rate, as the case may be, will occur. The range of voltage is called the "plateau" region. This range is determined experimentally, and a voltage value in this range is selected as the "operating voltage." This plateau makes an ion chamber appear electrically as a constant-current source for circuit considerations. The dynamic resistance ($\Delta E/\Delta I$) along the plateau usually ranges from 10^8 ohms at 100×10^{-6} amp to 2×10^9 ohms at 10^6 amp. It is highest at the upper plateau voltages.



NOTES

1. nv AT INSTRUMENT LOCATION IS NORMALLY 10^{-4} X AVERAGE REACTOR nv
2. USEFUL nv RANGE EXTENSION OBTAINED BY USING A COMPENSATED CHAMBER IF HIGH GAMMA RADIATION IS ENCOUNTERED.

Fig. 7.4.27 — Range of Nuclear-reactor Sensing Elements. Submitted by Argonne National Laboratory, Sept. 1952.

Chamber capacity is normally small compared to that of the leads between the chamber and measuring instrument. For fast chamber response, locate preamplifiers as close to the chamber as practical.

Ion collection time may effectively increase the time constant of the chamber and its associated circuits. This effect can be eliminated by using electrode voltages which are near the upper range of the plateau region. This collection time is affected by the type of gas used to fill the chamber.^{39,40}

For very low *nv* measurement, proportional counters are used, and associated circuits are designed to discard pulses of low magnitude resulting from gamma radiation. In principle, this makes the assembly sensitive only to neutrons because pulses from single gammas are low valued. The neutron sensitivity in counts per second per *nv* is reduced when counter assemblies are used in a gamma field near the limit value of 10^2 r/hr. Fission counters have a very high current pulse owing to fissions and are useful for discrimination against gamma up to 10^5 r/hr.

INSTRUMENT CHANNELS

GAS-FILLED COUNTER CHANNELS

The type of indicating and recording instrument used with a radiation counter is dependent upon the nature of the counting problem involved. Figure 7.4.28 illustrates some of the possible arrangements of electronic equipment used to indicate and record the output signal from a radiation counter. The figure shows various counting "channels" which are formed by combining elements represented by blocks. The following paragraphs discuss each element or block in the order in which it appears, beginning with the simplest channel shown at the top of Fig. 7.4.28.

AMPLIFIERS

The output signal of a radiation counter tube appears in the form of voltage pulses which are variable in magnitude and random with respect to time. The pulses are not of sufficient magnitude to operate indicating and recording instruments directly, and amplification is necessary. The characteristics of the amplifier are varied to suit the particular measurement problem involved. Pulse amplifiers, as applied to radiation counting problems, are treated along with typical practical circuits in references (41), pp 124-170, and in reference (42), pp 185-192. Figure 7.4.29 shows typical pre-amplifiers and Fig. 7.4.30, a typical linear amplifier, both of which are used with counters for a reactor instrumentation system. The linear amplifier is designed to amplify small pulses from an ionization chamber, proportional counter, or similar device to a level where the pulses can be seen on an oscilloscope or counted with a scaler. The amplifier is provided with a bandwidth switch to permit fast counting of large signals or somewhat slower counting of small signals. Up to 160,000 counts/sec can be amplified with medium bandwidth operation. One-hundred-volt pulses are obtained at the amplifier output. Further information is obtained in reference (43).

COUNTER CIRCUITS

Pulse heights within a certain range are identified with a particular type of radiation. The counter channel is made selective by discriminating against pulse heights not associated with a particular radiation. The pulse amplifier is modified to provide discrimination either by allowing it to saturate or by adding a discriminator circuit to pass pulses within a certain range of magnitude. Amplitude discriminators are discussed in reference (41), pp 202-206.

A scaler is used to count and indicate the number of pulses. Mechanical registers are

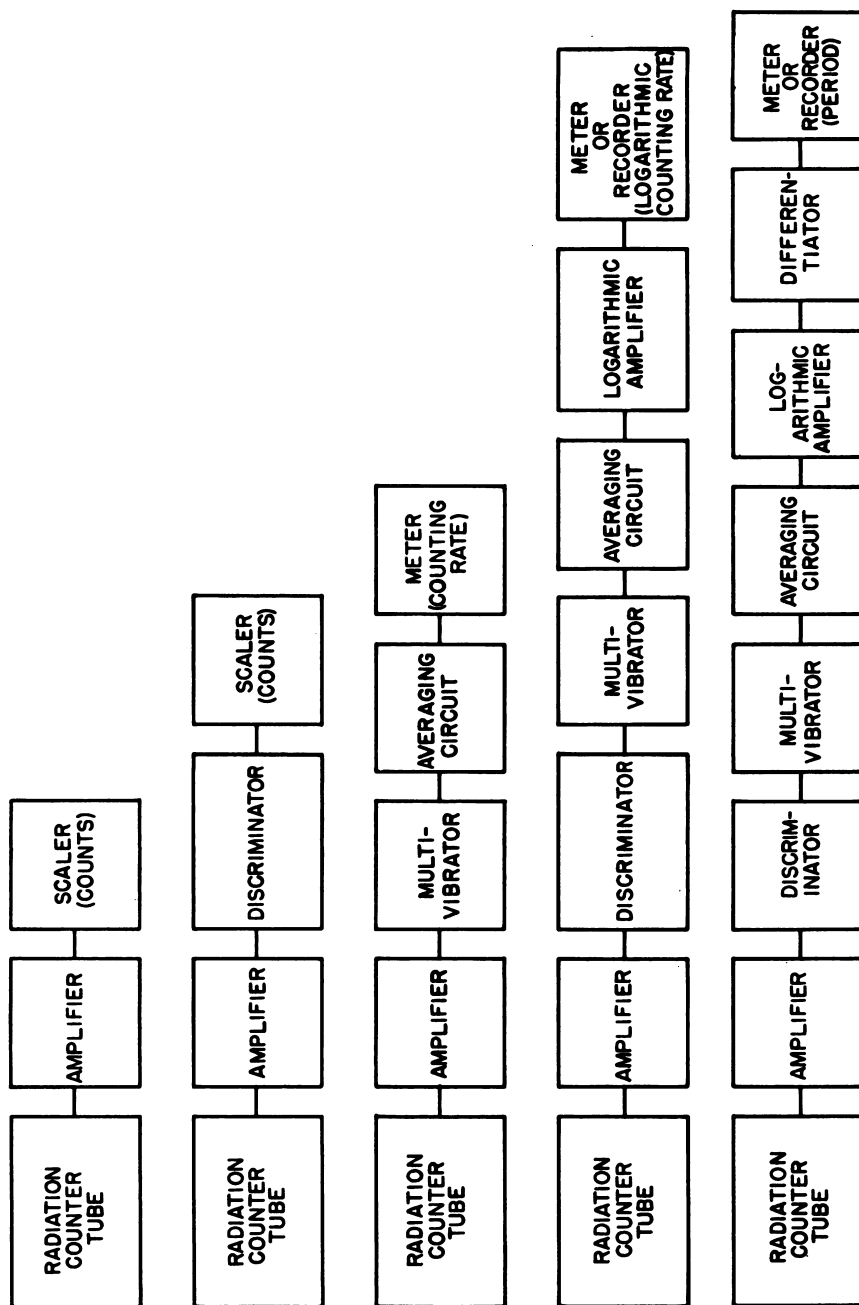
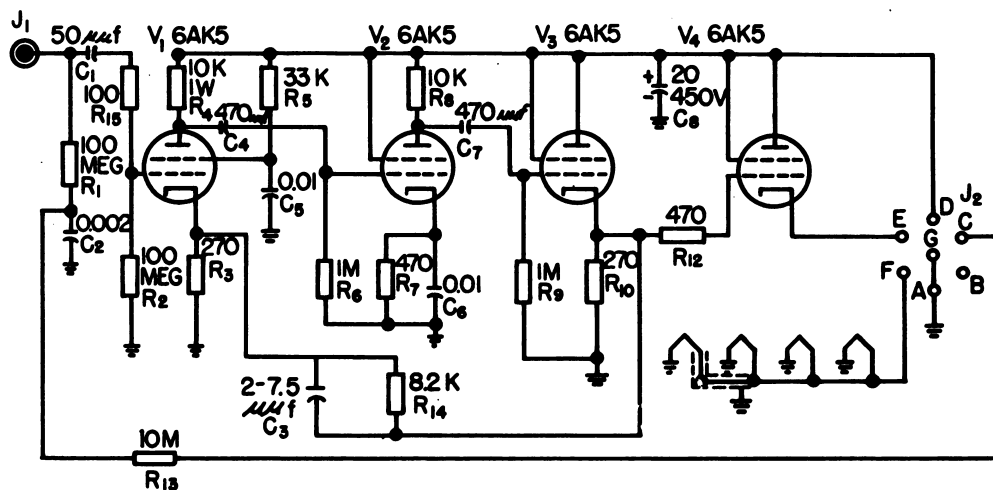
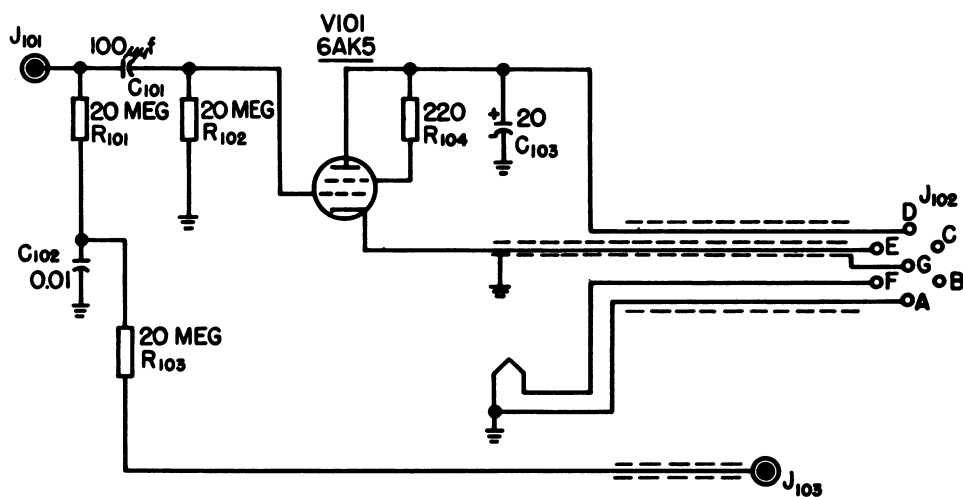


Fig. 7.4.28—Counting Channels. Submitted by Argonne National Laboratory, Oct. 1952.



AI A PREAMPLIFIER
FIG. A



AI B PREAMPLIFIER
FIG. B

Fig. 7.4.29 — Pulse Preamplifier. Redrawn from W. H. Jordan and P. R. Bell, Instructions For Use of A-1 Amplifier and Preamplifier, Mon.-P 323, Jan. 1949.

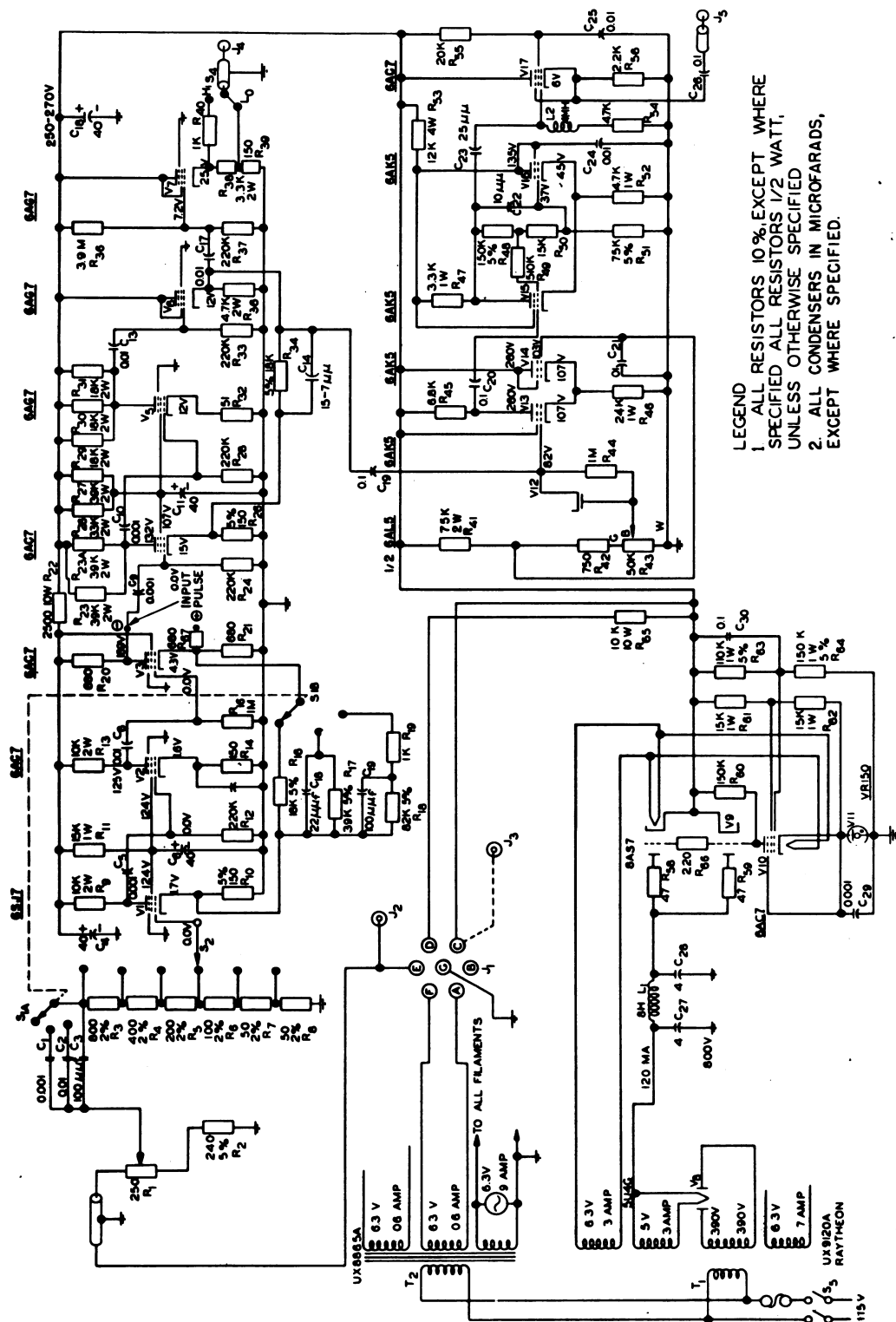


Fig. 7.4.30—Linear Amplifier. Redrawn from W. H. Jordan and P. R. Bell, Instructions for Use of A-1 Amplifier and Preamplifier, Mon.-P 323, Jan. 1949

slow and are preceded by electronic scaling circuits. Some scaler circuits and a description of operation are presented in reference (41), pp 206-212.

COUNTING-RATE CIRCUITS

The desired measurement is the number of pulses occurring in a unit time. This is obtained either by counting the total number of pulses registered in a measured time interval or by indicating a counting rate directly. In a counting-rate meter, the pulses from the amplifier are used to trigger a multivibrator, the output of which consists of current pulses of uniform duration and magnitude but still random with respect to time and initiated by the trigger pulses. An R-C circuit is so arranged that each multivibrator pulse causes a definite amount of charge to be placed on a capacitor in a time which is short compared with the average spacing of pulses. The charge on the capacitor leaks off through a high resistor, making the average potential across the capacitor proportional to the counting rate. A basic circuit of a counting-rate meter is presented in reference (41), p 251. Commercial units registering 100,000 counts/sec or more are available either as scalars or counting-rate meters.

LOG COUNTING RATE CIRCUITS

Pulse counters are used for reactor control to indicate three to four decades of operation near source strength n_v , especially when discriminating against high gamma-radiation. By including a logarithmic amplifier in the counting channel, a single meter will show several decades of n_v change. A typical logarithmic counting-rate meter-circuit is illustrated in Fig. 7.4.31. The counting rate is obtained by allowing the charge of the counting-rate capacitor to leak off through a diode producing an average current through the diode proportional to the number of pulses per second.⁴⁴ The voltage across the diode is proportional to the logarithm of the current through it and is measured by a means of vacuum tube voltmeter. Diode characteristics are presented in reference (44), p 41. A more complete description of Fig. 7.4.31 is contained in reference (44), p 62.

PERIOD CIRCUITS

Measurement of the reactor period is frequently desirable (for a definition see "Reactor Time Dependent Behavior"). A resistor-capacitor differentiating circuit placed after a logarithmic amplifier will provide an output signal proportional to the inverse period. Period circuit time response is an important control consideration. A discussion is contained in reference (45).

GAS-FILLED IONIZATION CURRENT CHAMBER CHANNELS

BASIC CIRCUITS

The equipment used with an ionization current chamber is designed to measure a continuous current instead of counting discrete pulses as in counters. Figure 7.4.32 illustrates some of the possible circuit arrangements or "channels" that are used with current ionization chambers.

Beginning at the top of Fig. 7.4.32, the simplest circuit arrangement is a chamber operating a sensitive relay. This channel is used in protective-circuit operation. At reactor power levels, a sensitive galvanometer is used to give an indication of chamber current. The addition of a shunt in this channel allows the galvanometer to be operated over a greater range of current. A galvanometer has about a 3-sec period, which is slow compared to the response obtainable with an electronic amplifier circuit. A typical feedback

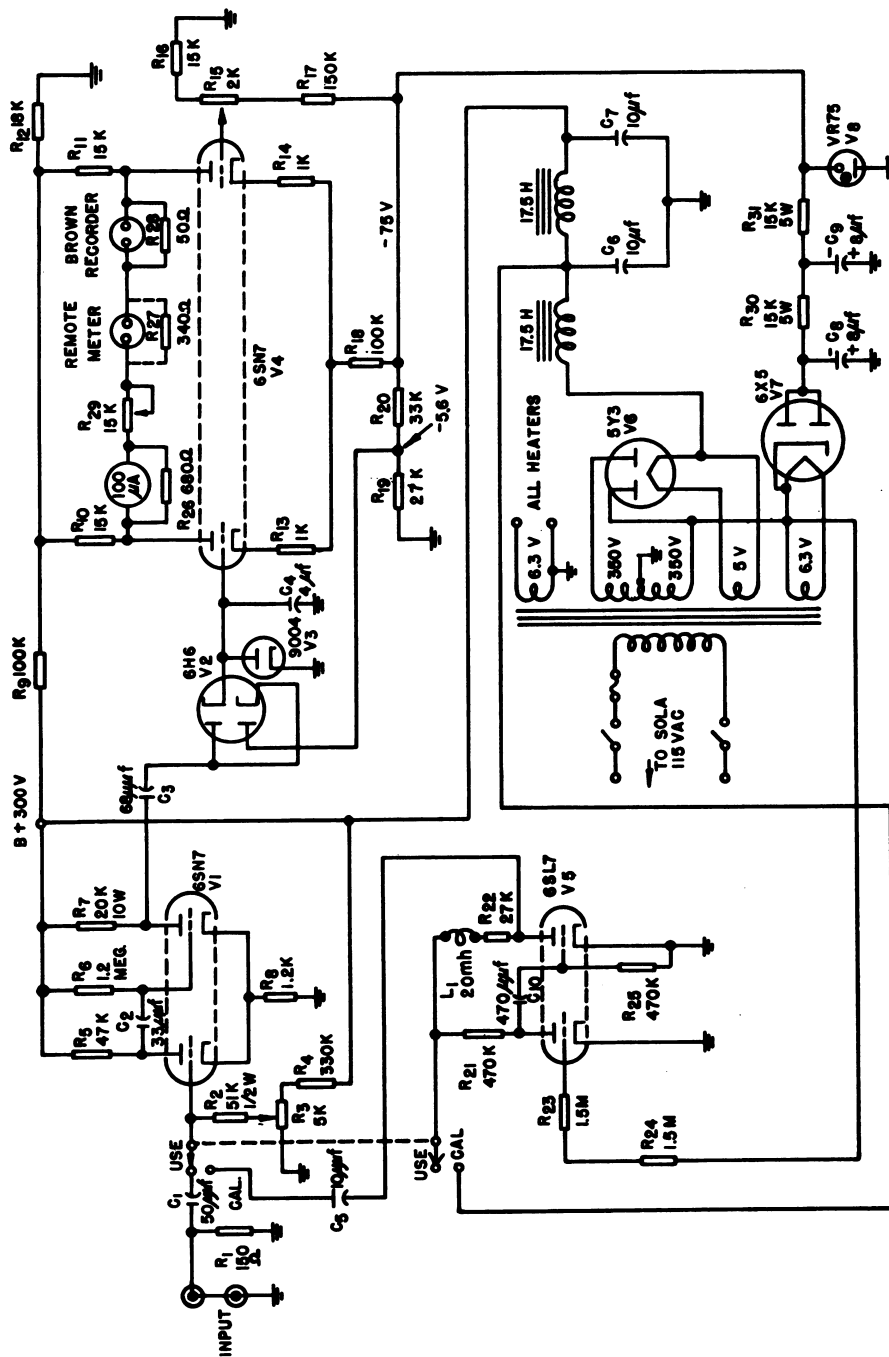


Fig. 7.4.31—Logarithmic Counting-rate Meter. Redrawn from W. H. Jordan, G. Kelley, and H. B. Frey, Logarithmic Counting-rate Meter, Physics Division Quarterly Report, CNL-35, Mar. 1948.

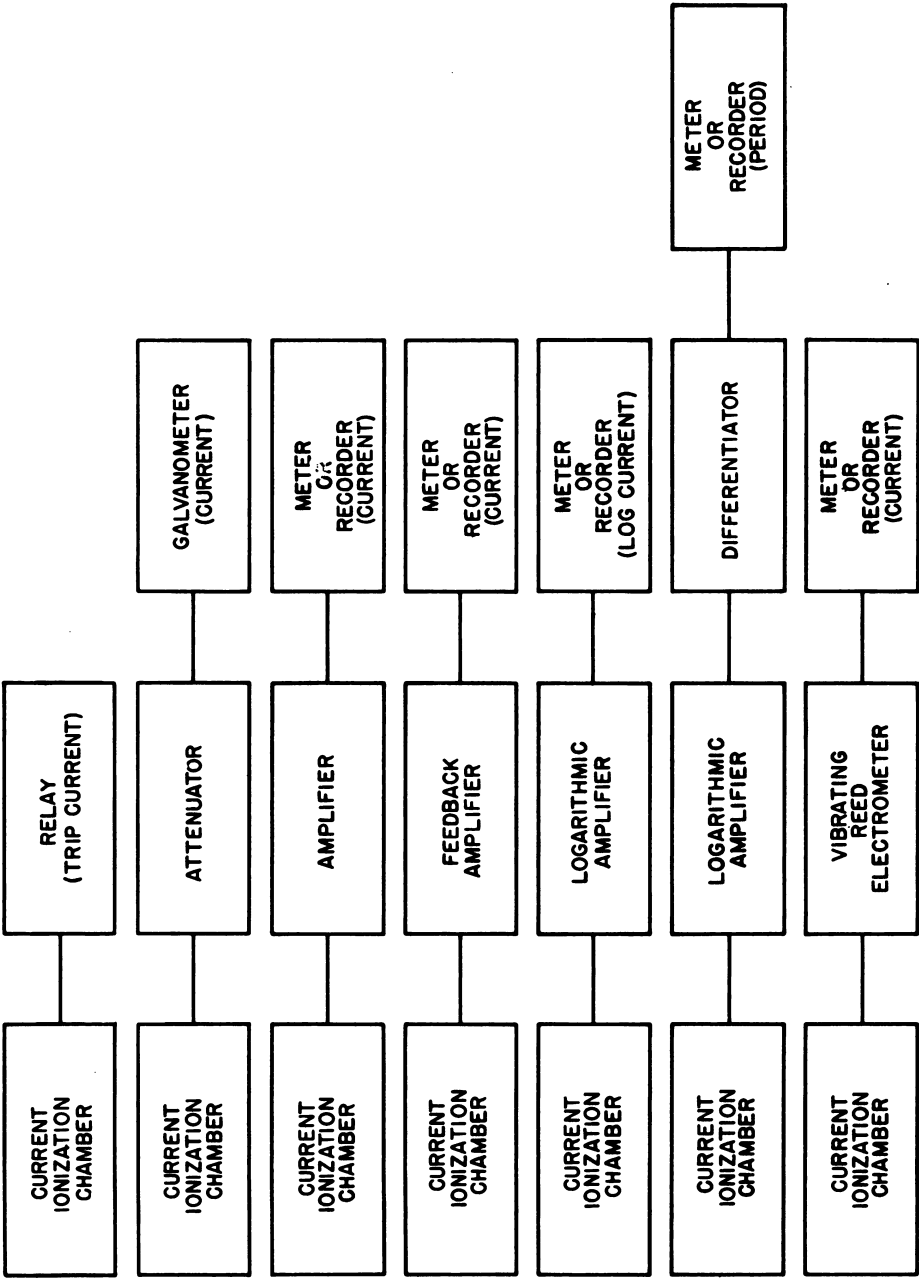


Fig. 7.4.32 — Current Channels. Submitted by Argonne National Laboratory, Oct. 1952.

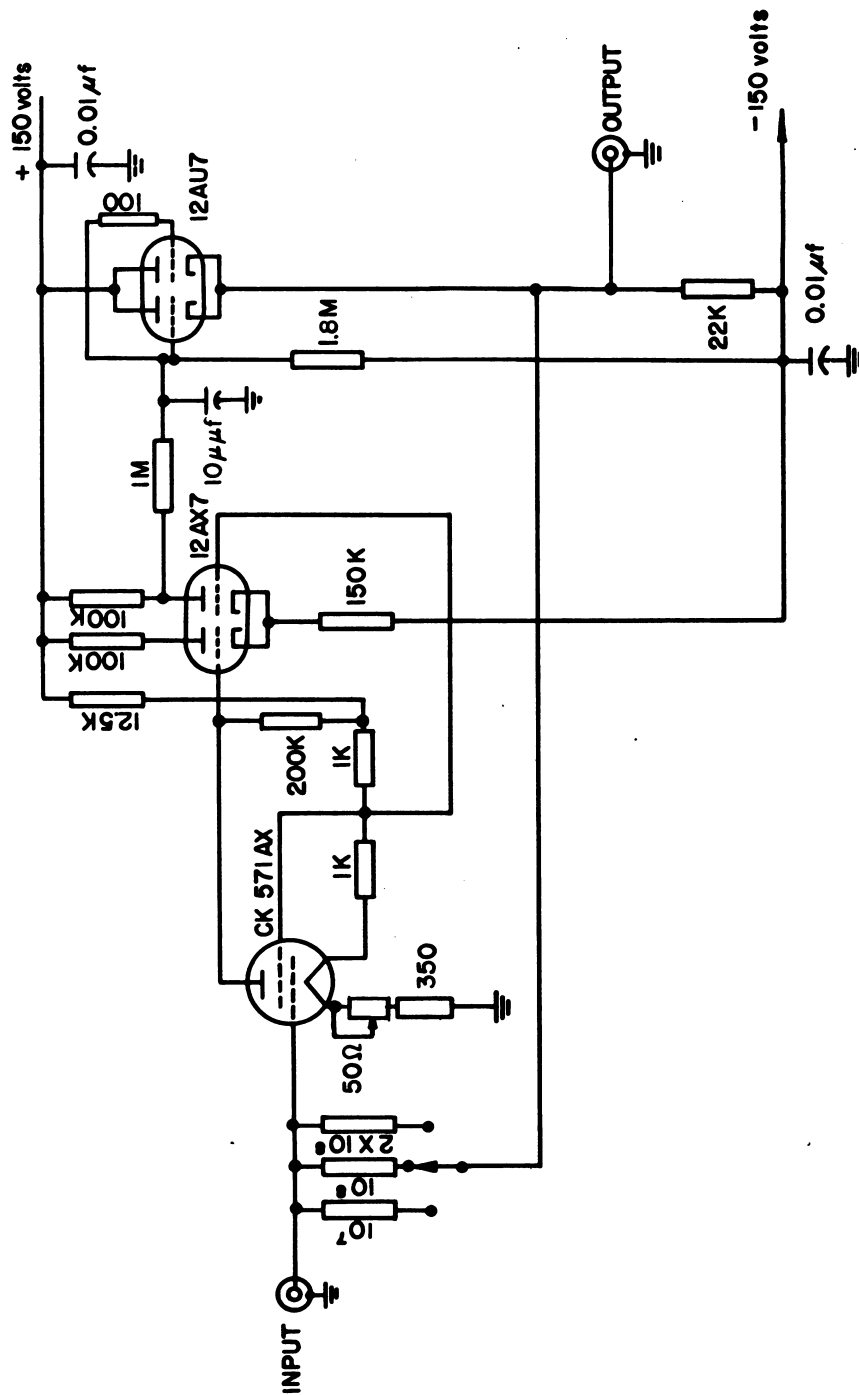


Fig. 7.4.33 — Feedback Amplifier. Submitted by Argonne National Laboratory, Oct. 1952.

amplifier circuit is illustrated in Fig. 7.4.33. For an amplifier of gain A and negative feedback, the amplifier input time constant is reduced by a factor of $1 + A$. For example, if the chamber plus cable capacitance is as low as $100 \mu\text{f}$, the input time constant for an amplifier with a 10^9 -ohm input resistor would be 0.1 sec, but by using a feedback amplifier with a gain of 100, the time constant is reduced to 0.00099 sec. Although the amplifier gain may be 100, the over-all circuit gain from amplifier input to amplifier output is very nearly unity. Another method of feedback can be employed to obtain capacitance neutralization and thus reduce the time constant of the circuit. The chamber cannot be grounded for this method, and it is necessary to provide an underground power supply for the chamber. For this reason, this method presents somewhat more complex problems than those encountered with the circuit of Fig. 7.4.32 when considered for reactor instrument applications. A general discussion of feedback amplifiers is contained in reference (41), p 187.

The measurement of direct currents of 10^{-11} amp or less by using circuits employing ordinary vacuum tubes is not practicable. A number of special electrometer-tube manufacturing techniques have been developed to circumvent this difficulty. With special manufacture, the grid current of an electrometer tube can be reduced to 10^{-17} amp, which permits detection of currents of the order of 60 electrons/sec. A discussion of electrometer tubes is contained in reference (41), pp 180-190.

A vibrating-reed electrometer is used to detect small ionization chamber current. This type of instrument assembly is commercially available, a principal advantage being the use of AC amplifiers which are more stable than the DC type.

Operation of the chamber with an alternating voltage applied to the plates is practicable.⁴⁶ Development of a method similar to the referenced method⁴⁶ may circumvent many design problems now encountered in the use of DC amplifiers in the nuclear-reactor control circuits.

LOGARITHMIC AMPLIFIER

Several decades of reactor power-level readings can be compressed into the same meter by using a logarithmic diode in the amplifier input circuit. A discussion of diode characteristics is covered under "Log Counting Rate Circuits." Figure 7.4.34 shows a logarithmic amplifier for use with a current ion chamber.

PERIOD AMPLIFIER

Reactor period (discussed under "Reactor Time Dependent Behavior") is obtained by differentiating the output of the logarithmic amplifier with a resistance capacitor network. A typical period meter circuit is shown in Fig. 7.4.35.

RECORDERS

The output signal of the various counter and current channels shown in Figs. 7.4.27 and 7.4.31 is available as a voltage proportional to the quantity being measured. A variety of commercial instruments which have the proper sensitivity, input impedance, and time response for use with nuclear reactor instrument assemblies can be obtained to record this signal.

POWER SUPPLY

An essential auxiliary device of a radiation-detecting chamber is a source of regulated voltage of proper magnitude. Chamber voltage may be supplied by the use of batteries, vibrator supplies, conventional 60-cycle power supplies, or radio-frequency oscillator supplies. High-voltage fluctuation is avoided by using voltage regulator tubes or a supply of the degenerative type. A discussion of power supplies is contained in reference (41), pp 363-396.

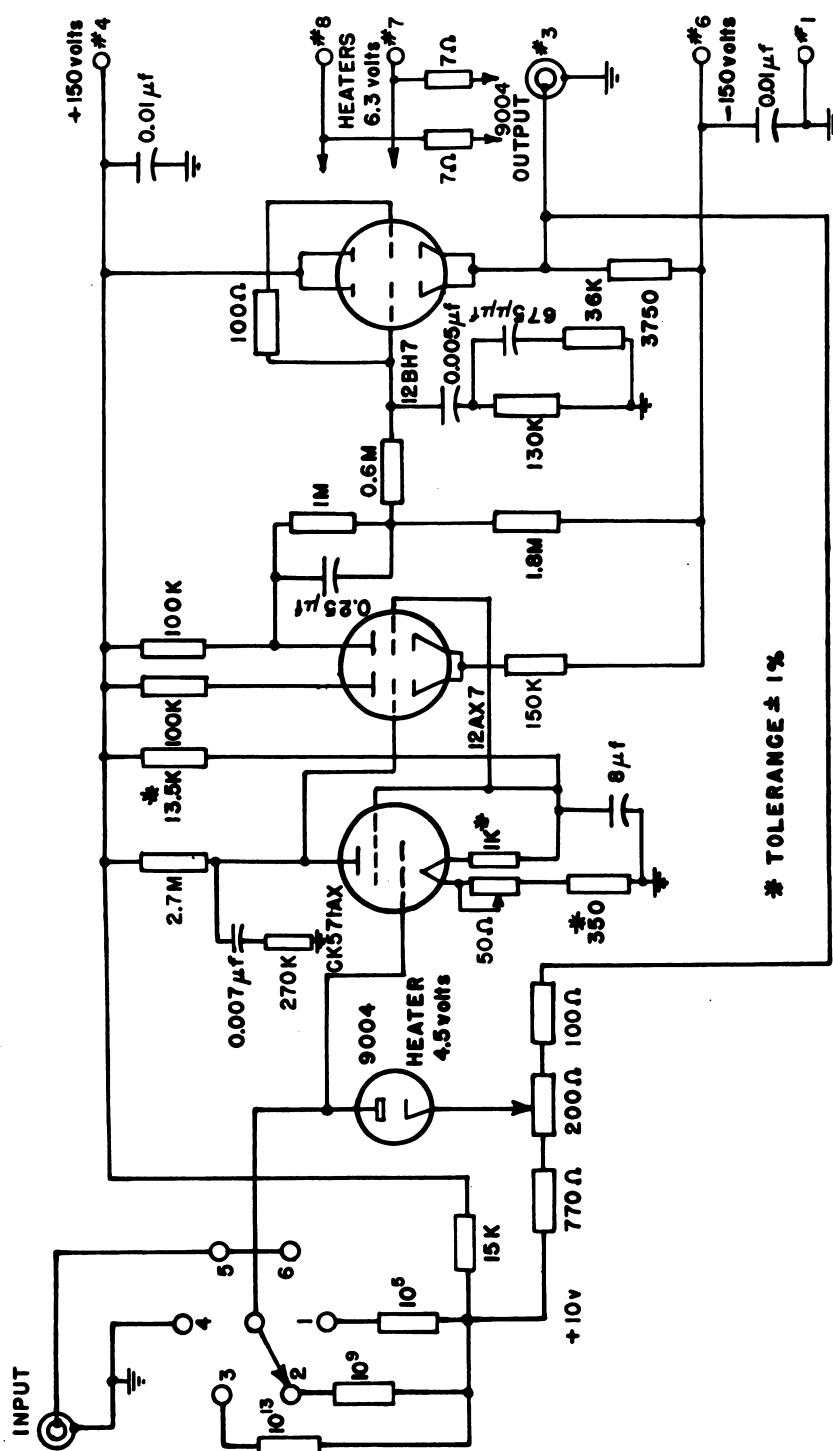


Fig. 7.4.34 — Logarithmic Amplifier Circuit. Submitted by Argonne National Laboratory, Oct. 1952.

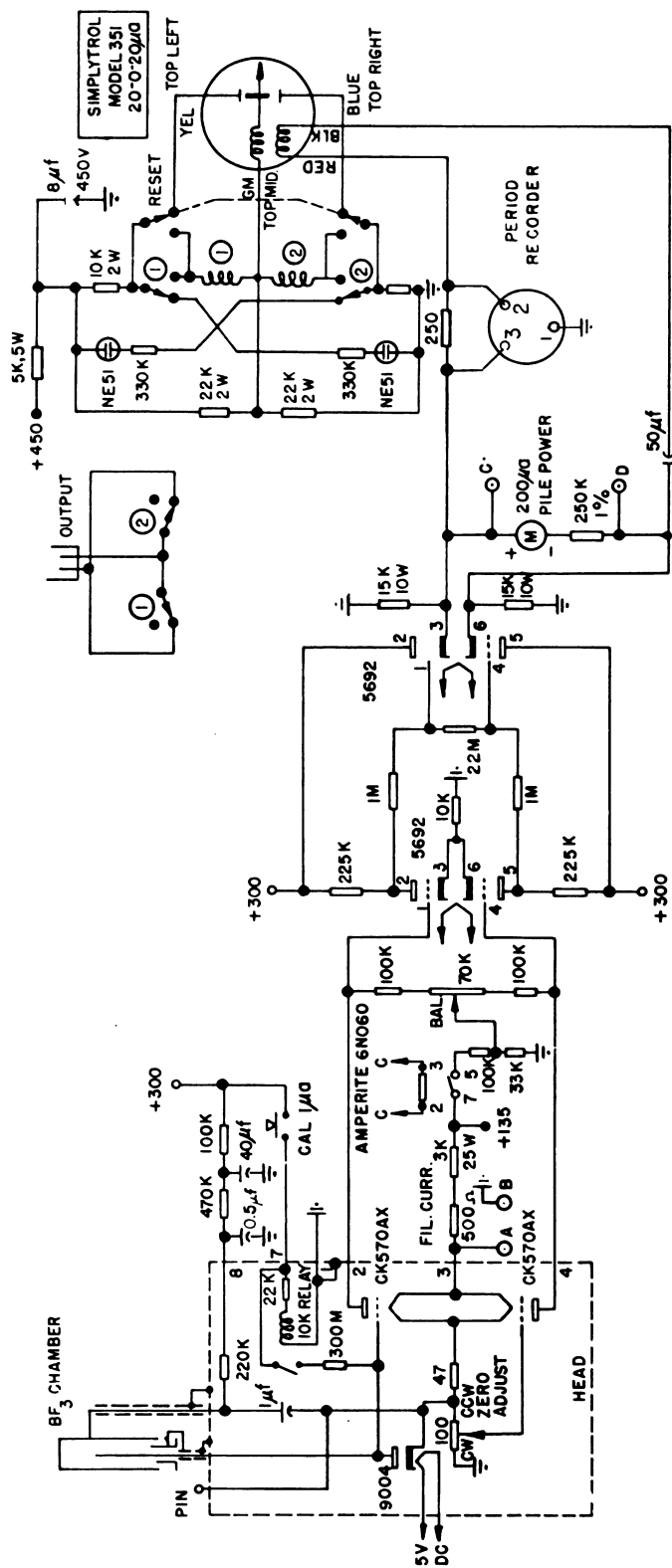


Fig. 7.4.35 — Period Meter Circuit. Submitted by Argonne National Laboratory, Oct. 1952.

LEGEND

FILL. CURR.- ADJUST TO GIVE 6.75 v ACROSS A-B.
BALANCE - WITH ZERO ADJUST CCW AND DIODE SHORTED,
ADJUST TILL PILE POWER METER READS ZERO
ZERO ADJ.- WITH CAL. 1 a BUTTON DEPRESSED, ADJUST TO
GIVE DESIRED READING (ABOUT 3/4 FS.) ON
PILE POWER METER.

REFERENCES

1. J. C. Simons, Jr., WAPD-RM-82, July 5, 1951 (classified).
2. Walter Pagels, WAPD-RM-75, Jan. 1952 (classified).
3. Soodak and Campbell, Elementary Pile Theory, AECD-2201, Aug. 4, 1948.
4. R. G. Dumas, WAPD-RM-62, Aug. 1951 (classified).
5. J. M. Harter, R. E. Boyar, and D. Krucoff, Transfer Function of Argonne CP-2 Reactor, *Nucleonics* 10, N8, Aug. 1952.
6. WAPD-40 (classified).
7. J. H. Buck and C. F. Leyse, ORNL-963 (classified).
8. R. S. Kelley and Roy L. Roberts, M-4428 Engineering Report 41 MIT Servomechanisms Laboratory, Aug. 1948 (classified).
9. D. Krucoff, An Electromagnetic Rod-position Indicator, ANL-4818, June 1952.
10. H. A. Straus, ORNL-2, Dec. 1948 (classified).
11. F. A. Hadden, M-4430 Engineering Report No. 57, Servomechanism Laboratory Mass. Inst. Tech., Feb. 1949 (classified).
12. LeRoy A. McColl, Fundamental Theory of Servomechanisms, D. Van Nostrand Co., Inc., Nov. 1945.
13. Ralph J. Kochenburger, A Frequency Response Method for Analyzing and Synthesizing Contacter Servomechanisms, *AIEE Transactions* 69, 1950.
14. J. A. DeShong, Performance of Servo Motors for Reactor Regulating Rods, ANL-4614, Feb. 1951.
15. Vol. II, Chapt. V, HKF-12, M-4416 (classified).
16. Section B, Chapt. 6 and 7 HW-10475 (classified).
17. ANL-4641, Mar. 1, 1951 to May 31, 1951, p 87 (classified).
18. Bruno B. Rossi and Hans H. Staub, *Ionization Chambers and Counters*, McGraw-Hill Book Company, Inc., 1949, pp 210 through 218.
19. A. C. Lapsley, Saturation Properties of Uranium Fission Chambers, ANL-4806, Mar. 31, 1952.
20. Clark Drouillard Goodman, *The Science and Engineering of Nuclear Power*, Addison-Wesley Press, Inc., Cambridge, Mass., 1947, p 261.
21. G. Barbaras, J. Farr, J. Kuranz, et al, The Design and Construction of Boron Coated Thermopiles for use in Neutron Fields, AECD-2485, Feb. 28, 1949.
22. Robert Hofstadter, Alkali Halide Scintillation Counters, *Phys. Rev.* 74, 1948, p 100.
23. Robert Hofstadter, Detection of Gamma-rays with Thallium-activated Sodium Iodide Crystals, *Phys. Rev.* 75, 1949, p 796.
24. L. Reiffel, C. A. Stone, and F. G. Rest, Protective Containers for NaI (TL), Vol. 22, 1951, p 1026.
25. R. K. Swank and J. S. Moenich, Packaging of NaI (Ti) Crystals for Scintillation Spectrometry, AECU-1905 (VAC-513).
26. R. Hofstadter, J. A. McIntyre, H. Roderick, and H. L. West, Detection of Slow Neutrons, *Phys. Rev.* 82, 1951, p 749.
27. W. Bernstein and A. W. Schardt, Activation of LiI Crystals Phosphors, *Phys. Rev.* 85, 1952, p 919.
28. James Schenck and R. L. Heath, Tin Activation of LiI, *Phys. Rev.* 85, 1952, p 923.
29. Fitz-Hugh Marshall, J. W. Coltman, and A. I. Bennett, Photo-multiplier Radiation Detector, *Rev. Sci. Inst.* 19, 1948, p 744.
30. W. F. Hornyak, A Fast Neutron Detector, BNL-1029.
31. R. H. Gillette, Calcium and Cadmium Tungstate As Scintillation Counter Crystals for Gamma-ray Detection, *Rev. Sci. Inst.* 21, 1950, p 294.
32. R. F. Leininger, On the Preparation of Stilbene Crystals, *Rev. Sci. Inst.* 23, 1952, p 127.
33. R. F. Post, Decay Time and Efficiency of a Liquid Scintillator, *Phys. Rev.* 79, 1950, p 735.
34. Hartmut Kallmann and Milton Furst, Fluorescence of Solutions Bombarded with High-energy Radiation (Energy Transport in Liquids), *Phys. Rev. Part I*, 79, 1950, p 857; *Part II*, 81, 1951, p 853; *Part III*, 85, 1952, p 816.
35. W. L. Buck and R. K. Swank, Plastic Phosphors for Scintillation Counters, *Bull. Amer. Phys. Soc.* 27, May 1, 1952, p 15.
36. George A. Morton, Photo-multipliers for Scintillation Counting, *R. C. A. Rev.* 10, No. 4, 1949, p 526.
37. Walter Heitler, *The Quantum Theory of Radiation*, Oxford University Press.
38. T. A. Perle, Electrical Noise From Instrument Cables Subject to Shock and Vibration, *Jour. Applied Phys.* 23, June 1952, p. 694.
39. Bruno B. Rossi and Hans H. Staub, op. cit., pp 10-19.
40. L. Colli and U. Facchini, Drift Velocity of Electrons in Argon, *Rev. Sci. Inst.* 23, Jan. 1952, p 39.
41. William C. Elmore and Matthew Sands, *Electronics*, McGraw-Hill Book Company, Inc., 1949.
42. Serge A. Kroft, *Electron and Nuclear Counters*, D. Van Nostrand Co., Inc., 1946.
43. W. H. Jordan and P. R. Bell, Instructions for Use of A1 Amplifier and Preamplifier, MonP-323, Jan. 1949.
44. CNL-35, Mar. 1948 (classified).
45. W. W. Ramaze, WAPD-RM-69 (part of WAPD-34) Dec. 1951 (classified).
46. ANL-4683, Sept. 1951, p 86 (classified).

Section 8

REACTOR DESIGNS

Prepared under the direction of
N. E. HUSTON
NORTH AMERICAN AVIATION, INC.

AUTHOR'S PREFACE

During the past decade, reactor designs have grown from the few early reactors to a considerable number of designs of varied component combinations and diverse purposes. Not only are the data for different reactors to be found only in different publications, but in some cases the gathering of information on any one reactor requires a laborious search through many documents. This situation demands an integrated reference in which the basic specification and operating characteristics of reactors can be found. The treatment need not and should not be exhaustive, since a requirement for detailed information can best be satisfied by published reports on the individual reactors, and since the voluminous compilation that would result from a complete survey of the field would be awkward both in presentation and use.

It is in this spirit, then, that the reactor data compilation presented here was made. The preparation was governed by three constraints: brevity, omission of any material of an educational nature, and avoidance of the use of illustrations. The last constraint is unfortunate in that it places an undue burden upon the reader in trying to comprehend textual descriptions of complex apparatus. It is hoped that this condition will be remedied in forthcoming revisions to the Handbook.

In general, the compilation of data in this section covers the Project literature up to February 1953.

CHAPTER 8.1

Introduction

In the following chapters, brief descriptions of a number of reactors are presented. The basic criterion for the inclusion of a reactor was that it should be in operation, under construction, or have reached an advanced stage of design. This criterion was necessarily tempered by additional conditions. For example, it was necessary to omit certain foreign reactors, which either have been or are being built, because detailed information regarding these reactors was lacking. In general, design-study reactors were considered qualified for this category if sufficient information were available to indicate most of the tabulated parameters and characteristics. Finally, reactors in a design-study stage that had unique features (such as the helium-cooled, Daniels Power Pile, or the North American homogeneous, graphite reactor) were favored for inclusion, whereas design-study reactors which were quite similar to existing or designed reactors were usually omitted. A more complete listing of reactor designs is presented in Table 8.1.1., a quick reference reactor chart. The references listed do not necessarily contain the most recent information on the reactors but are rather the most complete single references available—in most cases a feasibility report.

For convenience in presentation of the design compilations, the reactors are separated into two major groups, heterogeneous and homogeneous. The classification of Clementine and the EBR as heterogeneous was rather arbitrary. In these two major groups, the reactors are sub-divided according to moderator, each moderator group comprising one chapter. The description of each reactor consists of a tabular presentation followed by a descriptive text.

In general, the data for each reactor have been taken directly from reports of the responsible organizations. Blank spaces in the tables imply that the omitted information was not available. Some easily calculable items, such as fuel inventory and average power parameters, have been calculated when explicit values were not given. The numerical values for the parameters listed under physics are direct reproductions of the published values without heed to possible variations in the manner in which the data were calculated or measured. These data, for the most part, are to be found in the listed references, although an occasional item was taken from other reports.

The tabulation of "CAPITAL INVESTMENT" was done on the basis of a complete charge for the reactor, reactor building, heat removal system, administration buildings, site development, and all other charges common to reactors in general. No charge was included for fuel, heavy water, or facilities indirectly associated with the reactor, such as hot laboratories, separations facilities, and power conversion equipment. The investments were all corrected to 1951 costs.

The descriptive texts were made as brief as possible while retaining sufficient detail to afford a complete portrayal of the reactor systems. The details which are likely to be of the most interest are stressed, and subjects such as corrosion, heat transfer, and control are not discussed from a general viewpoint.

Table 8.1.1 — Reactor Chart*

Reactor	Purpose	Fuel	Reflector	Coolant	Status	Reference	Remarks
Graphite moderator							
Chicago reactor, No. 1	Res	Nat U	Graph	None	Dismantled	AECD-3289	†
Chicago reactor, No. 2	Res	Nat U	Graph	None	Operating	CP-2459	† To be dismantled
ORNL graphite reactor	Res	Nat U	Graph	Air	Operating	NNES-IV-5a	†
Brookhaven graphite research reactor	Res	Nat U	Graph	Air	Operating	BNL-18	†
Low power research reactor	Res	Enr U	Graph	D ₂ O	Design	In preparation	† Homogeneous
Graphite low energy experimental reactor	Res	Nat U	Graph	Air	Operating	AERE-N/R-126	†
British experimental reactor	Res	Nat U	Graph	Air	Operating	POC-A-1	
Mon.-Un-PuPt	Prod & power	Enr U	Graph	Na	...	Reactor Sci & Tech 2, 3	Preliminary economic study
Com.Ed-P.S.-It	Prod & power	Nat U	Graph	He	...	Reactor Sci & Tech 2, 3	Preliminary economic study
Beryllium moderator							
Brookhaven liquid fuel reactor	Prod & power	U ²³⁵ in Bi	Thorium	Fluid fuel	Design	BNL-111	Preliminary study
Beryllium oxide moderator							
Daniels power reactor	Prod & power	Enr U	BeO	He	Abandoned	MonN-383	† Design study only
H ₂ O moderator							
Low intensity training reactor	Res	Enr U	Be	H ₂ O	Operating	ORNL-701	† Initially an MTR mock-up
Bulk shielding reactor	Res	Enr U	BeO & H ₂ O	H ₂ O	Operating	ORNL-991	†
Materials testing reactor	Res	Enr U	Be & graph	H ₂ O	Operating	ORNL-963	†

Table 8.1.1 — (Continued)

Los Alamos water boiler	Res	Enr U	Graph	H ₂ O	Operating	LA-1301	† Homogeneous
Water boiler neutron source	Res	Enr U	Graph	None	Operating	Reactor Sci & Tech 2, 2	† Homogeneous
North Carolina research reactor	Res	Enr U	Graph	H ₂ O	Constr	NCS-46	† Homogeneous
Homogeneous reactor experiment	Exp	Enr U	D ₂ O	Fluid fuel	Operating	ORN-730	† Homogeneous
D ₂ O moderator							
French zero energy reactor	Res	Nat U	Graph	None	Operating	NP-2038	
Norwegian heavy water reactor	Res	Nat U	Graph	D ₂ O	Operating	Y-F33-2	
Zero energy experimental reactor	Res	Nat U	Graph	None	Operating	PD-207	
Canadian heavy water reactor	Res	Nat U	Graph	H ₂ O	Operating	E-JRH-94	†
Chicago reactor, No. 3'	Res	Enr U	D ₂ O & graph	D ₂ O	Operating	ANL-WHZ-250	†
Chicago reactor, No. 5	Res	Enr U	D ₂ O & graph	D ₂ O	Constr	ANL-4779	†
Com.Ed-P.S.-II*	Prod & power	Nat U	D ₂ O	D ₂ O	...	Reactor Sci & Tech 2, 3	Preliminary economic study
PGE-BC-I*	Prod & power	Nat U	H ₂ O	H ₂ O	...	Reactor Sci & Tech 2, 3	Preliminary economic study
No moderator							
Los Alamos fast reactor	Res	Pu	Nat U blanket	Hg	Operating	LAMS-567	†
Experimental breeder reactor	Res	Enr U	Nat U blanket	NaK	Operating	ANL-4356	†
PGE-BC-II†	Prod & power	Enr U	Nat U blanket	Na	...	Reactor Sci & Tech 2, 3	†
Unconventional moderator							
Thermal test reactor	Res	Enr U	Graph	None	Operating	KAPL-436	† H ₂ O and oil moderated

* All reactors listed are heterogeneous unless otherwise noted under remarks

† Indicates this reactor described in following chapters

† Industrial participation groups: Monsanto Chemical Company and Union Electric Company of Missouri; Commonwealth Edison Company and Public Service Company of Northern Illinois; Pacific Gas and Electric Company and Bechtel Corporation

CHAPTER 8.2

Graphite-moderated Heterogeneous Reactors

CHICAGO PILE NO. 1 (CP-1)

The graphite structure was made chiefly of $4\frac{1}{8}$ - by $4\frac{1}{8}$ -in. blocks (with some 4- by 4-in.) of various lengths. These were stacked in a crisscross fashion with a wooden support structure to approximate a sphere. The actual shape was approximately a flattened ellipsoid of revolution (24 ft across by 19 ft high) since criticality was reached with a smaller structure than had been anticipated. The fuel elements were fabricated in five forms:

- (1) Uranium metal in $2\frac{1}{4}$ -in.-diameter by $2\frac{1}{4}$ -in.-long cylinders.
- (2) UO_2 in $3\frac{1}{4}$ -in.-diameter by $3\frac{1}{4}$ -in.-long cylinders with edges beveled at 45° to simulate spheres.
- (3) UO_2 in 3-in.-diameter by 3-in.-long cylinders.
- (4) and (5) U_3O_8 in the same forms as (2) and (3).

A total of 19,480 fuel elements, predominantly of form (2), were contained in recesses bored in some of the graphite blocks on either $8\frac{1}{4}$ -in. or 8-in. center-to-center spacings. In stacking, filler blocks containing no fuel were interspersed between fuel-bearing blocks to effect a cubical lattice array. The types of graphite used from the center outward were AGOT, Speer, and AGX.

One side of the reactor was supported on a graphite pier rather than on the wooden structure to make sure that a stable structure would be available for inserting the control rods. Ten slots were provided through the pier, three of which were for safety, shim, and regulator rods. In addition, a removable stringer traversed the reactor parallel to the slots. The safety and shim rods were scrambled by a weight-and-pulley system which pulled them through the reactor.

Uranium metal was cast in finished cylindrical form without cladding. Uranium oxide elements were formed by compressing loose, dry uranium oxide powder in a die with a hydraulic press at a pressure of 35,000 to 45,000 psi. The die was lubricated with a dilute solution of stearic acid in acetone with a small amount of ethylene glycol as a wetting agent.

CHICAGO PILE NO. 2 (CP-2)

The graphite structure is a 22- by 20- by 19-ft rectangular stack constructed chiefly of $4\frac{1}{8}$ - by $4\frac{1}{8}$ -in. blocks (with some 4 by 4 in.) of various lengths laid horizontally in a crisscross fashion. About 17,700 fuel elements are contained in recesses bored in some of the blocks on either $8\frac{1}{4}$ - or 8-in. center-to-center spacings. The fuel elements are fabricated in three forms:

- (1) Uranium metal in $2\frac{1}{4}$ -in.-diameter by $2\frac{1}{4}$ -in.-long cylinders.
- (2) UO_2 in $3\frac{1}{4}$ -in.-diameter by $3\frac{1}{4}$ -in.-long cylinders with edges beveled at 45° to simulate a sphere.
- (3) U_3O_8 in the same form as (2).

Table 8.2.1—Chicago Pile No. 1 (CP-1)

LOCATION	University of Chicago Chicago, Illinois	Diffusion length squared (clean and cold) ^a	342 b cm ² 296 c cm ² 330 d cm ²
RESPONSIBLE ORGANIZATION	Metallurgical Laboratory, University of Chicago	Age (clean and cold) ^a	370 cm ²
Design	Metallurgical Laboratory, University of Chicago	Buckling (clean and cold)	45 b x 10 ⁻⁶ cm ⁻² 58.9 c x 10 ⁻⁶ cm ⁻² 101.2 d x 10 ⁻⁶ cm ⁻²
Construction	Metallurgical Laboratory, University of Chicago	Prompt neutron lifetime	About 1 x 10 ⁻³ sec
Operation	Metallurgical Laboratory, University of Chicago	k _∞ (clean and cold)	1.055 (average) 1.032 b 1.039 c 1.07 d
PURPOSE	In operation from Dec., 1942 to Feb., 1943	k _{eff} (clean and cold)	1.0005 a
STATUS		δ k (temperature)	-0.0001/°C
MATERIALS		δ k (poisons)	Negligible
Fuel	Natural uranium; 5.6 metric tons as metal 32.9 metric tons as UO ₂ 3.7 metric tons as U ₃ O ₈ Graphite; 266 metric tons Graphite; 84 metric tons	δ k (pressure)	About -6.4 x 10 ⁻⁶ /mb
Moderator	Graphite; 266 metric tons	NEUTRON FLUX DENSITY	
Reflector	Graphite; 84 metric tons	Fast	
Structural material	Graphite; 84 metric tons	Thermal	
Reactor atmosphere	Air	EXPERIMENTAL FACILITIES. 1 - 4 1/8 x 4 1/8 in. removable stringer 7 - foil along	
Shield	None	CAPITAL INVESTMENT ^a	\$2.7 x 10 ⁶
LATTICE TYPE	Pseudospheres in 8 1/4 in. and 8 in. cubical arrays	REFERENCES . . . Experimental Production of a Divergent Chain Reaction, E. Fermi, AEC-D-3269, 47 pp, January 4, 1952	
DIMENSIONS		a. Estimated	
Core (effective)	Polar radius; 10 ft 2 in. Equatorial radius; 12 ft 9 in. 1 ft thick	b. Uranium oxide in Speer graphite	
Reflector	24 1/2 x 24 1/2 x 19 1/2 ft high	c. Uranium oxide in AGOT graphite	
Over-all	24 1/2 x 24 1/2 x 19 1/2 ft high	d. Uranium metal in AGOT graphite	
STRATEGIC MATERIAL			
Fissionable Material	U235; 296 kg		
Consumption	Negligible		
Burn-up	Negligible		
Average cycle time	None		
COOLING SYSTEM	None		
AUXILIARY FACILITIES	None		
OPERATING CONDITIONS			
Total heat power	200 watts		
Useful power output	0		
Innage	Indefinite		
Heat flux	Negligible		
Power density (average)	10.7 x 10 ⁻⁶ kw/l		
Specific power (average)	6.8 x 10 ⁻⁴ kw/kg 25		
Maximum fuel temperature	Negligible rise		
Maximum moderator temperature	Negligible rise		
CONTROLS			
Shim	1 horizontal 1/8 x 3 1/2 in. cadmium strip on steel rod		
Regulating	1 horizontal 1/4 x 3 1/2 in. steel clad boron steel rod		
Safety	1 horizontal cadmium on steel rod		
Reactivity change			
PHYSICS			
Cell radius	13 cm (8 1/4 in. spacing) 12.6 cm (8 in. spacing)		
Resonance escape (clean and cold)	0.896 d		
Thermal utilization (clean and cold)	0.866 b 0.869 c 0.871 d		

Table 8.2.2—Chicago Pile No. 2 (CP-2)

LOCATION	Argonne National Laboratory Chicago, Illinois	Diffusion length squared (clean and cold)	342 ^b cm ² 296 ^c cm ² 330 ^d cm ²
RESPONSIBLE ORGANIZATIONS			
Design	Metallurgical Laboratory, University of Chicago	Age (clean and cold) ^a	45.5 x 10 ⁻⁶ cm ²
Construction	Metallurgical Laboratory, University of Chicago	Buckling (clean and cold)	58.9 ^c x 10 ⁻⁶ cm ⁻² 101.2 ^d x 10 ⁻⁶ cm ⁻²
Operation	Argonne National Laboratory	Prompt neutron lifetime	About 1 x 10 ⁻⁵ sec
PURPOSE	Research	k _∞ (clean and cold)	1.055 (average) 1.032 ^b 1.039 ^c 1.07 ^d
STATUS	In operation since Mar., 1943	k _{eff} (clean and cold)	1.004
MATERIALS		Δk (temperature)	-0.0001/°C
Fuel	Natural uranium; 9.1 metric tons as metal a 29.5 metric tons as UO ₂ a 1.3 metric tons as U ₃ O ₈ a	Δk (poisons)	Negligible
Moderator	Graphite; 314 metric tons	Δk (pressure)	-6.4 x 10 ⁻⁶ /mb
Reflector	Graphite; 115 metric tons	NEUTRON FLUX DENSITY	
Structural material	Graphite	Fast	
Reactor atmosphere	Air	Thermal: maximum	4.5 x 10 ⁵ n/(cm ²)(sec)(watt) ^a
Shield	Ordinary concrete, wood, and lead	average	1.5 x 10 ⁵ n/(cm ²)(sec)(watt) ^a
LATTICE TYPE	Pseudospheres in 8 1/4 in. and 8 in. cubical arrays	EXPERIMENTAL FACILITIES	34 x 34 in. x 20 ft long removable horizontal core 5 x 5 ft thermal column
DIMENSIONS			
Core	20 x 18 x 17 ft high		
Reflector	1 ft thick		
Shield	5 ft of ordinary concrete on sides 6 in. lead plus 40 in. wood on top		
Over-all	32 x 30 x 23 ft high (excluding thermal column)		
STRATEGIC MATERIAL			
Fissionable material	U ₂₃₅ ; 280 kg ^a		
Consumption	2.7 x 10 ⁻³ gm/day ^a		
Burn-up	Indefinite		
Average cycle time	Indefinite		
COOLING SYSTEM	None		
AUXILIARY FACILITIES			
Reactor atmosphere	Ventilating system		
OPERATING CONDITIONS			
Total heat power	10 kw (nominal)		
Useful power output	0		
Innage	Approx. 0.1		
Heat flux	Negligible		
Power density (average)	6.4 x 10 ⁻⁴ kw/l		
Specific power (average)	3.6 x 10 ⁻² kw/kg 25		
Average fuel temperature	About 25°F rise		
Average moderator temperature	About 15°F rise		
CONTROLS			
Shim	1 horizontal, steel supported, cadmium strip		
Regulating	2 horizontal, strip supported, cadmium strips		
Safety	3 horizontal, steel supported, cadmium strips		
Reactivity Change	0.005		
PHYSICS			
Cell radius	13 cm (8 1/4 in. spacing) 12.6 cm (8 in. spacing)		
Resonance escape (clean and cold)	0.896 ^b		
Thermal utilization (clean and cold)	0.866 ^b 0.869 ^c 0.871 ^d		

REFERENCES . . . Experimental Production of a Divergent Chain Reaction
E. Fermi, AEC-D-3269, 47 pp, January 4, 1952
A Brief General Description of the Argonne Uranium-
Graphite Pile (CP-2), H. E. Metcalf, CP-2459,
11 pp, Secret, Dec. 20, 1944

- a. Estimated
b. Uranium oxide in Speer graphite
c. Uranium oxide in AGOT graphite
d. Uranium metal in AGOT graphite

The graphite was stacked in such manner that the blocks containing fuel were separated by filler blocks containing no fuel, yielding a cubical lattice array. The types of graphite used from the center of the reactor outward are AGOT, Speer, and AGX.

Three control (shim and regulator) rods enter the reactor horizontally, parallel to the long dimension, spaced at 7 ft 11 in. in a horizontal line slightly above center. The removable core and stringers extend through the reactor in the same direction. Three safety rods are inserted horizontally into the left side of the reactor (facing the side that the shim and regulator rods enter), centrally spaced on a horizontal line. These are scrambled by gravity through systems of weights and pulleys that pull the rods through the reactor. The thermal column is built on top of the reactor and extends through the upper shield.

SHIELDING

The sides of the reactor are shielded by 5 ft of ordinary concrete. The top shield consists of 6 in. of lead plus $39\frac{3}{4}$ in. of wood. At higher power levels, the reactor room is not occupied. The openings required in the shield are plugged with concrete blocks. A special laboratory enclosure has been constructed around the thermal column.

REACTOR ATMOSPHERE

A low-capacity ventilating system has been installed for removing the radioactive gases. This unit draws about 100 cfm of air into the reactor around safety-rod, control-rod, and removable-stringer openings and exhausts it through a stack via a duct and filter bank near the top of the upper shield.

FUEL PREPARATION

The uranium metal was cast in finished cylinders without cladding. The uranium oxide elements were formed by compressing loose, dry uranium oxide powder in a die with a hydraulic press at a pressure of 35,000 to 45,000 psi. The die was lubricated with a dilute solution of stearic acid in acetone with a small amount of ethylene glycol as a wetting agent.

ORNL GRAPHITE REACTOR (X-10)

The 24- by 24- by $24\frac{1}{3}$ -ft graphite structure is constructed of layers of 4- by 4-in. blocks of lengths up to 4 ft laid on a concrete foundation. The blocks are oriented with parallel horizontal axes except for occasional transverse stringers, and the whole structure is keyed for stability. The graphite used, in order of quality, is AGOT, AGNT, and AGX. In the 73 courses of blocks, $1\frac{3}{4}$ -in.-square fuel channels (formed by V cuts in adjoining blocks) are provided in the even-numbered layers. There are 1247 standard fuel channels in 35 horizontal rows of 35 channels each, plus a centered 23-channel row at the top. One of the central channels is oversize to accommodate uranium doughnuts. An axial core is completely removable from the discharge face of the reactor. This contains eight standard fuel channels, the oversized doughnut channel, four circular-cross-section experimental channels, and an axial foil slot. Shim rods enter the right side of the reactor (looking at the charging face) in a centered, 4-ft-square array. Regulator rods enter the same face on the vertical center line, centrally spaced at 9 ft 6 in. Safety rods are suspended in the upper shield in an 8-ft 4-in. by 4-ft 8-in. rectangular array and drop by gravity into the reactor. The vertical boron-steel shot wells are approximately in the transverse central plane, 8 ft 8 in. apart. The experimental holes and foil slots extend transversely through the reactor except for the central-plane foil slots, which are obstructed by the removable-core section.

Table 8.2.3 — ORNL Graphite Reactor (X-10)

LOCATION	Oak Ridge National Laboratory Oak Ridge, Tennessee	Coolant pressure	Sub-atmosphere
RESPONSIBLE ORGANIZATIONS		Coolant pressure drop through reactor	19.25 in. of H ₂ O
Design	DuPont	Pumping rate	7,200 lb/min
Construction	DuPont	Pumping power required	800 hp
Operation	ORNL	CONTROLS	
PURPOSE	Research and radioisotope production	Shim	4 - 1 3/4 x 1 3/4 in. x 19 ft horizontal boron-steel rods
STATUS	In operation since Nov., 1943	Regulator	2 - 1 3/4 x 1 3/4 in. x 19 ft horizontal boron-steel rods
MATERIALS		Safety	4 - 1 1/2 in. dia. x 8 ft vertical boron-steel rods 2 - 1 3/4 in. dia. x 17 ft 2 in. vertical tubes for 3/8 in. boron-steel shot
Fuel	Natural uranium; 47.63 metric tons (typical)	Reactivity change (late 1944 loading)	0.0389
Fuel cladding	Aluminum; 0.035 in. wall, 0.060 in. end cap	FUEL HANDLING	
Moderator (and reflector)	Graphite; 612.5 metric tons	Charging	Hand charging, straight push through of slugs
Coolant	Air	Discharging	Slugs drop into canal
Fertile material	Varied	PHYSICS	
Structural material	Graphite	Cell radius	11.46 cm
Reactor atmosphere	Air	Resonance escape (clean and cold)	0.886
Shield	Ordinary and beryllite-haydite concrete, plus waterproofing pitch	Thermal utilization (clean and cold)	0.890
LATTICE TYPE	1.1 in. dia. rods in 8 in. square array	Diffusion length squared (clean and cold)	297 cm ²
DIMENSIONS		Age (clean and cold); axial	398 cm ²
Core	24 x 24 x 24 1/3 ft (including reflector)	Buckling (clean and cold)(experimental)	386 cm ²
Reflector	Depends upon loading	Prompt neutron lifetime	92 x 10 ⁻⁶ sec
Shield	2 ft of ordinary concrete retaining walls (waterproofed with pitch), 5 ft of beryllite-haydite concrete	k _∞ (clean and cold)	About 1 x 10 ⁻³
Over-all	47 x 38 x 35 ft	k _{eff} (clean and cold)(typical)	1.067
STRATEGIC MATERIAL		k _{eff} (temperature)(graphite plus fuel)	1.021
Fissionable material	U ²³⁵ ; 343 kg (typical)	δ k (poisons)(typical)	-2.86 x 10 ⁻⁵ /C°
Consumption	About 4.5 gms/day	δ k (pressure)	6.5 x 10 ⁻⁶ /mb
Burn-up	Indefinite	k _{eff} (hot and poisoned)(typical)	1.004
Average cycle time	Indefinite	NEUTRON FLUX DENSITY	
COOLING SYSTEM		Fast	3.2 x 10 ⁵ n/(cm ²)(sec)(watt) average 1.4 x 10 ⁵ n/(cm ²)(sec)(watt)
Type	Air: Once through	EXPERIMENTAL FACILITIES	20 x 24 in. x 24 ft removable axial core 7 - 2 3/4 x 3/8 in. x 24 ft foil slots 6 - 2 3/4 x 3/8 in. x 11 ft foil slots 4 - 1.684 in. dia. x 24 ft axial experimental holes 1 - 3 1/8 x 2 15/32 in. x 24 ft axial doughnut hole 10 - 4 x 4 in. x 24 ft experimental holes 2 - 14 1/2 x 14 in. animal tunnels in top shield, 6 - observation and experimental holes into discharge air plenum 1 - 5 x 5 ft thermal column 1 - drainable water filled core plug to accommodate additional thermal column or bulk material testing tank
Coolant treatment	Filtered	REFERENCES	Graphite Uranium Production Piles, AEC Technical Information Service, L. B. Borst, NNES-IV-5a, 457 pp, Secret, 1951 An Experimental and Theoretical Study of the Subcritical ENL Reactor, Brookhaven National Laboratory, J. Cherrick, et al, ENL-60, 109 pp Secret, June 15, 1950
Blowers	1 - 275 lb/min steam driven fan (stand-by) 2 - 3300 lb/min centrifugal blowers	a. Estimated	
OPERATING CONDITIONS (typical)			
Total heat power	3800 kw		
Useful power output	0		
Innage	Indefinite		
Rod power	7300 BTU/(sq ft)(hr) a		
Heat flux: maximum	3300 BTU/(sq ft)(hr) a		
Power density: maximum	4.4 kw/l		
Power density: average	1.9 kw/l		
Specific power: maximum	24.8 kw/kg 25 a		
Specific power: average	11.1 kw/kg 25 a		
Maximum fuel temperature	660°F		
Maximum sheath temperature	473°F		
Maximum moderator temperature	292°F		
Coolant inlet temperature	77°F		
Coolant outlet temperature	194°F		
Coolant velocity			

The experimental holes are on 2-ft 8-in. spacings in two rows 5 ft 6 in. apart. The foil slots are arrayed in a 6-ft-square array of three rows. A thermal column centered on the top of the reactor extends through the shield, expanding upward stepwise from a 5-ft square, to a 6-ft 7½-in. square.

SHIELDING

The vertical faces of the reactor are shielded by 5 ft of barytes-haydite concrete contained between two 1-ft ordinary-concrete retaining walls internally waterproofed with pitch. The top shield, separated by 10 in. from the top of the reactor, is self-supporting with 1½ ft of ordinary reinforced concrete (waterproofed) plus 5 ft of barytes-haydite concrete, covered with ½ ft of ordinary concrete. The side shields are separated from the reactor surface by 1-in. asbestos-rope packings. The 10-in. space at the top of the reactor is blocked by a lead- and neoprene-covered steel H beam. A 3-ft air plenum chamber is provided between the shield and reactor at the charging face. This is bridged by slotted 1¼-in. galvanized pipe for the fuel channels. The discharge face is provided with a 6-ft plenum chamber. The concrete of the shield at the back of the discharge plenum chamber is protected from the high-temperature air by a 2-in. insulating layer of cellamite, separated from the concrete by a 4-in. space through which cool air is circulated (comprising about 1 percent of the total air flow). The access holes through the shield for the fuel channels are shielded by two-step plugs of galvanized-iron pipe filled with lead shot and paraffin, with a 1-ft maple rod at the inner end of the plug. A two-step concrete-filled steel plug, stepped down to a smaller 1-ft maple extension at the inner end, offers access to the removable central core from the charging face. The core is removed through a drainable, water-filled, stepped tank plug at the discharge face. Experimental, observation, ionization-chamber, and foil-slot openings are shielded by graphite plus masonite-steel plugs. Three 4-in.-thick lead gates 6 ft 4½ in. apart are provided in each of the animal tunnels. There are 35 openings in the top shield above the discharge face for inserting an air-sampling device. These holes are shielded by plugs similar to the fuel-channel plugs. The control and safety rods cannot be completely removed from the shield, and the tips of the rods act as shield plugs for the openings. The upper thermal column is shielded by a cadmium sheet, 18 in. of concrete, and 4 in. of lead in that order upward. The discharge cooling air is shielded by 2 ft of concrete, and both inlet and outlet air channels make several 90° bends.

FUEL HANDLING

The fuel elements are 1.1-in.-diameter by 4-in.-long cylinders bonded with Al-Si to aluminum cans. Fuel slugs are inserted into the fuel channels and pushed manually into position by means of a steel rod. Spent slugs are forced out of the channels at the discharge face by the new slugs and drop to 45°-inclined planes (padded with neoprene rubber and canvas) which lead to a discharge chute and a deep water pit (19 ft 9 in. of water). The lower end of the discharge chute is movable, to facilitate sorting of the spent slugs into stainless-steel buckets. A 10-ft-deep canal from the deep pit communicates with a hot laboratory and the separations building.

COOLING SYSTEM

Cooling is effected by air drawn from the atmosphere through an inlet filter, the reactor, a venturi constriction, and the exit filter; after passing through the blowers, the air is exhausted through a 200-ft stack. The inlet filter consists of American Air Filter Company Air Mat Type PL-24 filter units loaded with ¾-in. Type G Air Mat Filters giving a total area of 1592 sq ft. After going through the venturi section, the air passes through the exit

filter [$\frac{1}{2}$ in. of FG No. 50 filter mediums, backed up with $\frac{1}{2}$ in. of FG No. 25 followed by a bank of CWS No. 6 (AEC-1) paper filters].

BROOKHAVEN GRAPHITE RESEARCH REACTOR (BGRR)

The graphite form of the Brookhaven reactor is that of a 25-ft cube separated into halves by a vertical gap, which may be varied from $2\frac{1}{4}$ to $3\frac{1}{4}$ in. Cooling air is introduced into this gap and flows out in both directions through the fuel channels, which are perpendicular to the gap. The graphite cube is made of 75 courses of 4- by 4-in. blocks of various lengths up to 45 in. AGOT, AGHT, CSO, and CSN graphites were used. With the exception of the blocks around control-rod and experimental openings, the block axes are parallel to the fuel channels. For stability, all joints are staggered, and the structure is keyed. Staggering of longitudinal joints was accomplished by making the outside blocks in the even-numbered layers 6 in. wide. The gap surfaces are divided into eight triangular portions by dividing the square faces into quadrants and then dividing these with the main diagonals. Alternate triangular portions are offset $2\frac{3}{4}$ in., with the raised portions on opposite sides of the gap alternating so that the two surfaces would interlock if brought together. To reduce coolant-pressure drop, the gap edges and the fuel-channel openings are flared and rounded. The reactor rests on the upper of two 3-in. steel bedplates, divided at the gap. The upper plate is separated from the lower by runners, and the half of the reactor opposite the charging face is arranged so that it can be moved to vary the gap width.

There are 1369 fuel channels in a 37- by 37-channel square, with the central one optional. The channels are formed by cutting semicircular-cross-section grooves in adjacent blocks and are 2.67 in. in diameter. The channels are on 8-in. centers in a square array. Each channel in each half of the reactor is provided with an annular groove to accommodate anchoring projections on the fuel elements. The fuel elements consist of 1.1-in.-diameter by 4-in. metal slugs encased in an 11-ft aluminum tubing provided with six longitudinal cooling fins.

The control rods enter the two discharge-face corners of the cube. The axes are horizontal, on 4-ft spacing, and parallel to the diagonal planes of the cube. Eight rods are inserted at each of the two corners in a 2- by 4-rod centered column. Two of the rods are used for control and are powered by induction motors. Each of the 14 emergency rods is powered by an electric-motor-driven hydraulic pump which in turn drives a hydraulic motor geared to the rod rack-drive pinion through a speed reducer. The electric motors also drive flywheels which store energy for emergency shutdown. The experimental holes traverse the reactor perpendicular to the fuel channels. In general, the holes are in a rectangular array of five rows, six holes to a row. The spacing in the rows is about 3 ft, and the spacing of rows is 4 ft. The array is centered horizontally but is slightly below center vertically. The holes in the middle row are displaced away from the central gap to accommodate an additional opening through the shield into the central gap. The middle row of experimental holes may or may not be blocked by the 12- by 12-in. removable axial core. The second hole from the charging face in the second row from the top is replaced by a sample conveyor system which consists of an endless chain of sample holders contained in two hollowed-out stringers separated by a 4-in. filler stringer. This endless chain is accessible through openings in the shield and is driven by an electrical mechanism located in the shield. Eleven pneumatic tubes parallel to the fuel channels are located in the half of the reactor opposite the charging face, and the other half of the reactor contains 30 inter-cell fuel channels. Two tunnels, one for animals and one for instruments, extend under the reactor perpendicular to the fuel channels to openings in the foundation for direct exposure. Each half of the reactor is provided with a vertical shot well that may be used for experimental purposes or for an additional safety device using boron-steel shot.

Table 8.2.4—Brookhaven Graphite Research Reactor (BGRR)

LOCATION	Brookhaven National Laboratory Upton, New York
RESPONSIBLE ORGANIZATIONS	
Design	H. K. Ferguson Company
Construction	H. K. Ferguson Company
Operation	Brookhaven National Laboratory
PURPOSE	Research and radioisotope production
STATUS	In operation since Aug., 1950
MATERIALS	
Fuel	Natural uranium; 52.5 metric tons (typical)
Fuel cladding	Aluminum; 0.030 in. wall, 6 - 0.6 in. fins; 0.232 lbs/ft
Moderator	Graphite; 350 metric tons
Reflector	Graphite; 382 metric tons
Coolant	Air
Fertile material	Varies
Structural material	Graphite
Reactor atmosphere	Air
Shield	Steel and limonite concrete
LATTICE TYPE	1.1 in. dia. rods in 8 in. square array
DIMENSIONS	
Core	7 ft dia. by 22 ft (typical)
Reflector	About 9 ft on sides, 1 1/2 ft on ends
Shield	9 in. steel; 4 ft 3 in. limonite concrete with iron aggregate
Over-all	37 1/2 x 55 x 33 1/2 ft high
STRATEGIC MATERIAL	
Fissionable material	U ²³⁵ ; 370 kg
Consumption	22.5 gm/day (average)
Burn-up	Up to 20%
Average cycle time	Indefinite
COOLING SYSTEM	
Type	Once through
Coolant source	Atmosphere
Coolant treatment	Inlet filter Outlet filter
Blowers	5 - 1,500 hp motor driven centrifugal fans 1 - 15 hp gasoline driven emergency blower
Pumps	3 - 4,500 gpm, motor driven centrifugal water pumps
AUXILIARY FACILITIES	
Ruptured slug detection	Positive helium pressure inside slug can
Reactor services	Slug canning facility
OPERATING CONDITIONS (typical)	
Total heat power	26,000 kw (28,000 kw design point)
Useful power output	0
Innage	0.9
Rod power (average)38 kw
Heat flux (average)	20,730 BTU/(sq ft)(hr)
Power density (average)	1.07 kw/l
Specific power (average)	70 kw/kg 25
Maximum fuel temperature	600°F
Maximum sheath temperature	441°F
Maximum moderator temperature	41°F
Coolant inlet temperature	265°F
Coolant outlet temperature (at reactor exit plenum)	265°F
Coolant pressure (inlet, i.e. across inlet filter)	1.7 in. H ₂ O
Coolant pressure drop through reactor	50.2 in. H ₂ O
Pumping rate	24,000 lbs/min
Pumping power required (air and water)	About 5700 kw
CONTROLS	
Regulator	2 - 2 x 2 in. x 25 1/2 ft, horizontal 1 3/4% boron steel rods
Shim and safety	14 - 2 x 2 in. x 25 1/2 ft, horizontal 1 3/4% boron steel rods
Reactivity change	2 - 3 1/2 in. dia. diagonal shot wells in gap 2 - 3 1/2 in. dia. x 25 ft shot wells
FUEL HANDLING	
Charging	By hand and remote grappeling equipment
Discharging	By hand and remote grappeling equipment
PHYSICS	
Cell radius	11.46 cm
Resonance escape (clean and cold)	0.884
Thermal utilization (clean and cold)	0.896
Diffusion length squared (clean and cold)(axial)	334 cm ²
Age (clean and cold)(axial)	316 cm ²
Buckling (experimental)	92.4 x 10 ⁻⁶ cm ⁻²
Prompt neutron lifetime	About 1 x 10 ⁻³ sec
k _∞ (clean and cold)	1.074
k _{eff} (clean and cold)(typical)	1.032
β k (temperature)(total)	-4 x 10 ⁻⁵ /°C
δ k (poisons)(typical)	-0.017
k _{eff} (hot and poisoned)(typical)	1.005
NEUTRON FLUX DENSITY	
Fast	2.59 x 10 ⁵ n/(cm ²)(sec)(watt)
Thermal (maximum)	29 - 4 x 4 in. x 25 ft experimental holes
EXPERIMENTAL FACILITIES	1 - 12 x 12 in. x 25 ft removable axial core 1 - 2 channel, 25 ft sample conveyor system 11 - 12 1/2 ft pneumatic tubes 1 - 20 x 20 ft section of removable shield 30 - intercell 12 1/2 ft fuel channels 2 - openings into central gap 2 - exposure tunnels under the reactor
CAPITAL INVESTMENT	\$19 x 10 ⁶
REFERENCES	Report on the Brookhaven Nuclear Reactor Brookhaven National Laboratory, BNL-18, 180 pp, Secret, June 22, 1948
	The Brookhaven Nuclear Reactor: Theory and Nuclear Design Calculations, Brookhaven National Laboratory, I. Kaplan and J. Chernick, BNL-152 80 pp, Secret, January, 1952

SHIELDING

The shielding consists of $4\frac{1}{4}$ ft of limonite, heavy-aggregate-concrete poured into forms made of 3-in. steel plate, with fuel-channel rifle barrels and sleeves for experimental holes welded in place. A 14-ft exhaust plenum is provided at the charging face, and a 6-ft exhaust plenum is provided at the opposite face. These are enclosed with large steel bellows for air seals. The shields on these faces are honeycombed with rifle barrels for fuel handling at the charging face and for push rods on the opposite face. An additional 3 in. of steel plate is used around the graphite to effect a total thermal shield of 6 in. This is supplemented with a 12- by 20-in. steel band encircling the reactor at the central gap. The concrete is shielded from the hot exhaust air in the plenum by a $4\frac{1}{2}$ -in. insulating layer of corrugated aluminum sheets, separated from the shield by a $2\frac{1}{2}$ -in. gap through which secondary cooling air is circulated. A similar insulation is provided in the exhaust ducts, which are shielded with heavy concrete as far as the outlet filters. A space of 12 to 15 in. is provided on the sides, top, and bottom of the reactor between the graphite and the shield for air flow from the inlet chambers near the ends of the pile to the central gap. The graphite is sealed by a $\frac{1}{4}$ -in. steel or $\frac{1}{8}$ -in. aluminum casing with metal bellows for the experimental openings. On the top face of the reactor, a 20- by 20-ft portion of the shield is made of interlocking stepped plugs which can be removed for experimental purposes. The top shield also has three rows of openings, two over the large plenum and one over the small plenum, which are used for scanning and for remote-grappling equipment during charging operations. All the reactor openings have stepped shield plugs of steel, graphite, and heavy-concrete combinations. The discharged slugs are dropped into a 4- by 13-ft-cross-section chute which leads down from the large plenum to a 13- by 13- by 20-ft-deep well. This has a 52-ft-long, 5-ft-deep canal for storage purposes which will be extended to the hot laboratory. The concrete walls of the canal are 18 in. thick and provided with three gate dams for isolation of contamination.

FUEL HANDLING

Fuel elements are removed from the reactor by placing a trough across the large plenum at the appropriate position. After removing the orificing and tube-retaining device from the opening, the helium tube is pinched off, and the element is withdrawn into the trough. From this position, it is picked up by two pneumatically operated grappling hooks lowered through the scanning openings in the top shield on cables. By means of push rods and hooks manipulated through openings at the sides, the element is positioned over the discharge chute and lowered into the deep well.

Fuel is placed into the reactor by bridging the large plenum gap with a trough as in discharging. An electrician's fishline is then inserted into the helium-tube conduit, which guides it into the fuel channel. The fishline is pushed through and connected to the helium tube on the element, and then the whole assembly is pulled and pushed into position.

COOLING SYSTEM

The cooling air is drawn through inlet filters to chambers encircling the ends of the reactors; past the lateral faces of the reactor to the control gap; into the gap and back to the ends of the reactor through the fuel channels; into the air plenums and down into discharge ducts that exit from the plenum floors; and through the exit filters, heat exchangers, and venturi constrictions. The two discharge ducts are then joined into a single manifold from which the fans in parallel exhaust the air through a silencer and a 320-ft (above grade) stack.

The air velocity in the gap averages about 200 ft/sec with a peak of about 250 ft/sec. The velocity in the fuel channels ranges from 160 to 275 ft/sec. Individual channels are orificed by slabs of various thicknesses which are clamped into the tapered outlet end of the channels. The fuel elements are also locked in position by these devices. Unloaded channels are blocked with graphite plugs to prevent unnecessary loading of the cooling system.

The inlet filter is a 53- by 8-ft bank of V filters, using a low-pressure-drop, bonded-glass filter medium. The outlet filters are banks of glass-tex cloth filters in the 13- by 19-ft outlet ducts. The air is cooled by passing it over helically finned copper tubes in a 19-ft by 11-ft by 20-in.-deep bank using 5300 gal of water per minute discharged at about 120°F. This water is circulated in a closed system and cooled to about 85°F in an induced-draft cooling tower.

CHAPTER 8.3

Beryllium-oxide-moderated Heterogeneous Reactors

DANIELS POWER PILE, NO. III (DPP)

This reactor represents a design study only, and no further development is anticipated. It consists of beryllium oxide bricks assembled as a right circular cylinder (72 in. diameter by 76 in. high). The bricks are fabricated as right hexagonal cylinders with 2-in. axial holes by hot pressing or by cold pressing followed by ceramic firing. The bricks are stacked with their axes vertical to form 517 continuous vertical channels. The horizontal joints between bricks of any one channel are staggered vertically by 2 in. relative to those of the adjacent channels. The vertical channels may be charged with fuel elements, reflector slugs, or fertile material.

Steel blocks are shaped to fit the irregular brick contour and form a cylinder. They consist of circular segments 1 ft long with an average width of 5 in. A 1-in.-thick steel retaining shell surrounds these forming blocks. Clearances of $\frac{1}{4}$ in. at the bottom and $\frac{3}{4}$ in. at the top are provided to allow for thermal expansion. The reactor is encased in a steel vessel, 8 ft OD, $1\frac{1}{2}$ in. thick, 22 $\frac{1}{2}$ ft in over-all length, and provided with elliptical heads.

A 6-in. steel plate serves as a base for the moderator-reflector bricks. This plate, in turn, is supported on pads mounted on the pressure shell. Holes are located in the plate to correspond to those in the brick assembly. These holes taper outward from a 2-in. diameter at the interface and are surrounded by an annular groove to engage the latch mechanism used to support the column of removable elements placed in the vertical channel. Weight is added to the top of the bricks (1) to resist the pressure drop across the reactor which tends to lift the bricks and (2) to retain the removable elements in the channels. The weight consists of cast-steel blocks 10 in. thick, each of which covers 7 vertical channels.

Each column of elements is held against the top weight by means of a replaceable spring element charged into the channel along with the fuel, reflector, or fertile elements. The retainer shell allows for a 34-in. space above the top weights to serve as the coolant outlet plenum. The support plate serves as the bottom of the retaining shell, and a space is left between this and the bottom of the pressure shell to accommodate the loading machine. The gas inlet plenum consists of a space between the top of the retaining shell and the pressure shell.

The control rods are supported above the core in a vertical position, the most reactive position being with the rods at the top of their travel. The regulating rod enters the central channel of the core; the shim rods are installed in a 21-in.-diameter concentric circle; and the safety rods are installed in a 57-in.-diameter concentric circle. The control rods are powered by electric motors, and the safety rods scram by gravity. The rods are cooled by helium.

Table 8.3.1 — Daniel Power Pile, No. III (DPP)

LOCATION	Maximum sheath temperature	1535° F
RESPONSIBLE ORGANIZATIONS	Maximum moderator temperature	500° F
Design	Coolant inlet temperature	1400° F
Construction	Coolant outlet temperature	132 psig
Operation	Coolant velocity	0.95 psi
PURPOSE	Coolant inlet pressure	12.3 lb/sec
STATUS	Coolant pressure drop through reactor	620 kw
MATERIALS	Pumping rate	
Fuel	Pumping power required	
Uranium (30% U235); 10.7 kg as UO ₂ dispersed in beryllium oxide	CONTROLS	
Fuel Cladding	Shim	6 - 1 1/2 in. OD, 1 in. ID, 1% boron steel
Coolant tubes	Regulator	vertical, hollow rods
Reflector	Safety	1 - 0.394 in. dia., 1% boron steel vertical rod
Beryllium oxide; 2.74 metric tons	Reactivity change	6 - 1 1/2 in. OD, 1 in. ID, 1% boron steel, vertical, hollow rods
Beryllium oxide; 7.96 metric tons	FUEL HANDLING	
Helium	Charging	Remotely operated, double pivot charging tube in lower gas plenum
Thorium; 5.38 metric tons as ThO ₂	Discharging	Remotely operated, double pivot charging tube in lower gas plenum
Beryllium oxide	PHYSICS a	
Helium	Cell radius	2.83 cm
Indefinite	Resonance escape (clean and cold)	0.98
Rods in 3 in. triangular array	Thermal utilization (clean and cold)	1.21
Core	Diffusion length squared (clean and cold)	2.58
49 in. dia. x 45 in. high	Age (clean and cold)	
5 3/4 in. thick on sides	Buckling (clean and cold)	
10 1/2 in. thick on top and bottom	k ₀₀ (clean and cold)	
5 in. thick on top and bottom	k _{eff} (clean and cold)	
Shield	8 k (temperature)	
Over-all (pressure shell only)	8 k (poisons)	
8 ft dia. x 22 1/2 ft high	k _{eff} (hot and poisoned)	
Indefinite	Conversion ratio	
STRATEGIC MATERIAL	NEUTRON FLUX DENSITIES	
Fissionable material	Fast	
Consumption	Thermal (average)	4.9 x 10 ¹³ n/(cm ²)(sec)
Burn-up	EXPERIMENTAL FACILITIES	
Average cycle time	CAPITAL INVESTMENT	Indefinite
29 days	REFERENCES	Summary Report on Design and Development of High Temperature Gas-Cooled Power Pile, Clinton Laboratories, C.R. McCullough, et al, MonN-383, 422 pp, Secret, September 15, 1947
COOLING SYSTEM		
Type		
Recirculated helium		
Continual purification		
4 - 5340 cfm, electrical motor driven, centrifugal blowers		
SAFETY FACILITIES		
Power conversion		
1 - 1,800 kw turbo-generator		
1 - 300 kw turbo-generator		
OPERATING CONDITIONS (Typical)		
Total heat power		
Useful power output		
1,800 kw		
Innage		
Rod power: maximum		
average		
78.8 kw		
52.5 kw		
Heat flux		
Power density: maximum		
average		
16.5 kw/l		
8.7 kw/l		
Specific power: maximum		
average		
3800 kw/kg 25		
2000 kw/kg 25		
Maximum fuel temperature		

a. Preliminary calculations in Appendix F of MonN-383

FUEL HANDLING

The fuel elements are fabricated in the form of honeycomb structures 5 in. long. These are charged into the reactor by means of a double-pivoted tube, the end of which may be positioned remotely at any fuel channel. A ram pushes the column of slugs from the charging tube into the fuel channel where a latch mechanism in the base plate supports the column. The slugs are introduced into the charging tube by means of a gas lock.

The elements are removed from the reactor by pushing the latch mechanism base about 1 in. into the taper of the matrix support plate against the compression of the support spring. This depresses and retains the latch, allowing the column of elements to be lowered into the charging tube by the ram.

COOLING SYSTEM

Helium enters the pressure shell through two 18-in.-diameter ducts located at the top of the shell. Most of the gas is directed by a baffle plate to the central portion of the top plate assembly. It then flows outward and down the annular passage between the retaining and pressure shells and into the space around the loading machine. From this lower plenum it flows upward through the reactor channels to the discharge plenum where it enters the two outgoing ducts. The two high-temperature ducts connect to duplicate boilers, the discharges from which connect to a common header. The four blowers in parallel draw the helium from this duct and discharge to another common header from which the two low-temperature ducts return it to the reactor. The high-temperature ducts are double-walled and cooled by helium circulated in the annulus.

POWER CONVERSION

Steam is conducted from the boilers at the rate of 20,500 lb/hr to a common header at 450 psig and 725°F. From this common header, steam is fed to the 1800-kw turbine-generator, the 300-kw turbine-generator, and two emergency steam condensers which will dispose of the total output of the boilers. The exhaust steam from the main turbine-generator is condensed in a 3800-sq-ft surface condenser. The cooling water system is a closed system containing a 14,000-gpm forced-draft cooling tower.

CHAPTER 8.4

Light-water-moderated Heterogeneous Reactors

MATERIALS TESTING REACTOR (MTR)

The active part of the reactor consists of closely packed vertical-plate assemblies, the individual plates being made of aluminum-clad uranium-aluminum alloy. The plates are spaced to allow water flow between them, the water thus serving as both coolant and moderator. Immediately surrounding the lattice is a reflector of water-cooled beryllium. This whole assembly of active lattice and beryllium reflector is mounted in a tank system through which the water flows and which contains the control rods and their bearings. Outside the tank system are a secondary reflector of graphite, a thermal shield, and a biological shield.

The fuel elements are made up of 18 plates supported in a stack, with 0.117-in. spacing between plates, by two grooved, aluminum side-plates. The fuel plates consist of cores of 10- to 20-percent-uranium (~ 90 percent U^{235})—aluminum alloys, $23\frac{3}{4}$ -by 2.50- by 0.021-in, clad with aluminum; final fuel-plate dimensions are $24\frac{5}{8}$ - by 2.845- by 0.060-in. (the external plates are lengthened to $28\frac{5}{8}$ in. by aluminum extensions). The plates are curved across their width to a $5\frac{1}{2}$ -in. radius and brazed into the aluminum side-plates. Tube-box adapters which mate with the upper and lower support grids are plug-welded to each end to complete the fuel element.

The tank system, approximately 30 ft tall, is made up of five sections. The tanks provide the means of funneling water through the active lattice and beryllium reflector and provide supports for the reactor assembly and the control rod bearings. They are bolted together and, by the use of aluminum gaskets, made into a watertight system. The sections from the top down are called the A, B, C, D, and E tanks. Sections A and E are made of stainless steel and are permanently imbedded in the concrete of the biological shield with a structural-steel framework support. Section E is $54\frac{1}{4}$ in. ID by 6 ft 5 in. with 2-in. walls. This section supports sections C and D and has two 24-in. water outlets. Section A is 70 in. ID by 11 ft 5 in. with $\frac{3}{4}$ -in. walls. It serves as a container for the water shielding above the lattice and is provided with two 24-in. water inlets (and overflow pipes). The diameter of this tank is large enough so that sections B, C, and D are removable through it.

Section C (4 ft $4\frac{3}{16}$ in. long) and section D (6 ft long) are made of 1-in. aluminum with a $54\frac{1}{4}$ -in. ID. Section D contains the active lattice and is bolted by external flanges to section E. Sections C and D are joined by internal flanges. Section D is pierced by several holes with aluminum thimbles welded in for experimental facilities. The resulting loss of strength in the tank wall is compensated by a 1-ft band of increased wall thickness ($1\frac{1}{8}$ in.) at the center. Section B is a bellows-type expansion joint of stainless steel, joined by an external flange to an internal flange at the bottom of section A and by internal flanges to section C.

A lower support casting, bolted to the bottom of section D, supports a lower assembly grid and a lower shim-rod-bearing grid. An upper support casting, which rests on an extension of the upper flanges of section D, supports a removable assembly of the upper assembly grid, the grid spacer, and the upper shim-rod-bearing grid.

Table 8.4.1 — Materials Testing Reactor (MTR)

LOCATION	National Reactor Testing Station	Heat flux (average)	294,000 BTU/(sq ft)(hr)
RESPONSIBLE ORGANIZATIONS	Arco, Idaho	Power density (average)	291 kw/l
Design	Oak Ridge National Laboratory, Argonne National Laboratory, and Blaw-Knox Construction Company	Specific power (average)	10,000 kw/kg 25
Construction	Fluor Corporation	Maximum fuel temperature	240° F
Operation	Phillips Petroleum Company	Maximum sheath temperature	125° F
PURPOSE	Research	Maximum moderator temperature	100° F
STATUS	In operation since April, 1952	Coolant inlet temperature	115° F
MATERIALS		Coolant outlet temperature	30 ft/sec
Fuel	Uranium (~90% U235) in uranium-aluminum alloy	Coolant inlet pressure	73 psia
Fuel Cladding	Aluminum; 0.020 in. thick	Coolant pressure drop through reactor	40 psi
Moderator	H ₂ O; 0.117 in. film	Pumping rate	20,000 gpm
Reflector	Beryllium; 2.61 metric tons	Pumping power required	
Graphite; 68.7 metric tons		CONTROL	
Coolant	H ₂ O; 0.117 in. film	Shim	4 - combination aluminum-cadmium box and fuel element rods
Fertile material	Aluminum, stainless steel, and concrete	Regulator	2 - 1 1/2 in. dia. aluminum-cadmium rods and beryllium rods
Structural material	H ₂ O, iron, and barytes concrete	Safety	Effectuated by all rods
Shield		Reactivity change	About 0.40
LATTICE TYPE	Slab type	FUEL HANDLING	
DIMENSIONS		Charging	Remote grappling devices from top of tank
Core	Up to 15 x 27 x 24 5/8 in.	Discharging	Remote grappling devices from top of tank. Spent fuel lowered through discharge chute to canal beneath reactor
Reflector	Beryllium, extends from core to 54 1/4 in. dia. cylinder	PHYSICS ^a	
Graphite; pebble zone out to 7 1/3 ft sq x 9 ft high		Resonance escape (clean and cold)	1.0
blocks out to 12 x 14 x 9 1/4 ft high		Thermal utilization (clean and cold)	0.76
8 in. iron; 9 ft barytes concrete;		Diffusion length squared (clean and cold)	3.5 cm ²
or 17 1/2 ft of H ₂ O plus top plug		Age (clean and cold)	64.2 cm ²
32 1/2 x 34 x 40 2/3 ft high		Buckling (clean and cold)	0.01 cm ⁻²
Over-all	32 1/2 x 34 x 40 2/3 ft high	Prompt neutron lifetime	2.63 x 10 ⁻⁴ sec
STRATEGIC MATERIAL		k _∞ (clean and cold)	1.61
Fissionable material	U235; 2.98 kg	k _{eff} (clean and cold)	
Consumption (at full power)	36 g/day	δ k (temperature)	-0.017/°C
Burn-up	Indefinite	δ k (poisons)	
Average cycle time	Indefinite	k _{eff} (hot and poisoned)	
COOLING SYSTEM		Conversion ratio	None
Type	Recirculated H ₂ O	NEUTRON FLUX DENSITIES ^a	
Coolant source	Wells	Fast (maximum)	1.2 x 10 ¹⁴ n/(cm ²)(sec)
Coolant treatment		Epithermal (maximum)	6 x 10 ¹⁴ n/(cm ²)(sec)
Pumps	3 (1 standby) - 10,000 gpm (97.5 psi), 700 hp horizontal, electrically driven, centrifugal pumps	Thermal (maximum)	2 x 10 ¹⁴ n/(cm ²)(sec)
Safety	2 - 850 gpm, electrically driven, centrifugal pumps	EXPERIMENTAL FACILITIES	
1 - 400 lb/min, electrically driven, blower		CAPITAL INVESTMENT	\$18 x 10 ⁶
1 - 400 lb/min, gasoline driven, centrifugal pump		REFERENCES	Materials Testing Reactor Project Handbook, Oak Ridge National Laboratory, J. H. Buck and C. F. Leyse, ORNL-963, 584 pp, Secret, May 7, 1951
1 - 150,000 gal, 170 ft head, working reservoir			
1 - 150,000 gal, 150 ft head storage tank			
2 - 360,000 gal storage ponds			
AUXILIARY FACILITIES			
Retention basin	750 kva Diesel-electric generator		
Standby equipment			
OPERATING CONDITIONS			
Total heat power	30,000 kw		
Useful power output	0		
Innage			

a. Preliminary calculations

The tube-box end-adapters of the fuel elements fit into the upper and lower assembly grids. A spring section of the upper end box allows each assembly to be held firmly and still allows for expansion and tolerance limitations. The assembly grids provide for a 5 by 9 array of fuel elements except that 8 centralized spaces (space numbers 2, 4, 6, and 8 of rows 2 and 4) are allotted as shim-rod spaces. The shim rods are lifted by electromagnetic clutches on drive shafts which extend through the top plug to the drive motors. The regulating rods enter the beryllium reflector portion of the reactor and are coupled to their drive shafts by quick-release mechanisms. The rods are guided by the upper and lower shim-rod-bearing grids. A further set of control-rod guide bearings, mounted in a spider, is fastened to the top plug by four long support tubes. When the top plug is lowered into place, the four corners of the spider fit over pins on the spider support ring which is bolted to the top flange of tank section B. The support, grid, and bearing castings are all made of aluminum.

The normal loading of the lattice is with fuel in a 3 by 9 array with four alternate spaces in the central row having combination fuel and poison shim-rods. The other lattice positions are filled with beryllium elements, and the other four shim positions use the combination poison and beryllium shim-rods.

The beryllium section of the reflector is all contained in tank section D, occupying the space between the active lattice and the tank wall. It is made of large blocks of hot-pressed beryllium powder, machined to fit together and around the beam holes and lattice. A discharge chute for unloading reactor components extends from the reactor (adjacent to the lattice region) to a canal system below the reactor. Access to this discharge chute is obtained by lifting out a section of the beryllium reflector. Adjacent to the tank wall and extending out a minimum of 40 cm to form a 7-ft 3-in. square is a 9-ft-high graphite pebble-zone containing about 700,000 one-in. balls of graphite. The pebbles rest on a base plate mounted on the lower thermal shield. Two discharge chutes in the pebble support plate can be opened into a discharge bin, allowing for removal of the pebbles. Around the pebble-zone, a graphite reflector, made up of 4- by 4-in. graphite blocks, is built out to a 12- by 14- by 9½-ft-high structure, keyed together, and with a 6- by 6-ft thermal column extending out through the shield to one side.

SHIELDING

The thermal shield is formed by two 4-in. steel plates separated by a gap through which cooling air is circulated. The outer plate is in contact with the concrete biological shield and cools this by direct thermal contact. Over-all dimensions of the thermal shield are 14 by 16 by 12½ ft high. Around this is the biological shield in the form of barytes concrete installed by the "prepack" method. The many experimental openings through the shield are shielded by stepped plugs of material which in general matches the surrounding shielding materials. These plugs are shielded by large lead coffins when they are withdrawn to provide access for the experimental facilities. A 6-ft by 6-ft by ¼-in. sheet of boral is used as a shielding curtain for the thermal column. This can be raised or lowered between the graphite reflector and the thermal column. A fixed 3-in.-thick sheet of lead in place of the thermal shield between the graphite reflector and the thermal column serves to attenuate the gamma radiation.

The process water is conveyed to and from the reactor tank through pipes imbedded in the biological shield and is carried in a pipe tunnel between the reactor building and the process-water building. The water in the reactor tank system along with the top and bottom tank plugs serves as a shield above and below the lattice.

The circulated air coolant is shielded by being conveyed in underground ducts. Handling of irradiated fuel elements is performed under about 17 ft of water in the canal below the reactor.

EXPERIMENTAL FACILITIES

Seventeen large experimental holes lead from the side shield faces to either the reactor tank wall or the active lattice as follows:

- (1) Six horizontal beam holes extend to the active lattice. Two of these are 8 in. in diameter to the tank wall and 6 in. in diameter from there to the active lattice. The other four holes are 6 in. in diameter all the way.
- (2) Six inclined holes of 6-in. diameter extend to the reactor tank wall. Inside the tank wall they are extended to the active lattice by 2-in.-ID, sealed, empty, aluminum cylinders.
- (3) Two horizontal, 6-in.-diameter holes extend to the reactor tank.
- (4) Two horizontal, 4-in.-diameter rabbit holes extend to the reactor tank.
- (5) One horizontal, $4\frac{11}{16}$ - by $4\frac{11}{16}$ -in. hole extends through the reactor adjacent to the active lattice

In addition, there are six horizontal through-holes, two 4 in. in diameter, two 8 in. in diameter, and two $10\frac{3}{4}$ in. in diameter, extending through the graphite block reflector.

There are 71 experimental and instrument holes accessible from the top of the reactor. These extend various distances into the graphite zones, pebble and block, and the biological shield.

The thermal column is made of GBF graphite and is covered by a thick lead door. The column is encased with a combination of lead, steel, and cadmium or boral shells. The column is penetrated by nine horizontal and two vertical experimental holes.

FUEL HANDLING

Fuel elements (or other reactor components) are loaded into the reactor by removing the top plug and maneuvering the components with long-handled grappling tools. Elements are discharged by lifting out the beryllium plugs over the discharge chute and lowering the elements into a canal system below the reactor. A hydraulically operated unloading mechanism effects the transfer between the two water systems and rotates the discharged components from a vertical to a horizontal position where the component is ejected onto a receiving table. From this point, the component is handled with long tongs or hooks and placed in storage racks in the canal.

COOLING-WATER SYSTEM

Water from the 150,000-gal working reservoir flows, under a normal head of 170 ft, directly to the reactor tank through a 30-in. stainless-steel pipe outside of the reactor building and a 36-in., stainless-steel pipe beneath the reactor building. The 36-in. pipe splits into two 24-in. stainless-steel pipes which convey the water up through diagonally opposite corners of the biological shield to the top of the reactor tank system. The water descends through the reactor tank sections, the active lattice, and the beryllium reflector and emerges from the bottom of the reactor tank into two 24-in. stainless-steel lines which join into a 36-in. line by which the water is conveyed to a 17,000-gal seal tank in the process-water building. Water from the seal tank is drawn into flash evaporators and, in being flashed at a pressure that yields 100°F effluent, falls from the flash evaporators into the 100,000-gal sump tank from which it is pumped to the working reservoir to complete the cooling cycle. The reactor heat, liberated in the flash evaporators, is carried away by cooling-tower water circulated in the condenser tubes of the evaporators. A demineralization system supplies the required make-up water.

COOLING-AIR SYSTEM

Air is drawn into the reactor building through coarse fiber-glass or wire-mesh prefilters. The air then goes through an electrostatic filter. The reactor building is pressurized to about $\frac{1}{2}$ in. of water so that leakage in through windows, doors, and the like is kept to a

minimum. The reactor building air is then drawn into the reactor through four airmat-type PL-24 glass-wool filters (except for the small amount leaking in around experimental openings). The air is channeled down between the two thermal shield plates from four 2- by 2- by 12-ft plenum chambers (on each side) by a series of 8-in. ducts leading to manifolds above the thermal shield. The air passes into plenum chambers beneath the graphite, rises up through the graphite reflector, and exits into a plenum chamber. The exit ducts consist of two 30- by 30-in. pipes which carry the air downward in diagonally opposed corners of the biological shield and join into a 48-in.-diameter duct leading to a plenum chamber beneath the blower and fan house. The blowers exhaust the air from this plenum to another plenum where it is mixed with contaminated air from the laboratory and discharged through a 250-ft stack.

MODIFICATIONS

The excess reactivity of the MTR has turned out to be less than anticipated. To compensate for this, the uranium content of the fuel core alloy is being raised to about 16.5 percent (168 gm of uranium per fuel element).

LOW-INTENSITY TRAINING REACTOR (LITR)

This reactor consists of an assembly of sandwich-plate fuel elements positioned in a slab-type lattice by upper and lower grids. Provision is made for enclosing this with beryllium blocks for reflection, and the whole assembly is contained in one section of a long, cylindrical tank structure having a vertical axis. The design represents a modified, full-scale mock-up of the MTR design current at the time of construction.

The fuel elements are made of 18 fuel plates supported in a stack, with 0.117-in. spacing between plates, by two grooved aluminum side-plates. The fuel plates consist of cores of 10 to 20 percent-uranium (~ 90 percent U^{235})—aluminum alloy, $23\frac{3}{4}$ by 2.50 by 0.021 in., clad with aluminum; final fuel-plate dimensions are $24\frac{5}{8}$ by 2.845 by 0.060 in. (the external plates are lengthened to $28\frac{5}{8}$ in. by aluminum extensions). The plates are curved across their width to a $5\frac{1}{2}$ -in. radius and brazed into the aluminum side-plates. Tube-box adapters which mate with the upper and lower support grids are plug-welded to each end to complete the fuel element.

The support grids provide for a 5 by 9 close-packed array of fuel elements except that three alternate spaces in the second row are allotted to coarse control rods. The spaces not used for fuel or control rods are filled with temporary beryllium reflector elements.

The tank structure is made up of six cylindrical sections which are designated, from the top down, the A, B, C, D, E, and F sections. All except C and D sections are made of mild steel and are Amercoated for corrosion protection. The tank support structure and housing is a steel girder framework with four main support columns. A sub-reactor room (15 by 15 ft) extends 12 ft below grade.

Section A is 70 in. ID by 11 ft $6\frac{1}{8}$ in. with a $\frac{5}{8}$ -in. wall. It has two 36-in. flanged openings for water inlets and is fitted with external flanges, at the top and bottom, by which it is supported. Section B is 55 in. ID by 5 ft $3\frac{1}{4}$ in. with a $\frac{1}{2}$ -in. wall. It is lowered through section A, from which it is supported by a lower internal flange mating with an upper external flange on section B.

Section D is made of $\frac{3}{4}$ -in. aluminum and is $54\frac{1}{4}$ in. ID by 6 ft. It encases the active lattice and forms the outer boundary of water flow through the reflector. This tank provides bearing surface and alignment for the upper and lower grid-support castings which are made of aluminum. Four offset and two central 6-in.-diameter horizontal aluminum thimbles are welded to the tank wall and terminate at the surface of the active-lattice region in the mid-plane. Lugs welded to the tank wall immediately above the reflector support the peripheral reflector-piece alignment ring.

Table 8.4.2 — Low-intensity Training Reactor (LITR)

LOCATION	Oak Ridge National Laboratory
RESPONSIBLE ORGANIZATIONS	Oak Ridge, Tennessee
Design	Oak Ridge National Laboratory
Construction	Oak Ridge National Laboratory
Operation	Oak Ridge National Laboratory
PURPOSE	Experimental and research
STATUS	In operation since Feb., 1950
MATERIALS	
Fuel	Uranium (~90% U ²³⁵); as 10 to 20% uranium-aluminum alloy
Fuel Cladding	Aluminum; 0.020 in. thickness
Moderator	H ₂ O; 0.117 in. film
Reflector	Beryllium; 1.5 metric tons
Coolant	H ₂ O; 0.117 in. film
Fertile material	None
Structural material	Aluminum
Shield	Concrete blocks, sand and borated plastic
LATTICE TYPE	Slab geometry
DIMENSIONS	
Core	up to 15 x 27 in. x 24 5/8 in. long
Reflector	8 in. thick (minimum)
Shield	12 ft thick (minimum)
Over-all	28 1/2 x 28 1/2 x 34 ft high
STRATEGIC MATERIAL	
Fissionable material	U ²³⁵ ; 2.8 kg
Consumption	1.5 g/day
Burn-up	Indefinite
Average cycle time	Indefinite
COOLING SYSTEM	
Type	Recirculated water
Coolant treatment	Demineralization and deaeration (batchwise)
Pumps	2 - 1000 gpm (at 78 psi) electrically driven centrifugal pumps (1 as standby)
Safety	Natural convection Gravity-fed water-spray system
OPERATING CONDITIONS	
Total heat power	1500 kw
Useful power output	0
Innage	0.93
Heat flux (average)	1.31 x 10 ⁴ BTU/(sq ft)(hr)
Power density (average)	15.7 kw/l
Specific power (average)	530 kw/kg 25
Maximum fuel temperature	122°F
Maximum sheath temperature	103.5°F
Maximum moderator temperature	112°F
Coolant inlet temperature	
Coolant outlet temperature	
Coolant velocity	
Coolant inlet pressure	2 1/2 psi ^a
Coolant pressure drop through reactor	1200 gpm
Pumping rate	55 kw
Pumping power required	

CONTROLS

Shim 3 - combination fuel and cadmium shim rods
Regulator 1 - 1 1/2 in. vertical aluminum rod with 20 in. cadmium tube insert

Safety Effected by shim rods
Reactivity change 0.18 a

FUEL HANDLING

Charging Remote grappelling devices
Discharging Remote grappelling devices. Depleted elements stored in top tank

PHYSICS^b

Resonance escape (clean and cold) 1.0
Thermal utilization (clean and cold) 0.76
Diffusion length squared (clean and cold) 3.65 cm²
Age (clean and cold) 64.2 cm²
Buckling (clean and cold) 10⁻² cm⁻²
Prompt neutron lifetime 2.63 x 10⁻⁴ sec
k_∞ (clean and cold) 1.61
k_{eff} (clean and cold) 1.05
δ k (temperature) -0.017/°C
δ k (poisons) Indefinite
k_{eff} (hot and poisoned) (typical) 1.011

NEUTRON FLUX DENSITIES

Fast (maximum) 9.5 x 10¹² n/(cm²)(sec)
Epithermal (maximum) 4.8 x 10¹³ n/(cm²)(sec)
Thermal: maximum (in lattice) 1.6 x 10¹³ n/(cm²)(sec)
 maximum (in reflector) 2 x 10¹³ n/(cm²)(sec)

EXPERIMENTAL FACILITIES. 2 - 3/4 in. ID pneumatic rabbit systems
6 - 6 in. dia. horizontal test holes
4 - 3 in. dia. vertical test holes (outside of tank)

CAPITAL INVESTMENT \$1 x 10⁶ a

REFERENCES Mock-up Design Report,
Oak Ridge National Laboratory, W. R. Gall and
D.J. Mallon, ORNL-701, 138 pp, Secret
October 27, 1949

Materials Testing Reactor Project Handbook
Oak Ridge National Laboratory, J.H. Buck
and C.F. Leyse, ORNL-963,
584 pp, Secret, May 7, 1951

a. Estimated

b. Preliminary calculations

Section E is a cylindrical steel shell, $55\frac{1}{4}$ in. ID by $47\frac{5}{16}$ in. with $\frac{3}{4}$ -in. walls, having two diametrically-opposed 16-in. flanged openings for water outlets and a 30-in. flanged opening for a manhole. These openings have been blocked off. There is an external flange at the top for connection to tank section D and an internal flange at the bottom for bolting to section F. Section F is the bottom of the tank and both closes the tank and supports the shim-rod shock absorbers and sections D and E of the tank. It consists of two flat plates, separated by a ring at the periphery and radial reinforcing ribs. The top plate is 2 in. thick and the bottom one is $1\frac{1}{2}$ in.

The two main portions of the tank structure, sections A and B supported from above, and sections D, E, and F supported from below are joined (by internal flanges) by section C, a stainless-steel bellows expansion section. The tank joints, except for the top plate, use aluminum wire gaskets. The top plate uses a neoprene gasket since it is frequently removed.

The inner assembly consists of upper and lower assembly grids and upper and lower control-rod guide grids. These are provided with support and spacer castings of aluminum. The lower grid support bears on a ring bolted to the lower tank flange, while the upper assembly support is born by lugs welded to the tank wall. The beryllium reflector is supported on a skirt-plate casting enveloping the lower grids.

The beryllium reflector is made up of bricks doweled and riveted together in the form of vertical columns. The reflector is 8 in. thick on the sides of the lattice but extends all the way to the tank wall at the ends. The beryllium on the 8-in.-thick sides is retained by aluminum side-plates. Unused lattice positions are also filled with beryllium elements to aid in reflection.

The regulator rod travels in the reflector immediately adjacent to the lattice. This, along with the three shim rods, extends up into tank section B to the electromagnetic suspensions. Shafts from the electromagnets extend upward through a positioning and bearing spider and through packing glands on the top plate to the rod drive mechanisms.

SHIELDING

Shielding directly above the tank is effected by the $17\frac{1}{2}$ -ft column of water above the active lattice. Around the B, C, and D sections of the tank, a 12-ft-thick shield is built. This consists of a wrapping of borated plastic, packed with sand, and concrete blocks with the uneven inner block surface filled in with sand. The six horizontal thimbles are stepped to 8 in. and provided with shield plugs. The outlet water lines are shielded with 3 in. of lead, the storage tank by about $1\frac{1}{2}$ ft of concrete, and the inlet water line by 1 in. of lead.

FUEL HANDLING

Fuel elements, reflector pieces, and internal reactor units are handled by long-shafted grappling devices from the top of the tank. Access to the lattice and reflector pieces is afforded by removing the top plate along with the control-rod shafts and positioning spider; the upper assembly and guide grids and supports are then raised and placed on a storage support on the control-rod-spider guide ring. Support is also provided in B section for storing irradiated fuel elements until they can be removed in a cask.

COOLING SYSTEM

Water is brought into the top tank section through an 8-in. aluminum header. After passing down through the tank structure, it is conveyed up past the active lattice and reflector through four 2-in. pipes. Above this section, these pipes are joined in two 6-in. pipes which pass up to the top section where the water is removed in a single 8-in. header. This conveys the outlet water to a 7000-gal seal tank and then to the pump. After leaving the

pump, the water passes through a Trane horizontal-bed forced-draft-cooled radiator using two 2-speed blower fans (40 or 10 hp). The radiator is a 4-pass bank of aluminum-finned aluminum tubes. After it is cooled, the water circulates back to the reactor tank. The water is treated by demineralization and deaeration of the make-up.

BULK SHIELDING REACTOR (BSR)

This thermal reactor is water cooled, water moderated, and partially beryllium-oxide reflected. It is suspended in a 40- by 20- by 20-ft pool of water. The fuel element is a box-like stack of 18 curved ($5\frac{1}{2}$ -in. radius across width) plates, each 3- by 24- by 0.060 in., spaced 0.117 in. apart, and braced into grooved aluminum side-plates. These plates are 0.060-in. sandwich structures of 14.1-percent-U-Al alloy between 0.020-in. aluminum cladding. Each fuel element is provided with an adapter tube at one end by means of which the fuel element is set into a hole in an aluminum support grid with the long axis of the element vertical. This grid is 28 by 19 by 5 in. deep. An aluminum can containing BeO blocks occupies 4 in. of the 19-in. dimension, leaving a free space of 27 by 15 in. which allows an array of 9 by 5 fuel elements (3- by 3-in. cross section).

For varying the loading pattern, aluminum cans with the same outline as the fuel elements and filled with beryllium oxide blocks are provided. The three control rods are vertical (scramming by gravity) and travel inside special fuel elements which have half of the fuel plates removed.

The aluminum support grid is suspended at a 16-ft depth by an aluminum framework from a bridge which spans the pool. This bridge also carries the controls and control panel, although the operator is located on a movable platform beside the pool. When in operation, the reactor bridge is locked to the rails with heavy clamps. The reactor travels along the long dimension of the pool without provision for vertical or lateral displacement.

The pool has a 14-ft by 14-ft by $5\frac{1}{2}$ -ft-deep well, centered 15 ft from one end of the pool. Adjoining this is a $7\frac{1}{2}$ -ft by 8-ft by 3-ft-deep extension well. These wells are normally filled with barytes-limonite concrete blocks. In addition to giving an adjustable floor level in the bottom of the pool, these blocks are used to piece out shielding samples. A 12- by 21-ft aluminum gate 10 ft from the opposite end of the pool can be lowered, blocking off this end of the pool and permitting the rest of the pool to be pumped dry.

SHIELDING

The standard shielding of the reactor is effected by at least 16 ft of water or by an equivalent shield with less water plus the concrete pool walls and the earth. For experiments with the reactor behind the aluminum barrier, the concrete blocks from the pool well may be stacked to supplement the shielding.

FUEL HANDLING

Fuel elements are inserted in and removed from the support grid by means of a long-handled grapping tool manipulated from the reactor bridge. Irradiated elements are stored on a rack in the pool under 8 ft of water.

COOLING SYSTEM

The pool contains about 100,000 gal of laboratory process water. It is filled by gravity flow and emptied by pumping. The outlet system has a "vacuum breaker" to ensure that the pool will not empty by syphoning action. Reactor heat is removed from the fuel elements by natural convection currents only. This cooling is estimated to be adequate for 1000-kw operation.

Table 8.4.3—Bulk Shielding Reactor (BSR)

LOCATION	Oak Ridge National Laboratory
RESPONSIBLE ORGANIZATIONS	Oak Ridge, Tennessee
Design	Oak Ridge National Laboratory
Construction	Oak Ridge National Laboratory
Operation	Oak Ridge National Laboratory
PURPOSE	Research
STATUS	In operation since Dec., 1950
MATERIALS	
Fuel	Uranium (~90% U ²³⁵); 2.4 to 4 kg, as 10 to 20% uranium-aluminum alloy
Fuel Cladding	Aluminum; 0.020 in. wall
Moderator	H ₂ O; 0.117 in. film
Reflector	Beryllium oxide and/or H ₂ O
Coolant	H ₂ O; 0.117 in. film
Fertile material	None
Structural material	Aluminum
Shield	H ₂ O
LATTICE TYPE	Slab geometry
DIMENSIONS	
Core	up to 15 x 27 in. x 24 in. high
Reflector	Depends upon loading
Shield	16 ft of H ₂ O, or equivalent
Over-all (pool)	40 x 20 x 20 ft
STRATEGIC MATERIAL	
Fissionable material	U ²³⁵ , 2.4 to 4 kg
Consumption	Indefinite
Burn-up	Indefinite
Average cycle time	Indefinite
COOLING SYSTEM	
Type	Water; natural convection
Coolant source	Process water
Coolant treatment	Sodium chromate as corrosion inhibitor
OPERATING CONDITIONS	
Total heat power	100 kw
Useful power output	0
Input	Indefinite
Heat flux (maximum)	1800 BTU/(sq ft)(hr)
Power density (average)	1.1 kw/l
Specific power (average)	30 kw/kg 25
Maximum fuel temperature	
Maximum sheath temperature	
Maximum moderator temperature	
Pumping power required	0

CONTROLS	
Shim	2 - 1 1/4 x 2 1/2 in. vertical, cadmium-lead rods
Regulator	1 - 1 1/4 x 2 1/2 in. vertical, cadmium-lead rod
Safety	All rods
Reactivity change	0.08
FUEL HANDLING	
Charging	Long handled grapppling device
Discharging	Long handled grapppling device; depleted elements stored in pool
PHYSICS ^a	
Resonance escape (clean and cold)	1.0
Thermal utilization (clean and cold)	0.76
Diffusion length squared (clean and cold)	3.5 cm ²
Age (clean and cold)	64.2 cm ²
Buckling (clean and cold)	0.01 cm ⁻²
Prompt neutron lifetime	1.61
k _∞ (clean and cold)	1.003
k _{eff} (clean and cold)	1.003
δk (temperature)	
δk (poisons)	
k _{eff} (hot and poisoned)	1.003
NEUTRON FLUX DENSITIES ^a	
Fast (average)	1 x 10 ¹¹ n/(cm ²)(sec)
Epithermal (average)	3 x 10 ¹¹ n/(cm ²)(sec)
Thermal: maximum	2 x 10 ¹² n/(cm ²)(sec)
Thermal: average	1 x 10 ¹² n/(cm ²)(sec)
EXPERIMENTAL FACILITIES	40 x 20 x 20 ft pool
CAPITAL INVESTMENT	\$217,000
REFERENCES	The New Bulk Shielding Facility at Oak Ridge National Laboratory; Oak Ridge National Laboratory, W.M. Breazeale, ORNL-991, 55 pp. Secret, May 8, 1951

a. Preliminary calculations

SHIELD TEST FACILITIES

An instrument bridge also spans the pool. A cart travels on a pair of rails on one side of the bridge, and a stainless-steel framework, suspended from the cart, reaches nearly to the bottom of the pool. A carriage which slides on the framework and is raised or lowered by a winch carries the various chambers associated with the measurements. It is also possible to rotate the framework about a vertical axis. The bridge and cart can be clamped to their rails, and the carriage can be clamped to the framework. In addition, by means of two telescoping tubes, the framework can be clamped to the bottom of the pool. A thin aluminum window in the pool barrier permits shielding studies in air by placing the reactor behind and close to the barrier and draining the remainder of the pool. Additional flexibility is obtained through the use of the well in the pool. In addition to affording an adjustable floor level, the blocks may be used to piece out and supplement shielding samples.

CHAPTER 8.5

Heavy-water-moderated Heterogeneous Reactors

ARGONNE HEAVY WATER REACTOR (CP-3')

This reactor consists of 122 fuel rods suspended vertically in an aluminum tank (6-ft OD with $\frac{3}{16}$ -in. walls, 8-ft 10-in. tall) through which D_2O coolant-moderator is circulated (the D_2O depth is 7 ft). The $1\frac{1}{2}$ -in.-thick stainless-steel support plate rests on a shoulder of the reactor tank, and the reflector graphite is stacked below the shoulder. A 12-in.-thick shield of lead blocks is also carried by the support plate. The fuel rods have flanges at the upper ends that bear on aluminum sleeves, which are threaded into holes in the support plate and extend upward through the lead-block shield. The lower ends of the fuel rods pass through a bottom grid-plate of aluminum that positions the rods without constraining their longitudinal freedom. Of the 136 lattice positions, 117 are loaded with standard fuel elements (one provided with a thermocouple). Three positions contain "poison rods" having $2\frac{1}{2}$ in. of cadmium at the lower end; two positions contain "spiked" elements containing a 12-in. length of 6-percent uranium-aluminum alloy in the center of the fuel section. The remaining lattice positions are occupied by 4 experimental thimbles, 2 burn-up thimbles, 3 control-rod thimbles, 1 aluminum thermocouple rod, and 4 blanking-off aluminum-pipe plugs. The portion of a fuel rod assembly which extends through the lead tank-plug is made up of a cadmium-lead shielding combination. The active portion of the rod is 66 in. long. The reactor tank rests upon and is enclosed by a 2-ft-thick layer of 4- by 4-in. cross-section graphite blocks stacked with staggered joints.

Two shim rods and two safety rods are pivoted from stainless-steel supports on the fuel-rod support plate near the periphery of the reactor tank and swing in four parallel, vertical planes between the fuel rods. The safety-rod planes of travel are $5\frac{3}{8}$ in. off the vertical axis of the reactor tank, whereas the shim-rod planes are $10\frac{3}{4}$ in. off the axis. These control rods are made of two concentric aluminum shells with a 0.015-in. cadmium layer between them. The cross section changes from a circular shape ($3\frac{1}{2}$ -in. OD) near the pivot end of the rod to approximately an ellipsoidal shape near the free end of the rod (major axis is the direction of motion). The shim-rod absorber sections are 5-ft 1-in. long, and the safety-rod absorber sections are 5-ft, $4\frac{3}{4}$ -in. long. These rods are driven by pivot shafts which extend out through the shielding to external drive-mechanisms. The shim rods are motor-driven, whereas the safety rods are pneumatically operated (fail-safe) and scram by gravity. In addition, there are three vertical control rods (one regulator and two safety) which operate in fuel-element positions. The safety rods are approximately diametrically opposed, with seven lattice spaces between them, and the regulator rod is approximately symmetrically placed with respect to the safety rods at a distance of five lattice spaces from the line joining their centers. The latter is composed of two aluminum tubes with a 0.015-in.-thick by 45-in.-long cadmium layer between them and is brought through the upper shield to the drive motor by an aluminum-steel extension. The safety-rod absorber sections are also made of concentric 36-in.-long aluminum shells with a 0.030-in.-layer of cadmium between them. The outside diameter is about $1\frac{1}{4}$ in. A $\frac{1}{2}$ -in.-

Table 8.5.1 — Argonne Heavy Water Reactor (CP-3')

LOCATION	Argonne National Laboratory Chicago, Illinois
RESPONSIBLE ORGANIZATIONS	
Design	Argonne National Laboratory
Construction	Argonne National Laboratory
Operation	Argonne National Laboratory
PURPOSE	Research
STATUS ^a	In operation from June, 1944 to Jan., 1950 with natural uranium as CP-3. Began operation with enriched fuel in July, 1950 as CP-3'
MATERIALS	
Fuel	Uranium (~90% U235), 4.2 kg as 2% uranium-aluminum alloy
Fuel Cladding	Aluminum, 0.059 in. wall
Coolant tubes	None
Moderator	D2O; 4.78 metric tons
Reflector	Top; D2O Sides and bottom; graphite
Coolant	D2O
Total D2O requirement	5.72 metric tons
Fertile material	None
Structural material	Aluminum
Reactor atmosphere	Helium
Shield	Lead and ordinary concrete
LATITUDE TYPE	0.850 in. dia. rods in 5/8 in. square array
DIMENSIONS	
Core	6 ft dia. x 5 1/2 ft
Reflector	2 ft thick on sides and bottom; 1 ft thick on top
Shield	4 in. of lead and 8 ft of concrete on sides; 1 ft of lead and 4 ft of laminated steel and masonite on top (modified right octagonal prism)
Over-all	26 ft across flats by 14 ft high
STRATEGIC MATERIAL	
Fissionable material	U235; ~3.8 kg
Consumption	0.29 g/day
Burn-up	Indefinite
Average cycle time	Indefinite
COOLING SYSTEM	
Type	D2O, recirculated
Coolant treatment	Filtering
Pumps	1 - canned rotor, sealed, electrically driven, 200 gpm
AUXILIARY FACILITIES	
Reactor atmosphere	1 - standby, sealed, centrifugal pump
OPERATING CONDITIONS	
Total heat power	275 kw
Useful power output	0
Innage	Indefinite
Rod power (average)	2.25 kw
Heat flux: maximum	13,300 BTU/(sq ft)(hr)
Power density: average	5,600 BTU/(sq ft)(hr)
Power density: maximum	0.12 kw/l
Specific power: maximum	0.05 kw/l
Specific power: average	168 kw/kg
Maximum fuel temperature	About 120°F
Maximum sheath temperature	About 110°F
Maximum moderator temperature	About 105°F
Coolant inlet temperature	91°F
Coolant outlet temperature	104°F
Coolant velocity	Indefinite
Coolant inlet pressure	Negligible
Coolant pressure drop through reactor	Negligible
Pumping rate	About 150 gpm
Pumping power required	Negligible
CONTROL	
Shim	2 - 4 1/8 x 2 1/2 x 61 in., aluminum-jacketed cadmium, signal-arm-type rods
Regulator	1 - 7/8 in. OD x 45 in., aluminum-jacketed cadmium, vertical rod
Safety	2 - 4 1/8 x 2 1/2 x 64 3/4 in. aluminum-jacketed cadmium, signal-arm-type rods
Reactivity change	2 - 1 1/4 in. OD x 36 in. aluminum-jacketed cadmium, vertical rods
FUEL HANDLING	
Charging	Manually charged initially
Discharging	Spent rods withdrawn into a lead coffin
PHYSICS	
Cell radius	4.35 cm
Resonance escape (clean and cold)	1.0
Thermal utilization (clean and cold)	0.8
Diffusion length squared (clean and cold)	465 cm ²
Age (clean and cold)	125 cm ²
Buckling (clean and cold)	882 x 10 ⁻⁶ cm ⁻²
Prompt neutron lifetime	2.3 x 10 ⁻³ sec
k _∞ (clean and cold)	1.6
k _{eff} (clean and cold)	About 1.016
δ k (temperature)	-5 x 10 ⁻⁴ /°C
δ k (poisons)(equilibrium xenon)	About -0.005
k _{eff} (hot and poisoned)	About 1.006
Conversion ratio	None
NEUTRON FLUX DENSITIES	
Fast	3.5 x 10 ¹¹ n/(cm ²)(sec)
Thermal: maximum	3.4 x 10 ¹² n/(cm ²)(sec)
Thermal: average	1.7 x 10 ¹² n/(cm ²)(sec)
EXPERIMENTAL FACILITIES	
1 - axial, 1 3/4 in. ID vertical thimble in reactor tank	
7 - horizontal, 3 7/8 in. to 10 13/16 in. square test holes	
1 - horizontal, 29 11/16 x 21 7/8 in. hole, filled with graphite, with 10 thimbles	
1 - horizontal 5 x 5 ft thermal column with beam hole	
CAPITAL INVESTMENT	A Report to the Atomic Energy Commission on the Proposed CP-3' Reactor, Argonne National Laboratory, ANL-WHZ-250, 96 pp, Secret, June 15, 1950
REFERENCES	

a. To be replaced by CP-5 in late 1953

diameter chromium-plated steel rod extension supports the absorber section from an electromagnetic suspension device located in the upper shield. This suspension device is mounted on a vertical endless-chain drive to effect the required travel for the safety rods. The vertical rods travel in aluminum thimbles and scram by gravity.

The horizontal experimental openings penetrate to or into the graphite reflector. There are no experimental openings on the side of the reactor toward the pump room, which is immediately adjacent to the reactor. In addition to the horizontal experimental openings, there are six vertical thimbles in fuel-rod positions. Two of these have cadmium burn-up elements which are used for long-time shim control. There is also an axial thimble (inter-cell).

SHIELDING

The reactor tank and reflector are encased by a 4-in.-thick layer of lead (poisoned with 1 percent cadmium). The inside of the lower 2 ft of this shell is covered by a water-tight lead sheet that serves as a drip-pan to reclaim leakage or spillage of D_2O . Two lead lines (2-in. and 1½-in. diameters) drain this pan to the D_2O drain tanks. The remainder of the principle shielding consists of concrete in the form of an octagonal prism enclosing the reactor-reflector assembly. The shield thickness is 7-ft 8-in. or more. On one side this thickness is partly provided by the pump room shielding-wall.

The shield above the reactor tank and lead plug is composed of 4 ft of laminated steel and masonite in the form of removable blocks, supported on a row of 15 removable 7-in. I-beams that rest on two 12-in. I-beams at their extremities. The pump and heat exchanger room is shielded by 2-ft-thick concrete walls. These walls also serve to shield the openings in the reactor shield through which the D_2O and helium pipe lines are carried.

The experimental openings which penetrate the shielding are stepped and provided with appropriate plugs. The thermal column and goat hole (filled with graphite) have lead and iron-masonite shielding; the exposure thimbles are curved and have fitted plugs.

COOLING SYSTEM

The D_2O enters the bottom of the reactor tank by way of a 2½-in. stainless-steel header and leaves the tank via a 4-in. stainless-steel line through the tank-plug which extends down to the top of the lattice. This line leads to a sealed, stainless-steel pump which circulates the D_2O through a tube-and-shell heat exchanger (cooled by a process-water and cooling-tower system). A 3-in.-diameter pipe branching from the return line to the reactor contains a quick-acting valve which permits dumping the D_2O from the reactor into the storage tank. The coolant system is provided with by-pass facilities for resin ion-exchange columns, filtering, distilling, and pD adjustment.

AUXILIARY SYSTEMS

A positive helium atmosphere is maintained above the D_2O in the reactor tank and the storage tanks. This is done to prevent contamination by the moisture (light water) contained in the atmosphere. This helium is circulated through a recombination system to reclaim D_2O which has been dissociated in the reactor.

ARGONNE RESEARCH REACTOR (CP-5)

This reactor is in the construction phase with essentially all components assembled or being ordered; future modifications are anticipated to be minor.

The fuel for this reactor is contained in sandwich plates (3- by 24½- by 0.060 in.) composed of a 0.020-in.-thick core of uranium-aluminum alloy clad with 0.020-in.-sheaths of

aluminum. These plates are curved to a $5\frac{1}{2}$ -in. radius across their width and maintained in a ten-plate stack, with 0.154-in. spaces between plates, by means of 0.112-in.-thick aluminum side-plates. Two 0.051-in.-thick aluminum end-plates are added as outside plates to complete the assembly of the grid-box with a cross section of about 2.4- by 3-in.

There are 17 locations on 6-in. centers for mounting the grid boxes vertically; these are spaced so that a full array of the boxes presents a cylindrical arrangement about 2 ft in diameter at the center of a 6-ft-diameter aluminum tank containing D_2O . A 10-in. helium plenum over the D_2O surface is formed by a tank plug fitting inside the upper $2\frac{1}{2}$ ft of the aluminum tank; the seal for this helium atmosphere is at the flange engagement at the top of the tank. The tank plug is partially supported on the $\frac{3}{8}$ -in. tank wall and partially by springs mounted in the $10\frac{1}{2}$ -ft-diameter top shield. This top shield in turn rests on an offset of a 10-ft-diameter steel tank which bears on steel base beams 2 ft below aluminum tank. A graphite zone 2 ft thick rests on these beams and supports the aluminum tank. The 2-ft-thick graphite reflector between the two tanks supports an annular shield at the same level as the tank plug.

Individual access to each fuel box is achieved by aligned holes in the tank plug and an inner plug of the top shield. Separate small weighing-plugs in the tank-plug holes hold the fuel boxes down against the coolant flow. The seals for the helium atmosphere are O-rings on the weighing plugs. The D_2O seal at the bottoms of fuel boxes is maintained by modified pipe-union-type of surfaces.

Four shim-safety rods, 1- by 5-in. rectangular cross section, swing in the spaces formed by five rows of fuel boxes. The rods are attached at bearings supported on a grid structure of the 6-ft-diameter aluminum tank. These rods are driven through a spline engagement by shafts which extend horizontally to seals and drive mechanisms outside the shielding. Safety movement of the rods is by combination gravity and spring action. A vertically actuated regulating rod can be positioned in any of eight thimble locations just external to the 17 fuel-box locations comprising the reactor core.

Aluminum thimbles for the experimental facilities are welded to the aluminum tank wall and extend inward to the core or through the tank. The thermal columns are horizontal and diametrically opposed.

SHIELDING

To minimize heating and gamma ray sources, the steel tank is lined with a boral-layer and enclosed by a 3- to $3\frac{1}{2}$ -in. layer of lead. Water circulated through copper coils buried in the lead removes the heat generated in the graphite and thermal shield. Around the thermal shield is the biological shield, consisting of limonite and heavy-aggregate concrete, in the form of a modified octagonal prism. An exception is the top shield external to its inner plug; this annular shell, $2\frac{1}{2}$ ft high, is filled with bags of borax and iron punchings. A layer of lead, 3 in. thick and 6 ft in diameter, covers the top shield to absorb radiation during transit of a spent fuel box being drawn into the 8-ton lead coffin.

Miscellaneous shielding includes a concrete mass for storing spent fuel and a 2-ft ceiling over D_2O system (main floor). Basement walls to isolate the recirculating D_2O will be erected after it is determined how completely the N^{16} decays in the reactor tank.

FUEL HANDLING

In loading, a fuel box, attached to its weighing plug and a safety loading washer, is lowered into position through an individual hole in the top shield. The final positioning of the fuel box is accomplished by disengaging the safety loading washer to permit the lower end of the box to engage its seat safely. A top plug is placed over the weighing plug.

On discharging, the top plug is removed and set aside. The safety washer is engaged, and the fuel box and weighing plug are raised approximately 1 in. The coffin is then posi-

Table 8.5.2—Argonne Research Reactor (CP-5)

LOCATION	Argonne National Laboratory Lemont, Illinois	Coolant pressure drop through reactor	About 2 psi
RESPONSIBLE ORGANIZATIONS		Pumping rate	1000 gal/min
Design	Argonne National Laboratory	Pumping power required	10 hp primary 30 hp secondary
Construction	Argonne National Laboratory		
Operation	Argonne National Laboratory		
PURPOSE	Scheduled to replace CP-3 late in 1953		
STATUS			
MATERIALS			
Fuel	Uranium (~90% U ²³⁵); in 10 to 20% uranium-aluminum alloy	Shim	4 - 1 x 5 1/2 x 60 in. aluminum-jacketed, cadmium, signal-arm type rods
Fuel Cladding	Aluminum; 0.020 in. thick	Regulator	1 - 1 1/2 in. OD, aluminum-jacketed cadmium, vertical rod
Coolant tubes	Aluminum; box type, 2 - 0.122 in. side plates and 2 - 0.051 in. side plates, about 2.4 x 3 in. over-all	Safety	Quick drain of D ₂ O to core level
Moderator	D ₂ O; 2 to 2 1/2 ft thick	Reactivity change (by safety rods)	Lowered through individual access holes in tank plug
Reflector: primary	Graphite; 29.5 metric tons	Charging	Drawn up into shielded coffin
Reflector: secondary	D ₂ O; 2 to 2 1/2 ft thick		
Coolant	D ₂ O		
Total D ₂ O requirement	6.8 metric tons		
Fertile material	None		
Structural material	Aluminum and steel		
Reactor atmosphere	Helium		
Shield	Boral, lead, and limonite-iron-aggregate concrete		
LATTICE TYPE	Grid box elements in 6 in. square array b		
DIMENSIONS			
Core (equivalent)	2 ft dia. x 2 ft		
Reflector: primary	2 to 2 1/2 ft of D ₂ O		
Reflector: secondary (sides and bottom)	2 ft of graphite		
Shield	3 1/2 in. of lead and 4 ft 8 1/2 in. of heavy concrete		
Over-all	20 1/3 ft across flats by 13 ft 6 1/2 in.		
STRATEGIC MATERIAL			
Fissionable material	U ²³⁵ ; 1.15 kg		
Consumption (average)	0.84 g/day		
Burn-up	About 20%		
Average cycle time	8 months		
COOLING SYSTEM			
Type	D ₂ O, recirculated		
Coolant treatment	Ion exchange columns (continuous)		
Pumps	2 - paralleled (1 standby), 1000 gpm, mechanical seals, electrically driven, centrifugal pumps		
AUXILIARY FACILITIES			
Reactor atmosphere	Helium, recirculated		
OPERATING CONDITIONS (Uniform loading)			
Total heat power	34,000 BTU/(sq ft)(hr)		
Useful power output	6 kw/l		
Innage	870 kw/kg 25		
Rod power (average)	148 F		
Heat flux (average)	146 F		
Power density (average)	117 F		
Specific power (average)	124 F		
Maximum fuel temperature	5.4 ft/sec		
Maximum sheath temperature	About 5 psi		
Coolant inlet temperature			
Coolant outlet temperature			
Coolant velocity			
Coolant inlet pressure			

a. Estimated
b. See text

Neutron flux densities
Fast (average) About 10¹² n/(cm²)(sec)
Epithermal (average) About 10¹³ n/(cm²)(sec)
Thermal: maximum 2.8 x 10¹³ n/(cm²)(sec)
average 2.3 x 10¹³ n/(cm²)(sec)
EXPERIMENTAL FACILITIES 10 - vertical thimbles in reactor tank: 6 - 1 in. dia., 1 - 6 in. dia. and 3 - 4 in. dia.
20 - vertical thimbles in graphite reflector: 13 - 3 in. dia. and 7 - 6 in. dia.
2 - 12 in. dia., horizontal beam holes
2 - 4 in. dia., horizontal beam holes
2 - 6 in. dia., horizontal test holes tangent to core
2 - 8 x 12 in., horizontal test holes in bottom graphite reflector
1 - 1 in. dia. horizontal pneumatic tube below lattice
1 - 2 in. dia. horizontal pneumatic tube below lattice
2 - 5 x 5 ft thermal columns with 16 3/4 in. sq axial test holes
CAPITAL INVESTMENT \$1.8 x 10⁶
REFERENCES Feasibility Report for the Argonne Research Reactor (CP-5), Argonne National Laboratory, J.M. West and J.T. Weills, ANL-4779, 23 pp, Secret May 7, 1951

tioned over the hole, and the fuel box and its weighing plug are drawn into the coffin. The flange of the washer stops the travel of the fuel box about 1 in. above its seat in the event the box is accidentally dropped.

COOLING SYSTEM

D₂O is fed into the reactor through an inlet header into a plenum chamber at the bottom of the reactor tank. Openings in the plenum chamber allow the D₂O to flow into the fuel boxes. The connecting adapter on the fuel box contains an orifice that distributes the flow. After passing upward through the active section, the D₂O is discharged into the moderator space through exit ports in the upper part of the fuel box. The D₂O level is maintained by an overflow line which drains into the D₂O storage tank. The D₂O is discharged from the tank by a vertical header at the bottom of the reactor tank and passes through a pump, two tube-and-shell heat exchangers, and then back into the reactor. Light water picks up the heat on the shell side of the heat exchangers and delivers it to a forced-draft cooling tower. Other features in the heavy-water system include a 500-gal dump tank to lower the D₂O moderator level just to the top of the reactor core and a 1400-gal storage tank for complete removal of D₂O from the reactor tank. Columns for continuous ion-exchange purification of the D₂O are provided.

AUXILIARY SYSTEMS

The 10-in. space above the D₂O in the reactor tank and all free space above the D₂O in the D₂O system is occupied by blower-recirculated helium. The helium carries decomposition gases over a catalyst for recombination of D₂O.

The graphite zone has a helium atmosphere to permit more heat to pass by conductivity from experimental plugs into the moderator near the reactor core. This atmosphere also assists in distributing graphite heat for removal in the coils of the thermal shield. A gas holder comprises the external part of this system.

The copper coils buried in the thermal shield lead are duplicated as an insurance feature. Distilled water is recirculated through the shell-and-tube heat exchanger, the heat being picked up by make-up water for the cooling-tower loop.

CHAPTER 8.6

Miscellaneous Heterogeneous Reactors

THERMAL TEST REACTOR (TTR)

This reactor was designed for the primary purpose of carrying out accurate, danger-coefficient experiments. An annular cylindrical can, constructed of aluminum, with an ID of 12 in. and an OD of 18 in. contains the 20 aluminum tubes (2 in. in diameter) that hold the fuel rods for the active section of the reactor. The interstices between these tubes and the can walls contain light water, whereas the tubes themselves are filled with a light paraffin-base oil. These two liquids (static) act as moderators. The central space in the annular cylinder is filled with graphite to form an internal thermal column which is constructed with a central slot for experimental samples. The neutron flux in the sample position is 2.3 times the average flux in the active lattice, and the cadmium ratio of indium activation is 5.9. A neutron cross section of 10^{-3} cm² can be measured by normal danger-coefficient methods.

Any six of eight $\frac{1}{2}$ -in.-diameter, vertical, aluminum tubes, which extend above and below the reactor, can be used as thimbles for the control and safety rods. The safety rods are suspended electromagnetically and scram into the reactor by gravity.

Each of the 20 fuel rods contain approximately 50 fuel discs. These washer-like discs have an outside diameter of 1.96 in. and an inside diameter of 0.194 in. The discs are 0.040 in. thick and contain about 2.7 gm of U²³⁵ as a 35-percent-uranium: aluminum alloy (~90 percent U²³⁵). These discs are placed on an 18-in. aluminum rod and spaced at 0.2 in. by polyethylene washers. The planes of the discs are canted 6° off the perpendicular to the rod axis to allow bubbles to escape freely.

A graphite reflector about $2\frac{1}{3}$ ft thick covers the sides and bottom of the core. This is extended out one side to form a horizontal thermal column.

SHIELDING

The reactor is placed in a 10-ft by 15-ft by 13-ft-high room. The three external walls of the room are made of 6 ft of ordinary concrete, and the ceiling is 1 ft of reinforced concrete. The fourth 6-ft-thick wall is built up of blocks of high-density concrete with an access opening and a thermal column opening provided.

Table 8.6.1 — Thermal Test Reactor (TTR)

LOCATION	Knolls Atomic Power Laboratory Schenectady, New York	FUEL HANDLING	Charging	Manually operated tongs
DISCHARGING		Discharging	Manually operated tongs	
RESPONSIBLE ORGANIZATIONS		PHYSICS		
Design	Knolls Atomic Power Laboratory	Resonance escape (clean and cold)	1.0	
Construction	Knolls Atomic Power Laboratory	Thermal utilization (clean and cold)		
Operation	Knolls Atomic Power Laboratory	Diffusion length squared (clean and cold)		
PURPOSE	Research	Age (clean and cold)		
STATUS	In operation since Jan., 1951	Prompt neutron lifetime	5×10^{-4} sec	
MATERIALS		Buckling (clean and cold)		
Fuel	Uranium (~90% U235); as ~35% uranium-aluminum alloy	k_{∞} (clean and cold)	Limited to about 1.002	
Fuel Cladding	None	k_{eff} (clean and cold)	About $8 \times 10^{-5}/^{\circ}\text{C}$	
Fuel tubes	Aluminum	δk (temperature)	Negligible	
Moderator	Paraffin base oil between fuel discs H ₂ O between fuel assemblies	δk (poisons)	Limited to about 1.002	
Reflector	Graphite	k_{eff} (hot and poisoned)		
Coolant	None	Conversion ratio	None	
Fertile material	None	NEUTRON FLUX DENSITIES		
Structural material	Aluminum	Fast	$3.6 \times 10^9 \text{ n}/(\text{cm}^2)(\text{sec})$	
Reactor atmosphere	None	Thermal: maximum (central column)	$1.6 \times 10^9 \text{ n}/(\text{cm}^2)(\text{sec})$	
Shield	Ordinary and high density concrete	average (in active section)	1 - 12 in. dia. internal, vertical, thermal column	
LATTICE TYPE	Cylindrical slab	EXPERIMENTAL FACILITIES	1 - external, horizontal thermal column	
DIMENSIONS		CAPITAL INVESTMENT		
Core	18 in. dia. x 18 in.	REFERENCES		
Reflector	About 2 1/3 ft thick	Feasibility Report for the KAPL Thermal Test Reactor, Knolls Atomic Power Laboratory, H.B. Stewart, et al, KAPL-436, 32 pp. Secret, Nov. 9, 1950		
Shield	6 ft thick	Supplement No. 1, Feasibility Report for the KAPL Thermal Test Reactor, Knolls Atomic Power Laboratory, H.B. Stewart, et al, Supplement No. 1 to KAPL-436, 25 pp, Secret, April 3, 1951		
Over-all	22 x 27 x 14 ft high			
STRATEGIC MATERIAL				
Fissionable material	U235; more than 2.6 kg			
Consumption	Negligible			
Burn-up	Negligible			
Average cycle time	Indefinite			
COOLING SYSTEM	None			
AUXILIARY FACILITIES				
OPERATING CONDITIONS				
Total heat power	100 watts			
Useful power output	0			
Innage	Indefinite			
Rod power (average)	5 watts			
Heat flux				
Power density (average)	2.4 watts			
Specific power (average)	0.04 kw/kg 25			
Maximum fuel temperature	Negligible			
Maximum moderator temperature	Negligible			
CONTROLS				
Shim	Provided by loading variation			
Regulator	2 - 1/2 in. dia., vertical, aluminum-clad cadmium rods			
Safety	4 - 1/2 in. dia., vertical, aluminum-clad cadmium rods			
Reactivity change	6 - 4 in. wide, 1/32 in. thick, iron-clad cadmium sheets			
	About 0.08			

CHAPTER 8.7

Unmoderated Heterogeneous Reactors

LOS ALAMOS FAST REACTOR (CLEMENTINE)

The fuel rods are held vertically in a close-packed array in a steel cage. Holes in the bottom and top plates of the cage allow mercury to flow from the bottom up around each slug and out the top plate. The over-all dimensions of the cage are $5\frac{7}{8}$ in. OD by $6\frac{7}{16}$ in. long. The fuel elements are located by recesses in the bottom plate and holes in the top plate. The cage is located at the bottom of a steel casing about 45 in. long. This casing, or pot, is closed by a top-tamper-plug 39 in. long made of uranium, steel, and shielding materials, which are enclosed in a steel shell welded close at both ends. Mercury enters the pot at the bottom from two tubes located on the outside of the pot, leading from above, and exits through an axial tube in the tamper plug.

Two steel plates, totalling 11 in., supported on a reinforced concrete pier serve as a base for the reactor. The tamper (reflector) volume, a 30-in. cube, contains the cage and pot in a column of uranium 8 in. by 8 in. by $17\frac{1}{2}$ in. high. On the four sides of the column are blocks of uranium (most of them silver plated) which are 5 in. thick. This, together with the pot tamper-plug, completes the $17\frac{1}{2}$ -in., cubical, uranium tamper, around which is a $\frac{1}{4}$ -in.-thick, water-cooled aluminum jacket. Surrounding the jacket are 6-in.-thick blocks of steel that complete the tamper to 30 in. Outside the tamper on the four sides and the top is a 4-in.-thick layer of lead and a $\frac{1}{32}$ -in., welded, aluminum jacket, encasing the entire tamper and lead shielding in a gas-tight envelope.

On one side of the reactor, a 4- by 4-in. block of bismuth extends through the tamper from the central uranium column to the gas-tight envelope. This serves as a window for the graphite thermal column, which steps up from about 30- by 30-in. to 6- by 6-ft over a 6-ft length. The thermal column has eight removable stringers and three transverse test holes. On the opposite face of the reactor a 6-in.-diameter by 11-in. thorium cylinder containing a $\frac{1}{2}$ -in.-diameter removable core extends from the central uranium column to the lead shield. One of the other faces has an 8- by 8-in. block of uranium containing a $\frac{3}{4}$ -in.-diameter removable core extending from the central uranium column to the lead shielding. The remaining face has a removable steel plug for a hole which extends in to the central uranium column. Four holes go completely through the tamper tangential to the central core and parallel to the uranium and steel windows. Ten vertical holes penetrate into various regions of the tamper.

Vertical control rods are located in the uranium tamper. These rods are driven by mechanisms located on the top shield and are scrambled through the reactor by gravity. The lower portions of the rods are made of uranium; the upper ends (of the control length) are made of sintered boron-10. This combination gives a maximum of control. Originally, as a safety feature, a portion of the uranium tamper below the core was designed to drop away from the assembly, but this system is no longer in use.

Table 8.7.1—Los Alamos Fast Reactor (Clementine)

LOCATION	Los Alamos Scientific Laboratory Los Alamos, New Mexico	Specific power (average)	
RESPONSIBLE ORGANIZATIONS		Maximum fuel temperature	266°F
Design	Los Alamos Scientific Laboratory	Maximum sheath temperature	
Construction	Los Alamos Scientific Laboratory	Coolant inlet temperature	86°F
Operation	Los Alamos Scientific Laboratory	Coolant outlet temperature	212°F
PURPOSE	Research	Coolant velocity	About 70 psia
STATUS	In operation since Nov., 1946	Coolant inlet pressure	7 psi
MATERIALS		Coolant pressure drop through reactor	9 l/min
Fuel	Plutonium	Pumping rate	5 kw
Fuel Cladding	Nickel coating 0.005 in. thick	Pumping power required	
Coolant tubes	Mild steel; 0.020 in. wall	CONTROLS	
Moderator	None	Shim	2 - 1 1/2 in. dia. vertical rods in reflector, half uranium and half sintered boron ¹⁰
Reflector	Uranium (natural); 1.36 metric tons	Regulator	2 - 1 1/2 in. dia. vertical rods in reflector, half uranium and half sintered boron ¹⁰
Coolant	Mercury	Safety	Reactivity change About 0.034
Fertile material	None	FUEL HANDLING	
Structural material	Steel	Charging	Remote grappling equipment
Reactor atmosphere	None	Discharging	Remote grappling equipment
Shield	Lead, iron, masonite, boron plastic and barytes concrete	NEUTRON FLUX DENSITIES ^a	
DIMENSIONS		Fast (maximum)	5 x 10 ¹²
Core	5 7/8 in. OD x 6 7/16 in.	Thermal (maximum)	5 x 10 ¹⁰
Reflector	Uranium; 5 3/4 in. Steel; 6 in.	EXPERIMENTAL FACILITIES	
Shield	About 11 x 15 x 9 ft high	1 - 0.55 in. dia., horizontal hole to core, enclosed by thorium cylinder through reflector	
Over-all		1 - 0.65 in. dia., horizontal hole to core, enclosed by thorium cylinder through reflector	
STRATEGIC MATERIAL		3 - 0.80 in. dia., horizontal holes, tangential to core	
Fissionable material		1 - 0.70 in. dia., horizontal hole, tangential to core	
Consumption	3 x 10 ⁻³ gm./day	4 - 0.90 in. dia., vertical holes in reflector	
Burn-up	Indefinite	1 - 30 x 30 in. horizontal, graphite thermal column with 8 removable stringers	
Average cycle time	Indefinite	3 - 2 x 2 in. horizontal, transverse holes through thermal column	
COOLING SYSTEM		CAPITAL INVESTMENT	Plutonium Fast Reactor at Los Alamos, Los Alamos Scientific Laboratory, Jane Hall, LAMS-567 (Revised), 45 pp, Secret, May 7, 1947
Type	Recirculated mercury	REFERENCES	
Coolant treatment	None		
Pumps	1 - AC electromagnetic pump		
AUXILIARY FACILITIES			
OPERATING CONDITIONS			
Total heat power	20 kw		
Useful power output	0		
Innage	0.5		
Rod power (average)	0.47 kw		
Heat flux (average)	20,800 BTU/(sq ft)(hr)		
Power density (average)	7.2 kw/l		

a. Estimated

SHIELDING

Outside the gas-tight aluminum casing are the laminated side shields comprised, from the center outward, of 3 in. of iron, 3 in. of masonite, 24 in. of iron and boron-plastic sheets alternated in 3-in. thicknesses, and 18 in. of poured barytes concrete. The top of the reactor is shielded by boron-plastic, iron, and removable concrete blocks.

The thermal column is shielded by $2\frac{1}{2}$ in. of boron-plastic, 0.040 in. of cadmium, and 8 in. of lead. The mercury coolant system is contained in a vault (in the main shield structure) provided with heavy lead doors supplemented by 12 in. of concrete blocks.

FUEL HANDLING

Fuel elements are removed from or placed in the core cage by removing sections of the top shield and the pot tamper-plug and handling the slugs with remotely operated grappling devices. After the core is partly unloaded, the entire pot may be removed and further dismantling done in a hot cell.

COOLING SYSTEM

Mercury is drawn from the heat exchanger by an AC electromagnetic pump which delivers the mercury to a reservoir tank at the top of the shielding. From the reservoir, the coolant flows through the reactor and then into the heat exchanger. The heat exchanger is made of helical coils cast in a copper cylinder. One coil is made of mild steel and carries the mercury; two are made of stainless steel and carry the water. To facilitate heat transfer, 1 ppm of titanium and 10 ppm of magnesium are added to the mercury.

EXPERIMENTAL BREEDER REACTOR (EBR)

The reactor structure is comprised of a bottom grid-plate (which positions the lower ends of the rods) hung by tie rods from a 4-in.-thick support and grid plate. Above this are the coolant inlet chamber, a separation plate, and the coolant outlet chamber. These components all fit inside a stainless-steel tank of double-wall construction. The bottom $24\frac{3}{4}$ in. of this tank fits closely around the uranium rod blanket to accommodate the external uranium blanket, which is made of stainless-steel-clad, uranium (natural) bricks stacked in the form of a cup $30\frac{1}{8}$ in. in diameter. Above this, the tank expands out to $23\frac{1}{2}$ in. ID over an 85-in. length with insulation bricks within the double wall structure. The external uranium cup is supported from below and is removed by lowering it into a sub-reactor room.

Twelve uranium rods, eight for safety and four for control, enter the external uranium cup from below; these are driven by mechanisms mounted on the cup elevator and are scrambled out of the reactor by compressed springs and cushioned pneumatically. Shim control is provided by height adjustment of the external uranium cup. An 8-in.-diameter plug of natural uranium at the bottom of the external blanket serves as a safety by dropping out of the blanket.

Around the reactor tank, a 19-in.-thick layer of graphite is built up as a reflector. This is extended out to effect the horizontal thermal column. Various experimental test and beam holes extend into and through the graphite.

SHIELDING

A steel thermal shield surrounds the graphite reflector. Around this is about $8\frac{1}{2}$ ft of concrete. The upper tank section is shielded by 2-in.-thick steel plates (drilled and broached to pass the fuel-elements) alternated with $8\frac{1}{2}$ -in. NaK-flooded spaces formed by

Table 8.7.2—Experimental Breeder Reactor (EBR)

LOCATION	National Reactor Testing Station Arco, Idaho	Innage	Indefinite
RESPONSIBLE ORGANIZATIONS		Rod power (average)	4.6 kw
Design	Argonne National Laboratory Austin Company of Cleveland, Ohio	Heat flux (average)	210,000 BTU/(sq ft)(hr)
Construction	Bechtel Corporation	Power density (average)	167 kw/l
Operation	Argonne National Laboratory	Specific power (average)	735°F
PURPOSE	Experimental	Maximum fuel temperature	635°F
STATUS	In operation	Maximum sheath temperature	482°F
MATERIALS		Coolant inlet temperature	662°F
Fuel	Uranium (~90% U235)	Coolant outlet temperature	6.7 ft/sec
Fuel Cladding	NaK (22.5 - 77.5%); 0.020 in. thick Stainless steel; 0.022 in. wall	Coolant inlet pressure	0.86 psi
Coolant tubes	None	Coolant pressure drop through reactor	300 gpm
Moderator	None	Pumping rate	
Reflector	Uranium (natural) blanket; 4.6 metric tons Graphite	Pumping power required	
Coolant	NaK (22.5 - 77.5%); 0.046 in. annulus U238 in blanket	CONTROL	
Fertile material	Stainless steel	Shim	Stainless steel clad, natural uranium, external reflector
Structural material	Argon	Regulator	4 - 1.584 in. dia., vertical, stainless steel clad, uranium rods in reflector
Reactor atmosphere	Concrete	Safety	8 - 1.584 in. dia., vertical, stainless steel 1 - 8 in. dia. movable section of uranium reflector beneath core
Shield		Reactivity change	0.062
DIMENSIONS		FUEL HANDLING	
Core	Uranium; about 9 in. thick Graphite; 19 in. thick	Charging	Inserted manually
Reflector	Modified octagon: 7 1/2 ft across flats by 14 ft high	Discharging	Withdrawn in inert gas atmosphere into lead coffin
Over-all		NEUTRON FLUX DENSITIES	
STRATEGIC MATERIAL		Fast (maximum)	$2 \times 10^{14} \text{ n}/(\text{cm}^2)(\text{sec})$
Fissionable material		Thermal	22 - vertical thimbles into graphite reflector and thermal column
Consumption	About 1 gm/day	EXPERIMENTAL FACILITIES	
Burn-up	About 50 days	2 - horizontal through holes in graphite reflector and thermal column	
Average cycle time	About 50 days	2 - horizontal, graphite thermal columns with 8 in. beam holes	
COOLING SYSTEM		2 - horizontal, 9 in. beam holes	
Type	Batchwise filtering	1 - horizontal, 10 in. beam hole	
Coolant treatment	1 - DC electromagnetic pump	5 - horizontal, 4 in. test holes	
Pumps	1 - tank type pump (stand-by)		
Safety	Convection air cooling of secondary coolant		
AUXILIARY FACILITIES		CAPITAL INVESTMENT	\$2.7 x 106
Power production	Steam generator and 125 kw turbo-generator	REFERENCES	Feasibility Report Fast Neutron Reactor for a Test of Conversion, Argonne National Laboratory, ANL-4356, 84 pp, Secret, October 14, 1949
Operating conditions			Physics of EBR, Letter to N.E. Huston, Argonne National Laboratory, H.H. Hummel, ANL-MH-67, 1 p, Secret, October 7, 1952
Total heat power	1400 kw		
Useful power output	200 kw		

spacer collars. The thermal columns are shielded by lead and laminated iron-masonite combinations. The experimental openings are shielded with appropriate plugs. The primary NaK circuit is shielded by $3\frac{1}{2}$ ft of concrete.

FUEL HANDLING

The internal rods are removed by withdrawing them upward into a lead coffin in an atmosphere of dry helium or nitrogen. The uranium cup is lowered into a sub-reactor room; it may then be removed to an adjacent shielded cell, provided with a remotely controlled crane, to disassemble the cup and place the bricks in suitable casks.

COOLING SYSTEMS

PRIMARY SYSTEM

NaK alloy (22.5 percent sodium, 77.5 percent potassium) for the reactor is contained in an upper storage tank with a capacity of approximately 3,000 gal. The coolant flows from this tank by gravity to the entrance chamber above the reactor core. From here it flows downward past the uranium blanket rods and then back up through the core. It leaves the reactor from an outlet chamber directly above the inlet chamber, although the surface of the NaK is near the top of the tank shield plug where an overflow line is provided. After leaving the reactor, the alloy drops into an expansion tank from which it flows through the heat exchanger to a receiver tank. A DC electromagnetic pump delivers the NaK from the receiver tank back to the storage tank to complete the circuit.

SECONDARY SYSTEM

The secondary NaK system is not shielded. The alloy flows from the heat exchanger either to a finned-tube air cooler or to a super-heater and steam generator when power production is desired.

CHAPTER 8.8

Graphite-moderated Homogeneous Reactors

LOW-POWER RESEARCH REACTOR (LPRR)

This reactor was designed specifically for private use, and accordingly the principle design emphasis was on safety. The reactor consists of a uranium-impregnated graphite core with a graphite reflector. Each fuel-element block measures 4.187- by 4.187- by 21 in. and is impregnated with uranium (~90 percent U^{235}). The blocks have 1.25-in.-diameter axial holes so that they may be slipped over vertical, bayonet-type cooling tubes, 1.25 in. in diameter and having $\frac{1}{8}$ -in. walls and $\frac{1}{8}$ -in. diametrical webs which divide the tubes into two chambers so that coolant may flow up one chamber and down the other. The 70 coolant tubes form an approximately circular pattern and are spaced on 4.248-in.-centers in a square array. This allows 0.060-in. clearance for expansion between the graphite blocks which slip over the tubes. Each coolant tube passes through two fuel-bearing blocks and two 24-in.-long plain-graphite blocks, one plain block above and one below the 42-in. active section to serve as top and bottom reflector, respectively. Additional odd-shaped blocks fill out the core assembly to form a 46-in.-diameter cylinder enclosed in a vacuum-tight 0.204-in.-wall aluminum tank. The bottom of the tank is made of three parallel 0.375-in. aluminum plates, $1\frac{1}{2}$ in. apart, forming inlet and outlet plenum chambers to which the double-chambered coolant tubes are appropriately welded. The coolant tubes are also welded to and support the top aluminum plate of the tank. Aluminum angles welded on the outside of the tank wall serve as stiffeners to prevent collapse of the tank when evacuated. At start-up, the tank is evacuated and then sealed under a helium atmosphere of 1 cm of Hg. The aluminum angles also support the transition reflector blocks which carry the circular cross section of the tank into the octagonal cross section of the reflector and shield.

An axial sleeve, occupying the space provided by the omission of two adjacent fuel elements, contains an unimpregnated graphite element flanked by two safety rods. The graphite element may be replaced with a standard fuel element to compensate for burn-up. On a centered 15-in.-radius circle are sleeves for four shim rods. These, like the central thimble, are welded to the top and bottom of the tank. All sleeves are cooled by D_2O circulated in $\frac{1}{4}$ -in. aluminum tubing welded to the corners of the sleeves. The regulator rod thimble is welded to the outside of the core tank.

A steel support plate at the top of the tank is provided with lifting lugs so that the whole tank unit can be raised. A thin perforated-aluminum jacket around the unit keeps the transition reflector blocks in place on their supports.

Around the core unit, graphite blocks are stacked permanently in the form of an octagonal ring. These complete the 28-in. reflector. The reflector and the core tank rest on a steel bed-plate which is accurately leveled. Through this bed-plate pass the D_2O coolant lines to disconnect joints in the sub-reactor room.

Table 8.8.1—Low Power Research Reactor (LPRR)

LOCATION	North American Aviation, Inc.
RESPONSIBLE ORGANIZATIONS	
Design	Construction
Operation	Research
PURPOSE	Design study
STATUS	
MATERIALS	
Fuel	Uranium (~90%); as UO ₂ in graphite
Fuel Cladding	Aluminum; 1/8 in. wall
Coolant tubes	Graphite; 1/3 metric tons
Moderator	Graphite; 20 metric tons
Reflector	D ₂ O
Coolant	270 kg
Total D ₂ O requirement	None
Fertile material	Aluminum and graphite
Structural material	Helium (low pressure)
Reactor atmosphere	Steel and iron-ore-colemanite concrete
Shield	Homogeneous
LATTICE TYPE	
DIMENSIONS	
Core	46 in. dia. x 42 in. high
Reflector	28 in. on sides; 24 in. on top and bottom
Shield	Steel; 1 in. Concrete; 72 in.
Over-all	Octagonal prism; 20 2/3 ft across flats x 14 1/3 ft high
STRATEGIC MATERIAL	
Fissionable material	U ²³⁵ ; 4 kg
Consumption	6.3 x 10 ⁻² gm/day
Burn-up	5%
Average cycle time	32,000 hrs
COOLING SYSTEM	
Type	Recirculated D ₂ O
Coolant treatment	Ion exchange demineralization
Pumps	Not specified
AUXILIARY FACILITIES	
OPERATING CONDITIONS	
Total heat power	150 kw
Useful power output	0
Innage	4100 BTU/(sq ft)(hr)
Heat flux (average)	0.18 kw/l
Power density (average)	37.5 kw/kg 25
Specific power (average)	465°F
Maximum fuel-block temperature	140°F
Coolant inlet temperature	158°F
Coolant outlet temperature	0.657 ft/sec
Coolant velocity	About 5 psig
Coolant inlet pressure	Negligible
Coolant pressure drop through reactor	50 gpm
Pumping rate (D ₂ O)	4 3/4 hp
Pumping power required (total)	

Shim	4 - 2 in. dia. vertical rod of boron carbide filled stainless steel tubing plus a moderator section
Regulator	1 - 1 in. dia. vertical rod of boron carbide filled stainless steel tubing
Safety	2 - 2 x 4 in. vertical rods of boron carbide filled stainless steel cans
Reactivity change	0.275
FUEL HANDLING	
Charging	Core tank with all fuel handled as a unit
Discharging	
PHYSICS a	
Resonance escape (clean and cold) b	0.8666
Thermal utilization (clean and cold)	0.8903
Diffusion length squared (clean and cold)	129 cm ²
Age (clean and cold)	383 cm ²
Buckling (clean and cold)	
Prompt neutron lifetime	1.15 x 10 ⁻³ sec
k _∞ (clean and cold)	1.9
k _{eff} (clean and cold)	1.095
β k (temperature)	-4 x 10 ⁻⁴ /°C
β k (poisons)	-0.0175
k _{eff} (hot and poisoned)	1.035
Conversion ratio	None
NEUTRON FLUX DENSITIES	
Fast: average	3.5 x 10 ¹² n/(cm ²)(sec)
Thermal (average)	1.2 x 10 ¹² n/(cm ²)(sec)
EXPERIMENTAL FACILITIES: 2 - 3 in. dia. horizontal holes tangential to core tank	
1 - 6 in. dia. horizontal hole extending to core tank	
6 - 3 1/2 in. dia. horizontal holes extending to core tank	
2 - 2 in. dia. horizontal pneumatic tubes tangential to core tank	
6 - 3 in. dia. vertical tubes in reflector for multiple specimen irradiations	
1 - 4 1/2 x 4 1/2 ft horizontal thermal column	
CAPITAL INVESTMENT	\$6 x 10 ⁵
REFERENCES	A Low Power Research Reactor Engineering Design Report, North American Aviation, Inc., in preparation

- a. Preliminary calculations
b. Escape from capture in epithermal region

SHIELDING

No thermal shield is required for this reactor. The biological shield consists of heavy-aggregate concrete poured in $\frac{1}{2}$ -in. steel form plates. Stepped plugs are used for experimental openings. An access plug in the top shield, over the reactor tank, can be lifted out as a unit. The D_2O system is located beneath the reactor and is shielded by 10-in. concrete walls.

FUEL HANDLING

The core tank is handled as a unit and is removed by removing the shielding access plug over the tank. A lead coffin is then inserted in the space provided by removal of the plug. After disconnecting the D_2O coolant lines, the entire core assembly is drawn up into the coffin in which it is transported to a hot-cell disassembly area. This is expected to occur only after about 15 years of operation.

COOLING SYSTEM

D_2O is pumped from the sump tank through the reactor, the heat exchangers, and back into the sump tank at a rate of 50 gal/min. Approximately 1 gal/min is by-passed through the ion-exchange columns for demineralization. Light water is pumped through the heat exchangers and a cooling tower at a rate of 138 gal/min as a secondary fluid. There is no treatment of the light water.

Light-water-moderated Homogeneous Reactors

LOS ALAMOS WATER BOILER (SUPO)

The core consists of a solution of uranium (88.7 percent U^{235}) as uranyl nitrate in water contained within (3.1 to 5 cm from the top) a stainless-steel sphere, 12 in. in diameter with a $\frac{3}{64}$ -in. wall. This sphere also contains three 20-ft-long coils of $\frac{1}{4}$ -in.-OD by $\frac{1}{32}$ -in.-wall stainless-steel tubing in parallel for cooling water, a 1-in.-ID "glory hole" tube, and two reentrant thimbles to accommodate $\frac{9}{16}$ -in.-diameter control rods. Above the sphere and joined to it is a pipe (or stack) containing a water-cooled condenser as part of the recombiner circuit through which air and decomposition gases are circulated. The inlet and outlet coolant tubes are welded into the upper half-shell, whereas the solution-transfer tube joins the bottom half-shell at its lowest point. The core is surrounded by the graphite reflector, which extends out to form two opposite thermal columns. The cadmium-sheet control rods enter the reflector vertically and are approximately tangent to the core. All rods scram into the reactor by gravity.

SHIELDING

Immediately around the reflector are layers of boron carbide, steel, and lead (except in the thermal columns which have bismuth windows). The shield is completed by poured concrete. The region above the reactor core contains the recombiner assembly, and the shielding is pieced out around this with steel, lead, and borax paraffin blocks and canned limonite-mix. The fixed shield on one thermal column is made of boron carbide-paraffin and lead blocks supplemented with an internal boron carbide-paraffin shutter. The shield for the other thermal column is mounted on wheels and consists of canned limonite-mix, boron carbide-paraffin, lead, and steel.

FUEL HANDLING

A transfer flask is located in a shielded vault above the reactor. By evacuating this flask, solution is drawn into the flask through a tube joining it and the bottom of the reactor tank. Conversely, air pressure applied to solution in the flask drives it into the reactor tank. Appropriate valves in the transfer tank allow samples to be removed or permit complete unloading of the core by transfer to shielded flasks of one-liter capacity.

COOLING SYSTEM

Process water, under a static head of 60 ft, is filtered and used to cool the core solution. No provision is made for decay retention.

RECOMBINER

A 120 1/min centrifugal blower circulates air drawn through a stainless-steel-wool trap from the core tank through one of two catalyst chambers, an external condenser, and down

Table 8.9.1 — Los Alamos Water Boiler (SUPO)

LOCATION	Los Alamos Scientific Laboratory
RESPONSIBLE ORGANIZATIONS	
Design	Los Alamos Scientific Laboratory
Construction	Los Alamos Scientific Laboratory
Operation	Los Alamos Scientific Laboratory
PURPOSE	In operation, with design variations, since May, 1944
STATUS	
MATERIALS	
Fuel	Uranium (88.7% U ²³⁵), 980 gm as uranyl nitrate solution
Coolant tubes	Stainless steel, 1/4 in. OD x 1/32 in. wall
Moderator	H ₂ O
Reflector	Graphite
Coolant	H ₂ O
Fertile material	None
Structural material	Stainless steel
Reactor atmosphere	Air
Shield	Boron carbide, paraffin, steel, lead and concrete
LATTICE TYPE	Homogeneous
DIMENSIONS	
Core	12 in. dia
Reflector	21 1/2 in. thick or greater
Shield	Boron carbide plus paraffin; 1/2 in. Steel; 2 in. Lead; 4 in. Concrete; 5 ft
Over-all	15 x 15 x 11 ft high
STRATEGIC MATERIAL	
Fissionable material	U ²³⁵ ; 895 gms
Consumption	About 5 x 10 ⁻³ gm/day
Burn-up	Indefinite
Average cycle time	Indefinite
COOLING SYSTEM	
Type	H ₂ O
Coolant source	Well water
Coolant treatment	Filtered
Pumps	None
Retention basin	None
AUXILIARY FACILITIES	
Reactor atmosphere	Recirculated air system
OPERATING CONDITIONS (typical)	
Total heat power	35 kw
Useful power output	0
Innage	0.3 to 0.4
Heat flux (average)	28,000 BTU/(sq ft)(hr)
Power density (average)	2.8 kw/l
Specific power (average)	39 kw/kg
Average fuel solution temperature	180°F
Coolant inlet temperature	60°F
Coolant outlet temperature	130°F
Coolant velocity	60 psi
Coolant inlet pressure	
Coolant pressure drop through reactor	About 60 psi
Pumping rate	3 1/4 gpm
Pumping power required	None
CONTROLS	
Shim	Solution concentration and regulator rods
Regulator	2 - 9/16 in. dia. x 18 in., vertical boron ¹⁰ steel jacketed (cadmium plated) rods extending into core
Safety	2 - 1/32 x 3 x 30 in., vertical, aluminum clad cadmium sheets
Reactivity change	1 - 1/32 x 3 x 30 in., vertical, aluminum clad cadmium sheet
FUEL HANDLING	
Charging	Transfer flask with fluid
Discharging	control by air pressure variation
PHYSICS	
Resonance escape (clean and cold)	0.71
Thermal utilization (clean and cold) ^a	1.47 cm ²
Diffusion length squared (clean and cold) ^a	33 cm ²
Age (clean and cold) ^a	1.44
Prompt neutron lifetime	
Buckling (clean and cold)	
k ₀₀ (clean and cold)	
k ₀₀ (clean and cold) ^a	
δk (temperature)(true)	-2.4 x 10 ⁻⁴ /°C
δk (temperature)(apparent at operating level)	-3.5 x 10 ⁻⁴ /°C
δk (poisons)	
k _{eff} (hot and poisoned)	
Conversion ratio	None
NEUTRON FLUX DENSITIES ^a	
Fast (maximum)	4.2 x 10 ² n/(cm ²)(sec)(watt)
Epithermal (maximum)	6.2 x 10 ² n/(cm ²)(sec)(watt)
Thermal (maximum)	3.8 x 10 ⁷ n/(cm ²)(sec)(watt)
EXPERIMENTAL FACILITIES	
1 - 1 in. dia., horizontal test hole through reactor core	
1 - 1 7/16 in. dia. horizontal test hole tangent to reactor core	
2 - horizontal, graphite thermal columns (1 - 4 x 4 ft and 1 - 5 x 5 ft), with several removable stringers	
CAPITAL INVESTMENT	The Los Alamos Homogeneous Reactor, Supo Model, Los Alamos Scientific Laboratory, L.D.P. King, LA-1301, October, 1951
REFERENCES	
a. Estimated	

through the stack of the core tank with its reflux condenser. Small bleed-valves permit fresh air to be admitted and cycled air to be discharged to an exhaust stack. The catalyst chambers contain platinized alumina pellets to recombine decomposed water.

HOMOGENEOUS REACTOR EXPERIMENT (HRE)

This is a light-water-moderated, heavy-water-reflected, circulating-fuel reactor designed to demonstrate the feasibility and to yield operational experience in the handling of such a system. A full, 50-liter spherical core, UO_2SO_4 (~90 percent U^{235}) concentration = 45 gm/liter, operates at 482°F and 1000 psi. A circulation of 100 gal/min through a 6-liter heat exchanger removes 1000 kw of heat in the form of 200-psi steam. Stainless steel is needed for all parts in contact with the fuel solution.

The spherical shell has a $\frac{3}{16}$ -in. wall and will withstand internal pressures in excess of 1000 psi if necessary. In operation, this shell is under a slight external pressure (about 20 psi) since the enveloping reflector is maintained at a higher pressure than the fuel solution. The inlet pipe is welded to the core and introduces the fuel tangentially in the horizontal diametrical plane to rotate the liquid within the core. This centrifugal action causes the bubbles formed in the solution to move rapidly to the vertical axis where they are drawn off through a gas tube and conveyed to a recombiner, which operates at atmospheric pressure.

The fuel outlet and the connection to the pressurizer are located at the top of the sphere, concentric to the gas outlet pipe. An outlet at the bottom of the core connects to the dump-tank system. This includes two dump-tanks, a heat exchanger, a pulsafeeder pump, an evaporator, a condensate tank, and finned water-to-air coolers for natural convection cooling of the material in the dump-tanks. Solution is pumped through the dump-tank circuit during normal operation at about 1 gal/min. This represents the working fluid for shim-ming by concentration variation.

The pressurizer for the reactor core consists of a cylindrical tank mounted above the core with an interconnecting line between the two. There is little solution hold-up, and the vapor space above the liquid provides ample space for any sudden pressure surges. The pressure is maintained and controlled by the equilibrium temperature between the liquid and vapor. The liquid in the pressurizer is heated by thermal circulation through a small heater tank mounted beside and connected to the pressurizer.

The reflector vessel is made of forged steel and designed (by ASME standards) for an internal pressure of 2000 psi, giving a total safety factor of 10 over the 1000 psi normal operating pressure. The cup for the pressure vessel supports the core, the pressurizer, and the control rods with their drive mechanisms. The lower part of the reflector tank is pierced by six instrument thimbles which extend in to the core tank. At the bottom of the reflector tank is the reflector outlet and dump line.

The safety and shim rod controls consist of clad boral plate assemblies, curved into spherical segments coaxial with the vertical core axis. These scram into the reflector by gravity plus spring loading. The regulator rod is similar but consists of only one poison plate.

SHIELDING

The shielding is comprised of barytes-concrete blocks stacked to form compartments which contain the core, fuel-solution system, reflector system, and steam-generating system. The inner blocks also contain colemanite ore and are unmortared. For gas-tightness and stability, the outer blocks are mortared. Access to the components is provided by removable shield plugs above the assembly.

Table 8.9.2 — Homogeneous Reactor Experiment (HRE)

LOCATION	Oak Ridge National Laboratory Oak Ridge, Tennessee	CONTROLS	Shim	1 - assembly of stainless steel clad, boron sheets in the form of cylindrical segments, tangential to core in reflector, Variation of fuel concentration Variation of reflector level
RESPONSIBLE ORGANIZATIONS		Regulator	1 - stainless steel clad, boron sheet in the form of a cylindrical segment, tangential to core in reflector	
Design	Oak Ridge National Laboratory	Safety	1 - assembly of stainless steel clad, boron sheets in the form of cylindrical segments, tangential to core in reflector	
Construction	Oak Ridge National Laboratory	Reactivity change (rods only)	Quick dump of core tank	0.014
Operation	Oak Ridge National Laboratory	FUEL HANDLING		
PURPOSE	Oak Ridge National Laboratory	Charging	Pump injection into circulating system	
STATUS	In operation since April, 1952	Discharging	Drain to dump tanks	
MATERIALS		PHYSICS ^a		
Fuel	Uranium (~90%); 1.6 to 2.1 kg as UO ₂ SO ₄ in water	Resonance escape	0.996	
Coolant tubes	None	Thermal utilization (clean and cold)		
Moderator	H ₂ O	Diffusion length squared (clean and cold)		
Reflector	D ₂ O	Age (clean and cold)	33 cm ²	
Total D ₂ O requirement	About 0.5 metric ton	Buckling (clean and cold)		
Coolant	Circulating fuel	Prompt neutron lifetime	7 x 10 ⁻⁵ sec	
Fertile material	None	k _∞ (clean and cold)	About 1.6	
Structural material	Stainless steel	k _{eff} (clean and cold)		
Reactor atmosphere	Decomposition and fission product gases	β _k (temperature)	About -6 x 10 ⁻⁴ /°C	
Shield	Steel and barytes concrete	β _k (poisons)		
LATTICE TYPE	Homogeneous	k _{eff} (hot and poisoned)		
DIMENSIONS		Conversion ratio	None	
Core	18 in. ID sphere	NEUTRON FLUX DENSITIES ^a		
Reflector	10 in. thick	Thermal: average	1.88 x 10 ¹³ n/(cm ²)(sec)	
Shield	7 ft thick or more	EXPERIMENTAL FACILITIES	None	
Over-all	22 x 26 x 18 2/3 ft high	CAPITAL INVESTMENT		
STRATEGIC MATERIAL		REFERENCES	Homogeneous Reactor Experiment Feasibility Report, Oak Ridge National Laboratory, ORNL-730, 108 pp, Secret, July 6, 1950	
Fissionable material (total)	U ₂₃₅ ; 2.7 to 3.6 kg		Homogeneous Reactor Project Quarterly Progress Report, Oak Ridge National Laboratory, ORNL-1318, 184 pp, Secret, Sept. 19, 1952	
Consumption	About 1 gm/day			
Burn-up	Indefinite			
Average cycle time	Indefinite			
COOLING SYSTEM				
Type	Recirculated liquid fuel			
Coolant treatment	Batch processing			
Pumps	1 - 100 gpm, Westinghouse Model 100A sealed armature, centrifugal pumps			
Safety	Natural convection cooling system			
AUXILIARY FACILITIES				
Moderator cooling	Circulation of D ₂ O through heat exchangers			
Power production	1 - 250 kw steam turbo-generator			
OPERATING CONDITIONS				
Total heat power	1000 kw			
Useful power output	About 120 kw (design)			
Innage	Indefinite			
Power density (average)	20 kw/l			
Specific power (average)	About 600 kw/kg 25 in core			
Fuel solution inlet temperature	407°F			
Fuel solution outlet temperature	482°F			
Fuel solution inlet pressure	1000 psia			
Fuel solution pressure drop through reactor	Negligible			
Pumping rate	100 gpm			
Pumping power required (total)	25 kw			

a. Estimated

COOLING SYSTEM

The fuel solution is pumped into the reactor core by a 100-gal/min centrifugal pump. From the core, the fuel passes through a heat exchanger and returns to the pump; about 1 gal/min is circulated through the feed line. The off-gases are circulated through a condenser, a flame recombiner, a catalytic recombiner, and final condenser; the condensate from the latter is returned to the dump tanks. The condensate from the first condenser is pumped into the fuel-circulating pump at about 1 gal/min to purge the bearings and reduce corrosion.

MODERATOR COOLING SYSTEM

D₂O is pumped from the reflector tank outlet through a heat exchanger and back into the reflector tank at about 30 gal/min. Off-gases are circulated through a condenser, catalytic combiner, and a final condenser, the condensate being returned to the D₂O feed-system which delivers about 1 gal/min to the circulating system. D₂O enters the reflector tank at 302°F and leaves it at 347°F.

POWER CONVERSION SYSTEM

The reflector heat exchanger preheats the boiler feed water from 125°F to 286°F at 200 psi. The fuel solution heat exchanger delivers 3000 lb/hr of 200 psi saturated steam to the 250-kw turbo-generators. When power is not being generated, the steam is by-passed directly to the condenser. Building steam may also be bled off the high-pressure steam line.

Appendix

APPENDIX

Table A.1 — Conversion Factors

Multiply	By	To obtain
Energy		
Btu	6.59×10^{15}	mev
Btu	1054.8	joules
Btu	2.930×10^{-4}	kw-hr
Btu	3.929×10^{-4}	hp-hr
Btu	252	gm-cal
cal (15°)	2.6126×10^{19}	ev
cal (15°)	4.1855×10^7	ergs
cal (15°)	4.1855	joules
ergs	6.2421×10^{11}	ev
ergs	10^{-7}	joules
ergs	2.3892×10^{-8}	cal (15°)
ev	1.60203×10^{-12}	ergs
ev	1.60203×10^{-19}	joules
ev	3.8276×10^{-20}	cal (15°)
gm	5.6095×10^{32}	ev
gm	8.9866×10^{20}	ergs
gm	8.9866×10^{13}	joules
gm	2.1471×10^{13}	cal (15°)
gm-cal	2.616×10^{13}	mev
gm-cal	4.186	joules
gm-cal	1.163×10^{-6}	kw-hr
gm-cal	1.559×10^{-6}	hp-hr
gm-cal	3.969×10^{-3}	Btu
hp-hr	1.677×10^{19}	mev
hp-hr	2.684×10^6	joules
hp-hr	0.7457	kw-hr
hp-hr	6.413×10^5	gm-cal
hp-hr	2545	Btu
joules	6.25×10^{12}	mev
joules	2.778×10^{-7}	kw-hr
joules	3.722×10^{-7}	hp-hr
joules	0.2389	gm-cal
joules	9.480×10^{-4}	Btu
joules	6.2421×10^{18}	ev
joules	1×10^7	ergs
joules	0.23892	cal (15°)
kw-hr	2.25×10^{19}	mev
kw-hr	3.6×10^6	joules
kw-hr	1.341	hp-hr
kw-hr	8.60×10^5	gm-cal
kw-hr	3.413×10^3	Btu
mev	1.6×10^{-13}	joules
mev	4.44×10^{-20}	kw-hr
mev	5.95×10^{-20}	hp-hr
mev	3.82×10^{-14}	gm-cal
mev	1.517×10^{-16}	Btu
Time		
days	2.738×10^{-3}	yr
days	24	hr
days	1440	min
days	8.640×10^4	sec
hr	1.141×10^{-4}	yr
hr	0.04167	days
hr	60	min
hr	3600	sec

ENGINEERING

Table A.1 — Continued

Multiply	By	To obtain
Time		
min	1.901×10^{-6}	yr
min	6.944×10^{-4}	days
min	1.667×10^{-2}	hr
min	60	sec
sec	3.169×10^{-8}	yr
sec	1.157×10^{-5}	days
sec	2.778×10^{-4}	hr
sec	1.667×10^{-2}	min
yr	365.26	days
yr	8766	hr
yr	5.260×10^5	min
yr	3.156×10^7	sec
Length		
cm	0.01	m
cm	.3937	in.
cm	.03281	ft
ft	.3048	m
ft	30.48	cm
ft	12	in.
in.	0.0254	m
in.	2.54	cm
in.	0.0833	ft
meters	100	cm
meters	39.37	in.
meters	3.281	ft.
microns	10^{-6}	meters
microns	10^{-4}	cm
microns	3.937×10^{-5}	in.
microns	3.281×10^{-6}	ft
Volume		
cu cm	10^{-6}	m ³
cu cm	6.102×10^{-2}	in. ³
cu cm	2.642×10^{-4}	gal
cu cm	3.531×10^{-5}	ft ³
cu cm	1.308×10^{-6}	yd ³
cu ft	2.832×10^{-2}	m ³
cu ft	2.832×10^4	cm ³
cu ft	1728	in. ³
cu ft	28.32	liters
cu ft	3.704×10^{-2}	yd ³
cu ft	7.481	gal
cu in.	1.639×10^{-5}	m ³
cu in.	16.39	cm ³
cu in.	5.787×10^{-4}	ft ³
cu meter	1×10^6	cm ³
cu meter	6.102×10^4	in. ³
cu yd	7.646×10^5	cm ³
cu yd	27	ft ³
cu yd	764.6	liters
cu yd	202	gal
gal	3785	cm ³
gal	0.1337	ft ³
gal	3.785	liters
gal	4.951×10^{-3}	yd ³
liters	1000	cm ³

APPENDIX

Table A.1 — Continued

Multiply	By	To obtain
Volume		
liters	3.531×10^{-2}	ft ³
liters	1.308×10^{-3}	yd ³
liters	0.2642	gal
Angular displacement		
deg	1.745×10^{-2}	rad
deg	2.778×10^{-3}	rev
rad	57.3	deg
rad	0.1592	rev
rev	360	deg
rev	6.283	rad
Pressure		
atm	76	cm Hg
atm	1033	gm/cm ²
atm	2177	lb/ft ²
atm	14.70	lb/in. ²
cm Hg	1.316×10^{-2}	atm
cm Hg	13.6	gm/cm ²
cm Hg	27.85	lb/ft ²
cm Hg	0.1934	lb/in. ²
gm/cm ²	9.678×10^{-4}	atm
gm/cm ²	7.356×10^{-2}	cm Hg
gm/cm ²	2.048	lb/ft ²
gm/cm ²	1.422×10^{-2}	lb/in. ²
lb/ft ²	4.725×10^{-4}	atm
lb/ft ²	3.591×10^{-2}	cm Hg
lb/ft ²	0.4882	gm/cm ²
lb/ft ²	6.944×10^{-3}	lb/in. ²
lb/in. ²	6.804×10^{-2}	atm
lb/in. ²	5.171	cm Hg
lb/in. ²	70.3	gm/cm ²
lb/in. ²	144	lb/ft ²
Density		
gm/cm ³	1×10^3	gm/liter
gm/cm ³	62.43	lb/ft ³
gm/liter	1×10^{-3}	gm/cm ³
gm/liter	6.243×10^{-2}	lb/ft ³
lb/ft ³	1.602×10^{-2}	gm/cm ³
lb/ft ³	16.02	gm/liter
Thermal conductivity		
Btu/(hr)(°F)(ft)	4.134×10^{-3}	gm-cal/(sec)(°C)(cm)
Btu/(hr)(°F)(ft)	12	Btu/(hr)(°F)(ft ² /in.)
Btu/(hr)(°F)(ft ² /in.)	3.44×10^{-4}	gm-cal/(sec)(°C)(cm)
Btu/(hr)(°F)(ft ² /in.)	8.33×10^{-2}	Btu/(hr)(°F)(ft)
gm-cal/(sec)(°C)(cm)	241.9	Btu/(hr)(°F)(ft)
gm-cal/(sec)(°C)(cm)	2903	Btu/(hr)(°F)(ft ² /in.)

Table A.2—Selected Physical Constants of the Elements

Element	Thermal-neutron absorption cross section, barns/atom	Density near 20°C, gm/cm ³	Melting point, °C	Boiling point, °C	Specific heat near 20°C, cal/(gm)(°C)	Coefficient of linear thermal expansion near 20°C, per °C × 10 ⁻⁶	Thermal conductivity near 20°C, cal/(sec)(cm)(°C)	Electrical resistivity, microhm-cm	Crystal structure*	Goldschmidt atomic radius, Å
Actinium	1,600
Aluminum	0.215	2.699	600.2	2,327	0.215	23.8	0.503	2.655 (20°C)	FCC	1.43
Americium
Antimony	6.4	6.62	630.5	1,440	0.049	8.5–10.8	0.045	39.0 (0°C)	R	1.61
Argon	0.62	1.6626 × 10 ⁻³	-189.4	-185.8	.125	...	0.406 × 10 ⁻⁴	...	FCC	1.92
Arsenic	4.1	5.73	814	610	.082	4.7	...	35 (0°C)	R	(1.25)
Barium	1.17	3.5	704	1,640	.068	BCC	2.24
Beryllium	0.0090	-1.85	1,315	2,970	.43	11.6	0.38	5.9 (0°C)	CPH	1.13
Bismuth	.032	9.80	271	1,627	.29	13.4	.019	106.8 (0°C)	R	1.82
Boron	750	2.3	2,000–2,300	2,550	.263	8.3	...	1.8 × 10 ⁻⁴ (0°C)	T-H	0.97
Bromine	6.5	3.12	-7.2	58	.070	O	(1.19)
Cadmium	2,400	8.65	321	765	.055	31.8	0.22	7.51 (18°C)	CPH	1.52
Calcium	0.43	1.55	850	1,440	.149	22	.3	3.43 (0°C)	FCC	1.97
Carbon (Graphite)	.0045	2.22	3,700	4,830	.165	0.6 × 4.3	.057	1,375 (0°C)	H	0.77 ₈
Cerium	.70	6.78	780	2,420	.043	75–90 (20°C)	FCC	1.82
Cesium	29.0	1.9	28	690	.052	97	...	18.83 (0°C)	BCC	2.70
Chlorine	31.6	...	-101	-34.7	.116	...	0.172 × 10	...	T	(1.07)
Chromium	2.9	7.19	1,890	2,500	.11	6.2	0.16	13 (28°C)	BCC	1.28
Cobalt	34.8	8.8	1,495	2,800	.102	14.2	.165	5.6 (0°C)	CPH	1.25
Columbium (Niobium)	1.1	8.57	2,415065	7.1	...	13.1 (18°C)	BCC	1.47
Copper	3.59	8.96	1,083	2,600	.092	16.5	0.94	1.673 (20°C)	FCC	1.28
Curium
Dysprosium	1,100	8.56	1,400	CPH	1.77
Erbium	166	9.16	>1,440	CPH	1.75
Europium	4,500	5.22	BCC	2.04
Fluorine	<0.010	...	-223	-188.2	0.18
Francium
Gadolinium	44,000	7.95	~1,200	CPH	1.80
Gallium	2.71	5.91	29.78	2,070	0.079	18	...	53.4 (0°C)	OFCC	2.7
Germanium	2.35	5.36	958073	89,000 (0°C)	DC	1.39
Gold	94	19.32	1,063	2,970	.031	14.2	0.71	2.19 (0°C)	FCC	1.44
Hafnium	115	13.36	2,130035	5.9	...	32.7 (0°C)	CPH	1.59
Helium	0.0068	0.1664 × 10 ⁻⁴	-271.4	-268.9	1.25	...	3.32 × 10 ⁻⁴	...	CPH	...
Holmium	64	8.76	~1,200	CPH	1.76
Hydrogen	0.330	0.08375 × 10 ⁻⁴	-259.4	-252.7	3.45	...	4.06 × 10 ⁻⁴	...	H	0.46
Illium
Iodine	180	7.31	156.4	...	0.057	33	0.067	8.37 (0°C)	FCT	1.57
Iridium	6.7	4.93	114	183	.052	93	10.4 × 10 ⁻⁴	1.3 × 10 ⁻⁴ (20°C)	O	(1.36)
Iridium	440	22.5	2,454	5,300	.031	6.8	0.14	5.3 (20°C)	FCC	1.35
Iron	2.43	7.87	1,539	2,740	.11	11.7	.18	9.71 (20°C)	BCC	1.28
Krypton	28	3.488 × 10 ⁻³	-157	-152	0.21 × 10 ⁻⁴	...	FCC	1.97
Lanthanum	8.9	6.19	966	4,340	0.048	65–75 (20°C)	CPH	1.87
Lead	0.17	11.34	327.4	1,740	.031	29.3	0.083	20.65 (20°C)	FCC	1.75
Lithium	67	0.53	186	1,370	.79	56	.17	8.55 (0°C)	BCC	1.87
Lutetium	108	9.74	CPH	1.73
Magnesium	0.059	1.74	650	1,120	0.25	26	0.38	4.46 (20°C)	CPH	1.60
Manganese	12.6	7.43	1,245	2,150	.115	22	...	185 (20°C)	C ₁₁	(1.60)
Mercury	380	13.55	-38.87	357	.033	...	0.0201	94.1 (0°C)	R	1.55
Molybdenum	2.4	10.2	2,622	4,804	.061	5.1	.32	5.17 (0°C)	BCC	1.40
Neodymium	44	6.98	820046	70 (20°C)	CPH	1.82
Neon	<2.8	0.6367 × 10 ⁻⁴	-248.6	-248.6	0.00011	...	FCC	1.60
Neptunium

APPENDIX

Table A.2— (Continued)

Element	Thermal-neutron absorption cross section, barns/atom	Density near 20°C, gm/cm ³	Melting point, °C	Boiling point, °C	Specific heat near 20°C, cal/(gm)(°C)	Coefficient of linear thermal expansion near 20°C, per °C × 10 ⁻⁴	Thermal conductivity near 20°C, cal/(sec)(cm)(°C)	Electrical resistivity, microhm-cm	Crystal structure*	Goldschmidt† atomic radius, Å
Nickel	4.5	8.90	1,455	2,730	0.105	13.3	0.22	6.84 (20°C)	FCC	1.25
Nitrogen	1.78	1.1649 × 10 ⁻³	-210.0	-195.8	.247000060	...	H	0.71
Osmium	14.7	22.5	2,700	5,500	.031	4.6	...	9.5 (20°C)	CPH	1.35
Oxygen	<0.0002	1.3318 × 10 ⁻³	-218.8	-183.0	.218	...	0.000059	...	C	0.69
Palladium	8.0	12.0	1,554	4,000	.058	11.8	.17	10.8 (20°C)	FCC	1.37
Phosphorus (yellow)	0.19	1.82	44.1	280	.177	125	...	10 ¹⁷ (11°C)	C	(1.69)
Platinum	8.1	21.45	1,773.5	4,410	.032	8.9	0.17	9.83 (0°C)	FCC	1.38
Plutonium	...	19.6	632	3,235	...	50.3 × 10 ⁻⁴
Polonium	...	9.51	254	912	...	24.4	...	140	M6	(1.40)
Potassium	1.97	0.86	63	770	0.177	83	0.24	6.15 (0°C)	BCC	2.38
Praseodymium	11.2	6.78	950	3,020	.049	75 (20°C)	CPH	1.83
Protactinium	3,600
Radium	...	5.0	700
Radon	...	4.40	-71	-61.8
Rhenium	84	20	3,170	...	0.033	CPH	1.38
Rhodium	150	12.41	1,966	4,500	.059	12.1	0.21	4.3 (0°C)	FCC	1.34
Rubidium	0.70	1.53	39	890	.090	90	...	12.5 (20°C)	BCC	2.51
Ruthenium	2.46	12.2	2,500	4,900	.057	9.1	...	7.6 (0°C)	CPH	1.34
Samarium	6,500	6.93	>1,300
Scandium	13	2.5	1,400	FCC	1.60
Selenium	11.8	4.81	220	680	0.084	37	H	(1.16)
Silicon	0.13	2.33	1,430	2,300	.162	2.8-7.3	0.20	10 ⁵ (0°C)	DC	(1.17)
Silver	60	10.49	960.5	2,212	.056	20.6	1.0	1.47 (10°C)	FCC	1.44
Sodium	0.49	0.97	97.7	892	.295	71	0.32	4.2 (0°C)	BCC	1.92
Strontium	1.16	2.6	770	1,380	0.176	23 (20°C)	FCC	2.15
Sulfur (yellow)	0.49	2.07	119.0	444.6	.175	64	6.31 × 10 ⁻⁴	2 × 10 ²³ (20°C)	FCO	(1.04)
Tantalum	21.3	16.6	2,996036	6.5	0.13	12.4 (18°C)	BCC	1.47
Tellurium	4.5	6.24	450	1,390	.047	16.8	.014	2 × 10 ⁵ (19.6°C)	H	(1.42)
Terbium	44	8.33	>1,400	CPH	1.77
Thallium	3.3	11.85	300	1,460	0.031	28	0.093	18 (0°C)	CPH	1.71
Thorium	...	11.71	1,690	>3,000	.028	11.15	.09	16 (20°C)	FCC	1.69
Thulium	118	9.35	CPH	1.74
Tin	0.65	7.298	231.9	2,270	0.054	23	0.16	11.5 (20°C)	BCT	1.58
Titanium	5.6	4.51	1,690	3,535	.137	8.5	.41	48 (20°C)	CPH	1.47
Tungsten	19.2	19.2	3,395	5,930	.032	4.4	.40	5.5 (20°C)	BCC	1.41
Uranium	...	19.1	1,133	3,900	.028	14.5	.060	25-50 (25°C)	O	(1.39)
Vanadium	4.7	6.1	1,710	3,400	.127	8.3	.07	25 (20°C)	BCC	1.36
Xenon	35	5.495 × 10 ⁻³	-112	-108.0	1.24 × 10 ⁻⁴	...	FCC	2.18
Ytterbium	36	7.01	1,800	FCC	1.83
Yttrium	1.38	5.51	1,475	CPH	1.61
Zinc	1.06	7.133	419.46	906	0.0915	39.7	0.27	5.916 (20°C)	CPH	1.37
Zirconium	0.18	6.5	1,845069	5	.057	41.0 (0°C)	CPH	1.60

*FCC = Face-centered cubic; R = Rhombohedral; BCC = Body-centered cubic; CPH = Close-packed hexagonal; O = Orthorhombic; H = Hexagonal; T = Tetragonal; DC = Diamond cubic; OFCO = One-face-centered orthorhombic; M = Monoclinic; BCT = Body-centered tetragonal

†Figures in parentheses are one-half the smallest interatomic distances

‡Complex cubic

§Probably monoclinic with $\beta = 92^\circ$

Table A.3—Thermal-neutron Absorption Cross-section of the Elements Arranged in Order of Atomic Number

(Neutron Cross Sections, AECU 2040)

Z	Element	Barns/atom		Cm ² /gram	Z	Element	Barns/atom		Cm ² /gram
		Value	Uncertainty				Value	Uncertainty	
1	H	0.330	±0.007	0.198	42	Mo	2.4	±0.2	0.0151
2	He	.006800102	43	Tc
3	Li	67	±2	5.8	44	Ru	2.46	±0.12	0.0146
4	Be	0.0090	±0.0005	0.00060	45	Rh	150	±7	.88
5	B	750	±10	42	46	Pd	8.0	±1.5	.045
6	C	0.0045	...	0.00022	47	Ag	60	±3	.34
7	N	1.78	±0.05	.076	48	Cd	2400	±200	12.9
8	O	<0.0002	...	<.0000075	49	In	190	10	1.00
9	F	<.010	...	<.00032	50	Sn	0.65	±0.05	0.0033
10	Ne	<2.8	...	<.084	51	Sb	6.4	±1.0	.032
11	Na	0.49	±0.02	.0128	52	Te	4.5	±0.2	.021
12	Mg	.059	±.004	.00146	53	I	6.7	±.6	.032
13	Al	.215	±.008	.0048	54	Xe	35		.161
14	Si	.13	±.03	.0028	55	Cs	29.0	±1.5	.132
15	P	.19	±.03	.0037	56	Ba	1.17	±0.10	.0051
16	S	.49	±.02	.0092	57	La	8.9	±.3	.039
17	Cl	31.6	±1	.54	58	Ce	0.70	±.08	.0030
18	A	0.62	±0.04	.0094	59	Pr	11.2	±.6	.048
19	K	1.97	±.06	.030	60	Nd	44	±2.0	.183
20	Ca	0.43	±.02	.0065	61	Pm
21	Sc	13	±2	.173	62	Sm	6500	±1000	26
22	Ti	5.6	±0.4	.070	63	Eu	4500	±500	17.9
23	V	4.7	±.2	.055	64	Gd	44000	±2000	169
24	Cr	2.9	±.1	.033	65	Tb	44	±4	0.166
25	Mn	12.6	±.6	.139	66	Dy	1100	±150	4.1
26	Fe	2.43	±.08	.026	67	Ho	64	±3	0.23
27	Co	34.8	±2.0	.35	68	Er	166	±16	.60
28	Ni	4.5	±0.2	.046	69	Tm	118	±6	.42
29	Cu	3.59	±.12	.034	70	Yb	36	±4	.125
30	Zn	1.06	±.05	.0098	71	Lu	108	±5	.37
31	Ga	2.71	±.12	.023	72	Hf	115	±15	.39
32	Ge	2.35	±.20	.0195	73	Ta	21.3	±1.0	.071
33	As	4.1	±.2	.033	74	W	19.2	±1.0	.063
34	Se	11.8	±.4	.090	75	Re	84	±4	.27
35	Br	6.5	±.5	.049	76	Os	14.7	±0.7	.047
36	Kr	28	±5	.20	77	Ir	440	±20	1.37
37	Rb	0.70	±0.07	.0049	78	Pt	8.1	±0.4	0.025
38	Sr	1.16	±.06	.0080	79	Au	94	±1	.29
39	Y	1.38	±.14	.0094	80	Hg	380	±20	1.14
40	Zr	0.18	±.02	.00119	81	Tl	3.3	±0.5	0.0098
41	Nb	1.1	±.1	.0071	82	Pb	0.17	±.01	.00050
					83	Bi	.032	±.003	.000092

APPENDIX

Table A.4—Thermal-neutron Absorption Cross-section of the Elements Arranged in Order of Increasing Cross-section
(Neutron Cross Sections, AECU 2040)

Element	Z	Cm ² /gram	Barns/atom	Element	Z	Cm ² /gram	Barns/atom
O	8	0.0000075	<0.0002	Ni	28	0.046	4.5
Bi	83	.000092	.032	Os	76	.047	14.7
C	6	.00022	.0045	Pr	59	.048	11.2
F	9	.00032	.010	Br	35	.049	6.5
Pb	82	.00050	.17	V	23	.055	4.7
Be	4	.00060	.0090	W	74	.063	19.2
He	2	.00102	.0068	Ti	22	.070	5.6
Zr	40	.00119	.18	Ta	73	.071	21.3
Mg	12	.00146	.059	N	7	.076	1.78
Si	14	.0028	.13	Ne	10	.084	<2.8
Ce	58	.0030	.70	Se	34	.090	11.8
Sn	50	.0033	.65	Yb	70	.125	36
P	15	.0037	.19	Cs	55	.132	29.0
Al	13	.0048	.215	Mn	25	.139	12.6
Rb	37	.0049	.70	Xe	54	.161	35
Ba	56	.0051	1.17	Tb	65	.166	44
Ca	20	.0065	0.43	Sc	21	.173	13
Nb	41	.0071	1.1	Nd	60	.183	44
Sr	38	.0080	1.16	H	1	.198	0.330
S	16	.0092	0.49	Kr	36	.20	28
Y	39	.0094	1.38	Ho	67	.23	64
A	18	.0094	0.62	Re	75	.27	84
Zn	30	.0098	1.06	Au	79	.29	94
Tl	81	.0098	3.3	Ag	47	.34	60
Na	11	.0128	0.49	Co	27	.35	34.8
Ru	44	.0146	2.46	Lu	71	.37	108
Mo	42	.0151	2.4	Hf	72	.39	115
Ge	32	.0195	2.35	Tm	69	.42	118
Te	52	.021	4.5	Cl	17	.54	31.6
Ga	31	.023	2.71	Er	68	.60	166
Pt	78	.025	8.1	Rh	45	.88	150
Fe	26	.026	2.43	In	49	1.00	190
K	19	.030	1.97	Hg	80	1.14	380
I	53	.032	6.7	Ir	77	1.37	440
Sb	51	.032	6.4	Dy	66	4.1	1100
Cr	24	.033	2.9	Li	3	5.8	67
As	33	.033	4.1	Cd	48	12.8	2400
Cu	29	.034	3.59	Eu	63	17.9	4500
La	57	.039	8.9	Sm	62	26	6500
Pd	46	.045	8.0	B	5	42	750
				Gd	64	169	44000

Table A.5—Corrosion Conversion Factors

Multiply	By	To obtain
mg/(cm ²)(mo)	100	mg/(dm ²)(mo)
mg/(cm ²)(mo)	3.3	mg/(dm ²)(day), [mdd]
mg/(cm ²)(mo)	0.0047	in. penetration per year, (ipy)
mg/(cm ²)(mo)	4.7/Density	mils/year
mg/(cm ²)(mo)	0.39/Density	mils/mo
mg/(dm ²)(mo)	0.01	mg/(cm ²)(mo)
mg/(dm ²)(day)	0.33	mg/(cm ²)(mo)
in. penetration per year	2.1 × 10 ³ × density	mg/(cm ²)(mo)

Index

INDEX

A

- Absorbing rods, 733
- Absorption, of helium, into fats, 498
- Abundance of helium, 496
- Acidity, of thorium nitrate, 642
 - of uranyl fluoride solutions, 585, 591
- Activation of oxygen, 235
- Activity, in helium stream, 496-498
 - in pumps and heat exchangers, 746
 - water, calculation of, 235-238
- Activity coefficient of aqueous thorium nitrate, 650
- Aerodynamic factors in gas dispersion, 484-486
- Age, 520
- Air, composition of, 386
 - cooling, induced activity in, 483-496
 - density of, 382, 850
 - entropy of, 383
 - heat capacity of, 391
 - internal energy of, 384
 - Mollier diagram for, 390
 - neutron cross section of, 371
 - Prandtl number for, 382, 391
 - pressure of, 385
 - properties of, 382-391, 399-407
 - specific heat of, 382, 389, 850
 - at constant pressure, 388
 - at constant volume, 387
 - specific-heat ratio for, 402
 - thermal conductivity of, 382, 391, 850
 - viscosity of, 382, 391, 850
 - empirical correlation for, 406, 407
- Alloying reaction, aluminum-uranium, 455
- Aluminum, 198-208, 451
 - corrosion of, effect of alloying on, 203-207
 - couple effect on, 203, 208
 - effect of irradiation on, 208
 - by NaOH, 841
 - protection against, 208
 - in water, 200-208
 - interface temperature, 455
- Aluminum fluoride, vapor pressure of, 839
- Aluminum oxide, corrosion by NaOH, 846, 847
- Aluminum oxide-aluminum mixtures, corrosion by NaOH, 847
- Aluminum oxide diffusion barrier, 453
- Aluminum oxide-magnesium oxide mixtures, corrosion by NaOH, 846, 847
- Aluminum-silicon bonding of fuel elements, 453
- Aluminum-uranium alloying reaction, 455
- Alundum (see Aluminum oxide)
- Analysis, of NaK, 293
 - of sodium, 293
- Analytical methods for transients, 152
 - (See also Lifetime, finite-difference solution)
- Angle of view, in mirror systems, 888, 889
 - in periscopes, 892, 893
 - through windows, 885
- Annuli, forced-convection heat transfer through,
 - basic equations for, 45, 47-49
 - single-phase-flow pressure drop in 55, 58-61
- Anodic coating on aluminum, 452
- Anodized film, 458
- Aqueous fuels, composition of, 509-510
- Aqueous homogeneous reactors, advantages of, 507-508
 - characteristics of, 507-510
 - control of, 679-685
 - power densities of, 507
 - problems of, 508-509
- Aqueous homogeneous systems, neutron chain reactions in, 511-553
- Aqueous slurry systems, properties of, 659-671
- Aqueous-solution reactors, 701
- Arc welding, 453
- Area, exclusion, for safety, 745
- Argon, 483
 - as beta-gamma emitter, 493
 - beta radiation from, 493
 - gamma radiation from, 496
 - in helium, 496, 497
- Argon-41 emission in Brookhaven reactor, 483-484
- Argonne Heavy Water Reactor, 1015-1017
 - cooling system, 1017
 - design data, 1016
 - fuel-element design, 242
 - neutron generation time, 143
 - shielding, 1017
 - temperature coefficient of reactivity, 144
 - water decomposition in, 188-189
- Argonne Research Reactor, 1017-1020
 - cooling system, 1020

Argonne Research Reactor, design data, 1019
 fuel elements, 1017-1018
 design, 244
 neutron generation time, 143
 shielding, 1018
 temperature coefficient of reactivity, 144
 Auxiliary equipment, 359, 360-361

B

- Bare reactors, 522-523
 effect of temperature on critical concentration, 523
 spherical, one-group equation for criticality of, 511-512
- Barium hydroxide, corrosion of metals and alloys by, 848
 heat capacity of, 848
 melting point of, 848
 strontium hydroxide system, constitution diagram of, 823
- Barium sulfate, growth in reactor, 622
 precipitation time in homogeneous reactor, 622
 solubility of, in uranyl sulfate, 633-634
 in water, 633
- Basic cycle equation, 312
- Basic equations, for forced-convection heat transfer, 45, 47-50
 through pipes, noncircular ducts, and annuli, 45, 47-50
 through randomly packed spheres, 50
 across single cylinder, flow normal to axis, 49-50
 across tube banks, flow normal to axis, 47, 49
 flow parallel to axis, 47
 for free-convection heat transfer, 43, 45, 46
- Bearings, 325-329
 anti-friction, 327-329
 journal, 325-327
- Bellows, corrosion of, 791
 life, 791
 effect of temperature on, 791
 tests, 791
- Bellows-type valve, 791
- Bend losses, pressure-drop system calculations for, 66, 68-70
- Beryllium, corrosion in water, 208-209
- Beryllium fluoride, vapor pressure of, 839
- Beryllium fluoride-lithium fluoride system, constitution diagram of, 825
- Beryllium fluoride-sodium fluoride system, constitution diagram of, 826
- Beryllium oxide crucible, corrosion by NaOH, 847
- Beta-gamma emitter, argon as, 493
- Beta radiation from argon, 493
- BGRR (see Brookhaven Graphite Research Reactor)
- Bismuth, molten, 793
 physical properties of, 773
 polonium formed from, 747
 pumping of, 789
 solubility of uranium in, 746
- Bismuth-lead-tin-uranium system, isothermal section of, 765
- Bismuth-lead-uranium system, 760, 761, 763
 isothermal section of, 761, 763
- Bismuth-sodium-uranium system, 760, 765
- Bismuth-thorium system, phase diagram of, 769
- Bismuth-tin-uranium system, 760, 763, 764
 isothermal section of, 763-764
- Bismuth-uranium system, 758-760
 phase diagram of, 758-759
- Blanket, breeder (see Breeder blanket)
- ThF₄, 747
 thickness, 536, 537-538
- Blanket concentration, 536
- Blanket power, effect on breeding gain, 546
 and higher isotopes, 536, 541-542
- Blower power, reactor, 477
- Blowers, 475
- Boiling heat transfer, 50-52
- Boiling point, of aqueous thorium nitrate, 649, 651
 of elements, 1044-1045
 of uranyl nitrate, 594
- Boiling reactors, heat removal from, 7
 kinetics, 551-552
 power removal from, 698
 vapor formation, 551
- Bonding, aluminum-silicon, of fuel elements, 453
- Borescopes (see Periscopes)
- Boron, addition to thermal shield, reduction of secondary gammas by, 118, 119
 corrosion by NaOH, 842
- Boron carbide, corrosion by NaOH, 847
- Boundary conditions, 513
- Brass, corrosion by NaOH, 842
- Breeder blanket, 513
 processing of, 854-856
 (See also Reactor breeder blankets)
- Breeder reactors, fuel systems, 805, 809
 moderators, 809
- Breeding gain, 513, 536
 effect of breeder size on, 536
- Bronze, corrosion of, by NaOH, 842
 in water, 210
- Brookhaven Graphite Research Reactor, 997-1000
 cooling system, 999-1000
 design data, 998
 fuel handling, 999
 shielding, 999
 A⁴¹ emission from, 483-484
- BSR (see Bulk Shielding Reactor)

INDEX

- Bubbles, 746
 - Build-up, in core, of U^{235} , 517
 - of U^{238} , 518
 - of higher isotopes, 514-519
 - from thorium, in blanket, 514
 - from U^{233} , 514-515
 - from U^{235} fuel, 516-517
 - Bulk Shielding Reactor, 1012-1014
 - cooling system, 1012
 - design data, 1013
 - fuel elements, 1012
 - shielding, 1012
 - Buoyancy effect, 485
- C
- Cadmium sulfate, solubility of, in uranyl sulfate, 637-638
 - in water, 637
 - Calcium oxide, corrosion by NaOH, 847
 - Calculation, methods of, 511-512
 - for 50-mw exchanger, 697
 - of water activity, 235-238
 - Calking compound for sealing filters, 499
 - Canning, 451-453
 - Carboloys (see Tungsten carbide)
 - Carbon dioxide, heat capacity of, 398
 - Prandtl number for, 398
 - properties of, 396-407
 - specific-heat ratio for, 402
 - thermal conductivity of, 398
 - viscosity of, 398
 - empirical correlation for, 396-407
 - Casings, 469
 - Catalytic recombiner, 705-707
 - Caves (see Hot laboratories)
 - Cells (see Hot laboratories)
 - Central transverse gap, effect on critical size, 466
 - Ceramics, corrosion of, by NaOH, 846, 847
 - Ceric sulfate, solubility of, in uranyl sulfate, 630-631
 - in water, 630-631
 - Cerium, corrosion by NaOH, 842
 - Cesium sulfate, solubility of, in uranyl sulfate, 628-629
 - in water, 628
 - CH_4 , specific-heat ratio for, 402
 - C_2H_4 , specific-heat ratio for, 402
 - Chain reactions, neutron, in aqueous homogeneous systems, 511-553
 - Chambers, B^{10} type, 946
 - cables and mountings, 969
 - circuit considerations, 969-971
 - compensated, 960-961
 - current, 948, 952-954
 - for neutron detection, 948-963
 - fission, 733, 948
 - Chambers, fission current, 948, 957, 959
 - gamma, 948
 - graphite, 733
 - location and range, 969
 - safety, 733
 - Channels, friction factor for, 58, 59
 - gas-filled ionization chamber, 975, 977-981
 - non-circular, single-phase-flow pressure drop in, 55, 58-61
 - pressure drop for, friction factor in, 58, 60
 - relative roughness for, 58, 59
 - Charcoal, activated, helium filtration through, 498
 - Charcoal filter, 498
 - Chemical decay, 514
 - Chemical loss, 516
 - Chemical processing, of thorium blanket, 514
 - Chemical properties, of uranyl fluoride, 581
 - of uranyl sulfate, 555-573
 - Chemical stability of gas coolants, 480
 - Chicago Pile No. 1, 991-992
 - design data, 992
 - fuel elements, 991
 - fuel preparation, 991
 - Chicago Pile No. 2, 991, 993-994
 - design data, 993
 - fuel elements, 991
 - fuel preparation, 994
 - reactor atmosphere, 994
 - shielding, 994
 - Chlorides, constitution diagrams of, 815-817
 - eutectic compositions of, 810, 828-829
 - as fuels for fast reactors, 807, 809
 - irradiation of, 838
 - melting points of, 810, 828-829
 - phase studies of, 810, 815-818
 - (See also Reactor coolants, fused-salt; Reactor fuels, fused-salt; and under specific compounds and systems)
 - Chromel (see Chromium-nickel alloys)
 - Chromium, corrosion of, by NaOH, 841, 843
 - in water, 209
 - Chromium alloys, corrosion by NaOH, 842
 - Chromium-nickel alloys, corrosion by NaOH, 841, 843
 - Circuit amplifiers, 971
 - Circuits, basic, 975
 - counter, 971
 - counting-rate, 975
 - log counting rate, 975, 976
 - logarithmic amplifier, 979, 980
 - period, 975
 - period amplifier, 979, 981
 - power supply, 979
 - Circulating system, external, 469
 - Clad fuel elements, 194
 - Clementine (see Los Alamos Fast Reactor)
 - Coatings, 451
 - Cobalt, corrosion of, by NaOH, 841
 - in water, 209

- Cobalt alloys, corrosion of, by NaOH, 841-843
 - in water, 209-211
 - couples of high corrosion resistance, 210, 211
- Coefficient of linear thermal expansion, of elements, 1044, 1045
- Coefficient of reactivity, negative temperature, for liquid fuel, 745
- Collisions to thermalize neutrons, 806
- Colmonoy (see Nickel alloys)
- Columbium, corrosion by NaOH, 842
- Complexes, uranyl carbonate, 607
- Composition, of air, 386
 - of filters, 501
- Compressors, 469
- Concentration, critical, 691
- Concentration control, HRE, 736
- Configuration, reactor, 691-699
 - basic, 691
- Constantan (see Copper-nickel alloys)
- Constants, for heavy water, 519
 - nuclear, 519-521
 - for $\text{ThO}_2\text{-D}_2\text{O}$ slurry, 519
 - for U^{233} producers, 519
 - uranium, 516
- Construction of hot laboratories, 909-923
- Construction materials, 2
 - activation of, 721
- Contamination of pumps and heat exchangers, 747
- Contraction, 427
- Contraction losses, pressure-drop system calculations for, 64, 66, 67
- Control, of aqueous homogeneous reactors, 679-685
 - concentration, 679
 - dumping fuel, 681
 - enrichment, 680-681
 - heat removal, 681
 - reflector-level, 681
 - by soluble poisons, 105
 - by temperature coefficient, 105
- Control elements, 322
 - effect on power distribution, 99
 - methods of control, 322
 - types of, 322
- Control mechanism, pressure in, 681
- Control methods, nonmechanical, 679-681
- Control rods, calculation methods for, 99, 114, 117
 - cell calculations, 100
 - channels, effect on flux distribution, 103-104
 - cross type, flux distribution around, 102, 103
 - distortion of, 167
 - eccentrically located, calculation methods for, 100-102
 - effect on power distribution, 99
 - heat generation in, 113
 - in MTR, 114
 - noncircular, methods of calculating, 102, 103
- Control rods, Nordheim-Scalett calculations, 100-102
 - partial insertion of, 102
 - tip effect, 114
- Control system, 926, 927
- Convection in boiling reactors, 697
- Conversion factors, angular displacement, 1043
 - corrosion, 1047
 - density, 1043
 - energy, 1047
 - length, 1042
 - pressure, 1043
 - thermal conductivity, 1043
 - time, 1041-1042
 - volume, 1042-1043
- Conversion ratio, 513, 533, 535
 - in bare reactors, effect of temperature on, 523
- Converter, two-region U^{233} , build-up of higher isotopes in, 518-519
- Converter reactors (see Breeder reactors)
- Coolant activity, water calculation of, 235-237
- Coolant, comparison of pumping-power requirements, 773-777
 - properties of, 772, 777
 - equations for, 477
 - physical, 772, 777
 - radioactivity in, 483-502
 - (See also Reactor coolants, fused-salt, and Reactor moderator-coolants, fused-hydroxide)
- Cooling, forced-convection, 697
 - of helium, 498
 - of solid-fuel reactors, design criteria for, 130-133, 138-139
 - design limitations for, 130-132, 138-139
 - heat balance in, 123
 - hot-spot factors in, 135-137
 - macroscopic study of, 123
 - methods of improving reactor performance, 138-139
 - microscopic study of, 125, 126
 - relation between design limitations and variables, 133-139
 - simple fuel-element geometries, 127, 128
 - steady-state heat removal, 123-139
 - temperature distribution in simple fuel geometries, longitudinal, 133, 134
 - transverse, 126-130
 - thermal-resistance concept, 127
 - thermal-resistance formulae, 127, 129
 - modified, 129-130
 - transient heat removal, 141-164
- Cooling-efficiency index of gases, 480
- Cooling system, Argonne Heavy Water Reactor, 1017
 - Argonne Research Reactor, 1020
 - Brookhaven Graphite Research Reactor, 999
 - Bulk Shielding Reactor, 1012

INDEX

- Cooling system, Daniels Power Pile, No. III, 1003
 - Experimental Breeder Reactor, 1027
 - Homogeneous Reactor Experiment, 1037
 - Los Alamos Fast Reactor, 1025
 - Los Alamos Water Boiler, 1033
 - Low-Intensity Training Reactor, 1011
 - Low-Power Research Reactor, 1031
 - Materials Testing Reactor, 1008-1009
 - ORNL Graphite Reactor, 996
- Copper, and alloys, corrosion in water, 210-211
 - corrosion of, by $\text{Ba}(\text{OH})_2$, 848
 - by NaOH , 841, 843
 - by $\text{Sr}(\text{OH})_2$, 848
- Copper-nickel alloys, corrosion by NaOH , 842
- Copper oxides, corrosion by NaOH , 847
- Core diameter, 536
- Core shell, effect on breeding gain, 545
- Core structures, reactor, thermal stress in, 169
- Core tank materials, properties of, 695, 696
- Correlations, thermal-conductivity, for gases, 405
- Corrosion, 295-307
 - of aluminum jacket, in air, 460
 - by aqueous thorium nitrate, 642
 - by bismuth, 302, 303
 - of construction materials, in water, 194, 198-201
 - conversion factors, 1047
 - definition of, 193
 - evaluation of data, 295
 - of fuel materials, in water, 198-201
 - by lead, 295, 302-303
 - by lead-bismuth, 295, 302-303
 - by liquid metals, 295-297
 - by lithium, 295, 299
 - mass-transfer, 793
 - by mercury, 295, 300
 - by NaK , 295-298, 301, 305
 - by sodium, 295-298, 301, 304-307
 - of stainless steel, in water, effect of nitriding on, 224
- in water, 193-233
 - alloying for improving resistance, 203, 204, 228, 229
- in water, crevice effect, 197-198
 - effect of corrosion products, 195
 - effect of gases, 195
 - effect of hydrogen, 195, 222
 - effect of impurities, 195, 229
 - alloying elements, 203, 228
 - gases dissolved in coolant, 195
 - hydrogen dissolved in coolant, 195
 - insoluble particles in coolant, 195
 - oxygen dissolved in coolant, 195
 - soluble salts in coolant, 196
 - effect of oxygen, 195, 214, 222, 229
 - effect of pH, 196, 200, 202-205, 207
 - effect of surface treatment, 222, 229
- Corrosion, in water, effect of temperature, 194
 - effect of velocity, 198, 224
 - effect on wearing parts, 194, 196, 198
 - general considerations, 193-194
 - heat treatment, effect on stainless steel, 224
 - effect on zirconium, 230
 - irradiation effect, 196, 208, 230
 - protection against, 208
 - rate of, 200
 - selection of materials, 198
 - use of inhibitors in, 208, 224
 - weight-change rate, 200
- Corrosion resistance, in water, of aluminum, 200-208
 - of beryllium, 208
 - of chromium, 209
 - of chromium plate, 199, 209
 - of cobalt alloys, 209-210
 - of constructional material, 198, 199
 - of copper and alloys, 210
 - of fuel materials, 198-201
 - of gold and alloys, 210-211
 - of magnesium and alloys, 211-212
 - of nickel and alloys, 212-213
 - of platinum and alloys, 210-211
 - of silver-cadmium alloys, 212, 214
 - of silver and alloys, 212, 214
 - of steel, carbon, 214
 - low-alloy, 214
 - stainless, 214
 - of structural materials, 198-201
 - of thorium and alloys, 224
 - of titanium, 225
 - of uranium, 225
 - of zirconium and alloys, 225, 228-230
- Counter amplifiers, 971-974
- Counter channels, gas-filled, 971-976
- Counter circuits, 971
- Counters, 946, 947-951
 - fission pulse, 948, 955, 956
 - scintillation, 966, 967, 968
- CP-1 (see Chicago Pile No. 1)
- CP-2 (see Chicago Pile No. 2)
- CP-3 (see Argonne Heavy Water Reactor)
- CP-3' (see Argonne Heavy Water Reactor)
- CP-5 (see Argonne Research Reactor)
- Creep and thermal stress, 171
- Critical concentration, of bare reactor, effect
 - of temperature on, 522-523
 - effect of breeder size, 536, 543
 - of uranium 235, and shell absorption, 533, 534
- Critical length of reactor, 463
- Critical mass, velocity in two-phase-flow
 - pressure drop, 77
- Critical properties, of heavy water, 22
 - of light water, 22
- Criticality, calculations, 511-546
 - and production data, 520

Cross-sectional flow area in reactor, 477
 Crystal structure of elements, 1044-1045
 Crystallography of uranium oxide, 661
 Cycle, power, flash-vaporization, 699
 Cylinder, single, forced-convection heat transfer across, 49-50
 Cystalon (see Silicon carbide)

D

- Daniels Power Pile, No. III, 1001-1003
 cooling system, 1003
 design data, 1002
 fuel handling, 1003
 power conversion, 1003
 Decomposition of water (see Water decomposition)
 Decomposition temperatures of sodium uranyl carbonates, 607
 Decontamination, of helium coolant, 498
 solutions for, 724
 Deflagration, 685
 limits, 685
 Delayed neutrons, effect of circulation on, 548
 effect on power oscillations, 550
 Density, of air, 382
 of aqueous thorium nitrate, 642, 647-648
 of elements, 1044-1045
 of heavy liquid water, 30
 of helium, 460, 462, 392, 394
 of light water, 39-40
 of Na_2CO_3 - UO_2CO_3 - H_2O system, 615, 617
 of slurries, 667
 of UO_2F_2 saturated solution, 591
 of UO_2F_2 - HF - H_2O system, 592
 of UO_2F_2 - H_2O system, 585
 of $\text{UO}_2(\text{NO}_3)_2$ - HNO_3 - H_2SO_4 - H_2O system, 599, 602
 of UO_2SO_4 - D_2O system, 574-578
 of UO_2SO_4 - H_2O system, 574-578
 of UO_3 - CO_2 - H_2O - K_2CO_3 system, 616
 of UO_3 - HF - H_2O system, 585
 of UO_3 - HNO_3 - H_2O system, 601
 of uranyl fluoride solutions, 592
 at 25°C, 592-593
 of uranyl nitrate, in H_2O , 594, 599, 600
 of uranyl nitrate solutions, 594, 599-602
 Density equation, for UO_2F_2 solutions, 593
 for $\text{UO}_2(\text{NO}_3)_2$ - H_2O solutions, 599
 Depth perception, with periscopes, 893
 in television, 903
 through windows, 876
 Design criteria for solid-fuel reactor, 130-133, 138-139
 Design data, Argonne Heavy Water Reactor, 1016
 Argonne Research Reactor, 1019
 Brookhaven Graphite Research Reactor, 998
 Design data, Bulk Shielding Reactor, 1013
 Chicago Pile No. 1, 992
 Chicago Pile No. 2, 993
 Daniels Power Pile, No. III, 1002
 Experimental Breeder Reactor, 1026
 Homogeneous Reactor Experiment, 1036
 Los Alamos Fast Reactor, 1024
 Los Alamos Water Boiler, 1034
 Low-Intensity Training Reactor, 1010
 Low Power Research Reactor, 1030
 Materials Testing Reactor, 1006
 ORNL Graphite Reactor, 995
 Thermal Test Reactor, 1022
 Design information, engineering, 691-739
 Design limitations for solid-fuel reactor, 130-132, 138-139
 Design of hot laboratories, 909
 Design temperature rise, 311
 Detonability, composition limits of, 686
 Detonation, 685
 Deuterium, as moderator for power reactor, 809
 Di-alkali-uranyl pyrophosphates, of Li and Na, preparation of, 615-616
 Dialkali-uranyl-sec.-phosphites, color of, 615
 preparation of, 615
 Diffusion barrier, aluminum oxide, 453
 Diffusion cascade, 498
 Diffusion constants, 520
 Dilution in atmosphere, 484
 Dispersions, 746-747
 under lapse conditions, 493
 under natural conditions, 493
 radiation effects on, 757
 in stable air, 489-490
 thermal effects on, 757
 in unstable air, 487
 Dissociation constant of uranyl tricarboxylate ion, 607
 Dissociation of water (see Water decomposition)
 Distortion, of control rods, 167
 of long prismatical shapes, 167-168
 thermal, in reactor core structures, 169
 δk control means, 933-935
 D_2O moderators, 523
 D_2O sample carrier for HRE reflector sampling, 729, 730
 D_2O sampler in HRE reflector system, 730, 731
 Dose rates, 493, 496
 DPP (see Daniels Power Pile, No. III)
 Ducts, noncircular, forced-convection heat transfer through, 45, 47-49
 Duriron (see Iron alloys)
 Dynamic viscosity, of heavy liquid water, 27, 35
 of light liquid water, 26-27, 35
 of light-water vapor, 36
 of steam, 36

INDEX

E

EBR (see Experimental Breeder Reactor)
 Effective stack height, 485
 Effectiveness, of regulating rods, 934
 of safety rods, 933
 of shim rods, 934
 Effluent concentrations, 491
 Effluent speed, 484
 Effluent temperature, 484
 Elastic thermal stress, 170
 Electrical resistivity of elements, 1044-1045
 Elements, physical constants of, 1044-1045
 thermal-neutron absorption cross sections of, 1044-1047
 Elgiloy (see Cobalt alloys)
 Empirical correlations, of gas-coolant properties, 381
 of heat-transfer coefficients, 497
 Enlargement losses, pressure-drop system calculations for, 64, 66
 Enriched reactors, fuel systems, 809
 nuclear properties of moderators, 806
 Enrichment, effect on water decomposition, 573
 Entrance pressure drop, 427, 429
 Entropy of air, 383
 Equations, for coolant properties, 477
 reactor, 926, 929
 Equilibrium concentration of higher isotopes, 514
 Equipment, arrangement of, 697
 cleaning of, 793-794
 decontamination of, 724
 sampling, 725, 727-728
 special, design of, 708-739
 Erosion, due to presence of solids, 747
 Erosion behavior of uranium oxide slurries, 668-669
 η , effect of critical radius on, 523
 Eucken equation for thermal conductivity, 406
 Examination (see Viewing)
 Exit pressure drop, 427, 429
 Expansion joint, 473, 475
 Expansion losses, 427
 Experimental Breeder Reactor, 1025-1027
 cooling system, 1027
 design data, 1026
 fuel elements, 1025
 shielding, 1025
 Experimental facilities, Materials Testing Reactor, 1008
 Explosion pressure, 685-687
 Explosions, gas, 685-687
 External circulating system, 469-475
 External recombiners, 701, 702-707
 Extraction of fission products, 747
 Extrusion pressure of finned tubing, 455
 Extrusion temperature of finned tubing, 455

F

Fabrication of control plates, 685
 Fast reactors, control, 805, 807
 fuel salts, fused chlorides, 807, 809-810
 fuel systems, 803, 807
 Fatigue and thermal stress, 171
 Fatigue fracture and thermal stress, 170
 Fermi age, 520
 Film coefficient, heat-transfer, 43
 Filters, composition of, 501
 glass-fiber, 499, 500
 pressure-drop build-up in, 499
 sealing, 499
 calking compound for, 499
 sintered stainless-steel, 795
 Filter house on downstream side of reactor, 500
 Filter systems for radioactive particles, 499-501
 Filtration, of helium, 498
 through activated charcoal, 498
 Finned surfaces, 427, 430-433
 Fission fragments, decomposition of water by, 674
 Fission products, 543-545
 aqueous, properties of, 622, 623-641
 continuous removal of, 745
 diffusion into helium, 496, 498
 estimated weights of, for reactor operating and cooling times, 622, 641
 extraction of, 747
 growth of, 622, 640
 references on, 622
 heats of solution in uranyl sulfate, 622, 639
 multiple, solubilities in aqueous uranyl sulfate, 622
 solubilities of, 622, 623-640
 Fissionable material, nonuniform distribution of, for flux and power flattening, 104
 Fissioning solutions, 560
 radiation stability of, 560, 574
 Flame recombiner, 702, 704, 705
 Flanged joint in piping, 793
 Flash vaporization, 699-701
 Flashbacks, recombiner, 705
 Flat-plate reactor, 464, 467
 Flattened zone, computation of, 106, 108, 110
 Flow diagram, 729, 730
 Flowmeters, 362-364
 electromagnetic, 796
 for liquid metals, 796
 Fluid flow, in gases, 409-449
 (See also Pressure drop)
 Fluid-flow passages, 461
 Fluid fuel, cooling of, 745
 Fluorides, as breeder blankets, 804, 830-834, 849
 as coolants, 849

- Fluorides, as fuels, 804, 809
 heat-transfer properties of, 824-827, 834
 melting points of, 834
 phase studies of, 810
 (See also Reactor coolants, fused-salt;
 Reactor fuels, fused-salt; and under
 specific compounds and systems)
 Flux distribution, local, in heterogeneous
 reactors, 109
 (See also Power distribution)
 Folded reactors, 433, 464, 468
 pressure drop in, 464
 turning losses in, 464
 Fracture and thermal stress, 170
 Free energy of dilution, of aqueous thorium
 nitrate, 642, 654
 Friction factor, for channels, 58, 59
 in pressure drop, 58-60
 for channels, 58, 60
 for randomly packed spheres, 62, 63
 Fuel compound, 520
 Fuel-element clad materials, 194
 corrosion requirements, 194
 Fuel-element design, 239-244
 Argonne Heavy Water Reactor, 242
 Argonne Research Reactor, 244
 Hanford reactors, 240
 Materials Testing Reactor, 243
 plutonium producer, 241
 Fuel elements, 321, 451
 Argonne Research Reactor, 1018
 Bulk Shielding Reactor, 1012
 heat-transfer requirements for, 451
 Low-Intensity Training Reactor, 1009
 Low-Power Research Reactor, 1029
 Materials Testing Reactor, 1005
 requirements of, 321
 general, 451
 rod-type, 451-460
 stress analysis of (see Thermal-stress
 analysis, of simple shapes)
 Thermal Test Reactor, 1021
 types of, 321-322
 Fuel handling, Brookhaven Graphite Research
 Reactor, 999
 Daniels Power Pile, No. III, 1003
 Los Alamos Water Boiler, 1033
 ORNL Graphite Reactor, 996
 (See also Remote handling)
 Fuel inventory, 782
 minimization of, 786
 Fuel plates, temperature distribution during
 exponential power rise, 145-152
 temperatures for, calculations of, 152-161
 Fuel preparation, Chicago Pile No. 1, 991
 Chicago Pile No. 2, 994
 Fuel-rod coating, 498
 Fuel sampler, for use in chemical laboratory,
 728
 Fuel slugs, Wilkins effect in, 109
 Fuel solution sampling apparatus, high-
 pressure, 725, 727
 Fuels, fluid, 745
 liquid-metal, 745
 composition of, 749-770
 properties of, 749-770
 liquid-metal-dispersion, 751, 757-770
 liquid-metal-solution, 751-757
 uranium-bismuth, 789,
 Fused salts, as breeder blankets, 849
 constitution diagrams of, 809-834
 corrosiveness of, 849
 as fuels, 803-807, 809
 irradiation of, 838, 846, 849
 as moderator, 803
 phase studies of, 810
 physical properties of, 838
 (See also Chlorides; Fluorides; Reactor
 coolants, fused-salt; Reactor fuels,
 fused-salt; and under specific com-
 pounds and systems)

G

- G, 560, 571-574, 707
 Gamma flux, effect on water decomposition,
 179-180
 Gamma radiation, from argon, 496
 Gamma rays, decomposition of water by, 674
 fission, heating by absorption of, 112
 probability of absorption within emitting
 body, 113
 secondary, heating by absorption of, 112
 Gas compressors, 469-470
 Gas coolants, chemical stability of, 480
 economic comparison of, 477-481
 physical properties of, 479
 pressure drop of, 477
 properties of, 381-407
 thermal-neutron-absorption cross sections
 of, 480
 thermal stability of, 480
 Gas-cooled reactors, general characteristics
 of, 371-373
 Gas handling systems, 701-707
 Gas-operated bearing, 469-475
 Gas passages, 461-468
 Gas sparging, xenon 135 removed by, 747
 Gas turbines, 469
 Gaseous fission products, 436
 Gases, effect on reactor criticality, 548
 fluid flow in, 409-449
 heat transfer in, 409-449
 induced radioactivity in, 484-493
 inert, 795
 production, 707
 solubility in water, 675

INDEX

- Gases, specific heats of, 403
 thermal conductivity of, 400-401
 velocity across stack orifice, 486
 viscosity of, 399-404
 effect of pressure on, 405
 empirical correlations for, 406-407
- Generation time, neutron, in H_2O - and D_2O -moderated reactors, 141-143
 in MTR, 143
 in specific reactors, 141-155
- Glass, effect of radiation on, 881-884, 890, 892
 properties of, 880
 for windows, 880-884
- Glass-fiber filters, 499-500
- Gold, corrosion of, by NaOH, 841, 843
 in water, 210
- Gold-platinum alloys, corrosion by NaOH, 841, 843
- Goldschmidt atomic radius, of elements, 1044-1045
- Graphitar (see Graphite)
- Graphite, corrosion by NaOH, 841-843
- Ground level, effluent at, 488
 dose rates, 491, 493-496
- Group methods, comparison with measured flux distribution, 96-97
- Growth, of fission products, 622
 particle-size, in uranium oxide slurries, 661-663
- H**
- Halides, as fuels, 809
- Handling, of liquid-metal systems, 795
 of radioactive materials (see Remote handling)
 (See also Hot laboratories)
- Handling apparatus, analytical laboratory, 728-729
- Hastelloy (see Nickel alloys)
- Haze in windows, 878, 879
- Header, gas, 464
- Heat, removal of (see Transients, reactor power)
 transient generation of (see Transients, reactor power)
- Heat balance, 477
 in stationary-fuel reactor, 123
- Heat capacity, of air, 391
 of carbon dioxide, 398
 of $UO_2(NO_3)_2 + NH_4NO_3$ solutions, 604
 of $UO_2(NO_3)_2 + NH_4NO_3 + HNO_3$ solutions, 604
 of UO_2SO_4 - D_2O system, 581, 582
 of UO_2SO_4 - H_2O system, 581-583
 of uranyl fluoride, 585
 of uranyl nitrate hexahydrate, 603
 solid, 599, 603
- Heat capacity, of uranyl nitrate solutions, 599, 602-604
 in butex, 604
 in HNO_3 , 604
- Heat dissipation, 8-10
 atmospheric or low-pressure systems, 8
 pressurized systems, 8-10
- Heat exchangers, 337-344, 474-475, 721, 723
 effect of changing from mercury to sodium, 784
 effect of tube design, 342, 344
 effect of tube diameter and spacing, 342, 343
 effect of tube wall conductance, 342, 344
 "hokey-stick" flat-tube, 338, 339
 HRE main, 721-724
 LMFR, calculated results of, 783
 design conditions for, 782, 783
 over-all coefficients for KAPL units, 338, 339
 proposed, for Homogeneous Reactor, 697, 698
 shell-and-tube, 338, 339
 spray-type, 778-779, 787-788
 advantages of, 788
 disadvantages of, 788
- Heat generation, by absorption of fission gammas, 112
 in control-rod tip, 114
 in control rods, 114-117
 by elastic collisions of neutrons, 111
 in fuel elements (see Flux distribution and Power distribution)
 by gammas from distributed secondary sources, 112
 by local $n-\alpha$ and $n-\beta$ reactions, 112
 by locally emitted secondary gammas, 112
 in moderator, 113
 in non-fuel-bearing core components, 109, 111-117
 in reactor, 477
 in reactor vessel, 118
 in reflector, 118
 in thermal shield, 118
 thermal stresses due to, 165-166
- Heat of decomposition, of uranyl nitrate, 593
- Heat of dilution, of aqueous thorium nitrate, 652-654
 of $UO_2(NO_3)_2 \cdot 6H_2O$, 606
 of uranyl nitrate solution, 604-606
- Heat of solution, of fission products, in uranyl sulfate, 622, 639
 of thorium nitrate, 652
 of $UO_2(NO_3)_2$, 604-605
 of $UO_2(NO_3)_2 \cdot H_2O$, 605
 of $UO_2(NO_3)_2 \cdot 2H_2O$, 604-606
 of $UO_2(NO_3)_2 \cdot 3H_2O$, 604-606
 of $UO_2(NO_3)_2 \cdot 6H_2O$, 604-606
 of uranyl nitrate, 606
 of uranyl nitrate solution, 604-606

- Heat production function, methods for obtaining, 695
- Heat release, 461
- Heat-removal processes, by boiling, 7
by sensible heat gain, 7
from solid-fuel reactors, 7-8
at supercritical pressure, 8
- Heat transfer, 477
boiling, 50-52
equipment, 778-780
film coefficients, 43
calculation of, 780
forced-convection, basic equations for, 45, 47-50
through pipes, noncircular ducts, and annuli, 45, 47-49
through randomly packed spheres, 50
across single cylinder, flow normal to axis, 49-50
across tube banks, flow normal to axis, 47, 49
flow parallel to axis, 47
free-convection, basic equations for, 43, 45, 46
fuel-element requirements, 451
fused-salt agents, 810, 824-827
in gases, 409-449
streamline flow, 414, 418, 419, 422, 423
turbulent flow, 423-426
helium, 425
hydrogen-nitrogen mixture, 425, 426
hydrogenous agents, 810, 819-823
in liquid-metal-fuel reactors, 771-788
nomenclature, 43, 44
through phase change, 778
and physics considerations, 461
properties of coolants, 850
rectangular ducts, 433, 437
roughness, 443, 445
in slurries, by forced convection, 665
at supercritical pressure, 52
trapezoidal ducts, 433, 438
(See also Reactor coolants)
- Heat-transfer coefficient, average, for gases, 419, 422-428
empirical correlations of, 477
entrance, for gases, 419-421
for gases, 409, 414
for light water, 47, 49
- Heat-transfer correlations for liquid metals, 277-286
- Heat-transfer equations for water, 43-54
- Heating, induction, 793
- Heating equipment, 793
- Heating wire, resistance, 793
- Heavy water, 574
constants for, 519
(See also Water, heavy)
- Helium, 371
absorption in fats, 498
abundance of, 496
argon in, 496, 497
cooling of, 498
density of, 392, 393
filtration of, 498
through activated charcoal, 498
fission-product diffusion into, 496, 498
heat-transfer data for, 425
impurities in, 393
induced activity in, 496-498
Prandtl number for, 392
properties of, 392-395, 399, 404-407
purification of, 498
specific heat of, 392, 394
temperature-entropy diagram for, 395
thermal conductivity of, 392, 394
thermal-neutron absorption cross section of, 496
thermodynamic properties of, 392-393
viscosity of, 392, 394
empirical correlations for, 406-407
- High-pressure recombination, 707
- Higher isotopes, and blanket power, 536, 541-542
build-up of, 514-519
effect on breeding gain, 543, 545
effect on critical concentration in breeder, 545
- H₂O moderators, 523
- Hold-up, 746
of fluid fuels, 745
- Homogeneous Reactor Experiment, 1035-1037
cooling system, 1037
design data, 1036
fuel sampler, 725, 727
manipulator for, 725, 727
fuel system, 735, 736
moderator cooling system, 1037
power conversion system, 1037
shielding, 1035
- Homogeneous reactors, hydrogenous fuel systems, 810
remote handling of equipment in, 721-726
- Hot cells (see Hot laboratories)
- Hot channels (see Hot-spot factors)
- Hot Laboratories, 909-923
- Hot-spot factors, 135-137
- HRE (see Homogeneous Reactor Experiment)
- Hydraulic radius, 461
- Hydrodynamic conversion factors, 57
- Hydrodynamics (see Pressure drop)
- Hydrogen, effect on water corrosion, 195, 222-224
as moderator for power reactors, 809
specific-heat ratio for, 402
yields, 560

INDEX

Hydrogen-nitrogen, heat-transfer data for, 425, 426
 Hydrolysis, of uranyl nitrate solutions, 594
 of uranyl sulfate solutions, 560, 566-570
 Hydroxides, constitution diagrams of, 810, 819-823
 corrosion of alloys and metals by, 840-848
 corrosiveness of, 810, 840-848
 as fuels, 804, 809, 835-838
 heat capacities of, 846, 848
 heat-transfer properties of, 810, 819-823
 irradiation of, 810, 839, 840
 melting points of, 846, 848
 as moderator-coolants, 839, 840-848
 as moderators, 840
 physical and thermal properties of, 846, 848-849
 solubility of UO_2 in, 835-837
 suspension of UO_2 in, 837
 (See also Reactor fuels, fused-hydroxide; Reactor moderator-coolants, fused-hydroxide; and under specific compounds and systems)

I

Illium corrosion by NaOH , 842
 Impurities, in commercial sodium, 288
 activating, 288
 affecting corrosion, 289
 hydrogen moderation, 288
 nuclear poisons, 287
 plugging, 289-291
 effect on water decomposition, 178, 182, 184
 in helium, 393
 in NaK , 288
 activating, 288
 affecting corrosion, 289
 hydrogen moderation, 288
 nuclear poisons, 287
 plugging, 289-291
 Induced radioactivity, 306-309
 from coolant metals, 306-307
 in cooling air, 483-496
 cyclical irradiation, equations for, 308
 in equipment, 686, 688-689
 in gases, 484-492
 in helium, 496-498
 in particulates, 491
 Inelastic thermal stress (see Elastic thermal stress)
 Inert atmosphere, 789
 Inert-gas purification, 293-294
 Inherent stability of aqueous reactor systems, 552
 Inspection (see Viewing)
 Instrument channels, 971, 972-981
 Instrument installation, 969-970

Instrumentation, 359, 362-365, 795-796, 946-970
 of aqueous homogeneous reactors, 729, 733-739
 electromagnetic pressure gauge, 795
 flowmeters, 362-364
 for liquid metals, 796
 of HRE, 735-739
 liquid-level indicators, 364-365, 796
 pressure measurements, 362
 properties affecting, 359, 362
 temperature measurements, 362
 of Water Boiler, 729, 733-734, 736
 Insulation, 360-361, 793
 Interface temperature, aluminum, 452
 Interlocks, operating procedure, 944
 Intermediate-cycle systems, 312, 314, 317
 no power conversion, 317
 power conversion, 317-319
 Internal energy of air, 384
 Interrupted plane fins, 430
 Invar (see Iron-nickel alloys)
 Inversion conditions in meteorology, 488-490
 Ion chambers, 797
 Ion exchange, method of corrosion control, 196
 Ion-exchange resins, use in reactors, 678
 Iridium-platinum alloys, corrosion by NaOH , 841, 843
 Iron, corrosion of, by $\text{Ba}(\text{OH})_2$, 848
 by NaOH , 841, 842
 by $\text{Sr}(\text{OH})_2$, 848
 Iron alloys, corrosion by NaOH , 841, 842
 Iron-nickel alloys, corrosion by NaOH , 842
 Iron oxide-nickel oxide-zinc oxide system, corrosion by NaOH , 847
 Irradiation, effect on water corrosion, 196, 203, 229, 230
 Irradiation effects, and thermal stress, 172
 on water (see Water decomposition)
 Irregular shapes, effect of thermal stress on, 171
 Isotopic ratios, critical radius for, 523, 526-529

J

Joints, 360-361
 Journal bearings, 469, 471, 475

K

KCl , 747
 KCl-LiCl eutectic, physical properties of, 773
 Kinetics, of boiling reactors, 551-552
 reactor, 926, 928-929
 in aqueous homogeneous systems, 545, 547-552

L

- Lag, in vapor formation, in boiling reactors, 551
- Lanthanum sulfate, solubility of, in uranyl sulfate, 625, 627
 - in water, 625-626
- Lapse conditions in meteorology, 486, 487
- Latent heat of vaporization, of heavy water, 31
- Lead, density of, 850
 - melting point of, 850
 - thermal conductivity of, 850
 - viscosity of, 850
- Lead-bismuth-tin-uranium system, 760, 765
- Lead fluoride, vapor pressure of, 839
- Lead-tin-uranium system, 760, 763, 764
 - isothermal section of, 764
- Lead-uranium system, 760, 761
 - phase diagram of, 761
- Leak detectors, 793
- Leak test, 458, 793
- Leakage probability for gamma sources, 112, 113
- Level indicators, continuous, 796
 - restrained-float type, 736, 737
- Lid Tank, thermal-shield experiments in, 118, 119
- Lifetime, finite-difference solution, explicit, 154-160
 - implicit, 160-161
 - of neutrons (see Generation time, neutron)
 - delayed, 141
 - time-average-implicit, 161, 162
 - instability of, 160
- Light water, 574
 - (See also Water, light)
- Lighting, for television, 908
 - with windows, 877-878, 885
- Liquid-level indicators, 364-365, 796
- Liquid-metal coolants, 249-252
 - activation, 250
 - availability of, 251
 - freezing point of, 251
 - heat-removal capacity of, 250
 - moderating ratio, 250-252
 - radiation damage, 250
- Liquid-metal dispersions, production of, 757
 - radiation effects on, 757
 - settling of, 757
 - thermal effects on, 757
 - types of, 757
 - viscosity of, 757
- Liquid-metal-fuel reactor (see LMFR)
- Liquid-metal fuels, applications of, 747-748
- Liquid metals, cross sections of, macroscopic, 262
 - microscopic, 262, 271-273
 - densities of, 254, 256, 263-264
 - electrical resistivities of, 255, 257, 259, 261
- Liquid metals, heat-transfer correlations for, 277-285
 - laminar flow through pipes, constant heat flux, 278
 - constant wall temperature, 278
 - latent heats of fusion, 254, 256, 258, 260
 - latent heats of vaporization, 254, 256, 258, 260
 - melting points of, 254, 256, 258, 260
 - natural convection from horizontal cylinders, 278, 281-283
 - nuclei/cc at melting point, 262
 - Prandtl numbers as function of temperature, 277, 279
 - properties of, 253-275
 - slug flow through rectangular duct, 278, 281
 - slug flow through triangular duct, 278, 281
 - specific heats of, 255, 257, 259, 261, 265-266
 - surface tension, 259, 261
 - thermal conductivities of, 255, 257, 269-270
 - thermal entry regions, 281, 284
 - turbulent cross flow to cylinders, 278
 - turbulent flow in annuli, 278
 - turbulent flow between parallel plates, 278
 - turbulent flow through pipes, constant heat flux, 278
 - constant wall temperature, 278
 - turbulent flow through unbaffled shell, 278, 281
 - unit prices, 255, 257
 - vapor pressures of, 254, 256, 258, 260
 - viscosities of, 255, 257, 267-268
 - volume change on fusion, 255, 257
- Lithium chloride, 747
- Lithium chloride-potassium chloride system, irradiation of, 838
- Lithium deuteride, as fuel for thermal power breeder, 809
- Lithium fluoride, vapor pressure of, 839
- Lithium fluoride-sodium fluoride system,
 - constitution diagram of, 824
 - phase studies of, 824
- Lithium fluoride-thorium fluoride system,
 - constitution diagram of, 830
 - phase studies of, 830
- Lithium fluoride-uranium(IV) fluoride system,
 - constitution diagram of, 811
 - phase studies of, 811
- Lithium hydroxide, corrosion of alloys by, 848
 - heat capacity of, 848
 - melting point of, 848
- Lithium hydroxide-potassium hydroxide system,
 - constitution diagram of, 820
- Lithium hydroxide-sodium hydroxide system,
 - constitution diagram of, 819
 - phase studies of, 819
- LITR (see Low-Intensity Training Reactor)
- LMFR, 747-748
 - plant designs, 780-788

INDEX

LMFR, power plant, 781, 784
 steam cycle, 782
 uranium-bismuth circuit in, 782, 783
 Loading of fissionable material, 461
 Local boiling, effect on two-phase-flow pressure drop, 76
 Local coefficients, for streamline flow of gases, 414
 Local heat-transfer coefficients for gases, 414-422
 Loop, thermal, graphite, 793
 Los Alamos Fast Reactor, 1023-1025
 cooling system, 1025
 design data, 1024
 shielding, 1025
 Los Alamos Water Boiler, 1033-1034
 boiling in, 698
 cooling system, 1033
 design data, 1034
 fuel handling, 1033
 recombiner, 1033
 shielding, 1033
 Loss, of neutrons, to higher isotopes, 516
 Loss coefficient, for bends, and angle of bend, in pressure-drop system calculation, 66, 68
 for 90° bends, in pressure-drop system calculation, 66, 68
 for sudden contraction, in pressure-drop system calculation, 66, 67
 for sudden enlargement, in pressure-drop system calculation, 64, 66
 Low-Intensity Training Reactor, 1009-1011
 cooling system, 1011
 design data, 1010
 fuel elements, 1009
 shielding, 1011
 Low-Power Research Reactor, 1029-1031
 cooling system, 1031
 design data, 1030
 fuel elements, 1029
 shielding, 1031
 LPRR (see Low-Power Research Reactor)

M

Machining of uranium, 455-457
 Magnesium, and alloys, corrosion in water, 211-212
 corrosion by NaOH, 842
 Magnesium fluoride, vapor pressure of, 839
 Magnesium fluoride-thorium fluoride system, constitution diagram of, 833
 phase studies of, 961
 Magnesium oxide, corrosion by NaOH, 847
 Magnification, in periscopes, 892
 of underwater objects, 876
 through windows, 877
 Manganese, corrosion by NaOH, 842

Manipulation (see Hot laboratories and Remote handling)
 Manipulators, catalog of, 863-873
 general-purpose, 859-873
 classification of, 860-862
 master-slave, 862, 870-873
 Mass velocity, 461
 Materials, mechanical behavior of, and thermal-stress problems, 165
 selection of, 695
 Materials Testing Reactor, 1005-1009
 cooling system, 1008-1009
 design data, 1006
 experimental facilities, 1008
 fuel elements, 1005
 design of, 243
 heating of control rods in, 114
 heating of reflector in, 118, 120
 neutron generation time, 143
 power distribution in, 96-97, 109
 shielding, 1007
 temperature coefficient of reactivity, 144
 Mechanical design of shim rods, 934
 Mechanical stability against thermal stresses, 451
 Mechanism, raising and lowering, 681, 683, 684
 regulating plate, 685
 safety plate, 685
 Melting point, of elements, 1044-1045
 of uranyl nitrate, 594-595
 Mercury, density of, 850
 physical properties of, 773
 thermal conductivity of, 850
 viscosity of, 850
 Mercury-uranium system, phase diagram of, 765, 766
 Meteorological factors in gas dispersion, 486-492
 Meteorology, effect of topography on, 488, 491, 492
 inversion conditions, 488-490
 lapse conditions, 486, 487
 neutral conditions, 486
 parameters, 486
 transitory conditions, 488
 wind variation, 491, 492
 Moderating ratio, 806
 Moderator cooling system, HRE, 1037
 Moderators, aqueous, decomposition by radiation, 673-678
 properties of, 673-678
 heat generation in, 113
 (See also Reactor moderators)
 Mollier diagram, for dry air, 390
 for mercury, 275
 Molybdenum, corrosion by NaOH, 842
 Molybdenum oxide, solubility in uranyl sulfate, 622
 Monel, corrosion by NaOH, 841-843
 (See also Nickel alloys)
 MTR (see Materials Testing Reactor)

N

- $\text{Na}_2\text{CO}_3\text{-UO}_2\text{CO}_3\text{-H}_2\text{O}$ system, density of, 616, 617
 $2\text{Na}_2\text{CO}_3\text{-UO}_2\text{CO}_3$, solubility of, 617
 Neptunium chain, 514
 Net efficiency of large nuclear power plants, 697
 Neutral conditions in meteorology, 486
 Neutral double orthophosphate, complexes of, 615
 preparation of, 615
 Neutron activations, reduction of, 721-722
 Neutron cross section, of air, 371
 of gases, 371
 Neutron detection, by counters and current chambers, 946-963
 temperature-type elements for, 961, 964-965
 Neutron detector, 797
 Neutron economy, 451, 520
 Neutron irradiation, effect on water decomposition, 179-180
 Neutrons, delayed, loss of, 745
 fast, decomposition of water by, 674
 heating by elastic collision of, 111
 Nickel, A, corrosion of, by LiOH , 848
 by $\text{Sr}(\text{OH})_2$, 848
 and alloys, corrosion in water, 212-213
 corrosion by NaOH , 840, 841
 L, corrosion by NaOH , 844
 mechanical properties of, 844, 845
 effect of NaOH on, 844, 845
 Z, corrosion of, by $\text{Ba}(\text{OH})_2$, 848
 by $\text{Sr}(\text{OH})_2$, 848
 Nickel alloys, corrosion of, by $\text{Ba}(\text{OH})_2$, 848
 by LiOH , 848
 by NaOH , 840-845
 by $\text{Sr}(\text{OH})_2$, 848
 Nitriding, effect on corrosion of stainless steel, 224
 Nitrogen, specific-heat ratio for, 402
 Nitrogen 15, 523
 Nomenclature, heat-transfer, 43, 44
 pressure-drop, 55-57
 Nomograms for Sutton equation, 493-495
 Norbide (see Boron carbide)
 Nordheim Scalett method for control-rod calculations, 100-102
 Nuclear constants, 519-521
 Nuclear instrumentation, of HRE, 736
 of Water Boiler, 733, 734
 Nuclear power equations, 547-548

O

- Observation (see Viewing)
 Off-gas system, HRE, 702-707
 general characteristics of, 702

- Oil-lubricated bearing, 469, 471
 One-group equation, for criticality of bare spherical reactor, 511, 512
 One-group theory, comparison of flux plots with two-group theory, 106, 110
 Operating time, of breeder, effect on breeding gain, 543
 effect on critical concentration, 543
 of reactor, 536
 Operational problems with bismuth and lithium, 797
 Orifice meters, 796
 Orifices, effect on two-phase-flow pressure drop, 82-84
 ORNL Graphite Reactor, 994-997
 cooling system, 996-997
 design data, 995
 fuel handling, 996
 shielding, 996
 Osmotic pressure of aqueous thorium nitrate, 650
 Oxidation, of uranium, 452
 in sodium, 293
 Oxygen, analysis of, in NaK, 293
 effect on corrosion by sodium, 289
 effect on water corrosion, 195, 214, 222
 neutron activation of, 235
 solubility of, in NaK, 289-290
 in sodium, 289-290
 specific-heat ratio for, 402

P

- Packed beds, 443, 444
 Packing, high-temperature, 793
 Palladium, corrosion by NaOH , 841, 843
 Parallel channels, two-phase-flow pressure drop in, 76, 78-84
 effect of orifices on, 82-84
 with flow in same horizontal plane, 79, 81
 with flow in same vertical plane, 81-82
 single-channel equations for, 78-80
 Parameters, lumped, method of, 152
 Particles, beryllium oxide, 499
 dust, 499
 graphite, 499
 uranium, 499
 uranium oxide, 499
 Particulates, 491
 induced radioactivity in, 491
 Period, inverse reactor, 929, 930
 Periscopes, 890-907
 applications of, 890
 design of, 890, 892-893
 examples of, 893-907
 Peroxide, decomposition in uranyl solution, 574
 (See also Uranium peroxide)

- pH, effect on water corrosion, 196, 200, 202-205, 207
 - of uranyl fluoride solutions, 585, 591
 - of uranyl sulfate solutions, 560, 566, 567, 569, 570
- Phosphoric acid, fuel solutions, 809
 - irradiation of, 809
- Physical constants, of elements, 1044-1045
- Physical properties, of gas coolants, 479
 - of light and heavy water, 21-42
 - of $\text{UO}_2\text{SO}_4\text{-D}_2\text{O}$ system, 574-584
 - of $\text{UO}_2\text{SO}_4\text{-H}_2\text{O}$ system, 574-584
- Piles (see Reactors)
- Pipe flow, pressure-drop system calculations for, 64
- Pipes, forced-convection heat transfer through,
 - basic equations for, 45, 47-49
 - relative roughness of, 58, 59
- Piping, 360-361, 793
 - expansion joints, 473, 475
 - flanged joint in, 793
- Plant efficiencies, 12-17
- Plates, mechanical, 681-685
 - thermal stress in, 166-167
- Platinum, corrosion of, by NaOH, 841, 843
 - in water, 210
- Plugs, freeze, 793
- Plume, 485
- Plutonium, liquid-metal dispersions of, 769
 - solubility of, in bismuth, 751, 756
- Plutonium chloride, as fuel, 809
- Plutonium fluoride, as fuel, 809
 - solubility in acid, 620
- Plutonium liquid-metal solutions, 757
- Plutonium nitrate, solubility in acid, 621
- Plutonium phosphate, solubility in acid, 620, 621
- Plutonium salt solutions, properties of, 617, 620, 621
 - solubilities of, 617, 620, 621
- Plutonium solutions in liquid metals, 751, 756-757
- Plutonyl chloride, solubility in acid, 621
- Plutonyl nitrate, solubility in acid, 621
- Poisoned catalyst, 707
- Poisons, 523
 - fission-product, 536
- Polonium, 797
 - as by-product, 746
 - formed from bismuth, 746
 - as hazard, 747
- Porous bodies, 441-442
- Position, measurement of, 935
 - remote indicators, 935
 - of rods, measurement of, 935
- Positioning, of regulating rods, 935
 - of safety rods, 933
 - of shim rods, 934
- Potassium chloride-uranium(III) chloride system, constitution diagram of, 817
- Potassium chloride-uranium(IV) chloride system, constitution diagram of, 816
- Potassium fluoride, vapor pressure of, 839
- Potassium fluoride-thorium fluoride system, constitution diagram of, 831
- Potassium fluoride-uranium(IV) fluoride system, constitution diagram of, 813
- Potassium fluoride-zirconium fluoride system, constitution diagram of, 827
- Potassium hydroxide, density of, 849
 - heat capacity of, 848
 - irradiation of, 840
 - melting point of, 848
 - vapor pressure of, 849
 - viscosity of, 849
- Potassium hydroxide-sodium hydroxide system, constitution diagram of, 821
- Potassium uranyl tricarbonate, solubility of, 607, 614
- Power, reactor, permissible, 522
- Power conversion, Daniels Power Pile, No. III, 1003
 - Homogeneous Reactor Experiment, 1037
- Power densities of aqueous homogeneous reactors, 507
- Power distribution, axial, 461
 - distortion by partly inserted control rods, 102
 - in bare and reflected reactors, 89-99
 - calculation of, 93, 96-99
 - in D_2O -moderated reactors, 99
 - effect of control elements, 99-103
 - effect of epithermal-flux/thermal-flux ratio on, 93, 94-95
 - effect of excess fuel loading, 93, 94-95
 - effect of moderating reflector on, 92, 93
 - effect of nonmoderating reflector on, 92, 93
 - effect of partly inserted control rods on, 102-103
 - effect of reflector saving on, 90-93
 - effect of water holes on, 103, 104-105
 - end effect in fuel slugs, 109
 - flattening of, 100-101, 104, 106, 108
 - in heterogeneous reactors, 106, 108-109
 - measured, in quasi-homogeneous reactors, 93, 96-99
 - methods of improving, 104-108, 109
 - in MTR, 96-97, 109
 - optimum, 461
 - radial, 461-462
 - in heterogeneous reactors, 106-109
 - during reactor transients, 141
 - in specific reactors, 109
 - Wilkins effect, 109
- Power plant, stationary vs. mobile, 311
- Power reactors, effect of temperature differences on, 7
 - fuel systems, 809
 - moderators, 803, 809

- Power reactors, stationary, fuel systems, 810
 - thermal cycles in, 7-20
- Power removal, 697
 - from boiling reactors, 698
 - by flash vaporization, 699-701
- Prandtl number, for air, 382, 391
 - for carbon dioxide, 398
 - for helium, 392
 - for light liquid water, 28-29, 37
 - for light-water vapor, 38
 - for liquid metals, as function of temperature, 278, 279
 - for steam, 38
- Pressure, of air, 385
 - effect on reactor criticality, 548
 - reactor, 477
- Pressure drop, 55-86, 371, 461, 466
 - build-up in filters, 499
 - for channels, friction factor in, 58, 60
 - of coolants, 477
 - data, average, for gases, 414-428
 - in duct components, 440
 - in ducts, 440
 - in folded reactor, 464
 - friction factor in, 58-60
 - for randomly packed spheres, 62, 63
 - across fuel-element channels, 508
 - for gases, turbulent flow, 495, 496
 - in headers, 440
 - nomenclature for, 55-57
 - in porous bodies, streamline flow, 441
 - turbulent flow, 441-442
 - rectangular ducts, 438-439
 - roughness, 443, 446
 - single-phase-flow, 55, 58-71
 - for flow inside tubes, non-circular channels, and annuli, 55, 58-61
 - for flow outside tube banks, normal to axis, 62
 - parallel to axis, 58, 60
 - for randomly packed spheres, 62, 63
 - trapezoidal ducts, 438-439
 - tube entrance, for gases, 419, 422
 - two-phase-flow, 69, 72-84
 - basic equations for, 69
 - critical mass velocity in, 77
 - effect of local boiling on, 76
 - methods of predicting, 72-76
 - sonic flow, 76, 77
 - in parallel channels, 76, 78-84
 - effect of orifices on, 82-84
 - with flow in same horizontal plane, 79, 81
 - with flow in same vertical plane, 81-82
 - single-channel equations, 78-80
 - velocity-head concept of, 62, 64-71
- Pressure-drop system calculations, for bend losses, 66, 68-70
 - for contraction losses, 64, 66, 67
 - for enlargement losses, 64, 66
- Pressure-drop system calculations, loss coefficient for bends, and angle of bend, 66, 68
 - loss coefficient for 90° bends, 66, 68
 - loss coefficient for sudden contraction, 66, 67
 - loss coefficient for sudden enlargement, 64, 66
 - for pipe flow, 64
 - for valves and fittings losses, 69, 71
 - velocity head of water, 64, 65
- Pressure gauge, electromagnetic, 795
- Pressure instrumentation, 795
- Pressure surges from nuclear power pulses, 549
- Pressurizer requirements for reactor stability, 548
- Prismatic shapes, effect of axial temperature gradients in, 169
 - long, distortion of, 167-168
 - thermal stress in, 168
- Process instrumentation, of HRE, 735-738
 - of Water Boiler, 733, 736
 - air-circulation safety, 736
 - catalytic recombination bed, 733
 - stack exhaust, 733
- Processing, of blanket, 536
 - rate, 545
- Production data, and criticality, 520
- Protactinium, 514
- Protective system, automatic, 942-944
- Pulsafeeder, HRE, 736
- Pumping power, 371
 - reactor, 477, 480
- Pumps, 342, 345-359, 708-716
 - applications, 345
 - bearings, 345
 - Byron Jackson, 789-790
 - canned-motor, 350
 - molten-metal, 790
 - canned-rotor, 350, 352, 708-717
 - for bismuth, 789
 - for molten salt, 789
 - small, 708-711
 - centrifugal, 789
 - DC Faraday, 358-359
 - diaphragm, 714, 716-717
 - electromagnetic, 345, 347, 350-359, 789, 791
 - General Electric, 791
 - helical-flow induction, 353, 357
 - linear-induction, 353-356
 - liquid metal, 788
 - for liquids, 788
 - magnetic, for bismuth, 789
 - mechanical, 345-346, 348-352, 789-793
 - positive displacement, 714, 716-717
 - pulsafeeder, 714, 716-717
 - requirements, general, 342
 - special, 342, 345

INDEX

Pumps, shaft-seal, 345, 351
 20,000-gpm Allis-Chalmers, 713-715, 717
 Westinghouse model 100 and 100A, 710, 712-713

Purification, of helium, 498

of NaK, 291-293

cold trap, 291-293

melt station, 291

of sodium, 291-293

cold trap, 291-293

melt station, 291

Purification process, 498

R

Radial thermal flux, 461-462

Radiation, decomposition of water by, 673-678

effect of pressure on, 675, 677

effect on glass, 881-884, 890, 892

effect on zinc bromide solution, 879

Radiation damage, by aqueous thorium nitrate, 642

metal solutions free from, 746

Radiation measurement, 797

Radiation stability, of fissioning solution, 560, 573-574

of uranyl carbonate, 607, 615-616

of uranyl fluoride, 585

Radioactive particles, 491, 499

filters for, 499-501

Radioactivity in coolants, 493-502

Radioargon, 483

Reactions, neutron, in water, 235-238

Reactivity, fluctuations of, 745

in reactor kinetics, 548-549

temperature coefficient of, 679

in CP-3', 144

in CP-5, 144

in MTR, 144

in water-cooled reactors, 141, 143-144

variations, and power flattening, 104, 106

Reactor atmosphere, Chicago Pile No. 2, 994

Reactor breeder blankets, fluorides, 805, 809, 830-833, 849

fused salts, 804-805

hydroxides, 804

Reactor coolants, fused-hydroxide (see Reactor moderator-coolants, fused-hydroxide)

fused-salt, irradiation of, 838, 846

properties of, 810, 824-827, 849

(See also Chlorides, Fluorides, and Fused salts)

Reactor equations, solution in phase plane, 550

Reactor fuels, fused-hydroxide, for breeders, 809

constitution diagrams of, 809, 819-823

corrosiveness of, 838

for homogeneous reactors, 810

irradiation of, 837

Reactor fuels, fused-hydroxide, properties of, 803, 835-838

(See also Hydroxides)

fused-salt, boiling points of, 805

constitution diagrams of, 811-818, 824-827, 830-833

melting points of, 805

properties of, 803, 809

(See also Chlorides, Fluorides, and Fused salts)

Reactor kinetics, in aqueous homogeneous systems, 545, 547-552

of circulating nonboiling systems, 547-550

and reactivity, 548-549

relations between nuclear and physical systems, 549

solution of equations, 549-550

Reactor moderator-coolants, fused-hydroxide, corrosiveness of, 840-848

irradiation of, 839

physical and thermal properties of,

810, 819-823, 846, 848-849

Reactor moderators, absorption cross-sections of, 806

fused-salt, 803-805

Reactor-power-plant system, optimizing, 697

Reactor vessels, one-core, design problems of, 691-696

two-core, design problems of, 691-696

Reactors, bare, power distribution in, 89-99

blower power, 477

chart of, 987-989

components, 321-329

cross-sectional flow area in, 477

design compilation, 987-989

diameter, 461

equivalent bare, use in control-rod calculations, 101-102

use in estimating flux distribution, 90, 109

heat generated in, 477

heterogeneous, power distribution in, 105, 106-109

liquid-metal-fuel, external cooling of, 771-772

internal cooling of, 771

MTR, refueling of, 855-859

output, 477

pressure in, 477

pumping power in, 477, 480

recharging of (see Remote handling)

reflected, power distribution in, 89-99

safety considerations, 552

single-region, 691, 692

typical arrangement for, 692

temperatures, 477, 536, 539-540

two-region, 691-693

design of core tank in, 695

typical arrangement for, 693

Recombiner, Los Alamos Water Boiler, 1033-1035

Recorders, 979
 Reduction of uranyl ion, 560
 Reflector saving, effect on power distribution, 90-93
 Refractive indices, of aqueous thorium nitrate, 642, 651
 of $\text{UO}_2\text{SO}_4\text{-H}_2\text{O}$ system, 581, 585
 Regulating rod assembly, HRE, 684
 Regulation, automatic power, 935-942
 Relative roughness, of channels, 58, 59
 of pipes, 58, 59
 Relaxation methods, use in control-rod calculations, 114, 117
 Release of safety rods, 933
 Remote handling, 855-873
 Remote maintenance, 721
 periscope in, 724
 replacement procedure in, 724-725
 shielding, 724
 tools for, 724-726
 Reprocessing, in LMFR, integrated with reactor, 747
 Residual heat removal, 334
 need for, 334
 Resistance welding, 452
 Resolution, visual, in periscopes, 893
 in television, 903
 through windows, 877
 Resonance absorption, 512
 Resonance absorption integral, 520
 Resonance escape probability, 520
 Reynolds number, and Stanton number, 430
 Rod-type fuel elements, 451-460
 Rods, control, drive requirements, 933
 long solid, thermal stress in, 166
 mechanical, 681-685
 position of, accurate measurement, 935
 position indexing, 935
 regulating, 935
 automatic operation, 942
 control, 936-942
 control loop, 936, 937
 characteristics, 938
 control-system components, 938
 normalized error, 936, 938-940
 performance evaluation, 941-942
 range, 936
 safety, 933
 shim, 934
 automatic operation, 942
 shim-safety, 935
 Rotameters, 796
 for liquid sodium and bismuth, 796
 Rotary pumps, 708-717
 Rotors, 469
 Roughness, 443, 445-446
 Roughness ratio, definition of, 443
 Rubidium fluoride, vapor pressure of, 839

Rubidium fluoride-thorium fluoride system, constitution diagram of, 832
 Rubidium fluoride-uranium(IV) fluoride system, constitution diagram of, 814

S

Safety considerations, reactor, 552
 Safety-rod assembly, HRE, 683
 Salts, molten, 789
 (See also Fused salts)
 Sampler, connection of, 729
 for high-pressure helium, in HRE pressurizing system, 729, 732
 molten-fuel, 794
 Sampling, 725-794
 of NaK, 293
 of sodium, 293
 Sampling apparatus, alternate, 729, 731
 for D_2O , 729, 731
 gas, 729, 732
 reflector, 729, 730
 Savannah River reactors, fuel-element design, 241
 Scanning, with periscopes, 893
 in mirror systems, 888
 Sealing of filters, 499
 Seals, 323-325
 frozen static, 323
 liquid trap, 324-325
 rotating, frozen, 323, 324
 rubber boot, 323, 324
 welded, 323-325
 wobble, 324-325
 Secondary coolant, arguments for and against, 777-778
 ideal, properties of, 772
 mercury, 781-782
 sodium, 782, 784
 Secular equations for heavy isotopes, 516
 Seeing (see Viewing)
 Self-welding, 295
 metal-to-metal, 791
 Separators, vapor, in boiling reactors, 697
 Shaft bearings, 469, 471-472, 475
 Shaft seals, 469, 471-472, 475
 Shell absorption, and U^{235} critical concentration, 533, 534
 Shielding, Argonne Heavy Water Reactor, 1017
 Argonne Research Reactor, 1018
 Brookhaven Graphite Research Reactor, 999
 Bulk Shielding Reactor, 1012
 Chicago Pile No. 2, 994
 Experimental Breeder Reactor, 1025
 gamma (see Hot laboratories)
 Homogeneous Reactor Experiment, 1253
 Los Alamos Fast Reactor, 1025

INDEX

- Shielding, Los Alamos Water Boiler, 1033
 - Low-Intensity Training Reactor, 1011
 - Low-Power Research Reactor, 1031
 - Materials Testing Reactor, 1007
 - ORNL Graphite Reactor, 996
 - Thermal Test Reactor, 1021
 - by water immersion, 875-876
 - by windows, 876
- Shutdown, nuclear reactor, 943
- Silicon, corrosion by NaOH, 842
- Silicon carbide, corrosion by NaOH, 847
- Silver, and alloys, corrosion in water, 212, 214
 - corrosion by NaOH, 841, 843
- Silver-cadmium alloys, corrosion in water, 212, 214
- Silver sulfate, solubility of, in uranyl sulfate, 635-636
 - in water, 635-636
- Single-channel equations, for two-phase-flow
 - pressure drop in parallel channels, 78-80
- Single-cycle systems, 312
- Slowing down of neutrons, heat generated by, 111
- Slurries, aqueous, properties of, 659-662
 - bentonite-stabilized, 662-663
 - density of, 666-668
 - heat transfer by forced convection, 665
 - stable, 662-664
 - thermal properties of, 665
 - ThO₂-D₂O, 533
 - thorium oxide, 669-670
 - corrosive-erosive behavior of, 670
 - radiation stability of, 670
 - unstable, 670
 - UO₃, characteristics of, 661, 662
 - U₂O₅, stable, 664
 - uranium, 659-669
 - uranium oxide, erosion behavior of, 668-669
 - particle-size growth in, 661-663
 - radiation stability of, 664-665
 - stability of, 659-669
 - under dynamic conditions, 659, 661
 - viscosity of, 666-668, 747
- Sodium, density of, 850
 - melting point of, 850
 - physical properties of, 773
 - thermal conductivity of, 850
 - viscosity of, 850
- Sodium antimonate, corrosion by NaOH, 847
- Sodium chloride-uranium(III) chloride system,
 - constitution diagram of, 818
- Sodium chloride-uranium(IV) chloride system,
 - constitution diagram of, 815
- Sodium fluoride, vapor pressure of, 839
- Sodium fluoride-uranium(IV) fluoride system,
 - constitution diagram of, 812
- Sodium hydroxide, corrosion of ceramics by, 846, 847
 - corrosion of metals and alloys by, 840-847
- Sodium hydroxide, corrosiveness of, 840
 - effect of impurities on, 846
 - density of, 849, 850
 - heat capacity of, 848
 - irradiation of, 839, 840
 - melting point of, 848, 850
 - thermal conductivity of, 846, 850
 - vapor pressure of, 849
 - viscosity of, 849, 850
- Sodium hydroxide-rubidium hydroxide system,
 - constitution diagram of, 822
- Sodium uranyl carbonate, preparation of, 607
 - solubility of, 607, 612-614
- Sodium uranyl tricarboxylate-sodium bicarbonate-water system, solid phases of, 611
 - solubility of, 611
- Solid-fuel reactors, heat dissipation in, 8-10
 - methods of heat removal, 7-8
 - steady-state heat removal, 123-139
 - (See also Cooling, of solid-fuel reactors)
- Solubility, of barium sulfate, in uranyl sulfate, 633-634
 - at 250°C, 633-634
 - in water, 633
- of cadmium sulfate, in uranyl sulfate, 637-638
 - in water, 637
- of ceric sulfate, in uranyl sulfate, 630-631
 - in water, 630-631
- of cesium sulfate, in uranyl sulfate, 628-629
 - in water, 628
- of gases, in water, 675
- of lanthanum sulfate, in uranyl sulfate, 625, 627
 - in water, 625-626
- of molybdenum oxide, in aqueous uranyl sulfate, 622
- of multiple fission products, in aqueous uranyl sulfate, 622
- of 2Na₂CO₃·UO₂CO₃, 617
- of plutonium fluoride, 620
- of plutonium nitrate, 621
- of plutonium phosphate, 620, 621
- of plutonium salts, 617, 620-621
- of plutonyl chloride, 621
- of plutonyl nitrate, 621
- of potassium uranyl tricarboxylate, 607, 614
- of silver sulfate, in uranyl sulfate, 635-636
 - in water, 635-636
- of sodium uranyl carbonate, 607, 612-614
 - of strontium sulfate, in water, 632
- of thorium nitrate, in water, 643, 645-646
- of UO₂F₂, in water, 591
- of UO₃, in uranyl fluoride, 581, 589
 - in uranyl sulfate, 560, 568-569
- in UO₃-CO₂-H₂O-K₂CO₃ system, 616
- of uranium, in bismuth, 746
- of uranyl sulfate, 555-565
- of yttrium sulfate, in uranyl sulfate, 623-624

- Solubility, of zinc sulfate, in water, 639
 of zirconium sulfate, in aqueous uranyl sulfate, 622
- Solutions, metal, free from radiation damage, 746
- Sonic flow, method of predicting, 76, 77
- Specific gravity, of UO_2F_2 solutions, 591
- Specific heat, of air, 382, 389
 at constant pressure, 388
 at constant volume, 387
 of elements, 1044-1045
 of gases, 403
 of heavy liquid water, 24, 32
 of helium, 392, 394
 of light liquid water, 22-23, 32
- Specific-heat ratio, 479
 for air, 402
 for carbon dioxide, 402
 for CH_4 , 402
 for C_2H_4 , 402
 for hydrogen, 402
 for nitrogen, 402
 for oxygen, 402
 for water, 402
- Specific power, maximum, 697
 of reactor, 479
- Spheres, randomly packed, forced-convection
 heat transfer through, 50
 pressure drop for, friction factor in, 62, 63
 single-phase-flow, 62, 63
- Spherical reactors, two-region, 523, 533-538
- Split flow, 433
- Split-flow design, 463-465
- Stability, chemical, of uranyl fluoride solutions, 581-593
 of uranyl sulfate solutions, 555-570
 of fuel elements, 451
 radiation, of uranium oxide slurries, 664-665
 of uranyl fluoride, 581
 of uranium oxide, 659-669
 under dynamic conditions, 659, 661
- Stack, gas velocity across, 486
- Stack design, 486
- Stack effluent, rise of, 484-485
- Stack parameters, 484
- Stainless steel, 451
 austenitic 300 series, corrosion in water, 215, 217-219
 cleaning of, 794
 corrosion of, by $\text{Ba}(\text{OH})_2$, 848
 by LiOH , 848
 by NaOH , 841, 842
 by $\text{Sr}(\text{OH})_2$, 848
 in water, 215-224
 decontamination of, 794
 ferritic 400 series, corrosion in water, 221
 heat-resistant, corrosion in water, 222
 high-alloy, corrosion in water, 222
- Stainless steel, martensitic 400 series, corrosion in water, 215
 precipitation-hardening, corrosion in water, 221
 radioactivity in, 688
 (See also Steel)
- Stanton number, and Reynolds number, 430
- Static rupture, of brittle material, 171
 of ductile material, 171
- Stationary-fuel reactor, steady-state heat removal, 123-139
- Steam, dynamic viscosity of, 36
 Prandtl number for, 38
 thermal conductivity of, 34
- Steam cycles available for power generation, 11-17
 compression process, 11
 expansion process, 12
 heat-addition process, 11
 heat-rejection process, 12
- Steam evaporator, HRE, 735
- Steam-generating equipment, 779-780
- Steam generators, 337-344
 EBR superheater performance, 342
 over-all coefficients for KAPL units, 338, 341
- Steam plant efficiencies, 12-17
- Steel, carbon, corrosion in water, 214-221
 corrosion by NaOH , 841, 842
 low-alloy, corrosion in water, 214
 (See also Stainless steel)
- Stellites (see Cobalt alloys)
- Stepped labyrinth glands, 469
- Storage for helium decay, 498
- Straight-through design, 463-466
 of light liquid water, 24-25, 33
 of light-water vapor, 34
 in solid-fuel reactors, 7-20
 of steam, 34
- Strain analysis, 165-173
- Stress analysis, 165-173
- Stress equations, solution of, 694
- Stresses, pressure, formulas for, 694
 principal types of, 691
 and temperature distributions, for spheres, rods, tubes, and plates, 695
 thermal, 691
- Strontium hydroxide, corrosion of alloys and metals by, 848
 heat capacity of, 848
 melting point of, 848
- Strontium sulfate, solubility in water, 632
- Structural materials, corrosion of, 193, 194
- Supercritical pressure, heat transfer at, 52
- Supercritical reactors, methods of heat removal, 8
- SUPO (see Los Alamos Water Boiler)
- Surface tension, of $\text{UO}_2\text{SO}_4\text{-D}_2\text{O}$ system, 581, 583-584

INDEX

Surface tension, of $\text{UO}_2\text{SO}_4\text{-H}_2\text{O}$ system, 581, 583-584
 of uranyl nitrate solutions, 600
 Sutton equation, 493
 nomograms for, 493-495

T

Tank assembly, HRE, 682
 Television, 903, 908
 Temperature, effect on reactor criticality, 548
 reactor, 477
 effect on U^{235} enrichment, 523, 532
 Temperature coefficient as control mechanism, 106
 Temperature-coefficient power regulation, 944-945
 Temperature differences, effect on power-reactor design, 13, 18
 Temperature distribution, clad fuel plate in
 flowing coolant, 147, 149
 clad fuel plate in stagnant coolant, 146-151
 in fuel plates, for arbitrary power distribution, 152-164
 during exponential power rise, 145-149
 in solid-fuel reactors, 126-130
 and stresses, for spheres, rods, tubes, and plates, 695
 unclad fuel plate in stagnant coolant, 145-147
 Temperature-entropy diagram for helium, 395
 Temperature gradients, axial, 169
 Tensile stress in spherical reactor core vessel, 696
 Thermal conductivity, of air, 382, 391
 of carbon dioxide, 398
 of elements, 1044-1045
 Eucken equation for, 406
 of gases, 400-401
 correlations for, 405
 of helium, 392, 394
 Thermal cycles, in gas-cooled reactors, 375-379
 Thermal decomposition, of uranyl nitrate, 593
 of uranyl nitrate solutions, 594, 597-598
 Thermal-gradient transfer, 295
 Thermal-neutron absorption cross section, of
 elements, 1044-1047
 of gas coolants, 480
 of helium, 496
 Thermal properties of slurries, 665
 Thermal reactors, control of, 805, 807
 fuel salts, 804
 fuel systems, 803, 809, 810
 hydrogenous fuels, 804, 809
 moderators, 803
 Thermal resistance, concept, 127
 formulae, 127, 129
 modified, 129-130

Thermal shield, heat generation in, 118
 Thermal shock, 330
 Thermal shock shields, 327-333
 cyclic uniaxial stresses, 330
 thermal stresses in, from thermal gradients, 327, 329
 estimate of, 329
 transient thermal gradients, 327
 Thermal stability of gas coolants, 480
 Thermal-strain analysis, 165-173
 Thermal stress, 451
 and creep, 171
 cyclic, 170
 due to heat generation, 165-166
 effects of, 171
 on irregular shapes, 171
 and fatigue, 171
 and fatigue fracture, 170
 formulas, 165-168
 and fracture, 170
 general considerations of, 169-170
 from growth due to irradiation, 172
 in hollow tube, 167
 and irradiation effects, 172
 in long solid rod, 166
 magnitude of, 169-170
 in multiply connected body, 169
 nature of, 169
 nomenclature, 166
 in plate, 166-167
 in prismatical shapes, 168
 in reactor core structures, 169
 significance of, 170-171
 units, 166
 Thermal-stress analysis, 165-173
 methods of, 165-169
 of simple shapes, 166-167
 Thermal Test Reactor, 1021-1022
 design data, 1022
 fuel elements, 1021
 shielding, 1021
 Thermodynamic properties, of helium, 392-393
 of light and heavy water, 21-42
 $\text{ThO}_2\text{-D}_2\text{O}$ slurry, constants for, 519
 Thorium, absorption cross section for, in fast
 region, 520
 and alloys, corrosion in water, 224
 build-up from, in blanket, 514
 concentration, 536-538
 liquid-metal dispersions of, 769, 770
 solubility of, in liquid metals, 751, 756
 in liquid metals and alloys, 751, 756
 Th^{232} , 514
 Th^{233} , 514
 Thorium-bismuth-lead system, isothermal
 section of, 769, 770
 Thorium compounds, ionic, 769
 Thorium fluoride as breeder blanket, 804, 849

- Thorium nitrate, aqueous, acidity of, 642
 activity coefficient of, 650
 boiling points of, 649, 651
 density of, 642, 647-648
 free energy of dilution of, 642, 652-654
 heat of dilution of, 642, 652-654
 osmotic pressure of, 650
 refractive indices of, 642, 651
 vapor pressure of, 642, 649-651
 work of dilution of, 642, 652-654
 corrosion by, 642
 heat of solution of, 642
 hydrolytic and phase stability of, 644
 radiation damage by, 642
 solubility in water, 643-646
 Thorium nitrate-water system, 642, 643-644
 Thorium oxide slurries, 669-670
 corrosive-erosive behavior of, 670
 radiation stability of, 670
 unstable, 670
 Thorium solutions in liquid metals, 751, 756
 Thorium-uranium-233 breeder reactors, 691
 Thrust bearing, 469, 475
 Time-dependent reactor behavior, 926, 928-932
 Tin-uranium system, 760-762
 phase diagram of, 761, 762
 Titanium, corrosion of, by NaOH, 842
 in water, 225
 Titanium carbide, corrosion by NaOH, 847
 Titanium carbide mixture, corrosion by NaOH, 847
 Titanium nitride, corrosion by NaOH, 847
 Titanium oxide, corrosion by NaOH, 847
 Topography, effect on meteorology, 488, 491, 492
 Transfer function, reactor, 929, 931-932
 Transients, calculation of thermal response, 161-164
 exponential temperature distributions, 145-152
 reactivity independent of power level, 141-143
 reactor power, 141-164
 Transitory conditions in meteorology, 488
 Triuranyl phosphate, crystal forms of, 617
 TTR (see Thermal Test Reactor)
 Tube banks, forced-convection heat transfer
 across, basic equations for, flow
 normal to axis, 47, 49
 flow parallel to axis, 47
 single-phase-flow pressure drop for, flow
 normal to axis, 62
 flow parallel to axis, 58, 60
 Tubes, hollow, thermal stress in, 181
 single-phase-flow pressure drop in, 55, 58-61
 Tungsten, corrosion by NaOH, 842
 Tungsten carbide, corrosion by NaOH, 847
 Turning losses, 433-436
 in folded reactor, 464
 Two-group critical equation, 512
 Two-liquid phase region, in acid-deficient systems, 555
 in acid-rich solutions, 555
 in uranyl fluoride solutions, 581, 589
 in uranyl sulfate solutions, 555
 Two-region reactors, 512-513
- ## U
- UF₆ fuel, 746
 UO₃-CO₂-H₂O-K₂CO₃ system, density in, 616
 solubility in, 616
 UO₂F₂-HF-H₂O system, 581, 589, 590
 densities in, 592
 UO₃-HNO₃-H₂O system, density of, 601
 UO₃·H₂O, polymorphic forms of, 594
 UO₂(NO₃)₂-HNO₃-H₂O, density of, 599
 UO₂(NO₃)₂-HNO₃-H₂SO₄-H₂O system, density of, 599, 602
 Uranium, corrosion in water, 225
 constants for, 516
 dispersions of, 758-769
 intermetallic-compound, properties of, 760
 ionic-compound, properties of, 768, 769
 isotopes of, higher, 545
 solubility of, in bismuth, 746
 in liquid bismuth-lead, 754
 in liquid metals and alloys, 751, 752
 U²³³, breeding, one-region reactor for, 523
 two-region reactors for, 536
 conversion, one-region reactor for, 523
 two-region reactors for, 533-542
 producers, constants for, 519
 in blanket, core fed with, 517
 U²³⁸, 517
 U²³⁷, 514
 Uranium-aluminum system, phase diagram of, 765, 767
 Uranium-bismuth solutions, 751, 755, 789
 corrosion of container materials by, 751
 Uranium-cadmium system, 766
 Uranium-calcium system, 760, 766
 Uranium-cerium system, 760, 766
 Uranium(III) chloride, phase studies of, 810, 817-818
 Uranium(IV) chloride, phase studies of, 810, 815-816
 Uranium chlorides (see Reactor fuels, fused-salt, and under specific compounds and systems)
 Uranium compounds, solubility in hydroxides, 835-837
 suspensions in hydroxides, 837
 U²³⁸ diluent, 518
 Uranium(IV) fluoride, vapor pressure of, 839
 Uranium fluorides, phase studies of, 809
 (See also Reactor fuels, fused-salt, and under specific compounds and systems)

INDEX

- Uranium oxide, conversion ratio, 523, 530
 - critical enrichment of, 523, 530
 - crystallography of, 661
- Uranium(VI) oxide, solubility in hydroxides, 835-837
 - suspensions in hydroxides, 837
- Uranium oxide-phosphoric acid-water system, thermal stability of, 617, 618
- Uranium oxide slurries, erosion behavior of, 668-669
 - particle-size growth in, 661-663
 - radiation stability of, 664-665
 - U_2O_5 , stable, 664
- Uranium oxide-sodium carbonate-water system, solid phases of, 610
 - solubility of, 610
- Uranium peroxide, decomposition in solution, kinetics of, 574
 - formation in fissioning solutions, 574
 - solubility of, 574
- Uranium slurries, 659-669
- Uranium solutions, fission-product activity of, 724
 - in liquid metals, 751-755
- Uranium trioxide, preparation of, 661
 - slurry characteristics, 661, 662
 - solubility of, 560, 568-569
 - in uranyl fluoride, 581, 589
- Uranyl carbonate, complexes, 607
 - gas and peroxide production of, 615, 616
 - preparation of, 606
 - radiation stability of, 607, 615-616
 - solubility of, 607
- Uranyl carbonate-sodium carbonate-water system, solid phases of, 607-609
 - solubility of, 607-609
- Uranyl complexes, new complex sodium-uranyl-carbonates, 607
 - uranyl-metal-carbonates, 607
- Uranyl fluoride, acid-rich system, 585, 589, 590
 - acidity of, 585, 591
 - heat capacity of, 585
 - hydrolysis of, 581
 - radiation stability of, 585
 - solubility of, 581-588
 - in water, 591
 - solubility of UO_3 in, 581, 585, 589
 - two-liquid phase region, 585, 589
- Uranyl fluoride solutions, density of, 592, 593
 - specific gravity of, 591
- Uranyl ion, reduction of, 560
- Uranyl nitrate, anhydrous, preparation of, 593
 - conversion ratio, 523, 531
 - critical enrichment of, 523, 531
 - density in H_2O , 594, 599, 600
 - dissociation in solution, 593
 - heat of decomposition of, 593
- Uranyl nitrate, hydrated, boiling points of, 594
 - melting points of, 594, 595
 - solubility in water, 594, 595
 - thermal decomposition pressures of, 593
- Uranyl nitrate hexahydrate, heat capacity of, 603
 - solid, heat capacity of, 599, 603
- Uranyl nitrate solutions, containing sulfuric and nitric acids, density of, 599, 602
 - density of, 594, 599-602
 - heat capacities of, 599, 602-604
 - heats of dilution of, 604-606
 - heats of solution of, 604-606
 - hydrolysis above $250^\circ C$, 594
 - stability at high temperatures, 594, 596
 - surface tension of, 600
 - thermal decomposition of, 594, 597-598
 - viscosity of, 600
- Uranyl phosphate, properties of, 615
- Uranyl sulfate, heat of solution of fission products in, 622
 - hydrolysis of, 560, 566-570
 - properties of, 560, 574
 - reduction of uranyl ion, 560
 - solubility of, in D_2O , 555
 - in H_2O , 555-556
 - solubility in, of barium sulfate, 633-634
 - at $250^\circ C$, 633-634
 - of cadmium sulfate, 637-638
 - of ceric sulfate, 630-631
 - of cesium sulfate, 628-629
 - of lanthanum sulfate, 625, 627
 - of molybdenum oxide, 622
 - of multiple fission products, 622
 - solubility in, of silver sulfate, 635-636
 - of UO_3 , 560, 568-569
 - of yttrium sulfate, 623-624
 - of zirconium sulfate, 622
- Uranyl tricarbonate ion, dissociation constant of, 607
 - evidence for, 607

V

- Valves, 359, 717-720, 791, 793
 - corrosion-resistant, 717
 - leakproof, 717
 - radiation-resistant, 717
- Valves and fittings losses, pressure-drop system calculations for, 69, 71
- Vanadium, corrosion by $NaOH$, 842
- Vapor pressure, of aqueous thorium nitrate, 642, 649-651
 - of heavy liquid water, 30
 - of light water, 41
- Vapor traps, 294

- Velocity, of regulating rods, 935
 of safety rods, 933
 of shim rods, 934
- Velocity distribution, for gases, 414, 415
 in triangular passages, 440
- Velocity head, of water, 64, 65
- Velocity-head concept of pressure drop, 62, 64-71
- Vessels, neutron absorbers in, 721
- Viewing, basic techniques of, 875
 through periscopes, 890, 891
 requirements in, 875
 by simple reflection, 888-889
 by television, 903, 908
 of underwater objects, 875-876
 through windows, 876-889
 (See also Hot laboratories)
- Viscosity, of air, 382, 391
 empirical correlation for, 406-407
 of carbon dioxide, 398
 empirical correlation for, 406-407
 of gases, 399, 404
 effect of pressure on, 405
 of gases, empirical correlations for, 406-407
 of helium, 392, 394
 empirical correlation for, 406-407
 of slurries, 666-668, 747
 of $\text{UO}_2\text{SO}_4\text{-D}_2\text{O}$ system, 575, 579-580
 of $\text{UO}_2\text{SO}_4\text{-H}_2\text{O}$ system, 575, 579-580
 of uranyl nitrate solutions, 599, 600, 602
- Vitallium, corrosion by NaOH, 841
- Volume, of heat-transfer passages, in reactor, 480

W

- Water, decomposition of, 560, 707
 by fast neutrons, 674
 by fission fragments, 674
 by fissioning solutions, 560, 571
 by gamma rays, 674
 by radiation, 673-678
 effect of pressure on, 675, 677
 effect of temperature on, 677-678
 and steady-state pressure, 675
 effect of temperature on, 677-678
- density of, 850
- heavy, critical properties of, 22
 latent heat of vaporization of, 31
 liquid, density of, 30
 dynamic viscosity of, 27, 35
 specific heat of, 24, 32
 vapor pressure of, 30
 physical and thermodynamic properties of, 21-42
 (See also Heavy water)
- ionization of, 176-177
- light, critical properties of, 22
 density of, 39-40

- Water, light, heat-transfer coefficient for, 47, 49
 liquid, dynamic viscosity of, 26-27, 35
 Prandtl number for, 28-29, 37
 specific heat of, 22-23, 32
 thermal conductivity of, 24-25, 33
 physical and thermodynamic properties of, 21-42
 vapor pressure of, 41
 (See also Light water)
- properties of aqueous moderators, 673-678
 reaction with alkali metal, 301, 306
 specific-heat ratio for, 402
 thermal conductivity of, 850
 thermal properties of, 678
 velocity head of, 64, 65
 for viewing, 875-876, 878
 viscosity of, 850
- Water activity, calculation of, 235-238
- Water corrosion (see Corrosion, in water)
- Water decomposition, 175-191
 Argonne Heavy Water Reactor, 188-190
 back reaction, 176
- Water holes, effect on flux distribution, 103, 104-105
- Water vapor, light, dynamic viscosity of, 36
 Prandtl number for, 38
 thermal conductivity of, 34
- Wave-shaped plates, 438-440
- Weld, bellows, 791
- Welding, 458
- Wilkins effect, 109
- Wind, variation of, 491, 492
- Wind-tunnel tests, 485
- Windows, applications of, 876-877
 defects of, 877-878
 shielding, 876
 construction of, 885-889
 design of, 881, 885
 materials for, 878-884
- Work in pumping coolants, 477
- Work of dilution, of aqueous thorium nitrate, 642, 654
- Worthite, corrosion by NaOH, 842
 (See also Iron alloys)

X

- X-10 (See ORNL Graphite Reactor)
- Xenon, equilibrium concentration in homogeneous reactor, 622
 growth in reactor, 622
- X^{135} , removed by gas sparging, 747

Y

- Yttrium sulfate, solubility of, in uranyl sulfate, 623-624
 in water, 623

INDEX

Z

- Zinc bromide solution, 878-880
- Zinc fluoride, vapor pressure of, 839
- Zinc oxide, corrosion by NaOH, 847
- Zinc sulfate, solubility in water, 639
- Zircaloy 1, 229
- Zircaloy 2, 229
- Zirconium, alloyed, corrosion in water, 228-229
 - corrosion of, by Ba(OH)₂, 848
- Zirconium, corrosion of, by NaOH, 841, 843
 - by Sr(OH)₂, 848
 - in water, 225, 228-230
 - effect of impurities on, 228
 - unalloyed, corrosion in water, 228
- Zirconium carbide, corrosion by NaOH, 847
- Zirconium fluoride, vapor pressure of, 839
- Zirconium oxide, corrosion by NaOH, 846, 847
- Zirconium shell, 523, 533
- Zirconium sulfate, solubility in aqueous uranyl sulfate, 622

